RENAL FUNCTION IN ACUTE AND CHRONIC KIDNEY DISEASES

EDITED BY: John D. Imig, Xueying Zhao and Md Abdul Hye Khan
PUBLISHED IN: Frontiers in Physiology, Frontiers in Medicine and Frontiers in Pharmacology

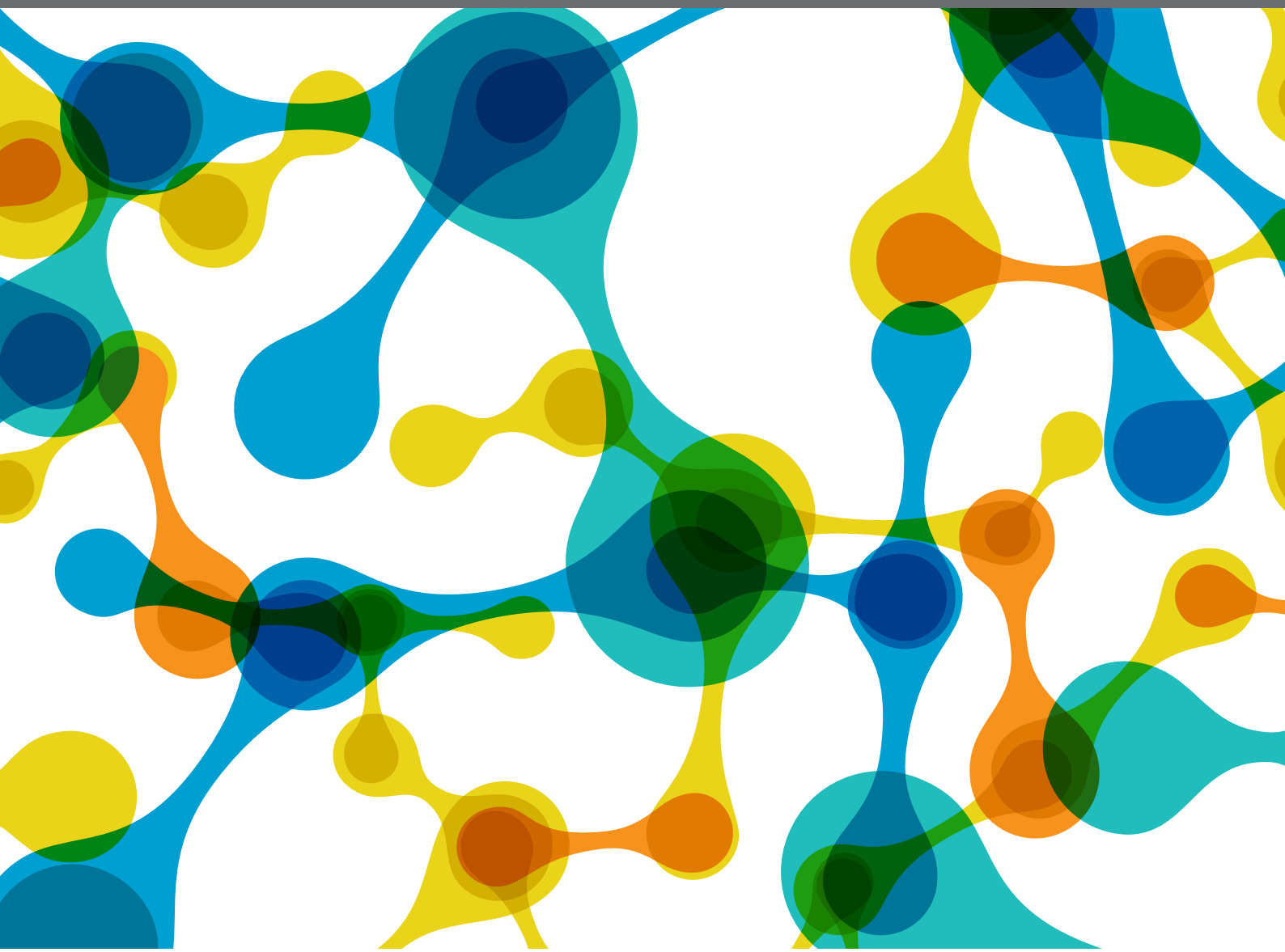

frontiers Research Topics

frontiers

Frontiers eBook Copyright Statement

The copyright in the text of individual articles in this eBook is the property of their respective authors or their respective institutions or funders. The copyright in graphics and images within each article may be subject to copyright of other parties. In both cases this is subject to a license granted to Frontiers.

The compilation of articles constituting this eBook is the property of Frontiers.

Each article within this eBook, and the eBook itself, are published under the most recent version of the Creative Commons CC-BY licence. The version current at the date of publication of this eBook is CC-BY 4.0. If the CC-BY licence is updated, the licence granted by Frontiers is automatically updated to the new version.

When exercising any right under the CC-BY licence, Frontiers must be attributed as the original publisher of the article or eBook, as applicable.

Authors have the responsibility of ensuring that any graphics or other materials which are the property of others may be included in the CC-BY licence, but this should be checked before relying on the CC-BY licence to reproduce those materials. Any copyright notices relating to those materials must be complied with.

Copyright and source acknowledgement notices may not be removed and must be displayed in any copy, derivative work or partial copy which includes the elements in question.

All copyright, and all rights therein, are protected by national and international copyright laws. The above represents a summary only. For further information please read Frontiers' Conditions for Website Use and Copyright Statement, and the applicable CC-BY licence.

ISSN 1664-8714
ISBN 978-2-88966-400-9
DOI 10.3389/978-2-88966-400-9

About Frontiers

Frontiers is more than just an open-access publisher of scholarly articles: it is a pioneering approach to the world of academia, radically improving the way scholarly research is managed. The grand vision of Frontiers is a world where all people have an equal opportunity to seek, share and generate knowledge. Frontiers provides immediate and permanent online open access to all its publications, but this alone is not enough to realize our grand goals.

Frontiers Journal Series

The Frontiers Journal Series is a multi-tier and interdisciplinary set of open-access, online journals, promising a paradigm shift from the current review, selection and dissemination processes in academic publishing. All Frontiers journals are driven by researchers for researchers; therefore, they constitute a service to the scholarly community. At the same time, the Frontiers Journal Series operates on a revolutionary invention, the tiered publishing system, initially addressing specific communities of scholars, and gradually climbing up to broader public understanding, thus serving the interests of the lay society, too.

Dedication to Quality

Each Frontiers article is a landmark of the highest quality, thanks to genuinely collaborative interactions between authors and review editors, who include some of the world's best academicians. Research must be certified by peers before entering a stream of knowledge that may eventually reach the public - and shape society; therefore, Frontiers only applies the most rigorous and unbiased reviews.
Frontiers revolutionizes research publishing by freely delivering the most outstanding research, evaluated with no bias from both the academic and social point of view. By applying the most advanced information technologies, Frontiers is catapulting scholarly publishing into a new generation.

What are Frontiers Research Topics?

Frontiers Research Topics are very popular trademarks of the Frontiers Journals Series: they are collections of at least ten articles, all centered on a particular subject. With their unique mix of varied contributions from Original Research to Review Articles, Frontiers Research Topics unify the most influential researchers, the latest key findings and historical advances in a hot research area! Find out more on how to host your own Frontiers Research Topic or contribute to one as an author by contacting the Frontiers Editorial Office: researchtopics@frontiersin.org

RENAL FUNCTION IN ACUTE AND CHRONIC KIDNEY DISEASES

Topic Editors:
John D. Imig, Medical College of Wisconsin, United States
Xueying Zhao, Morehouse School of Medicine, United States
Md Abdul Hye Khan, Medical College of Wisconsin, United States

Topic Editor John D Imig is a Co-founder of Diplos Therapeutics (Ann Arbor, MI) and Nephraegis (Milwaukee, WI). All other Topic Editors declare no competing interests with regards to the Research Topic subject.

Citation: Imig, J. D., Zhao, X., Khan, M. A. H., eds. (2021). Renal Function in Acute and Chronic Kidney Diseases. Lausanne: Frontiers Media SA.
doi: 10.3389/978-2-88966-400-9

Table of Contents

06 ***Editorial: Renal Function in Acute and Chronic Kidney Diseases***
John D. Imig, Md Abdul Hye Khan and Xueying Zhao

10 ***Resveratrol Protects Against Post-Contrast Acute Kidney Injury in Rabbits With Diabetic Nephropathy***
Yongfang Wang, Bin Wang, Xun Qi, Xin Zhang and Ke Ren

21 ***The Impact of Versatile Macrophage Functions on Acute Kidney Injury and Its Outcomes***
Jea-Hyun Baek

35 ***Combined Blockade of Smad3 and JNK Pathways Ameliorates Progressive Fibrosis in Folic Acid Nephropathy***
Mengjie Jiang, Jinjin Fan, Xinli Qu, Songhui Li, Susan K. Nilsson, Yu Bo Yang Sun, Yaping Chen, Di Yu, Dan Liu, Bi-Cheng Liu, Mingliang Tang, Wei Chen, Yi Ren, David J. Nikolic-Paterson, Xiaoyun Jiang, Jinhua Li and Xueqing Yu

52 ***Metabolomics Study of Metabolic Changes in Renal Cells in Response to High-Glucose Exposure Based on Liquid or Gas Chromatography Coupled With Mass Spectrometry***
Liang Wang, Yan Du, Bing-ju Xu, Xu Deng, Qing-hua Liu, Qiao-qiao Zhong, Chen-xiang Wang, Shuai Ji, Meng-zhe Guo and Dao-quan Tang

63 ***Inhibition of IL-1β by Aliskiren Improved Renal AQP2 Expression and Urinary Concentration Defect in Ureteral Obstruction and Release***
Shan Hu, Haixia Xie, Renfei Luo, Pinning Feng, Qiaojuan Liu, Mengke Han, Yonglun Kong, Xuenong Zou, Weidong Wang and Chunling Li

76 ***Renoprotection Provided by Additional Diuretic Treatment in Partially Nephrectomized Ren-2 Transgenic Rats Subjected to the Combined RAS and ET_A Blockade***
Ivana Vaněčková, Silvie Hojná, Zdenka Vernerová, Michaela Kadlecová, Hana Rauchová, Elzbieta Kompanowska-Jezierska, Zdeňka Vaňourková, Luděk Červenka and Josef Zicha

86 ***PINK1 Deficiency Ameliorates Cisplatin-Induced Acute Kidney Injury in Rats***
Li Zhou, Ling Zhang, Yu Zhang, Xuan Yu, Xiuping Sun, Tao Zhu, Xianglei Li, Wei Liang, Yunlin Han and Chuan Qin

98 ***The Behavior of the Type of Peritoneal Transport in the Inflammatory and Oxidative Status in Adults Under Peritoneal Dialysis***
Julio Alejandro Gutiérrez-Prieto, Javier Soto-Vargas, Renato Parra-Michel, Héctor Leonardo Pazarín-Villaseñor, Andrés García-Sánchez and Alejandra Guillermina Miranda-Díaz

108 ***Neferine Attenuates Acute Kidney Injury by Inhibiting NF-κB Signaling and Upregulating Klotho Expression***
Huihui Li, Wenhang Chen, Yusa Chen, Qiaoling Zhou, Ping Xiao, Rong Tang and Jing Xue

121 ***Refining the Mouse Subtotal Nephrectomy in Male 129S2/SV Mice for Consistent Modeling of Progressive Kidney Disease With Renal Inflammation and Cardiac Dysfunction***
James O'Sullivan, Sarah Louise Finnie, Oliver Teenan, Carolynn Cairns, Andrew Boyd, Matthew A. Bailey, Adrian Thomson, Jeremy Hughes, Cécile Bénézech, Bryan Ronald Conway and Laura Denby

138 ***Heat Strain, External Workload, and Chronic Kidney Disease in Tropical Settings: Are Endurance Athletes Exposed?***
Daniel Rojas-Valverde, Guillermo Olcina, Randall Gutiérrez-Vargas and Jennifer Crowe

142 ***Farrerol Attenuates Cisplatin-Induced Nephrotoxicity by Inhibiting the Reactive Oxygen Species-Mediated Oxidation, Inflammation, and Apoptotic Signaling Pathways***
Ning Ma, Wei Wei, Xiaoye Fan and Xinxin Ci

157 ***Urolithiasis is a Risk Factor for Uroseptic Shock and Acute Kidney Injury in Patients With Urinary Tract Infection***
Chih-Yen Hsiao, Tsung-Hsien Chen, Yi-Chien Lee, Meng-Chang Hsiao, Peir-Haur Hung, Yih-Yuan Chen and Ming-Cheng Wang

164 ***The δ-Opioid Receptor Differentially Regulates MAPKs and Anti-inflammatory Cytokines in Rat Kidney Epithelial Cells Under Hypoxia***
Fengbao Luo, Renfang Xu, Guanglai Song, Hao Lu, Xiaozhou He and Ying Xia

178 ***Endothelin-1/Nitric Oxide Ratio as a Predictive Factor of Response to Therapy With Terlipressin and Albumin in Patients With Type-1 Hepatorenal Syndrome***
Ahmed Abdel-Razik, Nasser Mousa, Mostafa Abdelsalam, Ahmed Abdelwahab, Mona Tawfik, Ahmed M. Tawfik, Ahmad S. Hasan, Rania Elhelaly, Niveen El-Wakeel and Waleed Eldars

187 ***Renal Glomerular Mitochondria Function in Salt-Sensitive Hypertension***
Mark Domondon, Iuliia Polina, Anna B. Nikiforova, Regina F. Sultanova, Claudia Kruger, Valeriia Y. Vasileva, Mikhail V. Fomin, Gyda C. Beeson, Anna-Liisa Nieminen, Nancy Smythe, Eduardo N. Maldonado, Krisztian Stadler and Daria V. Ilatovskaya

202 ***Effect of Calcitriol on the Renal Microvasculature Differentiation Disturbances Induced by AT_1 Blockade During Nephrogenesis in Rats***
Amanda L. Deluque, Lucas F. de Almeida, Heloísa D. C. Francescato, Cleonice G. A. da Silva, Roberto S. Costa, José Antunes-Rodrigues and Terezila M. Coimbra

211 ***Protective Effects of Amlodipine Pretreatment on Contrast-Induced Acute Kidney Injury And Overall Survival in Hypertensive Patients***
Wen-jun Yin, Ling-yun Zhou, Dai-yang Li, Yue-liang Xie, Jiang-lin Wang, Shan-ru Zuo, Kun Liu, Can Hu, Ge Zhou, Lin-hua Chen, Hui-qing Yang and Xiao-cong Zuo

222 ***Advances in Understanding the Effects of Erythropoietin on Renal Fibrosis***
Yangyang Zhang, Xiaoyu Zhu, Xiu Huang, Xuejiao Wei, Dan Zhao, Lili Jiang, Xiaoxia Zhao and Yujun Du

229 ***Dexmedetomidine Protects Against Lipopolysaccharide-Induced Acute Kidney Injury by Enhancing Autophagy Through Inhibition of the PI3K/AKT/mTOR Pathway***
Yuan Zhao, Xiujing Feng, Bei Li, Jichen Sha, Chaoran Wang, Tianyuan Yang, Hailin Cui and Honggang Fan

242 ***IL-4 Receptor α Chain Protects the Kidney Against Tubule-Interstitial Injury Induced by Albumin Overload***
Diogo B. Peruchetti, João Luiz Silva-Filho, Rodrigo P. Silva-Aguiar, Douglas E. Teixeira, Christina M. Takiya, Mariana C. Souza, Maria das Graças Henriques, Ana Acacia S. Pinheiro and Celso Caruso-Neves

256 ***Defective Mitochondrial Fatty Acid Oxidation and Lipotoxicity in Kidney Diseases***
Hee-Seong Jang, Mi Ra Noh, Jinu Kim and Babu J. Padanilam

264 **EDN1-AS*, A Novel Long Non-coding RNA Regulating Endothelin-1 in Human Proximal Tubule Cells***
Lauren G. Douma, Kristen Solocinski, Sarah H. Masten, Dominique H. Barral, Sarah J. Barilovits, Lauren A. Jeffers, Kareme D. Alder, Ravi Patel, Charles S. Wingo, Kevin D. Brown, Brian D. Cain and Michelle L. Gumz

274 ***Pharmacologic Blockade of 15-PGDH Protects Against Acute Renal Injury Induced by LPS in Mice***
Shuying Miao, Caihong Lv, Ying Liu, Jie Zhao, Ting Li, Chunjiang Wang, Yunfei Xu, Xiaoli Wang, Xianzhong Xiao and Huali Zhang

288 ***Recent Insights Into SREBP as a Direct Mediator of Kidney Fibrosis via Lipid-Independent Pathways***
Debra Dorotea, Daisuke Koya and Hunjoo Ha

304 ***Resolvin D1 Protects Against Ischemia/Reperfusion-Induced Acute Kidney Injury by Increasing Treg Percentages via the ALX/FPR2 Pathway***
Hong Luan, Chuanxiao Wang, Jianping Sun, Long Zhao, Lin Li, Bin Zhou, Shihong Shao, Xuefei Shen and Yan Xu

316 ***Baseline Soluble Anti-erythropoietin Antibody Level is an Independent Associated Factor for Follow-Up Erythropoietin Demand in Maintenance Dialysis Patients With End-Stage Renal Disease: A Prospective Cohort Study***
Ying Zhang, Shi-Zhu Bian, Kun Yang, Yiqing Wang, Sha Tang, Weili Wang, Daihong Wang, Ling Nie and Jinghong Zhao

328 ***NBCe2 (*Slc4a5*) is Expressed in the Renal Connecting Tubules and Cortical Collecting Ducts and Mediates Base Extrusion***
Dagne Barbuskaite, Fredrik D. Pedersen, Henriette L. Christensen, Laura Ø. Johnsen, Jeppe Praetorius and Helle H. Damkier

341 ***Enhanced Myogenic Constriction in the SHR Preglomerular Vessels is Mediated by Thromboxane A2 Synthesis***
Samera Nademi, Chao Lu and Jeffrey G. Dickhout

358 ***Trimetazidine Inhibits Renal Tubular Epithelial Cells to Mesenchymal Transition in Diabetic Rats* via *Upregulation of Sirt1***
Yong Yang, Yong Wang, Zuowen He, Yunchang Liu, Chen Chen, Yan Wang, Dao Wen Wang and Hong Wang

frontiers in Physiology

EDITORIAL
published: 03 December 2020
doi: 10.3389/fphys.2020.625353

Editorial: Renal Function in Acute and Chronic Kidney Diseases

John D. Imig[1†], Md Abdul Hye Khan[1†] and Xueying Zhao[2]*

[1] Drug Discovery Center and Cardiovascular Center, Medical College of Wisconsin, Milwaukee, WI, United States,
[2] Department of Physiology, Morehouse School of Medicine, Atlanta, GA, United States

Keywords: diabetic nephropathy, acute kidney injury, hypertension, renal epithelium, glomerulus

Editorial on the Research Topic

Renal Function in Acute and Chronic Kidney Diseases

INTRODUCTION

Acute and chronic kidney diseases have devastating consequences on human health. Renal vascular function, glomerular filtration, and epithelial transport are required for water and electrolyte homeostasis. Nephrotoxicity and diseases such as hypertension, diabetes, and metabolic syndrome contribute significantly to acute and chronic kidney diseases (Barnett and Cummings, 2018). These pathological states impact on renal vascular and epithelial function and the ability for the kidney to maintain water and electrolyte homeostasis. Experimental and clinical studies over the past decade determined that there is a transition from acute to chronic kidney injury (Fiorentino et al., 2018). Acute kidney injury in the clinical setting can cause sustained alterations in epithelial transport and renal hemodynamics that increase the risk for developing chronic kidney disease (Sharfuddin and Molitoris, 2011). Currently, there are extremely limited options to treat acute and chronic kidney diseases.

A Research Topic on acute and chronic kidney diseases is timely because this is a very fast-moving field that is focused on the tremendous need for kidney disease therapeutics. Articles in this Research Topic advance our understanding of organismal, cellular, and molecular mechanisms that contribute to acute and chronic kidney diseases. The Research Topic has broad interest since it covers acute kidney injury, chronic kidney disease, diabetic nephropathy, and hypertension mediated kidney disease. Research articles span cell signaling, animal studies, human and animal disease pathology studies, renal hemodynamics, glomerular filtration, and renal epithelial transport studies. Thirty contributions focus on novel developments defining renal vascular and epithelial mechanisms that contribute to acute and chronic kidney diseases.

REVIEWS

The Research Topic contains five review articles that discuss issues associated with acute and chronic kidney diseases. Macrophages and acute kidney disease are the focus of one review (Baek). Contributions to acute kidney injury for M1 pathogen destroying and inflammatory macrophages and the M2 immunosuppressive and tissue regeneration macrophages are discussed with an emphasis on the potential for therapeutic modulation (Baek). Mitochondrial fatty oxidation in acute and chronic kidney diseases that elicits tubular injury, inflammation, and fibrosis are explored in another review article (Jang et al.). Insight is provided on adenosine triphosphate (ATP)

OPEN ACCESS

Edited and reviewed by:
Carolyn Mary Ecelbarger, Georgetown University, United States

***Correspondence:**
John D. Imig
jdimig@mcw.edu

†ORCID:
John D. Imig
orcid.org/0000-0002-9668-2899
Md Abdul Hye Khan
orcid.org/0000-0001-5940-9300

Specialty section:
This article was submitted to Renal and Epithelial Physiology, a section of the journal Frontiers in Physiology

Received: *02 November 2020*
Accepted: *11 November 2020*
Published: *03 December 2020*

Citation:
Imig JD, Hye Khan MA and Zhao X (2020) Editorial: Renal Function in Acute and Chronic Kidney Diseases. Front. Physiol. 11:625353. doi: 10.3389/fphys.2020.625353

depletion, lipotoxicity, and mitochondrial energy metabolism in kidney diseases with a prospective for developing therapeutics. The theme of lipotoxicity and fibrosis in kidney diseases continues in a review article that focuses on sterol regulatory-element binding proteins (SREBPs) as mediators of kidney fibrosis via lipid-independent pathways (Dorotea et al.). Next, a mini-review examined the therapeutic potential for erythropoietin to combat renal fibrosis and chronic kidney disease (Zhang, Zhu et al.). Lastly, an opinion piece described heat strain, external workload, and chronic kidney disease in endurance athletes based in the tropical regions (Rojas-Valverde et al.). The authors advocate for more research for endurance athletes in the tropical regions to prevent chronic kidney disease in this population (Rojas-Valverde et al.). These reviews, mini-review, and opinion piece provide valuable insight on the pathology of acute kidney injury and chronic kidney disease, as well as, providing possible therapies to combat kidney diseases.

ACUTE KIDNEY INJURY

Mechanisms of acute kidney injury and potential therapeutic approaches were the emphasis of eight scientific articles in the Research Topic. The therapeutic potential for resolvin D1 to attenuate ischemia/reperfusion injury via the anaplastic lymphoma kinase/formyl-peptide receptor-2 (ALX/FPR2) pathway was demonstrated (Luan et al.). This article convincing evidence is presented that resolvin D1 protects against ischemia/reperfusion acute kidney injury by increasing regulatory T cell (Tregs) to reduce inflammation and renal tubular injury in mice (Luan et al.). Another therapeutic article described neferine, an alkaloid of the green seed of Lotus, on ischemia/reperfusion and lipopolysaccharide (LPS) induced acute kidney injury in mice (Li et al.). Pretreatment of neferine attenuated apoptosis and inflammation and increased kidney Klotho expression to mitigate acute kidney injury (Li et al.). Next, opioid regulation of rat renal epithelial cells exposed to hypoxia was evaluated (Luo et al.). This article found that δ-opioid receptor activation or inhibition regulates anti-inflammatory cytokines in renal epithelial cells exposed to hypoxia (Luo et al.). Anti-inflammatory cytokines were also the focus of a study in mice that had albumin overload induced acute kidney injury (Peruchetti et al.). The findings of this experimental study revealed that the interleukin-4 (IL-4) receptor α chain protects the kidney for albumin overload injury through modulation of the pro-inflammatory response (Peruchetti et al.). The acute kidney injury therapeutic theme continues with a study that demonstrates dexmedetomidine protects against LPS kidney injury in rats (Zhao et al.). Dexmedetomidine enhances kidney autophagy via the phosphoinositide 3-kinase/protein kinase B/mammalian target of rapamycin (PI3K/AKT/mTOR) pathway to decrease LPS induced renal damage (Zhao et al.). The attention on LPS renal injury in mice continued with an article on 15-hydroxyprostaglandin dehydrogenase (15-PGDH) treatment (Miao et al.). Inhibition of 15-PGDH with SW033291 decreased renal apoptosis, enhanced autophagy, and decreased oxidative stress rather than decreasing inflammation to reduce LPS induced acute kidney injury (Miao et al.). The last two acute kidney injury therapeutic articles utilized cisplatin-induced nephrotoxicity. The antioxidant, ferrerol was found to attenuate cisplatin induced kidney injury in mice through inhibiting reactive oxygen species-mediated oxidation, reducing inflammation, and decreasing apoptosis signaling pathways (Ma et al.). Another cisplatin-induced acute kidney injury study revealed that PTEN-induced kinase-1 (PINK1) knockout rats had ameliorated kidney damage via effects on mitochondrial fission and mitophagy (Zhou et al.). Taken together, this cadre of acute kidney injury articles provide several therapeutic targets and prospective drugs that could eventually improve outcomes in humans with acute kidney injury.

DIABETIC NEPHROPATHY

A trio of studies evaluated kidney damage associated with diabetes. The first of these experimental studies evaluated resveratrol in rabbits with diabetic nephropathy injected with the contrast dye, iohexol, to induce acute kidney injury (Wang Y. et al.). Resveratrol protected against renal injury by activating the sirtuin-1/peroxisome proliferator-activated receptor gamma coactivator 1-α/hypoxia inducible factor 1-α (SIRT1/PGC-1α/HIF-1α) signaling pathway to reduce hypoxia, mitochondrial dysfunction, and tubular cell apoptosis (Wang Y. et al.). Next, the therapeutic potential for trimetazidine in streptozotocin-induced diabetic nephropathy was evaluated (Yang et al.). Trimetazidine prevented diabetic kidney damage through anti-fibrotic and anti-oxidative stress mechanisms (Yang et al.). The last diabetic nephropathy study utilized renal tubular epithelial cells and glomerular mesangial cells in culture that were exposed to high glucose (Wang L. et al.). Metabolomics of renal epithelial and mesangial cells exposed to high glucose were compared to human plasma samples from diabetic nephropathy patients to reveal potential biomarkers for diabetic nephropathy (Wang L. et al.). Future studies are needed to further test the therapeutic approaches and validate biomarkers for diabetic nephropathy.

CHRONIC KIDNEY DISEASE

Four articles examining four different types of chronic kidney diseases are presented that tackle very different pathological aspects of chronic kidney disease. The first article tackles refining the mouse subtotal nephrectomy model to get consistent changes in chronic kidney disease (O'Sullivan et al.). Subtotal nephrectomy in male 129S2/SV mice resulted in progressive proteinuric renal disease, renal inflammation, and cardiac hypertrophy that was reliably reproducible (O'Sullivan et al.). Folic acid nephropathy and progressive fibrosis in mice was examined in response to Smad3 and c-Jun N-terminal kinase (JNK) pathway blockade (Jiang et al.). The Smad3 inhibitor, SIS3, and the JNK inhibitor, SP600125, given combined ameliorated progressive renal fibrosis through actions on PGC-1α (Jiang et al.). Bilateral ureteral obstruction and release in mice was used to determine the effects of the renin inhibitor, aliskiren (Hu et al.). This study found that aliskiren increased renal aquaporin 2

expression and suppressed NLR family pyrin domain containing 3 (NLPR3) inflammasome activation to improve the urinary concentration defect in ureteral obstruction and release (Hu et al.). Nephrogenesis disturbances induced by angiotensin type 1 (AT1) receptor blockade were the focus of the last chronic kidney disease article (Deluque et al.). Calcitriol treatment attenuated the AT1 receptor blockade altered renal microvascular differentiation (Deluque et al.). Overall, these four articles provide a snapshot of the wide variation in disease models and mechanisms that contribute to chronic kidney disease.

HYPERTENSION

Five articles in the Research Topic addressed hypertension and kidney disease. Hypertension and kidney disease in the Ren-2 transgenic rats focused on diuretic treatment (Vaněčková et al.). This study found that progressive proteinuria was lowered by combined AT1 receptor and endothelin type A (ET_A) receptor blockade that was further reduced by the diuretic, hydrochlorothiazide (Vaněčková et al.). Endothelin-1 (ET-1) regulation in human proximal tubule cells was the focus of an article investigating cellular proliferation (Douma et al.). This study identified a long, non-coding RNA (lncRNA) that is an antisense for the gene that encodes ET-1 (*EDN1-AS*) which increases renal epithelial cell ET-1 secretion (Douma et al.). In another article, salt-sensitive hypertension and renal glomerular mitochondrial function were evaluated (Domondon et al.). Glomerular mitochondria were structurally and functionally defective in salt-sensitive hypertension rats which contributes to glomerulosclerosis (Domondon et al.). Continuing with the glomerular theme, another article assessed preglomerular arterioles in spontaneously hypertensive rats (SHR) for myogenic constriction (Nademi et al.). The findings in this study revealed that enhanced myogenic constriction of preglomerular arterioles was due to thromboxane A2 synthesis (Nademi et al.). The fifth hypertension article focused on the electrogenic Na^+:HCO_3^- cotransporter NBCe2 (*Slc4a5*) in the renal epithelial cells of the connecting tubules and collecting ducts to blood pressure regulation (Barbuskaite et al.). Genetic deletion of NBCe2 resulted in net base extrusion and hypertension; however, hypertension was not observed in connecting tubule and intercalated cell NBCe2 knockout mice (Barbuskaite et al.). On the whole, these hypertension and kidney disease studies provide exciting and novel mechanisms responsible for blood pressure regulation and kidney disease progression.

CLINICAL STUDIES

A Research Topic on acute and chronic kidney diseases would not be complete without clinical studies that explore therapies. Treatment for contrast-induced acute kidney injury in hypertensive patients evaluated the calcium channel blocker amlodipine (Yin et al.). Amlodipine given prior to contrast exposure resulted in protecting a Chinese cohort of hypertensive patients from contrast-induced acute kidney injury and increased long-term survival (Yin et al.). Another article explored the risk for acute kidney injury in patients with urinary tract infections (Hsiao et al.). This study found that the urinary tract infection, urolithiasis, increased the risk for uroseptic shock and acute kidney injury (Hsiao et al.). The ability for an anti-erythropoietin antibody to predict the need for erythropoietin treatment in dialysis patients with end stage renal disease was the focus of another study (Zhang, Bian et al.). This study found that the anti-erythropoietin antibody combined with age and potassium levels prior to dialysis predicted the need and dose of erythropoietin required during maintenance dialysis (Zhang, Bian et al.). Dialysis was also the focus of a study that explored inflammation and oxidative stress (Gutiérrez-Prieto et al.). The findings of this study revealed that adults that undergo peritoneal dialysis have significant changes in inflammation, oxidative stress, and oxidative damage to DNA (Gutiérrez-Prieto et al.). The devastating disease, hepatorenal syndrome, was examined in the fifth clinical study (Abdel-Razik et al.). Type-1 hepatorenal syndrome patients with an early reduction in ET-1 to nitric oxide ratio had better outcomes when treated with terlipressin and albumin (Abdel-Razik et al.). These five clinical studies highlight advances in the treatment of acute and chronic kidney diseases and provide insight on the considerable demand for better therapies.

CONCLUSION

The Research Topic Renal Function in Acute and Chronic Kidney Diseases demonstrates emerging areas of research and clinical studies. This collection of 30 articles demonstrates that inflammation, mitochondrial dysfunction, and oxidative stress that contribute to the development and progression of renal diseases. Novel mechanisms and potential therapeutic targets are identified for acute kidney injury, hypertension induced kidney disease, diabetic nephropathy, and chronic kidney disease. Clinical studies highlighted the need for better kidney disease biomarkers and therapeutic approaches to improve kidney disease outcomes. Taken together, this Research Topic features recent advances and provides future directions for understanding renal function and treating acute and chronic kidney diseases.

AUTHOR CONTRIBUTIONS

JI conceived the content and drafted the manuscript. JI, MH, and XZ revised and approved the final manuscript. All authors contributed to the article and approved the submitted version.

ACKNOWLEDGMENTS

This work was supported by the National Institute of Diabetes and Digestive and Kidney Diseases DK103616 and Dr. Ralph and Marian Falk Medical Research Trust Bank of America, N.A., Trustee.

REFERENCES

Barnett, L. M. A., and Cummings, B. S. (2018). Nephrotoxicity and renal pathophysiology: a contemporary perspective. *Toxicol. Sci.* 164, 379–390. doi: 10.1093/toxsci/kfy159

Fiorentino, M., Grandaliano, G., Gesualdo, L., and Castellano, G. (2018). Acute kidney injury to chronic kidney disease transition. *Contrib. Nephrol.* 193, 45–54. doi: 10.1159/000484962

Sharfuddin, A. A., and Molitoris, B. A. Pathophysiology of ischemic acute kidney injury. *Nat. Rev. Nephrol.* (2011). 7, 189–200. doi: 10.1038/nrneph.2011.16

Conflict of Interest: The authors declare that the research was conducted in the absence of any commercial or financial relationships that could be construed as a potential conflict of interest.

Copyright © 2020 Imig, Hye Khan and Zhao. This is an open-access article distributed under the terms of the Creative Commons Attribution License (CC BY). The use, distribution or reproduction in other forums is permitted, provided the original author(s) and the copyright owner(s) are credited and that the original publication in this journal is cited, in accordance with accepted academic practice. No use, distribution or reproduction is permitted which does not comply with these terms.

frontiers in Pharmacology

ORIGINAL RESEARCH
published: 26 July 2019
doi: 10.3389/fphar.2019.00833

Resveratrol Protects Against Post-Contrast Acute Kidney Injury in Rabbits With Diabetic Nephropathy

Yongfang Wang[1,2†], Bin Wang[1†], Xun Qi[2], Xin Zhang[2] and Ke Ren[3]*

[1] Department of Radiology, First Hospital of Shanxi Medical University, Taiyuan, China, [2] Department of Radiology, First Hospital of China Medical University, Shenyang, China, [3] Department of Radiology, Xiang' an Hospital of Xiamen University, School of Medicine, Xiamen University, Xiamen, China

Resveratrol (Res) is a multi-functional polyphenol compound that has protective functions in acute kidney diseases. Here, we examined whether the resveratrol could ameliorate post-contrast acute kidney injury (PC–AKI) following diabetic nephropathy (DN), and explored any underlying mechanism(s) *in vivo* and *in vitro*. Twenty-four rabbits with DN were randomly divided into four groups: control (Cont), resveratrol (Res), iohexol (PC–AKI), and resveratrol plus iohexol (Res+PC–AKI) groups. Functional magnetic resonance imaging, renal histology, blood and urinary biomarkers, silent information regulator l (SIRT1), peroxisome proliferator-activated receptor gamma coactivator-1 alpha (PGC-1α), hypoxia-inducible transcription factor-1α (HIF-1α), and apoptosis-associated protein expression were assessed *ex vivo*. For *in vitro* experiments, renal tubular epithelial (HK-2) cells subjected to high glucose conditions were treated with resveratrol, Ex527, an SIRT1 inhibitor, or 2-methoxyestradiol (2-MeOE2), HIF-1α inhibitor, before treatment with iohexol. With regard to the rabbit model of acute renal injury in DN, compared to the PC–AKI group, the Res+PC–AKI group showed decreased levels of cystatin C and urinary neutrophil gelatinase-associated lipocalin, increased pure molecular diffusion (*D*) and the fraction of water flowing in capillaries (*f*), a decreased apparent relaxation rate (*R2**), renal injury score and apoptosis rate, increased protein expression levels of SIRT1 and PGC-1α, and decreased levels of HIF-1α and apoptosis-associated protein. In addition, iohexol decreased HK-2 cell survival and increased the cell apoptosis rate; results were reversed after treating cells with resveratrol. Resveratrol reduced renal hypoxia, mitochondrial dysfunction and renal tubular cell apoptosis by activating SIRT1–PGC–1α–HIF-1α signaling pathways in PC–AKI with DN.

Keywords: PC–AKI, diabetic nephropathy, SIRT1, PGC-1α, HIF-1α, apoptosis

OPEN ACCESS

Edited by:
John D. Imig,
Medical College of Wisconsin,
United States

Reviewed by:
Parames C. Sil,
Bose Institute, India
Isha Sharma,
Northwestern University,
United States

****Correspondence:***
Ke Ren
renke815@sina.com

†These authors have contributed equally to this work and share first authorship.

Specialty section:
This article was submitted to Renal Pharmacology, a section of the journal Frontiers in Pharmacology

Received: *16 April 2019*
Accepted: *28 June 2019*
Published: *26 July 2019*

Citation:
Wang Y, Wang B, Qi X, Zhang X and Ren K (2019) Resveratrol Protects Against Post-Contrast Acute Kidney Injury in Rabbits With Diabetic Nephropathy. Front. Pharmacol. 10:833. doi: 10.3389/fphar.2019.00833

INTRODUCTION

Post-contrast acute kidney injury (PC–AKI), described as a decrease in renal function that follows the intravascular administration of contrast medium, is one of the leading causes of hospital-acquired acute kidney injury (Takahashi et al., 2017; Van Der Molen et al., 2018). This type of injury is associated with adverse short- and long-term outcomes (Maioli et al., 2012; Chalikias et al., 2016). Overwhelming epidemiological and clinical evidence has demonstrated that diabetes mellitus may significantly contribute to the development of PC–AKI after the application of contrast medium

(Tziakas et al., 2014; Chalikias et al., 2016). Therefore, the identification of new molecular target(s) has been a major focus for the prevention of PC–AKI in high-risk patients.

Silent information regulator l (SIRT1) is a nicotinamide adenine dinucleotide-dependent protein deacetylase that is the human homolog of yeast silent information regulator 2 (Xu et al., 2016; Morigi et al., 2018). Resveratrol, as a chemical SIRT1 activator, can effectively repair SIRT1 activity. Accumulated experimental evidence suggests that resveratrol may inhibit the inflammatory response and tubular apoptosis, and scavenge oxygen free radicals in cisplatin-induced nephropathy, renal ischemic/reperfusion injury and diabetic nephropathy (Kim et al., 2011; Gu et al., 2016; Xiao et al., 2016).

Recent studies have shown that resveratrol promotes the activation of peroxisome proliferator-activated receptor-gamma coactivator-1 alpha (PGC-1α), and decreases oxidative stress and apoptosis in acute renal injury. PGC-1α is a nuclear-encoded transcriptional coactivator that regulates the expression of nuclear-encoded mitochondrial proteins (Ishimoto and Inagi, 2016). As reported, the overexpression of PGC-1α produces a robust increase in mitochondrial numbers, respiratory capacity and intracellular ATP concentration in cultured proximal tubular cells, and may promote repair and recovery after hypoxia damage (Rasbach and Schnellmann, 2007). Previous studies have shown that hypoxia-inducible transcription factors (HIFs), recognized as master regulators of hypoxic adaptation, are detected during the development of PC–AKI (Rosenberger et al., 2005). Many molecular pathways are involved in the protective effects of resveratrol, but the role of the SIRT1–PGC–1α–HIF-1α pathway in PC–AKI–based diabetic nephropathy has not yet been fully described. The aim of the present study was to assess the effect of resveratrol on the development of PC–AKI in diabetic models and to provide experimental evidence for the prevention and treatment of PC–AKI.

MATERIALS AND METHODS

Animals and Experimental Design

A total of 24 male white New Zealand rabbits (weighing 2.5–3.0 kg) were housed in an environment with a temperature of 22 ± 1°C, relative humidity of 50 ± 1% and a light/dark cycle of 12/12 h. All animal studies (including rabbit euthanasia) were conducted according to the China Medical University Application for Laboratory Animal Welfare and Ethical Review (201802 Edition). The protocol was approved by the Ethics Review Committee of China Medical University.

Abbreviations: Res, Resveratrol; SIRT1, Silent information regulator l; PC–AKI, Post-contrast acute kidney injury; DN, Diabetic nephropathy; PGC-1α, Peroxisome proliferator-activated receptor gamma coactivator-1 alpha; HIF-1α, Hypoxia-inducible transcription factor-1α; HK-2, Renal tubular epithelial cells; 2-MeOE2, 2-Methoxyestradiol; Cr, Serum creatinine; BUN, Urea nitrogen; CysC, Cystatin C; uNGAL, Urinary neutrophil gelatinase–associated lipocalin; fMRI, Functional magnetic resonance imaging; BOLD, Blood-oxygenation-level–dependent; *R2**, Apparent relaxation rate; IVIM, Intravoxel incoherent motion; *D*, Pure molecular diffusion; *D**, Flow velocity; *f*, The fraction of water flowing in capillaries; HG, High glucose; ROS, Reactive oxygen species; Cyt-C, Cytochrome C.

All animals were acclimatized for 7 days before the start of each experiment. Rabbits with diabetic nephropathy (DN) and renal impairment were established by a single intravenous injection of alloxan monohydrate (100 mg/kg) dissolved in 0.9% saline after 12 h of overnight fasting (Zhao et al., 2016). Furthermore, the rabbits were treated with 10% glucose solution for 24 h to get through the early stage of drug-induced hypoglycemia. Three days after alloxan injection, blood was collected and fasting blood glucose levels analyzed. A successful diabetes model was established when glucose levels were > 16.7 mmol/L (Zhao et al., 2016). Consequently, blood glucose levels were monitored once a week.

Twelve weeks after the induction of diabetic nephropathy (Wang et al., 2014), rabbits were randomly divided into four groups: saline–treated control group (Cont; $n = 6$), resveratrol alone–treated group (Res; $n = 6$), contrast medium–treated group (PC–AKI; $n = 6$), and contrast medium plus resveratrol–treated group (PC–AKI + Res; $n = 6$; **Figure S1**). The animals were treated with or without resveratrol (80 mg/kg/d, p.o.; Sigma, St Louis, MI, USA) once a day, for a total of 14 days before applying iohexol, a contrast agent (Li et al., 2016). Furthermore, iohexol (Omnipaque; 350 mg iodine/ml, 830 mOsm/kg H_2O; GE Healthcare, Shanghai, China) was intravenously injected at a dose of 2.5 g iodine/kg body weight *via* a venous cannula (24 G) inserted in the marginal ear vein (Bhargava et al., 1990; Lauver et al., 2014).

Functional MRI Mapping and Data Analysis

Animals underwent magnetic resonance imaging (MRI) 24 h after the injection of iohexol. MR imaging was performed on a 3.0-T scanner (General Electric Medical Systems, Milwaukee, WI, USA) using a cardiac matrix coil. An advanced workstation (General Electric Medical Systems) was used to extract intravoxel incoherent motion (IVIM) and blood oxygenation level–dependent (BOLD) parameters, including *D*, *D**, *f* and *R2** values. Quantitative regional IVIM parameters and *R2** measurements were performed, using manually defined region-of-interest (ROI) measurements, by two experienced radiologists who remained blinded to each group assignment. Regions of interest were manually placed in the renal cortex (CO) and outer medulla (OM; **Figure S2**) according to a previously described approach (Prasad et al., 2010).

IVIM parameters were consecutively calculated using a nonlinear biexponential fit based on the following equation: $S_b/S_0 = (1\text{-}f).\ \exp(\text{-}b\ D) + f.\ \exp[\text{-}b\ (D + D^*)]$, where S_0 = signal intensity in the absence of the diffusion weighting ($b = 0$); S_b = signal intensity with diffusion gradient b; slow diffusion coefficient (D) = pure molecular diffusion; fast diffusion coefficient (D^*) = flow velocity; and the perfusion fraction (f) = the fraction of water flowing in capillaries (Hu et al., 2015). BOLD parameters were able to indirectly measure the partial oxygen pressure by estimating the deoxyhemoglobin concentration in the renal parenchyma and blood vessels (Liu et al., 2013). Data acquisition of IVIM and BOLD parameters is shown in **Table 1**.

TABLE 1 | MRI parameters used for IVIM and BOLD parameters.

	IVIM	BOLD
Sequence type	DW–EPI	2D–GRE
Orientation	Coronal	Coronal
Repetition time, ms	4,050	96.2
Echo time, ms	95.5	4.4–48.7
Flip angle	–	30°
Bandwidth, hertz per pixel	–	41.67
Field of view, cm^2	16.0 × 16.0	16.0 × 16.0
Matrix	160 × 160	256 × 256
Section thickness, mm	3.0	3.0
Number of excitations	2.0	2.0
Acquisition time	6 min 41s	4 min 10 s
b-values (s/mm^2)	0, 10, 20, 50, 100, 200, 400, 600, 800, 1,200	–

MRI, magnetic resonance imaging; IVIM, intravoxel incoherent motion; BOLD, blood oxygenation level–dependent; DW–EPI, diffusion-weighted echo-planar imaging; 2D-GRE, two-dimensional gradient-recalled echo.

Renal Function Biomarkers

A total of 1.0–1.5 ml of blood and urine samples was collected from each animal after MRI. Blood samples were centrifuged and used to examine serum creatinine (Cr), blood urea nitrogen (BUN), and cystatin C (CysC) levels. Urine samples were collected for the assessment of urine creatinine and urinary neutrophil gelatinase-associated lipocalin (uNGAL). Concentrations of CysC and NGAL were assessed using an enzyme-linked immunosorbent assay (ELISA) kit (Yuanmu Biological Technology Co., Ltd, Shanghai, China) according to the manufacturer's instructions, and concentration levels of NGAL were normalized to the urine creatinine concentration (Li et al., 2014a; Li et al., 2014b). Serum Cr, BUN, and urine Cr were analyzed by a local clinical laboratory.

Histological Observations

After MRI, rabbits were sacrificed, and the right kidneys removed and fixed in 4% buffered paraformaldehyde for 72 h. Samples were then dehydrated, embedded in paraffin, cut into 5 μm sections, and finally stained with hematoxylin and eosin (H&E). Histological assessment of renal damage included observing tubular vacuolization and degeneration, renal tubular casts, inflammatory infiltration and obvious necrosis in the cortex, and the disruption of the tubular structures in the outer medulla after iohexol administration. Renal alterations were graded as follows: 0, normal kidney; 1, minimal injury (0–5%); 2, moderate injury (5–25%); 3, intermediate injury (25–75%), and 4, severe injury (75–100%) (Colbay et al., 2010). Two independent pathologists, who were blinded to the experimental conditions, evaluated the samples according to the scoring criteria. Renal cell apoptosis was assessed using terminal deoxynucleotidyl transferase dUTP nick-end labeling (TUNEL) staining (WL029a; Wanleibio, Shenyang, China) as previously described (Deng et al., 2015) and the percentage of apoptotic cells was quantified using ImageJ software.

In Vitro Experiments

Immortalized human proximal tubule (HK-2) cells were purchased from Basic Medical Cell Center of School of Basic Medicine, Peking Union Medical College (Beijing, China). Cells were grown in low-glucose (LG, 5.5 mM) RPMI 1640 medium (Gibco Laboratories, Grand Island, NY, USA) containing 10% fetal calf serum (Gibco Laboratories) and cultured in a humidified atmosphere containing 5% CO_2/95% air at 37°C. The culture medium was supplemented with a high level of glucose (HG, 25 mM) to induce a DN cell model. An *in vitro* model of contrast injury was constructed based on a previously described method (Billings et al., 2008). The SIRT1 inhibitor, Ex527, and HIF-1α inhibitor, 2-methoxyestradiol (2-MeOE2), were purchased from Selleckchem (Shanghai, China), while the SIRT1 activator, resveratrol, was obtained from Abcam (Cambridge, UK).

Well-differentiated HK-2 cells were divided into five groups: high glucose + resveratrol + iohexol (25 mmol/L glucose + 50 μmol/L Res + 100 mg/ml iohexol; Res), high glucose + Ex527 + iohexol (25 mmol/L glucose + 10 μmol/L Ex527 +100 mg/ml iohexol; Ex527), high glucose + iohexol (25 mmol/L glucose + 100 mg/ml iohexol; PC–AKI), high glucose + resveratrol + 2-MeOE2 + iohexol (25 mmol/L glucose + 50 μmol/L Res + 10 μmol/L 2-MeOE2 +100 mg/ml iohexol; 2-MeOE2), and low glucose (5.5 mmol/L glucose; Cont; **Figure S3)**. The cells were stimulated under high glucose conditions for 24 h (Chen et al., 2018). In order to evaluate the effect of activating SIRT1, the cells were pretreated with Ex527 for 24 h or 2-MeOE2 for 2 h before the iohexol treatment. After Res, Ex527 or 2-MeOE2 treatment, cells were exposed to iohexol for 16 h.

CCK-8 Cytotoxic Assay

In order to evaluate the protective effect of resveratrol, HK-2 cell viability in the five groups was quantified by a Cell Counting Kit-8 (CCK-8) assay (Dojindo Laboratories, Shanghai, China). Briefly, cells were incubated with 10 μl CCK-8 test solution for 2 h at 37°C. Absorbance values were measured at 450 nm using a microplate reader (Thermo Fisher Scientific, Waltham, MA, USA).

Flow Cytometry Analysis of Cell Apoptosis

HK-2 cells were seeded into 6-well plates at a density of 1×10^5 cells/well. The treated HK-2 cells were harvested and stained using an Annexin V- Light 650 Apoptosis Detection Kit (Wanleibio; WLA002b, Shenyang, China). After incubation for 15 min in the dark, the cell apoptosis ratio was measured using a flow cytometer (Acea Bio, San Diego, CA, USA).

Western Blot

Both kidney tissue and isolated HK-2 cells were centrifuged at 12,000 rpm for 20 min after homogenization in radio-immunoprecipitation assay lysis buffer containing a protease inhibitor cocktail. Total protein concentrations were determined by a bicinchoninic acid method. Afterward, protein samples were boiled at 95°C for 5 min. About 50 μg equal amounts of protein samples were separated by gel electrophoresis on an 8% to 12% sodium dodecyl sulfate–polyacrylamide gel and then transferred onto a polyvinylidene difluoride membrane using wet transfer at 80 V for 60 min, and 120 V for 60 min. Nonspecific binding sites

were blocked with 5% skim milk powder at room temperature for 2 h and the membrane then incubated with the following primary antibodies: SIRT1 (1:500, abs120289; absin, Shanghai, China), PGC-1α (1:500, TA343708; OriGene, Rockville, MD, USA), HIF-1α (1:500, NB100-105; Novus Biologicals, Centennial, CO, USA), Bax (1:5000, 50599-2-Ig; ProteinTech, Wuhan, China), Bcl-2 (1:2000, 12789-1-AP; ProteinTech, Wuhan, China), cleaved caspase-3 (1:1,000, ab2302; Abcam, UK), and cytochrome C (Cyt-C; 1:5,000, NB100-56503; Novus, Saint Charles, MI, USA) at 4°C overnight. After washing, films were incubated with horseradish peroxidase-labeled conjugated secondary antibodies (Proteintech) for 2 h. The immunostained protein bands were visualized with an enhanced chemiluminescence system and analyzed using Image J software. Beta-actin was used as an internal control.

Statistical Analysis

All values were analyzed with SPSS22.0 (SPSS Inc., Chicago, IL, USA) or GraphPad Prism 5 and expressed as mean ± standard deviation. Continuous data were analyzed with a one-way analysis of variance (ANOVA) followed by Fisher's least significance difference test between multiple groups, and unpaired data were analyzed with the Kruskal–Wallis test. The Mann–Whitney test was used for nonparametric comparisons between the two groups. $P < 0.05$ was considered statistically significant.

RESULTS

Effects of Resveratrol on Renal Function

Contrast medium significantly increased serum Cr, BUN, and CysC levels and the uNGAL level. In contrast, serum Cr, BUN and CysC levels were significantly lower in the Res+PC–AKI group compared to the PC–AKI group ($P = 0.038$; $P = 0.035$; $P = 0.048$, respectively), whereas there was no significant difference between Cont and Res groups ($P = 0.562$; $P = 0.631$; $P = 0.895$, respectively). Furthermore, compared with the Cont group, the urinary concentrations of NGAL were significantly increased 24 h after iohexol injection in the PC–AKI group ($P < 0.001$); however, resveratrol treatment markedly reduced levels of uNGAL induced by iohexol in the Res+PC–AKI group ($P = 0.04$; **Figure 1**). Thus, resveratrol ameliorated acute renal dysfunction after exposure to contrast medium in DN.

Effect of Resveratrol on Functional MRI Parameters

The IVIM parameters and *R2** values between the four groups of rabbits are presented in **Table 2** and their corresponding representative images are shown in **Figures 2, 3**.

After the injection of iohexol, *D* was significantly lower in the PC–AKI group compared with the Cont group in the CO ($P < 0.0001$) and OM ($P < 0.0001$). *D* was significantly higher

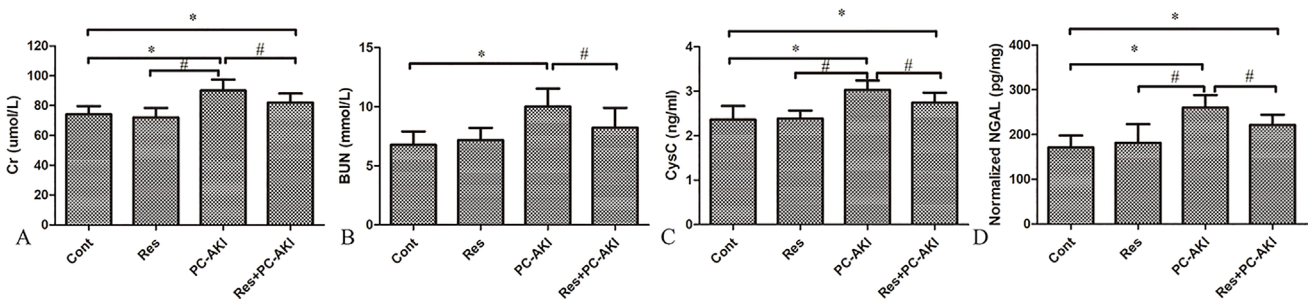

FIGURE 1 | Changes in renal function were evaluated after the injection of iohexol and co-administration of resveratrol in rabbits. Iohexol caused renal dysfunction in the PC–AKI group, while the co-administration of resveratrol decreased the level of Cr **(A)**, BUN **(B)**, CysC **(C)** and NGAL **(D)**. **P* < 0.05 vs. Cont; #*P* < 0.05 vs. PC–AKI. Cr, serum creatinine; BUN, urea nitrogen; CysC, cystatin C; NGAL, neutrophil gelatinase–associated lipocalin; Cont, control; Res, resveratrol; PC–AKI, post-contrast acute kidney injury.

TABLE 2 | Summary of IVIM parameters and *R2** for kidneys of rabbits with different treatments.

Kidney tissue	Groups	Cont	Res	PC–AKI	Res+PC–AKI
CO	D ($\times10^{-4}$ mm²/s)	3.99 ± 0.28	4.02 ± 0.30#	2.93 ± 0.33*	3.58 ± 0.34*#
	D* ($\times10^{-3}$ mm²/s)	9.86 ± 0.28	9.86 ± 0.30#	9.31 ± 0.35*	9.61 ± 0.38
	f (%)	39.13 ± 1.84	39.78 ± 1.90#	31.83 ± 1.67*	35.07 ± 2.91*#
	R2* (s^{-1})	23.42 ± 2.38	23.91 ± 4.92#	31.22 ± 3.07*	27.14 ± 1.58#
OM	D ($\times10^{-4}$ mm²/s)	3.74 ± 0.21	3.65 ± 0.42#	2.43 ± 0.28*	3.06 ± 0.46*#
	D* ($\times10^{-3}$ mm²/s)	8.97 ± 0.25	9.06 ± 0.27#	8.31 ± 0.32*	8.54 ± 0.42*
	f (%)	36.78 ± 1.78	37.20 ± 2.83#	28.75 ± 1.91*	33.28 ± 2.59*#
	R2* (s^{-1})	29.26 ± 4.85	28.65 ± 4.41#	41.32 ± 5.20*	35.40 ± 2.57*#

**P < 0.05 vs. Cont; #P < 0.05 vs. PC–AKI.*

Cont, control; PC–AKI, post-contrast acute kidney injury; Res, resveratrol; CO, renal cortex; OM, outer medulla.

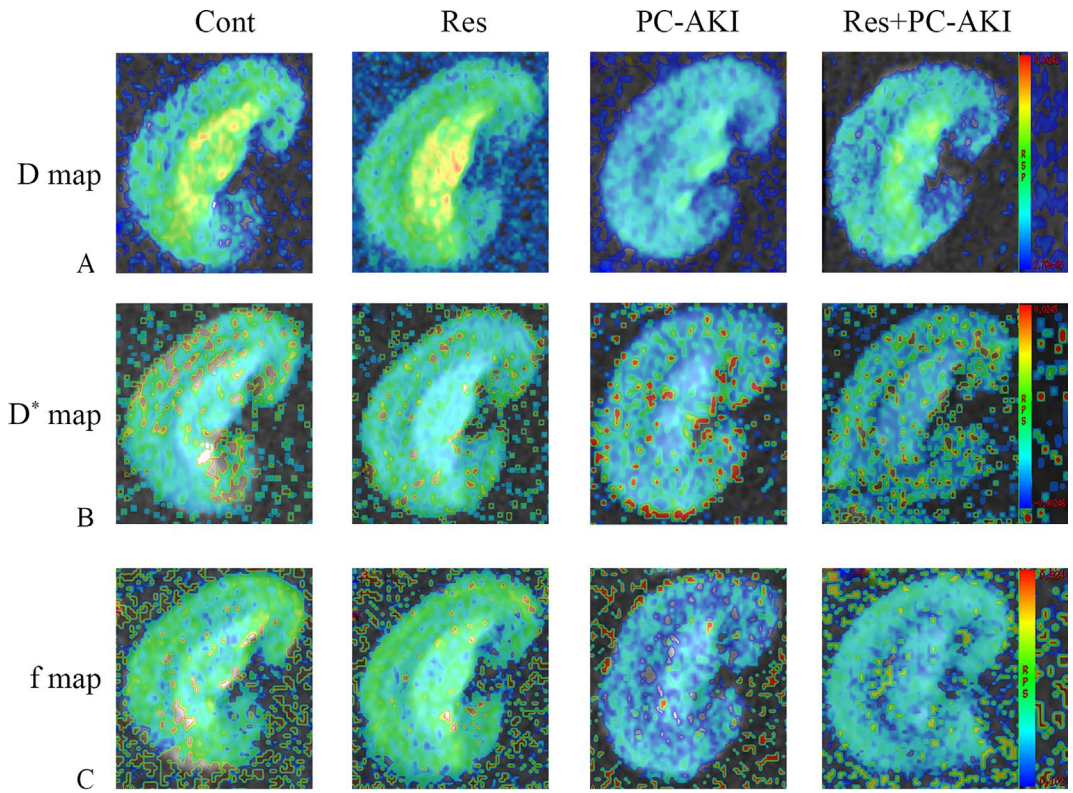

FIGURE 2 | Parametric images obtained from the intravoxel incoherent motion (IVIM) model for rabbit with different treatments. Representative IVIM images of *D* **(A)**, *D** **(B)**, and *f* **(C)** maps. The maximum *D, D** and *f* signal changes were observed in the PC–AKI group. The *D, D** and *f* values increased after the application of resveratrol. Cont, control; Res, resveratrol; PC–AKI, post-contrast acute kidney injury; IVIM, intravoxel incoherent motion.

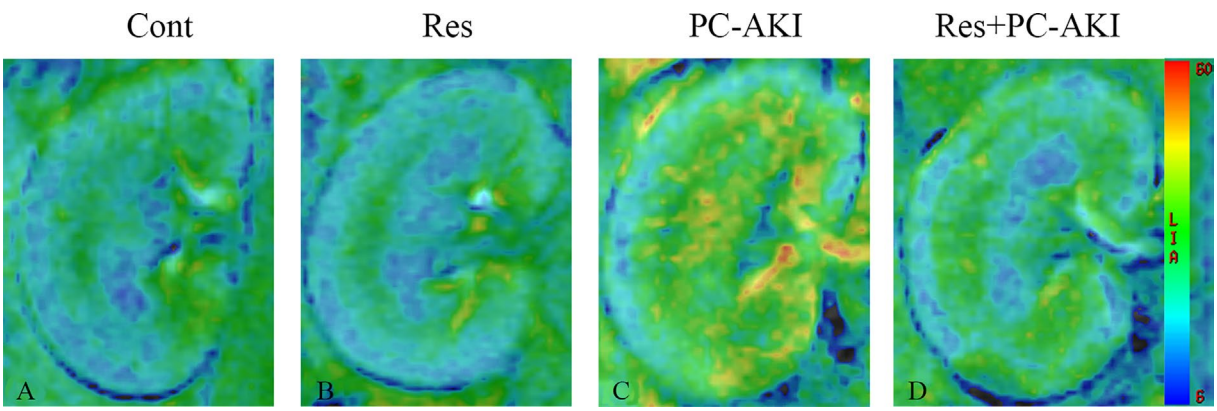

FIGURE 3 | Parametric images obtained from the BOLD model for rabbits with different treatments. The window and level settings for each map were kept the same. Compared to the control group, the brighter R2* maps in the PC–AKI group indicated increased hypoxia after iohexol injection. In the Res+PC–AKI group, the R2* values were significantly lower compared to the PC–AKI group, indicating increased oxygenation when using resveratrol before iohexol. **(A)** Control group, **(B)** Res group, **(C)** PC–AKI group, **(D)** Res+PC–AKI group. Cont, control; Res, resveratrol; PC–AKI, post-contrast acute kidney injury; BOLD, blood oxygenation level–dependent.

in the Res+PC–AKI group compared with the PC–AKI group in the CO (P = 0.002) and OM (P = 0.009). Perfusion-related parameters of D^* were slightly higher in the Res+PC–AKI group when compared with the PC–AKI group; however, significant differences were not found between the renal CO (P = 0.144) and OM (P = 0.214). In addition, the mean f values were significantly lower in the PC–AKI group compared to the Cont group in the CO ($P < 0.0001$) and OM ($P < 0.0001$). The mean f values significantly were greater in the Res+PC–AKI group compared with the PC–AKI group in the renal CO (P = 0.016) and OM

($P = 0.003$). The mean $R2^*$ values were significantly greater in the PC–AKI group compared with the Cont group in the renal CO ($P < 0.0001$) and OM ($P < 0.0001$), whereas $R2^*$ was lower in the Res+PC–AKI group when compared with the PC–AKI group in the renal CO ($P = 0.041$) and OM ($P = 0.030$). Thus, resveratrol increased oxygenation in kidney damage induced by exposure to contrast medium in DN.

Effects of Resveratrol on Histopathological Changes and Renal Cell Apoptosis

Histopathological examination showed no pathological alterations of the kidneys in the control group, whereas glomerular injury, tubular vacuolization–necrosis, and exfoliation of renal tubular epithelial cells, as well as the disruption of tubular structure scores were significantly greater in the PC–AKI group than in the other groups (**Figure 4**). Furthermore, the co-administration of resveratrol with iohexol (Res+PC–AKI) significantly decreased the severity score compared to the PC–AKI group ($P = 0.015$).

As shown in **Figure 5**, the number of TUNEL-positive cells was increased in iohexol-treated kidneys, while resveratrol substantially decreased the number of apoptotic cells in the Res+PC–AKI group compared with that in the kidneys of the PC–AKI group ($P = 0.001$, $P = 0.015$). In short, resveratrol ameliorated pathological changes in the kidney in response to contrast medium exposure in DN.

Effects of Resveratrol on Cell Toxicity Induced By Iohexol Under HG Conditions

As shown in **Table 3**, iohexol caused a marked elevation in HK-2 cell apoptosis when compared with controls ($P = 0.005$). In contrast, preincubation with resveratrol inhibited iohexol-mediated cell death ($P = 0.196$). Moreover, the HIF-1α inhibitor, 2-MeOE2, enhanced the renoprotective effect of resveratrol against cell apoptosis in iohexol-treated HK-2 cells under HG conditions ($P = 0.047$; **Figure 6**). In summary, resveratrol reduced cell cytotoxicity and apoptosis induced by contrast medium under HG conditions in a HIF-1α–mediated manner.

Effects of Resveratrol on SIRT1–PGC-1α–HIF-1α Signaling in DN Rabbits *In Vivo*

To investigate the molecular mechanisms associated with the renoprotective effects of resveratrol in DN rabbits with PC–AKI, the expression levels of SIRT1–PGC-1α–HIF-1α signaling proteins and those in its downstream pathway were analyzed (**Figure 7**).

Briefly, significantly higher levels of SIRT1 protein were detected in resveratrol-treated DN rabbits compared with rabbits in the control group [$P < 0.001$ (Res), $P = 0.008$ (Res+PC–AKI), respectively]. In addition, we found that the PGC-1α protein level was higher ($P = 0.447$) and the HIF-1α protein level lower ($P = 0.112$) in the Res+PC–AKI group compared to the PC–AKI group, but no statistical differences were observed between these

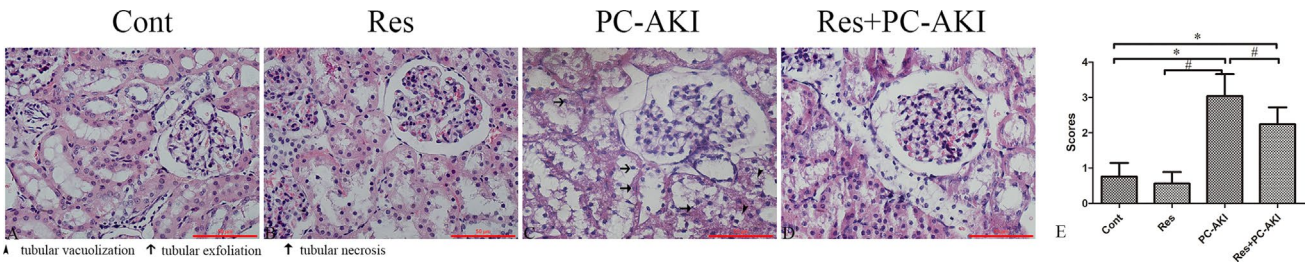

FIGURE 4 | Representative photomicrographs of HE-stained kidney sections in rabbits with different treatments. Iohexol induced obvious morphological alterations in kidneys of rabbits in the PC–AKI group. Resveratrol reduced contrast medium–induced morphological changes in the Res+PC–AKI group. **(A)** Cont group, **(B)** Res group, **(C)** PC–AKI group, and **(D)** Res+PC–AKI group. **(E)** Renal injury scores. Original magnifications: ×400. $^*P < 0.05$ vs. Cont; $^{\#}P < 0.05$ vs. PC–AKI. Cont, control; Res, resveratrol; PC–AKI, post-contrast acute kidney injury; HE, hematoxylin and eosin.

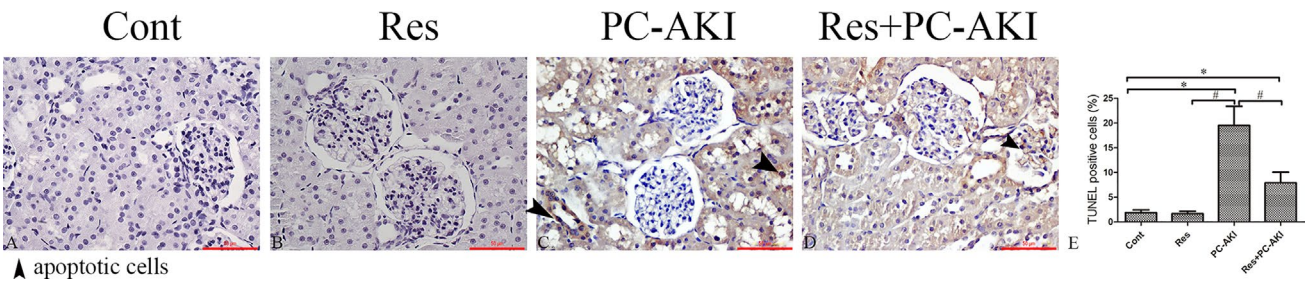

FIGURE 5 | Representative images of transferase dUTP nick-end labeling (TUNEL) staining for rabbits with different treatments. **(A–D)** TUNEL staining **(E)** Quantitative analysis of TUNEL-positive cells. A significant increase in TUNEL-positive cells was observed in the kidneys of rabbits with DN 24 h after contrast medium injection, whereas resveratrol inhibited renal tubular cell apoptosis. Original magnifications: ×400. $^*P < 0.05$ vs. Cont; $^{\#}P < 0.05$ vs. PC–AKI. TUNEL, terminal deoxynucleotidyl transferase dUTP nick-end labeling; DN, diabetic nephropathy; Cont, control; Res, resveratrol; PC–AKI, post-contrast acute kidney injury.

TABLE 3 | Quantitative analysis of the percentage of viable cells in different groups.

Groups	Res	Ex527	PC–AKI	2-MeOE2	Cont
	0.5498 ± 0.1161	0.3419 ± 0.1448*	0.4093 ± 0.1825*	0.6334 ± 0.1885	1.0176 ± 0.1345

**P < 0.05 vs. Cont.*

Cont, control; PC–AKI, post-contrast acute kidney injury; Res, resveratrol; Ex527, SIRT1 specific inhibitor; 2-MeOE2, HIF-1α specific inhibitor 2-methoxyestradiol; HG, high glucose; LG, low glucose.

Groups: Res, HG+res+iohexol; Ex527, HG+Ex527+iohexol; PC–AKI, HG+iohexol; 2-MeOE2, HG+res+2-MeOE2+iohexol; Cont, LG.

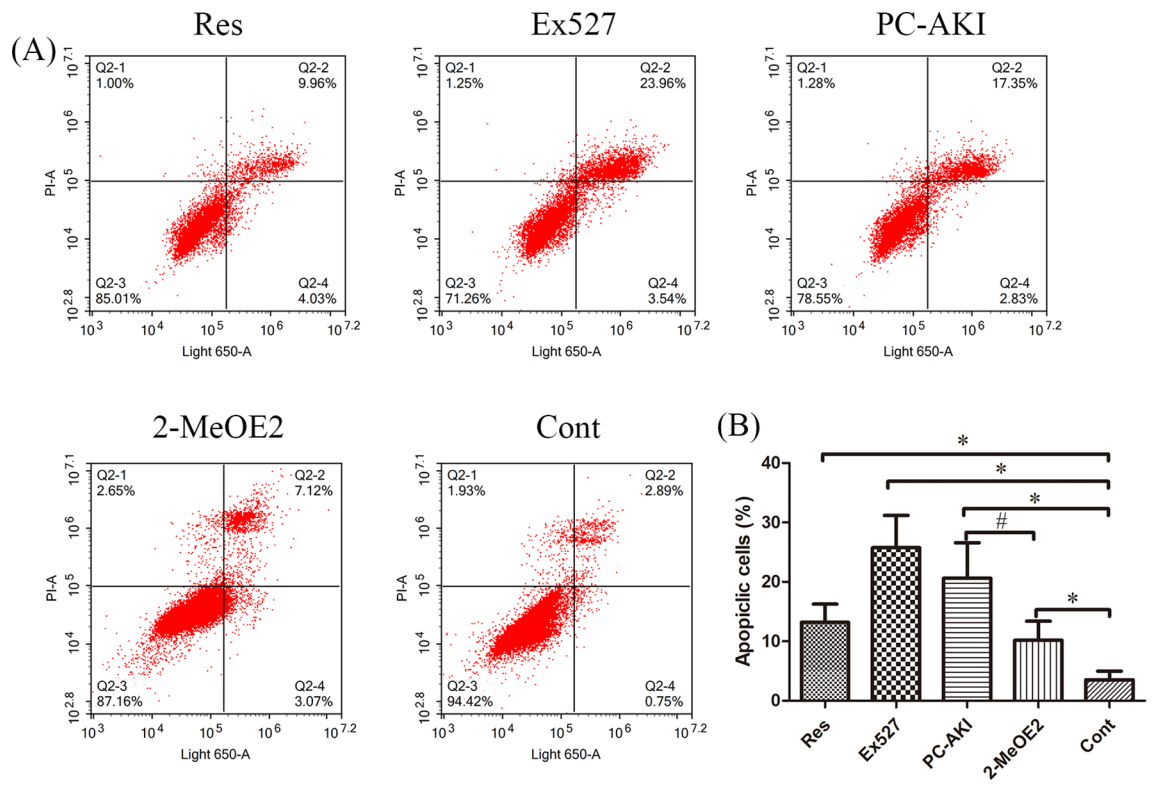

FIGURE 6 | Quantitative analysis of HK-2 cell apoptosis by flow cytometry. **(A)** HG-induced HK-2 cells were divided into five groups: Res, Ex527, PC–AKI, 2–MeOE2 and Cont groups. **(B)** Quantification of cell apoptosis in different groups. A significant increase in apoptotic cells was detected in the PC–AKI group; however, the up-regulation SIRT1 and silencing HIF-1α could both reduce iohexol-induced cell apoptosis. **P* < 0.05 vs. Cont; *#P* < 0.05 vs. PC–AKI. HG, high glucose; PC–AKI, post-contrast acute kidney injury; Cont, control; Res, resveratrol; SIRT1, silent information regulator l; HIF-1α, hypoxia-inducible transcription factor-1α; Ex527, SIRT1 specific inhibitor; 2-MeOE2, HIF-1α specific inhibitor 2-methoxyestradiol; LG, low glucose. Groups: Res, HG+res+iohexol; Ex527, HG+Ex527+iohexol; PC–AKI, HG+iohexol; 2-MeOE2, HG+res+2-MeOE2+iohexol; Cont, LG.

two groups. Furthermore, the protein level of Bcl-2 ($P = 0.515$) was slightly increased, and those of Bax ($P = 0.045$), cleaved caspase-3 ($P = 0.006$) and Cyt-C ($P < 0.001$) were significantly lower in the Res+PC–AKI group compared with the PC–AKI group. In summary, resveratrol modulated SIRT1–PGC-1α–HIF-1α signaling proteins and associated pathways in DN rabbits by upregulating SIRT1 and PGC-1α and by downregulating HIF-1α, Bax, cleaved caspase-3 and Cyt-C protein levels.

Effects of Resveratrol on SIRT1–PGC-1α–HIF-1α Signaling Under HG Conditions *In Vitro*

To further verify that SIRT1–PGC-1α–HIF-1α signaling was involved in renoprotection against PC–AKI under HG conditions, Ex527 and 2-MeOE2 were applied to HK-2 cells.

As shown in **Figure 8**, SIRT1 and PGC-1α protein levels were increased after treating cells with resveratrol. Resveratrol significantly reduced the protein levels of HIF-1α and its downstream factors, namely cleaved caspase-3, Bax and cytochrome C; co-treatment with 2-MeOE2 enhanced this reduction under HG conditions. However, the protective role of the SIRT1–PGC-1α–HIF-1α pathway was suppressed by the SIRT1 inhibitor, Ex527. The expression of SIRT1 ($P = 0.201$), PGC-1α ($P = 0.258$), and Bcl-2 ($P < 0.001$) proteins in cells treated with iohexol and Ex527 were decreased and the expression of HIF-1α ($P = 0.008$), Bax ($P < 0.001$), cleaved caspase-3 ($P = 0.001$), and cytochrome C ($P = 0.001$) were significantly increased compared to the control group. In summary, resveratrol also modulated SIRT1–PGC-1α–HIF-1α signaling proteins and associated pathways in HK-2 cells under HG by upregulating SIRT1 and PGC-1α, and by downregulating HIF-1α, Bax, cleaved caspase-3 and cytochrome C protein levels in a SIRT1-mediated manner.

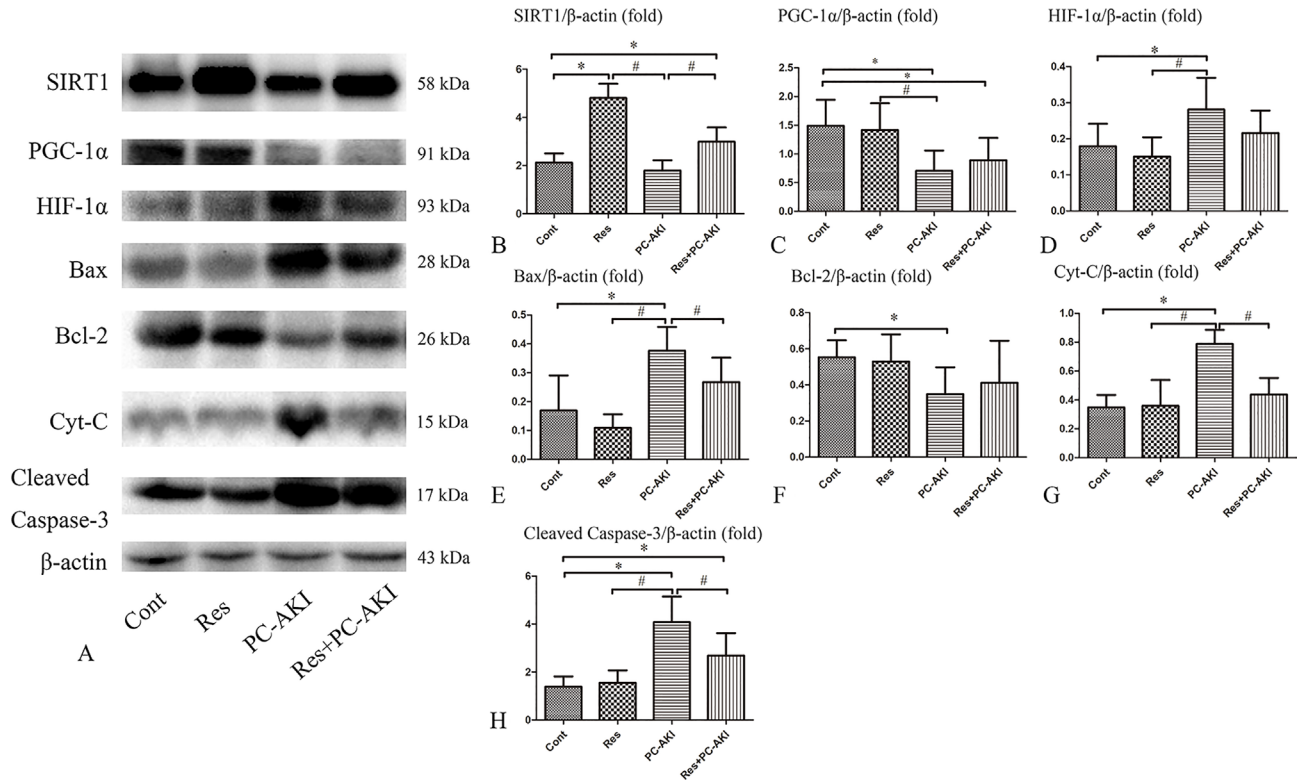

FIGURE 7 | Effects of resveratrol on the expression of SIRT1, PGC-1α, HIF-1α and apoptosis proteins *in vivo*. **(A)** Activation of the SIRT1–PGC-1α–HIF-1α signaling pathway in PC–AKI associated with DN in rabbits. Representative western blot images of proteins in the rabbits with DN treated with saline (Cont), resveratrol alone (Res), iohexol (PC–AKI), and co-treatment with resveratrol and iohexol (Res+PC–AKI). **(B–H)** Relative densitometry analysis of the ratios of SIRT1–PGC-1α–HIF-1α signaling proteins to β-actin were expressed as mean ± standard error. $^{*}P < 0.05$ vs. Cont; $^{\#}P < 0.05$ vs. PC–AKI. Cont, control; Res, resveratrol; PC–AKI, post-contrast acute kidney injury; SIRT1, silent information regulator l; HIF-1α, hypoxia-inducible transcription factor-1α; DN, diabetic nephropathy; PGC-1α, peroxisome proliferator-activated receptor gamma coactivator-1 alpha.

DISCUSSION

Post-contrast acute kidney injury is one of the leading causes of hospital-acquired acute kidney injury (Takahashi et al., 2017; Van Der Molen et al., 2018). Epidemiological and clinical evidence suggests that diabetes mellitus plays a part in the development of PC–AKI after the use of contrast medium (Tziakas et al., 2014; Chalikias et al., 2016). The identification of new molecular target(s) is thus crucial for the development of therapies for the prevention of PC–AKI in high-risk patients.

The development of PC–AKI with DN was found to lead to a decrease in the expression of SIRT1. Furthermore, we found that resveratrol could reverse the decrease in SIRT1 expression induced by PC–AKI with DN, which suggests that this may improve renal function, alleviate renal injury, and decrease iohexol-induced hypoxia and apoptosis in renal tubular cells. In addition, our findings also suggested that resveratrol may reduce iohexol-induced HK-2 cell apoptosis under HG conditions. Notably, resveratrol prevented the down-regulation of PGC-1α and up-regulation of HIF-1α in response to iohexol and DN in both a rabbit kidney and tissue culture model. These results indicate that resveratrol is an important survival mediator that protects against PC–AKI based DN complications by activating the SIRT1–PGC-1α–HIF-1α signaling pathway.

We found that resveratrol can protect the kidneys against damage induced by contrast medium in rabbits with DN. Suggested mechanisms for the protective action of resveratrol on PC–AKI with DN based on observations by us and others are as follows: 1) We found that resveratrol alleviates impaired renal hypoxia observed in PC–AKI as shown by observing functional MRI $R2^{*}$ parameters. 2) Resveratrol exerts a protective effect against contrast medium–induced injury by reducing oxidative stress and the excessive generation of reactive oxygen species (ROS) (Hussien et al., 2018). As reported, ROS may exert direct tubular and vascular endothelial injury, and further intensify renal parenchymal hypoxia by virtue of endothelial dysfunction and dysregulation of tubular transport (Andreucci et al., 2014). 3) We also found that resveratrol significantly alleviates tubular apoptosis in a PC–AKI animal model with DN.

PGC-1α has been characterized as a master regulator of mitochondrial biogenesis, which facilitates the combustion of stored energy by increasing its mitochondrial production (Dong et al., 2015; Ishimoto and Inagi, 2016). The deacetylation of PGC-1α ameliorates renal ischemic–reperfusion injury by

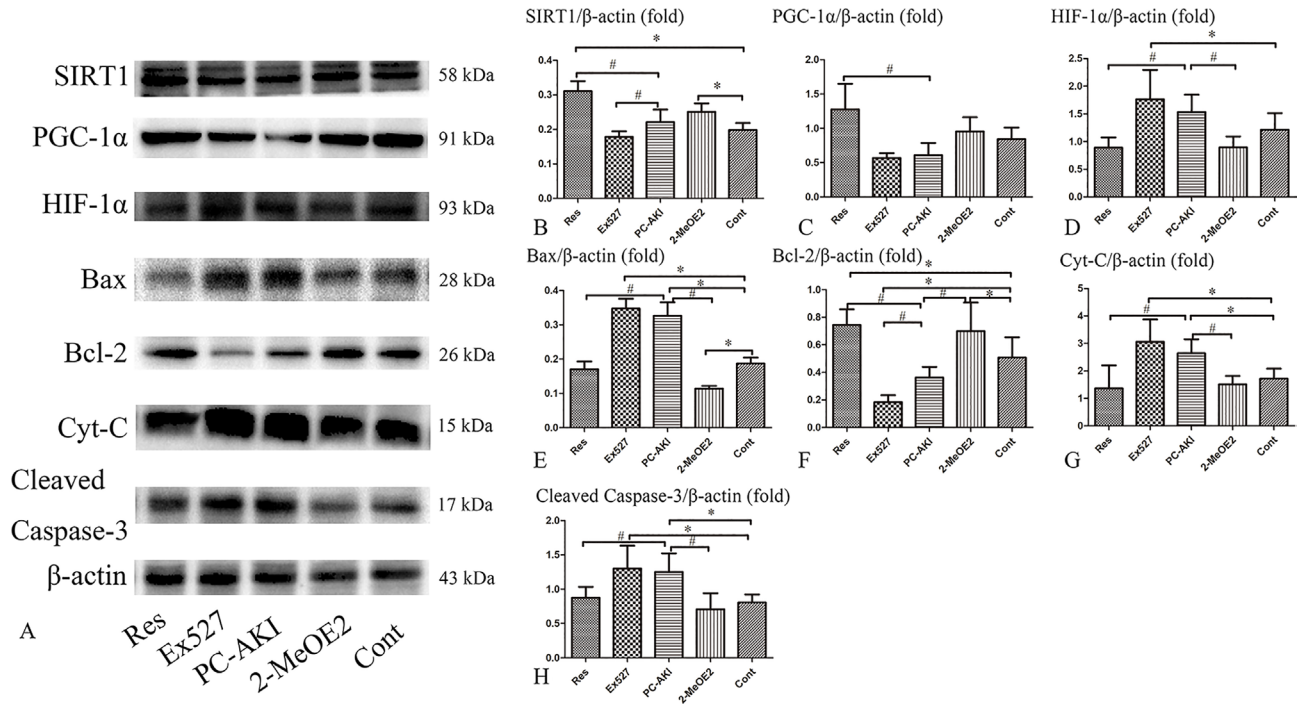

FIGURE 8 | Effects of resveratrol on the expression of SIRT1, PGC-1α, HIF-1α and apoptosis proteins *in vitro*. **(A)** The expression of SIRT1, PGC-1α, and Bcl-2 proteins were lower in iohexol treated HK-2 cells compared with control cells, which was reversed by treatment with resveratrol. The expression of HIF-1α, Bax, cleaved caspase-3, and Cyt-C were markedly increased after iohexol injection, which was reversed by treatment with resveratrol. Furthermore, this effect was enhanced by HIF-1α inhibitor, 2-MeOE2. **(B–H)** Relative densitometry of SIRT1–PGC-1α–HIF-1α signaling proteins expressed as mean ± standard error. $^{*}P < 0.05$ vs. Cont; $^{\#}P < 0.05$ vs. PC–AKI. Cont, control; Res, resveratrol; PC–AKI, post-contrast acute kidney injury; SIRT1, silent information regulator l; HIF-1α, hypoxia-inducible transcription factor-1α; Cyt-C, cytochrome C; PGC-1α, peroxisome proliferator-activated receptor gamma coactivator-1 alpha; Ex527, SIRT1 specific inhibitor; LG, low glucose. Groups: Res, HG+res+iohexol; Ex527, HG+Ex527+iohexol; PC–AKI, HG+iohexol; 2-MeOE2, HG+res+2-MeOE2+iohexol; Cont, LG.

recovering mitochondrial homeostasis (Funk and Schnellmann, 2013). As previously noted by Humes et al., contrast medium can impair mitochondrial energetics, resulting in a reduction in tubular ATP (Zager et al., 2003). We found that resveratrol countered the effect of contrast medium on mitochondrial function by increasing PGC-1α expression and therefore exerting a protective effect.

Previous studies have indicated that HIF-1α is upregulated in PC–AKI (Rosenberger et al., 2005). Accumulating evidence has also suggested that hypoxia has an important role in the development of PC–AKI (Wybraniec et al., 2015). In addition, diabetes mellitus with endothelial dysfunction may render the kidneys susceptible to further hypoxia by contrast medium (Calvin et al., 2010). Furthermore, hypoxia contributes to the formation of ROS and oxidative stress (Heyman et al., 2008). Similarly, contrast media can enhance oxidative stress leading to renal tubular epithelial cell apoptosis. In turn, that this may cause tissue hypoperfusion and hypoxia, which can aggravate the initial tissue damage caused by contrast medium, leading to a vicious circle (Liu et al., 2014; Patschan and Muller, 2016). It should be noted that resveratrol participates in PC–AKI with DN *via* a complex signaling network that includes PGC-1α, HIF-1α and other proteins, and that the inhibition of HIF-1α observed in our present study may be a dependent pathway through which resveratrol exerts its renal protective effects. Moreover, after treating cells with an inhibitor of HIF-1α, 2-MeOE2, the beneficial effect of resveratrol was greatly reinforced. Alternatively, given that SIRT1 expression and activity gradually decrease during hypoxia, HIF-1α may take over hypoxic signaling. In contrast to our results, Manotham et al. have suggested that HIF-1α has a role in a natural hypoxic adaptation to kidney ischemia that protects the medulla against ischemic insults (Manotham et al., 2005). Additionally, the potential protective impact of HIF upregulation has been extensively studied in AKI in a preclinical study (Loeffler and Wolf, 2015). Together with the discordant role of HIF-1α in AKI, we interpret these findings to mean that a "window of opportunity" for a HIF-dependent transcriptional response may exist. When the severity of hypoxia exceeds this, HIF-1α may begin to play a damaging role, resulting in the failure of this response and injury that may become irreversible.

In the present study, the elevated *D* observed in the renal cortex and medulla may be attributed to iohexol-induced tubular damage, renal tissue edema and inflammatory cell infiltration that may become alleviated after intervention with resveratrol. Meanwhile, we hypothesized that an increase in blood flow was responsible for increased D^{*} and *f* values observed in the kidneys of resveratrol-treated rabbits; resveratrol, as an activator of SIRT1, may significantly decrease renal vascular dysfunction. Moreover, the application of iohexol led to a prolonged increase of $R2^{*}$ values and HIF-1α expression, which suggested that hypoxia may be a major factor associated with the early

development of PC–AKI and was consistent with other studies (Li et al., 2015). The decrease in $R2^*$ values may be attributed to the inhibition of hypoxia production induced by resveratrol during the diabetes stage, and the amplification of secondary hypoxia signaling after iohexol injection. However, since there was very little blood flow change (the D^*) in Res+PC–AKI rabbits compared with PC–AKI rabbits, we think that resveratrol may have led to a decrease in oxygen consumption to ameliorate renal glomerular hyperfiltration. Regardless of the mechanism, our findings support the concept that resveratrol may have decreased the iohexol-induced renal hypoxia observed. Therefore, in this manner, resveratrol may promote the recovery of renal function after contrast injury in DN.

Nevertheless, potential limitations exist in the present study that require discussion. 1) The PC–AKI model we used was based on a DN procedure that increased the complexity of the model. 2) The sample size was small, and the SIRT1 inhibitor was not used in rabbits. Thus the current *in vivo* study could not adequately confirm the effect of resveratrol and subsequent apoptosis as observed in renal tubular cells. 3) We only explored the effects of resveratrol on HK-2 cells; a reduction in SIRT1 activity may also occur in other types of kidney cells and this should be addressed in future studies. 4) The mitochondrial membrane potential was not measured in our study so that the nature of the apoptosis and degree of mitochondrial dysfunction observed are yet to be elucidated.

In summary, our results suggest that resveratrol may prevent the development of post-contrast acute kidney injury. Increased SIRT1–PGC-1α–HIF-1α signaling is associated with renoprotection against PC–AKI with DN. Such beneficial effects are mainly mediated *via* anti-hypoxia, anti-apoptotic and energy maintenance effects. Consequently, understanding the relationship between resveratrol and PC–AKI following diabetic nephropathy may lead to a greater clinical perspective on tackling this disease.

DATA AVAILABILITY

The raw data supporting the conclusions of this manuscript will be made available by the authors, without undue reservation, to any qualified researcher.

ETHICS STATEMENT

All animal studies (including the rabbit euthanasia procedure) were done in compliance with the regulations and guidelines of our university institutional animal care and conducted according to the AAALAC and the IACUC guidelines.

AUTHOR CONTRIBUTIONS

Conceptualization: KR, YW; Project Administration: YW, XQ, XZ; Methodology: BW; Data Curation: BW; Writing the Original Draft: YW; Writing, Review and Editing: KR, BW.

FUNDING

The National Natural Science Foundation of China (Grant 81571635) and Scientific Research Foundation for Advanced Talents, Xiang'an Hospital of Xiamen University (NO. PM201809170011) supported this study.

ACKNOWLEDGMENTS

The authors gratefully appreciate the assistance of GuiboYu (Key Laboratory of Imaging Diagnosis and Interventional Radiology of Liaoning Province, Shenyang, Liaoning, China).

SUPPLEMENTARY MATERIAL

The Supplementary Material for this article can be found online at: https://www.frontiersin.org/articles/10.3389/fphar.2019.00833/full#supplementary-material

FIGURE S1 | Experimental flow chart for the in vivo model of contrast-induced kidney injury in DN.

FIGURE S2 | Positions of typical regions of interest (ROI). **(A)** T2-weighted image. **(B)** IVIM parametric images of D (b = 0 s/mm^2). CO, renal cortex; OM, outer medulla; IVIM, intravoxel incoherent motion; D, pure molecular diffusion.

FIGURE S3 | Experimental flow chart for the in vitro model of contrast-induced kidney cell injury in DN.

REFERENCES

Andreucci, M., Faga, T., Pisani, A. Sabbatini, M, and Michael, A. (2014). Acute kidney injury by radiographic contrast media: pathogenesis and prevention. *Biomed. Res. Int*. 2014, 362725. doi: 10.1155/2014/362725

Bhargava, A. S., Hofmeister, R., Siegmund, F., Schobel, C., and Gunzel, P. (1990). Effect of three non-ionic contrast media on rats and rabbits with regard to renal changes. Interspecies comparison. *Arzneimittelforschung* 40, 822–829.

Billings, F. T. T., Chen, S. W., Kim, M., Park, S. W., Song, J. H., Wang, S., et al. (2008). Alpha2-Adrenergic agonists protect against radiocontrast-induced nephropathy in mice. *Am. J. Physiol. Renal Physiol.* 295, F741–F748. doi: 10.1152/ajprenal.90244.2008

Calvin, A. D., Misra, S., and Pflueger, A. (2010). Contrast-induced acute kidney injury and diabetic nephropathy. *Nat. Rev. Nephrol.* 6, 679–688. doi: 10.1038/nrneph.2010.116

Chalikias, G., Drosos, I., and Tziakas, D. N. (2016). Contrast-induced acute kidney injury: an update. *Cardiovasc. Drugs Ther.* 30, 215–228. doi: 10.1007/s10557-015-6635-0

Chen, F., Sun, Z., Zhu, X., and Ma, Y. (2018). Astilbin inhibits high glucose-induced autophagy and apoptosis through the PI3K/Akt pathway in human proximal tubular epithelial cells. *Biomed. Pharmacother.* 106, 1175–1181. doi: 10.1016/j.biopha.2018.07.072

Colbay, M., Yuksel, S., Uslan, I., Acarturk, G., Karaman, O., Bas, O., et al. (2010). Novel approach for the prevention of contrast nephropathy. *Exp. Toxicol. Pathol.* 62, 81–89. doi: 10.1016/j.etp.2009.02.119

Deng, J., Wu, G., Yang, C., Li, Y., Jing, Q., and Han, Y. (2015). Rosuvastatin attenuates contrast-induced nephropathy through modulation of nitric oxide, inflammatory responses, oxidative stress and apoptosis in diabetic male rats. *J. Transl. Med.* 13, 53. doi: 10.1186/s12967-015-0416-1

Dong, W., Quo, W., Wang, F., Li, C., Xie, Y., Zheng, X., et al. (2015). Electroacupuncture upregulates SIRT1-dependent PGC-1alpha expression in SAMP8 mice. *Med. Sci. Monit.* 21, 3356–3362. doi: 10.12659/MSM.894864

Funk, J. A., and Schnellmann, R. G. (2013). Accelerated recovery of renal mitochondrial and tubule homeostasis with SIRT1/PGC-1alpha activation following ischemia-reperfusion injury. *Toxicol. Appl. Pharmacol.* 273, 345–354. doi: 10.1016/j.taap.2013.09.026

Gu, J., Yang, M., Qi, N., Mei, S., Chen, J., Song, S., et al. (2016). Olmesartan prevents microalbuminuria in db/db diabetic Mice through inhibition of angiotensin II/p38/SIRT1-induced podocyte apoptosis. *Kidney Blood Press Res.* 41, 848–864. doi: 10.1159/000452588

Heyman, S. N., Rosen, S., and Rosenberger, C. (2008). Renal parenchymal hypoxia, hypoxia adaptation, and the pathogenesis of radiocontrast nephropathy. *Clin. J. Am. Soc. Nephrol.* 3, 288–296. doi: 10.2215/CJN.02600607

Hu, G., Chan, Q., Quan, X., Zhang, X., Li, Y., Zhong, X., et al. (2015). Intravoxel incoherent motion MRI evaluation for the staging of liver fibrosis in a rat model. *J. Magn. Reson. Imaging* 42, 331–339. doi: 10.1002/jmri.24796

Hussien, N. I., Sorour, S. M., El-Kerdasy, H. I., and Abdelrahman, B. A. (2018). The glucagon-like peptide-1 receptor agonist Exendin-4, ameliorates contrast-induced nephropathy through suppression of oxidative stress, vascular dysfunction and apoptosis independent of glycaemia. *Clin. Exp. Pharmacol. Physiol.* 45, 808–818. doi: 10.1111/1440-1681.12944

Ishimoto, Y., and Inagi, R. (2016). Mitochondria: a therapeutic target in acute kidney injury. *Nephrol. Dial. Transplant* 31, 1062–1069. doi: 10.1093/ndt/gfv317

Kim, D. H., Jung, Y. J., Lee, J. E., Lee, A. S., Kang, K. P., Lee, S., et al. (2011). SIRT1 activation by resveratrol ameliorates cisplatin-induced renal injury through deacetylation of p53. *Am. J. Physiol. Renal Physiol.* 301, F427–F435. doi: 10.1152/ajprenal.00258.2010

Lauver, D. A., Carey, E. G., Bergin, I. L., Lucchesi, B. R., and Gurm, H. S. (2014). Sildenafil citrate for prophylaxis of nephropathy in an animal model of contrast-induced acute kidney injury. *PLoS One* 9, e113598. doi: 10.1371/journal.pone.0113598

Li, L. P., Lu, J., Zhou, Y., Papadopoulou, M. V., Franklin, T., Bokhary, U., et al. (2014a). Evaluation of intrarenal oxygenation in iodinated contrast-induced acute kidney injury-susceptible rats by blood oxygen level-dependent magnetic resonance imaging. *Invest. Radiol.* 49, 403–410. doi: 10.1097/RLI.0000000000000031

Li, L. P., Thacker, J., Lu, J., Franklin, T., Zhou, Y., Papadopoulou, M. V., et al. (2014b). Efficacy of preventive interventions for iodinated contrast-induced acute kidney injury evaluated by intrarenal oxygenation as an early marker. *Invest Radiol.* 49, 647–652. doi: 10.1097/RLI.0000000000000065

Li, L. P., Lu, J., Franklin, T., Zhou, Y., Solomon, R., and Prasad, P. V. (2015). Effect of iodinated contrast medium in diabetic rat kidneys as evaluated by blood-oxygenation-level-dependent magnetic resonance imaging and urinary neutrophil gelatinase-associated lipocalin. *Invest. Radiol.* 50, 392–396. doi: 10.1097/RLI.0000000000000141

Li, Y., Wang, P., Yang, X., Wang, W., Zhang, J., He, Y., et al. (2016). SIRT1 inhibits inflammatory response partly through regulation of NLRP3 inflammasome in vascular endothelial cells. *Mol. Immunol.* 77, 148–156. doi: 10.1016/j.molimm.2016.07.018

Liu, M., Guo, X., Wang, S., Jin, M., Wang, Y., Li, J., et al. (2013). BOLD-MRI of breast invasive ductal carcinoma: correlation of R2* value and the expression of HIF-1alpha. *Eur. Radiol.* 23, 3221–3227. doi: 10.1007/s00330-013-2937-4

Liu, T. Q., Luo, W. L., Tan, X., Fang, Y., Chen, J., Zhang, H., et al. (2014). A novel contrast-induced acute kidney injury model based on the 5/6-nephrectomy rat and nephrotoxicological evaluation of iohexol and iodixanol *in vivo*. *Oxid. Med. Cell. Longev.* 2014, 427560. doi: 10.1155/2014/427560

Loeffler, I., and Wolf, G. (2015). Morg1 heterozygous deficiency ameliorates hypoxia-induced acute renal injury. *Am. J. Physiol. Renal Physiol.* 308, F511–F521. doi: 10.1152/ajprenal.00236.2014

Maioli, M., Toso, A., Leoncini, M., Gallopin, M., Musilli, N., and Bellandi, F. (2012). Persistent renal damage after contrast-induced acute kidney injury: incidence, evolution, risk factors, and prognosis. *Circulation* 125, 3099–3107. doi: 10.1161/CIRCULATIONAHA.111.085290

Morigi, M., Perico, L., and Benigni, A. (2018). Sirtuins in renal health and disease. *J. Am. Soc. Nephrol.* 29, 1799–1809. doi: 10.1681/ASN.2017111218

Manotham, K., Tanaka, T., Ohse, T., Kojima, I., Miyata, T., Inagi, R., et al. (2005). A biologic role of HIF-1 in the renal medulla. *Kidney Int.* 67, 1428–1439. doi: 10.1111/j.1523-1755.2005.00220.x

Patschan, D., and Muller, G. A. (2016). Acute kidney injury in diabetes mellitus. *Int. J. Nephrol.* 2016, 6232909. doi: 10.1155/2016/6232909

Prasad, P., Li, L. P., Halter, S., Cabray, J., Ye, M., and Batlle, D. (2010). Evaluation of renal hypoxia in diabetic mice by BOLD MRI. *Invest. Radiol.* 45, 819–822. doi: 10.1097/RLI.0b013e3181ec9b02

Rasbach, K. A., and Schnellmann, R. G. (2007). Signaling of mitochondrial biogenesis following oxidant injury. *J Biol Chem.* 282, 2355–2362. doi: 10.1074/jbc.M608009200

Rosenberger, C., Heyman, S. N., Rosen, S., Shina, A., Goldfarb, M., Griethe, W., et al. (2005). Up-regulation of HIF in experimental acute renal failure: evidence for a protective transcriptional response to hypoxia. *Kidney Int.* 67, 531–542. doi: 10.1111/j.1523-1755.2005.67110.x

Takahashi, E. A., Kallmes, D. F., Fleming, C. J., Mcdonald, R. J., Mckusick, M. A., Bjarnason, H., et al. (2017). Predictors and outcomes of postcontrast acute kidney injury after endovascular renal artery intervention. *J. Vasc. Interv. Radiol.* 28, 1687–1692. doi: 10.1016/j.jvir.2017.07.038

Tziakas, D., Chalikias, G., Stakos, D., Altun, A., Sivri, N., Yetkin, E., et al. (2014). Validation of a new risk score to predict contrast-induced nephropathy after percutaneous coronary intervention. *Am. J. Cardiol.* 113, 1487–1493. doi: 10.1016/j.amjcard.2014.02.004

Van Der Molen, A. J., Reimer, P., Dekkers, I. A., Bongartz, G., Bellin, M. F., Bertolotto, M., et al. (2018). Post-contrast acute kidney injury - Part 1: definition, clinical features, incidence, role of contrast medium and risk factors: recommendations for updated ESUR contrast medium safety committee guidelines. *Eur. Radiol.* 28, 2845–2855. doi: 10.1007/s00330-017-5246-5

Wang, J. H., Ren, K., Sun, W. G., Zhao, L., Zhong, H. S., and Xu, K. (2014). Effects of iodinated contrast agents on renal oxygenation level determined by blood oxygenation level dependent magnetic resonance imaging in rabbit models of type 1 and type 2 diabetic nephropathy. *BMC Nephrol.* 15, 140. doi: 10.1186/1471-2369-15-140

Wybraniec, M. T., Mizia-Stec, K., and Wiecek, A. (2015). Contrast-induced acute kidney injury: the dark side of cardiac catheterization. *Pol. Arch. Med. Wewn.* 125, 938–949. doi: 10.20452/pamw.3218

Xiao, Y. D., Huang, Y. Y., Wang, H. X., Wu, Y., Leng, Y., Liu, M., et al. (2016). Thioredoxin-interacting protein mediates NLRP3 inflammasome activation involved in the susceptibility to ischemic acute kidney injury in diabetes. *Oxid. Med.Cell Longev.* 2016, 2386068. doi: 10.1155/2016/2386068

Xu, S., Gao, Y., Zhang, Q., Wei, S., Chen, Z., Dai, X., et al. (2016). SIRT1/3 activation by resveratrol attenuates acute kidney injury in a septic rat model. *Oxid. Med. Cell Longev*. 7296092. doi: 10.1155/2016/7296092

Zager, R. A., Johnson, A. C., and Hanson, S. Y. (2003). Radiographic contrast media-induced tubular injury: evaluation of oxidant stress and plasma membrane integrity. *Kidney Int.* 64, 128–139. doi: 10.1046/j.1523-1755.2003.00059.x

Zhao, Q., Li, J., Yan, J., Liu, S., Guo, Y., Chen, D., et al. (2016). Lycium barbarum polysaccharides ameliorates renal injury and inflammatory reaction in alloxan-induced diabetic nephropathy rabbits. *Life Sci.* 157, 82–90. doi: 10.1016/j.lfs.2016.05.045

Conflict of Interest Statement: The authors declare that the research was conducted in the absence of any commercial or financial relationships that could be construed as a potential conflict of interest.

Copyright © 2019 Wang, Wang, Qi, Zhang and Ren. This is an open-access article distributed under the terms of the Creative Commons Attribution License (CC BY). The use, distribution or reproduction in other forums is permitted, provided the original author(s) and the copyright owner(s) are credited and that the original publication in this journal is cited, in accordance with accepted academic practice. No use, distribution or reproduction is permitted which does not comply with these terms.

frontiers in Physiology

REVIEW
published: 06 August 2019
doi: 10.3389/fphys.2019.01016

The Impact of Versatile Macrophage Functions on Acute Kidney Injury and Its Outcomes

*Jea-Hyun Baek**

Research & Early Development, Biogen Inc., Cambridge, MA, United States

Acute kidney injury (AKI) is a common and devastating clinical condition with a high morbidity and mortality rate and is associated with a rapid decline of kidney function mostly resulting from the injury of proximal tubules. AKI is typically accompanied by inflammation and immune activation and involves macrophages (Mϕ) from the beginning: The inflamed kidney recruits "classically" activated (M1) Mϕ, which are initially poised to destroy potential pathogens, exacerbating inflammation. Of note, they soon turn into "alternatively" activated (M2) Mϕ and promote immunosuppression and tissue regeneration. Based on their roles in kidney recovery, there is a growing interest to use M2 Mϕ and Mϕ-modulating agents therapeutically against AKI. However, it is pertinent to note that the clinical translation of Mϕ-based therapies needs to be critically reviewed and questioned since Mϕ are functionally plastic with versatile roles in AKI and some Mϕ functions are detrimental to the kidney during AKI. In this review, we discuss the current state of knowledge on the biology of different Mϕ subtypes during AKI and, especially, on their role in AKI and assess the impact of versatile Mϕ functions on AKI based on the findings from translational AKI studies.

Keywords: macrophage, acute kidney damage, fibrosis, macrophage depletion, chronic kidney disease

OPEN ACCESS

Edited by:
Md Abdul Hye Khan,
Medical College of Wisconsin,
United States

Reviewed by:
Michael Hickey,
Monash University, Australia
Sara Calatayud,
University of Valencia, Spain

***Correspondence:**
Jea-Hyun Baek
jbaek.boston@gmail.com;
jeahyun.baek@biogen.com

Specialty section:
This article was submitted to Renal and Epithelial Physiology, a section of the journal Frontiers in Physiology

Received: *23 May 2019*
Accepted: *23 July 2019*
Published: *06 August 2019*

Citation:
Baek J-H (2019) The Impact of Versatile Macrophage Functions on Acute Kidney Injury and Its Outcomes. Front. Physiol. 10:1016. doi: 10.3389/fphys.2019.01016

INTRODUCTION

Severe AKI is a clinical condition closely linked with a high morbidity and mortality rate (Zuk and Bonventre, 2016). AKI manifests as a rapid decline of kidney function and is associated with CKD (Chawla et al., 2014; Fiorentino et al., 2018). AKI mostly results from the injury of proximal tubules and is accompanied by inflammation and immune activation (Zuk and Bonventre, 2019). Thereby, distinct Mϕ subtypes are involved across different stages of AKI (Huen and Cantley, 2017; Chen et al., 2019): (1) "Classically" activated (M1) Mϕ, which are poised to destroy potential pathogens, are recruited to the inflamed tissue and exacerbate inflammation in the initial stage of AKI; (2) "alternatively" activated (M2) Mϕ predominate in the injured tissue during the resolution phase of AKI and mediate immunosuppression and tissue regeneration; and (3) the last-mentioned also play

Abbreviations: AKI, acute kidney injury; CKD, chronic kidney disease; CLP, cecal ligation and puncture; CSF, colony-stimulating factor; DAMPs, damage-associated molecular patterns; DT, diphtheria toxin; (i)DTR, (inducible) diphtheria toxin receptor; ECM, extracellular matrix; IRI, ischemia-reperfusion injury/surgery; LPS, lipopolysaccharide; Mϕ, macrophage(s); PAMPs, pathogen-associated molecular patterns; PDGF, platelet-derived growth factor(s); PRR, pathogen recognition receptor(s); RA, retinoic acid; Th, T helper type; TLR, toll-like receptor; UUO, unilateral ureteral obstruction.

a role in the transition of AKI to CKD. As M2 Mϕ are found to be protective against AKI, there is a growing interest to use M2 Mϕ and Mϕ-modulating agents as therapeutic tools to treat patients with AKI (Chen et al., 2019). Whilst valuing its immense therapeutic potential, it is to acknowledge that the clinical translation of Mϕ-based therapies needs to be critically reviewed and questioned, especially since Mϕ act like double-edged swords being both beneficial and harmful to the injured tissue (**Figure 1**) (Braga et al., 2015). In this review, we discuss the current state of knowledge on the biology of different Mϕ subtypes during AKI and on the impact of global Mϕ and Mϕ subtypes on AKI based on the findings from *in vivo* Mϕ depletion studies. At the end, we outline Mϕ-based therapeutic strategies for the treatment of AKI.

KIDNEY Mϕ IN STEADY STATE AND INFLAMMATION

Mϕ are, as their name implies: [Greek: macrophage = $\mu\alpha\kappa\rho\acute{o}\varsigma$ (large) + $\varphi\alpha\gamma\varepsilon\acute{\iota}\nu$ (to eat)], cells highly specialized in phagocytosis, belonging to the mononuclear phagocytic system (MPS). They reside in virtually all organs and orchestrate tissue homeostasis and inflammation, being capable of both inducing and suppressing immune responses as well as promoting tissue repair. Mϕ are also the most abundant leukocytes in the resting and inflamed kidney, maintained by two main Mϕ survival factors, CSF-1 and interleukin-34 (IL-34), primarily expressed by tubular epithelial cells (Isbel et al., 2001; Menke et al., 2009; Zhang et al., 2012; Baek et al., 2015). Both cytokines are further up-regulated during renal inflammation and account for Mϕ expansion of in the kidney tissue (Baek et al., 2015). CSF-1 and IL-34 both signal through the CSF-1 receptor (CSF-1R), whereas the signaling via CSF-1R is the key pathway for Mϕ proliferation, differentiation, and survival (Baek et al., 2015). In addition to CSF-1R, IL-34 activates another receptor, which is receptor-type tyrosine-protein phosphatase zeta (PTP-ζ), (Nandi et al., 2013). However, there is so far no evidence that PTP-ζ is expressed by Mϕ (Baek et al., 2015).

Like Mϕ in other organs, first kidney Mϕ arise during organogenesis, derived from erythro-myeloid progenitors that are generated in the yolk sac before E8.5 and colonize the fetal liver of the embryo. These primitive progenitors give rise to pre-Mϕ, which simultaneously populate the whole embryo from E9.5 and differentiate to fetal and perinatal tissue-specific Mϕ activating tissue-dependent transcriptional machinery (Mass et al., 2016). Tissue-resident Mϕ are known to renew themselves *in situ* throughout the lifetime of the host (**Figure 2**). However, Mϕ arising from blood-circulating monocytes (also known as circulating Mϕ precursors) are also detected in resting adult kidneys, but they turn over within 14 days and do not substitute kidney-resident Mϕ unless kidney-resident Mϕ niches become available (Lever et al., 2019).

In the occurrence of inflammation, additional Mϕ are recruited from the blood circulation (Sere et al., 2012). Blood-circulating monocytes are attracted to the site of inflammation, where they differentiate to Mϕ and clear pathogens and cellular debris (**Figure 2**).

Mϕ exert multiple biological functions in health and disease. Most importantly, they are instrumental in both promoting and resolving inflammation, which are two contrasting features. Correspondingly, Mϕ are broadly classified into two subpopulations according to their phenotype and function: So-called "classically activated" Mϕ (M1) are the Mϕ subpopulation inducing cytotoxicity and tissue injury; conversely, "alternatively" activated (M2) Mϕ comprise the other subpopulation, which is involved in immunosuppression and tissue repair (Mills et al., 2000; Murray and Wynn, 2011). Overall, M1/M2 paradigm is a theoretical and oversimplified concept, which was firstly proposed by Mills et al. based on the observation that Mϕ from mouse strains with Th 1 (e.g., C57BL/6, B10D2) and Th2 (e.g., BALB/c, DBA/2) display distinctive activation profiles differing in metabolic programs (Mills et al., 2000). Correspondingly, both Mϕ phenotypes were named M1 and M2 and characterized *in vitro* by stimulating bone marrow or monocyte-derived Mϕ with either Th1 (e.g., LPS, Interferon γ) or Th2 stimuli (e.g., IL-4, IL-10, IL-13) (**Figure 3**). In addition,

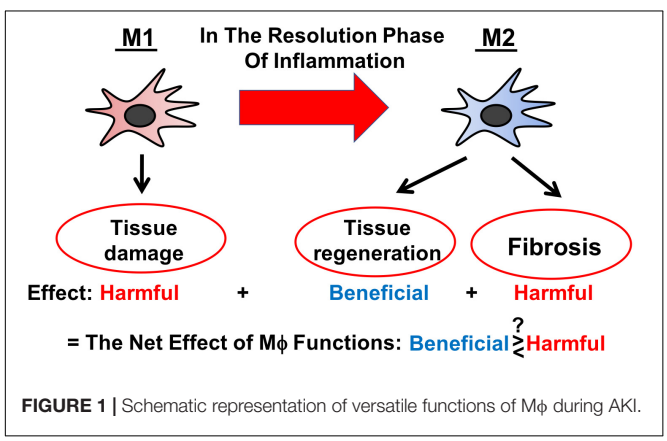

FIGURE 1 | Schematic representation of versatile functions of Mϕ during AKI.

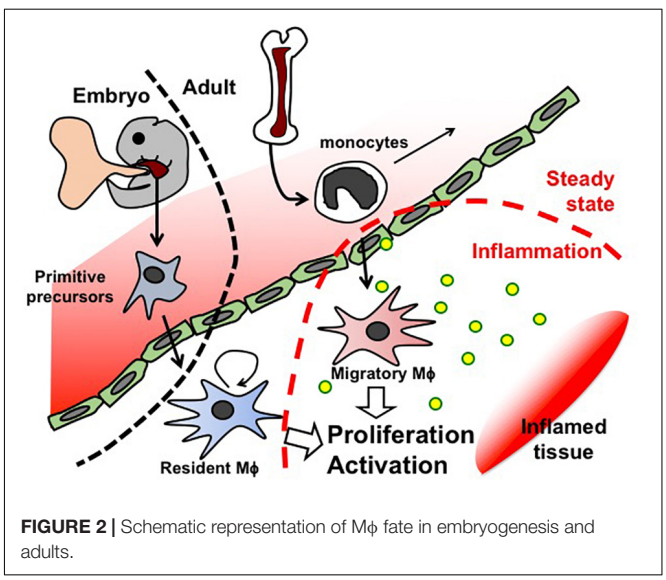

FIGURE 2 | Schematic representation of Mϕ fate in embryogenesis and adults.

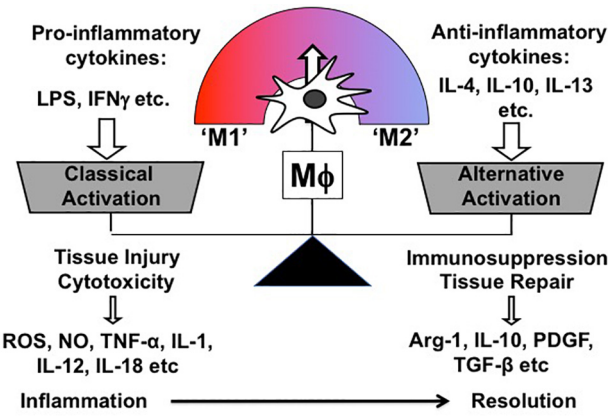

FIGURE 3 | Schematic representation of Mϕ polarization *in vitro*.

M2-activated Mϕ are further subdivided into different groups based on the Th2 stimulus, with which Mϕ are treated for M2 polarization. Of note, different M2 stimuli have distinct effects on transcriptional profiles and cellular functions of Mϕ (detailed information in Murray et al., 2014; Chen et al., 2019).

One of the unique characteristics of Mϕ is functional plasticity. In other words, Mϕ can easily change their phenotype from one activation state to the other. Thus, *in vivo* Mϕ are, in reality, somewhere along the continuum between the two *in vitro*-defined phenotypes (M1 and M2), and *in vitro* polarized Mϕ do not fully recapitulate *in vivo* Mϕ in pathologic conditions (**Figure 3**) (Geissmann et al., 2010).

As Mϕ play important roles in many biological processes, their malfunction is linked to various diseases. While Mϕ-mediated immune hyper-activation can lead to autoimmune and inflammatory diseases, unregulated tissue homeostasis can promote cancer growth and organ fibrosis. Accordingly, Mϕ are implicated in numerous renal diseases including lupus nephritis, glomerulonephritis as well as in AKI (Nikolic-Paterson and Atkins, 2001; Baek et al., 2018).

EXPERIMENTAL AKI MODELS

AKI is characterized by an abrupt loss of kidney function arising from different events, such as (1) sepsis/septic shock, (2) ureteral obstruction, (3) kidney ischemia, (4) hypoxia, (5) nephrotoxicity, (6) oxidative, and (7) metabolic stress. Of note, all etiologies share one common feature, which is the proximal tubular injury accompanied with inflammation and immune activation (Basile et al., 2012; Chevalier, 2016; Xu and Han, 2016). Proximal tubular injury can be acutely detrimental to the kidney as well as to the whole organism by impairing key kidney functions, such as reabsorption and secretion, and can lead to long-term problems (e.g., transitioning to CKD and increased risk of CKD and eventual death even after a complete recovery) (Bucaloiu et al., 2012; Jones et al., 2012). Of note, proximal tubules are highly vulnerable to injuries due to the high demand of oxygen consumption, which is required for multiple transport processes, and a relative paucity of endogenous antioxidant defenses (Chevalier, 2016). Thus, proximal tubules are the major target of AKI, and, in line with this, clinically relevant studies demonstrate that molecular targeting of the proximal tubule is sufficient to induce AKI and its transition to CKD (Chevalier, 2016).

For studying AKI, a number of experimental techniques have been developed to directly or indirectly target the kidney, including: (1) surgical approaches – UUO, IRI, CLP (via sepsis), etc.; (2) systemic administration of drugs or toxins inducing nephrotoxicity – injection of cisplatin, glycerol (via rhabdomyolysis), bacterial LPS (via sepsis) etc. (Ramesh and Ranganathan, 2014; Ortiz et al., 2015; Rabb et al., 2016; Bao et al., 2018; Johnson and Zager, 2018); and (3) selective depletion of proximal tubules in genetically modified mice, i.e., injecting mice with DT, which express human DT receptor (DTR) on proximal tubules – *Ggt1*-DTR (Zhang et al., 2012, 2017; Wang et al., 2015), *Ndgr1*-Cre^{ERT}:iDTR (Takaori et al., 2016), etc. Importantly, molecular mechanisms of AKI progression may differ depending on the type of insult to the proximal tubule. In effect, methods using (1) septic versus aseptic approaches, (2) systemic versus local, and (3) mild versus severe insults may involve different signaling pathways. This point is well illustrated in studies showing that the nucleotide-binding oligomerization domain, leucine rich repeat and pyrin domain containing 3 (NLRP3) inflammasome pathway is activated in ischemic, but not cisplatin-induced AKI (Kim et al., 2013). As AKI is a major risk factor for CKD progression, CKD is often assessed as a readout for AKI, and experimental AKI models are commonly utilized in the CKD research (detailed information in Tanaka et al., 2014; Chou et al., 2017; Fiorentino et al., 2018). Of note, not all experimental AKI are irreversible and lead to CKD (Chawla et al., 2011; Basile et al., 2012). Overall, it is important to determine the appropriate AKI model depending on the question being asked by giving consideration to the possibility that findings may not be transferable between experimental models. While designing the experiment, we need to consider the pathophysiology of mouse models and the mode of action of tested drugs and specify the model type, functional determination and time course of tissue collection (Ramesh and Ranganathan, 2014). Limitations and pitfalls of animal AKI models as well as the differences between AKI models have been recently described in several reviews. For a comparative overview of the various AKI animal models, please refer to the reviews: Ortiz et al. (2015), Rabb et al. (2016), and Bao et al. (2018).

Mϕ IN AKI

Infiltrating Mϕ in the Initial Phase of AKI

In experimental AKI models, blood-circulating Ly6C^{high} monocytes are recruited to the inflamed kidney as early as within 1 h (Li and Okusa, 2010; Zhang et al., 2012). The migration of Ly6C^{high} monocytes to the site of inflammation occurs through chemotactic mechanisms (e.g., via CCR2 and CX_3CR1). Therefore, deletion or blockage of chemotaxis receptors on monocytes is found to be protective against ischemia-induced AKI in mice (Furuichi et al., 2003; Li et al., 2008; Lu et al., 2008;

Oh et al., 2008; Yang et al., 2019). Monocyte infiltration occurs in the first 48 h (Lu et al., 2008) and completely ceases before day 3 of AKI. Accordingly, studies showed that the number of Ly6C^{high} monocytes and M1-like Mϕ drastically declines before day 3 of IRI (Lee et al., 2011; Lever et al., 2019) and CX_3CR1-dependent monocyte migration is not detectable at day 3 of UUO (Peng et al., 2015). Interestingly, the peak of tubular injury [e.g., following IRI (Lee et al., 2011) and glycerol injection (Bussolati et al., 2005)] timely overlaps with the maximum presence of infiltrating monocytes, indicating a close spatial and temporal relationship between the tissue destruction and the accumulation of infiltrating monocytes.

Ly6C^{high} monocytes differentiate into Mϕ, which are primarily skewed toward an M1 phenotype. M1 Mϕ polarization is mediated by pro-inflammatory cytokines [e.g., IFN-γ, IL-6, IL-1β, IL-23, IL-17, C3, C5a, and C5b (Rabb et al., 2016)] and DAMPs [e.g., high mobility group protein B1 (HMGB1), adenosine triphosphate (ATP), uric acid, or hypomethylated DNA (Anders, 2010; McDonald et al., 2010)] released by dying cells or damaged ECM (Anders and Schaefer, 2014). Most recently, soluble epoxide hydrolase was identified as a proximal tubular factor driving M1 polarization of Mϕ in IgA nephropathy (Wang Q. et al., 2018). DAMPs activate various PRRs [e.g., TLR families (Kulkarni et al., 2014; Leaf et al., 2017), NLRP3 and purinergic receptors (Anders and Schaefer, 2014)] on Mϕ and parenchymal cells (Leaf et al., 2017). The importance of DAMPs in inducing innate immune responses is highlighted by findings that the inhibition of PRR signaling suppresses immune responses in AKI (Kim et al., 2013; Leaf et al., 2017). Similar mechanisms are known from acute injuries in other organs, corroborating that DAMPs are central to the immune activation during tissue injury (Egawa et al., 2013; Wang et al., 2014; Groves et al., 2018). Interestingly, TLR4 activation was also shown to induce the expression of IL-22 in Mϕ, which is protective against AKI accelerating kidney regeneration (Kulkarni et al., 2014). M1 polarization of infiltrating Mϕ is additionally supported by parenchymal factors [e.g., Krüppel-like factor 5 (KLF5) expressed by collecting ducts (Fujiu et al., 2011) and suppressor of cytokine signaling 3 (SOCS3) upregulated by proximal tubules in AKI (Susnik et al., 2014)]. Both KLF5 and SOCS3 promote M1 activation of Mϕ and inhibit the expansion of M2 Mϕ in AKI (Fujiu et al., 2011; Susnik et al., 2014). M1-activated Mϕ largely produce pro-inflammatory cytokines and mediators (e.g., IL-1α, IL-6, IL-12, IL-18, TNF-α, nitric oxide), in turn, exacerbating the kidney inflammation (Li and Okusa, 2010).

M2 Polarization of Infiltrating Mϕ in the Resolution Phase of AKI

Inflammation following a transient insult is meant to prepare the tissue for healing. When the inflammation escalates (before day 3 of AKI), Mϕ seek to counteract overwhelming immune activation by skewing toward an immunosuppressive M2 Mϕ to restore tissue homeostasis (**Figure 3**) (Lee et al., 2011; Baek et al., 2015). However, this only depicts the global view of Mϕ dynamics and does not resolve how individual Mϕ subtypes change during AKI. Since Mϕ are highly plastic and rapidly adapt to the tissue microenvironment, it is difficult to trace the development of individual Mϕ subtypes during AKI. Nevertheless, we are steadily expanding our knowledge base through genetic fate mapping studies and parabiosis experiments. Earlier fate mapping studies revealed that Ly6C^{high} monocytes infiltrating the inflamed kidney give rise to Ly6C^{low} and Ly6C^{int} Mϕ, both phenotypically resembling tissue-resident Mϕ (Lin et al., 2009) (**Figure 4**). Several studies have shown that monocyte-derived Ly6C^{int} and Ly6C^{low} Mϕ populations display transcriptionally and functionally distinct M2 phenotypes, both implicated in immunosuppression and tissue regeneration. In the later stages of AKI, Ly6C^{low} Mϕ predominate over Ly6C^{int} Mϕ and are found to promote interstitial fibrosis (Lin et al., 2009; Clements et al., 2016; Lever et al., 2019; Yang et al., 2019) (**Figure 4**). More recent studies revealed that quiescent tissue-resident Mϕ remain in the tissue independently of monocyte-derived Ly6C^{low} Mϕ (Lin et al., 2009; Zhang et al., 2012; Lever et al., 2019) and are reprogramed in AKI toward a developmental state resembling perinatal Mϕ (Schulz et al., 2012; Mass et al., 2016), which are implicated in early kidney development (Lever et al., 2019). These cells display a unique transcriptional profile complying with neither canonical M1 nor M2 nor quiescent Mϕ phenotypes during the first 3 days after IRI. Interestingly, they activate the canonical wingless-type MMTV integration site family (Wnt) signaling by expressing Wnt ligand genes and downstream intracellular signaling mediators, implying that they mediate kidney healing after AKI (Lever et al., 2019). How reprogramed kidney-resident Mϕ further develop in the later stages of AKI and whether they are related to interstitial fibrosis following AKI deserve further investigation (**Figure 4**).

Beneficial Effects of M2-Activated Mϕ in AKI

Beneficial effects of M2-activated Mϕ in AKI are supported by many findings: (1) M2 Mϕ clear intraluminal debris (e.g., by apoptosis inhibitor of Mϕ [AIM]-dependent mechanisms) (Arai et al., 2016); (2) secrete tissue-reparative factors, which

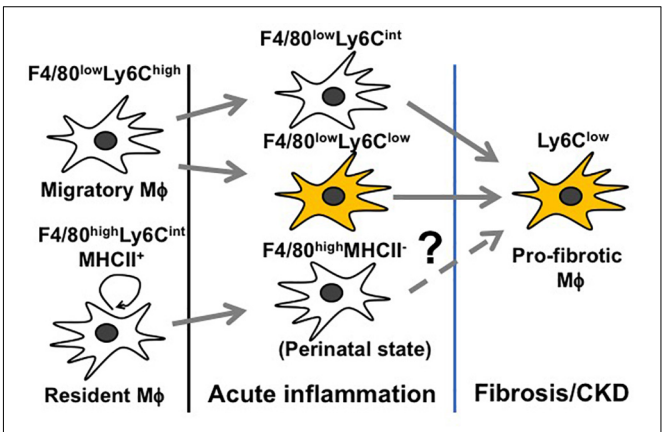

FIGURE 4 | Schematic representation of Mϕ subtypes throughout different stages of AKI.

limit cell cycle arrest (Lin et al., 2010) or apoptosis (Lin et al., 2010; Sola et al., 2011) or which support proliferation in tubular cells (Schmidt et al., 2013) [e.g., Wnt-7b (Lin et al., 2010), lipocalin-2 (Sola et al., 2011), breast regression protein 39 (BRP-39) (Schmidt et al., 2013)]; (3) secrete anti-inflammatory cytokines, which suppress effector T cells or activate regulatory T cells (e.g., IL-10, TGF-β) (Chen et al., 2019); and (4) reduce neutrophil infiltration by downregulating intracellular adhesion molecule-1 (ICAM-1) (Karasawa et al., 2015) and potentially also by sequestering the tissue damage through "cloaking" mechanisms as found in the peritoneal serosa (Uderhardt et al., 2019) etc. As M1 Mϕ are converted into M2 Mϕ in the resolution phase of AKI, a number of studies have focused on identifying stimuli driving Mϕ phenotypic switch during AKI. These stimuli include: (1) paracrine factors released from parenchymal and immune cells; (2) systemic factors, which are released into the blood circulation; and potentially (3) (tissue micro)environmental changes [e.g., apoptotic neutrophils (Filardy et al., 2010; Lee et al., 2011), oxygen (Raggi et al., 2017), and nutrient availability (Geeraerts et al., 2017)].

Paracrine Factors Released by Proximal Tubules

As mentioned above, proximal tubules are the main locale of the inflammation and potent producers of cytokines in AKI. Therefore, it would not be surprising if they substantially contributed to the phenotypic switch of Mϕ in AKI. In proximal tubule/Mϕ co-culture experiments (proximal tubules and Mϕ physically separated), quiescent proximal tubules are capable of polarizing both non- and M1-activated Mϕ toward an M2 Mϕ phenotype in a paracrine manner, similarly as known from mesenchymal stem cells (Lee et al., 2011; Huen et al., 2015). Unfortunately, the proximal tubular mechanisms of M2 polarization are still largely elusive, and it is also unclear whether the contribution of proximal tubules or proximal tubule-derived factors is indispensable for M2 Mϕ polarization in the resolution phase of AKI. Several studies suggest that proximal tubule-derived Mϕ survival factors (e.g., CSF-1, -2, IL-34) drive M2 Mϕ polarization, but these results remain controversial as discussed in the following paragraph. Proximal tubule-derived factors identified to polarize Mϕ toward an M2 phenotype are Wnt ligands and netrin-1, which are both upregulated during AKI (Reeves et al., 2008; Grenz et al., 2011; Ranganathan et al., 2013; Feng et al., 2018a,b). It has been shown that the blockade of Wnt/β-catenin signaling diminishes M2 Mϕ polarization also reducing interstitial fibrosis in AKI (Feng et al., 2018a,b). Netrin-1 deficiency was found to aggravate AKI, whereas the adoptive transfer of netrin-1-treated Mϕ was protective against AKI (Reeves et al., 2008; Grenz et al., 2011; Ranganathan et al., 2013). Proximal tubules also express both transforming growth factor β (TGF-β) and its receptors at high levels. While TGF-β with its pleiotropic effects acts on various cell types, it is known to polarize Mϕ toward an anti-inflammatory (Wang et al., 2005) and pro-fibrotic phenotype (Braga et al., 2015). However, it is unclear how beneficial the Mϕ-specific effects of TGF-β are on AKI as TGF-β can signal directly to proximal tubules and induce proximal tubular apoptosis (Nath et al., 2011; Gewin et al., 2012). In addition, TGF-β may promote the persistence of fibrotic M2 Mϕ and mediate interstitial fibrosis (Martinez et al., 2009; Lech and Anders, 2013; Chung et al., 2018).

Controversial Roles of Mϕ Survival Factors in Mϕ Polarization

CSF-1 and -2 are produced and up-regulated by proximal tubules during AKI. Many studies have pinpointed Mϕ survival factors, CSF-1 (Menke et al., 2009; Alikhan et al., 2011; Zhang et al., 2012; Wang et al., 2015) and -2 [also known as granulocyte-Mϕ CSF (GM-CSF)] (Huen et al., 2015), as factors driving the phenotypic switch toward an M2 phenotype, but this feature of Mϕ survival factors is highly controversial. CSF-1 and -2 are commonly used for generating *in vitro* Mϕ from bone marrow or blood monocytes, both being sufficient for Mϕ differentiation and maturation. Since CSF-1 and -2 mature and induce expression of distinct patterns of functional genes after a sufficient culture period, researchers have been incited to determine the polarization potential of CSF-1 and -2 and were led to propose that CSF-1 give rise to a more M2-like and CSF-2 to more M1-like expression patterns in Mϕ *in vitro* (Lacey et al., 2012). Nevertheless, it is important to understand that the translatability of *in vitro* data is limited as CSF-1 and -2 show *in vitro* M2 polarization potential only at high concentrations (Lutz et al., 2000; Hume and MacDonald, 2012; Huen et al., 2015) while being efficient at maintaining Mϕ already at low concentrations (Hamilton et al., 1988; Lutz et al., 2000; Meshkibaf et al., 2014). Whereas a number of studies have claimed that both CSF-1 and -2 drive M2 skewing of Mϕ in mice with AKI (Zhang et al., 2012; Huen et al., 2015; Wang et al., 2015), it was controversially found that IL-34, another ligand for CSF-1R, does not polarize Mϕ in murine AKI (Baek et al., 2015) and lupus model (Wada et al., 2019), indicating that CSF-1R signaling is dispensable in M2 Mϕ polarization. Supportive of this data, other studies have shown that: (1) increased CSF-1 expression in the resolution phase of AKI is not sufficient to prevent Mϕ from M1 polarization when Mϕ are exposed to an M1 stimulus or when they are deprived of an M2 stimulus during AKI (Fujiu et al., 2011; Susnik et al., 2014; Chiba et al., 2016); (2) quiescent and M2 Mϕ in the resolution phase of AKI differ in transcriptional profiles and functions (Lever et al., 2019; Yang et al., 2019); and (3) the sustained blockage of CSF-1R or the constitutive deletion of CSF-1 ameliorates AKI (Lenda et al., 2003; Ma et al., 2009; more discussion in *Assessing Mϕ functions by depleting Mϕ* section). Nevertheless, what is consistent throughout all studies (Zhang et al., 2012; Baek et al., 2015; Huen et al., 2015; Wang et al., 2015; Chiba et al., 2016) is that the deficiency in Mϕ survival factors reduces the number of Mϕ (including that of M2 Mϕ predominating in the resolution phase of AKI). It is interesting to note that the deletion of proximal tubule CSF-1 or the blockade of CSF-2 in AKI leads to a reduction in expression of M2 Mϕ-specific genes, which appears modest (<30%; except regarding *Arg1* expression), which may have resulted from the altered ratio of infiltrating and kidney-resident Mϕ, as blood-circulating Mϕ are not affected by the deletion of proximal tubule CSF-1

or the blockade of CSF-2 (Huen et al., 2015; Wang et al., 2015). The observation that clodronate-induced Mϕ depletion increased initial AKI and reduced recovery in the absence of proximal tubule CSF-1 (Wang et al., 2015) provided additional evidence that CSF-1 is not required or sufficient for M2 Mϕ polarization (also commented in Perry and Okusa, 2015). Taken together, CSF-1, -2 and IL-34 are likely not sufficient to polarize Mϕ toward M2 phenotype, but promote the expansion of M2 Mϕ post-AKI (Chiba et al., 2016). It would be interesting for future work to explore whether Mϕ survival factors have only redundant functions and, if not, what the unique, non-overlapping, functions of these Mϕ survival factors are.

Other Factors Inducing M2 Polarization of Mϕ

Th2 cytokines, IL-4, -10, and -13, are detected in the resolution phase of AKI, but they are not functionally expressed in proximal tubules (Andres-Hernando et al., 2017; Zhang et al., 2017). IL-4 and -13 are produced by Th2 T cells, basophils, mast cells, and granulocytes, whereas IL-10 is produced by regulatory T cells (Liu et al., 2011), B cells as well as Mϕ, induced by prostaglandins, glucocorticoids, apoptotic cells, and G protein-coupled receptor ligands (Zhang et al., 2017). IL-10, which is part of negative feedback response to inflammation and expressed along with pro-inflammatory cytokines, is released into the local tissue and blood circulation and contributes to the suppression of AKI (Deng et al., 2001; Wan et al., 2014; Greenberg et al., 2015; Zhang et al., 2015). Circulating pentraxin-2, also known as serum amyloid P, is found to facilitate the uptake of apoptotic cells and to bind to Fcγ receptors by opsonizing apoptotic cells. This process triggers IL-10 expression and M2 polarization in infiltrating Mϕ (Castano et al., 2009). IL-4 and -13 activate IL-4Rα and its downstream signaling molecule STAT6 and mediate tissue repair and IL-10 immunosuppression (Zhang et al., 2017). IL-4-stimulated Mϕ, not M1-stimulated Mϕ, promote tubular cell proliferation (Lee et al., 2011). Locally synthesized RA, most likely produced by peritubular Mϕ, represses M1 Mϕ and activates RA signaling in the injured tubular epithelium, which, in turn, promotes M2 polarization, thereby reducing Mϕ-dependent injury post-AKI (Chiba et al., 2016). As mentioned above, the proximal tubular mechanisms of M2 Mϕ polarization are only partially understood and deserve more investigation in the future.

M2 Mϕ in the Progression of CKD

AKI is reversible as long as the cause has been eliminated and the tissue has not been structurally damaged (Chawla et al., 2011; Basile et al., 2012). So far, it is largely unknown which mechanisms determine full recovery versus subsequent CKD after AKI. For a full recovery after AKI, two conditions regarding Mϕ need to be fulfilled: (1) re-transforming and/or removal of pro-fibrotic M2 Mϕ; and (2) the decline in Mϕ numbers to the basal level. Importantly, Mϕ numbers during AKI are supposed to be strictly controlled across all stages, and uncontrolled hyper-proliferation or inadequate removal of M2 Mϕ in the resolution phase of AKI may cause a non-resolving inflammation and chronic pathology as we observe in other disease areas (e.g., in muscle inflammation (Iwata et al., 2012; Baek et al., 2015; Baek et al., 2017). So far, virtually nothing is known about the fate of Mϕ after the tubular repair is complete, and this needs to be investigated in the future (Huen and Cantley, 2017). Since M2 Mϕ are considered to be protective in AKI, there is a growing interest to use M2 Mϕ and Mϕ-modulating agents as therapeutic tools to treat patients with AKI. However, it is to note that M2 Mϕ are considered to be instrumental in the development of pathological fibrosis and the progression of CKD (Duffield, 2010; Anders and Ryu, 2011). Especially, several studies have identified monocyte-derived Ly6C^{low} Mϕ, which predominate over Ly6C^{int} Mϕ in the later stages of AKI, as direct or indirect contributors to interstitial fibrosis (Lin et al., 2009; Anders and Ryu, 2011; Clements et al., 2016; Lever et al., 2019; Yang et al., 2019) and as a hallmark of CKD progression post-AKI. In line with this, CX_3CL1-CX_3CR1-mediated survival of Ly6C^{low} Mϕ correlates with interstitial fibrosis in obstructed kidneys (Peng et al., 2015). M2 Mϕ may take an important pro-fibrotic role (1) by promoting the formation of a provisional ECM (containing fibrin, fibrinogen, and fibronectin), which mediates the recruitment of fibrocytes, giving rise to myofibroblasts (= the effector cells in fibrosis, which, in turn, produce large amounts of ECM components); (2) by expressing matrix metalloproteases, some of which serve as essential drivers of fibrosis; and (3) by secreting large amounts of pro-fibrotic factors, which activate and differentiate resident fibroblasts and infiltrating fibrocytes into myofibroblasts [e.g., TGF-β1 and PDGF, vascular endothelial growth factor (VEGF), insulin-like growth factor 1 (IGF1), Galactin-3] (Vernon et al., 2010; Lech and Anders, 2013; Braga et al., 2015; Wynn and Vannella, 2016); and potentially (4) by directly transitioning into myofibroblasts to mediate interstitial fibrosis via a mechanism named "Mϕ-myofibroblast transition (MMT)" (Nikolic-Paterson et al., 2014; Meng et al., 2016; Wang et al., 2016; Wang Y.Y. et al., 2017; Liang et al., 2018; Tang et al., 2018).

ASSESSING Mϕ FUNCTIONS BY DEPLETING Mϕ

As discussed in detail above, Mϕ are highly implicated in AKI and in the progression of CKD, and Mϕ have versatile functions and are like double-edged swords being both tissue-destructive and -suppressive depending on circumstances. To successfully develop Mϕ-based therapeutic approaches for AKI and its outcomes, we need to precisely understand the role of Mϕ and Mϕ subtypes in AKI. To assess Mϕ functions in AKI, a number of studies have addressed how AKI is affected if global Mϕ or individual Mϕ subtypes are removed or reduced throughout different stages of AKI (**Figure 1**).

Acute kidney injury encompass both an injury phase and a resolution phase (Huen and Cantley, 2017). Mϕ change their functional phenotype throughout different stages of AKI: Mϕ are predominantly skewed toward M1 phenotypes at early stages of inflammation and toward M2 phenotypes in the resolution phase of AKI. As the phenotypic change of Mϕ during AKI has been

well characterized and is known to be a time-controlled process, the role of an individual Mϕ subtype can be assessed by depleting the individual Mϕ subtype by deleting the global Mϕ pool at a selected time point (i.e., when the Mϕ subtype predominates). A number of studies respectively pinpointed the role of M1 and M2 Mϕ using various Mϕ depletion strategies during and after the induction of AKI, including: (1) systemic administration of Mϕ-depleting clodronate or (2) neutralizing CSF-1R antibody; and (3) DT injection in mice expressing DTR on Mϕ. We note that in these studies investigators could not limit their depletion strategies to only M1 or M2 Mϕ as the time-specific removal of individual Mϕ subtypes only relates to the change in the relative abundance of the M1/M2 phenotypes at different time points. Of note, there may be a discrepancy between experimental AKI models in disease kinetics and reversibility and also a discrepancy between Mϕ depletion methods. In line with this, a study showed that Mϕ depletion by clodronate at a single dose effectively reduces blood monocytes, but not completely depletes tissue-resident Mϕ and depleted tissue-resident Mϕ are completely replenished within 72 h (Puranik et al., 2018). Other studies suggested that Mϕ depletion by anti-CSF-1R primarily depletes activated resident monocytes, not affecting the numbers of pro-inflammatory monocytes (MacDonald et al., 2010) and the injury (Wynn and Vannella, 2016).

Impact of Global Mϕ Depletion on AKI and Its Outcomes

To determine the role of global Mϕ, regardless of polarization state, in AKI, studies have been performed using depletion methods based on: (1) repeated administration of Mϕ-depleting agents (clodronate, small molecule CSF-1R inhibitors, neutralizing anti-CSF-1R antibodies, etc.); (2) genetic deletion of Mϕ survival factors (CSF-1, IL-34 or CSF-1R deficiency) (Lenda et al., 2003; Ma et al., 2009; Baek et al., 2015). In general, a (partial) global depletion of Mϕ was revealed to mitigate AKI in UUO and IRI experiments resulting in reduced tubular apoptosis (Lenda et al., 2003; Kitamoto et al., 2009; Ma et al., 2009; Baek et al., 2015) and interstitial fibrosis (Ma et al., 2009; Baek et al., 2015; Liu et al., 2018) (**Table 1**). In an experimental model of hypertension, the sustained depletion of global Mϕ was shown to attenuate hypertensive renal injury and fibrosis as well as to lower blood pressure (Huang et al., 2018). Much to our surprise, the reduced number of M2 Mϕ in *Il34*$^{-/-}$ mice did not show a delay in the kidney recovery, but prevented kidney fibrosis, being clearly beneficial to the injured kidney (Baek et al., 2015). Remarkably, a UUO experiment showed that the global depletion of Mϕ reduces tubular apoptosis, but does not affect interstitial fibrosis (Ma et al., 2009), but this may be due to the specificity of UUO, where the renal insult is irreversible and the suppression of the injury driving the fibrotic response is more difficult than in other models (Nikolic-Paterson et al., 2014).

When AKI was induced by cell-specific depletion of proximal tubules in *Ggt1*-DTR mice, global depletion of Mϕ led to opposite results, aggravating AKI. In this specific AKI model, global depletion of Mϕ resulted in reduced survival of mice (Zhang et al., 2012), delayed functional and structural recovery from AKI and increase in interstitial fibrosis (Wang et al., 2015) (**Table 1**). However, it is important to mention that this AKI model does not involve a prominent Mϕ infiltration as seen in other IRI models (Figure 6 in Zhang et al., 2012), indicating that the initial injury is independent of M1 Mϕ and depletion of global Mϕ mainly targets the resident Mϕ-derived M2 pool.

Overall, these studies indicate that (partial) general depletion of Mϕ is rather beneficial than harmful to the injured kidney, especially in AKI settings where Mϕ infiltration and M1 Mϕ are prominent features (e.g., IRI and UUO models). The significance of Mϕ in tissue repair after AKI is unquestioned as Mϕ are known as extremely potent phagocytes supposed to accelerate the tissue recovery by clearing debris. However, studies showed that the kidney epithelium possess its own mechanisms to self-heal, e.g., by producing autocrine factors, which mediate tubular regeneration [CSF-1 (Menke et al., 2009), TGF-β1 (Gewin et al., 2012) etc.], and Mϕ may not be the only phagocytes in the injured tissue. So far, we do not know whether Mϕ are indispensable in tissue repair after AKI.

TABLE 1 | Impact of global Mϕ depletion on AKI and its outcomes.

AKI model	Depletion method	Outcomes
Impact of global Mϕ depletion on AKI and its outcomes: beneficial		
UUO	Clodronate (before and at day 2 and 4 of UUO)	Reduced tubular apoptosis and fibrosis (Kitamoto et al., 2009)
UUO	Small molecule CSF-1R inhibitor (Fms-I; starting before UUO and 2× daily)	Reduced tubular apoptosis; no change in fibrosis (Ma et al., 2009)
UUO	CSF1 deficiency (knockout)	Reduced tubular apoptosis (Lenda et al., 2003)
Unilateral IRI	IL-34 deficiency (knockout)	Improved kidney function; reduced fibrosis (Baek et al., 2015)
Hypertension (high dose angiotensin II injections)	Clodronate (before and every 3 days till the end of the experiments)	Reduced renal injury and fibrosis; lowered blood pressure (Huang et al., 2018)
UUO	Clodronate (every 2 days starting day 1 before UUO)	Reduced fibrosis (Liu et al., 2018)
Impact of global Mϕ depletion on AKI and its outcomes: harmful		
DT-induced depletion of *Ggt1*-expressing proximal tubules	Clodronate or DT-induced depletion of CD11c^{+} cells	Reduced survival (Zhang et al., 2012)
DT-induced depletion of *Ggt1*-expressing proximal tubules or unilateral IRI	Proximal tubule-specific CSF1 deficiency (conditional knockout)	Delayed functional + structural recovery from AKI; increased fibrosis (Wang et al., 2015)

Impact of M1 Mϕ Depletion on AKI and Its Outcomes

To examine the impact of M1 Mϕ on AKI and its outcomes, Mϕ were depleted by injecting clodronate into mice before the induction of AKI by either uni- or bilateral IRI (Day et al., 2005; Jo et al., 2006; Vinuesa et al., 2008; Lee et al., 2011;

Ferenbach et al., 2012; Lu et al., 2012) or glycerol injection (Kim et al., 2014) (**Table 2**). All of these experiments demonstrated that reducing M1 Mϕ prevents immunopathology and improves kidney function in injured kidneys. In one of these studies, the depletion of M1 Mϕ paradoxically showed a reduced tubular regeneration at day 3 of bilateral IRI (Vinuesa et al., 2008); but, this may reflect that tubules were less damaged due to the depletion of M1 Mϕ. Independently, M1 Mϕ removal by immunotoxin (Fet et al., 2012) or neutralizing anti-CSF-1R antibody (Clements et al., 2016) prior to IRI uncovered similar findings including improved kidney function (Fet et al., 2012; Clements et al., 2016) and pathology and reduced oxidative stress (Fet et al., 2012) (**Table 2**). On the other hand, the reduction of M1 Mϕ by clodronate injection (Lu et al., 2008) and by DT injection in *Cd11b*-DTR mice (± clodronate) did not show any effect on cisplatin- and ischemia-induced AKI, respectively (Ferenbach et al., 2012; Lu et al., 2012) (**Table 2**). Interestingly, Mϕ depletion by clodronate injection improved AKI in the same IRI study (Ferenbach et al., 2012), indicating that DT-induced depletion of $CD11b^+$ cells in *Cd11b*-DTR mice may have affected a larger variety of immune cells including immunosuppressive cell types. Overall, the impact of M1 Mϕ depletion on AKI and its outcomes can be considered as protective in AKI.

TABLE 2 | Impact of M1 Mϕ depletion on AKI and its outcomes.

AKI model	Depletion method	Outcomes
Impact of M1 Mϕ depletion on AKI and its outcomes: beneficial		
Bilateral IRI	Clodronate (before IRI)	Reduced tubular necrosis, apoptosis; reduced inflammation (Day et al., 2005; Jo et al., 2006)
Bilateral IRI	Clodronate (before IRI)	Reduced tubular injury; improved kidney function; but also reduced tubular regeneration (at day 3 of IRI) (Vinuesa et al., 2008)
Unilateral IRI plus contralateral nephrectomy	Clodronate (before IRI)	Reduced tubular injury; improved kidney function (Lee et al., 2011)
Unilateral IRI plus contralateral nephrectomy	Immunotoxin H22(scFv)-ETA (at 6 h of IRI)	Improved histology; less oxidative stress; improved kidney function (Fet et al., 2012)
Unilateral IRI	Clodronate (before IRI)	Improved kidney function; reduced tubular apoptosis (Ferenbach et al., 2012; Lu et al., 2012)
Glycerol injection	Clodronate (before injection)	Reduced tubular apoptosis; reduced inflammation (Kim et al., 2014)
Bilateral IRI	Neutralizing anti-CSF1R antibody (before + at 30 min)	Improved kidney function (Clements et al., 2016)
Impact of M1 Mϕ depletion on AKI and its outcomes: none		
Cisplatin injection	Clodronate (before + at day 1)	None (Lu et al., 2008)
Unilateral IRI	Conditional (DT/DTR) ablation of $CD11b^+$ cells ± clodronate (before IRI)	None (Ferenbach et al., 2012; Lu et al., 2012)

Impact of M2 Mϕ Depletion on AKI and Its Outcomes

It may be easy to assume that the expansion of reparative M2 Mϕ in the resolution phase of inflammation would be beneficial to the injured tissue, but, in reality, M2 Mϕ can be both friends and foes in AKI (Braga et al., 2015). Indeed, studies focusing on evaluating the effect of M2 Mϕ depletion in AKI have led to controversial results. On the one hand, depletion of M2 Mϕ (e.g., by clodronate injection or DT-mediated conditional ablation of $CD11b^+$ cells) was found to decrease kidney fibrosis (Lin et al., 2009; Kim et al., 2015; Yang et al., 2019), improve the kidney function and reduce the production of inflammatory and pro-fibrotic cytokines in some IRI and UUO experiments (Ko et al., 2008). In addition, M2 Mϕ depletion starting as early as at day 1 after UUO showed an improvement of the immunopathology limiting tissue injury (Yang et al., 2019) (**Table 3**). Notably, renal fibrosis was found to be reduced in all experiments where M2 Mϕ depletion improves the renal pathology after AKI, indicating that the most undesirable feature of M2 Mϕ in Mϕ-based therapeutic approaches for AKI and CKD is the capability to promote renal fibrosis. Some IRI and septic AKI experiments, on the other hand, led to completely opposite results suggesting that M2 Mϕ depletion is harmful to injured kidneys (**Table 3**). In these experiments, M2 Mϕ depletion worsened AKI (Li et al., 2018) or delayed the recovery from AKI (Jang et al., 2008; Lee et al., 2011); increased tubular damage and apoptosis (Jang et al., 2008; Menke et al., 2009; Clements et al., 2016) and oxidative stress (Jang et al., 2008); and impaired of kidney function (Menke et al., 2009; Lee et al., 2011; Karasawa et al., 2015; Li et al., 2018). In one study, M2 Mϕ depletion by DT-mediated ablation of $CD11b^+$ cells even aggravated kidney fibrosis following IRI, which was contrary to the observations previously mentioned (Menke et al., 2009). In addition, DT-mediated depletion of $CD169^+$ cells, which represent tissue-resident M2 Mϕ, markedly worsened the kidney injury and increased the lethality in mice after IRI, which, but, could be rescued by the adoptive transfer of $Ly6C^-$ monocytes (Karasawa et al., 2015). Notwithstanding of all above, there was also a study showing that M2 Mϕ depletion (by conditional ablation in CD11b- or CD11c-DTR) does not have any impact on the development of fibrosis after unilateral IRI (Kim et al., 2015) (**Table 3**). In summary, the impact of M2 Mϕ depletion on AKI and its outcomes was not consistent throughout the experiments, illustrating that M2 Mϕ can be both beneficial and harmful to the injured kidney. These controversial results from AKI studies focusing on elucidating the role of M2 Mϕ corroborate the dual nature of M2 Mϕ. It is interesting to note that M2 Mϕ can to be rather disturbing than useful in the recovery process after AKI depending on the conditions given.

Mϕ-BASED THERAPEUTIC STRATEGIES

Mϕ are instrumental in maintaining immune homeostasis and mediating inflammation. Therefore, modulation of Mϕ functions is widely considered as a promising approach for various kidney

TABLE 3 | Impact of M2 Mϕ depletion on AKI and its outcomes.

AKI model	Depletion method	Outcomes
Impact of M2 Mϕ depletion on AKI and its outcomes: beneficial		
Unilateral IRI plus contralateral nephrectomy	Clodronate (starting on day 3)	Improved kidney function; reduced production of inflammatory and pro-fibrotic cytokines (Ko et al., 2008)
UUO	Conditional (DT/DTR) ablation of CD11b$^+$ cells (at day 7–9)	Reduced fibrosis (Lin et al., 2009)
Unilateral IRI	Clodronate (starting on day 3)	Reduced fibrosis (Kim et al., 2015)
Unilateral IRI	Clodronate (starting on day 1)	Improved histology; reduced kidney injury; reduced fibrosis (Yang et al., 2019)
Impact of M2 Mϕ depletion on AKI and its outcomes: harmful		
Bilateral IRI	Clodronate (at day 6)	Increased tubular damage; increased oxidative stress; delayed recovery from AKI (?) (Jang et al., 2008)
Unilateral IRI plus CSF-1 injection	Conditional (DT/DTR) ablation of CD11b$^+$ cells (at day 1–3)	Increased fibrosis; decreased kidney function; increased apoptosis (Menke et al., 2009)
Unilateral IRI plus contralateral nephrectomy	Clodronate (at day 2 and 3)	Less improvement in glomerular filtration; impaired tubular regeneration (Lee et al., 2011)
Unilateral IRI ± contralateral nephrectomy	Conditional (DT/DTR) ablation of CD169$^+$ cells (24–36 h before IRI)	Lethality, failed kidney function, increased inflammation (Karasawa et al., 2015)
Bilateral IRI	Neutralizing anti-CSF1R antibody (at day 1–3)	Increased apoptosis (Clements et al., 2016)
CLP	Clodronate	Worsening AKI; decreased kidney function (Li et al., 2018)
Impact of M2 Mϕ depletion on AKI and its outcomes: none		
Unilateral IRI	Conditional (DT/DTR) ablation of CD11b$^+$ or CD11c$^+$ cells (starting on day 3)	No change in fibrosis (Kim et al., 2015)

diseases. Different Mϕ-based strategies have been suggested for the treatment of AKI, including: (1) adoptive transfer of *ex vivo* Mϕ that are M2-activated via (a) treatment with M2 stimuli (Wang et al., 2007; Cao et al., 2010; Ranganathan et al., 2013; Geng et al., 2014) or (b) genetic manipulation (Wilson et al., 2002; Ferenbach et al., 2010; Jung et al., 2012, 2016); (2) adoptive transfer of immunomodulatory cells (such as bone marrow-derived mesenchymal stem cells, umbilical cord-derived stromal cells (Li et al., 2013; Geng et al., 2014; Rota et al., 2018) and type 2 innate lymphoid cells (Huang et al., 2015; Cao et al., 2018); (3) systemic administration of M2-polarizing agents (Cao et al., 2011; Chen et al., 2017; Wang Q. et al., 2017; Wang S. et al., 2017; Barrera-Chimal et al., 2018) [for more detailed information on this topic, please refer to the comprehensive review (Chen et al., 2019)]. Of note, most of these proposed strategies are based on the modulation of Mϕ functions favoring M2 anti-inflammatory state. In such a strategy, the risk of triggering renal fibrosis with M2 Mϕ can be a critical issue (Braga et al., 2015). Thus, studies have also focused on developing genetic modification of *ex vivo* Mϕ to suppress the development of kidney fibrosis. It has been found that the adoptive transfer of Mϕ overexpressing neutrophil gelatinase-associated lipocalin-2 (NGAL) (Guiteras et al., 2017) or lacking legumain (Wang D. et al., 2018) can attenuate renal interstitial fibrosis.

Interestingly, the reduction in the number of global and M2 Mϕ can be beneficial to the injured kidney and a promising approach to treatment of AKI. Actually, Mϕ-depleting clodronate and anti-CSF-1R neutralizing antibodies are used in different clinical areas (Frediani and Bertoldi, 2015; Peyraud et al., 2017; Frediani et al., 2018; Goldvaser and Amir, 2019). A potential target for depleting Mϕ is CSF-1R signaling. *Csf1r*$^{-/-}$ mice and mice deficient in functional CSF-1 (*Csf1*$^{op/op}$ mice) completely lack Mϕ, but also exhibit other severe non-Mϕ-related physiological abnormalities (Wei et al., 2010), illustrating that spatiotemporal expression of CSF-1 is crucial to many important biological processes. It has been found that genetic deletion of IL-34 partially removes Mϕ in injured kidneys and is beneficial in AKI (Baek et al., 2015) as well as in lupus nephritis (Wada et al., 2019). As *Il34*$^{-/-}$ mice show no gross phenotype in steady state (Greter et al., 2012; Wang et al., 2012), targeting of IL-34 appears to be more tolerable than that of CSF-1R or CSF-1. IL-34 may be useful for the partial removal of global Mϕ throughout all stages of AKI or for reducing M2 Mϕ in the later stages of AKI.

CONCLUSION AND OUTLOOK

This review has provided insights into the net effect of versatile Mϕ functions in AKI by Mϕ removal studies (**Figure 1**). Interestingly, several studies suggest that the (partial) depletion of global Mϕ in AKI can be beneficial to the injury kidney. In addition, this review has assessed the current literature on the impact of the depletion of individual Mϕ subtypes on AKI and its outcomes and found that M1 Mϕ depletion has been shown to be generally protective against AKI, whereas M2 Mϕ depletion has led to controversial results.

How can we translate findings from animal AKI models into clinical practice? M1 Mϕ instantly enter the tissue within an hour after AKI and phenotypically switch to M2 Mϕ within a couple of days. In most AKI cases, the onset cannot be predicted (e.g., unless patients are scheduled for a kidney transplant or other relevant surgery) and precedes the diagnose. Thus, therapeutic intervention via targeting of M1 Mϕ can be challenging. As M2 Mϕ can resolve inflammation, there is a growing interest to use M2 Mϕ and Mϕ-modulating agents as therapeutic tools to treat patients with AKI (Chen et al., 2019); however, we may not underestimate that M2 Mϕ can contribute to interstitial fibrosis and facilitate the AKI-to-CKD transition. Overall, M2 Mϕ act as double-edged swords being both beneficial and harmful to the inflamed kidney tissue (Braga et al., 2015), and the dual nature of M2 Mϕ is well recapitulated in the results from M2 Mϕ depletion

studies. As uncontrolled hyper-proliferation or inadequate removal of Mϕ in the resolution phase of inflammation can cause chronic inflammation and eventual organ failure, we need to simultaneously consider two avenues, when developing therapeutic approaches targeting Mϕ, including: (1) modulation of Mϕ activation and functions and (2) removal of excess Mϕ. Previous studies investigating the role of Mϕ in AKI mostly focused on the mechanism of Mϕ survival, proliferation and polarization, we do not understand by which mechanisms Mϕ disappear in the resolution phase of inflammation. Future studies need to investigate the fate of individual Mϕ subtypes after the tissue repair is completed.

AUTHOR CONTRIBUTIONS

J-HB conceptualized and wrote the manuscript.

FUNDING

The author declares that this study received funding from the Biogen. Biogen is paying for the publication fee of this review manuscript. Biogen has no role in the study design, data collection and analysis, decision to publish, or preparation of this manuscript.

REFERENCES

Alikhan, M. A., Jones, C. V., Williams, T. M., Beckhouse, A. G., Fletcher, A. L., Kett, M. M., et al. (2011). Colony-stimulating factor-1 promotes kidney growth and repair via alteration of macrophage responses. *Am. J. Pathol.* 179, 1243–1256. doi: 10.1016/j.ajpath.2011.05.037

Anders, H. J. (2010). Toll-like receptors and danger signaling in kidney injury. *J. Am. Soc. Nephrol.* 21, 1270–1274. doi: 10.1681/ASN.2010030233

Anders, H. J., and Ryu, M. (2011). Renal microenvironments and macrophage phenotypes determine progression or resolution of renal inflammation and fibrosis. *Kidney Int.* 80, 915–925. doi: 10.1038/ki.2011.217

Anders, H. J., and Schaefer, L. (2014). Beyond tissue injury-damage-associated molecular patterns, toll-like receptors, and inflammasomes also drive regeneration and fibrosis. *J. Am. Soc. Nephrol.* 25, 1387–1400. doi: 10.1681/ASN.2014010117

Andres-Hernando, A., Okamura, K., Bhargava, R., Kiekhaefer, C. M., Soranno, D., Kirkbride-Romeo, L. A., et al. (2017). Circulating IL-6 upregulates IL-10 production in splenic CD4(+) T cells and limits acute kidney injury-induced lung inflammation. *Kidney Int.* 91, 1057–1069. doi: 10.1016/j.kint.2016.12.014

Arai, S., Kitada, K., Yamazaki, T., Takai, R., Zhang, X., Tsugawa, Y., et al. (2016). Apoptosis inhibitor of macrophage protein enhances intraluminal debris clearance and ameliorates acute kidney injury in mice. *Nat. Med.* 22, 183–193. doi: 10.1038/nm.4012

Baek, J. H., Gomez, I. G., Wada, Y., Roach, A., Mahad, D., and Duffield, J. S. (2018). Deletion of the mitochondrial complex-IV cofactor heme a:farnesyltransferase causes focal segmental glomerulosclerosis and interferon response. *Am. J. Pathol.* 188, 2745–2762. doi: 10.1016/j.ajpath.2018.08.018

Baek, J. H., Many, G. M., Evesson, F. J., and Kelley, V. R. (2017). Dysferlinopathy promotes an intramuscle expansion of macrophages with a cyto-destructive phenotype. *Am. J. Pathol.* 187, 1245–1257. doi: 10.1016/j.ajpath.2017.02.011

Baek, J. H., Zeng, R., Weinmann-Menke, J., Valerius, M. T., Wada, Y., Ajay, A. K., et al. (2015). IL-34 mediates acute kidney injury and worsens subsequent chronic kidney disease. *J. Clin. Invest.* 125, 3198–3214. doi: 10.1172/JCI81166

Bao, Y. W., Yuan, Y., Chen, J. H., and Lin, W. Q. (2018). Kidney disease models: tools to identify mechanisms and potential therapeutic targets. *Zool. Res.* 39, 72–86. doi: 10.24272/j.issn.2095-8137.2017.055

Barrera-Chimal, J., Estrela, G. R., Lechner, S. M., Giraud, S., El Moghrabi, S., Kaaki, S., et al. (2018). The myeloid mineralocorticoid receptor controls inflammatory and fibrotic responses after renal injury via macrophage interleukin-4 receptor signaling. *Kidney Int.* 93, 1344–1355. doi: 10.1016/j.kint.2017.12.016

Basile, D. P., Anderson, M. D., and Sutton, T. A. (2012). Pathophysiology of acute kidney injury. *Compr. Physiol.* 2, 1303–1353. doi: 10.1002/cphy.c110041

Braga, T. T., Agudelo, J. S., and Camara, N. O. (2015). Macrophages during the fibrotic process: M2 as friend and foe. *Front. Immunol.* 6:602. doi: 10.3389/fimmu.2015.00602

Bucaloiu, I. D., Kirchner, H. L., Norfolk, E. R., Hartle, J. E. II, and Perkins, R. M. (2012). Increased risk of death and de novo chronic kidney disease following reversible acute kidney injury. *Kidney Int.* 81, 477–485. doi: 10.1038/ki.2011.405

Bussolati, B., Bruno, S., Grange, C., Buttiglieri, S., Deregibus, M. C., Cantino, D., et al. (2005). Isolation of renal progenitor cells from adult human kidney. *Am. J. Pathol.* 166, 545–555. doi: 10.1016/S0002-9440(10)62276-62276

Cao, Q., Wang, C., Zheng, D., Wang, Y., Lee, V. W., Wang, Y. M., et al. (2011). IL-25 induces M2 macrophages and reduces renal injury in proteinuric kidney disease. *J. Am. Soc. Nephrol.* 22, 1229–1239. doi: 10.1681/ASN.2010070693

Cao, Q., Wang, Y., Niu, Z., Wang, C., Wang, R., Zhang, Z., et al. (2018). Potentiating tissue-resident Type 2 innate lymphoid cells by IL-33 to prevent renal ischemia-reperfusion injury. *J. Am. Soc. Nephrol.* 29, 961–976. doi: 10.1681/ASN.2017070774

Cao, Q., Wang, Y., Zheng, D., Sun, Y., Wang, Y., Lee, V. W., et al. (2010). IL-10/TGF-beta-modified macrophages induce regulatory T cells and protect against adriamycin nephrosis. *J. Am. Soc. Nephrol.* 21, 933–942. doi: 10.1681/ASN.2009060592

Castano, A. P., Lin, S. L., Surowy, T., Nowlin, B. T., Turlapati, S. A., Patel, T., et al. (2009). Serum amyloid P inhibits fibrosis through Fc gamma R-dependent monocyte-macrophage regulation in vivo. *Sci. Transl. Med.* 1:5ra13. doi: 10.1126/scitranslmed.3000111

Chawla, L. S., Amdur, R. L., Amodeo, S., Kimmel, P. L., and Palant, C. E. (2011). The severity of acute kidney injury predicts progression to chronic kidney disease. *Kidney Int.* 79, 1361–1369. doi: 10.1038/ki.2011.42

Chawla, L. S., Eggers, P. W., Star, R. A., and Kimmel, P. L. (2014). Acute kidney injury and chronic kidney disease as interconnected syndromes. *N. Engl. J. Med.* 371, 58–66. doi: 10.1056/NEJMra1214243

Chen, L., Sha, M. L., Li, D., Zhu, Y. P., Wang, X. J., Jiang, C. Y., et al. (2017). Relaxin abrogates renal interstitial fibrosis by regulating macrophage polarization via inhibition of Toll-like receptor 4 signaling. *Oncotarget* 8, 21044–21053. doi: 10.18632/oncotarget.15483

Chen, T., Cao, Q., Wang, Y., and Harris, D. C. H. (2019). M2 macrophages in kidney disease: biology, therapies, and perspectives. *Kidney Int.* 95, 760–773. doi: 10.1016/j.kint.2018.10.041

Chevalier, R. L. (2016). The proximal tubule is the primary target of injury and progression of kidney disease: role of the glomerulotubular junction. *Am. J. Physiol. Renal. Physiol.* 311, F145–F161. doi: 10.1152/ajprenal.00164.2016

Chiba, T., Skrypnyk, N. I., Skvarca, L. B., Penchev, R., Zhang, K. X., Rochon, E. R., et al. (2016). Retinoic acid signaling coordinates macrophage-dependent injury and repair after AKI. *J. Am. Soc. Nephrol.* 27, 495–508. doi: 10.1681/ASN.2014111108

Chou, Y. H., Huang, T. M., and Chu, T. S. (2017). Novel insights into acute kidney injury-chronic kidney disease continuum and the role of renin-angiotensin system. *J. Formos Med. Assoc.* 116, 652–659. doi: 10.1016/j.jfma.2017.04.026

Chung, S., Overstreet, J. M., Li, Y., Wang, Y., Niu, A., Wang, S., et al. (2018). TGF-beta promotes fibrosis after severe acute kidney injury by enhancing renal macrophage infiltration. *JCI Insight* 3:e123563. doi: 10.1172/jci.insight.123563

Clements, M., Gershenovich, M., Chaber, C., Campos-Rivera, J., Du, P., Zhang, M., et al. (2016). Differential Ly6C expression after renal ischemia-reperfusion identifies unique macrophage populations. *J. Am. Soc. Nephrol.* 27, 159–170. doi: 10.1681/ASN.2014111138

Day, Y. J., Huang, L., Ye, H., Linden, J., and Okusa, M. D. (2005). Renal ischemia-reperfusion injury and adenosine 2A receptor-mediated tissue protection: role of macrophages. *Am. J. Physiol. Renal. Physiol.* 288, F722–F731. doi: 10.1152/ajprenal.00378.2004

Deng, J., Kohda, Y., Chiao, H., Wang, Y., Hu, X., Hewitt, S. M., et al. (2001). Interleukin-10 inhibits ischemic and cisplatin-induced acute renal injury. *Kidney Int.* 60, 2118–2128. doi: 10.1046/j.1523-1755.2001.00043.x

Duffield, J. S. (2010). Macrophages and immunologic inflammation of the kidney. *Semin. Nephrol.* 30, 234–254. doi: 10.1016/j.semnephrol.2010.03.003

Egawa, M., Mukai, K., Yoshikawa, S., Iki, M., Mukaida, N., Kawano, Y., et al. (2013). Inflammatory monocytes recruited to allergic skin acquire an anti-inflammatory M2 phenotype via basophil-derived interleukin-4. *Immunity* 38, 570–580. doi: 10.1016/j.immuni.2012.11.014

Feng, Y., Liang, Y., Zhu, X., Wang, M., Gui, Y., Lu, Q., et al. (2018a). The signaling protein Wnt5a promotes TGFbeta1-mediated macrophage polarization and kidney fibrosis by inducing the transcriptional regulators Yap/Taz. *J. Biol. Chem.* 293, 19290–19302. doi: 10.1074/jbc.RA118.005457

Feng, Y., Ren, J., Gui, Y., Wei, W., Shu, B., Lu, Q., et al. (2018b). Wnt/beta-Catenin-Promoted macrophage alternative activation contributes to kidney fibrosis. *J. Am. Soc. Nephrol.* 29, 182–193. doi: 10.1681/ASN.2017040391

Ferenbach, D. A., Ramdas, V., Spencer, N., Marson, L., Anegon, I., Hughes, J., et al. (2010). Macrophages expressing heme oxygenase-1 improve renal function in ischemia/reperfusion injury. *Mol. Ther.* 18, 1706–1713. doi: 10.1038/mt.2010.100

Ferenbach, D. A., Sheldrake, T. A., Dhaliwal, K., Kipari, T. M., Marson, L. P., Kluth, D. C., et al. (2012). Macrophage/monocyte depletion by clodronate, but not diphtheria toxin, improves renal ischemia/reperfusion injury in mice. *Kidney Int.* 82, 928–933. doi: 10.1038/ki.2012.207

Fet, N. G., Fiebeler, A., Klinge, U., Park, J. K., Barth, S., Thepen, T., et al. (2012). Reduction of activated macrophages after ischaemia-reperfusion injury diminishes oxidative stress and ameliorates renal damage. *Nephrol. Dial. Transplant.* 27, 3149–3155. doi: 10.1093/ndt/gfr792

Filardy, A. A., Pires, D. R., Nunes, M. P., Takiya, C. M., Freire-de-Lima, C. G., Ribeiro-Gomes, F. L., et al. (2010). Proinflammatory clearance of apoptotic neutrophils induces an IL-12(low)IL-10(high) regulatory phenotype in macrophages. *J. Immunol.* 185, 2044–2050. doi: 10.4049/jimmunol.1000017

Fiorentino, M., Grandaliano, G., Gesualdo, L., and Castellano, G. (2018). Acute kidney injury to chronic kidney disease transition. *Contrib. Nephrol.* 193, 45–54. doi: 10.1159/000484962

Frediani, B., and Bertoldi, I. (2015). Clodronate: new directions of use. *Clin. Cases Miner. Bone Metab.* 12, 97–108. doi: 10.11138/ccmbm/2015.12.2.097

Frediani, B., Giusti, A., Bianchi, G., Dalle Carbonare, L., Malavolta, N., Cantarini, L., et al. (2018). Clodronate in the management of different musculoskeletal conditions. *Minerva Med.* 109, 300–325. doi: 10.23736/S0026-4806.18.05688-5684

Fujiu, K., Manabe, I., and Nagai, R. (2011). Renal collecting duct epithelial cells regulate inflammation in tubulointerstitial damage in mice. *J. Clin. Invest.* 121, 3425–3441. doi: 10.1172/JCI57582

Furuichi, K., Wada, T., Iwata, Y., Kitagawa, K., Kobayashi, K., Hashimoto, H., et al. (2003). CCR2 signaling contributes to ischemia-reperfusion injury in kidney. *J. Am. Soc. Nephrol.* 14, 2503–2515. doi: 10.1097/01.asn.0000089563.63641.a8

Geeraerts, X., Bolli, E., Fendt, S. M., and Van Ginderachter, J. A. (2017). Macrophage metabolism as therapeutic target for cancer, atherosclerosis, and obesity. *Front. Immunol.* 8:289. doi: 10.3389/fimmu.2017.00289

Geissmann, F., Manz, M. G., Jung, S., Sieweke, M. H., Merad, M., and Ley, K. (2010). Development of monocytes, macrophages, and dendritic cells. *Science* 327, 656–661. doi: 10.1126/science.1178331

Geng, Y., Zhang, L., Fu, B., Zhang, J., Hong, Q., Hu, J., et al. (2014). Mesenchymal stem cells ameliorate rhabdomyolysis-induced acute kidney injury via the activation of M2 macrophages. *Stem Cell Res. Ther.* 5:80. doi: 10.1186/scrt469

Gewin, L., Vadivelu, S., Neelisetty, S., Srichai, M. B., Paueksakon, P., Pozzi, A., et al. (2012). Deleting the TGF-beta receptor attenuates acute proximal tubule injury. *J. Am. Soc. Nephrol.* 23, 2001–2011. doi: 10.1681/ASN.2012020139

Goldvaser, H., and Amir, E. (2019). Role of bisphosphonates in breast cancer therapy. *Curr. Treat. Options Oncol.* 20:26. doi: 10.1007/s11864-019-0623-628

Greenberg, J. H., Whitlock, R., Zhang, W. R., Thiessen-Philbrook, H. R., Zappitelli, M., Devarajan, P., et al. (2015). Interleukin-6 and interleukin-10 as acute kidney injury biomarkers in pediatric cardiac surgery. *Pediatr. Nephrol.* 30, 1519–1527. doi: 10.1007/s00467-015-3088-3084

Grenz, A., Dalton, J. H., Bauerle, J. D., Badulak, A., Ridyard, D., Gandjeva, A., et al. (2011). Partial netrin-1 deficiency aggravates acute kidney injury. *PLoS One* 6:e14812. doi: 10.1371/journal.pone.0014812

Greter, M., Lelios, I., Pelczar, P., Hoeffel, G., Price, J., Leboeuf, M., et al. (2012). Stroma-derived interleukin-34 controls the development and maintenance of langerhans cells and the maintenance of microglia. *Immunity* 37, 1050–1060. doi: 10.1016/j.immuni.2012.11.001

Groves, A. M., Johnston, C. J., Williams, J. P., and Finkelstein, J. N. (2018). Role of infiltrating monocytes in the development of radiation-induced pulmonary fibrosis. *Radiat. Res.* 189, 300–311. doi: 10.1667/RR14874.1

Guiteras, R., Sola, A., Flaquer, M., Hotter, G., Torras, J., Grinyo, J. M., et al. (2017). Macrophage overexpressing NGAL ameliorated kidney fibrosis in the UUO mice model. *Cell Physiol. Biochem.* 42, 1945–1960. doi: 10.1159/000479835

Hamilton, J. A., Vairo, G., Nicola, N. A., Burgess, A., Metcalf, D., and Lingelbach, S. R. (1988). Activation and proliferation signals in murine macrophages: synergistic interactions between the hematopoietic growth factors and with phorbol ester for DNA synthesis. *Blood* 71, 1574–1580.

Huang, L., Wang, A., Hao, Y., Li, W., Liu, C., Yang, Z., et al. (2018). Macrophage depletion lowered blood pressure and attenuated hypertensive renal injury and fibrosis. *Front. Physiol.* 9:473. doi: 10.3389/fphys.2018.00473

Huang, Q., Niu, Z., Tan, J., Yang, J., Liu, Y., Ma, H., et al. (2015). IL-25 Elicits innate lymphoid cells and multipotent progenitor Type 2 cells that reduce renal ischemic/reperfusion injury. *J. Am. Soc. Nephrol.* 26, 2199–2211. doi: 10.1681/ASN.2014050479

Huen, S. C., and Cantley, L. G. (2017). Macrophages in renal injury and repair. *Annu. Rev. Physiol.* 79, 449–469. doi: 10.1146/annurev-physiol-022516-034219

Huen, S. C., Huynh, L., Marlier, A., Lee, Y., Moeckel, G. W., and Cantley, L. G. (2015). GM-CSF Promotes macrophage alternative activation after renal ischemia/reperfusion injury. *J. Am. Soc. Nephrol.* 26, 1334–1345. doi: 10.1681/ASN.2014060612

Hume, D. A., and MacDonald, K. P. (2012). Therapeutic applications of macrophage colony-stimulating factor-1 (CSF-1) and antagonists of CSF-1 receptor (CSF-1R) signaling. *Blood* 119, 1810–1820. doi: 10.1182/blood-2011-09-379214

Isbel, N. M., Hill, P. A., Foti, R., Mu, W., Hurst, L. A., Stambe, C., et al. (2001). Tubules are the major site of M-CSF production in experimental kidney disease: correlation with local macrophage proliferation. *Kidney Int.* 60, 614–625. doi: 10.1046/j.1523-1755.2001.060002614.x

Iwata, Y., Bostrom, E. A., Menke, J., Rabacal, W. A., Morel, L., Wada, T., et al. (2012). Aberrant macrophages mediate defective kidney repair that triggers nephritis in lupus-susceptible mice. *J. Immunol.* 188, 4568–4580. doi: 10.4049/jimmunol.1102154

Jang, H. S., Kim, J., Park, Y. K., and Park, K. M. (2008). Infiltrated macrophages contribute to recovery after ischemic injury but not to ischemic preconditioning in kidneys. *Transplantation* 85, 447–455. doi: 10.1097/TP.0b013e318160f0d1

Jo, S. K., Sung, S. A., Cho, W. Y., Go, K. J., and Kim, H. K. (2006). Macrophages contribute to the initiation of ischaemic acute renal failure in rats. *Nephrol. Dial. Transplant.* 21, 1231–1239. doi: 10.1093/ndt/gfk047

Johnson, A. C., and Zager, R. A. (2018). Plasma and urinary p21: potential biomarkers of AKI and renal aging. *Am. J. Physiol. Renal. Physiol.* 315, F1329–F1335. doi: 10.1152/ajprenal.00328.2018

Jones, J., Holmen, J., De Graauw, J., Jovanovich, A., Thornton, S., and Chonchol, M. (2012). Association of complete recovery from acute kidney injury with incident CKD stage 3 and all-cause mortality. *Am. J. Kidney Dis.* 60, 402–408. doi: 10.1053/j.ajkd.2012.03.014

Jung, M., Brune, B., Hotter, G., and Sola, A. (2016). Macrophage-derived Lipocalin-2 contributes to ischemic resistance mechanisms by protecting from renal injury. *Sci. Rep.* 6:21950. doi: 10.1038/srep21950

Jung, M., Sola, A., Hughes, J., Kluth, D. C., Vinuesa, E., Vinas, J. L., et al. (2012). Infusion of IL-10-expressing cells protects against renal ischemia through induction of lipocalin-2. *Kidney Int.* 81, 969–982. doi: 10.1038/ki.2011.446

Karasawa, K., Asano, K., Moriyama, S., Ushiki, M., Monya, M., Iida, M., et al. (2015). Vascular-resident CD169-positive monocytes and macrophages control neutrophil accumulation in the kidney with ischemia-reperfusion injury. *J. Am. Soc. Nephrol.* 26, 896–906. doi: 10.1681/ASN.2014020195

Kim, H. J., Lee, D. W., Ravichandran, K., OKeys, D., Akcay, A., Nguyen, Q., et al. (2013). NLRP3 inflammasome knockout mice are protected against ischemic but not cisplatin-induced acute kidney injury. *J. Pharmacol. Exp. Ther.* 346, 465–472. doi: 10.1124/jpet.113.205732

Kim, J. H., Lee, D. W., Jung, M. H., Cho, H. S., Jeon, D. H., Chang, S. H., et al. (2014). Macrophage depletion ameliorates glycerol-induced acute kidney injury in mice. *Nephron Exp. Nephrol.* 128, 21–29. doi: 10.1159/000365851

Kim, M. G., Kim, S. C., Ko, Y. S., Lee, H. Y., Jo, S. K., and Cho, W. (2015). The role of M2 macrophages in the progression of chronic kidney disease following acute kidney injury. *PLoS One* 10:e0143961. doi: 10.1371/journal.pone.0143961

Kitamoto, K., Machida, Y., Uchida, J., Izumi, Y., Shiota, M., Nakao, T., et al. (2009). Effects of liposome clodronate on renal leukocyte populations and renal fibrosis in murine obstructive nephropathy. *J. Pharmacol. Sci.* 111, 285–292. doi: 10.1254/jphs.09227fp

Ko, G. J., Boo, C. S., Jo, S. K., Cho, W. Y., and Kim, H. K. (2008). Macrophages contribute to the development of renal fibrosis following ischaemia/reperfusion-induced acute kidney injury. *Nephrol. Dial. Transplant.* 23, 842–852. doi: 10.1093/ndt/gfm694

Kulkarni, O. P., Hartter, I., Mulay, S. R., Hagemann, J., Darisipudi, M. N., Kumar Vr, S., et al. (2014). Toll-like receptor 4-induced IL-22 accelerates kidney regeneration. *J. Am. Soc. Nephrol.* 25, 978–989. doi: 10.1681/ASN.2013050528

Lacey, D. C., Achuthan, A., Fleetwood, A. J., Dinh, H., Roiniotis, J., Scholz, G. M., et al. (2012). Defining GM-CSF- and macrophage-CSF-dependent macrophage responses by in vitro models. *J. Immunol.* 188, 5752–5765. doi: 10.4049/jimmunol.1103426

Leaf, I. A., Nakagawa, S., Johnson, B. G., Cha, J. J., Mittelsteadt, K., Guckian, K. M., et al. (2017). Pericyte MyD88 and IRAK4 control inflammatory and fibrotic responses to tissue injury. *J. Clin. Invest.* 127, 321–334. doi: 10.1172/JCI87532

Lech, M., and Anders, H. J. (2013). Macrophages and fibrosis: how resident and infiltrating mononuclear phagocytes orchestrate all phases of tissue injury and repair. *Biochim. Biophys. Acta* 1832, 989–997. doi: 10.1016/j.bbadis.2012.12.001

Lee, S., Huen, S., Nishio, H., Nishio, S., Lee, H. K., Choi, B. S., et al. (2011). Distinct macrophage phenotypes contribute to kidney injury and repair. *J. Am. Soc. Nephrol.* 22, 317–326. doi: 10.1681/ASN.2009060615

Lenda, D. M., Kikawada, E., Stanley, E. R., and Kelley, V. R. (2003). Reduced macrophage recruitment, proliferation, and activation in colony-stimulating factor-1-deficient mice results in decreased tubular apoptosis during renal inflammation. *J. Immunol.* 170, 3254–3262. doi: 10.4049/jimmunol.170.6.3254

Lever, J. M., Hull, T. D., Boddu, R., Pepin, M. E., Black, L. M., Adedoyin, O. O., et al. (2019). Resident macrophages reprogram toward a developmental state after acute kidney injury. *JCI Insight* doi: 10.1172/jci.insight.125503 [Epub ahead of print].

Li, L., Huang, L., Sung, S. S., Vergis, A. L., Rosin, D. L., Rose, C. E., et al. (2008). The chemokine receptors CCR2 and CX3CR1 mediate monocyte/macrophage trafficking in kidney ischemia-reperfusion injury. *Kidney Int.* 74, 1526–1537. doi: 10.1038/ki.2008.500

Li, L., and Okusa, M. D. (2010). Macrophages, dendritic cells, and kidney ischemia-reperfusion injury. *Semin. Nephrol.* 30, 268–277. doi: 10.1016/j.semnephrol.2010.03.005

Li, W., Zhang, Q., Wang, M., Wu, H., Mao, F., Zhang, B., et al. (2013). Macrophages are involved in the protective role of human umbilical cord-derived stromal cells in renal ischemia-reperfusion injury. *Stem Cell Res.* 10, 405–416. doi: 10.1016/j.scr.2013.01.005

Li, X., Mu, G., Song, C., Zhou, L., He, L., Jin, Q., et al. (2018). Role of M2 macrophages in sepsis-induced acute kidney injury. *Shock* 50, 233–239. doi: 10.1097/SHK.0000000000001006

Liang, H., Xu, F., Zhang, T., Huang, J., Guan, Q., Wang, H., et al. (2018). Inhibition of IL-18 reduces renal fibrosis after ischemia-reperfusion. *Biomed. Pharmacother.* 106, 879–889. doi: 10.1016/j.biopha.2018.07.031

Lin, S. L., Castano, A. P., Nowlin, B. T., Lupher, M. L. Jr., and Duffield, J. S. (2009). Bone marrow Ly6Chigh monocytes are selectively recruited to injured kidney and differentiate into functionally distinct populations. *J. Immunol.* 183, 6733–6743. doi: 10.4049/jimmunol.0901473

Lin, S. L., Li, B., Rao, S., Yeo, E. J., Hudson, T. E., Nowlin, B. T., et al. (2010). Macrophage Wnt7b is critical for kidney repair and regeneration. *Proc. Natl. Acad. Sci. U.S.A.* 107, 4194–4199. doi: 10.1073/pnas.0912228107

Liu, G., Ma, H., Qiu, L., Li, L., Cao, Y., Ma, J., et al. (2011). Phenotypic and functional switch of macrophages induced by regulatory CD4+CD25+ T cells in mice. *Immunol. Cell Biol.* 89, 130–142. doi: 10.1038/icb.2010.70

Liu, Y., Wang, K., Liang, X., Li, Y., Zhang, Y., Zhang, C., et al. (2018). Complement C3 produced by macrophages promotes renal fibrosis via IL-17A secretion. *Front. Immunol.* 9:2385. doi: 10.3389/fimmu.2018.02385

Lu, L., Faubel, S., He, Z., Andres Hernando, A., Jani, A., Kedl, R., et al. (2012). Depletion of macrophages and dendritic cells in ischemic acute kidney injury. *Am. J. Nephrol.* 35, 181–190. doi: 10.1159/000335582

Lu, L. H., Oh, D. J., Dursun, B., He, Z., Hoke, T. S., Faubel, S., et al. (2008). Increased macrophage infiltration and fractalkine expression in cisplatin-induced acute renal failure in mice. *J. Pharmacol. Exp. Ther.* 324, 111–117. doi: 10.1124/jpet.107.130161

Lutz, M. B., Suri, R. M., Niimi, M., Ogilvie, A. L., Kukutsch, N. A., Rossner, S., et al. (2000). Immature dendritic cells generated with low doses of GM-CSF in the absence of IL-4 are maturation resistant and prolong allograft survival in vivo. *Eur. J. Immunol.* 30, 1813–1822. doi: 10.1002/1521-4141(200007)30:7<1813::aid-immu1813>3.0.co;2-8

Ma, F. Y., Liu, J., Kitching, A. R., Manthey, C. L., and Nikolic-Paterson, D. J. (2009). Targeting renal macrophage accumulation via c-fms kinase reduces tubular apoptosis but fails to modify progressive fibrosis in the obstructed rat kidney. *Am. J. Physiol. Renal Physiol.* 296, F177–F185. doi: 10.1152/ajprenal.90498.2008

MacDonald, K. P., Palmer, J. S., Cronau, S., Seppanen, E., Olver, S., Raffelt, N. C., et al. (2010). An antibody against the colony-stimulating factor 1 receptor depletes the resident subset of monocytes and tissue- and tumor-associated macrophages but does not inhibit inflammation. *Blood* 116, 3955–3963. doi: 10.1182/blood-2010-02-266296

Martinez, F. O., Helming, L., and Gordon, S. (2009). Alternative activation of macrophages: an immunologic functional perspective. *Annu. Rev. Immunol.* 27, 451–483. doi: 10.1146/annurev.immunol.021908.132532

Mass, E., Ballesteros, I., Farlik, M., Halbritter, F., Gunther, P., Crozet, L., et al. (2016). Specification of tissue-resident macrophages during organogenesis. *Science* 353:aaf4238. doi: 10.1126/science.aaf4238

McDonald, B., Pittman, K., Menezes, G. B., Hirota, S. A., Slaba, I., Waterhouse, C. C., et al. (2010). Intravascular danger signals guide neutrophils to sites of sterile inflammation. *Science* 330, 362–366. doi: 10.1126/science.1195491

Meng, X. M., Wang, S., Huang, X. R., Yang, C., Xiao, J., Zhang, Y., et al. (2016). Inflammatory macrophages can transdifferentiate into myofibroblasts during renal fibrosis. *Cell Death Dis.* 7:e2495. doi: 10.1038/cddis.2016.402

Menke, J., Iwata, Y., Rabacal, W. A., Basu, R., Yeung, Y. G., Humphreys, B. D., et al. (2009). CSF-1 signals directly to renal tubular epithelial cells to mediate repair in mice. *J. Clin. Invest* 119, 2330–2342. doi: 10.1172/JCI39087

Meshkibaf, S., Gower, M. W., Dekaban, G. A., and Kim, S. O. (2014). G-CSF preferentially supports the generation of gut-homing Gr-1high macrophages in M-CSF-treated bone marrow cells. *J. Leukoc. Biol.* 96, 549–561. doi: 10.1189/jlb.1A0314-172R

Mills, C. D., Kincaid, K., Alt, J. M., Heilman, M. J., and Hill, A. M. (2000). M-1/M-2 macrophages and the Th1/Th2 paradigm. *J. Immunol.* 164, 6166–6173. doi: 10.4049/jimmunol.164.12.6166

Murray, P. J., Allen, J. E., Biswas, S. K., Fisher, E. A., Gilroy, D. W., Goerdt, S., et al. (2014). Macrophage activation and polarization: nomenclature and experimental guidelines. *Immunity* 41, 14–20. doi: 10.1016/j.immuni.2014.06.008

Murray, P. J., and Wynn, T. A. (2011). Protective and pathogenic functions of macrophage subsets. *Nat. Rev. Immunol.* 11, 723–737. doi: 10.1038/nri3073

Nandi, S., Cioce, M., Yeung, Y. G., Nieves, E., Tesfa, L., Lin, H., et al. (2013). Receptor-type protein-tyrosine phosphatase zeta is a functional receptor for interleukin-34. *J. Biol. Chem.* 288, 21972–21986. doi: 10.1074/jbc.M112.442731

Nath, K. A., Croatt, A. J., Warner, G. M., and Grande, J. P. (2011). Genetic deficiency of Smad3 protects against murine ischemic acute kidney injury. *Am. J. Physiol. Renal Physiol.* 301, F436–F442. doi: 10.1152/ajprenal.00162.2011

Nikolic-Paterson, D. J., and Atkins, R. C. (2001). The role of macrophages in glomerulonephritis. *Nephrol. Dial. Transplant.* 16(Suppl. 5), 3–7. doi: 10.1093/ndt/16.suppl_5.3

Nikolic-Paterson, D. J., Wang, S., and Lan, H. Y. (2014). Macrophages promote renal fibrosis through direct and indirect mechanisms. *Kidney Int. Suppl.* 4, 34–38. doi: 10.1038/kisup.2014.7

Oh, D. J., Dursun, B., He, Z., Lu, L., Hoke, T. S., Ljubanovic, D., et al. (2008). Fractalkine receptor (CX3CR1) inhibition is protective against ischemic acute renal failure in mice. *Am. J. Physiol. Renal Physiol.* 294, F264–F271. doi: 10.1152/ajprenal.00204.2007

Ortiz, A., Sanchez-Nino, M. D., Izquierdo, M. C., Martin-Cleary, C., Garcia-Bermejo, L., Moreno, J. A., et al. (2015). Translational value of animal models

of kidney failure. *Eur. J. Pharmacol.* 759, 205–220. doi: 10.1016/j.ejphar.2015.03.026

Peng, X., Zhang, J., Xiao, Z., Dong, Y., and Du, J. (2015). CX3CL1-CX3CR1 interaction increases the population of Ly6C(-)CX3CR1(hi) macrophages contributing to unilateral ureteral obstruction-induced fibrosis. *J. Immunol.* 195, 2797–2805. doi: 10.4049/jimmunol.1403209

Perry, H. M., and Okusa, M. D. (2015). Driving change: kidney proximal tubule CSF-1 polarizes macrophages. *Kidney Int.* 88, 1219–1221. doi: 10.1038/ki.2015.324

Peyraud, F., Cousin, S., and Italiano, A. (2017). CSF-1R inhibitor development: current clinical status. *Curr. Oncol. Rep.* 19:70. doi: 10.1007/s11912-017-0634-631

Puranik, A. S., Leaf, I. A., Jensen, M. A., Hedayat, A. F., Saad, A., Kim, K. W., et al. (2018). Kidney-resident macrophages promote a proangiogenic environment in the normal and chronically ischemic mouse kidney. *Sci. Rep.* 8:13948. doi: 10.1038/s41598-018-31887-31884

Rabb, H., Griffin, M. D., McKay, D. B., Swaminathan, S., Pickkers, P., Rosner, M. H., et al. (2016). Inflammation in AKI: current understanding, key questions, and knowledge gaps. *J. Am. Soc. Nephrol.* 27, 371–379. doi: 10.1681/ASN.2015030261

Raggi, F., Pelassa, S., Pierobon, D., Penco, F., Gattorno, M., Novelli, F., et al. (2017). Regulation of human macrophage M1-M2 polarization balance by hypoxia and the triggering receptor expressed on myeloid cells-1. *Front. Immunol.* 8:1097. doi: 10.3389/fimmu.2017.01097

Ramesh, G., and Ranganathan, P. (2014). Mouse models and methods for studying human disease, acute kidney injury (AKI). *Methods Mol. Biol.* 1194, 421–436. doi: 10.1007/978-1-4939-1215-5_24

Ranganathan, P. V., Jayakumar, C., and Ramesh, G. (2013). Netrin-1-treated macrophages protect the kidney against ischemia-reperfusion injury and suppress inflammation by inducing M2 polarization. *Am. J. Physiol. Renal Physiol.* 304, F948–F957. doi: 10.1152/ajprenal.00580.2012

Reeves, W. B., Kwon, O., and Ramesh, G. (2008). Netrin-1 and kidney injury. *II. Netrin*-1 is an early biomarker of acute kidney injury. *Am. J. Physiol. Renal Physiol.* 294, F731–F738. doi: 10.1152/ajprenal.00507.2007

Rota, C., Morigi, M., Cerullo, D., Introna, M., Colpani, O., Corna, D., et al. (2018). Therapeutic potential of stromal cells of non-renal or renal origin in experimental chronic kidney disease. *Stem Cell Res. Ther.* 9:220. doi: 10.1186/s13287-018-0960-968

Schmidt, I. M., Hall, I. E., Kale, S., Lee, S., He, C. H., Lee, Y., et al. (2013). Chitinase-like protein Brp-39/YKL-40 modulates the renal response to ischemic injury and predicts delayed allograft function. *J. Am. Soc. Nephrol.* 24, 309–319. doi: 10.1681/ASN.2012060579

Schulz, C., Gomez Perdiguero, E., Chorro, L., Szabo-Rogers, H., Cagnard, N., Kierdorf, K., et al. (2012). A lineage of myeloid cells independent of Myb and hematopoietic stem cells. *Science* 336, 86–90. doi: 10.1126/science.1219179

Sere, K., Baek, J. H., Ober-Blobaum, J., Muller-Newen, G., Tacke, F., Yokota, Y., et al. (2012). Two distinct types of langerhans cells populate the skin during steady state and inflammation. *Immunity* 37, 905–916. doi: 10.1016/j.immuni.2012.07.019

Sola, A., Weigert, A., Jung, M., Vinuesa, E., Brecht, K., Weis, N., et al. (2011). Sphingosine-1-phosphate signalling induces the production of Lcn-2 by macrophages to promote kidney regeneration. *J. Pathol.* 225, 597–608. doi: 10.1002/path.2982

Susnik, N., Sorensen-Zender, I., Rong, S., von Vietinghoff, S., Lu, X., Rubera, I., et al. (2014). Ablation of proximal tubular suppressor of cytokine signaling 3 enhances tubular cell cycling and modifies macrophage phenotype during acute kidney injury. *Kidney Int.* 85, 1357–1368. doi: 10.1038/ki.2013.525

Takaori, K., Nakamura, J., Yamamoto, S., Nakata, H., Sato, Y., Takase, M., et al. (2016). Severity and frequency of proximal tubule injury determines renal prognosis. *J. Am. Soc. Nephrol.* 27, 2393–2406. doi: 10.1681/ASN.2015060647

Tanaka, S., Tanaka, T., and Nangaku, M. (2014). Hypoxia as a key player in the AKI-to-CKD transition. *Am. J. Physiol. Renal Physiol.* 307, F1187–F1195. doi: 10.1152/ajprenal.00425.2014

Tang, P. M., Zhou, S., Li, C. J., Liao, J., Xiao, J., Wang, Q. M., et al. (2018). The proto-oncogene tyrosine protein kinase Src is essential for macrophage-myofibroblast transition during renal scarring. *Kidney Int.* 93, 173–187. doi: 10.1016/j.kint.2017.07.026

Uderhardt, S., Martins, A. J., Tsang, J. S., Lammermann, T., and Germain, R. N. (2019). Resident macrophages cloak tissue microlesions to prevent neutrophil-driven inflammatory damage. *Cell* 177, 541–555.e17. doi: 10.1016/j.cell.2019.02.028

Vernon, M. A., Mylonas, K. J., and Hughes, J. (2010). Macrophages and renal fibrosis. *Semin. Nephrol.* 30, 302–317. doi: 10.1016/j.semnephrol.2010.03.004

Vinuesa, E., Hotter, G., Jung, M., Herrero-Fresneda, I., Torras, J., and Sola, A. (2008). Macrophage involvement in the kidney repair phase after ischaemia/reperfusion injury. *J. Pathol.* 214, 104–113. doi: 10.1002/path.2259

Wada, Y., Gonzalez-Sanchez, H. M., Weinmann-Menke, J., Iwata, Y., Ajay, A. K., Meineck, M., et al. (2019). IL-34-Dependent intrarenal and systemic mechanisms promote lupus nephritis in MRL-Fas(lpr) Mice. *J. Am. Soc. Nephrol.* 30, 244–259. doi: 10.1681/ASN.2018090901

Wan, X., Huang, W. J., Chen, W., Xie, H. G., Wei, P., Chen, X., et al. (2014). IL-10 deficiency increases renal ischemia-reperfusion injury. *Nephron Exp. Nephrol.* 128, 37–45. doi: 10.1159/000366130

Wang, D., Xiong, M., Chen, C., Du, L., Liu, Z., Shi, Y., et al. (2018). Legumain, an asparaginyl endopeptidase, mediates the effect of M2 macrophages on attenuating renal interstitial fibrosis in obstructive nephropathy. *Kidney Int.* 94, 91–101. doi: 10.1016/j.kint.2017.12.025

Wang, Q., Liang, Y., Qiao, Y., Zhao, X., Yang, Y., Yang, S., et al. (2018). Expression of soluble epoxide hydrolase in renal tubular epithelial cells regulates macrophage infiltration and polarization in IgA nephropathy. *Am. J. Physiol. Renal Physiol.* 315, F915–F926. doi: 10.1152/ajprenal.00534.2017

Wang, M., You, Q., Lor, K., Chen, F., Gao, B., and Ju, C. (2014). Chronic alcohol ingestion modulates hepatic macrophage populations and functions in mice. *J. Leukoc. Biol.* 96, 657–665. doi: 10.1189/jlb.6A0114-004RR

Wang, Q., Su, Y. Y., Li, Y. Q., Zhang, Y. F., Yang, S., Wang, J. L., et al. (2017). Atorvastatin alleviates renal ischemia-reperfusion injury in rats by promoting M1-M2 transition. *Mol. Med. Rep.* 15, 798–804. doi: 10.3892/mmr.2016.6074

Wang, S., Zhang, C., Li, J., Niyazi, S., Zheng, L., Xu, M., et al. (2017). Erythropoietin protects against rhabdomyolysis-induced acute kidney injury by modulating macrophage polarization. *Cell Death Dis.* 8:e2725. doi: 10.1038/cddis.2017.104

Wang, Y. Y., Jiang, H., Pan, J., Huang, X. R., Wang, Y. C., Huang, H. F., et al. (2017). Macrophage-to-Myofibroblast transition contributes to interstitial fibrosis in chronic renal allograft injury. *J. Am. Soc. Nephrol.* 28, 2053–2067. doi: 10.1681/ASN.2016050573

Wang, S., Meng, X. M., Ng, Y. Y., Ma, F. Y., Zhou, S., Zhang, Y., et al. (2016). TGF-beta/Smad3 signalling regulates the transition of bone marrow-derived macrophages into myofibroblasts during tissue fibrosis. *Oncotarget* 7, 8809–8822. doi: 10.18632/oncotarget.6604

Wang, W., Huang, X. R., Li, A. G., Liu, F., Li, J. H., Truong, L. D., et al. (2005). Signaling mechanism of TGF-beta1 in prevention of renal inflammation: role of Smad7. *J. Am. Soc. Nephrol.* 16, 1371–1383. doi: 10.1681/ASN.2004121070

Wang, Y., Chang, J., Yao, B., Niu, A., Kelly, E., Breeggemann, M. C., et al. (2015). Proximal tubule-derived colony stimulating factor-1 mediates polarization of renal macrophages and dendritic cells, and recovery in acute kidney injury. *Kidney Int.* 88, 1274–1282. doi: 10.1038/ki.2015.295

Wang, Y., Szretter, K. J., Vermi, W., Gilfillan, S., Rossini, C., Cella, M., et al. (2012). IL-34 is a tissue-restricted ligand of CSF1R required for the development of Langerhans cells and microglia. *Nat. Immunol.* 13, 753–760. doi: 10.1038/ni.2360

Wang, Y., Wang, Y. P., Zheng, G., Lee, V. W., Ouyang, L., Chang, D. H., et al. (2007). Ex vivo programmed macrophages ameliorate experimental chronic inflammatory renal disease. *Kidney Int.* 72, 290–299. doi: 10.1038/sj.ki.5002275

Wei, S., Nandi, S., Chitu, V., Yeung, Y. G., Yu, W., Huang, M., et al. (2010). Functional overlap but differential expression of CSF-1 and IL-34 in their CSF-1 receptor-mediated regulation of myeloid cells. *J. Leukoc. Biol.* 88, 495–505. doi: 10.1189/jlb.1209822

Wilson, H. M., Stewart, K. N., Brown, P. A., Anegon, I., Chettibi, S., Rees, A. J., et al. (2002). Bone-marrow-derived macrophages genetically modified to produce IL-10 reduce injury in experimental glomerulonephritis. *Mol. Ther.* 6, 710–717. doi: 10.1006/mthe.2002.0802

Wynn, T. A., and Vannella, K. M. (2016). Macrophages in tissue repair, regeneration, and fibrosis. *Immunity* 44, 450–462. doi: 10.1016/j.immuni.2016.02.015

Xu, Y., and Han, J. (2016). The necrosome in acute kidney injury. *Semin. Nephrol.* 36, 199–207. doi: 10.1016/j.semnephrol.2016.03.007

Yang, Q., Wang, Y., Pei, G., Deng, X., Jiang, H., Wu, J., et al. (2019). Bone marrow-derived Ly6C(-) macrophages promote ischemia-induced chronic kidney disease. *Cell Death Dis.* 10:291. doi: 10.1038/s41419-019-1531-1533

Zhang, M. Z., Wang, X., Wang, Y., Niu, A., Wang, S., Zou, C., et al. (2017). IL-4/IL-13-mediated polarization of renal macrophages/dendritic cells to an M2a phenotype is essential for recovery from acute kidney injury. *Kidney Int.* 91, 375–386. doi: 10.1016/j.kint.2016.08.020

Zhang, M. Z., Yao, B., Yang, S., Jiang, L., Wang, S., Fan, X., et al. (2012). CSF-1 signaling mediates recovery from acute kidney injury. *J. Clin. Invest.* 122, 4519–4532. doi: 10.1172/JCI60363

Zhang, W. R., Garg, A. X., Coca, S. G., Devereaux, P. J., Eikelboom, J., Kavsak, P., et al. (2015). Plasma IL-6 and IL-10 concentrations predict AKI and long-term mortality in adults after cardiac surgery. *J. Am. Soc. Nephrol.* 26, 3123–3132. doi: 10.1681/ASN.2014080764

Zuk, A., and Bonventre, J. V. (2016). Acute kidney injury. *Annu. Rev. Med.* 67, 293–307. doi: 10.1146/annurev-med-050214-13407

Zuk, A., and Bonventre, J. V. (2019). Recent advances in acute kidney injury and its consequences and impact on chronic kidney disease. *Curr. Opin. Nephrol. Hypertens.* 28, 397–405. doi: 10.1097/MNH.0000000000000504

Conflict of Interest Statement: J-HB is an employee of Biogen.

Copyright © 2019 Baek. This is an open-access article distributed under the terms of the Creative Commons Attribution License (CC BY). The use, distribution or reproduction in other forums is permitted, provided the original author(s) and the copyright owner(s) are credited and that the original publication in this journal is cited, in accordance with accepted academic practice. No use, distribution or reproduction is permitted which does not comply with these terms.

frontiers in Pharmacology

ORIGINAL RESEARCH
published: 09 August 2019
doi: 10.3389/fphar.2019.00880

Combined Blockade of Smad3 and JNK Pathways Ameliorates Progressive Fibrosis in Folic Acid Nephropathy

Mengjie Jiang[1,2], Jinjin Fan[3,4], Xinli Qu[2], Songhui Li[5,6], Susan K. Nilsson[5,6], Yu Bo Yang Sun[2], Yaping Chen[7], Di Yu[7], Dan Liu[8], Bi-Cheng Liu[8], Mingliang Tang[9], Wei Chen[3,4], Yi Ren[10], David J. Nikolic-Paterson[11], Xiaoyun Jiang[1], Jinhua Li[2,4,12]* and Xueqing Yu[4,12,13]**

[1] Department of Pediatrics, the First Affiliated Hospital, Sun Yat-sen University, Guangzhou, China, [2] Department of Anatomy and Developmental Biology, Monash Biomedicine Discovery Institute, Monash University, Clayton, VIC, Australia, [3] Department of Nephrology, the First Affiliated Hospital, Sun Yat-sen University, Guangzhou, China, [4] Key Laboratory of Nephrology, National Health Commission and Guangdong Province, Guangzhou, China, [5] Biomedical Manufacturing Commonwealth Scientific and Industrial Research Organisation (CSIRO), Melbourne, VIC, Australia, [6] Australian Regenerative Medicine Institute, Monash University, Clayton, VIC, Australia, [7] Infection and Immunity Program, Monash Biomedicine Discovery Institute and Department of Biochemistry and Molecular Biology, Monash University, Clayton, VIC, Australia, [8] Institute of Nephrology, Zhong Da Hospital, Southeast University, Nanjing, China, [9] Key Laboratory for Developmental Genes and Human Disease, Ministry of Education, Institute of Life Sciences, Southeast University, Nanjing, China, [10] Florida State University College of Medicine, Tallahassee, FL, United States, [11] Department of Nephrology, Monash Health and Monash University Department of Medicine, Clayton, VIC, Australia, [12] The Second Clinical College and Shunde Women and Children Hospital, Guangdong Medical University, Shunde, China, [13] Guangdong Academy of Medical Science, Guangdong Provincial People's Hospital, Guangzhou, China

OPEN ACCESS

Edited by:
Xueying Zhao,
Morehouse School of Medicine,
United States

Reviewed by:
Isha Sharma,
Northwestern University,
United States
Zhengrong Guan,
University of Alabama at Birmingham,
United States

***Correspondence:**
Jinhua Li
jinhua.li@monash.edu
Xiaoyun Jiang
xyjiang-3208@163.com
Xueqing Yu
yuxq@mail.sysu.edu.cn

Specialty section:
This article was submitted to Renal Pharmacology, a section of the journal Frontiers in Pharmacology

Received: *02 May 2019*
Accepted: *10 July 2019*
Published: *09 August 2019*

Citation:
Jiang M, Fan J, Qu X, Li S, Nilsson SK, Sun YBY, Chen Y, Yu D, Liu D, Liu B-C, Tang M, Chen W, Ren Y, Nikolic-Paterson DJ, Jiang X, Li J and Yu X (2019) Combined Blockade of Smad3 and JNK Pathways Ameliorates Progressive Fibrosis in Folic Acid Nephropathy. Front. Pharmacol. 10:880. doi: 10.3389/fphar.2019.00880

Acute kidney injury leading to chronic kidney disease through tubulointerstitial fibrosis is a major challenge in nephropathy. Several signaling pathways promote interstitial fibrosis; however, effective suppression of fibrosis may require blockade of more than one pathway. This study investigated whether blockade of Smad3 and c-Jun N-terminal kinase (JNK) signaling gives added suppression of interstitial fibrosis in folic acid nephropathy. A single high dose of folic acid (FA) causes acute tubular damage in C57BL/6J mice followed by interstitial fibrosis and chronic renal impairment. Co-activations of Smad3 and JNK signaling occur in both tubular epithelial cells and myofibroblasts in areas of tubulointerstitial damage and fibrosis in both murine FA-induced nephropathy and human IgA nephropathy. Groups of mice were treated with a Smad3 inhibitor (SIS3), a JNK inhibitor (SP600125), or a combination from day 6 after FA administration until being killed on day 28. Each drug efficiently inhibited its specific target (Smad3 phosphorylation or c–Jun phosphorylation) without affecting the other pathway. Given alone, each drug partially reduced renal fibrosis, whereas the combination therapy gave an additive and profound protection from renal fibrosis and improved renal function. Inhibition of Smad3 and/or JNK signaling activities prevented down-regulation of PGC-1α in tubular epithelial cells and up-regulation of PGC-1α in myofibroblasts during FA-induced renal fibrosis and inflammation. The expression of PGC-1α was upregulated in *Smad3*$^{-/-}$ NRK52E cells while downregulated in *Smad3*$^{-/-}$NRK49F cells, suggesting that Smad3 signaling may regulate expression of PGC-1α in renal tubular epithelial cells and fibroblasts in distinct

fashion. *In vivo* and cell culture studies also indicate that Smad3 and JNK signaling cooperate to cause mitochondrial dysfunction and cell damage in tubular epithelial cells *via* direct actions on the transcription of PGC-1α. These pathways also act cooperatively to promote renal fibroblast proliferation in tempo-spatial fashion. In conclusion, we have identified a potential combination therapy for progressive renal fibrosis which operates, in part, through modifying mitochondrial function.

Keywords: tubulointerstitial fibrosis, Smad3, JNK1/2, PGC-1α, mitochondrial dysfunction

INTRODUCTION

There is increasing evidence that acute kidney injury (AKI) is often followed by tubulointerstitial damage due to incomplete renal recovery. Renal tubulointerstitial damage, characterized by tubular atrophy, inflammatory cell infiltration, fibrogenesis, and peritubular capillary rarefaction, is considered the final common pathway leading from chronic kidney disease (CKD) to end-stage renal disease (ESRD) (Takaori and Yanagita, 2016; Kaballo et al., 2017). Many patients develop CKD or even subsequent ESRD due to incomplete recovery after an AKI episode (Takaori and Yanagita, 2016; Kaballo et al., 2017). The progression of CKD to ESRD is a complex process involving various intracellular signaling pathways operating in a tempo-spatial manner. We lack specific anti-fibrotic treatments to stop or retard the progression of CKD to ESRD. A better understanding of the role that signaling pathways play in tubulointerstitial damage will enable rational intervention strategies for CKD.

Inflammation and fibrogenesis are two major determinants in the progression of CKD. The c-Jun N-terminal kinase (JNK) and Smad3 signaling pathways have been implicated in the production of proinflammatory mediators and in the fibrogenesis, respectively. Blockade of JNK signaling reduces the degree of interstitial fibrosis in the obstructed kidney (Ma et al., 2007), and JNK activation in the tubulointerstitium correlates with interstitial fibrosis and loss of renal function in human kidney disease (De Borst et al., 2007). On the other hand, blockade of Smad3 signaling has also been shown to suppress the development of renal interstitial fibrosis (Sato et al., 2003; Li et al., 2010).

Kidney function involves a high metabolic demand in which tubular cells require mitochondrial ATP production to move solutes against electrochemical gradients (Sjostrand and Rhodin, 1953; Weidemann and Krebs, 1969; Tran et al., 2011). Tubular ATP depletion due to mitochondrial dysfunction is a hall mark of AKI and cause of tubular cell injury and death (Thadhani et al., 1996). Disruption of mitochondrial homeostasis and suppression of mitochondrial biogenesis (MB) persists after AKI (Funk and Schnellmann, 2012) and may be a driver of CKD. PPARγ coactivator–1α (PGC-1α) (Puigserver et al., 1998; Wu et al., 1999), the regulator of MB and metabolism, is highly expressed in the kidney. The expression of PGC-1α is markedly suppressed during AKI induced by folic acid (FA), ischemia/reperfusion, or glycerol, while overexpression of PGC-1α in tubular epithelial cells can restore mitochondrial and cellular function and decrease epithelial–mesenchymal transition after oxidative stress (Rasbach and Schnellmann, 2007; Hallman et al., 2008; Yuan et al., 2012), suggesting that PGC-1α may play a pivotal role in the recovery after AKI and in the fibrotic response. Of note, Smad3 deficiency promotes MB and increases basal respiration in adipocytes and Smad3 acts as a repressor of PGC-1α expression. In addition, use of an anti-TGF-β1 neutralizing antibody to block TGF-β/Smad3 signaling protects mice from obesity, diabetes, and hepatic steatosis (Tan et al., 2011; Yadav et al., 2011). We have also demonstrated that Smad3 deficiency decreases high-fat diet–induced mitochondrial injury in podocytes (Sun et al., 2015). Activation of the JNK/c-Jun pathway by potassium deprivation down-regulates PGC-1α expression in cerebellar granule neurons (Liang et al., 2010), and JNK inhibition protects LPS-treated mice from fatty acid oxidation reduction and cardiac dysfunction (Drosatos et al., 2011). Taken together, the above studies indicate that blockade of Smad3 and/or JNK signaling has the potential to reduce mitochondrial dysfunction in AKI. The unanswered question is whether JNK and/or Smad3 signaling pathways modulate the expression of PGC-1α and mitochondrial function during the transition of AKI to CKD.

Here, we report that combined blockade of JNK and Smad3 signaling provides a significant added benefit in suppressing tubular damage and interstitial fibrosis in the AKI to CKD transition in the mouse model of folic acid nephropathy. This protection against ongoing tubular damage was associated with increased PGC-1α expression and improved mitochondrial function *in vivo*, while cell culture studies identified that both pathways modulate PGC-1α promoter activity in tubular epithelial cells. These data identify a novel combination therapy to halt the progression of AKI to CKD and propose a new mechanism of action by which JNK and Smad3 signaling promote renal interstitial fibrosis.

METHODS

Experimental Animals

C57BL6/J mice of 8 weeks old weighing 20–30 g were purchased from Animal Services, Sun Yat-sen University, Guangzhou, China. Mice were administered FA (Sigma-Aldrich, St. Louis, MO), by intraperitoneal injection (i.p). at the dose of 250-mg/kg body weight dissolved in 0.3 mmol/L sodium bicarbonate. The dose of FA-induced acute tubular necrosis achieved a low mortality rate (about 5%) within 3 days after FA injection. Control mice were administered an equivalent volume of sodium bicarbonate (buffer) by i.p. Body weight of each mouse

was measured every day for the whole course of experiment after injection. FA and control mice were sacrificed at 2 days, 6 days, 2 weeks, and 4 weeks after injection, and blood, urine, and kidney tissue were collected at the time of the sacrifice for analysis (n = 6/group/time point). In the intervention study, FA mice received JNK-specific inhibitor (SP600125, 15 μg/g/day, Abcam, Cambridge, UK) or/and Smad3-specific inhibitor (SIS3, 5 μg/g/day, Sigma-Aldrich) dissolved in 0.5% carboxymethylcellulose sodium (vehicle) or given vehicle alone by daily i.p. on day 7 after FA injection for 3 weeks. In the co-administration group, the drugs were combined together so that the number and volume of i.p. injections were the same across all groups. Mice were killed at 4 weeks after FA injection (n = 6/group). Blood, urine, and kidney samples were collected from each animal. All mice were acclimated in metabolic cages with free access to food and water for collection of 24-h urine samples. Measurement of urine protein and creatinine were determined using a detergent compatible protein assay kit (Bio-Rad, Hercules, CA) and Creatinine Assay Kit (Cayman Chemical, Ann Arbor, MI) according to instructions. Proteinuria was normalized for creatinine excretion. Each kidney was divided into three parts for (Kaballo et al., 2017) immunoprecipitation/Western blotting; (Takaori and Yanagita, 2016) 10% buffered formalin-fixed, paraffin-embedded tissue; and (Ma et al., 2007) periodate-lysine-paraformaldehyde, OCT-embedded tissue. All experiments were performed at Animal Services, Sun Yat-sen University and approved by the Sun Yat-sen University Animal Ethics Committee.

Human Renal Biopsy Specimens

Studies using human tissue were approved by the Human Ethics Committee of Monash Medical Centre and the Human Ethics Committee of the 1st Affiliated Hospital, Sun Yat-sen University. Human ethics committee approval and written informed consent from the patients were obtained in both institutions. Cryostat sections of snap-frozen tissue, excess to that required for diagnosis, were examined in five cases of IgA nephropathy. Normal kidney tissue was obtained from the non-involved pole of nephrectomies performed as the result of renal carcinoma.

Histology and Confocal Microscopy

Kidneys were fixed in 10% buffered formalin, and paraffin-embedded tissue sections (4 μm) stained with Masson trichrome. Cryostat sections of tissues (4 μm) fixed in periodate-lysine paraformaldehyde were blocked with 2% BSA in PBS and incubated with the following antibodies: rabbit anti-fibronectin (Sigma) or rabbit anti-collagen IV (Southern Biotechnology, Birmingham, AL) followed by goat anti-rabbit Alexa Fluor 488 (Invitrogen, Mount Waverly, Australia) and Cy3-conjugated mouse anti-α-SMA antibody (Sigma) or Alexa Fluor 488-conjugated Rabbit Anti-Tomm20 antibody (Abcam); rat anti-Smad3 (R&D Systems, Minneapolis, MN) followed by goat anti-rat Alexa Fluor 488, rabbit anti-phosphorylated JNK1/2 (Cell Signaling Technology, Danvers, MA) followed by goat anti-rabbit Alexa Fluor 647, and Cy3-conjugated mouse anti-α-SMA antibody; or rat anti-CD11b (Abcam) followed by goat anti-rat Alexa Fluor 488. Sections were counterstained with 4,6-diamidino-2-phenylindole (DAPI, Sigma) to visualize nuclei and analyzed with an Olympus FluoView 1000 Confocal Microscope (Olympus, Tokyo, Japan) under an oil UPLFL × 60 or × 40 objective (NA 1.25; Olympus) using the FV10-ASW software (V1.3c; Olympus). The percentage of staining area was counted in blinded slides. The number of infiltrating interstitial CD11b(+)/DAPI(+) cells was quantified in 20 non-overlapping cortical fields/each kidney and expressed as cells per mm^2 of cortical interstitium. Images were analyzed by ImageJ (http://rsb.info.nih.gov/ij/).

Cell Culture

Wild-type C57BL6/J (WT) mouse renal fibroblasts, NRK52E cells, and NRK49F cells were cultured as previously described (Li et al., 2010; Qu et al., 2012).

Western Blot Analysis

Kidneys (~20 mg) were homogenized and suspended in 0.4 ml of lysis buffer containing 10 mmol/L Tris-HCL, pH 7.4, 1% Triton X-100, 0.5% deoxycholate, 1 mmol/L phenylmethyl sulfonyl fluoride, and cOmplete™, EDTA-free Protease Inhibitor Cocktail (Roche, Castle Hill, Australia). Cultured cells (~2×10^6) were lysed in 0.3 ml RIPA lysis buffer and sonicated. Protein concentration estimations were performed with a detergentcompatible protein assay kit (Bio-Rad, Hercules, CA). Proteins (~50 μg) were separated by 10% sodium dodecyl sulfate-polyacrylamide gel electrophoresis and transferred to a polyvinylidene difluoride membrane. After blocking for 30 min at 4°C in 5% bovine serum albumin in phosphate-buffered saline with 0.1% Tween 20, the membrane was incubated overnight with rabbit anti-JNK, p-JNK (Cell Signaling Technology), or rabbit anti-Smad3, p-Smad3 (Biorbyt, Cambridge, UK). Blots were then incubated with peroxidase-conjugated goat anti-rabbit IgG for 1 h at room temperature, and bound antibody was detected using an ECL Kit (Amersham Pharmacia Biotech, Arlington, IL) and the Kodak 4000MM Image Station. Band density was quantified using ImageJ (http://rsb.info.nih.gov/ij/).

Enzyme-Linked Immunosorbent Assay (ELISA)

Mouse Cystatin C DuoSet ELISA Kit (R&D Systems) was used to measure the protein level of cystatin c in serum according to the instruction supplied.

Collagen I/PGC-1α Promoter Luciferase Assay

1 day after collagen I promoter luciferase plasmid or PGC-1α promoter luciferase plasmid was transfected NRK52E cells or NRK49F cells by lipofectamine 2000. Cells were treated with or without TNF-α, TGF-β1, DMSO, Sp600125, and/or SIS3 for 18 h. Wild-type *Renilla luciferase* was used for normalization in Reporter Assays. Then, cells were harvested and luciferase assay was performed according to the instruction in Luciferase Assay Kit (Promega).

Isolation of Mitochondria From Tissues and Cells

We isolated mitochondria using the *Mitochondria Isolation Kit* for fresh tissue (Thermo Scientific, cat. no. 89801) and cells (Thermo Scientific, cat. no. 89874).

Cell Proliferation Assay

Cell proliferation assay was performed using Cell Proliferation ELISA, BrdU (colorimetric) Kit (Roche Applied Science, Indianapolis, IN). Briefly, the cells were cultured in 96-well plates at a density of 6,000 cells/100 µl/well in complete growth media. The sense sequence of rat PGC-1α siRNA was: 5'AAGACGGATTGCCCTCATTTG. The negative control (scramble) siRNA sequence was: 5'AAGCTTCATAAGGCGC ATAGC. The SiRNA was transfected into NRK52E cells or NRK49F cells by using lipofectamine transfection reagent according to manufacturer's instructions. After 24 h, NRK52E cells and NRK49F cells were treated with epidermal growth factor (EGF) (50 ng/ml; R&D Systems, MN, USA) or PDGF-BB (20 ng/ml; R&D Systems), respectively. After 48 h, the cells were labeled using 10 µM BrdU per well and cultured for another 24 h. The detection and measurement of cell proliferation were performed according to the instruction in Cell Proliferation ELISA Kit.

Lentiviral CRISPR/Cas9 Constructs

For the inducible Smad3 sgRNA constructs, the previously described FgH1tUTG plasmid was modified to contain the rat Smad3 sgRNA (5'TCCCTACAAGGCGGCACATTGGGA3' and 5' AAACTCCCAATGTGCCGCCTTGTA') cassette, which was inserted into bi-directional Bsmb1 sites linked to the GFP fluorescent protein (Aubrey et al., 2015). The constitutive Cas9 expression vectors were derived from the pFUGW, Cas9 protein linked *via* the T2A peptide to the mCherry fluorescent reporter protein (Aubrey et al., 2015).

Statistical Analysis

Data are expressed as mean ± SD with statistical analyses performed using two-way analysis of variance or one-way analysis of variance, with *post hoc* analysis with Tukey's multiple comparison test using GraphPad Prism 6.0 (Graph-Pad Software, San Diego, CA). A probability (P) value below 0.05 was accepted as statistically significant.

RESULTS

Development and progression of tubulointerstitial fibrosis and inflammation following FA-induced acute kidney failure

Masson trichrome staining and immunostaining showed that administration of FA to mice resulted in severe tubulointerstitial injury, development, and progression of tubulointerstitial fibrosis and inflammation (**Figures 1A–C, E**). Levels of serum cystatin c dramatically increased by 2 days after FA administration and then dropped but remained at a higher level than that of vehicle administration throughout the study period (**Figure 1D**), demonstrating acute renal failure followed by incomplete tubulointerstitial recovery and the development and progression of CKD.

Smad3 and JNK Signaling Co-activation in FA-Induced Nephropathy and in Tubulointerstitial Fibrosis in Human IgA Nephropathy

Confocal microscopy demonstrated co-localization of p-Smad3 and p-JNK in tubulointerstitial cells, including tubular epithelial cells and α-smooth muscle actin (α-SMA)-positive myofibroblasts in FA-treated but not in buffer-treated mouse kidney (**Figures 2A–I**). Western blotting further demonstrated that phosphorylated Smad3 (p-Smad3) and JNK (p-JNK) levels were significantly upregulated 2 days after administration of FA, and this upregulation persisted during the progression of renal inflammation and fibrosis (**Figures 2J–M).** Confocal microscopy also demonstrated that few p-Smad3(+) and p-JNK(+) cells were seen in normal human kidney from the uninvolved pole of carcinoma nephrectomy samples (**Figures 3A–E)**. However, numerous tubular cells and α-SMA(+) myofibroblasts exhibited p-Smad3(+) or/and p-JNK(+) staining in biopsy specimens of IgA nephropathy (**Figures 3F–J**), suggesting that co-activation of Smad3 and JNK1/2 signaling in the tubulointerstitium persisted during the development and progression of CKD.

Inhibition of Smad3 and/or JNK Signaling Activities Protected Mice From FA-Induced Development and Progression of Renal Fibrosis and Inflammation

To investigate the functional role of Smad3 and/or JNK signaling pathways in the pathogenesis of FA-induced renal tubulointerstitial fibrosis and inflammation, a Smad3-specific inhibitor (SIS3) and/or a JNK inhibitor (SP600125) were administered daily to mice, beginning on day 6 days after FA injection. Western blotting demonstrated that SIS3 and SP600125 abrogated phosphorylation of Smad3 and c-Jun, respectively (**Figures 4A, B**), indicating that a maximally effective drug dose was used in each case. However, SIS3 did not affect c-Jun phosphorylation, and SP600125 did not affect Smad3 phosphorylation (**Figures 4A, B**), indicating that these signaling pathways operate in a largely independent fashion.

Co-administration of SIS3 and SP600125 inhibited both Smad3 and JNK signaling activations (**Figures 4A, B**). Masson trichrome and confocal microscopy demonstrated that administration of SIS3 alone or SP600125 alone partially reduced tubulointerstitial fibrosis and macrophage infiltration. Co-administration of SIS3 and SP600125 further protected mice from fibrosis and inflammation. Serum cystatin c levels also confirmed the salutary effects of SIS3 and/or SP600125 on renal function (**Figures 5A–E**). Collagen I promoter luciferase assay further demonstrated that TNF-α

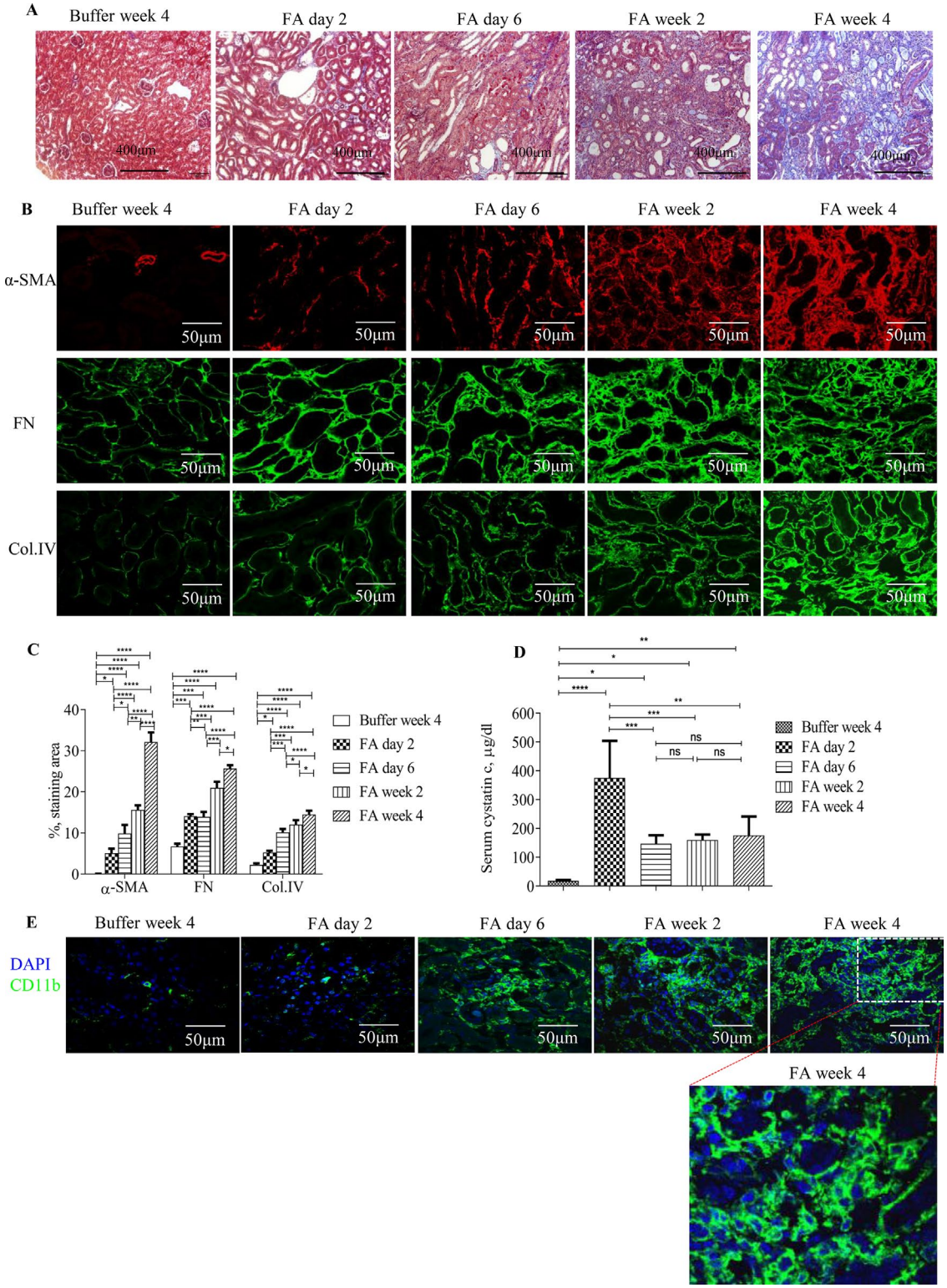

FIGURE 1 | Development and progression of tubulointerstitial fibrosis and inflammation following folic acid (FA)–induced acute kidney failure. **(A)** Masson trichrome staining showing histological changes in the kidneys 2 days, 6 days, 2 weeks, and 4 weeks after folic acid or buffer injection. **(B)** Confocal microscopy showing expression of α-SMA, fibronectin (FN), and collagen IV (Col. IV) and **(E)** CD11b in the kidneys 2 days, 6 days, 2 weeks, and 4 weeks after folic acid or buffer injection. **(C)** Quantification of α-SMA, FN, and Col. IV staining area in the kidneys 2 days, 6 days, 2 weeks, and 4 weeks after folic acid or buffer injection. **(D)** Time course of serum cystatin c changes from mice after folic acid or buffer injection. **(E)** Confocal microscopy showing expression of CD11b after folic acid or buffer injection. Original magnification; ×400 **(A** and **E)**; ×600 **(B)**. Data are mean ± SD (n = 6/group). $^{*}P < 0.05$, $^{**}P < 0.01$, $^{***}P < 0.001$, $^{****}P < 0.0001$.

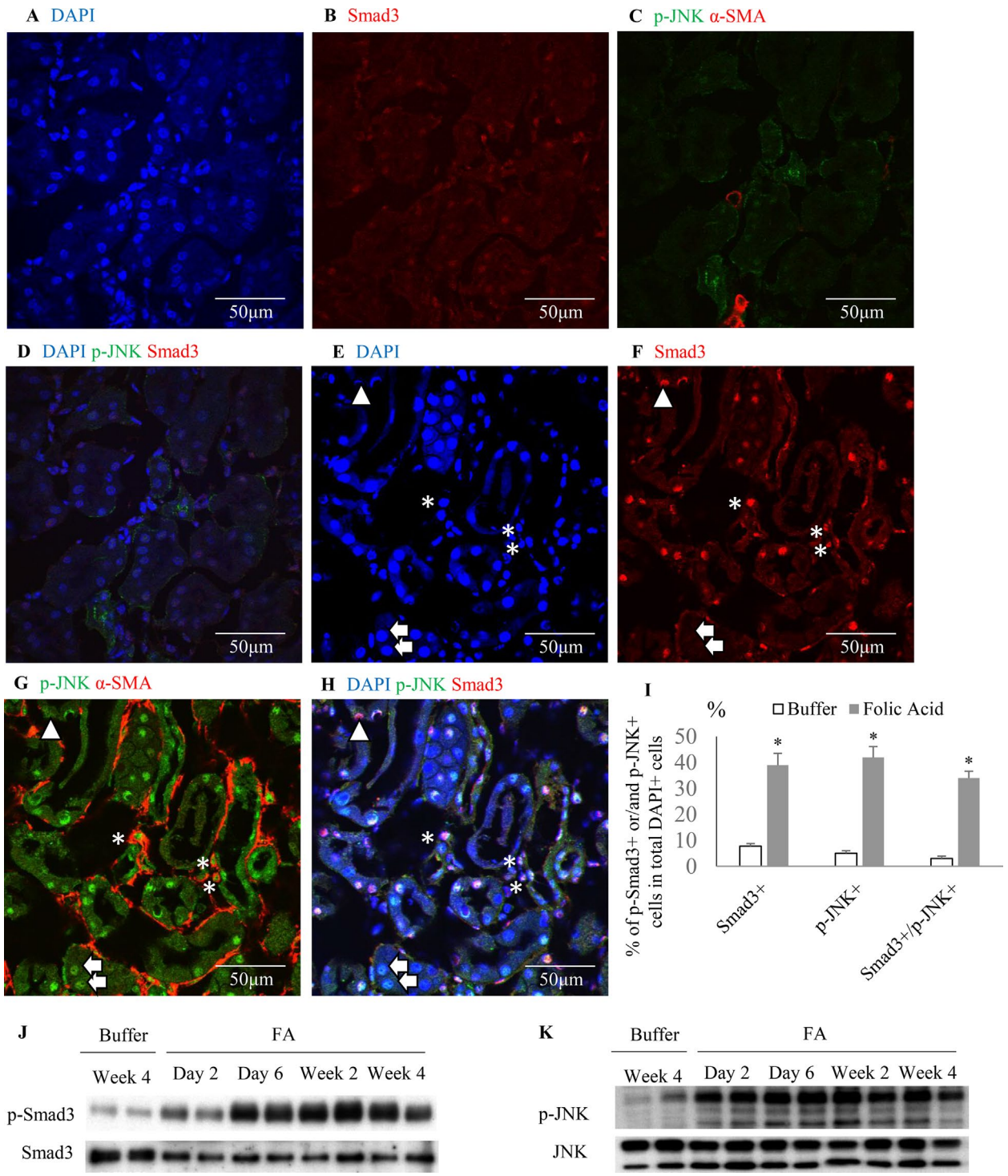

FIGURE 2 | Continued

has additive effect on TGF-β1-induced fibrotic response while blockade Smad3 and/or JNK signaling pathway almost abrogated this fibrotic response in renal fibroblasts (**Figure 6**). Taken together, all these data suggested that Smad3 and JNK signaling pathways may play an essential role in the pathogenesis of tubulointerstitial fibrosis and inflammation and that inhibition of Smad3 and JNK signaling may retard the development and progression of CKD.

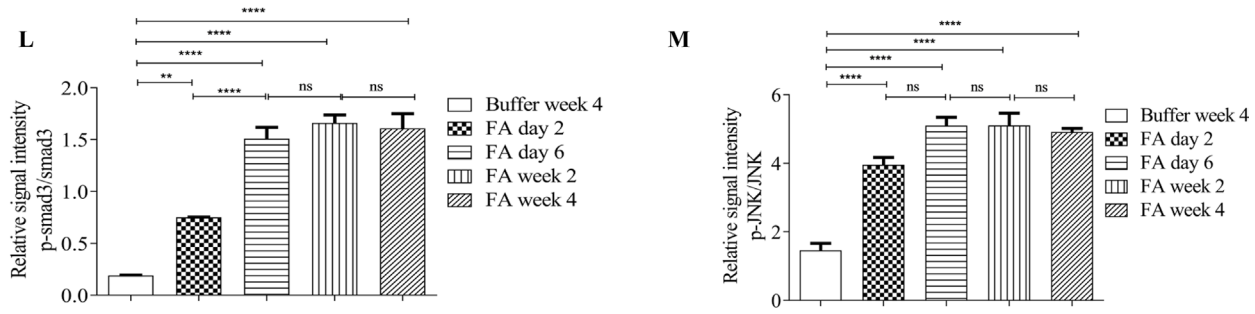

FIGURE 2 | Smad3 and JNK signaling activation after folic acid (FA)–induced acute kidney injury. Confocal microscopy demonstrated same fields in buffer-treated kidney **(A–D)** or kidney 6 days after folic acid treatment **(E–H)**. **(A)** DAPI, blue. **(B)** Nuclear staining of Smad3, red. **(C)** p-JNK, green and α-SMA, red. **(D)** Merged with DAPI (blue), nuclear staining of Smad3 (red) and p-JNK (green). **(E)** DAPI, blue. **(F)** Nuclear staining of Smad3, red. **(G)** p-c-Jun N-terminal kinases (JNK), green and α-SMA, red. **(H)** Merged with DAPI (blue), nuclear staining of Smad3 (red) and p-JNK (green). Arrows indicate nuclear Smad3(–)/p-JNK(+) cells; arrow head shows a nuclear Smad3(+)/p-JNK(–) cell; asterisks show interstitial α-SMA(+)/nuclear Smad3(+)/p-JNK(+) cells. **(I)** Quantification of nuclear staining of nuclear Smad3(+), p-JNK(+), and nuclear Smad3(+)/p-JNK(+) cells. *$^*P < 0.05$ vs.* buffer-treated kidney. Western blotting shows p-Smad3 **(J)** and p-JNK **(K)** in kidneys 2 days, 6 days, 2 weeks, and 4 weeks after folic acid or buffer injection. Quantification of relative signal intensities of p-Smad3/Smad3 **(L)** and p-JNK/JNK **(M)** in kidneys after folic acid or buffer injection. Original magnification (×600). Data are mean ± SD (n = 6/group). $^{**}P < 0.01$; $^{****}P < 0.0001$; ns, not significant.

Inhibition of Smad3 and/or JNK Signaling Activities Reduced Mitochondrial Dysfunction and Promoted Renal Tubular Epithelial Cell Recovery From Folic Acid-Induced Kidney Damage

Administration of FA to mice resulted in a rapid reduction of mitochondrial cytochrome c (**Figures 7A, B**) during the early phase of injury and this down-regulation of mitochondrial cytochrome c further reduced 2 weeks after FA administration. The increase protein expression of cytosol cytochrome c, a mitochondrial injury indicator, was demonstrated by WB in which a 3.5-, 3.5-, 1.5-, and 1-fold increase was observed in the kidneys of FA-injected mice at 2, 6, 14, and 28 days, respectively, compared with buffer-treated mice. This dynamic changes of mitochondrial activity demonstrated mitochondrial damage persisted and mitochondria incompletely recovered after FA-induced kidney injury.

Administration of SP600125 alone or SIS3 alone prevented cytochrome c release from mitochondria and decreased the interaction between Apaf-1 and cytosol cytochrome c and the protein expression level of active caspase-3 when compared to vehicle-treated group (**Figures 7C, D**), suggesting that both SP600125 and SIS3 are reducing mitochondrial dysfunction and resultant cell damage, including cell death through apoptosis. Co-administration of SP600125 and SIS3 almost recovered the expression of mitochondrial cytochrome c, significantly decreased the complex of Apaf-1 and cytosol cytochrome c and the formation of active caspase-3 and TUNEL(+) cells (**Figures 7C–G**). Furthermore, administration of SP600125 alone or SIS3 alone decreased the loss of E-cadherin, the tubular epithelial marker (**Figures 7E, F**). Co-administration of SP600125 and SIS3 almost prevented the loss of E-cadherin, an indicator of tubular cell damage, when compared to buffer-treated group (**Figures 7E, F**). Taken together, these studies demonstrated the relationship between Smad3 and JNK signaling pathways, mitochondrial function, and tubular epithelial recovery.

Inhibition of Smad3 and/or JNK Signaling Activities Prevented Down-Regulation of PGC-1α in Tubular Epithelial Cells and Up-Regulation of PGC-1α in Myofibroblasts During FA-induced Renal Fibrosis and Inflammation

To further investigate the impact of Smad3 and JNK signaling activation on mitochondrial dysfunction, the expression of cytochrome c, the mitochondrial marker, and PGC-1α, the MB marker, were examined. Confocal microscopy demonstrated that there was a rapid reduction of cytochrome c in tubular epithelial cells 2 days after FA injection, and the decrease persisted (**Figures 8A, C**) until the experimental endpoint. Confocal microscopy also demonstrated that the administration of SP600125 or SIS3 reduced loss of cytochrome c and PGC-1α in tubular epithelial cells and decreased the expression of PGC-1α in myofibroblasts (**Figures 8B, D–H**), suggesting co-administration of SP600125 and SIS3 further enhanced the impact on PGC-1α expression.

Smad3 and JNK1/2 Signaling Pathways Regulated Expression of PGC-1α in Renal Tubular Epithelial Cells and Fibroblasts in Distinct Fashion

To knockout Smad3 in NRK52E cells and NRK49F cells, the inducible Smad3 sgRNA was constructed in Lentiviral CRISPR/Cas9 system. Western blotting demonstrated that Smad3 was knockout in NRK52E cells and NRK49F cells (**Figures 9A, B**). The expression of PGC-1α was upregulated in *Smad3*$^{-/-}$ NRK52E cells while downregulated in *Smad3*$^{-/-}$ NRK49F cells (**Figures 9A–D**), suggesting that Smad3 signaling may regulate expression of PGC-1α in renal tubular epithelial cells and fibroblasts in distinct fashion. TGF-β1 or TNF-α decreased the expression of PGC-1α in rat tubular epithelial cells (NRK52E) while TGF-β1 + TNF-α further enhanced the inhibitive effects on NRK52E cells (**Figures 9E–G**). Administration of SP600125

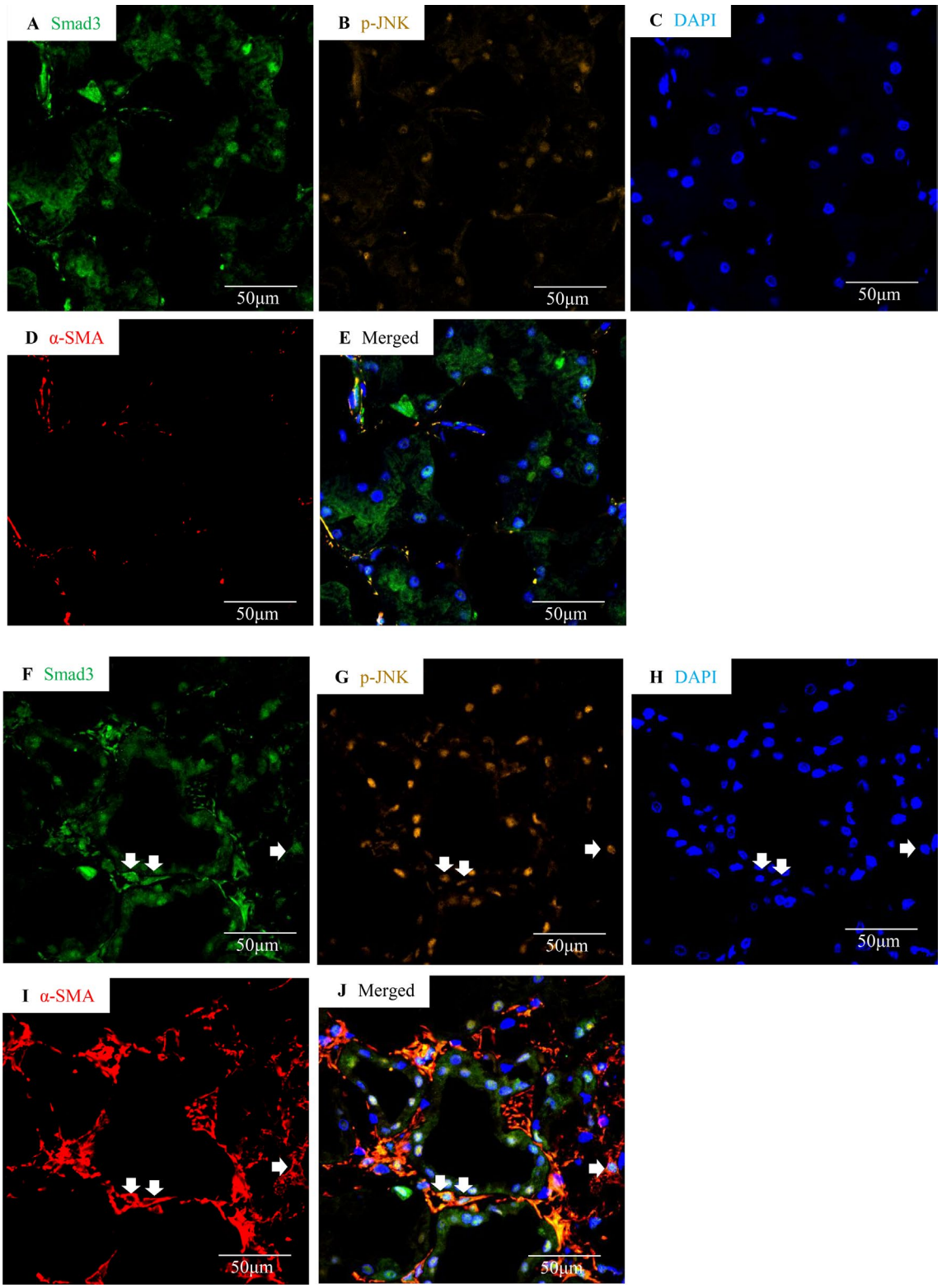

FIGURE 3 | Smad3 and JNK signaling co-activation in human IgA nephropathy. Multi-color confocal microscopy of the cortical interstitium in normal human kidney **(A–E)** and an area of tubulointerstitial fibrosis in a case of IgA nephropathy **(F–J)**. **(A** and **F)** nuclear staining of Smad3, green; **(B** and **G)** p-JNK, yellow; **(C** and **H)** DAPI, blue; **(D** and **I)** α-smooth muscle actin, α-SMA, red; **(E** and **J)** merged with nuclear Smad3 (green), p-JNK (yellow), DAPI (blue), and α-SMA (red). Arrows indicate interstitial α-SMA(+)/nuclear Smad3(+)/p-JNK(+) cells. Original magnification (x600).

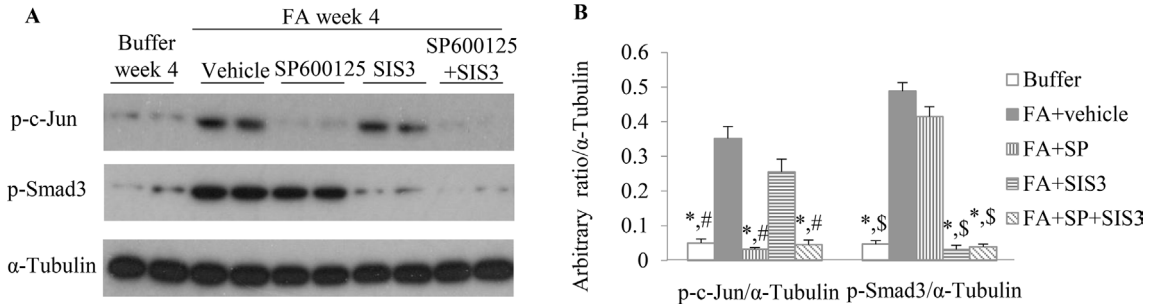

FIGURE 4 | The impact of blockade of JNK and/or Smad3 signaling on folic acid (FA)–induced kidney injury. **(A** and **B)** Western blotting shows p-c-Jun, p-Smad3, and α-tubulin in kidneys from buffer-treated kidneys and FA-induced kidney disease treated with vehicle, SP600125, SIS3, or SP600125 + SIS3. **(B)** Quantification of Western blot results. *$P < 0.05$ *vs.* FA+vehicle-treated group; $^{\#}P < 0.05$ *vs.* FA+SIS3-treated group; $^{\$}P < 0.05$ *vs.* FA+SP-treated group.

or/and SIS3 prevented TGF-β1-induced or TNF-α-induced down-regulation of PGC-1α in NRK52E cells (**Figure 9H**). TGF-β is known to cause damage to tubular cells. The cell culture findings are consistent with the confocal staining results in the kidney in which there is down-regulation of PGC-1α in tubular cells. TGF-β1 increased the expression of PGC-1α in rat renal fibroblasts (NRK49F). Low dose of TNF-α increased while higher dose TNF-α inhibited the expression of PGC-1α in NRK49F cells. Administration of SP600125 or/and SIS3 prevented the impacts of TGF-β1 and TNF-α on the expression of PGC-1α in NRK49F cells (**Figures 9I–L**). To investigate the relationship between PGC-1α expression and cell proliferation, the expression of PGC-1α was knocked down by PGC-1α siRNA. Knockdown of PGC-1α decreased the EGF-induced proliferation in NRK52E cells (**Figures 9M, O**) and PDGF-BB-induced proliferation in NRK49F cells (**Figures 9N, P**).

Smad3 and JNK Signaling Pathways Modulated PGC-1α Promoter Activity in Renal Tubular Epithelial Cells and Fibroblasts.

To further investigate the mechanism(s) how Smad3 and JNK1/2 signaling modulates the expression of PGC-1α, we employed PGC-1α promoter luciferase assay. Both TGF-β1 and TNF-α decreased PGC-1α promoter activity in a dose-dependent fashion in NRK52E cells (**Figure 10A**). TGF-β1 and TNF-α had additive effects on PGC-1α promoter activity and SIS3, and Sp600125 can reduce the inhibitive effects TGF-β1 and TNF-α on PGC-1α promoter activity in NRK52E cells (**Figure 10B**). TGF-β1 increased PGC-1α promoter activity in a dose-dependent fashion in NRK49F cells. Low dose of TNF-α increased while high dose of TNF-α decreased PGC-1α promoter activity in NRK49F cells (**Figures 10C, D**). Treatment with low dose of TGF-β1 and TNF-α had an additive effects on PGC-1α promoter activity while SIS3 and SP600125 blocked the effects of TGF-β1 and TNF-α on PGC-1α promoter activity in NRK49F cells (**Figures 10C, D**).

DISCUSSION

Tubulointerstitial damage is the common pathway to ESRD while inflammation and fibrogenesis are the two major determinants of the progression from CKD to ESRD (Li et al., 2006; Picken et al., 2016). The roles of JNK and Smad3 signaling pathways in inflammation and fibrogenesis have been studied on an individual basis (Sato et al., 2003; De Borst et al., 2007; Ma et al., 2007; Li et al., 2010). In the present study, we demonstrated that activated JNK and Smad3 signaling pathways were co-localized in the tubulointerstitial compartment after FA-induced kidney damage, which provided rationale that blockade of both Smad3 and JNK signaling pathways may provide better protection from FA-induced progressive CKD than single blockade of Smad3 signaling or JNK signaling. Co-administration of SP600125 and SIS3 was highly effective in blocking each signaling pathways and protected tubular epithelial cells from apoptosis and promoted tubular epithelial cell but decreased renal fibroblast proliferation through modulation expression of PGC-1α in both tubular epithelial cells and renal fibroblasts at transcriptional level. Co-administration of SP600125 and SIS3 achieved better renal function protection from FA-induced progressive fibrosis and inflammation than that of single blockade.

Tubular atrophy is an important characteristic of progressive CKD. In the present study, we demonstrated dynamic changes of mitochondrial cytochrome c, which reflects mitochondrial function, and cytosol cytochrome c, which indicates mitochondrial injury after FA-induced kidney damage. We further demonstrated that blockade of Smad3 or/and JNK signaling increased mitochondrial cytochrome c and decreased the interaction between cytochrome c and Apaf-1. The interaction between cytosol cytochrome c and Apaf-1 is the initial step in the cytochrome c/Apaf-1/procaspase-9/procaspase-3 activation sequence in the apoptosis pathway (Li et al., 1997; Zou et al., 1997). Tournier et al. demonstrated that JNK signaling activation is required for stress-induced activation of the cytochrome c-mediated apoptosis in primary murine embryonic fibroblasts (Tournier et al., 2000) while Smad3/Nox4-mediated mitochondrial dysfunction plays a critical role in puromycin-induced podocyte injury (Yu et al., 2014). In our study, blockade of Smad3 and JNK signaling pathways further decreased the production of cytosol cytochrome c, the interaction between Apaf-1 and cytochrome

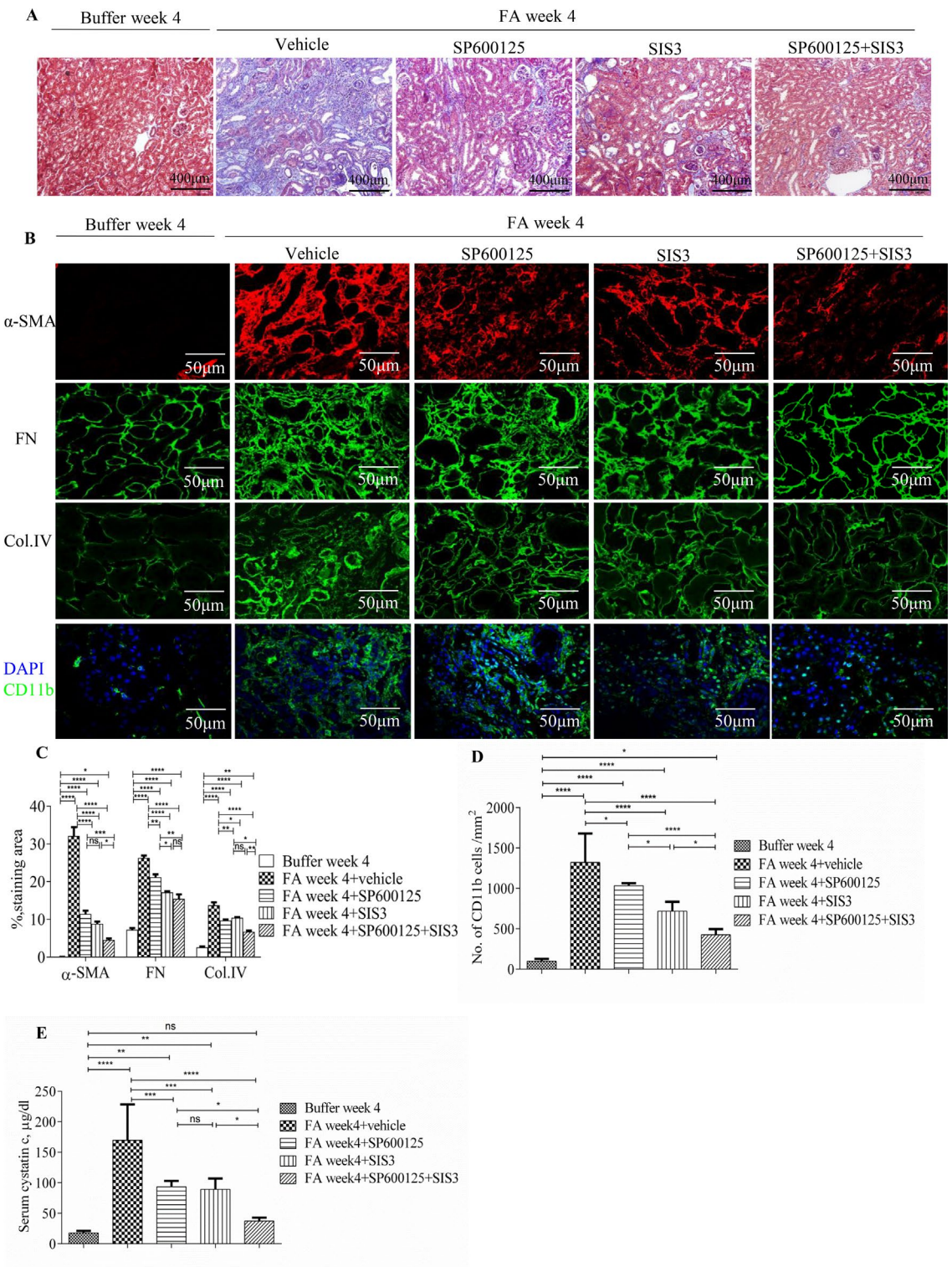

FIGURE 5 | Inhibition of Smad3 and/or JNK signaling reduces renal fibrosis and inflammation in folic acid (FA)–induced kidney injury. **(A)** Masson trichrome staining shows histological changes in the kidneys 4 weeks after buffer or folic acid injection with SP600125, SIS3, or combined SP600125+SIS3 treatment. **(B)** Confocal microscopy shows staining of α-SMA, fibronectin (FN), Col IV, and CD11b in the kidneys 4 weeks after buffer or folic acid injection with different treatments. Magnification: ×400 **(A)**, ×600 **(B** and **E)**. **(C)** Quantification of α-SMA, FN, and Col IV interstitial staining area. **(D)** The number of CD11b(+) macrophages in the kidneys 4 weeks after buffer or folic acid injection with different treatments. **(E)** Serum cystatin c levels in mice 4 weeks after buffer or folic acid injection with different treatments. Data are mean ± SD, (n = 6/group). $^{*}P < 0.05$, $^{**}P < 0.01$, $^{***}P < 0.001$, $^{****}P < 0.0001$.

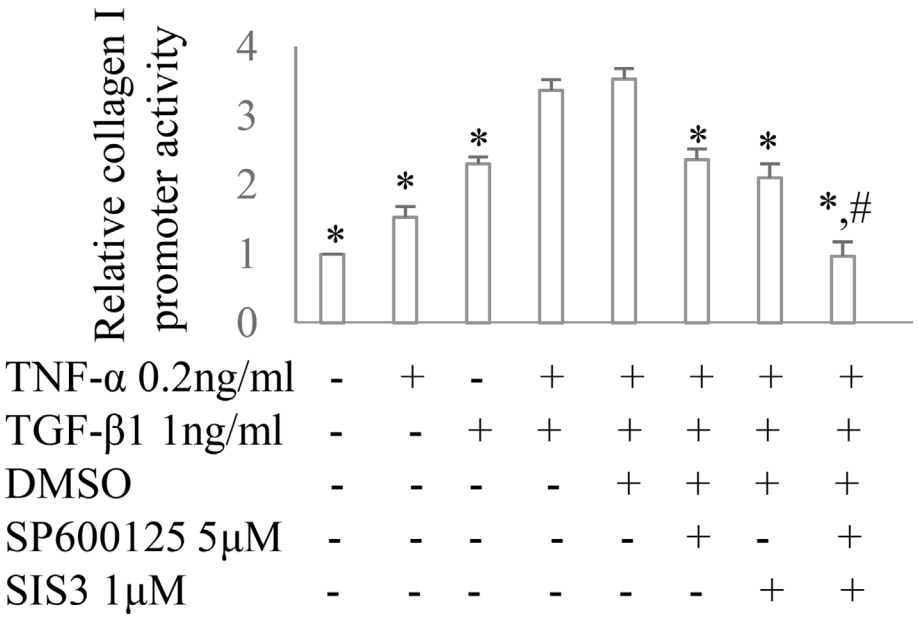

FIGURE 6 | The impact of Smad3 and JNK signaling on TNF-α and/or TGF-β1-induced fibrotic response. Collagen I promoter luciferase activity assay in cultured renal fibroblasts. *$P < 0.05$ *vs.* TNF-α 0.2 ng/ml + TGF-β1 1 ng/ml or TNF-α 0.2 ng/ml + TGF-β1 1 ng/ml +DMSO; #$P < 0.05$ *vs.* TNF-α 0.2 ng/ml + TGF-β1 1 ng/ml + SP600125 or TNF-α 0.2 ng/ml + TGF-β1 1 ng/ml + SIS3. Data are mean ± SD. Experiments were repeated three times.

c and active caspase-3 production, which accounted for the reduction in tubular epithelial cell apoptosis in FA-induced CKD. Thus, blockade of JNK and Smad3 signaling may rescue tubular epithelial cells from apoptosis.

Fully functional mitochondria is essential to the preservation of normal renal function (Tabara et al., 2014; Ralto and Parikh, 2016). PGC-1α plays an essential role in controlling MB and function (Wu et al., 1999). Downregulation of PGC-1α mRNA or/and protein levels was observed in several models of early stage AKI, including FA-induced, cisplatin-induced, and ischemia-reperfusion-induced kidney injury (Funk and Schnellmann, 2013; Ruiz-Andres et al., 2016). PGC-1α-deficient mice suffered persistent injury following endotoxemia while overexpression of PGC-1α after oxidative stress accelerated recovery of tubular cells (Rasbach and Schnellmann, 2007; Tran et al., 2011). Thus, the insufficiency of PGC-1α in tubular cells may contribute to persistence of injury and tubular atrophy. However, the upregulation of PGC-1α was also observed in UUO (Hickey et al., 2011) and recovery phase of ischemia––reperfusion-induced kidney injury (Funk and Schnellmann, 2012; Funk and Schnellmann, 2013). Our *in vivo* studies clearly demonstrated that the expression of PGC-1α was decreased in tubular epithelial cells while increased in myofibroblasts in FA-induced progressive tubulointerstitial damage. This up- *versus* down-regulation of PGC-1α in the two cell types reflects the pathologic changes during tubulointerstitial damage, tubular epithelial cell atrophy, and fibroblast proliferation. Our *in vitro* studies further showed that knockdown of PGC-1α reduced EGF-induced epithelial cell proliferation and PDGF-BB-induced fibroblast proliferation. Thus, our study provided evidence that the expression level of PGC-1α was correlated with proliferation of both tubular epithelial cells and renal fibroblasts. The tempo-spatial changes of PGC-1α expression are correlated with pathological changes in progressive CKD: tubular atrophy, and myofibroblast proliferation and accumulation. Co-administration of SP600125 and SIS3 prevented the up-regulation of PGC-1α expression in myofibroblasts and down-regulation of PGC-1α expression in tubular epithelial cells in FA-induced progressive tubulointerstitial injury. *In vitro* studies further demonstrated that both TGF-β1 and TNF-α downregulated PGC-1α expression in tubular epithelial cells while upregulated PGC-1α expression in renal fibroblasts. JNK inhibitor SP600125 and Smad3 inhibitor SIS3 abrogated the impact of TGF-β1 and TNF-α on the expression of PGC-1α in tubular epithelial cells and renal fibroblasts, which accounted for increased tubular proliferation with better repair and less fibroblast proliferation with the reduced accumulation of myofibroblasts and less fibrosis. Taken together, our study demonstrated a whole picture of tempo-spatial expression of PGC-1α in progressive CKD model and the exact role of PGC-1 in tubular epithelial cells and renal fibroblasts. Our studies also suggested that blockade of JNK and Smad3 signaling may promote tubular epithelial proliferation but inhibit fibroblast proliferation through modulation expression of PGC-1α.

PGC-1α is a transcriptional coactivator that regulates genes involved in MB and energy metabolism and provides a direct link between external stimuli and the modulation of mitochondrial function (Lin et al., 2005). Smad3 directly binds to Smad-binding elements (SBEs) on gene promoters to regulate target gene transcription (Feng and Derynck, 2005) while activation of JNK signaling leads to phosphorylated c-Jun binding to AP-1 binding site (Chung et al., 1996). Sequence analysis revealed the presence of SBE

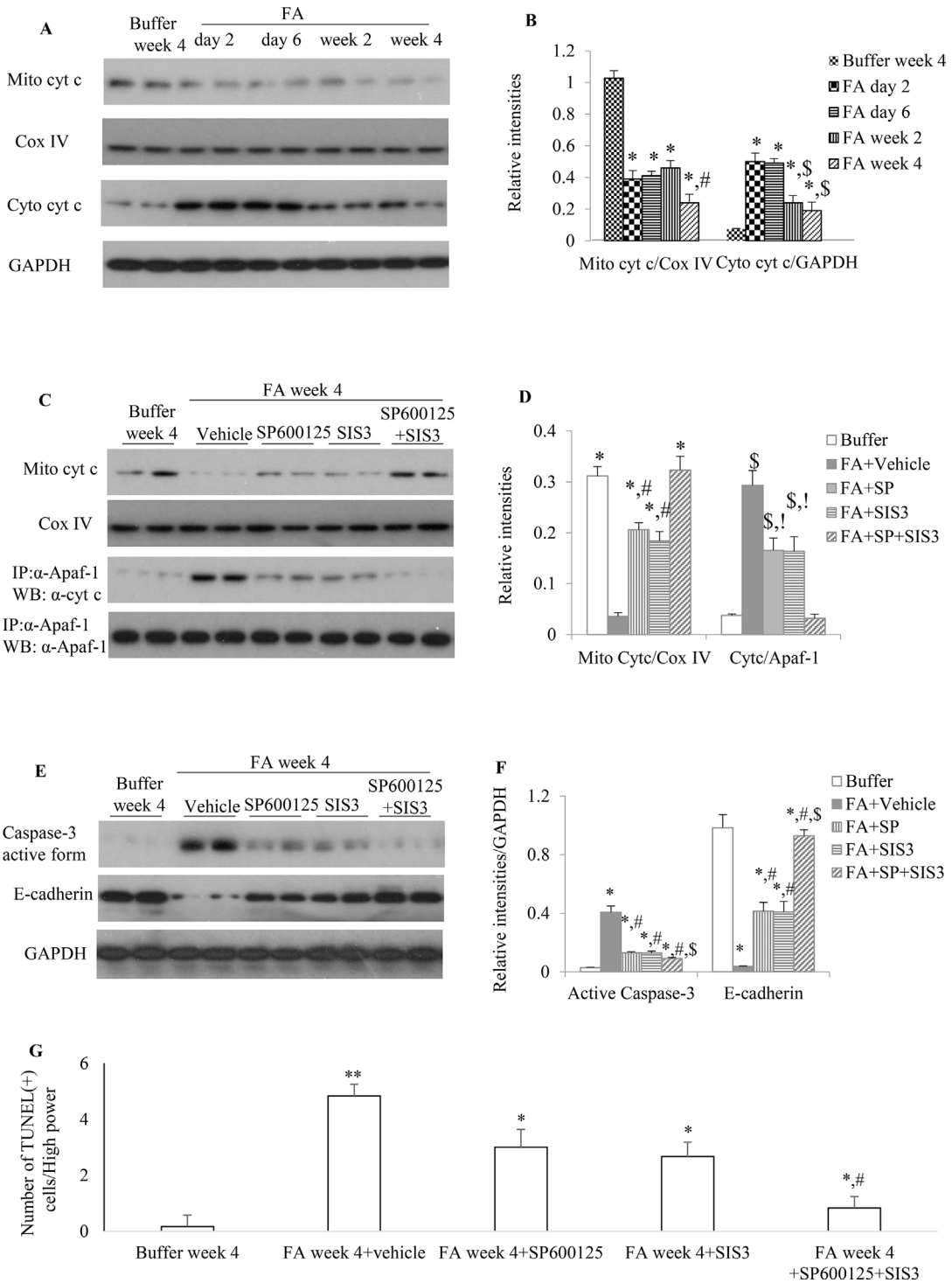

FIGURE 7 | The impact of blockade of JNK and/or Smad3 signaling on folic acid (FA)–induced kidney injury. **(A** and **B)** Western blotting shows mitochondrial cytochrome c and cytosol cytochrome c in buffer-treated or a time-course of FA-treated kidneys. **(B)** Quantification of Western blot results. *$^{*}P < 0.05$ *vs.* buffer week 4. $^{\#}P < 0.05$ *vs.* FA day 2, FA day 6, or FA week 2; $^{\$}P < 0.05$ *vs.* FA day 2 or FA day 6. **(C** and **D)** Western blotting (WB, upper two panels) and immunoprecipitation/WB (IP/WB, lower two panels) show the effect of treatment with SP600125 alone, SIS3 alone, and SP600125 + SIS3 on mitochondrial cytochrome c and interaction of cytochrome c with Apaf-1 in 4-week FA-induced kidney injury. **(D)** Quantification of blots. *$^{*}P < 0.05$ *vs. FA+vehicle;* $^{\#}P < 0.05$ *vs. FA+SP+SIS3;* $^{\$}P < 0.05$ *vs. Buffer week4;* $^{!}P < 0.05$ *vs. FA+SP+SIS3.* **(E** and **F)** West blotting shows effect of treatment with SP600125 alone, SIS3 alone, and SP600125 + SIS3 on caspase-3 activation and E-cadherin in 4-week FA-induced kidney injury. **(F)** Quantification of blots. *$^{*}P < 0.05$ *vs.* buffer week 4. $^{\#}P < 0.05$ *vs.* FA + vehicle; $^{\$}P < 0.05$ *vs.* FA+SP600125 or FA + SIS3. Data are mean ± SD. **(G)** Quantitation of TUNEL(+) cells per high power field (100×). *$^{*}P < 0.05$ *vs.* FA week 4; **$^{**}P < 0.01$ *vs.* buffer week 4; $^{\#}P < 0.05$ *vs.* FA week 4 + SP600125 or FA week 4 + SIS3. Data are mean ± SD (n = 6/group).

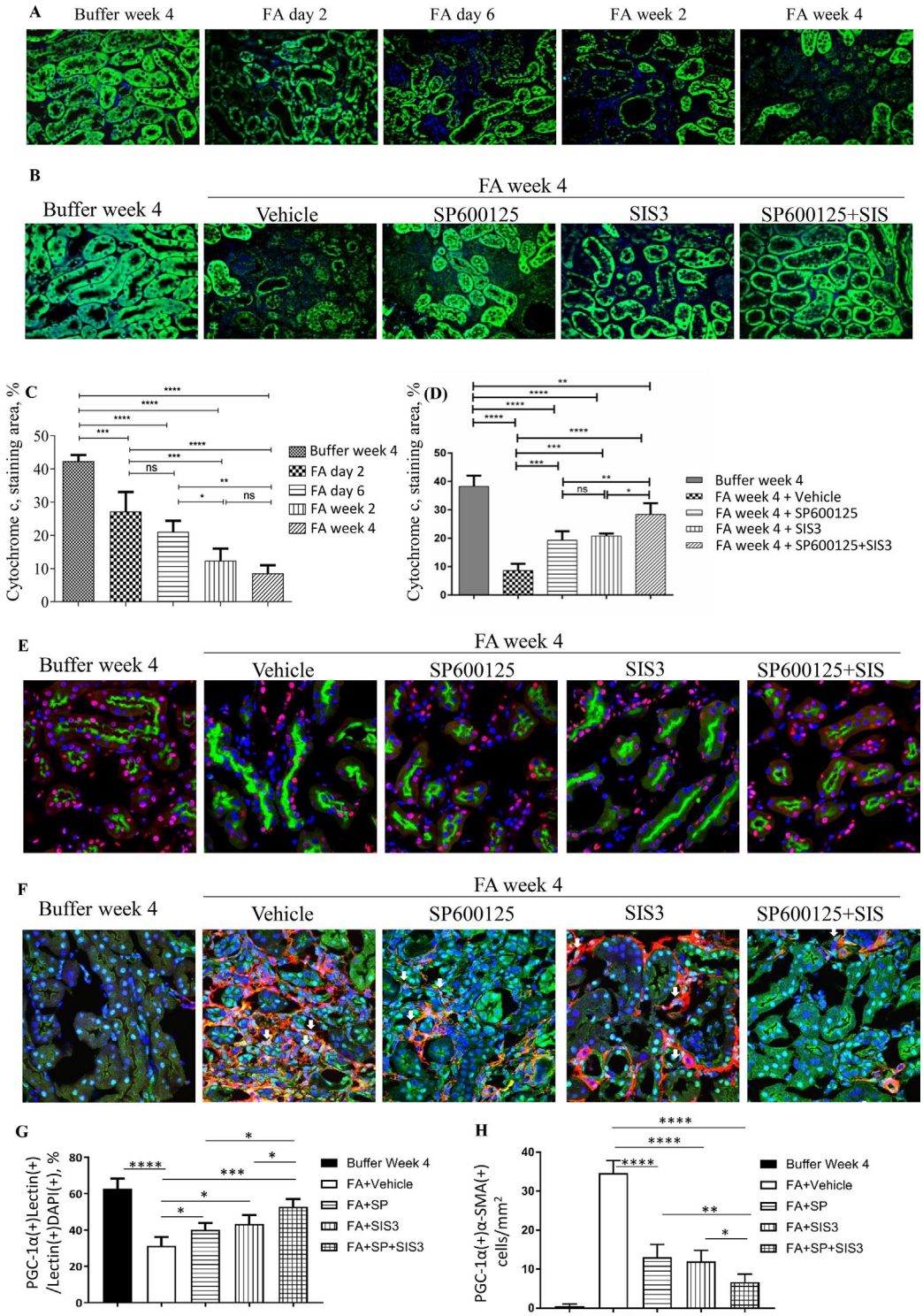

FIGURE 8 | Inhibition of Smad3 and/or JNK signaling reduces mitochondrial dysfunction in folic acid (FA)–induced kidney injury. Confocal microscopy shows cytochrome c (green) and nuclear staining DAPI (blue) in buffer-treated or FA-treated kidneys **(A)** and in kidneys 4 weeks after buffer or FA injection and treated with vehicle, SP600125 (SP), SIS3, or SP+SIS3 **(B)**. Quantification of staining area of cytochrome c **(C** and **D)**. Data are mean ± SD (n = 6/group), *$P < 0.05$; **$P < 0.01$; ***$P < 0.001$; ****$P < 0.0001$. **(E)** Confocal microscopy showing staining of lectin in tubular epithelial cells (green), PGC-1α (red), and nuclear staining DAPI (blue) in kidneys 4 weeks after buffer or folic acid injection and treated with vehicle, SP600125 (SP), SIS3, or SP+SIS3. **(F)** Confocal microscopy showing staining of PGC-1α (green) in myofibroblasts (red), and nuclear staining DAPI (blue) in kidneys 4 weeks after buffer or folic acid injection and treated with vehicle, SP600125 (SP), SIS3, or SP+SIS3. **(G)** Quantification of percentages of PGC-1α(+)lectin(+) cells in total lectin(+)DAPI(+) cells. **(H)** Quantification of numbers of PGC-1α(+)α-smooth muscle actin (α-SMA)(+) cells/mm^2. Data are mean ± SD (n = 6/group). *$P < 0.05$; **$P < 0.01$; ***$P < 0.001$; ****$P < 0.0001$.

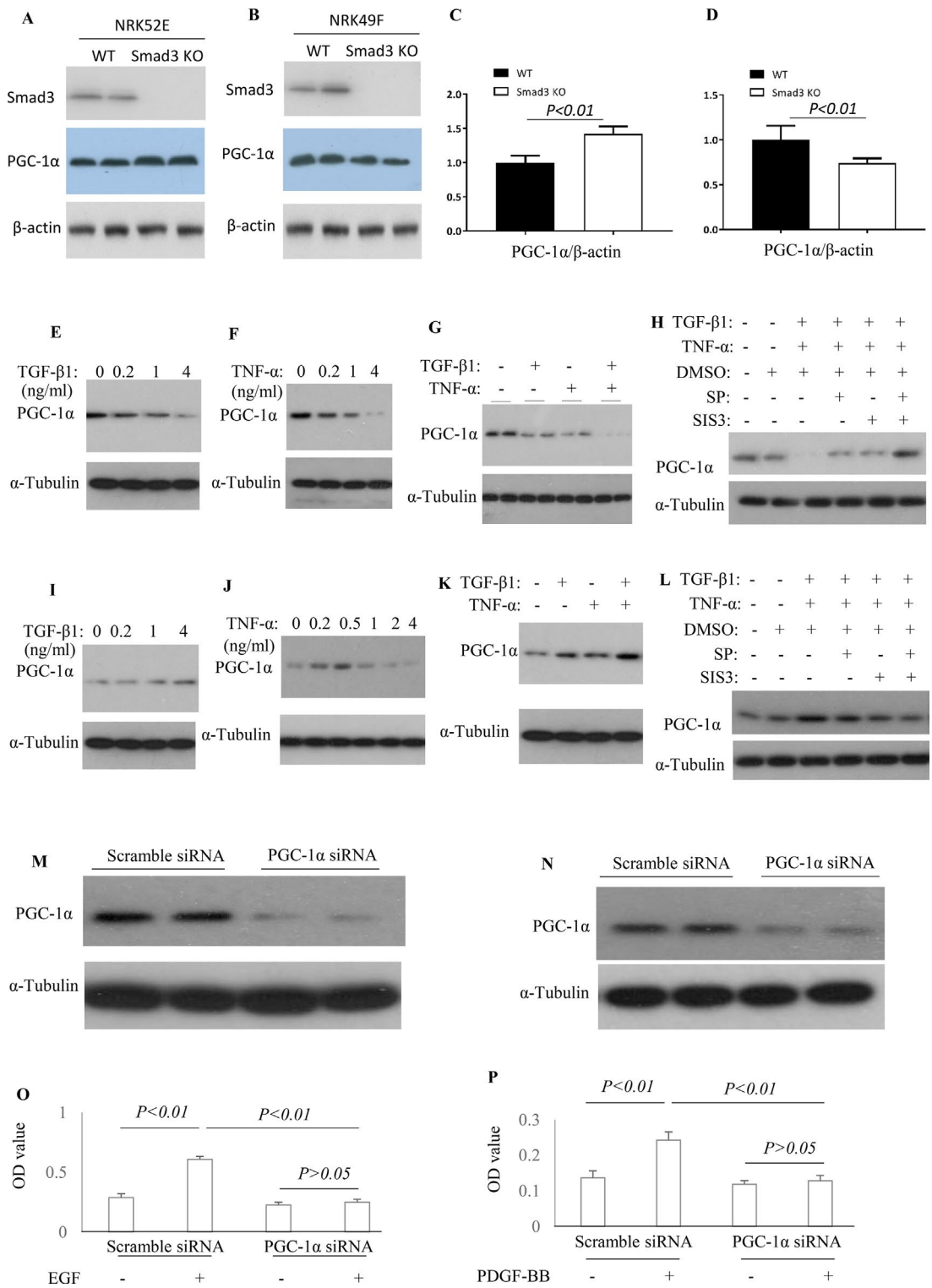

FIGURE 9 | Differential effect of JNK and Smad3 inhibition on PGC-1α expression and proliferation in renal tubular epithelial cells *versus* fibroblasts. Western blotting demonstrated expression of Smad3, PGC-1α, and β-actin in wild type (WT) and *Smad3*$^{-/-}$ NRK52E cells **(A)** and NRK49F cells **(B)**. Quantification of PGC-1α/β-actin in NRK52E cells **(C)** and NRK49F cells **(D)**. Western blotting identifies PGC-1α expression levels in NRK52E tubular epithelial cells **(E–H)** and NRK49F fibroblasts **(I–L)** after TGF-β1 and/or TNF-α treatment, with or without addition of SP600125 (SP) and/or SIS3. Experiments were repeated three times. Western blotting demonstrates a marked knock-down of PGC-1α by siRNA treatment in both NRK52E tubular epithelial cells **(M)**, and NRK49F fibroblasts **(N)**. Quantification of EGF-induced proliferation of NRK52E cells **(O)** and of PDGF-BB induced proliferation of NRK49F cells **(P)**, following scramble or PGC-1α siRNA treatment. Data are mean ± SD. Experiments were repeated three times.

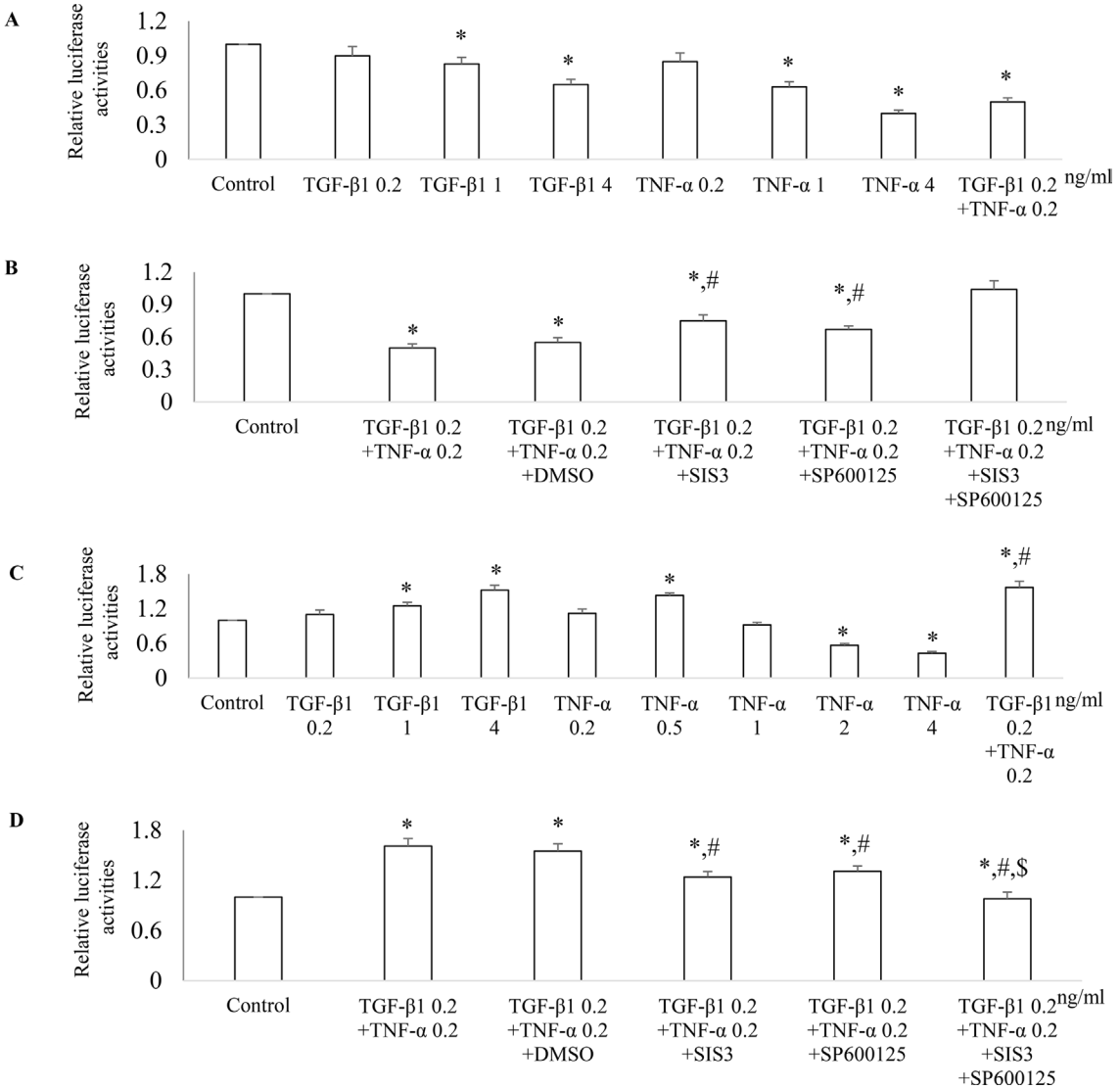

FIGURE 10 | Differential effect of JNK and Smad3 inhibition on PGC-1α promoter activity in renal tubular epithelial cells *versus* fibroblasts. NRK52E tubular epithelial cells **(A** and **B)** and NRK49F fibroblasts **(C** and **D)** were transfected with a PGC-1α promoter luciferase plasmid. 24 h after transfection, NRK52E cells **(A)** and NRK49F cells **(C)** were treated with TGF-β1 and/or TNF-α for 18 h then luciferase activity assay was performed. *$P < 0.05$ *vs.* control; #$P < 0.05$ *vs.* TGF-β1 0.2 ng/ ml. 24 h after transfection, NRK52E cells **(B)** and NRK49F cells **(D)** were incubated with vehicle (DMSO), SIS3 1 μM, or/and SP600125 10 μM for 30 min then treated with or without TGF-β1 and/or TNF-α for 18 h. The cells were harvested, and the luciferase activity assay was performed. Data are mean ± SD. *$P < 0.05$ *vs.* control; #$P < 0.05$ *vs.* TGF-β1 0.2 ng/ml + TNF-α 0.2 ng/ml; $$P < 0.05$ *vs.* TNF-α 0.2 ng/ml + TGF-β1 0.2 ng/ml + SP600125 or TNF-α 0.2 ng/ml + TGF-β1 0.2 ng/ml + SIS3. Experiments were repeated three times.

and AP-1 binding sequence and other transcription factor binding sequence on the PGC-1α promoter (Handschin et al., 2003). In the present study, we demonstrated that TGF-β1 or TNF-α modulated PGC-1α promoter activity in a cellular type-dependent fashion, suggesting that other factors in the transcription complex are involved which either enhance or block transcription. Blockade of both Smad3 and JNK signaling pathways increased or decreased PGC-1α transcriptional activities in tubular epithelial cells or fibroblasts, respectively, further supported the notion that blockade of both JNK and Smad3 signaling pathways provides better protection from progressive tubulointerstitial damage than single blockade.

In conclusion, our studies demonstrated that blockade of both JNK and Smad3 signalings achieved better protection from FA-induced progressive renal tubulointerstitial damage than single blockade. Inhibition of Smad3 and JNK signaling decreased cytosol cytochrome c production and apoptosis, modulated PGC-1α expression and mitochondrial metabolism, promoted tubular recovery, and reduced fibroblast accumulation. Our study suggested that blockade of both JNK and Smad3 signaling pathways may be a novel therapeutic strategy for progressive CKD.

DATA AVAILABILITY

All datasets generated for this study are included in the manuscript.

ETHICS STATEMENT

This study was carried out in accordance with the recommendations of the Human Ethics Committee of Monash Medical Centre and the Human Ethics Committee of the 1st Affiliated Hospital, Sun Yat-sen University with written informed consent from all subjects. All subjects gave written informed consent in accordance with the Declaration of Helsinki. The protocol was approved by the Human Ethics Committee of Monash Medical Centre and the Human Ethics Committee of the 1st Affiliated Hospital, Sun Yat-sen University. This animal study was carried out in accordance with the recommendations of the Sun Yat-sen University Animal Ethics Committee. The protocol was approved by the the Sun Yat-sen University Animal Ethics Committee.

AUTHOR CONTRIBUTIONS

Conceived and designed the experiments: JL. Performed the experiments: MJ, JF, XQ, SL, YS, YC, JL. Analyzed the data: MJ, JF, XQ, SL, SN, YS, YC, DY, DL, B-CL, MT, WC, YR, DN-P, XJ, JL, XY. Contributed reagents/materials/analysis tools: JL. Wrote the paper: JL, DN-P.

FUNDING

This study was supported by the National Natural Scientific Foundation of China (NSFC No. 81670667 to JL, 81670648 to XJ, 81800605 to MJ and 81600513 to DL), Guangdong Medical University of Provincial and Municipal Construction of Colleges and Universities Project (NO. 4SG18001Ga to JL) and the National Health and Medical Research Council (NHMRC) of Australia (APP1057581 to JL). MJ was supported by the International Program for Ph.D. Candidates, Sun Yat-sen University. DN-P has previously received funding from Celgene for studies of JNK inhibitors. The funder played no part in this study.

ACKNOWLEDGMENTS

Confocal imaging was performed at the Monash Micro Imaging Facility, and histology was performed at the Monash Histology Platform. The Australian Regenerative Medicine Institute is supported by grants from the State Government of Victoria and the Australian Government.

REFERENCES

Aubrey, B. J., Kelly, G. L., Kueh, A. J., Brennan, M. S., O'Connor, L., Milla, L., et al. (2015). An inducible lentiviral guide RNA platform enables the identification of tumor-essential genes and tumor-promoting mutations *in vivo*. *Cell. Rep.* 10 (8), 1422–1432. doi: 10.1016/j.celrep.2015.02.002

Chung, K. Y., Agarwal, A., Uitto, J., and Mauviel, A. (1996). An AP-1 binding sequence is essential for regulation of the human alpha2(I) collagen (COL1A2) promoter activity by transforming growth factor-beta. *J. Biol. Chem.* 271, 3272–3278. doi: 10.1074/jbc.271.6.3272

De Borst, M. H., Prakash, J., Melenhorst, W. B., van den Heuvel, M. C., Kok, R. J., Navis, G., et al. (2007). Glomerular and tubular induction of the transcription factor c-Jun in human renal disease. *J. Pathol.* 213 (2), 219–228. doi: 10.1002/path.2228

Drosatos, K., Drosatos-Tampakaki, Z., Khan, R., Homma, S., Schulze, P. C., Zannis, V. I., et al. (2011). Inhibition of c-Jun-N-terminal kinase increases cardiac peroxisome proliferator-activated receptor alpha expression and fatty acid oxidation and prevents lipopolysaccharide-induced heart dysfunction. *J. Biol. Chem.* 286, 36331–36339. doi: 10.1074/jbc.M111.272146

Feng, X. H., and Derynck, R. (2005). Specificity and versatility in tgf-beta signaling through Smads. *Annu. Rev. Cell. Dev. Biol.* 21, 659–693. doi: 10.1146/annurev.cellbio.21.022404.142018

Funk, J. A., and Schnellmann, R. G. (2012). Persistent disruption of mitochondrial homeostasis after acute kidney injury. *Am. J. Physiol. Renal Physiol.* 302, F853–F864. doi: 10.1152/ajprenal.00035.2011

Funk, J. A., and Schnellmann, R. G. (2013). Accelerated recovery of renal mitochondrial and tubule homeostasis with SIRT1/PGC-1alpha activation following ischemia-reperfusion injury. *Toxicol. Appl. Pharmacol.* 273, 345–354. doi: 10.1016/j.taap.2013.09.026

Hallman, M. A., Zhuang, S., and Schnellmann, R. G. (2008). Regulation of dedifferentiation and redifferentiation in renal proximal tubular cells by the epidermal growth factor receptor. *J. Pharmacol. Exp. Ther.* 325, 520–528. doi: 10.1124/jpet.107.134031

Handschin, C., Rhee, J., Lin, J., Tarr, P. T., and Spiegelman, B. M. (2003). An autoregulatory loop controls peroxisome proliferator-activated receptor gamma coactivator 1alpha expression in muscle. *Proc. Natl. Acad. Sci. U. S. A.* 100 (12), 7111–7116. doi: 10.1073/pnas.1232352100

Hickey, F. B., Corcoran, J. B., Docherty, N. G., Griffin, B., Bhreathnach, U., Furlong, F., et al. (2011). IHG-1 promotes mitochondrial biogenesis by stabilizing PGC-1alpha. *J. Am. Soc. Nephrol.* 22, 1475–1485. doi: 10.1681/ASN.2010111154

Kaballo, M. A., Elsayed, M. E., and Stack, A. G. (2017). Linking acute kidney injury to chronic kidney disease: the missing links. *J. Nephrol.* 30 (4), 461–475. doi: 10.1007/s40620-016-0359-5

Li, P., Nijhawan, D., Budihardjo, I., Shibata, T., and Yasuhiko, Y. (1997). Cytochrome c and dATP-dependent formation of Apaf-1/caspase-9 complex initiates an apoptotic protease cascade. *Cell* 91, 479–489. doi: 10.1016/S0092-8674(00)80434-1

Li, J., Campanale, N. V., Liang, R. J., Deane, J. A., Bertram, J. F., and Ricardo, S. D. (2006). Inhibition of p38 Mitogen-Activated Protein Kinase and Transforming Growth Factor-β1/Smad Signaling Pathways Modulates the Development of Fibrosis in Adriamycin-Induced Nephropathy. *Am. J. Pathol.* 169 (5), 1527–1540. doi: 10.2353/ajpath.2006.060169

Li, J., Qu, X., Ricardo, S. D., Bertram, J. F., and Nikolic-Paterson, D. J. (2010). Resveratrol inhibits renal fibrosis in the obstructed kidney: potential role in deacetylation of Smad3. *Am. J. Pathol.* 177, 1065–1071. doi: 10.2353/ajpath.2010.090923

Li, J., Qu, X., Yao, J., Caruana, G., Ricardo, S. D., Yamamoto, Y., et al. (2010). Blockade of endothelial-mesenchymal transition by a Smad3 inhibitor delays the early development of streptozotocin-induced diabetic nephropathy. *Diabetes.* 59 (10), 2612–2624. doi: 10.2337/db09-1631

Liang, J., Yang, Y., Zhu, X., Wang, X., and Chen, R. (2010). Down-expression of PGC-1alpha partially mediated by JNK/c-Jun through binding to CRE site during apoptotic procedure in cerebellar granule neurons. *J. Neurosci. Res.* 88, 1918–1925. doi: 10.1002/jnr.22354

Lin, J., Handschin, C., and Spiegelman, B. M. (2005). Metabolic control through the PGC-1 family of transcription coactivators. *Cell Metab.* 1, 361–370. doi: 10.1016/j.cmet.2005.05.004

Ma, F. Y., Flanc, R. S., Tesch, G. H., Han, Y., Atkins, R. C., Bennett, B. L., et al. (2007). A pathogenic role for c-Jun amino-terminal kinase signaling in renal fibrosis and tubular cell apoptosis. *J. Am. Soc. Nephrol.* 18 (2), 472–484. doi: 10.1681/ASN.2006060604

Picken, M., Long, J., Williamson, G. A., and Polichnowski, A. J. (2016). Progression of chronic kidney disease after acute kidney injury: role of self-perpetuating versus hemodynamic-induced fibrosis. *Hypertension.* 68 (4), 921–928. doi: 10.1161/HYPERTENSIONAHA.116.07749

Puigserver, P., Wu, Z., Park, C. W., Graves, R., Wright, M., and Spiegelman B. M. (1998). A cold-inducible coactivator of nuclear receptors linked to adaptive thermogenesis. *Cell* 92 (6), 829–839. doi: 10.1016/S0092-8674(00)81410-5

Qu, X., Zhang, X., Yao, J., Song, J., Nikolic-Paterson, D. J., and Li, J. (2012). Resolvins E1 and D1 inhibit interstitial fibrosis in the obstructed kidney *via* inhibition of local fibroblast proliferation. *J. Pathol.* 228, 506–519. doi: 10.1002/path.4050

Ralto, K. M., and Parikh, S. M. (2016). Mitochondria in Acute Kidney Injury. *Semin. Nephrol.* 36, 8–16. doi: 10.1016/j.semnephrol.2016.01.005

Rasbach, K. A., and Schnellmann, R. G. (2007). PGC-1alpha over-expression promotes recovery from mitochondrial dysfunction and cell injury. *Biochem. Biophys. Res. Commun.* 355, 734–739. doi: 10.1016/j.bbrc.2007.02.023

Ruiz-Andres, O., Suarez-Alvarez, B., Sanchez-Ramos, C., Monsalve, M., Sanchez-Niño, M. D., Ruiz-Ortega, M., et al. (2016). The inflammatory cytokine TWEAK decreases PGC-1alpha expression and mitochondrial function in acute kidney injury. *Kidney Int.* 89, 399–410. doi: 10.1038/ki.2015.332

Sato, M., Muragaki, Y., Saika, S., Roberts, A. B., and Ooshima, A. (2003). Targeted disruption of TGF-beta1/Smad3 signaling protects against renal tubulointerstitial fibrosis induced by unilateral ureteral obstruction. *J. Clin. Invest.* 112 (10), 1486–1494. doi: 10.1172/JCI200319270

Sjostrand, F., and Rhodin, J. (1953). The ultrastructure of the proximal convoluted tubules of the mouse kidney as revealed by high resolution electron microscopy. *Exp. Cell. Res.* 4 (2), 426–456. doi: 10.1016/0014-4827(53)90170-0

Sun, Y. B., Qu, X., Howard, V., Dai, L., Jiang, X., Ren, Y., et al. (2015). Smad3 deficiency protects mice from obesity-induced podocyte injury that precedes insulin resistance. *Kidney Int.* 88, 286–298. doi: 10.1038/ki.2015.121

Tabara, L. C., Poveda, J., Martin-Cleary, C., Selgas, R., Ortiz, A., and Sanchez-Niño, M. D. (2014). Mitochondria-targeted therapies for acute kidney injury. *Expert. Rev. Mol. Med.* 16, e13. doi: 10.1017/erm.2014.14

Takaori, K., and Yanagita, M. (2016). Insights into the Mechanisms of the Acute Kidney Injury-to-Chronic Kidney Disease Continuum. *Nephron.* 134 (3), 172–176. doi: 10.1159/000448081

Tan, C. K., Leuenberger, N., Tan, M. J., Yan, Y. W., Chen, Y., Kambadur, R., et al. (2011). Smad3 deficiency in mice protects against insulin resistance and obesity induced by a high-fat diet. *Diabetes* 60, 464–476. doi: 10.2337/db10-0801

Thadhani, R., Pascual, M., and Bonventre, J. V. (1996). Acute renal failure. *N. Engl. J. Med.* 334 (22), 1448–1460. doi: 10.1056/NEJM199605303342207

Tournier, C., Hess, P., Yang, D. D., Xu, J., Turner, T. K., Nimnual, A., et al. (2000). Requirement of JNK for stress-induced activation of the cytochrome c-mediated death pathway. *Science* 288, 870–874. doi: 10.1126/science.288.5467.870

Tran, M., Tam, D., Bardia, A., Bhasin, M., Rowe, G. C., Kher, A., et al. (2011). PGC-1alpha promotes recovery after acute kidney injury during systemic inflammation in mice. *J. Clin. Invest* 121, 4003–4014. doi: 10.1172/JCI58662

Weidemann, M. J., and Krebs, H. A. (1969). The fuel of respiration of rat kidney cortex. *Biochem. J.* 112 (2), 149–166. doi: 10.1042/bj1120149

Wu, Z., Puigserver, P., Andersson, U., Zhang, C., Adelmant, G., Mootha, V., et al. (1999). Mechanisms controlling mitochondrial biogenesis and respiration through the thermogenic coactivator PGC-1. *Cell.* 98 (1), 115–124. doi: 10.1016/S0092-8674(00)80611-X

Yadav, H., Quijano, C., Kamaraju, A. K., Gavrilova, O., Malek, R., Chen, W., et al. (2011). Protection from obesity and diabetes by blockade of TGF-beta/Smad3 signaling. *Cell. Metab.* 14, 67–79. doi: 10.1016/j.cmet.2011.04.013

Yu, L., Liu, Y., Wu, Y., Liu, Q., Feng, J., Gu, X., et al. (2014). Smad3/Nox4-mediated mitochondrial dysfunction plays a crucial role in puromycin aminonucleoside-induced podocyte damage. *Cell Signal* 26, 2979–2991. doi: 10.1016/j.cellsig.2014.08.030

Yuan, Y., Huang, S., Wang, W., Wang, Y., Zhang, P., Zhu, C., et al. (2012). Activation of peroxisome proliferator-activated receptor-gamma coactivator 1alpha ameliorates mitochondrial dysfunction and protects podocytes from aldosterone-induced injury. *Kidney Int.* 82, 771–789. doi: 10.1038/ki.2012.188

Zou, H., Henzel, W. J., Liu, X., Lutschg, A., and Wang, X. (1997). Apaf-1, a human protein homologous to C. elegans CED-4, participates in cytochrome c-dependent activation of caspase-3. *Cell* 90, 405–413. doi: 10.1016/S0092-8674(00)80501-2.

Conflict of Interest Statement: The authors declare that the research was conducted in the absence of any commercial or financial relationships that could be construed as a potential conflict of interest.

Copyright © 2019 Jiang, Fan, Qu, Li, Nilsson, Sun, Chen, Yu, Liu, Liu, Tang, Chen, Ren, Nikolic-Paterson, Jiang, Li and Yu. This is an open-access article distributed under the terms of the Creative Commons Attribution License (CC BY). The use, distribution or reproduction in other forums is permitted, provided the original author(s) and the copyright owner(s) are credited and that the original publication in this journal is cited, in accordance with accepted academic practice. No use, distribution or reproduction is permitted which does not comply with these terms.

frontiers in Pharmacology

ORIGINAL RESEARCH
published: 20 August 2019
doi: 10.3389/fphar.2019.00928

Metabolomics Study of Metabolic Changes in Renal Cells in Response to High-Glucose Exposure Based on Liquid or Gas Chromatography Coupled With Mass Spectrometry

Liang Wang[1,2†], Yan Du[1,3†], Bing-ju Xu[1†], Xu Deng[1], Qing-hua Liu[1], Qiao-qiao Zhong[1], Chen-xiang Wang[1], Shuai Ji[1,3], Meng-zhe Guo[1,3] and Dao-quan Tang[1,3]*

[1] Jiangsu Key Laboratory of New Drug Research and Clinical Pharmacy, School of Pharmacy, Xuzhou Medical University, Xuzhou, China, [2] Department of Bioinformatics, School of Medical Informatics, Xuzhou Medical University, Xuzhou, China, [3] Deparment of Pharmaceutical Analysis, School of Pharmacy, Xuzhou Medical University, Xuzhou, China

OPEN ACCESS

Edited by:
John D. Imig,
Medical College of Wisconsin,
United States

Reviewed by:
John William Newman,
United States Department of Agriculture, United States
Guoxiang Xie,
University of Hawaii Cancer Center, United States

***Correspondence:**
Dao-quan Tang
tangdq@xzhmu.edu.cn
tdq993@hotmail.com

[†]These authors contribute equally to the study

Specialty section:
This article was submitted to Renal Pharmacology, a section of the journal Frontiers in Pharmacology

Received: 17 April 2019
Accepted: 22 July 2019
Published: 20 August 2019

Citation:
Wang L, Du Y, Xu B-j, Deng X, Liu Q-h, Zhong Q-q, Wang C-x, Ji S, Guo M-z and Tang D-q (2019) Metabolomics Study of Metabolic Changes in Renal Cells in Response to High-Glucose Exposure Based on Liquid or Gas Chromatography Coupled With Mass Spectrometry. Front. Pharmacol. 10:928. doi: 10.3389/fphar.2019.00928

Diabetic nephropathy (DN) is one of the most serious microvascular complications and the leading causes of death in diabetes mellitus (DM). To find biomarkers for prognosing the occurrence and development of DN has significant clinical value for its prevention, diagnosis, and treatment. In this study, a non-targeted cell metabolomics–based ultra-performance liquid chromatography coupled with quadrupole time of flight mass spectrometry and gas chromatography coupled with mass spectrometry was developed and performed the dynamic metabolic profiles of rat renal cells including renal tubular epithelial cells (NRK-52E) and glomerular mesangial cells (HBZY-1) in response to high glucose at time points of 12 h, 24 h, 36 h, and 48 h. Some potential biomarkers were then verified using clinical plasma samples collected from 55 healthy volunteers, 103 DM patients, and 57 DN patients. Statistical methods, such as principal component analysis and partial least squares to latent structure-discriminant analysis were recruited for data analyses. As a result, palmitic acid and linoleic acid (all-cis-9,12) were the potential indicators for the occurrence and development of DN, and valine, leucine, and isoleucine could be used as the prospective biomarkers for DM. In addition, rise and fall of leucine and isoleucine levels in plasma could be used for prognosing DN in DM patients. Through this study, we established a novel non-targeted cell dynamic metabolomics platform and identified potential biomarkers that may be applied for the diagnosis and prognosis of DM and DN.

Keywords: dynamic metabolomics, diabetic nephropathy, diabetes mellitus, renal cell, biomarker identification

INTRODUCTION

Diabetic nephropathy (DN), with the characteristic of proteinuria, is one of the most serious microvascular complications in diabetes mellitus (DM) (Aldukhayel, 2017). The etiology and pathogenesis of DN are sophisticated and have not been fully elucidated yet. It is generally believed that, once formed, DN is difficult to be reversed. Thus, researchers have been committing to identify biologically specific biomarkers that can prognose DN in the stage of DM. Microalbuminuria is widely accepted as a clinically diagnostic indicator of early DN. However, relative studies have shown

that only about 30% of DM patients with microalbuminuria will eventually develop into DN (Rossing et al., 2005). A considerable number of DM patients with microalbuminuria can actually change back to non-proteinuria state (Perkins et al., 2003). Moreover, when excess protein is present in urine, severe structural changes in the glomerular basement membrane will occur, leading to serious kidney damage (Fioretto et al., 1994). Therefore, exploration of laboratory biomarkers that are earlier than microalbuminuria or those appearing at the same time has remarkable significance for the early diagnosis and treatment of DN.

Metabolomics is an analytical technique for studying metabolic pathways by examining the overall changes of small metabolites in body fluids or tissues after exogenous stimulation or gene mutation in biological systems. Among them, biomarker discovery and determination of content changes over disease formation and progression are often referred to as dynamic metabolomics (You et al., 2018), the development of which provides us with an important research strategy for exploring biomarkers in the early formation of DN. In the *in vivo* metabolomics study of animals and humans, differences between species are often significant, and these are easily disturbed by factors such as diet, environment, age, and other diseases. Thus, enabling high-throughput identification of potential biomarkers is rather difficult. In contrast, *in vitro* cell metabolomics can be easily regulated in terms of experimental conditions, by which protein expression, cell signaling, and metabolism in discrete physiological processes could have higher repeatability than animal or human experiments. *In vitro* cellular experiments also require fewer sample sizes, which can reduce the experimental costs. Cells are normally more tolerant to unfavorable environments, hence generation of more abundant metabolome information. Metabolomics studies of cell samples can dynamically monitor changes of metabolites during disease progression (Zhang et al., 2013; Acunha et al., 2018). Therefore, the use of cellular dynamic metabolomics, combined with multiple statistical analysis methods, to investigate the dynamic changes of potential biomarkers in the process of cell metabolism under normal conditions and pathological conditions becomes an important approach to explore the pathogenesis of diseases. Commonly used techniques in metabolomics include gas chromatography coupled with mass spectrometry (GC-MS), liquid chromatography tandem with mass spectrometry (LC-MS/MS), nuclear magnetic resonance (NMR), and capillary electrophoresis coupled with mass spectrometry (CE-MS), *etc*. (Chan et al., 2011). With the rapid development of high-resolution mass spectrometry, GC-MS and LC-MS/MS have become the mainstream technology in dynamic metabolomics (Smilde et al., 2010).

In DN, inflammatory lesions caused by high glucose, hemodynamic abnormalities, oxidative stress, and extracellular matrix accumulation can initially result in tubulointerstitial fibrosis and glomerulosclerosis, etc., which could then develop into kidney failure (Zheng et al., 2016). Mesangial cells, the main cells in the mesangial area, play an important role in maintaining the structural integrity of the glomerular microvascular bed, providing mesangial matrix homeostasis, and regulating glomerular filtration and can be selected as the major target cells in the study of DN (Qiu et al., 2015; Lu et al., 2018). On the other hand, in the process of tubulointerstitial fibrosis, the main effector cells are fibroblasts, and 36% of the newly added fibroblasts are derived from renal tubular epithelial cells (Forino et al., 2006; Li et al., 2015). Thus, we used two cell lines, rat renal tubular epithelial cells (NRK-52E), and glomerular mesangial cells (HBZY-1), as the objects in our study of dynamic metabolomics that are suitable to explore biomarkers in the occurrence and development of DN.

In this study, NRK-52E and HBZY-1 treated with high glucose were used as a model. Non-targeted metabolomics investigation of cells cultured *in vitro* at different time points were performed using ultra-performance liquid chromatography coupled with quadrupole time of flight mass spectrometry (UPLC-Q/TOF-MS/MS) and GC-MS. Moreover, in order to verify our initial screening results, clinical samples from healthy volunteers and DM and DN patients were used to quantify the levels of some identified biomarkers. According to our study, several novel biomarkers for prognosing DN in DM patients were identified, which may have the potential for further clinical applications.

MATERIALS AND METHODS

Chemicals, Reagents, and Materials

HPLC-grade methanol, acetonitrile, formic acid, and chloroform were purchased from MREDA (MA, USA). Low glucose (5.56 mmol/L) and high glucose (25 mmol/L) Gibco® Dulbecco's modified Eagle medium (DEME) were purchased from Nanjing KeyGen Biotech Co., Ltd. (Nanjing, China). Fetal bovine serum was purchased from Zhejiang Tianhang Biotechnology Co., Ltd. (Hangzhou, China).

Cell Culture

NRK-52E and HBZY-1 cells were purchased form Cell Bank of Chinese Academy of Science (Shanghai, China). They were initially cultured in low-dose glucose DEME medium including 10% fetal bovine serum (v/v), 100 U/ml penicillin, and 100 μg/ml streptomycin at 37°C with 5% CO_2. When the cell density reached approximately 80% or 90% confluence, the original culture solution was discarded. Cells were washed twice with 2 ml phosphate-buffered saline (PBS) buffer. 2.5% (v/v) trypsin (Vicmed, China) is gently tilted to make the cells immersed in the solution for complete digestion. Cells were then centrifuged at 1,000 rpm for 3 min after adding 2 ml DEME medium, and supernatants were discarded. Cells were then resuspended in 8 ml DEME medium and transferred to 50-ml centrifuge tube. Cell density was adjusted to around 0.5×10^5/ml to 1×10^5/ml with low glucose DEME medium and mixed by gently blowing. Then, 2 ml of cell suspension were respectively added to each well of two six-well plates and placed in cell culture incubator (Thermo Scientific Forma 3111 Water Jacketed CO_2 Incubator). After culturing for 12 h, the two plates were given high glucose (HG group, n = 6) and low glucose (LG group, n = 6) DMEM medium containing 1% (v/v) fetal bovine serum, respectively, which

were continuously cultured for 12, 24, 36, and 48 h until cellular extracts were measured. Cell morphologies were observed under light microscope.

Sample Preparation for Metabolomic Study

For LC-MS, cells were harvested at each time point and rinsed with normal saline for three times. Liquid nitrogen was then added to quench the cells immediately. Quenched cells were rinsed by methanol-water solution (4:1 v/v) and then transferred to 1.5-ml centrifuge tubes with repeated freezing and thawing for six times in liquid nitrogen and 37°C water bath. After centrifugation at 12,000 rpm for 2 min, 800 μl supernatant and 200 μl methanol-water solution (4:1 v/v) were mixed, which was then vortexed for 30 s and centrifuged at 12,000 rpm, 4°C for 10 min. Two-microliter sample was injected into UPLC-Q/TOF-MS for further analysis. For GC-MS, cells were quenched as described above. 800 μl of supernatant from cell extract was freeze-dried and then mixed with 50 μl methoxyamine hydrochloride (MOX) pyridine solution (15 mg/ml). After 60°C oil bath for 2 h, 100 μl *N,O*-bis(trimethylsilyl)trifluoroacetamide (BSTFA) [containing 1% trimethylchlorosilane (TMCS)] was then added to the mixed solution. After 1-min vortex and 60-min oil bath (65°C), the mixed solution was centrifuged at 10,000 rpm for 10min and then injected for GC-MS analysis. At each time point, there will be a set of quality control samples, which were obtained by mixing cell extracts from three-well low-dose glucose and three-well high-dose glucose DMEM media, respectively.

LC-MS Metabolic Profiling Analysis

UPLC-Q/TOF-MS/MS analysis was carried out using a 1290 system from Agilent (Agilent Technologies, Santa Clara, CA, USA) coupled with a quadrupole-time-of-flight mass spectrometer Agilent 6550 equipped with an orthogonal electrospray ionization (ESI) source (Agilent Jet Stream, AJS). The metabolomic profiling analysis was performed on a Fortis column (2.1 × 100 mm, 1.7 μm) using 0.1% (v/v) formic acid water solution (A) and 0.1% (v/v) formic acid acetonitrile solution (B) as mobile phase with a gradient program as follows: 5–45% B in 0–3 min, 45–65% B in 3–10 min, 65–95% B in 10–12 min, and 95% B in 12–14 min. Before each run, columns were re-equilibrated for 11 min using the initial solvent composition. The flow rate was set constant at 0.3 ml/min, and the column temperature was maintained at 40°C for all separations. Two microliters of samples solution were injected for each analysis, and metabolic profiling analyses were achieved in positive mode. MS operation conditions were as follows: capillary voltages, 4,000 V; nebulizer pressure, 28 psi; nozzle voltage, 300 V; drying gas flow rate, 12 L/min, drying gas temperature, 350°C; sheath gas temperature, 400°C; and sheath gas flow, 12 L/min. All analyses were performed in full-scan mode, and acquisition mass range was from m/z 50 to m/z 1,000.

GC-MS Metabolic Profiling Analysis

GC-MS analysis was performed using an Agilent 7890A GC system coupled to an Agilent 5975C single-quadrupole mass spectrometer equipped with electron ionization (EI). The metabolomic profiling analysis was performed on an Agilent HP-5MS-UI column (60 m× 0.25 mm i.d., liquid film thickness of 0.25 μm). Helium was used as carrier gas with a flow rate of 1.0 ml/min. The injector temperature was 280°C, and the prepared sample (1 μl) was injected in the splitless mode. The initial column temperature was maintained at 70°C for 1 min, then increased at a rate of 10°C/min to 150°C and held at this temperature for 2 min, then increased at a rate of 20°C/min to 300°C and held at this temperature for 6.5 min. The EI source energy was set at 70 eV, and full-scan range was form m/z 40 to m/z 600. The source temperature was set at 230°C. Mass spectral signals were recorded after a 5.5-min solvent delay to avoid derivatization interferences.

Clinical Validation of Some Potential Biomarkers

Sample Collection

Three cohorts of adults were recruited from the 2nd Affiliated Hospital of Xuzhou Medical University, which included 55 healthy volunteers (21 males and 34 females), 103 DM patients (54 males and 49 females), and 57 DN patients (25 males and 32 females), diagnosed by clinical physician by the fasting plasma glucose and urine protein levels according to WHO criteria. Other relevant diseases are excluded through the collection of medical history and routine laboratory biochemical tests, such as malignant tumors, active bleeding, peptic ulcers, and hepatic failure, *etc*. Biochemical indicators of DM and DN patients were checked on the test day by searching patient's hospital admission number. Biochemical indicators of healthy volunteers (NC group) were obtained by looking up corresponding physical examination reports. Relevant information such as gender, age, systolic blood pressure, diastolic blood pressure, blood glucose (BG), high-density lipoprotein cholesterol (HDLc), low-density lipoprotein cholesterol (LDLc), triglyceride (TG), total cholesterol (TC), creatinine (CREA), and urea is thoroughly collected. For detailed analysis of biochemical indicators, please refer to **Supplementary Table S1**. During research, the medication or treatment of patients from the clinical physician were not intervened. 2 ml of EDTA-anticoagulated fasting whole-blood samples collected from the upper limb vein of the subjects were centrifuged at 3,000 rpm for 10 min, and supernatants were transferred to 2 ml Eppendorf (EP) tube, which were then transported to -80°C freezer on ice pack for storage. The study was approved by the Medical Ethics Committee of Xuzhou Medical University and its 2nd affiliated hospital (Approval number: XYFY2016-KL088). All patients provided written informed consent.

The pre-column derivatization combined with GC-MS was used for the quantification of selected fatty acids and amino acids in human plasma referred to our previous method (Du et al., 2019) with a slight modification. The detailed characters of GC-MS were listed in the Supplementary Materials.

MS Data Processing and Statistical Analysis

For cell metabolomics, raw LC-MS and GC-MS data were processed using Agilent Mass Hunter, GC-MSD Analysis, and ProFinder 6.0. Alignment of drift (by retention time and mass)

and data filtering were performed with Mass Profiler Professional (MPP, version 14.5, Agilent Technologies). Principal component analysis (PCA) and partial least squares to latent structure–discriminant analysis (PLS-DA) were recruited by MPP for pattern discriminant analyses. Metabolites and structures of potential biomarkers were identified by using METLIN and NIST 11.0 database. A p-value <0.05 was considered significant to select metabolites.

For quantitative analysis of potential biomarkers in clinical samples, the general condition, biochemical data, and linear discriminant analysis (LDA) were processed by SPSS l6.0. CREA was expressed by mean (min-max). Other measurement data were assessed by mean ± standard deviation (SD). Gender statistics was applied to χ^2 test, and the remaining indicators were analyzed by one-way ANOVA.

RESULTS

In the present study, a multiplatform metabolomics study has been carried out using UHPLC-Q/TOF-MS/MS and GC-MS to investigate dynamic metabolite changes in renal cells in response to high glucose. Some potential biomarkers obtained in metabolomics were simply validated using clinical sample.

Effects of HG Interventions on Cell Morphologies

NRK-52E and HBZY-1 cells were cultured as previously described and exposed to by HG and LG media for 12, 24, 36, and 48 h, respectively. Effects of glucose interventions on NRK-52E and HBZY-1 cell morphologies were studies at each time point. It was observed under the light microscope that there are no significant changes in the morphologies of NRK-52E and HBZY-1 cells in LG group, inferring that low glucose medium might not affect cell growth and metabolism. In contrast, shape distortion and cell debris were observed in HG groups, which suggests that the HG medium has effects on growth and metabolism of the two types of cells with a probable time-dependent manner (**Supplementary Figure S1** and **Figure S2**). However, further metabolomics methods should be used for validating these observations.

Effects of HG and LG Interventions on Metabolic Profiles of NRK-52E and HBZY-1 Cells Based on Optimized UPLC-Q/TOF-MS or GC-MS

The QC data were illustrated in **Supplementary Figure S3** and **Figure S4**. The chromatograms showed that the overlap of six QC samples was good, and the variation of retention time and peak response was little, and 3D-PCA score plot showed that QC samples were centralized in the same quarter, which meant that the developed LC-MS and GC-MS methods were suitable for the metabolomics study of renal cells.

Typical LC-MS and GC-MS chromatograms of NRK-52E and HBZY-1 cells in response to LG and HG were shown in **Supplementary Figures S5–S8**. It can be seen that the metabolites of NRK-52E and HBZY-1 cells from HG and LG media at each time point have multiple differences. The results from unsupervised PCA (**Supplementary Figures S9–S12**) showed that the obvious separation trend between HG samples and LG samples could be found at every time points, which hinted that there were obvious difference between the metabolomic profiles of HG group and LG group.

The supervised PLS-DA model can effectively eliminate the effects of individual outliers and be predicted to characterize the contribution of each sample. Thus, PLS-DA was used to analyze the data obtained by LC-MS or GC-MS in this study. From **Figures 1** to **4**, spatial distributions of LG and HG sample points were obviously separated at each time point, suggesting that there were significant differences in terms of metabolite profiles between the two groups. For the data obtained by LC-MS, the predictive ability scores of PLS-DA model whether for NRK-52E or HBZY-1 cells were all 100%; while for the data obtained by GC-MS, the predictive ability scores of PLS-DA model were greater than 83.3% for NRK-52E and 66.6% for HBZY-1 (**Supplementary Tables S2–S5**), which indicated that the PLS-DA model was stable and reliable. Statistically differential metabolites with persistent changes between LG group and HG group at 12, 24, 36, and 48 h in the two cell lines were listed in **Table 1**. It can be seen that the increased compounds in HG group compared with LG group in NRK-52E from 12 h were ceramide (Cer, d18:0/12:0), Cer (d18:0/14:0), and Cer (d18:0/16:0). Compound phosphatidylethanolamine (PE, 16:0/0:0) and glycine had a decreasing trend from 24 h while Cer (d20:0/16:0), and isoleucine tended to increase. The compounds that continuously declined were hypoxanthine, phosphatidylserine (PS, 14:0/12:0), PS (20:0/0:0), and PS (16:0/16:0) while leucine, palmitic acid, and phosphatidylglycerol (PG, 20:5/0:0) kept increasing. As for the HBZY-1 cells, compound LysoPE (0:0/22:6) decreased from 24 h while PG (20:5/0:0), leucine, and valine increased persistently. The compounds oleic acid, stearic acid, linoleic acid, PG (15:1/15:0), Cer (t18:0/16:0), Cer (d18:0/14:0), glucose, and galactose had a continuous rise from 36 h while sphingosine C16 and PE (19:0/0:0) kept declining. These results were partly consistent with the previous finding (Jensen et al., 2019).

Clinical Verification of Biomarkers Identified in Cell Metabolomics

Because the quantitative method of potential biomarkers in human plasma was based on our previous method (Du et al., 2019), partial validation was performed, and validation data such as regression equation, correlation coefficient, linear range, and mass fraction corresponding to each fatty acid and amino acid were shown in **Supplementary Tables S6** and **S7**.

In order to effectively distinguish the three groups, data was analyzed using supervised LDA. Overall difference between the groups was distinguished by a linear combination of all compound characteristics, as shown in **Figure 5**. Each point in the figure represented a sample. The closer the sample points were, the closer the content of each compound was. The figure showed that the distribution of sample points in the NC, DM, and DN groups had a clear aggregation trend, while the sample points between the groups showed a good distinction.

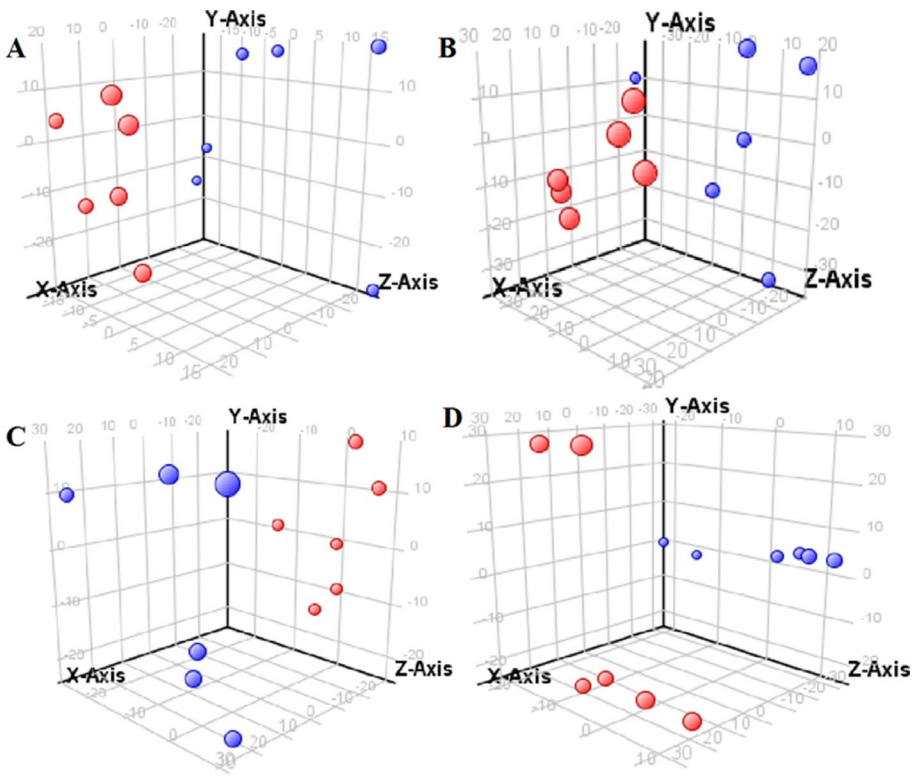

FIGURE 1 | Partial least-square discriminant analysis score plot for NRK-52E cells in response to high glucose (HG, 25 mmol/L, red dot) and low glucose (LG, 5.56 mmol/L, green dot) for 12 h **(A)**, 24 h **(B)**, 36 h **(C)**, and 48 h **(D)** using LC-MS data.

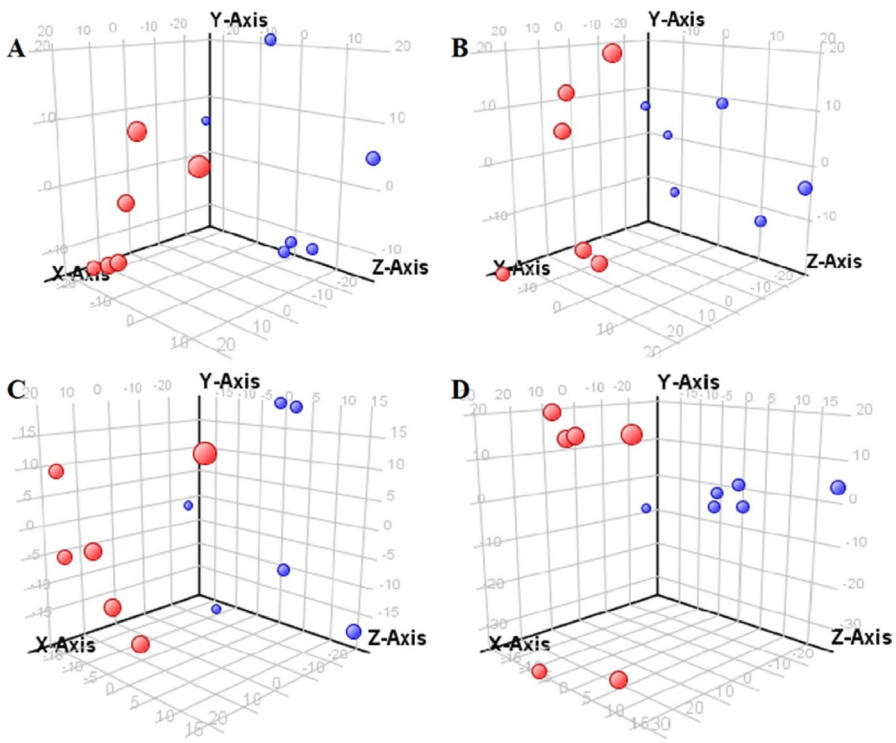

FIGURE 2 | Partial least-square discriminant analysis score plot for HBZY-1 cells in response to high glucose (HG, 25 mmol/L, red dot) and low glucose (LG, 5.56 mmol/L, green dot) for 12 h **(A)**, 24 h **(B)**, 36 h **(C)**, and 48 h **(D)** using LC-MS data.

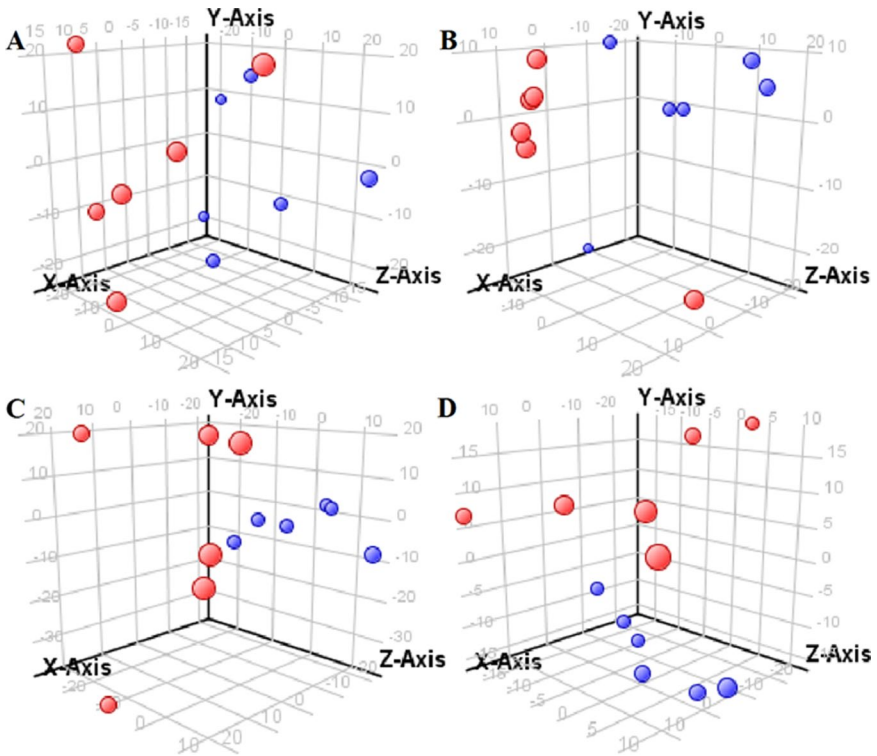

FIGURE 3 | Partial least-square discriminant analysis score plot for NRK-52E cells in response to high glucose (HG, 25 mmol/L, red dot) and low glucose (LG, 5.56 mmol/L, green dot) for 12 h **(A)**, 24 h **(B)**, 36 h **(C)**, and 48 h **(D)** using GC-MS data.

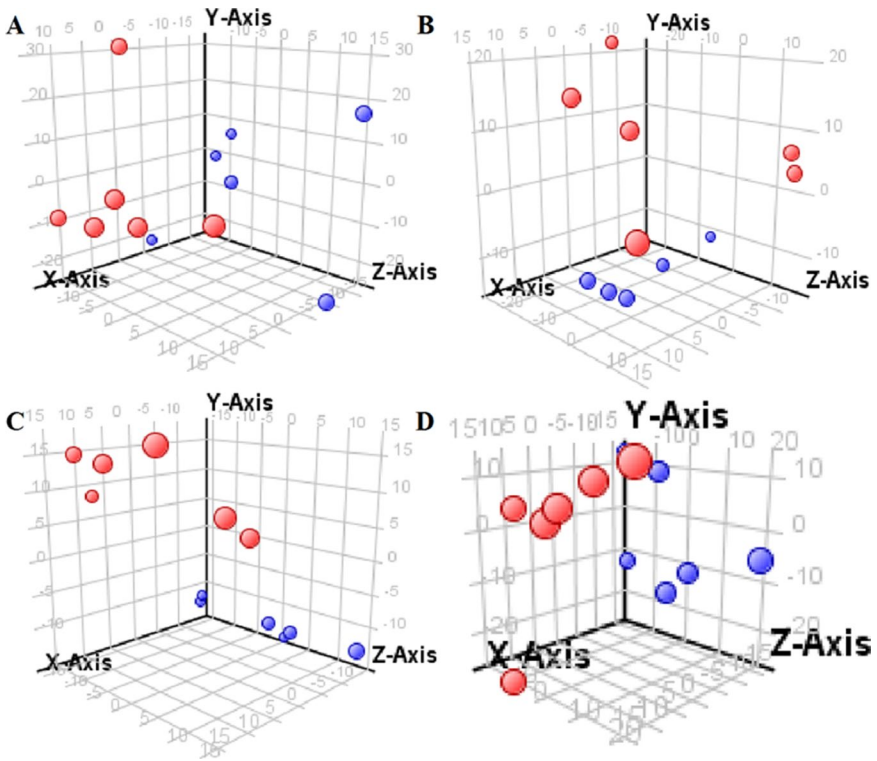

FIGURE 4 | Partial least-square discriminant analysis score plot for HBZY-1 cells in response to high glucose (HG, 25 mmol/L, red dot) and low glucose (LG, 5.56 mmol/L, green dot) for 12 h **(A)**, 24 h **(B)**, 36 h **(C)**, and 48 h **(D)** using GC-MS data.

TABLE 1 | The statistically differential metabolites with persistent changes from NRK-52E and HBZY-1 cells in response to high glucose at different time points based on UHPLC-Q/TOF-MS or GC-MS.

Renal cell	Class, subclass	Metabolites	Significances (*p* value, *vs*. low glucose)				Analytical method
			12 h	24 h	36 h	48 h	
	Amino acids						
	Branched chain AA	Leucine	NS [a]	NS	Up ($P < 0.01$)	Up ($P < 0.05$)	LC-MS
	Branched chain AA	Isoleucine	NS	Up ($P < 0.01$)	Up ($P < 0.01$)	Up ($P < 0.01$)	GC-MS
	AA	Glycine	NS	Down ($P < 0.01$)	Down ($P < 0.01$)	Down ($P < 0.01$)	GC-MS
	Fatty acids						
	FA (straight chain)	Palmitic acid	NS	NS	Up ($P < 0.01$)	Up ($P < 0.05$)	GC-MS
	Imidazopyrimidines						
	Purine derivatives	Hypoxanthine	NS	NS	Down ($P < 0.01$)	Down ($P < 0.01$)	LC-MS
NRK-52E	**Glycerophospholipids**						
	Glycerophosphoserine	PS (14:0/12:0)	NS	NS	Down ($P < 0.01$)	Down ($P < 0.01$)	LC-MS
	Glycerophosphoserine	PS (20:0/0:0)	NS	NS	Down ($P < 0.01$)	Down ($P < 0.01$)	LC-MS
	Glycerophosphoserine	PS (16:0/16:0)	NS	NS	Down ($P < 0.01$)	Down ($P < 0.01$)	LC-MS
	Diacylglycero phosphoglycerol	PG (20:5/0:0)	NS	NS	Up ($P < 0.01$)	Up ($P < 0.01$)	LC-MS
	Glycerophosphoethanolamine	PE (16:0/0:0)	NS	Down ($P < 0.01$)	Down ($P < 0.01$)	Down ($P < 0.01$)	LC-MS
	Sphingolipids						
	Ceramide	Cer (d20:0/16:0)	NS	Up ($P < 0.01$)	Up ($P < 0.01$)	Up ($P < 0.01$)	LC-MS
	Ceramide	Cer (d18:0/12:0)	Up ($P<0.01$)	Up ($P < 0.01$)	Up ($P < 0.01$)	Up ($P < 0.01$)	LC-MS
	Ceramide	Cer (d18:0/14:0)	Up ($P<0.01$)	Up ($P < 0.01$)	Up ($P < 0.01$)	Up ($P < 0.01$)	LC-MS
	Ceramide	Cer (d18:0/16:0)	Up ($P<0.01$)	Up ($P < 0.01$)	Up ($P < 0.01$)	Up ($P < 0.01$)	LC-MS
	Amino acids (AA)						
	Branched chain AA	Leucine	NS	Up ($P < 0.01$)	Up ($P < 0.01$)	Up ($P < 0.01$)	GC-MS
	Branched chain AA	Valine	NS	Up ($P < 0.01$)	Up ($P < 0.01$)	Up ($P < 0.01$)	GC-MS
HBZY-1	**Fatty acids (FA)**						
	FA (unsaturated)	Oleic acid	NS	NS	Up ($P < 0.01$)	Up ($P < 0.01$)	GC-MS
	FA (straight chain)	Stearic acid	NS	NS	Up ($P < 0.01$)	Up ($P < 0.01$)	GC-MS
	FA (unsaturated)	Linoleic acid	NS	NS	Up ($P < 0.01$)	Up ($P < 0.01$)	GC-MS
	Glycerophospholipids						
	Glycerophosphoethanolamine	PE (19:0/0:0)	NS	NS	Down ($P < 0.01$)	Down ($P < 0.01$)	LC-MS
	Diacylglycerophosphoglycerol	PG (15:1/15:0)	NS	NS	Up ($P < 0.01$)	Up ($P < 0.01$)	LC-MS
	Diacylglycerophosphoglycerol	PG (20:5/0:0)	NS	Up ($P < 0.01$)	Up ($P < 0.01$)	Up ($P < 0.01$)	LC-MS
	Sphingolipids						
	Ceramide	Cer (t18:0/16:0)	NS	NS	Up ($P < 0.01$)	Up ($P < 0.01$)	LC-MS
	Ceramide	Cer (d18:0/14:0)	NS	NS	Up ($P < 0.01$)	Up ($P < 0.01$)	LC-MS
	Sphingoid base	Sphingosine C16	NS	NS	Down ($P < 0.01$)	Down ($P < 0.01$)	LC-MS
	Lysophospholipid	LysoPE (0:0/22:6)	NS	Down ($P < 0.01$)	Down ($P < 0.01$)	Down ($P < 0.01$)	LC-MS
	Other metabolites						
		Glucose	NS	NS	Up ($P < 0.05$)	Up ($P < 0.05$)	GC-MS
		Galactose	NS	NS	Up ($P < 0.01$)	Up ($P < 0.01$)	GC-MS

[a]*NS: This metabolite was not statistically significant between HG group and LG group; PE: phosphatidylethanolamine; PG: phosphatidylglycerol; PS: phosphatidylserine.*

The contents of selected potentially biomarkers in clinical plasma were shown in **Table 2**. From the results, we could find that compared with NC group, the DM group plasma content of stearic acid was significantly decreased while valine, leucine, and isoleucine were obviously increased; DN group plasma contents of stearic acid and linoleic acid were obviously reduced while palmitic acid and leucine were significantly enhanced higher than that of NC group, respectively. When compared with DM group, the plasma contents of palmitic acid in DN group was obviously increased while the plasma contents of stearic acid, valine, leucine, and isoleucine were significantly decreased. Moreover, persistent increasing or decreasing could be found for palmitic acid or stearic acid and linoleic acid from NC to DM and then DN, while first increment in DM and then decrement in DN happened for valine, leucine, and isoleucine.

DISCUSSION

Optimization of Sample Treatment and Analytical Method

It is essential to quench the cells during cell collection and metabolite extraction in order to prevent compositional changes of intracellular metabolites. The principle of cell quenching is to terminate all enzyme activities as quickly as possible because many metabolites can be degraded in a short time under the catalysis

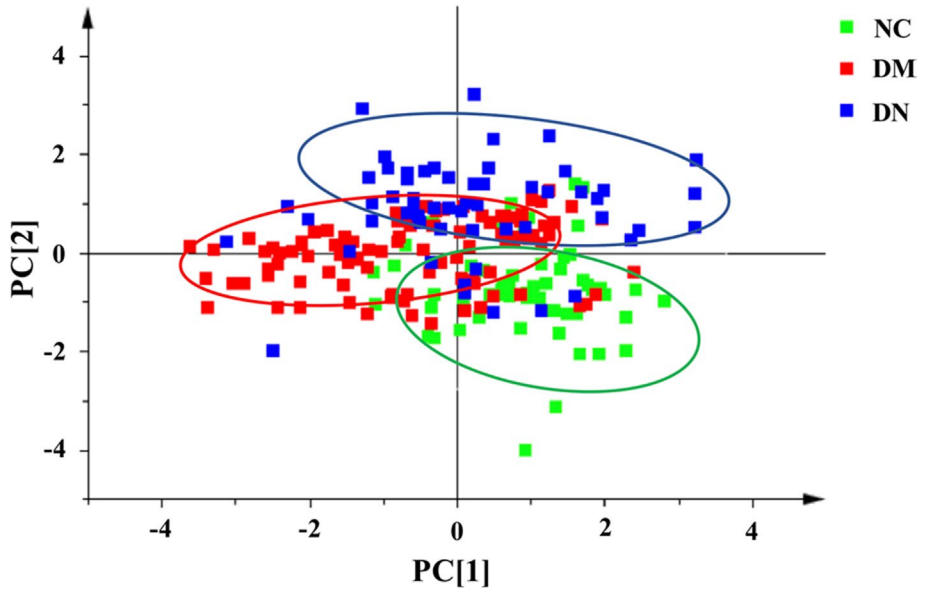

FIGURE 5 | Linear discriminant analysis score plot of plasma samples from three group of subjects (NC: healthy control group; DM: diabetes mellitus group; DN: diabetic nephropathy group).

TABLE 2 | The concentrations of some metabolites in the plasma of subjects (mean ± SD, μg/ml).

Metabolites	NC (n = 55)	DM (n = 103)	DN (n = 57)
Palmitic acid (C16:0)	272.68 ± 111.81	309.55 ± 133.90	371.01 ± 107.63*#
Stearic acid (C18:0)	259.07 ± 69.63	207.01 ± 77.27*	166.98 ± 52.94*#
Oleic acid (cis-9-C18:1)	109.06 ± 36.66	111.10 ± 100.67	97.46 ± 57.41
Linoleic acid (all-cis-9,12-C18:2)	462.94 ± 129.75	402.56 ± 248.23	360.54 ± 171.86*
Glycine	17.92 ± 6.10	16.05 ± 5.02	16.33 ± 6.47
Valine	26.31 ± 3.88	29.89 ± 6.71*	24.82 ± 6.36#
Leucine	17.91 ± 2.88	21.96 ± 4.86*	20.33 ± 4.86*#
Isoleucine	7.46 ± 1.33	9.21 ± 2.54*	7.57 ± 1.86#

$P < 0.05$ vs. NC; #$P < 0.05$ vs. DM.

of enzymes. A common method for cell quenching is to rapidly change the temperature or pH value. Since the characteristics of the cell itself may affect the quenching efficiency and the rate of metabolite leakage (Wu and Li, 2013), it is necessary to select suitable quenching methods for specific types of cells, in our situation, NRK-52E and HBZY-1 cells. In this study, two methods, liquid nitrogen and -80°C extraction solvent, were investigated for quenching effects, respectively. After GC-MS and LC-Q/TOF-MS analyses, we considered that quenching by liquid nitrogen is better based on the number of peaks and variation of the response values.

Disruption of quenched cells is also important during metabolomics analysis. Usually, a variety of cell disruption methods are selectable depending on cell types or compounds. However, non-targeted metabolomics studies require that metabolites in the biological samples and the response values should meet certain requirements. For example, the extracted metabolite components should represent as much as possible the overall metabolite profile. Two cell disruption methods, sonication and repeated cycles of liquid nitrogen and 37°C water bath for three times, were recruited to investigate cell disruption efficiencies. Results showed that there was no significant difference between the two methods, but a large amount of heat was generated during cell disruption by sonication. Thus, repeatedly freezing and thawing in liquid nitrogen and 37°C water bath were used for this study. For the two analytical platforms, GC-MS and LC-Q/TOF-MS, this experiment examined the effects of methanol, methanol/water (4:1, v/v), methanol/water/chloroform (4:1:1, v/v/v), and acetonitrile for metabolite extraction efficiencies. It was concluded that, as the extraction solvent, methanol/water/chloroform (4:1:1, v/v/v) was better used for GC-MS analysis while LC-Q/TOF-MS analysis preferred to methanol/water (4:1, v/v). In addition, MOX and BSTFA were used as derivatization reagents. Temperature and dosage were optimized, respectively. The investigated dosages were 30 μl MOX and 50 μl BSTFA (containing 1% TMCS) and 50 μl MOX and 100 μl BSTFA (containing 1% TMCS) while reaction temperatures were 60°C and 65°C. After analysis, it was found that the derivatization conditions used in this experiment, which were 50 μl MOX, 100 μl BSTFA (containing 1% TMCS), and 65°C, were preferred.

This experiment also examined three chromatographic columns, which were Agilent DB-23 (60 m×0.25 mm×0.15 μm), Agilent HP-5MS (30 m×0.25 mm×0.25μm), and Agilent HP-5MS UI (60 m×0.25 mm×0.25 μm). Results of the analysis showed that

HP-5MS was able to detect more metabolites and had better separation capacity among metabolites than the other two columns. Therefore, the HP-5MS column was used in this study. In order to make the small molecular metabolites in the cells have better resolution in GC-MS, we also investigated various heating procedures. Temperature program is described as below. Initial temperature was 70°C, which is maintained for 1 min, then increased at 5°C/min until 150°C, kept for 2 min, increased to 300°C at 20°C/min, and finally kept for 2 min. In order to make the small molecular metabolites in the cells have good resolution in LC-Q/TOF-MS, a variety of gradient elution procedures were investigated in this experiment, and the optimal procedure used in this study was finally obtained.

Potential Biomarkers

DN is one of the major complications of DM, which is a group of metabolic syndromes characterized by gradual increase of BG level. The pathogenesis of DN has not yet been elucidated. It is generally believed that the pathogenesis of DN involves multiple factors such as hyperglycemia, hemodynamics disturbance, oxidative stress, and inflammatory responses (Xiu et al., 2017). In the process of progression from DM to DN, changing patterns of small molecular metabolites in the body will occur, which may play distinct roles in the occurrence and development of DN.

In this study, non-targeted cell metabolomics was first performed, and the obtained results suggested that the constant changes of small molecular metabolites such as lipids, fatty acids, amino acids, carbohydrates, and nucleosides were involved in the process. In those potential biomarkers, fatty acids and amino acids had attracted extensive attention and been proved to be closely related to DM or DN (Campion et al., 2017; Welsh et al., 2018). Thus, differential metabolites with persistent changes including fatty acids (palmitic acid, stearic acid, oleic acid, and linoleic acid) and amino acids (glycine, valine, leucine, and isoleucine) in cell metabolomics were further selected as target to validate their clinically significance in DM or DN patients. The results hinted that plasma contents of palmitic acid, stearic acid, linoleic acid, valine, leucine, and isoleucine were significantly changed in DM or DN patients. However, those biomarkers validated in the subject plasma may reflect not only renal damage but also together with other tissues, as non-renal cell types were not used as the control.

Studies have shown that non-esterified fatty acids have certain toxic effects on pancreatic β cells (Giacca et al., 2011), which can further lead to insulin resistance. Palmitic acid and stearic acid are saturated fatty acid that play harmful roles in human body (Rogiers, 1981). Carnitine, together with palmitic acid, can be transferred into mitochondria in the form of fatty acylcarnitine to complete β-oxidation. Insulin resistance may inhibit β-oxidation of fatty acids (Lu et al., 2016a), resulting in the accumulation of palmitic acid and stearic acid in DM or DN, which in latter causes kidney damage (Lim et al., 2010; Chu et al., 2013; Lu et al., 2016b). In our study, elevated palmitic acid and stearic acid in the renal cells induced by high glucose and increased palmitic acid in the plasma of DM and DN patients were observed, which was consistent with the previous findings (Chu et al., 2013; Lu et al., 2016a; Lu et al., 2016b; Du et al., 2019). However, the plasma level of stearic acid obtained in DM and DN patients was contrary to that in cell and previous study (Chu et al., 2013; Lu et al., 2016a; Lu et al., 2016b). We speculated that these results may be related to the diet and medicine of the subjects and may be accidental.

Linoleic acid is recognized as an essential fatty acid. Low linoleate intake is associated with DN (Dos Santos et al., 2018), and its metabolites including γ-linoleic acid, the hydroxyoctadecadienoic acid (HODEs), and oxo-octadecadienoic acids (oxo-ODEs) have potent biological effects (Bull et al., 2003; Itoh et al., 2008). For instance, the 9-HODE and 13-HODE and their alcohol dehydrogenase–dependent ketone metabolites, 9-oxo-ODE and 13-oxo-ODE, are potent PPAR-γ ligands (Bull et al., 2003; Itoh et al., 2008). Therefore, the DN-associated reduction in the all-cis-9,12 linoleic acid may reflect a reduction in cellular linoleate, and when the content of linoleic acid (all-cis-9,12) is lowered, the levels of these PPAR-γ ligands may also be reduced, aggravating insulin resistance and inflammatory reaction, eventually causing damage to the kidney. In addition, cytochrome-P450-dependent metabolism of linoleate has been shown to be modulated during the regulation of renal sodium handling (Dreisbach et al., 2008). Therefore, low level of linoleic acid in DM or DN may decrease renal Na^+ excretion, which could itself promote renal damage. It is also possible that shunting of linoleate away from γ-linoleate production, and thus reducing availability of intracellular arachidonate, prostandoids, and other key lipid autocoids, may in and of itself promote renal damage, as supplementation with γ-linoleic acid has been shown to positively impact DN (Jamal, 1994) regardless of the mechanisms. These results suggest that linoleic acid (all-cis-9,12) levels may be an important biomarker during the development of DN.

Under normal conditions, the constant conversion between proteins and amino acids is in a state of equilibrium. The input and output rates of amino acids in blood are almost equal, thereby maintaining a stable amino acid concentration. During the development of DN, the metabolism of the body is disordered, and the amino acid level is bound to change. Valine, leucine, and isoleucine are all branched-chain amino acids (BCAA) that are essential in cellular metabolism. They are not only involved in protein synthesis, but also play an important role in glucose metabolism. Different pathological stages of DNs mirror changed metabolic statuses of BCAA. Studies have shown that, during insulin resistance and DM states, BCAA content increases (Gimble et al., 2010; Lynch and Adams, 2014), while in the early stage of chronic kidney disease, BCAA content decreases (Kumar et al., 2012). By monitoring the levels of leucine and isoleucine in plasma of T2DM patients by Raman spectroscopy, Birech et al. found that both compounds were significantly increased (Multhoff et al., 2017), which provide a basis for rapid screening and early intervention of T2DM patients. In addition, the causal relationship between BCAA and insulin resistance has attracted widespread attention during the development of DM. It was confirmed that, when the level of high-fat diet or insulin-like growth factor is low, protein decomposition increases, and BCAA level in the body rises. It was initially thought that enhanced BCAA leads to activation of the mTOR/S6K1 kinase signaling pathway and phosphorylation of serine residues on IRS-1, which further cause insulin resistance (Newgard et al., 2009). However,

many studies now confirm that activation of the mTOR/S6K1 kinase signaling pathway is not a sufficient condition to cause insulin resistance. In contrast, it is believed that elevated levels of CBAA are caused by protein degradation due to insulin resistance. At present, the hypothesis about BCAA metabolic disorder mechanism has been widely recognized. In specificity, metabolic disorder of BCAA causes accumulation of toxic metabolites such as branched α-keto acid and acyl-CoA, resulting in mitochondrial damage in β-cells. In addition, stress kinase is also activated, ultimately causing insulin resistance and DM (Lynch and Adams, 2014). The results of this study showed that the levels of valine, leucine, and isoleucine in the plasma of DM patients were higher than those of the NC group, which is consistent with the above theory. In the DN state, when the kidney is damaged, the protein in the body is elevated by the efflux of the kidney, breaking the balance between its synthesis and decomposition. Levels of valine, leucine, and isoleucine are all reduced. Therefore, BCAA can be used as a biomarker for DM in the body, and up and down trends of BCAA level can also serve as an early warning for the occurrence of DN. Moreover, as the medication or treatment of the patients was not intervened during whole research, the results of potential biomarkers may hint that there were not obvious associations between the medication or treatment of patients and the metabolic pathway with related to those potential biomarkers.

CONCLUSION

In this study, we established UPLC-Q/TOF-MS and GC-MS non-targeted cell dynamic metabolomics platforms for the initial exploration of potential biomarkers in the occurrence and development of DN. Through combined analysis of amino acids and fatty acids metabolites in clinical samples, we identified that (1) palmitic acid and linoleic acid (all-cis-9,12) can be used as potential biomarkers during the development of DN; (2) valine, leucine, and isoleucine can be considered as potential biomarkers of DM; and (3) fluctuation of valine, leucine, and isoleucine, that is, first increment and then decrement, may have an early warning effect on kidney damage in DM patients.

DATA AVAILABILITY

All datasets generated for this study are included in the manuscript and/or the **Supplementary files**.

ETHICS STATEMENT

This study was carried out in accordance with the recommendations of "Ethics committee of Xuzhou Medical University Affiliated Hospital" with written informed consent from all subjects. All subjects gave written informed consent in accordance with the Declaration of Helsinki. The protocol was approved by the "Ethics committee of Xuzhou Medical University Affiliated Hospital."

AUTHOR CONTRIBUTIONS

LW, YD, B-JX, and D-QT participated in research design. LW, YD, B-JX, XD, Q-HL, Q-QZ, C-XW, SJ, and M-ZG performed the experiments and(or) data analysis. LW, YD, B-JX, Q-HL and D-QT contributed to the writing of the manuscript.

FUNDING

This study was supported by Natural Science Foundation of Jiangsu Province (BK2011211 and BK20181147), the Program for Distinguished Talents of Six Domains in Jiangsu Province (2012-YY-013), Innovative and Entrepreneurial Talent Scheme of Jiangsu Province (2017), and Jiangsu University Natural Science Foundation of China (16KJA350001 and 16KJB180028).

SUPPLEMENTARY MATERIAL

The Supplementary Material for this article can be found online at: https://www.frontiersin.org/articles/10.3389/fphar.2019.00928/full#supplementary-material

REFERENCES

Acunha, T., García-Cañas, V., Valdés, A., Cifuentes, A., and Simó, C. (2018). Metabolomics study of early metabolic changes in hepatic HepaRG cells in response to rosemary diterpenes exposure. *Anal. Chim. Acta* 1037, 140–151. doi: 10.1016/j.aca.2017.12.006

Aldukhayel, A. (2017). Prevalence of diabetic nephropathy among type 2 diabetic patients in some of the Arab countries. *Int. J. Health Sci. (Qassim)* 11, 1–4.

Bull, A. W., Steffensen, K. R., Leers, J., and Rafter, J. J. (2003). Activation of PPAR gamma in colon tumor cell lines by oxidized metabolites of linoleic acid, endogenous ligands for PPAR gamma. *Carcinogenesis* 24, 1717–1722. doi: 10.1093/carcin/bgg131

Campion, C. G., Sanchez-Ferras, O., and Batchu, S. N. (2017). Potential role of serum and urinary biomarkers in diagnosis and prognosis of diabetic nephropathy. *Can. J. Kidney Health Dis.* 4, 2054358117705371. doi: 10.1177/2054358117705371

Chan, E. C., Pasikanti, K. K., and Nicholson, J. K. (2011). Global urinary metabolic profiling procedures using gas chromatography-mass spectrometry. *Nat. Protoc.* 6, 1483–1499. doi: 10.1038/nprot.2011.375

Chu, X., Liu, L., Na, L., Lu, H., Li, S., Li, Y., et al. (2013). Sterol regulatory element-binding protein-1c mediates increase of postprandial stearic acid, a potential target for improving insulin resistance, in hyperlipidemia. *Diabetes* 62, 561–571. doi: 10.2337/db12-0139

Dos Santos, A. L. T., Duarte, C. K., Santos, M., Zoldan, M., Almeida, J. C., Gross, J. L., et al. (2018). Low linolenic and linoleic acid consumption are associated with chronic kidney disease in patients with type 2 diabetes. *PLoS One* 13, e0195249. doi: 10.1371/journal.pone.0195249

Dreisbach, A. W., Rice, J. C., Japa, S., Newman, J. W., Sigel, A., Gill R. S., et al. (2008). Salt loading increases urinary excretion of linoleic acid diols and triols in healthy human subjects. *Hypertension* 51, 755–761. doi: 10.1161/HYPERTENSIONAHA.107.100123

Du, Y., Xu, B. J., Deng, X., Wu, X. W., Li, Y. J., Wang, S. R., et al. (2019). Predictive metabolic signatures for the occurrence and development of diabetic nephropathy and the intervention of Ginkgo biloba leaves extract based on gas or liquid chromatography with mass spectrometry. *J. Pharm. Biomed. Anal.* 166, 30–39. doi: 10.1016/j.jpba.2018.12.017

Fioretto, P., Steffes, M. W., and Mauer, M. (1994). Glomerular structure in nonproteinuric IDDM patients with various levels of albuminuria. *Diabetes* 43, 1358–1364. doi: 10.2337/diab.43.11.1358

Forino, M., Torregrossa, R., Ceol, M., Murer, L., Della Vella, M., Del Prete, D., et al. (2006). TGFbeta1 induces epithelial-mesenchymal transition,

but not myofibroblast transdifferentiation of human kidney tubular epithelial cells in primary culture. *Int. J. Exp. Pathol.* 87, 197–208. doi: 10.1111/j.1365-2613.2006.00479.x

Giacca, A., Xiao, C., Oprescu, A. I., Carpentier, A. C., and Lewis, G. F. (2011). Lipid-induced pancreatic β-cell dysfunction: focus on *in vivo* studies. *Am. J. Physiol. Endocrinol. Metab.* 300, E255–E262. doi: 10.1152/ajpendo.00416.2010

Gimble, J. M., Fiehn, O., Garvey, W. T., Newman, J. W., Lok, K. H., Hoppel, C. L., et al. (2010). Plasma metabolomic profiles reflective of glucose homeostasis in non-diabetic and type 2 diabetic obese African-American women. *PLoS One* 5, e15234. doi: 10.1371/journal.pone.0015234

Itoh, T., Fairall, L., Amin, K., Inaba, Y., Szanto, A., Balint, B. L., et al. (2008). Structural basis for the activation of PPARgamma by oxidized fatty acids. *Nat. Struct. Mol. Biol.* 15, 924–931. doi: 10.1038/nsmb.1474

Jamal, G. A. (1994). The use of gamma linolenic acid in the prevention and treatment of diabetic neuropathy. *Diabet. Med.* 11, 145–149. doi: 10.1111/j.1464-5491.1994.tb02010.x

Jensen, P. N., Fretts, A. M., Yu, C., Hoofnagle, A. N., Umans, J. G., Howard, B. V., et al. (2019). Circulating sphingolipids, fasting glucose, and impaired fasting glucose: the Strong Heart Family Study. *EBioMedicine* 41, 44–49. doi: 10.1016/j.ebiom.2018.12.046

Kumar, M. A., Bitla, A. R., Raju, K. V., Manohar, S. M., Kumar, V. S., and Narasimha, S. R. (2012). Branched chain amino acid profile in early chronic kidney disease. *Saudi J. Kidney Dis. Transpl.* 23, 1202–1207. doi: 10.4103/1319-2442.103560

Li, Y., Li, Y. J., Li, Z., Qiu, J. Y., Zheng, X. X., Bian, T. T., et al. (2015). Screening for potential bioactive components in Ginkgo biloba extract by the rat renal tubular epithelial cell extraction and LC-MS/MS. *Comb. Chem. High Throughput Screen.* 18, 514–523. doi: 10.2174/1386207318666150430114022

Lim, J. C., Lim, S. K., Han, H. J., and Park, S. H. (2010). Cannabinoid receptor 1 mediates palmitic acid-induced apoptosis *via* endoplasmic reticulum stress in human renal proximal tubular cells. *J. Cell. Physiol.* 225, 654–663. doi: 10.1002/jcp.22255

Lu, H., Hao, L., Li, S., Lin, S., Lv, L., Chen, Y., et al. (2016b). Elevated circulating stearic acid leads to a major lipotoxic effect on mouse pancreatic beta cells in hyperlipidaemia *via a* miR-34a-5p-mediated PERK/p53-dependent pathway. *Diabetologia* 59, 1247–1257. doi: 10.1007/s00125-016-3900-0

Lu, Q., Zhou, Y., Hao, M., Li, C., Wang, J., Shu, F., et al. (2018). The mTOR promotes oxidative stress-induced apoptosis of mesangial cells in diabetic nephropathy. *Mol. Cell. Endocrinol.* 473, 31–43. doi: 10.1016/j.mce.2017.12.012

Lu, Y., Wang, Y., Ong, C. N., Subramaniam, T., Choi, H. W., Yuan, J. M., et al. (2016a). Metabolic signatures and risk of type 2 diabetes in a Chinese population: an untargeted metabolomics study using both LC-MS and GC-MS. *Diabetologia* 59, 2349–2359. doi: 10.1007/s00125-016-4069-2

Lynch, C. J., and Adams, S. H. (2014). Branched-chain amino acids in metabolic signalling and insulin resistance. *Nat. Rev. Endocrinol.* 10, 723–736. doi: 10.1038/nrendo.2014.171

Multhoff, G., Birech, Z., Mwangi, P. W., Bukachi, F., and Mandela, K. M. (2017). Application of Raman spectroscopy in type 2 diabetes screening in blood using leucine and isoleucine amino-acids as biomarkers and in comparative anti-diabetic drugs efficacy studies. *PLoS One* 12, e0185130. doi: 10.1371/journal.pone.0185130

Newgard, C. B., An, J., Bain, J. R., Muehlbauer, M. J., Stevens, R. D., Lien, L. F., et al. (2009). A branched-chain amino acid-related metabolic signature that differentiates obese and lean humans and contributes to insulin resistance. *Cell Metab.* 9, 311–326. doi: 10.1016/j.cmet.2009.02.002

Perkins, B. A., Ficociello, L. H., Silva, K. H., Finkelstein, D. M., Warram, J. H., and Krolewski, A. S. (2003). Regression of microalbuminuria in type 1 diabetes. *N. Engl. J. Med.* 348, 2285–2293. doi: 10.1056/NEJMoa021835

Qiu, J. Y., Chen, X., Zheng, X. X., Jiang, X. L., Yang, D. Z., Yu, Y. Y., et al. (2015). Target cell extraction coupled with LC-MS/MS analysis for screening potential bioactive components in Ginkgo biloba extract with preventive effect against diabetic nephropathy. *Biomed. Chromatogr.* 29, 226–232. doi: 10.1002/bmc.3264

Rogiers, V. (1981). Long chain non-esterified fatty acid patterns in plasma of healthy children and young adults in relation to age and sex. *J. Lipid. Res.* 22, 1–6.

Rossing, P., Hougaard, P., and Parving, H. H. (2005). Progression of microalbuminuria in type 1 diabetes: ten-year prospective observational study. *Kidney Int.* 68, 1446–1450. doi: 10.1111/j.1523-1755.2005.00556.x

Smilde, A. K., Westerhuis, J. A., Hoefsloot, H. C., Bijlsma, S., Rubingh, C. M., Vis, D. J., et al. (2010). Dynamic metabolomic data analysis: a tutorial review. *Metabolomics* 6, 3–17. doi: 10.1007/s11306-009-0191-1

Welsh, P., Rankin, N., Li, Q., Mark, P. B., Würtz, P., Ala-Korpela, M., et al. (2018). Circulating amino acids and the risk of macrovascular, microvascular and mortality outcomes in individuals with type 2 diabetes: results from the ADVANCE trial. *Diabetologia* 61, 1581–1591. doi: 10.1007/s00125-018-4619-x

Wu, Y., and Li, L. (2013). Development of isotope labeling liquid chromatography-mass spectrometry for metabolic profiling of bacterial cells and its application for bacterial differentiation. *Anal. Chem.* 85, 5755–5763. doi: 10.1021/ac400330z

Xiu, Z. M., Wang, L. P., Fu, J., Xu, J., and Liu, L. (2017). 1-Acetyl-5-phenyl-1H-pyrrol-3-ylacetate: an aldose reductase inhibitor for the treatment of diabetic nephropathy. *Bioorg. Med. Chem. Lett.* 27, 4482–4487. doi: 10.1016/j.bmcl.2017.08.002

You, R., Dai, J., Zhang, P., Barding, G. A., Jr., and Raftery, D. (2018). Dynamic metabolic response to adriamycin-induced senescence in breast cancer cells. *Metabolites* 8, pii: E95. doi: 10.3390/metabo8040095

Zhang, A., Sun, H., Xu, H., Qiu, S., and Wang, X. (2013). Cell metabolomics. *OMICS* 17, 495–501. doi: 10.1089/omi.2012.0090

Zheng, S., Powell, D. W., Zheng, F., Kantharidis, P., and Gnudi, L. (2016). Diabetic nephropathy: proteinuria, inflammation, and fibrosis. *J. Diabetes. Res.* 2016, 5241549. doi: 10.1155/2016/5241549

Conflicts of Interests Statement: The authors declare that the research was conducted in the absence of any commercial or financial relationships that could be construed as a potential conflict of interest.

Copyright © 2019 Wang, Du, Xu, Deng, Liu, Zhong, Wang, Ji, Guo and Tang. This is an open-access article distributed under the terms of the Creative Commons Attribution License (CC BY). The use, distribution or reproduction in other forums is permitted, provided the original author(s) and the copyright owner(s) are credited and that the original publication in this journal is cited, in accordance with accepted academic practice. No use, distribution or reproduction is permitted which does not comply with these terms.

frontiers in Physiology

ORIGINAL RESEARCH
published: 13 September 2019
doi: 10.3389/fphys.2019.01157

Inhibition of IL-1β by Aliskiren Improved Renal AQP2 Expression and Urinary Concentration Defect in Ureteral Obstruction and Release

Shan Hu[1], Haixia Xie[1], Renfei Luo[1], Pinning Feng[2], Qiaojuan Liu[1], Mengke Han[1], Yonglun Kong[1], Xuenong Zou[3], Weidong Wang[1,4]† and Chunling Li[1]*†*

[1] Institute of Hypertension, Zhongshan School of Medicine, Sun Yat-sen University, Guangzhou, China, [2] Department of Clinical Laboratory, The First Affiliated Hospital, Sun Yat-sen University, Guangzhou, China, [3] Guangdong Provincial Key Laboratory of Orthopedics and Traumatology, The First Affiliated Hospital, Sun Yat-sen University, Guangzhou, China, [4] Department of Nephrology, The Seventh Affiliated Hospital, Sun Yat-sen University, Shenzhen, China

OPEN ACCESS

Edited by:
John D. Imig,
Medical College of Wisconsin,
United States

Reviewed by:
Nirupama Ramkumar,
The University of Utah, United States
Zhanjun Jia,
Nanjing Medical University, China

***Correspondence:**
Weidong Wang
wangwd6@mail.sysu.edu.cn
Chunling Li
lichl3@mail.sysu.edu.cn

†These authors have contributed equally to this work

Specialty section:
This article was submitted to Renal and Epithelial Physiology, a section of the journal Frontiers in Physiology

Received: 18 July 2019
Accepted: 28 August 2019
Published: 13 September 2019

Citation:
Hu S, Xie H, Luo R, Feng P, Liu Q, Han M, Kong Y, Zou X, Wang W and Li C (2019) Inhibition of IL-1β by Aliskiren Improved Renal AQP2 Expression and Urinary Concentration Defect in Ureteral Obstruction and Release. Front. Physiol. 10:1157. doi: 10.3389/fphys.2019.01157

We previously demonstrated that ureteral obstruction is associated with a urinary concentrating defect and reduced expression of renal aquaporins (AQPs), in which the renin–angiotensin system (RAS) may play an important role. The aims of the present study were to examine whether the renin inhibitor aliskiren could prevent the reduction in AQP expression and improve the urinary concentrating capacity in mice with bilateral ureteral obstruction (BUO) and BUO release. BUO was performed for 24 h, and BUO release was performed for 1 (B-R1D) or 3 days (B-R3D) with or without aliskiren treatment. Aliskiren prevented polyuria and decreased urine osmolality induced by B-R3D. In mice with BUO and BUO release, aliskiren attenuated the reduction in AQP2 protein and mRNA expression in the obstructed kidneys. B-R3D increased the protein expression of NLRP3 inflammasome components ASC, caspase-1, and interleukin-1β in the obstructed kidneys, which was markedly prevented by aliskiren. Moreover, the NF-κB inhibitor Bay 11-7082 blocked NLRP3 inflammasome activation and attenuated the decrease in AQP2 protein expression in primary cultured rat inner medullary collecting duct cells treated with angiotensin II. These results indicate that the renin inhibitor aliskiren increases water channel AQP2 expression at least partially by suppressing NLRP3 inflammasome activation in the obstructed kidneys of mice with BUO and BUO release.

Keywords: renin inhibition, urinary concentration, ureteral obstruction, IL-1β, AQP, inflammasome, renin

INTRODUCTION

Obstruction nephropathy is associated with reduced glomerular and tubular function as well as long-term impaired urinary concentrating capacity. Release of both unilateral and bilateral ureteral obstruction (UUO and BUO) causes marked changes in the glomerular-tubular balance and so-called postobstructive diuresis (Frokiaer and Zeidel, 2011). Clinical observations have indicated that patients with obstructive nephropathy experience massive vasopressin-insensitive polyuria after the

release of the obstruction, suggesting that BUO is associated with nephrogenic diabetes insipidus. We previously demonstrated that ureteral obstruction (both bilateral and unilateral) and its release in rats is associated with significant downregulation of aquaporin (AQP) protein expression in the kidneys, providing a molecular basis for the urinary concentrating defect (Li et al., 2001, 2003). The expression of the vasopressin-regulated collecting duct water channel AQP2 was reduced in BUO for 24 h in rats, which persisted 24–48 h after the release of the obstruction, accompanied by marked postobstructive polyuria (Frokiaer et al., 1996b). Rats with UUO showed downregulated AQP2 expression similar to that observed in rats with BUO (Li et al., 2003). This finding indicates that local/intrarenal factors may play important roles in the downregulation of AQP expression in obstructive nephropathy.

Recently, the intrarenal renin–angiotensin system (RAS) in the kidneys has been demonstrated to play an important role in cellular homeostasis. For example, local RAS activation in the kidneys may induce structural and functional changes in tubular epithelial cells independent of those elicited by the classical renin–angiotensin endocrine system (De Mello and Frohlich, 2014). Angiotensin II (Ang II) is synthesized *de novo* in the kidneys and may directly modulate renal hemodynamic and tubular transport (Braam et al., 1993; Reams et al., 1993). Obstructed kidneys have been reported to show increased intrarenal Ang II levels (Okabe et al., 2015), which may play a role in the reduction of the glomerular filtration rate (GFR) and renal blood flow (RBF) in ureteral obstruction. Reportedly, angiotensin-converting enzyme inhibitors (ACEIs) or Ang II type 1 receptor blockers (ARBs) partly prevent the reduction in GFR and RBF (Frokiaer et al., 1996a) and improve the expression and intracellular trafficking of renal AQP2 and several key sodium transporters in ureteral obstruction (Jensen et al., 2006, 2009; Topcu et al., 2007), indicating that Ang II contributes to the urinary concentrating defect of obstructed kidneys. In addition, Ang II infusion has been reported to induce the infiltration of monocytes and the release of inflammatory factors in the kidneys (Crowley et al., 2010), probably due to activation of the intracellular NF-κB pathway (Muller et al., 2000). RAS blockade attenuates the expression of an array of cytokines and growth factors, which potentially impair renal function in rats with UUO (Ishidoya et al., 1995; Wu et al., 2010; Soliman et al., 2011; Wang W. et al., 2015). Compared with ACEIs or ARBs, direct renin inhibitors (DRIs), such as aliskiren, can block the RAS at an early stage in the cascade and potently suppress the formation of Ang I and Ang II via both ACE and non-ACE pathways (Segall et al., 2007). Aliskiren is therefore an alternative option to inhibit RAS activation beside ACEi and ARB. A recent clinical trial showed that aliskiren improved renal and systemic hemodynamics (Kwakernaak et al., 2017), providing an effective treatment in hypertensive, cardiovascular, and renal diseases.

NOD-, LRR-, and pyrin domain-containing 3 (NLRP3) inflammasome is a cytosolic signaling macromolecular complex comprising a sensor molecule [NOD-like receptors (NLRs)], the adaptor apoptosis-associated speck-like protein containing a CARD (ASC), and the effector protease caspase 1, which processes pro-interleukin (IL-1β) into its mature form IL-1β that causes inflammation and tissue damage (Mangan et al., 2018). Recent studies have suggested that NLRP3 inflammasome and downstream cytokines contribute to several types of kidney disease, including crystalline nephropathy (Mulay et al., 2013; Wang et al., 2018), obstructive nephropathy (Wang W. et al., 2015), and obesity-related kidney diseases (Ke et al., 2018). We previously demonstrated that IL-1β directly inhibits AQP2 expression in the collecting duct principal cells of the kidneys (Wang W. et al., 2015), suggesting that inflammatory cytokines downregulate the expression of water channels and sodium transporters, resulting in altered water and sodium regulation in the kidneys. The present study aimed to investigate whether aliskiren alleviates the abnormal water regulation in the kidneys of mice with BUO and BUO release and attenuates the reduction in water channel expression and the activation of NLRP3 inflammasome.

MATERIALS AND METHODS

Reagents

For semiquantitative immunoblotting and immunocyto chemistry, previously characterized affinity-purified polyclonal antibodies to AQP2 and AQP3 were used (Wang et al., 2018). Antibodies to AQP1 were obtained from BOSTER (Wuhan, China); antibodies to IL-1β, p-NF-κB p65, and NF-κB p65 from Cell Signaling Technology; caspase-1 from Abcam; antibodies to ASC from Santa Cruz; and NLRP3 from Novus. Human IL-1β was obtained from Peprotech and Bay 11-7082 was purchased from Sigma–Aldrich. Ang II and valsartan were purchased from MCE (Shanghai, China).

Animals and Treatments

All animal procedures were approved by the Animal Care and Use Committee of Sun Yat-sen University. In brief, 8-week-old male C57BL/6 mice were purchased from the animal facility center of Sun Yat-sen University (Guangzhou, China), were maintained on a light/dark (12/12 h) cycle at 24°C, and received food and water *ad libitum* before experimentation.

To prepare for the surgery to establish BUO, the mice were anesthetized with pentobarbital sodium and placed on a heated table to maintain their rectal temperature at 37–38°C. A midline abdominal incision was then made to expose both ureters, and the ureters were occluded by ligating a 5-0 silk suture at the midportion. For BUO release, ureters were occluded by vascular clamps (#14120, World Precision Instruments Inc., Sarasota, FL, United States) at the midportion. Mice were intraperitoneally injected with aliskiren twice per day (40 mg/kg body weight/day). BUO was released by removing the vascular clamps after 16 h. By using this technique, the ureters of the mice could be completely occluded for 16 h without any subsequent impairment of ureteral function. The mice were sacrificed 1 or 3 days after BUO release.

Mice were allocated to the protocols indicated below. Age- and time-matched sham-operated controls were prepared and observed in parallel with each BUO group and BUO release

(B-R) group. *Protocol 1* included BUO for 24 h (BUO), BUO with aliskiren injection (BUO + Ali), and sham-operated (Sham) groups (n = 9 in each group). *Protocol 2* included BUO for 16 h followed by 1-day release (B-R1D), and B-R1D with aliskiren injection (B-R1D + Ali) and Sham groups (n = 9 in each group). *Protocol 3* included BUO for 16 h followed by 3-day release (B-R3D), and B-R3D with aliskiren injection (B-R3D + Ali), and Sham groups (n = 9 in each group).

All mice were maintained in metabolic cages during experimentation. Their daily water and food intake was monitored. Mice were placed in metabolic cages immediately after BUO or BUO release. Urine samples for clearance studies were collected (BUO-1D and BUO-3D) over 24-h periods. On the sacrifice day, all mice were anesthetized with pentobarbital sodium, and both kidneys were removed from each animal and prepared for protein, mRNA measurement, or histologic analysis.

Blood and Urine Chemistry

Urine was collected and clearance studies were performed during periods throughout the study. At the end of each protocol, blood samples were collected into heparinized tubes for the determination of serum creatinine and osmolality when the mice were sacrificed. The osmolality of urine and serum was determined by freezing-point depression (OM 806, Osmometer, Loser, Germany). The serum and urine creatinine were determined by using an ELISA kit according to the manufacturer's instructions (BioAssay System, United States). Creatinine clearance Ccr (μL/min/g BW) is calculated based on the following formula: Ccr = [urinary creatinine concentration (mmol/L) × urine output (μL/min/g)]/[plasma creatinine concentration (mmol/L)]. Urine and serum potassium concentrations were analyzed by using a flame photometer.

Electrophoresis and Immunoblotting

At the sacrifice day, mice were anesthetized with pentobarbital sodium, and kidneys were frozen in liquid nitrogen immediately after removal. Tissue was minced finely and homogenized in dissecting buffer (0.3 M sucrose, 25 mM imidazole, 1 mM EDTA, pH 7.2, containing the following protease inhibitors: 8.5 μM leupeptin, 1 mM phenylmethylsulfonyl fluoride). This homogenate was centrifuged at 4,000 × g for 15 min at 4°C. The supernatants were assayed for protein concentration using the BCA method (Pieces, Rockford, IL, United States). Gel samples were made from this pellet. Samples of membrane fractions were run on 12% polyacrylamide minigels. After transferring by electroelution to PVDF membranes, blots were blocked with 5% milk in PBS-T (80 mM Na_2HPO_4, 20 mM NaH_2PO_4, 100 mM NaCl, 0.1% Tween 20, pH 7.5) for 1 h and incubated with primary antibodies overnight at 4°C. After being washed with PBS-T, the blots were incubated with horseradish peroxidase-conjugated secondary antibody (Pieces, Rockford, IL, United States). After a final washing as above, corresponding secondary antibodies were visualized using enhanced chemiluminescence (Pierce, Rockford, IL, United States). The signals were quantified with a chemiluminescence detector and the accompanying densitometry software (UVP, Upland, CA, United States).

Immunohistochemistry and Immunofluorescence

The kidneys from mice were fixed by retrograde perfusion via the left ventricle with 0.01 M PBS buffer. The left kidney blocks containing all kidney zones were dehydrated and embedded in paraffin. For immunoperoxidase microscopy, sections (4 μm thick) cut from paraffin-embedded kidney samples were used for immunostaining of AQP2 (Wang et al., 2018). Briefly, after dewaxing and rehydration, a microwave pretreatment in citrate buffer (pH 6.2) was performed to unmask antigens present in the renal tissue. Tissue sections were then incubated overnight at 4°C with primary antibodies. After rinsing in PBS, slides were exposed to the secondary antibody for 1 h. The sections were later washed with PBS, followed by incubation with diaminobenzidine for 10 min. The microscopic examination was carried out by using a Leica DM2000 light microscope (Leica, Heidelberg, Germany). For sections prepared for immunofluorescence, AQP2 (Santa Cruz, sc-515770) and ASC (Abcam, ab64808) were used for primary antibodies. Secondary fluorescent antibodies were obtained from Santa Cruz. Fluorescence microscopy was carried out on a Leica DMI4000B fluorescence inverse microscope (Heidelberg, Germany).

RNA Extraction and Quantitative Real-Time PCR

Total RNA was extracted from the kidneys according to the manufacturer's instructions for Trizol reagent (Invitrogen, CA, United States). Total RNA (500 ng) was used for reverse transcription using PrimeScript® RT reagent Kit Perfect Real Time kit (Takara Bio Inc., Japan). The cDNA was used for quantitative real-time PCR (qRT-PCR) analysis using SYBR® Premix Ex Taq™ (Perfect Real Time, Takara Bio Inc., Japan). Target mRNA was determined using the comparative cycle threshold method of relative quantitation. The calibrator sample was selected from PBS-treated tissue, and GAPDH was used as an internal control. Primer sequences used are provided in **Table 1**.

Primary Rat Inner Medullary Collecting Duct Cell Culture Studies

Primary cultures of renal inner medullary collecting duct (IMCD) cells were generated with a modification of a previous study (Luo et al., 2019). In brief, Wistar rats (8–10 weeks) were killed by cervical dislocation, and kidneys were quickly removed under sterile condition. The renal medulla was dissected, minced, and digested for 60 min in 10 mL of medium (DMEM) containing 0.2% collagenase type I, 0.2% hyaluronidase, and 0.025% trypsin-EDTA at 37°C with shaking. The IMCD cells were cultured in 6-well plates for 48 h. In protocol 1, the IMCD cells were treated with or without IL-1β (5 ng/mL) for 6 h. In protocol 2, the IMCD cells were pretreated with or without Bay 11-7082 (10^{-6} M) or valsartan (10^{-6} M) for 30 min, and then incubated with Ang II (10^{-9} M) for 24 h. After incubation, cells were then centrifuged at 1,000 rpm for 5 min, the supernatant was discarded, and the pellet was resuspended in the modified medium (DMEM, and 100 U/mL penicillin G-streptomycin sulfate).

TABLE 1 | Primer sequences for RT-PCR (mouse).

Target gene	Primer sequence	Target gene	Primer sequence
GAPDH F	TGACCTCAACTACATGGTCTACA	AGT F	ATGCACAGATCGGAGATGACT
GAPDH R	CTTCCCATTCTCGGCCTTG	AGT R	CATGCAGGGTCTTCTCATTCAC
AQP2 F	GGACCTGGCTGTCAATGCTC	Renin F	CACACTCAGCAGTACGGACTACGT
AQP2 R	GCGGGCTGGATTCATGGAG	Renin R	CAGTGGGTGGTGGGATGTC
IL-1β F	GAAATGCCACCTTTTGACAGTG	ReninR F	CCGTAAACGCCTGTTTCAAG
IL-1β R	TGGATGCTCTCATCAGGACAG	ReninR R	TAGCACTTGCAGTTCGGAGA
KIM-1 F	ACATATCGTGGAATCACAACGAC	NGAL F	ACGGACTACAACCAGTTCGC
KIM-1 R	ACTGCTCTTCTGATAGGTGACA	NGAL R	AATGCATTGGTCGGTGGGG
V2R F	GCTGTGGCTCTGTTTCAAGTG		
V2R R	CCAGGATCATGTAGGAAGAGGC		

GAPDH, glyceraldehyde-3-phosphate dehydrogenase; AQP, aquaporin; IL, interleukin; AGT, angiotensinogen; reninR, renin receptor; KIM-1, kidney injury molecule-1; NGAL, neutrophil gelatinase-associated lipocalin; V2R, vasopressin type 2 receptor; F, forward; R, reverse.

Measurement of Ang II

Urinary and plasma Ang II concentration was determined using an Ang II magnetic particle-based chemiluminescence assay kit (Autobio Diagnostics Co., Ltd.).

Statistical Analysis

Results are presented as the means ± SE. Data were analyzed by ANOVA and Student–Newman–Keuls test for multiple comparisons. Statistical significance was accepted at the $P < 0.05$ level. Values represent means ± SE of three independent sets of experiments in primary cell culture studies.

RESULTS

Aliskiren Prevented the Downregulation of AQP2 Expression in the Obstructed Kidneys of BUO Mice

Bilateral ureteral obstruction was performed for 24 h in mice treated with or without aliskiren. As shown in **Figure 1**, western blot analyses revealed that the abundance of renal AQP2 and AQP1 proteins was significantly lower in the obstructed kidneys of BUO mice than in the kidneys of Sham mice, and the reduction in AQP2 protein expression was markedly prevented by aliskiren treatment (**Figures 1A,B**). Notably, AQP3 protein expression was not significantly different between the three groups (BUO, BUO + Ali, and Sham).

Aliskiren Prevented Polyuria and Reduction in AQP2 Expression in the Obstructed Kidneys of B-R1D Mice

Release of BUO causes postobstructive diuresis (Frokiaer et al., 1996b). As shown in **Table 2**, urine output was dramatically increased and urine osmolality was markedly decreased in mice with BUO that was released for 1 day (B-R1D), both of which were found to be prevented by aliskiren treatment in B-R1D + Ali mice (**Table 2**). The abundance of renal AQP1, AQP2, and AQP3 proteins was significantly lower in the obstructed kidneys of B-R1D mice than in the kidneys of Sham mice, and the reduction was prevented by aliskiren treatment in B-R1D + Ali mice (**Figures 1C,D**).

Aliskiren Prevented the Reduction in AQP2 Expression in the Obstructed Kidneys of B-R3D Mice

Urine output persistently increased in mice with BUO that was released for 3 days (B-R3D) compared with that in Sham mice (**Figure 2A**). This increase was prevented by aliskiren treatment in B-R3D + Ali mice (**Figure 2A**). The abundance of AQP2 protein was significantly lower in the obstructed kidneys of B-R3D mice than in the kidneys of Sham mice (**Figures 2B,C**). This decrease was significantly reversed by aliskiren treatment in B-R3D + Ali mice (**Figures 2B,C**). Immunohistochemistry revealed that the overall decrease in AQP2 labeling intensity observed in the inner medulla of the kidneys of B-R3D mice was clearly prevented by aliskiren treatment in B-R3D + Ali mice (**Figure 2D**). The expression of both AQP1 and AQP3 proteins was also markedly downregulated in B-R3D mice, but aliskiren treatment prevented the reduction in only AQP1 protein expression in B-R3D + Ali mice (**Figures 2B,C**).

Aliskiren Inhibited IL-1β Production in the Obstructed Kidneys of B-R3D Mice

Inflammasome activates caspase 1, which proteolytically activates the pro-inflammatory cytokines IL-1β and IL-18 (Martinon et al., 2002). Production of cleaved IL-1β was therefore examined in this study. The protein expression of the inflammasome components ASC and cleaved IL-1β (17 kDa) was increased in the obstructed kidneys of BUO and B-R1D mice; in comparison, BUO + Ali and B-R1D + Ali mice showed mild, insignificant decreases in ASC and IL-1β expression because of aliskiren treatment (**Figures 3A–D**). The expression of ASC, caspase-1, and IL-1β proteins was markedly upregulated by approximately 1. 3-, 2. 5-, and 1.8-folds, respectively, in the kidneys of B-R3D mice, whereas aliskiren treatment markedly blocked this upregulation in B-R3D + Ali mice (**Figures 3E,F**). Immunofluorescence showed ASC-positive staining in principal cells of the collecting ducts. The increased staining of ASC specks in principal cells of B-R3D + Ali mouse kidneys was abolished by aliskiren treatment (**Figure 3G**).

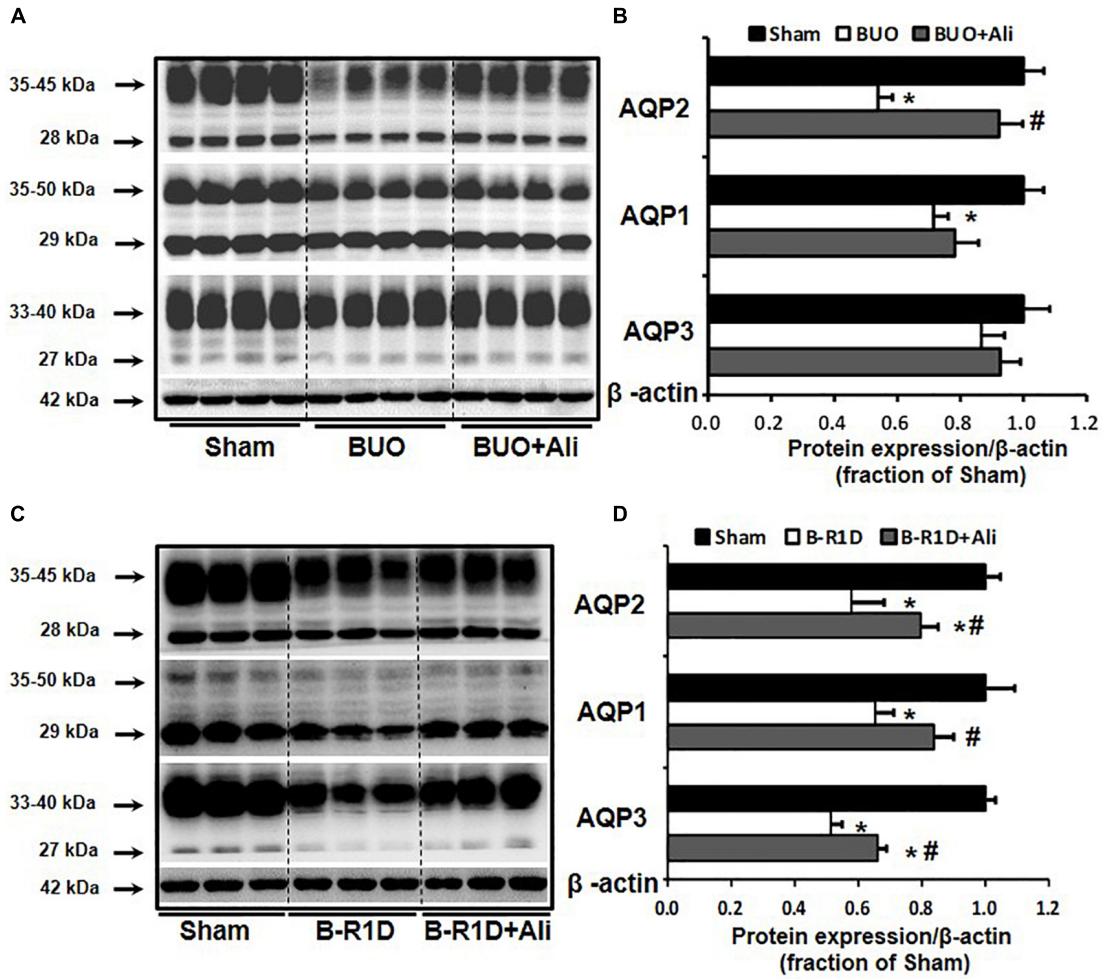

FIGURE 1 | Aliskiren treatment prevented the reduction in water channel AQP2 expression in the obstructed kidneys of BUO and B-R1D mice. Semi-quantitative immunoblots probed with anti-AQP2, -AQP1, -AQP3, and -β-actin antibodies in the whole kidneys of BUO mice **(A)** and in the whole kidneys of B-R1D mice **(C)**. Corresponding densitometric analyses of AQP2, AQP1, and AQP3 protein expression corrected for β-actin in BUO mice **(B)** and in B-R1D mice **(D)**. Sham, sham-operated mice; BUO, bilateral ureteral obstruction for 24 h; BUO + Ali, BUO mice treated with aliskiren; B-R1D, bilateral ureteral obstruction for 16 h followed by 1-day release; B-R1D + Ali, B-R1D mice treated with aliskiren. *$p < 0.05$ compared with the sham group; #$p < 0.05$ compared with the BUO/B-R1D group.

The time-course changes in cleaved IL-1β and AQP2 protein and mRNA expression during BUO, as well as BUO followed by release for 1–3 days (B-R1D and B-R3D), are shown in **Figure 4**. The renal abundance of AQP2 protein was maintained at the lowest level in the obstructed kidneys of the BUO group compared with the abundance in the two other groups. Notably, in the BUO-R1D + Ali and B-R3D + Ali groups, AQP2 protein expression was nearly maintained as that in the Sham group (**Figure 4A**), indicating that aliskiren treatment attenuated the reduction in AQP2 protein expression in the obstructed kidneys. In addition, aliskiren inhibited IL-1β expression by approximately 20–50% of that in the BUO, B-R1D, and B-R3D groups (**Figure 4B**), suggesting that local inflammatory cytokines (e.g., IL-1β) associated with kidney obstruction contribute to the downregulation of water channel AQP2 expression. AQP2 mRNA expression gradually increased in BUO, B-R1D, and B-R3D mice. At day 3 after release, AQP2 mRNA expression in the obstructed kidneys was higher than that in the kidneys of Sham mice, likely indicating the occurrence of a compensatory response after release (**Figure 4C**). Consistent with the expression pattern of IL-1β protein, IL-1β mRNA expression was higher in the obstructed kidneys than in the kidneys of Sham mice (**Figure 4D**). **Figure 4E** shows a potential linear correlation between IL-1β and AQP2 protein expression in the Sham, B-R3D, and B-R3D + Ali groups.

Interleukin-1β reduced binding of vasopressin to its receptor *in vitro* (Grinevich et al., 2004), indicating impairment of vasopressin action in the kidney during inflammation. Vasopressin-V2R and its corresponding signaling pathway are important for regulation of AQP2; we therefore examined mRNA expression of V2R in the obstructed kidneys. Compared with sham mice, mRNA levels of V2R dramatically decreased to about 15% in BUO and 50% in BUO-1D mice, which was prevented partially by aliskiren treatment (**Figure 4F**). In the obstructed

TABLE 2 | KIM-1 and NGAL mRNA levels (arbitrary units) in BUO, B-R1D, and B-R3D kidney with or without aliskiren treatment.

	KIM-1	NGAL
Sham	1 ± 0.3	1 ± 0.3
BUO	446 ± 45.2*	167 ± 51.5*
BUO + Ali	236 ± 3.2*#	152 ± 10.6*
Sham	1 ± 0.1	1 ± 0.2
B-R1D	152 ± 6.9*	112 ± 21.4*
B-R1D + Ali	125 ± 13.4*	34.5 ± 5.8*#
Sham	1 ± 0.2	1 ± 0.2
B-R3D	19.4 ± 2.6*	16.6 ± 3.9*
B-R3D + Ali	18.9 ± 1.6*	15.3 ± 1.4*

*KIM-1, kidney injury molecule-1; NGAL, neutrophil gelatinase-associated lipocalin; Sham, sham-operated groups; BUO, bilateral ureteral obstruction for 24 h; B-R1D, bilateral ureteral obstruction for 16 h followed by 1 day release; B-R3D, bilateral ureteral obstruction for 16 h followed by 3 days release. *$p < 0.05$ compared with Sham group; #$p < 0.05$ compared with obstructed kidney group.*

kidneys of BUO-3D mice, V2R mRNA was increased by 37% compared to sham mice (**Figure 4F**). The pattern of V2R gene changes in the obstructed kidneys was similar to that seen in changes of AQP2 expression. Next we examined whether IL-1β directly affects V2R expression in primary cultured IMCD cells (protocol 1). IL-1β markedly decreased the mRNA level of V2R by 25% (0.75 ± 0.05 vs. 1.00 ± 0.05 in controls, $p < 0.05$, $n = 6$ in controls and $n = 7$ in IL-1β treatment group). These data suggested that inflammatory factors (e.g., IL-1β) induced by ureteral obstruction not only downregulate AQP2 expression, but also decrease V2R gene expression, potentially affecting the V2R intracellular signaling pathway.

RAS in the Obstructed Kidneys of BUO, B-R1D, and B-R3D Mice

Gene expression levels of several RAS components in the obstructed kidneys were examined in BUO, B-R1D, and B-R3D mice. Angiotensinogen (AGT) mRNA expression reduced by 30% in BUO mice and increased by 1.4- and 1.5-folds in B-R1D and B-R3D mice, respectively, compared with that in the sham mice (**Figure 5A**). Renin mRNA levels were also reduced in BUO mice but returned to sham levels in B-R3D mice. Renin mRNA levels dramatically increased after aliskiren treatment, probably due to the inhibition of renin activity by aliskiren (**Figure 5B**). Renin receptor mRNA levels decreased in BUO mice and gradually returned to sham levels after BUO release in B-R1D and B-R3D mice (**Figure 5C**). Notably, aliskiren treatment had negligible effects on renin receptor mRNA expression in the obstructed kidneys (**Figure 5D**). Plasma and urinary levels of Ang II were measured. As shown in **Figure 5D**, plasma Ang II levels were ∼42% higher in BUO mice and ∼46% higher in B-R1D mice than those in sham mice – these increases were attenuated by aliskiren treatment. After release by 3 days, the plasma Ang II concentration returned to baseline level (**Figure 5D**). In B-R1D mice, urinary Ang II levels remained unchanged, whereas aliskiren treatment slightly reduced urinary Ang II concentration, although it did not reach statistical significance. Urinary Ang II levels were ∼60% higher in B-R3D mice than those in sham mice, which were completely suppressed by aliskiren treatment in B-R3D + Ali mice (**Figure 5E**).

Interestingly the observed changes of RAS components were associated with tubular injuries. mRNA levels of kidney injury molecule-1 (KIM-1) and neutrophil gelatinase-associated lipocalin (NGAL), two markers of tubular injuries, were dramatically increased in the obstructed kidneys. Aliskiren treatment decreased KIM-1 and NGAL mRNA levels, respectively (**Table 2**), indicating intervention by RAS blockade may ameliorate tubular injuries associated with obstruction. In B-R3D mice both KIM-1 and NGAL mRNA levels decreased markedly when compared to BUO or B-R1D, suggesting a potential recovery of tubular function, coincidently paralleling with recovered protein expression of AQPs. Aliskiren treatment is sometimes associated with hyperkalemia (Parving et al., 2012). In BUO and BUO + Ali mice, plasma potassium concentration showed an approximately 1.6-fold increase, but it markedly reduced after release of ureteral obstruction. Three days after release, plasma potassium concentrations returned to sham levels, but about a 20% increase was still found in B-R3D mice with aliskiren treatment (**Table 3**), likely due to inhibition of Ang II production.

Bay 11-7082 and Valsartan Prevented the Reduction in AQP2 Expression in Ang II-Treated Primary Cultured Rat Inner Medullary Collecting Duct Cells

The activation of NLRP3 inflammasome has been associated with the NF-κB signaling pathway (Kong et al., 2016a); we therefore investigated whether the inhibition of NLRP3-associated inflammatory response by blocking the NF-κB pathway affects AQP2 protein expression. In primary cultured rat IMCD cells, Ang II treatment increased the p-NF-κB p65/NF-κB p65 ratio by 1.8-folds, which was markedly reduced by the NF-κB inhibitor Bay 11-7082 (**Figures 6A,B**). Ang II treatment also increased the protein expression of the NLRP3 inflammasome components NLRP3 and IL-1β and markedly decreased that of AQP2, both of which were prevented by Bay 11-7082 (**Figures 6C–F**). This finding suggests that Bay 11-7082 improves AQP2 expression via its local anti-inflammatory role. In order to examine a role of local Ang II in induction of inflammation that reduces AQP2 protein expression, ARBs valsartan, but not aliskiren that inhibits Ang II production, was therefore used to block effects of Ang II in primary cultured IMCD cells. As expected, valsartan showed effects that inhibited IL-1β and increased AQP2 expression, similar to those of Bay 11-7082 on Ang II-treated IMCD cells (**Figure 6**).

DISCUSSION

In this study, we demonstrated that aliskiren, a DRI, prevented the reduction in AQP2 mRNA and protein expression in the obstructed kidneys of BUO, B-R1D, and B-R3D mice. Ureteral obstruction caused RAS activation in the kidneys and NLRP3

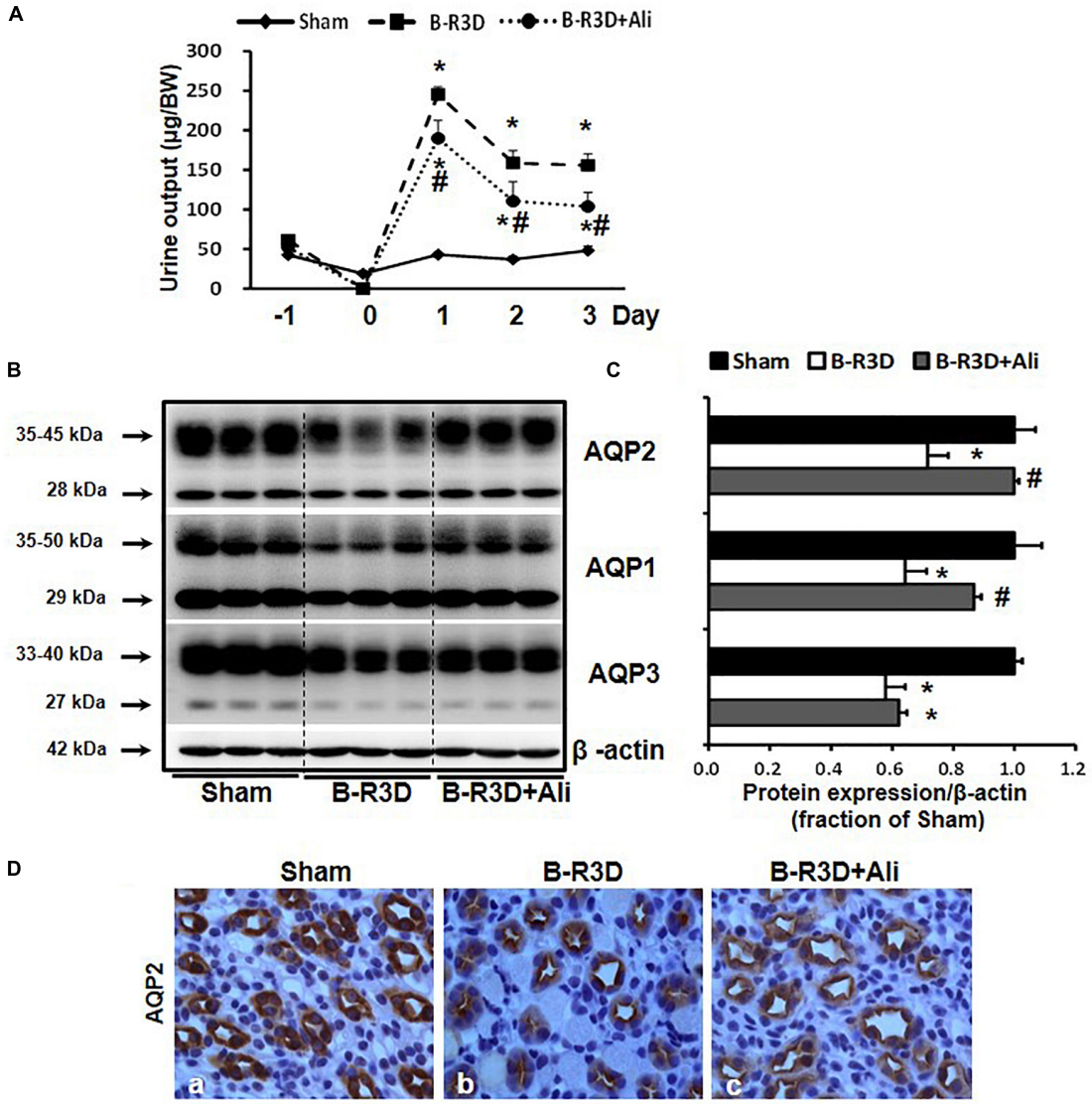

FIGURE 2 | Aliskiren treatment prevented polyuria and the reduction in water channel AQP2 and AQP1 expression in the obstructed kidneys of B-R3D mice. **(A)** Urine output was collected from sham, B-R3D, and aliskiren-treated mice. **(B)** Semi-quantitative immunoblots probed with anti-AQP2, -AQP1, -AQP3, and β-actin antibodies. **(C)** Corresponding densitometric analyses of the AQP2, AQP1, and AQP3 protein expression corrected for β-actin. **(D)** Immunohistochemistry of AQP2 in the kidneys of aliskiren-treated or non-treated B-R3D mice. Sham, sham-operated groups; B-R3D, bilateral ureteral obstruction for 16 h followed by 3 days release; B-R3D + Ali, B-R3D group with aliskiren treatment. $^{*}p < 0.05$ compared with sham group; $^{\#}p < 0.05$ compared with B-R3D groups.

inflammasome-induced IL-1β production, which is likely to have contributed to the downregulation of AQP2 expression in mice with BUO and BUO release.

Long-term impairment of urinary concentrating ability was observed in mice with BUO and BUO release (Frokiaer and Zeidel, 2011), which is probably attributable to reduced AQP2 protein expression in the obstructed kidneys (Frokiaer et al., 1996b). Recent evidence has demonstrated that in addition to systemic RAS, local RAS is involved in renal water metabolism and blood volume regulation (Wang F. et al., 2015). ACEIs, ARBs, and DRIs have been shown to prevent renal fibrosis and inflammation induced by UUO, suggesting that RAS is activated in ureteral obstruction (Kaneto et al., 1994; Ishidoya et al., 1995; Kellner et al., 2006; Wu et al., 2010; Sakuraya et al., 2014). RAS activation also plays a role in the downregulation of AQP2 protein expression associated with ureteral obstruction. In several studies, ARB significantly prevented the decrease in AQP2 protein expression in the postobstructed kidneys (Jensen et al., 2006; Topcu et al., 2007), prevented the downregulation of vasopressin V2 receptor complex, and reversed the obstruction-induced inhibition of stimulated cAMP generation in the inner medulla of obstructed kidneys (Jensen et al., 2009). The DRI aliskiren blocks RAS at an early stage in the RAS cascade and has

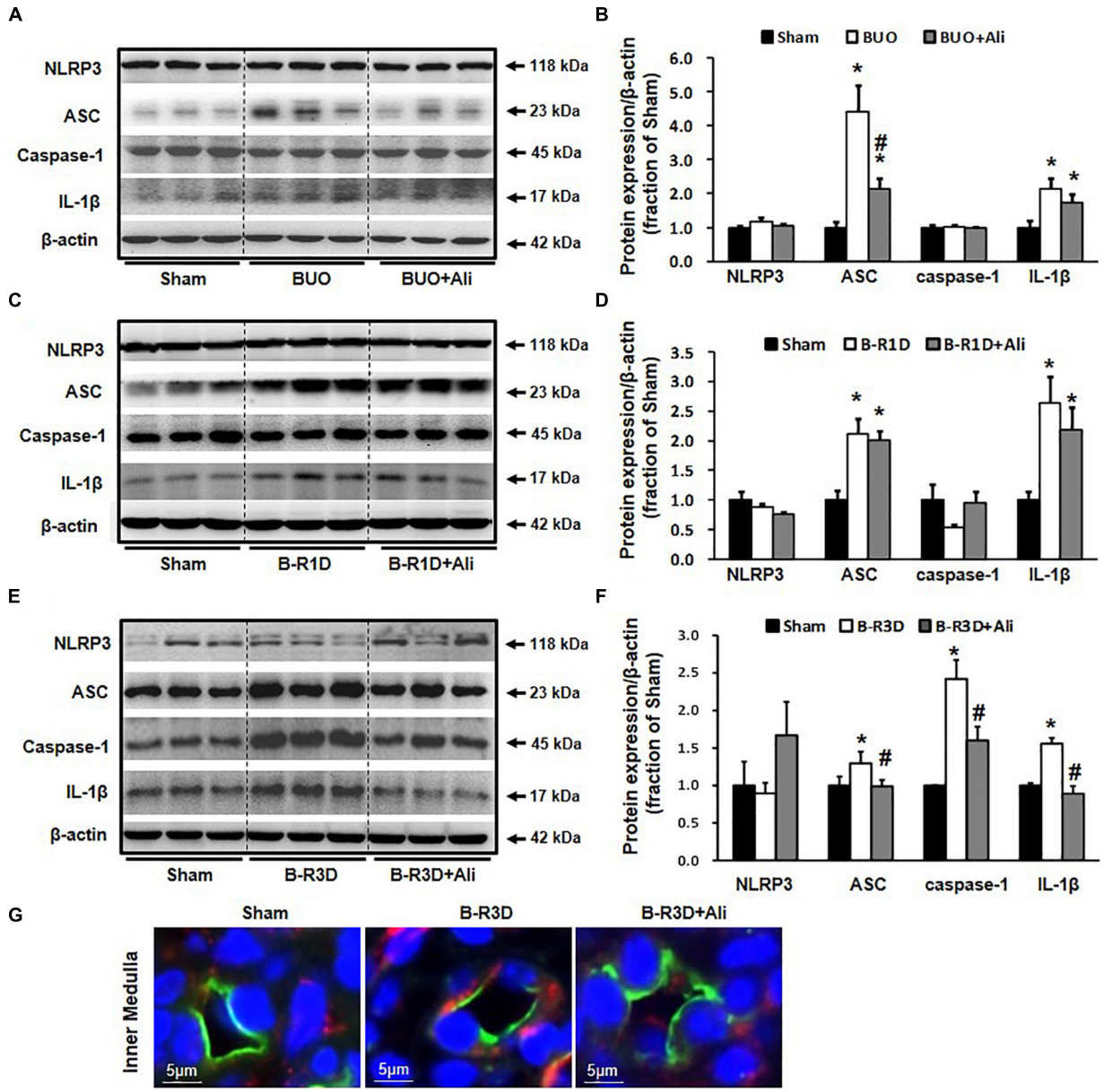

FIGURE 3 | Expression of inflammasome components in the obstructed kidneys of BUO, B-R1D, and B-R3D mice. **(A,C,E)** Semi-quantitative immunoblots probed with anti-NLRP3, -ASC, -caspase-1, and -IL-1β antibodies. **(B,D,F)** Corresponding densitometric analyses of the NLRP3, ACS, caspase-1, and IL-1β protein expression corrected for β-actin. **(G)** Immunofluorescence staining of AQP2 (in green) and ASC (in red) in principal cells of the collecting duct in the kidneys of B-R3D and B-R3D + Ali mice. NLRP3, NOD-like receptor pyrin domain containing 3; ASC, apoptosis-associated speck-like protein containing a caspase recruitment domain; Caspase-1, an evolutionarily conserved enzyme that proteolytically cleaves other proteins; IL-1β, interleukin-1β; Sham, sham-operated groups; BUO, bilateral ureteral obstruction for 24 h; BUO + Ali, BUO group with aliskiren treatment; B-R1D, bilateral ureteral obstruction for 16 h followed by 1 day release; B-R1D + Ali, B-R1D group with aliskiren treatment; B-R3D, bilateral ureteral obstruction for 16 h followed by 3 days release; B-R3D + Ali, B-R3D group with aliskiren treatment. $^{*}p < 0.05$ compared with Sham group; $^{\#}p < 0.05$ compared with OBS groups.

been widely used for treating cardiovascular diseases. We previously demonstrated that RAS suppression with aliskiren prevented the downregulation of AQP2 expression in the UUO kidneys; consistent with the results of previous studies (Eskild-Jensen et al., 2007) demonstrating that RAS blockade by ARB prevented the reduction in AQP2 expression after partial UUO in pigs.

Increased intrarenal Ang II secretion actively contributes to afferent vasoconstriction and reduction in the GFR following the release of ureteral obstruction. AGT mRNA expression was increased in the kidneys after BUO release, suggesting an activation of intrarenal RAS in these conditions, which was supported by increased urinary Ang II excretion at the third day after release. In the kidney of B-R3D + Ali mice, renin mRNA

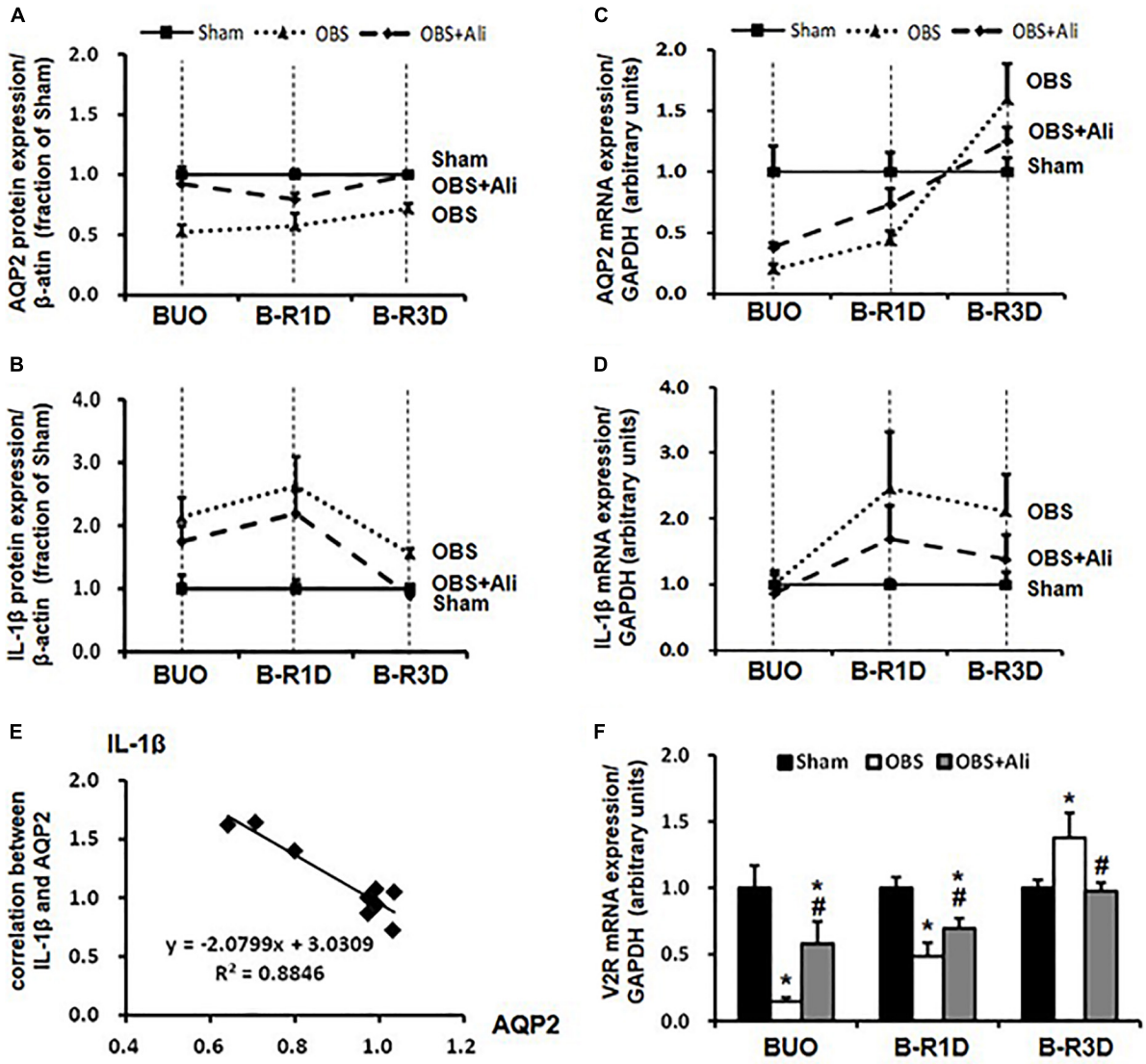

FIGURE 4 | Time-course changes in AQP2 **(A,C)** and IL-1β **(B,D)** protein and mRNA levels in the kidneys of BUO, B-R1D, and B-R3D mice. **(E)** Correlation between AQP2 and IL-1β protein expression in the obstructed kidneys of B-R3D mice (n = 9). **(F)** V2R mRNA levels in the kidneys of BUO, B-R1D, and B-R3D mice. IL-1β, interleukin-1β; V2R, vasopressin type 2 receptor; Sham, sham-operated groups; BUO, bilateral ureteral obstruction for 24 h; BUO + Ali, BUO group with aliskiren treatment; B-R1D, BUO for 16 h followed by 1 day release; B-R1D + Ali, B-R1D group with aliskiren treatment; B-R3D, BUO for 16 h followed by 3 days release; B-R3D + Ali, B-R3D group with aliskiren treatment; OBS, obstructed group; OBS + Ali, obstructed group with aliskiren treatment.

levels were dramatically increased after aliskiren treatment, probably due to a compensatory response, as observed in other animal studies (Wu et al., 2010).

Interestingly, local RAS activation in the kidneys was associated with downregulated AQP2 protein expression and increased urine output after BUO release, which was also prevented by aliskiren, as aliskiren decreases Ang II production by suppressing renin activity. The mechanism by which intrarenal RAS activation decreases AQP2 protein expression is not completely clear. One suggested mechanism is that Ang II stimulates inflammatory responses associated with obstruction. Ang II may activate several transcriptional factors (e.g., NF-κB) modulating gene expressions of proinflammatory factors within the nucleus of tubular cells. This ultimately leads to tubulointerstitial inflammation, fibrosis, and permanent loss of renal function, which may continue to progress after the obstruction has been relieved (Frokiaer and Zeidel, 2011).

Upon activation, NF-κB is translocated into the nucleus, where its p65 subunit is phosphorylated; this induces the transcription and translation of proinflammatory cytokines, e.g., IL-1β (Tak and Firestein, 2001). A recent study demonstrated marked increases of the transcript abundances of NF-κB family genes in the kidney of rats with lithium-induced NDI, which is believed to contribute to downregulation of AQP2. Induction of NF-κB signaling and an inflammatory-like response may repress AQP2 transcription in lithium-induced NDI (Sung et al., 2019),

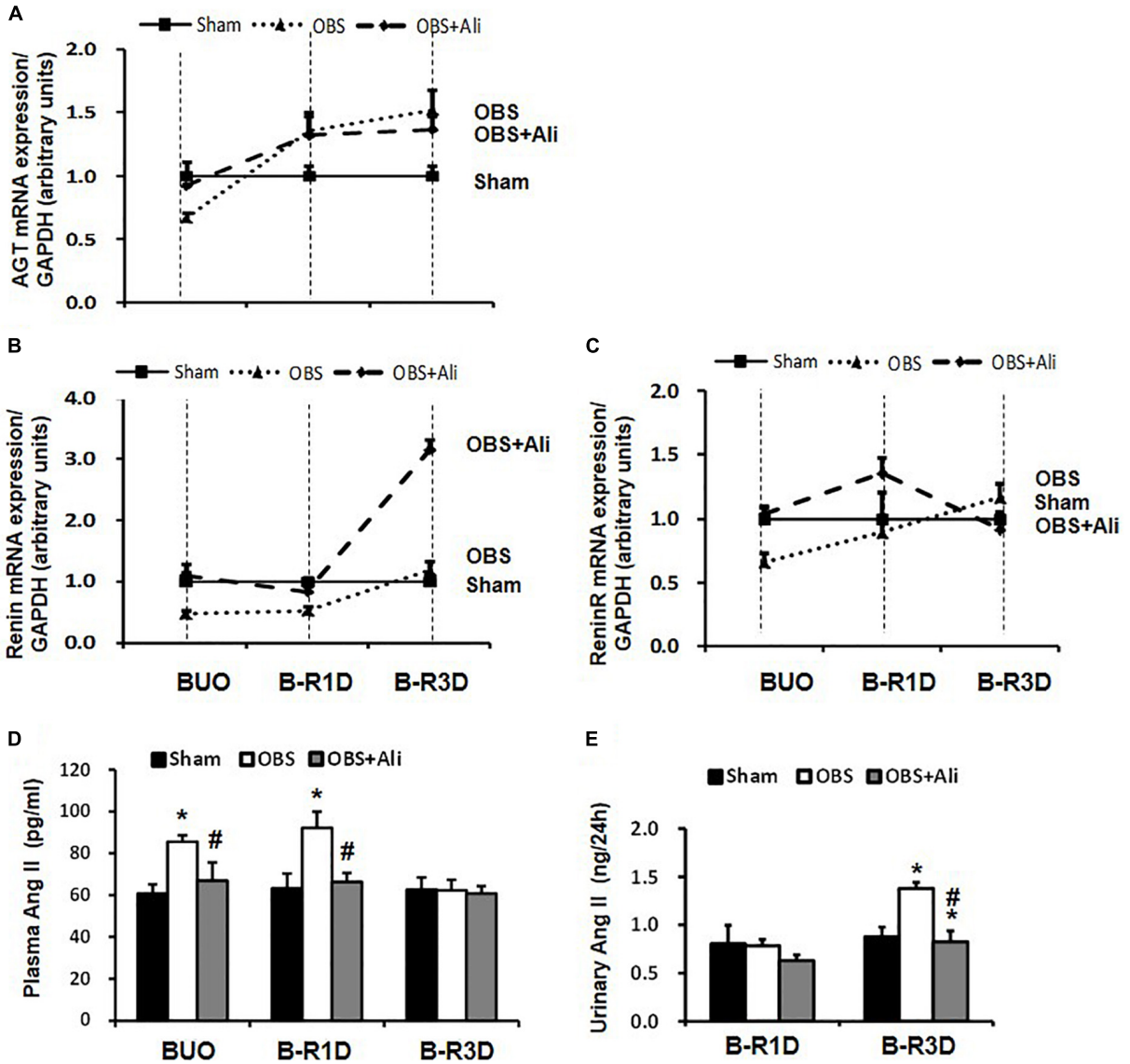

FIGURE 5 | Dynamic changes in AGT, renin, and renin receptor mRNA expression in the kidneys and plasma and urinary Ang II levels in aliskiren-treated or non-treated BUO, B-R1D, and B-R3D mice. **(A,B,C)** Analysis of AGT, renin, and renin receptor mRNA expression by real-time PCR. **(D,E)** Plasma and urinary Ang II levels in aliskiren-treated or non-treated BUO, B-R1D, and B-R3D mice. Ang II, angiotensin II; AGT, angiotensinogen; ReninR, renin receptor; Sham, sham-operated groups; BUO, bilateral ureteral obstruction for 24 h; BUO + Ali, BUO group with aliskiren treatment; B-R1D, BUO for 16 h followed by 1 day release; B-R1D + Ali, B-R1D group with aliskiren treatment; B-R3D, BUO for 16 h followed by 3 days release; B-R3D + Ali, B-R3D group with aliskiren treatment; OBS, obstructed group; OBS + Ali, obstructed group with aliskiren treatment. $^{*}p < 0.05$ compared with Sham group; $^{\#}p < 0.05$ compared with B-R3D groups.

TABLE 3 | Renal functional data in BUO, B-R1D, and B-R3D mice with or without aliskiren treatment.

	Sham	BUO	BUO + Ali	Sham	B-R1D	B-R1D + Ali	Sham	B-R3D	B-R3D + Ali
BW (g)	22.5 ± 1.0	22.5 ± 0.6	22.8 ± 0.5	22.0 ± 0.8	22.7 ± 0.6	22.4 ± 0.5	21.2 ± 0.4	21.6 ± 0.3	20.5 ± 0.5
P_K (mmol/L)	3.3 ± 0.09	5.8 ± 0.33*	5.5 ± 0.15*	3.5 ± 0.05	4.5 ± 0.48*	4.6 ± 0.34*	3.5 ± 0.04	3.7 ± 0.02	4.3 ± 0.04*#
C_{Cr} (μL/min/g bw)				4.93 ± 1.03	2.27 ± 0.51*	2.70 ± 0.20*	4.91 ± 0.13	4.32 ± 0.54	3.67 ± 0.20
UO (μl/24 h/g bw)				34.0 ± 4.7	241.1 ± 9.7*	206.4 ± 10.9*#	48.2 ± 5.2	155.7 ± 10.2*	103.7 ± 14.1*#
U_{Osm} (mOsm/kg·H_2O)				2403 ± 244	413 ± 19*	531 ± 26*#	2684 ± 321	1215 ± 103*	1333 ± 135*

BW, body weight; P_K, plasma potassium; C_{Cr}, creatinine clearance rate; UO, urine output; U_{Osm}, urine osmolality; Sham, sham-operated groups; BUO, bilateral ureteral obstruction for 24 h; B-R1D, bilateral ureteral obstruction for 16 h followed by 1 day release; B-R3D, bilateral ureteral obstruction for 16 h followed by 3 days release. $^{*}p < 0.05$ compared with Sham group; $^{\#}p < 0.05$ compared with obstructed kidney group.

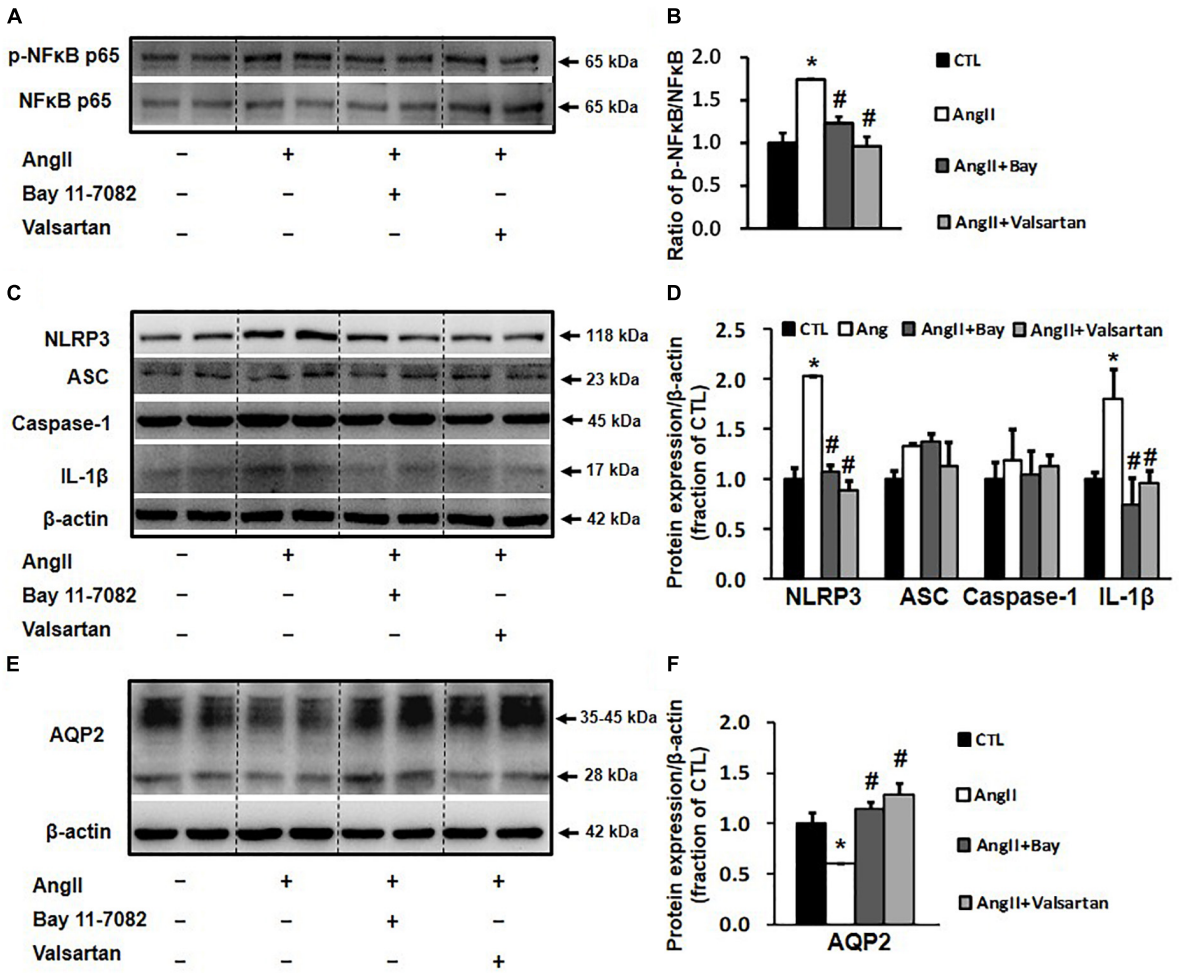

FIGURE 6 | Western blot analysis of NLRP3 inflammasome components and AQP2 in primary cultured rat IMCD cells incubated with Ang II (1 nM) and co-treated with the NF-κB inhibitor Bay 11-7082 (100 μM) or the AT1 receptor blocker valsartan (100 μM). **(A)** Semi-quantitative immunoblots probed with anti-p-NF-κB and NF-κB antibodies. **(B)** The p-NF-κB/NF-κB ratio. **(C)** Semi-quantitative immunoblots probed with anti -NLRP3, -ACS, -caspase-1, -IL-1β and -β-actin antibodies. **(D)** Corresponding densitometric analyses of NLRP3, ACS, caspase-1 and IL-1β protein expression corrected for β-actin. **(E)** Semi-quantitative immunoblots probed with anti-AQP2 and -β-actin antibodies. **(F)** Corresponding densitometric analyses of AQP2 protein expression corrected for β-actin. NF-κB, transcription factors of the nuclear factor κB; p-NF-κB, phosphorylated-NF-κB (Ser536); NLRP3, Nod-like receptor pyrin domain containing 3; ASC, apoptosis-associated speck-like protein containing a caspase recruitment domain; Caspase-1, an evolutionarily conserved enzyme that proteolytically cleaves other proteins; IL-1β, interleukin-1β; $^{*}p < 0.05$ compared with control group; $^{\#}p < 0.05$ compared with Ang II group.

since NF-κB binds to the AQP2 gene promoter and represses AQP2 transcription induced by vasopressin or hypertonicity (Hasler et al., 2008).

Our data showed that Ang II not only stimulated the NF-κB inflammatory pathway in rat IMCD cells, as indicated by increased NF-κB expression and phosphorylation, but also activated NLRP3 inflammasome and promoted IL-1β protein expression in rat IMCD suspensions. NF-κB may be involved in the regulation of NLRP3 inflammasome transcription (Qiao et al., 2012) and NLRP3 inflammasome participates in NF-κB-mediated inflammatory processes (Kong et al., 2016b). Interestingly, both Bay 11-7082 and valsartan inhibited Ang II-induced NF-κB activation and NLRP3/IL-1β protein expression (**Figure 6**), indicating potential links between the intrarenal RAS, NLRP3 inflammasome, and NF-κB pathways during inflammatory responses. Importantly, NLRP3 or NF-κB suppression by Bay 11-7082 or valsartan at least partially prevented the reduction in AQP2 expression after Ang II treatment in IMCD cells, which is likely attributable to the inhibition of IL-1β production. Changes in gene and protein expression during BUO and BUO release clearly showed a causal relationship between IL-1β and AQP2 expression (**Figure 4**). In general, at individual time points after BUO and BUO release, markedly increased IL-1β expression was associated with reduced AQP2 protein and gene expression. These alterations in IL-1β and AQP2 expression were prevented by aliskiren, indicating that RAS blockade increases AQP2 expression by suppressing inflammation. It is noted that there may be several other mechanisms by which IL-1β regulates AQP2. IL-1β downregulated V2R gene expression and reduced binding of

vasopressin to V2R (Grinevich et al., 2004), thus inhibiting the V2R intracellular signaling pathway and downregulating AQP2 gene and protein expression.

Protein expressions of AQP1 and AQP3 were also downregulated in BUO and BUO-R, consistent with earlier studies (Li et al., 2001), which was partially prevented by aliskiren if at all. The molecular mechanism of AQP3 and AQP1 regulation in the kidney is not fully understood. Altered AQP2 expression is not always paralleled with AQP3 in some conditions. The ARB candesartan prevented the reduced AQP2 protein expression in obstructed kidneys of rats with bilateral ureter obstruction and release, but the reduction of AQP3 expression persisted (Jensen et al., 2006), indicating a different signaling pathway in AQP3 regulation from AQP2 in the kidney. Interestingly, aliskiren showed a slightly better protection in AQP1 expression than AQP3 in BUO and BUO-R, but the underlying mechanism was not investigated. Recovery of AQP1 in the kidney may in fact protect tubules from further injuries induced by BUO and BUO-R. In endotoxin-related acute kidney injury, mice with AQP1 knockout showed severe tubular injury histologically and functionally compared with wild-type mice, indicating a protective role of AQP1 in tubular injury and healing (Wang et al., 2008).

Although aliskiren increased AQP2 protein expression in BUO and BUO release, likely by inhibiting the expression of inflammatory cytokines – in particular, IL-1β production induced by intrarenal RAS activation – aliskiren may also directly stimulate AQP2 expression and thus water metabolism in the kidneys. Our recent study demonstrated that aliskiren upregulates AQP2 protein expression in IMCD principal cells via cAMP-PKA pathways. Aliskiren can also improve lithium-induced urinary concentration defect and polyuria (Lin et al., 2017). Thus, there are multiple mechanisms in the kidneys contributing to the observed protective role of aliskiren in UUO, BUO, and BUO release.

In summary, the results of this study show that RAS blockade with the renin inhibitor aliskiren prevented drastic reduction in AQP2 protein expression, probably by inhibiting inflammatory responses, especially IL-1β expression, in the kidneys of mice with BUO and BUO release. The results indicate that intrarenal RAS activation plays a potential role in inflammasome maturation during ureteral obstruction. In addition to blocking RAS activation, inhibition of both NLRP3 inflammasome and NF-κB pathways may be a promising therapeutic strategy for obstructive nephropathy.

DATA AVAILABILITY

All datasets generated for this study are included in the manuscript and/or the supplementary files.

ETHICS STATEMENT

The animal study was reviewed and approved by the Committee on the Management and Use of Laboratory Animals, Sun Yat-sen University.

AUTHOR CONTRIBUTIONS

SH, HX, RL, PF, QL, MH, and YK performed the experiments. SH, RL, WW, and CL analyzed the data. SH, HX, WW, and CL interpreted the results of experiments. SH and CL prepared the figures. SH, WW, and CL drafted the manuscript. SH, XZ, WW, and CL edited and revised the manuscript. WW and CL approved the final version of the manuscript.

FUNDING

This work was supported by the National Natural Science Foundation of China (Grant Nos. 81870465, 81570635, 81670646, and 81370822) and the Natural Science Foundation of Guangdong Province, China (Grant Nos. 2014A020212623, 2014A030313168, and 2016A020215034).

REFERENCES

Braam, B., Mitchell, K. D., Fox, J., and Navar, L. G. (1993). Proximal tubular secretion of angiotensin II in rats. *Am. J. Physiol.* 264(5 Pt 2), F891–F898. doi: 10.1152/ajprenal.1993.264.5.F891

Crowley, S. D., Song, Y. S., Sprung, G., Griffiths, R., Sparks, M., Yan, M., et al. (2010). A role for angiotensin II type 1 receptors on bone marrow-derived cells in the pathogenesis of angiotensin II-dependent hypertension. *Hypertension* 55, 99–108. doi: 10.1161/HYPERTENSIONAHA.109.144964

De Mello, W. C., and Frohlich, E. D. (2014). Clinical perspectives and fundamental aspects of local cardiovascular and renal Renin-Angiotensin systems. *Front. Endocrinol.* <refvol> 5:16. doi: 10.3389/fendo.2014.00016

Eskild-Jensen, A., Paulsen, L. F., Wogensen, L., Olesen, P., Pedersen, L., Frokiaer, J., et al. (2007). AT1 receptor blockade prevents interstitial and glomerular apoptosis but not fibrosis in pigs with neonatal induced partial unilateral ureteral obstruction. *Am. J. Physiol. Renal Physiol.* 292, F1771–F1781. doi: 10.1152/ajprenal.00479.2006

Frokiaer, J., Djurhuus, J. C., Nielsen, M., and Pedersen, E. B. (1996a). Renal hemodynamic response to ureteral obstruction during converting enzyme inhibition. *Urol. Res.* 24, 217–227. doi: 10.1007/bf00295895

Frokiaer, J., Marples, D., Knepper, M. A., and Nielsen, S. (1996b). Bilateral ureteral obstruction downregulates expression of vasopressin-sensitive AQP-2 water channel in rat kidney. *Am. J. Physiol.* 270(4 Pt 2), F657–F668. doi: 10.1152/ajprenal.1996.270.4.F657

Frokiaer, J., and Zeidel, M. (2011). "Urinary Tract Obstruction," in *Brenner & Rector's "The Kidney"*, ed. M. W. Taal, (Philadelphia, PA: Elsevier Saunders), 1383–1410.

Grinevich, V., Knepper, M. A., Verbalis, J., Reyes, I., and Aguilera, G. (2004). Acute endotoxemia in rats induces down-regulation of V2 vasopressin receptors and aquaporin-2 content in the kidney medulla. *Kidney Int.* 65, 54–62. doi: 10.1111/j.1523-1755.2004.00378.x

Hasler, U., Leroy, V., Jeon, U. S., Bouley, R., Dimitrov, M., Kim, J. A., et al. (2008). NF-kappaB modulates aquaporin-2 transcription in renal collecting duct principal cells. *J. Biol. Chem.* 283, 28095–28105. doi: 10.1074/jbc.M708350200

Ishidoya, S., Morrissey, J., McCracken, R., Reyes, A., and Klahr, S. (1995). Angiotensin II receptor antagonist ameliorates renal tubulointerstitial fibrosis caused by unilateral ureteral obstruction. *Kidney Int.* 47, 1285–1294. doi: 10.1038/ki.1995.183

Jensen, A. M., Bae, E. H., Fenton, R. A., Norregaard, R., Nielsen, S., Kim, S. W., et al. (2009). Angiotensin II regulates V2 receptor and pAQP2 during ureteral

obstruction. *Am. J. Physiol. Renal Physiol.* 296, F127–F134. doi: 10.1152/ajprenal.90479.2008

Jensen, A. M., Li, C., Praetorius, H. A., Norregaard, R., Frische, S., Knepper, M. A., et al. (2006). Angiotensin II mediates downregulation of aquaporin water channels and key renal sodium transporters in response to urinary tract obstruction. *Am. J. Physiol. Renal Physiol.* 291, F1021–F1032. doi: 10.1152/ajprenal.00387.2005

Kaneto, H., Morrissey, J., McCracken, R., Reyes, A., and Klahr, S. (1994). Enalapril reduces collagen type IV synthesis and expansion of the interstitium in the obstructed rat kidney. *Kidney Int.* 45, 1637–1647. doi: 10.1038/ki.1994.215

Ke, B., Shen, W., Fang, X., and Wu, Q. (2018). The NLPR3 inflammasome and obesity-related kidney disease. *J. Cell Mol. Med.* 22, 16–24. doi: 10.1111/jcmm.13333

Kellner, D., Chen, J., Richardson, I., Seshan, S. V., El Chaar, M., Vaughan, E. D., et al. (2006). Angiotensin receptor blockade decreases fibrosis and fibroblast expression in a rat model of unilateral ureteral obstruction. *J. Urol.* 176, 806–812. doi: 10.1016/j.juro.2006.03.076

Kong, F., Ye, B., Cao, J., Cai, X., Lin, L., Huang, S., et al. (2016a). Curcumin represses nlrp3 inflammasome activation via tlr4/myd88/nf-kappab and p2x7r signaling in pma-induced macrophages. *Front. Pharmacol.* 7:369. doi: 10.3389/fphar.2016.00369

Kong, F., Ye, B., Lin, L., Cai, X., Huang, W., and Huang, Z. (2016b). Atorvastatin suppresses NLRP3 inflammasome activation via TLR4/MyD88/NF-kappaB signaling in PMA-stimulated THP-1 monocytes. *Biomed. Pharmacother.* 82, 167–172. doi: 10.1016/j.biopha.2016.04.043

Kwakernaak, A. J., Roksnoer, L. C., Lambers Heerspink, H. J., van den Berg-Garrelds, I., Lochorn, G. A., van Embden Andres, J. H., et al. (2017). Effects of direct renin blockade on renal & systemic hemodynamics and on raas activity, in weight excess and hypertension: a randomized clinical trial. *PLoS One* 12:e0169258. doi: 10.1371/journal.pone.0169258

Li, C., Wang, W., Knepper, M. A., Nielsen, S., and Frokiaer, J. (2003). Downregulation of renal aquaporins in response to unilateral ureteral obstruction. *Am. J. Physiol. Renal. Physiol.* 284, F1066–F1079. doi: 10.1152/ajprenal.00090.2002

Li, C., Wang, W., Kwon, T. H., Isikay, L., Wen, J. G., Marples, D., et al. (2001). Downregulation of AQP1, -2, and -3 after ureteral obstruction is associated with a long-term urine-concentrating defect. *Am. J. Physiol. Renal. Physiol.* 281, F163–F171. doi: 10.1152/ajprenal.2001.281.1.F163

Lin, Y., Zhang, T., Feng, P., Qiu, M., Liu, Q., Li, S., et al. (2017). Aliskiren increases aquaporin-2 expression and attenuates lithium-induced nephrogenic diabetes insipidus. *Am. J. Physiol. Renal. Physiol.* 313, F914–F925. doi: 10.1152/ajprenal.00553.2016

Luo, R., Hu, S., Liu, Q., Han, M., Wang, F., Qiu, M., et al. (2019). Hydrogen sulfide upregulates renal AQP-2 protein expression and promotes urine concentration. *FASEB J.* 33, 469–483. doi: 10.1096/fj.201800436R

Mangan, M. S. J., Olhava, E. J., Roush, W. R., Seidel, H. M., Glick, G. D., and Latz, E. (2018). Targeting the NLRP3 inflammasome in inflammatory diseases. *Nat. Rev. Drug. Discov.* 17, 588–606. doi: 10.1038/nrd.2018.97

Martinon, F., Burns, K., and Tschopp, J. (2002). The inflammasome: a molecular platform triggering activation of inflammatory caspases and processing of proIL-beta. *Mol. Cell* 10, 417–426.

Mulay, S. R., Kulkarni, O. P., Rupanagudi, K. V., Migliorini, A., Darisipudi, M. N., Vilaysane, A., et al. (2013). Calcium oxalate crystals induce renal inflammation by NLRP3-mediated IL-1beta secretion. *J. Clin. Invest.* 123, 236–246. doi: 10.1172/JCI63679

Muller, D. N., Mervaala, E. M., Schmidt, F., Park, J. K., Dechend, R., Genersch, E., et al. (2000). Effect of bosentan on NF-kappaB, inflammation, and tissue factor in angiotensin II-induced end-organ damage. *Hypertension* 36, 282–290. doi: 10.1161/01.hyp.36.2.282

Okabe, M., Miyazaki, Y., Niimura, F., Pastan, I., Nishiyama, A., Yokoo, T., et al. (2015). Unilateral ureteral obstruction attenuates intrarenal angiotensin II generation induced by podocyte injury. *Am. J. Physiol. Renal. Physiol.* 308, F932–F937. doi: 10.1152/ajprenal.00444.2014

Parving, H. H., Brenner, B. M., McMurray, J. J., de Zeeuw, D., Haffner, S. M., Solomon, S. D., et al. (2012). Cardiorenal end points in a trial of aliskiren for type 2 diabetes. *N. Engl. J. Med.* 367, 2204–2213. doi: 10.1056/NEJMoa1208799

Qiao, Y., Wang, P., Qi, J., Zhang, L., and Gao, C. (2012). TLR-induced NF-kappaB activation regulates NLRP3 expression in murine macrophages. *FEBS Lett.* 586, 1022–1026. doi: 10.1016/j.febslet.2012.02.045

Reams, G., Villarreal, D., Wu, Z., and Bauer, J. H. (1993). Renal tissue angiotensin II: response to infusions of angiotensin I and an angiotensin-converting enzyme inhibitor. *Am. J. Kidney Dis.* 22, 851–857. doi: 10.1016/s0272-6386(12)70345-1

Sakuraya, K., Endo, A., Someya, T., Hirano, D., Murano, Y., Fujinaga, S., et al. (2014). The synergistic effect of mizoribine and a direct renin inhibitor, aliskiren, on unilateral ureteral obstruction induced renal fibrosis in rats. *J. Urol.* 191, 1139–1146. doi: 10.1016/j.juro.2013.10.053

Segall, L., Covic, A., and Goldsmith, D. J. (2007). Direct renin inhibitors. the dawn of a new era, or just a variation on a theme? *Nephrol. Dial. Transplant.* 22, 2435–2439. doi: 10.1093/ndt/gfm363

Soliman, S. A., Shokeir, A. A., Mosbah, A., Abol-Enein, H., Barakat, N., Abou-Bieh, E., et al. (2011). Recoverability of renal function after relief of chronic partial unilateral ureteric obstruction: the effect of an angiotensin-converting enzyme inhibitor (enalapril). *Arab J. Urol.* 9, 67–71. doi: 10.1016/j.aju.2011.03.016

Sung, C. C., Chen, L., Limbutara, K., Jung, H. J., Gilmer, G. G., Yang, C. R., et al. (2019). RNA-Seq and protein mass spectrometry in microdissected kidney tubules reveal signaling processes initiating lithium-induced nephrogenic diabetes insipidus. *Kidney Int.* 96, 363–377. doi: 10.1016/j.kint.2019.02.015

Tak, P. P., and Firestein, G. S. (2001). NF-kappaB a key role in inflammatory diseases. *J. Clin. Invest.* 107, 7–11. doi: 10.1172/JCI11830

Topcu, S. O., Pedersen, M., Norregaard, R., Wang, G., Knepper, M., Djurhuus, J. C., et al. (2007). Candesartan prevents long-term impairment of renal function in response to neonatal partial unilateral ureteral obstruction. *Am. J. Physiol. Renal. Physiol.* 292, F736–F748. doi: 10.1152/ajprenal.00241.2006

Wang, F., Liu, Q., Jin, L., Hu, S., Luo, R., Han, M., et al. (2018). Combination exposure of melamine and cyanuric acid is associated with polyuria and activation of NLRP3 inflammasome in rats. *Am. J. Physiol. Renal. Physiol.* 315, F199–F210. doi: 10.1152/ajprenal.00609.2017

Wang, F., Lu, X., Liu, M., Feng, Y., Zhou, S. F., and Yang, T. (2015). Renal medullary (pro)renin receptor contributes to angiotensin II-induced hypertension in rats via activation of the local renin-angiotensin system. *BMC Med.* 13:278. doi: 10.1186/s12916-015-0514-1

Wang, W., Luo, R., Lin, Y., Wang, F., Zheng, P., Levi, M., et al. (2015). Aliskiren restores renal AQP2 expression during unilateral ureteral obstruction by inhibiting the inflammasome. *Am. J. Physiol. Renal. Physiol.* 308, F910–F922. doi: 10.1152/ajprenal.00649.2014

Wang, W., Li, C., Summer, S. N., Falk, S., Wang, W., Ljubanovic, D., et al. (2008). Role of AQP1 in endotoxemia-induced acute kidney injury. *Am. J. Physiol. Renal Physiol.* 294, F1473–F1480. doi: 10.1152/ajprenal.00036.2008

Wu, W. P., Chang, C. H., Chiu, Y. T., Ku, C. L., Wen, M. C., Shu, K. H., et al. (2010). A reduction of unilateral ureteral obstruction-induced renal fibrosis by a therapy combining valsartan with aliskiren. *Am. J. Physiol. Renal Physiol.* 299, F929–F941. doi: 10.1152/ajprenal.00192.2010

Conflict of Interest Statement: The authors declare that the research was conducted in the absence of any commercial or financial relationships that could be construed as a potential conflict of interest.

Copyright © 2019 Hu, Xie, Luo, Feng, Liu, Han, Kong, Zou, Wang and Li. This is an open-access article distributed under the terms of the Creative Commons Attribution License (CC BY). The use, distribution or reproduction in other forums is permitted, provided the original author(s) and the copyright owner(s) are credited and that the original publication in this journal is cited, in accordance with accepted academic practice. No use, distribution or reproduction is permitted which does not comply with these terms.

frontiers in Physiology

ORIGINAL RESEARCH
published: 18 September 2019
doi: 10.3389/fphys.2019.01145

Renoprotection Provided by Additional Diuretic Treatment in Partially Nephrectomized Ren-2 Transgenic Rats Subjected to the Combined RAS and ET_A Blockade

Ivana Vaněčková[1], Silvie Hojná[1], Zdenka Vernerová[2], Michaela Kadlecová[1], Hana Rauchová[1], Elzbieta Kompanowska-Jezierska[3], Zdeňka Vaňourková[4], Luděk Červenka[4] and Josef Zicha[1]*

[1] Department of Experimental Hypertension, Institute of Physiology, Czech Academy of Sciences, Prague, Czechia, [2] Department of Pathology, Third Faculty of Medicine, Charles University, Prague, Czechia, [3] Department of Renal and Body Fluid Physiology, Mossakowski Medical Research Centre, Polish Academy of Sciences, Warsaw, Poland, [4] Institute for Clinical and Experimental Medicine, Prague, Czechia

OPEN ACCESS

Edited by:
Xueying Zhao, Morehouse School of Medicine, United States

Reviewed by:
Siddhartha Ghosh, Virginia Commonwealth University, United States
Tetsuo Nakata, Kyoto Pharmaceutical University, Japan

***Correspondence:**
Ivana Vaněčková
ivana.vaneckova@fgu.cas.cz

Specialty section:
This article was submitted to Renal and Epithelial Physiology, a section of the journal Frontiers in Physiology

Received: *24 May 2019*
Accepted: *22 August 2019*
Published: *18 September 2019*

Citation:
Vaněčková I, Hojná S, Vernerová Z, Kadlecová M, Rauchová H, Kompanowska-Jezierska E, Vaňourková Z, Červenka L and Zicha J (2019) Renoprotection Provided by Additional Diuretic Treatment in Partially Nephrectomized Ren-2 Transgenic Rats Subjected to the Combined RAS and ET_A Blockade. Front. Physiol. 10:1145. doi: 10.3389/fphys.2019.01145

Objective: Our previous study in heterozygous Ren-2 transgenic rats (TGR) demonstrated that long-term treatment with endothelin receptor A (ET_A) blocker atrasentan added to the renin-angiotensin system (RAS) blockade had renoprotective effects in a model of chronic kidney disease (CKD) induced by partial nephrectomy. Since ET_A blockade is known to cause edema, we were interested whether diuretic treatment added to this therapy would be beneficial.

Design and Methods: Partial nephrectomy (NX) was performed at the age of 3 months in TGR rats which were subjected to: (i) RAS blockade alone (angiotensin receptor blocker losartan and angiotensin converting enzyme inhibitor trandolapril), (ii) combined RAS (losartan and trandolapril) and ET_A receptor blockade (atrasentan), or (iii) diuretic (hydrochlorothiazide) added to the combined RAS + ET_A blockade for 50 weeks following NX.

Results: At the end of the study systolic blood pressure and cardiac hypertrophy were similarly decreased in all treated groups. Survival was significantly improved by ET_A receptor blockade added to RAS blockade with no further effects of diuretic treatment. However, additional diuretic treatment combined with RAS + ET_A blockade decreased body weight and had beneficial renoprotective effects – reductions of both kidney weight and kidney damage markers. Proteinuria gradually increased in rats treated with RAS blockade alone, while it was substantially lowered by additional ET_A blockade. In rats treated with additional diuretic, proteinuria was progressively reduced throughout the experiment.

Conclusion: A diuretic added to the combined RAS and ET_A blockade has late renoprotective effects in CKD induced by partial nephrectomy in Ren-2 transgenic rats. The diuretic improved: renal function (evaluated as proteinuria and creatinine clearance), renal morphology (kidney mass, glomerular volume), and histological markers of kidney damage (glomerulosclerosis index, tubulointerstitial injury).

Keywords: hydrochlorothiazide, renoprotection, nephrectomy, atrasentan, chronic kidney disease, losartan, trandolapril

INTRODUCTION

Chronic kidney disease (CKD) is often associated with hypertension, diabetes and obesity. Due to its increasing occurrence, it represents an important burden for a healthcare system. Since the symptoms are often unrecognized, it is usually found later in life as it progresses to end-stage renal disease (Zhong et al., 2017). Moreover, as the world population is living longer, the prevalence of CKD increases. The most widely used therapy of CKD, the "gold standard," is provided by the inhibition of the renin-angiotensin system (RAS) exerting both antihypertensive and nephroprotective effects (Raij, 2005). However, this therapy is not able to halt the progression of CKD to end-stage renal disease (ESRD) and, therefore, new additive/combination therapies are strongly needed (Breyer and Susztak, 2016; Komers and Plotkin, 2016).

One of the treatment possibilities is the blockade of endothelin receptor A (ET_A) since the activation of these receptors with endothelin-1 (Yanagisawa et al., 1988; Davenport et al., 2016, 2018) is associated with inflammation, proliferation, fibrosis and renal cell injury (including podocyte injury) which ultimately leads to proteinuria. Many experimental as well as clinical studies indicated favorable potential of endothelin receptor antagonists (ERAs) – "sentans" – in the treatment of CKD especially due to their renoprotective capacities (for review see Kohan and Pollock, 2013; Kohan and Barton, 2014; Culshaw et al., 2015; Czopek et al., 2016; Vaněčková et al., 2018; Dhaun and Webb, 2019).

Ren-2 transgenic rats are a model of angiotensin II-dependent hypertension associated with an inappropriately activated RAS due to the insertion of mouse renin-2 gene into the Hannover Sprague-Dawley rats (Mullins et al., 1990). In combination with subtotal nephrectomy (Morrison, 1962) severe renal impairment is induced not only due to a markedly activated RAS but also due to highly elevated endothelin levels (Vaněčková et al., 2012; Čertíková Chábová et al., 2014; Sedláková et al., 2017). Thus, this model is of critical importance since it combines high blood pressure and activated renin-angiotensin and endothelin systems, which contribute to the progression of CKD to ESRD.

Our studies in this particular model of CKD (5/6 NX in Ren-2 transgenic rats) revealed that the chronic sole endothelin receptor A blockade with atrasentan improved survival rate, prevented the development of enhanced hypertension following subtotal nephrectomy, and attenuated end-organ damage (Vaněčková et al., 2012). Moreover, if chronic atrasentan treatment was combined with RAS blockade (maximal doses of angiotensin receptor blocker losartan and angiotensin converting enzyme inhibitor trandolapril), it exerted beneficial antiproteinuric effects. However, these effects were seen only after a very long treatment (44 weeks) (Čertíková Chábová et al., 2014), while they were not demonstrated after a shorter period (20 weeks) (Vaněčková et al., 2012). The beneficial effects of additional ET_A blockade were also lost when the treatment was postponed to the phase of established CKD, i.e., when the therapy was started 6 weeks after the induction of CKD by the subtotal nephrectomy (Sedláková et al., 2017).

The benefits of the therapy with endothelin receptor A antagonists are limited not only by their tolerability profile, but also by fluid retention which led to the termination of several big studies, including ASCEND (Mann et al., 2010) and RADAR (de Zeeuw et al., 2014). The final results of the SONAR clinical trial (Heerspink et al., 2019) demonstrated positive effect of atrasentan in the reduction of renal events in patients with type 2 diabetes and CKD although fluid retention in a number of patients still occurred. Moreover, the DUET study (Komers et al., 2017) in patients with focal segmental glomerulosclerosis (FSGS) (Trachtman et al., 2018) demonstrated better renoprotection by sparsentan (dual RAS and ET_A blocker) compared to irbesartan following 8 weeks of treatment: sparsentan being well tolerated and safe.

Apart from the liver toxicity and anemia the most significant side effect associated with endothelin receptor antagonists is fluid retention. A possible mechanism is the redistribution of body fluids within the body due to an increase in vascular permeability following the activation of ET_B receptors during ET_A receptor blockade (Vercauteren et al., 2017). Since the body weight (BW) gain and peripheral edema have been encountered to a certain degree with all endothelin receptor A antagonists, the use of diuretics to circumvent this problem was considered to be reasonable. Additionally, diuretics are inexpensive and efficient antihypertensives which can be used even in the advanced stages of CKD. Specifically, the concomitant use of thiazides (in combination with the inhibitors of the RAS) is now being revised in the treatment of this disease (Sinha and Agarwal, 2015) based on the clinical studies showing their positive effects on BP and proteinuria (Cirillo et al., 2014; Morales et al., 2015; Fuwa et al., 2016). However, there are almost no experimental data showing the positive effects of ET_A receptor antagonists in combination with diuretics. The only information available is that chlorthalidone combined with atrasentan exerted an antiproteinuric effect in Dahl rats fed a high fat/high salt diet which is a model of a metabolic syndrome (Jin et al., 2014).

Therefore, in the present study, we hypothesized whether the use of a diuretic alleviates the negative side effects of ET_A receptor blockade leading to fluid retention and whether the use

of hydrochlorothiazide is beneficial in a model of CKD induced by partial nephrectomy in hypertensive Ren-2 transgenic rats.

MATERIALS AND METHODS

Animals

Adult male heterozygous (mRen-2)27 transgenic (TGR) rats were housed at 23°C under a 12 h light/dark cycle, fed an Altromin diet (0.45% NaCl) and given tap water *ad libitum*. Partial nephrectomy (removal of the right kidney and both poles of the contralateral kidney) was performed in rats under anesthesia (tiletamine + zolazepam, Virbac SA, Carros Cedex, France, 8 mg/kg; and xylazine, Spofa, Czechia, 4 mg/kg intramuscularly), as described previously (Vaněčková et al., 2012; Čertíková Chábová et al., 2014) at the age of 3 months.

All the procedures and experimental protocols were approved by the Ethical Committee of the Institute of Physiology, Czech Academy of Sciences, and conformed to the European Convention on Animal Protection and Guidelines on Research Animal Use.

Chronic Treatment in Subtotally Nephrectomized TGR

We used three different therapies: (i) RAS blockade alone – angiotensin receptor blocker losartan (10 mg/kg/day; Lozap, Zentiva, Czechia) and angiotensin converting enzyme inhibitor trandolapril (0.6 mg/kg/day; Gopten, Abbott, Germany), (ii) combined RAS (losartan and trandolapril) and ET_A receptor blockade (atrasentan – 5 mg/kg/day; ABT-627, a generous gift from AbbVie, IL, United States), and (iii) diuretic hydrochlorothiazide (6 mg/kg/day; Léčiva, Czechia) given with the combined RAS + ET_A blockade. All these treatments started immediately after nephrectomy and lasted 50 weeks. The drug dosages were selected on the basis of previous studies (Vaněčková et al., 2012; Arias et al., 2013; Čertíková Chábová et al., 2014). The concentration of atrasentan was adjusted weekly according to the actual water intake to achieve a constant dose of atrasentan (5 mg/kg/day); this dosage was previously found to effectively block ET_A receptors (Vaněčková et al., 2012, 2018).

The following experimental groups were investigated:

1. Sham-operated TGR + water ($n = 12$).
2. 5/6 NX TGR + water ($n = 18$).
3. 5/6 NX TGR + RAS blockade ($n = 10$).
4. 5/6 NX TGR + RAS blockade + ET_A blockade ($n = 10$).
5. 5/6 NX TGR + RAS blockade + ET_A blockade + diuretic ($n = 10$).

Systolic BP, diastolic BP, and heart rate were measured by a direct cannulation of the carotid artery under isoflurane anesthesia (1.5% isoflurane) using a pressure transducer and a multichannel recorder (ADInstruments, Bella Vista, Australia) at the end of the experiment. Body weight and survival were monitored throughout the experiment. At weeks 1, 5, 9, 13, 17, 20, 30, 40 and 50, the animals were placed in individual metabolic cages for 24-h urine collection and proteinuria and creatinine excretion were determined. At these same measurement points, blood samples were withdrawn for the determination of creatinine concentration in plasma. This approach is regularly used and validated in our laboratory (Vaněčková et al., 2012; Čertíková Chábová et al., 2014). Urinary protein was measured using the Folin method with bovine serum albumin as a standard (Lowry et al., 1951). Plasma creatinine was measured by a FUJI DRI-CHEM analyzer using appropriate slides for creatinine CRE-P III (FUJIFILM Corp., Tokyo, Japan). Urine creatinine was determined using a Liquick Cor-CREATININE kit that is based on the modified Jaffe's method, without deprotenization (PZ CORMAY S.A., Poland). In an alkaline solution picrate reacts with creatinine to form a yellow-red 2,4,6-trinitrocyclohexadienate. The color intensity, measured by a photometer at 500 nm, is proportional to the creatinine concentration. Clearance of creatinine was calculated using a standard formula and was normalized per body weight. At the end of the study, the kidney and heart were weighed. The central part of the left kidney was always used to assess renal glomerular damage.

Histological Examination

The kidneys for histological analysis were fixed in 4% formaldehyde, dehydrated and embedded in paraffin. The sections stained with hematoxylin-eosin and PAS (periodic acid, for Schiff reaction) were examined and evaluated in a blind-test fashion. Fifty glomeruli in each kidney were examined on a semi-quantitative scale as described previously (Saito et al., 1987): grade 0, all glomeruli normal; grade 1, sclerotic area up to 25% (minimal sclerosis); grade 2, sclerotic area 25 to 50% (moderate sclerosis); grade 3, sclerotic area 50 to 75% (moderate-to-severe sclerosis); and grade 4, sclerotic area 75 to 100% (severe sclerosis). The glomerulosclerosis index (GSI) was calculated using the following formula: $GSI = [(1 \times n1) + (2 \times n2) + (3 \times n3) + (4 \times n4)]/(n0 + n1 + n2 + n3 + n4)$, where nx is the number of glomeruli in each grade of glomerulosclerosis. Renal cortical tubulointerstitial injury was evaluated on the basis of inflammatory cell infiltration, tubular atrophy, and interstitial fibrosis, using the semi-quantitative scoring method: for tubular atrophy: grade 0, no atrophy; grade 1, mild (<25% of the tubuli atrophic); grade 2, moderate (25–50% of the tubuli atrophic); and grade 3, severe (>50% of the tubuli atrophic) (Nakano et al., 2008). Inflammatory infiltrate and interstitial fibrosis were graded as mild (grade 1), moderate (grade 2) and severe (grade 3). The lesions were assessed in at least 30 random and non-overlapping fields in the renal cortex. Morphometric evaluation of the cross-sectional area of glomeruli (glomerular area) was performed on the same kidney sections that were examined for morphological changes with the method employed in our previous study (Rakusan et al., 2010), using the Nikon NIS-Elements AR 3.1 morphometric program (Nikon, Tokyo, Japan).

Statistics

The data are presented as the means ± SEM. Statistical analysis was done by Student's *t*-test, Wilcoxon's signed-rank test for unpaired data, or one-way analysis of variance (ANOVA) when appropriate, using the Graph-Pad Prism software (Graph Pad

Software, San Diego, CA, United States), and ANOVA for repeated measurements, followed by Student–Newman–Keuls test performed for the analysis within groups, when appropriate. Comparison of the survival curves was performed using a log-rank (Mantel–Cox) test followed by a Gehan–Breslow–Wilcoxon test. In order to obtain reliable data regarding the effects of treatment regimens on the survival rate, high initial *n* values were used to enable valid comparison of the long-term survival rate. These initial *n* values were estimated by statistical power analyses method developed by Cohen (2013).

RESULTS

While 80% of the sham-operated TGR survived until the end of the experiment, untreated TGR-NX rats began to die at week 4 and no TGR-NX rat survived 18 weeks following nephrectomy (**Figure 1A**). In contrast, RAS blockade alone substantially improved survival to the point that 55% of the animals were alive at the end of the study (52 weeks after surgery). Moreover, combined RAS + ET_A blockade without or with additional diuretic further increased the survival of these animals, reaching almost 90% at the end of the study.

Partial nephrectomy resulted in a substantial reduction of body weight gain in all groups but the treatments used in our experiments enabled a significant, subsequent increase in body weight, although the body weight in all treated groups of TGR-NX animals was still lower compared to the sham-operated TGR rats (**Figure 1B**). The body weight of partially nephrectomized rats, which were treated with a diuretic given with the combined RAS + ET_A blockade, was significantly lower than in rats treated with RAS blockade alone or with combined RAS + ET_A blockade during the study, suggesting reduced fluid retention.

Although systolic BP was similarly reduced by all three therapies showing the prevailing BP effect of RAS blockade, there was a mild tendency for a further drop of BP in diuretic-treated rats (110 ± 3 mm Hg in RAS blockade alone; 111 ± 4 mm Hg in combined RAS + ET_A blockade; 99 ± 2 mm Hg in combined RAS + ET_A blockade + diuretic) (**Figure 2A**). The sham-operated TGR exhibited distinct cardiac hypertrophy evaluated as heart weight/body weight ratio (2.62 ± 0.02 g/kg BW) (**Figure 2B**). Consistent with the normalization of BP following the treatments, relative cardiac weight was similarly decreased in all treated groups (2.24 ± 0.06 g/kg BW in RAS blockade alone; 2.29 ± 0.08 g/kg BW in combined RAS + ET_A blockade; 2.27 ± 0.08 g/kg BW in combined RAS + ET_A blockade + diuretic). Similarly, there were no differences in cardiac or left ventricular weights related to tibial length among TGR-NX animals subjected to the above treatments (data not shown).

There was only a gradual increase of proteinuria in sham-operated TGR during the study (16.4 ± 1.2 mg/24 h at week 1 vs. 41 ± 2 mg/24 h at week 50) (**Figure 3A**). In contrast, proteinuria in untreated TGR-NX rats rose steeply between weeks 1 and 5 after nephrectomy (13.4 ± 0.7 mg/24 h vs. 37.8 ± 3.0) and remained high until the death of the animals (47.3 ± 4.2 mg/24 h). On the other hand, all three treatments

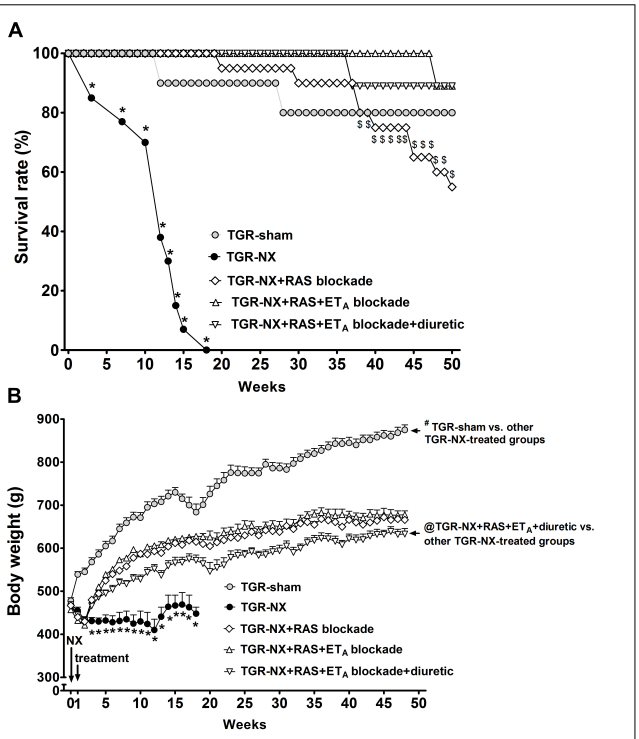

FIGURE 1 | The effect of diuretic treatment added to combined RAS and ET_A blockade on survival and body weight. Survival rate **(A)** and body weight **(B)** in sham-operated TGR (TGR-sham), nephrectomized TGR (TGR-NX) untreated receiving water or treated with the renin-angiotensin system (RAS) blockade alone (TGR-NX + RAS blockade), combined RAS + ET_A blockade (TGR-NX + RAS + ET_A blockade) or diuretic given with the combined RAS + ETA blockade (TGR-NX + RAS + ET_A blockade + diuretic). # $P < 0.05$ TGR-sham vs. other TGR-NX-treated groups, $ $P < 0.05$ TGR-NX + RAS treated vs. other TGR-NX-treated groups, @ $P < 0.05$ TGR-NX + RAS + ETA + diuretic vs. other TGR-NX-treated groups, *$P < 0.05$ untreated TGR-NX group compared with all other treated TGR-NX groups at the same time point.

slightly attenuated proteinuria during the first month of therapy (week 1 vs. week 5: 14 ± 2.5 mg/24 h vs. 7 ± 0.8 mg/24 h in RAS blockade alone; 15.6 ± 4.8 mg/24 h vs. 7.7 ± 0.3 mg/24 h in the combined RAS + ET_A blockade; and 15.5 ± 4.6 mg/24 h vs. 7.5 ± 0.4 mg/24 h in the combined RAS + ET_A blockade + diuretic) and proteinuria was significantly lowered when compared with sham-operated TGR (16.5 ± 0.9 mg/24 h). The treatment with RAS blockade alone was able to prevent the dramatic increase in proteinuria observed in untreated TGR-NX rats until week 20 after nephrectomy (10.2 ± 1.1 mg/24 h in TGR-NX + RAS at week 20 vs. 47.3 ± 4.2 mg/24 h in TGR-NX at week 13). However, after 30 weeks following nephrectomy a late, gradual increase in proteinuria occurred in the TGR-NX + RAS group, reaching 55.3 ± 2.7 mg/24 h at week 50. In contrast, additional ET_A blockade partially reversed this trend and diuretic treatment given with the combined RAS + ET_A blockade maintained proteinuria at low levels throughout the entire experiment (30 ± 2.5 mg/24 h in RAS + ET_A blockade and 12.4 ± 3 mg/24 h in RAS + ET_A blockade + diuretic at week 50) (**Figure 3A**).

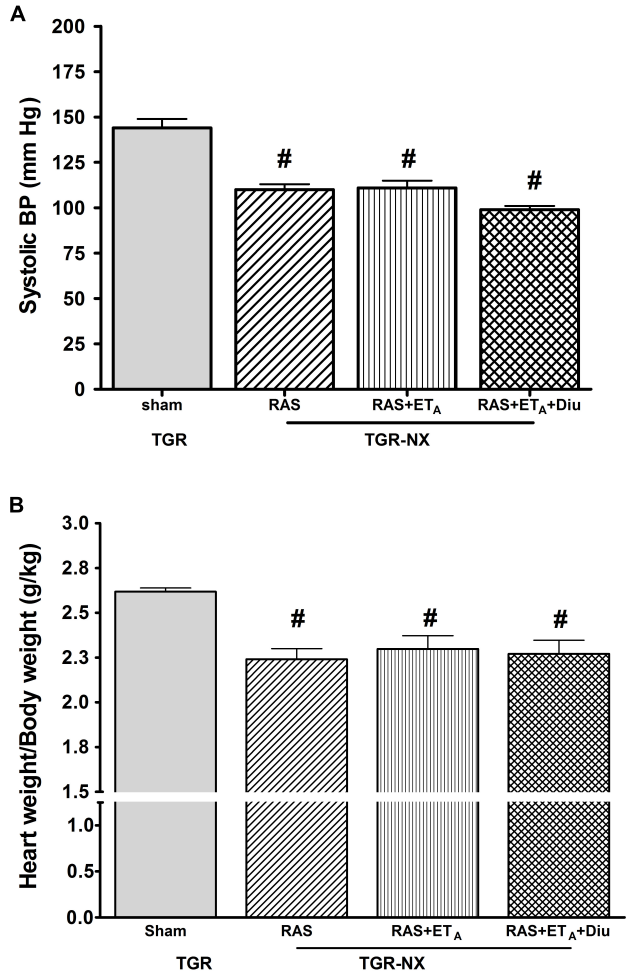

FIGURE 2 | The effect of diuretic treatment added to combined RAS and ET_A blockade on SBP and cardiac hypertrophy. Systolic blood pressure **(A)** and cardiac hypertrophy **(B)** in sham-operated heterozygous Ren-2 transgenic rats (TGR-sham), nephrectomized TGR (TGR-NX) treated with the renin-angiotensin system blockade alone (RAS), combined RAS + ET_A blockade (RAS + ET_A); or diuretic given with the combined RAS + ET_A blockade (RAS + ET_A + Diu). # $P < 0.05$ TGR-sham vs. other TGR-NX-treated groups, Diu – diuretic.

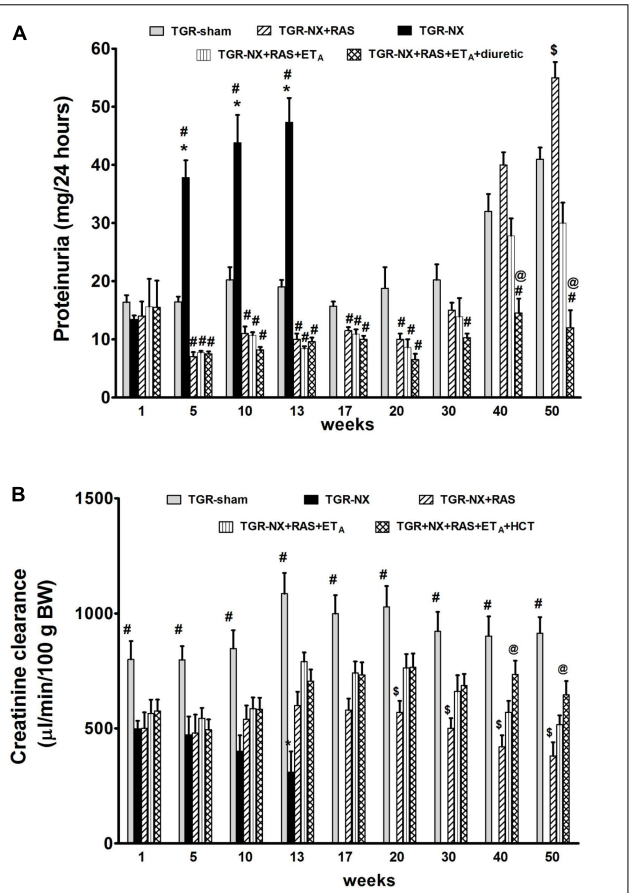

FIGURE 3 | The effect of diuretic treatment added to combined RAS and ETA blockade on proteinuria and creatinine clearance. Proteinuria **(A)** and creatinine clearance **(B)** in sham-operated TGR (TGR-sham), nephrectomized TGR (TGR-NX) untreated receiving water or treated with the renin-angiotensin system (RAS) blockade alone (TGR-NX + RAS), combined RAS + ET_A blockade (TGR-NX + RAS + ET_A), or diuretic given with the combined RAS + ET_A blockade (TGR-NX + RAS + ET_A blockade + diuretic). # $P < 0.05$ TGR-sham vs. other TGR-NX-treated groups, $ $P < 0.05$ TGR-NX + RAS treated vs. other TGR-NX-treated groups, @ $P < 0.05$ TGR-NX + RAS + ET_A + diuretic vs. other TGR-NX-treated groups, *$P < 0.05$ untreated TGR-NX group compared with all other treated TGR-NX groups at the same time point.

Creatinine clearance was stable in the sham-operated TGR rats during the entire experiment (**Figure 3B**). By contrast, creatinine clearance dramatically decreased after partial nephrectomy in all groups. In untreated animals, it rapidly declined with time, while all three treatments were able to partially reverse this drop of creatinine clearance. Moreover, creatinine clearance gradually decreased in the TGR-NX rats with RAS blockade alone, while additional ET_A blockade partly prevented this decrease. It is important to emphasize that the beneficial effects of diuretic added to RAS + ET_A blockade on glomerular filtration were observed especially in the late phase of the study (weeks 40 to 50) (**Figure 3B**).

The relative kidney weights (evaluated as kidney weight/body weight) (**Figure 4A**) in all treated nephrectomized TGR groups were significantly lower than those in sham-operated TGR (4.0 ± 0.18 g/kg BW in RAS blockade alone; 4.1 ± 0.24 mg/kg BW in the combined RAS + ET_A blockade and 3.39 ± 0.12 g/kg BW in RAS + ET_A blockade + diuretic vs. 5.8 ± 0.28 g/kg BW in TGR-sham). It is important to note that the addition of a diuretic strongly reduced kidney enlargement which is a crucial process underlying CKD progression. A similar effect was also observed using histological examination – the glomerular area (**Figure 4B**) of rats treated with additional hydrochlorothiazide was substantially smaller in comparison with animals treated with RAS blockade alone or with the combined RAS + ET_A blockade. The RAS blockade alone was not able to diminish the renal alterations caused by partial nephrectomy (glomerulosclerosis index and tubulointerstitial injury) (**Figure 5**) to a substantial degree but the addition of ET_A receptor blocker atrasentan to

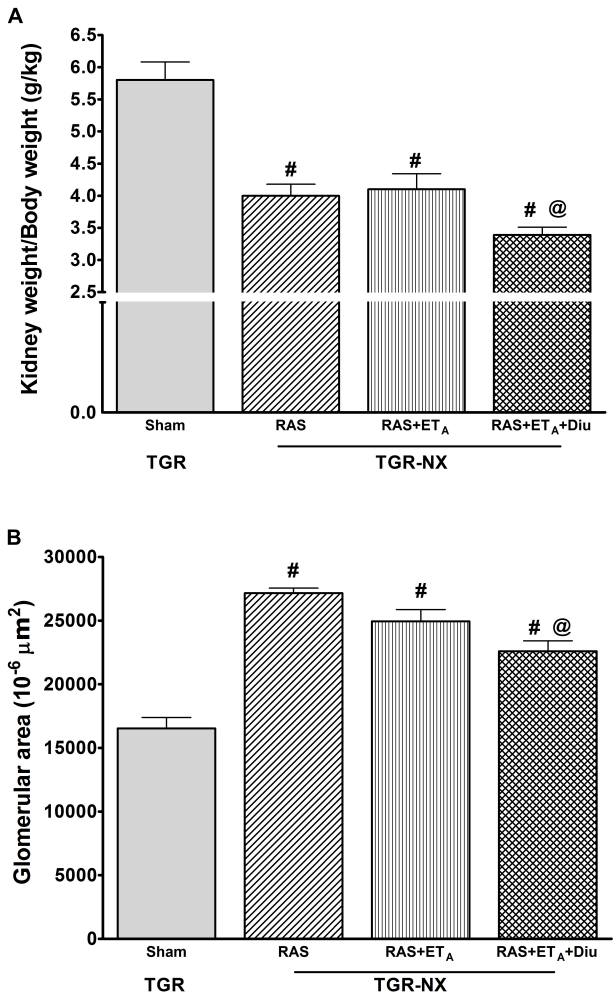

FIGURE 4 | The effect of diuretic treatment added to combined RAS and ET_A blockade on relative kidney weight and glomerular area. Relative kidney weight **(A)** and glomerular area **(B)** in sham-operated heterozygous Ren-2 transgenic rats (TGR-sham), nephrectomized TGR (TGR-NX) treated with the renin-angiotensin system blockade alone (RAS), combined RAS + ET_A blockade (RAS + ET_A); or diuretic given with the combined RAS + ET_A blockade (RAS + ET_A + Diu). # $P < 0.05$ TGR-sham vs. other TGR-NX-treated groups, Diu – diuretic. # $P < 0.05$ TGR-sham vs. other TGR-NX-treated groups, @ $P < 0.05$ TGR-NX + RAS + ET_A + diuretic vs. other TGR-NX-treated groups.

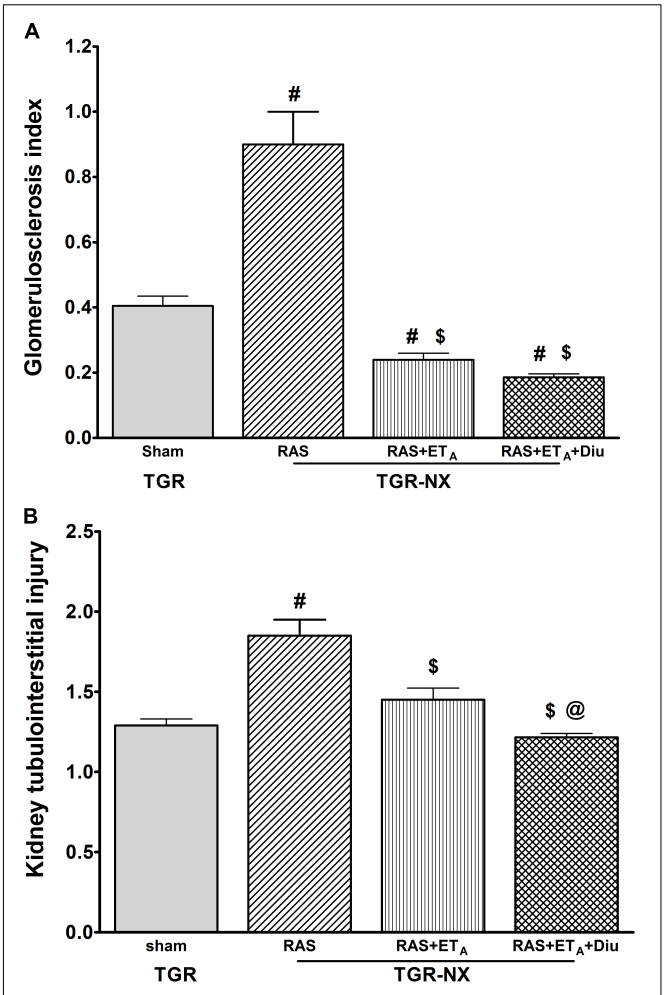

FIGURE 5 | The effect of diuretic treatment added to combined RAS and ET_A blockade on histological markers of renal damage. Glomerulosclerosis index **(A)** and kidney tubulointerstitial injury **(B)** in sham-operated heterozygous Ren-2 transgenic rats (TGR-sham), nephrectomized TGR (TGR-NX) treated with the renin-angiotensin system blockade alone (RAS), combined RAS + ET_A blockade (RAS + ET_A); or diuretic given with the combined RAS + ET_A blockade (RAS + ET_A + Diu). Diu – diuretic # $P < 0.05$ TGR-sham vs. other TGR-NX-treated groups, $ $P < 0.05$ TGR-NX + RAS treated vs. other TGR-NX-treated groups, @ $P < 0.05$ TGR-NX + RAS + ET_A + diuretic vs. other TGR-NX-treated groups.

RAS therapy significantly attenuated both parameters. Finally, diuretic treatment caused a further drop in the glomerulosclerosis index and kidney tubulointerstitial injury. Representative kidney slices stained with periodic acid-Schiff (PAS) are depicted in **Figure 6**.

DISCUSSION

This is the first study showing the beneficial effects of a diuretic added to a combination of the RAS inhibitors and endothelin receptor A antagonist atrasentan in a model of CKD which was induced by subtotal nephrectomy in hypertensive heterozygous Ren-2 transgenic rats. While the ET_A receptor blockade added to the RAS blockade improved survival, decreased proteinuria and reduced indices of renal injury (glomerulosclerosis index and tubulointerstitial injury), the addition of hydrochlorothiazide had further profound effects on the proteinuria and creatinine clearance, and substantially reduced the kidney weight and the glomerular area. However, the beneficial effects of diuretic therapy on proteinuria and creatinine clearance were evident only after a very long treatment (40–50 weeks). This is consistent with our previous study in which we demonstrated no additional renoprotective effects of ET_A receptor blockade combined with RAS blockade if the treatment lasted only 20 weeks (Vaněčková et al., 2012). In contrast, the positive

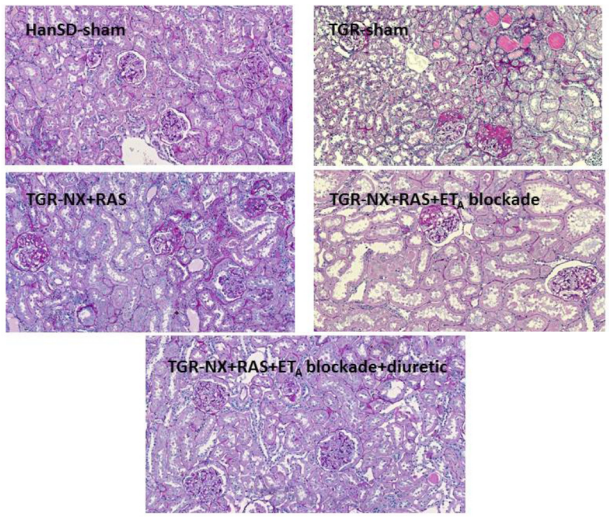

FIGURE 6 | Representative images of renal histology. Renal parenchyma without morphological alterations in control sham-operated HanSD rats (HanSD-sham). Extensive secondary focal segmental glomerulosclerosis and small zone of atrophic tubules (the upper right part) in sham-operated heterozygous Ren 2 transgenic rats (TGR-sham). RAS blockade only partially improved morphology of renal parenchyma; focal segmental glomerulosclerosis persists as well as glomerular enlargement in nephrectomized TGR (TGR-NX + RAS). Combined RAS and ETA blockade substantially atenuated renal injury in nephrectomized TGR; glomeruli contain segmental tuft sclerosis only sporadically (TGR-NX + RAS + ET_A blockade). Treatment with diuretic added to the combined RAS+ETA blockade most significantly protected renal parenchyma from injury in nephrectomized TGR (TGR-NX + RAS + ET_A blockade + diuretic). Periodic acid-Schiff staining. Magnification 200×.

effects, observed both in the earlier study (Čertíková Chábová et al., 2014) and in this one, were seen after the same treatment which lasted 40–50 weeks. Considering the importance for clinical practice, one should bear in mind that such a lifelong treatment resembles the antihypertensive treatment which is provided to patients for many decades. This should be considered in the design of clinical studies to ensure that they are of sufficient duration (i.e., adequately prolonged) in order to observe the benefits of such therapies in patients. It is evident that the translation of experimental results into clinical practice is difficult and sometimes not successful as has been described with the dual RAS blockade in CKD (Čertíková Chábová and Červenka, 2017).

It seems that there is a critical moment, i.e., at 20–30 weeks of treatment, when the sole RAS inhibition fails to be a sufficient therapy of CKD and additional therapeutic interventions are necessary. Such decreased efficiency of the treatment with RAS inhibitors and therefore the necessity of additional therapy were observed not only in the present study but also in the previous one (Čertíková Chábová et al., 2014). Moreover, similar findings of a substantial increase in proteinuria associated with an increased mortality after 30 weeks of treatment were also observed in TGR rats in which the treatment was postponed to the established phase of CKD (Sedláková et al., 2017). The results of our studies suggest some structural or functional changes in the kidney that are sensitive to additional treatments. Unfortunately, there are no other experimental studies with such long treatments that could enable us to discuss this idea. Therefore, further studies are needed to elucidate this issue.

As has been already discussed, the animals treated with RAS blockade alone started to die dramatically after 30 weeks of therapy. Although we did not determine the cause of death in rats subjected to partial nephrectomy in this particular study, the comparison of survival curve with the development of proteinuria or creatinine clearance indicates that the early death of untreated TGR-NX rats at 10–15 weeks after surgery as well as the late death of TGR-NX rats subjected to RAS blockade alone at 35–50 weeks after surgery was associated with a major reduction of GFR and a substantial increase of albuminuria. Thus, renal failure rather than heart failure might be the cause of their deaths. Nevertheless, a previous study of our colleagues, Kujal and Vernerová (unpublished results), who analyzed the cause of deaths following 5/6 nephrectomy demonstrated that about 50% of animals subjected to 5/6 nepherectomy died from heart failure during the 16 weeks of their study. The additional ET_A receptor therapy (with or without a diuretic) substantially increased survival, suggesting the importance of ET_A therapy. However, since we did not include the groups with diuretic added to RAS blockade (without ET_A receptor blockade) and diuretic added to ET_A receptor blockade (without RAS blockade), we are not able to determine which particular blockade would be more efficient. The reason for why we did not include these groups was the fact that the blockade of the RAS is the standard therapy of CKD; so that all therapies used in our study were based on RAS blockade. Nevertheless, on the basis of the better nephroprotective effects of therapy with a diuretic added to the combined RAS + ET_A blockade especially at the final stages of our study, one would anticipate that the survival in this particular group would improve significantly if the study were to be further prolonged.

Creatinine clearance in sham-operated TGR was 800–1000 μl/min/100 g BW, which was reduced to 500 after NX with a further drop to 300 at week 13. Similarly low value (380 μl/min/100 g BW) was found in TGR-NX treated with RAS blockade at week 50 after the surgery. In contrast, the addition of diuretics increased creatinine clearance to 600–700 μl/min/100 g BW throughout the study. According to CKD Guidelines, stage 3 is defined as a 50–75% reduction in GFR. It could be implied from our extrapolations that subtotally nephrectomized animals had GFR reduced by 50% (approximately stage 3) and that the diuretics added to the combined RAS + ET_A blockade were able to increase it by 25%. In other words, the addition of a diuretic improved the stage 3 to stage 2 of experimental CKD.

Interestingly, the positive effects of a combination of diuretic chlorthalidone with ET_A receptor blockade on albuminuria were demonstrated in Dahl rats on a high-fat/high-salt diet, a model of metabolic syndrome, after 4 weeks of treatment (Jin et al., 2014). In the same experimental model, the combination of enalapril (angiotensin enzyme inhibitor) and atrasentan was used in animals kept on a high-salt diet for 12 weeks. While a combination of both drugs reduced cardiac hypertrophy,

atrasentan (but not enalapril) attenuated proteinuria and serum creatinine level (Samad et al., 2015).

Although there was a tendency to lower BP in rats with additional diuretic treatment, the blood pressure and cardiac hypertrophy were similarly attenuated in all three groups of treated rats. These findings are not surprising as the maximal RAS blockade with losartan and trandolapril was employed in our study and hence the effective lowering of blood pressure to normotension was already achieved by RAS blockade alone. It seems that the beneficial renoprotective effects of diuretics on renal function (proteinuria and creatinine clearance) and renal damage (glomerular area and kidney weight together with tubulointerstitial changes) were achieved beyond those exerted by a normalization of blood pressure. Similar effects of different classes of RAS blockers (including direct renin inhibitor aliskiren) on BP normalization were also demonstrated in TGR rats without nephrectomy (Vaněčková et al., 2016).

Concerning the body weight, a diuretic added to the combined RAS + ET_A blockade significantly decreased body weight while no significant body weight gain was observed in rats with combined RAS + ET_A blockade. However, to determine whether edema is present, the volume and distribution of body fluids should be measured. Nevertheless, a significantly higher urine production in the diuretic-treated TGR with combined RAS + ET_A blockade was discerned at weeks 13, 40 and 50 (31 ± 2 vs. 24 ± 1 ml/24 h at week 13, 31 ± 2 vs. 25 ± 2 ml/24 h at week 40 and 27 ± 1 vs. 23 ± 1 ml/24 h at week 50) as compared with TGR treated only with RAS + ET_A blockade. Importantly, kidney weights (both absolute and relative) were greatly reduced in the rats treated with an additional diuretic. This finding together with a substantially smaller glomerular area in diuretic-treated rats is consistent with a glomerular hypertrophy concept (Brenner et al., 1996) suggesting that glomerular hyperfiltration and hypertension are major factors contributing to CKD development. Future studies are needed to elucidate whether podocytes are involved in this process (Kriz and Lemley, 2015).

It remains to be determined, whether the combination of other diuretics and RAS blockers would be similarly effective, since a combination of losartan with hydrochlorothiazide, but not with furosemide, was beneficial in rats with subtotal nephrectomy (Arias et al., 2013, 2016). Moreover, the benefits of hydrochlorothiazide against furosemide were demonstrated also in human studies (Fuwa et al., 2016). Although thiazides were previously not recommended in CKD patients, their use even in advanced stages of CKD is now being reconsidered (Sinha and Agarwal, 2015) because in combination with RAS blockade they were effective in reducing BP (Cirillo et al., 2014) and proteinuria (Morales et al., 2015). The superiority of losartan (ARB) has been documented not only in an earlier study in animals with subtotal nephrectomy (Fujihara et al., 2005) but also in a recent study (Maquigussa et al., 2018) showing the ability of losartan to restore anti-fibrotic molecules Klotho and PPAR gamma and thus to reduce tubulointerstitial fibrosis which is one of the key factors underlying the progression of CKD to ESRD (Zoja et al., 2006). In addition, newer thiazide-like diuretics (chlorthalidone and indapamide) might also be considered although their usage has not been supported by clinical data (Thomopoulos et al., 2015).

DATA AVAILABILITY

The datasets generated for this study are available on request to the corresponding author.

ETHICS STATEMENT

The animal study was reviewed and approved by Ethical Committee of the Institute of Physiology, Czech Academy of Sciences.

AUTHOR CONTRIBUTIONS

IV conceived and designed the project and wrote the manuscript. SH, HR, ZVa, and MK performed the experiments. ZVe examined the histology. IV and JZ analyzed the data and interpreted the results. JZ, LČ, and EK-J edited the manuscript. All authors read and approved the final version of the manuscript.

FUNDING

This work was supported by a research grant of the Ministry of Health of the Czech Republic (15-25396A) and also partially supported by the Bilateral mobility project of the Czech Academy of Sciences and the Polish Academy of Sciences (PAN-17-13), and by an institutional support (RVO: 67985823).

ACKNOWLEDGMENTS

The technical assistance of Zdeňka Kopecká and Alena Charvátová is highly appreciated. Atrasentan was generously provided from AbbVie (Grant No. 11116). The authors are grateful to Mr. Robert Kotanchik for his help in editing the manuscript.

REFERENCES

Arias, S. C., Souza, R. A., Malheiros, D. M., Fanelli, C., Fujihara, C. K., and Zatz, R. (2016). An association of losartan-hydrochlorothiazide, but not losartan-furosemide, completely arrests progressive injury in the remnant kidney. *Am. J. Physiol. Renal Physiol.* 310, F135–F143. doi: 10.1152/ajprenal.00388.2015

Arias, S. C., Valente, C. P., Machado, F. G., Fanelli, C., Origass, C. S., de Brito, T., et al. (2013). Regression of albuminuria and hypertension and arrest of severe renal injury by a losartan-hydrochlorthiazide association in a model of very advanced nephropathy. *PLoS One* 8:e56215. doi: 10.1371/journal.pone.0056215

Brenner, B. M., Lawler, E. V., and Mackenzie, H. S. (1996). The hyperfiltration theory: a paradigm shift in nephrology. *Kidney Int.* 49, 1774–1777. doi: 10.1038/ki.1996.265

Breyer, M. D., and Susztak, K. (2016). Developing treatments for chronic kidney disease in the 21st century. *Semin. Nephrol.* 36, 436–447. doi: 10.1016/j.semnephrol.2016.08.001

Čertíková Chábová, V., and Červenka, L. (2017). The dilemma of dual renin-angiotensin system blockade in chronic kidney disease: why beneficial in animal experiments but not in the clinic? *Physiol. Res.* 66, 181–192.

Čertíková Chábová, V., Vernerová, Z., Kujal, P., Husková, Z., Škaroupková, P., Tesař, V., et al. (2014). Addition of ETA receptor blockade increases renoprotection provided by renin-angiotensin system blockade in 5/6 nephrectomized Ren-2 transgenic rats. *Life Sci.* 118, 297–305. doi: 10.1016/j.lfs.2013.12.018

Cirillo, M., Marcarelli, F., Mele, A. A., Romano, M., Lombardi, C., and Bilancio, G. (2014). Parallel-group 8-week study on chlorthalidone effects in hypertensives with low kidney function. *Hypertension* 63, 692–697. doi: 10.1161/HYPERTENSIONAHA.113.02793

Cohen, J. (2013). *Statistical Power Analysis for the Behavioral Sciences*. Cambridge, MA: Academic press.

Culshaw, G. J., MacIntyre, I. M., Dhaun, N., and Webb, D. J. (2015). Endothelin in nondiabetic chronic kidney disease: preclinical and clinical studies. *Semin. Nephrol.* 35, 176–187. doi: 10.1016/j.semnephrol.2015.03.002

Czopek, A., Moorhouse, R., Webb, D. J., and Dhaun, N. (2016). Therapeutic potential of endothelin receptor antagonism in kidney disease. *Am. J. Physiol. Renal Physiol. Regul. Integr. Comp. Physiol.* 310, R388–R397. doi: 10.1152/ajpregu.00478.2015

Davenport, A. P., Hyndman, K. A., Dhaun, N., Southan, C., Kohan, D. E., Pollock, J. S., et al. (2016). Endothelin. *Pharmacol. Rev.* 68, 357–418. doi: 10.1124/pr.115.011833

Davenport, A. P., Kuc, R. E., Southan, C., and Maguire, J. J. (2018). New drugs and emerging therapeutic targets in the endothelin signaling pathway and prospects for personalized precision medicine. *Physiol. Res.* 67(Suppl. 1), S37–S54.

de Zeeuw, D., Coll, B., Andress, D., Brennan, J. J., Tang, H., Houser, M., et al. (2014). The endothelin antagonist atrasentan lowers residual albuminuria in patients with type 2 diabetic nephropathy. *J. Am. Soc. Nephrol.* 25, 1083–1093. doi: 10.1681/ASN.2013080830

Dhaun, N., and Webb, D. J. (2019). Endothelins in cardiovascular biology, and therapeutics. *Nat. Rev. Cardiol.* 16, 491–502. doi: 10.1038/s41569-019-0176-173

Fujihara, C. K., Velho, M., Malheiros, D. M., and Zatz, R. (2005). An extremely high dose of losartan affords superior renoprotection in the remnant model. *Kidney Int.* 67, 1913–1924. doi: 10.1111/j.1523-1755.2005.00290.x

Fuwa, D., Fukuda, M., Ogiyama, Y., Sato, R., Mizuno, M., Miura, T., et al. (2016). Addition of hydrochlorothiazide to angiotensin receptor blocker therapy can achieve a lower sodium balance with no acceleration of intrarenal renin angiotensin system in patients with chronic kidney disease. *J. Renin Angiotens. Aldoster. Syst.* 17:1470320316652032. doi: 10.1177/1470320316652032

Heerspink, H. J. L., Parving, H. H., Andress, D. L., Bakris, G., Correa-Rotter, R., Hou, F. F., et al. (2019). SONAR committees and investigators. atrasentan and renal events in patients with type 2 diabetes and chronic kidney disease (SONAR): a double-blind, randomised, placebo-controlled trial. *Lancet* 393, 1937–1947. doi: 10.1016/S0140-6736(19)30772-X

Jin, C., Jeon, Y., Kleven, D. T., Pollock, J. S., White, J. J., and Pollock, D. M. (2014). Combined endothelin a blockade and chlorthalidone treatment in a rat model of metabolic syndrome. *J. Pharmacol. Exp. Ther.* 351, 467–473. doi: 10.1124/jpet.114.215566

Kohan, D. E., and Barton, M. (2014). Endothelin and endothelin antagonists in chronic kidney disease. *Kidney Int.* 86, 896–904. doi: 10.1038/ki.2014.143

Kohan, D. E., and Pollock, D. M. (2013). Endothelin antagonists for diabetic and non-diabetic chronic kidney disease. *Br. J. Clin. Pharmacol.* 76, 573–579. doi: 10.1111/bcp.12064

Komers, R., Gipson, D. S., Nelson, P., Adler, S., Srivastava, T., Derebail, V. K., et al. (2017). Efficacy and safety of sparsentan compared with irbesartan in patients with primary focal segmental glomerulosclerosis: randomized, controlled trial design (DUET). *Kidney Int. Rep.* 2, 654–664. doi: 10.1016/j.ekir.2017.02.019

Komers, R., and Plotkin, H. (2016). Dual inhibition of renin-angiotensin-aldosterone system and endothelin-1 in treatment of chronic kidney disease. *Am. J. Physiol. Regul. Integr. Comp. Physiol.* 310, R877–R884. doi: 10.1152/ajpregu.00425.2015

Kriz, W., and Lemley, K. V. (2015). A potential role for mechanical forces in the detachment of podocytes and the progression of CKD. *J. Am. Soc. Nephrol.* 26, 258–269. doi: 10.1681/ASN.2014030278

Lowry, O. H., Rosebrough, N. J., Farr, A. L., and Randall, R. J. (1951). Protein measurement with the folin phenol reagent. *J. Biol. Chem.* 193, 265–275.

Mann, J. F., Green, D., Jamerson, K., Ruilope, L. M., Kuranoff, S. J., Littke, T., et al. (2010). ASCEND study group. avosentan for overt diabetic nephropathy. *J. Am. Soc. Nephrol.* 21, 527–535. doi: 10.1681/ASN.2009060593

Maquigussa, E., Paterno, J. C., de Oliveira Pokorny, G. H., da Silva Perez, M., Varela, V. A., da Silva Novaes, A., et al. (2018). Klotho and PPAR Gamma activation mediate the renoprotective effect of losartan in the 5/6 nephrectomy model. *Front. Physiol.* 9:1033. doi: 10.3389/fphys.2018.01033

Morales, E., Caro, J., Gutierrez, E., Sevillano, A., Aunon, P., Fernandez, C., et al. (2015). Diverse diuretics regimens differentially enhance the antialbuminuric effect of renin-angiotensin blockers in patients with chronic kidney disease. *Kidney Int.* 88, 1434–1441. doi: 10.1038/ki.2015.249

Morrison, A. B. (1962). Experimentally induced chronic renal insufficiency in the rat. *Lab. Invest.* 11, 321–333.

Mullins, J. J., Peters, J., and Ganten, D. (1990). Fulminant hypertension in transgenic rats harbouring the mouse Ren-2 gene. *Nature* 344, 541–544. doi: 10.1038/344541a0

Nakano, Y., Hirano, T., Uehara, K., Nishibayashi, S., Hattori, K., Aihara, M., et al. (2008). New rat model induced by anti-glomerular basement membrane antibody shows severe glomerular adhesion in early stage and quickly progress to end-stage renal failure. *Pathol. Int.* 58, 361–370. doi: 10.1111/j.1440-1827.2008.02237.x

Raij, L. (2005). The pathophysiological basis for blocking the renin-angiotensin system in hypertensive patients with renal disease. *Am. J. Hypertens.* 18, 95S–99S. doi: 10.1016/j.amjhyper.2004.11.040

Rakusan, D., Kujal, P., Kramer, H. J., Husková, Z., Vanourková, Z., Vernerová, Z., et al. (2010). Persistent antihypertensive effect of aliskiren is accompanied by reduced proteinuria and normalization of glomerular area in Ren-2 transgenic rats. *Am. J. Physiol. Renal Physiol.* 299, F758–F766. doi: 10.1152/ajprenal.00259.2010

Saito, T., Sumithran, E., Glasgow, E. F., and Atkins, R. C. (1987). The enhancement of aminonucleoside nephrosis by the co-administration of protamine. *Kidney Int.* 32, 691–699. doi: 10.1038/ki.1987.262

Samad, M. A., Kim, U. K., Kang, J. J., Ke, Q., and Kang, P. M. (2015). Endothelin a receptor antagonist, atrasentan, attenuates renal and cardiac dysfunction in dahl salt-hypertensive rats in a blood pressure independent manner. *PLoS One* 10:e0121664. doi: 10.1371/journal.pone.0121664

Sedláková, L., Čertíková Chábová, V., Doleželová, Š, Škaroupková, P., Kopkan, L., Husková, Z., et al. (2017). Renin-angiotensin system blockade alone or combined with ETA receptor blockade: effects on the course of chronic kidney disease in 5/6 nephrectomized Ren-2 transgenic rats. *Clin. Exp. Hypertens.* 39, 183–195. doi: 10.1080/10641963.2016.1235184

Sinha, A. D., and Agarwal, R. (2015). Thiazide diuretics in chronic kidney disease. *Curr. Hypertens. Rep.* 17:13. doi: 10.1007/s11906-014-0525-x

Thomopoulos, C., Parati, G., and Zanchetti, A. (2015). Effects of blood pressure lowering on outcome incidence in hypertension: 4. effects of various classes of antihypertensive drugs–overview and meta-analyses. *J. Hypertens.* 33, 195–211. doi: 10.1097/HJH.0000000000000447

Trachtman, H., Nelson, P., Adler, S., Campbell, K. N., Chaudhuri, A., Derebail, V. K., et al. (2018). DUET study group. DUET: a phase 2 study evaluating the efficacy and safety of sparsentan in patients with FSGS. *J. Am. Soc. Nephrol.* 29, 2745–2754. doi: 10.1681/ASN.2018010091

Vaněčková, I., Hojná, S., Kadlecová, M., Vernerová, Z., Kopkan, L., Červenka, L., et al. (2018). Renoprotective effects of ETA receptor antagonists therapy in experimental non-diabetic chronic kidney disease: is there still hope for the future? *Physiol. Res.* 67(Suppl. 1), S55–S67.

Vaněčková, I., Kujal, P., Husková, Z., Vaňourková, Z., Vernerová, Z., Čertíková Chábová, V., et al. (2012). Effects of combined endothelin a receptor and renin-angiotensin system blockade on the course of end-organ damage in 5/6 nephrectomized Ren-2 hypertensive rats. *Kidney Blood Press. Res.* 35, 382–392. doi: 10.1159/000336823

Vaněčková, I., Řezáčová, L., Kuneš, J., and Zicha, J. (2016). Moderate additive effects of endothelin receptor a blockade in Ren-2 transgenic rats subjected to various types of RAS blockade. *Life Sci.* 159, 127–134. doi: 10.1016/j.lfs.2016.01.020

Vercauteren, M., Trensz, F., Pasquali, A., Cattaneo, C., Strasser, D. S., Hess, P., et al. (2017). Endothelin ETA receptor blockade, by activating ETB receptors, increases vascular permeability and induces exaggerated fluid retention. *J. Pharmacol. Exp. Ther.* 361, 322–333. doi: 10.1124/jpet.116.234930

Yanagisawa, M., Kurihara, H., Kimura, S., Tomobe, Y., Kobayashi, M., Mitsui, Y., et al. (1988). A novel potent vasoconstrictor peptide produced by vascular endothelial cells. *Nature* 332, 411–415. doi: 10.1038/332411a0

Zhong, J., Yang, H. C., and Fogo, A. B. (2017). A perspective on chronic kidney disease progression. *Am. J. Physiol. Renal. Physiol.* 312, F375–F384. doi: 10.1152/ajprenal.00266.2016

Zoja, C., Abbate, M., and Remuzzi, G. (2006). Progression of chronic kidney disease: insight from animal models. *Curr. Opin. Nephrol. Hypertens.* 15, 250–257. doi: 10.1097/01.mnh.0000222691.53970.83

Conflict of Interest Statement: The authors declare that the research was conducted in the absence of any commercial or financial relationships that could be construed as a potential conflict of interest.

Copyright © 2019 Vaněčková, Hojná, Vernerová, Kadlecová, Rauchová, Kompanowska-Jezierska, Vaňourková, Červenka and Zicha. This is an open-access article distributed under the terms of the Creative Commons Attribution License (CC BY). The use, distribution or reproduction in other forums is permitted, provided the original author(s) and the copyright owner(s) are credited and that the original publication in this journal is cited, in accordance with accepted academic practice. No use, distribution or reproduction is permitted which does not comply with these terms.

frontiers in Physiology

ORIGINAL RESEARCH
published: 25 September 2019
doi: 10.3389/fphys.2019.01225

PINK1 Deficiency Ameliorates Cisplatin-Induced Acute Kidney Injury in Rats

*Li Zhou[1,2], Ling Zhang[1,2], Yu Zhang[1,2], Xuan Yu[1,2], Xiuping Sun[1,2], Tao Zhu[1,2], Xianglei Li[1,2], Wei Liang[1,2], Yunlin Han[1,2] and Chuan Qin[1,2]**

[1] Key Laboratory of Human Disease Comparative Medicine, Chinese Ministry of Health, Institute of Laboratory Animal Science, Chinese Academy of Medical Sciences (CAMS), Beijing, China, [2] Key Laboratory of Human Diseases Animal Models, State Administration of Traditional Chinese Medicine, Peking Union Medicine College (PUMC), Beijing, China

Mitophagy plays a key role in cleaning damaged and depolarized mitochondria to maintain cellular homeostasis and viability. Although it was originally found in neurodegenerative diseases, mitophagy is reported to play an important role in acute kidney injury. PINK1 and Parkin are key molecules in mitophagy pathway. Here, we used PINK1 knockout rats to examine the role of PINK1/Parkin-mediated mitophagy in cisplatin nephrotoxicity. After cisplatin treatment, PINK1 knockout rats showed lower plasma creatinine and less tubular damage when compared with wild-type rats. Meanwhile, mitophagy indicated by autophagosome formation and LC3B-II accumulation was also attenuated in PINK1 knockout rats. Renal expression of PINK1 and Parkin were down-regulated while BNIP3L was up-regulated by cisplatin treatment, indicating a major role of BNIP3/BNIP3L pathway in cisplatin-induced mitophagy. Transmission electron microscopy showed that PINK1 deficiency inhibited cisplatin-induced mitochondrial fragmentation indicating an involvement of mitochondrial fusion and fission. Renal expression of mitochondrial dynamics related proteins including *Fis1*, *Drp1*, *Mfn1*, *Mfn2*, and *Opa1* were checked by real-time PCR and western blots. The results showed PINK1 deficiency distinctly prevented cisplatin-induced up-regulation of DRP1. Finally, PINK1 deficiency alleviated cisplatin-induced tubular apoptosis indicated by TUNEL assay as well as the expression of caspase3 and cleaved caspase3. Together, these results suggested PINK1 deficiency ameliorated cisplatin-induced acute kidney injury in rats, possibly via inhibiting DRP1-mediated mitochondrial fission and excessive mitophagy.

Keywords: PINK1, nephrotoxicity, mitophagy, DRP1, mitochondrial dynamics

OPEN ACCESS

Edited by:
Xueying Zhao,
Morehouse School of Medicine, United States

Reviewed by:
Shaolin Shi,
Nanjing University, China
Daria Ilatovskaya,
Medical University of South Carolina, United States

****Correspondence:***
Chuan Qin
qinchuan@pumc.edu.cn

Specialty section:
This article was submitted to Renal and Epithelial Physiology, a section of the journal Frontiers in Physiology

Received: *10 June 2019*
Accepted: *09 September 2019*
Published: *25 September 2019*

Citation:
Zhou L, Zhang L, Zhang Y, Yu X, Sun X, Zhu T, Li X, Liang W, Han Y and Qin C (2019) PINK1 Deficiency Ameliorates Cisplatin-Induced Acute Kidney Injury in Rats. Front. Physiol. 10:1225. doi: 10.3389/fphys.2019.01225

Abbreviations: BNIP3, BCL2/adenovirus E1B 19 kDa protein-interacting protein 3; BNIP3L, Bcl-2/adenovirus E1B 19 kDa-interacting protein 3-like protein, also known as Nix; BUN, blood urea nitrogen; DAPI, 4′,6-diamidino-2-phenylindole; Drp1, dynamin related protein 1; Fis1, mitochondrial fission 1 protein; KO, knockout; LC3B, microtubule-associated protein light chain 3B; Mfn1, Mitofusin 1; Mfn2, Mitofusin 2; Opa1, optic atrophy 1; PAS, periodic acid schiff reaction; PINK1, PTEN induced putative kinase 1; TUNEL, TdT-mediated dUTP Nick-End Labeling; WT, wild-type.

INTRODUCTION

Cisplatin is a widely used chemotherapy drug. It is highly effective against numerous cancers including bladder, testicular, ovarian, head and neck, uterine cervical carcinoma, non-small cell lung carcinoma and so forth. However, the use of cisplatin is limited by numerous undesirable side effects in normal tissues. Nephrotoxicity is a common side effect that occurs in up to one-third of patients receiving cisplatin therapy (Dilruba and Kalayda, 2016). Despite extensive study, the mechanism underlying cisplatin-induced nephrotoxicity remains unclear.

Mitochondrial damage and dysfunction is closely related to the pathogenesis of acute kidney injury (AKI), especially for the damage and death of renal tubular cells (Ishimoto and Inagi, 2016). Mitochondrial injury can cause a series of cell dysfunction including oxidative stress, inflammation, and cell death (Che et al., 2014). The researches in the past decade have revealed that mitochondrial dysfunction may play a central pathogenic role in cisplatin nephrotoxicity (Yang et al., 2014). In an aqueous environment, cisplatin is subject to nucleophilic displacement of chloride forming aquated species to generate a positively charged electrophile. This electrophile preferentially accumulates within the negatively charged mitochondria. Due to less efficient DNA repair mechanisms, mitochondrial DNA is more susceptible to cisplatin than nuclear DNA. Studies have shown that the cellular sensitivity to cisplatin-induced cell death appears to correlate with both the mitochondrial membrane potential and the density of mitochondria (Miller et al., 2010). Our previous study also showed that improving mitochondrial function could ameliorate cisplatin-induced nephrotoxicity in mice (Zhou et al., 2017).

Mitophagy is a fundamental process of purging damaged or excessive mitochondria to maintain intracellular homeostasis (Kaushal and Shah, 2016). Up-regulation of autophagy or mitophagy in the kidney has been observed in several animal experimental models including ischemia-reperfusion injury (Decuypere et al., 2015; Tang et al., 2018), cisplatin nephropathy (Zhao et al., 2017a,b; Ichinomiya et al., 2018; Wang et al., 2018), cyclosporine nephropathy (Pallet et al., 2008) and protein overload (Hartleben et al., 2010).

A large number of studies have shown that autophagy is a double-edged sword. It may play a pro-survival or a pro-death role (Shintani and Klionsky, 2004). In most studies, autophagy plays a protective role in kidney injury. Autophagy suppression by the PtdIns3K inhibitor 3-methyladenine (3-MA) or proximal tubule specific Atg5 or Atg7 KO and the lysosomal inhibitor chloroquine aggravated kidney damage in renal ischemia-reperfusion mice models (Jiang et al., 2010, 2012; Kimura et al., 2011; Liu et al., 2012). However, despite abundant evidences of the protective properties, autophagy has also been shown to be detrimental. In uninephrectomized rats, adenoviral vector carrying Bcl-2 and Bcl-XL protected renal ischemia-reperfusion injury by both the anti-apoptotic and anti-autophagic mechanisms (Chien et al., 2007). Besides, the mTOR inhibitor everolimus stimulated autophagy in rat kidney and aggravated renal ischemia-reperfusion injury (Chien et al., 2007). Moreover, ischemic and repetitive hypoxic preconditioning was reported to have protective effects in renal ischemia rats, accompanied by a decrease of autophagy (Wu et al., 2009; Yeh et al., 2010). The role of autophagy and mitophagy in cisplatin-induced kidney injury is still not fully understood.

In mammalian cells, the PINK1/Parkin pathway is considered the main pathway of mitophagy under cell stress. When mitochondria are healthy, PINK1 is imported to the inner mitochondrial membrane to be cleaved and degraded. In damaged mitochondria, the import of PINK1 into mitochondria is suppressed, leading to the accumulation of PINK1 on mitochondrial outer membrane where it recruits cytosolic Parkin. Then Parkin is activated and ubiquitinates a series of mitochondrial outer membrane proteins. These ubiquitin-tagged proteins are then recognized as a signal for the sequestration and degradation of damaged mitochondria (McWilliams and Muqit, 2017).

Here we used PINK1 knockout (KO) rats and found that PINK1 deficiency ameliorated cisplatin-induced acute kidney injury. Surprisingly, the results were contrary to the protective role of PINK1 that previous observed in mice models (Wang et al., 2018). This study may indicate a bidirectional role of PINK1 as well as a probable different mechanism between rats and mice in cisplatin nephrotoxicity.

MATERIALS AND METHODS

Animals and Models of Cisplatin Injury

PINK1 KO and WT rats on Sprague Dawley background were obtained from Institute of Laboratory Animal Science, Peking Union Medical College and Chinese Academy of Medical Sciences, and these rat lines were previously described (Dave et al., 2014). Quantitative real-time PCR analysis of *Pink1* expression from WT and KO rats was determined using the Power Up SYBR Green master mix (Thermo Fisher Scientific) with *Pink1* expression normalized to *Actb*. Male rats of 24–28 weeks age were used in this study. The rats were housed in cages at temperature 22 ± 2°C, humidity 40 ± 5%, under a 12-hour light/dark cycle, and received sterilized maintenance diet (Beijing HFK Bioscience Co. Ltd., cat. no. 1022) and water *ad libitum*. All animal experiments were approved by the Institutional Animal Care and Use Committee of the Institute of Laboratory Animal Science of Peking Union Medical College (ILAS-QC19001). The animals were divided into four groups: WT rats control group (WT + saline; $n = 4$), KO rats control group (KO + saline; $n = 4$), WT rats treated with cisplatin group (WT + cisplatin; $n = 6$), and KO rats treated with cisplatin group (KO + cisplatin; $n = 6$). Cisplatin (Sigma-Aldrich Co. LLC., cat. no. P4394) was freshly prepared in saline at 1 mg/ml just before use. Cisplatin group rats received a single intraperitoneal injection of cisplatin at a dose of 5 mg/kg body weight, and control group rats received the equal volume of saline (Goulding and Johns, 2015). All rats were sacrificed at 96 h after cisplatin injection. Blood samples were collected from inferior vena cava for plasma creatinine and blood urea nitrogen (BUN) measurement, and renal tissues were obtained for histological and immunoblot analysis.

Creatinine and BUN

After 96 h cisplatin treatment, all rats were anesthetized with 3% pentobarbital sodium (50mg/kg), 4 ml blood samples were collected from the inferior vena cave and anticoagulated with EDTA. The plasma was isolated by centrifugation at 4000 rpm for 10 min at 4°C. The plasma creatinine and BUN were analyzed using creatinine assay kit (Leagene Biotechnology Co. Ltd., Beijing, China) and urea assay kit (Biosino Bio-Technology and Science Inc., Beijing, China) according to the instruction of the manufactures.

Histopathological Examination

Rat kidneys were immersion-fixed in 4% paraformaldehyde solution (PFA) overnight, and then dehydrated and embedded in paraffin. 4 μm thick sections were prepared and stained with periodic acid schiff reaction (PAS) using routine method. Renal tubular injury was indicated by tubular epithelial cell flattening, brush border loss, cytoplasmic vacuolization, cell necrosis, sloughing of cells into tubular lumen and formation of tubular casts. The degree of tissue damage was scored based on the percentage of damaged tubules by a pathologist as previously described: 0, no damage; 1, < 25%; 2, 25–50%; 3, 50–75%; 4, > 75% (Jia et al., 2011; Liu et al., 2013).

Immunofluorescence Staining

The tissues were fixed in 4% PFA for 24 h and then embedded in paraffin. After dewaxing and rehydration, heat-mediated epitope retrieval was performed by microwave pretreatment in citrate buffer (pH 6.0). The slides were blocked in goat serum for 1 h and then incubated overnight at 4°C with anti-LC3B (Cell Signaling Technology, cat. no. 2775). After washing off the primary antibody, sections were incubated for 1 h at room temperature with Alexa Fluor 594-conjugated AffiniPure Goat Anti-Rabbit IgG (H + L) (Life Technologies, Grand Island, NY, United States). Finally, the slides were counterstained with DAPI (Sigma-Aldrich, D9542). Immunofluorescence images were obtained using a laser confocal microscope (TCS LSI, Leica, Mannheim, Germany).

Transmission Electron Microscopy

Kidney tissues were prepared for transmission electron microscopy as previously described (Gu et al., 2018). Briefly, Fresh renal cortex was fixed in 3% glutaraldehyde solution (buffered pH 7.4) overnight at 4°C, washed with 0.1 M PBS for three times, and then post-fixed in 1% osmium tetroxide for another 2 h at 4°C. After several washes with PBS, the specimens were dehydrated and embedded in Epon 812. Ultra-thin sections were cut with a diamond knife, stained with uranium acetate and lead citrate and examined by transmission electron microscope. The lengths and widths of individual mitochondrion in proximal tubular cells were measured by Image-Pro Plus 6.0 software. Approximately 50 mitochondria in a representative area of one cell and totally 200 mitochondria of each group were measured. The ratios of mitochondria lengths to widths were calculated for statistical analysis.

Real-Time PCR

Total RNA was extracted from renal cortex tissues using Trizol following the manufacturer's instructions. 1 μg of total RNA was denatured at 65°C for 5 min, and subjected to reverse transcription reaction using the oligo$(dT)_{20}$ primer and SuperScript^{TM} III Reverse Transcriptase (Invitrogen^{TM}) at 50°C for 1 h. Real-time PCR was performed by the Prism 7500 Real-Time PCR Detection System (Applied Biosystems) with SYBR Green Master Mix (Thermo Fisher Scientific). The reaction conditions were 95°C for 10 min, followed by 40 repeats of 95°C for 15 s and 60°C for 1 min. The sequence of oligonucleotides used in the study are listed as follows: *Actb* sense: 5′-GG CATCCTGACCCTGAAGTA-3′ and antisense: 5′-GGGGTGT TGAAGGTCTCAAA-3′; *Pink1* sense: 5′-CATGGCTTTGGATG GAGAGT-3′ and antisense: 5′-TGGGAGTTTGCTCTTCAA GG-3′; *Parkin* sense: 5′-CTGGCAGTCATTCTGGACAC-3′ and antisense: 5′-CTCTCCACTCATCCGGTTTG-3′; *Drp1* sense: 5′-ACTGGCCCCCGTCCAGCTTA-3′ and antisense: 5′-TGAT CCACATCTGCTGGAAGGT-3′; *Fis1* sense: 5′-GCACGCA GTTTGAATACGCC-3′ and antisense: 5′-CTGCTCCTCTTT GCTACCTTTGG-3′; *Mfn1* sense: 5′-TGGGGAGGTGCTGTC TCGGA-3′ and antisense: 5′-ACCAATCCCGCTGGGGA GGA-3′; *Mfn2* sense: 5′-CTGCCAACCCCAGCATGCCA-3′ and antisense: 5′-GGCGCTTGAAGGCCCTCTCC-3′; *Opa1* sense: 5′-ATCATCTGCCACGGGT TGTT-3′ and antisense: 5′-GAGAGCGCGTCAT CATCTCA-3′.

Western Blotting Assay

The renal cortex was homogenized with RIPA Lysis Buffer. After centrifugation, protein concentration was determined by bicinchoninic acid (BCA) protein assay kit. The protein samples were then denatured in boiling water for 10 min. Equal amounts of proteins were resolved by sodium dodecyl sulfate (SDS)-polyacrylamide gel electrophoresis and transferred onto nitrocellulose membranes. The membranes were blocked with 3% bovine serum albumin in tris-buffered saline (TBS) for 1 h and incubated overnight at 4°C with following antibodies: Parkin (Cell Signaling Technology, cat. no. 2132), DRP1 (Abcam, cat. no. ab184247), LC3B (Cell Signaling Technology, cat. no. 2775), BNIP3L/Nix (Cell Signaling Technology, cat. no. 12396), caspase3 (Cell Signaling Technology, cat. no. 9662), cleaved caspase3 (Cell Signaling Technology, cat. no. 9661), and β-actin (Sigma, cat. no. A1978). Then, the membranes were incubated with horseradish peroxidase-conjugated secondary antibodies, followed by enhanced chemiluminescence reaction. Quantification was performed by the Gel and Graph Digitizing System. The full western blot bands of LC3B, Parkin, BNIP3L, DRP1, caspase3, cleaved caspase3 were shown in **Supplementary Figures S1–S6**.

Analysis of Apoptosis

Apoptosis was determined by TUNEL assay by using the *In Situ* Cell Death Detection Kit (Roche, Basel, Switzerland) in rat kidney sections. Briefly, following deparaffinization and rehydration, the sections were pretreated with 0.1 M sodium citrate (pH 6.0) at 65°C for 30 min. After washing, sections were blocked with

bovine serum albumin and then incubated with TUNEL reaction mixture for 1 h at 37°C in a moist chamber. DAPI was used to label the nuclei. Sections were observed with a Laser Scanning Confocal Microscope (TCS LSI, Leica, Mannheim, Germany). The numbers of the TUNEL-positive cells in the five fields of renal cortex region for each section were counted at ×40 magnification of objective, and the average was calculated. Besides, to evaluate apoptosis, the expression of caspase3 and cleaved caspase3 was also assessed by immunoblot analysis.

Statistical Analysis

All data are presented as means ± SE. For BUN, plasma creatinine and pathology score analyses, statistical analysis was performed with two-way ANOVA followed by Tukey test for multiple comparisons. For other experiments, statistical analysis was performed with the two-tailed student's *t*-test. A probability of less than 0.05 was considered to be statistically significant.

RESULTS

Cisplatin-Induced Kidney Injury Was Ameliorated in PINK1 KO Rats

Under unchallenged conditions, BUN and plasma creatinine were at low levels in both PINK1 KO rats and WT rats, indicating that PINK1 deficiency did not affect renal function in normal state. However, BUN and plasma creatinine levels were significantly lower in PINK1 KO rats than in WT rats at 96 h after cisplatin injection (**Figures 1A,B**). Next, we assessed the tubular injury via PAS staining. Histologically, the structure of renal tissues in the WT + saline group and KO + saline group was normal. Following the cisplatin treatment, WT rats displayed severe pathological changes, characterized by the distortion of the overall renal morphology, severe tubular necrosis, brush border loss and appearance of protein casts. In contrast, the cisplatin-induced damage was significantly ameliorated in PINK1 KO rats (**Figures 1C,D**). These results indicated that PINK1 KO rats were resistant to cisplatin-induced acute kidney injury.

PINK1 Deficiency Prevented Cisplatin-Induced Mitophagy in Renal Tubular Epithelial Cells

To address the effect of PINK1 deficiency on mitophagy during cisplatin treatment, we checked the expression of LC3B by western blot and immunofluorescence. As expected, cisplatin treatment significantly increased the expression of LC3B in renal proximal tubular epithelial cells and PINK1 deficiency blocked the up-regulation of LC3B (**Figures 2A,E,F**). We further verified cisplatin-induced autophagy by electron microscopy. As shown in **Figure 2B**, there were many autophagic vacuoles or vesicles in proximal tubular epithelial cells of WT rats after cisplatin treatment. Moreover, we found large vacuoles containing numerous autophagosomes and mitophagosomes in WT + cisplatin group (**Figure 2D**). Besides, after cisplatin treatment, many small and round mitochondria were observed and the ratios of mitochondrial lengths to widths were significantly decreased in proximal tubular cells of WT rats, indicating mitochondrial fragmentation (**Figures 2B,C**). Notably, all of these changes seemed to be attenuated by PINK1 deficiency.

The Expression of PINK1 and Parkin During Cisplatin Treatment

Real-time PCR detected very little *Pink1* mRNA in PINK1 KO rats. This indicated that PINK1 KO was effective. In WT rats, cisplatin treatment significantly decreased the expression of *Pink1* (**Figure 3A**). However, we were unable to confirm the protein expression of PINK1 due to lack of specific antibodies against PINK1 protein in rats (Dave et al., 2014). For Parkin, cisplatin treatment decreased the mRNA and protein expression significantly but PINK1 KO increased the expression of Parkin both under cisplatin treatment conditions and unchallenged conditions (**Figures 3B,C,E**). The down-regulation of PINK1 and Parkin indicated that PINK1/Parkin pathway might not take the major responsibility for the active of mitophagy in cisplatin-induced kidney injury. BNIP3/BNIP3L pathway is another main mechanism of mitophagy (Ney, 2015). We checked the expression of BNIP3L by western blot. The results showed that cisplatin treatment distinctly increased the renal expression of BNIP3L, but there was no difference between PINK1 KO rats and WT rats (**Figures 3D,E**).

The Effect of PINK1 Deficiency on Mitochondrial Dynamics During Cisplatin Treatment

Results from electron microscope showed mitochondrial fragmentation after cisplatin treatment indicated the change of mitochondrial dynamics from fusion to fission. So, we checked the mRNA expression of mitochondrial dynamics related genes including *Fis1*, *Drp1*, *Opa1*, *Mfn1*, and *Mfn2* by realtime PCR (**Figures 4A–E**). The results showed that mitochondrial fusion related genes *Mfn1* and *Mfn2* decreased significantly after cisplatin treatment both in WT and KO rats. However, *Drp1* which is critical for mitochondrial fission was significantly down-regulated in PINK1 KO rats both under cisplatin treatment conditions and unchallenged conditions. Subsequently, we double checked the protein expression of DRP1 by western blots. As shown in **Figures 4F,G**, cisplatin treatment induced an evident increase of DRP1 in renal cortex of WT rats, but it was largely attenuated in PINK1 KO rats, suggesting a key role of PINK1/Parkin in DRP1-mediated mitochondrial fission during cisplatin treatment.

PINK1 Deficiency Attenuated Cisplatin-Induced Renal Tubular Cell Apoptosis

Apoptosis and autophagy are highly coordinated mechanisms in response to various intrinsic and/or extrinsic stresses to maintain cellular homeostasis and it is well known that apoptosis contributes to cisplatin nephrotoxicity. We evaluated renal tubular cell apoptosis by TUNEL assay (**Figures 5A,B**). The results revealed that there were significantly less TUNEL-positive tubular cells in KO rats than WT rats after cisplatin treatment.

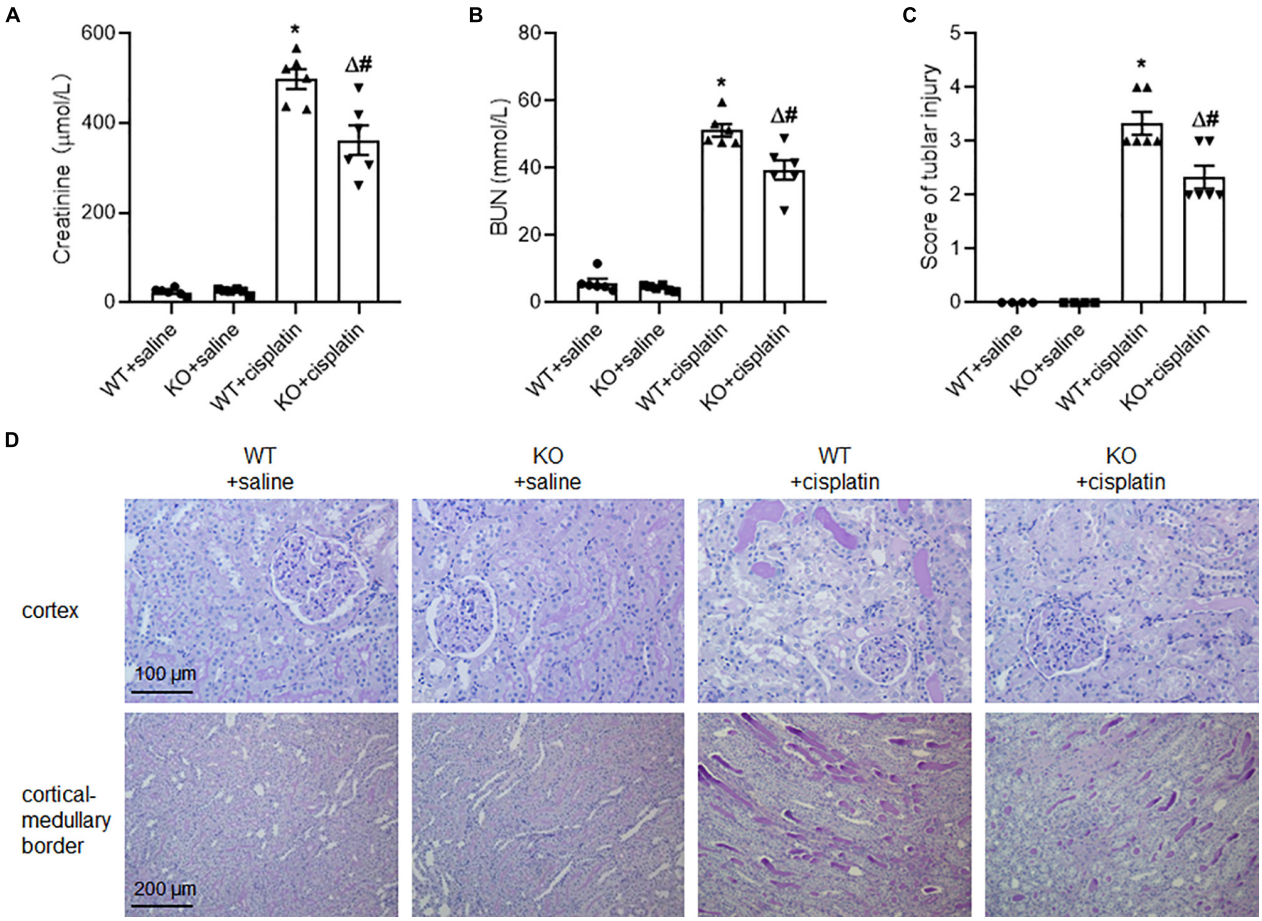

FIGURE 1 | PINK1 deficiency attenuated cisplatin-induced acute kidney injury. PINK1 KO and WT rats were injected with 5 mg/kg cisplatin or saline for 72 h. **(A)** Plasma level of BUN in PINK1 WT and KO rats after cisplatin treatment. **(B)** Plasma level of creatinine in PINK1 WT and KO rats after cisplatin treatment. **(C)** Pathological score of tubular damage. **(D)** Representative histology of kidney cortex by PAS staining. $N = 6$ in each group. $^{*}P < 0.05$, WT + cisplatin vs. WT + saline; $^{\#}P < 0.05$, KO + cisplatin vs. WT + cisplatin; $^{\Delta}P < 0.05$, KO + cisplatin vs. KO + saline. Data are mean ± SE.

Next, we checked the expression of caspase3 and cleaved caspase3 by western blots. Consistent with TUNEL assay, immunoblot analysis also showed a lower induction of caspase3 and cleaved caspase3 in renal cortex after cisplatin treatment in PINK1 KO rats (**Figures 5C–E**).

DISSCUSION

Many previous studies have clearly demonstrated mitochondrial damage and dysfunction as a key pathophysiological component in cisplatin nephrotoxicity. The pathological changes of mitochondria in cisplatin nephrotoxicity are mainly triggered by DNA damage response, disruption of mitochondrial dynamics, pro-apoptotic protein attack and oxidative stress (Yang et al., 2014). There is evidence that mitochondrial DNA and other mitochondrial targets are perhaps more important than nuclear DNA damage in mediating cisplatin-induced cell death and the sensitivity of cells to cisplatin seems to correlate well with mitochondrial density and mitochondrial membrane potential (Peres and da Cunha, 2013). Mitochondrial damage and dysfunction would then result in abnormal energy metabolism, oxidative stress, inflammation, and cell death, inducing a rapid deterioration in renal function (Manohar and Leung, 2018). Therefore, maintenance of a cohort of healthy mitochondria is crucial for the homeostasis and viability of renal tubular cells in cisplatin-induced kidney injury.

PINK1/Parkin-mediated mitophagy pathway is one of the best studied mechanisms for mitophagy in mammalian cells (Eiyama and Okamoto, 2015). Recently, Wang et al. (2018) demonstrated that renal PINK1 and Parkin were increased in cisplatin treated mice and indicated that PINK1/Parkin-mediated mitophagy had a protective role against kidney injury. Besides, there is evidence that PINK1-parkin pathway of mitophagy protects against contrast-induced acute kidney injury via decreasing mitochondrial ROS and NLRP3 inflammasome activation (Lin et al., 2019). However, in our present study, we found renal PINK1 and Parkin were significantly down-regulated in cisplatin treated rats. This is surprising but not impossible. In streptozotocin-induced diabetic mice and db/db

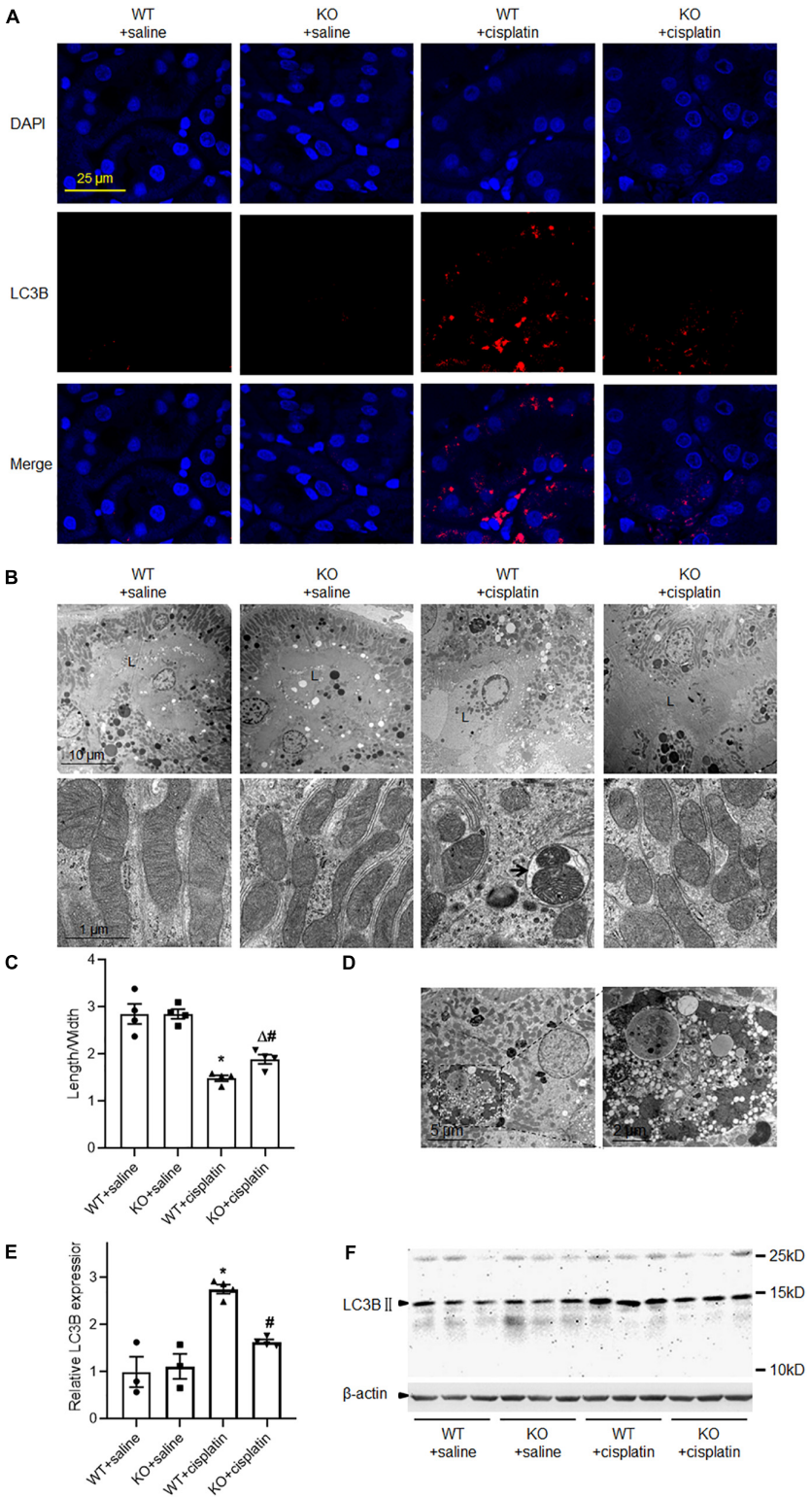

FIGURE 2 | PINK1 deficiency prevented cisplatin-induced mitophagy. **(A)** Representative images of LC3B immunostaining. **(B)** Representative transmission electron microscope images of renal proximal tubular cells and mitochondria. L indicated the proximal tubular lumen. The arrow indicated a representative mitophagosome. **(C)** Quantitative analysis of the length/width of mitochondria in proximal tubular cells. **(D)** Transmission electron microscope images of large vacuoles containing numerous autophagosomes and mitophagosomes in cisplatin treated WT rats. **(E)** Quantitative analysis of the western blotting of LC3BII. **(F)** Representative western blot bands of LC3BII in renal cortex. $N = 3$ in WT + saline group and KO + saline group, $N = 4$ in WT + cisplatin group and KO + cisplatin group. $^{*}P < 0.05$, WT + cisplatin vs. WT + saline; $^{\#}P < 0.05$, KO + cisplatin vs. WT + cisplatin; $^{\Delta}P < 0.05$, KO + cisplatin vs. KO + saline. Data are mean ± SE.

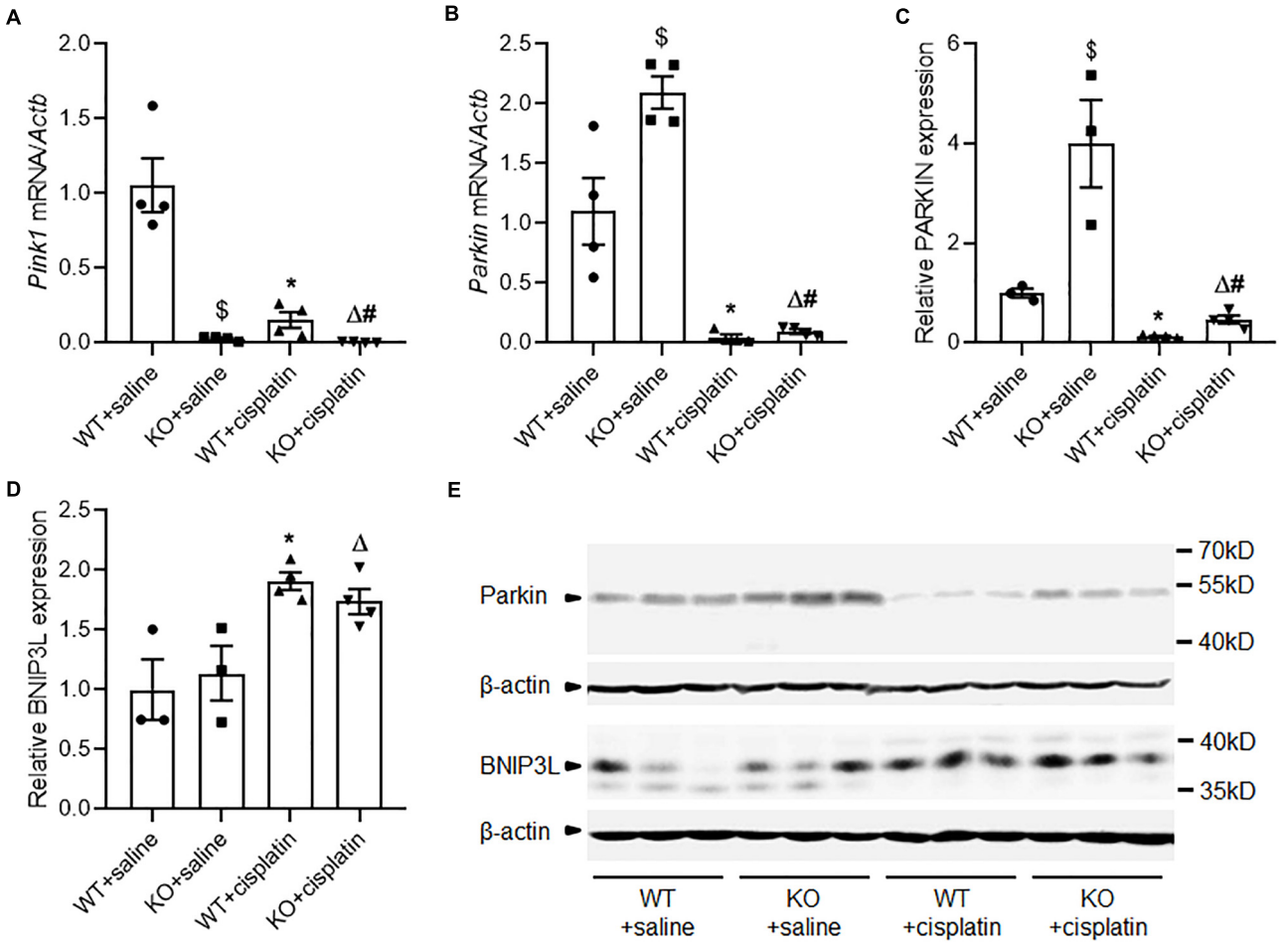

FIGURE 3 | Altered expression of PINK1, Parkin and BNIP3L during cisplatin treatment in PINK1 WT and KO rats. **(A)** Real-time quantitative PCR analysis of *Pink1* mRNA expression in renal cortex. **(B)** Real-time quantitative PCR analysis of *Parkin* mRNA expression in renal cortex. **(C)** Quantitative analysis of the western blotting of Parkin. **(D)** Quantitative analysis of the western blotting of BNIP3L. **(E)** Representative western blot bands of Parkin and BNIP3L in renal cortex. $N = 3$ in WT + saline group and KO + saline group, $N = 4$ in WT + cisplatin group and KO + cisplatin group. $^{*}P < 0.05$, WT + cisplatin vs. WT + saline; $^{\#}P < 0.05$, KO + cisplatin vs. WT + cisplatin; $^{\Delta}P < 0.05$, KO + cisplatin vs. KO + saline; $^{\$}P < 0.05$, KO + saline vs. WT + saline. Data are mean ± SE.

mice, Li et al. and Sun et al. found mitochondrial abnormalities occurred in the kidney accompanied by reduced PINK1 and Parkin expression, while BNIP3 and LC3B were significantly increased in the renal tubular cells (Huang et al., 2016; Li et al., 2017; Xiao et al., 2017). There are many possible reasons for the different pattern of PINK1 expression and role between cisplatin treated mice and rats. First, autophagy may be a double-edged sword. Indeed, stimulation of autophagy has been described to both improve and exacerbate ischemia-reperfusion injury in the kidney and a hypothesis has been put forward that autophagy can switch roles depending on the severity of the kidney injury and the phase of the injury process (Decuypere et al., 2015). Moderate level of autophagy may improve kidney injury and excessive autophagy may exacerbate kidney injury (Decuypere et al., 2015). The different cisplatin doses and differential accumulation of cisplatin in mitochondria between rats and mice in the absence of PINK1 in mitochondria may result in different mitochondria injury severity between rats and mice. In fact, we found a number of autophagic vacuoles or vesicles as well as large vacuoles containing numerous autophagosomes and mitophagosomes in cisplatin treated WT rats, indicating excessive autophagy. And the excessive mitochondria damage and autophagy might have negative feedback inhibition effect on the expression of PINK1 and Parkin. Second, most of evidences that autophagy exacerbated renal ischemia-reperfusion injury were found in rats models (Decuypere et al., 2015). Considered the difference that we used PINK1 KO rats and Wang et al. (2018) used PINK1 KO mice, it may also indicate species difference between mice and rats. Besides, aging are associated with dysfunctional autophagy, which may reduce the threshold for detrimental autophagy (Filfan et al., 2017). Furosemide is frequently used in patients with acute kidney injury to promote diuresis. Interestingly, furosemide can induce autophagosomes in the thick ascending loop and it has been reported that the detrimental effect of furosemide only occurs in adult rats but partially protective in young rats during renal

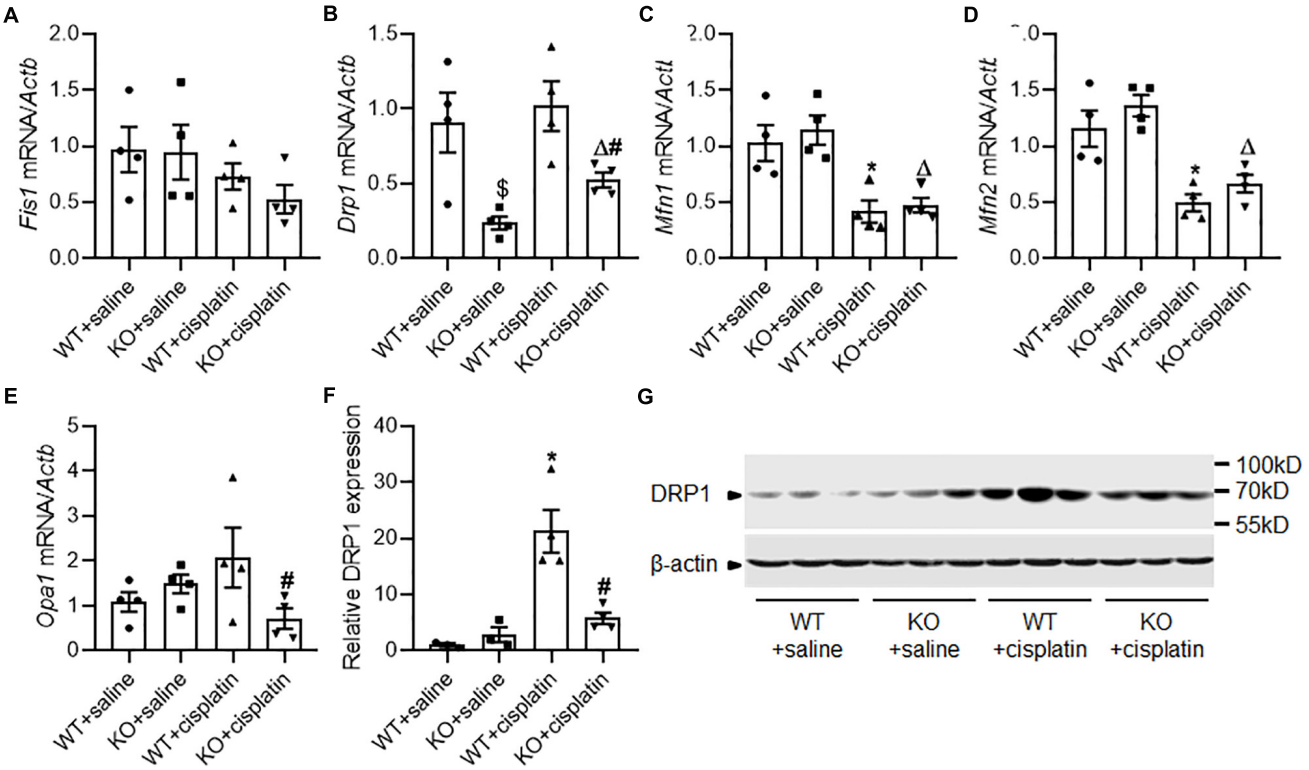

FIGURE 4 | The effect of PINK1 deficiency on mitochondrial dynamics related proteins during cisplatin treatment. **(A–E)** Real-time quantitative PCR analysis of *Fis1*, *Drp1*, *Mfn1*, *Mfn2*, and *Opa1* mRNA expression in renal cortex. **(F)** Quantitative analysis of the western blotting of DRP1. **(G)** Representative western blot bands of DRP1 in renal cortex. $N = 3$ in WT + saline group and KO + saline group, $N = 4$ in WT + cisplatin group and KO + cisplatin group. $^{*}P < 0.05$, WT + cisplatin vs. WT + saline; $^{\#}P < 0.05$, KO + cisplatin vs. WT + cisplatin; $^{\Delta}P < 0.05$, KO + cisplatin vs. KO + saline; $^{\$}P < 0.05$, KO + saline vs. WT + saline. Data are mean ± SE.

ischemia-reperfusion injury (Fleck and Heller, 1993). The age of rats (24–28 week old) may also contribute to the protective effects of PINK1 deficiency that observed in present study. In addition, the different gene targeting strategies between KO rats and KO mice that result in different products of transcription from *Pink1* locus could also be a reason.

In present study, electron-microscopy and LC3B expression indicated mitophagy was activated in cisplatin-induced acute kidney injury. However, real-time PCR and western blots showed a down-regulation of PINK1 and Parkin by cisplatin treatment, suggesting other mechanisms of mitophagy. There are substantial evidences that BNIP3 and BNIP3L can promote mitochondrial depolarization and mitophagy (Ney, 2015). Ishihara et al. reported that BNIP3 might regulate mitophagy in the proximal tubules of ischemia-reperfusion injury rats (Ishihara et al., 2013). In this study, we checked the expression of BNIP3L and found that cisplatin significantly up-regulated the expression of BINP3L, indicating BNIP3/BNIP3L pathway may play a major role for the elevated mitophagy in cisplatin treated rats.

Mitochondria are highly dynamic organelles that shift between fragmented and tubule like morphologies by the control of mitochondria fission and fusion. A number of biochemical and genetic studies link the PINK1/Parkin pathway to mitochondrial fission and fusion (Voigt et al., 2016). It has been demonstrated that normally tubule like mitochondria in the proximal tubules rapidly fragment in response to insults such as cisplatin and ischemia-reperfusion injury (Hall et al., 2013). Emerging evidences suggest that the mitochondrial fragmentation caused by changes of mitochondria fusion and fission balance has a pathogenic role in acute kidney injury. In line with those studies, electron-microscopy showed increased mitochondrial fragmentation after cisplatin treatment in WT rats while PINK1 deficiency seemed to decrease mitochondrial fragmentation in present study. The molecular machinery governing mitochondrial dynamics is determined by fission proteins, such as DRP1 and FIS1, and fusion proteins, such as MFN1, MFN2, and OPA1 (Meyer et al., 2017). Brooks et al. demonstrated in both cell and mouse models that DRP1 is rapidly recruited to fragmented mitochondria in the proximal tubule and inhibition of DRP1 was protective against mitochondrial fragmentation and kidney damage (Brooks et al., 2009). In present study, PINK1 deficiency remarkably restrained cisplatin-induced DRP1 up-regulation, indicating the regulation of DRP1 by PINK1/Parkin pathway might play a key role in cisplatin-induced acute kidney injury. A number of studies demonstrated that the PINK1/Parkin pathway is pro-fusion as overexpression of PINK1 leads to elongated mitochondria while knockdown of PINK1 leads to fragmented mitochondria (Dagda et al., 2009; Lutz et al., 2009). Accordantly, in present study cisplatin-induced mitochondrial

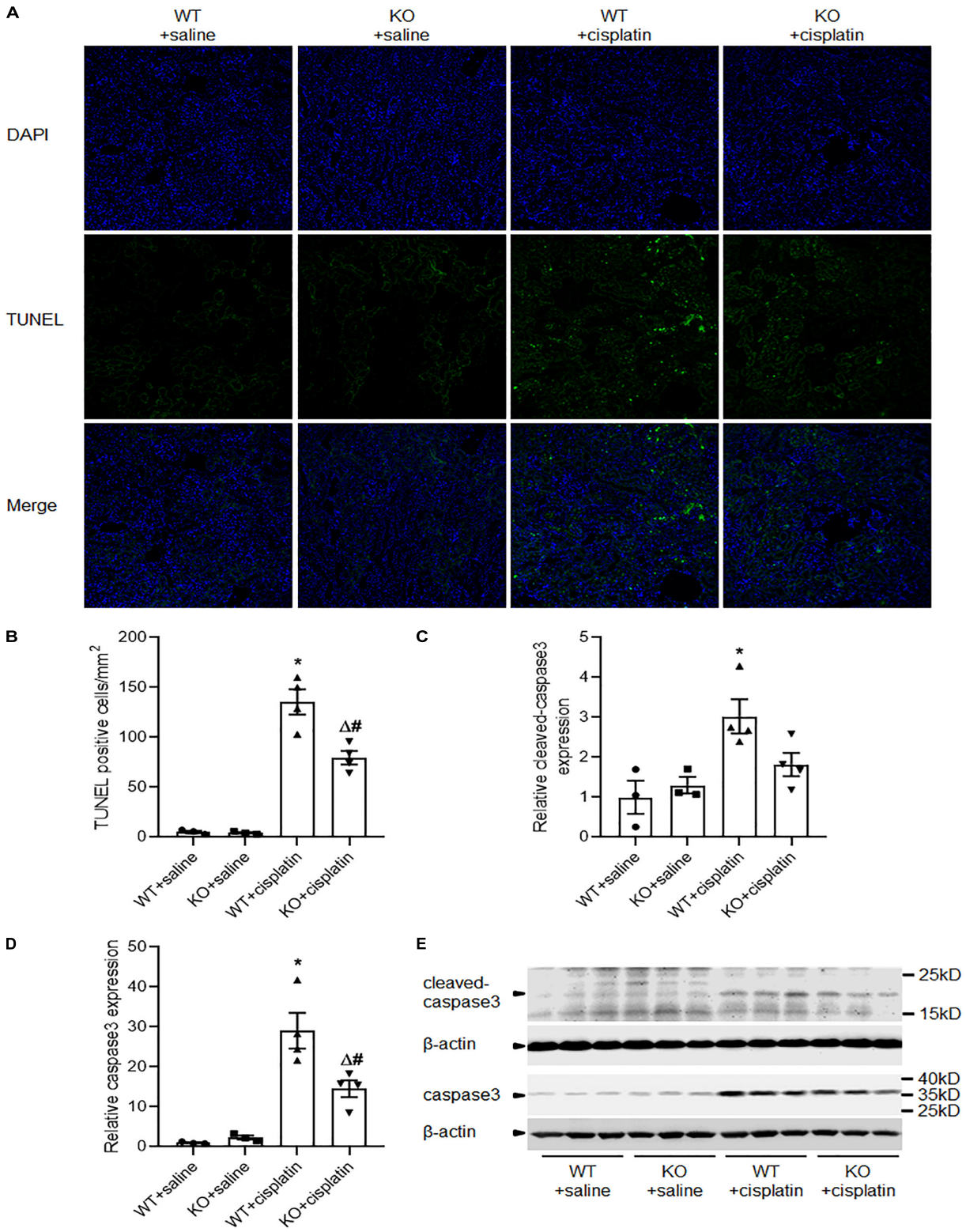

FIGURE 5 | PINK1 deficiency attenuated cisplatin-induced renal tubular cell apoptosis. **(A)** Presented are the representative photographs of TUNEL staining of kidney tissues in PINK1 WT and KO rats after cisplatin treatment. **(B)** Quantitative analysis of TUNEL-positive cells among the various groups. **(C,D)** Quantitative analysis of the western blotting of cleaved caspase3 and caspase3. **(E)** Representative western blot bands of cleaved caspase3 and caspase3. $N = 3$ in WT + saline group and KO + saline group, $N = 4$ in WT + cisplatin group and KO + cisplatin group. $^{*}P < 0.05$, WT + cisplatin vs. WT + saline; $^{\#}P < 0.05$, KO + cisplatin vs. WT + cisplatin; $^{\Delta}P < 0.05$, KO + cisplatin vs. KO + saline; $^{\$}P < 0.05$, KO + saline vs. WT + saline. Data are mean ± SE.

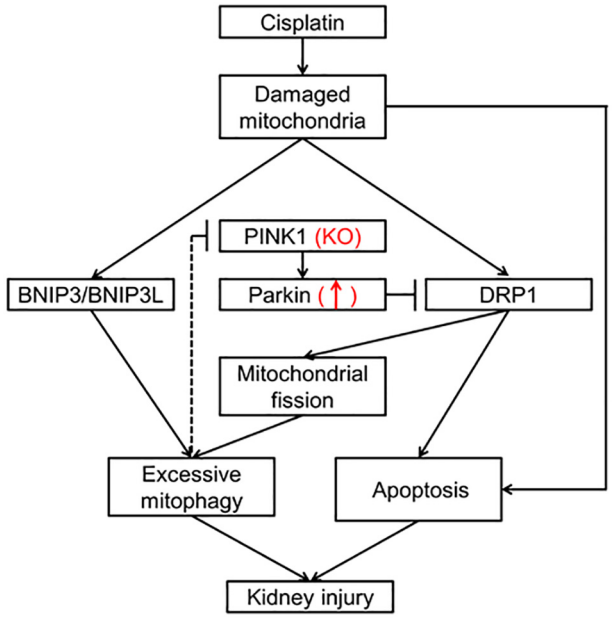

FIGURE 6 | Schematic representation of possible mechanism related to mitophagy in cisplatin-induced kidney injury in PINK1 KO rats. Cisplatin causes the mitochondrial damage of renal tubular epithelial cells, which induces BNIP3/BNIP3L-mediated mitophagy, DRP1-mediated mitochondrial fission and apoptosis leading to kidney injury. And the excessive mitophagy may have negative feedback inhibition effect on the expression of PINK1 and Parkin and result in the down-regulation of PINK1 and Parkin in WT rats. In PINK1 KO rats, PINK1 deficiency causes a compensatory increase of Parkin and significantly inhibits the up-regulation of DRP1, which regulates mitochondrial fission and apoptosis, and therefore to inhibit the excessive mitophagy and overall kidney damage.

fragmentation was accompanied by a down-regulation of PINK1 and Parkin. Interesting, we found PINK1 deficiency induced a compensatory increase of Parkin expression both under cisplatin treatment conditions and unchallenged conditions. And this compensatory increase of Parkin might account for the decrease of mitochondrial fragmentation and DRP1 expression in PINK1 KO rats during cisplatin treatment. In agree with this, Buhlman et al. (2014) demonstrated that Parkin-mediated mitochondrial fission depends on DRP1 and at least in part independently of PINK1. Additionally, mitochondria need to be fragmented before mitophagy to occur. Zhao et al. (2017a) demonstrated that DRP1 dependent mitochondrial fission was required for mitophagy in cisplatin treated tubular epithelial cells. Consistently, Li et al. (2018) showed that renal ischemia-reperfusion induced mitophagy also depended on DRP1-mediated mitochondrial fragmentation. Besides, *Drp1* mRNA expression was unchanged but DRP1 protein level was significantly up-regulated by cisplatin treatment in WT rats, indicating a main role of post-transcriptional regulation. However, PINK1 deficiency significantly inhibited *Drp1* mRNA expression both under cisplatin treatment conditions and unchallenged conditions, indicating a main role of transcriptional regulation. And the different pattern of *Drp1* mRNA expression and DRP1 protein level might suggest that *Drp1* mRNA expression was ample under normal conditions and the effect of PINK1 deficiency on *Drp1* transcriptional regulation was covered up. Under cisplatin treatment conditions, *Drp1* mRNA were extensively transformed into DRP1 proteins and then the effect of PINK1 deficiency on *Drp1* transcriptional regulation appeared. Interesting, it has been reported that Parkin could also act as a transcription factor and modulate various genes (Alves da Costa et al., 2018). Thus, there was high possibility that the effect of PINK1 deficiency on *Drp1* transcriptional regulation was related to the compensatory increase of Parkin expression. Taken together, it was probable that PINK1 deficiency caused a compensatory increase of Parkin and affected DRP1 dependent mitochondrial fission to protect against mitochondrial fragmentation, mitophagy and overall kidney damage.

It is well known that apoptosis contributes to cisplatin nephrotoxicity and some studies suggest that apoptosis and autophagy are co-ordinated processes in the pathogenesis of acute kidney injury (Zhou et al., 2018). The dual role of autophagy or mitophagy under stimulating factor may depend on the balance between pro-survival and pro-death processes. Generally, when cell is exposed to modest stress and just produce a few damaged mitochondria, the cell can easily remove those abnormal mitochondria via mitophagy. However, if plenty of mitochondria are damaged leading to insufficient scavenging capacity, the cell is beyond rescue and apoptosis will become the dominant pathway (Kubli and Gustafsson, 2012). Therefore, it is not surprising that both apoptosis and mitophagy/autophagy were attenuated in PINK1 KO rats in present study and this may also indicate excessive mitophagy/autophagy during cisplatin-induced acute kidney injury. Besides, mitochondrial dynamics are integrated with mitophagy and cell death. Studies have shown that excessive DRP1-mediated mitochondrial fission contributes to apoptosis (Frank et al., 2001). It has been found that DRP1 and Bax are co-localized on the mitochondrial membrane at the onset of apoptosis and inhibition of DRP1 protected against irradiation and senecionine induced apoptosis (Wang et al., 2015; Zhang et al., 2016; Yang et al., 2017). However, there is also evidence that DRP1-mediated fission is not necessary for apoptosis process but it increases sensitivity to apoptotic signals possibly by enhancing cytochrome c release (Sugioka et al., 2004; Parone et al., 2006). Therefore, the reduced apoptotic level in PINK1 KO rats may partly due to the inhibition of DRP1 and mitochondrial fission during cisplatin-induced acute kidney injury.

In summary, our results showed that renal mitophagy was activated in cisplatin treated rats and PINK1 deficiency ameliorated cisplatin-induced acute kidney injury accompanied by a decrease of mitophagy. Mechanistically, cisplatin treatment decreased the renal expression of PINK1 and Parkin while increased the expression of BNIP3L, indicating PINK1/Parkin mediated mitophagy might not play a major role in cisplatin nephrotoxicity rat models. Nevertheless, PINK1 deficiency caused a compensatory increase of Parkin and significantly inhibited cisplatin-induced up-regulation of DRP1, suggesting a renal protection mechanism by regulating DRP1 dependent mitochondrial fission and therefore to inhibit the excessive mitophagy and overall kidney damage (**Figure 6**).

DATA AVAILABILITY STATEMENT

The raw data supporting the conclusions of this manuscript will be made available by the authors, without undue reservation, to any qualified researcher.

ETHICS STATEMENT

The animal study was reviewed and approved by Institutional Animal Care and Use Committee of the Institute of Laboratory Animal Science of Peking Union Medical College.

AUTHOR CONTRIBUTIONS

LZho performed the research, analyzed the data and wrote the manuscript. YZ, XY, and XL performed the animal experiments. YH contributed to the histopathological examination. LZha and WL performed the Western blotting. TZ and XS performed other experiments. CQ designed and funded the research. All authors have read and agreed with the manuscript.

FUNDING

This work was supported by CAMS Innovation Fund for Medical Sciences (CIFMS) grants (2016-I2M-2-006 and 2016-12M-1-10) and National Natural Science Foundation of China Grants (81803858 and 31970510).

SUPPLEMENTARY MATERIAL

The Supplementary Material for this article can be found online at: https://www.frontiersin.org/articles/10.3389/fphys.2019.01225/full#supplementary-material

REFERENCES

Alves da Costa, C., Duplan, E., Rouland, L., and Checler, F. (2018). The transcription factor function of parkin: breaking the dogma. *Front. Neurosci.* 12:965. doi: 10.3389/fnins.2018.00965

Brooks, C., Wei, Q., Cho, S. G., and Dong, Z. (2009). Regulation of mitochondrial dynamics in acute kidney injury in cell culture and rodent models. *J. Clin. Invest.* 119, 1275–1285. doi: 10.1172/JCI37829

Buhlman, L., Damiano, M., Bertolin, G., Ferrando-Miguel, R., Lombes, A., Brice, A., et al. (2014). Functional interplay between parkin and drp1 in mitochondrial fission and clearance. *Biochim. Biophys. Acta* 1843, 2012–2026. doi: 10.1016/j.bbamcr.2014.05.012

Che, R., Yuan, Y., Huang, S., and Zhang, A. (2014). Mitochondrial dysfunction in the pathophysiology of renal diseases. *Am. J. Physiol. Renal Physiol.* 306, F367–F378. doi: 10.1152/ajprenal.00571.2013

Chien, C. T., Shyue, S. K., and Lai, M. K. (2007). Bcl-xL augmentation potentially reduces ischemia/reperfusion induced proximal and distal tubular apoptosis and autophagy. *Transplantation* 84, 1183–1190. doi: 10.1097/01.tp.0000287334.38933.e3

Dagda, R. K., Cherra, S. J. III, Kulich, S. M., Tandon, A., Park, D., and Chu, C. T. (2009). Loss of PINK1 function promotes mitophagy through effects on oxidative stress and mitochondrial fission. *J. Biol. Chem.* 284, 13843–13855. doi: 10.1074/jbc.M808515200

Dave, K. D., De Silva, S., Sheth, N. P., Ramboz, S., Beck, M. J., Quang, C., et al. (2014). Phenotypic characterization of recessive gene knockout rat models of Parkinson's disease. *Neurobiol. Dis.* 70, 190–203. doi: 10.1016/j.nbd.2014.06.009

Decuypere, J. P., Ceulemans, L. J., Agostinis, P., Monbaliu, D., Naesens, M., Pirenne, J., et al. (2015). Autophagy and the kidney: implications for ischemia-reperfusion injury and therapy. *Am. J. Kidney Dis.* 66, 699–709. doi: 10.1053/j.ajkd.2015.05.021

Dilruba, S., and Kalayda, G. V. (2016). Platinum-based drugs: past, present and future. *Cancer Chemother. Pharmacol.* 77, 1103–1124. doi: 10.1007/s00280-016-2976-z

Eiyama, A., and Okamoto, K. (2015). PINK1/Parkin-mediated mitophagy in mammalian cells. *Curr. Opin. Cell. Biol.* 33, 95–101. doi: 10.1016/j.ceb.2015.01.002

Filfan, M., Sandu, R. E., Zavaleanu, A. D., GresiTa, A., Glavan, D. G., Olaru, D. G., et al. (2017). Autophagy in aging and disease. *Rom. J. Morphol. Embryol.* 58, 27–31.

Fleck, C., and Heller, J. (1993). Age-dependent differences in the effect of ischaemia on the rat kidney: prevention of the postischaemic damage by different drugs. *Exp. Toxicol. Pathol.* 45, 381–387. doi: 10.1016/S0940-2993(11)80434-3

Frank, S., Gaume, B., Bergmann-Leitner, E. S., Leitner, W. W., Robert, E. G., Catez, F., et al. (2001). The role of dynamin-related protein 1, a mediator of mitochondrial fission, in apoptosis. *Dev. Cell.* 1, 515–525. doi: 10.1016/s1534-5807(01)00055-7

Goulding, N. E., and Johns, E. J. (2015). Neural regulation of the kidney function in rats with cisplatin induced renal failure. *Front. Physiol.* 6:192. doi: 10.3389/fphys.2015.00192

Gu, Y. Y., Huang, P., Li, Q., Liu, Y. Y., Liu, G., Wang, Y. H., et al. (2018). YangXue qingnao wan and silibinin capsules, the two chinese medicines, attenuate cognitive impairment in aged LDLR (+/-) golden syrian hamsters involving protection of blood brain barrier. *Front. Physiol.* 9:658. doi: 10.3389/fphys.2018.00658

Hall, A. M., Rhodes, G. J., Sandoval, R. M., Corridon, P. R., and Molitoris, B. A. (2013). In vivo multiphoton imaging of mitochondrial structure and function during acute kidney injury. *Kidney Int.* 83, 72–83. doi: 10.1038/ki.2012.328

Hartleben, B., Godel, M., Meyer-Schwesinger, C., Liu, S., Ulrich, T., Kobler, S., et al. (2010). Autophagy influences glomerular disease susceptibility and maintains podocyte homeostasis in aging mice. *J. Clin. Invest.* 120, 1084–1096. doi: 10.1172/JCI39492

Huang, C., Zhang, Y., Kelly, D. J., Tan, C. Y., Gill, A., Cheng, D., et al. (2016). Thioredoxin interacting protein (TXNIP) regulates tubular autophagy and mitophagy in diabetic nephropathy through the mTOR signaling pathway. *Sci. Rep.* 6:29196. doi: 10.1038/srep29196

Ichinomiya, M., Shimada, A., Ohta, N., Inouchi, E., Ogihara, K., Naya, Y., et al. (2018). Demonstration of mitochondrial damage and mitophagy in cisplatin-mediated nephrotoxicity. *Tohoku J. Exp. Med.* 246, 1–8. doi: 10.1620/tjem.246.1

Ishihara, M., Urushido, M., Hamada, K., Matsumoto, T., Shimamura, Y., Ogata, K., et al. (2013). Sestrin-2 and BNIP3 regulate autophagy and mitophagy in renal tubular cells in acute kidney injury. *Am. J. Physiol. Renal. Physiol.* 305, F495–F509. doi: 10.1152/ajprenal.00642.2012

Ishimoto, Y., and Inagi, R. (2016). Mitochondria: a therapeutic target in acute kidney injury. *Nephrol. Dial Transplant.* 31, 1062–1069. doi: 10.1093/ndt/gfv317

Jia, Z., Wang, N., Aoyagi, T., Wang, H., Liu, H., and Yang, T. (2011). Amelioration of cisplatin nephrotoxicity by genetic or pharmacologic blockade of prostaglandin synthesis. *Kidney Int.* 79, 77–88. doi: 10.1038/ki.2010.331

Jiang, M., Liu, K., Luo, J., and Dong, Z. (2010). Autophagy is a renoprotective mechanism during in vitro hypoxia and in vivo ischemia-reperfusion injury. *Am. J. Pathol.* 176, 1181–1192. doi: 10.2353/ajpath.2010.090594

Jiang, M., Wei, Q., Dong, G., Komatsu, M., Su, Y., and Dong, Z. (2012). Autophagy in proximal tubules protects against acute kidney injury. *Kidney Int.* 82, 1271–1283. doi: 10.1038/ki.2012.261

Kaushal, G. P., and Shah, S. V. (2016). Autophagy in acute kidney injury. *Kidney Int.* 89, 779–791. doi: 10.1016/j.kint.2015.11.021

Kimura, T., Takabatake, Y., Takahashi, A., Kaimori, J. Y., Matsui, I., Namba, T., et al. (2011). Autophagy protects the proximal tubule from degeneration and acute ischemic injury. *J. Am. Soc. Nephrol.* 22, 902–913. doi: 10.1681/ASN.2010070705

Kubli, D. A., and Gustafsson, A. B. (2012). Mitochondria and mitophagy: the yin and yang of cell death control. *Circ. Res.* 111, 1208–1221. doi: 10.1161/CIRCRESAHA.112.265819

Li, N., Wang, H., Jiang, C., and Zhang, M. (2018). Renal ischemia/reperfusion-induced mitophagy protects against renal dysfunction via drp1-dependent-pathway. *Exp. Cell. Res.* 369, 27–33. doi: 10.1016/j.yexcr.2018.04.025

Li, W., Du, M., Wang, Q., Ma, X., Wu, L., Guo, F., et al. (2017). FoxO1 Promotes Mitophagy in the Podocytes of Diabetic Male Mice via the PINK1/Parkin Pathway. *Endocrinology* 158, 2155–2167. doi: 10.1210/en.2016-1970

Lin, Q., Li, S., Jiang, N., Shao, X., Zhang, M., Jin, H., et al. (2019). PINK1-parkin pathway of mitophagy protects against contrast-induced acute kidney injury via decreasing mitochondrial ROS and NLRP3 inflammasome activation. *Redox Biol.* 26:101254. doi: 10.1016/j.redox.2019.101254

Liu, S., Hartleben, B., Kretz, O., Wiech, T., Igarashi, P., Mizushima, N., et al. (2012). Autophagy plays a critical role in kidney tubule maintenance, aging and ischemia-reperfusion injury. *Autophagy* 8, 826–837. doi: 10.4161/auto.19419

Liu, S., Jia, Z., Zhou, L., Liu, Y., Ling, H., Zhou, S. F., et al. (2013). Nitro-oleic acid protects against adriamycin-induced nephropathy in mice. *Am. J. Physiol. Renal Physiol.* 305, F1533–F1541. doi: 10.1152/ajprenal.00656.2012

Lutz, A. K., Exner, N., Fett, M. E., Schlehe, J. S., Kloos, K., Lammermann, K., et al. (2009). Loss of parkin or PINK1 function increases Drp1-dependent mitochondrial fragmentation. *J. Biol. Chem.* 284, 22938–22951. doi: 10.1074/jbc.M109.035774

Manohar, S., and Leung, N. (2018). Cisplatin nephrotoxicity: a review of the literature. *J. Nephrol.* 31, 15–25. doi: 10.1007/s40620-017-0392-z

McWilliams, T. G., and Muqit, M. M. (2017). PINK1 and Parkin: emerging themes in mitochondrial homeostasis. *Curr. Opin. Cell. Biol.* 45, 83–91. doi: 10.1016/j.ceb.2017.03.013

Meyer, J. N., Leuthner, T. C., and Luz, A. L. (2017). Mitochondrial fusion, fission, and mitochondrial toxicity. *Toxicology* 391, 42–53. doi: 10.1016/j.tox.2017.07.019

Miller, R. P., Tadagavadi, R. K., Ramesh, G., and Reeves, W. B. (2010). Mechanisms of cisplatin nephrotoxicity. *Toxins* 2, 2490–2518. doi: 10.3390/toxins2112490

Ney, P. A. (2015).). Mitochondrial autophagy: origins, significance, and role of BNIP3 and NIX. *Biochim. Biophys. Acta* 1853(10 Pt B), 2775–2783. doi: 10.1016/j.bbamcr.2015.02.022

Pallet, N., Bouvier, N., Legendre, C., Gilleron, J., Codogno, P., Beaune, P., et al. (2008). Autophagy protects renal tubular cells against cyclosporine toxicity. *Autophagy* 4, 783–791. doi: 10.4161/auto.6477

Parone, P. A., James, D. I., Da Cruz, S., Mattenberger, Y., Donze, O., Barja, F., et al. (2006). Inhibiting the mitochondrial fission machinery does not prevent Bax/Bak-dependent apoptosis. *Mol. Cell. Biol.* 26, 7397–7408. doi: 10.1128/MCB.02282-05

Peres, L. A., and da Cunha, A. D. Jr. (2013). Acute nephrotoxicity of cisplatin: molecular mechanisms. *J. Bras. Nefrol.* 35, 332–340. doi: 10.5935/0101-2800.20130052

Shintani, T., and Klionsky, D. J. (2004). Autophagy in health and disease: a double-edged sword. *Science* 306, 990–995. doi: 10.1126/science.1099993

Sugioka, R., Shimizu, S., and Tsujimoto, Y. (2004). Fzo1, a protein involved in mitochondrial fusion, inhibits apoptosis. *J. Biol. Chem.* 279, 52726–52734. doi: 10.1074/jbc.M408910200

Tang, C., Han, H., Yan, M., Zhu, S., Liu, J., Liu, Z., et al. (2018). PINK1-PRKN/PARK2 pathway of mitophagy is activated to protect against renal ischemia-reperfusion injury. *Autophagy* 14, 880–897. doi: 10.1080/15548627.2017.1405880

Voigt, A., Berlemann, L. A., and Winklhofer, K. F. (2016). The mitochondrial kinase PINK1: functions beyond mitophagy. *J. Neurochem.* 139(Suppl. 1), 232–239. doi: 10.1111/jnc.13655

Wang, P., Liu, B., Zhao, J., Pang, Q., Agrawal, S. G., Jia, L., et al. (2015). Dynamin-related protein Drp1 is required for bax translocation to mitochondria in response to irradiation-induced apoptosis. *Oncotarget* 6, 22598–22612. doi: 10.18632/oncotarget.4200

Wang, Y., Tang, C., Cai, J., Chen, G., Zhang, D., Zhang, Z., et al. (2018). PINK1/Parkin-mediated mitophagy is activated in cisplatin nephrotoxicity to protect against kidney injury. *Cell. Death Dis.* 9:1113. doi: 10.1038/s41419-018-1152-1152

Wu, H. H., Hsiao, T. Y., Chien, C. T., and Lai, M. K. (2009). Ischemic conditioning by short periods of reperfusion attenuates renal ischemia/reperfusion induced apoptosis and autophagy in the rat. *J. Biomed. Sci.* 16:19. doi: 10.1186/1423-0127-16-19

Xiao, L., Xu, X., Zhang, F., Wang, M., Xu, Y., Tang, D., et al. (2017). The mitochondria-targeted antioxidant MitoQ ameliorated tubular injury mediated by mitophagy in diabetic kidney disease via Nrf2/PINK1. *Redox Biol.* 11, 297–311. doi: 10.1016/j.redox.2016.12.022

Yang, X., Wang, H., Ni, H. M., Xiong, A., Wang, Z., Sesaki, H., et al. (2017). Inhibition of Drp1 protects against senecionine-induced mitochondria-mediated apoptosis in primary hepatocytes and in mice. *Redox Biol.* 12, 264–273. doi: 10.1016/j.redox.2017.02.020

Yang, Y., Liu, H., Liu, F., and Dong, Z. (2014). Mitochondrial dysregulation and protection in cisplatin nephrotoxicity. *Arch. Toxicol.* 88, 1249–1256. doi: 10.1007/s00204-014-1239-1

Yeh, C. H., Hsu, S. P., Yang, C. C., Chien, C. T., and Wang, N. P. (2010). Hypoxic preconditioning reinforces HIF-alpha-dependent HSP70 signaling to reduce ischemic renal failure-induced renal tubular apoptosis and autophagy. *Life Sci.* 86, 115–123. doi: 10.1016/j.lfs.2009.11.022

Zhang, Z., Liu, L., Wu, S., and Xing, D. (2016). Drp1, Mff, Fis1, and MiD51 are coordinated to mediate mitochondrial fission during UV irradiation-induced apoptosis. *FASEB J.* 30, 466–476. doi: 10.1096/fj.15-274258

Zhao, C., Chen, Z., Qi, J., Duan, S., Huang, Z., Zhang, C., et al. (2017a). Drp1-dependent mitophagy protects against cisplatin-induced apoptosis of renal tubular epithelial cells by improving mitochondrial function. *Oncotarget* 8, 20988–21000. doi: 10.18632/oncotarget.15470

Zhao, C., Chen, Z., Xu, X., An, X., Duan, S., Huang, Z., et al. (2017b). Pink1/Parkin-mediated mitophagy play a protective role in cisplatin induced renal tubular epithelial cells injury. *Exp. Cell. Res.* 350, 390–397. doi: 10.1016/j.yexcr.2016.12.015

Zhou, J., Fan, Y., Zhong, J., Huang, Z., Huang, T., Lin, S., et al. (2018). TAK1 mediates excessive autophagy via p38 and ERK in cisplatin-induced acute kidney injury. *J. Cell. Mol. Med.* 22, 2908–2921. doi: 10.1111/jcmm.13585

Zhou, L., Wei, X. H., Pan, C. S., Yan, L., Gu, Y. Y., Sun, K., et al. (2017). QiShenYiQi pills, a compound chinese medicine, prevented cisplatin induced acute kidney injury via regulating mitochondrial function. *Front. Physiol.* 8:1090. doi: 10.3389/fphys.2017.01090

Conflict of Interest: The authors declare that the research was conducted in the absence of any commercial or financial relationships that could be construed as a potential conflict of interest.

Copyright © 2019 Zhou, Zhang, Zhang, Yu, Sun, Zhu, Li, Liang, Han and Qin. This is an open-access article distributed under the terms of the Creative Commons Attribution License (CC BY). The use, distribution or reproduction in other forums is permitted, provided the original author(s) and the copyright owner(s) are credited and that the original publication in this journal is cited, in accordance with accepted academic practice. No use, distribution or reproduction is permitted which does not comply with these terms.

frontiers in Medicine

ORIGINAL RESEARCH
published: 27 September 2019
doi: 10.3389/fmed.2019.00210

The Behavior of the Type of Peritoneal Transport in the Inflammatory and Oxidative Status in Adults Under Peritoneal Dialysis

Julio Alejandro Gutiérrez-Prieto[1], *Javier Soto-Vargas*[1], *Renato Parra-Michel*[1], *Héctor Leonardo Pazarín-Villaseñor*[1,2], *Andrés García-Sánchez*[2] *and Alejandra Guillermina Miranda-Díaz*[2*]

[1] *Servicio de Nefrología, Hospital General Regional No. 46, Instituto Mexicano del Seguro Social, Guadalajara, Mexico,*
[2] *Instituto de Terapéutica Experimental y Clínica, Centro Universitario de Ciencias de la Salud, Universidad de Guadalajara, Guadalajara, Mexico*

Peritoneal dialysis (PD) is an alternative for managing the end-stage renal disease (ESRD). The peritoneal membrane (PM) is not just a membrane that passively responds to diffusion and convection. The characteristics of PM result in the peritoneal equilibrium test (PET) and with this test is possible to obtain the type of peritoneal transport (PT). The patient on PD can be classified in different types of PT as; Low, Low Average, High Average, and High. The aim of the study was to compare the inflammatory cytokines, oxidants, antioxidants, and oxidative DNA damage markers in the different types of PT. A cross-sectional analytical study of 77 adult PD patients was performed. Levels of lipoperoxides (LPO) were higher in all types of PT vs. healthy volunteer controls (HC) ($p < 0.0001$). Nitric oxide (NO) levels were found significantly down-regulated in all types of PT ($p < 0.0001$). The activity of the superoxide dismutase enzyme (SOD) was found to be significantly increased in all types of PT vs. the HC ($p < 0.0001$). The levels of the DNA repair enzyme were found to be decreased in all types of PT. The levels of the pro-inflammatory cytokines TNF-α, IL-6, the marker of oxidative DNA damage, 8-IP and the total antioxidant capacity (TAC) were all significantly decreased, contrary to the levels in HC, possibly by the clearance in the dialysis fluid in all types of PT or due to down-regulation of their expression. In conclusion, we found significant changes in markers of inflammation, oxidative stress, and oxidative damage to DNA in all types of PT; Low, low average, high average, and high PT in the values of D/P creatinine at 4 h compared to HC.

Keywords: peritoneal dialysis, peritoneal transport, oxidative stress, oxidative DNA damage, inflammation

OPEN ACCESS

Edited by:
John D. Imig,
Medical College of Wisconsin, United States

Reviewed by:
Víctor Manuel Mendoza-Núñez, Universidad Nacional Autónoma de México, Mexico
Rümeyza Turan Kazancioglu, Bezmiâlem Vakif Üniversitesi, Turkey

***Correspondence:**
Alejandra Guillermina Miranda-Díaz
kindalex1@outlook.com

Specialty section:
This article was submitted to Nephrology, a section of the journal Frontiers in Medicine

Received: *10 July 2019*
Accepted: *10 September 2019*
Published: *27 September 2019*

Citation:
Gutiérrez-Prieto JA, Soto-Vargas J, Parra-Michel R, Pazarín-Villaseñor HL, García-Sánchez A and Miranda-Díaz AG (2019) The Behavior of the Type of Peritoneal Transport in the Inflammatory and Oxidative Status in Adults Under Peritoneal Dialysis. Front. Med. 6:210. doi: 10.3389/fmed.2019.00210

INTRODUCTION

End-stage renal disease (ESRD) is a clinical morbidity given the increasing prevalence of diseases as diabetes mellitus (DM) and hypertension. Mortality in patients with ESRD has decreased 30% since 1999 (1). In Jalisco (Mexico), nearly half of the patients (49.4%) are on PD (2). The adequacy of initial and maintenance PD prescription it is usually based on Twardowski's peritoneal equilibrium

test (PET) result and KT/V. PET is used to evaluate the transport function of the peritoneal membrane (PM) of each patient, in which the solute transport rates (creatinine, sodium, urea, glucose) are evaluated by the speed of the equilibrium reached between the dialysate and the peritoneal capillaries. According to the PET result, the patient on PD can be classified in different types of peritoneal transport (PT) as; Low, Low Average, High Average and High (3, 4). Some studies refer to High PT as a risk factor for mortality and technique failure in PD patients (5, 6). However, other authors showed that a high PT by itself is not an independent risk factor for either mortality or technique failure and exposed that other factors, like peritoneal protein clearance, residual renal function and age, are better predictors for survival rather than peritoneal membrane (PM) permeability (7–9). Hence, the effect of PM solute transport rate on these findings remains unclear. Cardiovascular disease (CVD) is the leading cause of death among patients in hemodialysis (HD) or peritoneal dialysis (PD) (10). Inflammation is one of the earliest events in situations of cardiac stress which implies high levels of endothelial adhesion molecules, increased production and release of inflammatory cytokines and chemokines (11). Studies have reported inflammation as an independent risk factor for all causes of cardiovascular mortality in HD and PD patients (12). Oxidative stress (OS) is characterized by an imbalance between oxidants and antioxidants (13). OS is implicated as a unifying factor between chronic kidney disease (CKD) and CVD (14), and it is involved in mechanism related to vascular calcification, oxidation of low-density cholesterol, and low endothelial nitric oxide (NO) which lead to atherosclerosis (15–18). The increase in reactive oxygen species (ROS) and the decrease in antioxidants among PD patients in counterpart with matched controls have been previously reported (19, 20). The marker of oxidative damage to DNA; 8-hydroxy-2-deoxyguanosine (8-OHdG) is considered as an independent predictor of all-cause mortality in patients undergoing dialysis (21). An increase of OS may lead to increased risk for cardiovascular disease in patients in DP regardless of the type of PT, however, there is no clear association, whereas OS is clearly associated with PM permeability rate.

The aim of the study was to compare the serum/plasma levels of inflammatory cytokines, oxidants, antioxidants, and oxidative DNA damage markers in the different types of PT.

Abbreviations: ESRD, End-stage renal disease; DM, Diabetes mellitus; CVD, Cardiovascular disease; HD, Hemodialysis; PD, Peritoneal dialysis; OS, Oxidative stress; CKD, Chronic kidney disease; ROS, Reactive oxygen species; 8-OHdG, 8-hydroxy-2′-deoxyguanosine; DNA, Deoxyribonucleic acid; PET, Peritoneal equilibrium test; KT/V, K, elimination of urea and other waste, from the dialyzer. The t time, the period of each treatment, V is the volume of fluid in the body; PT, Peritoneal transport; PM, Peritoneal membrane; D/P, Transport across the PM for a given solute; HC, Healthy volunteer control; IL-6, Interleukin 6; TNF-α, Tumor necrosis factor alpha; LPO, Products of Lipid peroxidation; MDA, Malondialdehyde; 8-IP, 8-Isoprostane; AChE, Acetyl cholinesterase; NO, Nitric Oxide; SOD, Superoxide Dismutase; O_2^-, Radical superoxide; TAC, Total antioxidant capacity; HRP, Horseradish peroxidase; TMB, Tetramethylbenzidine; SOD, Superoxide dismutase; HDL, Cholesterol of high density; CAPD, Continuous ambulatory peritoneal dialysis; APD, Ambulatory peritoneal dialysis; BMI, Body mass index; TSAT, Transferrin saturation; LDL, Cholesterol of low-density; VLDL, Cholesterol of very low-density; HCI_3, Bicarbonate; CRP, C reactive protein.

PATIENTS AND METHODS

An analytical cross-sectional study was conducted. Seventy-seven ESRD patients receiving PD at Hospital General Regional No. 46 of the Instituto Mexicano del Seguro Social in Jalisco, Mexico were included. Patients were seen in the PD outpatient clinic and were sent to perform the PET. Patients were eligible of the PD program and never had have a PET performed before. Patients with episodes of peritonitis in the last 6 months with dysfunction of the PD catheter, with a current infectious, inflammatory, or malignant process were excluded.

Data Collection

Demographic and clinical data were obtained through medical records the day that PET was performed. An extra venous blood sample during PET was obtained to assess the following: hemoglobin, white blood cell count, blood urea nitrogen, creatinine, glucose, albumin, sodium, potassium, chloride, calcium, phosphorus, uric acid, total cholesterol, high-density lipoprotein cholesterol, low-density lipoprotein cholesterol, very low-density cholesterol, triglyceride, bicarbonate, serum iron, and transferrin saturation.

Peritoneal Equilibrium Test

The PET was performed and the patients were classified based on the result of dialysate to plasma/creatinine ratio at 4 h as Low, Low Average, High Average, and High PT. The PET was performed in 149 patients a minimum of sixteen patients were collected in each group of type of PT. For the calculation of sample size, we used the formula to compare two means. We assumed a risk of making two tail type I and type II errors of 5–20%, respectively. Previous data of OS markers measured in this study were not available in the populations of Low, Low Average, High Average, and High PT. Thus, we took as reference the variation of NO between PD patients and HC as reported by Uzun et al. (22). An additional 20% sample was added for possible withdrawals, missing data, loss of sample while processing, etc.

For the measurement of metabolites, blood samples were drawn when PET blood samples were taken and centrifuged at 10,000 rpm for 10 min at room temperature; supernatants were stored in aliquots at −80°C until final processing. We included 10 mL of extra blood from 10 blood donors [healthy volunteer controls (HC)] to establish the normal value of the metabolites. For the selection of blood donors, we considered subjects who are not known to suffer any relevant illness to the proposed study and be within normal range of body measurements (23). Also, efficient measures were implemented to improve the sample result among them; a better examination of donors through microbiological tests has led to the reduction of transfusion-related infections (1 in 8 million for HIV, 1 in 6.7 million hepatitis C viruses and 1 in 1.7 million for hepatitis B viruses) (24).

Inflammation Cytokines

TNF-α and IL6

The ELISA kit was used to determine the IL-6 and TNF-α level. We followed the instructions of the kit manufacturer (Peprotech, Rocky Hill, NJ 08553, USA®). Both cytokines had a detection

limit of 32 pg/mL. First, 100 μL of diluted capture antibody was added, followed by incubation overnight at room temperature. Then, 300 μL of blocking buffer was added to the wells and it was incubated for 1 h at room temperature. Plasma and standards were added, followed by incubation for 2 h at room temperature. After several washings, 100 μL of diluted detection antibody was added. The plate was incubated at room temperature for 2 h. Then, 100 μL diluted HRP-Avidin-conjugate was added, followed by incubation for 30 min at room temperature. Finally, 100 μL of substrate solution was added to each well. The plate was read at a wavelength of 405 nm with correction set at 650 nm. The TNF-α intra-assay coefficient of variation was 2.1% and the intra-assay IL-6 was 4.7%. For all of the technical readings of optical density the Synergy HT (BIOTEK) microplate reader was used.

Oxidative Stress Markers

Products of Lipid Peroxidation

The serum levels of LPO were measured through the FR22 assay kit (Oxford Biomedical Research Inc., Oxford, MI, USA®) according to the manufacturer's instructions. The limit of detection for this test was 0.1 nmol/mL. The chromogenic reagent reacts with malondialdehyde (MDA) and 4-hydroxy-alkenals to form a stable chromophore. One hundred and forty microliter of plasma with 455 μL of N-methyl-2-phenylindole in acetonitrile (Reagent 1) was diluted with ferric iron in methanol. Samples were agitated, after 105 μL 37%, HCl was added, followed by incubation at 45°C for 60 min, and centrifugation at 12,791 rpm for 10 min. One hundred and fifty microliter of the supernatant was added to a microplate and absorbance was measured at 586 nm. The standard curve with known concentrations of 1,1,3,3-Tetramethoxypropane in Tris-HCl was used. The intra-assay CV was 8.5%.

8-Isoprostane

The immunoassay reagent kit from Cayman Chemical Company® (Michigan, USA) was used according to the manufacturer's instructions. The limit of detection was 0.8 pg/mL. The 8-IP assay was based on the principle of competitive binding between sample 8-IP, 8-IP acetyl cholinesterase (AChE) conjugate, and 8-IP tracer. Fifty microliter of serum samples or standard were added to each well and 50 μL of 8-IP AChE tracer was added to all wells except the total activity and blank wells. Fifty microliter of 8-IP enzyme immunoassay antiserum was added to all wells except the total activity and blank wells. Fifty microliter of 8-IP antiserum was added to all wells except total activity, non-specific binding, and blank wells. The plate was covered and incubated at 4°C for 18 h and then washed 5 times with buffer. Absorbance was read at 420 nm. The intra-assay CV was 12.5%.

Nitric Oxide

The serum samples were de-proteinized by the addition of zinc sulfate; 6 mg of zinc sulfate was added to 400 μL of sample, vortexed for one min and the samples were centrifuged at 10,000 × g for 10 min at 4°C. For the determination of NO, the colorimetric method was used according to the kit (Nitric Oxide Assay Kit, User protocol 482650, Calbiochem®). Eighty five microliter of the standard or sample were added to the wells of the plate, 10 μL of nitrate reductase was added to each well and 10 μL of 2 mM NADH. The plate was shaken for 20 min at room temperature. Fifty microliter of dye 1 was added and shaken briefly; 50 μL of dye 2 was added and again shaken for 5 min at room temperature. Finally, the plate was read at 540 nm in a spectrophotometer within the first 20 min after the procedure was finished.

Antioxidants

Superoxide Dismutase (SOD)

The kit manufacturer's instructions were followed (SOD No. 706002, Cayman Chemical Company®, USA) for the detection of O_2^- generated by xanthine oxidase and hypoxanthine enzymes through the reaction of tetrazolium salts. The serum samples were diluted 1:5 in sample buffer, 200 μL of the radicals' detector diluted 1:400, was placed, and 10 μL of the sample was added. After slow agitation, 20 μL of xanthine oxidase was added to the wells. The microplate was incubated for 20 min at room temperature and the absorbency was read at a wavelength of 440 nm. The levels are reported in U/mL.

Total Antioxidant Capacity

The total antioxidant capacity (TAC) evaluation were made following the instructions of the kit manufacturer (Total Antioxidant Power Kit, No. TA02.090130, Oxford Biomedical Research®), to obtain the concentration in mM equivalents of trolox (an analog of vitamin E). The detection limit was 0.075 mM. The serum samples and standards were diluted 1:40, and 200 μL were placed in each well. The plate was read at 450 nm as a reference value, 50 μL of copper solution was added, and the plate was incubated at room temperature for 3 min. Fifty microliter of stop solution was added and the plate was read again at 450 nm. The dilution factor was considered in the result. The intra-assay CV was 7.8%.

8-hydroxy-2′-deoxyguanosine (8-OHdG)

The method by the manufacturer of the ELISA kit was followed (8-hydroxy-2′-deoxyguanosine No. ab201734 Abcam®, Cambridge, United Kingdom). An 8-OHdG-coated 96-well plate was used. Fifty μL of sample or standard were added to each well and were detected with horseradish peroxidase (HRP) conjugated 8-OHdG antibody. Tetramethylbenzidine (TMB) substrate was used to obtain a color signal measured at 450 nm using a spectrophotometer reader. The value of the samples was plotted on the standard curve to interpolate sample concentrations.

8-oxoguanine-DNA-N-glycosylase-1 (hOGG1)

Repair of the oxidative damage of DNA was determined with a commercial kit (hOGG1 MBS702793 My BioSource®, San Diego, CA). The manufacturer's instructions were followed. One hundred microliter of plasma and standards were added to the wells and the plate was incubated at 37°C. The biotinylated antibody was added and incubated under the same conditions.

The corresponding washings were done and the HRP-avidin was added, followed by the substrate and the stop solution at the corresponding times. The optical density was read at 450 nm.

Statistical Analysis

All data were expressed as mean ± standard deviation (SD), standard error (SEM), or percentages. Kolmogorov-Smirnov test was used to analyze distribution normality of measured parameters. Differences between the four groups for continuous variables we used Kruskall-Wallis or a way ANOVA test according to the normality distribution. The *post-hoc* Dunn-Bonferroni correction was used for pairwise comparison and was considered significant at $p \leq 0.05$. For categorical variables, the difference between the groups using Chi^2 or Fisher's exact test for categorical variables. To evaluate relationships between oxidative stress markers and PET results Pearson's correlation test was used. $p \leq 0.05$ was considered statistically significant. SPSS for Windows version 18.0 (IBM SPSS statics Inc., Chicago, IL, USA) was used.

Ethical Considerations

The research complies with the ethical principles for medical research in human beings stipulated in the Declaration of Helsinki 64th General Assembly, Fortaleza, Brazil, October 2013. To adhering to the standards of Good Clinical Practices. All procedures were performed according to regulations stipulated in the General Health Legal Guidelines for Health care Research in Mexico, 2nd Title, in Ethical Aspects for Research in Human Beings, Chapter 1, and Article 17. All patients gave and signed informed consent form in the presence of signed witnesses. The study was evaluated and approved by the Local Ethics, and Research Committee, at the Hospital General Regional No. 110, Instituto Mexicano del Seguro Social (R-2017-1303-117).

RESULTS

Baseline Demographic and Clinical Characteristics

Of 77 patients who met the inclusion criteria; 15 were Low (It was not possible to complete 16 patients of this group), 23 Low Average, 23 High Average, and 16 were classified as High PT. The median age was 42 (IQR 27–60) years, 53 (65%) patients were male, and the etiology of CKD was of unknown and DM kidney disease predominantly. The average time on PD program was ∼40 months. Albumin ($p = 0.05$) and Triglycerides levels ($p = 0.007$) were lower in the High PT compared to the rest of the transporters. The PET was significant in the High PT patients ($p < 0.0001$). Hypertension was found more frequently in the High Average group ($p = 0.016$). Uric acid increased in patients with Low/Low Average PT rates compared with those with High Average/High PT rates ($p = 0.016$). Baseline demographic and characteristics of PD therapy according to the type of PT are shown in **Tables 1**, **2**.

Inflammatory Cytokines According the Type of PT

TNF-α and IL-6

The TNF-α level in the different types of PT were found to be significantly decreased. Low PT, 28.94 ± 5.23 pg/mL, Low Average, 27.90 ± 4.20 pg/mL, High Average, 32.56 ± 6.18 pg/mL and High, 66.28 ± 21.12 pg/mL vs. levels found in HC, 631.38 ± 125.40 pg/mL ($p < 0.0001$ Mann Whitney *U*-test and Kruskall-Wallis test).

The different types of PT showed lower serum levels of IL-6; Low PT, 326.13 ± 287.75 pg/mL, Low Average, 124.89 ± 47.25 pg/mL, High Average 357.21 ± 126.47 pg/mL and High PT, 272.02 ± 164.65 pg/mL vs. serum levels of IL-6 in HC, 498.45 ± 93.96 pg/mL ($p < 0.0001$ Mann Whitney *U*-test and Kruskall-Wallis test) (**Table 3**).

Oxidative Damage of DNA and Repair

Levels of the oxidative DNA damage marker were significantly reduced in Low PT, 38.25 ± 15.10 ng/mL, Low Average, 38.09 ± 20.68 ng/mL ($p = 0.042$), High Average, 11.20 ± 3.05 ng/mL, and High PT 31.05 ± 8.02 ng/mL ($p = 0.046$) in contrast to HC, 65.21 ± 19.14 ng/mL ($p = 0.004$).

The hOGG1 levels in HC obtained 3.53 ± 2.09 ng/mL. The different types of PT obtained lower levels (NS); Low PT, 0.29 ± 0.17 ng/mL, Low Average, 0.30 ± 0.12 ng/mL, High Average, 0.07 ± 0.01 ng/mL, and High 0.23 ± 0.09 ng/mL (**Table 3**).

Oxidants

The serum levels of the 8-IP were significantly reduced ($p < 0.0001$) in all types of PT in relation to the levels of HC, 22.88 ± 3.80 pg/mL. The serum levels of LPO in the HC were 3.05 ± 0.18 μM, however, significantly increased levels of LPO were found ($p < 0.0001$) in Low PT, 160.01 ± 30.39 μM, Low Average, 157.83 ± 35.48 μM, High Average, 223.77 ± 90.26 μM, and High PT, 101.80 ± 21.94 μM.

In contrast, the levels of NO metabolites were found significantly decreased in the different types of PT; Low 20.13 ± 4.79 μM, Low Average 23.53 ± 5.35 μM, High Average 6.82 ± 1.44, and High 10.59 ± 3.52 μM vs. levels of HC, 197.97 ± 34.20 μM ($p < 0.0001$) (**Table 3**).

Antioxidants

Serum activity of SOD was found increased in all types of PT; Low 3.02 ± 0.38 U/mL, Low Average, 3.40 ± 0.37 U/mL, High Average, 3.36 ± 0.35 U/mL, and High 3.41 ± 0.22 U/mL. In contrast, the activity of the enzyme in HC obtained 0.23 ± 0.02 U/mL ($p < 0.0001$) (**Table 3**).

The levels of TAC were found to be significantly consumed in all types of PT; Low 0.71 ± 0.05 mM, Low Average 0.68 ± 0.02 mM, High Average 0.64 ± 0.03 mM, and High PT, 0.68 ± 0.05 mM vs. the HC, 2.62 ± 0.17 mM ($p < 0.0001$) (**Table 3**).

Correlations

Table 4 shows correlations found between the markers of inflammation and oxidative stress with PET values. Only NO presented a low negative correlation with PET ($r = -0.269$, $p = 0.021$).

TABLE 1 | Clinical data of different type of peritoneal transport.

	Low n-15	Low average n-23	High average n-23	High n-16	*p*
Antihypertensive therapy *n* (%)					
Enalapril	0	2 (8.7)	2 (8.7)	1(6.2)	0.57
Losartan	12 (80)	17 (73.9)	15 (65.2)	11 (68.8)	0.001*
No treated	3 (20)	4 (17.4)	6 (26.1)	4 (25)	0.049*
Dialysis dose *n* (%)					
2,000 mL 1.5% every 6 h	6 (39)	11 (47.8)	9 (39.1)	5 (31.2)	0.002*
2,000 mL 1.5% and 2.25% every 6 h alternating	7 (46.7)	6 (26.1)	8 (34.8)	7 (43.8)	0.13
2,000 mL 2.25% every 6 h	2 (13.3)	6 (26.1)	6 (26.1)	4 (25)	0.049*
Type of PD *n* (%)					
APD	4 (26.7)	3 (13)	5 (21.7)	3 (18.8)	0.35
CAPD	11 (73.3)	20 (87)	18 (78.3)	13 (81.2)	<0.001*
CKD etiology *n* (%)					
Unknown	5 (33.3)	11 (47.8)	12 (52.2)	8 (50)	0.004*
Nephrolithiasis	1 (6.7)	0	0	0	1.000
Diabetes mellitus	7 (46.6)	12 (52.2)	8 (34.8)	7 (43.8)	0.002*
Preeclampsia with CKD	0	0	2 (8.7)	0	0.56
Polycystic kidney disease	1 (6.7)	0	0	0	1.00
Hypertension	1 (6.7)	0	1 (4.3)	1 (6.2)	0.67

*CKD, Chronic Kidney Disease, Values are media ± SD or percent; PD, peritoneal dialysis; APD, ambulatory peritoneal dialysis; CAPD, continuous ambulatory peritoneal dialysis. *Chi^2 test.*

DISCUSSION

In this study, we investigated the behavior between the types of PT and the levels of diverse markers of inflammation and OS in patients with ESRD on PD. The levels of the above-mentioned markers were altered in the totality of the 77 patients in comparison with the levels of these markers in HC. Uremic inflammation commonly affects patients with CKD and is characterized by increased expression of pro-inflammatory cytokines (25, 26). Overexpression of TNF-α and IL-6 has been previously reported in patients with ESRD (27). Systemic pro-inflammatory cytokines is a significant risk factor suggestive of infection in patients with PD (28). However, recently it was reported that circulating pro-inflammatory cytokines TNF-α and IL-6 decreased significantly after 3 months of PD and remained low at 6 months of follow-up in patients with heart failure undergoing PD due to overflow (29). The patients included in the study did not have heart failure, but the information could partially explain the behavior of the pro-inflammatory cytokines in the included patients. According to the types of PT, the serum levels of TNFα and IL-6 were significantly reduced. In this finding, we can hypothesize that the systemic inflammatory state was not present or that in the PD process the cytokines were purified in the dialysis fluid or is the result of a change in its expression (TNF-α and IL-6 in the dialysis fluid were not determined).

The circulating levels of 8-OHdG were first described in 1984 (30). 8-OHdG is considered a robust and sensitive marker of the OS; it reflects the oxidative decomposition of DNA (18). The 8-OHdG marker is considered an independent predictor of all-cause mortality in HD patients (21). Overexpression of 8-OHdG produces erroneous readings by converting A to C and form G to T capable of producing mutagenic alterations (31). Circulating and urinary concentrations of the 8-OHdG marker are increased in patients with chronic diseases such as cancer, chronic hepatitis, DM, CVD, and ESRD (32–34). In a study reported in 2015, the authors analyzed the levels of 83 PD patients and found higher levels of 8-OHdG than the control population without significant difference between the types of PD. In other reports, the higher levels were found in patients on HD, which underscores the importance of the role of other factors involved in oxidative status (19). Contrary to previous reports, we found significantly decreased levels of the 8-OHdG marker in Low Average PT, High Average and High PT in contrast to levels obtained in HC. Our findings could be due to the possible depuration of this marker during PD sessions due to greater biocompatibility of the PD solutions in the PM (19). Other studies have shown moderate positive correlation between the ratio of creatinine D/P at 4 h and the levels of 8-OHdG in the peritoneal effluent as a marker of damage to the PM. However, the authors did not measure plasma levels and did not explain whether the correlation is due to increased local production of 8-OHdG or to a better clearance of it (35). The clearance of this marker in the dialyzed effluent is only speculative. We did not find in the available literature low systemic levels of 8-OHdG as in our study.

In the present study, the levels of the DNA repair enzyme (hOGG-1) were found to be decreased in all types of PT (NS), in contrast to levels obtained in HC, suggesting the inactivity or consumption of the enzyme in an attempt to avoid

TABLE 2 | Demographic and biochemical data according to the type of peritoneal transport.

	Low n-15	Low average n-23	High average n-23	High n-16	*p*
Gender *n* (%)					
Male	11 (73.33)	16 (69.56)	18 (78.26)	8 (50)	<0.000ŧ
Female	4 (26.67)	7 (30.44)	5 (21.74)	8 (50)	0.475
Age (years)	47.33 ± 16.97	44.45 ± 18.62	43.88 ± 19.66	46.59 ± 17.60	0.894
Weight (kg)	67.06 ± 14.15	72.12 ± 13.41	68.63 ± 11.25	71.68 ± 10.68	0.408
Height (m)	1.63 ± 0.07	1.64 ± 0.09	1.66 ± 0.08	1.61 ± 0.11	0.163
BMI kg/m^2	25.37 ± 5.37	26.70 ± 4.3	24.86 ± 3.61	28.13 ± 6.32	0.067
Hypertension *n* (%)	6 (40.00)	10 (43.06)	14 (60.29)	8 (51.39)	0.016ŧ
Residual urine (mL)	813.89 ± 566.93	655.26 ± 587.34	697.00 ± 579.32	582.35 ± 451.71	0.687
PET	0.55 ± 0.04^a	0.66 ± 0.03^b	0.78 ± 0.03^c	0.90 ± 0.04^d	<0.000**
Hemoglobin (g/dL)	12.04 ± 1.95	11.13 ± 2.17	11.02 ± 2.07	10.22 ± 1.99	0.086
Urea (mg/dL)	113.22 ± 26.10	116.95 ± 30.09	107.51 ± 37.16	125.73 ± 32.38	0.254
Creatinine (mg/dL)	10.44 ± 5.06	10.75 ± 4.54	11.52 ± 4.83	11.49 ± 4.88	0.809
Glucose (mg/dL)	137.98 ± 88.64	124.71 ± 59.76	114.25 ± 43.53	102.90 ± 33.72	0.195
Phosphorus (mg/dL)	5.05 ± 1.68	4.85 ± 1.73	4.66 ± 1.88	5.62 ± 1.44	0.284
Calcium (mg/dL)	9.40 ± 0.91	9.52 ± 1.16	9.22 ± 1.07	9.28 ± 0.99	0.422
Magnesium (mg/dL)	2.23 ± 0.47	2.21 ± 0.37	2.26 ± 0.53	2.24 ± 0.46	0.976
Potassium (mEq/L)	4.49 ± 0.60	4.32 ± 0.63	4.23 ± 0.71	4.49 ± 0.70	0.437
Sodium (mEq/L)	139.47 ± 3.43	138.86 ± 3.00	138.68 ± 3.82	136.64 ±3.82	0.159
Albumin (g/dL)	3.80 ± 0.51	3.58 ± 0.67	3.40 ± 0.70	3.25 ± 0.46	0.053
Uric acid (mg/dL)	6.85 ± 1.65^{a,b}	6.92 ± 1.55^a	5.99 ± 0.86^b	6.13 ± 0.91^{a,b}	0.016**
Iron (mcg/dL)	92.91 ± 45.15	65.27 ± 28.08	76.05 ± 28.87	80.71 ± 44.22	0.063
TSAT %	41.25 ± 7.93	28.7 ± 23.77	40.56 ± 23.22	18.67 ± 0.58	0.330
Cholesterol (mg/dL)	193.24 ± 46.74	166.42 ± 50.68	161.89 ± 42.5	179.51 ± 44.27	0.100
HDL (mg/dL)	37.11 ± 9.17	40.51 ± 13.43	45.88 ± 15.20	50.46 ± 17.0	0.033**
LDL (mg/dL)	112.93 ± 30.56	93.04 ± 41.12	93.43 ± 35.25	96.58 ± 30.00	0.333
Triglycerides (mg/dL)	226.69 ± 159.22^a	158.61 ± 87.03^{a,b}	127.53 ± 68.38^b	129.99 ±74.92^b	0.007*
VLDL (mg/dL)	45.71 ± 32.63^a	32.93 ± 19.08^{a,b}	25.44 ± 13.71^b	26.06 ±15.05^{a,b}	0.010*
HCO_3 (mEq/L)	20.19 ± 2.93	21.01 ± 3.21	21.47 ± 3.32	20.37 ± 3.81	0.574
CRP (mg/L)	4.293 ± 3.29	8.78 ± 10.90	3.58 ± 4.84	5.12 ± 5.81	0.113

*Values are mean ± SD or percent. PET, peritoneal equilibration tests; BMI, body mass index; TSAT, transferrin saturation; HDL, high-density lipoprotein; LDL, low-density lipoprotein; VLDL, very low-density lipoprotein; HCO_3, bicarbonate; CRP, C reactive protein; ŧ Chi^2 test; * K-W, Kruskall Wallis test; ** ANOVA. a,b,c,d: different letter denote statistically significant difference using Dunn-Bonferroni pairwise test at $p \leq 0.05$.*

over-production of the 8-OHdG. We can speculate that the results may be due to the inactivity of the enzyme or down-regulation of its expression. The repair of DNA containing oxidized bases, involves complex pathways (36). One mechanism of repair that eliminates 8-OHdG is characterized by the cleavage of the glycosidic bond of the 8-OHdG residue by breaking the phosphodiester bond at the resulting apurinic site by β-elimination (37). There is a lack of data in the literature about hOGG-1 in dialysis patients. We previously evaluated the long-term behavior of hOGG-1 in patients with renal transplantation and we found low levels of hOGG-1 in HC compared with patients in HD or DP before transplantation. However, these measures were made with no distinction of type of PT or renal replacement therapy (38).

LPO are molecules that result from the reactions of ROS (39). The production of ROS by mitochondria is important because it underlies oxidative damage in many pathologies and contributes to retrograde redox signaling from the matrix of mitochondria to the cytosol and nucleus (40). MDA is a final compound of the LPO process and is useful as an indicator of OS in patients with CKD where its elimination is decelerated (41). The lipid peroxidation process is involved in the genesis of atherosclerotic lesions and cardiovascular complications in CKD (42–44). Higher levels of MDA have been reported in patients with ESRD, HD, PD vs. HC (45, 46). There are also reports where no differences in MDA levels in patients with PD and HC (47). In our study, we found increased levels of LPO in all types of PT (48) and no correlation with the value of PET. Stepanova et al. previously reported the association of MDA with some PD parameters, they also found no correlation with D/P creatinine ratio but a negatively correlation with total KT/V (49).

NO is produced by an NOS family and consists of three identified isoforms (neuronal, inducible, and endothelial NOS). NO is an important molecule in physiological processes

TABLE 3 | Inflammation cytokines, oxidative DNA damage, oxidants and antioxidants according to the type of peritoneal transportation of patients in peritoneal dialysis.

	Healthy controls n-10	Low n-15	Low average n-23	High average n-23	High n-16	*p* K-W
Inflammatory cytokines						
TNF-α (pg/mL)	631.38 ± 125.40[b]	28.94 ± 5.23[a]	27.90 ± 4.20[a]	32.56 ± 6.18[a]	66.28 ± 21.12[a]	<0.0001
IL-6 (pg/mL)	498.45 ± 93.96[b]	326.13 ± 287.75[a]	124.89 ± 47.25[a]	357.21 ± 126.47[a]	272.02 ± 164.65[a,b]	0.001
Oxidative DNA damage						
8-OHdG (ng/mL)	65.21 ± 19.14[b]	38.25 ± 15.10[a,b]	38.09 ± 20.68[a,b]	11.20 ± 3.05[a]	31.05 ± 8.02[a]	0.046
hOGG1 (ng/mL)	3.53 ± 2.09	0.29 ± 0.17	0.30 ± 0.12	0.07 ± 0.01	0.23 ± 0.09	0.38
Oxidants						
8-Isoprostanes (pg/mL)	22.88 ± 3.80[b]	19.05 ± 15.83[a]	4.76 ± 0.79[a]	3.54 ± 0.42[a]	6.06 ± 1.46[a]	<0.0001
Lipoperoxides (μM)	3.05 ± 0.18[b]	160.01 ± 30.39[a]	157.83 ± 35.48[a]	223.77 ± 90.26[a]	101.80 ± 21.94[a]	<0.0001
Nitric oxide (μM)	197.97 ± 34.20[b]	20.13 ± 4[a]	23.53 ± 5.35[a]	6.82 ± 1.44[a]	10.59 ± 3.52[a]	<0.0001
Antioxidants						
Superoxide dismutase (U/mL)	0.23 ± 0.02[b]	3.02 ± 0.38[a]	3.40 ± 0.37[a]	3.36 ± 0.35[a]	3.41 ± 0.22[a]	<0.0001
Total antioxidant capacity (mM)	2.62 ± 0.17[b]	0.71 ± 0.05[a]	0.68 ± 0.02[a]	0.64 ± 0.03[a]	0.68 ± 0.05[a]	<0.0001

Values are media ± SEM, K-W, Kruskall Wallis test. a,b: different letter denote statistically significant difference using Dunn-Bonferroni pairwise test at $p \leq 0.05$.

as in neuronal transmission, reproduction, apoptosis and predominantly in endothelial vasodilatation. NO also actively participates in pathological processes such as inflammation, septic shock, asthma, and nitrosative stress. NOS produces O_2^- by NOS decoupling phenomenon (50). The generation of O_2^- occurs mainly when the NOS is not coupled with its cofactor or substrate due to depletion of L-arginine (10). Vascular endothelial dysfunction is due to the decoupling of NOS, phagocytic activation of vascular membrane oxidases and mitochondrial. NO is capable of increasing vascular stiffness and compromising cardiac output (51). The decrease in OS is directly related to endothelial dysfunction by reducing the bioavailability of NO to produce alterations in vascular permeability and favoring the entry of low-density cholesterol into the vascular intima where it is oxidized. In this process, the migration of inflammatory cells in the sub-endothelial space takes place after the expression of adhesion molecules by the dysfunctional endothelium (52). In our study, NO levels were significantly decreased in all types of PT vs. the levels found in HC. Additionally, a negative correlation between NO and PET was found. These explained that patient with High and High Average PT tents to have lower levels of NO, which could suggest alterations in the bioavailability of NO in the vascular endothelium (53). Schmidt et al., showed that patients in PD have low levels of NO vs. HC when both are undergoing a controlled dietary NO intake (54). Uzun et al., also found that patients in PD, without HD, have lower levels of NO compared with HC (22). However, Kovačević et al., found increased levels of NO in CAPD (55). The reason of these different outcomes may be explained by the effect of PM solute transport rate among the patient in PD.

8-IP are a bioactive product of peroxidation of arachidonic acid (56). In our study, significantly decreased serum levels were found in the patients studied in comparison to HC. However, in the available literature, one study reported decreased plasma levels of F2-isoprostans in patients with CAPD compared to patients in HD (57). It has been reported down-regulation of this metabolite in people with high consumption of polyunsaturated fatty acids via NOX (58). The enhanced levels of 8-IP has been reported in patients with ESRD receiving HD and CAPD (59). Other studies have found higher levels of 8-IP in CAPD patients vs. healthy matches (60). Currently, there is no defined behavior of 8-IP and its serum levels, as well as the clearance of these in the PD effluent. It would be necessary to determine the levels of this metabolite in the dialytic effluent.

TABLE 4 | Pearson correlation coefficient between the oxidative stress markers and PET value.

	r	*p*
8-OH-dG ng/mL	−0.040	0.735
hOGG1 ng/mL	−0.053	0.642
LPO μM	−0.034	0.766
Nitric oxide μM	−0.269*	0.021
8-isoprostane pg/mL	−0.175	0.129
SOD U/mL	0.086	0.447
Total antioxidant capacity mM	−0.090	0.429
TNF-α pg/mL	0.221	0.055
IL-6 ng/mL	0.048	0.682
SOD U/mL	0.086	0.447

As a defense mechanism against oxidative damage, the organism possesses compounds with antioxidant capacity such as the SOD enzyme. The SOD is a metallo-enzyme that catalyzes the dismutation of O_2^-, this enzyme is considered crucial in the beginning of the enzymatic mechanisms of defense against OS (61). The determination of SOD levels turns out to be an important indicator for the analysis of the OS in various pathologies such as DM and CKD. The activity of SOD enzyme in all types of PT was significantly increased compared to HC in agreement with other studies demonstrating the alteration the OS

balance favoring the pro-oxidant state (43). The SOD enzyme contains selenium that is traditionally been considered as the main mediator of antioxidant enzymatic protection (61). In the present study, we found greater activity of the SOD enzyme in all types of PT vs. HC, possibly in an attempt to compensate the increase in LPO products (62, 63). Some studies suggest patients in PD have an increased activity of SOD vs. HC (64).

The main antioxidant defenses in extracellular fluids against OS are bilirubin, uric acid, and albumin; which makes it possible to measure them as a whole by determining the TAC reagent. Albumin, bilirubin and urates prevent free radicals from reacting by sequestering transition metal ions (65–67). We found TAC decreased in all types of PT by contrast to HC, which is consistent with other study that showed low TAC in PD also compared to HC. Other studies demonstrated contrary; higher TAC in patients in PD vs. HC (68). This finding could suggest that these extracellular antioxidants are possibly being cleared in the dialysate effluent.

As strengths, we point out that the present study is one of the largest studies carried out so far at an international level in the PD population with an adequate number of patients in each group according to the type of PT, in addition to being a homogeneous sample as to the baseline, clinical, and therapeutic characteristics. Most of the data available in the literature is focus between binominals of mixed population of Low-Low Average PT and High Average-High PT. In our study, we aimed to show the behavior for each individual group. These data give tools to understand the behavior of the oxidative status in relation of the PM permeability rate, which may contribute to the design of new studies with therapeutic or risk assessment approaches.

In terms of limitations of the study, we accept that it is a cross-sectional study; thus, only one sample was used to decide about the inflammation and OS markers. The levels of the markers do not have a static behavior and a follow up throughout study with multiple determinations in time is required to corroborate these findings.

In conclusion, we found statistically significant changes in the markers of OS, DNA damage, and inflammation in all type of PT, Low, Low Average, High Average, and High PT compared to HC. All patients included had increased levels of LPO and the SOD suggesting compensatory antioxidant activity. Important down-regulation of serum levels of NO with the ability to influence the bioavailability of NO in the renal and systemic vascular endothelium. The decreased levels in hOGG1 was possible due to the down-regulation of the expression or excretion in the dialysis fluid.

DATA AVAILABILITY STATEMENT

The datasets generated for this study are available on request to the corresponding author.

ETHICS STATEMENT

The study was evaluated and approved by the Local Ethics and Research Committee, at the Hospital General Regional No. 110, IMSS (R-2017-1303-117). The patients/participants provided their written informed consent to participate in this study.

AUTHOR CONTRIBUTIONS

JG-P, HP-V, and AM-D: conception and design. AG-S, RP-M, HP-V, and JS-V: analysis and interpretation of data. JG-P, HP-V, AM-D, AG-S, RP-M, and JS-V: document writing and critical review.

FUNDING

Program 1.1.4.8.6 Strengthening Research and Postgraduate Studies, 2017. Ministry of Public Education, Mexico.

REFERENCES

1. Delanaye P, Mariat C, Glassock RJ. Safety of living kidney donation: another brick in the wall and a solid (physiologic) one. *Am J Kidney Dis.* (2015) 66:1–3. doi: 10.1053/j.ajkd.2015.04.005
2. U.S. Renal Data System. *USRDS 2013 Annual Data Report: Atlas of Chronic Kidney Disease and End-Stage Renal Disease in the United States*. National Institutes of Health, National Institute of Diabetes and Digestive and Kidney Diseases, Bethesda, MD (2013).
3. Twardowski ZJ, Nolph K, Khanna R. Peritoneal equilibration test. *Perit Dial Bull.* (1987) 3:138–47.
4. Gotch FA, Sargent JA. A mechanistic analysis of the National Cooperative Dialysis Study (NCDS). *Kidney Int.* (1985) 28:526–34. doi: 10.1038/ki.1985.160
5. Brimble KS, Walker M, Margetts PJ, Kundhal KK, Rabbat CG. Meta-analysis: peritoneal membrane transport, mortality, and technique failure in peritoneal dialysis. *J Am Soc Nephrol.* (2006) 17:2591–8. doi: 10.1681/ASN.2006030194
6. Rumpsfeld M, McDonald SP, Johnson DW. Higher peritoneal transport status is associated with higher mortality and technique failure in the Australian and New Zealand peritoneal dialysis patient populations. *J Am Soc Nephrol.* (2006) 17:271–8. doi: 10.1681/ASN.2005050566
7. Lee CC, Chen KH, Tian YC, Weng CM, Yang CW, Hung CC. Initial high peritoneal transport status is not a predictor of mortality in peritoneal dialysis patients. *Ren Fail.* (2010) 32:788–95. doi: 10.3109/0886022X.2010.493981
8. Perl J, Huckvale K, Chellar M, John B, Davies SJ. Peritoneal protein clearance and not peritoneal membrane transport status predicts survival in a contemporary cohort of peritoneal dialysis patients. *Clin J Am Soc Nephrol.* (2009) 4:1201–6. doi: 10.2215/CJN.01910309
9. Reyes MJ, Bajo MA, Hevía C, Del Peso G, Ros S, de Miguel AG, et al. Inherent high peritoneal transport and ultrafiltration deficiency: their mid-term clinical relevance. *Nephrol Dial Transplant.* (2007) 22:218–23. doi: 10.1093/ndt/gfl529
10. United States Renal Data System. *2017 USRDS Annual Data Report: Epidemiology of Kidney Disease in the United States*. National Institutes of Health, National Institute of Diabetes and Digestive and Kidney Diseases, Bethesda, MD (2017). Available online at: https://www.usrds.org/2017/view/Default.aspx
11. Glezeva N, Baugh JA. Role of inflammation in the pathogenesis of heart failure with preserved ejection fraction and its potential as a therapeutic target. *Heart Fail Rev.* (2014) 19:681–94. doi: 10.1007/s10741-013-9405-8

12. Wang AY, Wang M, Woo J, Lam CW, Lui SF, Li PK, et al. Inflammation, residual kidney function, and cardiac hypertrophy are interrelated and combine adversely to enhance mortality and cardiovascular death risk of peritoneal dialysis patients. *J Am Soc Nephrol.* (2004) 15:2186–94. doi: 10.1097/01.ASN.0000135053.98172.D6
13. Blake PG. What is the problem with high transporters? *Perit Dial Int. (*1997) 17:317–20.
14. Himmelfarb J, Stenvinkel P, Ikizler TA, Hakim RM. The elephant in uremia: oxidant stress as a unifying concept of cardiovascular disease in uremia. *Kidney Int. (*2002) 62:1524–38. doi: 10.1046/j.1523-1755.2002.00600.x
15. Farrar EJ, Huntley GD, Butcher J. Endothelial-derived oxidative stress drives myofibroblastic activation and calcification of the aortic valve. *PLoS ONE.* (2015) 10:e0123257. doi: 10.1371/journal.pone.0123257
16. Byon CH, Javed A, Dai Q, Kappes JC, Clemens TL, Darley VM, et al. Oxidative stress induces vascular calcification through modulation of the osteogenic transcription factor Runx2 by AKT signaling. *J Biol Chem.* (2008) 283:15319–27. doi: 10.1074/jbc.M800021200
17. Maiolino G, Rossitto G, Caielli P, Bisogni V, Rossi GP, Calò LA. The role of oxidized low-density lipoproteins in atherosclerosis: the myths and the facts. *Mediat Inflamm.* (2013) 2013:714653. doi: 10.1155/2013/714653
18. Förstermann U, Xia N, Li H. Roles of vascular oxidative stress and nitric oxide in the pathogenesis of atherosclerosis. *Circ Res.* (2017) 120:713–35. doi: 10.1161/CIRCRESAHA.116.309326
19. Sundl I, Roob JM, Meinitzer A, Tiran B, Khoschsorur G, Haditsch B, et al. Antioxidant status of patients on peritoneal dialysis: associations with inflammation and glycoxidative stress. *Perit Dial Int.* (2009) 29:89–101.
20. Bonnefont-Rousselot D, Jaudon MC, Issad B, Cacoub P, Congy F, Jardel C, et al. Antioxidant status of elderly chronic renal patients treated by continuous ambulatory peritoneal dialysis. *Nephrol Dial Transplant. (*1997) 12:1399–405. doi: 10.1093/ndt/12.7.1399
21. Xu H, Watanabe M, Qureshi AR, Heimbürger O, Bárány P, Anderstam B, et al. Oxidative DNA damage and mortality in hemodialysis and peritoneal dialysis patients. *Perit Dial Int.* (2015) 35:206–15. doi: 10.3747/pdi.2013.00259
22. Uzun H, Konukoglu D, Besler M, Erdenen F, Sezgin C, Muderrisoglu C. The effects of renal replacement therapy on plasma, asymmetric dimethylarginine, nitric oxide and C-reactive protein levels. *Clin Invest Med.* (2008) 31, 490–6. doi: 10.25011/cim.v31i1.3135
23. Posner J. Chapter 4: Exploratory development. In: Griffin JP, O'Grady J, editors. *The Textbook of Pharmaceutical Medicine*, 6th ed. Oxford, UK: Wiley-Blackwell Publishing (2009). p. 137–66.
24. O'Brien SF, Yi Q-L, Fan W, Scalia V, Fearon MA, Allain J-P. Current incidence and residual risk of HIV, HBV and HCV at Canadian Blood Services. *Vox Sang.* (2012) 103:83–6. doi: 10.1111/j.1423-0410.2012.01584.x
25. Rodríguez-Carrizalez AD, Castellanos-González JA, Martínez-Romero EC, Miller-Arrevillaga G, Villa-Hernández D, Hernández-Godínez PP, et. al. Oxidants, antioxidants and mitochondrial function in non-proliferative diabetic retinopathy. *J Diabetes. (*2014) 6:167–75. doi: 10.1111/1753-0407.12076
26. Cantón-Romero JC, Miranda-Díaz AG, Bañuelos-Ramírez JL, Carrillo-Ibarra S, Sifuentes-Franco S, Castellanos-González JA, et al. Markers of oxidative stress and inflammation in ascites and plasma in patients with platinum-sensitive, platinum-resistant, and platinum-refractory epithelial ovarian cancer. *Oxid Med Cell Longev. (*2017) 2017:1–8. doi: 10.1155/2017/2873030
27. Pecoits-Filho R, Heimbürger O, Bárány P, Suliman M, Fehrman-Ekholm I, Lindholm B, et al. Associations between circulating inflammatory markers and residual renal function in CRF patients. *Am J Kidney Dis.* (2003) 41:1212–8. doi: 10.1016/S0272-6386(03)00353-6
28. Kang E, Kim S, Lee HJ, Park I, Kim H, Shin GT. Tumor necrosis factor α is a risk factor for infection in peritoneal dialysis patients. *Kor J Intern Med.* (2016) 31:722–9. doi: 10.3904/kjim.2015.230
29. Kunin M, Carmon V, Arad M, Levin-Iaina N, Freimark D, Holtzman EJ, et al. Inflammatory biomarkers in refractory congestive heart failure patients treated with peritoneal dialysis. *Biomed Res Int.* (2015) 2015:590851. doi: 10.1155/2015/590851
30. Kasai H, Tanooka H, Nishimura S. Formation of 8-hydroxyguanine residues in DNA by X-irradiation. *Gann.* (1984) 75:1037–9.
31. Kasai H. Analysis of a form of oxidative DNA damage, 8-hydroxy-2′-deoxyguanosine, as a marker of cellular oxidative stress during carcinogenesis. *Mutat Res.* (1997) 387:147–63. doi: 10.1016/S1383-5742(97)00035-5
32. Wu LL, Chiou CC, Chang PY, Wu JT. Urinary 8-OHdG: a marker of oxidative stress to DNA and a risk factor for cancer, atherosclerosis and diabetics. *Clin Chim Acta.* (2004) 339:1–9. doi: 10.1016/j.cccn.2003.09.010
33. Tarng DC, Huang TP, Wei YH, Liu TY, Chen HW, Wen Chen T, et al. 8-Hydroxy-2′-deoxyguanosine of leukocyte DNA as a marker of oxidative stress in chronic hemodialysis patients. *Am J Kidney Dis.* (2000) 36:934–44. doi: 10.1053/ajkd.2000.19086
34. Mastalerz-Migas A, Steciwko A, Pokorski M, Pirogowicz I, Drobnik J, Bunio A, et al. What influences the level of oxidative stress as measured by 8-hydroxy-2′-deoxyguanosine in patients on hemodialysis? *J Physiol Pharmacol.* (2006) 57:199–205.
35. Morishita Y, Watanabe M, Hirahara I, Shigeaki Muto T, Eiji Kusano S, Akimotio T. Level of 8-OHdG in drained dialysate appears to be a marker of peritoneal damage in peritoneal dialysis. *Int J Nephrol Renovasc Dis.* (2012) 5:9–14. doi: 10.2147/IJNRD.S27553
36. Nash HM, Bruner SD, Schärer OD, Kawate T, Addona TA, Spooner E, et al. Cloning of a yeast 8-oxoguanine DNA glycosylase reveals the existence of a base-excision DNA-repair protein superfamily. *Curr Biol.* (1996) 6:968–80. doi: 10.1016/S0960-9822(02)00641-3
37. van der Kemp PA, Thomas D, Barbey R, de Oliveira R, Boiteux S. Cloning and expression in *Escherichia coli* of the OGG1 gene of *Saccharomyces cerevisiae*, which codes for a DNA glycosylase that excises 7,8-dihydro-8-oxoguanine and 2.6-diamino-4-hdroxy-5–*n*-methylformamidopyrimidine. *Proc Natl Acad Sci USA.* (1996) 93:5197–202. doi: 10.1073/pnas.93.11.5197
38. Cerrillos-Gutiérrez JI, Miranda-Díaz AG, Preciado-Rojas P, Gómez-Navarro B, Sifuentes-Franco S, Carrillo-Ibarra S, et al. The beneficial effects of renal transplantation on altered oxidative status of ESRD patients. *Oxid Med Cell Longev.* (2016) 2016:5757645. doi: 10.1155/2016/5757645
39. Ghezzi P, Floridi L, Boraschi D, Cuadrado A, Manda G, Levic S, et al. Oxidative stress and inflammation induced by environmental and psychological stressors: a biomarker perspective. *Antioxid Redox Signal.* (2018) 28:852–87. doi: 10.1089/ars.2017.7147
40. Droge W. Free radicals in the physiological control of cell function. *Physiol Rev.* (2002) 82:47–95. doi: 10.1152/physrev.00018.2001
41. Daschner M, Lenhartz H, Bötticher D, Schaefer F, Wollschläger M, Mehls O, et al. Influence of dialysis on plasma lipid peroxidation products and antioxidant levels. *Kidney Int.* (1996) 50:1268–72. doi: 10.1038/ki.1996.437
42. Loeper J, Goy J, Rozensztajn L, Bedu O, Moisson P. Lipid peroxidation and protective enzymes during myocardial infarction. *Clin Chim Acta. (*1991) 196:119–25. doi: 10.1016/0009-8981(91)90064-J
43. Steinbrecher P. Role of lipoprotein peroxidation in the pathogenesis of atherosclerosis. *Clin Cardiol. (*1991) 14:865–7. doi: 10.1002/clc.4960141102
44. Locatelli F, Canaud B, Eckardt K-U, Stenvinkel P, Wanner C, Zoccali C. Oxidative stress in end-stage renal disease: an emerging threat to patient outcome. *Nephrol Dial Transplant. (*2003) 18:1272–80. doi: 10.1093/ndt/gfg074
45. De Vecchi AF, Bamonti F, Novembrino C, Ippolito S, Guerra L, Lonati S, et al. Free and total plasma malondialdehyde in chronic renal insufficiency and in dialysis patients. *Nephrol Dial Transplant. (*2009) 24:2524–9. doi: 10.1093/ndt/gfp102
46. Ozden M, Maral H, Akaydin D, Cetinalp P, Kalender B. Erythrocyte glutathione peroxidase activity, plasma malondialdehyde and erythrocyte glutathione levels in hemodialysis and CAPD patients. *Clin Biochem. (*2002) 35:269–73. doi: 10.1016/S0009-9120(02)00307-7
47. Montazerifar F, Karajibani M, Sanadgol H, Hashemi M. Effect of peritoneal dialysis on antioxidant defense system and oxidative stress. *Hong Kong J Nephrol. (*2012) 14:33–7. doi: 10.1016/j.hkjn.2012.09.004
48. Ledwozyw A, Michalak J, Stępien A, Kadziołka A. The relationship between plasma triglycerides, cholesterol, total lipids and lipid peroxidation products during human atherosclerosis. *Clin Chim Acta. (*1986) 155:275–83. doi: 10.1016/0009-8981(86)90247-0
49. Stepanova N, Korol L, Burdeyna O. Oxidative stress in peritoneal dialysis patients: association with the dialysis adequacy and technique survival. *Indian J Nephrol.* (2019) 10:1–8. doi: 10.4103/ijn.IJN_242_18

50. Ahmad A, Dempsey SK, Daneva Z, Azam M, Li N, Li PL, et al. Role of nitric oxide in the cardiovascular and renal systems. *Int J Mol Sci.* (2018) 19:E2605. doi: 10.3390/ijms19092605
51. Ungvari Z, Gupte S, Recchia F, Batkai S, Pacher P. Role of oxidative-nitrosative stress and downstream pathways in various forms of cardiomyopathy and heart failure. *Curr Vasc Pharmacol.* (2005) 3:221–9. doi: 10.2174/1570161054368607
52. Li H, Horke S, Forstermann U. Vascular oxidative stress, nitric oxide and atherosclerosis. *Atherosclerosis.* (2014). 237:208–19. doi: 10.1016/j.atherosclerosis.2014.09.001
53. De Keyzer D, Karabina SA, Wei W, Geeraert B, Stengel D, Marsillach J, et al. Increased PAFAH and oxidized lipids are associated with inflammation and atherosclerosis in hypercholesterolemic pigs. *Arterioscler Thromb Vasc Biol.* (2009) 29:2041–6. doi: 10.1161/ATVBAHA.109.196592
54. Schmidt RJ, Yokota S, Tracy TS, Sorkin MI, Baylis C. Nitric oxide production is low in end-stage renal disease patients on peritoneal dialysis. *Am J Physiol.* (1999) 276:F794–7. doi: 10.1152/ajprenal.1999.276.5.F794
55. Kovačević P, Dragić S, Rajkovača Z, Veljković S, Kovačević T. Serum levels of nitric oxide and endothelin-1 in patients treated with continuous ambulatory peritoneal dialysis. *Ren Fail.* (2014) 36:437–40. doi: 10.3109/0886022X.2013.867812
56. Lim PS1, Chang YM, Thien LM, Wang NP, Yang CC, Chen TT, et al. 8-iso-prostaglandin F2alpha as a useful clinical biomarker of oxidative stress in ESRD patients. *Blood Purif.* (2002) 20:537–42. doi: 10.1159/000066962
57. Puchades MJ, Saez G, Muñoz MC, Gonzalez M, Torregrosa I, Juan I, et al. Study of oxidative stress in patients with advanced renal disease and undergoing either hemodialysis or peritoneal dialysis. *Clin Nephrol.* (2013) 80:177–86. doi: 10.5414/CN107639
58. Chen J, Wei Y, Chen X, Jiao J, Zhang Y. Polyunsaturated fatty acids ameliorate aging via redox-telomere-antioncogene axis. *Oncotarget*. (2017) 8:7301–14. doi: 10.18632/oncotarget.14236
59. Kim KM, Jung BH, Paeng K-J, Kim SW, Chung BC. Alteration of plasma total F2-isoprostanes before and after hemodialysis in end-stage renal disease patients. *Prostaglandins Leukot Essent Fat Acids.* (2004) 70:475–8. doi: 10.1016/j.plefa.2003.10.001
60. Vaziri ND. Oxidative stress in uremia: nature, mechanisms, and potential consequences. *Semin Nephrol.* (2004) 24:469–73. doi: 10.1016/j.semnephrol.2004.06.026
61. Yilmaz MI, Saglam M, Caglar K, Cakir E, Sonmez A, Ozgurtas T, et al. The determinants of endothelial dysfunction in CKD: oxidative stress and asymmetric dimethylarginine. *Am J Kidney Dis.* (2006) 47:42–50. doi: 10.1053/j.ajkd.2005.09.029
62. Martin-Mateo MC, del Canto-Jafiez E, Barrero-Martinez MJ. Oxidative stress and enzyme activity in ambulatory renal patients undergoing continuous peritoneal dialysis. *Ren Fail.* (1998) 20:117–24. doi: 10.3109/08860229809045094
63. Ertan NZ, Bozfakioglu S, Ugurel E, Sinan M, Yalcin O. Alterations of erythrocyte rheology and cellular susceptibility in end stage renal disease: effects of peritoneal dialysis. *PLoS ONE*. (2017) 12:e0171371. doi: 10.1371/journal.pone.0171371
64. Filiopoulos V, Hadjiyannakos D, Takouli L, Metaxaki P, Sideris V, Vlassopoulos D. Inflammation and oxidative stress in end-stage renal disease patients treated with hemodialysis or peritoneal dialysis. *Int J Artif Organs.* (2009) 32:872–82. doi: 10.1177/039139880903201206
65. Sies H. Oxidative stress: oxidants and antioxidants. *Exp Physiol.* (1997) 82:291–5. doi: 10.1113/expphysiol.1997.sp004024
66. Samouilidou E, Grapsa E. Effect of dialysis on plasma total antioxidant capacity and lipid peroxidation products in patients with end-stage renal failure. *Blood Purif.* (2003) 21:209–12. doi: 10.1159/000070691
67. Teixidó J. Clinical implications of peritoneal transport. *Nefrologia.* (2000) 20:53–61.
68. Ahmadpoor P, Eftekhar E, Nourooz-Zadeh J, Servat H, Makhdoomi K, Ghafari A. Glutathione, glutathione-related enzymes, and total antioxidant capacity in patients on maintenance dialysis. *Iran J Kidney Dis.* (2009) 3:22–7.

Conflict of Interest: The authors declare that the research was conducted in the absence of any commercial or financial relationships that could be construed as a potential conflict of interest.

Copyright © 2019 Gutiérrez-Prieto, Soto-Vargas, Parra-Michel, Pazarín-Villaseñor, García-Sánchez and Miranda-Díaz. This is an open-access article distributed under the terms of the Creative Commons Attribution License (CC BY). The use, distribution or reproduction in other forums is permitted, provided the original author(s) and the copyright owner(s) are credited and that the original publication in this journal is cited, in accordance with accepted academic practice. No use, distribution or reproduction is permitted which does not comply with these terms.

frontiers in Pharmacology

ORIGINAL RESEARCH
published: 15 October 2019
doi: 10.3389/fphar.2019.01197

Neferine Attenuates Acute Kidney Injury by Inhibiting NF-κB Signaling and Upregulating Klotho Expression

Huihui Li[1], Wenhang Chen[1], Yusa Chen[1], Qiaoling Zhou[1], Ping Xiao[1], Rong Tang[1] and Jing Xue[2,3]*

[1] Department of Nephrology, Xiangya Hospital, Central South University, Changsha, China, [2] Institute of Hospital Administration, Xiangya Hospital, Central South University, Changsha, China, [3] Department of Scientific Research, Xiangya Hospital, Central South University, Changsha, China

Purpose: Morbidity associated with and mortality from acute kidney injury (AKI) is gradually increasing, and no efficient drug is available. We explored whether neferine, a bisbenzylisoquinoline alkaloid, attenuated AKI, and the possible mechanisms in play *in vivo* and *in vitro*.

Methods: We induced AKI using ischemia-reperfusion (I/R) or lipopolysaccharide (LPS) *in vivo*. C57 BL/6 male mice were randomized into two groups each containing four subgroups: control, neferine, I/R or LPS, and I/R or LPS + neferine. Mice were sacrificed 24 h after AKI induction and kidneys and sera were collected. NRK-52E cells were exposed to hypoxia/reoxygenation (H/R) or LPS *in vitro*.

Results: Neferine pretreatment significantly alleviated kidney functional loss and pathological damage. In the AKI mouse models induced by I/R or LPS, neferine inhibited the infiltration of inflammatory cells, including granulocytes and macrophages. Both *in vivo* and *in vitro*, neferine attenuated apoptosis, suppressed inflammatory cytokine production, decreased degradation of IκB-α, and inhibited nuclear translocation of NF-κB. Furthermore, it also upregulated Klotho expression in AKI.

Conclusion: Neferine mitigated renal injury in AKI models, perhaps by suppressing the activation of NF-κB and upregulating the expression of Klotho.

Keywords: acute kidney injury (AKI), neferine, NF-κB, Klotho, apoptosis, inflammation

OPEN ACCESS

Edited by:
John D. Imig,
Medical College of Wisconsin, United States

Reviewed by:
Ana Belen Sanz,
Health Research Institute Foundation Jimenez Diaz (IIS-FJD), Spain
Marta Ruiz-Ortega,
Autonomous University of Madrid, Spain

***Correspondence:**
Wenhang Chen
wenhangchen@csu.edu.cn

Specialty section:
This article was submitted to Renal Pharmacology, a section of the journal Frontiers in Pharmacology

Received: *28 May 2019*
Accepted: *17 September 2019*
Published: *15 October 2019*

Citation:
Li H, Chen W, Chen Y, Zhou Q, Xiao P, Tang R and Xue J (2019) Neferine Attenuates Acute Kidney Injury by Inhibiting NF-κB Signaling and Upregulating Klotho Expression. Front. Pharmacol. 10:1197. doi: 10.3389/fphar.2019.01197

INTRODUCTION

Acute kidney injury (AKI) is a heterogeneous group of disorders manifested by increased levels of serum creatinine (Scr) and/or oliguria. AKI is becoming more prevalent worldwide, associated with high mortality and morbidity (Ali et al., 2007; Bellomo et al., 2012; Wen et al., 2013). A systematic review of data from 2004 to 2012 found that the pooled adult AKI rate was 21.6% [95% confidence interval (CI) 19.3 to 24.1%], while the pooled mortality of AKI patients was 23.9% (95% CI 22.1 to 25.7%) (Susantitaphong et al., 2013). The multinational AKI–epidemiologic prospective investigation found that AKI developed in over half of all intensive care unit patients (Hoste et al., 2015). AKI was associated with prolonged hospitalization, more resource utilization, and an unfavorable prognosis. AKI prevention and treatment are thus urgent. Generally, AKI develops after the contraction of another acute or chronic disease such as a critical illness, sepsis, circulatory shock, or complications

associated with medication (Levey and James, 2017). When the kidneys are exposed to risk factors, various cellular reactions causing tissue injury commence. Inflammation plays a key role in AKI emergence, exacerbation, and prognosis (Akcay et al., 2009; Dellepiane et al., 2016; Coelho et al., 2018); it involves the release of inflammatory mediators by endothelial and tubular cells, infiltration of inflammatory cells, and the damaging effects of toxic molecules on renal tubules. Nuclear factor kappa B (NF-κB) activation has been recorded both *in vitro* and *in vivo* models of AKI. Research increasingly suggests that NF-κB plays a pivotal role in AKI-associated inflammation and other cellular events (Guijarro and Egido, 2001; Sanz et al., 2010; Panah et al., 2018). Renal tubular epithelial cells stimulated by lipopolysaccharide (LPS) produce inflammatory mediators, free radicals, and other disruptive agents; express various proinflammatory cytokines after NF-κB activation; and, ultimately, contribute greatly to renal dysfunction. The level of Klotho, a single-pass transmembrane protein, correlates with the levels of aging suppressors (Kuro-O et al., 1997) and the extent of calcium/phosphorus metabolism (Huang and Moe, 2011). Klotho is synthesized principally by the distal renal tubules. AKI is associated with greatly reduced Klotho production, in turn aggravating kidney damage (Hu et al., 2010; Hu et al., 2012).

Neferine (**Figure 1**), a bisbenzylisoquinoline alkaloid from the seed embryo of *Nelumbo nucifera*, is widely used in traditional Chinese medicine to treat nervous exhaustion, bacillosis, helminthiasis, and cardiovascular and pulmonary diseases (Sharma et al., 2017; Marthandam Asokan et al., 2018). Neferine exhibits anti-cancer properties (Qin et al., 2011; Deng et al., 2017), relaxes smooth muscles; inhibits platelet aggregation and arrhythmia; retards the development of atherosclerosis (Zheng et al., 2014), diabetes, and Alzheimer's disease; and reduces scarring and cisplatin nephrotoxicity (Li et al., 2017), and the like. Neferine attenuates the inflammatory response and fibrosis by inhibiting cytokine production and NF-κB activation both *in vivo* and *in vitro* (Zhao et al., 2010; Baskaran et al., 2016; Baskaran et al., 2017; Priya et al., 2017; Guolan et al., 2018). Thus, we speculated that neferine might protect the kidney from acute injury. We established two AKI models to explore this topic.

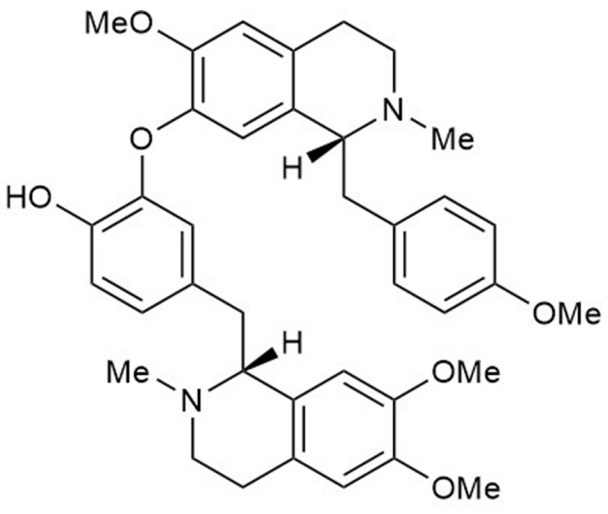

FIGURE 1 | The chemical structure of neferine ($C_{38}H_{44}N_2O_6$).

MATERIALS AND METHODS

Animals

C57BL/6 male mice with 10 weeks of age (20–25 g in weight) were purchased from the Department of Laboratory Animals of Central South University and were individually housed at a standard temperature (22 ± 2°C) and humidity (50–60%) under a 12-h/12-h photoperiod. The study was approved by the Institutional Animal Care and Use Committee of Central South University. All animal experimental procedures met the criteria of the National Institutes of Health (NIH) Guide for the Care and Use of Laboratory Animals.

AKI was induced by ischemia-reperfusion (I/R) or LPS injection as described previously (Savransky et al., 2006; Cao et al., 2008). The mice were randomized into two major groups and each group then divided into four subgroups (n = 6 mice per subgroup): (1) control, (2) neferine (Purechem-Standard Co. Ltd., Chengdu, China), (3) I/R or LPS, and (4) I/R or LPS + neferine. The I/R model was established by clipping both kidney pedicles (using microarterial clamps; model FST 18055-04: Fine Science Tools Inc., Foster City, CA, USA) for 30 min. LPS-induced AKI was generated *via* intraperitoneal injection of 10 mg/kg LPS. Neferine was administrated *via* intraperitoneal injection for 3 days prior to model establishment (20 mg/kg/d) (Huang et al., 2007); mice were sacrificed 24 h later. Normal saline was used instead of neferine in control and model groups. Anesthesia was induced by an intraperitoneal injection of pentobarbital (0.7 mg/kg) prior to surgery. Kidneys and sera were stored at −80°C prior to analysis.

Histology

Kidneys were fixed in 4% (v/v) paraformaldehyde for 48 h at room temperature. Paraffin-embedded sections (4 μm thick) were stained with hematoxylin and eosin and periodic acid–Schiff. The extent of tubular injury was scored as the percentage of damaged tubules in the outer medulla (Savransky et al., 2006). All scoring was performed by a renal pathologist (blinded to mouse subgroup) under the high-power field of a light microscope. Ten random non-overlapping fields were examined for each sample.

Serum Biochemistry and Enzyme-Linked Immunosorbent Assay (ELISA)

Scr and blood urine nitrogen (BUN) levels were measured using a Hitachi model 7180 automatic analyzer (Hitachi Ltd., Tokyo, Japan). Serum levels of neutrophil gelatinase-associated lipocalin (NGAL) were measured with the aid of an ELISA kit following the manufacturer's instructions (Abcam, Cambridge, UK).

Immunohistochemical Staining

Kidney sections were sequentially deparaffinized, rehydrated, and subjected to antigen retrieval and inactivation of endogenous

enzyme activity. After blocking in 5% (w/v) bovine serum album (BSA) for 30 min, tissues were incubated with a primary antibody targeting Ly6G (Servicebio, Wuhan, China; 1:200), and F4/80 (Servicebio; 1:200) and Klotho (Abcam; 1:200) at 4°C overnight. Biotinylated secondary antibodies (ZsBio, Beijing, China) were then added; the samples were incubated at room temperature for 30 min and analyzed using a biotin-streptavidin horseradish peroxidase (HRP) detection system.

Cell Culture

NRK-52E cells (American Type Culture Collection, Rockville, MD, USA) were cultured in high-glucose Dulbecco's modified Eagle's medium (DMEM) containing 10% fetal bovine serum (FBS) at 37°C in a humidified incubator with an atmosphere containing 5% CO2. Two cell-based models of AKI were established—hypoxia/reoxygenation (H/R)– and LPS (5 μg/ml, Sigma)-mediated cell injuries. Cells were pretreated with the indicated concentrations of neferine for 2 h, followed by H/R or administration of LPS. For H/R, the cells were cultured in glucose- and FBS-free DMEM containing antimycin A (100 nM, Abcam) for 2 h to imitate hypoxia. The cells were subsequently cultured in normal medium until being harvested.

Cell Counting Kit-8 Assay

A Cell Counting Kit-8 (CCK8) (Selleck, Shanghai, China) was used to assay cell proliferation. NRK-52E cells were seeded in 96-well plates at a density of 4×10^3/well and incubated overnight. When the cells reached 50% confluence, neferine was added at the indicated concentrations (1, 2, 4, 8, 10, 20, 40, 100μM), and the cells were incubated for 24 h. Next, 10 ml of CCK-8 reagent was added to each well, and the plate was incubated at 37°C for 2 h. Finally, the absorbance at 450 nm was measured. Each experiment was conducted independently three times.

Flow Cytometry

An Annexin V-Fluorescein Isothiocyanate (FITC)/Propidium Iodide (PI) Apoptosis Detection Kit (BD Pharmingen, CA, USA) was used to assay the rate of apoptosis of cultured cells. Cells were collected by trypsinization 12 h after H/R. After washing twice with cold PBS, the cells were resuspended in 300 ml of 1× binding buffer and stained with 5 ml of Annexin V-FITC plus 5 ml of PI for 15 min in the dark. Fluorescence signals were detected using a FACScan Flow Cytometer (BD Biosciences, CA, USA). Each experiment was conducted independently three times.

Quantitative Reverse Transcription-PCR

Total RNAs were isolated from kidney tissue NRK-52E cells exposed to the TransZol Up reagent (TransGen Biotech, Beijing, China) and reverse-transcribed into complementary DNA using the EasyScript One-Step gDNA Removal and cDNA Synthesis SuperMix system (TransGen Biotech). Quantitative PCR employed Hiff qPCR SYBR Green Master Mix (Low ROX Plus) (Yeasen, Shanghai, China) and the following primers: M-Klotho, forward 5′-TTTGCCCTATTTCACCGAAG-3,′ reverse 5′-CCTGACT GGGAGAGTTGAGC-3′; M-tumor necrosis factor-α (TNF-α), forward 5′-TATGGCTCAGGGTCCAACTC-3,′ reverse 5′-CTCCC TTTGCAGAACTCAGG-3′; M-interleukin-6 (IL-6), forward 5′-AGTTGCCTTCTTGGGACTGA-3,′ reverse 5′-TCCACGATTT CCCAGAGAAC-3′; M-cyclooxygenase 2 (COX2), forward 5′-TGCAGAATTGAAAGCCCTCT-3,′ reverse 5′-GCTCGGCT TCCAGTATTGAG-3′; and M-β-actin, forward 5′-CGTTGAC ATCCGTAAAGACC-3,′ reverse 5′-AACAGTCCGCCTAGAA GCAC-3′; R-Klotho, forward 5′-AGCTGCTTGTGTTGTGA TGC-3,′ reverse 5′-TACGGGGGTGCTGTAGAAAC-3′; R-TNF-α, forward 5′-AACTCCCAGAAAAGCAAGCA-3,′ reverse 5′-CGAG CAGGAATGAGAAGAGG-3′; and R-β-actin, forward 5′-CACCC GCGAGTACAACCTTC-3,′ reverse 5′-CCCATACCCACCAT CACACC-3.′

Western Blotting

Total protein was extracted from mouse kidneys and cultured cells using RIPA Lysis Buffer (Beyotime Biotechnology, Nanjing, China). Nucleoproteins were extracted using a commercial kit (Beyotime Biotechnology). Samples (20–40 μg of protein/lane) were separated on 12% (w/v) sodium dodecyl sulfate-polyacrylamide gels; the proteins were electrotransferred to 0.22-μm pore-sized polyvinylidene fluoride membranes (Millipore Sigma, Burlington, MA, USA) and immunoblotted with primary antibodies against Klotho (Abcam; 1:1,000; Santa Cruz Biotechnology, Dallas, TX, USA; 1:200), NF-κB p65 (Cusabio, Wuhan, China; 1:1,000), IκB-α (Abcam; 1:5,000), phosphorylated-IκB-α (Abcam; 1:1,000), COX2 (Proteintech, Rosemont, IL, USA; 1:300), caspase-3 (Proteintech; 1:1,000), Bax (Proteintech; 1:2,000), Bcl2 (Cell Signaling Technology, Danvers, MA, USA; 1:1,000), histone 3 (Cell Signaling Technology; 1:1,000), and β-actin (Servicebio; 1:2,000). They were then incubated with HRP-conjugated secondary antibodies (Proteintech; 1:10,000). The Western blots were developed using a ChemiDoc MP Imaging System (Bio-Rad, Hercules, CA, USA); band intensities were quantified with the aid of Quantity One ver. 4.6.7 software (Bio-Rad).

Immunofluorescence Staining

Cultured cells were incubated with anti-NF-κB p65 (Cusabio, 1:200) antibodies at 4°C overnight, then with CY3-labeled secondary antibodies (Servicebio; 1:500) for 1 h at room temperature and counterstained with 4′,6-diamidino-2-phenylindole (DAPI; Servicebio) for 10 min. Images were taken under a fluorescence microscope (Olympus Corp., Tokyo, Japan).

Terminal Deoxynucleotidyl Transferase-Mediated Nick-End Labeling (TUNEL) Assay

We used the TUNEL assay to detect apoptotic cells in kidney sections; we employed an *in situ* Cell Death Detection Kit (Roche, Basel, Switzerland) following the manufacturer's instructions. After deparaffinization and rehydration, kidney tissues were incubated with proteinase K (20 μg/ml) for 20 min at room temperature and with the TUNEL reaction mixture for 1 h at 37°C, stained with DAPI, and observed under a fluorescence microscope.

Cytometric Bead Array (CBA)

A CBA Mouse Th1/Th2/Th17 Cytokine Kit (Becton Dickinson, Franklin Lakes, NJ, USA) was used to measure serum TNF-α and IL-6 levels. Standards were reconstituted in 2.0-ml amounts of assay diluent and serially diluted to 1:2, 1:4, 1:8, 1:16, 1:32, 1:64, 1:128, and 1:256; mixed capture beads (10 μl volumes) were added to all tubes, followed by 50-μl amounts of standard dilutions and sera, and then 50-μl amounts of the Th1/Th2/Th17 PE detection reagent. The tubes were incubated for 2 h at room temperature; next, 300 μl of wash buffer was added to each tube to resuspend the beads, and the beads were subjected to flow cytometry. Data were analyzed with the aid of FCAP Array Software.

Statistical Analysis

All data are expressed as means ± standard deviations (SDs). Student's *t*-test was used to compare pairs of groups; a one-way ANOVA followed by Tukey's test was employed to compare multiple groups. We used SPSS ver. 19 software (IBM Corp., Armonk, NY, USA). A P-value <0.05 was taken to indicate statistical significance.

RESULTS

Neferine Attenuated AKI Induced by I/R and LPS

In mice with AKI induced by I/R, the renal tubular epithelium was severely injured; the brush border was lost, and necrosis, cast deposition, and renal tubule dilatation were evident (**Figure 2A**). In the LPS-induced AKI model, tubular cell damage included vacuolization, brush border loss, cast deposition, and necrosis (**Figure 2D**). These pathological changes were most obvious in the external medulla. We calculated tubular injury scores (**Figures 2B**, **E**). No mesangial proliferation and fibrosis were observed in mouse AKI models. Renal insufficiency (reflected by increases in serum SCr, BUN, and NGAL levels) was evident in both AKI models (**Figures 2C, F**). Neferine pretreatment effectively mitigated kidney injury and renal insufficiency in both AKI models.

Neferine Suppressed Apoptosis in Mouse AKI Models

Above, we showed that neferine afforded renal protection; we thus explored whether the drug affected apoptosis. Apoptosis was in play in both AKI mouse models as revealed by the TUNEL assay which detects DNA fragmentation (**Figures 3A** and **4A**). We further verified the apoptotic phenotype by showing that Bcl2 expression was decreased, while the Bax and activated caspase-3 levels were increased in model groups, compared to the control values (**Figures 3B** and **4B**). Neferine pretreatment significantly reduced DNA breakage and the changes in the expression levels of Bcl2, Bax, and cleaved caspase-3 induced by I/R and LPS (**Figures 3** and **4**).

Neferine Attenuated the Expression of Inflammatory Cytokines in Mouse AKI Models

Inflammation can be triggered by various stimuli, including I/R and LPS. Inflammatory factors play important roles in AKI emergence and development. The levels of mRNAs encoding TNF-α, IL-6, and COX2 in the kidney increased significantly 24 h after I/R or LPS injection (**Figures 5C**, **D**), as did the serum levels of TNF-α and IL-6 (**Figures 5E**, **F**) and the kidney COX2 level (as revealed by

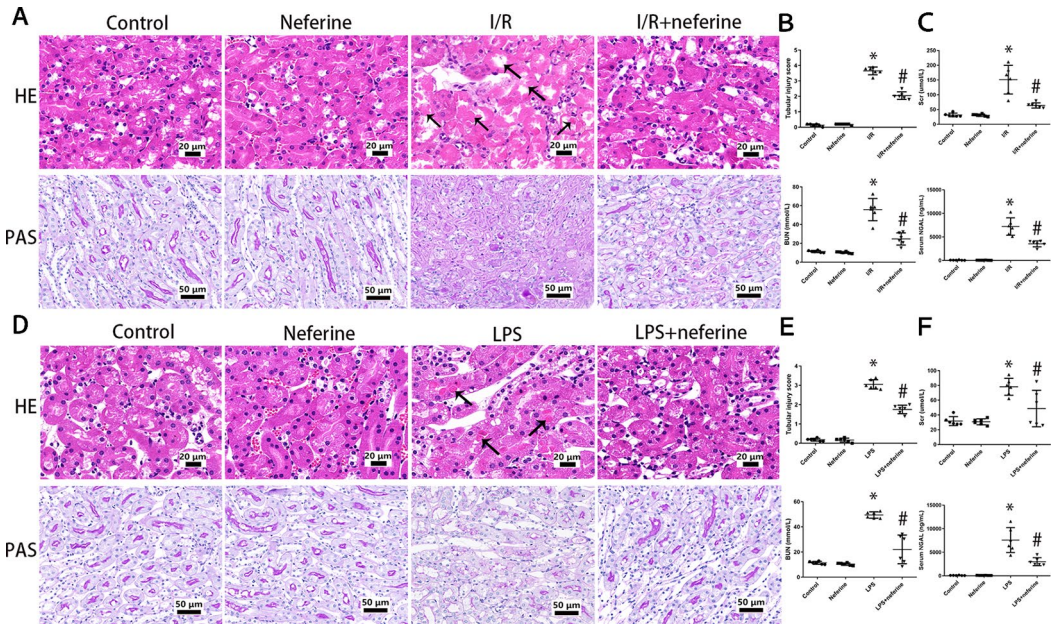

FIGURE 2 | Neferine attenuated AKI induced by I/R and LPS *in vivo*. **(A**, **D)** Representative photomicrographs of kidney sections stained by hematoxylin–eosin and periodic acid–Schiff. Black arrows indicated tubular injury, comprising cast deposition, brush border loss, necrosis, tubular dilatation, and vacuolization. **(B**, **E)** The tubular injury scores of **(A** and **D)**. Data was presented as the percentage of damaged renal tubules over the total visible tubules in the outer medulla. **(C**, **F)** Serum levels of Scr, BUN, and NGAL in four subgroups. Data are represented as means ± SD (n = 6). *P < 0.05 *vs*. control, #P < 0.05 *vs*. I/R or LPS.

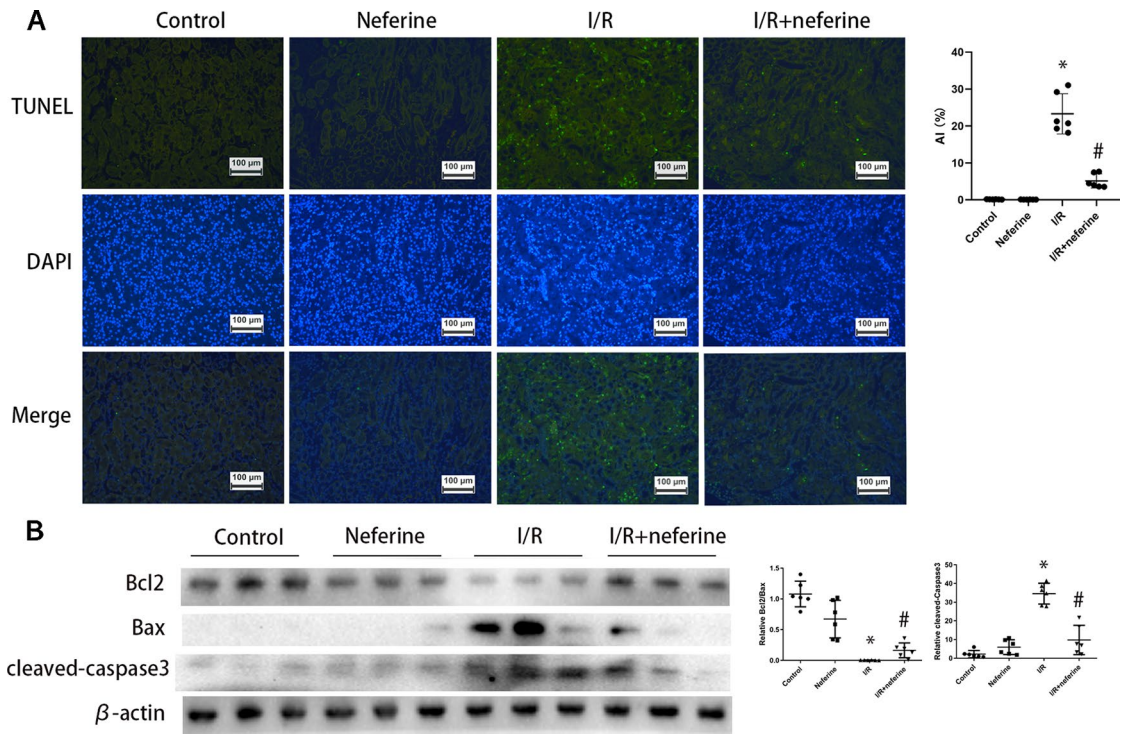

FIGURE 3 | Neferine suppressed apoptosis in I/R-AKI. **(A)** Apoptosis induced by I/R in kidney cells was detected by TUNEL assays. Apoptosis index was calculated according to TUNEL results. **(B)** Renal protein levels of Bcl2, Bax, and cleaved caspase-3 assayed by Western blotting (three randomly samples selected from each subgroup were shown). The corresponding quantifications were shown as well. Data are represented as means ± SD (n = 6). *P < 0.05 *vs*. control, #P < 0.05 *vs*. I/R.

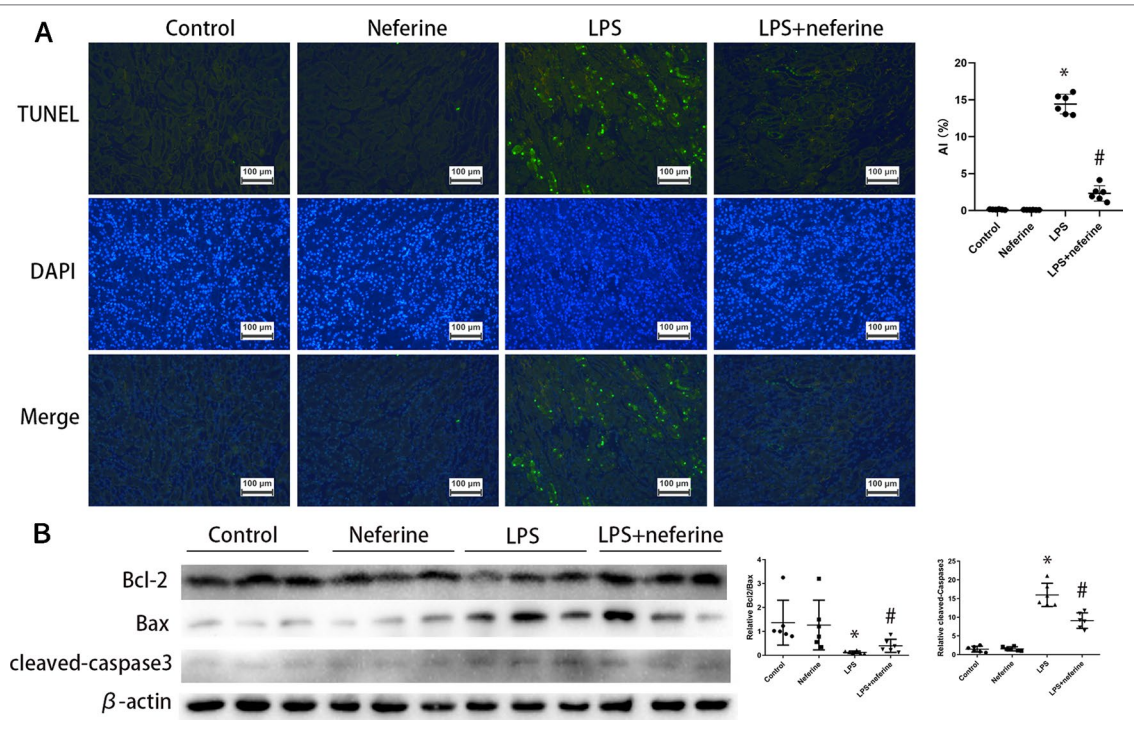

FIGURE 4 | Neferine suppressed apoptosis in LPS-AKI. **(A)** Apoptosis induced by LPS in kidney cells was detected by TUNEL assays. Apoptosis index was calculated according to TUNEL results. **(B)** Renal protein levels of Bcl2, Bax, and cleaved caspase-3 assayed by Western blotting (three randomly samples selected from each subgroup were shown). The corresponding quantifications were shown as well. Data are represented as means ± SD (n = 6). *P < 0.05 *vs*. control, #P < 0.05 *vs*. LPS.

immunoblotting; **Figures 5A**, **B**). Neferine pretreatment effectively mitigated the abnormal expression of inflammatory mediators.

Neferine Inhibited the Infiltration of Inflammatory Cells in Models of AKI

The various leukocyte subgroups contribute to AKI in different ways. Upon the development of AKI, granulocytes and macrophages successively accumulate in kidney tissue (Bonventre and Zuk, 2004; Joannes-Boyau et al., 2010). We performed immunohistochemical staining for Ly6G and F4/80 as markers of granulocytes and macrophages, respectively. As shown in **Figures 6A–D**, granulocyte and macrophage infiltrations were negligible in the control and neferine subgroups. However, the expressions of Ly6G and F4/80 in both cortex and outer medulla were increased by I/R or administration of LPS. Neferine reduced the number of Ly6G- and F4/80-positive cells, suggesting inhibition of inflammatory cells infiltration.

Neferine Inhibited the Nuclear Translocation of NF-κB in Both AKI Mouse Models

NF-κB activation is triggered by both I/R and LPS. NF-κB is activated principally *via* nuclear translocation. To explore whether neferine modulated NF-κB activity, we used Western blotting to measure the levels of NF-κB p65 in the nucleus and cytoplasm. The immunoblotting of p65 in nucleus and cytoplasm (**Figures 7A**, **B**) confirmed that neferine inhibited the nuclear translocation of NF-κB. Neferine reduced IκB-α phosphorylation and degradation after I/R or LPS injection (**Figures 5A**, **B**), which further revealed that neferine inhibited the activation of NF-κB pathway.

Effect of Neferine on the Expression Levels of Klotho in AKI Models

We confirmed that both I/R (Panah et al., 2018) and LPS (Bi et al., 2018) downregulated Klotho expression. As mentioned above, Klotho levels decreased 3 h after I/R and attained a nadir 24 h after reperfusion (Hu et al., 2010). We thus performed assays at this time. The levels of Klotho-encoding mRNA and the protein *per se* were high in normal kidney tissues; both I/R (**Figures 8A–C**) and LPS (**Figures 8D–F**) triggered Klotho deficiencies. Neferine pretreatment attenuated such changes in both AKI models.

Effect of Neferine on Apoptosis of NRK-52E Cells Exposed to H/R and LPS

The above results suggest that neferine protects against AKI in mouse models in a manner involving tubular cells. Next, we investigated the mechanism of protection *in vitro* using NRK-52E cells. To determine the optimum concentration of neferine, a CCK8 assay of cell viability was performed using 1, 2, 4, 8, 10, 20, 40, and 100 μM neferine (**Figure 9A**), then neferine treatment with 2, 4, and 8 μM was employed in the following experiments. The morphological characteristics and the rate of apoptosis determined by flow cytometry (**Figures 9B**, **C**) suggested that neferine rescued the cell death induced by H/R. Moreover, Western blotting for Bcl2, Bax, and cleaved-caspase3 (**Figure 9D**) confirmed that neferine suppressed apoptosis. Although only a few apoptotic cells was observed after 24 h of LPS administration, the expression of Bcl2 and Bax protein levels revealed the protective effect of neferine in LPS-induced tubular cell injury (**Figure 9E**).

Neferine Inhibits the Production of Inflammatory Cytokines and the Activation of NF-κB Pathway Induced by H/R and LPS in NRK-52E Cells

Neferine dose-dependently inhibited the expression of TNF-α induced by H/R and LPS (**Figures 10B** and **11B**). Neferine inhibits the NF-κB signaling pathway *in vivo*; therefore, we next investigated the underlying mechanisms *in vitro*. Immunofluorescence staining (**Figures 10A** and **11A**) and Western blotting (**Figures 10C** and **11C**) showed the protein levels of p65 in the nucleus and cytoplasm, suggesting that neferine suppressed the nuclear translocation of NF-κB in a dose-dependent manner. Also, neferine reduced the phosphorylation and degradation of IκB-α induced by H/R and LPS (**Figures 10D** and **11D**), consistent with the *in vivo* findings.

Effect of Neferine on Klotho Expression in NRK-52E Cells

The gene that encodes Klotho is expressed mainly in distal renal tubules, while Klotho protein is present in proximal renal tubules. We investigated the expression of the Klotho-encoding gene using NRK-52E cells (Hsu et al., 2014a). The expression level of Klotho in NRK-52E cells was reduced by exposure to H/R and LPS. Administration of neferine significantly increased the Klotho mRNA and protein levels in a dose-dependent manner (**Figures 12A–D**).

DISCUSSION

A multicenter, retrospective Chinese cohort study (Xu et al., 2015) found that the overall incidence of AKI was 11.6% and in-hospital mortality 8.8%. AKI is thus a major problem; no effective drug is available, and such a drug is urgently required. We showed that neferine, a bisbenzylisoquinoline alkaloid, effectively alleviated AKI by inhibiting apoptosis, inflammation, and nuclear translocation of NF-κB while preserving Klotho expression.

AKI caused by I/R and sepsis develops secondarily to several clinical conditions. We explored this topic using I/R and LPS AKI models, which were reliable and reproducible. AKI is characterized by kidney apoptosis and inflammation; a drug ameliorating these symptoms would be very useful. Neferine was renoprotective in AKI mouse models, as evidenced both pathologically and biochemically. Neferine accumulates to high levels in the kidneys, perhaps explaining the beneficial effects afforded by the drug (Huang et al., 2007). Neferine highly penetrates tissues by passive diffusion due to its highly lipophilicity. The drug then plays various pharmacological roles. This is the first report to discover the potential therapeutic value of neferine for AKI.

In I/R-AKI, proximal tubule epithelial cells are extremely susceptible to apoptosis, and loss of tubular cells causes increased backleak and reduced glomerular filtration rate (GFR) (Havasi and Borkan, 2011). Although the pathogenesis of septic AKI is multifactorial, renal cell apoptosis is definitely involved

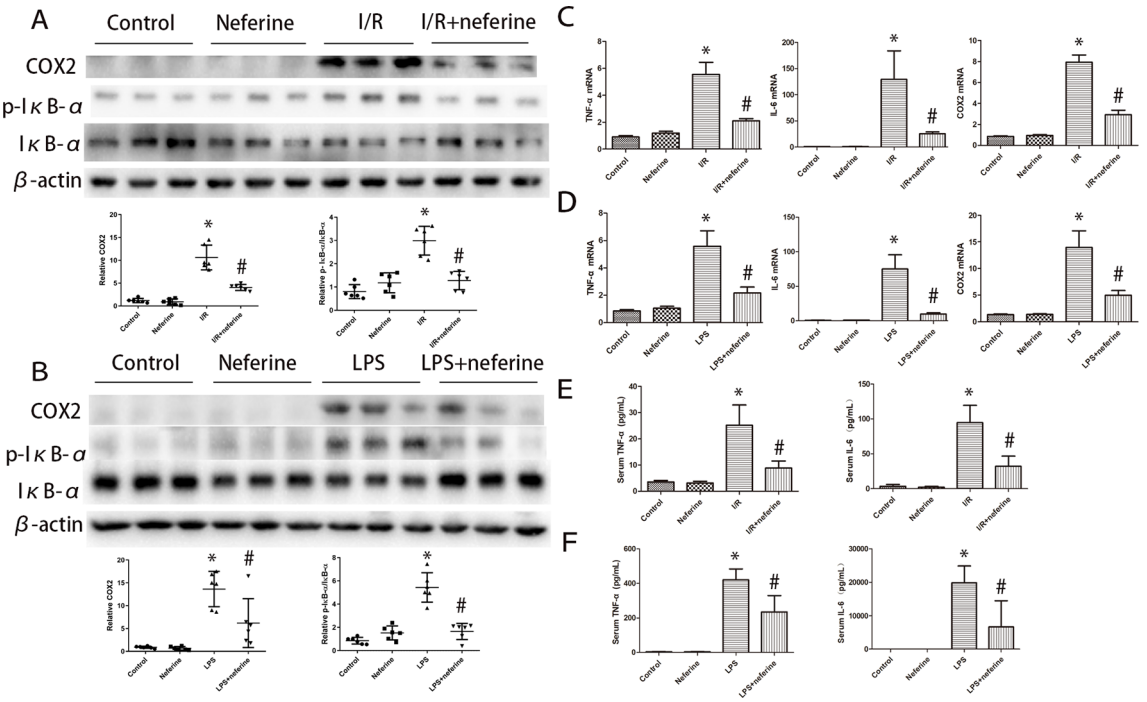

FIGURE 5 | Neferine inhibited the phosphorylation of IκB-α and the expression of inflammation cytokines in AKI models. **(A, B)** Renal protein levels of COX2, p-IκB-α, and IκB-α assayed by Western blotting (three randomly samples selected from each subgroup were shown). The corresponding quantifications were shown as well. **(C, D)** Renal mRNA levels of TNFα, IL-6, and COX2 were assayed by qRT-PCR and quantified as fold changes. **(E, F)** Serum levels of TNFα and IL-6 in different subgroups. Data are represented as means ± SD (n = 6). *P < 0.05 *vs*. control, #P < 0.05 *vs*. I/R or LPS.

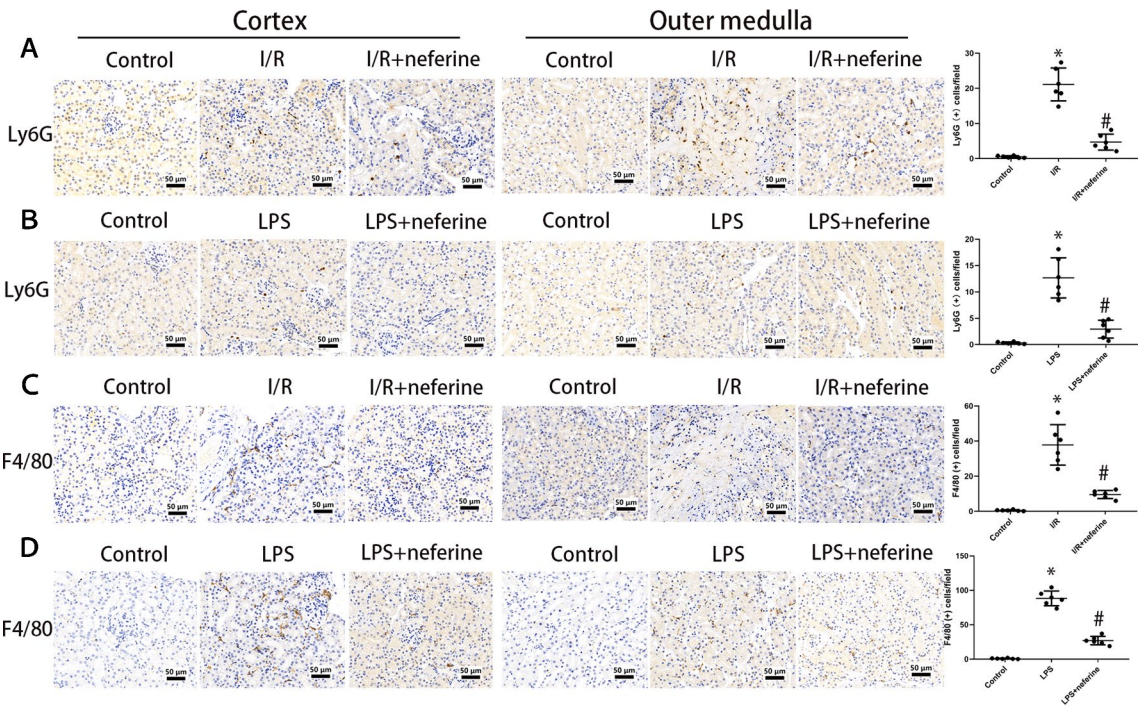

FIGURE 6 | Neferine inhibited the infiltration of inflammatory cells in AKI models. The figures in cortex and outer medulla were listed respectively. **(A, B)** Photomicrographs of Ly6G-stained kidney sections and the corresponding quantifications. **(C, D)** Photomicrographs of F4/80-stained kidney sections and the corresponding quantifications. Data are represented as means ± SD (n = 6). *P < 0.05 *vs*. control, #P < 0.05 *vs*. I/R or LPS.

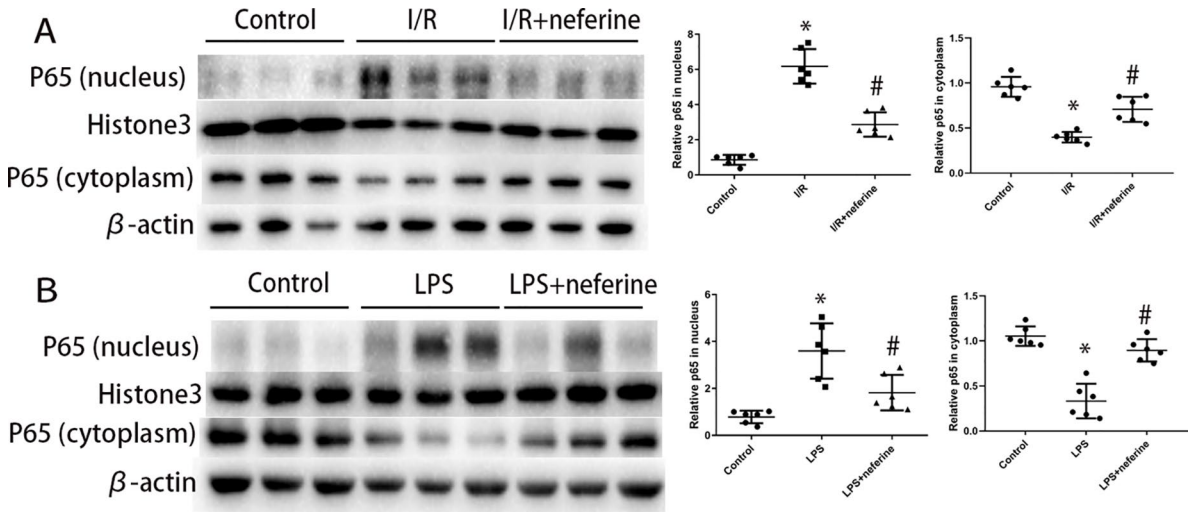

FIGURE 7 | Neferine inhibited the nuclear translocation of NF-κB in AKI models. **(A, B)** P65 levels in nuclear extract and cytoplasm assayed by Western blotting (three randomly samples selected from each subgroup were shown). The corresponding quantifications were shown. Data are represented as means ± SD (n = 6). *P < 0.05 *vs*. control, #P < 0.05 *vs*. I/R or LPS.

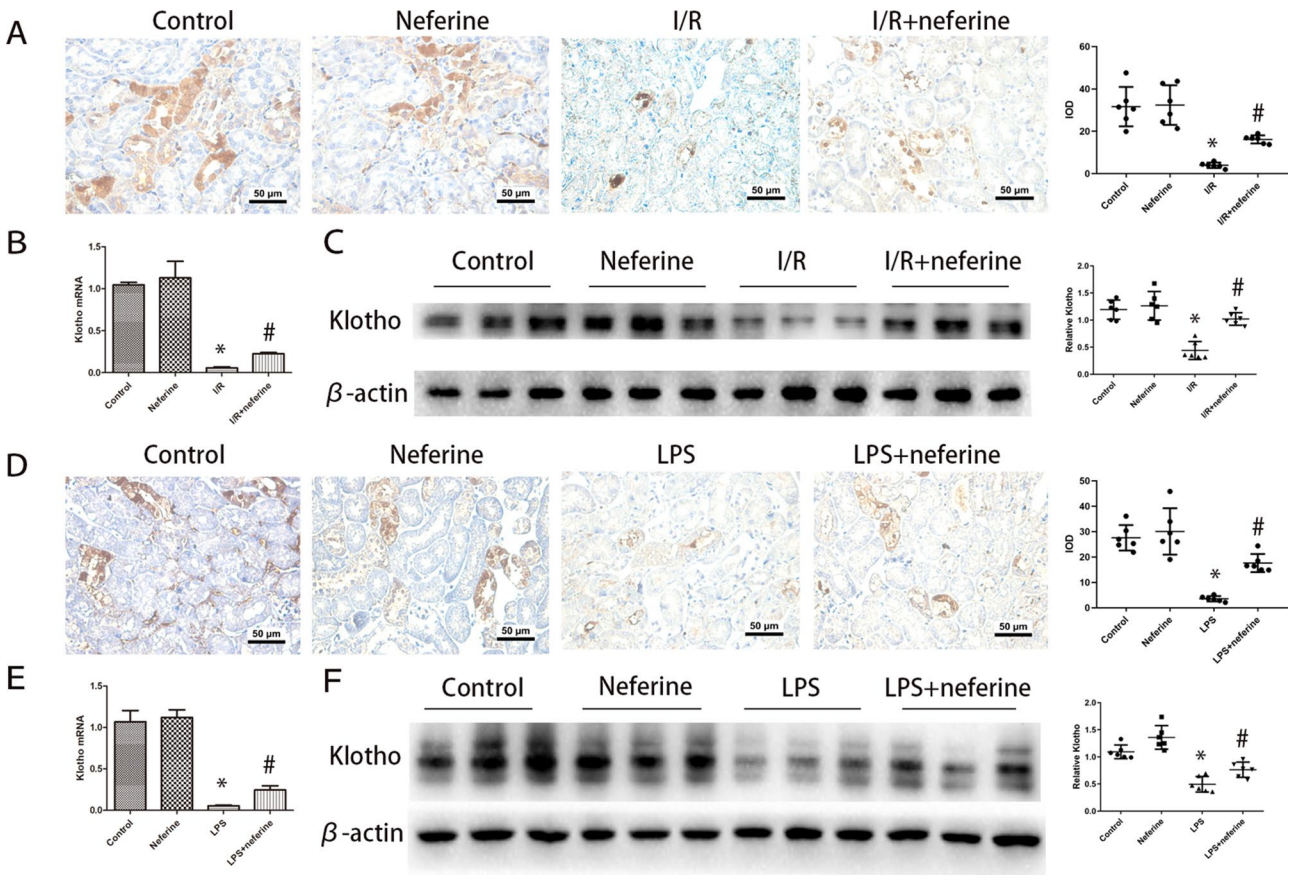

FIGURE 8 | Effect of neferine on the expression levels of Klotho in AKI models. **(A, D)** Representative expression levels of Klotho by immunohistochemistry in different groups and the corresponding quantifications. **(B, E)** Renal mRNA levels of Klotho was assayed by qRT-PCR and quantified as fold changes. **(C, F)** Renal protein levels of Klotho assayed by Western blotting (three randomly samples selected from each subgroup were shown). The corresponding quantifications were shown as well. Data are represented as means ± SD (n = 6). *P < 0.05 *vs*. control, #P < 0.05 *vs*. I/R or LPS.

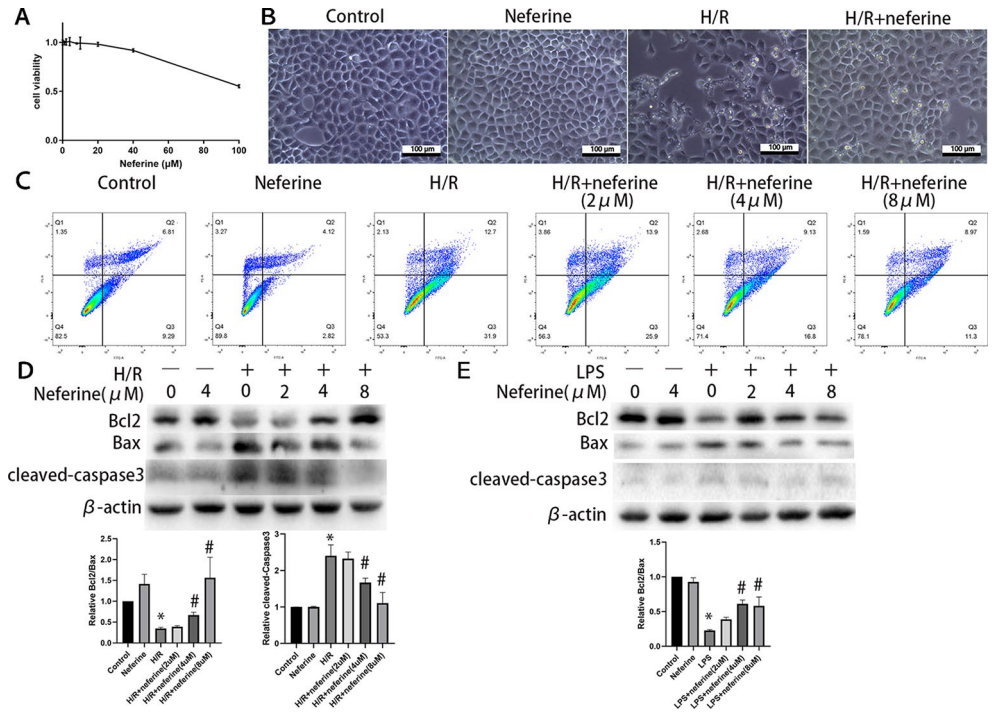

FIGURE 9 | Neferine suppressed apoptosis in NRK-52E cells exposed to H/R or LPS. **(A)** Cell viability was measured by CCK8 in NRK-52E cells after 24 h of treatment with neferine. **(B)** The microscope image of NRK-52E cells. Cells were treated with H/R in the absence or presence of neferine (8 μM) for 12 h. **(C)** Cell apoptosis was detected by flow cytometry. NRK-52E cells were treated with H/R in the absence or presence of neferine (2, 4, 8 μM) for 12 h. **(D, E)** Western blotting of Bcl2, Bax, and cleaved caspase3. NRK-52E cells were treated with H/R or LPS in the absence or presence of neferine (2, 4, 8 μM) for 12 h. Each experiment was conducted independently three times. *P < 0.05 *vs*. control, #P < 0.05 *vs*. H/R or LPS.

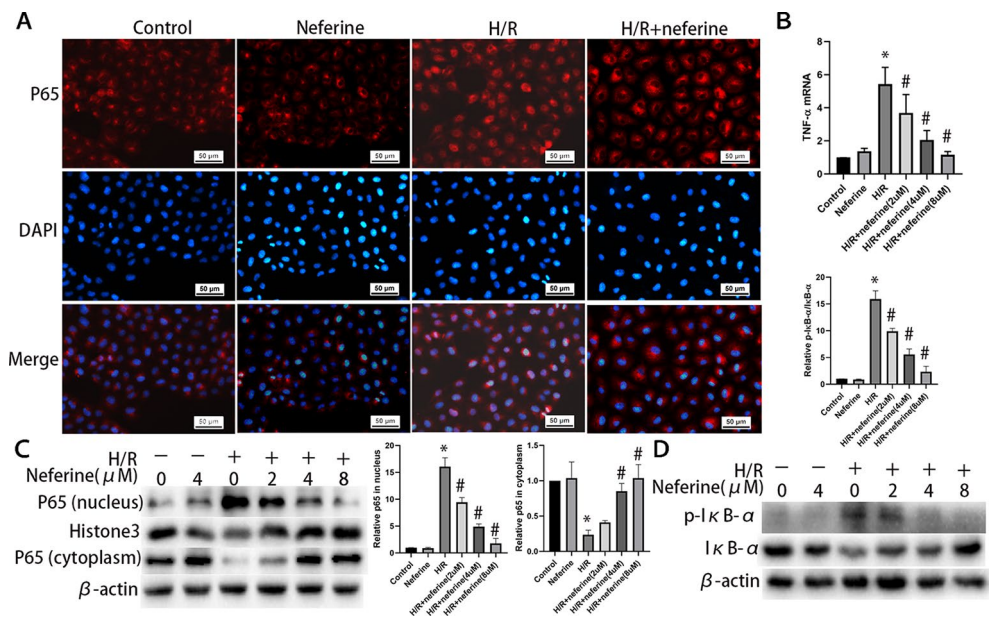

FIGURE 10 | Neferine inhibited NF-κB signaling pathway and the production of inflammatory cytokine induced by H/R in NRK-52E cells. **(A)** Immunofluorescent staining of p65. NRK-52E cells were treated with H/R in the absence or presence of neferine (8 μM) for 12 h. The cells were stained with anti-p65 antibody (top panel) and counter-stained with DAPI (middle panel), and figures were merged (lower panel). **(B)** The TNF-α mRNA levels of NRK-52E cells assayed by qRT-PCR and quantified as fold changes. Cells were treated with H/R in the absence or presence of neferine (2, 4, 8 μM) for 12 h. **(C)** Western blotting of p65 in nucleus and cytoplasm. The corresponding quantifications were presented as well. **(D)** Western blotting of p-IκB-α and IκB-α in NRK-52E cells. Each experiment was conducted independently three times. *P < 0.05 *vs*. control, #P < 0.05 *vs*. H/R.

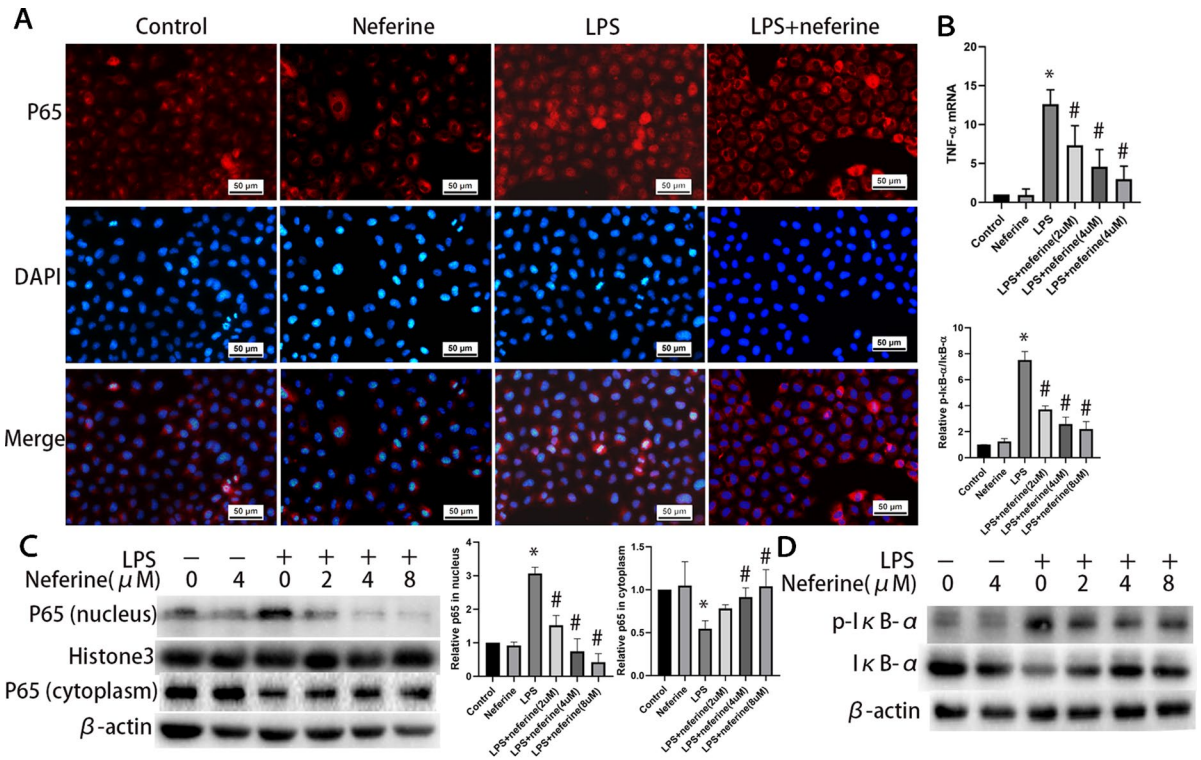

FIGURE 11 | Neferine inhibited NF-κB signaling pathway and the production of inflammatory cytokine induced by LPS in NRK-52E cells. **(A)** Immunofluorescent staining of p65. NRK-52E cells were treated with LPS in the absence or presence of neferine (8 μM) for 12 h. The cells were stained with anti-p65 antibody (top panel) and counter-stained with DAPI (middle panel), and figures were merged (lower panel). **(B)** The TNF-α mRNA levels of NRK-52E cells assayed by qRT-PCR and quantified as fold changes. Cells were treated with LPS in the absence or presence of neferine (2, 4, 8 μM) for 12 h. **(C)** Western blotting of p65 in nucleus and cytoplasm. The corresponding quantifications were presented as well. **(D)** Western blotting of p-IκB-α and IκB-α in NRK-52E cells. Each experiment was conducted independently three times. *P < 0.05 *vs*. control, #P < 0.05 *vs*. LPS.

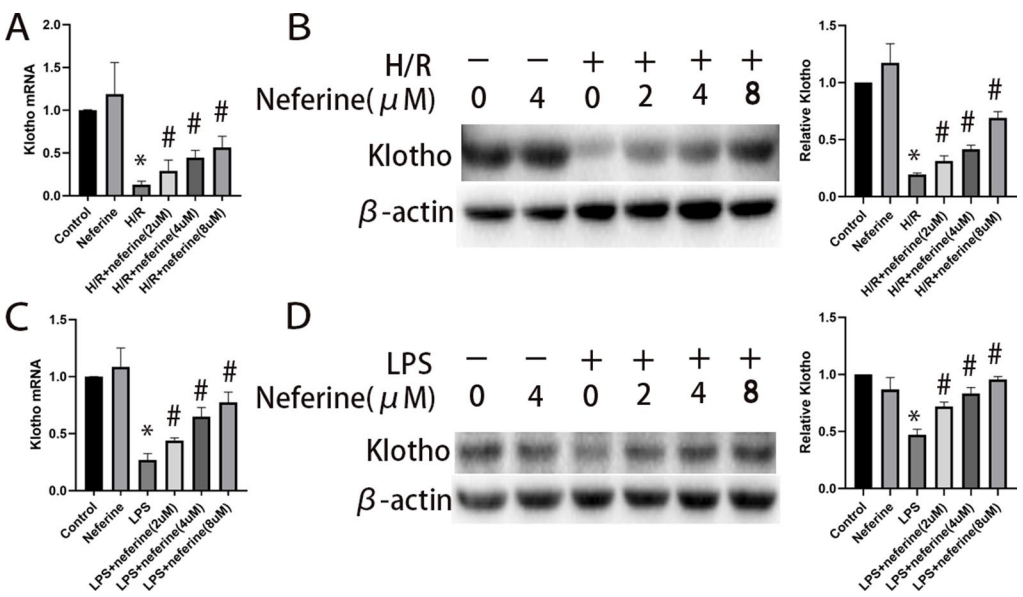

FIGURE 12 | Effect of neferine on the expression levels of Klotho in NRK-52E cells exposed to H/R or LPS. Cells were treated with H/R or LPS in the absence or presence of neferine (2, 4, 8 μM) for 12 h. **(A, C)** The Klotho mRNA levels of NRK-52E cells assayed by qRT-PCR and quantified as fold changes. **(B, D)** Protein levels of Klotho assayed by Western blotting and the corresponding quantifications. Each experiment was conducted independently three times. *P < 0.05 *vs*. control, #P < 0.05 *vs*. H/R or LPS.

(Joannes-Boyau et al., 2010). In our study, neferine decreased the ratio of Bax/Bcl2 *in vivo* and *in vitro* and dramatically attenuated the apoptosis of tubular cells in AKI, which suggested that anti-apoptosis may be one of the mechanisms of kidney protection from neferine. Pyroptosis is a new cell death pathway drawing substantial attention in recent years (Yang et al., 2014). It was reported that neferine inhibited LPS-ATP-induced endothelial cell pyroptosis (Tang et al., 2019), indicating the effect of prohibiting pyroptosis of neferine. Therefore, further studies focused on pyroptosis should be evaluated to explore the functional mechanism of neferine in AKI.

The NF-κB family of transcription factors integrates extracellular stimuli with intracellular signal transduction pathways, transcriptionally regulating genes involved in inflammation, immunity, and apoptosis. NF-κB is a potential target of anti-inflammatory therapy. Various etiologies of AKI, including I/R and LPS, can trigger the activation of NF-κB through distinct pathway in tubular cells (Sanz et al., 2010; Panah et al., 2018). The classic activation pathway features three consecutive steps: phosphorylation/ubiquitination, proteolytic degradation of IκB, and NF-κB nuclear translocation. As most NF-κB target genes are regulated by RelA (p65)/p50 (Sanz et al., 2010), we measured p65 levels when exploring the effects of NF-κB. We found that neferine clearly inhibited NF-κB nuclear translocation, indicating that suppression of NF-κB activation may explain the renoprotective action of the drug. Neferine reduced IκB-α phosphorylation and degradation, suggesting that the drug affected the classical NF-κB activation pathway. The results were consistent with the conclusions in osteoclast differentiation (Chen et al., 2019). Moreover, unlike other types of cells, neferine also suppressed NF-κB pathway by inhibiting the p65 expression in renal cancer cells (Kim et al., 2019).

TNF-α, IL-6, and COX2, all of which are involved in the AKI inflammatory response (Lemay et al., 2000; Grigoryev et al., 2008; Feitoza et al., 2010; Wang et al., 2016), are downstream regulators of NF-κB (Baskaran et al., 2016). Expression of the genes encoding these proinflammatory proteins is upregulated after NF-κB enters the nucleus and therein binds to the corresponding promoters. We found that the serum levels of TNF-α, IL-6, and COX-2 expressions in the kidney increased substantially in both AKI models. Neferine pretreatment inhibited cytokine upregulation in AKI, accompanied by the inhibition of NF-κB activation. We thus suggest that neferine relieves AKI inflammation by preventing NF-κB nuclear translocation.

The Klotho protein comes in two different forms: transmembrane and soluble Klotho (sKL). Transmembrane Klotho serves as a co-receptor for fibroblast growth factor-23 (FGF23) and thus regulates both calcium and phosphorus metabolism. sKL, the extracellular domain of the transmembrane form of Klotho, protects the kidney by exerting anti-oxidative (Mitobe et al., 2005), anti-apoptosis (Hu et al., 2012), anti-inflammation (Oh et al., 2015; Bi et al., 2018), anti-fibrotic effects (Sugiura et al., 2012). Klotho expression was reduced after the induction of AKI by I/R, LPS, cisplatin (Panesso et al., 2014), and folic acid (Moreno et al., 2011). Low-level Klotho is both a biomarker of and a contributor to AKI pathogenesis. Klotho is upregulated by resveratrol (Hsu et al., 2014a), testosterone (Hsu et al., 2014b), statins (Kuwahara et al., 2008), Rhein (Zhang et al., 2017), and hydrogen-rich saline (Chen et al., 2017) in both the cells and tissues of animals with kidney disease. Klotho restoration exerted impressive renal protective roles on pathological injury. We found that the Klotho levels fell in AKI, consistent with previous work. Notably, the present study demonstrated that neferine significantly prevented Klotho loss from AKI, supporting the scenario that the renoprotective effect of neferine might be mediated by the upregulation of Klotho expression.

The relationship between the Klotho protein and NF-κB pathway activity is critical. TNF-α downregulates Klotho expression *via* an NF-κB-dependent mechanism in renal tubular cells (Moreno et al., 2011). Preservation of Klotho expression attenuates inflammation induced by LPS *via* inhibition of the TLR4/NF-κB pathway (Bi et al., 2018). We found that neferine not only inhibited NF-κB nuclear translocation but also reversed the decrease in Klotho expression. The function mechanisms of neferine were supposed to be one of the following three ways. Neferine may inhibit the NF-κB pathway directly. Alternatively, neferine may inhibit the NF-κB pathway by increasing Klotho expression. Finally, neferine may affect NF-κB activation and Klotho expression *via* two different signaling pathways. Further researches should be performed to explore the exact mechanisms.

In summary, we found that neferine protected against AKI by inhibiting both apoptosis and inflammation. The renoprotection afforded by the drug may be attributable to inhibition of NF-κB activation and preservation of Klotho expression. Neferine may be a valuable prophylactic therapy for AKI.

DATA AVAILABILITY STATEMENT

The raw data supporting the conclusions of this manuscript will be made available by the authors, without undue reservation, to any qualified researcher.

ETHICS STATEMENT

The animal study was reviewed and approved by The Institutional Animal Care and Use Committee of Central South University.

AUTHOR CONTRIBUTIONS

Conceived and designed the experiments: HL and QZ. Performed the experiments: HL, YC and WC. Analyzed the data: HL and WC. Contributed reagents/materials/analysis tools: PX, JX and RT. Wrote the manuscript: HL and WC.

FUNDING

This study was financially supported by the National Youth Science Foundation of China (No. 81600536) and the Natural Science Foundation of Hunan Province of China (No. 2018JJ3833; No. 2018JJ3818).

REFERENCES

Akcay, A., Nguyen, Q., and Edelstein, C. L. (2009). Mediators of inflammation in acute kidney injury. *Mediators Inflammation* 2009, 137072. doi: 10.1155/2009/137072

Ali, T., Khan, I., Simpson, W., Prescott, G., Townend, J., Smith, W., et al. (2007). Incidence and outcomes in acute kidney injury: a comprehensive population-based study. *J. Am. Soc. Nephrol.* 18, 1292–1298. doi: 10.1681/ASN.2006070756

Baskaran, R., Poornima, P., Huang, C. Y., and Padma, V. V. (2016). Neferine prevents NF-kappaB translocation and protects muscle cells from oxidative stress and apoptosis induced by hypoxia. *Biofactors* 42, 407–417. doi: 10.1002/biof.1286

Baskaran, R., Priya, L. B., Kalaiselvi, P., Poornima, P., Huang, C. Y., and Padma, V. V. (2017). Neferine from *Nelumbo nucifera* modulates oxidative stress and cytokines production during hypoxia in human peripheral blood mononuclear cells. *Biomed. Pharmacother.* 93, 730–736. doi: 10.1016/j.biopha.2017.07.003

Bellomo, R., Kellum, J. A., and Ronco, C. (2012). Acute kidney injury. *Lancet* 380, 756–766. doi: 10.1016/S0140-6736(11)61454-2

Bi, F., Chen, F., Li, Y., Wei, A., and Cao, W. (2018). Klotho preservation by Rhein promotes toll-like receptor 4 proteolysis and attenuates lipopolysaccharide-induced acute kidney injury. *J. Mol. Med.* 96: 915–927. doi: 10.1007/s00109-018-1644-7

Bonventre, J. V., and Zuk, A. (2004). Ischemic acute renal failure: an inflammatory disease? *Kidney Int.* 66, 480–485. doi: 10.1111/j.1523-1755.2004.761_2.x

Cao, W., Bao, C., Padalko, E., and Lowenstein, C. J. (2008). Acetylation of mitogen-activated protein kinase phosphatase-1 inhibits toll-like receptor signaling. *J. Exp. Med.* 205, 1491–1503. doi: 10.1084/jem.20071728

Chen, J., Zhang, H., Hu, J., Gu, Y., Shen, Z., Xu, L., et al. (2017). Hydrogen-rich saline alleviates kidney fibrosis following AKI and retains Klotho expression. *Front. Pharmacol.* 8, 499. doi: 10.3389/fphar.2017.00499

Chen, S., Chu, B., Chen, Y., Cheng, X., Guo, D., et al. (2019). Neferine suppresses osteoclast differentiation through suppressing NF-κB signal pathway but not MAPKs and promote osteogenesis. *J. Cell. Physiol.* 234: 22960–22971. doi: 10.1002/jcp.28857

Coelho, S., Cabral, G., Lopes, J. A., and Jacinto, A. (2018). Renal regeneration after acute kidney injury. *Nephrology (Carlton)* 23, 805–814. doi: 10.1111/nep.13256

Dellepiane, S., Marengo, M., and Cantaluppi, V. (2016). Detrimental cross-talk between sepsis and acute kidney injury: new pathogenic mechanisms, early biomarkers and targeted therapies. *Crit. Care* 20, 61. doi: 10.1007/978-3-319-27349-5_9

Deng, G., Zeng, S., Ma, J., Zhang, Y., Qu, Y., Han, Y., et al. (2017). The anti-tumor activities of Neferine on cell invasion and oxaliplatin sensitivity regulated by EMT *via* snail signaling in hepatocellular carcinoma. *Sci. Rep.* 7, 41616. doi: 10.1038/srep41616

Feitoza, C. Q., Semedo, P., Goncalves, G. M., Cenedeze, M. A., Pinheiro, H. S., Dos Santos, O. F., et al. (2010). Modulation of inflammatory response by selective inhibition of cyclooxygenase-1 and cyclooxygenase-2 in acute kidney injury. *Inflamm. Res.* 59, 167–175. doi: 10.1007/s00011-009-0083-x

Grigoryev, D. N., Liu, M., Hassoun, H. T., Cheadle, C., Barnes, K. C., and Rabb, H. (2008). The local and systemic inflammatory transcriptome after acute kidney injury. *J. Am. Soc. Nephrol.* 19, 547–558. doi: 10.1681/ASN.2007040469

Guijarro, C., and Egido, J. (2001). Transcription factor-kappa B (NF-kappa B) and renal disease. *Kidney Int.* 59, 415–424. doi: 10.1046/j.1523-1755.2001.059002415.x

Guolan, D., Lingli, W., Wenyi, H., Wei, Z., Baowei, C., and Sen, B. (2018). Anti-inflammatory effects of neferine on LPS-induced human endothelium *via* MAPK, and NF-kappabeta pathways. *Pharmazie* 73, 541–544. doi: 10.1691/ph.2018.8443

Havasi, A., and Borkan, S. C. (2011). Apoptosis and acute kidney injury. *Kidney Int.* 80, 29–40. doi: 10.1038/ki.2011.120

Hoste, E. A., Bagshaw, S. M., Bellomo, R., Cely, C. M., Colman, R., Cruz, D. N., et al. (2015). Epidemiology of acute kidney injury in critically ill patients: the multinational AKI-EPI study. *Intensive Care Med.* 41, 1411–1423. doi: 10.1007/s00134-015-3934-7

Hsu, S. C., Huang, S. M., Chen, A., Sun, C. Y., Lin, S. H., Chen, J. S., et al. (2014a). Resveratrol increases anti-aging Klotho gene expression *via the* activating transcription factor 3/c-Jun complex-mediated signaling pathway. *Int. J. Biochem. Cell Biol.* 53, 361–371. doi: 10.1016/j.biocel.2014.06.002

Hsu, S. C., Huang, S. M., Lin, S. H., Ka, S. M., Chen, A., Shih, M. F., et al. (2014b). Testosterone increases renal anti-aging klotho gene expression *via the* androgen receptor-mediated pathway. *Biochem. J.* 464, 221–229. doi: 10.1042/BJ20140739

Hu, M. C., Kuro-O, M., and Moe, O. W. (2012). The emerging role of Klotho in clinical nephrology. *Nephrol. Dial. Transplant* 27, 2650–2657. doi: 10.1093/ndt/gfs160

Hu, M. C., Shi, M., Zhang, J., Quinones, H., Kuro-O, M., and Moe, O. W. (2010). Klotho deficiency is an early biomarker of renal ischemia-reperfusion injury and its replacement is protective. *Kidney Int.* 78, 1240–1251. doi: 10.1038/ki.2010.328

Huang, C. L., and Moe, O. W. (2011). Klotho: a novel regulator of calcium and phosphorus homeostasis. *Pflugers Arch.* 462, 185–193. doi: 10.1007/s00424-011-0950-5

Huang, Y., Bai, Y., Zhao, L., Hu, T., Hu, B., Wang, J., et al. (2007). Pharmacokinetics and metabolism of neferine in rats after a single oral administration. *Biopharm. Drug Dispos.* 28, 361–372. doi: 10.1002/bdd.556

Joannes-Boyau, O., Honore, P. M., Boer, W., and Rose, T. (2010). Septic acute kidney injury and tubular apoptosis: never a lone ranger. *Intensive Care Med.* 36, 385–388. doi: 10.1007/s00134-009-1725-8

Kim E. A., Sung, E. G., Song, I. H., Kim, J. Y., Sung, H. J., et al. (2019) Neferine-induced apoptosis is dependent on the suppression of Bcl-2 expression via downregulation of p65 in renal cancer cells. *Acta biochimica et biophysica Sinica.* 51: 734–742. doi: 10.1093/abbs/gmz061

Kuro-O, M., Matsumura, Y., Aizawa, H., Kawaguchi, H., Suga, T., Utsugi, T., et al. (1997). Mutation of the mouse klotho gene leads to a syndrome resembling ageing. *Nature* 390, 45–51. doi: 10.1038/36285

Kuwahara, N., Sasaki, S., Kobara, M., Nakata, T., Tatsumi, T., Irie, H., et al. (2008). HMG-CoA reductase inhibition improves anti-aging klotho protein expression and arteriosclerosis in rats with chronic inhibition of nitric oxide synthesis. *Int. J. Cardiol.* 123, 84–90. doi: 10.1016/j.ijcard.2007.02.029

Lemay, S., Rabb, H., Postler, G., and Singh, A. K. (2000). Prominent and sustained up-regulation of gp130-signaling cytokines and the chemokine MIP-2 in murine renal ischemia-reperfusion injury. *Transplantation* 69, 959–963. doi: 10.1097/00007890-200003150-00049

Levey, A. S., and James, M. T. (2017). Acute kidney injury. *Ann. Intern. Med.* 167, Itc66–itc80. doi: 10.7326/AITC201711070

Li, H., Tang, Y., Wen, L., Kong, X., Chen, X., Liu, P., et al. (2017). Neferine reduces cisplatin-induced nephrotoxicity by enhancing autophagy *via the* AMPK/mTOR signaling pathway. *Biochem. Biophys. Res. Commun.* 484, 694–701. doi: 10.1016/j.bbrc.2017.01.180

Marthandam Asokan, S., Mariappan, R., Muthusamy, S., and Velmurugan, B. K. (2018). Pharmacological benefits of neferine—a comprehensive review. *Life Sci.* 199, 60–70. doi: 10.1016/j.lfs.2018.02.032

Mitobe, M., Yoshida, T., Sugiura, H., Shirota, S., Tsuchiya, K., and Nihei, H. (2005). Oxidative stress decreases klotho expression in a mouse kidney cell line. *Nephron Exp. Nephrol.* 101, e67–e74. doi: 10.1159/000086500

Moreno, J. A., Izquierdo, M. C., Sanchez-Nino, M. D., Suarez-Alvarez, B., Lopez-Larrea, C., Jakubowski, A., et al. (2011). The inflammatory cytokines TWEAK and TNFalpha reduce renal klotho expression through NFkappaB. *J. Am. Soc. Nephrol.* 22, 1315–1325. doi: 10.1681/ASN.2010101073

Oh, H. J., Nam, B. Y., Lee, M. J., Kim, C. H., Koo, H. M., Doh, F. M., et al. (2015). Decreased circulating klotho levels in patients undergoing dialysis and relationship to oxidative stress and inflammation. *Perit. Dial. Int.* 35, 43–51. doi: 10.3747/pdi.2013.00150

Panah, F., Ghorbanihaghjo, A., Argani, H., Asadi Zarmehri, M., and Nazari Soltan Ahmad, S. (2018). Ischemic acute kidney injury and klotho in renal transplantation. *Clin. Biochem.* 55, 3–8. doi: 10.1016/j.clinbiochem.2018.03.022

Panesso, M. C., Shi, M., Cho, H. J., Paek, J., Ye, J., Moe, O. W., et al. (2014). Klotho has dual protective effects on cisplatin-induced acute kidney injury. *Kidney Int.* 85, 855–870. doi: 10.1038/ki.2013.489

Priya, L. B., Baskaran, R., Huang, C. Y., and Padma, V. V. (2017). Neferine ameliorates cardiomyoblast apoptosis induced by doxorubicin: possible role in modulating NADPH oxidase/ROS-mediated NFkappaB redox signaling cascade. *Sci. Rep.* 7, 12283. doi: 10.1038/s41598-017-12060-9

Qin, Q., Chen, X. P., Yang, Z. S., Xiao, Y. H., Min, H., and Li, Y. J. (2011). Neferine increases STI571 chemosensitivity *via* inhibition of P-gp expression in STI571-resistant K562 cells. *Leuk. Lymphoma* 52, 694–700. doi: 10.3109/10428194.2010.550075

Sanz, A. B., Sanchez-Nino, M. D., Ramos, A. M., Moreno, J. A., Santamaria, B., Ruiz-Ortega, M., et al. (2010). NF-kappaB in renal inflammation. *J. Am. Soc. Nephrol.* 21, 1254–1262. doi: 10.1681/ASN.2010020218

Savransky, V., Molls, R. R., Burne-Taney, M., Chien, C. C., Racusen, L., and Rabb, H. (2006). Role of the T-cell receptor in kidney ischemia-reperfusion injury. *Kidney Int.* 69, 233–238. doi: 10.1038/sj.ki.5000038

Sharma, B. R., Gautam, L. N., Adhikari, D., and Karki, R. (2017). A comprehensive review on chemical profiling of *Nelumbo Nucifera*: potential for drug development. *Phytother Res.* 31, 3–26. doi: 10.1002/ptr.5732

Sugiura, H., Yoshida, T., Shiohira, S., Kohei, J., Mitobe, M., Kurosu, H., et al. (2012). Reduced Klotho expression level in kidney aggravates renal interstitial fibrosis. *Am. J. Physiol. Renal. Physiol.* 302, F1252–F1264. doi: 10.1152/ajprenal.00294.2011

Susantitaphong, P., Cruz, D. N., Cerda, J., Abulfaraj, M., Alqahtani, F., Koulouridis, I., et al. (2013). World incidence of AKI: a meta-analysis. *Clin. J. Am. Soc. Nephrol.* 8, 1482–1493. doi: 10.2215/CJN.00710113

Tang, Y. S., Zhao, Y. H., Zhong, Y., Li, X. Z., Pu, J. X., et al. (2019). Neferine inhibits LPS-ATP-induced endothelial cell pyroptosis via regulation of ROS/NLRP3/Caspase-1 signaling pathway. *Inflamm Res.* 68: 727–738. doi: 10.1007/s00011-019-01256-6

Wang, Q., Zhang, B., and Yu, J. L. (2016). Farrerol inhibits IL-6 and IL-8 production in LPS-stimulated human gingival fibroblasts by suppressing PI3K/AKT/NF-kappaB signaling pathway. *Arch. Oral. Biol.* 62, 28–32. doi: 10.1016/j.archoralbio.2015.11.007

Wen, Y., Jiang, L., Xu, Y., Qian, C. Y., Li, S. S., Qin, T. H., et al. (2013). Prevalence, risk factors, clinical course, and outcome of acute kidney injury in Chinese intensive care units: a prospective cohort study. *Chin. Med. J. (Engl.)* 126, 4409–4416. doi: 10.3760/cma.j.issn.0366-6999.20132065

Xu, X., Nie, S., Liu, Z., Chen, C., Xu, G., Zha, Y., et al. (2015). Epidemiology and clinical correlates of AKI in Chinese hospitalized adults. *Clin. J. Am. Soc. Nephrol.* 10, 1510–1518. doi: 10.2215/CJN.02140215

Yang, J. R., Yao, F. H., Zhang, J. G., Ji, Z. Y., Li, K. L., Zhan, J., et al. (2014). Ischemia-reperfusion induces renal tubule pyroptosis *via the* CHOP-caspase-11 pathway. *Am. J. Physiol. Renal. Physiol.* 306, F75–F84. doi: 10.1152/ajprenal.00117.2013

Zhang, Q., Liu, L., Lin, W., Yin, S., Duan, A., Liu, Z., et al. (2017). Rhein reverses Klotho repression *via* promoter demethylation and protects against kidney and bone injuries in mice with chronic kidney disease. *Kidney Int.* 91, 144–156. doi: 10.1016/j.kint.2016.07.040

Zhao, L., Wang, X., Chang, Q., Xu, J., Huang, Y., Guo, Q., et al. (2010). Neferine, a bisbenzylisoquinline alkaloid attenuates bleomycin-induced pulmonary fibrosis. *Eur. J. Pharmacol.* 627, 304–312. doi: 10.1016/j.ejphar.2009.11.007

Zheng, L., Cao, Y., Liu, S., Peng, Z., and Zhang, S. (2014). Neferine inhibits angiotensin II-induced rat aortic smooth muscle cell proliferation predominantly by downregulating fractalkine gene expression. *Exp. Ther. Med.* 8, 1545–1550. doi: 10.3892/etm.2014.1952

Conflict of Interest: The authors declare that the research was conducted in the absence of any commercial or financial relationships that could be construed as a potential conflict of interest.

Copyright © 2019 Li, Chen, Chen, Zhou, Xiao, Tang and Xue. This is an open-access article distributed under the terms of the Creative Commons Attribution License (CC BY). The use, distribution or reproduction in other forums is permitted, provided the original author(s) and the copyright owner(s) are credited and that the original publication in this journal is cited, in accordance with accepted academic practice. No use, distribution or reproduction is permitted which does not comply with these terms.

frontiers in Physiology

ORIGINAL RESEARCH
published: 15 November 2019
doi: 10.3389/fphys.2019.01365

Refining the Mouse Subtotal Nephrectomy in Male 129S2/SV Mice for Consistent Modeling of Progressive Kidney Disease With Renal Inflammation and Cardiac Dysfunction

*James O'Sullivan[1], Sarah Louise Finnie[1], Oliver Teenan[1], Carolynn Cairns[1], Andrew Boyd[1], Matthew A. Bailey[1], Adrian Thomson, Jeremy Hughes[2], Cécile Bénézech[1], Bryan Ronald Conway[1] and Laura Denby[1]**

[1] Centre for Cardiovascular Science, Queen's Medical Research Centre, The University of Edinburgh, Edinburgh, United Kingdom, [2] Centre for Inflammation, Queen's Medical Research Centre, The University of Edinburgh, Edinburgh, United Kingdom

OPEN ACCESS

Edited by:
Xueying Zhao, Morehouse School of Medicine, United States

Reviewed by:
Jaap Joles, Utrecht University, Netherlands
Tetsuro Kusaba, Kyoto Prefectural University of Medicine, Japan

***Correspondence:**
Laura Denby
Laura.Denby@ed.ac.uk

Specialty section:
This article was submitted to Renal and Epithelial Physiology, a section of the journal Frontiers in Physiology

Received: *24 July 2019*
Accepted: *14 October 2019*
Published: *15 November 2019*

Citation:
O'Sullivan J, Finnie SL, Teenan O, Cairns C, Boyd A, Bailey MA, Thomson A, Hughes J, Bénézech C, Conway BR and Denby L (2019) Refining the Mouse Subtotal Nephrectomy in Male 129S2/SV Mice for Consistent Modeling of Progressive Kidney Disease With Renal Inflammation and Cardiac Dysfunction. Front. Physiol. 10:1365. doi: 10.3389/fphys.2019.01365

Chronic kidney disease (CKD) is prevalent worldwide and is associated with significant co-morbidities including cardiovascular disease (CVD). Traditionally, the subtotal nephrectomy (remnant kidney) experimental model has been performed in rats to model progressive renal disease. The model experimentally mimics CKD by reducing nephron number, resulting in renal insufficiency. Presently, there is a lack of translation of pre-clinical findings into successful clinical results. The pre-clinical nephrology field would benefit from reproducible progressive renal disease models in mice in order to avail of more widely available transgenics and experimental tools to dissect mechanisms of disease. Here we evaluate if a simplified single step subtotal nephrectomy (STNx) model performed in the 129S2/SV mouse can recapitulate the renal and cardiac changes observed in patients with CKD in a reproducible and robust way. The single step STNx surgery was well-tolerated and resulted in clinically relevant outcomes including hypertension, increased urinary albumin:creatinine ratio, and significantly increased serum creatinine, phosphate and urea. STNx mice developed significant left ventricular hypertrophy without reduced ejection fraction or cardiac fibrosis. Analysis of intra-renal inflammation revealed persistent recruitment of Ly6C^{hi} monocytes transitioning to pro-fibrotic inflammatory macrophages in STNx kidneys. Unlike 129S2/SV mice, C57BL/6 mice exhibited renal fibrosis without proteinuria, renal dysfunction, or cardiac pathology. Therefore, the 129S2/SV genetic background is susceptible to induction of progressive proteinuric renal disease and cardiac hypertrophy using our refined, single-step flank STNx method. This reproducible model could be used to study the systemic pathophysiological changes induced by CKD in the kidney and the heart, intra-renal inflammation and for testing new therapies for CKD.

Keywords: chronic kidney disease (CKD), modeling disease, cardiac hypertrophy, renal fibrosis and inflammation, monocytes/macrophages

INTRODUCTION

Chronic kidney disease (CKD) is increasing in prevalence (Eckardt et al., 2013) and is a significant public health problem due to its associated economic burden (Kerr et al., 2012). Multiple clinical etiologies result in CKD with hypertension and diabetes being the leading causes (Horowitz et al., 2015; Alicic et al., 2017; Obrador and Levin, 2019). CKD progression is staged via estimated glomerular filtration rate (eGFR) and urinary albumin-creatinine ratio (ACR) (Stevens and Levin, 2013). Patients with CKD are at increased risk of cardiovascular disease (CVD) and this risk increases as renal function declines. Once patients reach end-stage kidney disease (ESKD) requiring dialysis or transplantation, the risk of CVD is 10–30x that of the general population with cardiovascular events accounting for almost 50% of deaths in CKD patients (Di et al., 2015).

The common end-pathway of progressive CKD is the deposition of fibrotic scar tissue that replaces the functional renal parenchyma in the form of tubulointerstitial fibrosis and glomerulosclerosis. The underlying mechanisms of fibrosis remain incompletely understood as it is a complex process involving a diverse array of cell types and molecular pathways, with cross-talk between cell types being evident (Gewin et al., 2017). These cell types include fibroblasts, tubular epithelial cells, macrophages, endothelial cells, dendritic cells, and lymphocytes (Boor et al., 2010). For example, fibroblasts differentiate into myofibroblasts, proliferate, and deposit extracellular matrix components (Mack and Yanagita, 2015). The sources of myofibroblasts within the injured kidney have been the subject of intense study, perivascular Gli^+ progenitor cells have been suggested to be particularly important (Kramann et al., 2015). Another notable feature of CKD is tubular atrophy and loss of tubular epithelial cells (Venkatachalam et al., 2015; Schelling, 2016; Webster et al., 2017). The renal tubule has long been thought of as a target of renal injury, however it may also function as a propagator of injury as tubular cells may undergo cell-cycle arrest, de-differentiation, and acquire a pro-secretory phenotype (Gewin, 2018). Cytokines secreted by tubular cells may act as paracrine factors to promote the production of collagenous matrix by surrounding myofibroblasts (Gewin, 2018).

Subtotal nephrectomy, or 5/6 nephrectomy, is used as a rodent model of progressive CKD (Yang et al., 2010). Historically, the subtotal nephrectomy model was performed in rats, although it has more recently been conducted in mice (Ma and Fogo, 2003; Kennedy et al., 2008; Siedlecki et al., 2009; Yang et al., 2010; Gava et al., 2012; Oosterhuis et al., 2017). The effectiveness of STNx to produce experimental-CKD in mice has been found to vary depending on the strain of mouse used (Leelahavanichkul et al., 2010), with C57BL/6 mice being more resistant (Kren and Hostetter, 1999; Ma and Fogo, 2003; Leelahavanichkul et al., 2010) and SV129/CD1 mice being permissive (Ma and Fogo, 2003; Kennedy et al., 2008; Siedlecki et al., 2009; Leelahavanichkul et al., 2010). However, the results in mice have been inconsistent and there is a lack of technical information about how the model was performed, any power calculation data, mortality rates, information on post-surgery animal welfare and whether the ARRIVE guidelines were followed. This lack of standardization in the model in mice likely contributes to the inconsistencies reported (Chatzimanouil et al., 2018).

We sought with this paper to standardize the STNx model in mice, to improve animal welfare standards and define the renal and cardiac effects to enable consistent modeling of the pathophysiological changes induced during progressive CKD.

MATERIALS AND METHODS

Single Step Flank Subtotal Nephrectomy Model

The refined STNx model involves a single anesthetic and surgery (∼40 min), performed via flank incisions that result in improved animal condition scores, reduced mortality with reproducible outcomes between studies.

Male 129S2/SV mice were obtained from Envigo and used when 6–8 weeks old (weighing 24.7 ± 0.37 g SEM). Male Gli1 × Ai14 mice on a C57BL/6 genetic background were used at 9 ± 3 weeks old (weighing 31.9 ± 1.1 g SEM). Mice were group-housed and provided with *ad lib* access to water and fed with Rm1 standard chow (Special Diets Services) with the following content 0.25% Na, 0.67% K, 0.38% Cl. Mice were also given environmental enrichment. A 12-h light–dark cycle was maintained. During the study, mice were weighed weekly and had their condition recorded. ARRIVE guidelines were adhered to at all times. Only male mice were selected as unlike in other organs, notable sex difference in myeloid cells, including macrophages have been documented in the kidney (Bain et al., 2016).

Animals were randomized to receive sham or subtotal nephrectomy surgery (STNx) using a random number generator website[1]. Prior to surgery, mice had a timed overnight urine sample collected (single housed metabolic cage), blood sample taken (superficial vein) and blood pressure measured (tail cuff). Immediately prior to surgery, mice were weighed and a total of four studies including two pilot studies were performed.

Surgery was performed in a sterile surgical environment using inhalational isoflurane for anesthesia. Once anesthetised, the mouse was shaved and received perioperative s.c. analgesia.

The mouse was initially placed on the left lateral side and an incision was made on the flank over the right kidney. The right kidney was located and carefully maneuvred out of the incision site. The adrenal gland was carefully blunt dissected away from the kidney to avoid adrenalectomy. The right renal pedicle was clamped and a nephrectomy performed. The vascular clamp was removed, the renal bed checked for signs of bleeding and the abdominal wall sutured closed and skin clips applied to close the outer skin incision.

The left kidney was then located and adrenal gland blunt-dissected away. The renal artery and vein were isolated and clamped ensuring ischemic time was less than 5 min. Renal poles (approximately 2/3 renal mass) were then surgically removed and spongostan applied. The vascular clamp was released and once hemostasis had been achieved, the kidney was placed back into the abdomen and the incisions closed. For sham surgery, animals

[1] http://random.org

were prepared the same way, had bilateral flank incisions and both kidneys isolated and manipulated.

At the end of surgery, mice were immediately placed in a fresh cage with littermates in a hotbox at 28°C, where they remained for 7 days. During this time, the mice were checked three times daily and scored using bespoke animal condition scoring sheets (**Supplementary Table 1**). After this time the mice were weighed, skin clips removed and placed in a regular animal holding room and maintained under normal conditions.

For quality control purposes, the weight of kidney removed was calculated to estimate how much residual kidney was left (with the caveat that the kidneys have a small mismatch in weights). The weight of the whole right kidney was measured and compared to the weight of the two pole sections of kidney removed from the left kidney. In order to maintain consistency in this model we ensured that the percentage remaining was as consistent as possible. Residual kidney mass was calculated by the following:

$$\%\ \text{left renal mass remaining} = 100 - [(\text{left kidney sections weight}/\text{whole right kidney weight}) * 100]$$

Animals were schedule 1 culled in compliance with United Kingdom Home Office regulations. Upon confirmation of death, blood was obtained via cardiac puncture and the animal perfused with PBS and tibia length recorded. For isolation of serum, blood was allowed to clot and spun down at 3000G for 20 min at 4°C. Organs were removed and weighed, prior to being cut into predefined sections with sections for RNA and protein snap frozen in liquid nitrogen, while those for histology were placed in 10% formalin for 24-h, before embedding in paraffin to produce FFPE sections. For flow cytometry studies kidney portions were collected in PBS on ice prior to processing.

Histology

Three μM thick FFPE sections were cut and deparaffinized prior to staining with picrosirius red in accordance with manufacturer's guidelines (Abcam, ab150681). Slides were imaged using ZEISS Axio Scan.Z1 Slide Scanner. Quantification of images was carried out using Image-Pro Premier 9.2.

RNA Extraction, Gene and miRNA Expression

Tissue was homogenized using Qiagen TissueLyser II. RNA was extracted from homogenized tissue with the RNeasy Mini Kit (Qiagen 74106) and RNA yields were quantified using NanoDrop 1000 (Thermo Fisher). Reverse transcription was carried out using high-capacity cDNA synthesis kit (Applied Biosystems, 4368814). Quantitative real-time PCR (qRT-PCR) was carried out using specific Taqman gene probes (**Table 1**).

Renal Function Analysis

Timed overnight collections of urine (18 h) were performed at baseline, 6-weeks post-STNx and 10-weeks post-STNx from mice housed singly in metabolic cages. Blood was collected at baseline and at termination. Urine and serum were stored at −20°C prior to analysis by an in-house biochemical analysis service[2].

TABLE 1 | Taqman gene and miRNA expression assays used for qRT-PCR in these studies.

Gene	Probe/assay ID
Col1a1	Mm00801666_g1
Col3a1	Mm01254476_m1
Col4a1	Mm01210125_m1
Acta2	Mm00725412_s1
Mmp2	Mm00439498_m1
Tgfb1	Mm01178820_m1
Il1b	Mm00434228_m1
Tnf	Mm00443258_m1
Ppia	Mm02342430_g1
Nppa	Mm01255747_g1
Nppb	Mm01255770_g1
Gapdh	Mm99999915_g1
miR-21-5p	000397
miR-214-3p	002306
u6	001973

Mouse urine albumin measurements were determined using a commercial Microalbumin Kit (DiaSys Diagnostics Systems, Germany) adapted for use on a Cobas Mira analyzer (Roche Diagnostics, Ltd., Welwyn Garden City, United Kingdom). The immunoturbidimetric assay was standardized against purified mouse albumin standards (Sigma Chemical, Co., Poole, United Kingdom) with samples diluted in phosphate buffer saline as appropriate. Within run precision was CV $<$ 5% while intra-batch precision was CV $<$ 7.1%.

Urine ion concentration was determined using ion-selective electrodes using the SPOTCHEM^{TM} E-Plate with the SPOTCHEM^{TM} EL Analyzer. Urine osmolality was measured by freezing-point depression on a Micro-Digital i-Osmometer (Type 16M, CamLab, United Kingdom).

Echocardiography for Cardiac Structure and Function

Echocardiography was carried out by University of Edinburgh pre-clinical imaging facility under isoflurane anesthesia at 6 and 10-weeks post-surgery as previously published (Respress and Wehrens, 2010; Gao et al., 2011; Lindsey et al., 2018). A parasternal long-axis view of the heart was used to obtain EKV (ECG-gated Kilohertz Visualization) over one cardiac cycle. Spectral Doppler was carried out in parasternal short-axis view and used to assess mitral valve and blood-flow. Doppler sample volume was placed across the mitral valve for measurement of E (early) and A (late, atrial) wave velocity. Doppler sample volume was placed at mid-left ventricular level to measure isovolumic relaxation (IV RT).

Blood-Pressure Analysis

Systolic blood-pressure was measured via a non-invasive tail-cuff method in a customized machine (Wang et al., 2017).

[2]https://surf.ed.ac.uk/facilities/specialist-assay-service/

Mice were trained prior to the start of the study. The mice were placed in a hot-box at 32°C for 5–10 min prior to blood-pressure measurement.

Flow Cytometry

Tissue was placed in gentleMACS^{TM} C Tubes with digestion buffer (Collagenase Type II 0.425 mg/mL, Collagenase D 0.625 mg/mL, Dispase 1 mg/mL and DNAse 30 μg/mL) and dissociated using the gentleMACS^{TM} Dissociator. Cellular suspensions were digested at 37°C for 30 min then gentleMACS^{TM} dissociated for a second time. The cellular suspensions were then put through 100, 70, and 40 μM sieves sequentially and red blood lysis performed with Red Blood Cell Lysing Buffer (Sigma). The concentration of the resultant single cell suspension was determined using a cell counter and cells dispensed into 96-well round-bottom plate and incubated with appropriate rat anti-mouse antibodies (**Table 2**). Unstained samples, compensation beads for each antibody, FMO samples and cell suspensions were run on the six laser LSR Fortessa cell analyzer (BD Biosciences) using DAPI to determine live cells. Data was analyzed using FlowJo software.

Statistical Analysis

A pilot study was performed using Col1a1 gene expression as the outcome measure. Power calculations derived from the pilot study determined that $n = 9$ mice in each group were required to ensure sufficient power (95%) to detect a 30% difference of in Col1a1 expression at a 5% level of significance. To account for mortality at 9% (combined anesthetic and model mortality), $n = 10$ mice/group was employed. For C57BL/6 study the results are from a pilot study performed on group size $n = 6$.

All data was assessed for normal distribution using the D'Agostino-Pearson normality test. Comparisons between two, normally-distributed, data points were carried out via Student's *t*-test. Comparisons between two unpaired, non-normally distributed data points were carried out via Mann–Whitney test. All data generated was subjected to Grubbs outlier test, outliers were removed from analysis. ACR at 6 and 10-weeks post-surgery (**Figure 1D**) was assessed for statistical significance via two-way ANOVA for repeat measures with Sidak's multiple comparison test. Gene and miRNA expression at 6 and 10-weeks post-surgery (**Figures 2D,E**) were compared via ordinary two-way ANOVA with Tukey's multiple comparison test.

TABLE 2 | Antibodies utilized in flow cytometry.

Antibody	Clone/flurochrome/final concentration
Live	DAPI/1:1000
CD45	30-F11/APC or BV650/1:100
F4/80	BM8/Pe-Cy7/1:200
MHCII	M5/114.15.2/APC-Cy7/1:400
Ly6G	1A8/e450/1:200
Ly6C	HK1.4/AF700/1:200
CD11b	M1_70/PE Dazzle/1:1000
CD11c	N418/BV605/1:100
CD206	MR5D3/APC/1:200

RESULTS

Effect of One-Step Flank STNx on Renal Function

We utilized initially male 129S2/SV mice because they have been shown to be sensitive to developing renal dysfunction in previous studies. Following our refined single step flank subtotal nephrectomy (STNx) procedure there was no significant difference in body weight between the sham and STNx animals during the 10-week study run (**Supplementary Figure 1A**). The use of a single surgery procedure was well-tolerated. In total across four studies (pilot and full studies), 53 male 129S2/SV mice aged 7–10 weeks (weights 24.7 ± 0.37 g SEM) and 10 male Gli1 × Ai14 mice on a C57BL/6 genetic background aged 9 ± 3 weeks (weights 31.9 ± 1.1 g SEM) were subjected to STNx or sham surgery. There was an overall model failure rate of 9% (5% mortality, 2% anesthetic death, and 2% early termination rate due to deteriorating animal body condition scoring). Group housing the mice post-surgery resulted in improved animal condition scores and faster recovery compared to single housing (**Supplementary Figure 1B**). Animal stress peaked day 3 post-surgery as assessed by body condition score for single and grouped house, which may suggest analgesia up to day 2 post-surgery may be warranted (**Supplementary Figure 1B**). Across the studies the mean percentage of residual left kidney mass was 32.9 ± 0.98% SEM (**Supplementary Figure 1C**).

Initially we examined the effect of the STNx performed on 129S2/SV male mice on renal excretory function and proteinuria as patients with CKD have increased serum creatinine (Jha et al., 2013; Levey et al., 2014; Hill et al., 2016), urea (Jörres et al., 2004; Almeras and Argilés, 2009; Lau and Vaziri, 2016; Vanholder et al., 2018), and phosphate (Martin and González, 2011; Felsenfeld et al., 2015; Ritter and Slatopolsky, 2016; Vervloet et al., 2017) levels as well as proteinuria. Biochemical analysis of blood samples from mice 10-weeks post-STNx consistently revealed significant increases in serum creatinine (9.29 vs. 4 μmol/l) (**Figure 1A**), phosphate (2.74 vs. 1.84 mmol/L) (**Figure 1B**) and urea (11.62 vs. 6.35 mmol/L) (**Figure 1C**) compared to sham operated mice indicating a reduction of renal excretion. Total urinary albumin excretion was significantly increased 123-fold in STNx mice compared to controls (**Table 3**). STNx mice had a significant increase in urinary albumin:creatinine ratio (ACR) at 6 and 10-weeks post-surgery, with ACR significantly increasing from 6 to 10-weeks post-surgery indicating progressive proteinuria (**Figure 1D**). Renal sodium excretion was not significantly different between STNx and sham operated mice at both 6-weeks (174 ± 24 vs. 121 ± 26 μmol/18 h) and 10-weeks (167 ± 20 vs. 132 ± 24 μmol/18 h; **Table 3**). Chloride excretion was also not different between groups at 6-weeks (372 ± 38 vs. 290 ± 61 μmol/18 h) and 10-weeks (255 ± 21 vs. 271 ± 25 μmol/18 h; **Table 3**). Potassium excretion was significantly different between groups, reflecting an increase in excretion in STNX mice at 6-weeks (380 ± 32

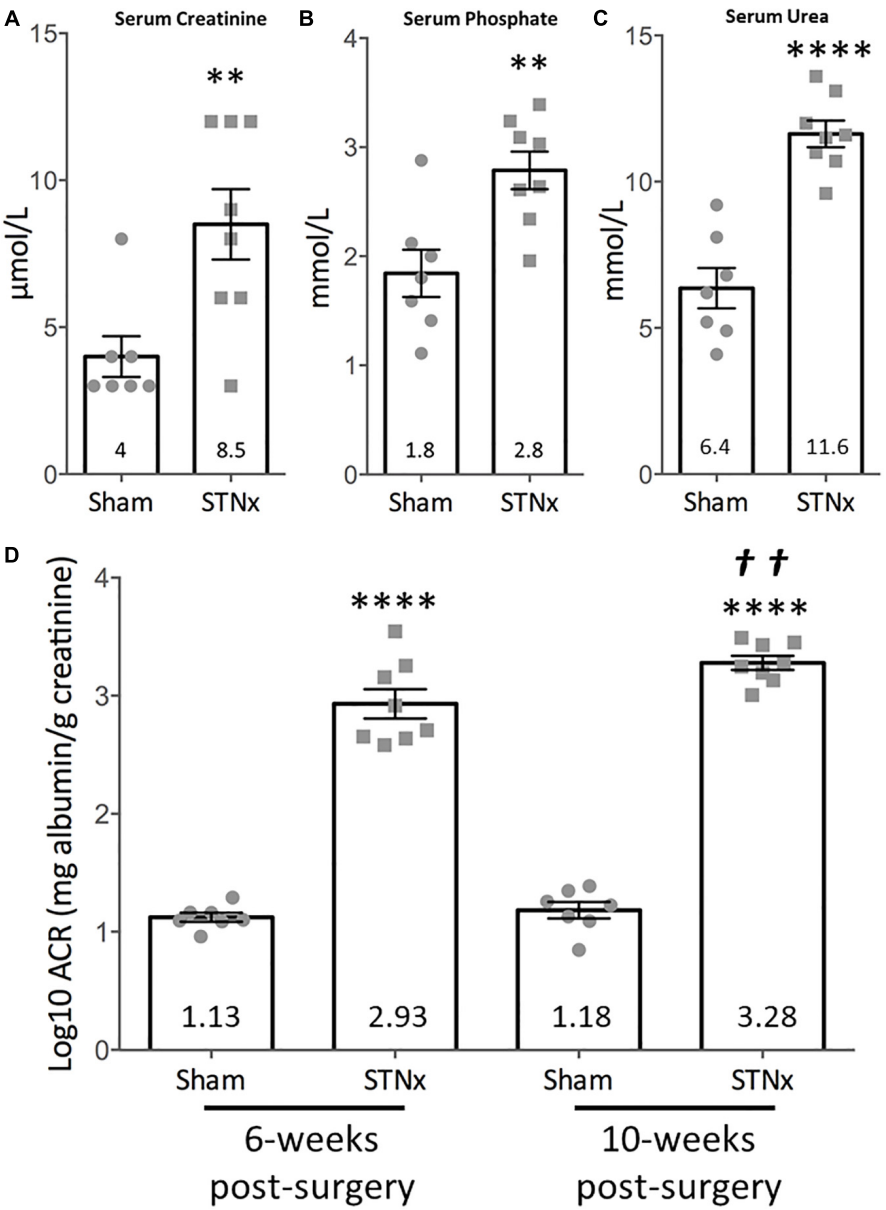

FIGURE 1 | Effect of single-step subtotal nephrectomy on renal function. 129S2/SV mice were subjected to flank single-step STNx or sham surgery and were culled 10-weeks post-surgery. Urine and blood at 10-weeks post-STNx or sham surgery was analyzed for renal function parameters. **(A)** Serum creatinine, **(B)** phosphate, **(C)** urea. Sham: $n = 7$, STNx: $n = 8$. Student's t-test was used for statistical analysis. $^{**}P \leq 0.01$, $^{****}P \leq 0.0001$. Plotted as mean ± SEM. **(D)** Urinary albumin:creatinine ratios (log10) were calculated from timed overnight (18 h) collections from animals 6 and 10-weeks post-surgery. Sham: $n = 7$, STNx: $n = 8$. All comparisons made via two-way ANOVA for repeat measures, with Sidak's multiple comparisons test. $^{****}P \leq 0.0001$ vs. sham (of same timepoint), $^{††}P \leq 0.01$ vs. STNx 6-week. Plotted as mean ± SEM.

vs. 260 ± 45 μmol/18 h, $P = 0.019$); potassium excretion was not different between groups at 10-weeks (234 ± 15 vs. 218 ± 28 μmol/18 h; **Table 3**). Urine osmolarity was also measured with no significant difference at 6-weeks between sham and STNx groups (1272.7 vs. 1157.5 mOsm) but by 10-weeks post-STNx there was significantly lower osmolarity compared with sham animals (**Table 3**).

Renal fibrosis remains one of the best histological markers of progressive kidney disease (Ito et al., 2004; Hewitson, 2009; Hewitson et al., 2017). At 10-weeks post-STNx, renal fibrosis as measured by picrosirius red staining was increased 3.4-fold (increasing from 0.62 ± 0.12% in sham kidneys to 2.11 ± 0.37% in STNx kidneys) (**Figures 2A,B**). Evidence of tubulointerstitial fibrosis and glomerulosclerosis was observed along with tubular dilation (**Figure 2A**). 6-weeks post-STNx surgery, when ACR was already increased, there were no significant pro-fibrotic gene expression changes (**Supplementary Figure 2**). However, by 10-weeks post-STNx surgery, gene expression analysis revealed

TABLE 3 | Urine parameters measured in male 129S2/SV mice 10-weeks post-STNx.

Urine parameters	Sham (10-weeks)	STNx (10-weeks)
Na excretion	131.94 ± 24 μM/18 h	166.77 ± 20 μM/18 h
K excretion	271.78 ± 28 μM/18 h	164.45 ± 21 μM/18 h
Cl excretion	270.84 ± 25 μM/18 h	225.75 ± 11 μM/18 h
Total albumin	3.39 ± 0.48 μg/18 h	418.16 ± 89 μg/18 h ***
Osmolality	1347 ± 89 mOsm	914.5 ± 63 mOsm ***

*Ion excretion, total albumin and osmolality was measured in 18 h-timed urine collection from mice 10-weeks post-surgery or age-matched sham mice. ***P < 0.001 unpaired t-test.*

significant increases in the expression of pro-fibrotic genes (*Col1a1, Col3a1, Col4a1, Acta2, Mmp2, Tgfβ1*) (**Figure 2C**). When gene expression of pro-inflammatory genes (*Il1β* and *Tnfα*) were examined there was no difference in expression compared to sham animals at 6 weeks but a significant increase from 6 to 10-weeks post-STNx (**Figure 2D**). We have previously reported that miR-21 and miR-214 are consistently elevated in the kidney following injury (Denby et al., 2011), however, these miRs have not been assessed in progressive renal dysfunction induced by STNx in 129S2/SV mice. We found that the pro-fibrotic miRNA miR-214-3p (Denby et al., 2014; Bai et al., 2019) was significantly upregulated 6-weeks post-STNx surgery (**Figure 2E**), prior to pro-fibrotic gene expression changes, with no change in the pro-fibrotic miRNA miR-21-5p expression (Denby et al., 2011; Chau et al., 2012; Gomez et al., 2015; Hennino et al., 2016). At 10-weeks post-STNx surgery, miR-21-5p was significantly upregulated 2.4-fold and miR-214-3p remained significantly elevated with a 3.5-fold higher expression compared to sham kidneys (**Figure 2E**). Significant increases in miR-214-3p and miR-21-5p expression were detected in the kidneys of STNx group animals between the 6 and 10-week post-surgery timepoints (**Figure 2E**).

Effect of One-Step Flank STNx on Intra-Renal Inflammation

As we observed an increase in pro-inflammatory gene expression markers 10-weeks post-STNx, we sought to further characterize the nature of the inflammatory cells in kidneys from mice that underwent STNx. Analysis by flow cytometry (gating strategy provided in **Supplementary Figure 3A**) revealed that at 10-weeks post-STNx there was a significant increase in the proportion of cells in the kidney that expressed $CD45^+$ compared to sham kidneys (2.23% STNx vs. 0.96% Sham, **Figures 3A,B** and **Supplementary Figure 3B**). Similarly, a significant increase in $CD45^+$ cells was also observed in the hearts of animals subjected to STNx (**Supplementary Figure 3C**). Further analysis of the $CD45^+$ population in the kidney revealed no significant difference in the proportion of $CD45^+$ inflammatory cells constituted by neutrophils (7.9% STNx vs. 4.5% Sham; **Figure 3C**), $CD11b^+$ $F4/80^{lo}$ macrophages (monocyte derived), or $CD11b^+$ $F4/80^{hi}$ macrophages (resident population) (**Figures 3D,E**). However, further subset analysis of the $CD11b^+$ $F4/80^{lo}$ population revealed a clear waterfall effect in the STNx kidneys with $Ly6C^{hi}$ monocytes transitioning to $Ly6C^{lo}$ $MHCII^+$ macrophages, an effect which was absent in the sham kidney (**Figure 3F**). Furthermore, the percentage of $CD45^+$ $CD11b^+$ $F4/80^{lo}$ $Ly6C^{hi}$ cells was significantly increased in the STNx kidneys (**Figure 3G**). Analysis of the $CD11b^+$ $F4/80^{hi}$ resident macrophages population revealed that there was significantly increased expression of CD206 in these resident macrophages in the STNx kidneys (**Figure 3H**).

Effect of One-Step Flank STNx on Vascular and Cardiac Parameters

We next determined the effect of the STNx surgery on vascular and cardiac function in the 129S2/SV mice we had measured renal excretory function and proteinuria. We determined systolic blood pressure using tail vein plethysmograph in trained conscious mice at baseline, at 6-weeks post-surgery and at study end. The mean systolic blood pressure at 6-weeks was not significantly different in STNx mice compared with sham animals, but was significantly increased from 115 ± 2.6 mmHg in sham animals to 153.1 ± 4.6 mmHg in STNx animals 10-weeks post-STNx surgery (**Figure 4A**). The STNx mice also had significantly increased heart mass compared to sham animals at 10-weeks post-STNx surgery (**Figure 4B**). Therefore, we sought to determine the effects of the progressive loss of renal function induced by our one-step STNx surgery in the 129S2/SV mice on cardiac function as measured by echocardiography (ECHO) carried out at baseline, 6- and 10-weeks post-surgery (**Figure 4C** and **Table 4**). No significant differences in percentage ejection fraction were detected, although there was a trend for a reduction 10-weeks post-STNx. At 6-weeks, changes were detected in % fractional area change (FAC) and area change, indicating that adaption had begun to occur at this point (**Table 4**), but no statistical difference was detected in heart weight (data not shown). By 10-weeks, STNx animals had increased cardiac wall thickness (0.88 ± 0.02 to 1.05 ± 0.04 mm) and left-ventricle mass (182.7 ± 9.06 to 234.6 ± 17.75 mm) compared with sham animals (**Table 4**), which mirrored the increased heart weights measured at 10-weeks post-STNx (**Figure 4B**). Doppler imaging performed on the mitral valve revealed a significantly increased left ventricle isovolumetric relaxation time (IV RT) at 10-weeks post-STNx, but not 6-weeks post-STNx, suggesting STNx induced renal dysfunction may lead to diastolic dysfunction over time (Lindsey et al., 2018; Schnelle et al., 2018). As ECHO analysis suggested cardiac hypertrophy and diastolic dysfunction had occurred, cardiac fibrosis was assessed histologically. At 10-weeks post-STNx there was no significant increase in total collagen deposition in the heart (**Figures 4D,E**). At 6-weeks post-STNx, no change in expression for fibrillar collagen genes *Col1a1* and *Col3a1* was observed (**Figure 4F**), however *Col3a1* expression was significantly increased at 10-weeks compared with sham animals (**Figure 4G**). There was significantly higher expression of the cardiac hypertrophy markers ANP (Nppa) and BNP (Nppb) in the STNx compared with sham animals at 6-weeks with ANP remaining increased a 10-weeks (**Figures 4F,G**).

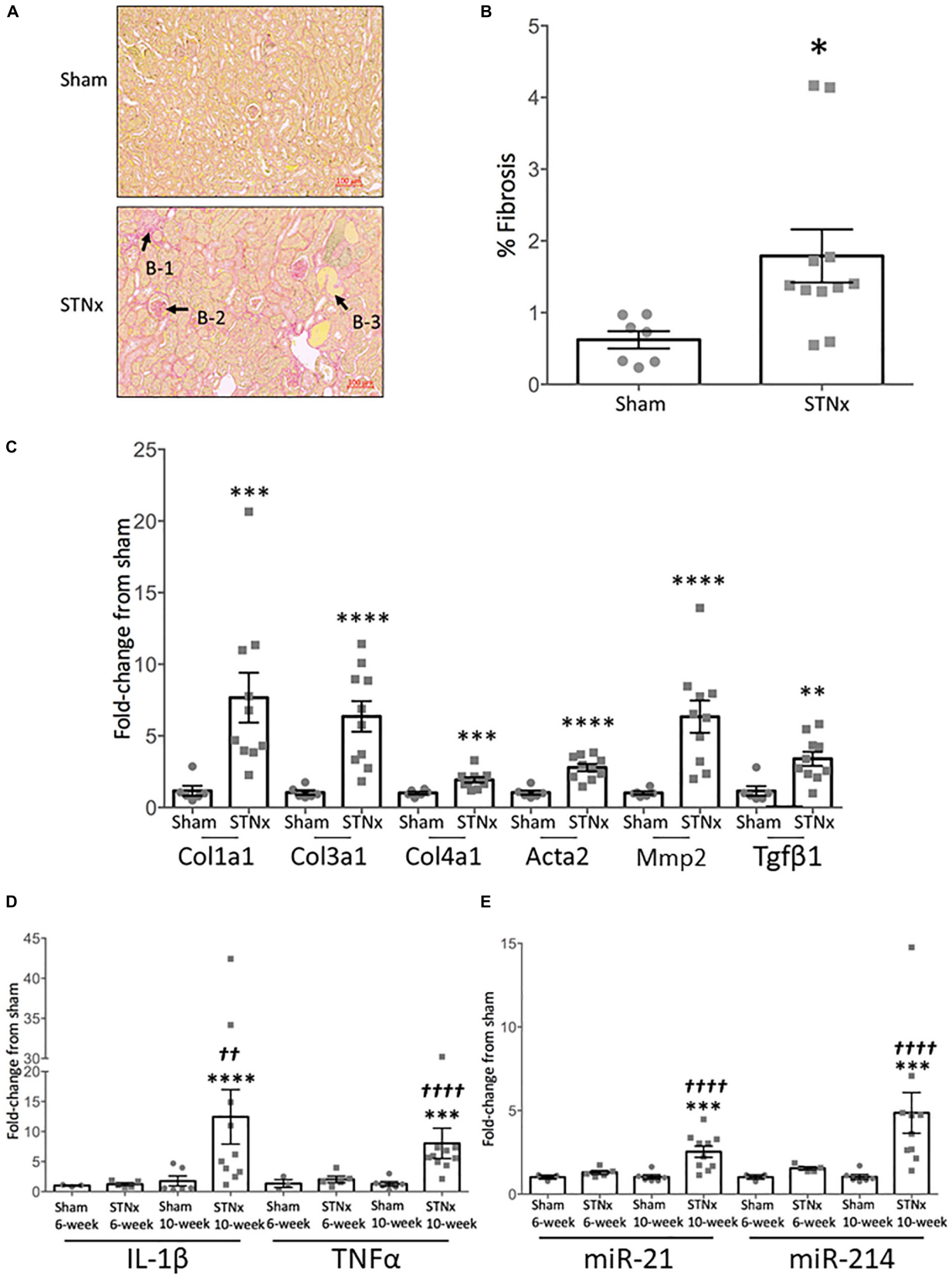

FIGURE 2 | Continued

FIGURE 2 | Single-step subtotal nephrectomy induces significant renal fibrosis. 129S2/SV mice were subjected to flank single-step STNx or sham surgery and were culled 10-weeks post-surgery. At sacrifice kidney sections were snap frozen for RNA analysis and to prepare FFPE 3 μM sections. **(A)** Picrosirius red staining for total collagen in kidneys. Exemplar images are provided at 5x magnification, scale bar 100 μM. B-1 = Tubulointerstitial fibrosis, B-2 = glomerulosclerosis, B-3 = tubular dilation. **(B)** Quantification of fibrosis (% PSR staining). Sham: $n = 7$, STNx: $n = 11$. Student's t-test was used for statistical analysis. $^{*}P < 0.05$. Plotted as mean ± SEM. **(C)** Pro-fibrotic gene expression in whole kidney tissue was determined by quantitative real-time PCR (qRT-PCR) carried out with specific Taqman probes for each gene, normalized to housekeeper Ppia. Sham: $n = 6$, STNx: $n = 10$. Col1a1 was found to have non-parametric distribution, therefore Mann–Whitney test was used, Student's t-test was used for other genes. $^{****}P < 0.0001$, $^{***}P < 0.001$, $^{**}P < 0.01$. Plotted as RQ mean ± SEM. **(D)** Inflammatory gene expression in whole kidney tissue at 6 and 10-weeks post-surgery was determined by quantitative real-time PCR (qRT-PCR) carried out with specific Taqman probes for each gene, normalized to housekeeper Ppia. Sham 6-week: $n = 3$, STNx 6-week: $n = 5$, Sham 10-week: $n = 6$, STNx 10-week: $n = 10$. All comparisons made via an ordinary two-way ANOVA with Tukey's multiple comparisons test. $^{***}P < 0.001$ vs. sham (of same timepoint), $^{****}P < 0.0001$ vs. sham (of same timepoint), $^{††}P < 0.01$ vs. STNx 6-week, $^{††††}P < 0.0001$ vs. STNx 6-week. Plotted as mean ± SEM. **(E)** Renal fibrosis-associated miRNA expression in whole kidney tissue at 6 and 10-weeks post-surgery was determined by quantitative real-time PCR (qRT-PCR) carried out with specific Taqman probes for each miRNA, normalized to housekeeper U6. Sham 6-week: $n = 3$, STNx 6-week: $n = 5$, Sham 10-week: $n = 6$, STNx 10-week: $n = 10$. All comparisons made via an ordinary two-way ANOVA with Tukey's multiple comparisons test. $^{***}P < 0.001$ vs. sham (of same timepoint), $^{††††}P < 0.0001$ vs. STNx 6-week. Plotted as mean ± SEM.

To demonstrate consistent outputs from the STNx model presented in this manuscript, two independent studies were compared in male 129S2/SV mice run 1.5 years apart (**Figure 5**). Between the two studies there were no significant differences in the amount of renal fibrosis detected, the increase in ACRs induced, amount of LVH (measured by heart weight:normalized to tibia) or gene expression of collagen 1 in renal tissue (**Figure 5**).

Effect of Genetic Background on One-Step Flank STNx Induced Renal and Cardiac Dysfunction

Subtotal nephrectomy is known to be a strain-dependent model, with C57BL/6 mice being resistant to developing fibrosis (Ma and Fogo, 2003; Leelahavanichkul et al., 2010). However, this strain is commonly used as a background for the production of transgenic animals. To assess how the single step STNx performs in this genetic background, a Gli1 reporter mouse (Gli1 × Ai14) on a C57BL/6 background was used. An increase in total collagen expression (sham: 0.81 ± 0.03%, STNx: 2.57 ± 0.42%) along with histological hallmarks of renal fibrosis (tubulointerstitial fibrosis and glomerulosclerosis) was observed (**Supplementary Figures 4A,B**), as well as a significant increase in pro-fibrotic genes and inflammatory genes (**Supplementary Figure 4C**). However, the urinary ACRs of STNx animals were not different to sham at 6 or 10-weeks post-surgery (**Supplementary Figure 4D**) and there was no increase in heart weight observed (**Supplementary Figure 4E**).

DISCUSSION

Clinically, CKD is characterized by worsening excretory function with or without proteinuria and renal biopsies typically show glomerulosclerosis, tubulointerstitial fibrosis, and inflammatory cell infiltrates. In addition, CKD is associated with the development of CVD, characterized by hypertension and cardiac and vascular dysfunction. Therefore, we set out to establish if a one-step flank STNx performed in male 129S2/SV mice could model these clinical CKD parameters in a consistent and robust manner.

Urinary albumin to creatinine ratio (ACR) is an important prognostic indicator for progression of renal disease (Feldman et al., 2014; Vassalotti et al., 2016), and cardiovascular events (Waheed et al., 2012). Furthermore, regression of albuminuria is associated with improved renal outcomes (Perkins et al., 2007) and hence represents a therapeutic target in CKD patients (Heerspink and Gansevoort, 2015). Hence, the significantly increased ACR in STNx mice compared to sham operated mice represents an important clinically-relevant readout for testing novel therapeutics in this model. Indeed, this was a key readout used to demonstrate the efficacy of ACE inhibition in seminal studies in the rat subtotal nephrectomy model (Meyer et al., 1985; Anderson et al., 1986), which represents one of the few therapies that have been successfully translated from rodent models to human CKD. Urinary excretion of sodium, chloride and potassium were largely comparable between sham-operated and STNx mice at both time points. Although GFR was not directly measured here, the major reduction in filtration following STNx would significantly reduce the filtered load for sodium, chloride and potassium and our data indicate a proportionate decline tubular reabsorption. Thus, over this time course, the renal tubule adapted to maintain electrolyte excretion and preserve balance. The STNx group showed a progressive decline in urine osmolarity, indicating a reduced concentrating capacity in the remnant kidney.

Male 129S2/SV mice subjected to the refined one-step STNx developed increased serum creatinine, BUN and phosphate which are important clinical manifestations of renal disease. There was approximately a twofold increase in both creatinine and urea by 10-weeks post-STNx, however, the coefficient of variation (CV) for urea was only 11.1% compared to 39.8% for creatinine suggesting that serum urea measurements are more reliable as kidney injury markers in rodents. In this context, it would be interesting to measure some newer markers of renal function such as Cystatin C (Song et al., 2009) to further validate this model of progressive renal dysfunction in mice. The increase in serum phosphate is important as hyperphosphatemia is observed in late-stage CKD and is a driver of secondary hyperparathyroidism (Locatelli et al., 2002), mineral bone disorder and vascular calcification (Felsenfeld et al., 2015). Hyperphosphatemia is also thought to contribute to cardiac hypertrophy and calcification of heart valves and conduction system (Di et al., 2015).

The serum urea levels recorded in the mice following the single step flank STNx procedure were significantly increased compared to age matched sham controls, however, these levels

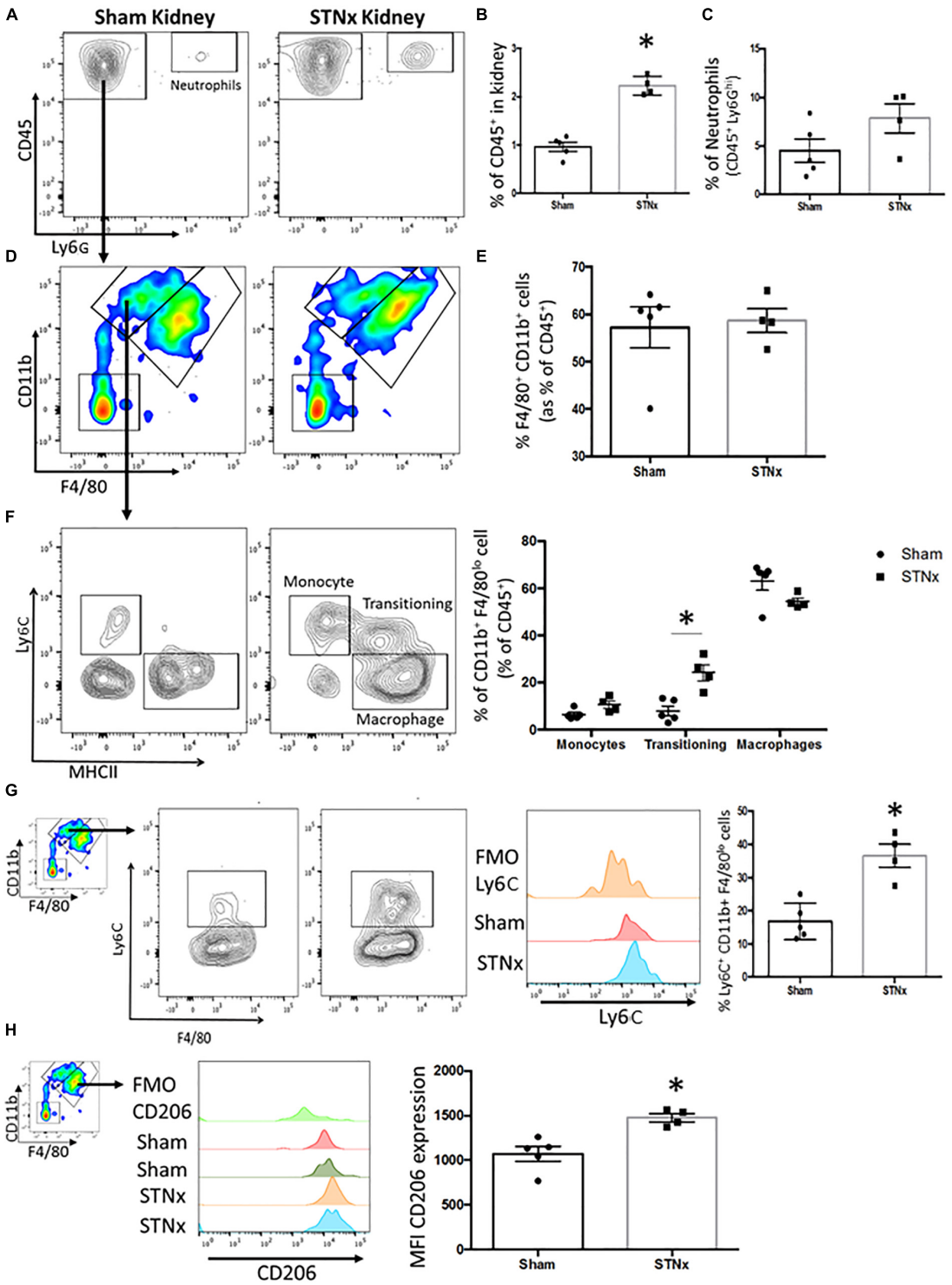

FIGURE 3 | Analysis of inflammatory infiltrate in the STNx kidney. 129S2/SV mice were subjected to flank single-step STNx or sham surgery and were culled 10-weeks post-surgery. At sacrifice $n = 5$ Sham and $n = 4$ STNx kidneys were perfused and kidneys digested for flow cytometry and analyzed on the 6L Fortessa Flow Analyzer. **(A)** Plot of $CD45^+$ cells and neutrophils (CD45 + $Ly6G^{hi}$) in kidney. **(B)** Quantification of the percentage of total cells that express $CD45^+$ in the kidney. **(C)** Quantification of Neutrophils ($CD45^+$ $Ly6G^{hi}$) in the kidney. **(D)** Analysis of $CD45^+$ $Ly6G^-$ $CD11b^+$ $F4/80^+$ population in the kidney. **(E)** Quantification of $CD45^+$ $Ly6G^-$ $CD11b^+$ $F4/80^+$ population in the kidney. **(F)** Subset analysis and quantification of $CD45^+$ $Ly6G^-$ $CD11b^+$ $F4/80^{lo}$ population into monocytes ($Ly6C^{hi}$ $MHCII^-$), transitioning monocyte-macrophages and macrophages ($Ly6C^-$ $MHCII^+$). **(G)** Expression and quantification of the proportion of $CD45^+$ $Ly6G^-$ $CD11b^+$ $F4/80^{lo}$ that express Ly6C. **(H)** Analysis and quantification of CD206 expression in the resident macrophage population $CD45^+$ $Ly6G^-$ $CD11b^+$ $F4/80^{hi}$. $N = 5$ Sham $N = 4$ STNx statistical analysis by Mann–Whitney test $^*P < 0.05$.

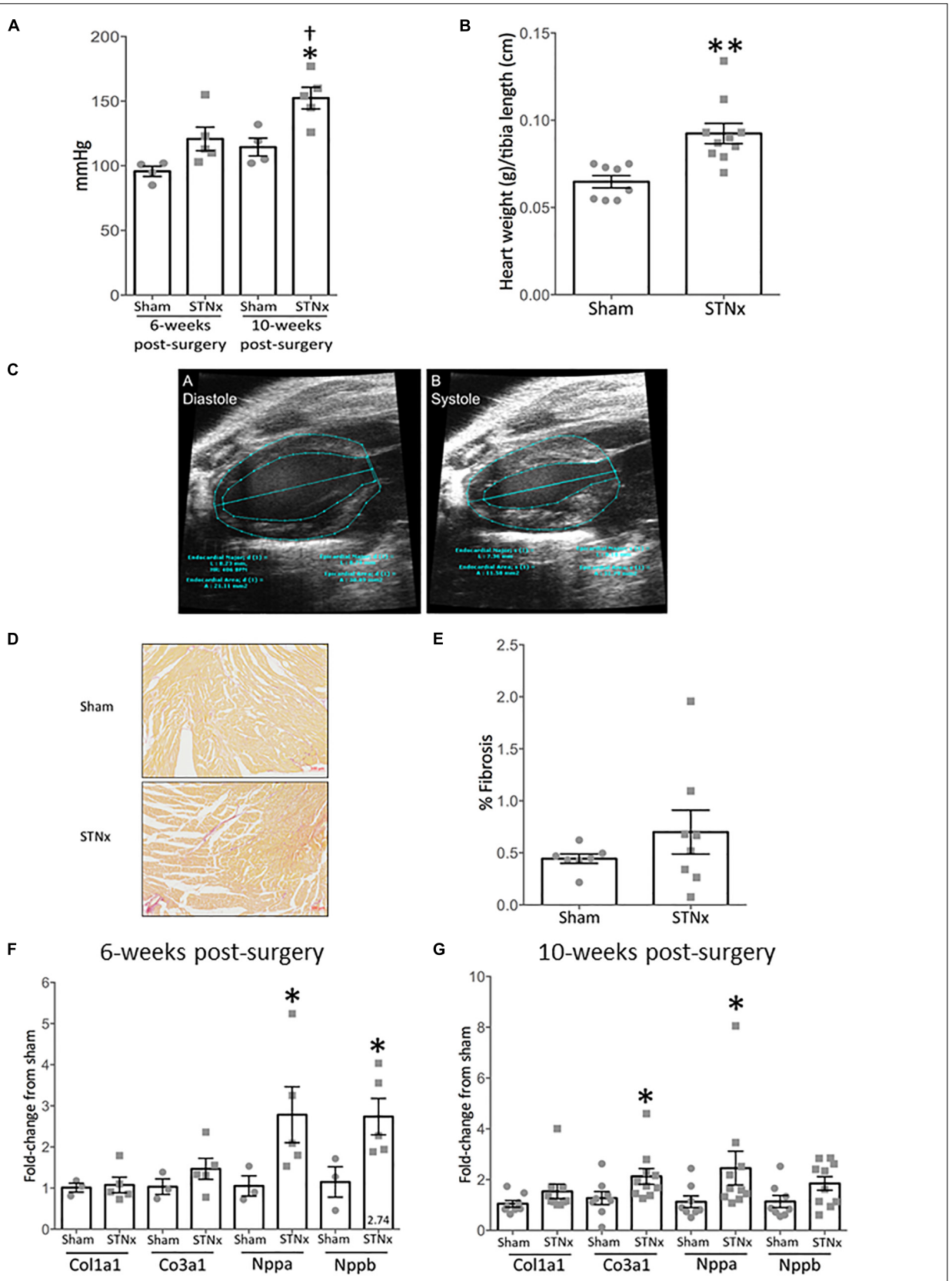

FIGURE 4 | Continued

FIGURE 4 | Single-step flank STNx induces cardiac dysfunction and hypertrophy but not cardiac fibrosis. 129S2/SV mice were subjected to flank single-step STNx or sham surgery and were culled 10-weeks post-surgery. At sacrifice heart sections were taken and snap frozen for RNA analysis and to prepare FFPE 3 μM sections. **(A)** Systolic blood pressure was measured via tail cuff at 6 and 10-weeks post-surgery. Sham: $n = 4$, STNx: $n = 5$. One way-ANOVA with Tukey's multiple comparison test, all compared to sham. $^{*}P \leq 0.05$, $^{\dagger}P < 0.05$ vs. STNx at 6 weeks. Plotted as mean ± SEM. **(B)** Heart weight at cull normalized to tibia length. Sham: $n = 7$, STNx: $n = 11$. Student's *t*-test was used for statistical analysis. $^{**}P \leq 0.01$. Plotted as mean ± SEM. **(C)** Exemplar images of the analysis of EKV echocardiography via VisualSonics software. A = diastole, B = systole. Trace lines were drawn along the epicardial and endocardial borders at both end systole and end diastole. Left ventricle (LV) major axes were also traced at end systole and end diastole by drawing a line from the LV apex endocardium or LV apex epicardium, to the mitral valve line. **(D)** Picrosirius red stain for total collagen in hearts. Exemplar images are provided at 5x magnification. **(E)** Quantification of fibrosis (% PSR staining) carried out via Image-Pro Plus 7. Sham: $n = 7$, STNx: $n = 8$. Student's *t*-test was used for statistical analysis. Plotted as mean ± SEM. **(F)** Gene expression in whole heart tissue was assessed 6 weeks post-STNx using quantitative real-time PCR (qRT-PCR) using specific Taqman probes for each gene, normalized to housekeeper Gapdh. Sham: $n = 3$, STNx: $n = 5$. Student's *t*-test was used for statistical analysis. $^{*}P \leq 0.05$. Plotted as mean ± SEM. **(G)** Gene expression in whole heart tissue 10-weeks post-STNx or sham surgery was assessed using quantitative real-time PCR (qRT-PCR) using specific Taqman probes for each gene, normalized to housekeeper Gapdh. Sham: $n = 8$, STNx: $n = 10$. Col1a1, Col3a1, and Nppa expression were determined to have non-parametric distribution. Mann–Whitney test was used for statistical analysis on Col1a1, Col3a1 and Nppa, Student's *t*-test was used on Nppb. $^{*}P \leq 0.05$. Plotted as mean ± SEM.

TABLE 4 | Cardiac echocardiography measurements in STNX and Sham animals at 6 and 10-weeks post-surgery.

	6-weeks post-surgery		10-weeks post-surgery	
	Sham	**STNx**	**Sham**	**STNx**
EKV:	$n = 8$	$n = 10$	$n = 8$	$n = 10$
Ejection fraction (%)	59.1 ± 1.5	48.8 ± 4.4	54.4 ± 4	45.9 ± 2.8
Fractional area change (%)	40.5 ± 0.8	32.2 ± 3.3 *	37.2 ± 3.2	29.8 ± 2.3
Area change (mm^2)	9.21 ± 0.8	7.21 ± 0.64 *	8.73 ± 0.86	6.91 ± 0.34 †
Cardiac wall thickness (mm)	0.92 ± 0.03	1.02 ± 0.04	0.88 ± 0.02	1.04 ± 0.04 ††
LV mass (mg)	189.1 ± 10.7	215.8 ± 16.3	182.7 ± 9.1	234.6 ± 17.7 †
Mitral valve spectral doppler:	$n = 8$	$n = 9$	$n = 8$	$n = 9$
E wave (mm/s)	770 ± 27.4	650 ± 41.7*	747 ± 25.6	663 ± 38.9
A wave (mm/s)	457 ± 24.5	479 ± 44.3	443 ± 39.9	471 ± 45.5
LV IV RT	24.5 ± 1.24	28.2 ± 1.75	24.1 ± 0.82	28.6 ± 1.38 †

Echocardiography measurements were obtained under isoflurane anesthesia at 6 and 10-week post-STNx or sham surgery. Sham: n = 8, STNx: n = 10. Student's t-test was used for statistical analysis of difference between sham and STNx groups at 6 or 10-weeks post-surgery. $^{*}P \leq 0.05$ at 6-weeks vs. sham. $^{\dagger}P \leq 0.05$, $^{\dagger\dagger}P \leq 0.01$ at 10-weeks vs. sham.

are lower than those observed in some other studies which might suggest this surgery resulted in less tissue being taken and a less severe renal dysfunction being induced which resulted in less mortality. The lack of a statistical difference in body weight appears to support this too. There are very few studies that document the amount of tissue taken beyond those studies that showed the relationship between renal function and the amount of tissue removed (Rambausek et al., 1985). In our studies in male SV129/SV mice, when on average 32.9% of left renal tissue remained, all mice developed renal dysfunction with significant alterations in renal excretory function and proteinuria. Importantly, the low mortality rate in this STNx model means animals survived to pre-defined study end-points which maintained statistical power in the studies.

The relationship between CKD and hypertension is bidirectional. CKD is known to cause hypertension and hypertension is a known risk factor for CKD (Gosmanova and Kovesdy, 2016). 86% of CKD patients have hypertension (Gosmanova and Kovesdy, 2016). Blood pressure lowering strategies have been shown to decrease progression of kidney disease and all-cause mortality in patients with CKD (Peters et al., 2017). At 10-weeks post-STNx, a significant increase in systolic blood pressure was detected using tail vein plethysmograph. This was in agreement with several other studies (Kennedy et al., 2008; Leelahavanichkul et al., 2010; Gava et al., 2012). However, this is contrast to subtotal nephrectomy two-step models run in 129SV and FVB mice, where no change in blood pressure was observed (Siedlecki et al., 2009; Dilauro et al., 2010). Interestingly, sham mice from the 129SV study had higher systolic blood pressures than recorded in our study (129 ± 4 mmHg; Siedlecki et al., 2009 sham versus 115 ± 2.6 mmHg sham operated in our study). The mice in this study were trained prior to blood pressure measurements to ensure the results were not affected by stress of the procedure, potentially explaining the lower conscious blood pressures obtained. However, the diet of the mice differing between studies could also explain these effects as increased dietary NaCl is known to aggravate hypertension. Similarly, group housing of the animals may also have affected our results, as this is a less stressful environment for the animals that may have led to our sham animals having lower systolic blood pressure.

The refined single-step flank STNx performed on 129S2/SV mice results in significant renal fibrosis, accompanied by histological hallmarks tubulointerstitial fibrosis (TIF) and glomerulosclerosis (GS) by 10-weeks post-surgery. Both TIF and GS are observed in CKD patients (Nakagawa et al., 2015), with TIF being an important predictor of disease progression (Nath, 1992). Increases in three collagen genes mirror what can be seen histologically. *Col1a1* and *Col3a1* encode fibrillar collagens (Delella et al., 2017) which are important extracellular

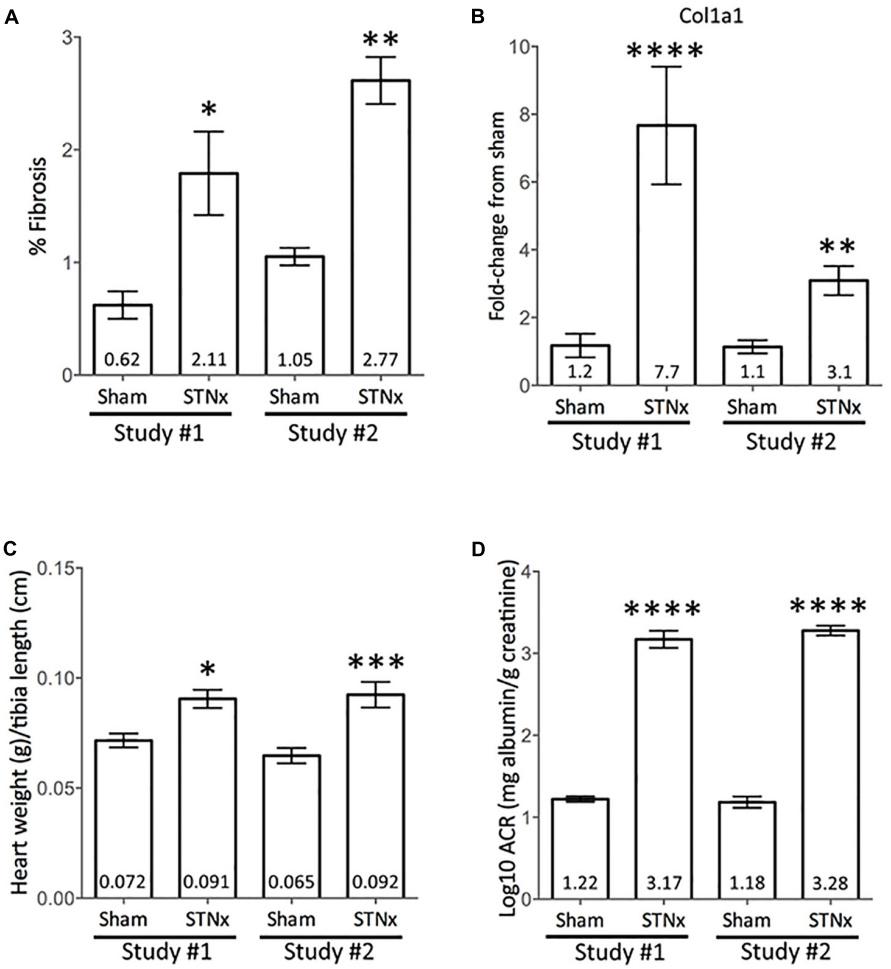

FIGURE 5 | Comparison between independent STNx studies conducted in male 129S2/SV mice. Male 129S2/SV mice (bought from Envigo) were subjected to STNx in two separate studies, 1.5 years apart (Study 1 – March 2017; Study 2 – September 2018). Plotted as mean ± SEM. **(A)** Quantification of picrosirius red stain for total renal collagen, via Image-Pro Plus. Study #1 Sham: $n = 7$, study #1 STNx: $n = 11$, Study #2 Sham: $n = 7$, study #2 STNx: $n = 6$. **(B)** Renal Col1a1 gene expression at 10-weeks post-surgery. Study #1 Sham: $n = 6$, study #1 STNx: $n = 10$, Study #2 Sham: $n = 8$, study #2 STNx: $n = 10$. **(C)** Heart weight normalized to tibia length at cull, 10-weeks post-surgery. Study #1 Sham: $n = 7$, study #1 STNx: $n = 11$, Study #2 Sham: $n = 8$, study #2 STNx: $n = 10$. **(D)** Log10 albumin:creatinine ratio (ACR) at 10-weeks post-surgery. Study #1 Sham: $n = 7$, Study #1 STNx: $n = 11$, Study #2 Sham: $n = 7$, study #2 STNx: $n = 8$. Statistical analysis carried out via ordinary one-way ANOVA with Tukey's multiple comparisons test. $^{*}P < 0.05$ vs. sham (same study), $^{**}P < 0.01$, $^{***}P < 0.001$, $^{****}P < 0.0001$.

matrix components (Nakagawa and Duffield, 2013). *Col4a1* is an important basement membrane component (Jones et al., 2016), suggesting possible basement membrane expansion in STNx kidneys. *Acta2* encodes α-smooth muscle actin, a marker of activated myofibroblasts, which increase in number in renal fibrosis (Bernard et al., 2014) and secrete excess extracellular matrix components (Bernard et al., 2014). The increased expression of miR-21 and miR-214 is of interest given the pro-fibrotic role these miRNAs are known to have in the kidney (Denby et al., 2014). Importantly, miR-21 and miR-214 have also been shown to be up-regulated in the kidneys of patients with CKD, indicating that the STNx model mimics the mechanisms that promote fibrosis in human disease (Lv et al., 2018). Taken together, increased expression of these genes and miRNAs in the kidney suggests a pro-fibrotic environment is present in the kidneys of mice subjected to STNx on both the histological and molecular level.

Gene expression of the cardiac hypertrophy marker ANP (Kerkelä et al., 2015; Riaz et al., 2015) was increased in hearts at both 6 and 10-weeks post-STNx whilst BNP (Kerkelä et al., 2015) was only significantly increased at 6-weeks. This coupled with the increased heart weight detected at 10-weeks post-STNx and increased average cardiac wall thickness and left-ventricular mass detected by ECHO at 10-weeks post-STNx suggests significant hypertrophy had taken place, although cardiac fibrosis had not manifested at the histological level at this time-point. However, no significant change in these measures was detected at 6-weeks post-STNx, indicating the development of this cardiac hypertrophy in the STNx model is time dependent. Prolonged isovolumic relaxation time (IV RT) was observed at 10-weeks

post-STNx (but not at 6-weeks), indicating diastolic dysfunction is present in these mice via impairment of myocardial relaxation (Schnelle et al., 2018). No significant decrease in ejection fraction was observed, indicating that adaptive measures taken by the heart to overcome the increased stress have been successful up until 10-weeks post-STNx. It is likely necessary to extend the timeline of the model past 10-weeks post-surgery in order to observe diastolic dysfunction and fibrosis.

The STNx model has been extensively reviewed from the point of heart-kidney interactions (Bongartz et al., 2012; Hewitson et al., 2015; Liu, 2019). A common comment in reviews of the literature is that in mice this model is highly variable if not uniformly performed and you can get conflicting results depending on the strain. Here we are able to present data which shows that in 129S2/SV male mice you can achieve reproducible physiological readouts using the single step STNx model described, with the added advantage of low mortality and improved animal welfare. The model is amenable to echocardiography studies which allow longitudinal studies of cardiac structure and function. Utilizing the 129S2/SV mouse also allows for the inflammatory cell profile to be examined in detail as multiple validated antibodies are available for mouse unlike rat.

Low grade inflammation is common in CKD patients (Amdur et al., 2016), with patients typically exhibiting elevated CRP, TNFα, and IL-6 levels (Panichi et al., 2001; Lacson and Levin, 2004). Furthermore, macrophage infiltration into the kidney in CKD has been found to correlate with a decline in kidney function (Eardley et al., 2006; Amdur et al., 2016). The analysis of the inflammatory cell content of the STNx mice revealed there is increased $CD45^+$ hematopoietic cell content in the STNx kidney and heart. The STNx model mimics the findings in human CKD of increased inflammation, with flow cytometry data demonstrating persistent $Ly6C^{hi}$ monocyte recruitment to the STNx kidney where they transition into pro-inflammatory macrophages. Previous work has identified a $CD11b^+$ $Ly6C^{hi}$ population to be induced with the onset of renal injury following ischemia reperfusion injury and unilateral ureteric obstruction (Lin et al., 2009; Clements et al., 2016). Importantly, in our study we excluded $Ly6G^+$ neutrophils and found that significantly more $CD45^+$ $Ly6G^-$ $CD11b^+$ $F4/80^{lo}$ cells express Ly6C. This population has been previously shown to have a pro-inflammatory gene signature (Clements et al., 2016), and promote fibrosis in other organs such as the liver (Ramachandran et al., 2012). Within the $CD45^+$ $CD11b^+$ $F4/80^{hi}$ resident macrophage population there was a significantly greater expression of CD206 (Mannose receptor 1, Mrc1). This C-type lectin is expressed predominantly by tissue macrophages and is involved in phagocytosis and acts as a scavenger receptor (Taylor et al., 2005). CD206 is classically thought of as an alternatively activated or M2 macrophage marker (Murray et al., 2014). The increase in the Mrc1 expression is confined to the resident macrophage population that may suggest that resident macrophages may play an important role in scavenging of debris and scar tissue. Hence, this STNx model in mice affords an opportunity in future studies to perform detailed mechanistic studies of the role of each immune cell subset in progressive CKD.

A number of refinements to traditional methods of undertaking subtotal nephrectomy were employed in the refined single-step STNx surgery used in this study with a key focus on animal welfare. One of the key differences between the surgical methods presented in this paper and the majority of previously published studies is the use of a single-surgery via flank incisions to perform both the nephrectomy and contralateral partial nephrectomy. Multiple papers have been published where nephrectomy is performed in one surgery, then 1–2 weeks later, resection of the poles or renal artery ligation is performed in a separate surgery (Kren and Hostetter, 1999; Ma and Fogo, 2003; Soler et al., 2008; Windt et al., 2008; Leelahavanichkul et al., 2010; Yang et al., 2010; Babelova et al., 2012; Gava et al., 2012; Li et al., 2012; Purnomo et al., 2013; Hyde et al., 2014; Ucero et al., 2014; Vavrinec et al., 2016; Rosendahl et al., 2018). Reducing the number of surgeries to which the mice are subjected, by performing the single-step STNx surgery has a number of benefits for animal welfare including: the animals undergo anesthesia on one less occasion, the length of time the mice are on-procedure is decreased, and requirement for analgesics is reduced. Our approach also avoids hypertrophy of the remaining kidney or remnant kidney (depending on the surgical order) between surgeries. Renal tissue during this phase could be argued to be in the "regenerative mode" and thus may be more resistant to the development of fibrosis which would not be present in this refined STNx model. Animal welfare in response to STNx was monitored weekly throughout the study using an animal condition scoring sheet (**Supplementary Table 1**), which included body condition scoring. A cumulative score of 5 or higher resulted in a mandatory schedule 1 termination of the animal. We found that group housing resulted in improved animal welfare scores, therefore group housing animals is recommended. Decreased weight and body condition score in mice is an important determinant of health status (Foltz and Ullman-Culleré, 1999; Ullman-Culleré and Foltz, 1999; Burkholder et al., 2012) and mice subjected to STNx were found not to differ in weight in comparison to sham animals at any time-point during the 10-weeks between surgery and sacrifice. In studies which use traditional two-step subtotal nephrectomy protocols, most (Leelahavanichkul et al., 2010; Gava et al., 2012; Zeng et al., 2018) but not all (Siedlecki et al., 2009), report a reduction in body weight with subtotal nephrectomized animals compared to sham controls. The lack of a difference in body weight may be due to this model inducing milder progressive renal disease as systolic blood pressure and ACRs were not significantly increased until 6-weeks post-surgery. However, this may also be in part due to improved animal welfare brought about by group housing. This study could have benefited from a side by side comparison with the traditional two-step STNx to fully demonstrate its advantages, however, the mortality rates for this surgery can be high and in a recent study shown to be 60% 4 weeks post-surgery (Tan et al., 2019). Therefore, in the interests of animal welfare it is not appropriate to run such a study.

The mortality following subtotal nephrectomy has been poorly reported in the literature, but is often high, for example 43% by 12-weeks post-surgery (Ma and Fogo, 2003). Other studies report no mortality but it is not clear if this included animals that either

did not develop significant renal dysfunction or were terminated prematurely due to animal welfare concerns. In our model in total 9% of animals did not complete the study due to a combination of mortality during follow-up ($n = 3$), exceeding animal welfare scoring limits ($n = 2$) or failure to recover from anesthetic ($n = 2$). These data suggest that the single-step STNx surgery is well-tolerated by the mice, although a small mortality rate needs to be factored into power calculations.

The subtotal nephrectomy is known to be a strain-dependent model. Both the 129S2/SV and CD1 strain have been reported to be permissive to injury (Ma and Fogo, 2003; Kennedy et al., 2008; Siedlecki et al., 2009; Leelahavanichkul et al., 2010). In our 129S2/SV mice no cardiac fibrosis was detected *per se* but on the gene expression level Collagen III was increased by 10-weeks post-surgery. Using the CD1 strain of mice, cardiac fibrosis can be induced with the added insult of additional dietary salt (Fontes et al., 2015) which may be required in this model too. In a pilot study in this genetic background, the refined STNx model resulted in significant renal fibrosis and increased pro-fibrotic gene expression in the kidney which matches that previously observed (Ma and Fogo, 2003). However, there were no functional alterations detectable, e.g., increased ACR or changes in heart weight. This indicates that STNx in C57BL/6 mice may not be the best pre-clinical model to test novel therapies where clinically relevant renal and cardiac outcomes are required. These results mirror the experience of other groups with subtotal nephrectomy in C57BL/6 mice (Ma and Fogo, 2003; Leelahavanichkul et al., 2010), with additional stimuli such as angiotensin II infusion required to produce hard renal outcomes (Leelahavanichkul et al., 2010). The resistance to development of albuminuria in the C57BL/6 mice is well-recognized, albumin overloaded 129S2/SV mice develop abundant albuminuria whereas C57BL/6 show none despite increased serum albumin (Ishola et al., 2006). The significant increase in fibrosis observed, however, suggests that for studies into renal fibrosis, the STNx model could be further utilized to understand the precise pathophysiology of progressive renal fibrosis using genetic knockout mice on the C57BL/6 genetic background.

Summary

Together, these data provide evidence that conducting the subtotal nephrectomy model with our refined protocol in male 129S2/SV mice results in renal dysfunction, renal inflammation, and fibrosis with systemic pathologies akin to what is observed in patients.

This model is also suitable for testing new therapies for CKD given its progressive nature, clinically relevant biochemical measurements and cardiac dysfunction. In addition, these therapies can be given with standard therapy of ACEi to examine physiological effects beyond those offered by blood pressure reduction alone.

C57BL/6 mice as previously reported are refractory to proteinuric renal dysfunction, blood pressure and cardiac changes but do develop significant renal fibrotic disease. Therefore, for pathophysiological studies of fibrosis the STNx model in C57BL/6 background may offer some insight when using genetic knockout models on this genetic background.

DATA AVAILABILITY STATEMENT

All datasets generated for this study are included in the article/**Supplementary Material**.

ETHICS STATEMENT

The animal study was reviewed and approved by University of Edinburgh Animal Welfare and Ethical Review Board.

AUTHOR CONTRIBUTIONS

JO'S contributed to the investigation, analysis, the writing and revising of the original draft of the manuscript. SF contributed to the investigation, analysis, the writing and editing of the original draft of the manuscript. OT and AB contributed to the investigation and analysis. CC contributed to the investigation, analysis, and the editing of the original draft of the manuscript. MB contributed to the analysis and the editing of revised manuscript. AT contributed to the investigation, methodology, and analysis of the study. JH contributed to the conceptualization and methodology of the study. CB contributed to the methodology, analysis, and the writing, the review and the editing of the manuscript. BC contributed to the conceptualization, methodology, analysis, and the writing, the review and the editing of the manuscript. LD contributed to the funding acquisition, supervision, conceptualization, project administration, methodology, investigation, analysis, the writing, the review and the editing original, and revised draft of the manuscript.

FUNDING

This study was funded by Medical Research Scotland 789_Ph.D._2014, Kidney Research UK Fellowships PDF6/2012, SF_001_20181122, and BBSRC Ph.D. studentship BB/R505638/1, and British Heart Foundation Ph.D. studentship FS/15/63/32033 awarded to LD.

ACKNOWLEDGMENTS

Thanks to Lorraine Bruce for urine osmolality measurements. Flow cytometry data was generated with support from the QMRI Flow Cytometry and Cell Sorting Facility, University of Edinburgh.

SUPPLEMENTARY MATERIAL

The Supplementary Material for this article can be found online at: https://www.frontiersin.org/articles/10.3389/fphys.2019.01365/full#supplementary-material

REFERENCES

Alicic, R. Z., Rooney, M. T., and Tuttle, K. R. (2017). Diabetic kidney disease: challenges, progress, and possibilities. *Clin. J. Am. Soc. Nephrol.* 12, 2032–2045. doi: 10.2215/CJN.11491116

Almeras, C., and Argilés, À (2009). The general picture of uremia. *Semin. Dial.* 22, 329–333. doi: 10.1111/j.1525-139X.2009.00575.x

Amdur, R. L., Feldman, H. I., Gupta, J., Yang, W., Kanetsky, P., Shlipak, M., et al. (2016). Inflammation and progression of CKD: the CRIC study. *Clin. J. Am. Soc. Nephrol.* 11, 1546–1556. doi: 10.2215/CJN.13121215

Anderson, S., Rennke, H. G., and Brenner, B. M. (1986). Therapeutic advantage of converting enzyme inhibitors in arresting progressive renal disease associated with systemic hypertension in the rat. *J. Clin. Invest.* 77, 1993–2000. doi: 10.1172/jci112528

Babelova, A., Avaniadi, D., Jung, O., Fork, C., Beckmann, J., Kosowski, J., et al. (2012). Role of Nox4 in murine models of kidney disease. *Free Radic. Biol. Med.* 53, 842–853. doi: 10.1016/j.freeradbiomed.2012.06.027

Bai, M., Chen, H., Ding, D., Song, R., Lin, J., Zhang, Y. Y., et al. (2019). MicroRNA-214 promotes chronic kidney disease by disrupting mitochondrial oxidative phosphorylation. *Kidney Int.* 95, 1–16. doi: 10.1016/j.kint.2018.12.028

Bain, C. C., Hawley, C. A., Garner, H., Scott, C. L., Schridde, A., Steers, N. J., et al. (2016). Long-lived self-renewing bone marrow-derived macrophages displace embryo-derived cells to inhabit adult serous cavities. *Nat. Commun.* 7:ncomms11852. doi: 10.1038/ncomms11852

Bernard, M., Dieude, M., Yang, B., Hamelin, K., Underwood, K., and Hebert, M.-J. (2014). Autophagy fosters myofibroblast differentiation through MTORC2 activation and downstream upregulation of CTGF. *Autophagy* 10, 2193–2207. doi: 10.4161/15548627.2014.981786

Bongartz, L. G., Braam, B., Gaillard, C. A., Cramer, M. J., Goldschmeding, R., Verhaar, M. C., et al. (2012). Target organ cross talk in cardiorenal syndrome: animal models. *Am. J. Physiol. Ren. Physiol.* 303, 1253–1263. doi: 10.1152/ajprenal.00392.2012

Boor, P., Ostendorf, T., and Floege, J. (2010). Renal fibrosis: novel insights into mechanisms and therapeutic targets. *Nat. Rev. Nephrol.* 6, 643–656. doi: 10.1038/nrneph.2010.120

Burkholder, T., Foltz, C., Karlsson, E., Linton, C. G., and Smith, J. M. (2012). Health evaluation of experimental laboratory mice. *Curr. Protoc. Mouse Biol.* 2, 145–165. doi: 10.1002/9780470942390.mo110217

Chatzimanouil, M. K. T., Wilkens, L., and Anders, H.-J. (2018). Quantity and reporting quality of kidney research. *J. Am. Soc. Nephrol.* 30, 13–22. doi: 10.1681/ASN.2018050515

Chau, B. N., Xin, C., Hartner, J., Ren, S., Castano, A. P., Linn, G., et al. (2012). MicroRNA-21 promotes fibrosis of the kidney by silencing metabolic pathways. *Sci. Transl. Med.* 4:121ra18. doi: 10.1126/scitranslmed.3003205

Clements, M., Gershenovich, M., Chaber, C., Campos-Rivera, J., Du, P., Zhang, M., et al. (2016). Differential Ly6C expression after renal ischemia-reperfusion identifies unique macrophage populations. *J. Am. Soc. Nephrol.* 27, 159–170. doi: 10.1681/ASN.2014111138

Delella, F. K., de Almeida, F. L. A., Nunes, H. C., Rinaldi, J. C., and Felisbino, S. L. (2017). Fibrillar collagen genes are not coordinately upregulated with TGF β1 expression in finasteride-treated prostate. *Cell Biol. Int.* 41, 1214–1222. doi: 10.1002/cbin.10787

Denby, L., Ramdas, V., Lu, R., Conway, B. R., Grant, J. S., Dickinson, B., et al. (2014). MicroRNA-214 antagonism protects against renal fibrosis. *J. Am. Soc. Nephrol.* 25, 65–80. doi: 10.1681/ASN.2013010072

Denby, L., Ramdas, V., McBride, M. W., Wang, J., Robinson, H., McClure, J., et al. (2011). miR-21 and miR-214 are consistently modulated during renal injury in rodent models. *Am. J. Pathol.* 179, 661–672. doi: 10.1016/j.ajpath.2011.04.021

Di, L., Andrew, L., Antonio, H., Santoboni, A., Russo, D., and Ronco, C. (2015). Chronic kidney disease and cardiovascular complications. *Hear. Fail Rev.* 20, 259–272.

Dilauro, M., Zimpelmann, J., Robertson, S. J., Genest, D., and Burns, K. D. (2010). Effect of ACE2 and angiotensin-(1–7) in a mouse model of early chronic kidney disease. *Am J Physiol Ren. Physiol.* 298, F1523–F1532. doi: 10.1152/ajprenal.00426.2009

Eardley, K. S., Zehnder, D., Quinkler, M., Lepenies, J., Bates, R. L., Savage, C. O., et al. (2006). The relationship between albuminuria, MCP-1/CCL2, and interstitial macrophages in chronic kidney disease. *Kidney Int.* 69, 1189–1197. doi: 10.1038/sj.ki.5000212

Eckardt, K., Coresh, J., Devuyst, O., Johnson, R. J., Levey, A. S., and Levin, A. (2013). Evolving importance of kidney disease: from subspecialty to global health burden. *Lancet* 382, 158–169. doi: 10.1016/S0140-6736(13)60439-0

Feldman, H. I., Peralta, C. A., Inker, L. A., Lash, J. P., Fox, C. H., Kurella Tamura, M., et al. (2014). KDOQI US commentary on the 2012 KDIGO clinical practice guideline for the evaluation and management of CKD. *Am. J. Kidney Dis.* 63, 713–735. doi: 10.1053/j.ajkd.2014.01.416

Felsenfeld, A. J., Levine, B. S., and Rodriguez, M. (2015). Pathophysiology of calcium, phosphorus, and magnesium dysregulation in chronic kidney disease. *Semin. Dial.* 28, 564–577. doi: 10.1111/sdi.12411

Foltz, C. J., and Ullman-Culleré, M. (1999). Guidelines for assessing the health and condition of mice. *Lab. Anim.* 28, 28–32.

Fontes, M. S. C., Papazova, D. A., Van Koppen, A., De Jong, S., Korte, S. M., Bongartz, L. G., et al. (2015). Arrhythmogenic remodeling in murine models of deoxycorticosterone acetate-salt-induced and 5/6-subtotal nephrectomy-salt-induced cardiorenal disease. *CardioRenal Med.* 5, 208–218. doi: 10.1159/000430475

Gao, S., Ho, D., Vatner, D. E., and Vatner, S. F. (2011). Murine echocardiography. *Curr. Protoc. Mouse Biol.* 1, 71–83. doi: 10.1002/9780470942390.mo100130

Gava, A. L., Freitas, F. P., Balarini, C. M., Vasquez, E. C., and Meyrelles, S. S. (2012). Effects of 5/6 nephrectomy on renal function and blood pressure in mice. *Int. J. Physiol. Pathophysiol. Pharmacol.* 4, 167–173.

Gewin, L., Zent, R., and Pozzi, A. (2017). Progression of chronic kidney disease: too much cellular talk causes damage. *Kidney Int.* 91, 552–560. doi: 10.1016/j.kint.2016.08.025

Gewin, L. S. (2018). Renal fibrosis: primacy of the proximal tubule. *Matrix Biol.* 6, 248–262. doi: 10.1016/j.matbio.2018.02.006

Gomez, I. G., Mackenna, D. A., Johnson, B. G., Kaimal, V., Roach, A. M., Ren, S., et al. (2015). Anti–microRNA-21 oligonucleotides prevent Alport nephropathy progression by stimulating metabolic pathways. *J. Clin. Invest.* 125, 141–156. doi: 10.1172/jci75852

Gosmanova, E. O., and Kovesdy, C. P. (2016). Blood pressure targets in CKD: lessons learned from sprint and previous observational studies. *Curr. Cardiol. Rep.* 18:88. doi: 10.1007/s11886-016-0769-y

Heerspink, H. J. L., and Gansevoort, R. T. (2015). Albuminuria Is an appropriate therapeutic target in patients with CKD: the pro view. *Clin. J. Am. Soc. Nephrol.* 10, 1079–1088. doi: 10.2215/CJN.11511114

Hennino, M.-F., Buob, D., Van der Hauwaert, C., Gnemmi, V., Jomaa, Z., Pottier, N., et al. (2016). miR-21-5p renal expression is associated with fibrosis and renal survival in patients with IgA nephropathy. *Sci. Rep.* 6:27209. doi: 10.1038/srep27209

Hewitson, T. D. (2009). Renal tubulointerstitial fibrosis: common but never simple. *Am. J. Physiol. Ren. Physiol.* 296, F1239–F1244. doi: 10.1152/ajprenal.90521.2008

Hewitson, T. D., Holt, S. G., and Smith, E. R. (2015). Animal models to study links between cardiovascular disease and renal failure and their relevance to human pathology. *Front. Immunol.* 6:465. doi: 10.3389/fimmu.2015.00465

Hewitson, T. D., Holt, S. G., and Smith, E. R. (2017). Progression of tubulointerstitial fibrosis and the chronic kidney disease phenotype - role of risk factors and epigenetics. *Front. Pharmacol.* 8:520. doi: 10.3389/fphar.2017.00520

Hill, N. R., Fatoba, S. T., Oke, J. L., Hirst, J. A., O'Callaghan, C. A., Lasserson, D. S., et al. (2016). Global prevalence of chronic kidney disease – a systematic review and meta-analysis. *PLoS One* 6:e0158765. doi: 10.1371/journal.pone.0158765

Horowitz, B., Miskulin, D., and Zager, P. (2015). Epidemiology of hypertension in CKD. *Adv. Chronic Kidney Dis.* 22, 88–95. doi: 10.1053/j.ackd.2014.09.004

Hyde, G. D., Taylor, R. F., Ashton, N., Borland, S. J., Wu, H. S. G., Gilmore, A. P., et al. (2014). Axl tyrosine kinase protects against tubulo-interstitial apoptosis and progression of renal failure in a murine model of chronic kidney disease and hyperphosphataemia. *PLoS One* 9:e102096. doi: 10.1371/journal.pone.0102096

Ishola, D. A., van der Giezen, D. M., Hahnel, B., Goldschmeding, R., Kriz, W., Koomans, H. A., et al. (2006). In mice, proteinuria and renal inflammatory responses to albumin overload are strain-dependent. *Nephrol. Dial. Transplant.* 21, 591–597. doi: 10.1093/ndt/gfi303

Ito, K., Chen, J., El Chaar, M., Stern, J. M., Seshan, S. V., Khodadadian, J. J., et al. (2004). Renal damage progresses despite improvement of renal function after

relief of unilateral ureteral obstruction in adult rats. *Am. J. Physiol. Ren. Physiol.* 287, F1283–F1293.

Jha, V., Garcia-Garcia, G., Iseki, K., Li, Z., Naicker, S., Plattner, B., et al. (2013). Chronic kidney disease: global dimension and perspectives. *Lancet* 382, 260–272. doi: 10.1016/S0140-6736(13)60687-X

Jones, F. E., Bailey, M. A., Murray, L. S., Lu, Y., Mcneilly, S., Lennon, R., et al. (2016). ER stress and basement membrane defects combine to cause glomerular and tubular renal disease resulting from Col4a1 mutations in mice. *Dis. Model. Mech.* 9, 165–176. doi: 10.1242/dmm.021741

Jörres, A., Lemke, H. D., Henle, T., Descamps-Latscha, B., De Smet, R., Glorieux, G., et al. (2004). Review on uremic toxins: classification, concentration, and interindividual variability. *Kidney Int.* 63, 1934–1943. doi: 10.1046/j.1523-1755.2003.00924.x

Kennedy, D. J., Elkareh, J., Shidyak, A., Shapiro, A. P., Smaili, S., Mutgi, K., et al. (2008). Partial nephrectomy as a model for uremic cardiomyopathy in the mouse. *Am. J. Physiol. Ren. Physiol.* 294, F450–F454.

Kerkelä, R., Ulvila, J., and Magga, J. (2015). Natriuretic peptides in the regulation of cardiovascular physiology and metabolic events. *J. Am. Heart Assoc.* 4, 1–13.

Kerr, M., Bray, B., Medcalf, J., O'Donoghue, D. J., and Matthews, B. (2012). Estimating the financial cost of chronic kidney disease to the NHS in England. *Nephrol. Dial. Transplant.* 27(Suppl. 3):iii73-80. doi: 10.1093/ndt/gfs269

Kramann, R., Schneider, R. K., Dirocco, D. P., Machado, F., Fleig, S., Bondzie, P. A., et al. (2015). Perivascular Gli1+ progenitors are key contributors to injury-induced organ fibrosis. *Cell Stem Cell* 16, 51–66. doi: 10.1016/j.stem.2014.11.004

Kren, S., and Hostetter, T. H. (1999). The course of the remnant kidney model in mice. *Kidney Int.* 56, 333–337. doi: 10.1046/j.1523-1755.1999.00527.x

Lacson, E., and Levin, N. (2004). C-reactive protein and end-stage renal disease. *Semin. Dial.* 17, 438–448.

Lau, W. L., and Vaziri, N. D. (2016). Urea, a true uremic toxin: the empire strikes back. *Clin. Sci.* 131, 3–12. doi: 10.1042/cs20160203

Leelahavanichkul, A., Yan, Q., Hu, X., Eisner, C., Huang, Y., Chen, R., et al. (2010). Angiotensin II overcomes strain-dependent resistance of rapid CKD progression in a new remnant kidney mouse model. *Kidney Int.* 78, 1136–1153. doi: 10.1038/ki.2010.287

Levey, A. S., Inker, L. A., and Coresh, J. (2014). GFR estimation: from physiology to public health. *Am. J. Kidney Dis.* 63, 820–834. doi: 10.1053/j.ajkd.2013.12.006

Li, K. L., He, Y. N., Chen, J., Zhan, J., Li, Z. H., and Zhao, L. (2012). P53 negatively regulates the osteogenic differentiation of vascular smooth muscle cells in mice with chronic kidney disease. *Cardiovasc. J. Afr.* 23, e1–e9. doi: 10.5830/CVJA-2011-069

Lin, G. H. Y., Sedgmen, B. J., Moraes, T. J., Snell, L. M., Topham, D. J., and Watts, T. H. (2009). Endogenous 4-1BB ligand plays a critical role in protection from influenza-induced disease. *J. Immunol.* 182, 934–947. doi: 10.4049/jimmunol.182.2.934

Lindsey, M. L., Kassiri, Z., Virag, J. A. I., de Castro Brás, L. E., and Scherrer-Crosbie, M. (2018). Guidelines for measuring cardiac physiology in mice. *Am. J. Physiol. Circ. Physiol.* 314, H733–H752. doi: 10.1152/ajpheart.00339.2017

Liu, S. (2019). Heart-kidney interactions: mechanistic insights from animal models. *Am. J. Physiol. Ren. Physiol.* 316, F974–F985. doi: 10.1152/ajprenal.00624.2017

Locatelli, F., Cannata-Andia, J. B., Drueke, T. B., Horl, W. H., Fouque, D., Heimburger, O., et al. (2002). Management of disturbances of calcium and phosphate metabolism in chronic renal insufficiency, with emphasis on the control of hyperphosphataemia. *Nephrol. Dial. Transplant.* 17, 723–731. doi: 10.1093/ndt/17.5.723

Lv, W., Fan, F., Wang, Y., Gonzalez-Fernandez, E., Wang, C., Yang, L., et al. (2018). Therapeutic potential of microRNAs for the treatment of renal fibrosis and CKD. *Physiol. Genom.* 50, 20–34. doi: 10.1152/physiolgenomics.00039.2017

Ma, L.-J., and Fogo, A. B. (2003). Model of robust induction of glomerulosclerosis in mice: importance of genetic background. *Kidney Int.* 64, 350–355. doi: 10.1046/j.1523-1755.2003.00058.x

Mack, M., and Yanagita, M. (2015). Origin of myofibroblasts and cellular events triggering fibrosis. *Kidney Int.* 87, 297–307. doi: 10.1038/ki.2014.287

Martin, K. J., and González, E. A. (2011). Prevention and control of phosphate retention/ hyperphosphatemia in CKD-MBD: what is normal, when to start, and how to treat? *Clin. J. Am. Soc. Nephrol.* 6, 440–446. doi: 10.2215/CJN.05130610

Meyer, T. W., Anderson, S., Rennke, H. G., and Brenner, B. M. (1985). Converting enzyme inhibitor therapy limits progressive glomerular injury in rats with renal insufficiency. *Am. J. Med.* 79, 31–36. doi: 10.1016/0002-9343(85)90077-4

Murray, P. J., Allen, J. E., Biswas, S. K., Fisher, E. A., Gilroy, D. W., Goerdt, S., et al. (2014). Macrophage activation and polarization: nomenclature and experimental guidelines. *Immunity* 41, 14–20. doi: 10.1016/j.immuni.2014.06.008

Nakagawa, N., and Duffield, J. S. (2013). Myofibroblasts in fibrotic kidneys. *Curr. Pathobiol. Rep.* 1, 189–198. doi: 10.1007/s40139-013-0025-8

Nakagawa, S., Nishihara, K., Miyata, H., Shinke, H., Tomita, E., Kajiwara, M., et al. (2015). Molecular markers of tubulointerstitial fibrosis and tubular cell damage in patients with chronic kidney disease. *PLoS One* 10:e0136994. doi: 10.1371/journal.pone.0136994

Nath, K. A. (1992). Tubulointerstitial changes as a major determinant in the progression of renal damage. *Am. J. Kidney Dis.* 20, 1–17. doi: 10.1016/s0272-6386(12)80312-x

Obrador, G. T., and Levin, A. (2019). CKD hotspots: challenges and areas of opportunity. *Semin. Nephrol.* 39, 308–314. doi: 10.1016/j.semnephrol.2019.02.009

Oosterhuis, N. R., Papazova, D. A., Gremmels, H., Joles, J. A., and Verhaar, M. C. (2017). T-cells contribute to hypertension but not to renal injury in mice with subtotal nephrectomy. *BMC Nephrol.* 18:153. doi: 10.1186/s12882-017-0555-0

Panichi, V., Migliori, M., De Pietro, S., Taccola, D., Bianchi, A. M., Norpoth, M., et al. (2001). C reactive protein in patients with chronic renal diseases. *Ren. Fail.* 23, 551–562. doi: 10.1081/jdi-100104737

Perkins, B. A., Ficociello, L. H., Ostrander, B. E., Silva, K. H., Weinberg, J., Warram, J. H., et al. (2007). Microalbuminuria and the risk for early progressive renal function decline in type 1 diabetes. *J. Am. Soc. Nephrol.* 18, 1353–1361. doi: 10.1681/asn.2006080872

Peters, R., Staessen, J. A., Cheung, A. K., Beckett, N., Nadkarni, G. N., Mant, J., et al. (2017). Association between more intensive vs less intensive blood pressure lowering and risk of mortality in chronic kidney disease stages 3 to 5. *JAMA Intern. Med.* 177:1498. doi: 10.1001/jamainternmed.2017.4377

Purnomo, E., Emoto, N., Nugrahaningsih, D. A. A., Nakayama, K., Yagi, K., Heiden, S., et al. (2013). Glycosaminoglycan overproduction in the aorta increases aortic calcification in murine chronic kidney disease. *J. Am. Heart Assoc.* 2, 1–18. doi: 10.1161/JAHA.113.000405

Ramachandran, P., Pellicoro, A., Vernon, M. A., Boulter, L., Aucott, R. L., Ali, A., et al. (2012). Differential Ly-6C expression identifies the recruited macrophage phenotype, which orchestrates the regression of murine liver fibrosis. *Proc. Natl. Acad. Sci. U.S.A.* 109, E3186–E3195. doi: 10.1073/pnas.1119964109

Rambausek, M., Ritz, E., Mall, G., Mehls, O., and Katus, H. (1985). Myocardial hypertrophy in rats with renal insufficiency. *Kidney Int.* 28, 775–782. doi: 10.1038/ki.1985.197

Respress, J. L., and Wehrens, X. H. T. (2010). Transthoracic echocardiography in mice. *J. Vis. Exp.* 39:1738. doi: 10.3791/1738

Riaz, N., Wolden, S. L., Gelblum, D. Y., and Eric, J. (2015). Atrial natriuretic peptide in cardiovascular biology and disease (NPPA). *Gene* 569, 1–6. doi: 10.1016/j.gene.2015.06.029

Ritter, C. S., and Slatopolsky, E. (2016). Phosphate toxicity in CKD: the killer among us. *Clin. J. Am. Soc. Nephrol.* 11, 1088–1100. doi: 10.2215/CJN.11901115

Rosendahl, A., Kabiri, R., Bode, M., Cai, A., Klinge, S., Ehmke, H., et al. (2018). Adaptive immunity and IL-17A are not involved in the progression of chronic kidney disease after 5/6 nephrectomy in mice. *Br. J. Pharmacol.* 176, 2002–2014. doi: 10.1111/bph.14509

Schelling, J. R. (2016). Tubular atrophy in the pathogenesis of chronic kidney disease progression. *Pediatr. Nephrol.* 31, 693–706. doi: 10.1007/s00467-015-3169-4

Schnelle, M., Catibog, N., Zhang, M., Nabeebaccus, A. A., Anderson, G., Richards, D. A., et al. (2018). Echocardiographic evaluation of diastolic function in mouse models of heart disease. *J. Mol. Cell. Cardiol.* 114, 20–28. doi: 10.1016/j.yjmcc.2017.10.006

Siedlecki, A. M., Jin, X., and Muslin, A. J. (2009). Uremic cardiac hypertrophy is reversed by rapamycin but not by lowering of blood pressure. *Kidney Int.* 75, 800–808. doi: 10.1038/ki.2008.690

Soler, M. J., Wysocki, J., and Batlle, D. (2008). Angiotensin-converting enzyme 2 and the kidney. *Exp. Physiol.* 93, 549–556.

Song, S., Meyer, M., Türk, T. R., Wilde, B., Feldkamp, T., Assert, R., et al. (2009). Serum cystatin C in mouse models: a reliable and precise marker for renal function and superior to serum creatinine. *Nephrol. Dial. Transplant.* 24, 1157–1161. doi: 10.1093/ndt/gfn626

Stevens, P. E., and Levin, A. (2013). Evaluation and management of chronic kidney disease: synopsis of the kidney disease: improving global outcomes 2012 clinical practice guideline. *Ann. Intern. Med.* 158, 825–830. doi: 10.7326/0003-4819-158-11-201306040-00007

Tan, R. Z., Zhong, X., Li, J. C., Zhang, Y. W., Yan, Y., Liao, Y., et al. (2019). An optimized 5/6 nephrectomy mouse model based on unilateral kidney ligation and its application in renal fibrosis research. *Ren. Fail.* 41, 555–566. doi: 10.1080/0886022X.2019.1627220

Taylor, P. R., Martinez-Pomares, L., Stacey, M., Lin, H.-H., Brown, G. D., and Gordon, S. (2005). Macrophage receptors and immune recognition. *Annu. Rev. Immunol.* 23, 901–944. doi: 10.1146/annurev.immunol.23.021704.115816

Ucero, A. C., Benito-Martin, A., Izquierdo, M. C., Sanchez-Niño, M. D., Sanz, A. B., Ramos, A. M., et al. (2014). Unilateral ureteral obstruction: beyond obstruction. *Int. Urol. Nephrol.* 46, 765–776. doi: 10.1007/s11255-013-0520-1

Ullman-Culleré, M. H., and Foltz, C. J. (1999). Body condition scoring: a rapid and accurate method for assessing health status in mice. *Lab. Anim. Sci.* 49, 319–323.

Vanholder, R., Gryp, T., and Glorieux, G. (2018). Urea and chronic kidney disease: the comeback of the century? (in uraemia research). *Nephrol. Dial. Transplant.* 33, 4–12. doi: 10.1093/ndt/gfx039

Vassalotti, J. A., Centor, R., Turner, B. J., Greer, R. C., Choi, M., and Sequist, T. D. (2016). Practical approach to detection and management of chronic kidney disease for the primary care clinician. *Am. J. Med.* 129:153-162.e7. doi: 10.1016/j.amjmed.2015.08.025

Vavrinec, P., Buikema, H., Vettoretti, S., Deelman, L. E., De Zeeuw, D., Henning, R. H., et al. (2016). Renal endothelial function is associated with the anti-proteinuric effect of ACE inhibition in 5/6 nephrectomized rats. *Am. J. Physiol. Physiol.* 310, F1047–F1053. doi: 10.1152/ajprenal.00325.2015

Venkatachalam, M. A., Weinberg, J. M., Kriz, W., and Bidani, A. K. (2015). Failed tubule recovery, AKI-CKD transition, and kidney disease progression. *J. Am. Soc. Nephrol.* 26, 1765–1776. doi: 10.1681/ASN.2015010006

Vervloet, M. G., Sezer, S., Massy, Z. A., Johansson, L., Cozzolino, M., and Fouque, D. (2017). The role of phosphate in kidney disease. *Nat. Rev. Nephrol.* 13, 27–38. doi: 10.1038/nrneph.2016.164

Waheed, S., Matsushita, K., Sang, Y., Hoogeveen, R., Ballantyne, C., Coresh, J., et al. (2012). Combined association of albuminuria and cystatin C-based estimated GFR with mortality, coronary heart disease, and heart failure outcomes: the atherosclerosis risk in communities (ARIC) study. *Am. J. Kidney Dis.* 60, 207–216. doi: 10.1053/j.ajkd.2012.03.011

Wang, Y., Thatcher, S. E., and Cassis, L. (2017). Measuring blood pressure using a noninvasive tail cuff method in mice. *Methods Mol. Biol.* 1614, 69–73. doi: 10.1007/978-1-4939-7030-8_6

Webster, A. C., Nagler, E. V., Morton, R. L., and Masson, P. (2017). Chronic kidney disease. *Lancet* 389, 1238–1252. doi: 10.1016/S0140-6736(16)32064-5

Windt, W. A. K. M., van Dokkum, R. P. E., Kluppel, C. A., Jeronimus-Stratingh, C. M., Hut, F., de Zeeuw, D., et al. (2008). Therapeutic resistance to angiotensin converting enzyme (ACE) inhibition is related to pharmacodynamic and -kinetic factors in 5/6 nephrectomized rats. *Eur. J. Pharmacol.* 580, 231–240. doi: 10.1016/j.ejphar.2007.10.060

Yang, H.-C., Zuo, Y., and Fogo, A. B. (2010). Models of chronic kidney disease. *Drug Discov. Today Dis. Model.* 7, 13–19.

Zeng, L., Mathew, A. V., Byun, J., Atkins, K. B., Brosius, F. C., and Pennathur, S. (2018). Myeloperoxidase-derived oxidants damage artery wall proteins in an animal model of chronic kidney disease–accelerated atherosclerosis. *J. Biol. Chem.* 293, 7238–7249. doi: 10.1074/jbc.ra117.000559

Conflict of Interest: LD is an awardee and JO'S is a recipient of an MRS Ph.D. studentship co-funded by Regulus Therapeutics. Regulus Therapeutics had no input on the studies contained in this manuscript.

The remaining authors declare that the research was conducted in the absence of any commercial or financial relationships that could be construed as a potential conflict of interest.

Copyright © 2019 O'Sullivan, Finnie, Teenan, Cairns, Boyd, Bailey, Thomson, Hughes, Bénézech, Conway and Denby. This is an open-access article distributed under the terms of the Creative Commons Attribution License (CC BY). The use, distribution or reproduction in other forums is permitted, provided the original author(s) and the copyright owner(s) are credited and that the original publication in this journal is cited, in accordance with accepted academic practice. No use, distribution or reproduction is permitted which does not comply with these terms.

frontiers in Physiology

OPINION
published: 21 November 2019
doi: 10.3389/fphys.2019.01403

Heat Strain, External Workload, and Chronic Kidney Disease in Tropical Settings: Are Endurance Athletes Exposed?

Daniel Rojas-Valverde[1,2*†], *Guillermo Olcina*[2], *Randall Gutiérrez-Vargas*[1] and *Jennifer Crowe*[3]

[1] Centro de Investigación y Diagnóstico en Salud y Deporte, Escuela Ciencias del Movimiento Humano y Calidad de Vida, Universidad Nacional, Heredia, Costa Rica, [2] Grupo en Avances en el Entrenamiento Deportivo y Acondicionamiento Físico (GAEDAF), Facultad Ciencias del Deporte, Universidad de Extremadura, Cáceres, Spain, [3] Instituto Regional de Estudios en Sustancias Tóxicas (IRET), Universidad Nacional, Heredia, Costa Rica

OPEN ACCESS

Edited by:
Xueying Zhao,
Morehouse School of Medicine,
United States

Reviewed by:
Yue Zhang,
Nanjing Medical University, China

***Correspondence:**
Daniel Rojas-Valverde
drojasv@hotmail.com

†ORCID:
Daniel Rojas-Valverde
orcid.org/0000-0002-0717-8827

Specialty section:
This article was submitted to Renal and Epithelial Physiology, a section of the journal Frontiers in Physiology

Received: 30 September 2019
Accepted: 31 October 2019
Published: 21 November 2019

Citation:
Rojas-Valverde D, Olcina G, Gutiérrez-Vargas R and Crowe J (2019) Heat Strain, External Workload, and Chronic Kidney Disease in Tropical Settings: Are Endurance Athletes Exposed? Front. Physiol. 10:1403. doi: 10.3389/fphys.2019.01403

Keywords: sport, physical endurance, heat strain, acute kidney injury, running

INTRODUCTION

Tropical regions are currently facing a great challenge regarding very high prevalence of chronic kidney disease (CKD). In recent years, a condition called chronic kidney disease of unknown etiology (CKDu), also called CKD of non-traditional origin (CKDnt) or Mesoamerican Nephropathy has been reported (Wesseling et al., 2013, 2015; Wegman et al., 2015). This renal condition has been clearly documented in several so-called hot spots around the globe, typically in low-altitude communities near the western coast of the American continent. Though CKDu presents as typical CKD (Jha et al., 2013), CKDu patients do not present typical risk factors such as obesity, advanced age, hypertension, or diabetes. Instead, they tend to be young, otherwise healthy individuals that often live and work where dehydration and high internal and external physical loads are common. Although the etiology of the disease remains unclear (González-Quiroz et al., 2018; Chapman et al., 2019; Pearce and Caplin, 2019), most researchers agree that CKDu etiology is likely multifactorial and that chronic heat exposure, high external workload, and dehydration are associated with the disease (Wegman et al., 2015; Kupferman et al., 2018). Until now, CKDu in Mesoamerica has been studied mostly in agricultural populations (Crowe et al., 2013, 2015; García-Trabanino et al., 2015; Laws et al., 2016; Wesseling et al., 2016; Butler-Dawson et al., 2018; Kupferman et al., 2018).

Recently, the possibility of elevated rates of CKD in other populations exposed to high external heat and heavy internal heat loads from work/exercise has been raised. These populations could include endurance athletes (Eichner, 2017) in sports such as running, cycling, triathlon, open swimming, adventure races, and other long-duration disciplines. Such athletes usually undertake tremendous physical effort under high heat and humidity during a large number of hours and even consecutive days in multi-stage events in tropical settings (Gutiérrez-Vargas et al., 2018; McDermott et al., 2018; Rojas-Valverde, 2019). Although there are clear differences between CKDu occupational populations and athletes including socio-economic levels, non-optimal working conditions, poor access to health services, lack of recovery time, and low educational levels, there are notable environmental and contextual similarities between both populations.

Since people living and working in agricultural communities often face a wide range of social-economic determinants of health and are exposed to wide variety agents that could feasibly be on the etiologic pathway to CKDu, methodologies to study the effect of heat load on the kidney are complex. The athletes who participate in endurance events represent a privileged sample that could allow the isolation of factors that lead to CKD and provide insights into how external workload, dehydration and heat strain could contribute to the development of adverse renal conditions in athletes as well as populations in more vulnerable populations.

The existing evidence between heat exposure and CKDu in addition to imminent changes in temperature due to global warming have already prompted the question of whether athletes might also be at risk for kidney damage (Eichner, 2017). The sum of external workload and internal factors leading to thermal strain is of great concern, particularly when environmental temperature exceeds normal body temperature. The effect of high thermal stress (e.g., rise in internal temperature, heat loss restriction due to high humidity, and other factors) on the health and performance of athletes has been previously reported (Che Muhamed et al., 2016; Gutiérrez-Vargas et al., 2018; McDermott et al., 2018; Omassoli et al., 2019). Although these conditions are similar to those presented by populations in which CKDu has been diagnosed (see **Figure 1**). AKI leading to CKD has not been directly related to sports practice. However, there is evidence about increasing cases of acute kidney injury (AKI) in endurance sports related to external workload, heat and dehydration (Junglee et al., 2013; Hou et al., 2015; Kao et al., 2015; Bongers et al., 2018), although there remains a lack of information about whether AKI in sports could lead to CKD.

Recently, it has been shown that the practice of endurance sports can cause exertional rhabdomyolysis conditions (Hoffman et al., 2012; Kim et al., 2015), and that this can trigger transitional AKI (Boulter et al., 2011; Chlíbková et al., 2015; Hoffman and Weiss, 2016) due to the release of sarcoplasmic proteins into the bloodstream as a consequence of damage and disintegration of striated muscle during strenuous physical exertion (Bosch et al., 2009; Tietze and Borchers, 2014; Olcina et al., 2018). The preferred biomarkers to diagnose both conditions are serum creatinine and cystatin C levels for kidney function and creatine kinase and lactate dehydrogenase for muscle damage. According to the RIFLE (Risk, Injury, Failure, Loss of Kidney Function, and End-stage kidney disease) categorization, a risk of renal injury exists when serum creatinine (S-Cr) increases 1.5 times; a lesion when S-Cr 2 times, and failure when the S-Cr increases 3 times or values >4 mg/dL (Bellomo et al., 2004). Another classification system, the Acute Kidney Injury Network (AKIN) classification considers AKI to occur when at least one of the following conditions are met in the last 48 h: (a) absolute increase of ≥0.3 mg/dL, (b) increase of 1.5 times above the baseline, or (3) oliguria (urination <0.5 mL/kg per hour per >6 h) (Lopes and Jorge, 2013). In addition, other biomarkers have been recently proposed in order to differentiate functional and subclinical AKI as: cystatin-C, serum albumin, neutrophil gelatinase-associated lipocalin, and kidney injury molecule 1 (McCullough et al., 2013).

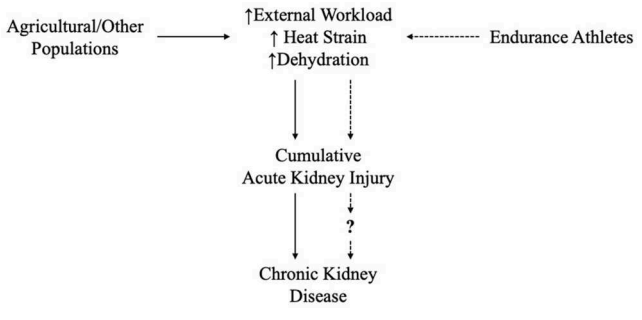

FIGURE 1 | Chronic Kidney Disease common risk factors between agricultural populations and endurance athletes in tropical settings. Dotted line flow needs more longitudinal research and evidence.

Athletes experiencing AKI according to these definitions have been documented to regain baseline renal function in a matter of 1–15 days (Kim et al., 2015; Abbas et al., 2019; Rojas-Valverde et al., 2019), however, documentation also exists of more serious consequences, leading to the death of the athlete in combination to other potential risks (Asserraji et al., 2014). Due to the lack of information about whether the repeated AKI can lead to future CKD (Hoffman and Weiss, 2016), there is a need for studies that shed light on the potential of the combination of environment and physical thermal load in athletes to trigger future CKD, especially in tropical settings, where conditions of high thermal stress exist almost year-round in some regions (Gutiérrez-Vargas et al., 2017, 2018). Unfortunately, in order to observe whether AKI caused by heat exposure and prolonged physical exercise provokes CKD on the long-term requires cohort studies in a long timeframe; such a timeframe could be too late for affected athletes (Eichner, 2017). Other contextual factors that could influence AKI incidence should be explored as internal thermal load indicators, slope variations, age, finish time, carried weight during running, dehydration status and other contextual variables.

DISCUSSION

Existing evidence regarding AKI in hospitalized and occupational (working) populations, as well as the similarities in thermal load experienced by CKDu-affected occupational populations and athlete populations in the tropics, beg the question of whether athletes in hot environments might be experiencing AKI and eventually CKD. Currently available technological tools and methods allow to objectively study cases of AKI and CKD, improving parameters for accurate diagnosis (Clarkson et al., 2006; Stahl et al., 2019) and new markers and methods have been used for their identification (Colombini et al., 2012; McCullough et al., 2013).

Enough is known about the potential risk that we must call on authorities, including universities, ministries, federations, sports committees and other involved institutions, to study, and take preventative regulatory actions in the tropical and Mesoamerican region to protect athletes who compete for prolonged periods at high levels of thermal stress. This is of particular urgency given

the recent increase in popularity and quantity of this type of event and the fact that there is no regional and organizational platform in place to insure implementation of endurance events in a secure manner. Regulation of aspects such as the time of events, heat-exposure, stricter participation criteria, regular medical check-ups, among others, are essential to avoid a regional health problem related to physical exercise.

Through this call for attention, the regional and international scientific community is urged not to wait for the first cases of CKD in athletes related to the combination of three above mentioned factors: heat strain, dehydration, and high external workload, to be documented before acting, since preliminary evidence (i.e., frequent reports of exertional rhabdomyolysis, AKI) are more than enough to demonstrate the need to take timely measures. Since cumulative AKI events have been shown to make individuals more likely to develop CKD in the future (Heung et al., 2016; Hsu and Hsu, 2016), it is highly probable that the same phenomenon is occurring in athletes.

Endurance athletes in tropical regions are exposed to conditions (heat strain, dehydration, and high external workload) similar to those experienced by working populations known to suffer from AKI and CKDu (Gutiérrez-Vargas et al., 2018; Rojas-Valverde et al., 2019), which is why attention should be paid to this factor as a determining point for the monitoring and treatment of this condition in endurance athletes who they carry out long-term activities at moderate to high intensities. We therefore advocate more research in athlete populations in tropical settings in order to (1) protect athletes who may be exposed under the current lack of regulation and (2) provide possible mechanistic insights that might help understand and intervene with CKDu-affected working populations.

AUTHOR CONTRIBUTIONS

DR-V and JC contributed to the conceptualization, the preparation, and the writing of the original draft. DR-V contributed to the literature search. JC, GO, and RG-V critically revised the manuscript and contributed to the supervision. DR-V, JC, GO, and RG-V contributed to the final manuscript approval.

REFERENCES

Abbas, M., Brown, V., Rietveld, A., and Hoek, A. (2019). A marathon runner with rhabdomyolysis. *Ned. Tijdschr. Geneeskd.* 163:D2848.

Asserraji, M., Benameur, I., Maoujoud, O., Kharras, A. E., Hajbi, H., and Filali, K. (2014). Late care in marathon runs leading to exertional heat stroke with multiple organ failure. *Asian J. Sport Med.* 5, 136–138.

Bellomo, R., Ronco, C., Kellum, J. A., Mehta, R. L., Palevsky, P., and Acute Dialysis Quality Initiative workgroup (2004). Acute renal failure - definition, outcome measures, animal models, fluid therapy and information technology needs: the Second International Consensus Conference of the Acute Dialysis Quality Initiative (ADQI) Group. *Crit. Care* 8, R204–R212. doi: 10.1186/cc2872

Bongers, C. C. W. G., Alsady, M., Nijenhuis, T., Tulp, A. D. M., Eijsvogels, T. M. H., Deen, P. M. T., et al. (2018). Impact of acute versus prolonged exercise and dehydration on kidney function and injury. *Physiol. Rep.* 6:e13734. doi: 10.14814/phy2.13734

Bosch, X., Poch, E., and Grau, J. M. (2009). Rhabdomyolysis and acute kidney injury. *N. Engl. J. Med.* 361, 62–72. doi: 10.1056/NEJMra0801327

Boulter, J., Noakes, T., and Hew-Butler, T. (2011). Acute renal failure in four Comrades Marathon runners ingesting the same electrolyte supplement: coincidence or causation? *S. Afr. Med. J.* 101, 876–878.

Butler-Dawson, J., Krisher, L., Asensio, C., Cruz, A., Tenney, L., Weitzenkamp, D., et al. (2018). Risk factors for declines in kidney function in sugarcane workers in Guatemala. *J. Occup. Environ. Med.* 60, 548–558. doi: 10.1097/JOM.0000000000001284

Chapman, E., Haby, M. M., Illanes, E., Sanchez-Viamonte, J., Elias, V., and Reveiz, L. (2019). Risk factors for chronic kidney disease of non-traditional causes: a systematic review. *Rev. Panam. Salud Pública* 43:e35. doi: 10.26633/RPSP.2019.35

Che Muhamed, A. M., Atkins, K., Stannard, S. R., Mündel, T., and Thompson, M. W. (2016). The effects of a systematic increase in relative humidity on thermoregulatory and circulatory responses during prolonged running exercise in the heat. *Temperature* 3, 455–464. doi: 10.1080/23328940.2016.1182669

Chlíbková, D., Knechtle, B., Rosemann, T., Tomášková, I., Novotný, J., Žákovská, A., et al. (2015). Rhabdomyolysis and exercise-associated hyponatremia in ultra-bikers and ultra-runners. *J. Int. Soc. Sports Nutr.* 12:29. doi: 10.1186/s12970-015-0091-x

Clarkson, P. M., Kearns, A. K., Rouzier, P., Rubin, R., and Thompson, P. D. (2006). Serum creatine kinase levels and renal function measures in exertional muscle damage. *Med. Sci. Sports Exerc.* 38, 623–627. doi: 10.1249/01.mss.0000210192.49210.fc

Colombini, A., Corsetti, R., Graziani, R., Lombardi, G., Lanteri, P., and Banfi, G. (2012). Evaluation of creatinine, cystatin C and eGFR by different equations in professional cyclists during the Giro d'Italia 3-weeks stage race. *Scand. J. Clin. Lab. Invest.* 72, 114–120. doi: 10.3109/00365513.2011.642305

Crowe, J., Nilsson, M., Kjellstrom, T., and Wesseling, C. (2015). Heat-Related symptoms in sugarcane harvesters. *Am. J. Ind. Med.* 58, 541–548. doi: 10.1002/ajim.22450

Crowe, J., Wesseling, C., Solano, B. R., Umaña, M. P., Ramírez, A. R., Kjellstrom, T., et al. (2013). Heat exposure in sugarcane harvesters in Costa Rica. *Am. J. Ind. Med.* 56, 1157–1164. doi: 10.1002/ajim.22204

Eichner, E. R. (2017). Is heat stress nephropathy a concern for endurance athletes? *Curr. Sports Med. Rep.* 16, 299–300. doi: 10.1249/JSR.0000000000000408

García-Trabanino, R., Jarquín, E., Wesseling, C., Johnson, R. J., González-Quiroz, M., Weiss, I., et al. (2015). Heat stress, dehydration, and kidney function in sugarcane cutters in El Salvador–A cross-shift study of workers at risk of Mesoamerican nephropathy. *Environ. Res.* 142, 746–755. doi: 10.1016/j.envres.2015.07.007

González-Quiroz, M., Pearce, N., Caplin, B., and Nitsch, D. (2018). What do epidemiological studies tell us about chronic kidney disease of undetermined cause in Meso-America? A systematic review and meta-analysis. *Clin. Kidney J.* 11, 496–506. doi: 10.1093/ckj/sfx136

Gutiérrez-Vargas, R., Martín-Rodríguez, S., Sánchez-Ureña, B., Rodríguez-Montero, A., Salas-Cabrera, J., Gutiérrez-Vargas, J. C., et al. (2018). Biochemical and muscle mechanical postmarathon changes in hot and humid conditions. *J. Strength Cond. Res.* doi: 10.1519/JSC.0000000000002746. [Epub ahead of print].

Gutiérrez-Vargas, R., Ugalde-Ramírez, J. A., Rojas-Valverde, D., Salas-Cabrera, J., Rodríguez-Montero, A., and Gutiérrez-Vargas, J. C. (2017). La termografía infrarroja como herramienta efectiva para detectar áreas músculares dañadas después de correr una maratón. *Rev. Fac. Med.* 65, 601–607. doi: 10.15446/revfacmed.v65n4.60638

Heung, M., Steffick, D. E., Zivin, K., Gillespie, B. W., Banerjee, T., Hsu, C.-Y., et al. (2016). Acute kidney injury recovery pattern and subsequent risk of CKD: an analysis of veterans health administration data. *Am. J. Kidney Dis.* 67, 742–752. doi: 10.1053/j.ajkd.2015.10.019

Hoffman, M. D., Ingwerson, J. L., Rogers, I. R., Hew-Butler, T., and Stuempfle, K. J. (2012). Increasing creatine kinase concentrations at the 161-km Western States Endurance Run. *Wilderness Environ. Med.* 23, 56–60. doi: 10.1016/j.wem.2011.11.001

Hoffman, M. D., and Weiss, R. H. (2016). Does acute kidney injury from an ultramarathon increase the risk for greater subsequent injury? *Clin. J. Sport Med.* 26, 417–422. doi: 10.1097/JSM.0000000000000277

Hou, S.-K., Chiu, Y.-H., Tsai, Y.-F., Tai, L.-C., Hou, P. C., How, C.-K., et al. (2015). Clinical impact of speed variability to identify ultramarathon runners at risk for acute kidney injury. *PLoS ONE* 10:e0133146. doi: 10.1371/journal.pone.0133146

Hsu, R. K., and Hsu, C. (2016). The role of acute kidney injury in chronic kidney disease. *Semin. Nephrol.* 36, 283–292. doi: 10.1016/j.semnephrol.2016.05.005

Jha, V., Garcia-Garcia, G., Iseki, K., Li, Z., Naicker, S., Plattner, B., et al. (2013). Chronic kidney disease: global dimension and perspectives. *Lancet* 382, 260–272. doi: 10.1016/S0140-6736(13)60687-X

Junglee, N. A., Di Felice, U., Dolci, A., Fortes, M. B., Jibani, M. M., Lemmey, A. B., et al. (2013). Exercising in a hot environment with muscle damage: effects on acute kidney injury biomarkers and kidney function. *Am. J. Physiol. Renal Physiol.* 305, F813–F820. doi: 10.1152/ajprenal.00091.2013

Kao, W.-F., Hou, S.-K., Chiu, Y.-H., Chou, S.-L., Kuo, F.-C., Wang, S.-H., et al. (2015). Effects of 100-km ultramarathon on acute kidney injury. *Clin. J. Sport Med.* 25, 49–54. doi: 10.1097/JSM.0000000000000116

Kim, D., Ko, E.-J., Cho, H., Park, S. H., Lee, S. H., Cho, N., et al. (2015). Spinning-induced rhabdomyolysis: eleven case reports and review of the literature. *Electrolytes Blood Press.* 13, 58–61. doi: 10.5049/EBP.2015.13.2.58

Kupferman, J., Ramírez-Rubio, O., Amador, J. J., López-Pilarte, D., Wilker, E. H., Laws, R. L., et al. (2018). Acute kidney injury in sugarcane workers at risk for mesoamerican nephropathy. *Am. J. Kidney Dis.* 72, 475–482. doi: 10.1053/j.ajkd.2018.04.014

Laws, R. L., Brooks, D. R., Amador, J. J., Weiner, D. E., Kaufman, J. S., Ramírez-Rubio, O., et al. (2016). Biomarkers of kidney injury among nicaraguan sugarcane workers. *Am. J. Kidney Dis.* 67, 209–217. doi: 10.1053/j.ajkd.2015.08.022

Lopes, J. A., and Jorge, S. (2013). The RIFLE and AKIN classifications for acute kidney injury: a critical and comprehensive review. *Clin. Kidney J* 6, 8–14. doi: 10.1093/ckj/sfs160

McCullough, P. A., Shaw, A. D., Haase, M., Bouchard, J., Waikar, S. S., Siew, E. D., et al. (2013). "Diagnosis of acute kidney injury using functional and injury biomarkers: workgroup statements from the tenth acute dialysis quality initiative consensus conference," in *Contributions to Nephrology*, eds P. A. McCullough, J. A. Kellum, R. L. Mehta, P. T. Murray, and C. Ronco (Basel: S. KARGER AG), 13–29. doi: 10.1159/000349963

McDermott, B. P., Smith, C. R., Butts, C. L., Caldwell, A. R., Lee, E. C., Vingren, J. L., et al. (2018). Renal stress and kidney injury biomarkers in response to endurance cycling in the heat with and without ibuprofen. *J. Sci. Med. Sport* 21, 1180–1184. doi: 10.1016/j.jsams.2018.05.003

Olcina, G., Timón, R., Brazo-Sayavera, J., Martínez-Guardado, I., Marcos-Serrano, M., and Crespo, C. (2018). Changes in physiological and performance variables in non-professional triathletes after taking part in an Olympic distance triathlon. *Res. Sports Med.* 26, 323–331. doi: 10.1080/15438627.2018.1447472

Omassoli, J., Hill, N. E., Woods, D. R., Delves, S. K., Fallowfield, J. L., Brett, S. J., et al. (2019). Variation in renal responses to exercise in the heat with progressive acclimatisation. *J. Sci. Med. Sport* 22, 1004–1009. doi: 10.1016/j.jsams.2019.04.010

Pearce, N., and Caplin, B. (2019). Let's take the heat out of the CKDu debate: more evidence is needed. *Occup. Environ. Med.* 2018:105427. doi: 10.1136/oemed-2018-105427

Rojas-Valverde, D. (2019). Brief historical review of distance and ultradistance runnig in Costa Rica and the world. *Rev. Educ. Física* 8, 1–19. Available online at: https://aprendeenlinea.udea.edu.co/revistas/index.php/viref/article/viewFile/335559/20792730

Rojas-Valverde, D., Sánchez-Ureña, B., Pino-Ortega, J., Gómez-Carmona, C., Gutiérrez-Vargas, R., Timón, R., et al. (2019). External workload indicators of muscle and kidney mechanical injury in endurance trail running. *Int. J. Environ. Res. Publ. Health* 16:3909. doi: 10.3390/ijerph16203909

Stahl, K., Rastelli, E., and Schoser, B. (2019). A systematic review on the definition of rhabdomyolysis. *J. Neurol*. doi: 10.1007/s00415-019-09185-4. [Epub ahead of print].

Tietze, D. C., and Borchers, J. (2014). Exertional rhabdomyolysis in the athlete: a clinical review. *Sports Health* 6, 336–339. doi: 10.1177/1941738114523544

Wegman, D., Crowe, J., Hogstedt, C. H., Jakobsson, K., and Wesseling, C. (2015). *Mesoamerican Nephropathy: Report From the Second International Research Workshop on MeN, 1st Edn.* Heredia: SALTRA/IRET; Universidad Nacional.

Wesseling, C., Aragón, A., González, M., Weiss, I., Glaser, J., Rivard, C. J., et al. (2016). Heat stress, hydration and uric acid: a cross-sectional study in workers of three occupations in a hotspot of Mesoamerican nephropathy in Nicaragua. *BMJ Open* 6:e011034. doi: 10.1136/bmjopen-2016-011034

Wesseling, C., Crowe, J., Hogstedt, C., Jakobsson, K., Lucas, R., and Wegman, D. (2013). The epidemic of chronic kidney desease of unknown etiology in mesoamerica: a call for interdisciplinary research and action. *Am. J. Public Health* 103, 1927–1930. doi: 10.2105/AJPH.2013.301594

Wesseling, C., van Wendel de Joode, B., Crowe, J., Rittner, R., Sanati, N. A., Hogstedt, C., et al. (2015). Mesoamerican nephropathy: geographical distribution and time trends of chronic kidney disease mortality between 1970 and 2012 in Costa Rica. *Occup. Environ. Med.* 72, 714–721. doi: 10.1136/oemed-2014-102799

Conflict of Interest: The authors declare that the research was conducted in the absence of any commercial or financial relationships that could be construed as a potential conflict of interest.

Copyright © 2019 Rojas-Valverde, Olcina, Gutiérrez-Vargas and Crowe. This is an open-access article distributed under the terms of the Creative Commons Attribution License (CC BY). The use, distribution or reproduction in other forums is permitted, provided the original author(s) and the copyright owner(s) are credited and that the original publication in this journal is cited, in accordance with accepted academic practice. No use, distribution or reproduction is permitted which does not comply with these terms.

frontiers in Physiology

ORIGINAL RESEARCH
published: 26 November 2019
doi: 10.3389/fphys.2019.01419

Farrerol Attenuates Cisplatin-Induced Nephrotoxicity by Inhibiting the Reactive Oxygen Species-Mediated Oxidation, Inflammation, and Apoptotic Signaling Pathways

Ning Ma[1,2†], Wei Wei[1†], Xiaoye Fan[1] and Xinxin Ci[1]*

[1]Institute of Translational Medicine, The First Hospital, Jilin University, Changchun, China, [2]Department of Urology, The First Hospital, Jilin University, Changchun, China

OPEN ACCESS

Edited by:
Md Abdul Hye Khan,
Medical College of Wisconsin,
United States

Reviewed by:
Rehan Khan,
Mayo Clinic Arizona,
United States
Zi Wang,
Jilin Agriculture University, China
Li Gao,
Anhui Medical University, China

***Correspondence:**
Xinxin Ci
cixinxin@jlu.edu.cn

[†]These authors have contributed equally to this work

Specialty section:
This article was submitted to Renal and Epithelial Physiology, a section of the journal Frontiers in Physiology

Received: 18 July 2019
Accepted: 04 November 2019
Published: 26 November 2019

Citation:
Ma N, Wei W, Fan X and Ci X (2019) Farrerol Attenuates Cisplatin-Induced Nephrotoxicity by Inhibiting the Reactive Oxygen Species-Mediated Oxidation, Inflammation, and Apoptotic Signaling Pathways. Front. Physiol. 10:1419. doi: 10.3389/fphys.2019.01419

Cisplatin is a chemotherapy drug that is often used in clinical practice, but its frequent use often leads to nephrotoxicity. Therefore, we urgently need a drug that reduces the nephrotoxicity induced by cisplatin. Farrerol reportedly has antioxidant potential, but its renal protective effects and potential mechanisms remain unclear. In this study, we used both cell and mouse models to determine the mechanism of farrerol in cisplatin-induced nephrotoxicity. The *in vitro* experiments revealed that farrerol improved cisplatin-induced nephrotoxicity and reactive oxygen species (ROS) production *via* nuclear factor erythrocyte 2-related factor 2 (Nrf2) activation. Moreover, farrerol effectively activated Nrf2 and subsequently increased the expression of Nrf2-targeted antioxidant enzymes, including heme oxygenase-1 (HO-1) and NAD(P)H quinone oxidoreductase-1 (NQO1), but inhibited Kelch-like ECH-associated protein 1 (Keap1) and NADPH oxidase type 4 (NOX4). Furthermore, farrerol attenuated the phosphorylation of C-Jun N-terminal kinase (JNK), extracellular signal-regulated kinase (ERK), and p38 mitogen-activated protein kinase (p38); the activation of phosphorylated nuclear factor-κB (p-NF-κB) and nucleotide-binding domain (NOD)-like receptor protein 3 (NLRP3); and the expression of phosphorylated p53 (p-p53), Bax, and cleaved caspase-3. *In vivo*, farrerol significantly improved cisplatin-induced renal damage, as demonstrated by the recovery of blood urea nitrogen (BUN), serum creatinine (SCr), kidney injury molecule-1 (KIM-1), neutrophil gelatinase-associated lipocalin (NGAL), and pathological damage. Moreover, farrerol inhibited inflammatory and apoptotic protein expression *in vivo*. Notably, farrerol exerted slight protection in Nrf2-knockout mice compared with wild-type mice. These findings indicate that farrerol can effectively activate Nrf2 and can serve as a therapeutic target in the treatment of acute kidney injury (AKI).

Keywords: farrerol, cisplatin, acute kidney injury, reactive oxygen species, Nrf2, oxidative stress, inflammation, apoptosis

INTRODUCTION

Cisplatin is an inorganic platinum chemotherapy drug that is commonly used in clinical chemotherapy treatment (Yang et al., 2018) because it can effectively treat a wide range of solid tumors, including lung, ovarian, and bladder cancers. However, cisplatin has many serious side effects, such as myelosuppression, nephrotoxicity, and ototoxicity (Stojic et al., 2018), and these toxic side effects limit the clinical application of cisplatin as part of standard cancer treatment. The kidney is considered the main pathway for cisplatin excretion and the main site of its accumulation (Arany and Safirstein, 2003). Cisplatin is heavily absorbed by proximal tubular cells, and this absorption leads to renal pathophysiological disorders (Pan et al., 2009). Although the pre-hydration effects of diuretics in patients during chemotherapy reduce the nephrotoxicity of cisplatin, the incidence of cisplatin nephrotoxicity remains high, with an incidence of approximately one-third (Pabla and Dong, 2008). At present, AKI treatment is mainly supportive, and there is no treatment with curative effects (Bagshaw and Wald, 2016). The current diagnostic criteria include the BUN and SCr levels, which primarily reflect the late manifestations of the disease, and thus, early intervention is critical for the effective treatment of AKI (Moledina and Parikh, 2018; Fu et al., 2019).

The generation of ROS is induced after cisplatin enters renal tubular cells, and the levels of generated ROS exceeds the level that can be scavenged by the body, resulting in an imbalance in the redox system (Kim et al., 2019). Excessive ROS can cause oxidative stress, increase the malondialdehyde (MDA) and myeloperoxidase (MPO) levels, and inhibit antioxidant enzymes such as superoxide dismutase (SOD) and glutathione (GSH) (Ma et al., 2015). NADPH oxidase can produce many free radicals, and NOX4 is abundantly produced and leads to excessive ROS production; thus, cisplatin induces significant damage to renal tubular epithelial cells (Ma et al., 2017; Meng et al., 2018b). Nrf2 is a transcription factor that plays a decisive role in the regulation of cellular oxidative defense and redox homeostasis (Li et al., 2018a). In general, Keap1 is an inhibitory molecule that promotes Nrf2 ubiquitination by binding to Nrf2 in the cytoplasm. The activation of Nrf2 enhances the activity of the antioxidant response element (ARE) promoter and thereby simultaneously upregulates the expression of HO-1 and NQO1 and downregulates NOX4 and Keap1 to attenuate cisplatin-induced kidney damage (Babelova et al., 2012; Sedeek et al., 2013). In addition, Nrf2-deficient mice are more vulnerable to oxidative damage than normal mice and also exhibit increased susceptibility to diabetic nephropathy (Jiang et al., 2010), lupus nephritis (Chin et al., 2018), and ischemic AKI (Liu et al., 2009).

Stimulation of the renal tubules by cisplatin significantly increases the production of ROS and thereby the activation of a series of signaling proteins, including JNK (Jaiman et al., 2013), ERK (So et al., 2007), and p38 (Ma et al., 2017). In addition, cisplatin can aggravate AKI by inducing the phosphorylation of ERK and p38 and thereby upregulating the phosphorylation of NF-κB and p53 (Okada et al., 2014; Buendia et al., 2016; Chen et al., 2019). NF-κB, a heterodimer composed of two DNA-binding subunits, namely, p50 and p65, activates the NLRP3 inflammasome and mediates the inflammatory response (Ke et al., 2018). Notably, the mitochondrial pathway underlying the p53-medaited induction of apoptosis can be regulated *via* Bax (a pro-apoptotic protein) and Bcl2 (an anti-apoptotic protein) (Jiang et al., 2009; Okada et al., 2014). Excessive amounts of Bax protein can result in increased binding of Bax to the mitochondrial membrane, and this binding induces the release of cytochrome C from the mitochondria and activates caspase-3, which eventually results in the acceleration of apoptosis (Wei et al., 2007; Ma et al., 2017). Accordingly, Bcl2 can stabilize the mitochondrial membrane potential through a series of inhibitory effects. Consistently, Bcl2 enhances the mitochondrial membrane potential by inhibiting the release of Bax and caspase-3 and thereby blocking the mitochondrial pathway of apoptosis (Arany et al., 2004; Li et al., 2019). Therefore, apoptosis and inflammatory pathways can also be inhibited through the inhibition of ROS production. In addition, Nrf2-targeting molecules provide a new strategy for the treatment of kidney disease.

As major Nrf2 activators, some natural products counteract oxidative stress by modulating the Nrf2/ARE signaling pathway. Farrerol, which was isolated from azaleas, is a novel 2,3-dihydroflavonoid (Wang et al., 2019). We previously showed that farrerol has anti-inflammatory, antibacterial, and antioxidant properties (Ci et al., 2012; Liu et al., 2015; Wang et al., 2019) and that farrerol can activate Nrf2 in RAW 264.7 cells to resist oxidative stress (Ci et al., 2015). Thus far, the protective effect of farrerol on cisplatin-induced AKI has not been reported. Here, we used both cellular and mice models to study the effects and underlying mechanisms of farrerol on cisplatin-induced nephrotoxicity.

MATERIALS AND METHODS

Reagents and Chemicals

Farrerol was purchased from Chengdu Pufei De Biotech Co., Ltd. (Chengdu, China). Anti-phosphorylated c-Jun NH2-terminal kinase (JNK), β-actin, and NOX4 antibodies were obtained from Sungene Biotech Co., Ltd. (Tianjin, China) and Abcam (Cambridge, MA, USA). Primary antibodies against Nrf2, Keap1, HO-1, NQO1, P53, caspase-3, Bax, Bcl2, phospho-JNK, phospho-ERK, phospho-p38, and NF-κB were purchased from Abcam (Cambridge, MA, USA) and Cell Signaling (Boston, MA, USA). Phosphatase p53 was purchased from ImmunoWay. KIM-1- and NGAL-specific antibodies were purchased from R&D Systems, and the BCA protein assay kit (Beyotime, China) was used to evaluate the protein concentrations. The cell culture medium DMEM, antibiotic-antimycotic, and trypsin-EDTA were purchased from Corning, MBI, and Biofil, respectively. Dimethyl sulfoxide (DMSO) and DCFH-DA were purchased from Sigma Chemical Co. (St. Louis, MO, USA). In addition, BUN, SCr, MDA, MPO, GSH, and SOD detection kits were obtained from Nanjing Jiancheng Bioengineering Institute (Nanjing, China).

Cell Culture and CCK-8 Analysis

Mouse tubular epithelial cells (MTECs) and human proximal tubule cells (HK-2) were purchased from the Chinese Cell

Bank (Beijing, China). MTECs were cultured in DMEM containing 10% fetal bovine serum (FBS), 100 U/ml penicillin, 100 U/ml streptomycin, and 3 mM glutamine at 37°C in an environment with 95% air and 5% carbon dioxide. We used the CCK-8 assay kit to detect viability of the cells. MTECs and HK2 were seeded in 96-well plates (1.5×10^4 cells/well), and after 24 h of culture, the cells were treated with farrerol and cisplatin for 18 h and incubated with 10 μl of CCK-8 reagent for 2 h in an incubator at 37°C. The absorbance at 450 nm was then measured to determine the cell viability.

Intracellular Reactive Oxygen Species Measurement

The active oxygen scavenging activity of farrerol was determined using the oxidant-sensitive fluorescent probe DCFH-DA. MTECs were plated in 96-well plates (1.5×10^4 cells/well), pretreated with or without farrerol (5, 10, and 20 μM) for 18 h, and then stimulated with cisplatin (20 μM) for 30 min. The cells were then incubated with 50 mM DCFH-DA for 20 min. The fluorescence intensity was measured with an excitation wavelength of 485 nm and an emission wavelength of 535 nm.

Quantitative Real-Time Polymerase Chain Reaction

The mRNA expression levels of Nrf2 in MTECs and HK2 were detected by qPCR. Total RNA was extracted from the cells using the TransGen Biotech (Beijing, China) reagent according to the manufacturer's instructions. EasyScript First-Strand cDNA Synthesis SuperMix was used to obtain the cDNA templates (TransGen Biotech, Beijing, China), and mRNA transcription was determined using SYBR Green qPCR kits and analyzed using real-time PCR systems. Each analysis was repeated three times.

Hoechst 33342/PI Double Staining

MTECs were seeded in 12-well plates (3×10^5 cells/well) and cultured for 24 h, and the medium was then aspirated and replaced with low-sugar serum-free DMEM. The cells were pretreated with farrerol for 1 h prior to stimulation with cisplatin for 18 h. We subsequently added 2 μl of Hoechst 33342 solution and 6 μl of PI staining solution, heated the cells in a warm water bath at 37°C for 15 min, and examined the cells by fluorescence microscopy.

EXPERIMENTAL DESIGN AND ANIMAL PROCEDURES OF ACUTE KIDNEY INJURY

An animal model of cisplatin-induced AKI was established in male C57BL/6 mice. The mice were randomized into the following four groups (n = 10/group): control (saline), farrerol (20 mg/kg), cisplatin only (20 mg/kg), and cisplatin (20 mg/kg) + farrerol (20 mg/kg). Prior to the *in vivo* experiments, all the mice were starved for 12 h. After fasting, the mice belonging to the cisplatin (20 mg/kg) + farrerol (20 mg/kg) group were treated with 20 mg/kg farrerol and administered 20 mg/kg cisplatin *via* intraperitoneal injection1 hour later. Farrerol was re-administered 24 and 48 h after the cisplatin injection, and the mice were sacrificed 24 h after the last dose of farrerol. C57BL/6 wild-type mice were purchased from Liaoning Changsheng Technology Industrial Co., Ltd. (Certificate SCXK2010-0001; Liaoning, China), and C57BL/6 Nrf2-knockout mice were purchased from The Jackson Laboratory (Bar Harbor, ME, United States). All the animals were housed in a specific pathogen-free facility, and this experiment was approved by the Animal Health and Research Ethics Committee of Jilin University.

Histopathology Assessment

Paraffin-embedded mouse kidneys were prepared and cut into 3-μm-thick sections. The degree of representativeness of each histological sections of kidney tissue was determined by H&E staining (Huang et al., 2017). Histological damage was determined according to necrosis, cast formation, brush border loss, tubular degeneration, and vacuolization. Tissue scores are indicated by damaged tubules. Scored as a percentage of 0, 1, 2, 3, and 4, indicating damage to tissues of normal, 1–25%, 26–50, 51–75, and ≥ 75%, respectively (Wang et al., 2018).

Blood Measurements

The renal function was measured based on the BUN and SCr levels. Blood samples were collected from the mice immediately after sacrifice. The levels of BUN and SCr in the blood samples were measured using kits purchased from Nanjing Jiancheng Bioengineering Institute (Nanjing, China) according to the instructions provided with the kits.

Measurement of the Myeloperoxidase, Malondialdehyde, Glutathione, and Superoxide Dismutase Levels in Kidney Tissues

All the mice were sacrificed by anesthesia with ether, and the bilateral kidneys were excised 3 days after stimulation with cisplatin. The kidney tissue was homogenized and dissolved in extraction buffer for analysis of the MPO, MDA, SOD, and GSH levels. To examine the neutrophil accumulation and the lipid peroxidation levels in kidney tissue, the MPO and MDA levels were assessed using commercially available assay kits (Nanjing Jiancheng Bioengineering Institute, China) according to the manufacturer's instructions. In addition, to further measure the antioxidant enzyme activity in lung tissue, the SOD and GSH levels were measured using kits (Keygen Biotech. Co., Ltd., Nanjing, China) according to the manufacturer's instructions.

Western Blot Analysis

Renal tissue and MTECs were collected and lysed on ice for 30 min, and the protein concentrations were analyzed using a BCA Protein Assay Kit. Equal amounts of protein were separated on 10 or 12.5% SDS-polyacrylamide gels and transferred to PVDF membranes. The membranes were blocked in 5% nonfat milk on a shaker for 1 h at room temperature, incubated with the corresponding primary antibodies overnight at 4°C, and probed

with the corresponding secondary antibody at room temperature. The bands were then observed using ECL, and the band intensities were quantified using ImageJ gel analysis software.

Statistical Analysis

All the above-mentioned data are expressed as the means ± SEMs and were analyzed using SPSS 19.0 (IBM). The experimental data were compared by one-way analysis of variance (ANOVA). Statistical significance was defined as $p < 0.05$.

RESULTS

The Effects of Farrerol on Cisplatin-Induced Reactive Oxygen Species Depend on Nuclear Factor Erythrocyte 2-Related Factor 2

To identify the signals involved in the effects, we initially focused on ROS, which are associated with cisplatin nephrotoxicity. We first observed the cytotoxic effects induced by cisplatin and the protective effects of farrerol using the CCK8 method. As shown in **Figure 1A**, farrerol (0–20 μM) did not exert cytotoxicity in MTECs. Furthermore, cisplatin reduced the viability of the cells after culture for 18 h with an IC_{50} of 20 μM (**Figure 1B**). Based on these data, MTECs were pretreated with farrerol (0–20 μM) for 1 h and then incubated with 20 μM cisplatin for 18 h. The farrerol pretreatment, particularly at a concentration of 20 μM, attenuated the cytotoxicity of cisplatin (**Figure 1C**). In addition, a fluorescence microscopy analysis showed that high levels of ROS were produced after cisplatin treatment, but farrerol (20 μM) pretreatment significantly reduced the production of ROS (**Figures 1D,E**). In addition, the results obtained from the treatment of HK2 cells with farrerol and cisplatin were consistent with the previous results (**Figures 1F,G**). Nrf2 is an important regulator of cell resistance to oxidants. Specifically, Nrf2 controls the baseline and induced expression of a range of antioxidant response element-dependent genes

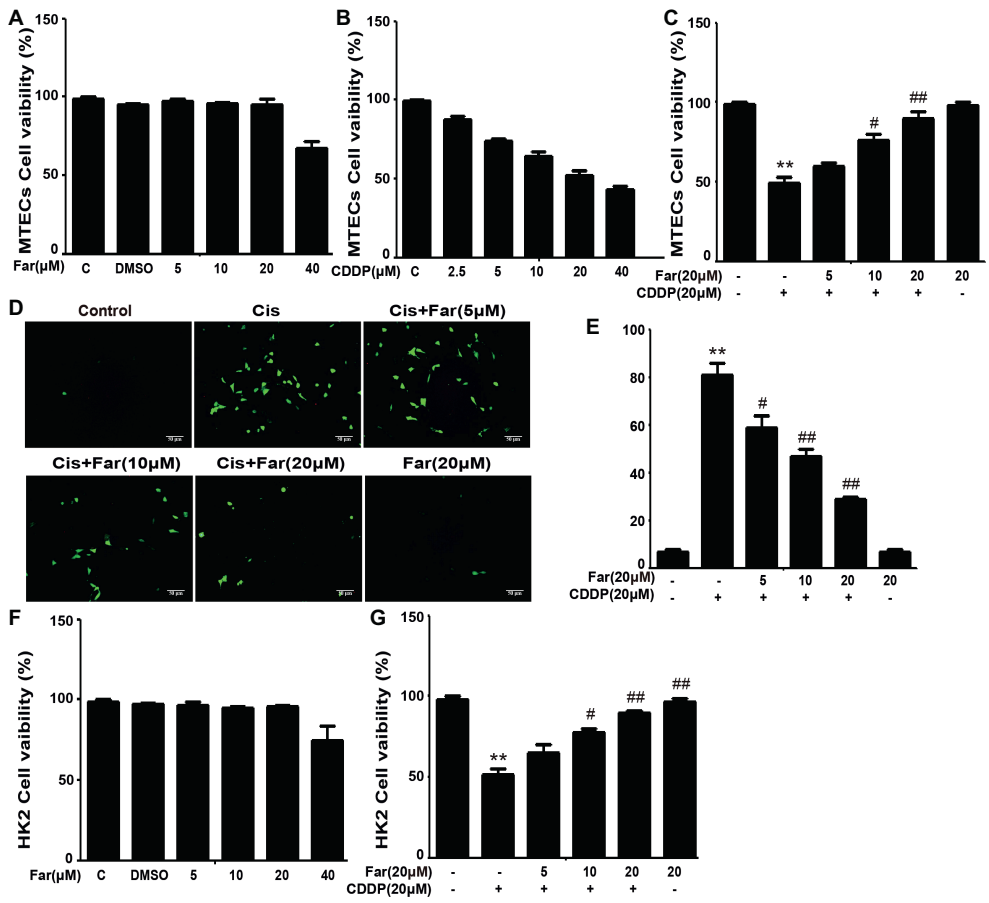

FIGURE 1 | Farrerol affects cisplatin-induced oxidative stress by inhibiting ROS production *in vitro*. MTECs were treated with the specified concentration of farrerol **(A)** or cisplatin **(B)** for 18 h, and the cell viability was then determined through the CCK-8 assay. **(C)** MTECs were treated with various concentrations of farrerol (5, 10 and 20 μM) for 1 h and then with cisplatin (20 μM) for 18 h, and the CCK-8 assay was then used for the assessment of cell viability. MTECs were stained with 50 mM ROS fluorescent probe for 30 min, and the resulting fluorescence was detected using a fluorescence microscope **(D)** and multiple detection readers **(E)**. **(F,G)** HK2 cells were treated as in **(A)** and **(C)**, and the cell viability was measured with the CCK-8 assay. All of the data displayed represent the mean of three independent experiments. $^{*}p < 0.05$ and $^{**}p < 0.01$ vs. the control group; $^{\#}p < 0.05$ and $^{\#\#}p < 0.01$ vs. the CDDP group.

to regulate the damage caused by oxidant exposure (Ma, 2013). To investigate whether the protective effect of farrerol on cisplatin-induced cytotoxicity is related to Nrf2, we investigated the influence of Nrf2 inhibitors on this process through a CCK-8 assay. The experimental results suggested that the mechanism through which farrerol protects against CDDP cytotoxicity might be related to the activation of Nrf2 expression (**Figures 2A,B**). As shown in **Figures 2C,D**, a qPCR analysis showed that Nrf2 mRNA expression was markedly induced *in vitro* by treatment with different concentrations of farrerol. To further confirm that farrerol inhibited ROS production by activating Nrf2, we subsequently inhibited cisplatin nephrotoxicity and found that inhibitors of Nrf2 effectively inhibited the protective effect of farrerol against cisplatin and eliminated the farrerol-induced clearance of ROS (**Figures 2E,F**).

Farrerol Attenuates Cisplatin-Induced Oxidation and Inflammation *in vitro*

We performed *in vitro* Western blotting analyses to further investigate the potential mechanism of farrerol, and the results indicated that farrerol activated Nrf2 in a dose-dependent manner and enhanced the levels of the downstream proteins HO-1 and NQO1. In contrast, farrerol alleviated the levels of Keap1 and Nox4 in a concentration-dependent manner (**Figures 3A,B**). These results also confirmed that the protective effects of farrerol on AKI might be related to Nrf2 activation. The mitogen-activated protein kinase (MAPK) pathway plays a crucial role in both inflammation and apoptosis (Okada et al., 2014). Farrerol reduced the cisplatin-induced phosphorylation of JNK, p38, and ERK to inhibit the MAPK pathway (**Figures 3C,D**) and downregulated the protein expression of p-NF-κB and NLRP3 to inhibit inflammation (**Figures 3C,E**).

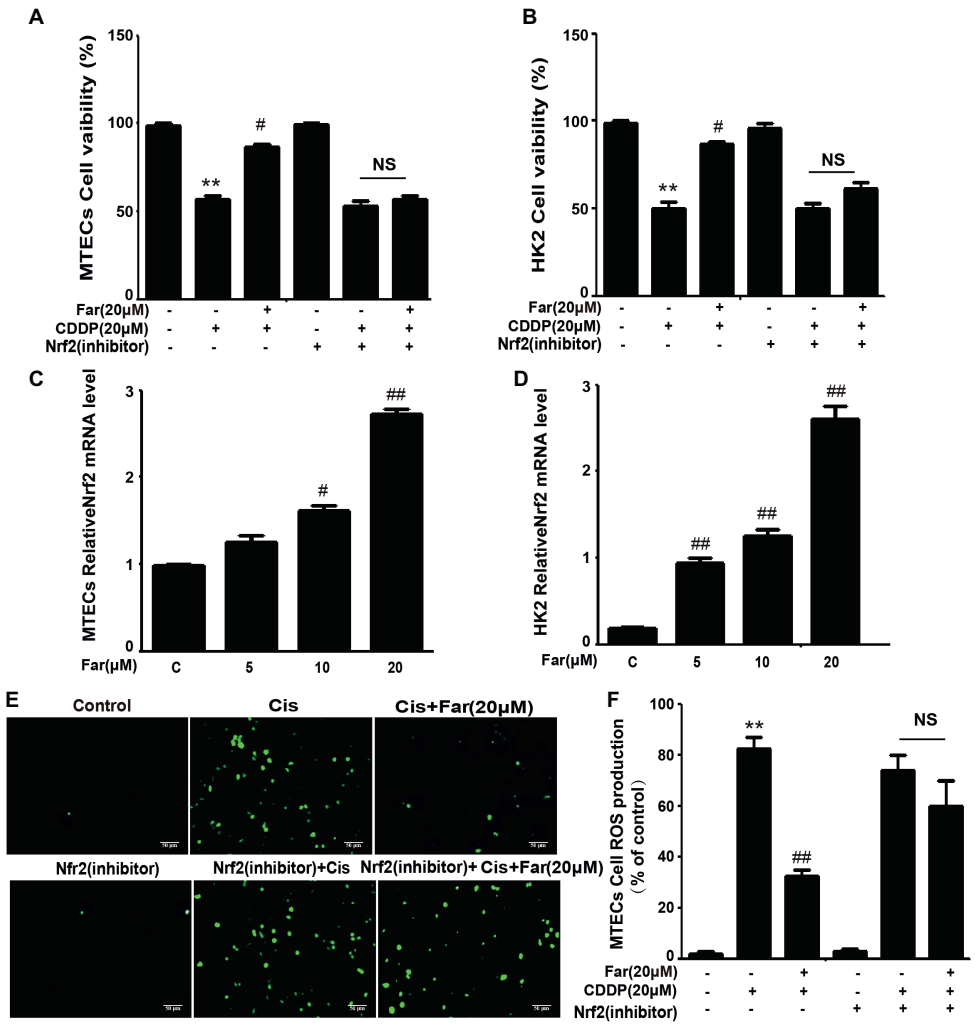

FIGURE 2 | The effects of farrerol on ROS production depend on Nrf2 *in vitro*. Effect of farrerol on MTECs **(A)** and HK2 cell **(B)** viability in the presence or absence of a Nrf2 inhibitor. Nrf2 mRNA expression in MTECs **(C)** and HK2 **(D)** treated with different concentrations of farrerol (5, 10, and 20 μM). **(E)** The production of ROS by MTECs was examined using the same protocol shown in **Figure 1D**, with or without pretreatment with a Nrf2 inhibitor. **(F)** Quantitative and statistical analysis of ROS-positive cells. All experiments were repeated three times. $^{*}p < 0.05$ and $^{**}p < 0.01$ vs. the control group; $^{\#}p < 0.05$ and $^{\#\#}p < 0.01$ vs. the CDDP group. NS, no specificity.

Farrerol Regulates Cisplatin-Induced Mouse Tubular Epithelial Cells Apoptosis

During activation of the MAPK pathway, ERK and P38 phosphorylation can effectively stimulate p-p53 production to induce apoptosis (Li et al., 2018b), which is consistent with the Western blot results obtained in our study. Pretreatment with farrerol inhibited the expression of p-p53, Bax, and cleaved caspase-3 and activated the expression of Bcl2 in a concentration-dependent manner *in vitro* (**Figures 4A,B**). In addition, the cells were stained with PI and Hoechst dyes, and their apoptosis was observed using a fluorescence microscope. The results showed that farrerol significantly reduced the number of PI-positive cells and effectively inhibited apoptosis in a dose-dependent manner (**Figures 4C,D**). Similarly, the same experimental results were obtained by flow cytometric analysis (**Figures 4E,F**).

Effects of Farrerol on Cisplatin-Induced Kidney Dysfunction

To determine the effect of farrerol on AKI, we established an experimental model of cisplatin-treated mice (**Figure 5A**). After

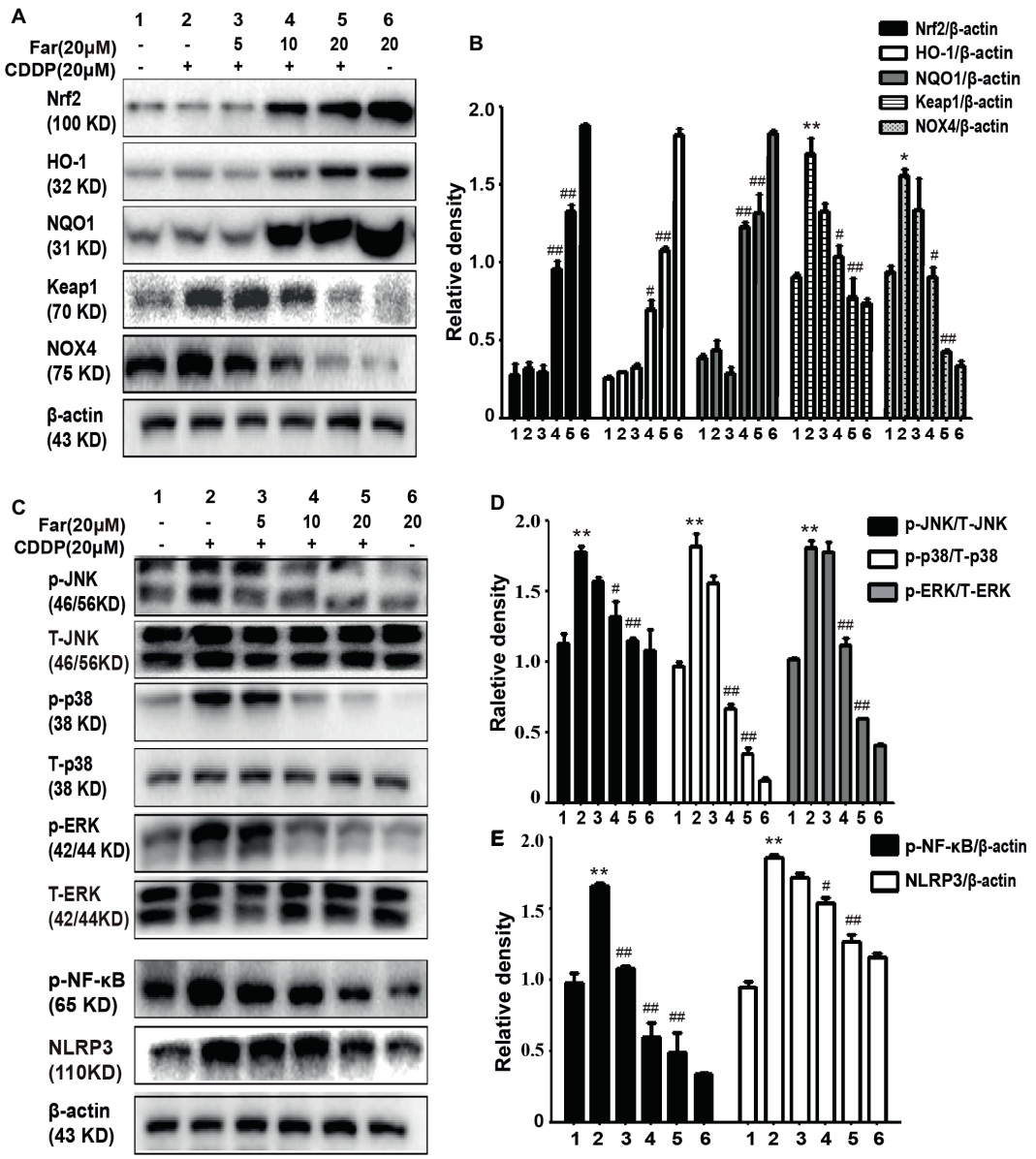

FIGURE 3 | Effects of farrerol on cisplatin-induced oxidation and inflammation pathway *in vitro*. MTECs were treated with different concentrations of farrerol (5, 10, or 20 μM) for 1 h and then with cisplatin (20 μM) for 18 h, and whole cell lysates were collected for Western blotting. **(A,B)** Quantification of the relative Nrf2, HO-1, NQO1, Keap1, and NOX4 protein levels obtained by Western blotting. **(C–E)** Representative Western blots showing the p- JNK/T-JNK, p-ERK/T-ERK, p-p38/T-p38, p- NF-κB (p-p65), and NLRP3 protein levels. All experiments were repeated three times. $^{*}p < 0.05$ and $^{**}p < 0.01$ compared with the control group; $^{\#}p < 0.05$ and $^{\#\#}p < 0.01$ compared with the CDDP group. β-actin was used as an internal control.

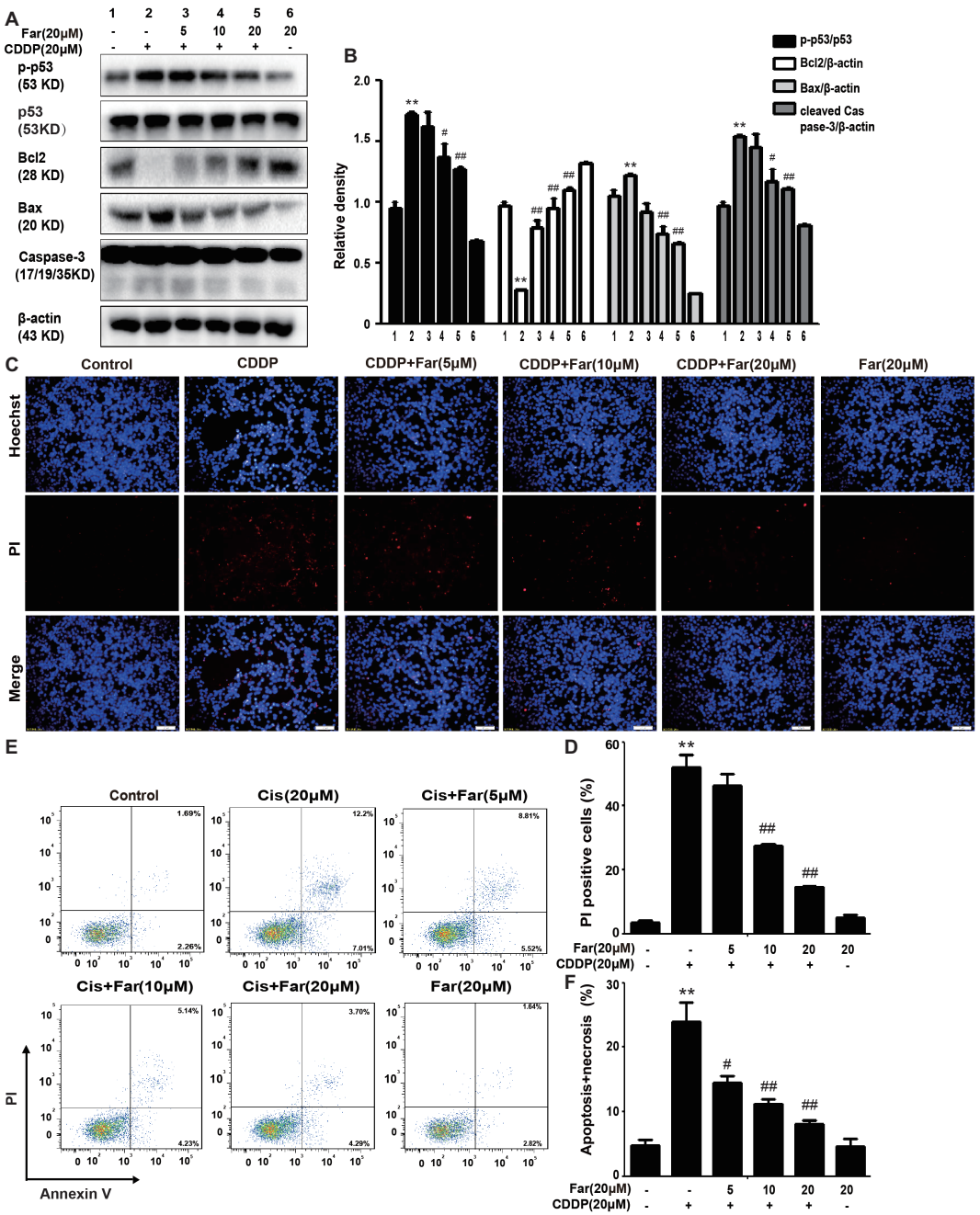

FIGURE 4 | Effects of farrerol on inhibition of the apoptosis of cisplatin-treated MTECs. MTECs were plated in six-well plates, preincubated with farrerol (5, 10, or 20 μM) for 1 h and then stimulated with cisplatin (20 μM) for 18 h. **(A,B)** The expression of the representative proteins p-p53, p53, Bcl2, Bax, and caspase-3 was assessed by Western blotting. **(C,D)** MTECs were stained with Hoechst/PI for 15 min, and the fluorescence was then rapidly detected with a fluorescence microscope. **(E,F)** The percentages of apoptotic and necrotic cells were determined by flow cytometry. All experiments were duplicated three times. $^{*}p < 0.05$ and $^{**}p < 0.01$ vs. the control group; $^{\#}p < 0.05$ and $^{\#\#}p < 0.01$ vs. the CDDP group. β-actin was used as an internal control.

12 h of fasting, the mice received an individual intraperitoneal injection of cisplatin (20 mg/kg) to induce AKI. Morphological observations revealed that the kidneys of the cisplatin group showed significant edema, mainly characterized by an increased kidney volume and a pale kidney color. However, the morphology of the kidneys of the mice belonging to the treatment group was significantly improved (**Figure 5B**). Furthermore, we measured and analyzed changes in the body weights of the mice, and the results showed that the weights of the stimulated group were significantly decreased. In addition, no evident difference in body weight was found between the farrerol and control groups (**Figure 5C**). Our analysis of the

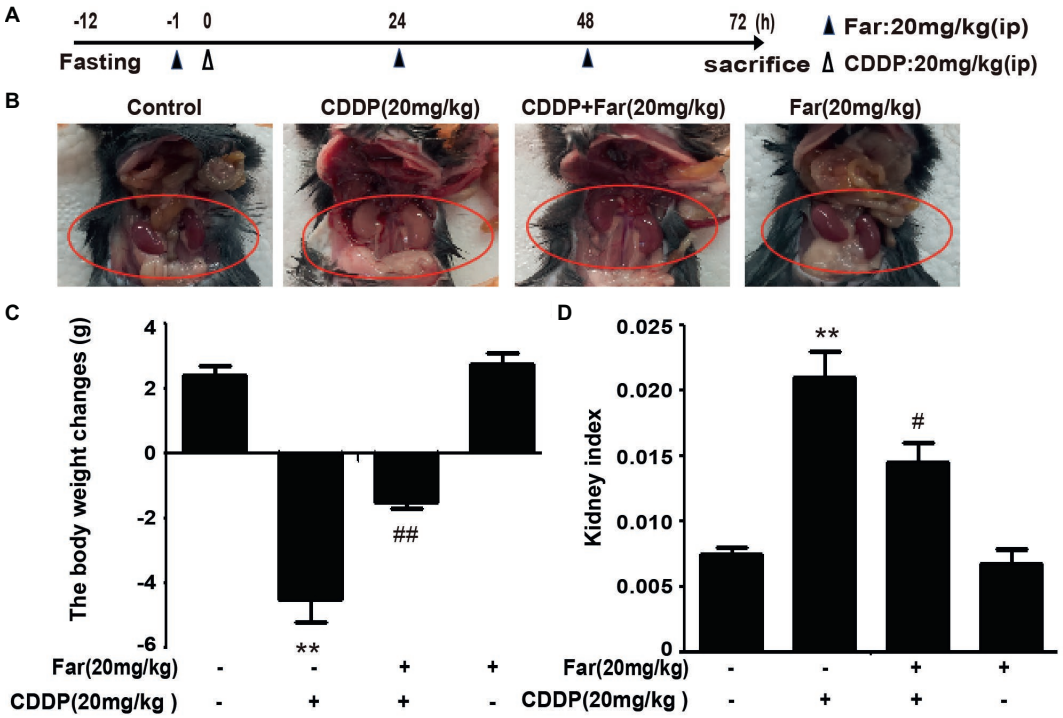

FIGURE 5 | Effects of farrerol on cisplatin-induced AKI. **(A)** Experimental design and schedule for treatment with cisplatin alone or in combination with farrerol. After 12 h of fasting, C57BL/6 mice were treated with farrerol (20 mg/kg) and administered 20 mg/kg cisplatin or vehicle 1 h later *via* intraperitoneal injection. Farrerol was administered 24 and 48 h after injection, and the mice were sacrificed 24 h after the last dose of farrerol. **(B)** Images of kidneys without magnification. **(C)** The changes in body weight were calculated by subtracting the body weight at 72 h from and the body weight 1 h prior to treatment. **(D)** The kidney index is expressed as the weight of the kidney divided by the body weight at 72 h. All the data are presented as the means ± SEM (n = 10 per group). All experiments were duplicated three times. $^{*}p < 0.05$ and $^{**}p < 0.01$ vs. the control group; $^{\#}p < 0.05$ and $^{\#\#}p < 0.01$ vs. the CDDP group.

kidney index also revealed that farrerol significantly improved the cisplatin-induced kidney damage (**Figure 5D**). To understand the mechanism of action of farrerol, we performed H&E staining and scored the stained sections. Compared with the control group, the cisplatin group showed more morphological damage, including necrosis, cast formation, brush border loss, tubular degeneration, and vacuolization. Notably, these histological lesions were significantly attenuated in the farrerol-treated mice (**Figures 6A,B**). Consistent with the improvements in the kidney morphology, farrerol significantly reversed the increase in the BUN and SCr levels observed after 72 h of cisplatin treatment (**Figures 6C,D**). Moreover, farrerol improved the significant upregulation of renal KIM1 and NGAL (proximal tubular injury markers) caused by cisplatin, as shown in **Figures 6E,F**.

Farrerol Improves Cisplatin-Induced Oxidative Stress and Inflammation *in vivo*

Because oxidative stress plays a key role in cisplatin-induced mice, we evaluated the extent of cisplatin-induced oxidative damage by measuring various oxidation markers. The data demonstrate that cisplatin can increase the MPO and MDA concentrations while reducing the SOD and GSH levels. Consistently, we observed that farrerol attenuated cisplatin-induced AKI in mice by reducing the MPO and MDA levels and increasing the SOD and GSH levels compared with the levels obtained with cisplatin treatment only (**Figures 7A–D**). To assess the antioxidant mechanism of farrerol in a cisplatin-induced AKI model, we extracted protein from kidney tissue and performed Western blotting. The results showed that farrerol efficiently activated Nrf2 and increased the levels of the downstream proteins HO-1 and NQO1. In contrast, farrerol attenuated the expression of Keap1 and NOX4 (**Figures 7E,F**). These data indicated that the antioxidant ability of farrerol involves activation of the Nrf2/ARE pathway, and this finding was examined further in the subsequent experiments.

Farrerol Ameliorates Cisplatin-Induced Inflammation and Apoptosis in Mice

We then investigated whether farrerol regulates the MAPK pathway in the AKI model. As shown in **Figures 8A,B**, the protein expression of p-JNK, p-ERK, and p-p38 was evidently upregulated in the cisplatin group compared with the control group, and farrerol pretreatment effectively reduced the expression levels of these proteins. The MAPK pathway plays a crucial role in both inflammation and apoptosis (Okada et al., 2014). We subsequently investigated the role of farrerol in the inflammatory and apoptotic pathways *in vivo*, and the results indicated that farrerol can inhibit inflammation by inhibiting

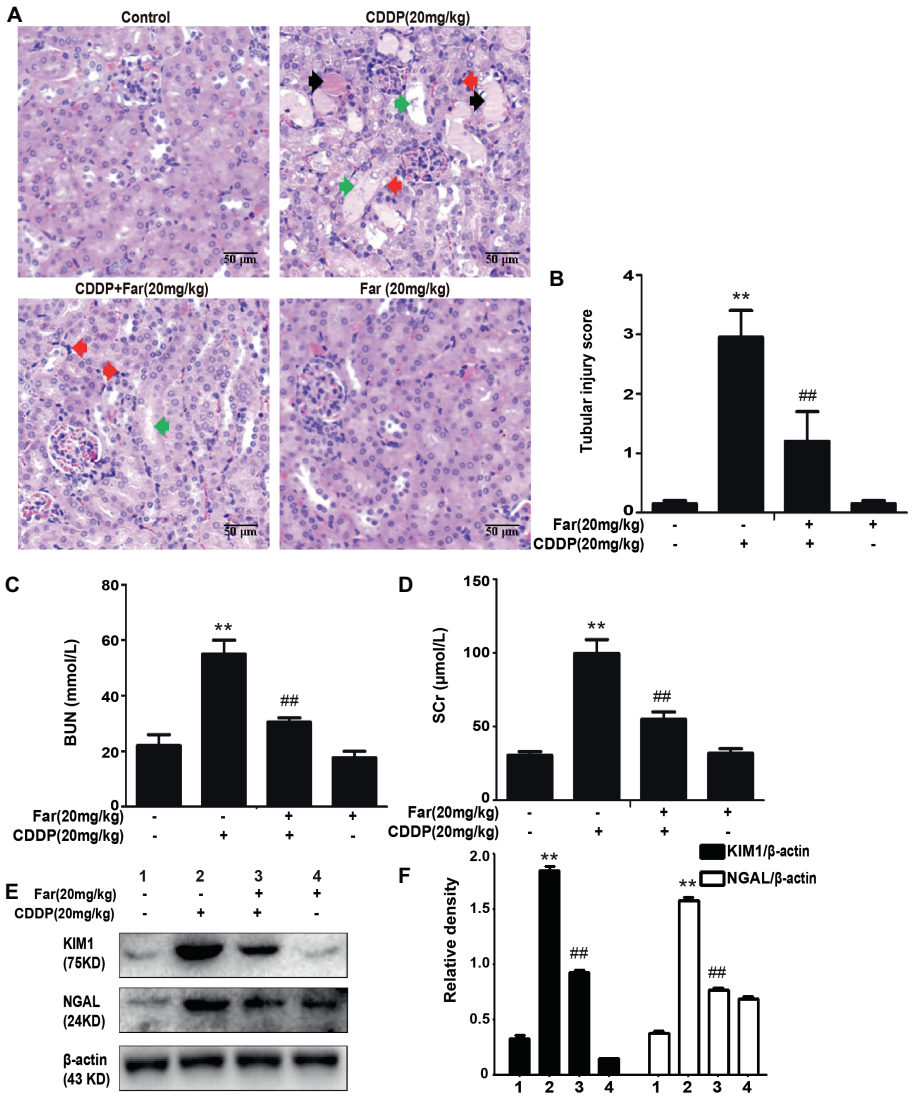

FIGURE 6 | Effects of farrerol on cisplatin-induced kidney dysfunction. **(A)** Representative tissue sections of kidneys stained with H&E. Necrosis (red arrow); Cast formation (black arrow); brush border loss, tubular degeneration, and vacuolization (green arrow). **(B)** Tissue damage score by percentage of damaged tubules (0, no damage; 1, <25% damage; 2, 25–50% damage; 3, 50–75% damage; and 4, >75% damage). The collected blood was used for calculation of the BUN **(C)** and SCr **(D)** levels. Data are presented as means ± SEM (n = 10 in each group). **(E,F)** The kidney tissue was homogenized and dissolved in extraction buffer, and Western blotting was performed to evaluate the protein expression of the proximal tubular injury markers, including KIM1 and NGAL. All experiments were repeated three times. $^{*}p < 0.05$ and $^{**}p < 0.01$ compared with the control group; $^{\#}p < 0.05$ and $^{\#\#}p < 0.01$ compared with the CDDP group.

the expression of p-NF-κB and NLRP3 (**Figures 8A,C**). In addition, farrerol increased the Bcl2 protein levels compared with the levels obtained with cisplatin treatment alone and reduced the levels of p-p53, Bax, and cleaved caspase-3 (**Figures 8D,E**). To further confirm this hypothesis, the kidney specimens were subjected to immunohistochemical staining of caspase-3. As shown in **Figure 8F**, the expression of caspase-3 in the kidney tissues of the mice exposed to CDDP was elevated compared with that found in the control group, and farrerol pretreatment significantly reduced these levels. All the results confirm that treatment with farrerol can improve CDDP-induced inflammation and the apoptotic pathway.

Nuclear Factor Erythrocyte 2-Related Factor 2 Deficiency Aggravates Cisplatin-Induced Acute Kidney Injury *in vivo*

To test whether the improvements mediated by Nrf2 in CDDP-induced AKI contribute to the protective effects of farrerol, we also induced AKI in wild-type and Nrf2-knockout C57BL/6 mice using a similar approach to that used to obtain the data shown in **Figure 4A**. The expression of the antioxidant response gene Nrf2 and that of its downstream related genes HO-1 and NQO1 were significantly increased in the wild-type mice, but no significant expression was observed in the Nrf2-knockout mice (**Figures 9A,B**). We

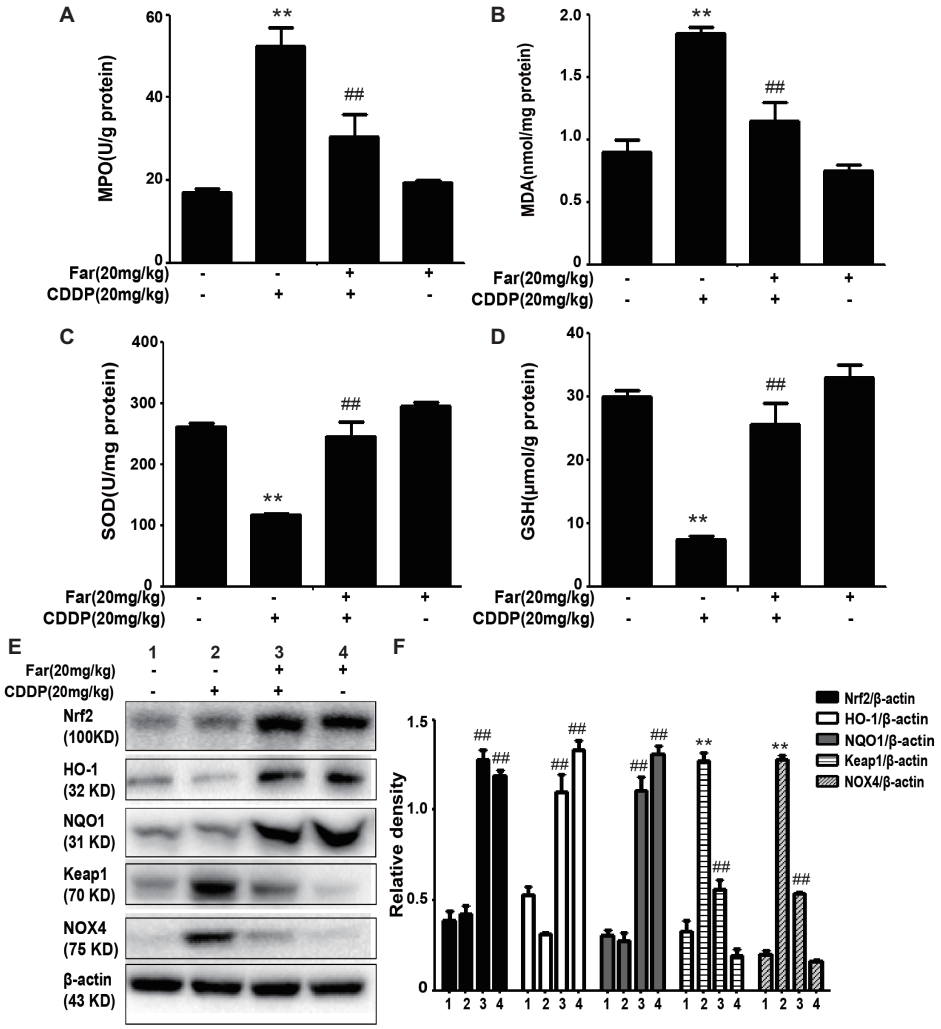

FIGURE 7 | Effects of farrerol on the levels of oxidative pathway-related proteins induced by cisplatin. **(A–D)** Renal tissues were collected from the mice to measure the production of MPO, MDA, SOD, and GSH. Data are expressed as mean ± SEM (n = 10 per group). **(E,F)** Representative Western blots showing the effect of farrerol on the levels of oxidative pathway-related proteins (including Nrf2, HO-1, NQO1, Keap1, and NOX4) in mouse kidney tissues. All experiments were duplicated three times. $^{*}p < 0.05$ and $^{**}p < 0.01$ vs. the control group; $^{\#}p < 0.05$ and $^{\#\#}p < 0.01$ vs. the CDDP group.

then assessed renal function by measuring the body weight changes, kidney index, and levels of BUN, SCr, KIM1 and NGAL. Compared with the control group, kidney function was significantly reduced in the cisplatin group, and Nrf2 knockout mice have worsened symptoms than the wild-type mice (**Figures 9C–H**). Notably, the results presented in **Figures 9A–H** showed that farrerol exerted no obvious protective effect on Nrf2-deficient mice.

DISCUSSION

Acute kidney injury (AKI) caused by sepsis, ischemia, or nephrotoxic agents is characterized by abrupt and reversible kidney dysfunction (Doi and Rabb, 2016). The pathogenesis of AKI is complex and diverse and is mainly related to oxidative stress, inflammation, and apoptosis. Among these symptoms, nephrotoxicity is a main side effect of cisplatin chemotherapy, and this side effect limits the usage of cisplatin for the treatment of cancer patients (Ozkok and Edelstein, 2014). It has been reported that the entry of cisplatin into the proximal tubules of the kidney induces the production of a large amount of ROS, which might destroy the balance of the body's redox system (Yen et al., 2019). Some studies have shown that antioxidants can prevent cisplatin-induced nephrotoxicity through their effects on inflammation and apoptosis (Shen et al., 2019), and other studies have shown that antioxidants can improve cisplatin-induced cytotoxicity by inhibiting inflammatory responses and reducing apoptosis (Lin et al., 2019).

Under various pathological conditions, ROS produced by oxidative stress are inseparable from renal damage (Nath and Norby, 2000). The treatment of mice with cisplatin significantly increases the BUN, SCr, KIM1, and NGAL levels (**Figures 6C–F**)

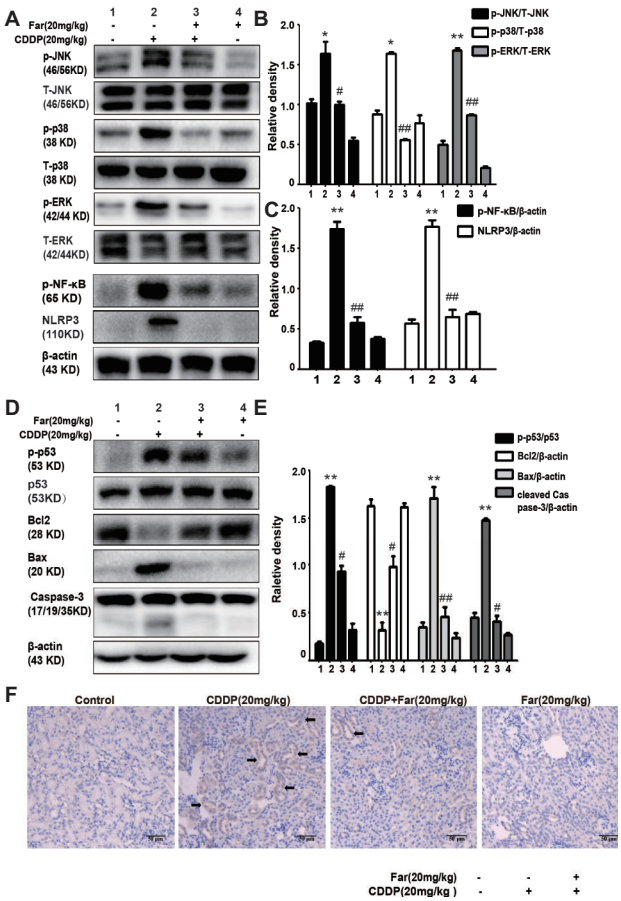

FIGURE 8 | Effects of farrerol on cisplatin-induced inflammation and apoptosis in AKI. **(A–C)** p-JNK / T-JNK, p-ERK / T-ERK and p-p38 / T-p38, p-NF-κB (p-p65) and NLRP3 protein levels were analyzed by Western blot. **(D,E)** Representative Western blot showing the expression of p-p53, p53, Bax, caspase-3 and Bcl2 in the kidney. **(F)** Representative photographs of immunohistochemical analysis of Caspase3 (black arrow) for kidney sections of the control, CDDP, CDDP + Far, and Far groups. Data are presented as the means ± SEM (n = 10 per group). All of the data displayed represent the mean of three independent experiments. $^{*}p < 0.05$ and $^{**}p < 0.01$ vs. the control group; $^{\#}p < 0.05$ and $^{\#\#}p < 0.01$ vs. the CDDP group. NS, no specificity. β-actin was used as an internal control.

and significantly worsens the histopathology results mainly including necrosis, cast formation, and brush border loss (**Figures 6A,B**). Therefore, we concluded that ROS-mediated oxidative stress is associated with cisplatin-induced AKI. Farrerol is a novel 2,3-dihydroflavonoid isolated from rhododendron (Wang et al., 2019) that reportedly exerts antioxidant effects (Liu et al., 2015; Wang et al., 2019). The administration of 20 mg/kg cisplatin was adjusted based on the protocol used for farrerol administration (**Figure 4A**). CDDP-induced oxidative stress is characterized by elevated MDA and MPO levels and decreased SOD and GSH levels (Ma et al., 2015), and these effects were reversed by farrerol in our experiments (**Figures 7A–D**). Based on these data, farrerol can effectively inhibit oxidative stress, but the specific mechanism remains unclear. Farrerol also reportedly activates Nrf2 to alle*via*te oxidative lesions in RAW 264.7 cells (Liu et al., 2015). Inspired by these observations, we utilized antioxidant molecules to investigate the possible relationship between Nrf2 and antioxidant activity to further explore the pharmacological effects of farrerol. The activation of the Nrf2 pathway plays an important role in the cellular redox status and oxidative stress (Dodson et al., 2015). Notably, a Nrf2 inhibitor abolished farrerol-induced Nrf2 activation and increased cisplatin-induced cytotoxicity, which indicated that farrerol might protect against cisplatin-induced toxicity through Nrf2 activation (**Figures 2A,B**). In addition, we observed that farrerol failed to attenuate the production of ROS in cisplatin-treated tubular cells in which Nrf2 was inhibited (**Figures 2E,F**), and these results suggested that farrerol inhibited ROS production by activating Nrf2 and subsequently inhibited cisplatin nephrotoxicity *in vitro*. In addition, qPCR and Western blotting assays were performed to detect the expression of Nrf2, and the results demonstrated that farrerol upregulated the expression of Nrf2 in a dose-dependent manner *in vitro* (**Figures 2C,D**). Our results also showed that farrerol dose-dependently upregulates the levels of HO-1 and NQO1 proteins and downregulates the expression of Keap1 and NOX4 *in vitro* (**Figures 3A,B**) and *in vivo* (**Figures 7E,F**). To support these findings, we used Nrf2-knockout and wild-type mice models to further explore the mechanism through which Nrf2 protects against CDDP-induced AKI. Our findings revealed that the cisplatin group

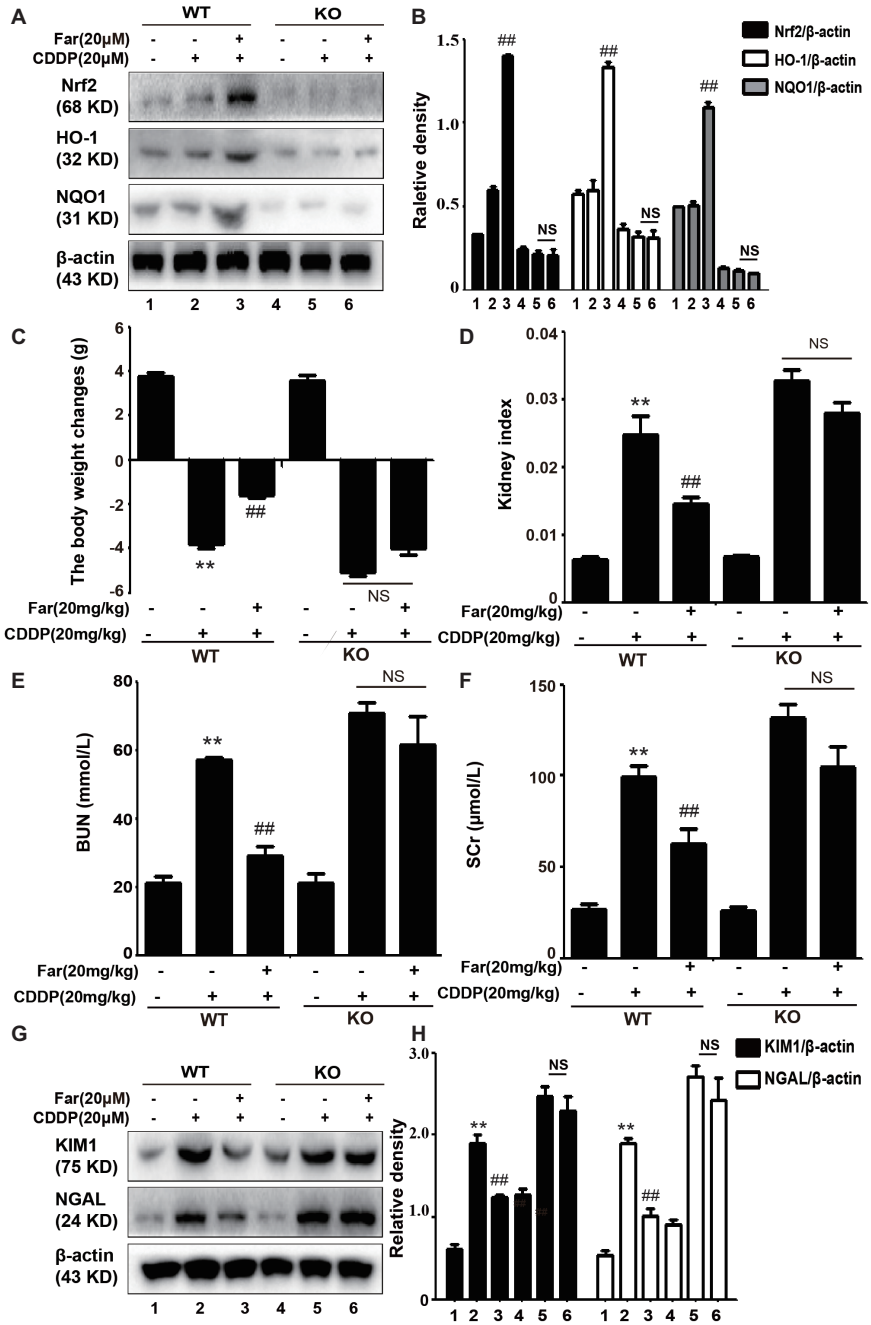

FIGURE 9 | The effects of farrerol on cisplatin-induced AKI depend on Nrf2 *in vivo*. After 12 h of fasting, wild-type and Nrf2-knockout C57BL/6 mice were injected intraperitoneally with farrerol (20 mg/kg), and cisplatin (20 mg/kg) was administered by intraperitoneal injection 1 h later. Farrerol was then administered at 24 and 48 h after the injection, and the mice were sacrificed 24 h after the last farrerol administration. After recording the body and kidney weights, the kidneys and blood from all the tested mice were collected. **(A,B)** Protein expression of Nrf2, HO-1, and NQO1 in the wild-type and Nrf2-knockout mice. The body weight changes **(C)**, kidney injury index **(D)**, BUN **(E)**. and SCr levels **(F)** in the wild-type and Nrf2-knockout mice were measured. All the data are presented as the means ± SEM (n = 10 per group). **(G,H)** Western blot analysis of KIM1 and NGAL protein expression in the kidneys. All experiments were duplicated three times. $^{*}p < 0.05$ and $^{**}p < 0.01$ compared with the control group; $^{\#}p < 0.05$ and $^{\#\#}p < 0.01$ compared with the CDDP group. β-actin was used as an internal control, NS, no specificity; WT, wild-type C57BL/6 mice; KO, Nrf2-knockout C57BL/6 mice.

exhibited significantly reduced kidney function (including body weight changes; kidney index; BUN, SCr, KIM1, and NGAL levels) and that Nrf2-knockout mice exhibited lower kidney function compared with the wild-type mice (**Figures 9C–H**). We also found that farrerol exerted only a slight protective effect on Nrf2-deficient mice, and no significant expression of Nrf2, HO-1, and NQO1 was detected in the Nrf2-knockout mice (**Figures 9A,B**).

Furthermore, increasing lines of evidence show that ROS produced by cisplatin mediate inflammatory pathways by activating the MAPK and NF-κB pathways (Baker et al., 2011; Li et al., 2014). NF-κB, which is a central regulator of the kidney inflammatory response mechanism (Meng et al., 2018a), can effectively control the expression of the inflammation-related signaling molecule NLRP3 and thereby regulate the inflammatory pathway. In brief, the MAPK family consists of three major serine/threonine kinase proteins, namely, JNK, ERK and p38. Previous studies have shown that members of the MAPK family are activated after cisplatin exposure (Malik et al., 2015). The phosphorylation of MAPK exacerbates renal function and further causes apoptosis and inflammation (Pabla and Dong, 2008). Here, we discovered that farrerol substantially declined cisplatin-induced MAPK phosphorylation and p-NF-κB activation *in vitro* (**Figures 3C–E**) and *in vivo* (**Figures 8A–C**). As described above, ROS can also induce the phosphorylation of ERK and p38 to regulate apoptosis *via* p53 (Martindale and Holbrook, 2002), which is a tumor-suppressor protein that plays a key role in the induction of apoptosis in various cell types (Jiang et al., 2007). Here, we detected the levels of p53, Bax, caspase-3, and Bcl2 by Western blot analysis and found that the expression levels of p-p53, Bax, and caspase-3 were significantly increased in the cisplatin group and that Bcl2 expression was increased after pretreatment with farrerol (**Figures 4A,B,D,E**). In addition, TUNEL staining (**Figures 4C,D**) and flow cytometry (**Figures 4E,F**) assays indicated that farrerol evidently alleviated apoptosis compared with cisplatin treatment alone. Therefore, the scavenging of ROS by farrerol could prevent cisplatin-induced p-p53 activation and effectively decrease MTECs apoptosis. In short, we concluded that farrerol can alle*via*te the cisplatin-induced inflammatory response and apoptotic pathway by inhibiting ROS production *in vitro* and *in vivo*.

CONCLUSION

In summary, our study demonstrated that farrerol can improve cisplatin-induced nephrotoxicity by ameliorating the oxidative, inflammatory, and apoptotic pathways (**Figure 10**). This mechanism of kidney protection further alleviates the generation of ROS by activating Nrf2, which in turn regulates the signaling pathways associated with oxidation, inflammation, and apoptotic factors. These experiments demonstrated that farrerol, as a natural Nrf2 activator, has potential for the treatment of clinical AKI.

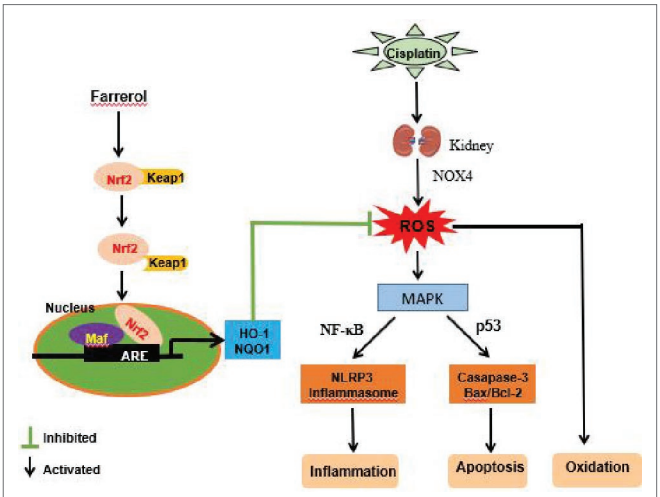

FIGURE 10 | Protective effects of farrerol on CDDP-induced AKI and the underlying mechanism. Cisplatin enters the kidney and induces the production of a large amount of ROS. On the one hand, ROS can directly cause oxidative stress, and on the other hand, ROS activate NF-κB and p53 *via* the MAPK pathway and thereby induce changes in inflammation and apoptosis. Farrerol alleviates the generation of ROS by activating Nrf2, which in turn regulates the oxidation, inflammation, and apoptosis signaling pathways.

DATA AVAILABILITY STATEMENT

All datasets analyzed for this study are included in the article/supplementary material.

ETHICS STATEMENT

The animal study was reviewed and approved by the Animal Health and Research Ethics Committee of Jilin University.

AUTHOR CONTRIBUTIONS

NM, WW, and XC designed the study. NM, WW, and XF performed the study. XF and XC helped in analyzing the data. NM and WW wrote the manuscript.

FUNDING

This study was funded by the National Natural Science Foundation of China (grant/award number 81603174) and the China Postdoctoral Science Fund for General Economic Assistance (grant/award number 2018T110257).

REFERENCES

Arany, I., Megyesi, J. K., Kaneto, H., Price, P. M., and Safirstein, R. L. (2004). Cisplatin-induced cell death is EGFR/src/ERK signaling dependent in mouse proximal tubule cells. *Am. J. Physiol. Renal Physiol.* 287, F543–F549. doi: 10.1152/ajprenal.00112.2004

Arany, I., and Safirstein, R. L. (2003). Cisplatin nephrotoxicity. *Semin. Nephrol.* 23, 460–464. doi: 10.1016/S0270-9295(03)00089-5

Babelova, A., Avaniadi, D., Jung, O., Fork, C., Beckmann, J., Kosowski, J., et al. (2012). Role of Nox4 in murine models of kidney disease. *Free Radic. Biol. Med.* 53, 842–853. doi: 10.1016/j.freeradbiomed.2012.06.027

Bagshaw, S. M., and Wald, R. (2016). Acute kidney injury: timing of renal replacement therapy in AKI. *Nat. Rev. Nephrol.* 12, 445–446. doi: 10.1038/nrneph.2016.92

Baker, R. G., Hayden, M. S., and Ghosh, S. (2011). NF-kappaB, inflammation and metabolic disease. *Cell Metab.* 13, 11–22. doi: 10.1016/j.cmet.2010.12.008

Buendia, I., Michalska, P., Navarro, E., Gameiro, I., Egea, J., and Leon, R. (2016). Nrf2-ARE pathway: an emerging target against oxidative stress and neuroinflammation in neurodegenerative diseases. *Pharmacol. Ther.* 157, 84–104. doi: 10.1016/j.pharmthera.2015.11.003

Chen, Y., Zheng, Y., Xin, L., Zhong, S., Liu, A., Lai, W., et al. (2019). 15-epi-lipoxin A4 inhibits TNF-alpha-induced tissue factor expression *via* the PI3K/AKT/ NF-kappaB axis in human umbilical vein endothelial cells. *Biomed. Pharmacother.* 117:109099. doi: 10.1016/j.biopha.2019.109099

Chin, M. P., Bakris, G. L., Block, G. A., Chertow, G. M., Goldsberry, A., Inker, L. A., et al. (2018). Bardoxolone methyl improves kidney function in patients with chronic kidney disease stage 4 and type 2 diabetes: post-hoc analyses from bardoxolone methyl evaluation in patients with chronic kidney disease and type 2 diabetes study. *Am. J. Nephrol.* 47, 40–47. doi: 10.1159/000486398

Ci, X., Chu, X., Wei, M., Yang, X., Cai, Q., and Deng, X. (2012). Different effects of farrerol on an OVA-induced allergic asthma and LPS-induced acute lung injury. *PLoS One* 7:e34634. doi: 10.1371/journal.pone.0034634

Ci, X., Lv, H., Wang, L., Wang, X., Peng, L., Qin, F. X., et al. (2015). The antioxidative potential of farrerol occurs *via* the activation of Nrf2 mediated HO-1 signaling in RAW 264.7 cells. *Chem. Biol. Interact.* 239, 192–199. doi: 10.1016/j.cbi.2015.06.032

Dodson, M., Redmann, M., Rajasekaran, N. S., Darley-Usmar, V., and Zhang, J. (2015). KEAP1-NRF2 signalling and autophagy in protection against oxidative and reductive proteotoxicity. *Biochem. J.* 469, 347–355. doi: 10.1042/BJ20150568

Doi, K., and Rabb, H. (2016). Impact of acute kidney injury on distant organ function: recent findings and potential therapeutic targets. *Kidney Int.* 89, 555–564. doi: 10.1016/j.kint.2015.11.019

Fu, H., Zhou, D., Zhu, H., Liao, J., Lin, L., Hong, X., et al. (2019). Matrix metalloproteinase-7 protects against acute kidney injury by priming renal tubules for survival and regeneration. *Kidney Int.* 95, 1167–1180. doi: 10.1016/j.kint.2018.11.043

Huang, Y. C., Tsai, M. S., Hsieh, P. C., Shih, J. H., Wang, T. S., Wang, Y. C., et al. (2017). Galangin ameliorates cisplatin-induced nephrotoxicity by attenuating oxidative stress, inflammation and cell death in mice through inhibition of ERK and NF-kappaB signaling. *Toxicol. Appl. Pharmacol.* 329, 128–139. doi: 10.1016/j.taap.2017.05.034

Jaiman, S., Sharma, A. K., Singh, K., and Khanna, D. (2013). Signalling mechanisms involved in renal pathological changes during cisplatin-induced nephropathy. *Eur. J. Clin. Pharmacol.* 69, 1863–1874. doi: 10.1007/s00228-013-1568-7

Jiang, T., Huang, Z., Lin, Y., Zhang, Z., Fang, D., and Zhang, D. D. (2010). The protective role of Nrf2 in streptozotocin-induced diabetic nephropathy. *Diabetes* 59, 850–860. doi: 10.2337/db09-1342

Jiang, M., Wang, C. Y., Huang, S., Yang, T., and Dong, Z. (2009). Cisplatin-induced apoptosis in p53-deficient renal cells *via* the intrinsic mitochondrial pathway. *Am. J. Physiol. Renal Physiol.* 296, F983–F993. doi: 10.1152/ajprenal.90579.2008

Jiang, M., Wei, Q., Pabla, N., Dong, G., Wang, C. Y., Yang, T., et al. (2007). Effects of hydroxyl radical scavenging on cisplatin-induced p53 activation, tubular cell apoptosis and nephrotoxicity. *Biochem. Pharmacol.* 73, 1499–1510. doi: 10.1016/j.bcp.2007.01.010

Ke, B., Shen, W., Fang, X., and Wu, Q. (2018). The NLPR3 inflammasome and obesity-related kidney disease. *J. Cell. Mol. Med.* 22, 16–24. doi: 10.1111/jcmm.13333

Kim, J., Perera, N. C. N., Godahewa, G. I., Priyathilaka, T. T., and Lee, J. (2019). Characterization of a catalase from red-lip mullet (Liza haematocheila): demonstration of antioxidative activity and mRNA upregulation in response to immunostimulants. *Gene* 712:143945. doi: 10.1016/j.gene.2019.143945

Li, H., Huang, K., Liu, X., Liu, J., Lu, X., Tao, K., et al. (2014). Lithium chloride suppresses colorectal cancer cell survival and proliferation through ROS/GSK-3β/NF-κB signaling pathway. *Oxidative Med. Cell. Longev.* 2014:241864. doi: 10.1155/2014/241864

Li, Y., Kakkar, R., and Wang, J. (2018a). *In vivo* and *in vitro* approach to anti-arthritic and anti-inflammatory effect of crocetin by alteration of nuclear factor-E2-related factor 2/hem oxygenase (HO)-1 and NF-kappaB expression. *Front. Pharmacol.* 9:1341. doi: 10.3389/fphar.2018.01341

Li, Z., Xu, K., Zhang, N., Amador, G., Wang, Y., Zhao, S., et al. (2018b). Overexpressed SIRT6 attenuates cisplatin-induced acute kidney injury by inhibiting ERK1/2 signaling. *Kidney Int.* 93, 881–892. doi: 10.1016/j.kint.2017.10.021

Li, R. Y., Zhang, W. Z., Yan, X. T., Hou, J. G., Wang, Z., Ding, C. B., et al. (2019). Arginyl-fructosyl-glucose, a major Maillard reaction product of red ginseng, attenuates cisplatin-induced acute kidney injury by regulating nuclear factor kappaB and phosphatidylinositol 3-kinase/protein kinase B signaling pathways. *J. Agric. Food Chem.* 67, 5754–5763. doi: 10.1021/acs.jafc.9b00540

Lin, Q., Li, S., Jiang, N., Shao, X., Zhang, M., Jin, H., et al. (2019). PINK1-parkin pathway of mitophagy protects against contrast-induced acute kidney injury *via* decreasing mitochondrial ROS and NLRP3 inflammasome activation. *Redox Biol.* 26:101254. doi: 10.1016/j.redox.2019.101254

Liu, M., Grigoryev, D. N., Crow, M. T., Haas, M., Yamamoto, M., Reddy, S. P., et al. (2009). Transcription factor Nrf2 is protective during ischemic and nephrotoxic acute kidney injury in mice. *Kidney Int.* 76, 277–285. doi: 10.1038/ki.2009.157

Liu, E., Liang, T., Wang, X., Ban, S., Han, L., and Li, Q. (2015). Apoptosis induced by farrerol in human gastric cancer SGC-7901 cells through the mitochondrial-mediated pathway. *Eur. J. Cancer Prev.* 24, 365–372. doi: 10.1097/CEJ.0000000000000104

Ma, Q. (2013). Role of nrf2 in oxidative stress and toxicity. *Annu. Rev. Pharmacol. Toxicol.* 53, 401–426. doi: 10.1146/annurev-pharmtox-011112-140320

Ma, Z. N., Liu, Z., Wang, Z., Ren, S., Tang, S., Wang, Y. P., et al. (2017). Supplementation of American ginseng berry extract mitigated cisplatin-evoked nephrotoxicity by suppressing ROS-mediated activation of MAPK and NF-kappaB signaling pathways. *Food Chem. Toxicol.* 110, 62–73. doi: 10.1016/j.fct.2017.10.006

Ma, P., Zhang, S., Su, X., Qiu, G., and Wu, Z. (2015). Protective effects of icariin on cisplatin-induced acute renal injury in mice. *Am. J. Transl. Res.* 7, 2105–2114

Malik, S., Suchal, K., Gamad, N., Dinda, A. K., Arya, D. S., and Bhatia, J. (2015). Telmisartan ameliorates cisplatin-induced nephrotoxicity by inhibiting MAPK mediated inflammation and apoptosis. *Eur. J. Pharmacol.* 748, 54–60. doi: 10.1016/j.ejphar.2014.12.008

Martindale, J. L., and Holbrook, N. J. (2002). Cellular response to oxidative stress: signaling for suicide and survival. *J. Cell. Physiol.* 192, 1–15. doi: 10.1002/jcp.10119

Meng, X. M., Li, H. D., Wu, W. F., Ming-Kuen Tang, P., Ren, G. L., Gao, L., et al. (2018a). Wogonin protects against cisplatin-induced acute kidney injury by targeting RIPK1-mediated necroptosis. *Lab. Investig.* 98, 79–94. doi: 10.1038/labinvest.2017.115

Meng, X. M., Ren, G. L., Gao, L., Yang, Q., Li, H. D., Wu, W. F., et al. (2018b). NADPH oxidase 4 promotes cisplatin-induced acute kidney injury *via* ROS-mediated programmed cell death and inflammation. *Lab. Investig.* 98, 63–78. doi: 10.1038/labinvest.2017.120

Moledina, D. G., and Parikh, C. R. (2018). Phenotyping of acute kidney injury: beyond serum creatinine. *Semin. Nephrol.* 38, 3–11. doi: 10.1016/j.semnephrol.2017.09.002

Nath, K. A., and Norby, S. M. (2000). Reactive oxygen species and acute renal failure. *Am. J. Med.* 109, 665–678. doi: 10.1016/S0002-9343(00)00612-4

Okada, M., Matsuzawa, A., Yoshimura, A., and Ichijo, H. (2014). The lysosome rupture-activated TAK1-JNK pathway regulates NLRP3 inflammasome activation. *J. Biol. Chem.* 289, 32926–32936. doi: 10.1074/jbc.M114.579961

Ozkok, A., and Edelstein, C. L. (2014). Pathophysiology of cisplatin-induced acute kidney injury. *Biomed. Res. Int.* 2014:967826. doi: 10.1155/2014/967826

Pabla, N., and Dong, Z. (2008). Cisplatin nephrotoxicity: mechanisms and renoprotective strategies. *Kidney Int.* 73, 994–1007. doi: 10.1038/sj.ki.5002786

Pan, H., Shen, Z., Mukhopadhyay, P., Wang, H., Pacher, P., Qin, X., et al. (2009). Anaphylatoxin C5a contributes to the pathogenesis of cisplatin-induced nephrotoxicity. *Am. J. Physiol. Renal Physiol.* 296, F496–F504. doi: 10.1152/ajprenal.90443.2008

Sedeek, M., Nasrallah, R., Touyz, R. M., and Hebert, R. L. (2013). NADPH oxidases, reactive oxygen species, and the kidney: friend and foe. *J. Am. Soc. Nephrol.* 24, 1512–1518. doi: 10.1681/ASN.2012111112

Shen, Y., Chen, S., and Zhao, Y. (2019). Sulfiredoxin-1 alleviates high glucose-induced podocyte injury though promoting Nrf2/ARE signaling *via* inactivation of GSK-3beta. *Biochem. Biophys. Res. Commun.* 516, 1137–1144. doi: 10.1016/j.bbrc.2019.06.157

So, H., Kim, H., Lee, J. H., Park, C., Kim, Y., Kim, E., et al. (2007). Cisplatin cytotoxicity of auditory cells requires secretions of proinflammatory cytokines

via activation of ERK and NF-kappaB. *J. Assoc. Res. Otolaryngol.* 8, 338–355. doi: 10.1007/s10162-007-0084-9

Stojic, I. M., Jakovljevic, V. L., Zivkovic, V. I., Srejovic, I. M., Nikolic, T. R., Jeremic, J. N., et al. (2018). The perfusion of cisplatin and cisplatin structural analogues through the isolated rat heart: the effects on coronary flow and cardiodynamic parameters. *Gen. Physiol. Biophys.* 37, 515–525. doi: 10.4149/gpb_2018004

Wang, Y., Tang, C., Cai, J., Chen, G., Zhang, D., Zhang, Z., et al. (2018). PINK1/Parkin-mediated mitophagy is activated in cisplatin nephrotoxicity to protect against kidney injury. *Cell Death Dis.* 9:1113. doi: 10.1038/s41419-018-1152-2

Wang, L., Wei, W., Xiao, Q., Yang, H., and Ci, X. (2019). Farrerol ameliorates APAP-induced hepatotoxicity *via* activation of Nrf2 and autophagy. *Int. J. Biol. Sci.* 15, 788–799. doi: 10.7150/ijbs.30677

Wei, Q., Dong, G., Franklin, J., and Dong, Z. (2007). The pathological role of Bax in cisplatin nephrotoxicity. *Kidney Int.* 72, 53–62. doi: 10.1038/sj.ki.5002256

Yang, Y., Adebali, O., Wu, G., Selby, C. P., Chiou, Y. Y., Rashid, N., et al. (2018). Cisplatin-DNA adduct repair of transcribed genes is controlled by two circadian programs in mouse tissues. *Proc. Natl. Acad. Sci. USA* 115, E4777–E4785. doi: 10.1073/pnas.1804493115

Yen, C. C., Chang, W. H., Tung, M. C., Chen, H. L., Liu, H. C., Liao, C. H., et al. (2019). Lactoferrin protects hyperoxia-induced lung and kidney systemic inflammation in an *in vivo* imaging model of NF-kappaB/luciferase transgenic mice. *Mol. Imaging Biol.* 11, 5197–5211. doi: 10.1007/s11307-019-01390-x

Conflict of Interest: The authors declare that the research was conducted in the absence of any commercial or financial relationships that could be construed as a potential conflict of interest.

Copyright © 2019 Ma, Wei, Fan and Ci. This is an open-access article distributed under the terms of the Creative Commons Attribution License (CC BY). The use, distribution or reproduction in other forums is permitted, provided the original author(s) and the copyright owner(s) are credited and that the original publication in this journal is cited, in accordance with accepted academic practice. No use, distribution or reproduction is permitted which does not comply with these terms.

frontiers in Medicine

ORIGINAL RESEARCH
published: 05 December 2019
doi: 10.3389/fmed.2019.00288

Urolithiasis Is a Risk Factor for Uroseptic Shock and Acute Kidney Injury in Patients With Urinary Tract Infection

*Chih-Yen Hsiao [1,2], Tsung-Hsien Chen [1], Yi-Chien Lee [3,4], Meng-Chang Hsiao [5], Peir-Haur Hung [1,6], Yih-Yuan Chen [7] and Ming-Cheng Wang [8]**

[1] Division of Nephrology, Department of Internal Medicine, Ditmanson Medical Foundation Chia-Yi Christian Hospital, Chiayi, Taiwan, [2] Department of Hospital and Health Care Administration, Chia Nan University of Pharmacy and Science, Tainan, Taiwan, [3] Department of Internal Medicine, Fu Jen Catholic University Hospital, Fu Jen Catholic University, New Taipei City, Taiwan, [4] School of Medicine, College of Medicine, Fu Jen Catholic University, New Taipei City, Taiwan, [5] The Jackson Laboratory for Genomic Medicine, Farmington, CT, United States, [6] Department of Applied Life Science and Health, Chia Nan University of Pharmacy and Science, Tainan, Taiwan, [7] Department of Biochemical Science and Technology, National Chiayi University, Chiayi, Taiwan, [8] Division of Nephrology, Department of Internal Medicine, National Cheng Kung University Hospital, College of Medicine, National Cheng Kung University, Tainan, Taiwan

Urinary tract infection (UTI) is a common complication in patients with urolithiasis. This study aimed to compare clinical manifestations and treatment outcomes among UTI patients with or without urolithiasis. It also focused on identifying relationships among urolithiasis, uroseptic shock, and acute kidney injury (AKI). This retrospective study enrolled hospitalized UTI patients who underwent imaging in an acute care setting from January 2006 to March 2015. Of 662 participants enrolled, 113 (17.1%) had urolithiasis, 107 (16.2%) developed uroseptic shock, and 184 (27.8%) developed AKI. A multivariate logistic regression analysis showed that in UTI patients, urolithiasis is associated with an increased risk of uroseptic shock (OR 1.80, 95% CI: 1.08–3.02, $P = 0.025$), AKI (OR 1.95, 95% CI: 1.22–3.12, $P = 0.005$), and bacteremia (OR 1.68, 95% CI: 1.08–2.64, $P = 0.022$). Urolithiasis is common in UTI patients and is associated with an increased risk of uroseptic shock and AKI.

Keywords: urolithiasis, urinary tract infection, uroseptic shock, acute kidney injury, bacteremia

OPEN ACCESS

Edited by:
John D. Imig,
Medical College of Wisconsin,
United States

Reviewed by:
Bassam G. Abu Jawdeh,
University of Cincinnati, United States
Ankana Daga,
Harvard Medical School,
United States

***Correspondence:**
Ming-Cheng Wang
tsutsugamushi8901@gmail.com

Specialty section:
This article was submitted to Nephrology, a section of the journal Frontiers in Medicine

Received: *27 August 2019*
Accepted: *22 November 2019*
Published: *05 December 2019*

Citation:
Hsiao C-Y, Chen T-H, Lee Y-C, Hsiao M-C, Hung P-H, Chen Y-Y and Wang M-C (2019) Urolithiasis Is a Risk Factor for Uroseptic Shock and Acute Kidney Injury in Patients With Urinary Tract Infection. Front. Med. 6:288. doi: 10.3389/fmed.2019.00288

INTRODUCTION

Urolithiasis is a global problem with an increasing incidence and prevalence rate (1, 2). The global prevalence of urolithiasis ranges from 2 to 20% and varies based on geographical locations and socioeconomic conditions of different populations (3, 4). Urolithiasis is a well-known risk factor of urinary tract infection (UTI), and a vicious cycle leading to several clinical consequences is observed seen as follows: stones → obstruction → stasis → infection → stones (5). Furthermore, urolithiasis is associated with an increased risk of chronic kidney disease (CKD), hypertension, and myocardial infarction (6–8).

Urolithiasis can lead to urinary stasis, which enables bacteria to adhere to the urothelium and multiply, thereby causing UTI (9). Complicated UTI related to obstructive uropathy can progress to urosepsis and may cause septic shock and disseminated intravascular coagulopathy (10). However, only a few studies have demonstrated the correlation among urolithiasis, uroseptic shock, and

acute kidney injury (AKI) in UTI patients. Hence, we conducted a study to investigate whether urolithiasis is an important risk factor for uroseptic shock and AKI in UTI patients.

MATERIALS AND METHODS

Study Design and Patient Selection

The data for this retrospective observational study were collected between January 2006 and March 2015 from patients visiting Chiayi Christian Hospital in southern Taiwan, which consists of 1,077 inpatient beds and an outpatient department serving ∼4,110 patients per day. This study was conducted after obtaining ethical approval from the Institutional Review Board of Chiayi Christian Hospital (approval no. CYCH-IRB-100015).

In total, 662 consecutively hospitalized UTI patients without any other concurrent infectious disease were enrolled in the study. All patients were adults and presented with UTI symptoms such as pain on urination, lumbago, or fever with bacterial isolation of $>10^5$ colony-forming units/mL from a urine specimen. All patients underwent imaging studies, such as ultrasonography, intravenous urography (IVU), or computed tomography (CT), to identify urolithiasis and urinary tract obstruction. The patients were divided into two groups based on the presence or absence of urolithiasis. The clinical characteristics and laboratory data were collected using a standard form for further analysis.

Assessment of the Subjects

Data on demographic characteristics (age and sex), comorbidities [diabetes mellitus (DM), hypertension, coronary artery disease, congestive heart failure (CHF), stroke, and long-term indwelling Foley catheter], vital signs (blood pressure and temperature), laboratory results [white blood cell (WBC) count, platelet count, serum creatinine, and estimated glomerular filtration rate (eGFR) at baseline and after hospitalization], causative microorganisms and antimicrobial resistance pattern, and imaging of patients were collected and analyzed.

Definitions

The diagnosis of urolithiasis was based on imaging studies. Urolithiasis was defined as the presence of any stone formation in the urinary tract that was detected during imaging studies such as ultrasonography, CT with or without enhancement, or IVU. Uroseptic shock was defined as sepsis-induced hypotension [systolic blood pressure (SBP) <90 mmHg or mean arterial pressure <70 mmHg or a decrease in SBP by >40 mmHg and lasting for at least 1 h, despite adequate fluid resuscitation and in the absence of other causes of hypotension] (11). eGFR was determined using the Chronic Kidney Disease Epidemiology Collaboration (CKD-EPI) creatinine equation (12, 13). For patients without recognized CKD, the estimation of baseline creatinine level was performed using the CKD-EPI creatinine equation assuming a GFR of 75 ml/min/1.73 m^2 (14). AKI was defined as an increase in serum creatinine level to ≥1.5 times the baseline values according to the KDIGO Clinical Practice Guideline criteria for serum creatinine value for AKI stages 1, 2, and 3 (15). Afebrile status was defined as a body temperature of ≤38.3°C (101°F) during hospitalization. Multiple drug resistance (MDR) was defined as non-susceptibility of the isolates to at least one agent in three or more antimicrobial categories (16).

Statistical Analyses

The patients were grouped into two categories: those with or without urolithiasis. The continuous variables were expressed as mean ± SD, and the categorical variables were expressed as number (percentage). The data were analyzed using Student's *t*-test or chi-square test depending on the type of variables. Multivariate logistic regression analyses were performed to identify factors associated with urolithiasis, septic shock, and AKI post-admission. Only variables significant at the 0.15 level in the univariate analysis were selected for consecutive multivariate analyses. The goodness-of-fit of the logistic regression model was assessed using the Cox and Snell test, and the explanatory power was reported using Nagelkerke's pseudo-R-square. A *P*-value of <0.05 was considered statistically significant. All analyses were performed using SPSS software for Windows (SPSS Science, v. 17.0, Chicago, IL).

RESULTS

The demographic and clinical characteristics of 662 hospitalized UTI patients are shown in **Table 1**. The mean age on admission was 67 ± 17 years. A majority of the patients [468 (70.7%)] were females, and 229 (34.6%) had a prior history of UTI. There were 107 patients (16.2%) with uroseptic shock and 184 patients (27.8%) with AKI during hospitalization. The overall mortality rate was 0.45% (3/662). Among UTI patients, 113 (17.1%) had urolithiasis and 41 had ureteral stone with urinary tract obstruction. The ureteral stones were located at the upper ureter or ureteropelvic junction in 18 patients (43.9%), mid ureter in 5 (12.2%), and distal ureter and ureterovesical junction in 18 (43.9%). Thirty (16.3%) and 81 patients (16.9%) underwent radiologic examinations using contrast media (IVU or CT) in the AKI and non-AKI groups, respectively. The prevalence of male sex (40.7 vs. 27.0%, $P = 0.003$), bacteremia (57.5 vs. 40.3%, $P = 0.001$), uroseptic shock (26.5 vs. 14.0%, $P = 0.001$), AKI (40.7 vs. 25.1%, $P = 0.001$) and *Proteus* spp. isolates (10.6 vs. 2.6%, $P < 0.001$) was higher, while *Escherichia coli* isolates (61.1 vs. 75.8%, $P = 0.002$) was lower in patients with urolithiasis than in those without. Among UTI patients with urolithiasis, the incidences of AKI were 60.0 and 33.7%, respectively, in patients with and without uroseptic shock. The top five bacteria identified in UTI patients with urolithiasis were *E. coli* (61.1%), *Proteus* spp. (10.6%), *Klebsiella* spp. (8.8%), *Pseudomonas* spp. (8.0%), and *Enterococcus* spp. (3.5%). The top five bacteria identified in UTI patients without urolithiasis were *E. coli* (75.8%), *Klebsiella* spp. (7.7%), *Pseudomonas* spp. (7.1%), *Enterococcus* spp. (4.6%), and *Proteus* spp. (2.6%).

CHF (OR 2.43, 95% CI: 1.03–5.77, $P = 0.043$), urolithiasis (OR 1.80, 95% CI: 1.08–3.02, $P = 0.025$), and AKI (OR 2.30, 95% CI: 1.45–3.65, $P < 0.001$) were independently associated with an increased risk of uroseptic shock (**Table 2**). Patients with DM (OR 1.78, 95% CI: 1.21–2.60, $P = 0.003$), afebrile during hospitalization (OR 1.63, 95% CI: 1.08–2.44, $P = 0.019$),

TABLE 1 | Characteristics of hospitalized patients with urinary tract infection with respect to urolithiasis.

	All (n = 662)	Non-urolithiasis (n = 549)	Urolithiasis (n = 113)	P-value
Age (year)	67 ± 17	67 ± 18	67 ± 15	0.603*
Sex (male)	194 (29.3)	148 (27.0)	46 (40.7)	0.003¥
Diabetes mellitus	282 (42.6)	232 (42.3)	50 (44.2)	0.697¥
Hypertension	335 (50.6)	275 (50.1)	60 (53.1)	0.561¥
Congestive heart failure	28 (4.2)	23 (4.2)	5 (4.4)	0.802¥
Coronary artery disease	64 (9.7)	55 (10.0)	9 (8.0)	0.501¥
Stroke	157 (23.7)	134 (24.4)	23 (20.4)	0.356¥
Prior history of UTI				0.726¥
None	433 (65.4)	357 (65.0)	76 (67.3)	
Once	123 (18.6)	105 (19.1)	18 (15.9)	
Twice	59 (8.9)	50 (9.1)	9 (8.0)	
Thrice or more	47 (7.1)	37 (6.7)	10 (8.8)	
Indwelling Foley catheter	58 (8.8)	46 (8.4)	12 (10.6)	0.443¥
Afebrile	270 (40.8)	231 (42.1)	39 (34.5)	0.136¥
Bacteremia	286 (43.2)	221 (40.3)	65 (57.5)	0.001¥
Uroseptic shock	107 (16.2)	77 (14.0)	30 (26.5)	0.001¥
Acute kidney injury	184 (27.8)	138 (25.1)	46 (40.7)	0.001¥
Acute kidney injury stage				0.004¥
Stage 1	99 (15.0)	78 (14.2)	21 (18.6)	
Stage 2	58 (8.8)	41 (7.5)	17 (15.0)	
Stage 3	27 (4.1)	19 (3.5)	8 (7.1)	
Baseline serum creatinine (mg/dL)	1.1 ± 0.8	1.1 ± 0.8	1.1 ± 0.8	0.665*
Baseline eGFR (mL/min/1.73 m^2)	70.5 ± 28.7	70.4 ± 29.7	71.2 ± 23.6	0.755*
Hospitalized serum creatinine (mg/dL)	1.6 ± 1.4	1.6 ± 1.4	1.7 ± 1.4	0.561*
Hospitalized eGFR (mL/min/1.73 m^2)	58.2 ± 36.4	56.0 ± 32.2	50.9 ± 27.1	0.076*
White blood cell ($10^3/\mu L$)	13.4 ± 6.1	13.4 ± 5.9	13.7 ± 7.3	0.649*
Platelets ($10^3/\mu L$)	207 ± 124	209 ± 130	202 ± 92	0.600*
Escherichia coli	485 (73.3)	416 (75.8)	69 (61.1)	0.002¥
Proteus species	26 (3.9)	14 (2.6)	12 (10.6)	<0.001¥
Klebsiella species	52 (7.9)	42 (7.7)	10 (8.8)	0.811¥
Enterococcus species	29 (4.4)	25 (4.6)	4 (3.5)	0.803¥
Pseudomonas species	48 (7.3)	39 (7.1)	9 (8.0)	0.903¥
MDR isolate	234 (35.3)	190 (34.6)	44 (38.9)	0.381¥

**Student's t-test; ¥ Chi-square test or Fisher's exact test.*
Data are expressed as mean ± SD or number (percentage).
MDR, multiple drug resistance; eGFR, estimated glomerular filtration rate.

bacteremia (OR 2.19, 95% CI: 1.47–3.26, $P < 0.001$), uroseptic shock (OR 2.44, 95% CI: 1.51–3.93, $P < 0.001$), urolithiasis (OR 1.95, 95% CI: 1.22–3.12, $P = 0.005$), and higher WBC count (OR 1.04, 95% CI: 1.00–1.07, $P = 0.025$) were independently associated with an increased risk of AKI. Conversely, higher eGFR (OR 0.99, 95% CI: 0.98–0.99, $P < 0.001$) was independently associated with a decreased risk of AKI in UTI patients (**Table 3**). **Figure 1** shows a reduction in eGFR in UTI patients with uroseptic shock and urolithiasis. The reduction in eGFR values in uroseptic shock patients with or without urolithiasis, and UTI patients with or without urolithiasis were 28.35 (95% CI: 19.23–37.46), 20.78 (95% CI: 16.58–24.97), 17.05 (95% CI: 13.72–20.39), and 13.28 (95% CI: 12.05–14.50) mL/min/1.73 m^2, respectively. Significant differences were observed between uroseptic shock patients with urolithiasis and UTI patients with urolithiasis, uroseptic shock patients without urolithiasis and UTI patients without urolithiasis, uroseptic patients with urolithiasis and UTI patients without urolithiasis, and UTI patients with urolithiasis and UTI patients without urolithiasis. Urolithiasis (OR 1.68, 95% CI: 1.08–2.64, $P = 0.022$), AKI (OR 1.87, 95% CI: 1.26–2.78, $P = 0.002$), and higher WBC count (OR 1.04, 95% CI: 1.01–1.07, $P = 0.006$) were independently associated with an increased risk of bacteremia, while afebrile status (OR 0.32, 95% CI: 0.22–0.46, $P < 0.001$) and higher platelet count (OR 1.00, 95% CI: 0.99–1.00, $P < 0.001$) were independently associated with a decreased risk of bacteremia in UTI patients (**Table 4**).

DISCUSSION

The relationship between urolithiasis and UTI is complex. UTI is a common complication in patients with urolithiasis, and it promotes the formation of urolithiasis (5). Our study

TABLE 2 | Univariate and multivariate logistic regression analyses of factors related to uroseptic shock in patients with urinary tract infection.

Covariate	Univariate		Multivariate	
	OR (95% CI)	*P*-value	OR (95% CI)	*P*-value
Age (year)	1.01 (1.00–1.03)	0.038	1.01 (0.99–1.02)	0.230
Sex (male)	1.48 (0.96–2.29)	0.077	1.49 (0.94–2.37)	0.093
Diabetes mellitus	0.93 (0.61–1.42)	0.736		
Hypertension	0.83 (0.55–1.26)	0.382		
Congestive heart failure	3.08 (1.38–6.86)	0.006	2.43 (1.03–5.77)	0.043
Coronary artery disease	2.04 (1.12–3.71)	0.019	1.54 (0.80–2.94)	0.195
Stroke	1.31 (0.82–2.09)	0.252		
Indwelling Foley catheter	0.95 (0.45–1.99)	0.889		
Afebrile	0.66 (0.43–1.03)	0.065	0.62 (0.38–1.02)	0.060
Bacteremia	1.95 (1.28–2.96)	0.002	1.34 (0.84–2.15)	0.216
Acute kidney injury	2.76 (1.80–4.22)	<0.001	2.30 (1.45–3.65)	<0.001
Urolithiasis	2.22 (1.37–3.59)	0.001	1.80 (1.08–3.02)	0.025
Baseline eGFR (mL/min/1.73 m^2)	1.00 (0.99–1.00)	0.292		
White blood cell ($10^3/\mu L$)	1.02 (0.99–1.06)	0.157		
Platelets ($10^3/\mu L$)	1.00 (1.00–1.00)	0.024	1.00 (1.00–1.00)	0.166

eGFR, estimated glomerular filtration rate.

TABLE 3 | Univariate and multivariate logistic regression analyses of factors related to acute kidney injury in patients with urinary tract infection.

Covariate	Univariate		Multivariate	
	OR (95% CI)	*P*-value	OR (95% CI)	*P*-value
Age (year)	1.03 (1.02–1.04)	<0.001	1.01 (0.99–1.03)	0.206
Sex (male)	0.80 (0.55–1.18)	0.260		
Diabetes mellitus	2.19 (1.55–3.10)	<0.001	1.78 (1.21–2.60)	0.003
Hypertension	1.95 (1.38–2.77)	<0.001	1.30 (0.87–1.95)	0.197
Congestive heart failure	2.73 (1.27–5.84)	0.010	1.84 (0.78–4.32)	0.161
Coronary artery disease	1.77 (1.04–3.02)	0.036	1.13 (0.62–2.05)	0.698
Stroke	1.02 (0.68–1.51)	0.941		
Indwelling Foley catheter	0.99 (0.54–1.81)	0.970		
Afebrile	1.45 (1.03–2.04)	0.035	1.63 (1.08–2.44)	0.019
Bacteremia	2.11 (1.50–2.99)	<0.001	2.19 (1.47–3.26)	<0.001
Uroseptic shock	2.76 (1.80–4.22)	<0.001	2.44 (1.51–3.93)	<0.001
Urolithiasis	2.04 (1.34–3.12)	0.001	1.95 (1.22–3.12)	0.005
Baseline eGFR (mL/min/1.73 m^2)	0.98 (0.98–0.99)	<0.001	0.99 (0.98–0.99)	<0.001
White blood cell ($10^3/\mu L$)	1.04 (1.01–1.07)	0.004	1.04 (1.00–1.07)	0.025
Platelets ($10^3/\mu L$)	1.00 (1.00–1.00)	0.568		

eGFR, estimated glomerular filtration rate.

demonstrated a higher prevalence of urolithiasis in UTI patients than in the general population. The presence of urolithiasis was associated with worse clinical outcomes in UTI patients, including an increased risk of bacteremia, uroseptic shock, and AKI. To the best of our knowledge, this is the first study to demonstrate that urolithiasis is associated with an increased risk of uroseptic shock and AKI in UTI patients.

Patients with septic shock are in a critical situation that requires significant healthcare resources. It is estimated that UTI is the underlying cause in 30% of patients with severe sepsis and septic shock (17). The rate of developing septic shock in patients with UTI can range from 20.8 to 32.9% based on different underlying conditions (18–20). In the current study, the incidence of uroseptic shock in UTI patients that necessitated admission was 16.2%. Multiple factors attributing to septic shock have previously been reported in patients with UTI. Indwelling urinary catheter and increased C-reactive protein levels were risk factors of septic shock in UTI patients with or without bacteremia (18, 21). Our study showed that urolithiasis could be a good predictor of the development of uroseptic shock in UTI patients. Previous studies showed that the rate of uroseptic shock in calculous acute pyelonephritis (APN) ranged from

20.8 to 36.2% (22, 23). Here, we found a similar incidence (26.5%) of uroseptic shock in UTI patients with urolithiasis. UTI with urinary tract obstruction can lead to urosepsis in ∼10% of cases (24), and the presence of urinary tract obstruction is a risk factor for septic shock in patients with bacteremic APN (19, 25). A lack of decompression leads to an increased risk of mortality for patients with sepsis and ureteral stone (26). It is important to decompress the renal collecting system by ureteral stent or pyelonephrostomy for UTI patients with severe urinary tract obstruction (27). Because urolithiasis is an independent risk factor for the development of septic shock in UTI patients, early imaging for sepsis patients with clinical suspicion of urinary source and decompressing the urinary collecting system for those with obstruction is recommended. For patients identifying severe sepsis or septic shock, administration of effective intravenous antibiotics within an hour is critical according to the recommendation of Surviving Sepsis Campaign guidelines (11).

The primary mechanism of urolithiasis-associated AKI is obstructive nephropathy (28). However, urolithiasis is a rare cause of adult AKI, accounting for ∼1–2% of all AKI events only (28). One of the common causes of AKI in critically ill patients is sepsis (29), and ∼60% of patients with septic shock develop AKI (30). Urolithiasis is a risk factor for UTI, and UTI is one of the common causes of sepsis, which may lead to uroseptic shock and deterioration of renal function. Our study found a high incidence of AKI (46.7%) among the patients with uroseptic shock, and uroseptic shock was an independent risk factor for AKI. UTI patients with urolithiasis were more prone to develop uroseptic shock and tended to have a greater reduction in eGFR than those without urolithiasis, regardless of the presence of uroseptic shock. Because patients with urolithiasis or uroseptic shock are both predisposed to develop more severe AKI, nephrotoxic agents, including non-steroidal anti-inflammatory drugs, contrast media, and aminoglycosides should be avoided in patients with a high risk of AKI.

The presence of bacteremia in complicated APN patients results in an increased risk of developing severe sepsis or uroseptic shock (31). Previous studies have indicated that specific clinical features in UTI patients, such as old age, low SBP, high body temperature, and high procalcitonin levels, were significantly associated with bacteremia (32). Our study showed that UTI patients with urolithiasis, AKI, and higher WBC count were at a higher risk of developing bacteremia. Urolithiasis *per se* is an important source of secondary infection (33). A previous study reported that the incidence of bacteria isolated from urine and stone matrices of stone formers was 24 and 32%, respectively (34). Traditionally, UTI with urease-producing bacteria, in most cases belonging to *Proteus* spp., can split urinary urea and increase urinary pH, thus, promoting the precipitation and aggregation of struvite crystals to form infective urolithiasis (5). However, UTIs are frequently associated with kidney stones of different chemical compositions other than struvite (34). Tavichakorntrakool et al. reported that the three most common bacteria in urine samples of patients with renal stones were *E. coli*, *Enterococcus* spp., and *Klebsiella*/*Enterobacter* spp. (34). Our data showed that the three most common pathogens in UTI patients with urolithiasis were *E. coli*, *Proteus* spp., and *Klebsiella* spp. There were more isolates of *Proteus* spp. but fewer isolates of *E. coli* in UTI patients with urolithiasis than in those without urolithiasis. Third-generation cephalosporin is a reasonable empirical antibiotic for stable community-acquired UTI associated with urolithiasis, while broader spectrum antimicrobial coverage is needed for patients with severe sepsis or septic shock (18). In addition, urolithiasis contains bacteria, and the number of bacteria on the stone surface can increase despite antibiotic therapy. Thus, eradication of the associated UTI is only possible after complete removal of the stone (35).

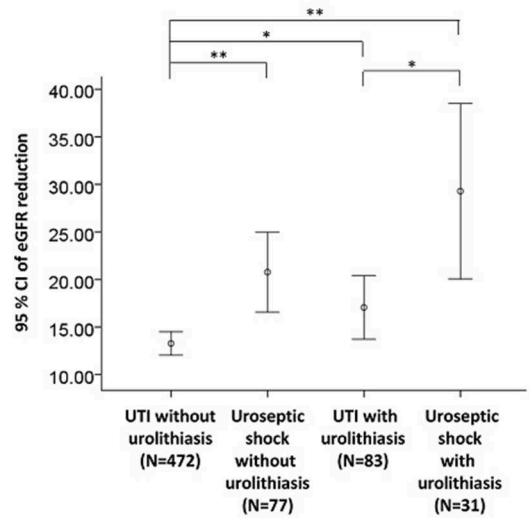

FIGURE 1 | eGFR reduction in UTI patients with respect to uroseptic shock and urolithiasis. eGFR, estimated glomerular filtration rate; UTI, urinary tract infection; eGFR reduction, baseline minus worst value of eGFR. *$p < 0.05$, **$p < 0.01$.

Our study had several limitations. First, the retrospective design involved a potential bias in data collection. Although we collected data using a standard form to reduce bias, the data regarding prior history of urolithiasis, as well as the type and size of urolithiasis were absent. A prospective study is needed to collect the above information to determine the associations between urolithiasis burden and urosepsis, as well as uroseptic shock and AKI. Second, this was a single-center study involving hospitalized patients with UTI, which limits the generalizability of the results. A multicenter study with a larger sample size will be needed to confirm our results. Third, in this study, the patient number with urinary tract obstruction was insufficient to evaluate it as a risk factor for causing uroseptic shock and AKI in UTI patients with urolithiasis. These limitations will be addressed in our future study.

In conclusion, we demonstrated that UTI patients with urolithiasis have a higher risk of developing uroseptic shock and AKI than those without urolithiasis. Therefore, careful medical history and imaging studies for urolithiasis are important for physicians to prevent and manage acute and severe complications in UTI patients.

TABLE 4 | Univariate and multivariate logistic regression analyses of factors related to bacteremia in patients with urinary tract infection.

Covariate	Univariate		Multivariate	
	OR (95% CI)	*P*-value	OR (95% CI)	*P*-value
Age (year)	1.00 (0.99–1.01)	0.499		
Sex (male)	0.95 (0.68–1.33)	0.755		
Diabetes mellitus	1.32 (0.97–1.81)	0.077	1.30 (0.91–1.85)	0.146
Hypertension	1.26 (0.92–1.71)	0.146	1.41 (0.99–2.00)	0.059
Congestive heart failure	0.99 (0.46–2.12)	0.970		
Coronary artery disease	1.18 (0.70–1.98)	0.533		
Stroke	0.66 (0.46–0.96)	0.030	0.70 (0.46–1.06)	0.088
Indwelling Foley catheter	0.73 (0.42–1.27)	0.262		
Afebrile	0.34 (0.24–0.47)	<0.001	0.32 (0.22–0.46)	<0.001
Uroseptic shock	1.95 (1.28–2.96)	0.002	1.42 (0.89–2.26)	0.138
Acute kidney injury	2.11 (1.50–2.99)	<0.001	1.87 (1.26–2.78)	0.002
Urolithiasis	2.01 (1.33–3.03)	0.001	1.68 (1.08–2.64)	0.022
Baseline eGFR (mL/min/1.73 m^2)	1.00 (0.99–1.00)	0.519		
White blood cell ($10^3/\mu L$)	1.03 (1.01–1.06)	0.017	1.04 (1.01–1.07)	0.006
Platelets ($10^3/\mu L$)	1.00 (1.00–1.00)	<0.001	1.00 (0.99–1.00)	<0.001

eGFR, estimated glomerular filtration rate.

DATA AVAILABILITY STATEMENT

The datasets generated for this study are available on request to the corresponding author.

ETHICS STATEMENT

This study was conducted in concordance with institutional patient safety laws and has been approved by the Institutional Review Board of Chiayi Christian Hospital (approval no. CYCH-IRB-100015). This study was performed in accordance with the Declaration of Helsinki. The patients/participants provided their written informed consent to participate in this study.

AUTHOR CONTRIBUTIONS

All authors: participated in the interpretation of the studies and analysis of the data and also reviewed and approved the final version of the manuscript. C-YH: protocol/project development. C-YH and Y-YC: data collection or management. C-YH and T-HC: manuscript writing/editing. T-HC and Y-CL: data analysis. M-CH, P-HH, and M-CW: manuscript review. M-CW: scientific advisor.

ACKNOWLEDGMENTS

The authors would like to acknowledge the support of Cheng-Lun Chiang.

REFERENCES

1. Moe OW. Kidney stones: pathophysiology and medical management. *Lancet*. (2006) 367:333–44. doi: 10.1016/S0140-6736(06)68071-9
2. Scales CD Jr, Smith AC, Hanley JM, Saigal CS, Urologic Diseases in America P. Prevalence of kidney stones in the United States. *Eur Urol*. (2012) 62:160–5. doi: 10.1016/j.eururo.2012.03.052
3. Yongzhi L, Shi Y, Jia L, Yili L, Xingwang Z, Xue G. Risk factors for urinary tract infection in patients with urolithiasis-primary report of a single center cohort. *BMC Urol*. (2018) 18:45. doi: 10.1186/s12894-018-0359-y
4. Raheem OA, Khandwala YS, Sur RL, Ghani KR, Denstedt JD. Burden of urolithiasis: trends in prevalence, treatments, and costs. *Eur Urol Focus*. (2017) 3:18–26. doi: 10.1016/j.euf.2017.04.001
5. Borghi L, Nouvenne A, Meschi T. Nephrolithiasis and urinary tract infections: 'the chicken or the egg' dilemma? *Nephrol Dial Transplant*. (2012) 27:3982–4. doi: 10.1093/ndt/gfs395
6. Keddis MT, Rule AD. Nephrolithiasis and loss of kidney function. *Curr Opin Nephrol Hypertens*. (2013) 22:390–6. doi: 10.1097/MNH.0b013e32836214b9
7. Madore F, Stampfer MJ, Rimm EB, Curhan GC. Nephrolithiasis and risk of hypertension. *Am J Hypertens*. (1998) 11:46–53. doi: 10.1016/S0895-7061(97)00371-3
8. Rule AD, Roger VL, Melton LJ III, Bergstralh EJ, Li X, Peyser PA, et al. Kidney stones associate with increased risk for myocardial infarction. *J Am Soc Nephrol*. (2010) 21:1641–4. doi: 10.1681/ASN.2010030253
9. Choe HS, Lee SJ, Yang SS, Hamasuna R, Yamamoto S, Cho YH, et al. Summary of the UAA-AAUS guidelines for urinary tract infections. *Int J Urol*. (2018) 25:175–85. doi: 10.1111/iju.13493
10. Tambo M, Okegawa T, Shishido T, Higashihara E, Nutahara K. Predictors of septic shock in obstructive acute pyelonephritis. *World J Urol*. (2014) 32:803–11. doi: 10.1007/s00345-013-1166-4
11. Dellinger RP, Levy MM, Rhodes A, Annane D, Gerlach H, Opal SM, et al. Surviving sepsis campaign: international guidelines for management of severe sepsis and septic shock: 2012. *Crit Care Med*. (2013) 41:580–637. doi: 10.1097/CCM.0b013e31827e83af
12. Levey AS, Stevens LA, Schmid CH, Zhang YL, Castro AF III, Feldman HI, et al. A new equation to estimate glomerular filtration rate. *Ann Intern Med*. (2009) 150:604–12. doi: 10.7326/0003-4819-150-9-200905050-00006

13. National Kidney F. K/DOQI clinical practice guidelines for chronic kidney disease: evaluation, classification, and stratification. *Am J Kidney Dis*. (2002) 39:S1–266.
14. Bellomo R, Ronco C, Kellum JA, Mehta RL, Palevsky P, Acute Dialysis Quality Initiative workgroup. Acute renal failure - definition, outcome measures, animal models, fluid therapy and information technology needs: the Second International Consensus Conference of the Acute Dialysis Quality Initiative (ADQI) Group. *Crit Care*. (2004) 8:R204–12. doi: 10.1186/cc2872
15. Kellum J, Lameire N, Aspelin P, MacLeod AM, Barsoum RS, Mehta RL, et al. Kidney disease: improving global outcomes (KDIGO) acute kidney injury work group. KDIGO clinical practice guideline for acute kidney injury. *Kidney Int Suppl*. (2012) 2:1–138. doi: 10.1038/kisup.2012.1
16. Magiorakos AP, Srinivasan A, Carey RB, Carmeli Y, Falagas ME, Giske CG, et al. Multidrug-resistant, extensively drug-resistant and pandrug-resistant bacteria: an international expert proposal for interim standard definitions for acquired resistance. *Clin Microbiol Infect*. (2012) 18:268–81. doi: 10.1111/j.1469-0691.2011.03570.x
17. Tandogdu Z, Johansen T, Bartoletti R, Florian Wagenlehner F. Management of the urologic sepsis syndrome. *Eur Urol Suppl*. (2016) 15:102–11. doi: 10.1016/j.eursup.2016.04.004
18. Shigemura K, Tanaka K, Osawa K, Arakawa S, Miyake H, Fujisawa M. Clinical factors associated with shock in bacteremic UTI. *Int Urol Nephrol*. (2013) 45:653–7. doi: 10.1007/s11255-013-0449-4
19. Lee JH, Lee YM, Cho JH. Risk factors of septic shock in bacteremic acute pyelonephritis patients admitted to an ER. *J Infect Chemother*. (2012) 18:130–3. doi: 10.1007/s10156-011-0289-z
20. Efstathiou SP, Pefanis AV, Tsioulos DI, Zacharos ID, Tsiakou AG, Mitromaras AG, et al. Acute pyelonephritis in adults: prediction of mortality and failure of treatment. *Arch Intern Med*. (2003) 163:1206–12. doi: 10.1001/archinte.163.10.1206
21. Yamamichi F, Shigemura K, Kitagawa K, Takaba K, Tokimatsu I, Arakawa S, et al. Shock due to urosepsis: a multicentre study. *Can Urol Assoc J*. (2017) 11:E105–9. doi: 10.5489/cuaj.4097
22. Koga S, Arakaki Y, Matsuoka M, Ohyama C. Calculous pyelonephritis. *Int Urol Nephrol*. (1992) 24:109–12. doi: 10.1007/BF02549636
23. Kakinoki H, Tobu S, Kakinoki Y, Udo K, Uozumi J, Noguchi M. Risk factors for uroseptic shock in patients with urolithiasis-related acute pyelonephritis. *Urol Int*. (2018) 100:37–42. doi: 10.1159/000481801
24. Reyner K, Heffner AC, Karvetski CH. Urinary obstruction is an important complicating factor in patients with septic shock due to urinary infection. *Am J Emerg Med*. (2016) 34:694–6. doi: 10.1016/j.ajem.2015.12.068
25. Kalra OP, Raizada A. Approach to a patient with urosepsis. *J Glob Infect Dis*. (2009) 1:57–63. doi: 10.4103/0974-777X.52984
26. Borofsky MS, Walter D, Shah O, Goldfarb DS, Mues AC, Makarov DV. Surgical decompression is lifesaving for patients with sepsis and ureteral calculi. *J Urol*. (2013) 189:946–51. doi: 10.1016/j.juro.2012.09.088
27. Yamamichi F, Shigemura K, Kitagawa K, Fujisawa M. Comparison between non-septic and septic cases in stone-related obstructive acute pyelonephritis and risk factors for septic shock: a multi-center retrospective study. *J Infect Chemother*. (2018) 24:902–6. doi: 10.1016/j.jiac.2018.08.002
28. Tang X, Lieske JC. Acute and chronic kidney injury in nephrolithiasis. *Curr Opin Nephrol Hypertens*. (2014) 23:385–90. doi: 10.1097/01.mnh.0000447017.28852.52
29. Zarbock A, Gomez H, Kellum JA. Sepsis-induced acute kidney injury revisited: pathophysiology, prevention and future therapies. *Curr Opin Crit Care*. (2014) 20:588–95. doi: 10.1097/MCC.0000000000000153
30. Plataki M, Kashani K, Cabello-Garza J, Maldonado F, Kashyap R, Kor DJ, et al. Predictors of acute kidney injury in septic shock patients: an observational cohort study. *Clin J Am Soc Nephrol*. (2011) 6:1744–51. doi: 10.2215/CJN.05480610
31. Hsu CY, Fang HC, Chou KJ, Chen CL, Lee PT, Chung HM. The clinical impact of bacteremia in complicated acute pyelonephritis. *Am J Med Sci*. (2006) 332:175–80. doi: 10.1097/00000441-200610000-00004
32. Lee H, Lee YS, Jeong R, Kim YJ, Ahn S. Predictive factors of bacteremia in patients with febrile urinary tract infection: an experience at a tertiary care center. *Infection*. (2014) 42:669–74. doi: 10.1007/s15010-014-0615-3
33. Zanetti G, Paparella S, Trinchieri A, Prezioso D, Rocco F, Naber KG. Infections and urolithiasis: current clinical evidence in prophylaxis and antibiotic therapy. *Arch Ital Urol Androl*. (2008) 80:5–12.
34. Tavichakorntrakool R, Prasongwattana V, Sungkeeree S, Saisud P, Sribenjalux P, Pimratana C, et al. Extensive characterizations of bacteria isolated from catheterized urine and stone matrices in patients with nephrolithiasis. *Nephrol Dial Transplant*. (2012) 27:4125–30. doi: 10.1093/ndt/gfs057
35. Miano R, Germani S, Vespasiani G. Stones and urinary tract infections. *Urol Int*. (2007) 79(Suppl 1):32–6. doi: 10.1159/000104439

Conflict of Interest: The authors declare that the research was conducted in the absence of any commercial or financial relationships that could be construed as a potential conflict of interest.

Copyright © 2019 Hsiao, Chen, Lee, Hsiao, Hung, Chen and Wang. This is an open-access article distributed under the terms of the Creative Commons Attribution License (CC BY). The use, distribution or reproduction in other forums is permitted, provided the original author(s) and the copyright owner(s) are credited and that the original publication in this journal is cited, in accordance with accepted academic practice. No use, distribution or reproduction is permitted which does not comply with these terms.

frontiers in Physiology

ORIGINAL RESEARCH
published: 21 January 2020
doi: 10.3389/fphys.2019.01572

The δ-Opioid Receptor Differentially Regulates MAPKs and Anti-inflammatory Cytokines in Rat Kidney Epithelial Cells Under Hypoxia

Fengbao Luo[1], Renfang Xu[1], Guanglai Song[1], Hao Lu[1], Xiaozhou He[1] and Ying Xia[2]**

[1] Department of Urology, The Third Affiliated Hospital of Soochow University, Changzhou, China, [2] Shanghai Key Laboratory of Acupuncture Mechanism and Acupoint Function, Fudan University, Shanghai, China

OPEN ACCESS

Edited by:
John D. Imig,
Medical College of Wisconsin,
United States

Reviewed by:
Hailin Zhao,
Imperial College London,
United Kingdom
Zhanjun Jia,
Nanjing Medical University, China

***Correspondence:**
Ying Xia
Y55738088@gmail.com
Xiaozhou He
czyyhxz@sina.com

Specialty section:
This article was submitted to Renal and Epithelial Physiology, a section of the journal Frontiers in Physiology

Received: 05 September 2019
Accepted: 16 December 2019
Published: 21 January 2020

Citation:
Luo F, Xu R, Song G, Lu H, He X and Xia Y (2020) The δ-Opioid Receptor Differentially Regulates MAPKs and Anti-inflammatory Cytokines in Rat Kidney Epithelial Cells Under Hypoxia. Front. Physiol. 10:1572. doi: 10.3389/fphys.2019.01572

Hypoxic injury is one of the most important factors in progressive kidney disorders. Since we have found that δ-opioid receptor (DOR) is neuroprotective against hypoxic stress through a differential regulation of mitogen-activated protein kinases (MAPKs) and anti-inflammatory cytokines, we asked if DOR that is highly expressed in the kidney can modulate renal MAPKs and anti-inflammatory cytokines under hypoxia. We exposed cultured rat kidney epithelial cells (NRK-52E) to prolonged hypoxia (1% O_2) with applications of specific DOR agonist or/and antagonist to examine if DOR affects hypoxia-induced changes in MAPKs and anti-inflammatory cytokines. The results showed that endogenous DOR expression remained unchanged under hypoxia, while DOR activation with UFP-512 (a specific DOR agonist) reversed the hypoxia-induced up-regulation of ERK1/2 and p38 phosphorylation. DOR inhibition with naltrindole had no appreciable effect on the hypoxia-induced changes in ERK1/2 phosphorylation, but increased p38 phosphorylation. DOR inhibition with naltrindole attenuated the effects of DOR activation on the changes in ERK1/2 and p38 phosphorylation in hypoxia. Moreover, DOR activation/inhibition differentially affected the expression of transcriptional repressor B-cell lymphoma 6 (Bcl-6), anti-inflammatory cytokines tristetraprolin (TTP), and interleukin-10 (IL-10). Taken together, our novel data suggest that DOR activation differentially regulates ERK1/2, p38, Bcl-6, TTP, and IL-10 in the renal cells under hypoxia.

Keywords: kidney, NRK-52E cell, hypoxia, DOR, MAPKs, Bcl-6

INTRODUCTION

Alteration in oxygenation induced tissue hypoxia in kidney has been identified as a final common pathway to the development and progression of diseases in both acute and chronic kidney injury (Nangaku et al., 2013; Singh et al., 2013; Fu et al., 2016), as well as renal cancer (Myszczyszyn et al., 2015; Schodel et al., 2016), and eventually leads to the end-stage kidney disease (ESKD).

The responses of individual cells to hypoxia include a range of changes in genetic and signaling regulations that facilitate them to adapt to the hypoxic conditions (Shoji et al., 2014). It is demonstrated that multiple signaling pathways, such as hypoxia inducible factor (HIF), Notch, NF-κB, PI3K/Akt, and mitogen-activated protein kinases (MAPKs), are involved in hypoxia response (Luo et al., 2016; Liu J. et al., 2017). The MAPKs are one of the most fascinating signaling pathways that have been frequently studied and involved in many hypoxic/ischemic kidney diseases (Kim et al., 2013; Liu et al., 2013).

In MAPK family, there are at least four members based on their sequence similarity, upstream activators, and to a lesser extent, substrate specificity (Kyriakis and Avruch, 2001). The classic extracellular signal-regulated kinases1 and 2 (ERK1 and ERK2) are identified in the context of growth factor-related signaling, whereas the c-Jun N-terminal kinase (JNK) and p38 families are described in the setting of cell response to stress and inflammation (Kyriakis and Avruch, 2012). All MAPK pathways include central three-tiered "core signaling modules" as MAPK-kinase-kinase, in which MAPKs are activated by associated Tyr and Thr phosphorylation (Kyriakis and Avruch, 2001). They are differentially involved in the regulation of inflammatory cytokines in the hypoxic/ischemic conditions (Tan et al., 2013; Wang et al., 2017; Wu et al., 2017).

Mitogen-activated protein kinases also participate in renal responses to hypoxic stress. The activation of MAPKs, especially ERK1/2 and p38, is detected under hypoxic condition in human kidney (Chen et al., 2013). Our recent studies on rat kidney epithelial cells have shown that the phosphorylation of both ERK1/2 and p38 is up-regulated under hypoxic stress (Luo et al., 2017). However, this is different from our observations on neuronal cells that showed an increase in p38 phosphorylation with a decrease in the level of ERK1/2 phosphorylation after prolonged exposure to severe hypoxia (Ma et al., 2005).

Our serial studies have proven that the δ-opioid receptor (DOR) has a protective effect on neurons under hypoxic/ischemic stress via the regulation of ERK1/2 and p38 as well as inflammatory cytokines (Ma et al., 2005). DOR is a G protein-coupled receptor and is a key player in pain control, hedonic homeostasis, mood, stress responses, and other function (Chu Sin Chung and Kieffer, 2013; Xia, 2015). Since DOR is highly expressed in the kidney (Peng et al., 2012), we wonder if DOR activation modulates survival process by interacting with MAPKs as well as anti-inflammatory cytokines such as transcriptional repressor B-cell lymphoma 6 (Bcl-6), anti-inflammatory cytokines tristetraprolin (TTP), and interleukin-10 (IL-10) in hypoxic renal cells. Based on our previous studies, we hypothesize that DOR activation may differentially regulate MAPKs and some anti-inflammatory cytokines in the kidney under hypoxia. To test this hypothesis, we conduct serial experiments on rat kidney epithelial cells in this work to determine DOR expression and the effects of DOR activation or/and inhibition on ERK1/2, p38, and some critical anti-inflammatory cytokines under prolonged hypoxia. The outcome results demonstrate that DOR signaling indeed differentially regulates ERK1/2, p38, Bcl-6, TTP, and IL-10 under hypoxic conditions.

MATERIALS AND METHODS

Cell Culture

NRK-52E cells (normal rat kidney epithelial cells) were acquired from Chinese Academy of Sciences (Shanghai, China). In brief, Dulbecco's Modified Eagle Medium (DMEM) (Gibco, Grand Island, NY, United States) was used as cell culture medium, containing 5% fetal bovine serum (FBS) (Gibco, Grand Island, NY, United States), 100 U/ml penicillin, and 100 mg/ml streptomycin (Gibco, Grand Island, NY, United States). NRK-52E cells were incubated in a humidified atmosphere at 37°C with 21% O_2 and 5% CO_2.

Establishment of Hypoxic Culture Condition

Cells were exposed to hypoxia by placing them in a mixed gas incubator filled with an atmosphere consisting of 94% N_2, 5% CO_2, and 1% O_2 for different durations (24, 48, and 72 h). Normoxic controls were incubated in parallel in a humidified incubator supplemented with 21% O_2 and 5% CO_2 at 37°C.

Drug Treatments

For drug treatments, UFP-512, a specific and effective DOR agonist, was synthesized by our research teams (Balboni et al., 2002; Chao et al., 2007), naltrindole, a particular DOR antagonist (Zhang et al., 2006; Granier et al., 2012), was purchased from Sigma (St. Louis, MO, United States), tumor necrosis factor-α (TNF-α) was purchased from R&D Systems (Minneapolis, MN, United States), they were added into the culture medium in demanded concentrations and exposed to normoxic or hypoxic conditions starting immediately before the onset of hypoxia (or at the same time-point in normoxia).

Cellular Proliferation Assay

The NRK-52E cells (1×10^4 cells/well) were seeded in a 96-well plate and incubated in normal culture condition for 24 h before hypoxia. After drug treatment, cell proliferation was determined by the CellTiter 96® AQueous One Solution Cell Proliferation Assay (MTS) kit (Promega, Madison, WI, United States) according to the manufacturer's instructions. MTS reagent (10 μl) was added to cultured cells in all wells followed by incubation for 1 h at 37°C. The absorbance was tested at the wavelength of 490 nm with a micro-plate reader (Bio-Rad Laboratories, Hercules, CA, United States).

Protein Extraction and Western Blot Analysis

Harvested cells were washed twice with ice-cold phosphate-buffered saline (PBS) and homogenized with lysis buffer (KeyGEN Biotech Co., Ltd., Nanjing, China) on ice. Cell lysates were centrifuged at 4°C for 15 min at 12,000 rpm, and then the supernatant was collected in fresh tubes and quantified using the bicinchoninic acid assay (BCA) method (KeyGEN Biotech Co., Ltd., Nanjing, China). Cell lysate proteins (30 μg) were separated by sodium dodecyl sulfate-polyacrylamide (Solarbio Science & Technology Co., Ltd., Beijing, China) gel electrophoresis

and electrophoretically transferred to polyvinylidene difluoride (PVDF) membranes (Millipore, Billerica, MA, United States). After blocking with 5% fat-free milk (Bio-Rad Laboratories, Hercules, CA, United States) in Tris-buffered saline tween-20 (TBST, Solarbio Science & Technology Co., Ltd., Beijing, China) buffer at room temperature for 1 h, the membranes were incubated overnight at 4°C with the indicated primary antibodies. β-Actin (1:3000), ERK1/2 (1:2000), and p38 (1:1000) were purchased from Cell Signaling Technologies (Danvers, MA, United States), rabbit polyclonal anti-DOR (1:1000) were from Millipore (Billerica, MA, United States), Bcl-6 (1:100) and TTP (1:200) were purchased from Santa Cruz Biotechnology (Santa Cruz, CA, United States), IL-10 (1:1000) were purchased from Abcam (Cambridge, United Kingdom). After repeated washing, they were reacted with the appropriate horseradish peroxidase (HRP)-conjugated secondary antibodies for 1 h at room temperature and enhanced chemiluminescence (ECL) detecting reagent (Thermo Scientific, Rockford, IL, United States). The images were analyzed with Quantity One software (Bio-Rad Laboratories, Hercules, CA, United States).

Statistics

The data were expressed as the changes in percentage compared to the control. At least three independent experiments were conducted in each group. The results were stated as the mean and standard error mean (SEM). Comparison between two groups (i.e., 24 h of normoxia vs. 24 h of hypoxia) was analyzed by unpaired *t*-test. Differences with a *P*-value < 0.05 were considered statistically significant. GraphPad Prism software (GraphPad Software, Inc., La Jolla, CA, United States) was used for statistical analyses.

RESULTS

Effect of Hypoxia on the Expression of DOR

We first examined DOR expression in NRK-52E cells under hypoxic conditions (1% O_2). As shown in **Figure 1**, hypoxia had no significant impact on the level of DOR protein (68, 52, and 42 KD) after 24–72 h of hypoxia ($P > 0.05$), suggesting that DOR protein expression of NRK-52E cells is resistant to prolonged hypoxic stress, which is very different from the observation made on neuronal cells in our previous study (Ma et al., 2005).

Effect of DOR Activation on ERK1/2 and p38 in Hypoxic Conditions

Our previous work showed that prolonged hypoxia can dramatically induce the activation of MAPKs (ERK1/2 and p38) in NRK-52E cells (Luo et al., 2017), while we also explored that MAPKs were managed by DOR function in neuronal cells under hypoxic tensions (Ma et al., 2005). To explore potential interactions between DOR and MAPKs in rat kidney epithelial cells under hypoxic conditions, we applied UFP-512 (1 μM), a potent and specific agonist of DOR (Balboni et al., 2002; Chao et al., 2008), to the culture medium and determined the effect of DOR activation on ERK1/2 and p38 phosphorylation. After 24–72 h of exposure to UFP-512 in hypoxic conditions, the total cellular content of phosphorylated ERK1/2 (P-ERK1/2) was significantly decreased to 24.73 ± 3.3, 31.99 ± 3.2, and 16.97 ± 2.05%, respectively, compared to those of hypoxic groups without UFP-512 treatment (100%, $P < 0.001$ at all three time points, **Figure 2**). Interestingly, UFP-512 did not change the ERK1/2 phosphorylation in the same cells under normoxic conditions. In sharp contrast to the changes in P-ERK1/2, the total ERK1/2 (T-ERK1/2) had no appreciable change after DOR activation in both hypoxic groups and normoxic groups after 24 and 48 h of exposure, though UFP-512 induced significant increase of T-ERK1/2 in both hypoxic groups (1.31-fold, $P < 0.05$) and normoxic groups (1.22-fold, $P < 0.05$) after 72 h of treatment (**Figure 2**). This data suggest that DOR activation can reverse the increase in ERK1/2 phosphorylation induced by hypoxia in rat kidney epithelial cells.

When DOR was activated, the hypoxic increase in phosphorylated p38 (P-p38) was reduced to 39.07 ± 7.01, 59.66 ± 25.65, and 55.45 ± 10.31% after 24, 48, and 72 h, respectively, compared to those of hypoxic groups without UFP-512 treatment (100%, $P < 0.01$ at 24 h and $P < 0.05$ at 48 and 72 h). In sharp contrast, P-p38 was markedly increased by 3.05-, 2.0-, and 2.3-fold at 24, 48, and 72 h, respectively, with UFP-512 treatment in the cells under normoxic conditions (**Figure 2**). DOR activation had no appreciable effect on the levels of total p38 protein (T-p38) under hypoxia or normoxia. This data suggest that DOR activation can largely reverse the effect of hypoxia on ERK1/2 and p38 phosphorylation. Meanwhile, UFP-512 significantly induced P-p38, but not P-ERK1/2, under normoxic conditions.

Effects of DOR Inhibition on ERK1/2 and p38 in Hypoxic Conditions

To further verify the roles of DOR in MAPK regulation in NRK-52E cells exposed to hypoxic stress, we tested the effects of naltrindole, a specific DOR antagonist (Zhang et al., 2006; Filizola and Devi, 2012; Granier et al., 2012), on the changes in ERK1/2 and p38 phosphorylation. As shown in **Figure 3**, incubation with naltrindole (1 μM) alone had no significant impact on ERK1/2 phosphorylation under normoxia or hypoxia ($P > 0.05$). However, it resulted in a significant increase in T-ERK1/2 expression in both hypoxic (1.28-fold, $P < 0.05$) and normoxic (1.30-fold, $P < 0.05$) conditions at 24 h, as well as 72 h after hypoxia (1.45-fold, $P < 0.05$).

The effect of DOR inhibition on p38 was different from that of ERK1/2. As shown in **Figure 3**, DOR inhibition by 1 μM naltrindole significantly up-regulated the levels of P-p38 by 1. 73-, 1.86-, and 2.29-fold at 24, 48, and 72 h, respectively, under normoxic conditions ($P < 0.05$). In the hypoxic groups, naltrindole increased p38 phosphorylation after 48 h, but not 24 or 72 h, of the drug treatment (1.43-fold, $P < 0.05$, **Figure 3**). The expression of T-p38 had no appreciable change after naltrindole administration except a large reduction at 48 h after hypoxia (decreased to 69.45 ± 14.71%, $P < 0.01$, **Figure 3**).

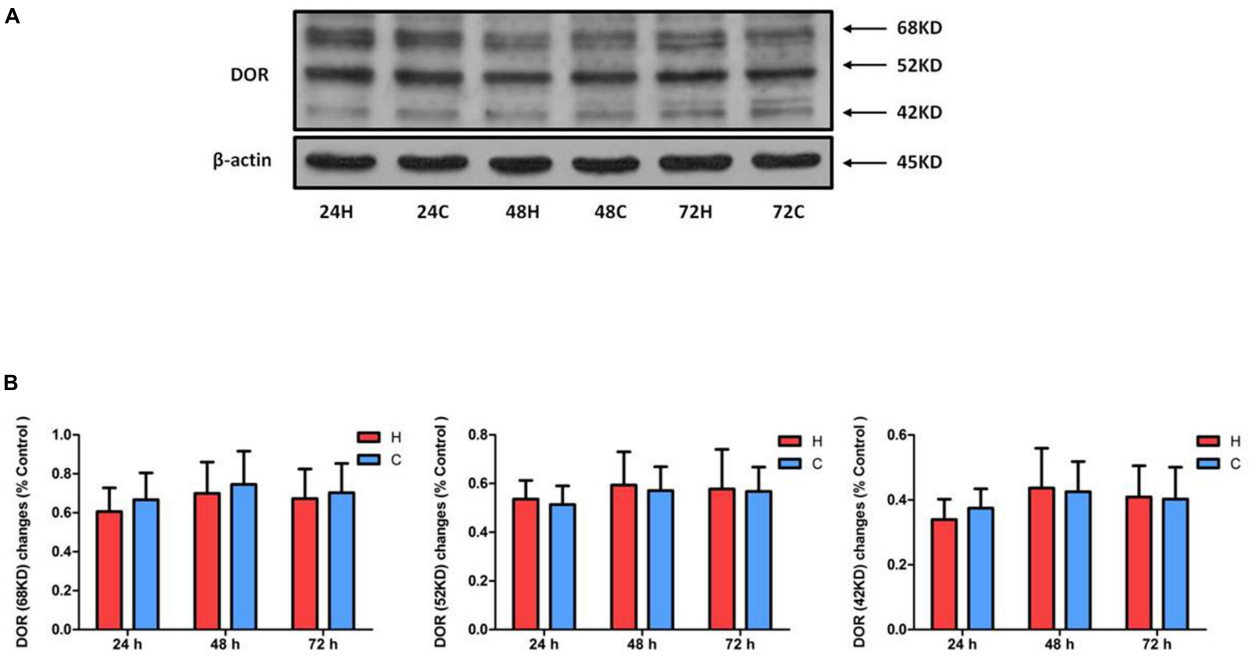

FIGURE 1 | Effect of hypoxia on DOR expression of NRK-52E cells. NRK-52E cells were exposed to hypoxia at 1% O_2 for 24–72 h. Representative Western blots **(A)** and relative quantitation **(B)** of DOR in the total protein of NRK-52 cells. H, hypoxia; C, normoxic control. At least three independent experiments were conducted in each group. Note that the DOR protein has three different signal bands (68, 52, and 42 KD) and did not change significantly in response to hypoxia at the whole cell level.

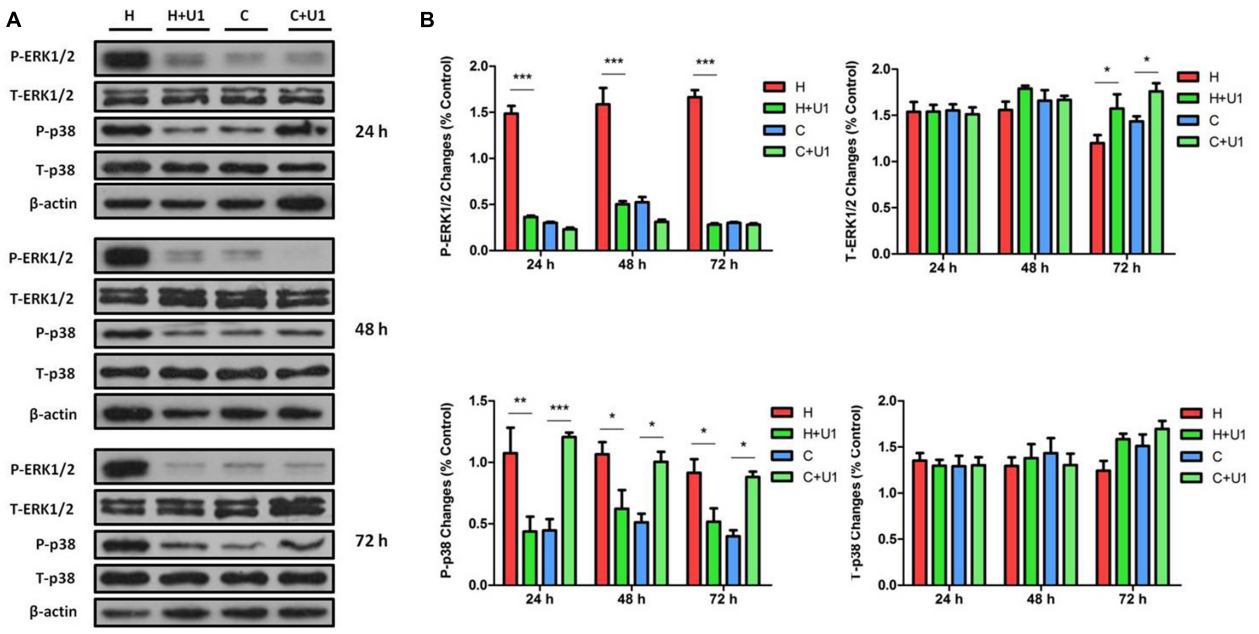

FIGURE 2 | ERK1/2 and p38 expression in NRK-52E cells under hypoxic condition with DOR activation. NRK-52E cells were exposed to hypoxia at 1% O_2 for 24–72 h and treated with 1 μM DOR agonist (UFP-512). **(A)** Representative Western blots of ERK1/2 and p38 protein. **(B)** Relative quantitation of ERK1/2 and p38. H, hypoxia; C, normoxic control. $^*P < 0.05$, $^{**}P < 0.01$, $^{***}P < 0.001$. U1, 1 μM UFP-512; C + U1, DOR activation with 1 μM UFP-512 treatment under normoxic conditions; H + U1, DOR activation with 1 μM UFP-512 treatment under hypoxic conditions. At least three independent experiments were carried out in all groups. Note that DOR activation with UFP-512 eliminated the hypoxia-induced changes on P-ERK1/2 and P-p38.

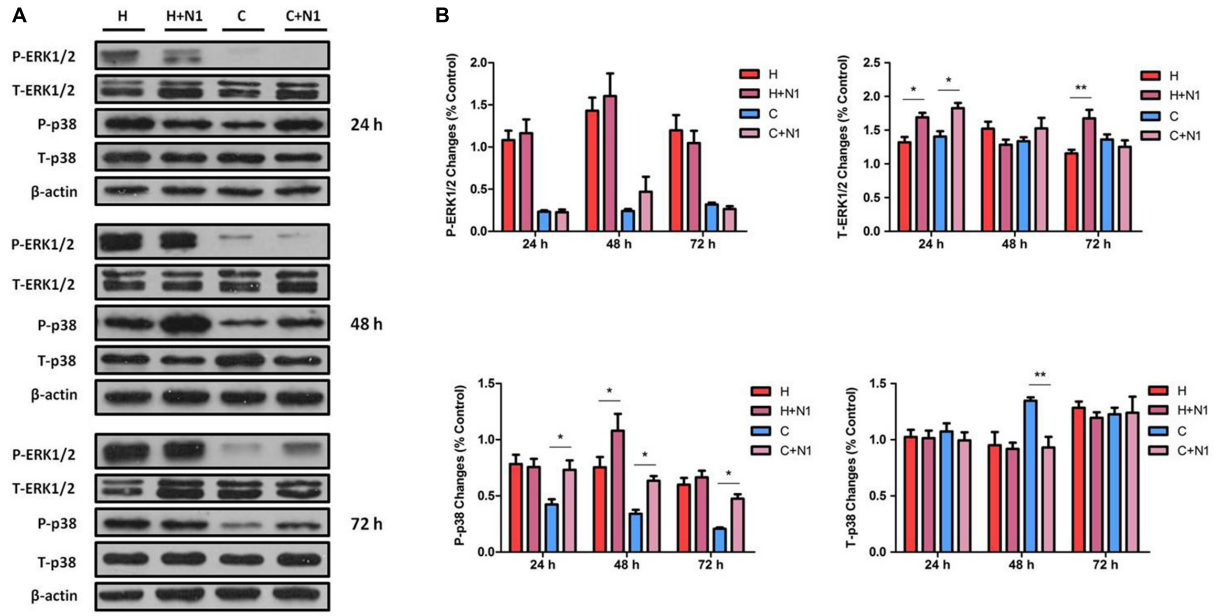

FIGURE 3 | ERK1/2 and p38 expression in NRK-52E cells under hypoxic condition with DOR inhibition. Cells were exposed to hypoxia at 1% O_2 for 24–72 h and treated with 1 μM DOR antagonist naltrindole. **(A)** Representative Western blots of ERK1/2 and p38 protein. **(B)** Relative quantitation of ERK1/2 and p38. H, hypoxia; C, normoxic control. *$P < 0.05$, **$P < 0.01$. N1, 1 μM naltrindole; C + N1, DOR inhibition with 1 μM naltrindole treatment under normoxic conditions; H + N1, DOR inhibition with 1 μM naltrindole treatment under hypoxic conditions. At least three independent experiments were performed. Note that DOR-inhibition with naltrindole had no obvious impact on the expression of P-ERK1/2 under either hypoxia or normoxia, whereas naltrindole can increase the T-ERK1/2 after 24 h of treatment using both hypoxia and normoxia, as well as after 72 h of treatment in the hypoxic group. The level of P-p38 was highly induced by the naltrindole treatment under normoxic and hypoxic condition (48 h), though the level of T-p38 only changed significantly in response to naltrindole at 48 h of treatment under normoxia.

Attenuated Effect of DOR Antagonist on DOR Activation Induced Changes in ERK1/2 and p38

We further investigated if DOR antagonist can mitigate the DOR activation induced effects stated above. When simultaneously treating the hypoxic cells with both UFP-512 (1 μM) and naltrindole (1 μM), the level of P-ERK1/2 was reduced to 75.38 ± 6.49% at 24 h ($P < 0.05$), 75.06 ± 22.37% at 48 h ($P < 0.05$), and 28.37 ± 14.13% at 72 h ($P < 0.001$), compared to those of hypoxia alone. In normoxic cells, the treatment did not change the P-ERK1/2 level at all. The co-treatment of UFP-512 and naltrindole elevated the levels of T-ERK1/2 in both hypoxic and normoxic groups, with a more remarkable increase after the first 24 h ($P < 0.05$, **Figure 4**). These observations suggest that DOR activation with UFP-512 can significantly reduce ERK1/2 phosphorylation and this effect was partly attenuated by co-exposure to naltrindole, although naltrindole treatment alone had no impact on the levels of P-ERK1/2.

P-p38 was dramatically increased by 2.02-, 2.51-, and 2.29-fold at 24, 48, and 72 h with the co-treatment of UFP-512 and naltrindole in the cells under normoxic conditions. The same treatment also increased T-p38 expression under hypoxia, but only occurred at 24 h (1.59-fold, $P < 0.01$, **Figure 4**). This data suggested that DOR activation with UFP-512 can remarkably decrease p38 phosphorylation under hypoxia though it increased p38 phosphorylation under normoxia, while naltrindole can attenuate the UFP-512-induced decrease in p38 phosphorylation under hypoxia.

Changes in ERK1/2 and p38 Phosphorylation in Response to TNF-α Exposure

Since the TNF-α has been thought as a pro-inflammatory mediator for hypoxic/ischemic injury (Park and Bowers, 2010; Watters and O'Connor, 2011; Liu and McCullough, 2013; Wang et al., 2014), we further examined the response of ERK1/2 and p38 to TNF-α exposure in the NRK-52E cells. We administered TNF-α to the medium at three increasing concentrations (0.1, 1, and 10 ng/ml) and examined their effects on ERK1/2 and p38 at 6, 12, 24, and 48 h in hypoxia and normoxia (**Figure 5**). After the first 12 h of TNF-α exposure in either hypoxia or normoxia, the MTS assay showed that the NRK-52E cells did not have any appreciable injury. After prolonging the duration of TNF-α exposure to 24 h, normoxic cells showed severe damage with a significant reduction of cell viability compared to those of normoxic cells without TNF-α treatment. As a comparison, the same treatment did not induce cell injury in hypoxia. After 48 h of exposure to TNF-α at 0.1 ng/ml, cell viability was significantly lower in the normoxic than hypoxic groups ($P < 0.01$). In the concentrations of 1 and 10 ng/ml TNF-α; however, there was no appreciable difference in cell viability between normoxic and hypoxic groups.

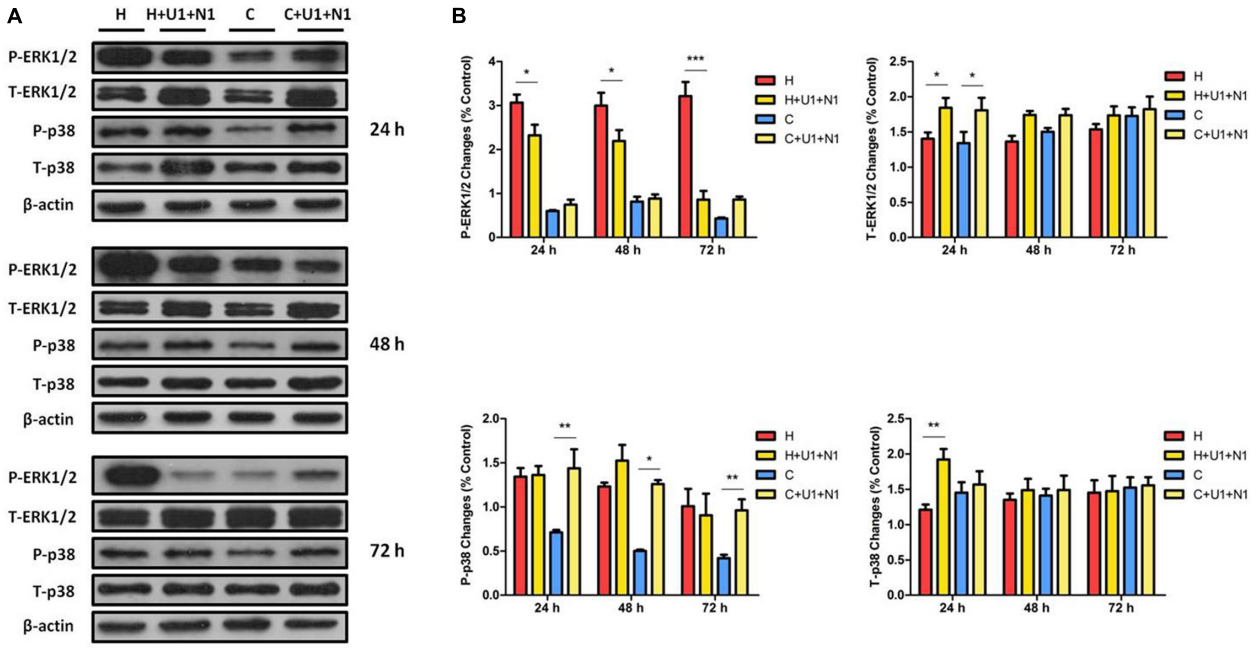

FIGURE 4 | The effects of DOR activation and inhibition on ERK1/2 and p38 in NRK-52E cells. NRK-52E cells were exposed to hypoxia with both DOR agonist UFP-512 (1 μM) and DOR antagonist naltrindole (1 μM) at 1% O_2 for 24–72 h. **(A)** Representative Western blots of ERK1/2 and p38 protein. **(B)** Relative quantitation of ERK1/2 and p38. H, hypoxia; C, normoxic control. $^*P < 0.05$, $^{**}P < 0.01$, $^{***}P < 0.001$. U1 + N1, simultaneous administration of 1 μM UFP-512 and 1 μM naltrindole; C + U1 + N1, 1 μM UFP-512 and 1 μM naltrindole treatment under normoxic conditions; and H + U1 + N1, 1 μM UFP-512 and 1 μM naltrindole treatment under hypoxic conditions. At least three independent experiments were conducted in each group. Note that naltrindole, along with UFP-512, reversed the efforts on ERK1/2 phosphorylation induced by hypoxia, especially after 72 h of treatment, whereas both the DOR agonist and antagonist induced the expression of T-ERK1/2 significantly after exposure for 24 h. The P-p38 was largely increased by naltrindole and UFP-512 treatment under normoxia, while the T-p38 protein levels had markedly increased under hypoxia after 24 h of treatment.

After exposure for 24 h to TNF-α with increasing concentrations (0.1, 1, and 10 ng/ml) in hypoxia, P-ERK1/2 was largely increased by hypoxia alone, while TNF-α treatment fully eliminated the hypoxic effect on ERK1/2 phosphorylation. In the condition of TNF-α, the P-ERK1/2 expression under normoxia was much lower than that under hypoxia (decreased to 71.62 ± 9.08% at 0.1 ng/ml TNF-α, $P < 0.05$; 35.49 ± 6.20% at 1 ng/ml TNF-α, $P < 0.01$; and 40.91 ± 6.15% at 10 ng/ml TNF-α, $P < 0.01$, **Figure 6**). There was a significant increase in T-ERK1/2 levels after TNF-α exposure, with no appreciable difference between hypoxic and normoxic groups.

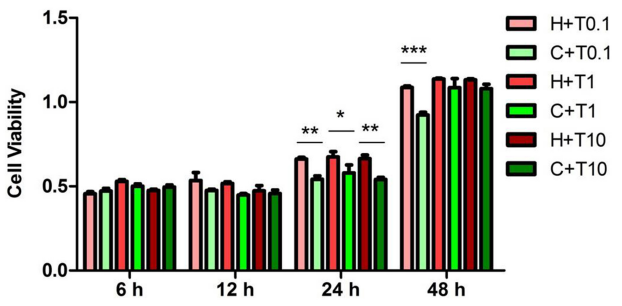

FIGURE 5 | Effects of TNF-α treatment on the viability of NRK-52E cells exposed to hypoxia. NRK-52E cells were exposed to hypoxia at 1% O_2 with TNF-α, and then the cell viability ($n = 4$) was measured by an MTS (3-[4,5-dimethylthiazol-2-yl]-5-[3-carboxymethoxypheny]-2-[4-sulfophenyl]-2H-tetrazolium) assay. H, hypoxia; C, normoxic control; T0.1, 0.1 ng/ml TNF-α; T1, 1 ng/ml TNF-α; T10, 10 ng/ml TNF-α. $^*P < 0.05$, $^{**}P < 0.01$, $^{***}P < 0.001$. Note that the cell viability treated by TNF-α under hypoxia was higher than under normoxia after 24 and 48 h (0.1 ng/ml TNF-α).

The P-p38 was decreased after TNF-α treatment under hypoxic conditions, there was no significant change between hypoxic and normoxic groups except after the exposure to 10 ng/ml TNF-α (decreased to 72.73 ± 7.7% in normoxia at 10 ng/ml TNF-α, compared to those of hypoxic groups at 10 ng/ml TNF-α, $P < 0.05$, **Figure 6**). The T-p38 protein level was significantly enhanced by TNF-α exposure at all concentrations. In short, TNF-α treatment reduced cell viability and the phosphorylation of ERK1/2 and p38 in rat kidney epithelial cells, but increased the expression of T-ERK1/2 and T-p38 protein levels. Interestingly, in all concentrations of TNF-α exposure, the P-ERK1/2 level was significantly elevated in hypoxia compared to that of normoxic group.

Effect of DOR Activation or/and Inhibition on Bcl-6, TTP, and IL-10

Since hypoxia significantly decreases the levels of Bcl-6 protein in the NRK-52E cells (Luo et al., 2017) and DOR is cytoprotective against hypoxic stress (Ma et al., 2005; Wang et al., 2014;

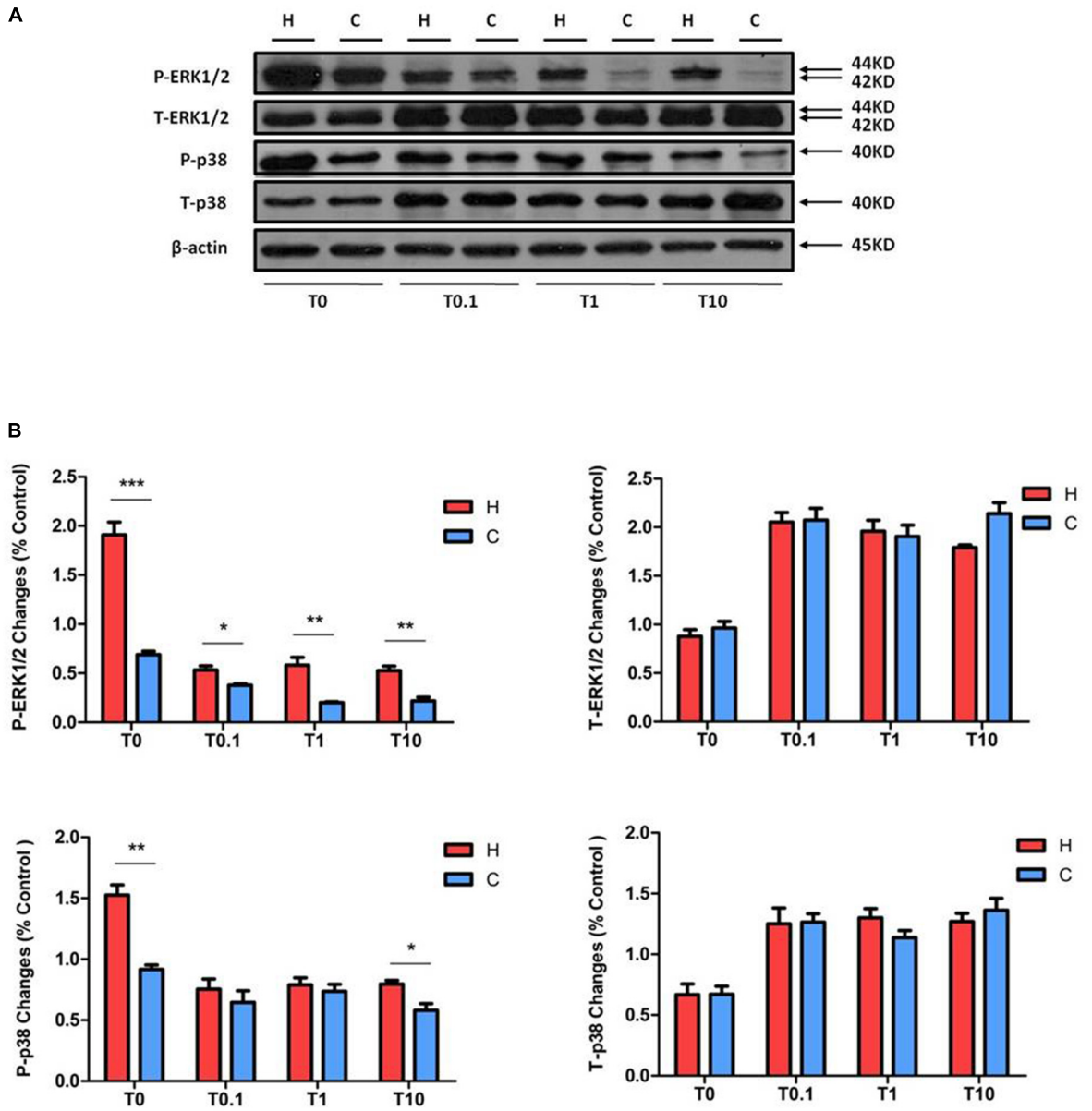

FIGURE 6 | Effects of TNF-α treatment on the expression of ERK1/2 and p38 in NRK-52E cells. Cells were exposed to media with different concentration of TNF-α at 1% O_2 for 24 h. The expressions of ERK1/2 and p38 were measured by a Western blot. **(A)** Representative Western blots of ERK1/2 and p38 protein. **(B)** Relative quantitation of ERK1/2 and p38. H, hypoxia; C, normoxic control; T0.1, 0.1 ng/ml TNF-α; T1, 1 ng/ml TNF-α; T10, 10 ng/ml TNF-α. $^{*}P < 0.05$, $^{**}P < 0.01$, $^{***}P < 0.001$. At least three independent experiments were performed. The levels of P-ERK1/2 treated with different concentrations of TNF-α were relatively elevated in the groups of hypoxia, compared to the groups treated with TNF-α under normoxia. Similar to P-ERK1/2, P-p38 under hypoxia was higher than under normoxia, but only occurred after treatment with 10 ng/ml TNF-α. TNF-α induced the total protein levels of ERK1/2 and p38; there was no significant change between the groups under hypoxia and normoxia.

Cao et al., 2015), we further examined if DOR plays a role in Bcl-6 protein expression. We found that DOR activation with 1 μM UFP-512 had no significant effect on Bcl-6 expression after 24 h of hypoxia; however, it down-regulated the level of Bcl-6 protein by 40.39 ± 1.13% under normoxic conditions ($P < 0.05$). At 48 h after adding the DOR agonist, Bcl-6 protein expression increased in the group of hypoxia (1.87-fold, $P < 0.05$), but did not change significantly in normoxia (**Figure 7A**). Moreover, the level of Bcl-6 protein was much lower than the control after naltrindole treatment for 24 h in normoxic conditions ($P < 0.05$). This reduction almost disappeared at 48 h. The hypoxic cells showed no significant differences in terms of Bcl-6 expression after DOR inhibition at 24 and 48 h (**Figure 7B**). In addition, Bcl-6 expression decreased after co-exposure of UFP-512 and naltrindole under normoxia both at 24 and 48 h ($P < 0.05$) and increased at 24 h under hypoxia ($P < 0.05$, **Figure 7C**). As shown

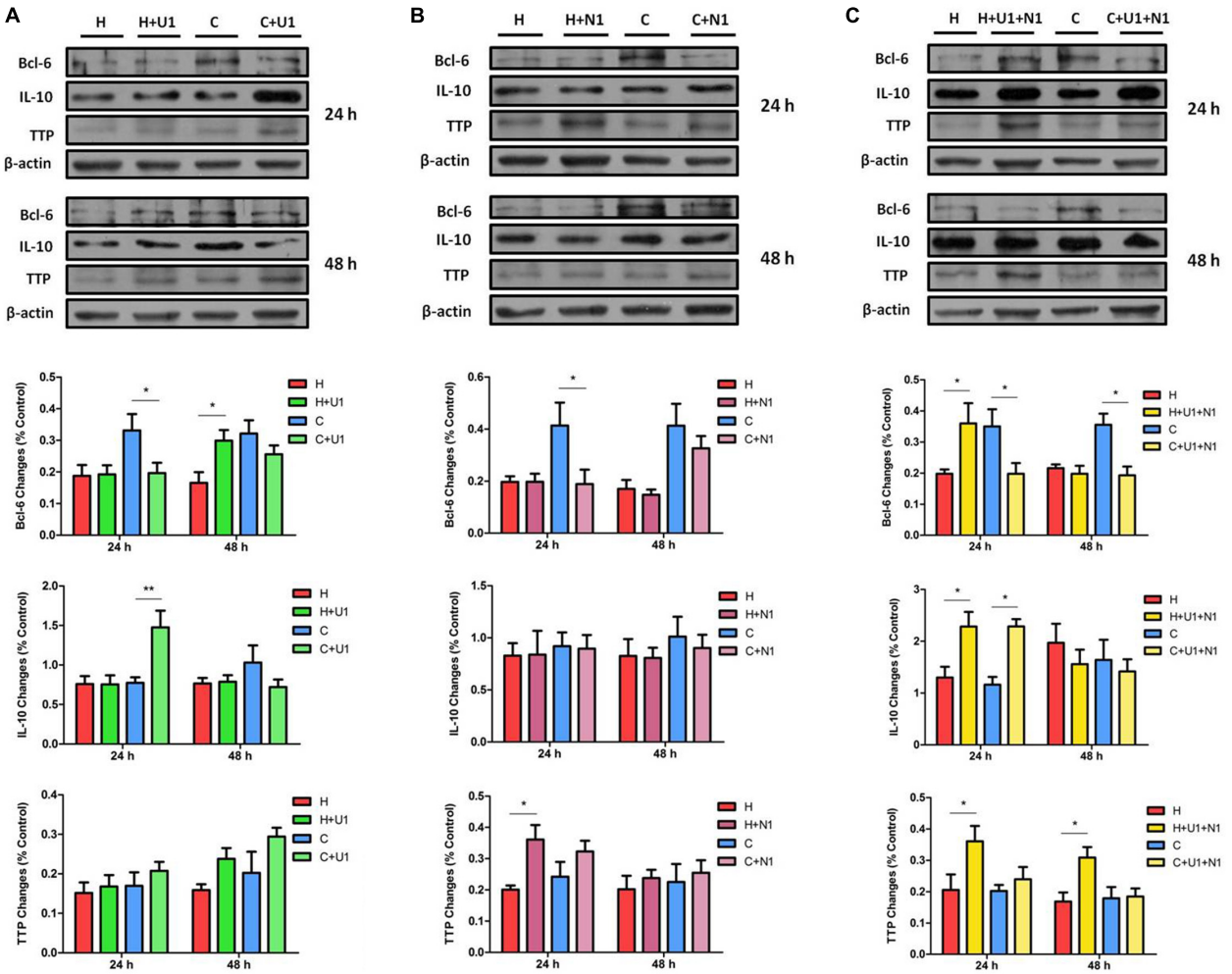

FIGURE 7 | The protein expression of Bcl-6, TTP, and IL-10 in NRK-52E cells under hypoxic condition with DOR activation or/and inhibition. Cells were exposed to hypoxia at 1% O_2 for 24–48 h and treated with 1 μM DOR agonist (UFP-512) or/and 1 μM DOR antagonist naltrindole. **(A)** Western blots of Bcl-6, TTP, and IL-10 after UFP-512 treatment. **(B)** Western blots of Bcl-6, TTP, and IL-10 after naltrindole treatment. **(C)** Western blots of Bcl-6, TTP, and IL-10 after UFP-512 and naltrindole treatment. H, hypoxia; C, normoxic control. $^{*}P < 0.05$, $^{**}P < 0.01$. U1, 1 μM UFP-512; C + U1, DOR activation with 1 μM UFP-512 treatment under normoxic conditions; H + U1, DOR activation with 1 μM UFP-512 treatment under hypoxic conditions; N1, 1 μM naltrindole; C + N1, DOR inhibition with 1 μM naltrindole treatment under normoxic conditions. U1 + N1, simultaneous administration of 1 μM UFP-512 and 1 μM naltrindole; C + U1 + N1, 1 μM UFP-512 and 1 μM naltrindole treatment under normoxic conditions; H + U1 + N1, 1 μM UFP-512 and 1 μM naltrindole treatment under hypoxic conditions.

in **Table 1**, it seems that the expression level of Bcl-6 is linked to MAPKs phosphorylation level, which can be managed by DOR function in rat kidney epithelial cells.

As a comparison, we also investigated the effects of DOR activation on TTP protein in the same cells. In normoxia, UFP-512 treatment did not significantly affect the expression of TTP at 24 h after the treatment, but intended to increase TTP protein levels at 48 h (**Figure 7A**). After naltrindole treatment, the expression of TTP seemed to increase under both normoxia and hypoxia at 24 h, though the phenotype was more significant under hypoxia (**Figure 7B**, $P < 0.05$). TTP was significantly increased by co-treatment of UFP-512 and naltrindole under hypoxic conditions, but did not change under normoxia (**Figure 7C**). Since the expression level of TTP remains steady under hypoxic stress, indicated in our previous (Luo et al., 2017), it is reasonable to believe that TTP is also regulated by DOR function in NRK-52E cells.

On the other hand, IL-10 protein level was significantly increased after exposure to UFP-512 for 24 h in normoxic conditions ($P < 0.01$), but not in hypoxic conditions. The increased IL-10 in normoxic conditions disappeared after treatment of UFP-512 for 48 h (**Figure 7A**). Meanwhile, IL-10 had no response to the DOR inhibition by naltrindole under either hypoxia or normoxia (**Figure 7B**). Interestingly, the co-treatment of UFP-512 and naltrindole for 24 h can enhance the expression of IL-10 in both normoxic and hypoxic conditions ($P < 0.05$), but not for those of 48 h of treatment (**Figure 7C**). Similar to TTP, the expression level of IL-10 may be conducted by the DOR function, since hypoxia alone has no appreciable impact on IL-10 in NRK-52E cells (Luo et al., 2017).

TABLE 1 | Effects of DOR activation/inhibition on ERK1/2, p38, Bcl-6, TTP, and IL-10.

Treatment	Condition	P-ERK1/2	P-p38	Bcl-6	TTP	IL-10
DOR activation with UFP-512	Hypoxia	↓(24–72 h)	↓(24–72 h)	↑(48 h)	–	–
	Normoxia	–	↑(24 h), ↑(48, 72 h)	↓(24 h)	–	↑(48 h)
DOR inhibition with Naltrindole	Hypoxia	–	↑(48 h)	–	↑(24 h)	–
	Normoxia	–	↑(24–72 h)	↓(24 h)	–	–
UFP-512 plus Naltrindole	Hypoxia	↓(24, 48 h), ↓(72 h)	–	↑(24 h)	↑(24, 48 h)	↑(24 h)
	Normoxia	–	↑(24, 72 h), ↑(48 h)	↓(24, 48 h)	–	↑(24 h)

↑, *increased and* $P < 0.05$; ↑, *increased and* $P < 0.01$; ↑, *increased and* $P < 0.001$; ↓, *decreased and* $P < 0.05$; ↓, *decreased and* $P < 0.001$.

Changes in Bcl-6, TTP, and IL-10 Expression in Response to TNF-α Exposure

We also checked the expressions of Bcl-6, TTP, and IL-10 in NRK-52E cells exposed to TNF-α under hypoxia. Compared to the hypoxic groups without TNF-α treatment, the protein levels of Bcl-6 in the groups with TNF-α were much higher. However, there was no significant difference in Bcl-6 levels between the hypoxic and normoxic groups when disregarding the concentration of TNF-α (**Figure 8**). The expression of TTP and IL-10, especially the latter, seemed to be higher after TNF-α treatment under both hypoxic and normoxic conditions.

DISCUSSION

This work presents the following key findings in rat kidney epithelial cells: (1) prolonged hypoxia increased the phosphorylation of ERK1/2 and p38 without any appreciable change in DOR expression, while DOR activation attenuate the hypoxia-induced phosphorylation of ERK1/2 and p38; (2) DOR inhibition with naltrindole had no significant impact on the change of P-ERK1/2 either under hypoxia or normoxia, but increased the phosphorylation of p38 after 48 h of hypoxia and 24–72 h of normoxia; (3) either DOR agonist or antagonist increased the activation of p38 under normoxic conditions, while DOR inhibition with naltrindole partly counteract the effect of DOR activation on the changes of ERK1/2 and p38 phosphorylation under hypoxic conditions; (4) TNF-α decreased the expression of P-ERK1/2; (5) the expression of Bcl-6 was negatively regulated by ERK1/2 and p38 phosphorylation, which could be controlled by DOR function; and (6) the expression of TTP and IL-10 was regulated by DOR administration though hypoxia alone had no significant effect on these two anti-inflammatory cytokines.

The delta-, mu-, and kappa-opioid receptors (DOR, MOR, and KOR) are three major subtypes of opioid receptors and belong to members of the rhodopsin subfamily in the superfamily of seven transmembrane nucleotide binding regulatory G-protein-coupled receptors (Law and Loh, 1999; Audet et al., 2008; Xia, 2015). A current study using absolute quantitative real-time illustrated that the kidney is principally a "DOR organ" since DOR expression is approximately 44.5-fold higher than that of KOR, without any detectable expression of MOR (Peng et al., 2012). Indeed, our studies (Chen et al., 2014; Cao et al., 2015) have shown DOR expression at both mRNA and protein levels in HEK293 cells. We have also found that DOR activation can modify microRNA expression in rat kidney under prolonged hypoxia (He et al., 2013b), suggesting an important role of DOR in renal adaptation to hypoxic stress.

We previously showed that DOR is highly expressed in cortical neurons (Ma et al., 2005) and plays a critical role in neuroprotection against hypoxic injury (Zhang et al., 2002). A severe and prolonged hypoxia (e.g., 1% oxygen for 72 h) largely reduced the level of DOR with severe injury in the cortical neurons (Ma et al., 2005). In sharp contrast, the same hypoxic stress only caused a mild cell injury in NRK-52E cells after long-term exposure as shown in our previous study (Luo et al., 2017) and this present work. This is likely attributed to, at least partially, the tolerance of DOR to the hypoxic stress in the rat kidney epithelial cells, since DOR remains the "normal" level in these cells after 24–72 h of hypoxic exposure as shown in this study. Indeed, the level of DOR expression is likely related to the tolerance of hypoxic stress because the high density of DOR in the turtle brain may make turtle neurons more tolerant to hypoxia than rat neurons (Xia et al., 1992; Xia and Haddad, 2001). Since hypoxia was not able to decrease the expression of DOR in the rat kidney epithelial cells, DOR may be more resistant to hypoxic stress in these renal cells than neurons, which may be one of the reasons that these kidney cells are more tolerant to hypoxic stress. The present data further suggest that DOR expression may be a critical determinant of renal cell survival during hypoxic stress and its activity may serve as a protective factor against hypoxic kidney injury.

The major differences between the kidney and neuronal cells in DOR expression and cell survival under prolonged hypoxia inspirited us to further explore the roles of DOR in the regulation of ERK1/2 and p38 in the kidney cells, since ERK1/2 and p38 are two critical and opposite signaling regulators in the DOR-mediated neuroprotection (Ma et al., 2005). A surprising finding is that both ERK1/2 and p38 are seriously up-regulated in terms of their phosphorylation by hypoxic stress, while both of them are largely suppressed by DOR activation in NRK-52E cells. This is very different from our observation on neuronal cells in which DOR activation by hypoxic preconditioning attenuated the

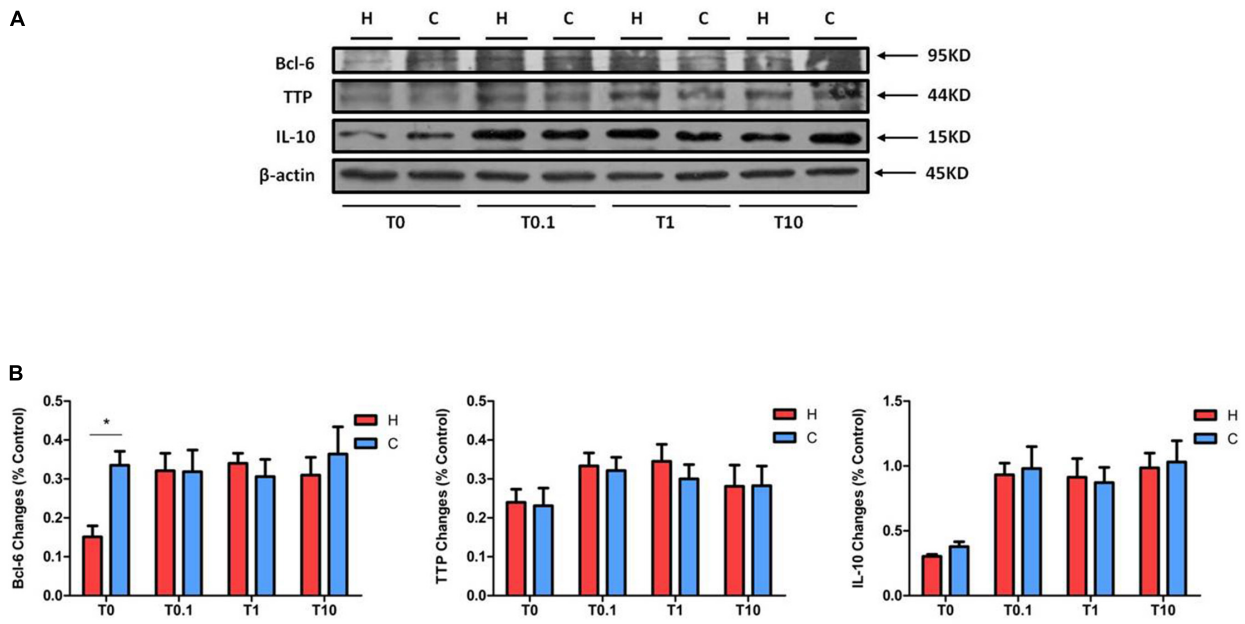

FIGURE 8 | The expression of Bcl-6, TTP, and IL-10 in NRK-52E cells after TNF-α treatment. NRK-52E cells were exposed to media with different concentrations of TNF-α at 1% O_2 for 24 h. The expressions of Bcl-6, TTP, and IL-10 were measured by Western blot. **(A)** Representative Western blots of Bcl-6, TTP, and IL-10 protein. **(B)** Relative quantitation of Bcl-6, TTP, and IL-10 protein ($n = 3$). H, hypoxia; C, normoxic control; T0.1, 0.1 ng/ml TNF-α; T1, 1 ng/ml TNF-α; T10, 10 ng/ml TNF-α. $^*P < 0.05$. Note that TNF-α can raise the protein levels of Bcl-6 under hypoxia, without changing them between hypoxia and normoxia. TNF-α tended to promote the expression of TTP and IL-10 under both hypoxia and normoxia, though there was no change between the groups under hypoxia and normoxia treated by TNF-α.

increase in P-p38 and partially reversed the decrease in P-ERK1/2 in severe hypoxia, suggesting different mechanisms in the DOR-mediated regulation of MAPKs between neuronal and renal cells.

In view of the fact that most of previous studies showing a harmful role of p38 (Li et al., 2016; Liu W.Y. et al., 2017) and protective role of ERK1/2 (Hung et al., 2003; Chen et al., 2015; Li et al., 2018) in cell survival under stress, the up-regulation of P-ERK1/2 in hypoxic renal cells is probably an adaptive response to overcome the hypoxia-induced increase in P-p38, rendering the cells a new balance between ERK1/2 and p38. Indeed, there is solid evidence indicating that P-ERK1/2 is a mediator of controlling cell survival in response to many stimuli including hypoxia in the kidney (di Mari et al., 1999; Kunduzova et al., 2002; Yang et al., 2003; Zou et al., 2016), while the p38 is considered as the major stress-activated protein kinases (Kyriakis and Avruch, 2012) and mediate a pro-inflammation effect in hypoxic condition (Wu et al., 2016). Based on our previous work, we believe that DOR, which was tolerant to hypoxia and was not down-regulated in the renal cells after hypoxia, plays a positive effect in the upstream signaling of P-ERK1/2 and a negative influence on p38, at least partially. On the other hand, DOR plays its protective role via multiple mechanisms (Ma et al., 2005; Chao and Xia, 2010; He et al., 2013a; Xia, 2015). When strengthening DOR signaling by adding DOR agonists, other mechanisms might be activated, which leads to a reduction in the hypoxia-induced increase in P-p38. Therefore, ERK1/2 is accordingly adjusted for the economy of cellular energy resources. Moreover, p38 is likely sensitive to DOR and DOR inhibition reverses the DOR-induced reduction of p38 phosphorylation because the level of P-p38 was high after the treatment with both DOR agonist and antagonist. The differential responses to DOR inhibition between p38 and ERK1/2 further suggest that there is a DOR-mediated mechanism(s) that affects p38 more than ERK1/2 in these cells. However, it is unknown why P-p38 was enhanced by UFP-512 or/and naltrindole treatment in normoxic conditions. It seems that p38 responds to DOR activation differently in hypoxia and normaxia.

Tumor necrosis factor-α is a potent pro-inflammatory molecule and can trigger downstream signaling cascades that control numerous cellular processes linked to cell viability and gene expression (Park and Bowers, 2010; Watters and O'Connor, 2011; Liu and McCullough, 2013). Our previous work showed that exogenous addition of TNF-α to the culture media worsened the hypoxia-induced damage in PC-12 cells (Wang et al., 2014). The present work further demonstrates that TNF-α can reduce the level of P-ERK1/2, suggesting that its insult to cell survival may be partially via down-regulating ERK1/2 signaling.

A large number of experimental data have confirmed that MAPK signal pathways are closely related to the regulation of anti-inflammatory cytokines, such as Bcl-6, TTP, and IL-10 (Pantoja-Escobar et al., 2019; Ronkina et al., 2019; Zhang et al., 2019) although there are still controversies with some showing an inhibitory effect of MAPKs on certain anti-inflammatory cytokines in BV2 cell line (Lee et al., 2015) and others having different opinions in bone marrow cells and microglial cells (Chi et al., 2006; Correa et al., 2010). In the kidney or renal

cells, however, there is a lack of information on the relationship between MAPKs and anti-inflammatory cytokines in hypoxic condition. Our present study represents the first investigation into the relationship between MAPKs and anti-inflammatory cytokines and demonstrated that Bcl-6 is sensitive to hypoxic stress and DOR activation in the renal cells.

Bcl-6 protein, a transcriptional repressor, is a critical regulator of germinal centers and involves in the development and progression of cancers with uncertain mechanism (Basso and Dalla-Favera, 2010; Yu et al., 2015) and is relevant to MAPK signaling process (Batlle et al., 2009). Our previous study showed that it was down-regulated after hypoxic exposure, in parallel with an up-regulation of both ERK1/2 and p38 MAPKs (Luo et al., 2017). An intriguing finding in the present work is that the expression of Bcl-6 is negatively correlated with the phosphorylation of MAPKs and modulated by DOR function. For example, when the levels of P-ERK1/2 and P-p38 were down-regulated by DOR activation, the level of Bcl-6 was increased after 48 h exposure to hypoxia. The same is true in normoxia. This is the first work to show the regulation of DOR in Bcl-6 expression via MAPKs in kidney epithelial cells. There is evidence suggesting that MAPKs can regulate the hypoxic exposure level of Bcl-6 by a rapid degradation through the ubiquitin/proteasome pathway (Niu et al., 1998). Therefore, the DOR-MAPK mechanisms may play a role in the regulation of Bcl-6 through ubiquitination and proteasomal degradation pathway. However, the downstream signaling in the interaction between MAPKs and Bcl-6 in kidney epithelial cells is not well acknowledged yet.

Tristetraprolin is an mRNA-destabilizing and RNA-binding protein and can enhance the decay of mRNAs, and plays as an anti-inflammatory cytokine (Patial and Blackshear, 2016). TTP can limit the expression of a number of critical genes for chronic inflammatory diseases (Brooks and Blackshear, 2013; Prabhala and Ammit, 2015). Some studies suggested that the RNA degradation activity of TTP is negatively regulated by p38 MAPK-dependent signaling (Stoecklin et al., 2004; Brook et al., 2006; Hitti et al., 2006). However, the impact of the p38 pathway on TTP expression and function remains controversial (O'Neil et al., 2018). TTP is found at sites of inflammation, and is co-localized with active p38 MAPK (Ross et al., 2017). It is implied that the strong expression of TTP protein may function as a suppressor of inflammation by down-regulating inflammatory cytokines, chemokines, as well as adhesion molecules (Bollmann et al., 2014). Based on the present work, TTP is insensitive to hypoxic stress, but it increased to other severe insults such as DOR inhibition and TNF-α exposure. We propose that the enhanced TTP expression may devote to combat cellular injury caused by DOR inhibition or TNF-α inflammation.

Interleukin-10 is produced by many kinds of cells including T and B cells as well as epithelial cells (Williams et al., 2004). It inhibits transcription of a subset of pro-inflammatory genes (Denys et al., 2002; Murray, 2005). However, the mechanisms underlying IL-10-mediated anti-inflammatory responses are not well known. Here we firstly report that DOR is a regulator of such anti-inflammatory mechanism because DOR activation increases the level of IL-10 in normaxia. Interestingly, hypoxia alone could not induce any changes in IL-10 expression (Luo et al., 2017) and the same was true for DOR activation under hypoxic condition. It seems that IL-10 is more sensitive to DOR activation in normoxia than hypoxic condition. The major results of the present work are summarized in **Table 1** and **Figure 9**. In brief, our data suggest that DOR may upregulate Bcl-6 via targeting MAPKs in rat kidney epithelial cells under hypoxia. In contrast, TTP and IL-10 are insensitive to DOR activation in hypoxia. Our data may provide a clue to the development of new therapeutic strategies for the prevention or/and treatment of hypoxic kidney injury as may occur in a range of clinically important conditions including ischemia–reperfusion injury and chronic kidney diseases.

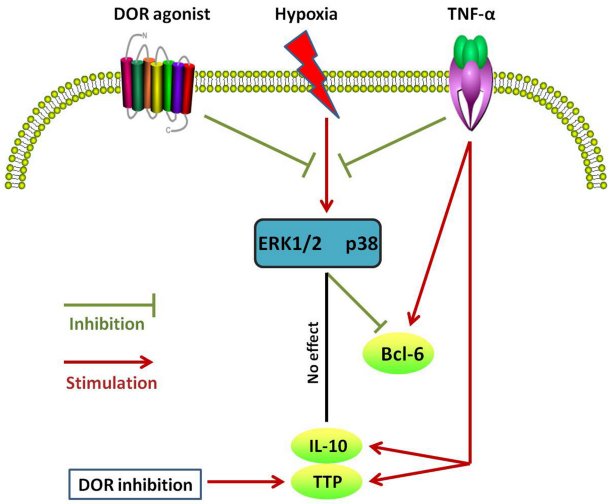

FIGURE 9 | Schematic diagram of different changes in Bcl-6, TTP, and IL-10 expression in response to DOR activation, hypoxia, and TNF-α in NRK-52E cells. Note that these anti-inflammatory cytokines differentially response to different cell treatments.

DATA AVAILABILITY STATEMENT

All datasets generated for this study are included in the article and original records are available upon request.

ETHICS STATEMENT

This study was carried out in accordance with the recommendations of the Ethics Committee of Soochow University.

AUTHOR CONTRIBUTIONS

FL and YX designed this study. FL and GS performed the experiments. FL and HL analyzed the results. RX coordinated the project. XH provided the research reagents. FL, XH, and YX wrote the manuscript. All authors approved the final version of manuscript.

FUNDING

This research was partially funded by the National Natural Science Foundation of China (81873361), the Science and Technology Commission of Shanghai Municipality (18401970100), and the Shanghai Key Laboratory of Acupuncture Mechanism and Acupoint Function (14DZ2260500).

REFERENCES

Audet, N., Gales, C., Archer-Lahlou, E., Vallieres, M., Schiller, P. W., Bouvier, M., et al. (2008). Bioluminescence resonance energy transfer assays reveal ligand-specific conformational changes within preformed signaling complexes containing delta-opioid receptors and Heterotrimeric G proteins. *J. Biol. Chem.* 283, 15078–15088. doi: 10.1074/jbc.M707941200

Balboni, G., Salvadori, S., Guerrini, R., Negri, L., Giannini, E., Jinsmaa, Y., et al. (2002). Potent delta-opioid receptor agonists containing the Dmt-Tic pharmacophore. *J. Med. Chem.* 45, 5556–5563. doi: 10.1021/jm020336e

Basso, K., and Dalla-Favera, R. (2010). BCL6: master regulator of the germinal center reaction and key oncogene in B cell lymphomagenesis. *Adv. Immunol.* 105, 193–210. doi: 10.1016/S0065-2776(10)05007-8

Batlle, A., Papadopoulou, V., Gomes, A. R., Willimott, S., Melo, J. V., Naresh, K., et al. (2009). CD40 and B-cell receptor signalling induce MAPK family members that can either induce or repress Bcl-6 expression. *Mol. Immunol.* 46, 1727–1735. doi: 10.1016/j.molimm.2009.02.003

Bollmann, F., Wu, Z., Oelze, M., Siuda, D., Xia, N., Henke, J., et al. (2014). Endothelial dysfunction in tristetraprolin-deficient mice is not caused by enhanced tumor necrosis factor-alpha expression. *J. Biol. Chem.* 289, 15653–15665. doi: 10.1074/jbc.M114.566984

Brook, M., Tchen, C. R., Santalucia, T., McIlrath, J., Arthur, J. S., Saklatvala, J., et al. (2006). Posttranslational regulation of tristetraprolin subcellular localization and protein stability by p38 mitogen-activated protein kinase and extracellular signal-regulated kinase pathways. *Mol. Cell Biol.* 26, 2408–2418. doi: 10.1128/mcb.26.6.2408-2418.2006

Brooks, S. A., and Blackshear, P. J. (2013). Tristetraprolin (TTP): interactions with mRNA and proteins, and current thoughts on mechanisms of action. *Biochim. Biophys. Acta* 1829, 666–679. doi: 10.1016/j.bbagrm.2013.02.003

Cao, S., Chao, D., Zhou, H., Balboni, G., and Xia, Y. (2015). A novel mechanism for cytoprotection against hypoxic injury: delta-opioid receptor-mediated increase in Nrf2 translocation. *Br. J. Pharmacol.* 172, 1869–1881. doi: 10.1111/bph.13031

Chao, D., Bazzy-Asaad, A., Balboni, G., Salvadori, S., and Xia, Y. (2008). Activation of DOR attenuates anoxic K+ derangement via inhibition of Na+ entry in mouse cortex. *Cereb. Cortex* 18, 2217–2227. doi: 10.1093/cercor/bhm247

Chao, D., Bazzy-Asaad, A., Balboni, G., and Xia, Y. (2007). delta-, but not mu-, opioid receptor stabilizes K(+) homeostasis by reducing Ca(2+) influx in the cortex during acute hypoxia. *J. Cell Physiol.* 212, 60–67. doi: 10.1002/jcp.21000

Chao, D., and Xia, Y. (2010). Ionic storm in hypoxic/ischemic stress: can opioid receptors subside it? *Prog. Neurobiol.* 90, 439–470. doi: 10.1016/j.pneurobio.2009.12.007

Chen, H. H., Lu, P. J., Chen, B. R., Hsiao, M., Ho, W. Y., and Tseng, C. J. (2015). Heme oxygenase-1 ameliorates kidney ischemia-reperfusion injury in mice through extracellular signal-regulated kinase 1/2-enhanced tubular epithelium proliferation. *Biochim. Biophys. Acta* 1852, 2195–2201. doi: 10.1016/j.bbadis.2015.07.018

Chen, J., Wang, W., Zhang, Q., Li, F., Lei, T., Luo, D., et al. (2013). Low molecular weight fucoidan against renal ischemia-reperfusion injury via inhibition of the MAPK signaling pathway. *PLoS One* 8:e56224. doi: 10.1371/journal.pone.0056224

Chen, T., Li, J., Chao, D., Sandhu, H. K., Liao, X., Zhao, J., et al. (2014). delta-Opioid receptor activation reduces alpha-synuclein overexpression and oligomer formation induced by MPP(+) and/or hypoxia. *Exp. Neurol.* 255, 127–136. doi: 10.1016/j.expneurol.2014.02.022

Chi, H., Barry, S. P., Roth, R. J., Wu, J. J., Jones, E. A., Bennett, A. M., et al. (2006). Dynamic regulation of pro- and anti-inflammatory cytokines by MAPK phosphatase 1 (MKP-1) in innate immune responses. *Proc. Natl. Acad. Sci. U.S.A.* 103, 2274–2279. doi: 10.1073/pnas.0510965103

Chu Sin Chung, P., and Kieffer, B. L. (2013). Delta opioid receptors in brain function and diseases. *Pharmacol. Ther.* 140, 112–120. doi: 10.1016/j.pharmthera.2013.06.003

Correa, F., Hernangomez, M., Mestre, L., Loria, F., Spagnolo, A., Docagne, F., et al. (2010). Anandamide enhances IL-10 production in activated microglia by targeting CB(2) receptors: roles of ERK1/2, JNK, and NF-kappaB. *Glia* 58, 135–147. doi: 10.1002/glia.20907

Denys, A., Udalova, I. A., Smith, C., Williams, L. M., Ciesielski, C. J., Campbell, J., et al. (2002). Evidence for a dual mechanism for IL-10 suppression of TNF-alpha production that does not involve inhibition of p38 mitogen-activated protein kinase or NF-kappa B in primary human macrophages. *J. Immunol.* 168, 4837–4845. doi: 10.4049/jimmunol.168.10.4837

di Mari, J. F., Davis, R., and Safirstein, R. L. (1999). MAPK activation determines renal epithelial cell survival during oxidative injury. *Am. J. Physiol.* 277, F195–F203. doi: 10.1152/ajprenal.1999.277.2.F195

Filizola, M., and Devi, L. A. (2012). Structural biology: how opioid drugs bind to receptors. *Nature* 485, 314–317. doi: 10.1038/485314a

Fu, Q., Colgan, S. P., and Shelley, C. S. (2016). Hypoxia: the force that drives chronic kidney disease. *Clin. Med. Res.* 14, 15–39. doi: 10.3121/cmr.2015.1282

Granier, S., Manglik, A., Kruse, A. C., Kobilka, T. S., Thian, F. S., Weis, W. I., et al. (2012). Structure of the delta-opioid receptor bound to naltrindole. *Nature* 485, 400–404. doi: 10.1038/nature11111

He, X., Sandhu, H. K., Yang, Y., Hua, F., Belser, N., Kim, D. H., et al. (2013a). Neuroprotection against hypoxia/ischemia: delta-opioid receptor-mediated cellular/molecular events. *Cell Mol. Life Sci.* 70, 2291–2303. doi: 10.1007/s00018-012-1167-2

He, X., Yang, Y., Zhi, F., Moore, M. L., Kang, X., Chao, D., et al. (2013b). delta-Opioid receptor activation modified microRNA expression in the rat kidney under prolonged hypoxia. *PLoS One* 8:e61080. doi: 10.1371/journal.pone.0061080

Hitti, E., Iakovleva, T., Brook, M., Deppenmeier, S., Gruber, A. D., Radzioch, D., et al. (2006). Mitogen-activated protein kinase-activated protein kinase 2 regulates tumor necrosis factor mRNA stability and translation mainly by altering tristetraprolin expression, stability, and binding to adenine/uridine-rich element. *Mol. Cell Biol.* 26, 2399–2407. doi: 10.1128/mcb.26.6.2399-2407.2006

Hung, C. C., Ichimura, T., Stevens, J. L., and Bonventre, J. V. (2003). Protection of renal epithelial cells against oxidative injury by endoplasmic reticulum stress preconditioning is mediated by ERK1/2 activation. *J. Biol. Chem.* 278, 29317–29326. doi: 10.1074/jbc.m302368200

Kim, H. D., Yu, S. J., Kim, H. S., Kim, Y. J., Choe, J. M., Park, Y. G., et al. (2013). Interleukin-4 induces senescence in human renal carcinoma cell lines through STAT6 and p38 MAPK. *J. Biol. Chem.* 288, 28743–28754. doi: 10.1074/jbc.M113.499053

Kunduzova, O. R., Bianchi, P., Pizzinat, N., Escourrou, G., Seguelas, M. H., Parini, A., et al. (2002). Regulation of JNK/ERK activation, cell apoptosis, and tissue regeneration by monoamine oxidases after renal ischemia-reperfusion. *FASEB J.* 16, 1129–1131. doi: 10.1096/fj.01-1008fje

Kyriakis, J. M., and Avruch, J. (2001). Mammalian mitogen-activated protein kinase signal transduction pathways activated by stress and inflammation. *Physiol. Rev.* 81, 807–869. doi: 10.1152/physrev.2001.81.2.807

Kyriakis, J. M., and Avruch, J. (2012). Mammalian MAPK signal transduction pathways activated by stress and inflammation: a 10-year update. *Physiol. Rev.* 92, 689–737. doi: 10.1152/physrev.00028.2011

Law, P. Y., and Loh, H. H. (1999). Regulation of opioid receptor activities. *J. Pharmacol. Exp. Ther.* 289, 607–624.

Lee, E. J., Ko, H. M., Jeong, Y. H., Park, E. M., and Kim, H. S. (2015). beta-Lapachone suppresses neuroinflammation by modulating the expression of cytokines and matrix metalloproteinases in activated microglia. *J. Neuroinflamm.* 12:133. doi: 10.1186/s12974-015-0355-z

Li, C., Wang, T., Zhang, C., Xuan, J., Su, C., and Wang, Y. (2016). Quercetin attenuates cardiomyocyte apoptosis via inhibition of JNK and p38 mitogen-activated protein kinase signaling pathways. *Gene* 577, 275–280. doi: 10.1016/j.gene.2015.12.012

Li, X., He, P., Wang, X. L., Zhang, S., Devejian, N., Bennett, E., et al. (2018). Sulfiredoxin-1 enhances cardiac progenitor cell survival against oxidative stress via the upregulation of the ERK/NRF2 signal pathway. *Free Radic. Biol. Med.* 123, 8–19. doi: 10.1016/j.freeradbiomed.2018.05.060

Liu, F., and McCullough, L. D. (2013). Inflammatory responses in hypoxic ischemic encephalopathy. *Acta Pharmacol. Sin.* 34, 1121–1130. doi: 10.1038/aps.2013.89

Liu, J., Wei, Q., Guo, C., Dong, G., Liu, Y., Tang, C., et al. (2017). Hypoxia, HIF, and associated signaling networks in chronic kidney disease. *Int. J. Mol. Sci.* 18:E0950. doi: 10.3390/ijms18050950

Liu, W. H., Liu, H. B., Gao, D. K., Ge, G. Q., Zhang, P., Sun, S. R., et al. (2013). ABCG2 protects kidney side population cells from hypoxia/reoxygenation injury through activation of the MEK/ERK pathway. *Cell Transplant.* 22, 1859–1868. doi: 10.3727/096368912X657206

Liu, W. Y., Liou, S. S., Hong, T. Y., and Liu, I. M. (2017). Protective effects of hesperidin (Citrus Flavonone) on high glucose induced oxidative stress and apoptosis in a cellular model for diabetic retinopathy. *Nutrients* 9:E1312. doi: 10.3390/nu9121312

Luo, F., Shi, J., Shi, Q., He, X., and Xia, Y. (2017). ERK and p38 upregulation versus Bcl-6 downregulation in rat kidney epithelial cells exposed to prolonged hypoxia. *Cell Transplant.* 26, 1441–1451. doi: 10.1177/0963689717720296

Luo, F., Shi, J., Shi, Q., Xu, X., Xia, Y., and He, X. (2016). Mitogen-activated protein kinases and hypoxic/ischemic nephropathy. *Cell Physiol. Biochem.* 39, 1051–1067. doi: 10.1159/000447812

Ma, M. C., Qian, H., Ghassemi, F., Zhao, P., and Xia, Y. (2005). Oxygen-sensitive {delta}-opioid receptor-regulated survival and death signals: novel insights into neuronal preconditioning and protection. *J. Biol. Chem.* 280, 16208–16218. doi: 10.1074/jbc.m408055200

Murray, P. J. (2005). The primary mechanism of the IL-10-regulated antiinflammatory response is to selectively inhibit transcription. *Proc. Natl. Acad. Sci. U.S.A.* 102, 8686–8691. doi: 10.1073/pnas.0500419102

Myszczyszyn, A., Czarnecka, A. M., Matak, D., Szymanski, L., Lian, F., Kornakiewicz, A., et al. (2015). The role of hypoxia and cancer stem cells in renal cell carcinoma pathogenesis. *Stem Cell Rev.* 11, 919–943. doi: 10.1007/s12015-015-9611-y

Nangaku, M., Rosenberger, C., Heyman, S. N., and Eckardt, K. U. (2013). Regulation of hypoxia-inducible factor in kidney disease. *Clin. Exp. Pharmacol. Physiol.* 40, 148–157. doi: 10.1111/1440-1681.12005

Niu, H., Ye, B. H., and Dalla-Favera, R. (1998). Antigen receptor signaling induces MAP kinase-mediated phosphorylation and degradation of the BCL-6 transcription factor. *Genes Dev.* 12, 1953–1961. doi: 10.1101/gad.12.13.1953

O'Neil, J. D., Ammit, A. J., and Clark, A. R. (2018). MAPK p38 regulates inflammatory gene expression via tristetraprolin: doing good by stealth. *Int. J. Biochem. Cell Biol.* 94, 6–9. doi: 10.1016/j.biocel.2017.11.003

Pantoja-Escobar, G., Morales-Martinez, M., Vega, G. G., Castro-Escarpulli, G., and Vega, M. I. (2019). Cytotoxic effect caspase activation dependent of a genetically engineered fusion protein with a CD154 peptide mimetic (OmpC-CD154p) on B-NHL cell lines is mediated by the inhibition of bcl-6 and YY1 through MAPK p38 activation. *Leuk. Lymphoma* 60, 1062–1070. doi: 10.1080/10428194.2018.1516286

Park, K. M., and Bowers, W. J. (2010). Tumor necrosis factor-alpha mediated signaling in neuronal homeostasis and dysfunction. *Cell Signal.* 22, 977–983. doi: 10.1016/j.cellsig.2010.01.010

Patial, S., and Blackshear, P. J. (2016). Tristetraprolin as a therapeutic target in inflammatory disease. *Trends Pharmacol. Sci.* 37, 811–821. doi: 10.1016/j.tips.2016.07.002

Peng, J., Sarkar, S., and Chang, S. L. (2012). Opioid receptor expression in human brain and peripheral tissues using absolute quantitative real-time RT-PCR. *Drug Alcohol. Depend.* 124, 223–228. doi: 10.1016/j.drugalcdep.2012.01.013

Prabhala, P., and Ammit, A. J. (2015). Tristetraprolin and its role in regulation of airway inflammation. *Mol. Pharmacol.* 87, 629–638. doi: 10.1124/mol.114.095984

Ronkina, N., Shushakova, N., Tiedje, C., Yakovleva, T., Tollenaere, M. A. X., Scott, A., et al. (2019). The Role of TTP Phosphorylation in the Regulation of Inflammatory Cytokine Production by MK2/3. *J. Immunol.* 203, 2291–2300. doi: 10.4049/jimmunol.1801221

Ross, E. A., Naylor, A. J., O'Neil, J. D., Crowley, T., Ridley, M. L., Crowe, J., et al. (2017). Treatment of inflammatory arthritis via targeting of tristetraprolin, a master regulator of pro-inflammatory gene expression. *Ann. Rheum. Dis.* 76, 612–619. doi: 10.1136/annrheumdis-2016-209424

Schodel, J., Grampp, S., Maher, E. R., Moch, H., Ratcliffe, P. J., Russo, P., et al. (2016). Hypoxia, hypoxia-inducible transcription factors, and renal cancer. *Eur. Urol.* 69, 646–657. doi: 10.1016/j.eururo.2015.08.007

Shoji, K., Tanaka, T., and Nangaku, M. (2014). Role of hypoxia in progressive chronic kidney disease and implications for therapy. *Curr. Opin. Nephrol. Hypertens.* 23, 161–168. doi: 10.1097/01.mnh.0000441049.98664.6c

Singh, P., Ricksten, S. E., Bragadottir, G., Redfors, B., and Nordquist, L. (2013). Renal oxygenation and haemodynamics in acute kidney injury and chronic kidney disease. *Clin. Exp. Pharmacol. Physiol.* 40, 138–147. doi: 10.1111/1440-1681.12036

Stoecklin, G., Stubbs, T., Kedersha, N., Wax, S., Rigby, W. F., Blackwell, T. K., et al. (2004). MK2-induced tristetraprolin:14-3-3 complexes prevent stress granule association and ARE-mRNA decay. *EMBO J.* 23, 1313–1324. doi: 10.1038/sj.emboj.7600163

Tan, J., Liu, D., Lv, X., Wang, L., Zhao, C., Che, Y., et al. (2013). MAPK mediates inflammatory response and cell death in rat pulmonary microvascular endothelial cells in an ischemia-reperfusion model of lung transplantation. *J. Heart Lung Transplant.* 32, 823–831. doi: 10.1016/j.healun.2013.05.005

Wang, Q., Chao, D., Chen, T., Sandhu, H., and Xia, Y. (2014). delta-Opioid receptors and inflammatory cytokines in hypoxia: differential regulation between glial and neuron-like cells. *Transl. Stroke Res.* 5, 476–483. doi: 10.1007/s12975-014-0342-1

Wang, Y., Hai, B., Niu, X., Ai, L., Cao, Y., Li, R., et al. (2017). Chronic intermittent hypoxia disturbs insulin secretion and causes pancreatic injury via the MAPK signaling pathway. *Biochem. Cell Biol.* 95, 415–420. doi: 10.1139/bcb-2016-0167

Watters, O., and O'Connor, J. J. (2011). A role for tumor necrosis factor-alpha in ischemia and ischemic preconditioning. *J. Neuroinflamm.* 8:87. doi: 10.1186/1742-2094-8-87

Williams, L. M., Ricchetti, G., Sarma, U., Smallie, T., and Foxwell, B. M. (2004). Interleukin-10 suppression of myeloid cell activation–a continuing puzzle. *Immunology* 113, 281–292. doi: 10.1111/j.1365-2567.2004.01988.x

Wu, S. H., Wang, M. J., Lu, J., and Chen, X. Q. (2017). Signal transduction involved in lipoxin A4induced protection of tubular epithelial cells against hypoxia/reoxygenation injury. *Mol. Med. Rep.* 15, 1682–1692. doi: 10.3892/mmr.2017.6195

Wu, X., Gu, W., Lu, H., Liu, C., Yu, B., Xu, H., et al. (2016). Soluble receptor for advanced glycation end product ameliorates chronic intermittent hypoxia induced renal injury, inflammation, and apoptosis via p38/jnk signaling pathways. *Oxid. Med. Cell Longev.* 2016:1015390.

Xia, Y. (ed.) (2015). *Neural Functions of the Delta-Opioid Receptor*. New York, NY: Springer.

Xia, Y., and Haddad, G. G. (2001). Major difference in the expression of delta- and mu-opioid receptors between turtle and rat brain. *J. Comp. Neurol.* 436, 202–210. doi: 10.1002/cne.1061.abs

Xia, Y., Jiang, C., and Haddad, G. G. (1992). Oxidative and glycolytic pathways in rat (newborn and adult) and turtle brain: role during anoxia. *Am. J. Physiol.* 262, R595–R603.

Yang, C. W., Ahn, H. J., Jung, J. Y., Kim, W. Y., Li, C., Choi, B. S., et al. (2003). Preconditioning with cyclosporine A or FK506 differentially regulates mitogen-activated protein kinase expression in rat kidneys with ischemia/reperfusion injury. *Transplantation* 75, 20–24. doi: 10.1097/00007890-200301150-00004

Yu, J. M., Sun, W., Hua, F., Xie, J., Lin, H., Zhou, D. D., et al. (2015). BCL6 induces EMT by promoting the ZEB1-mediated transcription repression of E-cadherin in breast cancer cells. *Cancer Lett.* 365, 190–200. doi: 10.1016/j.canlet.2015.05.029

Zhang, D., Li, N., Wang, Y., Lu, W., Zhang, Y., Chen, Y., et al. (2019). Methane ameliorates post-operative cognitive dysfunction by inhibiting microglia NF-kappaB/MAPKs pathway and promoting IL-10 expression in aged mice. *Int. Immunopharmacol.* 71, 52–60. doi: 10.1016/j.intimp.2019.03.003

Zhang, J., Gibney, G. T., Zhao, P., and Xia, Y. (2002). Neuroprotective role of delta-opioid receptors in cortical neurons. *Am. J. Physiol. Cell Physiol.* 282, C1225–C1234.

Zhang, J., Qian, H., Zhao, P., Hong, S. S., and Xia, Y. (2006). Rapid hypoxia preconditioning protects cortical neurons from glutamate toxicity through delta-opioid receptor. *Stroke* 37, 1094–1099. doi: 10.1161/01.str.0000206444.29930.18

Zou, Y. R., Zhang, J., Wang, J., Peng, L., Li, G. S., and Wang, L. (2016). Erythropoietin receptor activation protects the kidney from ischemia/reperfusion-induced apoptosis by activating erk/p53 signal pathway. *Transplant. Proc.* 48, 217–221. doi: 10.1016/j.transproceed.2016.01.009

Conflict of Interest: The authors declare that the research was conducted in the absence of any commercial or financial relationships that could be construed as a potential conflict of interest.

Copyright © 2020 Luo, Xu, Song, Lu, He and Xia. This is an open-access article distributed under the terms of the Creative Commons Attribution License (CC BY). The use, distribution or reproduction in other forums is permitted, provided the original author(s) and the copyright owner(s) are credited and that the original publication in this journal is cited, in accordance with accepted academic practice. No use, distribution or reproduction is permitted which does not comply with these terms.

frontiers in Pharmacology

ORIGINAL RESEARCH
published: 31 January 2020
doi: 10.3389/fphar.2020.00009

Endothelin-1/Nitric Oxide Ratio as a Predictive Factor of Response to Therapy With Terlipressin and Albumin in Patients With Type-1 Hepatorenal Syndrome

Ahmed Abdel-Razik[1], Nasser Mousa[1], Mostafa Abdelsalam[2], Ahmed Abdelwahab[2], Mona Tawfik[2], Ahmed M. Tawfik[3], Ahmad S. Hasan[4], Rania Elhelaly[4], Niveen El-Wakeel[5] and Waleed Eldars[5]*

[1] Tropical Medicine Department, Faculty of Medicine, Mansoura University, Mansoura, Egypt, [2] Nephrology and Dialysis Unit, Internal Medicine Department, Faculty of Medicine, Mansoura University, Mansoura, Egypt, [3] Diagnostic & Interventional Radiology Department, Faculty of Medicine, Mansoura University, Mansoura, Egypt, [4] Clinical Pathology Department, Faculty of Medicine, Mansoura University, Mansoura, Egypt, [5] Medical Microbiology and Immunology Department, Faculty of Medicine, Mansoura University, Mansoura, Egypt

OPEN ACCESS

Edited by:
Md Abdul Hye Khan, Medical College of Wisconsin, United States

Reviewed by:
Chiara Elia, Cardinal Massaia Asti Hospital, Italy
Flemming Bendtsen, University of Copenhagen, Denmark

***Correspondence:**
Ahmed Abdel-Razik
Ahmedabdelrazik76@gmail.com

Specialty section:
This article was submitted to Renal Pharmacology, a section of the journal Frontiers in Pharmacology

Received: *31 October 2019*
Accepted: *06 January 2020*
Published: *31 January 2020*

Citation:
Abdel-Razik A, Mousa N, Abdelsalam M, Abdelwahab A, Tawfik M, Tawfik AM, Hasan AS, Elhelaly R, El-Wakeel N and Eldars W (2020) Endothelin-1/Nitric Oxide Ratio as a Predictive Factor of Response to Therapy With Terlipressin and Albumin in Patients With Type-1 Hepatorenal Syndrome. Front. Pharmacol. 11:9. doi: 10.3389/fphar.2020.00009

Background and Purpose: Predictors of response to type-1 hepatorenal syndrome (HRS) therapy are urgently needed. This study's purpose is to evaluate the proposed predictors in these patients.

Methods: Forty-two type-1 HRS patients with cirrhosis were treated with albumin and terlipressin. Clinical, biochemical, and demographic parameters taken at the onset of therapy and changes in endothelin-1/nitric oxide (ET-1/NO) ratio during therapy were analyzed to check their predictive value.

Results: Response to treatment (serum creatinine level <1.5 mg/dL at the end of therapy) was shown in 20 patients (48%). Independent predictive variables of response to therapy were early reduction of ET-1/NO ratio ≥0.15 at day 3 of therapy and serum bilirubin baseline <8 mg/dL (area under the receiver operating characteristic curve, 0.751; $P < 0.001$; specificity, 55%; sensitivity, 85%). Response rates in patients with serum bilirubin level <8 and ≥8 mg/dL were 63% and 20%, respectively ($P = 0.008$). The corresponding values in patients with an early reduction of ET-1/NO ratio ≥0.15 and <0.15 on day 3 were 85% and 13.6%, respectively ($P < 0.001$).

Conclusions: Early reduction of ET-1/NO ratio and lower serum bilirubin baseline can predict response to type-1 HRS therapy with albumin and terlipressin. Alternative therapy should be investigated for nonresponder type-1 HRS patients.

Keywords: hepatorenal syndrome, endothelin-1, nitric oxide, liver cirrhosis, endothelin-1/nitric oxide ratio, terlipressin, albumin

INTRODUCTION

Hepatorenal syndrome (HRS) is a reversible cause of renal impairment that occurs in patients with cirrhotic ascites, as well as in patients with alcoholic hepatitis or acute liver failure who show no significant abnormalities in the kidneys morphology (Arroyo et al., 1996; Dagher and Moore, 2001; Angeli et al., 2015).

HRS is characterized by marked alterations in cardiovascular function, impaired renal function, and over-activity of renin-angiotensin systems that lead to severe renal vasoconstriction with a significant reduction of the glomerular filtration rate (GFR) as well as vigorous activation of the sympathetic nervous system (Arroyo et al., 1996; Dagher and Moore, 2001).

HRS predicts mortality in cirrhosis. The most important aspect of providing care to patients with HRS is an evaluation of candidacy for orthotopic liver transplantation (Gonwa et al., 1995; Jeyarajah et al., 1997; Nair et al., 2002). Current accessible therapies other than liver transplantation for HRS consist of albumin and the utilization of vasoconstrictors, for example, terlipressin (Angeli and Merkel, 2008).

Recently, only 52% of HRS patients have responded to therapy with terlipressin (Møller et al., 2000; Fabrizi et al., 2006; Gluud et al., 2010; Allegretti et al., 2017). Furthermore, few researches have reported some predictors of response to treatment in HRS patients treated with this regimen.

The endothelium release many vasoactive mediators that change the structure and function of the vascular smooth muscle in response to mechanical and humoral stimuli. Two of the most prominent are ET and NO (Cahill et al., 2001). ET-1 is released in response to infectious complications with an inflammatory response in the form of transcription mediators activation and proinflammatory cytokines (IL-1, IL-6, and TNF-α) production. It also plays an important role in the vascular disruption pathogenesis caused by infection (Charpin et al., 2001; Yeager et al., 2012; Freeman et al., 2014).

The pathophysiology of various disorders is closely related on the ET-1/NO imbalance (Alonso and Radomski, 2003). In cirrhosis and HRS, the ET system dysfunction causes hemodynamic disturbances (Moore et al., 1992; Uchihara et al., 1992).

The identification of patients with low therapeutic response probability is of imperative clinical importance, especially in patients waiting for transplantation. In our study, we evaluated the hypothesized predictors of response to albumin and terlipressin in type-1 HRS and cirrhosis patients treated with this protocol.

PATIENTS AND METHODS

Study Population

Starting 2015, patients with renal impairment and cirrhosis admitted to the Tropical Medicine Department (Mansoura, Egypt) were assessed using the same diagnostic algorithm (Gine`s et al., 2003), that involves evaluation of the possible causes of hypovolemia, diuretic withdrawal, possible infection, drug nephrotoxicity, and renal parenchymal disorders. To exclude the presence of volume depletion related renal failure, plasma expansion with I.V. albumin was tried. According to the International Ascites Club (Arroyo et al., 1996), patients who met the type-1 HRS criteria, were treated with albumin and terlipressin. The new HRS defining criteria were approved by this study protocol (Angeli et al., 2015). Some patients didn't receive therapy due to having advanced hepatocellular carcinoma, severe cardiovascular disorders and/or being terminal cases (death expected in less than 2 days).

All the differential diagnosis causes of cirrhotic acute kidney injury including: organic (including glomerulonephritis and acute tubular necrosis), prerenal (all accessible hypovolemic causes), and obstructive nephropathy (Garcia-Tsao et al., 2008; Møller et al., 2014) were excluded in this study by meticulous history taking and physical examination, together with complete biochemical analysis and radiological investigations.

The existence of infection was assessed by various methods, for example, culture and sensitivity testing for ascitic fluid, blood, sputum, and urine, evaluation of the ascitic fluid absolute polymorphonuclear (PMN) count, and chest radiography. Patients with infection were precluded from this study and received albumin and terlipressin only when renal failure continued after the infection was successfully treated. According to the type of infection, bacterial infections were initially treated with antibiotics as reported in detail elsewhere (Martin-Llahi et al., 2011; Fernandez et al., 2012). The antibiotic was changed according to the results of the cultures if there was no response to the initial therapy. In patients with negative cultures and not responding to the initial therapy, empiric antibiotics policy consisting of vancomycin and carbapenems combination was used (Barreto et al., 2014).

The current study included 42 consecutive cirrhosis/type-1 HRS patients who were subjected to treatment from March 2015 to February 2019. Twenty nine (69%) of them had bacterial infection induced type-1 HRS including 20 SBP cases, six soft tissue infection cases, and three patients with pneumonia as well as 13 patients with HRS without known risk factors.

Bacterial infections were categorized according to the following criteria: SBP is the presence of an ascitic fluid absolute polymorphonuclear count >250/mm^3 and/or a positive ascitic fluid bacterial culture with no apparent source of infection (Rimola et al., 2000); spontaneous bacteremia is positive blood cultures without an evident source of infection; local infections (skin infection, urinary tract infection, pneumonia, gastroenteritis, meningitis, and biliary tract infection) were evaluated utilizing standard criteria; sepsis with negative-culture is leukocytosis with/without band forms, the presence of fever (>38°C), together with negative cultures, after the exclusion of disorders other than infection that could be related to the systemic inflammatory response.

Improvement of SBP was defined as a reduction in polymorphonuclear cell count <250/mm^3, absence of clinical

Abbreviations: HRS, hepatorenal syndrome; ET-1/NO ratio, endothelin-1/nitric oxide ratio; GFR, glomerular filtration rate; PMN, polymorphonuclear; SBP, spontaneous bacterial peritonitis; IVCCI, inferior vena cava collapsibility index; CBC, complete blood count; MELD, Model for End-Stage Liver Disease.

signs of infection, negative cultures, and normal leukocyte count. The remaining infections were improved according to the conventional criteria. Septic shock was identified as a mean arterial pressure below 60 mmHg regardless of adequate volume resuscitation and need for vasopressor agents (Dellinger, 2003).

In this study, all specific therapy or treatment was delayed for type-1 HRS until the infection has been cured.

In addition, the control group included 42 cirrhotic patients without renal impairment who were sex- and age-matched subjects (male/female = 27/15).

Treatment Protocol

The response to treatment was considered a primary endpoint, determined by either a decline in serum creatinine level >50% of the pretreatment value, or >1.5 mg/dL during treatment with an end-of-therapy level of ≤1.5 mg/dL.

Terlipressin (Glypressin, Ferring S.A., Saint-Prex, Switzerland) was administrated as follows; 0.5–1 mg/4 h, as intravenous (i.v.) bolus for 3 days with an increase up to 2 mg/4 h for those whose values did not decrease by at least 25% of the pretreatment values. The maximum duration of therapy was 2 weeks. Once serum creatinine is reduced below 1.5 mg/dL, Terlipressin was withheld. If patients developed manifestations matching the ischemic complications, administration of Terlipressin was stopped.

All patients received albumin (Baxter Human Albumin 20%, Baxter AG, Industriestraße 67, A-1221 Vienna, Austria) at a dose of 1 g/kg BW. during the first day, followed by 40 g/d, given for a maximum of 15 days, in order to reach the inferior vena cava collapsibility index (*IVCCI*) ≥40% and ≤75%. Clinically, *IVCCI* was evaluated daily in a regular manner throughout the follow-up period. The dose of albumin was decreased to 20 g/d and/or was stopped if *IVCCI* was <40% (Brennan et al., 2006). All measurements were carried out by qualified ultrasound radiologists. Moreover, if radiological and clinical signs of pulmonary edema developed, the administration of albumin was withheld, and the patients received i.v. doses of furosemide with careful follow-up.

During therapy of HRS, any complications of cirrhosis were treated based on standardized therapeutic measures (Cardenas and Gine`s, 2005).

Sampling

Following an overnight fasting of 12 h, 4 to 8 mL blood *were withdrawn* through cannulas in superficial forearm *veins* for all patients [1 mL in EDTA for complete blood count (CBC), 5mL without anticoagulants for serum samples].

Methodology

CBC was assessed using the CELL-DYN Emerald cell counter (Abbott, Wiesbaden, Germany). Serum creatinine, blood urea nitrogen (BUN) and liver function tests were measured on a Dimension Xpand plus chemistry analyzer (Siemens Technology, Princeton, NJ, USA) using commercially available enzyme-based kit and reagents. Quantitative detection of plasma nitric oxide (NO) was measured using ELISA kits provided by MyBiosource (San Diego, CA 92195-3308, USA) Cat No. MBS264607, with detection range 1.56 to 100 nmol/mL (nmol/mL = μmol/L). Though the NO role in various disorders is debatable, the majority of researchers agree that evaluating serum levels of NOx are associated with NO production. (Andrukhov et al., 2013). Quantitative detection of plasma Endothelin-1 (ET-1) was measured using ELISA kits provided by MyBiosource (San Diego, CA 92195-3308, USA) Cat No. MBS025621, with detection range 6.25 to 200 pg/mL (pg/mL = ng/L). Plasma L-Arginine was quantitatively measured using ELISA kits provided by ALPCO (26G Keewaydin Drive, Salem, New Hampshire 3079, United States) Cat No. 30-7733, with detection range 12.5 to 300 μmol/L. The estimated glomerular filtration rate (eGFR) was calculated according to the following formula (Levey et al., 1999): $186 \times (\text{Creatinine}/88.4)^{-1.154} \times (\text{Age})^{-0.203}$ x (0.742 if female) x (1.210 if black). The ET-1/NO ratio was calculated and recorded for all patients.

Ethics

The protocol of this study was completed to acclimate with the Declaration of Helsinki and was affirmed by the Ethics Committee of the Mansoura University. Informed consent was obtained from all enrolled patients or their legal representatives.

Statistical Analysis

The analysis was carried out using SPSS version 20 for Windows (SPSS Inc., Chicago, IL). Results are expressed as the mean ± SD. Comparisons of continuous and categorical variables between patients were carried out using Student *t*- and X^2-tests respectively. A paired Wilcoxon test and Student *t*-test were used to compare the variables measured at various time points. The multivariate analysis was built using the univariate analysis parameters that had a significant predictive value ($P < 0.01$). The best cutoff values for variables with independent predictive value were measured using receiver operating characteristic curves. The probability of response was evaluated using the Kaplan–Meier method. The calculation of overall response involved patients who received a liver transplant (n = 3) and the results were viewed redacted at the time of transplantation. $P < 0.05$ was considered statistically significant.

RESULTS

Patient Characteristics

Only 42 out of the 121 patients with cirrhotic ascites and renal failure were included in this study. The etiology of renal failure was evaluated after admission and HRS was diagnosed following the diagnostic criteria reported by Angeli et al. Of all the excluded patients, 51 were due to previous infection exposure who were discharged from hospital with normal renal function after adequate therapy of infection (32 SBP, 12 soft tissue infections and 7 pneumonia), six due to nephrotoxic agents administration (four aminoglycosides and two contrast agents), seven due to hypovolemic causes (five GIT bleeding and two

severe vomiting), and three due to obstructive nephropathy. Also, the 12 patients who showed complete response and marked serum creatinine decline after receiving only albumin as a corrective measure for the pre-renal causes of renal failure were excluded.

Baseline characteristics of patients with type-1 HRS at the time of diagnosis before starting the treatment with albumin and terlipressin are reported in **Table 1**. Not surprisingly, most patients with type-1 HRS had severe liver failure, as demonstrated by increased international normalized ratio (INR), high Model for End-Stage Liver Disease (MELD) and Child-Pugh scores, low estimated GFR using Modification of Diet in Renal Disease equation, high levels of serum bilirubin, creatinine, L-arginine, NOx, serum ET-1, and ET-1/NO ratio *compared* to the control group.

Predictive Factors For Treatment Response

Twenty out of the 42 patients (48%) had a response to therapy. Generally, at the end of therapy, serum creatinine decreased below 1.5 mg/dL, while in two patients serum creatinine decreased >50% of the pretreatment levels but stayed above 1.5 mg/dL (4.8 decreased to 1.8 mg/dL and 3.7 to 1.7 mg/dL). The rest of the patients (52%) failed to reach the response to therapy criteria. Serum creatinine levels during the therapy period in non-responders and responders are summarized in **Figure 1**. During therapy, the probability of response in all patients is shown in **Figure 2**. The estimated period for response was approximately 2 weeks. Response to therapy was merely constant in most patients. Recurrence of HRS was 4/20 (20%) in patients who responded to therapy. The average period for recurrence was 2 weeks (range, 3–38 days).

At baseline, several parameters obtained were assessed for the predictive value of response to therapy (**Table 2**). Parameters related to response to therapy ($P < 0.05$) were WBCs count, AST level, serum bilirubin level, urine volume, and MELD score. Furthermore, neither ET-1/NO ratio nor serum creatinine level at baseline was related to response to treatment. The only parameter found to have an independent predictive value in the multivariate analysis was the serum bilirubin level (OR, 14.2; 95% CI, 1.256–160.77; $P = 0.032$). By receiver operating characteristic curves, serum bilirubin level has a cutoff value (< 8 mg/dL) that well-predicted response to therapy, (AUC = 0.751; $P < 0.001$; specificity = 55%; sensitivity = 85%; PPV = 63%; and NPV = 80%). Response rates in patients classified based on baseline serum bilirubin level <8 or ≥8 mg/dL were 63% (17/27) and 20% (3/15), respectively ($P = 0.008$).

Based on changes in the ET-1/NO ratio evaluated at day 3 of therapy, we analyzed response rates in all patients. The value of the ET-1/NO ratio used was the average value of all measurements of ET-1/NO ratio assessed at day 3; a reduction in ET-1/NO ratio of 0.15 was considered relevant and used as a cutoff value. Values of ET-1/NO ratio throughout therapy in non-responders and responders are summarized in **Figure 3**. Although the baseline ET-1/NO ratio was not a predictive factor of response, early changes of ET-1/NO ratio within the first days of therapy predicted response. Patients with a reduction in the ET-1/NO ratio equal to or greater than 0.15 at day 3 of therapy had a response rate at the end of treatment of 85% (17/20) compared to 13.6% (3/22) in patients with minimal decreases in the ET-1/NO ratio ($P < 0.001$). When this decrease in the ET-1/NO ratio of 0.15 or more at day 3 was enclosed in the multivariate analysis with the baseline parameters, the predictive factors of response to treatment were the baseline serum bilirubin level and the decrease in the ET-1/NO ratio ≥0.15 at day 3 (**Table 3**). Moreover, 2/5 patients (40%) responded if there was a reduction ET-1/NO ratio ≥0.15 in those with baseline serum bilirubin level ≥8 mg/dL, compared to a response in 1/10 (10%) in those with a change in the ET-1/NO ratio <0.15 with baseline serum bilirubin level ≥8 mg/dL (**Figure 4**).

In addition, Spearman's correlation analysis showed that there was a significant correlation between the ET-1/NO ratio and serum bilirubin level, serum creatinine level, creatinine clearance, MELD and Child-Pugh scores (*rho* = 0.63, $P < 0.001$; *rho* = 0.72, $P < 0.001$; *rho* = −0.66, $P < 0.001$; *rho* = 0.72, $P < 0.001$; *rho* = 0.69, $P < 0.001$respectively).

TABLE 1 | Baseline characteristics of patients with type-1 hepatorenal syndrome at the time of diagnosis.

Parameters	Cirrhotic patients with HRS (n = 42)	Cirrhotic patients without HRS (control group) (n = 42)	*P*
Age (years)	45 ± 9	44 ± 8.7	0.61
Sex (male/female)	29/13	27/15	0.889
BMI (kg/m^2)	27 ± 5.9	26.5 ± 5.4	0.686
Etiology of liver cirrhosis			
CHB-related liver cirrhosis	39 (92.8)	37 (88.1)	0.466
CHB-related liver cirrhosis	2 (4.8)	3 (7.2)	0.645
NASH-related liver cirrhosis	1 (2.4)	2 (4.7)	0.571
Hematocrit (%)	28 ± 7	30 ± 8.5	0.243
WBCs (×10^3/mm^3)	4.7 ± 2.4	4.5 ± 2.1	0.686
Platelet count (×10^3/mm^3)	95 ± 74	102 ± 69	0.655
AST (U/L)	60 ± 32	56 ± 27	0.538
ALT (U/L)	55 ± 27	50 ± 24	0.372
T. Bilirubin (mg/dL)	10.8 ± 8.3	1.9 ± 1.2	<0.001
Serum albumin (g/dL)	2.6 ± 0.6	2.5 ± 0.7	0.484
INR	2.2 ± 0.6	1.8 ± 0.5	0.001
Serum creatinine (mg/dL)	2.8 ± 1.4	1.1 ± 0.4	<0.001
eGFR (mL/min/1.73 m^2)	57 ± 2.9	74 ± 9.3	<0.001
BUN (mg/dL)	38.4 ± 8.4	37.7 ± 7.9	0.695
Urine volume (mL/d)	585 ± 279	968 ± 453	<0.001
Na (mmol/L)	129 ± 7	130 ± 11	0.621
K (mmol/L)	4.12 ± 0.7	4.23 ± 0.8	0.504
Child-Pugh score	11+1.5	9.75+1.3	<0.001
MELD score	28 ± 9	22+10	0.005
L-arginine (μmol/L)	92.5 ± 15.3	74.5 ± 10.2	<0.001
Oxide metabolites (NOx) (μmol/L)	70.6 ± 3.9	49.5 ± 1.1	<0.001
Endothelin-1 (ET-1) (ng/L)	29.1 ± 1.9	13.3 ± 0.9	<0.001
ET-1/NO ratio	0.42 ± 0.036	0.27 ± 0.02	<0.001

BMI, basal metabolic index; CHB, chronic hepatitis B; CHC, chronic hepatitis C; eGFR, estimated glomerular filtration rate; MELD score, Model for End-Stage Liver Disease score; NASH, nonalcoholic steatohepatitis; WBCs, white blood cells; ALT, alanine aminotransferase; AST, aspartate aminotransferase; INR, international normalized ratio; Na, sodium; K, potassium; ET-1/NO ratio, endothelin-1/nitric oxide ratio.

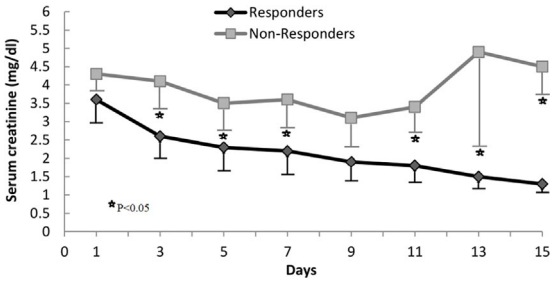

FIGURE 1 | Changes in serum creatinine concentration during treatment in responders and nonresponders.

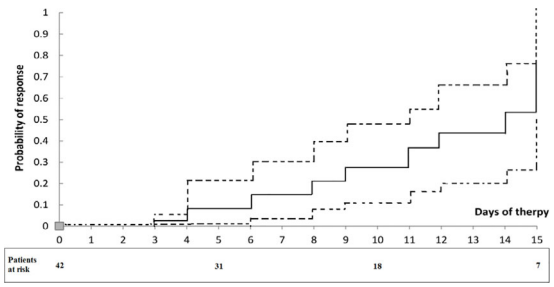

FIGURE 2 | Probability of response to treatment in patients with type 1 HRS treated with albumin and terlipressin. Dotted lines represent 95% confidence intervals. The numbers under the curve are patients at risk at each time.

During therapy, the early decrease in serum creatinine was also used as a predictor of response to treatment. Response to therapy was demonstrated in 15 of the 19 patients (79%) in whom serum creatinine decreased by at least 0.5 mg/dL at day 3, compared to only 5 of the 23 patients (22%) in whom serum creatinine did not decrease 0.5 mg/dL or elevated at day 3 compared to the baseline ($P < 0.001$). When the cutoff value for the change in serum creatinine used was 1 mg/dL instead of 0.5 mg/dL similar figures were demonstrated (89% and 36%, respectively; $P = 0.005$). The value of the reduction in serum creatinine at day 3 as a predictor of response to treatment was also approved in the multivariate analysis model (odds ratio, 9.46; $P = 0.048$).

Complications of Cirrhosis

A total of 47 major cirrhotic complications were developed in 37 patients (88%) during therapy: 32 patients with hepatic encephalopathy, five patients with GIT bleeding, and ten patients with bacterial infection. Bacterial infections between responders and non-responders showed no significant difference [4/20 (20%) vs. 6/22 (27%), respectively; $P = 0.6$]. The median value for WBCs count was 7,100/mm^3 and throughout therapy, the occurrence of bacterial infections was partially more common in patients higher count than in those with lower count [7/23 (30.4%) vs. 3/19 (15.8%), respectively; $P = 0.275$]. At the lower WBCs count baseline, patients acquired pneumonia (n = 1) and urinary tract infections (n = 2) after an average period of 6 days (range, 2–10 days), while at the higher WBCs count baseline, patients acquired pneumonia (n = 2) and sepsis (n = 5) after an average period of 6 days (range, 2–14 days).

Side Effects of Therapy

Eight patients (19%) developed albumin/terlipressin therapy-related side effects. Signs of circulatory overload developed in four patients, that improved after short-lived cessation of albumin but not of terlipressin and furosemide was added in small doses. Intestinal ischemia signs developed in two patients, that disappeared after cessation of therapy. Transient arrhythmia (ventricular extrasystolia) developed in two patients, that did not need persistent cessation of therapy, and improved after therapy withdrawal. We followed up with the patients for at least 3 months after their hospital discharge.

Survival

90 days after the initiation of treatment, 32 (76.2%) patients died, 6 (14.3%) patients were still alive, 3 (7.2%) participants had undergone liver transplantation, and 1 (2.4%) patient was lost to follow-up as well as the survival probability at that time was significantly higher in responders (40%) with median survival of 65 days compared to non-responders (9%) with median survival of 8 days; $P < 0.001$). Septic shock (n = 16), multiorgan failure (n = 11), liver failure (n = 4), and/or unknown (n = 1) were the *causes of death.*

Using the original MELD risk equation, Area Under the Receiver Operating Characteristic Curve (AUROC) analysis revealed that a MELD score threshold of 20 corresponded to median survival less than 3-months (**Figure 5**). Kaplan-Meier survival curves of patients stratified by baseline MELD score below or above 20, which represents threshold for 3-month median survival. Median survival of patients with baseline MELD score <20 significantly greater than those with baseline MELD scores ≥ 20 (62 vs. 15 days, $P < 0.001$).

DISCUSSION

This recent study reports that albumin with terlipressin are currently the accepted therapy for type-1 HRS, but over 50% of patients show a suboptimal to no response to treatment (Dagher and Moore, 2001; Angeli et al., 2015). It is therefore of paramount importance that we keep searching and investigating not only for adequate predictors of response but also prognostic factors before beginning the treatment or early afterward. Obviously, patients responding to treatment showed a statistically significant decline in ET-1/NO ratio at the end of therapy; probably because the low effective arterial blood volume of HRS was improved. These outcomes firmly recommend that the gainful impact of terlipressin in the treatment of HRS is identified with its ability to enhance systemic hemodynamics (Fabrizi et al., 2006; Moreau and Lebrec, 2006). We still don't

TABLE 2 | Univariate analysis of baseline parameters according to response to treatment with albumin and terlipressin.

Parameters	Responders (n = 20)	Non-responders (n = 22)	*P*
Age (y)	44 ± 10	43 ± 8	0.72
Sex (male/female)	14/6	15/7	0.97
BMI (kg/m^2)	25 ± 5.2	27 ± 6.1	0.26
Etiology of liver cirrhosis			
CHC-related liver cirrhosis	19 (95)	20 (91)	0.62
CHB-related liver cirrhosis	1 (5)	1 (4.5)	0.94
NASH-related liver cirrhosis	-	1 (4.5)	-
Hematocrit (%)	27 ± 6	29 ± 8	0.37
WBCs (×10^3/mm^3)	4.1 ± 2.2	5.8 ± 2.7	0.03
Platelet count (×10^3/mm^3)	108 ± 85	91 ± 69	0.48
AST (U/L)	49 ± 27	69 ± 34	0.04
ALT (U/L)	48 ± 23	63 ± 31	0.08
T. bilirubin (mg/dL)	5.5 ± 1.8	15.5 ± 9	<0.001
Serum albumin (g/dL)	2.5 ± 0.7	2.6 ± 0.8	0.67
INR	1.9 ± 0.6	1.8 ± 0.5	0.56
Serum creatinine (mg/dL)	2.3 ± 1.4	2.9 ± 1.6	0.21
eGFR (mL/min/1.73 m^2)	58 ± 2.5	56 ± 2.7	0.02
BUN (mg/dL)	38 ± 8.2	38.7 ± 8.8	0.792
Urine volume (mL/d)	475 ± 125	395 ± 90	0.02
Na (mmol/L)	129 ± 9	126 ± 7	0.23
K (mmol/L)	4 ± 0.9	4.11 ± 1	0.71
Child-Pugh score	11 ± 1	12 ± 2	0.051
MELD score	20 ± 6	25 ± 9	0.04
L-arginine (μmol/L)	89.4 ± 12.4	84.5 ± 11.3	0.19
Oxide metabolites (NOx) (μmol/L)	72 ± 2.8	69.5 ± 4.9	0.052
Endothelin-1 (ET-1) (ng/L)	29.7 ± 1.2	30.5 ± 1.4	0.055
ET-1/NO ratio	0.43 ± 0.016	0.44 ± 0.028	0.169

BMI, basal metabolic index; CHB, chronic hepatitis B; CHC, chronic hepatitis C; eGFR, estimated glomerular filtration rate; MELD score, Model for End-Stage Liver Disease score; NASH, nonalcoholic steatohepatitis; WBCs, white blood cells; ALT, alanine aminotransferase; AST, aspartate aminotransferase; INR, international normalized ratio; Na, sodium; K, potassium; ET-1/NO ratio, endothelin-1/nitric oxide ratio.

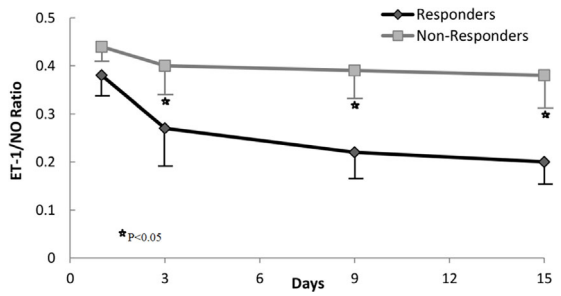

FIGURE 3 | Changes in ET-1/NO ratio during treatment in responders and nonresponders.

know why in some type-1 HRS patients the systemic hemodynamics were not enhanced when treated with terlipressin. This may be due to the presence of concomitant adrenal insufficiency, and latent infections associated with higher levels of ET-1 (Hocher et al., 1999).

Independent predictors of response to treatment were serum bilirubin levels at baseline and a decline in the ET-1/NO ratio ≥0.15 at day 3 of therapy. Eleven of the eleven patients (100%) with serum bilirubin at baseline <8 mg/dL who demonstrated a decline in the ET-1/NO ratio ≥0.15 at day 3 responded to our therapeutic protocol. While only one of the 10 (10%) patients with serum bilirubin at baseline ≥8 mg/dL and a reduction in the ET-1/NO ratio <0.15 had a response to therapy. In previous studies, predictive variables of response observed in patients with HRS involved MELD and Child-Pugh scores, arterial pressure, and serum creatinine level at the baseline (Moreau et al., 2002; Alessandria et al., 2007; Neri et al., 2008; Sanyal et al., 2008; Sharma et al., 2008). But some drawbacks may be observed as a small number of patients received therapy as well as analysis may have involved patients treated with different vasoconstrictors e.g. norepinephrine instead of terlipressin.

The association between the renal response to terlipressin and the presence of an early reduction of the ET-1/NO ratio shows the significance of the enhancement of systemic hemodynamics in accomplishing type-1 HRS reversal. ET-1 and NO are the most important local vasoconstrictor and vasodilator respectively. They seem to play a role in almost every tissue and organ (Hei et al., 2006). Recent researches reported that the important factors in identifying the harmful versus beneficial effects of NO are the site of NO production, duration of action, and its amount (Hon et al., 2002). It has been proposed that the disequilibrium of ET-1 and NO levels may have an impact on the pathophysiology of local and systemic circulation disorders. This imbalance in the renal microcirculation has been proposed to be in charge of the dynamic disintegration in kidney function in these patients and the development of HRS (Kayali et al., 2009).

ET-1 may be involved in both impaired glomerular perfusion and renal vasoconstriction which causes HRS (Moore, 2004). Renal blood flow is not the only factor contributing to changes in glomerular filtration rate as seen at the microcirculatory level. The enhanced production of vasoactive mediators including ET-1 causes reduction of the surface area available for glomerular filtration and contraction of mesangial cells which contributes to this phenomenon (Ring-Larsen, 1977; Simonson and Dunn, 1990). The intake of ETA and ETB receptors antagonists combination prevented and in sometimes reversed the pathogenesis of renal failure in different experiments (Anand et al., 2002). Physiologically, early reduction of the ET-1/NO ratio is considered a good prognostic marker in HRS patients with end stage liver disease or on the liver transplantation waiting list.

Interestingly, serum bilirubin level at baseline was considered an independent predictive factor of response to treatment. Poor response to therapy and elevated serum bilirubin levels association can't be explained, but looks to be unrelated to the hemodynamic response to terlipressin. The mechanisms explaining the lack of response to terlipressin related to high serum bilirubin levels are interesting and merits examination. The correlation between the ET-1/NO ratio and bilirubin noticed in this study demonstrates that the values of ET-1 are influenced by the excretory liver function. A correlation between ET-1 and

TABLE 3 | Parameters with independent predictive value of response to treatment with albumin and terlipressin in patients with type 1 HRS.

Parameters	Univariate analysis			Multivariate analysis		
	OR	95% CI	*P*	OR	95% CI	*P*
Baseline serum bilirubin	6.8	1.54–30.8	0.012	14.2	1.256–160.77	0.032
Δ ET-1/NO ratio at day 3 ≥1.5	35.9	6.37–202.2	< 0.001	59.3	5.98–586.92	< 0.001
Δ Serum creatinine at day 3 > 0.5 mg/dL	5.0	1.35–18.6	< 0.001	9.46	0.84–105.9	0.048

CI, confidence interval; OR, odds ratio; ET-1/NO ratio, endothelin-1/nitric oxide ratio.

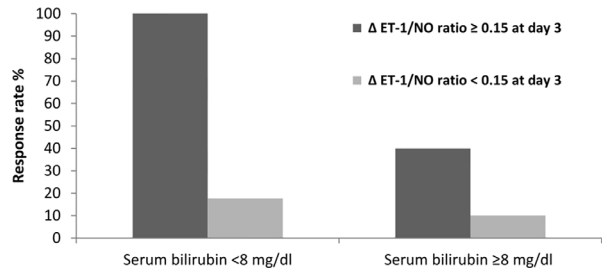

FIGURE 4 | Response rate according to levels of ET-1/NO ratio and its relationship to serum bilirubin at baseline.

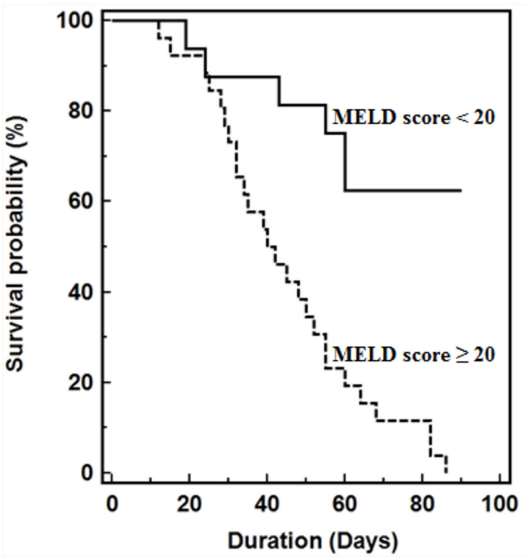

FIGURE 5 | Kaplan-Meier survival curves of patients stratified by baseline MELD score below or above 20, which represents threshold for 3-month median survival. Median survival of patients with baseline MELD score <20 significantly greater than those with baseline MELD scores ≥ 20 (62 vs. 15 days, $P < 0.001$).

bilirubin has been approved also by some (Nozue et al., 1995; Bachmann-Brandt et al., 2000), but not all authors (Isobe et al., 1993). The possible explanation, not determined by our data, maybe owing to indirect (excess pulmonary *arteriovenous* shunts that increased with the deterioration of liver condition) and direct (reduced clearance of ET-1 by the hepatic tissue) associations. Leakage of bile into the blood and/or disturbance of ET-1 degradation may result in increased serum ET-1 levels since ET-1 is excreted through the biliary system (Cai et al., 1999).

The multivariate analysis model showed that the reduction in serum creatinine level at day 3 can be considered a predictor of response to treatment. It should be noted that up to one-fourth of the patients showed response at the end of therapy though their serum creatinine level was not reduced by day 3. This may be due to increasing the dose of terlipressin in patients whom their serum creatinine level failed to reach an early reduction or showed a delayed renal response with respect to the improvement of hemodynamic status. In these patients, treatment with terlipressin was maintained after 3 days to achieve this delayed response effect. This finding is approved by Nazar et al. (2010).

In the current study, the 90-day survival probability in non-responders was 9% and in responders 40%. These results, in conjunction with the observation that patients with HRS where the albumin and terlipressin enhanced their renal capacity had marvelous posttransplantation results compared to patients without HRS (Restuccia et al., 2004), confirm that albumin plus terlipressin is a successful and helpful choice for HRS patients anticipating liver transplantation. The observations of this study were in accordance with previous reports which stated that type-1 HRS patients responding to therapy with albumin and terlipressin have longer survival expectancy compared to that of non-responders [(Ortega et al., 2002; Martín-Llahí et al., 2008; Neri et al., 2008; Sharma et al., 2008).

Moreover, to our knowledge, no studies published the role of changes in the ET-1/NO ratio as an independent predictor of response to albumin with terlipressin in type-1 HRS. Such results will certainly be much scrutinized, but there are some clear conclusions for the role of ET-1 and NO in the pathophysiology of HRS. Such findings add to our understanding and knowledge of the pathogenesis of HRS in a number of ways and provide a foundation for its management. This study's findings have a number of significant implications for future practice.

Of course, this study has some limitations that should be addressed. First, the sample size is small. Second, the current study is a single center study, and recruiting a large number of patients for such a meticulous study, is mandatory yet difficult due to the unavailability of terlipressin in many centers and type-1 HRS is not a common disorder. Third, the ET-1/NO ratio is not routinely measured in clinical practice. Furthermore, studies from multiple centers are needed to confirm these findings in HRS patients.

In conclusion, the outcomes of the current study, in type-1 HRS patients, indicate that a reduction in the ET-1/NO ratio and lower serum bilirubin baseline are considered good predictors of response to treatment with albumin and terlipressin. Future studies on treatment of type-1 HRS should discuss the possible mechanisms of declined response to pharmacological treatment and should search for new therapeutic options for non-responders.

DATA AVAILABILITY STATEMENT

The raw data supporting the conclusions of this article will be made available by the authors, without undue reservation, to any qualified researcher.

ETHICS STATEMENT

The study was reviewed and approved by the Ethics Committee of Mansoura University, Egypt. (Proposal code: R.19.06.534). The patients/participants provided their written informed consent to participate in this study.

AUTHOR CONTRIBUTIONS

All the authors have accepted responsibility for the entire content of this submitted manuscript and approved submission. AA-R and NM acquired, analyzed and interpreted data; performed statistical analysis; and wrote, edited and reviewed the manuscript. MA, AA, and MT recruited and followed up with patients; acquired, analyzed and interpreted data; performed statistical analysis; critically revised the manuscript. AT recruited and followed up with patients; acquired, analyzed and interpreted data; critically revised the manuscript. AH recruited and followed up with patients; acquired, analyzed and interpreted data; critically revised the manuscript. RE acquired, analyzed and interpreted data; underwent laboratory investigations and revised the manuscript. WE and NE-W acquired, analyzed and interpreted data; performed statistical analysis; underwent laboratory investigations; critically revised the manuscript. All authors approved the final version of the article, including the authorship list.

ACKNOWLEDGMENTS

The authors thank the staff and patients of the Tropical Medicine Department and the lab specialists for their significant aid.

REFERENCES

Alessandria, C., Ottobrelli, A., Debernardi-Venon, W., Todros, L., Cerenzia, M. T., Martini, S., et al. (2007). Noradrenalin vs terlipressin in patients with hepatorenal syndrome: a prospective, randomized, unblinded, pilot study. *J. Hepatol.* 47, 499–505. doi: 10.1016/j.jhep.2007.04.010

Allegretti, A. S., Israelsen, M., Krag, A., Jovani, M., Goldin, A. H., Schulman, A. R., et al. (2017). Terlipressin versus placebo or no intervention for people with cirrhosis and hepatorenal syndrome. *Cochrane Database Syst. Rev.* 6, CD005162. doi: 10.1002/14651858.CD005162.pub4

Alonso, D., and Radomski, M. W. (2003). The nitric oxide-endothelin-1 connection. *Heart Fail Rev.* 8, 107–115. doi: 10.1023/a:1022155206928

Anand, R., Harry, D., Holt, S., Milner, P., Dashwood, M., Goodier, D., et al. (2002). Endothelin is an important determinant of renal function in a rat model of acute liver and renal failure. *Gut* 50, 111–117. doi: 10.1136/gut.50.1.111

Andrukhov, O., Haririan, H., Bertl, K., Rausch, W. D., Bantleon, H. P., Moritz, A., et al. (2013). Nitric oxide production, systemic inflammation and lipid metabolism in periodontitis patients: possible gender aspect. *J. Clin. Periodontol.* 40 (10), 916–923. doi: 10.1111/jcpe.12145

Angeli, P., and Merkel, C. (2008). Pathogenesis and management of hepatorenal syndrome in patients with cirrhosis. *J. Hepatol.* 48 (Suppl.), S93–S103. doi: 10.1016/j.jhep.2008.01.010

Angeli, P., Ginès, P., Wong, F., Bernardi, M., Boyer, T. D., Gerbes, A., et al. (2015). Diagnosis and management of acute kidney injury in patients with cirrhosis: revised consensus recommendations of the International Club of Ascites. *J. Hepatol.* 62, 968–974. doi: 10.1016/j.jhep.2014.12.029

Arroyo, V., Gine`s, P., Gerbes, A. L., Dudley, F. J., Gentilini, P., Laffi, G., et al. (1996). Definition and diagnostic criteria of refractory ascites and hepatorenal syndrome in cirrhosis. *Int. Ascites Club. Hepatol.* 23, 164–176. doi: 10.1002/hep.510230122

Bachmann-Brandt, S., Bittner, I., Neuhaus, P., Frei, U., and Schindler, R. (2000). Plasma levels of endothelin-1 in patients with the hepatorenal syndrome after successful liver transplantation. *Transpl. Int.* 13, 357–362. doi: 10.1007/s001470050714

Barreto, R., Fagundes, C., Guevara, M., Solà, E., Pereira, G., Rodríguez, E., et al. (2014). Type1 hepatorenal syndrome associated with infections in cirrhosis: natural history, outcome of kidney function, and survival. *Hepatology* 59, 1505–1513. doi: 10.1002/hep.26687

Brennan, J. M., Ronan, A., Goonewardena, S., Blair, J. E., Hammes, M., Shah, D., et al. (2006). Handcarried ultrasound measurement of the inferior vena cava for assessment of intravascular volume status in the outpatient hemodialysis clinic. *Clin. J. Am. Soc Nephrol.* 1, 749–753. doi: 10.2215/CJN.00310106

Cahill, P. A., Redmond, E. M., and Sitzmann, J. V. (2001). Endothelial dysfunction in cirrhosis and portal hypertension. *Pharmacol. Ther.* 89, 273–293. doi: 10.1016/s0163-7258(01)00128-0

Cai, L., Wang, G. J., Mukherjee, K., Xu, Z. L., Khalil, M., Cherian, M. G., et al. (1999). Endothelins and their receptors in cirrhotics and neoplastic livers of Canadian and Chinese populations. *Anticancer Res.* 19, 2243–2247.

Cardenas, A., and Gine`s, P. (2005). Management of complications of cirrhosis in patients awaiting liver transplantation. *J. Hepatol.* 42, S124–S133. doi: 10.1016/j.jhep.2004.12.007

Charpin, J. M., Stern, M., Lebrun, G., Aubin, P., Grenet, D., and Israël-Biet, D. (2001). Increased endothelin-1 associated with bacterial infection in lung transplant recipients. *Transplantation* 71 (12), 1840–1847. doi: 10.1097/00007890-200106270-00022

Dagher, L., and Moore, K. (2001). The hepatorenal syndrome. *Gut* 49, 729–737. doi: 10.1136/gut.49.5.729

Dellinger, R. P. (2003). Cardiovascular management of septic shock. *Crit. Care* 31, 946–955. doi: 10.1097/01.CCM.0000057403.73299.A6

Fabrizi, F., Dixit, V., and Martin, P. (2006). Meta-analysis: terlipressin therapy for the hepatorenal syndrome. *Aliment Pharmacol. Ther.* 24, 935–944. doi: 10.1111/j.1365-2036.2006.03086.x

Fernandez, J., Acevedo, J., Castro, M., Garcia, O., de Lope, C. R., Roca, D., et al. (2012). Prevalence and risk factors of infections by multiresistant bacteria in cirrhosis: a prospective study. *Hepatology* 55, 1551–1561. doi: 10.1002/hep.25532

Freeman, B. D., Machado, F. S., Tanowitz, H. B., and Desruisseaux, M. S. (2014). Endothelin-1 and its role in the pathogenesis of infectious diseases. *Life Sci.* 118 (2), 110–119. doi: 10.1016/j.lfs.2014.04.021

Garcia-Tsao, G., Parikh, C. R., and Viola, A. (2008). Acute kidney injury in cirrhosis. *Hepatology* 48, 2064–2077. doi: 10.1002/hep.22605

Gine`s, P., Guevara, M., Arroyo, V., and Rodes, J. (2003). Hepatorenal syndrome. *Lancet* 362, 1819–1827. doi: 10.1016/S0140-6736(03)14903-3

Gluud, L. L., Christensen, K., Christensen, E., and Krag, A. (2010). Systematic review of randomized trials on vasoconstrictor drugs for hepatorenal syndrome. *Hepatology* 51 (2), 576–584. doi: 10.1002/hep.23286

Gonwa, T. A., Klintmalm, G. B., Levy, M., Jennings, L. S., Goldstein, R. M., and Husberg, B. S. (1995). Impact of pretransplant renal function on survival after liver transplantation. *Transplantation* 59, 361–365. doi: 10.1097/00007890-199502150-00010

Hei, Z. Q., Huang, H. Q., Luo, C. F., Li, S. R., and Luo, G. J. (2006). Changes of nitric oxide and endothelin, thromboxane A2 and prostaglandin in cirrh-otic patients undergoing liver transplantation. *World J. Gastroenterol.* 12, 4049–4051. doi: 10.3748/wjg.v12.i25.4049

Hocher, B., Brause, M., Mendes, U., Berger, D., Bulher, H., and Gross, P. (1999). Impact of endothelin system on water and sodium excretion in patients with liver cirrhosis. *Nephrol. Dial Transplant.* 14, 1133–1138. doi: 10.1093/ndt/14.5.1133

Hon, W. M., Lee, K. H., and Khoo, H. E. (2002). Nitric oxide in liver diseases: friend, foe, or just passerby? *Ann. N.Y. Acad. Sci.* 962, 275–295. doi: 10.1111/j.1749-6632.2002.tb04074.x

Isobe, H., Satoh, M., Sakai, H., and Nawata, H. (1993). Increased plasma endothelin-1 levels in patients with cirrhosis and esophageal varices. *J. Clin. Gastroenterol.* 17, 227–230. doi: 10.1097/00004836-199310000-00011

Jeyarajah, D. R., Gonwa, T. A., McBride, M., Testa, G., Abbasoglu, O., Husberg, B. S., et al. (1997). Hepatorenal syndrome: combined liver kidney transplants versus isolated liver transplant. *Transplantation* 64, 1760–1765. doi: 10.1097/00007890-199712270-00024

Kayali, Z., Herring, J., Baron, P., Franco, E., Ojogho, O., Smith, J., et al. (2009). Increased plasma nitric oxide, L-arginine, and arginase-1 in cirrhotic patients with progressive renal dysfunction. *J. Gastroenterol. Hepatol.* 24, 1030–1037. doi: 10.1111/j.1440-1746.2008.05757.x

Levey, A. S., Bosch, J. P., Lewis, J. B., Greene, T., Rogers, N., and Roth, D. (1999). A more accurate method to estimate glomerular filtration rate from serum creatinine: a new prediction equation. Modification of diet in renal disease study groupm. *Ann. Intern. Med.* 130, 461–470. doi: 10.7326/0003-4819-130-6-199903160-00002

Møller, S., Hansen, E. F., Becker, U., Brinch, K., Henriksen, J. H., and Bendtsen, F. (2000). Central and systemic haemodynamic effects of terlipressin in portal hypertensive patients. *Liver* 20 (1), 51–59. doi: 10.1034/j.1600-0676.2000.020001051.x

Møller, S., Krag, A., and Bendtsen, F. (2014). Kidney injury in cirrhosis: pathophysiological and therapeutic aspects of hepatorenal syndromes. *Liver Int.* 34, 1153–1163. doi: 10.1111/liv.12549

Martin-Llahi, M., Guevara, M., Torre, A., Fagundes, C., Restuccia, T., Gilabert, R., et al. (2011). Prognostic importance of the cause of renal failure in patients with cirrhosis. *Gastroenterology* 140, 488–496. doi: 10.1053/j.gastro.2010.07.043

Martín-Llahí, M., Pépin, M. N., Guevara, M., Díaz, F., Torre, A., Monescillo, A., et al. (2008). Terlipressin and albumin vs albumin in patients with cirrhosis and hepatorenal syndrome: a randomized study. *Gastroenterology* 134, 1352–1359. doi: 10.1053/j.gastro.2008.02.024

Moore, K., Wendon, J., Frazer, M., Karani, J., Williams, R., and Badr, K. (1992). Plasma endothelin immunoreactivity in liver disease and hepatorenal syndrome. *N. Engl. J. Med.* 327, 1774–1778. doi: 10.1056/NEJM199212173272502

Moore, K. (2004). Endothelin and vascular function in liver disease. *Gut* 53 (2), 159–161. doi: 10.1136/gut.2003.024703

Moreau, R., and Lebrec, D. (2006). The use of vasoconstrictors in patients with cirrhosis: type 1 HRS and beyond. *Hepatology* 43, 385–394. doi: 10.1002/hep.21094

Moreau, R., Durand, F., Poynard, T., Duhamel, C., Cervoni, J. P., Ichaı¨, P., et al. (2002). Terlipressin in patients with cirrhosis and type 1 hepatorenal syndrome: a retrospective multicenter study. *Gastroenterology* 122, 923–930. doi: 10.1053/gast.2002.32364

Nair, S., Verma, S., and Thuluvath, P. J. (2002). Pretransplant renal function predicts survival in patients undergoing orthotopic liver transplantation. *Hepatology* 35, 1179–1185. doi: 10.1080/00365521.2018.1526967

Nazar, A., Pereira, G. H., Guevara, M., Martín-Llahi, M., Pepin, M. N., Marinelli, M., et al. (2010). Predictors of response to therapy with terlipressin and albumin in patients with cirrhosis and type 1 hepatorenal syndrome. *Hepatology* 51, 219–226. doi: 10.1002/hep.23283

Neri, S., Pulvirenti, D., Malaguarnera, M., Cosimo, B. M., Bertino, G., Ignaccolo, L., et al. (2008). Terlipressin and albumin in patients with cirrhosis and type I hepatorenal syndrome. *Dig. Dis. Sci.* 53, 830–835. doi: 10.1007/s10620-007-9919-9

Nozue, T., Kobayashi, A., Uemasu, F., Takagi, Y., Endoh, H., and Sako, A. (1995). Plasma endothelin-1 levels of children with cirrhosis. *J. Pediatr. Gastroenterol. Nutr.* 21, 220–223. doi: 10.1097/00005176-199508000-00015

Ortega, R., Gine`s, P., Uriz, J., Cardenas, A., Calahorra, B., de las Heras, D., et al. (2002). Terlipressin therapy with and without albumin for patients with hepatorenal syndrome: results of a prospective, nonrandomized study. *Hepatology* 36, 941–948. doi: 10.1053/jhep.2002.35819

Restuccia, T., Ortega, R., Guevara, M., Gine`s, P., Alessandria, C., Ozdogan, O., et al. (2004). Effects of treatment of hepatorenal syndrome before transplantation on posttransplantation outcome. A case-control study. *J. Hepatol.* 40, 140–146. doi: 10.1016/j.jhep.2003.09.019

Rimola, A., García-Tsao, G., Navasa, M., Piddock, L. J., Planas, R., Bernard, B., et al. (2000). Diagnosis, treatment and prophylaxis of spontaneous bacterial peritonitis: a consensus document. *Int. Ascites Club. J. Hepatol.* 32, 142–153. doi: 10.1016/s0168-8278(00)80201-9

Ring-Larsen, H. (1977). Renal blood flow in cirrhosis: relation to systemic and portal haemodynamics and liver function. *Scand. J. Clin. Lab. Invest.* 37, 635–642. doi: 10.3109/00365517709100657

Sanyal, A. J., Boyer, T., Garcia-Tsao, G., Regenstein, F., Rossaro, L., Appenrodt, B., et al. (2008). A randomized, prospective, double-blind, placebo-controlled trial of terlipressin for type 1 hepatorenal syndrome. *Gastroenterology* 134, 1360–1368. doi: 10.1053/j.gastro.2008.02.014

Sharma, P., Kumar, A., Shrama, B. C., and Sarin, S. K. (2008). An open label, pilot, randomized controlled trial of noradrenaline versus terlipressin in the treatment of type 1 hepatorenal syndrome and predictors of response. *Am. J. Gastroenterol.* 103, 1689–1697. doi: 10.1111/j.1572-0241.2008.01828.x

Simonson, M. S., and Dunn, M. J. (1990). Endothelin-1 stimulates contraction of rat glomerular mesangial cells and potentiates beta-adrenergic-mediated cyclic adenosine monophosphate accumulation. *J. Clin. Invest.* 85 (3), 790–797. doi: 10.1172/JCI114505

Uchihara, M., Izumi, N., Sato, C., and Marumo, F. (1992). Clinical significance of elevated plasma endothelin concentration in patients with cirrhosis. *Hepatology* 16, 95–99. doi: 10.1002/hep.1840160117

Yeager, M. E., Belchenko, D. D., Nguyen, C. M., Colvin, K. L., Ivy, D. D., and Stenmark, K. R. (2012). Endothelin-1, the unfolded protein response, and persistent inflammation: role of pulmonary artery smooth muscle cells. *Am. J. Respir. Cell Mol. Biol.* 46, 14–22. doi: 10.1165/rcmb.2010-0506OC

Conflict of Interest: The authors declare that the research was conducted in the absence of any commercial or financial relationships that could be construed as a potential conflict of interest.

Copyright © 2020 Abdel-Razik, Mousa, Abdelsalam, Abdelwahab, Tawfik, Tawfik, Hasan, Elhelaly, El-Wakeel and Eldars. This is an open-access article distributed under the terms of the Creative Commons Attribution License (CC BY). The use, distribution or reproduction in other forums is permitted, provided the original author (s) and the copyright owner(s) are credited and that the original publication in this journal is cited, in accordance with accepted academic practice. No use, distribution or reproduction is permitted which does not comply with these terms.

frontiers in Physiology

ORIGINAL RESEARCH
published: 04 February 2020
doi: 10.3389/fphys.2019.01588

Renal Glomerular Mitochondria Function in Salt-Sensitive Hypertension

*Mark Domondon[1], Iuliia Polina[1], Anna B. Nikiforova[1,2], Regina F. Sultanova[1,3], Claudia Kruger[4], Valeriia Y. Vasileva[1,5], Mikhail V. Fomin[1], Gyda C. Beeson[6], Anna-Liisa Nieminen[6], Nancy Smythe[7], Eduardo N. Maldonado[6], Krisztian Stadler[4] and Daria V. Ilatovskaya[1]**

[1] Department of Medicine, Division of Nephrology, Medical University of South Carolina, Charleston, SC, United States, [2] Institute of Theoretical and Experimental Biophysics, Pushchino, Russia, [3] Saint-Petersburg State Chemical Pharmaceutical University, Saint Petersburg, Russia, [4] Oxidative Stress and Disease Laboratory, Pennington Biomedical Research Center, Baton Rouge, LA, United States, [5] Institute of Cytology Russian Academy of Science, Saint Petersburg, Russia, [6] Department of Drug Discovery & Biomedical Sciences, Medical University of South Carolina, Charleston, SC, United States, [7] Department of Pathology, Medical University of South Carolina, Charleston, SC, United States

OPEN ACCESS

Edited by:
John D. Imig,
Medical College of Wisconsin, United States

Reviewed by:
Joshua S. Speed,
University of Mississippi Medical Center, United States
Shengyu Mu,
University of Arkansas for Medical Sciences, United States
Ningjun Li,
Virginia Commonwealth University, United States

***Correspondence:**
Daria V. Ilatovskaya
ilatovskaya@musc.edu

Specialty section:
This article was submitted to Renal and Epithelial Physiology, a section of the journal Frontiers in Physiology

Received: 13 September 2019
Accepted: 19 December 2019
Published: 04 February 2020

Citation:
Domondon M, Polina I, Nikiforova AB, Sultanova RF, Kruger C, Vasileva VY, Fomin MV, Beeson GC, Nieminen A-L, Smythe N, Maldonado EN, Stadler K and Ilatovskaya DV (2020) Renal Glomerular Mitochondria Function in Salt-Sensitive Hypertension. Front. Physiol. 10:1588. doi: 10.3389/fphys.2019.01588

Salt-sensitive (SS) hypertension is accompanied with an early onset of proteinuria, which results from the loss of glomerular podocytes. Here, we hypothesized that glomerular damage in the SS hypertension occurs in part due to mitochondria dysfunction, and we used a unique model of freshly isolated glomeruli to test this hypothesis. In order to mimic SS hypertension, we used Dahl SS rats, an established animal model. Animals were fed a 0.4% NaCl (normal salt, NS) diet or challenged with a high salt (HS) 4% NaCl diet for 21 days to induce an increase in blood pressure (BP). Similar to previous studies, we found that HS diet caused renal hypertrophy, increased BP, glomerulosclerosis, and renal lesions such as fibrosis and protein casts. We did not observe changes in mitochondrial biogenesis in the renal cortex or isolated glomeruli fractions. However, Seahorse assay performed on freshly isolated glomeruli revealed that basal mitochondrial respiration, maximal respiration, and spare respiratory capacity were lower in the HS compared to the NS group. Using confocal imaging and staining for mitochondrial H_2O_2 using mitoPY1, we detected an intensified response to an acute H_2O_2 application in the podocytes of the glomeruli isolated from the HS diet fed group. TEM analysis showed that glomerular mitochondria from the HS diet fed group have structural abnormalities (swelling, enlargement, less defined cristae). Therefore, we report that glomerular mitochondria in SS hypertension are functionally and structurally defective, and this impairment could eventually lead to loss of podocytes and proteinuria. Thus, the glomerular–mitochondria axis can be targeted in novel treatment strategies for hypertensive glomerulosclerosis.

Keywords: kidney, glomeruli, hypertension, podocyte, mitochondria

INTRODUCTION

Salt-sensitive (SS) hypertension is characterized by elevated blood pressure (BP) resulting from increased dietary salt intake (Pilic et al., 2016; Rust and Ekmekcioglu, 2017). Available medications are insufficient to control BP in the SS subjects, and there is a need for the development of novel effective therapies (Elijovich et al., 2016; Laffer and Elijovich, 2018). To date, substantial

research efforts have been devoted to uncovering the mechanisms underlying salt sensitivity, a condition known to be associated with various physiological, environmental, demographic, and genetic factors (Pilic et al., 2016). Intricate studies on kidney transplantations discovered that salt sensitivity "follows" the kidney: SS rats, which received a kidney transplant from a normotensive rat, became salt resistant (Bianchi et al., 1974; Patschan et al., 1997), implying that salt sensitivity originates in the kidney. Glomerular damage, loss of podocytes, and subsequent proteinuria are among the primary signs of kidney disease initiation in SS hypertension, and it is especially compelling to assess the mechanisms underlying their impairment (Denic et al., 2016; Assady et al., 2017; Seccia et al., 2017).

Recent evidence demonstrated that mitochondrial fission/fusion, biogenesis, redox capacity, and homeostasis are implicated in the pathogenesis of hypertensive renal damage, acute kidney injury (AKI), and diabetic nephropathy (DN) (Eirin et al., 2017a; Galvan et al., 2017). Multiple studies (highlighted in recent excellent reviews by Drs. Schnellmann, Sharma, Lerman, Danesh, and other groups) were devoted to identifying mitochondria-related targets for renal dysfunction in CKD. Current knowledge suggests that an imbalance in mitochondrial dynamics and energetics in glomeruli and their components (mesangial cells, endothelial cells, or podocytes), can cause a decrease in ATP production, induction of ROS (reactive oxygen species) generation and the disruption of normal renal function (Zhan et al., 2013; Casalena et al., 2014; Daehn et al., 2014; Ayanga et al., 2016; Long et al., 2016; Szeto et al., 2016; Zhao et al., 2016; Bhargava and Schnellmann, 2017; Duann and Lin, 2017; Eirin et al., 2017a; Galvan et al., 2017; Qi et al., 2017; Sharma, 2017; Sweetwyne et al., 2017; Arif et al., 2019; Kruger et al., 2019; Zhang et al., 2019). However, very little is known about glomeruli and mitochondria in chronic hypertension.

The development of hypertension correlates with changes in mitochondrial dynamics and ROS production in the brain, vasculature, and kidney (Manucha et al., 2015; Dikalov and Dikalova, 2016; Lahera et al., 2017; Loperena and Harrison, 2017; Daneva et al., 2019; Ding et al., 2019). As a major source of ROS, mitochondria can increase sympathetic activity, promoting sodium and volume retention and enhancing vasoconstriction (Dikalov and Dikalova, 2016), although the complete mechanism remains unclear (Loperena and Harrison, 2017). The majority of hypertension-related studies have been focused on mitochondrial function in the tubules. For instance, increased sodium delivery in the medullary thick ascending limb (mTAL) was reported to stimulate mitochondrial H_2O_2 production, possibly contributing to SS hypertension (Ohsaki et al., 2012). Urinary mitochondrial DNA (mtDNA) copy number was shown to be elevated in hypertensive patients (Eirin et al., 2016, 2017b). Antioxidant activity of superoxide dismutase 2 (SOD2) attenuated hypertensive effects by scavenging excess renal ROS (Dikalov and Dikalova, 2016). Interestingly, mice deficient in SOD2 develop salt-induced hypertension associated with activation of intrarenal ROS generating pathways (Elliott et al., 1990; Rodriguez-Iturbe et al., 2007). Plenty of evidence support that overproduction of ROS and bioenergetic alterations during hypertension heavily implicate mitochondrial dysfunction and the resulting oxidative stress as key contributors promoting the disease (Manucha et al., 2015; Loperena and Harrison, 2017; Marshall et al., 2018). However, extensive additional mechanistic studies are required to confirm a cause–effect relationship between mitochondrial dysfunction and renal damage (Eirin et al., 2015, 2018).

Cowley et al. (2015) revealed that in the Dahl SS rat there is a natural shift in the redox balance between nitric oxide and ROS, while selective reduction of ROS production in the renal medulla reduces SS hypertension. In another study, they found that the p67(phox) subunit of NADPH oxidase 2 plays a role in the excessive production of renal medullary ROS (Salehpour et al., 2015; Zheleznova et al., 2016). Mitochondrial proteomic analysis and respirometry also revealed deficiencies in oxygen utilization in mTAL and differential expression of mitochondria-encoded proteins in the Dahl SS rat compared to the SS.13(BN) control (Zheleznova et al., 2012). In 2014, He et al. (2014) demonstrated that mitochondrial abnormalities can be observed in the mTAL of SS rats before the development of histologically detectable injury. Later, Wang et al. (2017) provided evidence that renal mitochondria of Dahl SS rats displayed metabolic alterations and dysfunctions, aggravated by an increase in salt intake. Through transcriptomic analyses of renal medullary biological pathways, they established that mitochondrial TCA cycle and cell energetics are crucial for the molecular networks relevant to salt-sensitivity (Cowley et al., 2014; Evans et al., 2018).

Therefore, mitochondrial structure and bioenergetics are critical for the renal mechanisms of SS hypertension development. However, not much is known about renal cortical mitochondria, especially their function in glomeruli. The current study is focused on assessing functional and structural properties of mitochondria in renal glomeruli during SS hypertension. We employed a variety of techniques to address this question in Dahl SS rats, using a preparation of the freshly isolated glomeruli. We hypothesized that glomerular mitochondria function is a central contributor to renal disease development in SS hypertension.

MATERIALS AND METHODS

Study Design and Animal Use

Male Dahl salt-sensitive (Dahl SS) rats were obtained from Charles River Laboratories (strain code 320) at 7 weeks of age, and they were switched to a normal salt (NS, 0.4% NaCl) AIN-76A-based diet upon arrival (Dyets, Inc., #D113755, Bethlehem, PA, United States). At 8 $\pm$ 0.3 weeks of age (265 $\pm$ 15 g body weight), rats were either maintained on a NS diet or provided a high salt (HS, 4% NaCl) AIN-76A-based chow (Dyets, Inc., D#113756) to induce hypertension development (**Figure 1A**). Rats were housed at the Medical University of South Carolina (MUSC) Department of Laboratory Animal Resources under 12 h light/dark cycle. Access to food and water and environmental enrichment were provided *ad libitum*. All animal experiments were conducted in accordance with the National Institutes of Health Guide for the Care and Use of Laboratory Animals

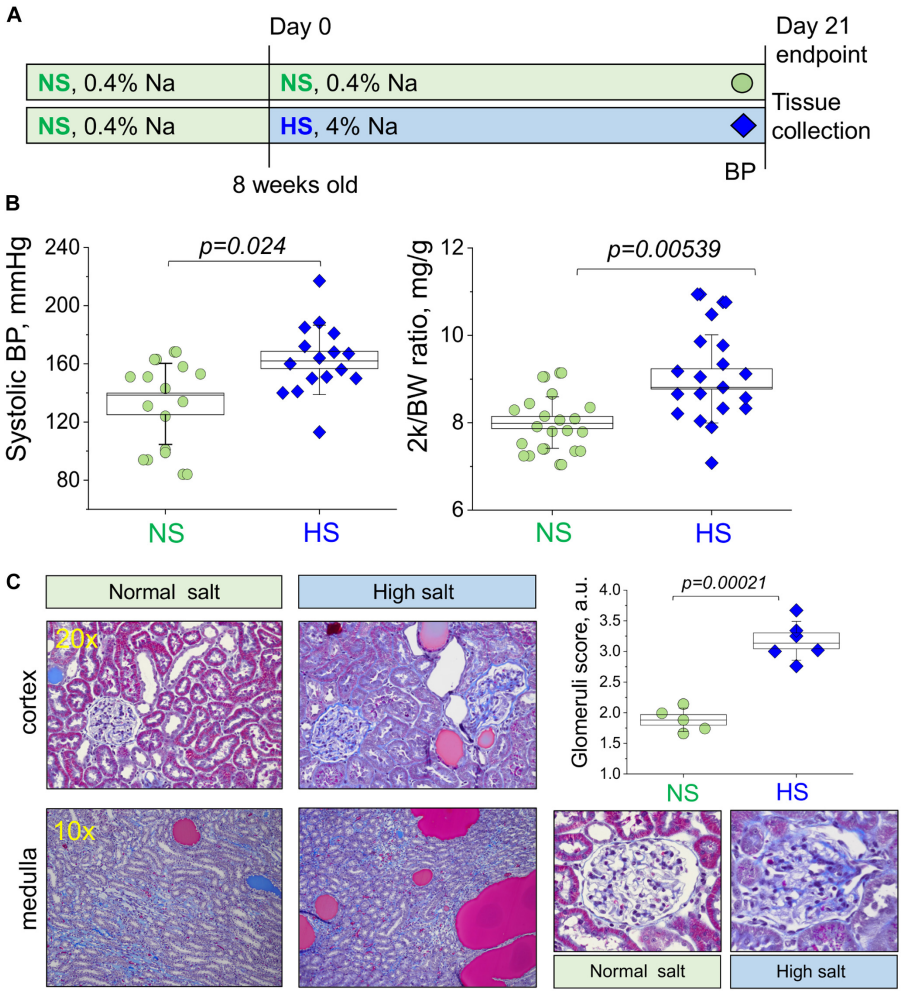

FIGURE 1 | Study protocol and development of the salt-sensitive (SS) hypertension in the Dahl SS rats. **(A)** Schematic representation of the experimental protocol used to induce SS hypertension in Dahl SS rats. **(B)** Graphs illustrating the observed increase in systolic blood pressure (systolic BP, **left**) and two kidney to body weight ratio (middle panel, 2 k/BW) in the NS diet fed group compared to a HS diet fed group (right). **(C)** Representative histological images showing cortical renal tissues (20×) and medullary tissues (10×) from NS and HS diet fed animals stained with Masson's trichrome. Graph illustrates summarized glomerular damage score (glomeruli examples are provided below for each experimental group). All data were compared using a one-way ANOVA with Holm–Sidak *post hoc* test. In Graphs **(B)**, each data point represents a single measurement from an experimental animal at the end of the protocol after the NS or HS challenges. For the glomerular damage score **(C)**, each point is an average of 100 glomeruli blindly scored in the renal tissue of each animal. NS, normal salt; HS, high salt.

following the protocol review and approval by the MUSC Institutional Care and Use Committee. Rats were randomly assigned to research groups; sample size was estimated using power analysis. Euthanasia and tissue collections were performed between 10 am and 2 pm.

Blood Pressure Measurements, Kidney Flush, and Glomeruli Isolation

Blood pressure measurements via tail cuff plethysmography (IITC Life Science Inc., United States) were obtained from each rat at 11 weeks old, immediately before endpoint kidney flush. For tissue collections, rats were anesthetized with 2.5% isoflurane, abdominal aorta was catheterized for blood collection, and kidneys were flushed with PBS (3 ml/min/kidney until blanched) as described previously (Ilatovskaya et al., 2015b). Then, tissues were snap-frozen for Western blotting or qPCR, fixed for subsequent histological or electron microscopy analyses, or used for immediate *ex vivo* experiments. For glomeruli isolation, renal cortex was excised and minced using a single-edged razor blade; then, isolation was performed with differential sieving as described previously (Ilatovskaya et al., 2011, 2015b; Ilatovskaya and Staruschenko, 2013). Briefly, the minced tissue was sequentially pushed through a steel 150-μm sieve and then pipetted through a 106-μm sieve (04-881-5Z and 04-881-5X; Fisher Scientific) using the culture medium solution RPMI1640 (Invitrogen, Inc., United States) with 5% BSA. This tissue homogenate was then pipetted onto a 75-μm sieve (S4145; Sigma), rinsed from the sieve surface, and stored on ice. Glomeruli were used within 3 h post isolation.

Histological Staining and Glomeruli Scoring

Tissues fixed with 10% NBF were routinely embedded, cut and mounted on slides, deparaffinized, rehydrated, and stained with Masson's trichrome. Glomeruli scoring was performed according to previously published protocols and scales (Raij et al., 1984; Palygin et al., 2017) using a Nikon Ti-2 microscope equipped with a 40× NA 0.7 objective and a DS-Fi2 color camera; glomeruli were blindly scored from zero (healthy) to four (diseased) (see Raij et al., 1984). At least 100 glomeruli were randomly scored in the cortical area of each experimental animal.

Plasma Creatinine and Electrolyte Measurements

Blood samples obtained from the abdominal aorta before kidney flushing, were centrifuged immediately after collection at 6000 rpm for 5 min to separate the plasma. The plasma was snap-frozen and stored at −80°C. Plasma creatinine levels were measured using the Quantichrom Creatinine Assay Kit (DICT-500). A standard curve was created from the stock 50 mg/dl creatinine standard. Concentrations of 6, 2, 1, 0.5, and 0 mg/dl were used to create the standard curve. Creatinine concentrations were determined by measuring absorbance per the manufacturer's instructions. Plasma electrolyte levels were measured with Carelyte analyzer (Diamond Diagnostics, United States).

Electron Microscopy

Samples were excised from the animal and fixed overnight in freshly made 2.5% glutaraldehyde in phosphate buffer (Electron Microscopy Sciences). The samples were rinsed in buffer 2× for 15 min and postfixed in 2% osmium tetroxide for 1 h on a rocker plate. Each sample was then dehydrated through a series of ethyl alcohol dilutions starting at 50, 70, 90, and 95%. Three 100% rinses for 15 min were used to complete the dehydration, and the samples were put into propylene oxide to start the infiltration with Embed 812 (Electron Microscopy Sciences) at ratios of 1:3, 2:2, and 3:1 for 1 h each. In the final stage the samples were then left in pure plastic overnight on the rocker plate and subsequently put into the mold and left in the oven overnight to polymerize. Once hardened, the blocks were trimmed, semi-thick sectioned at 0.5 μm, dried on a glass slide, stained with 1% toluidine Blue, and looked at under the microscope to determine the appropriate area to thin section. The block was trimmed again to reflect that area, and the thin sections were taken and placed on a 200-mesh cu grid, dried and stained with uranyl acetate for 10 min, and rinsed and stained with lead citrate for 10 min. The sections were observed on a JEOL 1010 transmission electron microscope running at 80 kV and imaged.

Protein and mRNA Isolation, Western Blotting, and Mitochondrial DNA Quantification

After excision, kidneys were cut into 1–2 mm slices, and the cortical kidney pieces were pulse sonicated in RIPA buffer containing a protease inhibitor cocktail (Roche) on ice for up to 10 s and then spin cleared at 10,000 × *g* for 10 min. The resulting supernatant was subjected to PAGE, transferred onto a nitrocellulose membrane (Bio-Rad, Hercules, CA, United States) for probing with antibodies, and subsequently visualized by enhanced chemiluminescence (ECL; Thermo Scientific, Waltham, MA, United States). The following antibodies were used: Total OXPHOS Rodent WB Antibody cocktail (ab110413, abcam, 1:500), PGC1α Polyclonal Antibody (PA5-38022, Invitrogen, Inc., United States); secondary anti-Mouse IgG HRP Conjugate (W402B, Promega, 1:5,000), and Goat anti-Rabbit IgG (H + L) (#31460, Invitrogen, Inc., United States). For qPCR, total DNA was extracted from rat kidney cortical tissues using a DNeasy Blood and Tissue kit (69504; Qiagen). The quality of each sample was determined using gel electrophoresis of 50 ng of total DNA following PCR on a C1000 Themocycler (Bio-Rad, Hercules, CA, United States) with a SuperScript First-Strand synthesis system for RT-PCR (11904; Invitrogen, Inc., United States), while the quantity was determined by spectrophotometry (Nanodrop). Real-time PCR analysis was performed with 50 ng total DNA using SYBR green chemistry on a CFX96 (Bio-Rad, Hercules, CA, United States). Primer sequences were as follows: *Nd1* F: ATGGCCTTCCTCACCCTAGT, R: GTTAGGGGGCGTATGGGTTC, *Nd6* F: TTGGGGTTGCGG CTATTTAT, R: ATCCCCGCAAACAATGACCA, with positive controls *B-actin* F: GCTCTATCACTGGGCATTGG and R: CGCAACTCTTAACTCGGAAGA.

Confocal Microscopy and Image Analysis

Isolated glomeruli were allowed to adhere onto glass bottom Mat-Tek dishes coated with poly-L-lysine for 5 min (P4707; Sigma) and immediately imaged in a solution containing (in mM): 145 NaCl, 4.5 KCl, 2 $CaCl_2$, 2 $MgCl_2$, 10 HEPES, pH 7.35. Fluorescence intensities were monitored using a confocal laser scanning microscope system Leica TCS SP 5. Detection was performed using an oil immersed 63×/NA 1.4 Oil objective with the argon laser excitation at 488 or 361 nm and emission filters 520/25 nm for MitoPY1 (Tocris, #4428, 10 μM loading for 30 min at RT) and 480/25 nm for Hoechst 33342 (ThermoFisher, H3570, 8 μM loading for 10 min at RT), respectively. Fluorescence images were collected with 0.125 Hz frequency and processed with open source software Fiji (ImageJ 1.47v, National Institute of Health, United States). Podocytes were located on the surface of capillaries by their morphology, body size, nuclei size, and structure in the focal plane next to the glass chip, similarly to what was done in previously published manuscripts (Ilatovskaya and Staruschenko, 2013; Ilatovskaya et al., 2015a,b, 2018). Please see **Figure 5A** for a detailed schematic.

Complex V Activity Assay

Mitochondrial Complex V activity was analyzed in isolated glomeruli pellets, normalized to 10 μg protein, and expressed as oxidation rate of NADH at 340 nm. The reaction mixture in a 1 cm cuvette contained: 500 μl of Buffer HEPES-Mg, 10 μl of 30 mM NADH, 50 μl of 50 mM phosphoenolpyruvic acid,

5 μl of 10 mg/ml of pyruvate kinase, 10 μl of 5 mg/ml of lactate dehydrogenase, and 10 μl of antimycin A. Ten micrograms of protein was added, and the mixture was incubated at 30°C for 2 min. The baseline kinetics were then recorded for 2 min. The reaction was started by adding 100 μl of 25 mM ATP, and kinetics were measured for 2 min (ΔAbs 340). Then 10 μl oligomycin (0.2 mg/ml in 50% ethanol) was added, and absorbance was measured again for 2 min. Complex V specific activity was calculated by comparing the Δabs with and without oligomycin.

Oxygen Consumption Rate Measurements

Equal volumes of freshly isolated glomeruli were plated onto Agilent Seahorse XF96 Microplates (Agilent Technologies, CA, United States, #101085-004). The Seahorse XF96 Analyzer (Agilent Technologies, CA, United States) was used to measure the basal levels of oxygen consumption rate (OCR) and OCR in the presence of electron transport chain (ETC) inhibitors and uncouplers (oligomycin, 1 μM; carbonyl cyanide-*p*-trifluoromethoxyphenylhydrazone, 1 μM; rotenone, 2 μM; antimycin A, 1 μM) using the standard software algorithm. The day before analysis, the sensor cartridge was placed in the calibration buffer provided by Seahorse Agilent. The following day, the medium was replaced with low phosphate DMEM buffer and warmed up in a 37°C non-CO_2 incubator. The injection ports of the sensor plate were filled with 25 μl of the compounds or vehicle diluted in buffer. The sensor plate was placed into the XF-96 instrument for calibration. After calibration, the calibration fluid plate was removed, and the cell plate was loaded for analysis. The measurement protocol was 2 min mix and 3 min measurement. There were three rate measurements post each injection (basal levels, oligomycin, FCCP, and antimycin/rotenone), and each injection had three measurement cycles. OCR was finally normalized to protein concentrations (a standard BCA assay was performed on tested wells and OCR results were normalized to protein content).

MitoSox Fluorescence Assay

Isolated glomeruli were incubated with 5 μM MitoSOX (M36008, Invitrogen, Inc., United States) for 25 min at room temperature with continuous mixing on a rotating shaker. Then, MitoSOX fluorescence (510-nm excitation/580-nm emission) was measured in multiple 96-well plates using a fluorescence plate reader (Novostar, BMG LabTechnologies, Offenburg, Germany). Fluorescence was normalized to 1 mg of protein.

Antioxidant Kit

Antioxidant Assay (Cayman Chemical, Item No. 709001) was used to measure the total antioxidant capacity of kidney cell lysates. Kidney tissue (∼10–15 mg/sample) from each studied group was sonicated in the assay buffer on ice, then cells were spinned down by centrifugation (10,000 × *g* for 15 min at 4°C). The supernatant was diluted 1:50 and used for further analysis according to the manufacturer's instructions. Absorbance was measured in 96-well plates with a Biotek Instruments plate reader at 405 nm. The capacity of the antioxidant system was compared with a standard curve obtained with Trolox (water-soluble tocopherol analog) and quantified as milliMolar (mM) Trolox equivalents.

RNA Isolation

RNA from rat glomeruli was isolated using TRIzol Reagent (Life Technologies) according to the manufacturer's instructions. In short, tubes containing glomeruli in TRIzol were thawed at room temperature. Fifty microliters of chloroform was added, and the contents were mixed by vortexing for 10 s before incubating at room temperature for 5 min. After centrifugation at 15,300 × *g* for 15 min at 4°C, the aqueous layer was carefully transferred to a new set of tubes and 1 μl glycogen (Thermo Fisher Scientific), 100 μl isopropanol (Fisher Scientific), and 10 μl 8 M LiCl (Sigma-Aldrich) were added to assist precipitation at −20°C overnight. The next morning centrifugation was performed at 21,000 × *g* for 40 min at 4°C, and the pellet was washed using 70% ethanol. After centrifugation at 15,300 × *g* for 30 min at 4°C all ethanol was removed, and the pellet was allowed to air dry. Then, the RNA pellet was dissolved in 20 μl nuclease-free water and incubated at 60°C for 15 min. RNA integrity was measured using the RNA 6000 Nano chip on the Agilent 2100 Bioanalyzer (Agilent Technologies, CA, United States). Acquired RNA integrity numbers (RIN) were >5.8 for all investigated samples.

Reverse Transcription

The High-Capacity cDNA Reverse Transcription Kit with RNase inhibitor (Applied Biosystems) was used to reverse transcribe 800 ng RNA from each sample into cDNA. In brief, the 20 μl reaction consists of 10 μl 2× RT Master Mix and 10 μl RNA sample. The Master Mix contains 2.0 μl 10× RT Buffer, 0.8 μl 25× dNTP Mix (100 mM), 2.0 μl 10× RT Random Primers, 1 μl MultiScribe Reverse Transcriptase, 1 μl RNase Inhibitor, and 3.2 μl Nuclease-free water. The thermal cycling conditions were as follows: 10 min at 25°C, 120 min at 37°C, 5 min at 85 and 4°C. After cycling, synthesized cDNA was transferred into a new tube and 60 μl nuclease-free water was added to a final concentration of 10 ng/μl for each sample.

Primers

Sequences of the target genes were downloaded from the Ensembl genome browser. Primer Express Software v3.0 (Applied Biosystems) was used in its default settings for primer pair design. Where possible, the amplicon was spanned across an exon–exon boundary to exclude potential contamination with genomic DNA. The locations and sequences of the primers are listed in **Table 2**. Synthesis of the primer sets was carried out by Integrated DNA Technologies (Coralville, IA, United States). Primers were reconstituted with low-TE (Thermo Fisher) to a concentration of 100 μM and diluted with nuclease-free water (Ambion) to a working solution with 10 μM concentration.

Quantitative Real-Time PCR

Quantitative Real-Time PCR was performed on the 7900HT Sequence Detection System (Applied Biosystem) with default

settings including dissociation curves for each assay. Using the epMotion 5075 (Liquid Handling Robot from Eppendorf), the PCR reactions were set up in a 384-well plate (Applied Biosystems) with 2 ng cDNA per reaction. Total volume was 10 μl per reaction [consisting of 3 μl cDNA, 5 μl iTaq Universal SYBR Green Supermix containing ROX as passive reference dye (Bio Rad), 1.8 μl water, 0.1 μl forward primer, and 0.1 μl reverse primer]. The thermal cycling reaction was started with 2 min at 50°C and 10 min at 95°C for optimal DNA polymerase activation. The PCR reactions consisted of a denaturation step of 15 s at 95°C, annealing and extension for 1 min at 60°C, for a total of 40 cycles. Reactions were run in triplicates, including no-template controls (water) for each gene. The comparative C_T method ($2^{-\Delta\Delta CT}$) was used for relative quantification of gene expression (User Bulletin #2, Applied Biosystems). For each primer set, the actual amplification efficiency (AE) was calculated and implemented in the formula to calculate fold-changes. The geometric means of measurements for peptidylprolyl isomerase B (Ppib) and Sod2 gene expression were used as the references for normalization to derive ΔC_t values. For each primer pair, the AE was calculated by applying the formula: $\Delta Rn_{cycle\ (n)}/\Delta Rn_{cycle\ (n-1)}$ over three consecutive cycles, starting at the determined C_t value in the geometric phase.

Statistical Analysis

All data are displayed as box plots showing all data points. The box represents SEM, the error bars show SD, and a horizontal line denotes the median value. One-way ANOVA with Holm–Sidak *post hoc* or one-way repeated-measures ANOVA with Holm–Bonferroni for *post hoc* means comparison was employed for statistical analysis; p-value <0.05 was considered statistically significant. Animal numbers in each group and the number of replicates, if applicable, as well as the statistical tests applied, are shown in the corresponding figure legends. Statistical analysis of comparisons between conditions in qPCR experiments was conducted using t-tests, assuming unequal variances and two-sided p-values. P-values <0.05 were considered significant. DataAssist software (Applied Biosystems) was used to identify possible outliers among triplicate measurements.

RESULTS

Hypertension and Renal Injury Development in Dahl SS Rats

Male Dahl SS rats (Charles River Laboratories) were placed on a 0.4% NaCl diet immediately after arrival. Animals were randomly assigned to NS and HS diet fed groups following the standard experimental protocol (**Figure 1A**). After 21 days on a HS diet, rats developed a typical hypertension. Systolic BP as measured with tail cuff technique was 132.4 ± 7.4 and 162.7 ± 5.9 mmHg in the NS and HS diet fed groups, respectively (**Figure 1B**). Two kidneys to body weight ratio was increased in the HS diet fed group (**Figure 1B**, right panel, 8.0 ± 0.1 vs. 9.0 ± 0.2 mg/g in the NS diet fed group). Additional physiological parameters measured at the end of the experimental protocol (plasma creatinine, electrolyte levels, heart weight, and body weight, reported in **Table 1**) were similar. To characterize the renal lesions in the experimental groups, we performed blinded glomerular damage score in the Masson's trichrome stained tissues. As shown in **Figure 1C**, there was an increase in renal protein cast formation in the HS diet fed animals as well as pronounced glomerular damage reflected in the overall enlarged glomeruli, reduced size of Bowman space, blocked capillaries, mesangial matrix expansion, loss of podocytes, and fibrosis. The glomerular damage score was 1.8 ± 0.1 vs. 3.2 ± 0.1 in the NS and HS diet fed groups, respectively. Therefore, the well-developed renal injury and BP increase in our model were in accordance with previously published studies (Endres et al., 2017; Palygin et al., 2017; Pavlov et al., 2017; Ilatovskaya et al., 2018; Kumar et al., 2019).

Dietary Salt Challenge Does Not Affect Mitochondrial Biogenesis and the Expression of ETC Complexes in Renal Cortex and Isolated Glomeruli

We first aimed to test if renal cortical mitochondria biogenesis was affected by a HS challenge. As reported in **Figure 2A**, the expression of PGC1α protein (Peroxisome Proliferator-Activated Receptor-Gamma Coactivator-1α), a transcriptional coactivator that regulates the genes involved in energy metabolism and a master regulator of mitochondrial biogenesis, was similar between groups. We further confirmed this finding by testing for another mitochondrial biogenesis factor (Gibbs et al., 2018; Cameron et al., 2019) – the mitochondria DNA content (mtDNA copy number) in the renal cortex by qPCR. As demonstrated in **Figure 2B**, this experiment did not reveal differences in the mitochondria-encoded *Nd1* and *Nd6* gene expression (normalized to genomic DNA encoded *Actb*). Next, we assessed the mitochondrial Complex V (the ATP synthase of the mitochondrial ETC) activity in isolated glomerular pellets (expressed as oxidation rate of NADH at 340 nm). As shown in **Figure 2C**, we did not report any significant changes in this parameter between the groups, which is supportive of the data reported above regarding similar biogenesis and mtDNA content in the HS and NS diet fed rats. We next tested the expression of the mitochondrial oxidative phosphorylation (OXPHOS) complexes in the renal cortex and glomeruli using a well-established cocktail of antibodies available from Abcam. We reported a slight decrease in Complex V (ATP synthase) and

TABLE 1 | Various physiological parameters measured at the end of the experimental protocol in the high salt (HS) and normal salt (NS) diet fed groups.

	NS diet	HS diet	*p*-value	*N*
Plasma [Na], mM/L	148.3 ± 6.0	146.4 ± 2.5	0.32	12
Plasma [K], mM/L	3.8 ± 0.4	3.9 ± 0.4	0.54	12
Plasma [Cl], mM/L	105.5 ± 3.2	107.7 ± 2.1	0.06	12
Plasma creatinine, mg/dl	0.93 ± 0.2	0.83 ± 0.1	0.24	6
Body weight, g	343.8 ± 16.9	348.5 ± 16.4	0.46	14
Heart weight, g	1.3 ± 0.1	1.3 ± 0.1	0.75	14

At least six animals per group, data are shown ± SEM.

TABLE 2 | Genes investigated in this study: primer location, sequences, and amplification efficiency.

Gene symbol	Ensembl ID	Gene name	Forward primer; sequence	Forward primer position
Atp5f1a	ENSRNOG00000017032	ATP synthase F1 subunit alpha	TGACCGAGCTGCTAAAGCAA	1,449–1,468
Cox4i1	ENSRNOG00000017817	Cytochrome c oxidase subunit 4i1	CCATGTTCTTCATCGGCTTCA	417–437
Cycs	LOC100363502-201	Cytochrome c, somatic-like	GGCTGCTGGATTCTCTTACACA	204–225
Gpx4	ENSRNOG00000013604	Glutathione peroxidase 4	AGGCAGGAGCCAGGAAGTAATC	496–517
Ppargc1a	ENSRNOG00000004473	PPARG coactivator 1 alpha	AAGGTCCCCAGGCAGTAGATC	1,906–1,926
Ppib	ENSRNOG00000016781	Peptidylprolyl isomerase B	GGCTCCCAGTTCTTCATAACTACAG	561–585
Sod2	ENSRNOG00000019048	Superoxide dismutase 2	TGCCGCCTGCTCTAATCAG	566–584

Gene symbol	Reverse primer; sequence	Reverse primer position	Exon–exon boundary	AE
Atp5f1a	TGACAGCCACCTGTTCTTCAAT	1,511–1,490	Yes	1.96
Cox4i1	GGGCCATACACGTAGCTCTTCT	480–459	Yes	1.91
Cycs	TTTCCAAATACTCCATCAGGGTATC	286–262	Yes	1.88
Gpx4	CAGATCTTGCTGTACATGTCAAACC	578–554	Yes	1.90
Ppargc1a	GGTGTCTGTAGTGGCTTGATTCAT	1,973–1,950	Yes	1.89
Ppib	ACCACATCCATGCCTTCCA	652–634	Yes	1.95
Sod2	CGTGCTCCCACACATCAATC	645–626	Yes	1.91

Gene sequences were taken from the Ensembl genome browser, and the positions corresponding to primer sequences (in 5′–3′ direction) are listed. Primer pairs were designed to span across an exon–exon boundary. The achieved amplification rate over three cycles in the geometric phase with each primer set is listed.

Complex IV (Cytochrome c oxidase) expression (**Figure 2D**), whereas other OXPHOS proteins [CIII (Q-cytochrome c oxidoreductase), CII (succinate-Q oxidoreductase), CI (NADH-coenzyme Q oxidoreductase)] were not affected. We further tested if OXPHOS expression changes in isolated glomeruli fraction (**Figure 2E**), and densitometry analysis showed that the expression of Complexes I, II, III, IV, and V was similar between groups. In addition, we supported these data with qPCR performed in the freshly isolated glomeruli (**Figure 3**): expression analysis of *Ppargc1a* (encoding for PGC1α), *Cycs* (encoding for Cytochrome C), *Atp5f1a* (encoding for mitochondrial ATP synthase, complex V), and *Cox4i1* (encoding for Cytochrome C Oxidase Subunit 4I1) did not reveal any differences in glomeruli isolated from the NS and HS diet fed rats.

Glomerular Mitochondrial Respiration Is Suppressed in Glomeruli Isolated From Rats Fed a HS Diet

Freshly isolated decapsulated glomeruli were used in the OCR experiments on an Agilent Seahorse assay, which is a standard procedure for analytical detection of mitochondrial respiration. Cellular oxygen consumption (respiration) causes changes to the concentrations of oxygen dissolved in the media, measured by solid state sensor probes. Different states of respiration are assessed in a so-called "mitochondrial stress test," where ETC proteins are targeted with specific inhibitors. In this standard assay, we added oligomycin [blocks the proton channel of ATP synthase (V), so phosphorylation of ADP is no longer possible], FCCP (uncoupler of OXPHOS, which allows the ETC to function at the maximal respiratory capacity), as well as antimycin and rotenone (complex III complex I inhibitors, which shut down the entire ETC). A schematic illustration of the experimental protocol is shown on an inset in **Figure 4A**. As seen from the summarized OCR transients in **Figure 4A** and dot plots derived from these curves (**Figure 4B**), glomeruli from the HS fed rats had significantly impaired respiration. Specifically, we observed higher basal respiration (oxygen consumption used to meet cellular ATP demand under baseline conditions, 176.0 ± 16.7 vs. 104.9 ± 8.9 OCR/mg protein) and ATP-linked respiration (the portion of basal respiration that was being used to drive ATP production, 85.3 ± 12.3 vs. 45.0 ± 8.9 OCR/mg protein) in the NS group vs. the HS groups. Both maximal respiration (FCCP stimulates the respiratory chain to operate at maximum capacity and causes rapid oxidation of substrates to meet the metabolic challenge: 248.7 ± 34.4 vs. 117.0 ± 12.7 OCR/mg protein) and spare respiratory capacity (difference between maximal and basal respiration, 88.7 ± 22.3 vs. 20.0 ± 4.8 OCR/mg protein) were higher in the NS group vs. the HS group, respectively. All data were normalized to protein content. Proton leak (remaining basal respiration not coupled to ATP production) was not found to be significantly different between the groups.

Glomerular Mitochondria From HS Diet Fed Rats Reveal Structural and Functional Changes as Well as Mitochondria-Derived Oxidative Stress

In order to examine mitochondrial function in renal glomeruli in further detail, we performed confocal imaging of podocytes from freshly isolated glomeruli. These samples were loaded with a MitoPY1 dye to label mitochondria-produced hydrogen peroxide. **Figure 5A** demonstrates a schematic of glomeruli imaging and representative staining of the podocytes in the glomerular sample [the technique for labeling and imaging podocytes in freshly isolated glomeruli was well established in our earlier publications (Ilatovskaya et al., 2015a,b, 2018; Spires et al., 2018)]. These experiments revealed a more fragmented staining pattern for mitochondrial H_2O_2 in the glomeruli from

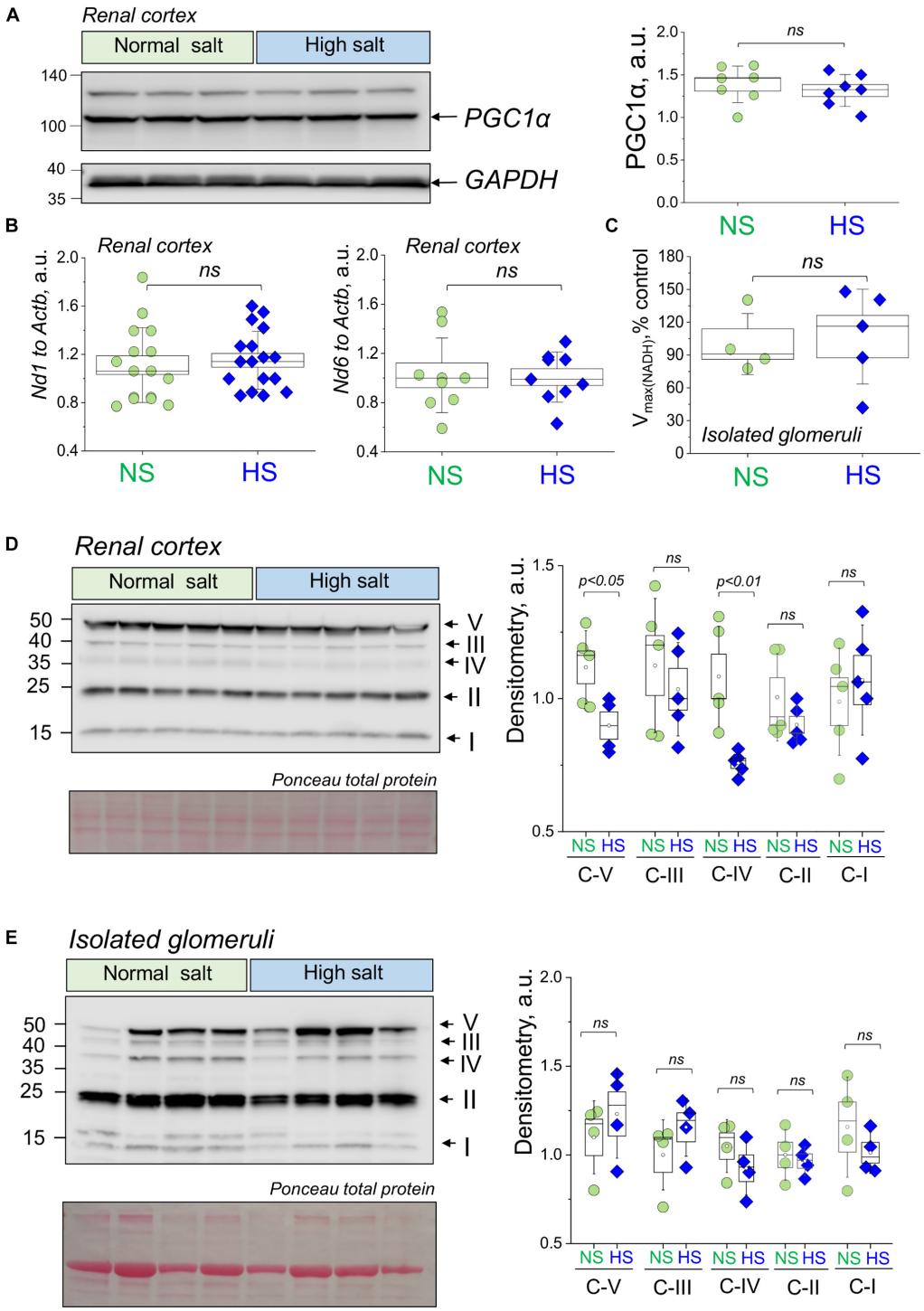

FIGURE 2 | Renal mitochondria biogenesis and electron transport chain (ETC) complexes expression and activity during salt-sensitive (SS) hypertension. **(A)** Representative Western blot showing expression of PGC1α in the renal cortex of the HS and NS diet fed animals. Graph on the right summarizes densitometry values from the Western blot shown on the left combined with another (independent) Western run on other samples (data not shown). All data were normalized to GAPDH expression level. $N = 7$ individual rats tested in each group. **(B)** Mitochondrial DNA content in the renal cortex of rats fed a HS or a NS diet. Shown are results of qPCR for mitochondria genome encoded genes *Nd1* and *Nd6* (values normalized to nuclei-encoded *Actb*). **(C)** ETC Complex V activity as measured in the glomeruli isolated from NS and HS diet fed rats. Data were normalized to protein level, $n = 5$ animals per group. **(D,E)** Western blot analysis illustrating the expression of ETC complexes V, IV, III, II, and I in the renal cortex **(D)** and isolated glomeruli **(E)** from HS and NS diet fed Dahl SS rats. Graph on the right summarizes densitometry values (normalized to total protein as measured with Ponceau stain). NS, normal salt; HS, high salt; ns, not statistically significant ($p > 0.05$). All data were compared using a one-way ANOVA with Holm–Sidak *post hoc* test. Each lane on the Western is a sample from a separate animal.

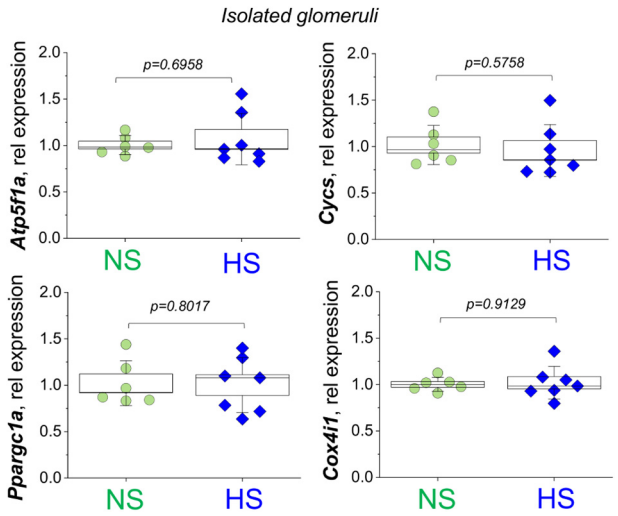

FIGURE 3 | Relative expression of the *Atp5f1a*, *Cycs*, *Ppargc1a*, and *Cox4i1* genes assessed in the fraction of the glomeruli isolated from normal salt (NS) and high salt (HS) diet fed Dahl SS rats. Each point on the graph is a sample from a separate animal. *P*-values were obtained with *t*-tests, assuming unequal variances.

the HS diet fed rats. We believe that the observed staining pattern indicates the enhanced H_2O_2 formation and is reflective of the ultrastructural changes in the mitochondria that are being observed with EM (formation of the mitophagosomes, which could result in staining artifacts, such as fragmentation). In addition, we assessed an acute effect of H_2O_2 on mitoPY1-stained glomeruli, and observed a significantly blunted response in the NS diet fed glomeruli, indicative of higher antioxidant capacity in this tissue. Next, isolated glomeruli TEM demonstrated a pronounced structural damage to the mitochondria in the podocytes from the HS diet fed animals (as shown by loss of cristae, swelling, and signs of mitophagy) compared to the NS glomeruli as seen in representative images in **Figure 5B**. Observations reported in **Figures 5A,B** led us to hypothesize that glomerular damage might result from mitochondria-derived ROS production. In order to test this, we measured mitochondrial superoxide anion production in isolated glomeruli using MitoSox fluorescent dye. **Figure 5C** shows that in the HS diet fed group, glomeruli had increased levels of MitoSox fluorescence intensity, indicative of differential mitochondrial ROS production between the NS and HS groups. Glomeruli isolated from rats fed a HS diet had elevated levels of superoxide production compared to NS, suggesting mitochondrial damage and/or their antioxidant system impairment, supporting the data described above. Interestingly, qPCR analysis (**Figure 5D**) revealed that in freshly isolated glomeruli the expression of *Gpx4* (encoding for glutathione peroxidase 4, which belongs to a family of proteins that catalyze the reduction of hydrogen peroxide, organic hydroperoxides, and lipid hydroperoxides, and protect cells against oxidative damage) was significantly reduced. We also reported the downregulation of the overall antioxidant system in the HS renal cortex (**Figure 5E**, measured with a Trolox-based assay), which is in line with data reported in **Figures 5A,C,D**.

DISCUSSION

The Dahl SS rat is a well-established and characterized rat model of SS hypertension, which displays renal lesions virtually identical to human hypertensive nephrosclerosis (Rapp, 1982; Rapp and Dene, 1985). We confirmed that rats obtained from Charles River recapitulated the phenotype typically observed after a HS diet challenge in this strain. We showed that these animals displayed an increase in systolic BP, kidney hypertrophy, and renal histological lesions (protein casts, glomerular scarring). This study focused on the role of renal cortical and particularly glomerular, mitochondria in the development of kidney injury, using a unique preparation of freshly isolated glomeruli.

It is widely accepted that in AKI and/or chronic kidney disease (CKD) such as DN, mitochondrial biogenesis is significantly affected, and thus could be one of the major reasons for renal tissue damage (Hall and Schuh, 2016; Bhargava and Schnellmann, 2017; Duann and Lin, 2017; Eirin et al., 2018). Surprisingly, little is known about mitochondrial function and biogenesis in SS hypertension. Here we demonstrate for the first time to our knowledge that while Dahl SS rats seem to have a largely preserved renal mitochondrial biogenesis, mitochondrial respiratory function declines in association with morphological changes in the mitochondrial glomeruli. We suggest this based on our data (**Figure 2**), which revealed very limited differences in mtDNA copy number, OXPHOS proteins, and PGC1α expression comparison between NS and HS diet fed groups. Consistent with this observation, we detected no differences in expression of *Atp5f1a*, *Cycs*, *Ppargc1a*, and *Cox4i1* genes in isolated glomeruli. Therefore, our data imply that the major mitochondrial changes in glomeruli during SS hypertension may be functional.

Indeed, the extracellular flux analyzer assay performed on freshly isolated glomeruli revealed dramatic differences in mitochondrial OCR, suggesting an impairment of glomerular mitochondrial function and inability to produce sufficient ATP to satisfy energy needs. We showed that the glomerular mitochondria from the HS group kidneys lost a significant portion of their reserve respiratory capacity. This is an important diagnostic parameter for mitochondrial bioenergetics, which can be indicative of mitochondrial stress, and help us determine how close to their functional limit the mitochondria are operating (Brand and Nicholls, 2011). In contrast to our bioenergetic data however, we did not detect any differences in Complex V activity between the groups. A possible explanation could be that while bioenergetic parameters were measured in intact glomeruli, Complex V activity was assessed in freeze–thawed glomerular pellets. In earlier studies, kidneys from Dahl SS rats were reported to display apoptosis related to mitochondrial release of cytochrome C and subsequent activation of caspase-9 and caspase-3 (Ying and Sanders, 2001). Zheleznova et al. (2012) reported that mTAL cells and mitochondria in the outer medulla of

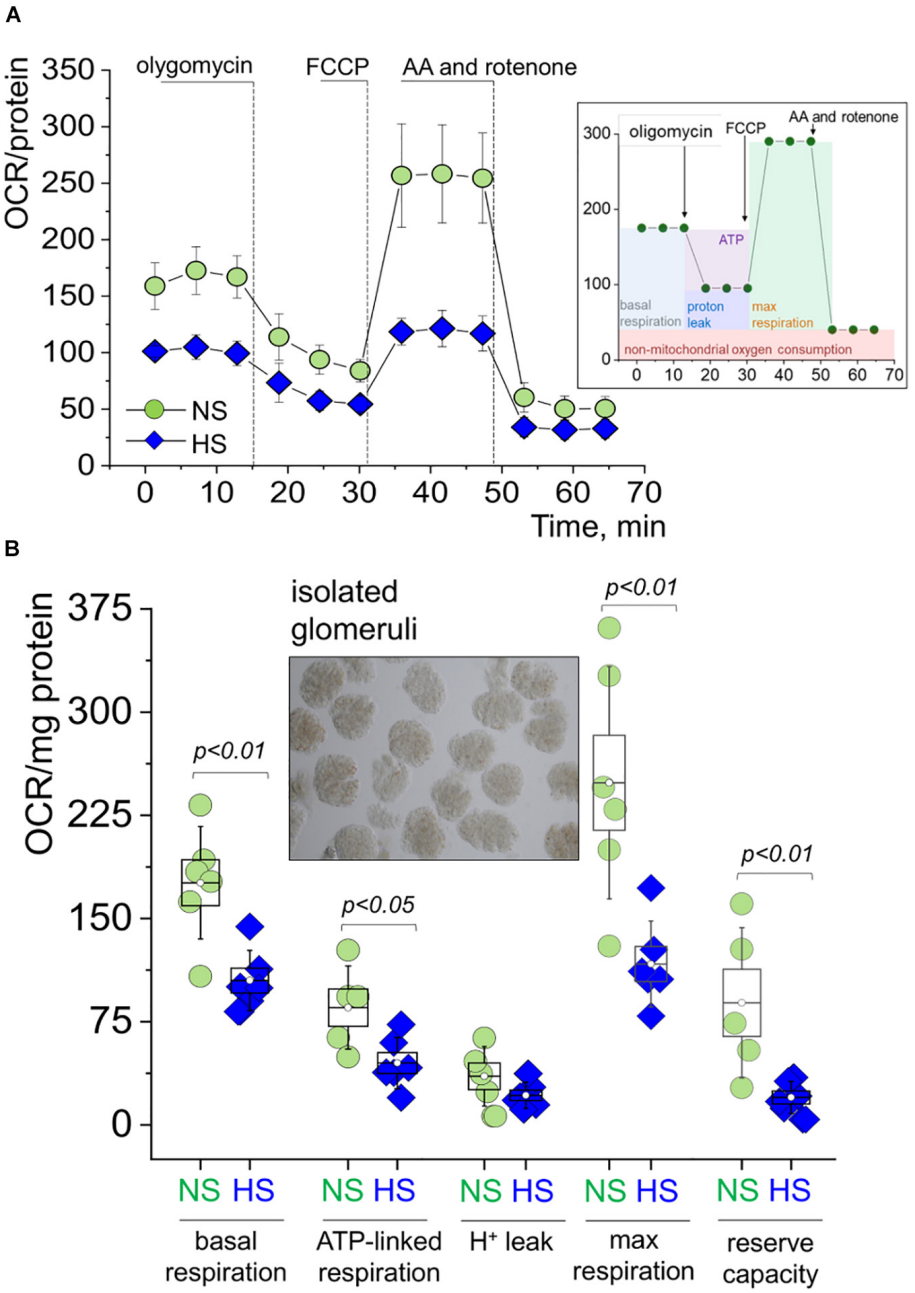

FIGURE 4 | Mitochondrial respiration in the freshly isolated glomeruli during SS hypertension. **(A)** Oxygen consumption rate (OCR, pmol/min/mg protein) values obtained in a Seahorse experiment from glomeruli freshly isolated from the renal cortex of rats fed a high salt (HS) or normal salt (NS) diet. Shown are curves summarized from at least five rats per group, three to five replicates per rat; error bars are SEM. Right inset panel illustrates the experimental design. **(B)** Summary for basal respiration, ATP production, proton leak, maximal respiration, and reserve respiratory capacity as measured in the seahorse experiment shown in Graph. OCR is expressed in pmol/min/mg protein **(A)**. Each data point is an average of at least three replicates per individual rat. An inset shows a typical preparation of isolated glomeruli. All data were compared using a one-way ANOVA with Holm–Sidak *post hoc* test. NS, normal salt; HS, high salt.

SS rats fed a HS diet (8% for 7 days) exhibited lower rates of oxygen utilization compared to those from the SS.13BN rats; the authors concluded that mTAL mitochondria energetics is changed in SS rats, which leads to a reduction in O_2 utilization efficiency. This is in accordance with our data demonstrating decreased basal, ATP-linked and maximal respiration, as well as spare respiratory capacity in isolated glomeruli from Dahl SS rats fed a HS diet vs. NS.

In our experiments, increased oxidative stress and reduced antioxidant capacity were observed in renal glomeruli from SS rats fed a HS diet, which can be a contributing factor in

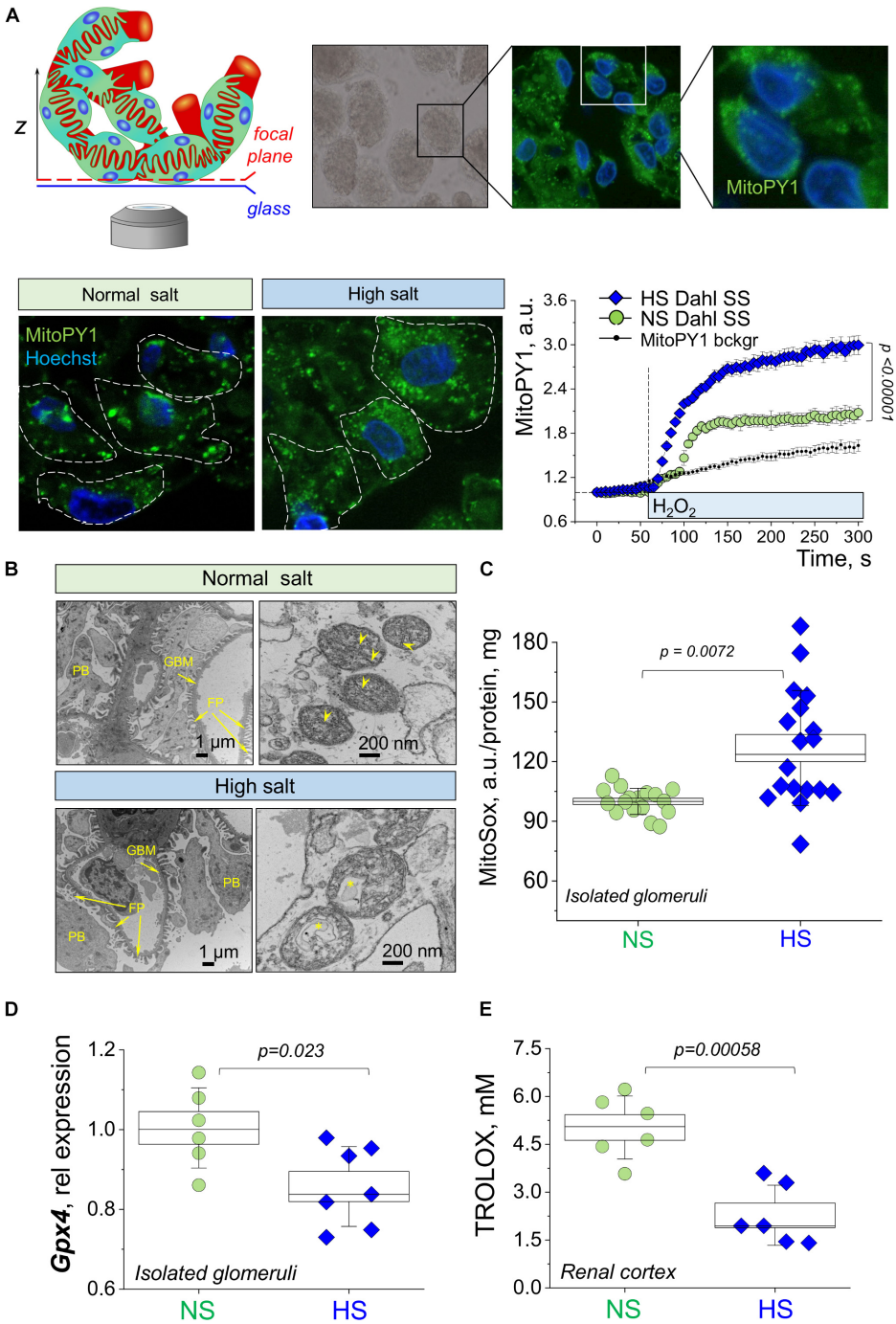

FIGURE 5 | Structural and functional properties of glomerular mitochondria in salt-sensitive (SS) hypertension. **(A)** A schematic illustration of the imaging configuration, as well as representative images of the podocytes in the isolated glomeruli stained with mitoPY1 to visualize H_2O_2 in mitochondria (green), and Hoechst (blue) to label nuclei. Images were obtained with a 63× oil objective, NA 1.4. Dotted lines show podocyte body outlines (obtained from TL images). Graph on the right summarizes the fluorescence transients obtained from mitoPY1-stained podocytes of freshly isolated glomeruli in response to acute addition of 10 μM H_2O_2. Background auto fluorescence of mitoPY1 is shown (transient obtained in the absence of H_2O_2). *N*, five rats per group, at least four glomeruli per animal, with five to nine ROIs (podocytes) analyzed per glomerulus. Statistical analysis performed using one-way repeated measures ANOVA with Holm–Bonferroni for *post hoc* means comparison. **(B)** Representative electron microscopy images of the mitochondria ultrastructure in the podocyte of the glomeruli isolated from NS and HS diet fed rats. Scale bar is shown on the graph; asterisk denotes autophagosome formation; arrowheads show cristae. FP, foot processes; GMB, glomerular basement membrane; PB, podocyte body. **(C)** Mitochondria of glomeruli of HS diet fed animals exhibit higher levels of super oxide, as shown by fluorescence of MitoSox, six rats in each group, three replicates were measured per each experimental animal. Data were compared using a one-way ANOVA with Holm–Sidak *post hoc* test. **(D)** Relative expression of *Gpx4* in the fraction of freshly isolated glomeruli. **(E)** The antioxidant capacity of renal cortical tissue compared in NS vs. HS diet fed animals (expressed in mM Trolox). Data were compared using a one-way ANOVA with Holm–Sidak *post hoc* test, each point represents a separate animal.

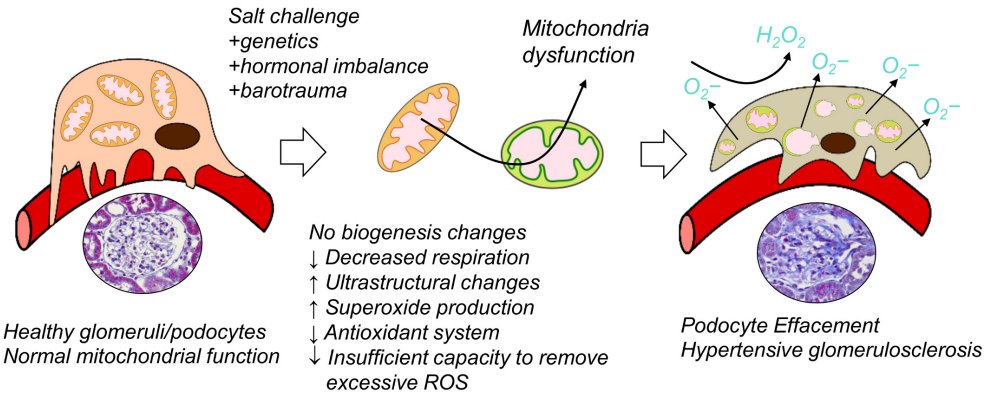

FIGURE 6 | Suggested schematic illustration of the contribution of renal mitochondrial dysfunction to glomerular damage occurring in salt-sensitive (SS) hypertension.

glomerulosclerosis development under a HS challenge. Excessive mitochondrial H_2O_2 production has been shown previously in kidney disease, for instance, in mice fed a high fat diet (Ruggiero et al., 2011) or in the urine of mice fed a Western diet (Decleves et al., 2011). Our results are in accordance with a hypothesis that excessive H_2O_2 production and mitochondrial ROS leakage may be a common mechanism underlying pathogenesis in many forms of kidney disease, including SS hypertensive nephrosclerosis. Mitochondrial structural changes observed with EM potentially implicate the podocyte as a target cell in the glomerulus, however, further studies are required to draw definite conclusions. Salehpour et al. (2015) revealed that kidneys of Dahl SS rats have reduced levels of mitochondrial ETC activity and enhanced oxidative stress; specifically, when fed a HS diet, this strain exhibited significantly lower tissue redox ratios compared to the NS fed rats (Salehpour et al., 2015). We observed Complex V and IV level reduction in the renal cortex (but no apparent changes in Complex V activity or OXPHOS expression in isolated glomeruli), which partially agrees with the data by Ying and Sanders (2001) that showed inappropriate mitochondria release of Cytochrome C in the kidney tissue of Dahl SS rat. Interestingly, Lee et al. (2014) found increased mitochondrial OXPHOS in the renal proximal tubule cells of SHR rats compared to Wistar rats and identified the pyruvate dehydrogenase complex as a determinant of such increased mitochondrial metabolism. We believe that these discrepancies may be attributed to mechanistic dissimilarities in the origin and progression of hypertension in SHR and Dahl SS rats. A recent manuscript by Wang et al. (2017) established that renal mitochondria from Dahl SS rats fed HS diet (8%, 2 weeks) exhibit a lower activity of fumarase, isocitrate dehydrogenase, and succinyl-CoA synthase compared with SS.13BN salt-resistant control rats, as well as reduced ATP production, membrane potential, and SOD activity. Our data indicated that similar mitochondrial impairment manifested in Dahl SS rats when a lesser salt challenge was introduced (4%, 3 weeks). An earlier study by He et al. (2014) using TEM analysis showed that mitochondrial and ER ultrastructural abnormalities occurred in the medullary TALs of SS rats prior to the development of histological injury, potentially contributing to the subsequent development of metabolic and functional renal dysfunction (He et al., 2014). However, that study was focused on renal tubules; therefore, our data are the first to demonstrate the ultrastructural changes in the mitochondria from the podocytes in the Dahl SS rat fed a HS diet, including swelling, loss of cristae, and, in some cases, mitophagy.

To sum up, our study is the first one to report reduced oxygen consumption, impairments in bioenergetics, downregulation of renal antioxidant system, and increased oxidative stress specifically in the renal cortical glomeruli from Dahl SS rats fed a HS diet (**Figure 6**). We demonstrated that bioenergetic changes are not necessarily correlated with mitochondrial biogenesis in the renal cortex of the Dahl SS rats developing hypertensive nephrosclerosis. However, additional studies should be devoted to the factors inducing mitochondrial damage in the glomeruli, the timeline of damage development, and the use of these phenomena as a potential diagnostic tool in clinics (especially targeting renal mitochondria biogenesis vs. mitochondrial function in SS hypertension).

DATA AVAILABILITY STATEMENT

The datasets generated for this study are available on request to the corresponding author.

ETHICS STATEMENT

The animal study was reviewed and approved by the MUSC Institutional Animal Care and Use Committee.

AUTHOR CONTRIBUTIONS

MD, IP, AN, VV, CK, RS, MF, GB, NS, A-LN, DI, and KS performed the experiments, and acquired, analyzed, and interpreted the data. DI, KS, and

EM designed the study, interpreted and analyzed the data, and drafted the manuscript. All authors provided approval for the publication of the final manuscript.

FUNDING

This study was supported by the National Institutes of Health (NIDDK) R00 DK105160 (to DI), 1R01 DK115749 (to KS), and NIH/NCI Grants R01 CA184456 to EM; Dialysis Clinic Inc. Reserve Fund, the MUSC SCTR support program via NIH/NCATS UL1TR001450 (DI); and the APS Research Career Enhancement and Lazaro J. Mandel awards to DI. The work was also partially supported by the P20-GM103542 South Carolina COBRE in Oxidants, Redox Balance, and Stress Signaling.

ACKNOWLEDGMENTS

The authors would like to thank Dr. Monika Gooz and Kareem Heslop (MUSC) for help with initial imaging experiments, and the MUSC Histology & Immunohistochemistry Laboratory and Research Electron Microscopy Service Laboratory for assistance with preparation of sample and staining of tissues for histology and TEM.

REFERENCES

Arif, E., Solanki, A. K., Srivastava, P., Rahman, B., Fitzgibbon, W. R., Deng, P., et al. (2019). Mitochondrial biogenesis induced by the beta2-adrenergic receptor agonist formoterol accelerates podocyte recovery from glomerular injury. *Kidney Int.* 96, 656–673. doi: 10.1016/j.kint.2019.03.023

Assady, S., Wanner, N., Skorecki, K. L., and Huber, T. B. (2017). New insights into podocyte biology in glomerular health and disease. *J. Am. Soc. Nephrol.* 28, 1707–1715. doi: 10.1681/ASN.2017010027

Ayanga, B. A., Badal, S. S., Wang, Y., Galvan, D. L., Chang, B. H., Schumacker, P. T., et al. (2016). Dynamin-related protein 1 deficiency improves mitochondrial fitness and protects against progression of diabetic nephropathy. *J. Am. Soc. Nephrol.* 27, 2733–2747. doi: 10.1681/ASN.2015101096

Bhargava, P., and Schnellmann, R. G. (2017). Mitochondrial energetics in the kidney. *Nat. Rev. Nephrol.* 13, 629–646. doi: 10.1038/nrneph.2017.107

Bianchi, G., Fox, U., Di Francesco, G. F., Giovanetti, A. M., and Pagetti, D. (1974). Blood pressure changes produced by kidney cross-transplantation between spontaneously hypertensive rats and normotensive rats. *Clin. Sci. Mol. Med.* 47, 435–448. doi: 10.1042/cs0470435

Brand, M. D., and Nicholls, D. G. (2011). Assessing mitochondrial dysfunction in cells. *Biochem. J.* 435, 297–312. doi: 10.1042/BJ20110162

Cameron, R. B., Gibbs, W. S., Miller, S. R., Dupre, T. V., Megyesi, J., Beeson, C. C., et al. (2019). Proximal Tubule beta 2-Adrenergic Receptor Mediates Formoterol-Induced Recovery of Mitochondrial and Renal Function after Ischemia-Reperfusion Injury. *J. Pharmacol. Exp. Ther.* 369, 173–180. doi: 10.1124/jpet.118.252833

Casalena, G., Krick, S., Daehn, I., Yu, L., Ju, W., Shi, S., et al. (2014). Mpv17 in mitochondria protects podocytes against mitochondrial dysfunction and apoptosis in vivo and in vitro. *Am. J. Physiol. Renal Physiol.* 306, F1372–F1380. doi: 10.1152/ajprenal.00608.2013

Cowley, A. W. Jr., Abe, M., Mori, T., O'Connor, P. M., Ohsaki, Y., and Zheleznova, N. N. (2015). Reactive oxygen species as important determinants of medullary flow, sodium excretion, and hypertension. *Am. J. Physiol. Renal Physiol.* 308, F179–F197. doi: 10.1152/ajprenal.00455.2014

Cowley, A. W. Jr., Moreno, C., Jacob, H. J., Peterson, C. B., Stingo, F. C., Ahn, K. W., et al. (2014). Characterization of biological pathways associated with a 1.37 Mbp genomic region protective of hypertension in Dahl S rats. *Physiol. Genom.* 46, 398–410. doi: 10.1152/physiolgenomics.00179.2013

Daehn, I., Casalena, G., Zhang, T., Shi, S., Fenninger, F., Barasch, N., et al. (2014). Endothelial mitochondrial oxidative stress determines podocyte depletion in segmental glomerulosclerosis. *J. Clin. Invest.* 124, 1608–1621. doi: 10.1172/JCI71195

Daneva, Z., Laubach, V. E., and Sonkusare, S. K. (2019). Novel regulators and targets of redox signaling in pulmonary vasculature. *Curr. Opin. Physiol.* 9, 87–93. doi: 10.1016/j.cophys.2019.04.026

Decleves, A. E., Mathew, A. V., Cunard, R., and Sharma, K. (2011). AMPK mediates the initiation of kidney disease induced by a high-fat diet. *J. Am. Soc. Nephrol.* 22, 1846–1855. doi: 10.1681/ASN.2011010026

Denic, A., Glassock, R. J., and Rule, A. D. (2016). Structural and functional changes with the aging kidney. *Adv. Chronic Kidney Dis.* 23, 19–28. doi: 10.1053/j.ackd.2015.08.004

Dikalov, S. I., and Dikalova, A. E. (2016). Contribution of mitochondrial oxidative stress to hypertension. *Curr. Opin. Nephrol. Hypertens.* 25, 73–80. doi: 10.1097/mnh.0000000000000198

Ding, L., Kang, Y., Dai, H. B., Wang, F. Z., Zhou, H., Gao, Q., et al. (2019). Adipose afferent reflex is enhanced by TNFalpha in paraventricular nucleus through NADPH oxidase-dependent ROS generation in obesity-related hypertensive rats. *J. Transl. Med.* 17:256. doi: 10.1186/s12967-019-2006-0

Duann, P., and Lin, P. H. (2017). Mitochondria damage and kidney disease. *Adv. Exp. Med. Biol.* 982, 529–551. doi: 10.1007/978-3-319-55330-6_27

Eirin, A., Lerman, A., and Lerman, L. O. (2015). Mitochondria: a pathogenic paradigm in hypertensive renal disease. *Hypertension* 65, 264–270. doi: 10.1161/hypertensionaha.114.04598

Eirin, A., Lerman, A., and Lerman, L. O. (2017a). The emerging role of mitochondrial targeting in kidney disease. *Handb. Exp. Pharmacol.* 240, 229–250. doi: 10.1007/164_2016_6

Eirin, A., Lerman, A., and Lerman, L. O. (2018). Enhancing mitochondrial health to treat hypertension. *Curr. Hypertens. Rep.* 20:89. doi: 10.1007/s11906-018-0889-4

Eirin, A., Saad, A., Tang, H., Herrmann, S. M., Woollard, J. R., Lerman, A., et al. (2016). Urinary mitochondrial DNA copy number identifies chronic renal injury in hypertensive patients. *Hypertension* 68, 401–410. doi: 10.1161/HYPERTENSIONAHA.116.07849

Eirin, A., Saad, A., Woollard, J. R., Juncos, L. A., Calhoun, D. A., Tang, H., et al. (2017b). Glomerular hyperfiltration in obese African American hypertensive patients is associated with elevated urinary mitochondrial-DNA copy number. *Am. J. Hypertens.* 30, 1112–1119. doi: 10.1093/ajh/hpx103

Elijovich, F., Weinberger, M. H., Anderson, C. A., Appel, L. J., Bursztyn, M., Cook, N. R., et al. (2016). Salt sensitivity of blood pressure: a scientific statement from the American heart association. *Hypertension* 68, e7–e46.

Elliott, L. H., Wilkinson, S. E., Sedgwick, A. D., Hill, C. H., Lawton, G., Davis, P. D., et al. (1990). K252a is a potent and selective inhibitor of phosphorylase kinase. *Biochem. Biophys. Res. Commun.* 171, 148–154. doi: 10.1016/0006-291x(90)91369-4

Endres, B. T., Sandoval, R. M., Rhodes, G. J., Campos-Bilderback, S. B., Kamocka, M. M., Mcdermott-Roe, C., et al. (2017). Intravital imaging of the kidney in a rat model of salt-sensitive hypertension. *Am. J. Physiol. Renal Physiol.* 313, F163–F173. doi: 10.1152/ajprenal.00466.2016

Evans, L. C., Dayton, A., Yang, C., Liu, P., Kurth, T., Ahn, K. W., et al. (2018). Transcriptomic analysis reveals inflammatory and metabolic pathways that are regulated by renal perfusion pressure in the outer medulla of Dahl-S rats. *Physiol. Genom.* 50, 440–447. doi: 10.1152/physiolgenomics.00034.2018

Galvan, D. L., Green, N. H., and Danesh, F. R. (2017). The hallmarks of mitochondrial dysfunction in chronic kidney disease. *Kidney Int.* 92, 1051–1057. doi: 10.1016/j.kint.2017.05.034

Gibbs, W. S., Collier, J. B., Morris, M., Beeson, C. C., Megyesi, J., and Schnellmann, R. G. (2018). 5-HT1F receptor regulates mitochondrial homeostasis and its loss potentiates acute kidney injury and impairs renal recovery. *Am. J. Physiol. Renal. Physiol.* 315, F1119–F1128. doi: 10.1152/ajprenal.00077.2018

Hall, A. M., and Schuh, C. D. (2016). Mitochondria as therapeutic targets in acute kidney injury. *Curr. Opin. Nephrol. Hypertens.* 25, 355–362. doi: 10.1097/MNH.0000000000000228

He, X., Liu, Y., Usa, K., Tian, Z., Cowley, A. W. Jr., and Liang, M. (2014). Ultrastructure of mitochondria and the endoplasmic reticulum in renal tubules of Dahl salt-sensitive rats. *Am. J. Physiol. Renal. Physiol.* 306, F1190–F1197. doi: 10.1152/ajprenal.00073.2014

Ilatovskaya, D. V., Blass, G., Palygin, O., Levchenko, V., Pavlov, T. S., Grzybowski, M. N., et al. (2018). A NOX4/TRPC6 pathway in podocyte calcium regulation and renal damage in diabetic kidney disease. *J. Am. Soc. Nephrol.* 29, 1917–1927. doi: 10.1681/ASN.2018030280

Ilatovskaya, D. V., Levchenko, V., Lowing, A., Shuyskiy, L. S., Palygin, O., and Staruschenko, A. (2015a). Podocyte injury in diabetic nephropathy: implications of angiotensin II-dependent activation of TRPC channels. *Sci. Rep.* 5:17637. doi: 10.1038/srep17637

Ilatovskaya, D. V., Palygin, O., Levchenko, V., and Staruschenko, A. (2015b). Single-channel analysis and calcium imaging in the podocytes of the freshly isolated glomeruli. *J. Vis. Exp.* 100:e52850. doi: 10.3791/52850

Ilatovskaya, D. V., Levchenko, V., Ryan, R. P., Cowley, A. W. Jr., and Staruschenko, A. (2011). NSAIDs acutely inhibit TRPC channels in freshly isolated rat Glomeruli. *Biochem. Biophys. Res. Commun.* 408, 242–247. doi: 10.1016/j.bbrc.2011.04.005

Ilatovskaya, D. V., and Staruschenko, A. (2013). Single-channel analysis of TRPC channels in the podocytes of freshly isolated Glomeruli. *Methods Mol. Biol.* 998, 355–369. doi: 10.1007/978-1-62703-351-0_28

Kruger, C., Nguyen, T. T., Breaux, C., Guillory, A., Mangelli, M., Fridianto, K. T., et al. (2019). Proximal tubular Cell-specific ablation of carnitine acetyltransferase causes tubular disease and secondary Glomerulosclerosis. *Diabetes Metab. Res. Rev.* 68, 819–831. doi: 10.2337/db18-0090

Kumar, V., Evans, L. C., Kurth, T., Yang, C., Wollner, C., Nasci, V., et al. (2019). Therapeutic suppression of mTOR (Mammalian Target of Rapamycin) signaling prevents and reverses salt-induced hypertension and kidney injury in Dahl salt-sensitive rats. *Hypertension* 73, 630–639. doi: 10.1161/HYPERTENSIONAHA.118.12378

Laffer, C. L., and Elijovich, F. (2018). Mechanisms of salt sensitivity of blood pressure: an unbiased approach to skinning a cat. *J. Hypertens.* 36, 702–703. doi: 10.1097/hjh.0000000000001636

Lahera, V., De Las Heras, N., Lopez-Farre, A., Manucha, W., and Ferder, L. (2017). Role of mitochondrial dysfunction in hypertension and obesity. *Curr. Hypertens. Rep* 19:11.

Lee, H., Abe, Y., Lee, I., Shrivastav, S., Crusan, A. P., Huttemann, M., et al. (2014). Increased mitochondrial activity in renal proximal tubule cells from young spontaneously hypertensive rats. *Kidney Int.* 85, 561–569. doi: 10.1038/ki.2013.397

Long, J., Badal, S. S., Ye, Z., Wang, Y., Ayanga, B. A., Galvan, D. L., et al. (2016). Long noncoding RNA Tug1 regulates mitochondrial bioenergetics in diabetic nephropathy. *J. Clin. Invest.* 126, 4205–4218. doi: 10.1172/JCI87927

Loperena, R., and Harrison, D. G. (2017). Oxidative stress and hypertensive diseases. *Med. Clin. North Am.* 101, 169–193. doi: 10.1016/j.mcna.2016.08.004

Manucha, W., Ritchie, B., and Ferder, L. (2015). Hypertension and insulin resistance: implications of mitochondrial dysfunction. *Curr. Hypertens. Rep.* 17:504. doi: 10.1007/s11906-014-0504-2

Marshall, J. D., Bazan, I., Zhang, Y., Fares, W. H., and Lee, P. J. (2018). Mitochondrial dysfunction and pulmonary hypertension: cause, effect, or both. *Am. J. Physiol. Lung. Cell Mol. Physiol.* 314, L782–L796. doi: 10.1152/ajplung.00331.2017

Ohsaki, Y., O'connor, P., Mori, T., Ryan, R. P., Dickinson, B. C., Chang, C. J., et al. (2012). Increase of sodium delivery stimulates the mitochondrial respiratory chain H2O2 production in rat renal medullary thick ascending limb. *Am. J. Physiol. Renal Physiol.* 302, F95–F102. doi: 10.1152/ajprenal.00469.2011

Palygin, O., Levchenko, V., Ilatovskaya, D. V., Pavlov, T. S., Pochynyuk, O. M., Jacob, H. J., et al. (2017). Essential role of Kir5.1 channels in renal salt handling and blood pressure control. *JCI Insight* 2:92331. doi: 10.1172/jci.insight.92331

Patschan, O., Kuttler, B., Heemann, U., Uber, A., and Rettig, R. (1997). Kidneys from normotensive donors lower blood pressure in young transplanted spontaneously hypertensive rats. *Am. J. Physiol.* 273, R175–R180.

Pavlov, T. S., Levchenko, V., Ilatovskaya, D. V., Li, H., Palygin, O., Pastor-Soler, N. M., et al. (2017). Lack of effects of metformin and AICAR chronic infusion on the development of hypertension in Dahl salt-sensitive rats. *Front. Physiol.* 8:227. doi: 10.3389/fphys.2017.00227

Pilic, L., Pedlar, C. R., and Mavrommatis, Y. (2016). Salt-sensitive hypertension: mechanisms and effects of dietary and other lifestyle factors. *Nutr. Rev.* 74, 645–658. doi: 10.1093/nutrit/nuw028

Qi, H., Casalena, G., Shi, S., Yu, L., Ebefors, K., Sun, Y., et al. (2017). Glomerular endothelial mitochondrial dysfunction is essential and characteristic of diabetic kidney disease susceptibility. *Diabetes Metab. Res. Rev* 66, 763–778. doi: 10.2337/db16-0695

Raij, L., Azar, S., and Keane, W. (1984). Mesangial immune injury, hypertension, and progressive glomerular damage in Dahl rats. *Kidney Int.* 26, 137–143. doi: 10.1038/ki.1984.147

Rapp, J. P. (1982). Dahl salt-susceptible and salt-resistant rats. A review. *Hypertension* 4, 753–763. doi: 10.1161/01.hyp.4.6.753

Rapp, J. P., and Dene, H. (1985). Development and characteristics of inbred strains of Dahl salt-sensitive and salt-resistant rats. *Hypertension* 7, 340–349. doi: 10.1161/01.hyp.7.3.340

Rodriguez-Iturbe, B., Sepassi, L., Quiroz, Y., Ni, Z., Wallace, D. C., and Vaziri, N. D. (2007). Association of mitochondrial SOD deficiency with salt-sensitive hypertension and accelerated renal senescence. *J. Appl. Physiol.* 102, 255–260. doi: 10.1152/japplphysiol.00513.2006

Ruggiero, C., Ehrenshaft, M., Cleland, E., and Stadler, K. (2011). High-fat diet induces an initial adaptation of mitochondrial bioenergetics in the kidney despite evident oxidative stress and mitochondrial ROS production. *Am. J. Physiol. Endocrinol. Metab.* 300, E1047–E1058. doi: 10.1152/ajpendo.00666.2010

Rust, P., and Ekmekcioglu, C. (2017). Impact of salt intake on the pathogenesis and treatment of hypertension. *Adv. Exp. Med. Biol.* 956, 61–84. doi: 10.1007/5584_2016_147

Salehpour, F., Ghanian, Z., Yang, C., Zheleznova, N. N., Kurth, T., Dash, R. K., et al. (2015). Effects of p67phox on the mitochondrial oxidative state in the kidney of Dahl salt-sensitive rats: optical fluorescence 3-D cryoimaging. *Am. J. Physiol. Renal Physiol.* 309, F377–F382. doi: 10.1152/ajprenal.00098.2015

Seccia, T. M., Caroccia, B., and Calo, L. A. (2017). Hypertensive nephropathy. Moving from classic to emerging pathogenetic mechanisms. *J. Hypertens.* 35, 205–212. doi: 10.1097/HJH.0000000000001170

Sharma, K. (2017). Mitochondrial dysfunction in the diabetic kidney. *Adv. Exp. Med. Biol.* 982, 553–562. doi: 10.1007/978-3-319-55330-6_28

Spires, D., Ilatovskaya, D. V., Levchenko, V., North, P. E., Geurts, A. M., Palygin, O., et al. (2018). Protective role of Trpc6 knockout in the progression of diabetic kidney disease. *Am. J. Physiol. Renal Physiol.* 315, F1091–F1097. doi: 10.1152/ajprenal.00155.2018

Sweetwyne, M. T., Pippin, J. W., Eng, D. G., Hudkins, K. L., Chiao, Y. A., Campbell, M. D., et al. (2017). The mitochondrial-targeted peptide, SS-31, improves glomerular architecture in mice of advanced age. *Kidney Int.* 91, 1126–1145. doi: 10.1016/j.kint.2016.10.036

Szeto, H. H., Liu, S., Soong, Y., Alam, N., Prusky, G. T., and Seshan, S. V. (2016). Protection of mitochondria prevents high-fat diet-induced glomerulopathy and proximal tubular injury. *Kidney Int.* 90, 997–1011. doi: 10.1016/j.kint.2016.06.013

Wang, Z., Sun, Q., Sun, N., Liang, M., and Tian, Z. (2017). Mitochondrial dysfunction and altered renal metabolism in Dahl salt-sensitive rats. *Kidney Blood Press. Res.* 42, 587–597. doi: 10.1159/000479846

Ying, W. Z., and Sanders, P. W. (2001). Cytochrome c mediates apoptosis in hypertensive nephrosclerosis in Dahl/Rapp rats. *Kidney Int.* 59, 662–672. doi: 10.1046/j.1523-1755.2001.059002662.x

Zhan, M., Brooks, C., Liu, F., Sun, L., and Dong, Z. (2013). Mitochondrial dynamics: regulatory mechanisms and emerging role in renal pathophysiology. *Kidney Int.* 83, 568–581. doi: 10.1038/ki.2012.441

Zhang, L. H., Zhu, X. Y., Eirin, A., Nargesi, A. A., Woollard, J. R., Santelli, A., et al. (2019). Early podocyte injury and elevated levels of urinary podocyte-derived extracellular vesicles in swine with metabolic syndrome: role of podocyte mitochondria. *Am. J. Physiol. Renal Physiol.* 317, F12–F22. doi: 10.1152/ajprenal.00399.2018

Zhao, M., Yuan, Y., Bai, M., Ding, G., Jia, Z., Huang, S., et al. (2016). PGC-1alpha overexpression protects against aldosterone-induced podocyte depletion: role of mitochondria. *Oncotarget* 7, 12150–12162. doi: 10.18632/oncotarget.7859

Zheleznova, N. N., Yang, C., and Cowley, A. W. Jr. (2016). Role of Nox4 and p67phox subunit of Nox2 in ROS production in response to increased tubular flow in the mTAL of Dahl salt-sensitive rats. *Am. J. Physiol. Renal Physiol.* 311, F450–F458. doi: 10.1152/ajprenal.00187.2016

Zheleznova, N. N., Yang, C., Ryan, R. P., Halligan, B. D., Liang, M., Greene, A. S., et al. (2012). Mitochondrial proteomic analysis reveals deficiencies in oxygen utilization in medullary thick ascending limb of Henle in the Dahl salt-sensitive rat. *Physiol. Genom.* 44, 829–842. doi: 10.1152/physiolgenomics.00060.2012

Conflict of Interest: The authors declare that the research was conducted in the absence of any commercial or financial relationships that could be construed as a potential conflict of interest.

Copyright © 2020 Domondon, Polina, Nikiforova, Sultanova, Kruger, Vasileva, Fomin, Beeson, Nieminen, Smythe, Maldonado, Stadler and Ilatovskaya. This is an open-access article distributed under the terms of the Creative Commons Attribution License (CC BY). The use, distribution or reproduction in other forums is permitted, provided the original author(s) and the copyright owner(s) are credited and that the original publication in this journal is cited, in accordance with accepted academic practice. No use, distribution or reproduction is permitted which does not comply with these terms.

frontiers in Medicine

BRIEF RESEARCH REPORT
published: 06 February 2020
doi: 10.3389/fmed.2020.00023

Effect of Calcitriol on the Renal Microvasculature Differentiation Disturbances Induced by AT_1 Blockade During Nephrogenesis in Rats

*Amanda L. Deluque[1], Lucas F. de Almeida[1], Heloísa D. C. Francescato[1], Cleonice G. A. da Silva[1], Roberto S. Costa[2], José Antunes-Rodrigues[3] and Terezila M. Coimbra[1]**

[1] Laboratory of Renal Physiology, Department of Physiology, Ribeirão Preto Medical School, University of São Paulo, São Paulo, Brazil, [2] Laboratory of Renal Pathology, Division of Nephrology, Department of Internal Medicine, Ribeirão Preto Medical School, University of São Paulo, São Paulo, Brazil, [3] Laboratory of Neuroendocrinology, Department of Physiology, Ribeirão Preto Medical School, University of São Paulo, São Paulo, Brazil*

OPEN ACCESS

Edited by:
John D. Imig, Medical College of Wisconsin, United States

Reviewed by:
Josef Zicha, Institute of Physiology (ASCR), Czechia
Tinte Itinteang, Ministry of Health and Medical Services, Kiribati
Li Zhou, Institute of Laboratory Animal Sciences (CAMS), China
Milan Ivanov, University of Belgrade, Serbia

***Correspondence:**
Terezila M. Coimbra
tmcoimbr@usp.br

Specialty section:
This article was submitted to Nephrology, a section of the journal Frontiers in Medicine

Received: *27 October 2019*
Accepted: *15 January 2020*
Published: *06 February 2020*

Citation:
Deluque AL, de Almeida LF, Francescato HDC, da Silva CGA, Costa RS, Antunes-Rodrigues J and Coimbra TM (2020) Effect of Calcitriol on the Renal Microvasculature Differentiation Disturbances Induced by AT_1 Blockade During Nephrogenesis in Rats. Front. Med. 7:23. doi: 10.3389/fmed.2020.00023

Alterations in the renal vasculature during fetal programming can cause disturbances in renal structure and function that persist into adulthood. Calcitriol can affect cellular differentiation and proliferation, and promote endothelial cell maintenance, each of which is a key event in nephrogenesis. Calcitriol is a negative endocrine regulator of the renin gene. Rats exposed to renin-angiotensin system (RAS) antagonists during lactation have been shown to develop renal disorders, which demonstrated that the RAS may play an important role in mammalian kidney development. We evaluated the effects of calcitriol administration on losartan [angiotensin II receptor antagonist (ANGII), AT_1]-induced changes in renal differentiation in rats during lactation. Rats treated with losartan showed alterations in renal function and structure that persisted into adulthood. These disruptions included hydronephrosis, papillary atrophy, endothelial dysfunction, and aberrant endothelial structure. These changes were mitigated by treatment with calcitriol. The results of our study showed that animals exposed to AT_1 blockade during lactation exhibited altered renal microvasculature differentiation in adulthood that was attenuated by treatment with calcitriol.

Keywords: calcitriol, cell differentiation, kidney development, renin-angiotensin system, renal microvasculature

INTRODUCTION

During renal development, a series of events occur that result in the formation of blood vessels (1). These processes include formation of the renal arterial tree and glomerular capillaries, and alignment of the vasa recta and peritubular capillaries (2). Three-dimensional organization and expansion of microvessels in the renal medulla are dependent on several signaling pathways that supply oxygen and nutrients to adjacent cells (2, 3). The renin-angiotensin system (RAS) plays an important role in expansion, migration, and formation of renal structure during nephrogenesis (4). Results from our studies and others have shown that pharmacological RAS inhibition or genetic deletion of downstream signaling components of RAS (1, 3, 5–8) result in impaired development

of glomeruli and preglomerular vasculature. Angiotensin II (ANGII) also affects the post-glomerular circulation. A study performed by Madsen et al. showed that treatment with an AT_1 receptor antagonist for 14 days during lactation reduced the volume, length, and surface area of capillaries in the kidney medulla, and resulted in disorganization of vasa recta bundles (3). In humans, nephrogenesis is complete by 34–36 weeks of gestation. In contrast, nephrogenesis continues after birth for about 2–3 weeks in mice and rats (1, 8). Therefore, neonatal rats are commonly used to study the mechanisms of renal development (5).

Several studies have reported that calcitriol (1α,25-dihydroxyvitamin D3; activated vitamin D) is involved in maintenance of endothelial function (9), cell proliferation, differentiation, apoptosis, and RAS modulation (5, 10, 11). We previously reported that treatment with calcitriol attenuated glomerular disturbances and promoted differentiation of tubular cells in the renal cortex in animals exposed to AT_1 blockade during nephrogenesis (5). Blockade of AT_1 with losartan during renal development resulted in overexpression of the renin gene and increased expression of ANGII (5), which resulted in disruption of nephrogenesis. Therefore, use of calcitriol in adulthood may mitigate losartan-induced effects on nephrogenesis through modulation of RAS. In addition, calcitriol may improve endothelial cell differentiation and function.

In the present study, we hypothesize that blockade of AT_1 during renal development can result in disturbances in cell differentiation, resulting in reduced vascular density, and that treatment with calcitriol can mitigate these changes. Calcitriol has received increased attention because of widespread vitamin D deficiency and the recent discovery that calcitriol can modulate the RAS. Further evaluation of the effects of calcitriol is important because losartan is a typical pharmacological treatment for hypertension, even in pregnancy. Therefore, the aim of our study was to evaluate the effects of calcitriol on losartan-induced disturbances in the renal microvasculature. Capillary density was evaluated in kidney tissue by immunohistochemical staining for aminopeptidase P (JG12). Associations between capillary density and parenchymal changes in the outer and inner medulla were analyzed using markers of cell differentiation (vimentin and α-SMA).

MATERIALS AND METHODS

Animals and Experimental Design

All experiments were performed in accordance with the ethical principles for animal experimentation of the Brazilian College of Animal Experimentation, and the Animal Experimentation Committee of the University of São Paulo at Ribeirão Preto Medical School approved the study protocol (COBEA/CETEA/FMRP-USP, protocol no. 178/2014).

The animals were housed in a controlled temperature (22°C) environment and exposed to a 12 h light/12 h dark cycle. The animals were provided chow diet and water *ad libitum*. Female and male Wistar rats (Animal House of the Campus of Ribeirao Preto, University of São Paulo, Ribeirao Preto, SP, Brazil) were housed together overnight to permit mating. Each male was housed with three females, and the first gestational day was determined based on the presence of copulatory plugs (12). Pregnant females were separated and monitored during of the entire gestation period and during lactation (21 days each). Male Wistar pups were randomly selected for this study. The litter was reduced to six per mother to ensure equal feeding. During lactation, rats were divided into the following groups: (1) offspring of mothers treated with 2% sucrose solution during lactation and (2) offspring of mothers treated with losartan during lactation (100 mg/kg/day; All Chemistry, Brazil) (5, 7). Each group received the treatment solutions in place of drinking water. Losartan was detected in breast milk at a concentration nearly half of that in maternal plasma in 75% of the rats (8).

After weaning, losartan or sucrose treatments were discontinued, and the animals were separated from their mothers and allowed to acclimate for 4 days. The rats were then separated into the following four experimental groups: (1) SUC (sucrose 2%, $n = 7$), (2) SUC + Calcitriol (sucrose 2% + calcitriol, $n = 7$), (3) LOS (losartan, $n = 8$), and (4) LOS + Calcitriol (losartan + calcitriol, $n = 8$). Calcitriol (6 ng/day, Calcijex, Abbott Laboratories, USA) or vehicle (0.9% NaCl) was administered using mini-osmotic pumps (Model 2004, Alzet, USA) implanted subcutaneously under anesthesia with isoflurane (Cristalia, Brazil). Calcitriol or vehicle supplementation was started following the end of nephrogenesis when losartan-induced lesions were established and continued for 4 weeks. The dose and duration of calcitriol treatment were selected according to previous studies (5, 13, 14).

Systolic Blood Pressure

Systolic blood pressure (SBP) was determined indirectly at 60 days of age using the tail—cuff method (CODA Non-Invasive Blood Pressure System, Kent Scientific Corporation, 2010). The animals were allowed to acclimate for 3 days prior to measurement of SBP. Twelve SBP measurements were averaged for each animal (15).

Evaluation of Renal Function

At 59 days of age, the animals were placed in metabolic cages for 24 h to collect urine samples for measurement of sodium (9180-electrolyte analyzer, Roche, Austria) and osmolality (Fiske OS Osmometer, Advanced Instruments, USA). On the next day, the rats were weighed, then anesthetized using sodium thiopental (0.1 ml/100 g, Brazil). Blood samples were collected from the abdominal artery for analysis of creatinine (Labtest Diagnostica, Brazil) and sodium. One kidney was removed and fixed using methacarn solution for histological and immunohistochemical analyses.

Determination of Nitric Oxide in Renal Tissue

Renal tissue was homogenized in 0.1 N acetic acid (3:1), centrifuged at 10,000 × g for 5 min, and aliquoted. The samples were deproteinated by addition of 95% ethanol (4°C) (1:2), then centrifuged at 4,000 × g for 5 min. The supernatants were analyzed for nitric oxide (NO) content by an NO/ozone technique described previously (16) using a Sievers analyzer

(Sievers 280 NOA, USA). Protein levels in renal tissue were also determined as described previously (17).

Histological Analysis

Tissues were embedded in paraffin and sliced into 4-μm-thick slices, then stained with Masson's Trichrome and visualized using a light microscope (AxioVision Rel. 4.3; Zeiss, Germany). The outer and inner medulla were identified by location and epithelial characteristics. The transition from the cortical region to the medullary region was observed. A representative image is presented in **Figure 1**.

Immunohistochemical Analysis

Kidney sections were deparaffinized and hydrated for immunohistochemical analysis. Non-specific antigen binding was blocked by incubation for 20 min with normal goat serum. The sections were then incubated with anti-vimentin (1:500, Dako Corporation M0725, Denmark), anti-aminopeptidase P (JG12, 1:1000, eBioScience BMS1104, USA), or anti-eNOS (1:100, Santa Cruz Biotechnology sc-376751, USA) antibodies for 60 min at room temperature, and anti-α-smooth muscle actin (α-SMA, 1:1000, Dako Corporation M0851, Denmark) antibody overnight at 4°C. Avidin-biotin-peroxidase complex (Vector Laboratories, USA) and DAB [3,3′-diaminobenzidine (Sigma Chemical Company, USA)] were used for detection. The sections were then counterstained with methyl green, dehydrated, and mounted.

The outer and inner medulla were evaluated. The images were randomly quantified using a Greek box system. Quantification was performed by a blinded analyst. The number of JG12-positive capillaries was counted and localization of α-SMA, vimentin, and eNOS was semi-quantitatively graded as follows: 0 = absent or <5% staining; 1 = 5–25% staining; 2 = 25–50% staining; 3 = 50–75% staining, and 4 ≥75% staining (18). Thirty consecutive fields (0.1 mm^2 each) were evaluated for the outer and inner medulla. Only the inner medulla is shown in the figures.

Western Blot Analysis

Kidneys were homogenized in lysis buffer (50 mM Tris–HCl, pH 7.4; 150 mM NaCl; 1% Triton X-100; 0.1% SDS; 1 μg/mL aprotinin; 1 μg/mL leupeptin; 1 mM phenylmethylsulfonyl fluoride; 1 mM sodium orthovanadate, pH 10; 1 mM sodium pyrophosphate; 25 mM sodium fluoride; and 0.001 M EDTA, pH 8), then centrifuged at 4°C for 15 min at 10,000 rpm. Proteins (60 μg) were separated by polyacrylamide gel electrophoresis, transferred to nitrocellulose membranes, incubated for 1 h in blocking buffer (TBS, 5% skim milk), washed with TBS-T (TBS,

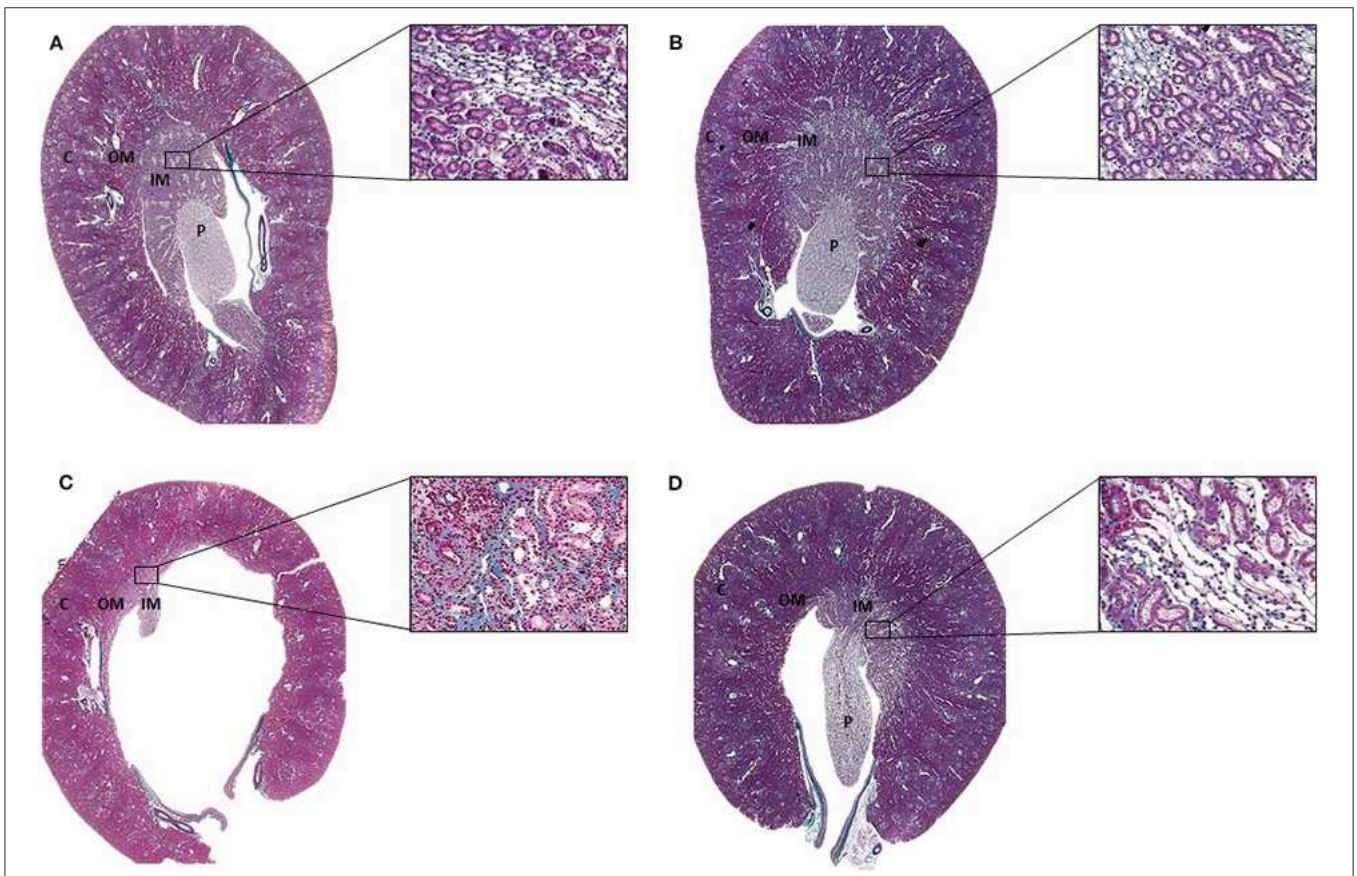

FIGURE 1 | Representative Masson's trichrome staining of histological sections of the **(A)** SUC, **(B)** SUC + Calcitriol, **(C)** LOS, and **(D)** LOS + Calcitriol groups. C, Renal cortex; OM, Outer medulla; IM, Inner medulla; P, Papilla. Magnification, 1X and 40X.

0.1% Tween 20, pH 7.6), then incubated with anti-AT_1 (1:500, Santa Cruz Biotechnology, USA) antibody overnight at 4°C. Membranes were incubated with anti-GAPDH monoclonal antibody (1:1000; Sigma Chemical Co, USA) overnight at 4°C as a loading control. The membranes were then washed and incubated with horseradish peroxidase-conjugated goat anti-mouse (1:5000; Dako, Denmark) antibody for 1 h at room temperature. The membrane-bound antibodies were detected using SuperSignal West Pico Chemiluminescent Substrate (Pierce Chemical, USA), and the blots were visualized using an imaging system (Kodak Gel Logic 2200, USA). Band intensity was quantified by densitometry using ImageJ NIH image software (http://www.nih.gov) and was reported in arbitrary units. Protein quantitation was performed as previously described (17).

Statistical Analysis

Nonparametric Kruskal—Wallis test followed by Dunn's post-test was used to analyze non-normally distributed data. Analysis of variance followed by the Newman—Keuls multiple comparisons test was used for analysis of normally distributed data. Statistical analyses were performed using GraphPad Prism version 7.0 for Windows (GraphPad Software, USA). The data were expressed as means ± standard error of the mean (S.E.M.). $P < 0.05$ were considered statistically significant.

RESULTS

Renal Function Evaluation

Calcitriol treatment improved kidney dysfunction caused by AT_1 receptor blockade during renal development. Rats treated with losartan had higher SBP than those in the SUC and SUC + Calcitriol groups. The rats in the LOS + Calcitriol group had higher SBP than the control groups but did not differ from the LOS group (**Table 1**). Body weight did not differ among the LOS (359.3 ± 9.5), SUC (381.6 ± 9.8), and SUC + Calcitriol (377.5 ± 3.5) groups at 60 days of age. However, body weight was higher in the LOS + Calcitriol group (399.7 ± 12.6) than that in the control group. Changes in water intake, urinary volume, fractional sodium excretion (FE^+_{Na}), and GFR levels were less pronounced in the LOS + Calcitriol group than those in the LOS group (**Table 1**). Urinary osmolality (U) was lower in the LOS and LOS + Calcitriol groups compared to that in the control group. Calcitriol treatment did not affect this parameter (**Table 1**).

Analysis of Renal Structure

The animals of the LOS group presented with renal alterations characterized by atrophic papilla, interstitial fibrosis, tubular atrophy, and tubular dilation. Calcitriol treatment reduced these structural changes induced by AT_1 blockade during renal development (**Figure 1**).

Immunohistochemistry Studies

The expression of α-SMA, a mesenchymal cell (myofibroblasts) marker, was increased in the outer medulla of the LOS group (1.23 ± 0.25) compared to that in the SUC (0.3 ± 0.03) and SUC+Calcitriol (0.26 ± 0.01) groups, which demonstrated lack of cellular differentiation in response to losartan. This increase was mitigated in the outer medulla of rats in the LOS + Calcitriol group (0.3 ± 0.04). Losartan also induced increased expression of α-SMA in the inner medulla, but treatment with calcitriol did not attenuate this increase (**Figure 2**).

The expression of vimentin, a marker of cell differentiation, was increased in the outer medullas of the LOS group (2.78 ± 0.31) compared to that in the SUC (1.05 ± 0.06) and SUC+Calcitriol (1.04 ± 0.07) groups. Losartan-induced increases in vimentin expression were mitigated by treatment with calcitriol (LOS+Calcitriol group; 1.08 ± 0.09). The expression of vimentin in inner medulla was higher in the LOS group than that in the SUC and SUC + Calcitriol groups. However, calcitriol treatment did not attenuate this increase (**Figure 2**).

Immunohistochemical analysis showed that the number of cells positive for JG12, an endothelial capillary cell marker, was reduced in the LOS group (20.73 ± 2.28) compared with that in the SUC (26.12 ± 2.89) and SUC+Calcitriol (23.88 ± 3.71) groups. These differences were not significant in the outer medulla. In the inner medulla, the number of endothelial cells was significantly lower in the LOS group than that in the SUC and SUC + Calcitriol groups. In addition, the LOS + Calcitriol exhibited significantly different expression of JG12 than the SUC + Calcitriol and LOS groups. Calcitriol treatment increased JG12 expression in the inner medullas of rats in the SUC + Calcitriol group compared with that in the SUC group (**Figure 2**).

Endothelial nitric oxide synthase (eNOS) expression was decreased in the kidneys of the LOS group (3.12 ± 0.24) compared with that in the SUC (3.80 ± 0.06) and SUC + Calcitriol (3.86 ± 0.02) groups. Calcitriol treatment did alter the expression of eNOS in the outer medulla. In contrast, in the inner medulla, the LOS + Calcitriol group exhibited higher eNOS expression than the LOS group. In addition, the levels of NO in renal tissue of rats in the LOS + Calcitriol group (7.71 ± 1.69 μM/μg protein) were higher than those in the SUC (4.21 ± 0.38_μM/μg protein), SUC + Calcitriol (2.97 ± 0.23 μM/μg protein), and LOS (5.59 ± 0.65 μM/μg protein) groups. These results showed that AT_1 receptor blockade resulted in disruption of endothelial cell structure and function, and that calcitriol affected neovasculogenesis (**Figure 2**).

Western Blot Studies

The expression of AT_1 was higher in the LOS group than that in the control groups and the LOS + Calcitriol group (**Figure 3**).

DISCUSSION

The results of this study showed that treatment with calcitriol attenuated disturbances in the renal microvasculature in adulthood induced by AT_1-ANGII receptor inhibition during renal development. Several events that occur during development may contribute to hypertension in adulthood. Fetal programming results from mechanisms that include regulation of blood volume and blood pressure (1). Inhibition of AT_1 in rats during renal development has been shown to result in

TABLE 1 | Systolic blood pressure, twenty-four-hour water intake, urine volume, urinary osmolality (U), fractional excretion of sodium (FE^{+}_{Na}), and GFR of 60-day-old pups in SUC, SUC + Calcitriol, LOS and LOS + Calcitriol groups.

	SUC	SUC + Calcitriol	LOS	LOS + Calcitriol
SBP (mmHg)	120.6 ± 6.3	122.5 ± 1.9	143.4 ± 1.8$^{**;\#\#}$	132.9 ± 1.9
Water intake (mL 100 g^{-1} 24 h^{-1})	54.6 ± 3.1	50.4 ± 1.9	120.8 ± 11.1$^{***;\#\#\#}$	88.9 ± 5.83$^{**;\#\#;\$\$}$
Urinary volume (mL 100 g^{-1} 24 h^{-1})	35.7 ± 2.5	35.3 ± 1.4	96 ± 7.5$^{**;\#\#}$	69.1 ± 4.6$^{*;\#}$
U_{osm}(mOsm kg H_2O^{-1})	1,475.0 ± 26.8	1,504.0 ± 24.8	632.4 ± 62.3$^{***;\#\#\#}$	754.4 ± 56.4$^{***;\#\#\#}$
GFR (ml min^{-1}100 g^{-1})	0.81 ± 0.09	0.84 ± 0.06	0.60 ± 0.16$^{*;\#}$	0.71 ± 0.19$^{*;\#;\$}$
FE^{+}_{Na} (%)	0.28 ± 0.04	0.33 ± 0.07	0.80 ± 0.05$^{***;\#\#\#}$	0.56 ± 0.04$^{***;\#\#\#;\$\$}$

*Data are expressed as means ± SEM. *P < 0.05 vs. SUC; **P < 0.01 vs. SUC; ***P < 0.001 vs. SUC; #P < 0.05 vs. SUC + Calcitriol; ##P < 0.01 vs. SUC + Calcitriol; ###P < 0.001 vs. SUC + Calcitriol; $P < 0.05 vs. LOS; $$P < 0.01 vs. LOS.*
SBP, systolic blood pressure.
GFR, glomerular filtration rate.

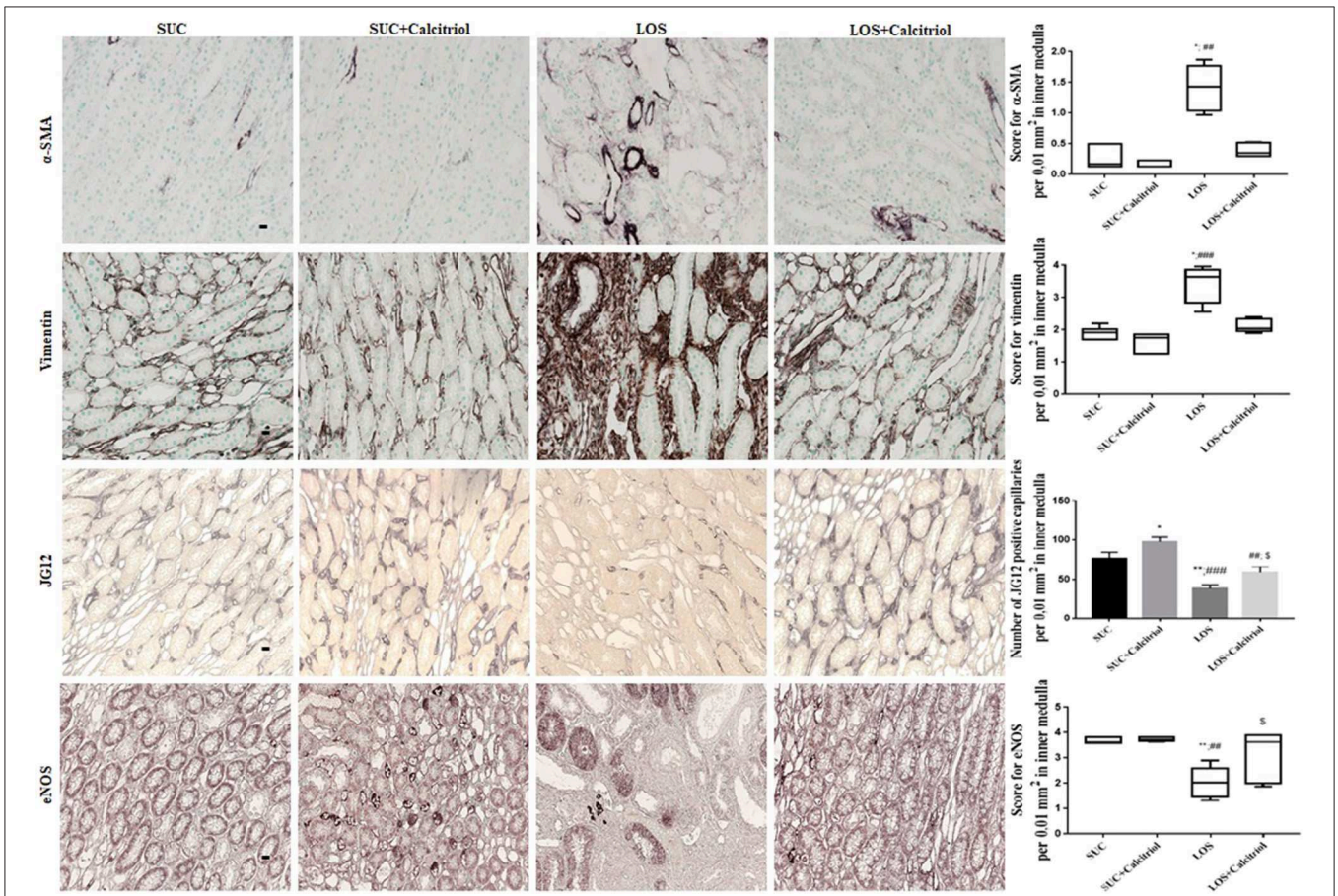

FIGURE 2 | Immunolocalization of α-SMA, vimentin, JG12, and eNOS in inner medulla sections from the SUC, SUC + Calcitriol, LOS, and LOS + Calcitriol groups. Immunohistochemical data are expressed as the median and interquartile range (25–75th) and the mean ± S.E.M. Scale bar = 20 μm, $n = 5$–7 for each group. These markers indicated a lack of tubular and endothelial cell differentiation, and dysfunction. *$P < 0.05$ vs. SUC; **$P < 0.01$ vs. SUC; ##$P < 0.01$ vs. SUC + Calcitriol; ###$P < 0.001$ vs. SUC + Calcitriol; $$P < 0.05$ vs. LOS.

increased blood pressure (8), reduced renal function, and altered renal structure in adulthood. These changes were associated with aberrant renal medulla microcirculation that resulted from losartan-induced reduction in urinary osmolality. Exposure to losartan reduced the ability to concentrate urine and increased urinary volume. This effect resulted from inner medulla and papillary atrophy-induced reductions in water reabsorption by the medullary collecting duct (19). These changes were exacerbated by decreased vasculature in the inner medulla, tubulointerstitial lesions, hydronephrosis, lack of differentiation

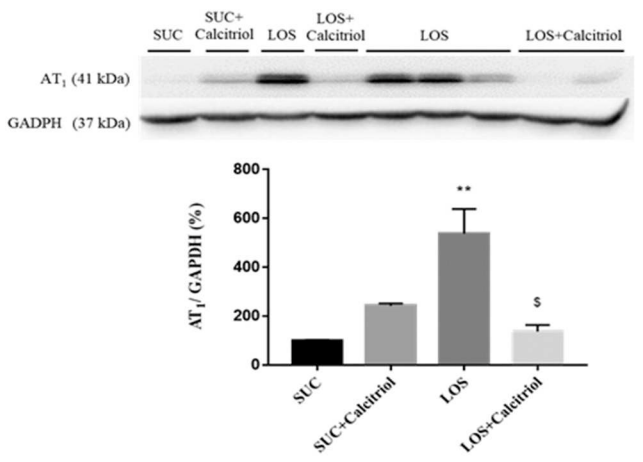

FIGURE 3 | Intrarenal expression of AT_1 receptor in the SUC, SUC+Calcitriol, LOS, and LOS + Calcitriol groups at 60 days of age. Immunoblot data are expressed as the mean ± S.E.M. $^{**}P < 0.01$ vs. SUC; $^{\$}P < 0.05$ vs. LOS.

of tubular cells, and formation of vascular medullar bundles, which resulted in disruption of the osmotic gradient. Expansion of renal medullary microcirculation during the embryonic stage in response to a properly functioning RAS (20) contributes to maintenance and control of sodium and water excretion (1). Reduced vessel density in the medulla resulting from renal development disorders that affect ANGII expression has been shown to induce changes in urinary concentration that could not be mitigated by calcitriol treatment. The integrity of vascular structures in the renal inner medulla is essential for urinary concentration (4), and is programmed in development, that could be dependent of arginine vasopressin (AVP), responsible to dipsogenic and pressor responses and to counter-current multiplier and exchange. The immature kidney from RAS inhibition to AVP may decrease water reabsorption in collecting duct and limit urine concentration. Impaired ANGII-AT_1 receptor signaling or treatment with an AT_1 receptor antagonist during kidney development results in reduced capillary density and impaired ability to concentrate urine that persists into adulthood. In our study, the urinary osmolality in the LOS + Calcitriol group was not significantly different from that in the LOS group, potentially because renal structure recovered and hydronephrosis induced by renal medulla loss was not complete. The absence of AT_1 receptor signaling or loss of AT_1 receptors can result in damage to ∼50% of the renal parenchyma (3). We also observed an increase in FE^{+}_{Na} in rats that received losartan during renal development, which indicated that renal sodium transport was altered. The changes in glomerular filtration rate observed in the present study were similar to those observed in other studies that used this model (5, 7, 20, 21).

Endothelial dysfunction has been shown to result in altered renal microvasculature with reduced peritubular capillary density (4). Serón et al. (22) and Bohle et al. (23) observed a negative correlation between the number of peritubular capillaries and renal function. We observed alterations in vascular bundles (**Figure 1**). Atrophic papilla and the presence of hydronephrosis and tubular dilation were characteristic of disruption of renal development by RAS blockade (4, 24). Calcitriol treatment attenuated these effects, likely through promotion of cell proliferation and differentiation. We previously showed that animals at 21 days postnatal exposed to losartan during lactation showed abnormalities in renal function, structure, hydronephrosis, and increased expression of mesenchymal markers (7, 20). Mecawi et al. (25) also observed hydronephrosis in animals exposed to captopril, an ACE (angiotensin-converting enzyme) inhibitor, characterized by distension and dilation of the renal pelvis. Based on these findings, hydronephrosis and alterations in medullar structure and function resulting from RAS inhibition were modulated, in part, by calcitriol. Morphometric changes have been previously evaluated only in the cortical region. The structures evaluated in previous studies included glomeruli, tubules, and cortical renal interstitium (5, 7, 20). As the RAS is important for renal development and AT_1 receptor blockade induced rarefaction of renal vessels in the outer and inner medullas, the aim of our study was to evaluate changes in the medullary region and to correlate structural abnormalities with functional changes, and to evaluate the ability of calcitriol to mitigate these changes. In this study, we showed representative histological sections from kidneys of rats treated with sucrose or losartan and saline or calcitriol at lower magnification for visualization of papillary atrophy and hydronephrosis. All animals in the losartan group showed significant papillary atrophy, and treatment with calcitriol mitigated this atrophy. However, calcitriol treatment did not restore renal function in this model.

Alpha-smooth muscle actin is only present on arterioles and vessel walls in healthy animals (7, 26). In a ureteral obstruction model, calcitriol treatment reduced renal interstitial fibrosis and α-SMA expression, and preserved cell—cell interactions and epithelial phenotype, which resulted in suppression of fibrotic factors (27). The RAS is important in establishment of cell—cell interactions and interactions with the extracellular matrix (28). The lack of differentiation of medullary renal tubules induced by losartan was less pronounced in the group that received calcitriol, which showed that vitamin D was important in restoring cellular differentiation (5, 29, 30). Under normal conditions, vimentin, a component of the cytoskeleton, is present in glomerular epithelial cells and vessel walls (7). However, vimentin is only present in tubular cells in adulthood when differentiation, or cell proliferation, does not occur. Blockade of the AT_1 receptor during renal development is associated with changes in α-SMA and vimentin expression in renal tissue, and results in lack of cell differentiation. Therefore, these proteins have been used as markers of impaired differentiation (5, 7, 20). Calcitriol treatment reduced vimentin expression in the outer medullas of the LOS group, and resulted in reduced mesenchymal cell expression. These results were consistent with those observed in other studies (5, 14, 31). These findings indicated that epithelial to mesenchymal transition (EMT) occurred in response to losartan, resulting in development of myofibroblasts. Tan et al. (27) showed that

paricalcitol treatment reduced EMT, as evidenced by decreased mesenchymal markers in a model of obstructive nephropathy. Vitamin D acts by inhibiting the Snail transcription factor (involved in EMT programming) and restoring VDR (vitamin D receptor) expression.

We also showed that exposure to losartan resulted in development of renal vasculature disorders that were attenuated by calcitriol. We observed lack of differentiation of endothelial cells, as evidenced by reduced expression of JG12, a marker of blood vessel endothelial cells with greater specificity than the common endothelial markers CD34 and CD31, which are present in blood and lymphatic vessels (32). The reduced expression of eNOS in the renal medullas of animals exposed to losartan resulted in disturbances in endothelial function and structure that were attenuated by calcitriol treatment. These findings demonstrate that calcitriol could modulate cell differentiation and vascular function. Yoo et al. (4) reported decreased JG12 expression in rats exposed to an ACE inhibitor for 8 days after birth. Several clinical and experimental studies have shown that vitamin D can confer endothelial protection (5, 6, 9, 33, 34). A previous study showed that vitamin D deficiency could induce changes in peritubular capillaries, resulting in reduced capillary density (6). Several clinical and experimental studies have shown that vitamin D induces beneficial effects on endothelial cells (31). Use of vitamin D has also been shown to affect smooth muscle cell proliferation and positive impact on cardiovascular disease (31). These findings showed that vitamin D increased the number and function of endothelial cells. We observed increases in the expression of JG12 and eNOS in the inner medullas of animals treated with calcitriol in adulthood compared with animals treated with losartan alone. The effect of calcitriol on neovasculogenesis has not been characterized, but it has been shown to promote cell differentiation and proliferation, and to positively affect endothelial function and structure.

Rats in the LOS + Calcitriol group exhibited increased NO production. Nitric oxide is involved in endothelial vascular growth factor signaling. These angiogenic pathways are coordinated by ANGII during kidney development under normal physiological conditions and are activated by eNOS-induced Akt/PI3K signaling (35) and endothelial NO production. Phosphorylation of eNOS by Akt resulted in activation, and increased production of NO. (36). *In vitro* and *in vivo* studies have shown that increased eNOS activity resulted in endothelial cell proliferation and migration, and increased angiogenesis (37, 38). Increased NO production in the LOS + Calcitriol group compared to that in the LOS group have resulted in decreased vasoconstriction induced by reduced AT_1 receptor activity in renal tissue from these animals. Decreased NO in the SUC + Calcitriol group may have been an artifact of small sample size. The expression of eNOS in the outer and inner medulla was equivalent between the SUC and SUC + Calcitriol groups. Previous studies have shown that vitamin D supplementation improved endothelial function in patients with chronic kidney disease (39). This effect was due to increased expression and activity of eNOS, which resulted in increased NO production (40, 41). Shear stress is reduced in chronic kidney disease due to reduced production of NO and growth factors such as VEGF and VEGFR2 (vascular endothelial growth factor and vascular endothelial growth factor receptor 2). Reduced shear stress results in induction of programmed cell death, resulting in a pro-inflammatory environment that contributes to reduced vascular density (42). Activated vitamin D can preserve the microvasculature and improve capillary blood flow and tissue perfusion (42), each of which were impaired following exposure to losartan during lactation. Recently, our group showed that vitamin D was important in maintenance of the renal microvasculature and played a key role in maintenance of homeostasis of growth factors such as VEGF and angiopoietins (angpt-1 and angpt-2), and the Tie-2 receptor (43).

The expression of the AT_1 receptor was increased in the LOS group, likely due to a compensatory mechanism resulting from recovery of RAS activity. This is particularly interesting because exposure to losartan during lactation resulted in alterations that persisted into adulthood despite recovery of RAS signaling. This demonstrated that fetal programming was critical to development of hypertension. Calcitriol treatment mitigated LOS-induced increases in ANGII cortical expression (5). This resulted from increased AT_2 receptor stimulation (21). Losartan treatment increased AT1 receptor expression which, after losartan withdrawal, reacted with increased cortical angiotensin II levels and that these effects were modulated by calcitriol. Blockade of AT_1 disrupted the balance between proliferation and apoptosis, which resulted in altered renal structure. Calcitriol mitigated these microvasculature disturbances, which resulted in improved cell differentiation and function.

In conclusion, the present study showed that calcitriol treatment attenuated disturbances in endothelial function and inner medulla structure induced by losartan treatment during lactation. Calcitriol contributed to maintenance of the renal microvasculature in the outer and inner medullas of rats exposed to AT_1 blockade during lactation, improved cellular differentiation, as evidenced by evaluation of α-SMA and vimentin. Calcitriol treatment also improved renal function and structure. Our study highlighted the importance of the renal medulla in development of proper kidney function.

DATA AVAILABILITY STATEMENT

All datasets generated for this study are included in the article/supplementary material.

ETHICS STATEMENT

The animal study was reviewed and approved by Animal Experimentation Committee of the University of São Paulo at Ribeirão Preto Medical School approved the study protocol (COBEA/CETEA/FMRP-USP, protocol no. 178/2014).

AUTHOR CONTRIBUTIONS

AD, LA, HF, and CS contributed to the design of the experiments. The manuscript was written by AD and LA. TC supervised the study. RC performed histology and immunohistochemical

staining. JA-R performed the NO/Ozone analyses. All authors contributed to review and approval of the manuscript.

FUNDING

This work was funded by the Fundação de Amparo à Pesquisa do Estado de São Paulo (FAPESP, grant number 2017/07118-8), the Conselho Nacional de Desenvolvimento Científico e Tecnológico (CNPq, grant number 302516/2017-4), and the Coordenação de Aperfeiçoamento de Pessoal de Nível Superior—Brasil (CAPES)—Finance Code 001.

ACKNOWLEDGMENTS

The authors would like to thank Milene Mantovani for assisting with nitric oxide analysis.

REFERENCES

1. Madsen K, Tinning AR, Marcussen N, Jensen BL. Postnatal development of the renal medulla; the role of the renin-angiotensin system. *Acta Physiol*. (2013) 208:41–9. doi: 10.1111/apha.12088
2. Herzlinger D, Hurtado R. Patterning the renal vascular bed. *Semin Cell Dev Biol*. (2014) 36:50–6. doi: 10.1016/j.semcdb.2014.08.002
3. Madsen K, Marcussen N, Pedersen M, Kjærsgaard G, Facemire C, Coffman TM, et al. Angiotensin II promotes development of the renal microcirculation through AT1 receptors. *J Am Soc Nephrol*. (2010) 21:448–59. doi: 10.1681/ASN.2009010045
4. Yoo KH, Yim HE, Bae ES, Hong YS. Capillary rarefaction and altered renal development: the imbalance between pro- and anti-angiogenic factors in response to angiotensin II inhibition in the developing rat kidney. *J Mol Histol*. (2018) 49:219–28. doi: 10.1007/s10735-018-9762-7
5. de Almeida LF, Francescato HDC, da Silva CGA, Costa RS, Coimbra TM. Calcitriol reduces kidney development disorders in rats provoked by losartan administration during lactation. *Sci Rep*. (2017) 7:11472. doi: 10.1038/s41598-017-11815-8
6. Almeida LF, Francescato HDC, Silva RS, Silva CGA, Antunes-Rodrigues J, de Paula FJA, et al. Renal developmental disturbances and their long-term consequences in female pups from vitamin D-deficient mothers: involved mechanisms. *J Dev Orig Health Dis*. (2019) 10:497–501. doi: 10.1017/S2040174418000909
7. Marin EC, Francescato HD, da Silva CG, Costa RS, Coimbra TM. Postnatal renal abnormalities in rats exposed to losartan during lactation. *Nephron Exp Nephrol*. (2011) 119:e49–57. doi: 10.1159/000328337
8. Spence SG, Zacchei AG, Lee LL, Baldwin CL, Berna RA, Mattson BA, et al. Toxicokinetic analysis of losartan during gestation and lactation in the rat. *Teratology*. (1996) 53:245–52. doi: 10.1002/(SICI)1096-9926(199604)53:4<245::AID-TERA7>3.0.CO;2-1
9. Tarcin O, Yavuz DG, Ozben B, Telli A, Ogunc AV, Yuksel M, et al. Effect of vitamin D deficiency and replacement on endothelial function in asymptomatic subjects. *J Clin Endocrinol Metab*. (2009) 94:4023–30. doi: 10.1210/jc.2008-1212
10. DeLuca HF. Vitamin D: historical overview. *Vitam Horm*. (2016) 100:1–20. doi: 10.1016/bs.vh.2015.11.001
11. Li YC, Kong J, Wei M, Chen ZF, Liu SQ, Cao LP. 1,25-dihydroxyvitamin D (3) is a negative endocrine regulator of the renin-angiotensin system. *J Clin Invest*. (2002) 110:229–38. doi: 10.1172/JCI0215219
12. Marcondes FK, Bianchi FJ, Tanno AP. Determination of the estrous cycle phases of rats: some helpful considerations. *Braz J Biol*. (2002) 62:609–14. doi: 10.1590/S1519-69842002000400008
13. Reis NG, Francescato HDC, de Almeida LF, Silva CGAD, Costa RS, Coimbra TM. Protective effect of calcitriol on rhabdomyolysis-induced acute kidney injury in rats. *Sci Rep*. (2019) 9:7090. doi: 10.1038/s41598-019-43564-1
14. Panichi V, Migliori M, Taccola D, Filippi C, De Nisco L, Giovannini L, et al. Effects of 1,25(OH)2D3 in experimental mesangial proliferative nephritis in rats. *Kidney Int*. (2001) 60:87–95. doi: 10.1046/j.1523-1755.2001.00775.x
15. Alvarez V, Quiroz Y, Nava M, Pons H, Rodriguez-Iturbe B. Overload proteinuria is followed by salt-sensitive hypertension caused by renal infiltration of immune cells. *Am J Physiol Renal Physiol*. (2002) 283:F1132–41. doi: 10.1152/ajprenal.00199.2002
16. Hampl V, Walters CL, Archer SL. Determination of nitric oxide by the chemiluminescence reaction with ozone. In: Feelisch M, Stamler JS, editors. *Methods in Nitric Oxide Research*. New York, NY: John Wiley and Sons (1996). p. 309–18.
17. Bradford MM. A rapid and sensitive method for the quantitation of microgram quantities of protein utilizing the principle of protein-dye binding. *Anal Biochem*. (1976) 72:248–54. doi: 10.1016/0003-2697(76)90527-3
18. Kliem V, Johnson RJ, Alpers CE, Yoshimura A, Couser WG, Koch KM, et al. Mechanisms involved in the pathogenesis of tubulointerstitial fibrosis in 5/6-nephrectomized rats. *Kidney Int*. (1996) 49:666–78. doi: 10.1038/ki.1996.95
19. Guron G, Nilsson A, Nitescu N, Nielsen S, Sundelin B, Frøkiaer J, et al. Mechanisms of impaired urinary concentrating ability in adult rats treated neonatally with enalapril. *Acta Physiol Scand*. (1999) 165:103–12. doi: 10.1046/j.1365-201x.1999.00477.x
20. Tufro-McReddie A, Romano LM, Harris JM, Ferder L, Gomez RA. Angiotensin II regulates nephrogenesis and renal vascular development. *Am J Physiol*. (1995) 269:F110–5. doi: 10.1152/ajprenal.1995.269.1.F110
21. Balbi APC, Marin ECS, Francescato, HDC, Costa RS, Coimbra TM. MAPK and angiotensin II receptor in kidney of newborn rats from losartan-treated dams. *Pediatr Nephrol*. (2008) 23:1433–44. doi: 10.1007/s00467-008-0830-1
22. Serón D, Alexopoulos E, Raftery MJ, Hartley B, Cameron JS. Number of interstitial capillary cross-sections assessed by monoclonal antibodies: relation to interstitial damage. *Nephrol Dial Transplant*. (1990) 5:889–93. doi: 10.1093/ndt/5.10.889
23. Bohle A, Mackensen-Haen S, Wehrmann M. Significance of postglomerular capillaries in the pathogenesis of chronic renal failure. *Kidney Blood Press Res*. (1996) 19:191–5. doi: 10.1159/000174072
24. Tinning AR, Jensen BL, Johnsen I, Chen D, Coffman TM, Madsen K. Vascular endothelial growth factor signaling is necessary for expansion of medullary microvessels during postnatal kidney development. *Am J Physiol Renal Physiol*. (2016) 311:F586–99. doi: 10.1152/ajprenal.00221.2016
25. Mecawi AS, Araujo IG, Rocha FF, Coimbra TM, Antunes-Rodrigues J, Reis LC. Ontogenetic role of angiontensin-converting enzyme in rats: thirst and sodium appetite evaluation. *Physiol Behav*. (2010) 99:118–24. doi: 10.1016/j.physbeh.2009.10.018
26. Yim HE, Yoo KH, Bae ES, Hong YS, Lee JW. Impaired angiogenesis in the enalapril-treated neonatal rat kidney. *Korean J Pediatr*. (2016) 59:8–15. doi: 10.3345/kjp.2016.59.1.8
27. Tan X, Li Y, Liu Y. Paricalcitol attenuates renal interstitial fibrosis in obstructive nephropathy. *J Am Soc Nephrol*. (2006) 17:3382–93. doi: 10.1681/ASN.2006050520
28. Marchesi C, Paradis P, Schiffrin EL. Role of the renin-angiotensin system in vascular inflammation. *Trends Pharmacol Sci*. (2008) 29:367–74. doi: 10.1016/j.tips.2008.05.003
29. Samuel S, Sitrin MD. Vitamin D's role in cell proliferation and differentiation. *Nutr Rev*. (2008) 66(10 Suppl. 2):S116–24. doi: 10.1111/j.1753-4887.2008.00094.x
30. Fujita H, Sugimoto K, Inatomi S, Maeda T, Osanai M, Uchiyama Y, et al. Tight junction proteins claudin-2 and−12 are critical for vitamin D-dependent Ca2+ absorption between enterocytes. *Mol Biol Cell*. (2008) 19:1912–21. doi: 10.1091/mbc.e07-09-0973
31. Cardus A, Panizo S, Encinas M, Dolcet X, Gallego C, Aldea M, et al. 1,25-dihydroxyvitamin D3 regulates VEGF production through a vitamin D response element in the VEGF promoter. *Atherosclerosis*. (2009) 204:85–9. doi: 10.1016/j.atherosclerosis.2008.08.020
32. Matsui K, Nagy-Bojarsky K, Laakkonen P, Krieger S, Mechtler K, Uchida S et al. Lymphatic microvessels in the rat remnant kidney model of renal

fibrosis: aminopeptidase p and podoplanin are discriminatory markers for endothelial cells of blood and lymphatic vessels. *J Am Soc Nephrol*. (2003) 14:1981–9. doi: 10.1097/01.ASN.0000076078.50889.43
33. Tare M, Emmett SJ, Coleman HA, Skordilis C, Eyles DW, Morley R, et al. Vitamin D insufficiency is associated with impaired vascular endothelial and smooth muscle function and hypertension in young rats. *J Physiol*. (2011) 589(Pt 19):4777–86. doi: 10.1113/jphysiol.2011.214726
34. Helle F, Iversen BM, Chatziantoniou C. Losartan increases NO release in afferent arterioles during regression of L-NAME-induced renal damage. *Am J Physiol Renal Physiol*. (2010) 298:F1170–7. doi: 10.1152/ajprenal.00056.2009
35. Feliers D, Chen X, Akis N, Choudhury GG, Madaio M, Kasinath BS. VEGF regulation of endothelial nitric oxide synthase in glomerular endothelial cells. *Kidney Int*. (2005) 68:1648–59. doi: 10.1111/j.1523-1755.2005.00575.x
36. Babaei S, Stewart DJ. Overexpression of endothelial NO synthase induces angiogenesis in a co-culture model. *Cardiovasc Res*. (2002) 55:190–200. doi: 10.1016/S0008-6363(02)00287-0
37. Bach MH, Sadoun E, Reed MJ. Defects in activation of nitric oxide synthases occur during delayed angiogenesis in aging. *Mech Ageing Dev*. (2005) 126:467–73. doi: 10.1016/j.mad.2004.10.005
38. Francescato HDC, Almeida LF, Reis NG, Faleiros CM, Papoti M, Costa RS, et al. Previous exercise effects in cisplatin-induced renal lesions in rats. *Kidney Blood Press Res*. (2018) 43:582–93. doi: 10.1159/000488964
39. Zoccali C, Curatola G, Panuccio V, Tripepi R, Pizzini P, Versace M, et al. Paricalcitol and endothelial function in chronic kidney disease trial. *Hypertension*. (2014) 64:1005–11. doi: 10.1161/HYPERTENSIONAHA.114.03748
40. Vanhoutte PM, Shimokawa H, Feletou M, Tang EH. Endothelial dysfunction and vascular disease - a 30th anniversary update. Acta Physiol. (2017) 219:22-96. doi: 10.1111/apha.12646
41. Ballermann BJ, Obeidat M. Tipping the balance from angiogenesis to fibrosis in CKD. *Kidney Int Suppl*. (2011) 4:45–52. doi: 10.1038/kisup.2014.9
42. Lundwall K, Jörneskog G, Jacobson SH, Spaak J. Paricalcitol, microvascular and endothelial function in non-diabetic chronic kidney disease: a randomized trial. *Am J Nephrol*. (2015) 42:265–73. doi: 10.1159/000441364
43. Almeida LF, Francescato HDC, Antunes-Rodrigues J, de Paula FJA Silva RS, Silva CGA, Costa RS et al. Imbalance of pro- and anti-angiogenic factors due to maternal vitamin D deficiency causes renal microvasculature alterations affecting the adult kidney function. *Nutrients*. (2019) 11:1929. doi: 10.3390/nu11081929

Conflict of Interest: The authors declare that the research was conducted in the absence of any commercial or financial relationships that could be construed as a potential conflict of interest.

Copyright © 2020 Deluque, de Almeida, Francescato, da Silva, Costa, Antunes-Rodrigues and Coimbra. This is an open-access article distributed under the terms of the Creative Commons Attribution License (CC BY). The use, distribution or reproduction in other forums is permitted, provided the original author(s) and the copyright owner(s) are credited and that the original publication in this journal is cited, in accordance with accepted academic practice. No use, distribution or reproduction is permitted which does not comply with these terms.

frontiers in Pharmacology

ORIGINAL RESEARCH
published: 11 February 2020
doi: 10.3389/fphar.2020.00044

Protective Effects of Amlodipine Pretreatment on Contrast-Induced Acute Kidney Injury And Overall Survival In Hypertensive Patients

Wen-jun Yin[1], *Ling-yun Zhou*[1], *Dai-yang Li*[1], *Yue-liang Xie*[1], *Jiang-lin Wang*[1], *Shan-ru Zuo*[1], *Kun Liu*[1], *Can Hu*[1], *Ge Zhou*[1], *Lin-hua Chen*[1], *Hui-qing Yang*[1] *and Xiao-cong Zuo*[1,2]*

[1] Department of Pharmacy, The Third Xiangya Hospital of Central South University, Changsha, China, [2] Center of Clinical Pharmacology, The Third Xiangya Hospital of Central South University, Changsha, China

OPEN ACCESS

Edited by:
Xueying Zhao,
Morehouse School of Medicine,
United States

Reviewed by:
Elena Lazzeri,
University of Florence, Italy
Guangbi Li,
Virginia Commonwealth University,
United States

***Correspondence:**
Xiao-cong Zuo
zuoxc08@126.com

Specialty section:
This article was submitted to Renal Pharmacology, a section of the journal Frontiers in Pharmacology

Received: 02 September 2019
Accepted: 14 January 2020
Published: 11 February 2020

Citation:
Yin W-j, Zhou L-y, Li D-y, Xie Y-l, Wang J-l, Zuo S-r, Liu K, Hu C, Zhou G, Chen L-h, Yang H-q and Zuo X-c (2020) Protective Effects of Amlodipine Pretreatment on Contrast-Induced Acute Kidney Injury And Overall Survival In Hypertensive Patients. Front. Pharmacol. 11:44. doi: 10.3389/fphar.2020.00044

Backgroud: Contrast-induced acute kidney injury (CI-AKI) is the most common adverse reaction caused by contrast media, which has been reported to prolong hospitalization and increase mortality and morbidity. The hypertensive population has proved susceptible to CI-AKI. Unfortunately, no therapeutic has been shown to prevent and cure CI-AKI effectively. A few studies have shown the protection of amlodipine on renal function, but the relationship between amlodipine and CI-AKI in hypertensive group is unknown, we aimed to study the effects of amlodipine on CI-AKI and overall survival in a large Chinese hypertensive cohort.
Methods: A retrospective, matched, cohort study was conducted among adults hospitalized at the Third Xiangya Hospital of Central South University from October 2007 to May 2017. CI-AKI was the primary end point of the trial, time-related all-cause mortality (including in-hospital) and length of hospital stay were the secondary end points. Propensity Score Matching was used to reduce the effect of selection bias and potential confounding.
Results: 868 patients with and 1,798 ones without amlodipine before contrast administration were included. The incidence of CI-AKI was 10.50%. The unadjusted, adjusted, and propensity-score matched incidence of CI-AKI were lower in patients treated with amlodipine (OR, 0.650; P = 0 .003; OR, 0.577; P = 0.007; OR, 0.687; P = 0.015, respectively), and the same results were found in the subgroups of diabetes, chronic kidney disease (CKD), non-CKD, low-osmolar, and elderly. Moreover, amlodipine reduced hospital stay, whether matched or not (7.08 ± 7.28 vs 7.77 ± 7.82, P = 0.027, before matching; vs 7.81 ± 7.58, P = 0.040, after matching). 1,046 patients finished follow-up including 343 amlodipine users and 703 non-users. The overall mortality was significantly lower among amlodipine users (10.79%) than controls (16.07%), the significant difference was found in survival between them (P = 0.024, log-rank test), amlodipine was associated with longer overall survival [HR, 0.623; 95% CI (0.430–0.908), P = 0.014].

Conclusion: In conclusion, we first found amlodipine treatment before contrast exposure played a role in protecting hypertensive patients from CI-AKI and prolonging survival.

Keywords: contrast media, contrast-induced acute kidney injury, acute kidney injury, risk factor, amlodipine, hypertension

INTRODUCTION

Contrast-induced acute kidney injury (CI-AKI) is the most common clinical complication of the intravascular administration of contrast media (CM) which can prolong hospitalization and increase morbidity and mortality. (Tepel et al., 2006) What's more, CI-AKI has become the third prevalent cause of all hospital-acquired renal failure, accounting for 10%. (Nash et al., 2002) According to the Contrast Media Safety Committee, CI-AKI was defined as an increase in serum creatinine (Scr) of 0.5 mg/dl (44.2 μmol/L) or 25% relative increase in Scr from the baseline value to 72 hours after exposure to CM.

Unfortunately, there is no strategy to effectively prevent and cure CI-AKI. Therefore, we should attach significance to identifying high-risk CI-AKI groups for earlier preventive measures as soon as possible to reduce CI-AKI. Hypertension is also a major risk factor of CI-AKI and increases the risk of two times, (Bartholomew et al., 2004) and it is a leading cause of chronic kidney disease (CKD), kidney disease progression, and end-stage kidney disease. (Klag et al., 1996; Fox et al., 2004; Carey et al., 2018) According to the 2015 Report on the Status of Nutrition and Chronic Diseases in China, the incidence of hypertension is greatly high, approximately 25.2% of adults suffer from hypertension. (Zhang et al., 2017) Although the hypertensive population is a huge group with high-risk of CI-AKI, CI-AKI in hypertensive patients has not been studied.

The precise mechanisms underlying CI-AKI are not well understood. However, the toxicity effect of CM on the tubular epithelial cells due to apoptosis has been reported to be related to the pathogenesis of CI-AKI. And the apoptosis of renal vasoconstriction and tubular induced by CM have been considered relevant to changes in calcium physiology. (Neumayer et al., 1989; Russo et al., 1990; Yang et al., 2008; Yang et al., 2013) Intracellular calcium overload followed by reactive oxygen species overproduction and caspase-3 overexpression was found to play a key role in renal tubular cytotoxicity induced by CM. (Duan et al., 2000) Although the physiological and pathophysiological mechanisms of Ca^{2+} overload in ischemic kidney and CI-AKI have not been fully elucidated, there is evidence that the increase of Ca^{2+} in cytoplasm may be an important mediator of epithelial cell apoptosis and necrosis. (Wilson et al., 1984) Therefore, in theory, calcium channel blockers (CCB) can selectively block Ca^{2+} channels in cell membranes, prevent Ca^{2+} from entering cells, and have a protective effect on CI-AKI.

Amlodipine, one of the most common used CCB drugs, is a dihydropyridine CCB that inhibits the slow channel transmembrane influx of calcium ions into vascular smooth muscle and into cardiac muscle with fewer side effects and a longer half-life than most antihypertensives, enabling once-daily dosing (Haria and Wagstaff, 1995). Some studies have shown that amlodipine has a protective effect on the kidney. In basic experimental study, amlodipine can inhibit the HKC apoptosis and protect the renal tubule cell from injury induced by meglumine diatrizoate, in the amlodipine group, the cell viability increased significantly, LDH levels decreased, and the apoptosis was lower than that of the model group, Bax protein expression and caspase 3 activity decreased. (Zhou et al., 2007) Duan et al. found calcium load played a role in producing renal function impairment induced by diatrizoate meglumine, and amlodipine protected the renal tissue from nephrotoxicity induced by diatrizoate. (Duan et al., 2000) Combined aliskiren and amlodipine reduced albuminuria via reduction in renal inflammation in diabetic rats. In clinical research, amlodipine offers protection against CI-AKI in elderly patients with coronary heart disease, (Owen et al., 2014) and the combination therapy with amlodipine and atorvastatin may exert additional beneficial effects on renal and vascular damages as well as blood pressure (BP) profile in addition to BP lowering in hypertension with CKD. (Azushima et al., 2014) However, it is unclear whether amlodipine can protect CI-AKI in hypertensive population and the long-term outcome of amlodipine in hypertensive population with contrast administration.

The purpose of this study was to determine the effect of amlodipine before contrast exposure on the CI-AKI and overall survival in a large Chinese hypertensive cohort.

MATERIALS AND METHODS

Ethics Statement

The Medical Ethical Committee in the Third Xiangya Hospital of Central South University approved this study (No. 2016-S160). All subjects were anonymized, thus the provision of informed consent was not required. This study complied with the ethical guidelines of the 1975 Declaration of Helsinki and Strengthening the Reporting of Observational Studies in Epidemiology guidelines.

Patient Population

A retrospective, matched, cohort study was conducted among adults hospitalized at the Third Xiangya Hospital of Central South University from October 2007 to May 2017. Patients were included if they were administered with CM procedure including coronary angiography, percutaneous coronary intervention, received intravenous CM such as for enhanced CT and intravascular surgery, and their admitting diagnosis is recognized as "hypertension", identified by the electronic medical record system. Patients with the following conditions were excluded: 1) preprocedure estimated glomerular filtration rate (eGFR) under 15 ml/(min 1.73 m^2); 2) treated with CCB drugs other than amlodipine

or levamlodipine; 3) the dosage regimen is not 2.5 mg/qd for levamlodipine or not 5.0 mg/qd for amlodipine; 4) age ≤ 18. Their detailed demographic and clinical characteristics were obtained from the structured hospital information system of The Third Xiangya Hospital (Changsha, China) included demographics, baseline and postoperative Scr, preoperative hemoglobin, diastolic blood pressure, systolic blood pressure, complication, discharge diagnosis, Killip scores, and medications included diuretic, ACEI, ARB, βblockers, aspirin, and alprostadil. In the survival analysis, we excluded the patients with missing or replacing telephone numbers and who refused to be followed up.

Study End Points and Definitions

The primary end point of the trial was the incidence of CI-AKI, the secondary end point was time-related all-cause mortality (including in- hospital) and length of hospital stay. CI-AKI was defined as an increase in Scr of 0.5 mg/dl (44.2 μmol/L) or 25% relative increase in Scr from the baseline value to 72 hours after exposure to CM in the absence of alternative causes for acute kidney injury. The earliest Scr concentration within 14 days prior to contrast was defined as baseline, and the highest Scr concentration within 72 hours after contrast was used as follow-up Scr to evaluate the incidence of CI-AKI. CKD was defined as eGFR < 60 ml/(min 1.73 m^2) calculated by the Modification of Diet in Renal Disease equation. (Matsushita et al., 2012; Palevsky et al., 2013) Anemia was defined as hemoglobin concentration <13 g/dl for men and <12 g/dl for women. (Nutritional Anaemias, 1968) The aged were equal to those over 60 years old.

Statistical Analysis

All of the analyses were performed using IBM SPSS Version 22.0 (SPSS, Inc., Chicago, IL) and R (version3.5.1). Continuous variables were presented as means and standard deviations (SDs). A t-test was used to compare the normally distributed continuous variables; otherwise, the Mann-Whiney U-test was performed. Categorical variables were performed by chi-squared test. Logistic regression analysis was performed to evaluate the efficacy of amlodipine treatment on CI-AKI, adjusting for various potential prognostic and confounding factors. A two-tailed value of $P < 0.05$ was established as the threshold of statistical significance.

In order to reduce the impact of selection bias and potential confounding in this study, we rigorously adjusted the differences in renal function and diabetes mellitus, which has been reported as independent risk factors for CI-AKI, by propensity score analysis between the two groups (amlodipine and no amlodipine) to assess the outcomes of CI-AKI. Propensity scores were calculated using logistic regression of age, sex, CKD, diabetes, baseline Scr, baseline GFR, since renal insufficiency and diabetes were reported as independent risk factors of CI-AKI in the previous studies. Propensity Score Matching is a technique that attempts to approximate a random experiment, eliminating many of the problems and reducing the bias due to confounding variables that come with observational data analysis by matching treated patients to controls that were similarly likely in the same group. The possibility of bias occurs because some characteristics instead of the effect of the treatment decides the apparent difference in outcome between these two groups that received the treatment versus those that did not. The randomization enables agonic estimation of curative effects in randomized experiments; according to the law of large numbers, randomization means that treatment-groups will be balanced on average on each covariate. While in observational studies, the treatments to research subjects are usually assigned at nonrandom. In order to imitate randomization, a unit sample which received the treatment that is equivalent on all observed covariates to a unit sample that did not receive the treatment is created by matching. (Ho et al., 2007) In this study, propensity matching was performed with a 1:1 genetic matching for case and control subjects in which the nearest neighbor was selected. (Diamond and Sekhon, 2013) The comparative risk of outcome was further adjusted for a conditional logistic-regression model, the adjusted variables included age, sex, body mass index (BMI), baseline eGFR, Scr, CKD, diabetes, Killip III, systolic blood pressure (SBP), diastolic blood pressure (DBP), hyperlipidemia, anemia, aspirin, diuretic, angiotensin-converting enzyme inhibitors (ACEI), angiotensin receptor blockers (ARB), β blockers, and alprostadil. To further study the reliability of the results, we also carried out subgroup analysis in CKD, diabetes, and the aged population. In addition, the effects of amlodipine dosage and duration were studied.

All patients were followed up until occurrence of death, end of the study period, or loss to follow-up. Time to all-cause mortality was analyzed using Cox proportional hazards models in our cohorts and hazard ratios with 95% CIs were estimated adjusting for baseline stratification factors. Survival time was calculated as time from contrast administration to death, loss to follow-up, or end of study period. Survival time was censored on December 26, 2018 or at the time a patient was lost to follow-up. The association of amlodipine and death were obtained by using Kaplan–Meier curves over the entire study period. Hazard ratios and odds ratios were reported relative to study participants without amlodipine.

RESULTS

Patient Characteristics

Among a total of initial 5,379 hypertensive patients with contrast administration, there were 3 juveniles (<18 years), 2,088 treated with CCB drugs other than amlodipine or levamlodipine, 229 with preprocedure eGFR under 15 ml/(min 1.73 m^2), and 392 without the dosage regimen of 2.5 mg/qd for levamlodipine or 5.0 mg/qd for amlodipine. After excluding the above-mentioned participants 2,666 patients were enrolled in the final analysis. The mean age of the total population was 63.53±9.45 years, and 1,647 (61.78%) of them were males. Of these, 868 patients received amlodipine (including levamlodipine) and 1,798 controls were selected. With the use of propensity score matching, 868 matched controls were identified. **Figure 1** showed the number of patients included in analysis after applying for exclusion

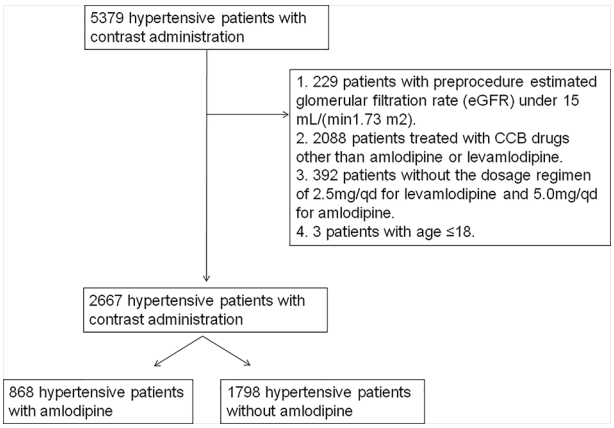

FIGURE 1 | Flow chart depicting number of patients who were included in analysis after exclusion criteria.

criteria. The baseline characteristics of the study population separated by amlodipine, controls, and matched controls are presented in **Table 1**. The Scr levels were significantly higher prior to matching and the CKD, diabetes, and male were significant prevalent in the amlodipine group in comparison to controls. After matching, these differences between the two groups were reduced. About 70% of patients used low-osmolar, 17% used iso-osmolar in this cohort.

Association Between Amlodipine and CI-AKI

The primary endpoint of CI-AKI occurred in 280 (10.50%) of the 2,667 group. The incidence of CI-AKI was significantly lower in amlodipine group (7.95%, 69 of 868, vs 11.74%, 211 of 1,798; $P = 0.003$). After matching, the same results were obtained between the amlodipine group and matched group (7.95%, 69 of 868, vs 11.87%, 103 of 868; $P = 0.006$). There was no significant difference between the two groups in the postoperative Scr levels between the two groups with or without matching. As is shown in the **Table 2**, amlodipine was associated with a significant shorten in hospital stay (7.08 ± 7.28 vs 7.77 ± 7.82; $P = 0.027$), and propensity score matching got the same result (7.08 ± 7.28 vs 7.81 ± 7.58; $P = 0.040$).

In the unadjusted model analysis, amlodipine reduced the risk of CI-AKI compared with controls [OR, 0.650; 95% confidence interval (CI), 0.489–0.864; $P = 0.003$], and this protection remained consistent after adjusting for baseline demographic characteristics, disease incidence, laboratory examination, and medication (OR, 0.687; 95% CI, 0.508–0.930; $P = 0.015$). After propensity score matching, amlodipine showed the same protection of CI-AKI whether using the unadjusted (OR, 0.577; 95% CI, 0.508–0.930; $P = 0.007$) or adjusted analysis (OR, 0.568; 95% CI, 0.402–0.802; $P < 0.001$, **Figure 2**). The multivariable logistic regression analysis also revealed that after amlodipine, age (OR, 1.204; $P = 0.001$), sex (OR, 0.748; $P < 0.001$), GFR (OR, 1.029; $P < 0.001$), Scr (OR, 1.010; $P < 0.001$), CKD (OR, 1.622; $P = 0.046$), DBP (OR, 0.990; $P = 0.011$), diuretic (OR, 2.077;

TABLE 1 | Baseline characteristics before and after propensity-score matching.

Characteristic	Amlodipine group (n = 868)	Control group (n = 1,798)	Matched control group (n = 868)	P_1	P_2
Age					
Mean (years)	63.66±9.51	63.46±9.45	63.79±9.92	0.613	0.778
Distribution					
<60 years	203 (23.39%)	696 (38.54%)	242 (27.88%)		
≥60 years	665 (76.61%)	1,102 (61.29%)	626 (72.12%)	<0.001	0.032
Sex (%)					
Male	537 (61.87%)	1,110 (61.74%)	542 (62.44%)	0.032	0.850
Female	331 (38.13%)	688 (38.26%)	326 (37.56%)		
Body mass index, kg/m^2	24.62±3.45	24.36±3.28	24.34±3.31	0.062	0.094
Scr	94.50±47.75	90.27±47.75	95.50±52.71	0.032	0.693
GFR	82.18±38.48	84.25±38.48	80.48±32.08	0.194	0.377
Contrast type					
Low-osmolar	673 (77.53%)	1,474 (82.39%)	708 (81.57%)	0.007	0.037
Iso-osmolar	151 (17.40%)	298 (16.66%)	152 (17.51%)	0.595	0.950
High-osmolar	1 (0.12%)	26 (1.45%)	8 (0.92%)	0.001	0.019
Diabetes	296 (34.10%)	501 (27.86%)	285 (32.83%)	0.001	0.576
Anemia	352 (40.55%)	823(45.77%)	436 (50.23%)	0.011	<0.001
Hyperlipidemia	92 (10.60%)	136 (7.56%)	73 (8.41%)	0.010	0.088
Killip III	94 (10.83%)	152 (8.45%)	76 (8.76%)	0.109	0.146
Medications					
Diuretic	159 (18.32%)	372 (20.69%)	188 (21.66%)	0.196	0.082
ACEI	417 (48.04%)	776 (43.16%)	380 (43.78%)	0.553	0.068
ARB	174 (20.04%)	227 (12.63%)	104 (11.98%)	<0.001	<0.001
β-blockers	473 (54.49%)	848 (47.16%)	414 (47.70%)	<0.001	0.005
Aspirin	552 (63.59%)	957 (53.23%)	465 (53.57%)	0.003	<0.001
Alprostadil	193 (22.24%)	351 (19.52%)	166 (19.12%)	0.087	0.123

eGFR, estimated glomerular filtration rate; SBP, systolic blood pressure; DBP, diastolic blood pressure; CKD, chronic kidney disease [defined as eGFR <60 mL/(min 1.73 m^2)]; ACEI, angiotensin converting enzyme inhibitor; ARB, angiotensin receptor blocker; CI-AKI, contrast-induced acute kidney injury; P_1, Amlodipine group vs Control group; P_2, Amlodipine group vs Matched control group.

$P < 0.001$), and ACEI (OR, 0.745; $P = 0.035$) were also independent predictors of CI-AKI development (**Figure 3**).

Subgroup Analysis and Duration–Response Analysis

The efficacy of amlodipine on the prevention of incidence of CI-AKI in the subgroups was shown in **Table 3**. Before matching, a significant reduction in CI-AKI was observed in the elderly (OR, 0.571; 95% CI, 0.410–0.794; $P < 0.001$), diabetes groups (OR, 0.598; 95% CI, 0.368–0.969; $P = 0.035$), non-CKD group (OR, 0.654; 95% CI, 0.473–0.905, $P = 0.01$), and low-osmolar group (OR, 0.652; 95% CI 0.475–0.896, $P = 0.008$) but not CKD group (OR, 0.634; 95% CI, 0.349–1.152; $P = 0.132$) and iso-osmolar group (OR, 0.590; 95%, 0.282–1.234; $P = 0.157$). However, after matching, this result was found in the elderly (OR, 0.486; 95% CI, 0.338–0.699; $P < 0.001$) and those with diabetes (OR, 0.549; 95% CI, 0.324–0.930; $P = 0.024$), CKD (OR, 0.480; 95% CI, 0.253–0.911; P=0.023), non-CKD (OR, 0.612; 95% CI, 0.426–0.880, P=0.008), and low-osmolar (OR, 0.554; 95% CI 0.391–0.785, P=0.001), but not in iso-osmolar group (OR, 0.648; 95%, 0.281–1.491; P=0.305). We also investigated the duration–response relationship between duration of amlodipine therapy and risk of CI-AKI (**Figure 4**). It was found that as the duration of amlodipine increased from 3 to 7 days to greater than 7 days, there was a decrease risk of the CI-AKI incidence (11.74%, 9.38%, 7.22%, 6.91%).

Survival Analysis

A total of 1,046 patients were followed up for survival analysis including 343 amlodipine users and 703 non-users, 702 patients failed to follow up because missing or replacing telephone numbers, and 342 patients or family members refused (**Figure 5**). The data regarding overall survival were analyzed at a cutoff date of December 26, 2018, with a median follow-up of 40.85 months. The overall mortality was significantly lower among amlodipine users (10.79%) than controls (16.07%, P=0.028), the significant difference was found in survival between them (P=0.024, log-rank test, **Figure 6**). Upon univariate analysis, amlodipine use before CM was associated with longer overall survival (HR, 0.654; 95% CI, 0.451–0.948; P=0.025, **Table 4**). This trend persisted after adjusting for age, sex, BMI, baseline eGFR, baseline Scr, CKD, and diabetes (HR, 0.623; 95% CI, 0.430–0.908; P=0.014, **Table 4**).

DISCUSSION

For the first time, our present study directly addresses the prevention of amlodipine for CI-AKI in the hypertensive population which is a huge group with high risk of CI-AKI. The major finding of this study was that in patients with hypertension, amlodipine treatment prior to exposure to CM was able to reduce the risk of CI-AKI, before and after propensity matching and additional adjustment, and the same results were found in the diabetes, CKD, and the elderly subgroups. What's more, the treatment with amlodipine resulted in longer overall survival than controls. Moreover, the longer the use of amlodipine, the lower the incidence, but the difference was not significant.

Hypertensives is a huge group in high risk of CI-AKI. Ischemic and hypoxic of kidney has been reported as an important pathogenesis of CI-AKI, leading to inflammation, ischemia, and apoptosis. Hypertension remains a powerful prognostic marker for this condition. (Palit et al., 2015; James et al., 2015) Disorders of vasoactive substances, RAS activation, changes in inflammatory factors, and increased reactive oxygen species were involved in the mechanisms of renal damage caused by hypertension. (Pietri et al., 2015) Endothelial function and arterial stiffness changed with a decrease in nitric oxide (NO) in inflammation-induced hypertension as inflammation inducing available NO decrease in hypertension. (Boos and Lip, 2006) Oxidative stress also appears to be an important feature of NO reduction and is aggravated by an increase in circulating angiotensin II (Ang II) levels. (Hansell et al.,

TABLE 2 | The incidence of CI-AKI and the length of hospital stay in the amlodipine and control group.

Outcome	Amlodipine group (n=868)	Control group (n=1,798)	Matched control group (n=868)	P_1	P_2
CI-AKI	69 (7.95%)	211 (11.74%)	103 (11.87%)	0.003	0.006
Hospital stay	7.08 ± 7.28	7.77 ± 7.82	7.81 ± 7.58	0.027	0.040

CI-AKI, contrast-induced acute kidney injury; P_1, Amlodipine group vs Control group; P_2, Amlodipine group vs Matched control group.

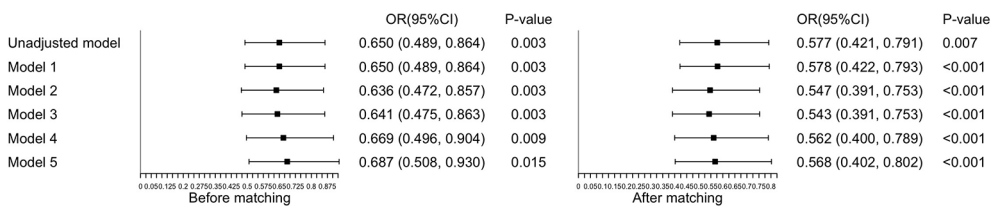

FIGURE 2 | The association between amlodipine and CI-AKI in the adjusted model. Model 1 adjusted for age, sex and BMI. Model 2 adjusted for age, sex, BMI, baseline eGFR and Scr. Model 3 adjusted for age, sex, BMI, baseline eGFR, Scr, CKD and diabetes. Model 4 adjusted for age, sex, BMI, baseline eGFR, Scr, CKD, diabetes, Killip III, SBP, DBP, hyperlipidema and anemia. Model 5 adjusted for age, sex, BMI, baseline eGFR, Scr, CKD, diabetes, Killip III, SBP, DBP, hyperlipidema, anemia, asipilin, diuretic, ACEI, ARB, β blockers and alprostadil.

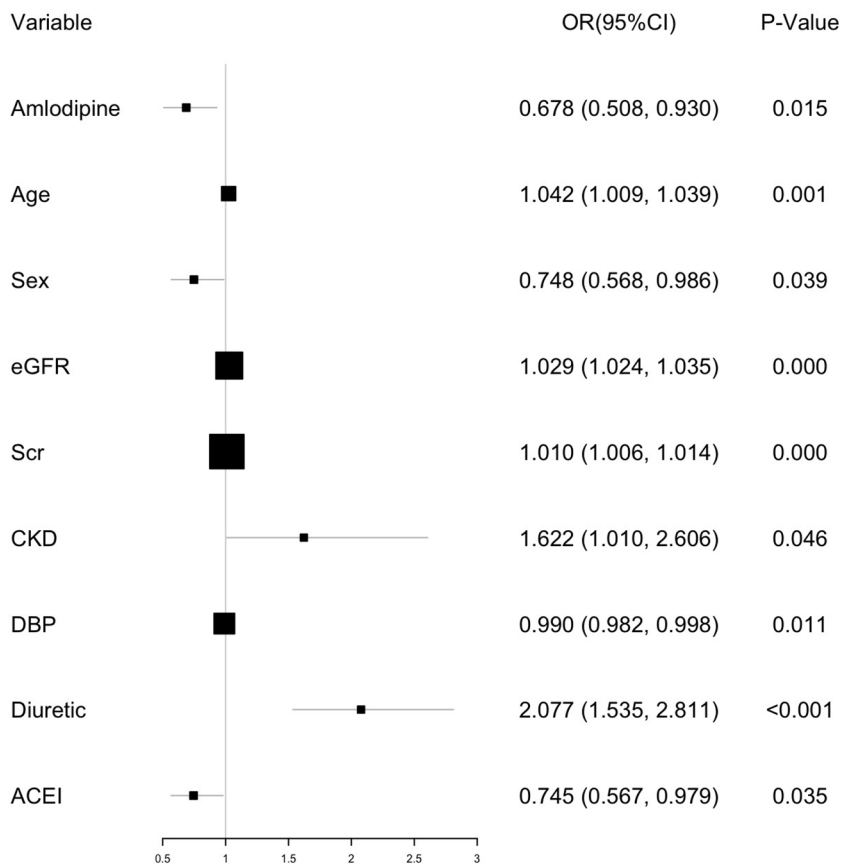

FIGURE 3 | Multivariable analysis for predictors of CI-AKI before matching.

TABLE 3 | The association between amlodipine and CI-AKI in the subgroups.

Outcome	Amlodipine group	Control group	Matched control group	P_1	P_2
No. of Diabetes	296	500	285		
CI-AKI	25 (8.45%)	67 (13.40%)	41 (12.89%)		
OR		0.598 (0.368–0.969)	0.549 (0.324–0.930)	0.035	0.024
No. of CKD	205	382	200		
CI-AKI	16 (7.80%)	45 (11.78%)	30 (13.79%)		
OR		0.634 (0.349–1.152)	0.480 (0.253–0.911)	0.132	0.023
No. of non-CKD	663	1,416	668		
CI-AKI	53 (7.99%)	166 (11.72%)	83 (12.43%)		
OR		0.654 (0.473–0.905)	0.612 (0.426–0.880)	0.01	0.008
No. of elderly	665 (7.52%)	1,331 (12.47%)	635 (14.33%)		
CI-AKI	50	166	91		
OR		0.571 (0.410–0.794)	0.486 (0.338–0.699)	<0.001	<0.001
No. of low-osmolar	673	1,474	708		
CI-AKI	55 (8.17%)	177 (12.01%)	98 (13.84%)		
OR		0.652 (0.475–0.896)	0.554 (0.391–0.785)	0.008	0.001
No. of iso-osmolar	151	298	152		
CI-AKI	10 (6.62%)	32 (10.74%)	15 (9.87%)		
OR		0.590 (0.282–1.234)	0.648 (0.281–1.491)	0.157	0.305

CI-AKI, contrast-induced acute kidney injury; P_1*, Amlodipine group vs Control group;* P_2*, Amlodipine group vs Matched control group.*

2013) Hypertension, combined with elevated levels of Ang II, and oxidative stress events, leading to renal damage.

Unfortunately, no specific therapeutic regimens exist to cure CI-AKI effectively. Thus, it is important to take precautions before CM administration. Amlodipine, one of the commonest CCB drugs for hypertension, has been reported to maintain renal function in patients with hypertension. (Nakamura et al., 2010; Honma et al., 2016) However, no study has reported the

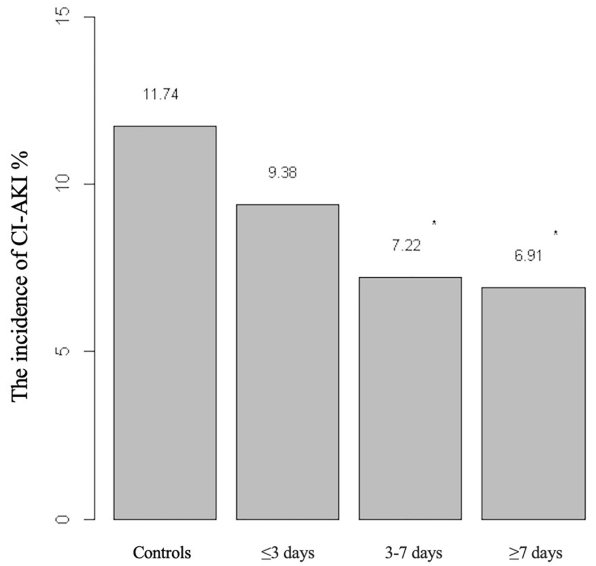

FIGURE 4 | Risk of CI-AKI associated with increasing duration of amlodipine. *$P < 0.05$ vs. controls.

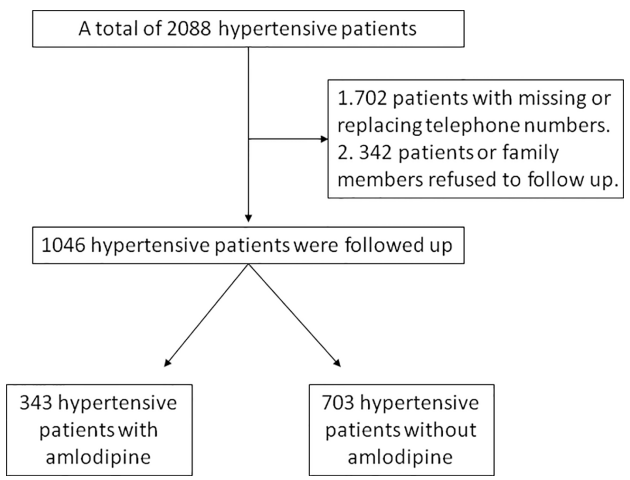

FIGURE 5 | Flow diagram of survival analysis in this study.

relationship between amlodipine and CI-AKI in hypertensives. The available data of these studies on the use of CCBs for the prevention of CI-AKI are contradictory and have not been clarified yet. Some studies have shown that CCB have a protective effect on the kidney and can prevent or reduce acute kidney injury caused by drugs *in vivo* and *vitro*. (Sepehr-Ara et al., 2010; Sepehr-Ara et al., 2011) A meta-analysis concluded that ACEI/ARB plus CCB (including amlodipine) is stronger than ACEI/ARB plus diuretics for maintaining renal function in hypertensive patients. (Cheng et al., 2016) The study by Russo et al. found that the renal plasma flow and GFR were increased in the group receiving nifedipine prior to injection of CM (n=30). (Russo et al., 1990) However, some other studies have reported the opposite. Oguzhan et al. objected to the benefit of a combination of an ARB and CCB in the treatment of CI-AKI in 90 CKD patients, the incidence of CI-AKI in patients undergoing coronary angiography received hydration along with amlodipine/valsartan (n = 45) increased when comparing to controls (n = 45), 17.8% vs 6.7%. (Oguzhan et al., 2013) In another study, among a total of 60 patients, isotonic sodium chloride, sodium bicarbonate, and isotonic sodium chloride with diltiazem application showed the same effect in prevention of CI-AKI. (Beyazal et al., 2014) But the sample size of the researches above is small, so in this study, we launched a much larger cohort: 2,667 hypertensive patients participated.

We first found amlodipine treatment before contrast exposure was able to reduce the risk of CI-AKI and prolong survival in the hypertensive population. Firstly, univariate analysis was carried out before matching. CKD and diabetes mellitus are known as the most important risk factors for CI-AKI, (Mccullough et al., 2016; Yin et al., 2017) and there were differences between the two groups at baseline eGFR, Scr, proportion of CKD, and diabetes, in order to reduce the effect of selection bias and potential confounding, we then matched controls on diabetes mellitus and renal function in 1:1 by propensity matching, in addition, age and sex were also matched. Because of the sample size, other antihypertensive drugs such as ACEI did not include in the matching analysis, we analyzed them in the conditional logistic regression. The protective effect of amlodipine was further confirmed by conditional logistic regression, adjusting for BMI, Killip III, SBP, DBP, complications, and combination medications. In this study, amlodipine was stable in reducing CI-AKI risk and shortening hospital stays, whether matched or adjusted. Finally, we conducted a subgroup analysis of the protective effects of amlodipine in high-risk groups such as diabetes, CKD, and the aged. Before matching, the morbidity was significant lower in the diabetes, non-CKD, low-osmolar, and aged amlodipine subgroups, and lower in subgroups of diabetes, CKD, non-CKD, low-osmolar, and the aged after matching.

The protective mechanism of amlodipine on CI-AKI is unclear, but some studies have studied the mechanism of renal protection by CCBs. It has been reported that renal tubular epithelial cells are associated with toxic effects of CM due to apoptosis, intrarenal hemodynamic disorder and medullary hypoxia, (Sadat, 2013) although the precise pathophysiological mechanism of CI-AKI also remains obscure. Current researches focus on contrast induced apoptosis caused by oxidative stress, increased Bcl-2/Bax, activation of caspase-3/9, and so on. (Romano et al., 2008; Gong et al., 2016; Kunak et al., 2016; Wang et al., 2017) Intracellular calcium overload which induced ROS overproduction and caspase-3 overexpression played an important role in the contrast-induced renal tubular cytotoxicity, and CCB plays a role in preventing calcium overload and inhibiting the opening of mitochondrial permeability transition pores (mPTP) by increasing calcium retention in protecting cardiomyocytes. (Ago et al., 2010; Mamou et al., 2015) Zhang et al. suggested that lacidipine treatment could protect human kidney cell against ischemia/reperfusion (I/R) injury by

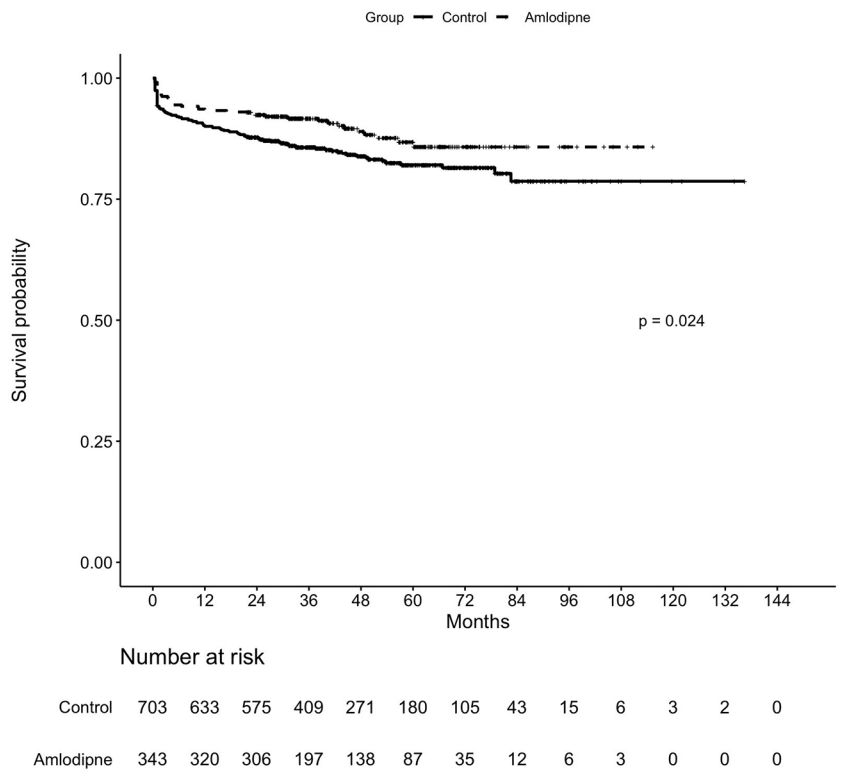

FIGURE 6 | Kaplan–Meier estimates for overall survival in hypertensive patients with contrast administration receiving amlodipine vs controls.

TABLE 4 | The association between amlodipine use and overall survival.

Variables	No amlodipine	Amlodipine	*P*
$HR_{unadjusted}$ (95% CI)	1.00	0.654 (0.451–0.948)	0.025
$HR_{adjusted\ 1}$ (95% CI)	1.00	0.657 (0.453–0.953)	0.027
$HR_{adjusted\ 2}$(95% CI)	1.00	0.632 (0.435–0.918)	0.016
$HR_{adjusted\ 3}$ (95% CI)	1.00	0.623 (0.430–0.908)	0.014

$HR_{adjusted\ 1}$ adjusted for age, sex, and BMI; $HR_{adjusted\ 2}$ adjusted for age, sex, BMI, baseline eGFR, and Scr; $HR_{adjusted\ 3}$ adjusted for age, sex, BMI, baseline eGFR, baseline Scr, CKD, and diabetes.

inhibiting the expression of Bax and Cytc proteins and by increasing Bcl-2 in an *in vitro* cell culture model to mimic I/R. (Zhang et al., 2013) And the caspase-3 pathway is involved in the protective mechanism. Caspase-3 activity peaked 30 min after ATP depletion and recovery, and it was attenuated by lacidipine. Yao et al. demonstrated that benidipine could ameliorate the AKI in rats due to the reduction of apoptosis in the tubular epithelial cells. (Yao et al., 2000).

What's more, substantial evidences showed that voltage-gated Ca^{2+} channel subtypes (L–, T–, N–, and P/Q–) exist in renal vessels and tubules, and blocking these channels play different effects on renal microcirculation. (Hayashi et al., 2007) L-Type calcium channel is widely distributed in renal vascular bed. L-Type CCB can significantly increase renal blood flow and glomerular filtration rate by blocking L-type calcium channel. Amlodipine, as a classical L-type calcium channel blocker, can also play a similar role. In summary, the underlying pathogenesis of amlodipine protection includes reduced apoptosis and inhibition of mPTP opening by preventing calcium overload, in addition, increase renal blood flow and glomerular filtration rate by blocking L-type calcium channel.

Cox proportional hazards models showed amlodipine before CM was a negative predictive risk factor for death after adjusting for age, sex, BMI, baseline eGFR, baseline Scr, CKD, and diabetes [HR 0.623, 95% CI (0.430–0.908), *P*=0.014]. CI-AKI has been shown associated with in-hospital need for dialysis (<1%), long-term kidney failure, and overall mortality (7–31%). (Azzalini et al., 2016) In this study, the mortality rate of hypertensive patients treated with contrast was 14.34%. A study involved 80 patients with CI-AKI after cardiac catheterization showed that CCB could reduce the mortality in CI-AKI patients. (Lai et al., 2013) Its role in ameliorating ischemic and toxic cell injury may play an important part in prolonging survival.

Multivariable analysis found that eGFR, Scr, and CKD were risk factors for CI-AKI. In previous studies, preexisting CKD has been reported to be the most important independent risk factor for CI-AKI. And the baseline eGFR, Scr, and potential kidney disease were included in many risk prediction models of CI-AKI. Our results were consistent with previous studies because baseline eGFR and Scr are two important indicators of renal function. Some studies have also shown that diabetes is a predictor of CI-AKI, and not all multivariable analyses have found it to be an independent risk factor because most diabetic

patients suffered from CKD at the same time. In this study, diabetes was not a major risk factor for CI-AKI.

We also studied the effects of duration of amlodipine. When the duration is greater than 3 days, there was a lower risk of CI-AKI, although, this difference seems not significant. Thus, we advocate amlodipine at least three days in advance for a better preventive effect.

Some limitations of our analysis should be considered. First, this was a nonrandomized retrospective study, whose inherent weakness cannot be avoided despite robust propensity-score matching. Second, this study was conducted in a single center and may therefore be weaker in methodology than studies using multicenter sampled populations. Third, the effects of many drugs have not been ruled out, especially some renal protective drugs such as N-acetylcysteine. Fourth, in the survival analysis, some important information about patients were missing such as if some patients underwent further procedure with CM during the 144 months, AKI episodes, renal diseases, renal function, progression of hypertension, which result in the lax survival analysis. In the future prospective research, those information should be collected.

CONCLUSIONS

Our data first demonstrate that the use of amlodipine may play a role in protecting patients from CI-AKI, and reducing the hospital stay in hypertensive population and the same results were found in the diabetes, CKD, and aged subgroups. We also found that amlodipine resulted in a statistically significant increase in overall survival among Chinese hypertensive patients with contrast for the first time. In addition, greater than 3 days duration and normal dose of levamlodipine 2.5 mg/qd or amlodipine 5.0 mg/qd before contrast administration show a better prevention from CI-AKI. This could provide guidance for medication for patients with hypertension.

DATA AVAILABILITY STATEMENT

The datasets generated for this study are available on request to the corresponding author.

ETHICS STATEMENT

The studies involving human participants were reviewed and approved by the Medical Ethical Committee in the Third Xiangya Hospital of Central South University (No. 2016-S160). Written informed consent for participation was not required for this study in accordance with the national legislation and the institutional requirements.

AUTHOR CONTRIBUTIONS

W-JY and X-CZ conceived and designed the study. W-JY, X-CZ, and D-YL performed data acquisition and statistical analyses. W-JY and L-YZ managed the patient database. All authors were involved in the data interpretation and discussion of the results. W-JY, H-QY, and Y-JX prepared the figures. W-JY and X-CZ drafted the manuscript. All authors approved the final version of the manuscript.

FUNDING

This study was supported by the National Natural Science Foundation of China (No. 81773822 and 81973400), the Hunan Traditional Chinese Medicine Research Program (No. 201760), the Hunan Pharmaceutical Society Scientific Research Funding Project (No. Hn2017003), and the Hunan Provincial Natural Science Foundation of China (No. 2018JJ6051).

ACKNOWLEDGMENTS

We thank Shanghai Lejiu Healthcare Technology Co., Ltd for their assistance in data extraction. Shanghai Lejiu Healthcare Technology Co., Ltd helped us establish a large clinical database of rational drug use based on the clinical data of the Third Xiangya Hospital. Based on this database, we were easily able to extract the data of this study.

REFERENCES

Ago, T., Yang, Y., Zhai, P., and Sadoshima, J. (2010). Nifedipine inhibits cardiac hypertrophy and left ventricular dysfunction in response to pressure overload. *J. Cardiovasc. Transl. Res.* 3, 304–313. doi: 10.1007/s12265-010-9182-x

Azushima, K., Uneda, K., Tamura, K., Wakui, H., Ohsawa, M., Kobayashi, R., et al. (2014). Effects of single pill-based combination therapy of amlodipine and atorvastatin on within-visit blood pressure variability and parameters of renal and vascular function in hypertensive patients with chronic kidney disease. *BioMed. Res. Int.* 2014, 437087. doi: 10.1155/2014/437087

Azzalini, L., Spagnoli, V., and Ly, H. Q. (2016). Contrast-induced nephropathy: from pathophysiology to preventive strategies. *Can. J. Cardiol.* 32, 247–255. doi: 10.1016/j.cjca.2015.05.013

Bartholomew, B. A., Harjai, K. J., Dukkipati, S., Boura, J. A., Yerkey, M. W., Glazier, S., et al. (2004). Impact of nephropathy after percutaneous coronary intervention and a method for risk stratification. *Am. J. Cardiol.* 93, 1515–1519. doi: 10.1016/j.amjcard.2004.03.008

Beyazal, H., Caliskan, Z., and Utac, C. (2014). Comparison of effects of isotonic sodium chloride with diltiazem in prevention of contrast-induced nephropathy. *Ren. Fail* 36, 351–355. doi: 10.3109/0886022X.2013.866016

Boos, C. J., and Lip, G. Y. (2006). Is hypertension an inflammatory process? *Curr. Pharm. Des.* 12, 1623–1635. doi: 10.2174/138161206776843313

Carey, R. M., Muntner, P., Bosworth, H. B., and Whelton, P. K. (2018). Prevention and control of hypertension: JACC health promotion series. *J. Am. Coll. Cardiol.* 72, 1278–1293. doi: 10.1016/j.jacc.2018.07.008

Cheng, Y., Huang, R., Kim, S., Zhao, Y., Li, Y., and Fu, P. (2016). Renoprotective effects of renin–angiotensin system inhibitor combined with calcium channel blocker or diuretic in hypertensive patients: a PRISMA-compliant meta-analysis. *Med. (Baltimore)* 95, e4167. doi: 10.1097/MD.0000000000004167

Diamond, A., and Sekhon, J. S. (2013). Genetic matching for estimating causal effects: a general multivariate matching method for achieving balance in observational studies. *Rev. Econ. Stat* 95, 932–945. doi: 10.1162/REST_a_00318

Duan, S. B., Liu, F. Y., Luo, J. A., Wu, H. W., Liu, R. H., Peng, Y. M., et al. (2000). Nephrotoxicity of high- and low-osmolar contrast media. the protective role of

amlodipine in a rat model. *Acta Radiol.* 41, 503–507. doi: 10.1080/028418500127345794

Duan, S. B., Liu, F. Y., Luo, J. A., Wu, H. W., Liu, R. H., Peng, Y. M., et al. (2000). Nephrotoxicity of high- and low-osmolar contrast media. The protective role of amlodipine in a rat model. *Acta Radiol.* 41, 503–507. doi: 10.1080/028418500127345794

Fox, C. S., Larson, M. G., Leip, E. P., Culleton, B., Wilson, P. W., and Levy, D. (2004). Predictors of new-onset kidney disease in a community-based population. *JAMA* 291, 844–850. doi: 10.1001/jama.291.7.844

Gong, X., Duan, Y., Zheng, J., Wang, Y., Wang, G., Norgren, S., et al. (2016). Nephroprotective effects of N-acetylcysteine amide against contrast-induced nephropathy through upregulating thioredoxin-1, inhibiting ASK1/p38MAPK pathway, and suppressing oxidative stress and apoptosis in rats. *Oxid. Med. Cell Longev.* 2016, 8715185. doi: 10.1155/2016/8715185

Hansell, P., Welch, W. J., Blantz, R. C., and Palm, F. (2013). Determinants of kidney oxygen consumption and their relationship to tissue oxygen tension in diabetes and hypertension. *Clin. Exp. Pharmacol. Physiol.* 40, 123–137. doi: 10.1111/1440-1681.12034

Haria, M., and Wagstaff, A. J. (1995). Amlodipine. A reappraisal of its pharmacological properties and therapeutic use in cardiovascular disease. *Drugs* 50, 560–586. doi: 10.2165/00003495-199550030-00009

Hayashi, K., Wakino, S., Sugano, N., Ozawa, Y., Homma, K., and Saruta, T. (2007). Ca^{2+} channel subtypes and pharmacology in the kidney. *Circ. Res.* 100, 342–353. doi: 10.1161/01.RES.0000256155.31133.49

Ho, D. E., Imai, K., King, G., and Stuart, E. A. (2007). Matching as nonparametric preprocessing for reducing model dependence in parametric causal inference. *Political Anal.* 15, 199–236. doi: 10.1093/pan/mpl013

Honma, S., Nakamura, K., Shinohara, M., Mitazaki, S., Abe, S., and Yoshida, M. (2016). Effect of amlodipine on mouse renal interstitial fibrosis. *Eur. J. Pharmacol.* 780, 136–141. doi: 10.1016/j.ejphar.2016.03.041

James, M. T., Grams, M. E., Woodward, M., Elley, C. R., Green, J. A., Wheeler, D. C., et al. (2015). A meta-analysis of the association of estimated GFR, albuminuria, diabetes mellitus, and hypertension with acute kidney injury. *Am. J. Kidney Dis.* 66, 602–612. doi: 10.1053/j.ajkd.2015.02.338

Klag, M. J., Whelton, P. K., Randall, B. L., Neaton, J. D., Brancati, F. L., Ford, C. E., et al. (1996). Blood pressure and end-stage renal disease in men. *N. Engl. J. Med.* 334, 13–18. doi: 10.1056/NEJM199601043340103

Kunak, C. S., Ugan, R. A., Cadirci, E., Karakus, E., Polat, B., Un, H., et al. (2016). Nephroprotective potential of carnitine against glycerol and contrast-induced kidney injury in rats through modulation of oxidative stress, proinflammatory cytokines, and apoptosis. *Br. J. Radiol.* 89, 1058. doi: 10.1259/bjr.20140724

Lai, H. M., Aronow, W. S., Chugh, S. S., Pudasaini, B., Goel, A., and Garrick, R. (2013). Risk factors for hemodialysis and mortality in patients with contrast-induced nephropathy. *Am. J. Ther.* 20, 607–612. doi: 10.1097/MJT.0b013e31822831e9

Mamou, Z., Chahine, M., Rhondali, O., Dehina, L., Chevalier, P., Descotes, J., et al. (2015). Effects of amlodipine and perindoprilate on the structure and function of mitochondria in ventricular cardiomyocytes during ischemia–reperfusion in the pig. *Fundam. Clin. Pharmacol.* 29, 21–30. doi: 10.1111/fcp.12070

Matsushita, K., Mahmoodi, B. K., Woodward, M., Emberson, J. R., Jafar, T. H., Jee, S. H., et al. (2012). Comparison of risk prediction using the CKD-EPI equation and the MDRD study equation for estimated glomerular filtration rate. *JAMA* 307, 1941–1951. doi: 10.1001/jama.2012.3954

Mccullough, P. A., Choi, J. P., Feghali, G. A., Schussler, J. M., Stoler, R. M., Vallabahn, R. C., et al. (2016). Contrast-induced acute kidney injury. *J. Am. Coll. Cardiol.* 68, 1465–1473. doi: 10.1016/j.jacc.2016.05.099

Nakamura, T., Sato, E., Fujiwara, N., Kawagoe, Y., Ueda, Y., Sugaya, T., et al. (2010). Comparative effects of benidipine and amlodipine on proteinuria, urinary 8-OHdG, urinary L-FABP, and inflammatory and atherosclerosis markers in early-stage chronic kidney disease. *Am. J. Med. Sci.* 339, 157–163. doi: 10.1097/MAJ.0b013e3181c643df

Nash, K., Hafeez, A., and Hou, S. (2002). Hospital-acquired renal insufficiency. *Am. J. Kidney Dis.* 39, 930–936. doi: 10.1053/ajkd.2002.32766

Neumayer, H. H., Junge, W., Kufner, A., and Wenning, A. (1989). Prevention of radiocontrast-media-induced nephrotoxicity by the calcium channel blocker nitrendipine: a prospective randomised clinical trial. *Nephrol. Dial. Transplant.* 4, 1030–1036. doi: 10.1093/ndt/4.12.1030

Nutritional Anaemias (1968). Report of a WHO scientific group. *World Health Organ. Tech. Rep. Ser.* 405, 5–37.

Oguzhan, N., Cilan, H., Sipahioglu, M., Unal, A., Kocyigit, I., Kavuncuoglu, F., et al. (2013). The lack of benefit of a combination of an angiotensin receptor blocker and calcium channel blocker on contrast-induced nephropathy in patients with chronic kidney disease. *Ren. Fail* 35, 434–439. doi: 10.3109/0886022X.2013.766566

Owen, R. J., Hiremath, S., Myers, A., Fraser-Hill, M., and Barrett, B. J. (2014). Canadian Association of Radiologists consensus guidelines for the prevention of contrast-induced nephropathy: update 2012. *Can. Assoc. Radiol. J.* 65, 96–105. doi: 10.1016/j.carj.2012.11.002

Palevsky, P. M., Liu, K. D., Brophy, P. D., Chawla, L. S., Parikh, C. R., Thakar, C. V., et al. (2013). KDOQI US commentary on the 2012 KDIGO clinical practice guideline for acute kidney injury. *Am. J. Kidney Dis.* 61, 649–672. doi: 10.1053/j.ajkd.2013.02.349

Palit, S., Chonchol, M., Cheung, A. K., Kaufman, J., Smits, G., and Kendrick, J. (2015). Association of BP with death, cardiovascular events, and progression to chronic dialysis in patients with advanced kidney disease. *Clin. J. Am. Soc. Nephrol.* 10, 934–940. doi: 10.2215/CJN.08620814

Pietri, P., Vlachopoulos, C., and Tousoulis, D. (2015). Inflammation and arterial hypertension: from pathophysiological links to risk prediction. *Curr. Med. Chem.* 22, 2754–2761. doi: 10.2174/0929867322666150420104727

Romano, G., Briguori, C., Quintavalle, C., Zanca, C., Rivera, N. V., Colombo, A., et al. (2008). Contrast agents and renal cell apoptosis. *Eur. Heart J.* 29, 2569–2576. doi: 10.1093/eurheartj/ehn197

Russo, D., Testa, A., Della, V. L., and Sansone, G. (1990). Randomised prospective study on renal effects of two different contrast media in humans: protective role of a calcium channel blocker. *Nephron* 55, 254–257. doi: 10.1159/000185971

Sadat, U. (2013). Radiographic contrast-media-induced acute kidney injury: pathophysiology and prophylactic strategies. *ISRN Radiol.* 2013, 496438. doi: 10.5402/2013/496438

Sepehr-Ara, L., Sepehr-Ara, M., and Mahmoudian, M. (2010). Effect of the two new calcium channel blockers mebudipine and dibudipine in comparison to amlodipine on vascular flow of isolated kidney of diabetic rat. *Acta Physiol. Hung* 97, 281–289. doi: 10.1556/APhysiol.97.2010.3.4

Sepehr-Ara, L., Mohajeri, S. A., and Mahmoudian, M. (2011). Effect of the two new calcium channel blockers mebudipine and dibudipine on vascular flow of isolated kidney of normal and diabetic rats. *Pathophysiology* 18, 175–184. doi: 10.1016/j.pathophys.2010.09.001

Tepel, M., Aspelin, P., and Lameire, N. (2006). Contrast-induced nephropathy: a clinical and evidence-based approach. *Circulation* 113, 1799–1806. doi: 10.1161/CIRCULATIONAHA.105.595090

Wang, K., Bei, W. J., Liu, Y. H., Li, H. L., Chen, S. Q., Lin, K. Y., et al. (2017). miR21 attenuates contrast-induced renal cell apoptosis by targeting PDCD4. *Mol. Med. Rep.* 16, 6757–6763. doi: 10.3892/mmr.2017.7426

Wilson, D. R., Arnold, P. E., Burke, T. J., and Schrier, R. W. (1984). Mitochondrial calcium accumulation and respiration in ischemic acute renal failure in the rat. *Kidney Int.* 25, 519–526. doi: 10.1038/ki.1984.48

Yang, D. P., Jia, R. H., Ding, G. H., and Yang, D. W. (2008). Felodipine attenuates NRK52E cell injury induced by contrast media. *Herald of Medicine*, 27 (10) 1153–1156.

Yang, D., Yang, D., Jia, R., and Ding, G. (2013). Selective inhibition of the reverse mode of Na+/Ca^{2+} exchanger attenuates contrast-induced cell injury. *Am. J. Nephrol.* 37, 264–273. doi: 10.1159/000348526

Yao, K., Sato, H., Ina, Y., Nagashima, K., Nishikawa, S., Ohmori, K., et al. (2000). Benidipine inhibits apoptosis during ischaemic acute renal failure in rats. *J. Pharm. Pharmacol.* 52, 561–568. doi: 10.1211/0022357001774200

Yin, W. J., Yi, Y. H., Guan, X. F., Zhou, L. Y., Wang, J. L., Li, D. Y., et al. (2017). Preprocedural prediction model for contrast-induced nephropathy patients. *J. Am. Heart Assoc.* 6, 2. doi: 10.1161/JAHA.116.004498

Zhang, A., Fu, S., Chen, L., Ren, L., Qu, S., Zhang, Y., et al. (2013). Lacidipine attenuates apoptosis via a caspase-3 dependent pathway in human kidney cells. *Cell. Physiol. Biochem.* 32, 1040–1049. doi: 10.1159/000354504

Zhang, N., Du, S. M., and Ma, G. S. (2017). Current lifestyle factors that increase risk of T2DM in China. *Eur. J. Clin. Nutr.* 71, 832–838. doi: 10.1038/ejcn.2017.41

Zhou, X. R., Duan, S. B., Peng, Y. M., Liu, F. Y., Ye, Y., Liu, R. H., et al. (2007). Protective effect of amlodipine on the cytotoxicity induced by contrast media in human kidney cells. *Zhong Nan Da Xue Xue Bao Yi Xue Ban* 32, 806–811.

Conflict of Interest: The authors declare that the research was conducted in the absence of any commercial or financial relationships that could be construed as a potential conflict of interest.

Copyright © 2020 Yin, Zhou, Li, Xie, Wang, Zuo, Liu, Hu, Zhou, Chen, Yang and Zuo. This is an open-access article distributed under the terms of the Creative Commons Attribution License (CC BY). The use, distribution or reproduction in other forums is permitted, provided the original author(s) and the copyright owner(s) are credited and that the original publication in this journal is cited, in accordance with accepted academic practice. No use, distribution or reproduction is permitted which does not comply with these terms.

frontiers in Medicine

MINI REVIEW
published: 21 February 2020
doi: 10.3389/fmed.2020.00047

Advances in Understanding the Effects of Erythropoietin on Renal Fibrosis

*Yangyang Zhang, Xiaoyu Zhu, Xiu Huang, Xuejiao Wei, Dan Zhao, Lili Jiang, Xiaoxia Zhao and Yujun Du**

Department of Nephrology, The First Hospital of Jilin University, Changchun, China

Renal fibrosis is the common manifestation of the pathogenesis of end-stage renal disease that results from different types of renal insult, and is a hallmark of chronic kidney disease (CKD). The main pathologic characteristics of renal fibrosis are renal interstitial fibroblast hyperplasia and the aberrant and excessive deposition of extracellular matrix, pathologies that lead to the destruction of normal renal tubules and interstitial structures. However, the biological significance of fibrosis during the progression of CKD is not clear, and there are no approved clinical treatments for delaying or reversing renal fibrosis. Studies of the mechanism of renal fibrosis and of potential measures of prevention and treatment have focused on erythropoietin (EPO), a hormone best known as a regulator of red blood cell production. These recent studies have found that EPO may also provide efficient protection against renal fibrosis. Future therapeutic approaches using EPO offer new hope for patients with CKD. The aim of the present review is to briefly discuss the role of EPO in renal fibrosis, to identify its possible mechanisms in preventing renal fibrosis, and to provide novel ideas for the use of EPO in future treatments of renal fibrosis.

Keywords: chronic kidney disease, renal fibrosis, erythropoietin, extracellular matrix, myofibroblasts

OPEN ACCESS

Edited by:
Xueying Zhao,
Morehouse School of Medicine,
United States

Reviewed by:
Norio Suzuki,
Tohoku University, Japan
Nikolina Basic-Jukic,
University Hospital Centre
Zagreb, Croatia

****Correspondence:***
Yujun Du
kjkduyujun@126.com

Specialty section:
This article was submitted to Nephrology, a section of the journal Frontiers in Medicine

Received: *25 November 2019*
Accepted: *30 January 2020*
Published: *21 February 2020*

Citation:
Zhang Y, Zhu X, Huang X, Wei X, Zhao D, Jiang L, Zhao X and Du Y (2020) Advances in Understanding the Effects of Erythropoietin on Renal Fibrosis. Front. Med. 7:47. doi: 10.3389/fmed.2020.00047

INTRODUCTION

The prevalence of chronic kidney disease (CKD) has risen significantly during the last several decades, and it is now a major public health issue that poses enormous economic challenges worldwide (1). According to recent epidemiological surveys, more than 500 million people worldwide currently have some stage of CKD (2, 3). The two principal causes of CKD are diabetes and hypertension; several additional conditions often accompany CKD, such as HIV infection, obesity, and primary kidney injury (4). The progression of CKD is accompanied by multiple complications and comorbidities that ultimately lead to renal fibrosis and end-stage renal disease, a condition associated with poor outcome and increased risk of death (5, 6).

Renal fibrosis is a progressive pathophysiological change that is associated with damage and functional loss of the kidney (7). Pathogenesis begins following stimulation by a variety of pathogenic factors, such as trauma, infection, inflammation, blood circulation disorders, and excessive immune responses. These insults damage healthy kidney cells, leading to the deposition and accumulation of large amounts of collagen as disease progresses. During the later stages of pathogenesis, there is a gradual hardening of the renal parenchyma and formation of scar tissue, and then the complete loss of kidney function (8). Renal fibrosis is simply the process of fibrosis and hardening of the formerly healthy cells of the kidney. It is also characterized by the abnormal deposition of extracellular matrix (ECM). Although previous studies have examined the main

molecular mediators of renal fibrosis, there are no approved therapies that directly target renal fibrosis (9, 10). Therefore, it is necessary to further study the pathogenesis of renal fibrosis to facilitate the development of new drugs that inhibit renal fibrosis and delay the progression to CKD.

In 1906, Carnot and Deflander first proposed the existence of a hormone primarily produced by the kidneys that regulates red blood cell production. This hormone, subsequently named erythropoietin (EPO), is now known to regulate the formation of red blood cells by stimulating bone marrow, and is widely used for the clinical treatment of anemia caused by various factors (11–13). Recent research in China and elsewhere has examined the non-hematopoietic aspects of EPO (14–16). There is now evidence that EPO is a multifunctional cytokine (17). Thus, in addition to regulating erythropoiesis (which increases tissue oxygen supply) EPO also has anti-apoptosis, anti-inflammatory, antioxidant, angiogenesis, cell proliferation, and anti-tumor effects (18).

The aims of this review were to briefly review the scientific evidence regarding the relationship of the therapeutic use of EPO with renal fibrosis.

EPO AND RELATED MOLECULES

EPO is an acidic glycoprotein containing sialic acid whose precursor has 193 amino acids. After post-translational processing, the active protein has 165 amino acids and is highly glycosylated (19, 20). The serum EPO level in healthy individuals ranges from 15 to 25 U/L (21), and the oxygenation state of tissues regulates its production. EPO is a glycoprotein hormone secreted by the kidneys whose biological effects occur after it binds to its receptor (EPO-R), which occurs on the plasma membranes of target cells (22). EPO primarily targets hematopoietic cells in the bone marrow, which has high concentrations of EPO, and this is its main site of action (23). The binding of EPO to EPO-R on erythrocytes activates a variety of signaling pathways (24), thus stimulating cell proliferation, differentiation, and maturation (13). EPO can improve anemia by inducing erythropoiesis, thus indirectly ameliorating organ damages. Studies have shown that in predialysis patients with non-severe anemia, the early initiation of erythropoietin significantly slows the progression of kidney disease and delays the initiation of renal replacement therapy (25). Initial studies found EPO-R in erythroid progenitor cells, so researchers considered its function was limited to these cells, and gave little consideration to the role of EPO in the kidney and other tissues (26). More recent studies have shown expression of EPO-R by renal cells (including renal tubular cells, mesangial cells, and collecting duct cells), gastric epithelial cells, and some neurogenic cells (27, 28). Other studies have shown that EPO has cellular protective effects, through its interaction with the EPO-R, in the kidneys, brain, heart, and blood vessels, in that it regulates mitosis, reduces oxidative stress, inhibits apoptosis, promotes vascular repair, and has several other effects (24, 29). The clinical application of erythropoiesis stimulating agents (ESAs) was a milestone in the treatment of renal anemia, because these drugs greatly improve the prognosis of patients with chronic renal failure and provide important renoprotective effects (30–32).

However, due to the poor specificity and sensitivity of existing anti-EPO-R antibodies, there is still controversy about the function of EPO beyond its effect on erythropoiesis. Elliott et al. found that EPO-R protein was below the detection limit in tissues and renal cells and no evidence of EPO-R expression and function in the kidneys (33). A subsequent meta-analysis of clinical trials by Elliott et al. showed that ESAs had no clear renoprotective effect, at least in the included subjects (34). Thus, it is currently controversial whether functional EPO-R occurs on the plasma membranes of renal cells. Moreover, multiple clinical studies showed that ESAs provided no improvement in renal function after transplantation or acute kidney injury (35, 36). However, due to the poor specificity of the EPO-R assay and the discordance of *in vitro* and *in vivo* data in animal models, this topic needs further study.

EPO AND RENAL FIBROSIS

Renal fibrosis is a key feature of CKD and is the common pathologic manifestation and pathogenic outcome of end-stage renal disease (37). Renal interstitial fibroblast proliferation and the aberrant and persistent deposition of ECM are the main pathological features of renal fibrosis. This process begins when an inflammatory stimulus accelerates the transformation of epithelial cells and interstitial fibroblasts into myofibroblasts, which together produce excess ECM. Then, because of the decreased activity of matrix proteolytic enzymes and increased activity of protease inhibitors, excessive deposition of ECM occurs, leading to the formation of permanent fibrotic scars, thereby accelerating the progression of tubulointerstitial fibrosis (38, 39).

It is now known that EPO is a major multifunctional glycoprotein hormone that has protective functions in various organs and tissues. For example, an animal study demonstrated that EPO attenuated cardiac dysfunction by inhibiting interstitial fibrosis in diabetic rats (40). Another animal study reported the beneficial effects of EPO in diverse liver injuries, such as carbon tetrachloride-induced hepatic fibrosis (41). EPO also has renoprotective effects (**Figure 1**) (42, 43), and early treatment of anemia with EPO in CKD patients slows the development in renal dysfunction (44). Extensive research during recent years demonstrated that EPO can improve recovery from acute kidney injury (45). Administration of recombinant human EPO (rhEPO) reduces the production of urinary proteins and biomarkers associated with kidney injury and even with CKD. We therefore believe that EPO may also play a critical role in the development of renal fibrosis, but the mechanism of this effect requires further examination.

EPO and Myofibroblasts

Myofibroblasts are fibroblasts containing actin, myosin, and other muscle-related proteins that provide these cells with contractile properties. Various stimuli and injuries can induce the activation and proliferation of renal interstitial fibroblasts, leading to the formation of active myofibroblasts. These

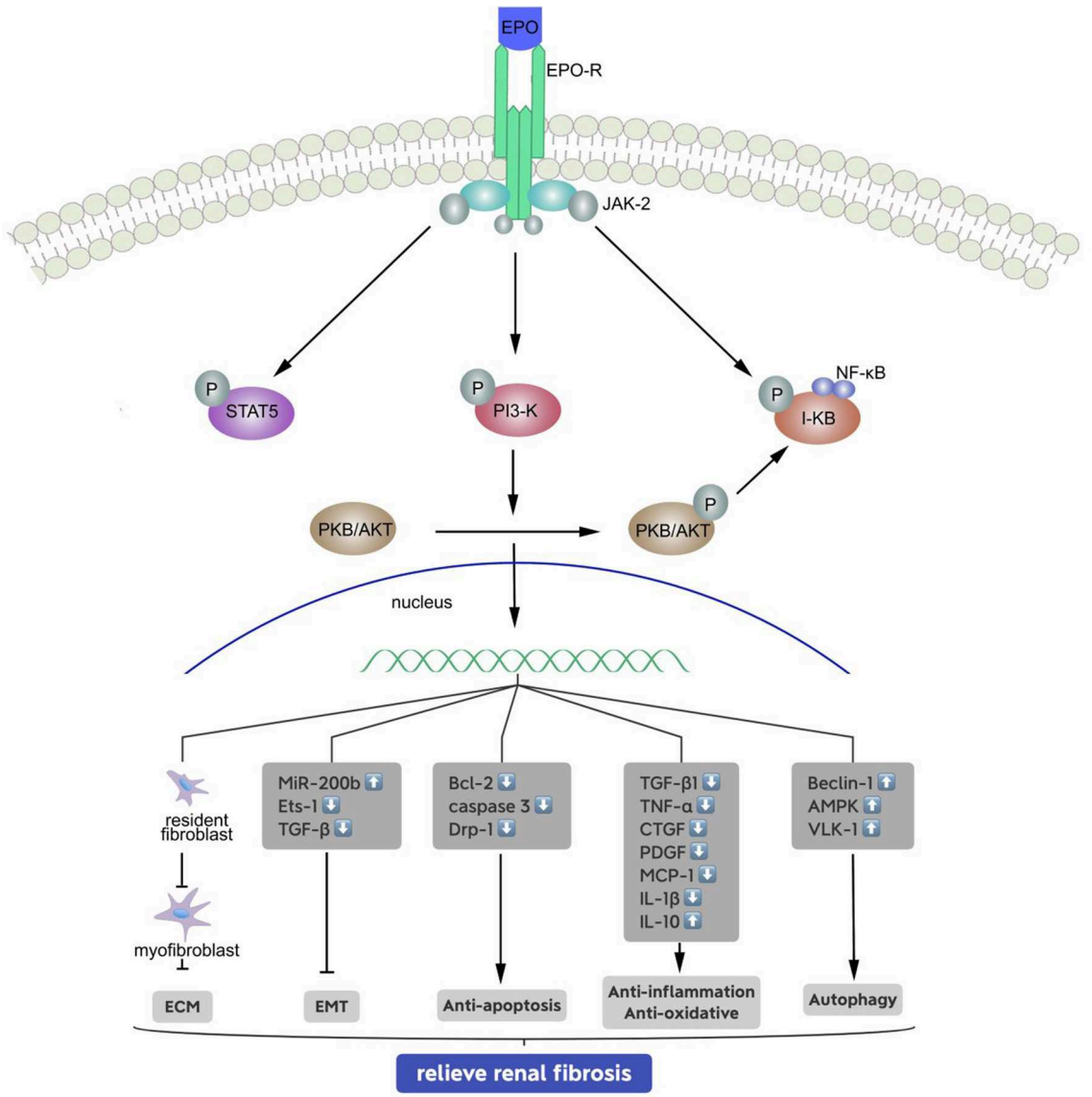

FIGURE 1 | Signal transduction pathways of the erythropoietin receptor and mechanisms of relieving renal fibrosis. Binding of erythropoietin (EPO) causes conformational changes to the EPO receptor, phosphorylation of associated JAK-2, PI-3 kinase and I-kB molecules, and activation of signaling molecules and target genes: (1) inhibits the generation of stromal mesenchymal fibroblasts; (2) inhibits the EMT by upregulating miR-200b, and reducing of Ets-1 and TGF-β; (3) phosphorylates and inactivates proapoptotic molecules; (4) reduces inflammation by inhibiting the release of pro-inflammatory cytokines and anti-oxidative, and (5) enhances autophagy to some extent.

renal myofibroblasts function as effector cells of the renal interstitial ECM, causing damage to the function of the kidney, and eventually leading to renal failure (46–48). Moreover, the population of novel myofibroblasts present in fibrotic kidneys can derive from renal tubular interstitial resident fibroblasts, bone marrow derived fibrocytes, vascular pericytes, the epithelial-mesenchymal transition (EMT), and the endothelial-mesenchymal transition (EndoMT) (49, 50).

There is an increasing body of evidence suggesting that interstitial myofibroblasts constitutively produce ECM, and that this leads to the development of glomerulosclerosis and tubulointerstitial fibrosis due to activation of TGF-β1 (51). The accumulation of matrix proteins, such as fibronectin and type I and III collagen, is a hallmark of renal fibrosis. Thus, under normal conditions, resident renal fibroblasts produce EPO in response to hypoxic insults to maintain physiological homeostasis. However, under pathologic conditions the resident renal fibroblasts transdifferentiate into myofibroblasts, which promote renal fibrosis by producing large amounts of extracellular matrix proteins rather than EPO (52). A study of mice showed that treatment with rhEPO significantly inhibited the accumulation of fibrocyte by

inhibition of α-SMA upregulation, and thereby attenuating renal interstitial fibrosis (53). Another study of transgenic mice found that enhanced signaling mediated by hypoxia-inducible factor (HIF) in myofibroblast-transformed renal EPO-producing cells reactivated the synthesis of EPO, without influencing renal fibrosis or inflammation (54). However, studies of type 2 diabetic mice found that a continuous erythropoietin receptor activator (CERA) enhanced tissue repair by inhibiting the generation of stromal mesenchymal fibroblasts, and thus had a non-hematopoietic and tissue-protective role (55).

EPO and the EMT

During the EMT, epithelial cells undergo a loss of cell-cell adhesion and apical-basal polarity. This is accompanied by increased expression of mesenchymal markers, rearrangement of the cytoskeleton, and increased cell dissociation, all of which contribute to development of the mesenchymal phenotype. The EMT is pathologically reactivated in, and contributes to, the progression of fibrosis (56). Tubulointerstitial fibroblasts, derived from tubular epithelial cells during the EMT, are among the most important effector cells facilitating the progression of renal fibrosis (57, 58). In the past few decades, many studies have examined the role of the EMT during organ fibrosis, wound healing, and cancer metastasis. These studies have demonstrated that TGF-β1 promotes renal fibrosis through the EMT by activation of Smad2/3 (59, 60). In support of this conclusion, animal studies have also shown that the renal EMT contributes to renal fibrosis. For example, Grande et al. concluded that the partial EMT drives renal fibrosis in mice (61). Therefore, it is important to identify interventions or drug therapies that could potentially reverse or inhibit the EMT in the kidney to improve clinical management of these patients.

Previous studies reported that EPO functions as an EMT inhibitor in the kidneys and was effective in ameliorating renal fibrosis (62). Imamura et al. reported that EPO inhibits tubulointerstitial fibrosis in remnant kidney by functioning as an inhibitor of the EMT (63). A recent study using HK-2 cells showed that administration of EPO markedly inhibited hypoxia-induced EMT by upregulating miR-200b expression via the repression of Ets-1. Another study of a unilateral ureteric obstruction (UUO) mouse model reported that rhEPO treatment reduced renal fibrosis by attenuating the EMT (64). Although the role of the EMT in renal fibrosis is not entirely clear, it is nonetheless important to identify therapeutic targets that may allow the prevention or reversal of the EMT and thereby slow the progression of CKD.

EPO and Apoptosis

Apoptosis is the spontaneous and orderly death of cells in multicellular organisms that is regulated by specific genes to maintain the stability of the internal environment. In contrast to the passive process of necrosis, apoptosis is an active process in which there are specific changes in the expression of multiple genes. It is not a phenomenon of self-injury that occurs during pathological conditions, but a process that eliminates cells so that the organism is better adapted to its microenvironment. There are several signal transduction pathways associated with apoptosis; the major pathways are mitochondrial mediated apoptosis, endoplasmic reticulum mediated apoptosis, and death receptor-mediated apoptosis (65).

Renal fibrosis is accompanied by a significant reduction of parenchymal cells, including podocytes, mesangial cells, and tubular epithelial cells, and increased apoptosis also plays an important role. During renal interstitial fibrosis, there is evidence that apoptosis of renal tubular epithelial cells is closely related to renal tubular atrophy, and the increased apoptosis index during this process is an indication of the formation of extracellular matrix (66). Therefore, a targeted inhibition of apoptosis may be an effective strategy to delay or inhibit renal fibrosis.

EPO has many biochemical effects, in addition to its promotion of red blood cell production, and these include anti-inflammatory and anti-apoptotic effects. For example, EPO is the main regulator of erythroid progenitor cell proliferation and differentiation, and these are mediated via its anti-apoptotic effect (67). Many recent animal experiments have shown that EPO may delay the development of CKD and protect the kidneys by reducing the extent of interstitial fibrosis. For example, one study showed that the extent of renal fibrosis correlated positively with the number of apoptotic cells (68). Another study demonstrated that EPO provided a renoprotective and antiapoptotic effects by activation of ERK/p53 signaling (26). A study of renal interstitial fibrosis in a rat model reported that EPO had renoprotective effects due to its due to its down-regulation of dynamin-related protein-1 (Drp-1) (69), a protein with a major role in the mitochondrial mediated apoptosis pathway. A study by Nakazawa et al. showed that EPO inhibited the apoptosis of renal tubular cells, thereby reducing the extent of renal interstitial fibrosis (70). In the context of ischemia-reperfusion (IR) injury, reduced levels of pro-apoptotic genes in the Bcl-2 family can ameliorate the destruction of mitochondrial integrity and tubular cell apoptosis, and consequently inhibit renal injury (71, 72). Sharples et al. studied a rat kidney model of severe IR injury and demonstrated that EPO inhibited the apoptosis of proximal tubular epithelial cells and promoted significant cell proliferation at high doses, despite serum starvation (73).

Anti-inflammatory Effects of EPO

Inflammation is a defensive response of living tissue that involves the vascular system and occurs following injury from factors such as infections, physical, chemical, or antigenic changes, or traumatic damage.

CKD is characterized by persistent renal inflammation that progresses to tubular interstitial fibrosis, renal failure, and end-stage renal disease (74). Elevated levels of inflammatory cytokines are associated with mortality, especially in patients with CKD. Various renal insults can activate tubulointerstitial cells and promote inflammatory cell infiltration, leading to the release of multiple vasoactive molecules and soluble cytokines that promote the progression of fibrosis. These molecules include TGF-β1, TNF-α, connective tissue growth factor, and platelet-derived growth factor. Secretion of these cytokines by tubulointerstitial and inflammatory cells alters the dynamic balance between synthesis and degradation of ECM proteins, eventually leading to the accumulation of ECM components and the development

of fibrosis. Renal innate cells (mesangial cells, podocytes, and endothelial cells) also secrete a variety of fibrogenic cytokines such as TGF-β1 and TNF-α.

EPO also has an important non-haematopoietic effects in that it can reduce inflammation caused by injury, toxins, or hypoxia. Mateus et al. reported the anti-inflammatory effect of EPO was due to its inhibition of TNF-α and IL-1β production and stimulation of IL-10 production in an animal model of TNBS-induced colitis (75). Chang et al. found that subcutaneous injection of EPO into rats with UUO significantly reduced the expression of TNF-α and mononuclear cell chemotactic protein-1 (MCP-1), decreased inflammatory cell infiltration, inhibited interstitial fibrosis, and protected kidney function (76). Heme oxygenase-1 (HO-1) is an important antioxidant protein, Katavetin et al. demonstrated that EPO induces expression of HO-1, thereby reducing oxidative stress and delaying CKD progression (77).

EPO and Autophagy

Autophagy is a conserved mechanism of cell self-degradation, in which lysosomes degrade damaged organelles and macromolecules so they can be reused. In general, autophagy is necessary to maintain cell homeostasis, and it has roles in slowing the progress of aging, promoting differentiation and development, increasing immunity and the clearance of microorganisms, and preventing the progression of tumors and other diseases (78, 79). However, excessive autophagy can have pathological effects. For example, Livingston et al., using pharmacological and genetic methods, demonstrated that sustained activation of autophagy in the proximal tubules promoted renal interstitial fibrosis in rats with UUO (80). In agreement, a study of an experimental model of neonatal necrotizing enterocolitis found that EPO reduced excessive autophagy, and contained cell damage (81). EPO also protects against rotenone-induced neurotoxicity in SH-SY5Y cells by enhancing autophagy-related signaling pathways (82). The renoprotective effects of ESAs in animal models may be due to their antiapoptotic effects. A study of kidney IR injury reported that ESAs had renoprotective effects by inducing autophagy (83). The antiapoptotic effects of EPO are dependent on JAK2 signaling and the phosphorylation of Akt by phosphatidylinositol 3-kinase. Increased Akt signaling is associated with suppression of cell apoptosis and promotion of renal fibrosis in IR injury-induced acute kidney injury (84). However, suppression of Akt phosphorylation accelerates tubular repair and inhibits renal fibrosis (85).

CONCLUSION

The classical role of EPO is the regulation of red blood cell production, but many studies have reported that EPO also has many non-erythroid effects. These findings underline the importance of investigating the global actions of rhEPO and its derivatives in pre-clinical and clinical settings. Thus, EPO may be useful for protection of the kidney because of its effects on multiple pathways, in addition to its effect on red blood cell production. More specifically, EPO can prevent the development of renal failure during the end-stages of various renal diseases, and can actively control the fibrosis of renal interstitial tissue. However, the mechanism of EPO in the prevention and treatment of renal interstitial fibrosis is not fully understood. For this reason, additional studies are required to determine the optimal dose and timing of EPO administration and how to best avoid possible adverse reactions, such as thrombosis. The recent research and development of new types of EPO for treatment of anemia and other conditions may increase the applications of EPO for additional conditions. The results of this new research may also provide new insights into the mechanism by which rhEPO prevents interstitial fibrosis and slows the progression of CKD. Lastly, we believe that the many developments and unremitting efforts from multiple medical disciplines will eventually establish a basis for the use of EPO as a treatment for renal fibrosis and will help guide future research in this area.

AUTHOR CONTRIBUTIONS

YZ, XZhu, XH, and YD contributed conception and design of the study. XW and DZ organized the database. YZ wrote the first draft of the manuscript. LJ and XZha wrote sections of the manuscript. All authors contributed to manuscript revision, read and approved the submitted version.

REFERENCES

1. Ng JK, Li PK. Chronic kidney disease epidemic: how do we deal with it? *Nephrology*. (2018) 23:116–20. doi: 10.1111/nep.13464
2. ForniOgna V, Ogna A, Ponte B, Gabutti L, Binet I, Conen D, et al. Prevalence and determinants of chronic kidney disease in the Swiss population. *Swiss Med Wkly*. (2016) 146:w14313. doi: 10.4414/smw.2016.14313
3. Liyanage T, Ninomiya T, Perkovic V, Woodward M, Stirnadel-Farrant H, Matsushita K, et al. Chronic kidney disease in Asia: protocol for a collaborative overview. *Nephrology*. (2017) 22:456–62. doi: 10.1111/nep.12821
4. Mehdi U, Toto RD. Anemia, diabetes, and chronic kidney disease. *Diabetes Care*. (2009) 32:1320–6. doi: 10.2337/dc08-0779
5. De Oliveira Junior WV, Sabino Ade P, Figueiredo RC, Rios DR. Inflammation and poor response to treatment with erythropoietin in chronic kidney disease. *J Bras Nefrol*. (2015) 37:255–63. doi: 10.5935/0101-2800.20150039
6. Zhang L, Wang F, Wang L, Wang W, Liu B, Liu J, et al. Prevalence of chronic kidney disease in China: a cross-sectional survey. *Lancet*. (2012) 379:815–22. doi: 10.1016/S0140-6736(12)60033-6
7. Mack M, Yanagita M. Origin of myofibroblasts and cellular events triggering fibrosis. *Kidney Int*. (2015) 87:297–307. doi: 10.1038/ki.2014.287
8. Sun YB, Qu X, Caruana G, Li J. The origin of renal fibroblasts/myofibroblasts and the signals that trigger fibrosis. *Differentiation*. (2016) 92:102–7. doi: 10.1016/j.diff.2016.05.008
9. Baues M, Dasgupta A, Ehling J, Prakash J, Boor P, Tacke F. Fibrosis imaging: current concepts and future directions. *Adv Drug Deliv Rev*. (2017) 121:9–26. doi: 10.1016/j.addr.2017.10.013
10. Chuang PY, Menon MC, He JC. Molecular targets for treatment of kidney fibrosis. *J Mol Med*. (2013) 91:549–59. doi: 10.1007/s00109-012-0983-z

11. Bai J, Xiao X, Zhang X, Cui H, Hao J, Han J, et al. Erythropoietin inhibits hypoxia-induced epithelial-to-mesenchymal transition via upregulation of miR-200b in HK-2 cells. *Cell Physiol Biochem*. (2017) 42:269–80. doi: 10.1159/000477327
12. Perreault AA, Venters BJ. Integrative view on how erythropoietin signaling controls transcription patterns in erythroid cells. *Curr Opin Hematol*. (2018) 25:189–95. doi: 10.1097/MOH.0000000000000415
13. Klingmüller U. The role of tyrosine phosphorylation in proliferation and maturation of erythroid progenitor cells. *Eur J Biochem*. (1997) 249:637–47. doi: 10.1111/j.1432-1033.1997.t01-1-00637.x
14. Ogunshola OO, Bogdanova AY. Epo and non-hematopoietic cells: what do we know? *Methods Mol Biol*. (2013) 982:13–41. doi: 10.1007/978-1-62703-308-4_2
15. Kimakova P, Solar P, Solarova Z, Komel R, Debeljak N. Erythropoietin and its angiogenic activity. *Int J Mol Sci*. (2017) 18:1519. doi: 10.3390/ijms18071519
16. Reinhardt M, Dey S, Noguchi CT, Zhang Y, Krakoff J, Thearle MS. Non-hematopoietic effects of endogenous erythropoietin on lean mass and body weight regulation. *Obesity*. (2016) 24:1530–36. doi: 10.1002/oby.21537
17. O'Leary OE, Canning P, Reid E, Bertelli PM, McKeown S, Brines M, et al. The vasoreparative potential of endothelial colony-forming cells in the ischemic retina is enhanced by cibinetide, a non-hematopoietic erythropoietin mimetic. *Exp Eye Res*. (2019) 182:144–55. doi: 10.1016/j.exer.2019.03.001
18. Zheng DH, Han ZQ, Wang XX, Ma D, Zhang J. Erythropoietin attenuates high glucose-induced oxidative stress and inhibition of osteogenic differentiation in periodontal ligament stem cell (PDLSCs). *Chem Biol Interact*. (2019) 305:40–7. doi: 10.1016/j.cbi.2019.03.007
19. Jelkmann W. Physiology and pharmacology of erythropoietin. *Transf Med Hemother*. (2013) 40:302–9. doi: 10.1159/000356193
20. Shih HM, Wu CJ, Lin SL. Physiology and pathophysiology of renal erythropoietin-producing cells. *J Formos Med Assoc*. (2018) 117:955–63. doi: 10.1016/j.jfma.2018.03.017
21. Baker JE. Erythropoietin mimics ischemic preconditioning. *Vascul Pharmacol*. (2005) 42:233–41. doi: 10.1016/j.vph.2005.02.004
22. Dunlop EA, Percy MJ, Boland MP, Maxwell AP, Lappin TR. Induction of signalling in non-erythroid cells by pharmacological levels of erythropoietin. *Neurodegener Dis*. (2006) 3:94–100. doi: 10.1159/000092099
23. Cao X, Chen Z, Yu Z, Ge Y, Zeng X. Pharmacokinetics of PEGylated recombinant human erythropoietin in rats. *J Anal Methods Chem*. (2014) 2014:918686. doi: 10.1155/2014/918686
24. Moore E, Bellomo R. Erythropoietin (EPO) in acute kidney injury. *Ann Intensive Care*. (2011) 1:3. doi: 10.1186/2110-5820-1-3
25. Gouva C, Nikolopoulos P, Ioannidis JP, Siamopoulos KC. Treating anemia early in renal failure patients slows the decline of renal function: a randomized controlled trial. *Kidney Int*. (2004) 66:753–60. doi: 10.1111/j.1523-1755.2004.00797.x
26. Zou YR, Zhang J, Wang J, Peng L, Li GS, Wang L. Erythropoietin receptor activation protects the kidney from ischemia/reperfusion-induced apoptosis by activating ERK/p53 signal pathway. *Transplant Proc*. (2016) 48:217–21. doi: 10.1016/j.transproceed.2016.01.009
27. Westenfelder C, Biddle DL, Baranowski RL. Human, rat, and mouse kidney cells express functional erythropoietin receptors. *Kidney Int*. (1999) 55:808–20. doi: 10.1046/j.1523-1755.1999.055003808.x
28. Hu MC, Shi M, Cho HJ, Zhang J, Pavlenco A, Liu S, et al. The erythropoietin receptor is a downstream effector of klotho-induced cytoprotection. *Kidney Int*. (2013) 84:468–81. doi: 10.1038/ki.2013.149
29. Rodrigues CE, Sanches TR, Volpini RA, Shimizu MH, Kuriki PS, Camara NO, et al. Effects of continuous erythropoietin receptor activator in sepsis-induced acute kidney injury and multi-organ dysfunction. *PLoS ONE*. (2012) 7:e29893. doi: 10.1371/journal.pone.0029893
30. Hung SC, Lin YP, Tarng DC. Erythropoiesis-stimulating agents in chronic kidney disease: what have we learned in 25 years? *J Formos Med Assoc*. (2014) 113:3–10. doi: 10.1016/j.jfma.2013.09.004
31. Kanbay M, Perazella MA, Kasapoglu B, Koroglu M, Covic A. Erythropoiesis stimulatory agent- resistant anemia in dialysis patients: review of causes and management. *Blood Purif*. (2010) 29:1–12. doi: 10.1159/000245041
32. Bamgbola O. Resistance to erythropoietin-stimulating agents: etiology, evaluation, and therapeutic considerations. *Pediatr Nephrol*. (2012) 27:195–205. doi: 10.1007/s00467-011-1839-4
33. Elliott S, Busse L, Swift S, McCaffery I, Rossi J, Kassner P, et al. Lack of expression and function of erythropoietin receptors in the kidney. *Nephrol Dial Transplant*. (2012) 27:2733–45. doi: 10.1093/ndt/gfr698
34. Elliott S, Tomita D, Endre Z. Erythropoiesis stimulating agents and reno-protection: a meta-analysis. *BMC Nephrol*. (2017) 18:14. doi: 10.1186/s12882-017-0438-4
35. Fernandez LM, Marcen R, Villafruela J, Teruel JL, Tato A, Rivera M, et al. Effect of rHuEpo therapy in dialysis patients on endogenous erythropoietin synthesis after renal transplantation. *Nephron*. (1996) 73:54–7. doi: 10.1159/000188998
36. Endre ZH, Walker RJ, Pickering JW, Shaw GM, Frampton CM, Henderson SJ, et al. Early intervention with erythropoietin does not affect the outcome of acute kidney injury (the EARLYARF trial). *Kidney Int*. (2010) 77:1020–30. doi: 10.1038/ki.2010.25
37. Locatelli F, Del Vecchio L. New strategies for anaemia management in chronic kidney disease. *Contrib Nephrol*. (2017) 189:184–8. doi: 10.1159/000450779
38. Chen P, Yang Q, Li X, Qin Y. Potential association between elevated serum human epididymis protein 4 and renal fibrosis: a systemic review and meta-analysis. *Medicine*. (2017) 96:e7824. doi: 10.1097/MD.0000000000007824
39. Park SH, Choi MJ, Song IK, Choi SY, Nam JO, Kim CD, et al. Erythropoietin decreases renal fibrosis in mice with ureteral obstruction: role of inhibiting TGF-β-induced epithelial-to-mesenchymal transition. *J Am Soc Nephrol*. (2007) 18:1497–507. doi: 10.1681/ASN.2005080866
40. Lu J, Yao YY, Dai QM, Ma GS, Zhang SF, Cao L, et al. Erythropoietin attenuates cardiac dysfunction by increasing myocardial angiogenesis and inhibiting interstitial fibrosis in diabetic rats. *Cardiovasc Diabetol*. (2012) 11:105. doi: 10.1186/1475-2840-11-105
41. Park SY, Lee JY, Tak WY, Kweon YO, Lee MS. Erythropoietin decreases carbon tetrachloride-induced hepatic fibrosis by inhibiting transforming growth factor-beta. *Chin Med J*. (2012) 125:3098–103. doi: 10.3760/cma.j.issn.0366-6999.2012.17.024
42. Sharples EJ, Yaqoob MM. Erythropoietin in experimental acute renal failure. *Nephron Exp Nephrol*. (2006) 104:e83–8. doi: 10.1159/000094546
43. Bagnis C, Beaufils H, Jacquiaud C, Adabra Y, Jouanneau C, Le Nahour G, et al. Erythropoietin enhances recovery after cisplatin-induced acute renal failure in the rat. *Nephrol Dial Transplant*. (2001) 16:932–8. doi: 10.1093/ndt/16.5.932
44. Togel FE, Ahlstrom JD, Yang Y, Hu Z, Zhang P, Westenfelder C. Carbamylated erythropoietin outperforms erythropoietin in the treatment of AKI-on-CKD and other AKI models. *J Am Soc Nephrol*. (2016) 27:3394–404. doi: 10.1681/ASN.2015091059
45. Gobe GC, Bennett NC, West M, Colditz P, Brown L, Vesey DA, et al. Increased progression to kidney fibrosis after erythropoietin is used as a treatment for acute kidney injury. *Am J Physiol Renal Physiol*. (2014) 306:F681–92. doi: 10.1152/ajprenal.00241.2013
46. Yan Y, Ma L, Zhou X, Ponnusamy M, Tang J, Zhuang MA, et al. Src inhibition blocks renal interstitial fibroblast activation and ameliorates renal fibrosis. *Kidney Int*. (2016) 89:68–81. doi: 10.1038/ki.2015.293
47. Liang H, Zhang Z, Yan J, Wang Y, Hu Z, Mitch WE, et al. The IL-4 receptor α has a critical role in bone marrow–derived fibroblast activation and renal fibrosis. *Kidney Int*. (2017) 92:1433–43. doi: 10.1016/j.kint.2017.04.021
48. Saliba Y, Karam R, Smayra V, Aftimos G, Abramowitz J, Birnbaumer L, et al. Evidence of a role for fibroblast transient receptor potential canonical 3 Ca^{2+} channel in renal fibrosis. *J Am Soc Nephrol*. (2015) 26:1855–76. doi: 10.1681/ASN.2014010065
49. Pakshir P, Hinz B. The big five in fibrosis: macrophages, myofibroblasts, matrix, mechanics, and miscommunication. *Matrix Biol*. (2018) 68–69:81–93. doi: 10.1016/j.matbio.2018.01.019
50. Diao W, Chen W, Cao W, Yuan H, Ji H, Wang T, et al. Astaxanthin protects against renal fibrosis through inhibiting myofibroblast activation and promoting CD8+ T cell recruitment. *Biochim Biophys Acta Gen Subj*. (2019) 1863:1360–70. doi: 10.1016/j.bbagen.2019.05.020
51. Nogueira A, Pires MJ, Oliveira PA. Pathophysiological Mechanisms of renal fibrosis: a review of animal models and therapeutic strategies. *In Vivo*. (2017) 31:1–22. doi: 10.21873/invivo.11019
52. Sato Y, Yanagita M. Resident fibroblasts in the kidney: a major driver of fibrosis and inflammation. *Inflam Regen*. (2017) 37:17. doi: 10.1186/s41232-017-0048-3

53. Geng XC, Hu ZP, Lian GY. Erythropoietin ameliorates renal interstitial fibrosis via the inhibition of fibrocyte accumulation. *Mol Med Rep*. (2015) 11:3860–5. doi: 10.3892/mmr.2015.3157
54. Souma T, Nezu M, Nakano D, Yamazaki S, Hirano I, Sekine H, et al. Erythropoietin synthesis in renal myofibroblasts is restored by activation of hypoxia signaling. *J Am Soc Nephrol*. (2016) 27:428–38. doi: 10.1681/ASN.2014121184
55. Fischer C, Deininger N, Wolf G, Loeffler I. CERA Attenuates kidney fibrogenesis in the db/db mouse by influencing the renal myofibroblast generation. *J Clin Med*. (2018) 7:E15. doi: 10.3390/jcm7020015
56. Lamouille S, Xu J, Derynck R. Molecular mechanisms of epithelial-mesenchymal transition. *Nat Rev Mol Cell Biol*. (2014) 15:178–96. doi: 10.1038/nrm3758
57. Li J, An C, Kang L, Mitch WE, Wang Y. Recent advances in magnetic resonance imaging assessment of renal fibrosis. *Adv Chronic Kidney Dis*. (2017) 24:150–53. doi: 10.1053/j.ackd.2017.03.005
58. Marquez-Exposito L, Lavoz C, Rodrigues-Diez RR, Rayego-Mateos S, Orejudo M, Cantero-Navarro E, et al. Gremlin regulates tubular epithelial to mesenchymal transition via VEGFR2: potential role in renal fibrosis. *Front Pharmacol*. (2018) 9:1195. doi: 10.3389/fphar.2018.01195
59. Ji X, Wang H, Wu Z, Zhong X, Zhu M, Zhang Y, et al. Specific inhibitor of Smad3 (SIS3) attenuates fibrosis, apoptosis, and inflammation in unilateral ureteral obstruction kidneys by inhibition of transforming growth factor beta (TGF-beta)/Smad3 signaling. *Med Sci Monit*. (2018) 24:1633–41. doi: 10.12659/MSM.909236
60. Zhang D, Sun L, Xian W, Liu F, Ling G, Xiao L, et al. Low-dose paclitaxel ameliorates renal fibrosis in rat UUO model by inhibition of TGFβ/Smad activity. *Lab Invest*. (2010) 90:436–47. doi: 10.1038/labinvest.2009.149
61. Grande MT, Sanchez-Laorden B, Lopez-Blau C, De Frutos CA, Boutet A, Arevalo M, et al. Snail1-induced partial epithelial-to-mesenchymal transition drives renal fibrosis in mice and can be targeted to reverse established disease. *Nat Med*. (2015) 21:989–97. doi: 10.1038/nm.3901
62. Chen CL, Chou KJ, Lee PT, Chen YS, Chang TY, Hsu CY, et al. Erythropoietin suppresses epithelial to mesenchymal transition and intercepts Smad signal transduction through a MEK-dependent mechanism in pig kidney (LLCPK1) cell lines. *Exp Cell Res*. (2010) 316:1109–18. doi: 10.1016/j.yexcr.2010.02.022
63. Imamura R, Isaka Y, Sandoval RM, Ichimaru N, Abe T, Okumi M, et al. A nonerythropoietic derivative of erythropoietin inhibits tubulointerstitial fibrosis in remnant kidney. *Clin Exp Nephrol*. (2012) 16:852–62. doi: 10.1007/s10157-012-0647-x
64. Tasanarong A, Kongkham S, Khositseth S. Dual inhibiting senescence and epithelial-to-mesenchymal transition by erythropoietin preserve tubular epithelial cell regeneration and ameliorate renal fibrosis in unilateral ureteral obstruction. *Biomed Res Int*. (2013) 2013:308130. doi: 10.1155/2013/308130
65. Abate M, Festa A, Falco M, Lombardi A, Luce A, Grimaldi A, et al. Mitochondria as playmakers of apoptosis, autophagy and senescence. *Semin Cell Dev Biol*. (2019) 98:139–53. doi: 10.1016/j.semcdb.2019.05.022
66. Yang T, Vesey DA, Johnson DW, Wei MQ, Gobe GC. Apoptosis of tubulointerstitial chronic inflammatory cells in progressive renal fibrosis after cancer therapies. *Transl Res*. (2007) 150:40–50. doi: 10.1016/j.trsl.2007.01.006
67. Lacombe C, Mayeux P. Biology of erythropoietin. *Haematologica*. (1998) 83:724–32.
68. Izquierdo MC, Sanz AB, Mezzano S, Blanco J, Carrasco S, Sanchez-Nino MD, et al. TWEAK (tumor necrosis factor-like weak inducer of apoptosis) activates CXCL16 expression during renal tubulointerstitial inflammation. *Kidney Int*. (2012) 81:1098–107. doi: 10.1038/ki.2011.475
69. Zhao XF, Liu YH, Han ZM, Xu YU. Effect of erythropoietin on the expression of dynamin-related protein-1 in rat renal interstitial fibrosis. *Exp Ther Med*. (2015) 9:2065–71. doi: 10.3892/etm.2015.2419
70. Nakazawa Y, Nishino T, Obata Y, Nakazawa M, Furusu A, Abe K, et al. Recombinant human erythropoietin attenuates renal tubulointerstitial injury in murine adriamycin-induced nephropathy. *J Nephrol*. (2013) 26:527–33. doi: 10.5301/jn.5000178
71. Sun PP, Yuan F, Xu J, Sai K, Chen J, Guan S. Cryptotanshinone ameliorates hepatic normothermic ischemia and reperfusion injury in rats by anti-mitochondrial apoptosis. *Biol Pharm Bull*. (2014) 37:1758–65. doi: 10.1248/bpb.b14-00389
72. Xu Y, Li D, Zeng L, Wang C, Zhang L, Wang Y, et al. Proteasome inhibitor lactacystin enhances cisplatin cytotoxicity by increasing endoplasmic reticulum stresseassociated apoptosis in HeLa cells. *Mol Med Rep*. (2015) 11:189–95. doi: 10.3892/mmr.2014.2683
73. Sharples EJ, Patel N, Brown P, Stewart K, Mota-Philipe H, Sheaff M, et al. Erythropoietin protects the kidney against the injury and dysfunction caused by ischemia-reperfusion. *J Am Soc Nephrol*. (2004) 15:2115–24. doi: 10.1097/01.ASN.0000135059.67385.5D
74. Morgado-Pascual JL, Marchant V, Rodrigues-Diez R, Dolade N, Suarez-Alvarez B, Kerr B, et al. Epigenetic modification mechanisms involved in inflammation and fibrosis in renal pathology. *Mediators Inflamm*. (2018) 2018:2931049. doi: 10.1155/2018/2931049
75. Mateus V, Rocha J, Alves P, Mota-Filipe H, Sepodes B, Pinto RMA. Anti-inflammatory effect of erythropoietin in the TNBS-induced colitis. *Basic Clin Pharmacol Toxicol*. (2017) 120:138–45. doi: 10.1111/bcpt.12663
76. Chang YK, Choi DE, Na KR, et al. Erythropoietin attenuates renal injury in an experimental model of rat unilateral ureteral obstruction via anti-inflammatory and anti-apoptotic effects. *J Urol*. (2009) 3:1434–43. doi: 10.1016/j.juro.2008.10.105
77. Katavetin P, Inagi R, Miyata T, Shao J, Sassa R, Adler S, et al. Erythropoietin induces heme oxygenase-1 expression and attenuates oxidative stress. *Biochem Biophys Res Commun*. (2007) 359:928–34. doi: 10.1016/j.bbrc.2007.05.207
78. Ryter SW, Mizumura K, Choi AM. The impact of autophagy on cell death modalities. *Int J Cell Biol*. (2014) 2014:502676. doi: 10.1155/2014/502676
79. Jing K, Lim K. Why is autophagy important in human diseases? *Exp Mol Med*. (2012) 44:69–72. doi: 10.3858/emm.2012.44.2.028
80. Livingston MJ, Ding HF, Huang S, Hill JA, Yin XM, Dong Z. Persistent activation of autophagy in kidney tubular cells promotes renal interstitial fibrosis during unilateral ureteral obstruction. *Basic Res Papers*. (2016) 12:976–98. doi: 10.1080/15548627.2016.1166317
81. Yu Y, Shiou SR, Guo Y, Lu L, Westerhoff M, Sun J, Petrof EO, et al. Erythropoietin protects epithelial cells from excessive autophagy and apoptosis in experimental neonatal necrotizing enterocolitis. *PLoS ONE*. (2013) 8:e69620. doi: 10.1371/journal.pone.0069620
82. Jang W, Kim HJ, Li H, Jo KD, Lee MK, Yang HO. The neuroprotective effect of erythropoietin on rotenone-induced neurotoxicity in SH-SY5Y cells through the induction of autophagy. *Mol Neurobiol*. (2016) 53:3812–21. doi: 10.1007/s12035-015-9316-x
83. Yang C, Xu Z, Zhao Z, Li L, Zhao T, Peng D, et al. A novel proteolysis-resistant cyclic helix B peptide ameliorates kidney ischemia reperfusion injury. *Biochim Biophys Acta*. (2014) 1842:2306–17. doi: 10.1016/j.bbadis.2014.09.001
84. Tang J, Liu N, Tolbert E, Ponnusamy M, Ma L, Gong R, et al. Sustained activation of EGFR triggers renal fibrogenesis after acute kidney injury. *Am J Pathol*. (2013) 183:160–72. doi: 10.1016/j.ajpath.2013.04.005
85. Yang C, Cao Y, Zhang Y, Li L, Xu M, Long Y, et al. Cyclic helix B peptide inhibits ischemia reperfusion-induced renal fibrosis via the PI3K/Akt/FoxO3a pathway. *Transl Med*. (2015) 13:355. doi: 10.1186/s12967-015-0699-2

Conflict of Interest: The authors declare that the research was conducted in the absence of any commercial or financial relationships that could be construed as a potential conflict of interest.

Copyright © 2020 Zhang, Zhu, Huang, Wei, Zhao, Jiang, Zhao and Du. This is an open-access article distributed under the terms of the Creative Commons Attribution License (CC BY). The use, distribution or reproduction in other forums is permitted, provided the original author(s) and the copyright owner(s) are credited and that the original publication in this journal is cited, in accordance with accepted academic practice. No use, distribution or reproduction is permitted which does not comply with these terms.

frontiers in Pharmacology

ORIGINAL RESEARCH
published: 25 February 2020
doi: 10.3389/fphar.2020.00128

Dexmedetomidine Protects Against Lipopolysaccharide-Induced Acute Kidney Injury by Enhancing Autophagy Through Inhibition of the PI3K/AKT/mTOR Pathway

Yuan Zhao, Xiujing Feng, Bei Li, Jichen Sha, Chaoran Wang, Tianyuan Yang, Hailin Cui and Honggang Fan *

Heilongjiang Key Laboratory for Laboratory Animals and Comparative Medicine, College of Veterinary Medicine, Northeast Agricultural University, Harbin, China

OPEN ACCESS

Edited by:
John D. Imig,
Medical College of Wisconsin, United States

Reviewed by:
Hyung Sik Kim,
Sungkyunkwan University, South Korea
Jonatan Barrera-Chimal,
Universidad Nacional Autónoma de México, Mexico

***Correspondence:**
Honggang Fan
fanhonggang2002@163.com

Specialty section:
This article was submitted to Renal Pharmacology, a section of the journal Frontiers in Pharmacology

Received: *09 November 2019*
Accepted: *29 January 2020*
Published: *25 February 2020*

Citation:
Zhao Y, Feng X, Li B, Sha J, Wang C, Yang T, Cui H and Fan H (2020) Dexmedetomidine Protects Against Lipopolysaccharide-Induced Acute Kidney Injury by Enhancing Autophagy Through Inhibition of the PI3K/AKT/mTOR Pathway. Front. Pharmacol. 11:128. doi: 10.3389/fphar.2020.00128

Background: Acute kidney injury (AKI) is often secondary to sepsis. Previous studies suggest that damaged mitochondria and the inhibition of autophagy results in AKI during sepsis, but dexmedetomidine (DEX) alleviates lipopolysaccharide (LPS)-induced AKI. However, it is uncertain whether the renoprotection of DEX is related to autophagy or the clearance of damaged mitochondria in sepsis-induced AKI.

Methods: In this study, AKI was induced in rats by injecting 10 mg/kg of LPS intraperitoneally (i.p.). The rats were also pretreated with DEX (30 μg/kg, i.p.) 30 min before the injection of LPS. The structure and function of kidneys harvested from the rats were evaluated, and the protein levels of autophagy-related proteins, oxidative stress levels, and apoptosis levels were measured. Further, atipamezole (Atip) and 3-Methyladenine (3-MA), which are inhibitors of DEX and autophagy, respectively, were administered before the injection of DEX to examine the protective mechanism of DEX.

Results: Pretreatment with DEX ameliorated kidney structure and function. DEX decreased the levels of blood urea nitrogen (BUN) and creatinine (Cre), urine kidney injury molecule-1 (KIM-1), neutrophil gelatinase-associated lipocalin (NGAL), reactive oxygen species (ROS), and apoptosis proteins (such as cleaved caspase-9 and cleaved caspase-3). However, DEX upregulated the levels of autophagy and mitophagy proteins, such as Beclin-1, LC3 II and PINK1. These results suggest that DEX ameliorated LPS-induced AKI by reducing oxidative stress and apoptosis and enhancing autophagy. To promote autophagy, DEX inhibited the phosphorylation levels of PI3K, AKT, and mTOR. Furthermore, the administration of Atip and 3-MA inhibitors blocked the renoprotection effects of DEX.

Conclusions: Here, we demonstrate a novel mechanism in which DEX protects against LPS-induced AKI. DEX enhances autophagy, which results in the removal of damaged

mitochondria and reduces oxidative stress and apoptosis in LPS-induced AKI through the α_2-AR and inhibition of the PI3K/AKT/mTOR pathway.

Keywords: acute kidney injury, dexmedetomidine, LPS, autophagy, apoptosis

INTRODUCTION

Sepsis, a systemic inflammatory response syndrome (SIRS), is caused by infection, can induce multiple organs dysfunction and even death (Bellomo et al., 2017). According to the 2018 World Health Organization report, more than 30 million people worldwide are diagnosed with sepsis each year (Kumar et al., 2019). The mortality rate of patients with sepsis is more than 10%, but increases to 40% in severe cases, such as septic shock (Assinger et al., 2019). The kidney is one of the most vulnerable organs during sepsis, and acute kidney injury (AKI) occurs in 40–50% of septic patients with a mortality rate of up to 60% (Plotnikov et al., 2019). The underlying pathogenesis of sepsis acute kidney injury (SAKI) is not well understood but includes oxidative stress (Chen et al., 2019), inflammation (Feng et al., 2019), and apoptosis (Kang et al., 2018). Recently, it was reported that autophagy played a key role in SAKI, and the inhibition of autophagy resulted in the development of AKI during sepsis (Ho et al., 2016). However, the specific role of autophagy in SAKI remains unclear.

Autophagy is a mechanism which recycles damaged organelles and cellular components in response to various stress conditions such as nutrient deprivation (Filomeni et al., 2015), metabolic balance (Maiuri et al., 2007), apoptosis (Maiuri et al., 2007) and inflammation (Kimura et al., 2017), and is beneficial for cell survival. Clinical and preclinical studies confirm that sepsis triggers autophagy in multiple organs, including the kidney (Wan et al., 2016; Chung et al., 2017; Kimura et al., 2017; Sun et al., 2019), and an increasing amount of evidence suggests that stimulating autophagy *via* pharmacological approaches protects the kidney during sepsis (Mei et al., 2016). Mitophagy, the selective removal of mitochondria by autophagy, also plays an important role in SAKI (Kaushal and Shah, 2016). Mitophagy is necessary to maintain cellular homeostasis and ensure healthy mitochondria. Mitophagy is regulated by two pathways, including the PTEN-induced putative protein kinase 1 (PINK1)/Parkin-dependent and PINK1/Parkin-independent (e.g., BNIP3 and FUNDC1) pathways (Ishimoto and Inagi, 2016). The PINK1/Parkin pathway is the main regulator of mitophagy and has been studied in multiple disease models (Kaushal and Shah, 2016; Sorrentino et al., 2017). Mitophagy can limit cell death from mitochondrial oxidant stress and promote the release of pro-apoptotic proteins (Sun et al., 2018). It has been demonstrated that mitophagy plays a critical role in mitochondrial quality control, tubular cell survival, and renal function during ischemic AKI (Tang et al., 2018). Therefore, autophagy and mitophagy may play key roles in SAKI by reducing oxidant stress and apoptosis.

Dexmedetomidine (DEX) is a highly selective alpha-2 adrenergic receptor (α_2-AR) agonist (Kawazoe et al., 2017). Our previous studies have shown that DEX exhibits anti-inflammatory and anti-oxidative effects in LPS-induced AKI (Chen et al., 2019; Feng et al., 2019; Yao et al., 2019). It has also demonstrated that DEX has anti-inflammatory and anti-apoptotic effects in LPS-induced AKI (Kang et al., 2018). In the macrophage cell line RAW 264.7, DEX alleviated LPS-induced apoptosis and inflammation through PINK1-mediated mitophagy, which eliminated damaged mitochondria (Wang et al., 2019). Furthermore, it has been shown that DEX alleviated LPS-induced acute lung injury through the PI3K/AKT/mTOR pathway (Meng et al., 2018). Inhibition of the kinase mammalian target of rapamycin (mTOR), a major modulator of autophagy, promotes the initiation of autophagy (Munson and Ganley, 2015). mTOR is a downstream target of the phosphatidylinositol 3 kinase (PI3K) and protein kinase B (AKT) pathway (Heras-Sandoval et al., 2014). AKT activates the mTOR complex 1 (mTORC1) to inhibit autophagy. In this study, we hypothesized that DEX regulates autophagy to alleviate SAKI *via* the PI3K/AKT/mTOR pathway.

Our studies aimed to determine the role of autophagy (including mitophagy) in SAKI, identify the relationship between DEX renoprotection and autophagy during sepsis, and determine how DEX regulates autophagy in SAKI using the autophagy inhibitor 3-Methyladenine (3-MA). Our studies provide a further understanding of the pharmacological mechanism of DEX and increase its clinical application value.

MATERIALS AND METHODS

Animals and Treatment

Adult male Sprague Dawley (SD) rats (weight 180–220 g) were procured from the Second Affiliated Hospital of Harbin Medical University (Harbin, China). Rats were housed under conditions of controlled temperature (21–25°C) and humidity (45–55%), with a 12 h light/dark cycle for 7 days to adjust to the environment. Rats were housed in groups (3 per cage) and received tap water and a standard rat chow diet ad libitum. All experimental procedures in this study adhered the requirements of the Animal Experimental Committee of Northeast Agricultural University and complied with the National Institutes of Health Guide for the Care and Use of Laboratory Animals.

Thirty-six rats were randomly divided into six groups (n = 6) as follow:

1. The CON group did not receive any treatments.
2. The CON+DEX group was injected intraperitoneally (i.p.) with DEX (30 μg/kg, American Pfizer) without any additional treatments.
3. The LPS group received LPS (10 mg/kg, i.p., *Escherichia coli* O111:B4, L2630, Sigma-Aldrich, USA) 4 h before sacrifice.
4. The DEX+LPS group was injected with DEX 30 min before the injection of LPS.

5. The Atip+DEX+LPS group was injected with atipamezole (Atip) (an α_2-AR antagonist) (300 mg/kg, i.p., American Pfizer) 30 min before injection of DEX; 30 min after the injection of DEX, injection of LPS.
6. The 3-MA+DEX+LPS group was injected with 3-MA (30 mg/kg, i.p., S1075, Selleck, Shanghai, China) 30 min before injection of DEX; 30 min after the injection of DEX, injection of LPS.

Four hours after the last treatment, all rats were quickly anesthetized with isoflurane (Yipin Pharmaceutical Co., Ltd., Hebei, China) to collect blood, urine, and kidney samples and no rats died until sacrificed.

Assessment of Kidney Function

Blood samples were collected quickly by heart puncture. After coagulating 30 min, the blood samples were centrifuged at 3,000 rpm for 10 min at room temperature to collect serum. Using an automated analyzer (Roche Diagnostics, Mannheim, Germany) detected Serum blood urea nitrogen (BUN) and creatinine (Cre) levels. Using enzyme-linked immunosorbent assay analyzed kidney injury molecule-1 (KIM-1) (RKM100, R&D Systems, USA) and neutrophil gelatinase-associated lipocalin (NGAL) (DY3508, R&D Systems, USA) levels of urine samples.

ELISA Assay for Serum Inflammation Cytokine

Using a commercial ELISA kit (Nanjing Jiancheng Bioengineering Institute, Nanjing, China) examined serum tumor necrosis factor-α (TNF-α) (H052), interleukin (IL)-1β (H002), IL-6 (H007), and IL-18 (H0015) according to the manufacturer's instructions.

Histological and Ultrastructural Observations

Kidney fixed in 10% neutral-buffered formalin solution were dehydrated, seeded, dipped in wax, embedded, sectioned and stained with hematoxylin and eosin stain and then observed by light microscopy (BX-FM; Olympus Corp, Tokyo, Japan). Renal tissue with the following histopathological changes were judged injured: loss of brush border, vacuolization, cast formation, tubular dilation and disruption, cell lysis, and cellular necrosis. Tissue damage was checked in a blinded manner and scored by the percentage of damaged tubules: 0, no damage; 1, 0–25%; 2, 25–50%; 3, 50–75%; 4, more than 75% (Tang et al., 2018).

The kidneys were fixed overnight with 3% glutaraldehyde, rinsed three times with 0.1 M phosphate buffer saline (PBS) for 15 min each time. The pellet was fixed with 1% osmic acid 90 min and then rinsed three times with 0.1 M PBS for 15 min each. Thereafter, the samples were dehydrated in different gradients of ethanol (50, 70, 90, and 100%) for 10 min. Then placed in fresh pure Epon resin and polymerized at 60°C for 2 h. Finally, the ultrathin sections (60 nm) were doubled stained with uranyl acetate and lead citrate. The observation was done on a transmission electron microscope (Tecnai, Hitachi, Tokyo, Japan) at 100 kV Electron Microscopy Film 4489 (Kodak, ESTAR thick base, San Francisco, CA)

Measurement of Oxidative Stress Markers

According to the manufacturer's instructions, using the corresponding assay kit (Nanjing Jiancheng Bioengineering Institute, Nanjing, China) measured the levels of reactive oxygen species (ROS) (E004-1-1), glutathione (GSH) (A006-1-1), and malondialdehyde (MDA) (A003-2-2) and tested the activity of superoxide dismutase (SOD) (A001-3-2) and catalase (CAT) (A007-1-1).

Western Blot Analysis

Equal amounts of protein samples were loaded onto sodium dodecyl sulfate-polyacrylamide gel, electrophoresed, and then transferred to polyvinylidene difluoride membranes. Membranes were blocked in 5% bull serum albumin or skim milk for 2 h at room temperature, incubated with the primary antibody in the anti-dilution buffer (Leagene Biotechnology, Beijing, China) overnight at 4°C. Primary antibodies and dilutions were as follows: Bax (1:500, sc-23959), Parkin (1:500, sc-32282), PINK1 (1:500, sc-517353), caspase-3 (1:500, sc-373730), caspase-9 (1:500, sc-56076), p62 (1:500, sc-48402) and p-AKT (1:500, sc-514032) from Santa Cruz Biotechnology, USA. Cytochrome C (Cyt C) (1:1000, WL02410); PI3 Kinase p85 (1:500, WL02240), GAPDH (1:2,000, WL01547), p-mTOR (1:500, WL03694), AKT (1:1,000, WL0003b) and Bcl-2 (1:500, WL01556) from Wanlei Bio, China. PI3 Kinase p85 (phospho-Tyr467/199) (1:750, #11508) from Signalway Antibody, USA. MAP1LC3B (1:1,000, A11280) from ABclonal, China. mTOR (1:1,000, A5866) from bimake, USA. Beclin-1(1:1,000, #3495) from Cell Signaling Technology, USA. After washed with Tris-buffered saline containing Tween (TBST), the membranes were incubated with horseradish peroxidase (HRP)-conjugated goat anti-rabbit IgG antibody (1:20,000, ZB-2301, ZSGB-Bio, Beijing, China) or anti-mouse IgG antibody (1:20,000, ZB-2305, ZSGB-Bio, Beijing, China) for 2 h at room temperature then washed with TBST. Protein bands were visualized using ECL plus Western Blot Detection Reagents (GE Healthcare).

Analysis of Apoptosis

Using TUNEL Apoptosis Assay kit (11684795910, Roche, Basel, Switzerland) measured apoptosis, according to the manufacturer's instructions. Then samples were examined under a fluorescence microscope after anti fluorescence quenching.

Real-time Polymerase Chain Reaction (RT-PCR) Analyses

According to the manufacturer's instructions, Using Eastep Super Total RNA Extraction Kit (Promega Biotech Co, Ltd, Beijing, China) extracted total RNA from kidney. Using NanoDrop2000 (Thermo Fisher Inc., Waltham, MA, USA) tested the purity and concentration of total RNA.

Then according to the manufacturer's instructions, using GoScript™ Reverse Transcription System (Promega Biotech Co, Ltd, Beijing, China) reversely transcribed total RNA into cDNA. **Table 1** shows the PCR primer sequences. Real-time PCR was implemented in the Roche 480 System (Roche, Switzerland) using SYBR Green PCR Core Reagents (Roche, Switzerland). GAPDH was used as the internal reference for relative quantitative analysis of gene mRNA expression level. Data were analyzed according to the $2^{-\Delta\Delta Ct}$ method.

TABLE 1 | Primer sequence in this study.

Gene	No.	Sequences
PINK1	NM_001106694.1	Forward: 5′GTATGAAGCCACCATGCCCA3′ Reverse: 5′ACGACATCTGGGCCTTTTCC3′
MAPLC3b	NM_022867.2	Forward: 5′AGCACTGGCTGTGTAAGACT3′ Reverse: 5′ TGCCTACGTTCTGATCTGTGG3′
Beclin-1 (Becn1)	NM_001034117.1	Forward: 5′ GATGGAGCAGAAGCCGACTC3′ Reverse: 5′TCGTGTCCAGTTTCAGAGGC3′
p62 (SQSTM1)	NM_175843.4	Forward:5′ TGGAGTCGGATAACTGCTCAGGAG3′ Reverse:5′ AGACTGGAGTTCACCTGTGGATGG3′
GADPH	NM_017008.4	Forward: 5′AGTGCCAGCCTCGTCTCATA3′ Reverse: 5′GATGGTGATGGGTTTCCCGT3′

Immunohistochemistry (IHC) and Immunofluorescence (IF) Staining

Expression of Beclin-1, LC3, p62 and Cyt C in kidney tissues was detected by IHC staining. Paraffin-embedded kidney tissue fraction (5 μm thickness) and xylene dewaxed, then dehydrated using graded concentrations of alcohol, and incubation with 3% H_2O_2 inhibited endogenous peroxidase. After blocked in 10% goat serum for 10 min at room temperature, incubated with the primary antibody in blocking solution overnight at 4°C. The primary antibodies for IHC were p62 (1:50, sc-48402), Beclin-1 (1:200, WL02508, Wanlei Bio), MAPLC3B (1:50, A11280), and Cyt C (1:200, WL02410). After slides were washed in PBS and applied HRP-labeled anti-rabbit IgG (1:100; Beyotime, China) for 30 min at 37°C, then washed with PBS again. Staining was visualized by reaction with 3,3'-diaminobenzidine (DAB) (Solarbio, Beijing, China) and counterstaining with hematoxylin. Sections were made transparent with xylene. Finally, using the DP73 type microscope (Olympus, Japan) observed sections. We also performed IF co-staining using PINK1 (1:50, sc-517353) and VDAC1 (1:50, sc-390996, Santa Cruz Biotechnology, USA) antibodies to delineate the mitophagy in the kidney. Then images were acquired with a Nikon Eclipse Ni inverted microscope (TE2000, Nikon, Tokyo, Japan).

Statistical Analysis

Data were expressed as mean ± SEM (standard error means). The data were analyzed by SPSS 18.0 (Chicago, IL, USA). A one-way analysis of variance (ANOVA) followed by Tukey's *post hoc* test was used to multi-group comparison. Using GraphPad Prism 7 software (GraphPad Software Inc., San Diego, CA, United States) made graphs. Statistically significant were considered to be significant when $p < 0.05$, and extremely significant when $p < 0.01$.

RESULTS

Effects of DEX on Renal Function and Structural Changes

BUN and Cre are important indicators of the severity of renal impairment. Furthermore, NGAL and KIM-1 have been identified as specific biomarkers of kidney injury (Han et al., 2002; Bolignano et al., 2008), and their increased expression is associated with early renal tubular injury in AKI (Chen et al., 2019). The levels of BUN (**Figure 1Aa**), Cre (**Figure 1Ab**), KIM-1 (**Figure 1Ac**), and NGAL (**Figure 1Ad**) were significantly increased after LPS injection, and DEX pretreatment significantly decreased the levels of these markers, which indicated that DEX alleviates LPS-induced kidney injury. However, the protective effects of DEX were reversed by treatment with Atip and 3-MA.

Analysis of the pathological sections of rat kidneys revealed intact glomerular and tubular structures in the CON group (**Figure 1B**). In contrast, there were substantial pathological changes in the LPS group, which included edema of renal tubular epithelial cells (green arrow), tubular necrosis (blue arrow), telangiectasia and severe congestion/hemorrhage (red arrow), and cast formation (yellow arrow) (**Figure 1B**). However, the LPS-induced kidney damage was significantly improved by pretreatment with DEX. In addition, the protective effect of DEX was reversed by Atip and 3-MA, and similar damage was observed in these two groups as in the LPS group.

Renal ultrastructure changes are shown in **Figure 2**. In the CON group, cells had an intact nuclear morphology, and cell mitochondria exhibited normal morphology with clearly discernible cristae. In the LPS group, we observed mitochondria defects, such as swelling, disorganization, and reduction or vanishing of the cristae (red arrow). We also observed typical apoptotic features, including chromatin margination, condensation, and fragmentation (orange arrow), in the LPS group. These results suggest damaged mitochondria induced apoptosis in LPS-induced AKI. DEX pretreatment alleviated cell mitochondria injury and apoptosis that were induced by LPS, and we also observed mitophagy (green arrow) and autolysosomes (blue arrow). However, the administration of Atip and 3-MA reversed the effects of DEX. These results suggest that DEX alleviates LPS-induced kidney injury *via* the α_2-AR and the enhancement of autophagy.

Effects of DEX on Renal Inflammation and Oxidative Stress

To further elucidate the relationship between DEX renoprotection and autophagy, we measured the levels of inflammatory cytokines and oxidative stress. LPS significantly elevated the levels of interleukin (IL)-6 (**Figure 3Aa**), tumor necrosis factor-alpha (TNF-α) (**Figure 3Ab**), IL-18 (**Figure 3Ac**), and IL-1β (**Figure 3Ad**), whereas DEX significantly decreased the levels of these four markers. Compared with the LPS+DEX group, the levels of these inflammatory cytokines were significantly increased in the Atip +DEX+LPS and 3-MA+DEX+LPS groups. These results suggest that DEX reduces the levels of inflammatory cytokines *via* the α_2-AR and the enhancement of autophagy.

We measured the levels of ROS, CAT, MDA, SOD, and GSH in kidney tissues. In the LPS group, the levels of ROS (**Figure 3Ba**) and MDA (**Figure 3Bb**) were significantly elevated, and the levels of CAT (**Figure 3Bc**), GSH (**Figure 3Bd**), and SOD (**Figure 3Be**) were markedly decreased. DEX not only significantly reduced ROS and MDA levels, but also increased SOD and CAT activity and increased GSH levels. However, 3-MA and Atip significantly reversed these DEX-induced changes, suggesting that DEX protects against oxidative stress *via* the α_2-AR and the enhancement of autophagy.

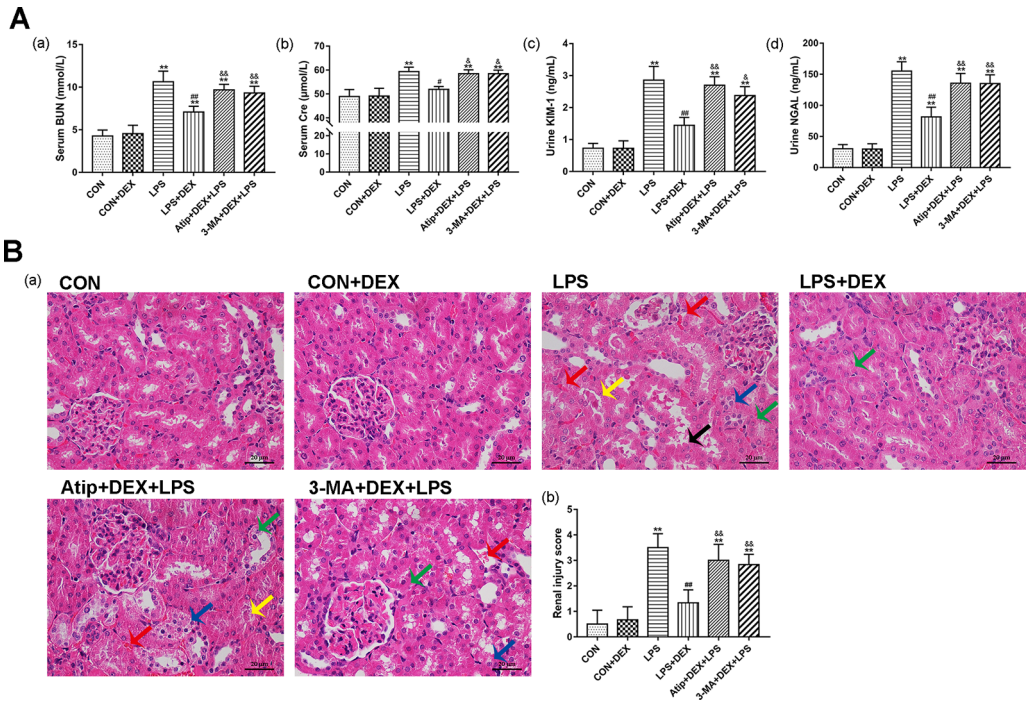

FIGURE 1 | Protective effect of DEX in LPS-induced AKI. **(A)** DEX improved renal dysfunction in LPS-induced AKI: the levels of serum BUN (a), serum Cre (b), urine KIM-1 (c), and urine NGAL (d) in rats. **(B)** Histopathological examination of the kidney: (a) Representative images from different groups. Green arrow indicates edema of renal tubular epithelial cells; blue arrow indicates tubular necrosis; yellow arrow indicates cast formation; red arrow indicates hemorrhage. Magnification: 400×, Bar: 20 μm. (b) Semiquantitative histopathological score of injury. Data are expressed as mean ± SEM (n = 6). **p < 0.01 versus CON group. #p < 0.05, ##p < 0.01 versus LPS group. &p < 0.05, &&p < 0.01 versus DEX + LPS group.

Effects of DEX on Renal Apoptosis

Using the terminal uridine nick-end labeling (TUNEL) assay, we measured apoptosis in kidney tissue sections. There were a few apoptotic cells in the CON group, but apoptosis was elevated in the LPS group. However, the levels of apoptosis were decreased in the DEX group compared with the LPS group, and the levels of apoptosis were significantly increased in the Atip+DEX+LPS and 3-MA+DEX+LPS groups compared with the LPS+DEX group (**Figures 4A, B**).

We also determined the expression of apoptosis-related proteins and the ratio of Bax/Bcl-2 (**Figure 5Ab**). The levels of apoptosis-related proteins, such as Bax (**Figure 5Aa**), Cyt C (**Figures 5Aa, c, B**), cleaved caspase-9 (**Figure 5Aa, d**), and cleaved caspase-3 (**Figure 5Aa, e**), were significantly elevated in the LPS group. However, DEX reduced the levels of these apoptosis-related proteins. Additionally, the administration of Atip and 3-MA reversed the effect of DEX. These results indicate that LPS induces mitochondrial apoptosis in AKI, and DEX reduces cell apoptosis *via* the α_2-AR and the enhancement of autophagy.

Effect of DEX on Renal Autophagy and the PINK1/Parkin Mitophagy

Beclin-1 is a key molecule that controls autophagic activity. LC3 is a marker of autophagosome formation, and the ratio of LC3 II/LC3 I correlates to the number of autophagosomes. The levels of Beclin-1 (**Figures 6A–C, E**) and LC3 II (**Figures 6A–C, E**) were decreased in the LPS group but increased after pretreatment with DEX. The polyubiquitin-binding protein p62/SQSTM1 (**Figures 6A–C, E**), which degraded during autophagy, showed the reverse trend. Treatment with Atip and 3-MA reversed the effect of DEX. Similar changes in the mRNA and protein of Beclin-1 and LC3 were observed (**Figures 6Da, b**), but p62 mRNA did not change in every group (**Figure 6Dc**). These results indicate that LPS inhibits autophagy, and DEX enhances autophagy *via* the α_2-AR.

Having observed mitophagy (**Figure 2**) from renal ultrastructure changes in the LPS+DEX group, we next measured the levels of mitophagy-related proteins. The amount of PINK1 was very low in the CON group. PINK1 largely accumulated on mitochondria in the LPS group, but the pretreatment with DEX decreased the amount of PINK1 (**Figures 7A, C**). The changes in Parkin (**Figure 7A**) were consistent with PINK1. The change in PINK mRNA (**Figure 7B**) was a reverse trend compared with the change of protein, which suggested LPS downregulated the transcription of PINK1, whereas DEX upregulated its transcription. Further, the use of Atip and 3-MA reversed the effects of DEX.

DEX Regulates Autophagy *via* Inhibiting the PI3K/AKT/mTOR Pathway

The mechanism underlying the protective effect of DEX through the modulation of autophagy was further investigated by assessing the levels of PI3K, AKT, and mTOR in kidney tissues

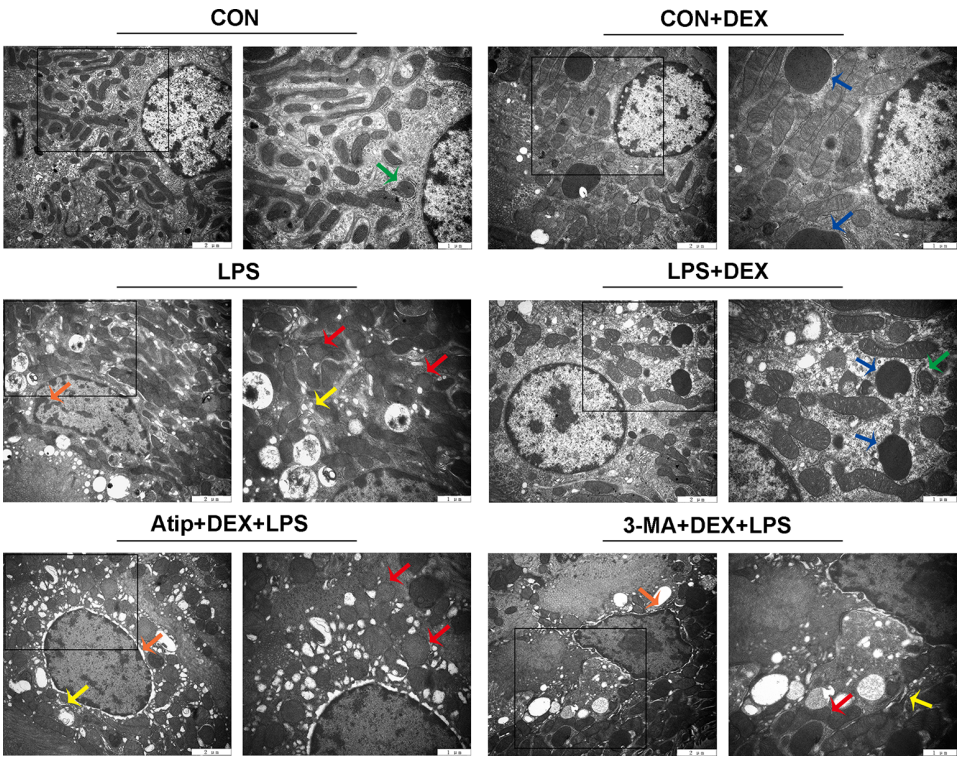

FIGURE 2 | The ultrastructure examination of the kidney. Representative ultrastructure samples from different groups. Red arrow indicates mitochondria appeared swelling, vacuolization and loss of cristae; orange arrow indicates chromatin margination, condensation, and fragmentation; yellow arrow indicates endoplasmic reticulum swelling; blue arrow indicates autolysosome; green arrow indicates mitophagy.

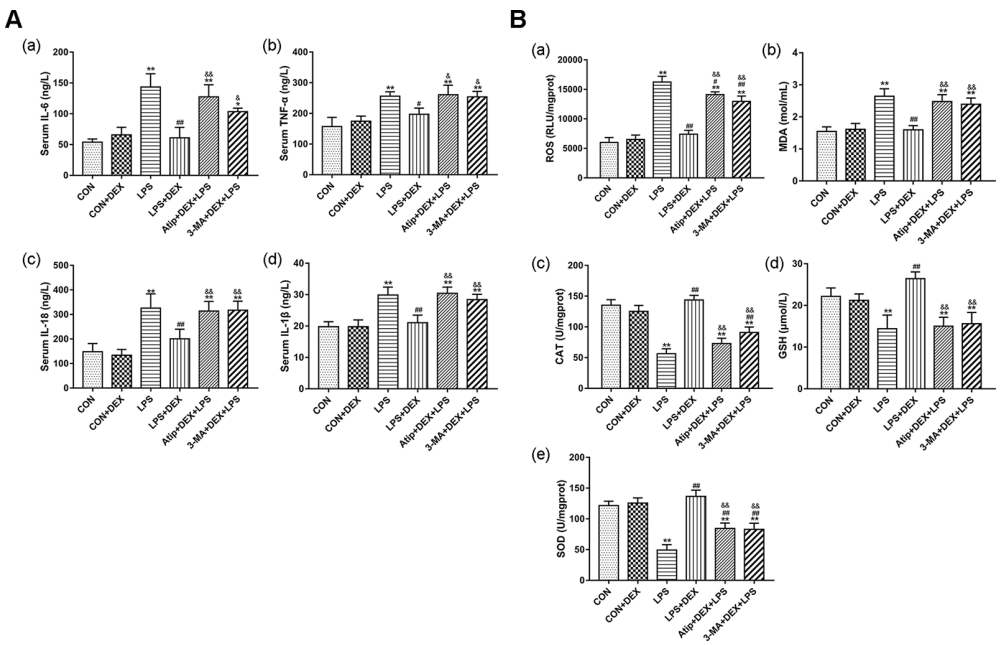

FIGURE 3 | DEX reduced inflammation and oxidative stress in LPS-induced AKI. **(A)** The content of inflammatory cytokines in serum, including IL-6 (a), TNF-α (b), IL-18 (c), IL-1β (d). **(B)** The content of ROS (a); the concentration of MDA (b); the activity of CAT (c); the content of GSH (d); the activity of SOD (e). Data are expressed as mean ± SEM (n = 6). *p < 0.05, **p < 0.01 versus CON group. #p < 0.5, ##p < 0.01 versus LPS group. &p < 0.05, &&p < 0.01 versus DEX + LPS group.

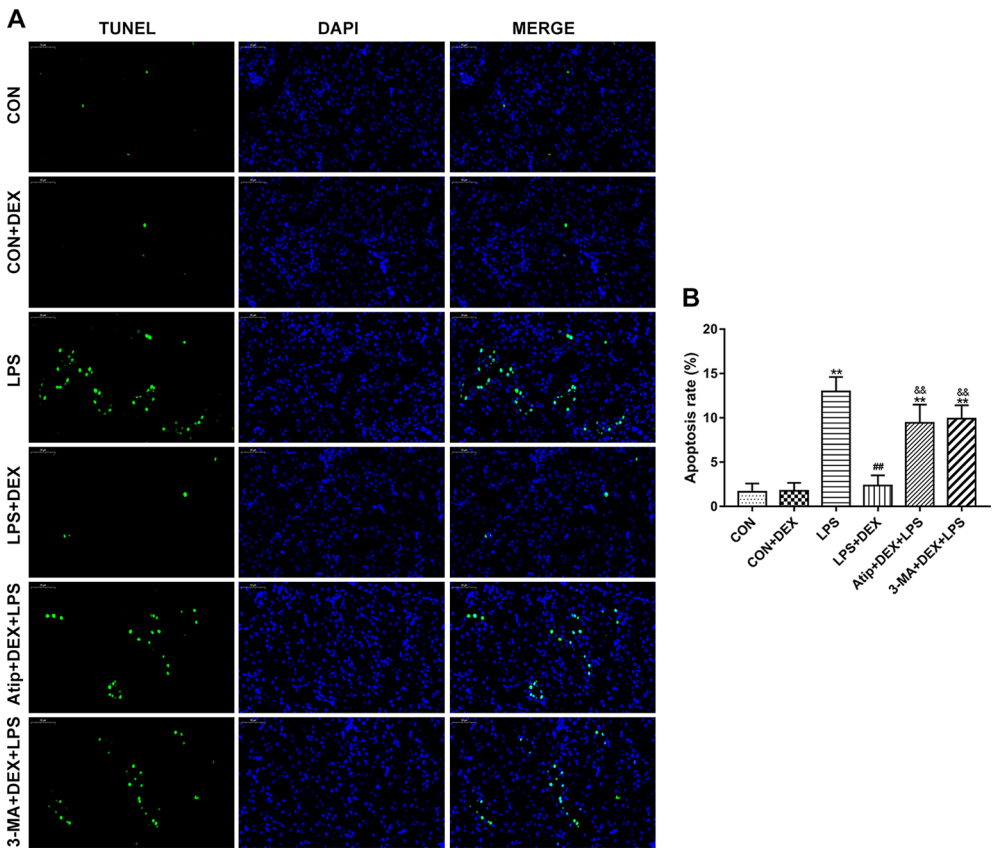

FIGURE 4 | Effect of DEX on renal apoptosis. **(A)** Representative images of TUNEL assay in renal tissue. Bar: 50 μm. **(B)** TUNEL-positive cells rate in kidney tissues. Data are expressed as mean ± SEM (n = 6). **p < 0.01 versus CON group. ##p < 0.01 versus LPS group. &&p < 0.01 versus DEX + LPS group.

(**Figure 8A**). In the LPS group, the phosphorylation levels of PI3K, AKT, and mTOR were increased compared with the CON group. However, pretreatment with DEX reduced these protein phosphorylation levels compared with the LPS group, and Atip reversed the effects of DEX. These results indicate that DEX inhibited the PI3K/AKT/mTOR pathway *via* the α_2-AR.

DISCUSSION

In our previous study, we demonstrated that DEX plays a protective role against SAKI *via* attenuating oxidative stress and downregulating inflammatory factors. Here, we further examined the mechanisms underlying the protective effect of DEX on SAKI by focusing on the potential involvement of DEX in the modulation of autophagy.

LPS, a known toxic component of Gram-negative bacteria, is widely used to induce SAKI in animal models (Jou-Valencia et al., 2018), and studies have confirmed that the intraperitoneal administration of LPS for 4 h induces AKI (Chen et al., 2019; Feng et al., 2019). After LPS treatment, the indicators of kidney injury (BUN, Cre, KIM-1, and NGAL) are significantly increased, suggesting renal dysfunction and kidney injury. Additionally, the integrity of glomerular and tubular structures is disrupted, and edema of renal tubular epithelial cells, tubular necrosis, and cast formation are observed. In renal tissue sections, telangiectasia, severe congestion, and hemorrhage also occur. These structural changes indicate that LPS destroys renal tissue structure and induces AKI.

Our results show that oxidative stress, inflammation, and apoptosis occur in the kidney after the administration of LPS. Meanwhile, the inhibition of autophagy occurs in the kidney. We observed the reduction of Beclin-1 and LC3 II and the accumulation of p62 in the kidney after treatment with LPS. However, another study showed that renal autophagy was rapidly induced by LPS, and this was followed by the progression from autophagosome to autolysosome, and finally by autophagic degradation (Mei et al., 2016).These results are different from ours, but differences in autophagy exist in many studies, and these differences are currently being studied by many research groups. These differences are likely associated with the use of various experimental models and the time-points monitored. Recently, Yuxiao Sun confirmed that in a mouse heart, autophagy increased in a dose-dependent manner at low doses of LPS (0.25–2.5 mg/kg), but this was followed by a gradual decline at higher doses of 5–15 mg/kg (Sun et al., 2018). This suggests that autophagy was upregulated in less severe or mild

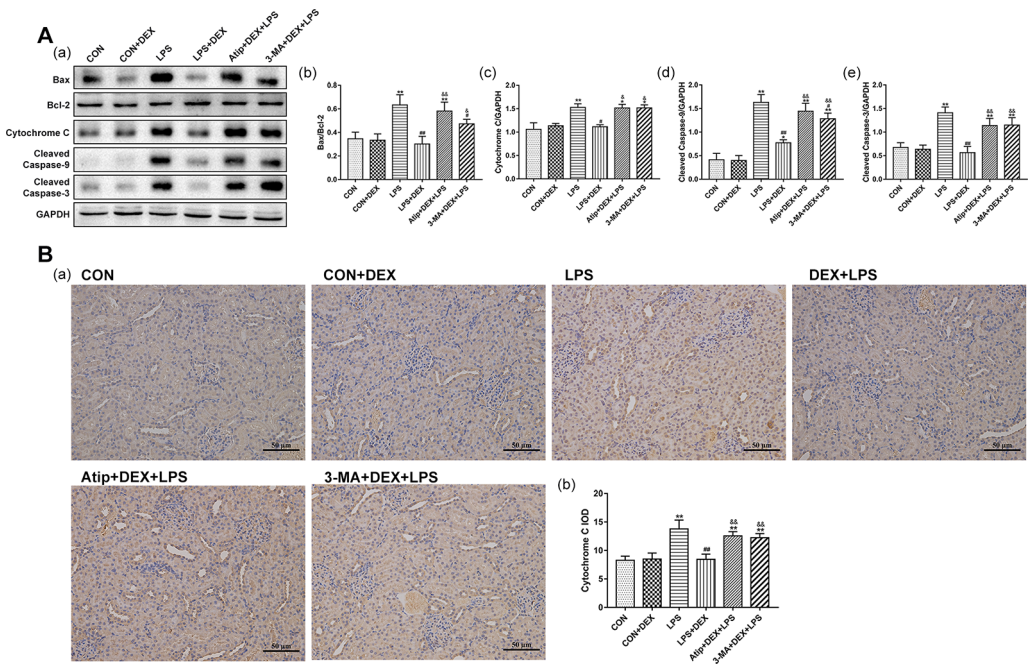

FIGURE 5 | Effects of DEX on apoptosis related proteins. **(A)** Representative blots (a) of Bax, Bcl-2, Cyt C, cleaved caspase-9, and cleaved caspase-3, and the densitometry of Bax/Bcl-2 (b), Cyt C (c), cleaved caspase-9 (d), and cleaved caspase-3 (e) signals. **(B)** Representative images of Cyt C IHC (a), and quantitative analysis of Cyt C (b) in kidney. Data are expressed as mean ± SEM (n = 6). **p < 0.01 versus CON group. #p < 0.05, ##p < 0.01 versus LPS group. &p < 0.05, &&p < 0.01 versus DEX + LPS group.

sepsis but inhibited during severe sepsis. Our results also show that the inhibition of autophagy occurred in LPS-induced AKI, and our model in which 10 mg/kg of LPS was administered for 4 h can also represent severe sepsis in rats.

Oxidative stress and apoptosis are known as the main pathological mechanisms of AKI. From the analysis of GSH, SOD, CAT, MAD, and ROS, it is clear that redox imbalance occurs in the kidney during sepsis. A large number of ROS triggers changes in mitochondrial structure and impairs mitochondrial function. As a result of the damage, mitochondria, the main source of ROS, produce more ROS (Lowes et al., 2013), which causes the body to enter a vicious cycle which aggravates kidney damage. At the same time, the damaged mitochondria also release mitochondrial-derived danger-associated molecular patterns (DAMPs), including Cyt C, which induces apoptosis (Sun et al., 2018).After the administration of LPS, mitochondria in kidney tubular cells were damaged and exhibited swelling, fragmentation, vacuoles in the mitochondrial matrix, and loss of cristae. Upon mitochondrial damage, Bax translocates from the cytosol to the mitochondria, increasing mitochondrial permeability and opening the mitochondrial permeability transition pore (MPTP). Concomitantly, Cyt C is released from mitochondria to the cytosol (Wei et al., 2001),which stimulates Apaf-1 (apoptotic protease-activating factor 1) to activate caspase-9. Once activated, caspase-9 activates downstream effector caspases, such as caspase-3, to promote apoptosis (Adams and Cory, 2007). The kidney is second only to the heart in its abundance of mitochondria and consumption of oxygen (Parikh et al., 2015; Kaushal and Shah, 2016). Mitochondria provide high energy for the processes of the excretion of waste products and electrolyte reabsorption. Therefore, for protection against LPS-induced AKI, abnormal mitochondria must be removed to maintain the quality control of mitochondria.

Autophagy can non-selectively or selectively eliminate damaged proteins and organelles by forming a double-membrane autophagosome, which fuses with lysosomes (Wu et al., 2019). Mitophagy is the selective autophagy of mitochondria. Under basal conditions, PINK1 targets mitochondria and is imported and degraded by healthy mitochondria (Whitworth and Pallanck, 2017), and PINK expression is also very low and not easily detected. Under stress conditions, PINK1 senses mitochondrial damage and activates Parkin by phosphorylating Parkin and ubiquitin. Activated Parkin then builds ubiquitin chains on damaged mitochondria to tag them for degradation in lysosomes (Bingol and Sheng, 2016).In this study, PINK1 largely accumulated on mitochondria in LPS-induced AKI, indicating LPS-induced abnormal mitochondria were recognized by PINK1. We also observed the reduction of LC3II and Beclin-1 and the accumulation of p62. It is well established that Beclin-1, p62, and LC3 are the key proteins of autophagy. Beclin-1 interacts with the class III phosphatidylinositol 3-kinase (PtdIns3K) to initiate autophagy and participates in later steps involving the fusion of autophagosomes to lysosomes (Zhong et al., 2009). LC3 binds to autophagosome membranes to form a complete autophagosome that fuses with lysosomes for degradation (Wu et al., 2019). P62 interacts with LC3 II to target aggregates for autophagy-specific degradation (Parzych and Klionsky, 2014). Therefore, our results

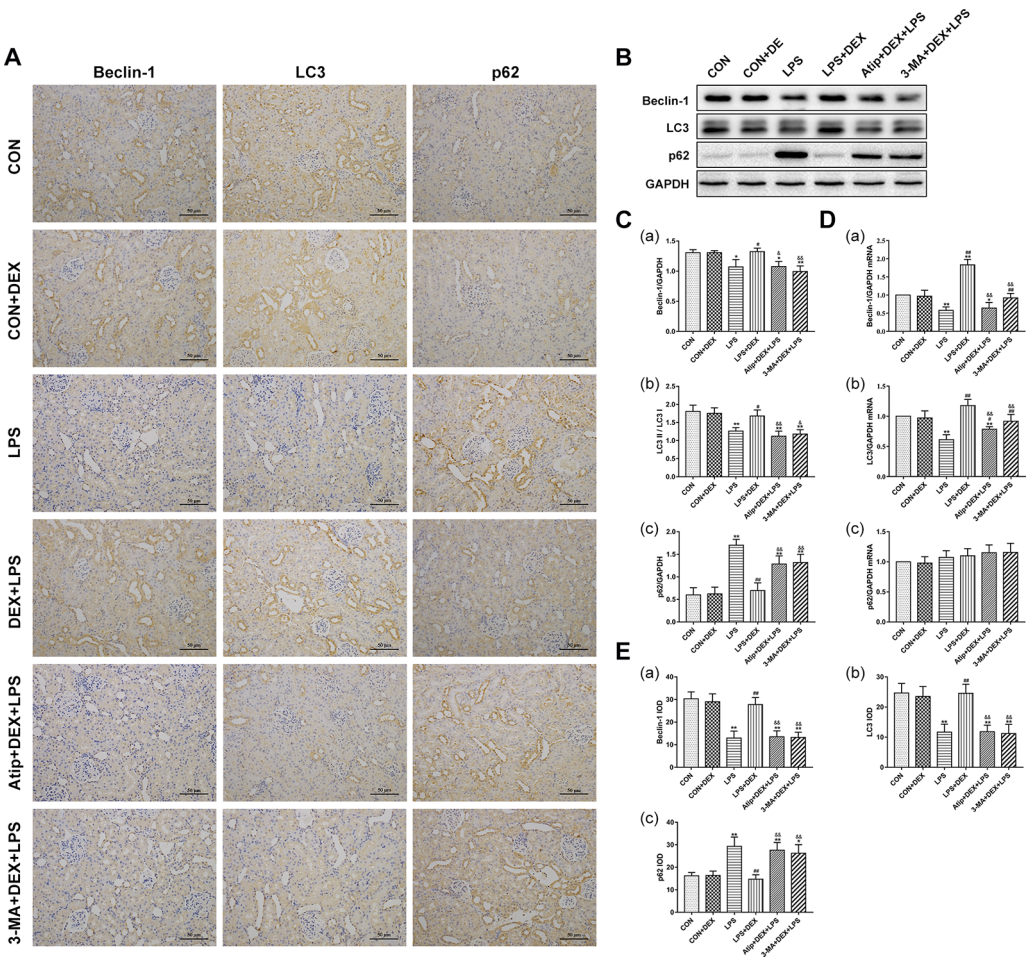

FIGURE 6 | Effects of DEX treatment on autophagy. **(A)** Representative images of Beclin-1 IHC, LC3 IHC, and p62 IHC. **(B)** Representative blots of Beclin-1, LC3, and p62. **(C)** Representative blots densitometry of Beclin-1 (a), LC3 (b), and p62 (c). **(D)** The expression of Beclin-1 (a), LC3 (b), and p62 (c)mRNA in renal tissues. **(E)** The quantitative analysis of Beclin-1 IHC (a), LC3 IHC (b), and p62 IHC (c) in kidney. Data are expressed as mean ± SEM (n = 6). *p < 0.05, **p < 0.01 versus CON group. #p < 0.05, ##p < 0.01 versus LPS group. &p < 0.05, &&p < 0.01 versus DEX + LPS group.

suggested that at the late stages of mitophagy, complete autophagosomes could not form and fuse with lysosomes for degradation, which is consistent with the inhibition of autophagy. Finally, damaged mitochondria were recognized by PINK1, but not degraded through autophagy, which allowed them to accumulate in the cell. These factors aggravated kidney damage. Therefore, the occurrence and development of LPS-induced AKI are associated with the inhibition of autophagy, and enhancing autophagy to remove abnormal mitochondria may be an important mechanism to ameliorate LPS-induced AKI.

We have confirmed that DEX protects against LPS-induced AKI *via* anti-inflammatory and anti-oxidative mechanisms (Chen et al., 2019; Feng et al., 2019; Yao et al., 2019). Also, we found that DEX regulated renal autophagy, a phenomenon that was accompanied by the amelioration of oxidative stress and cell apoptosis. Pretreatment with DEX significantly increased the transcription and translation of LC3 and Beclin-1. However, DEX reduced the level of PINK protein but increased its transcription. These results showed that in the presence of DEX, damaged mitochondria were recognized by PINK1, phagocytosed to form completed autophagosomes, and degraded in lysosomes, suggesting that autophagy had been restored (Parzych and Klionsky, 2014; Bingol and Sheng, 2016). To confirm that in LPS-induced AKI, the renoprotection of DEX is associated with enhanced autophagy, we used 3-MA to inhibit the effects of DEX on autophagy. 3-MA, a PtdIns3K inhibitor, is the most widely used autophagy inhibitor. After treatment with 3-MA, the increased production of ROS and activation of caspase-3 were observed, which indicated the renoprotection of DEX was reversed, and kidney damage was aggravated in LPS-induced AKI. The accumulation of PINK1 and p62 and the reduction of Beclin-1 and LC3 II were similar to the LPS group. These changes indicate that DEX enhances autophagy to reduce oxidative stress and apoptosis. Our data confirm that the inhibition of autophagy is one of the important pathogenesis mechanisms of LPS-induced AKI and that DEX enhances autophagy to alleviate kidney injury.

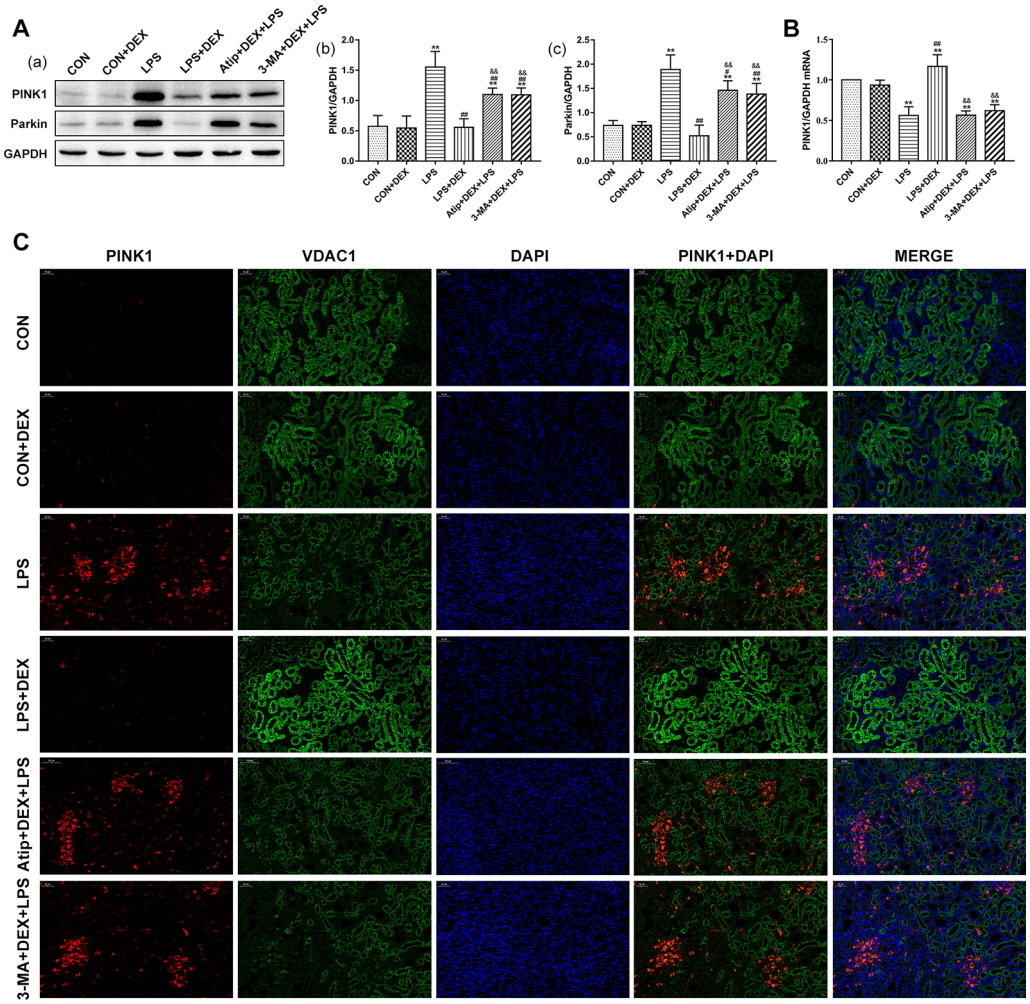

FIGURE 7 | Effects of DEX treatment on mitophagy. **(A)** Representative blots (a) and densitometry of PINK1 (b) and Parkin (c) signals. **(B)** The expression of PINK1 mRNA in renal tissue. **(C)** Representative images of PINK1 localization in renal tissues. Bar: 50 μm. Positive PINK1 cells were stained red, positive VDAC1 cells were stained green, with the sections counterstained with DAPI to visualize nuclei. Data are expressed as mean ± SEM (n = 6). **p < 0.01 versus CON group. #p < 0.05, ##p < 0.01 versus LPS group. &&p < 0.01 versus DEX + LPS group.

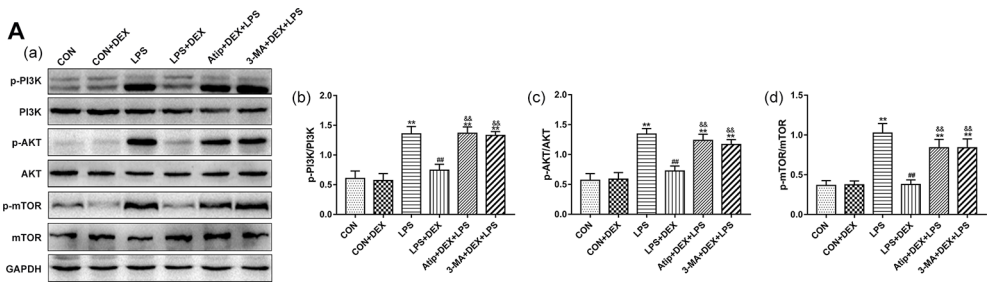

FIGURE 8 | Effects of DEX treatment on the PI3K/AKT/mTOR pathway. **(A)** Representative blots (a), and densitometry of p-PI3K/PI3K (b), p-AKT/AKT (b), and p-mTOR/mTOR (c) signals. Data are expressed as mean ± SEM (n = 6). **p < 0.01 versus CON group. ##p < 0.01 versus LPS group. &&p < 0.01 versus DEX + LPS group.

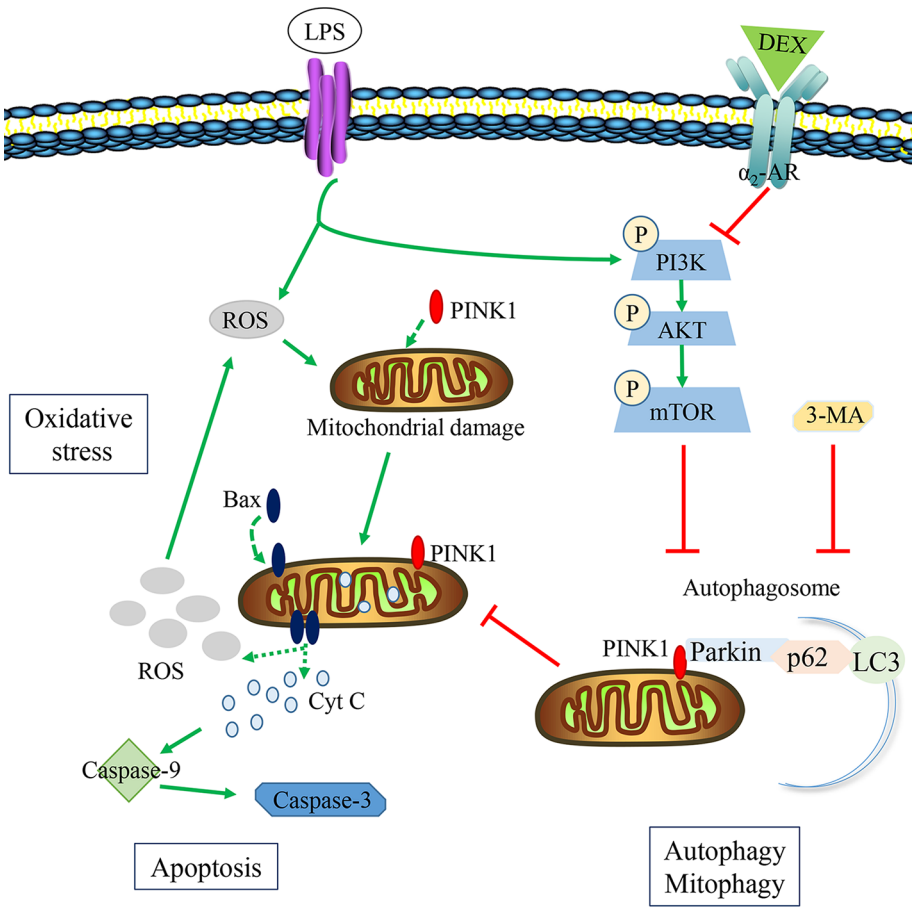

FIGURE 9 | The potential protective mechanisms of DEX in reducing oxidative stress and apoptosis in LPS-induced AKI. LPS could hold back the formation of autophagosome *via* activating the PI3K/AKT/mTOR pathway, inducing the accumulation of damaged mitochondria. Then ROS and Cyt C released from damaged mitochondria could induce oxidative stress and apoptosis. DEX could inhibit the PI3K/AKT/mTOR pathway to enhance autophagy by α_2-AR, reducing oxidative stress and apoptosis. 3-MA could inhibit the effect of DEX on autophagy.

We also investigated the molecular mechanisms by which DEX modulates renal autophagy in LPS-induced AKI. When activated, the kinase mTOR inhibits autophagy initiation (Munson and Ganley, 2015). The phosphorylation of mTOR was increased in LPS-induced AKI, and the upregulation of p-PI3K and p-AKT were also observed. Some studies have confirmed that during the severe stages of sepsis, beneficial autophagic activities are inhibited by mTOR activation (Sun et al., 2018). Therefore, the activation of the PI3K/AKT/mTOR pathway inhibits autophagy in LPS-induced AKI, whereas pretreatment with DEX reduced the phosphorylation of PI3K, AKT, and mTOR. The application of Atip, an α_2-AR antagonist, inhibits the effect of DEX on the phosphorylation of PI3K, AKT, and mTOR. These data suggest that DEX can inhibit the PI3K/AKT/mTOR pathway to activate autophagy through α_2-AR stimulation. However, our study did not determine how α_2-AR stimulation by DEX inhibits PI3K and downstream signaling and processes, and there are few reported studies on this mechanism. We will address this issue in future research.

In summary, this study provided substantial evidence for a novel mechanism in which DEX protects against LPS-induced AKI (summarized in **Figure 9**). LPS inhibited the formation of autophagosomes by activating mTOR, which subsequently inhibited autophagy. This resulted in increased oxidative stress and apoptosis, leading to kidney damage. The inhibition of autophagy is one of the vital pathogenesis of LPS-induced AKI. DEX inhibited the PI3K/AKT/mTOR pathway *via* the α_2-AR and restored autophagy. The enhancement of autophagy removed damaged mitochondria and reduced oxidative stress and apoptosis in LPS-induced AKI.

DATA AVAILABILITY STATEMENT

The datasets generated for this study are available on request to the corresponding author.

ETHICS STATEMENT

The animal study was reviewed and approved by the Animal Experimental Committee of Northeast Agricultural University.

AUTHOR CONTRIBUTIONS

HF and YZ contributed conception and design of the study. YZ, TY, and HC conducted experiments. YZ organized the database. JS and CW performed the statistical analysis. YZ wrote the first draft of the manuscript. XF and BL wrote sections of the manuscript. All authors contributed to manuscript revision, read and approved the submitted version.

FUNDING

This work was supported by the National Natural Science Foundation of China (Grant Nos. 31772806 and 31802251) and the National Key Research and Development Project of China (Grant No. 2016YFD0501008).

ACKNOWLEDGMENTS

We thank Melissa Crawford, PhD, from Liwen Bianji, Edanz Group China (www.liwenbianji.cn/ac), for editing the English text of a draft of this manuscript.

REFERENCES

Adams, J. M., and Cory, S. (2007). The Bcl-2 apoptotic switch in cancer development and therapy. *Oncogene* 26 (9), 1324–1337. doi: 10.1038/sj.onc.1210220

Assinger, A., Schrottmaier, W. C., Salzmann, M., and Rayes, J. (2019). Platelets in sepsis: an update on experimental models and clinical data. *Front. Immunol.* 10, 1687. doi: 10.3389/fimmu.2019.01687

Bellomo, R., Kellum, J. A., Ronco, C., Wald, R., Martensson, J., Maiden, M., et al. (2017). Acute kidney injury in sepsis. *Intensive Care Med.* 43 (6), 816–828. doi: 10.1007/s00134-017-4755-7

Bingol, B., and Sheng, M. (2016). Mechanisms of mitophagy: PINK1, Parkin, USP30 and beyond. *Free Radic. Biol. Med.* 100, 210–222. doi: 10.1016/j.freeradbiomed.2016.04.015

Bolignano, D., Donato, V., Coppolino, G., Campo, S., Buemi, A., Lacquaniti, A., et al. (2008). Neutrophil gelatinase-associated lipocalin (NGAL) as a marker of kidney damage. *Am. J. Kidney Dis.* 52 (3), 595–605. doi: 10.1053/j.ajkd.2008.01.020

Chen, Y., Luan, L., Wang, C., Song, M., Zhao, Y., Yao, Y., et al. (2019). Dexmedetomidine protects against lipopolysaccharide-induced early acute kidney injury by inhibiting the iNOS/NO signaling pathway in rats. *Nitric. Oxide* 85, 1–9. doi: 10.1016/j.niox.2019.01.009

Chung, K. W., Kim, K. M., Choi, Y. J., An, H. J., Lee, B., Kim, D. H., et al. (2017). The critical role played by endotoxin-induced liver autophagy in the maintenance of lipid metabolism during sepsis. *Autophagy* 13 (7), 1113–1129. doi: 10.1080/15548627.2017.1319040

Feng, X., Guan, W., Zhao, Y., Wang, C., Song, M., Yao, Y., et al. (2019). Dexmedetomidine ameliorates lipopolysaccharide-induced acute kidney injury in rats by inhibiting inflammation and oxidative stress *via the* GSK-3beta/Nrf2 signaling pathway. *J. Cell Physiol.* 234 (10), 18994–19009. doi: 10.1002/jcp.28539

Filomeni, G., De Zio, D., and Cecconi, F. (2015). Oxidative stress and autophagy: the clash between damage and metabolic needs. *Cell Death Differ.* 22 (3), 377–388. doi: 10.1038/cdd.2014.150

Han, W. K., Bailly, V., Abichandani, R., Thadhani, R., and Bonventre, J. V. (2002). Kidney Injury Molecule-1 (KIM-1): a novel biomarker for human renal proximal tubule injury. *Kidney Int.* 62 (1), 237–244. doi: 10.1046/j.1523-1755.2002.00433.x

Heras-Sandoval, D., Pérez-Rojas, J. M., Hernández-Damián, J., and Pedraza-Chaverri, J. (2014). The role of PI3K/AKT/mTOR pathway in the modulation of autophagy and the clearance of protein aggregates in neurodegeneration. *Cell. Signal.* 26 (12), 2694–2701. doi: 10.1016/j.cellsig.2014.08.019

Ho, J., Yu, J., Wong, S. H., Zhang, L., Liu, X., Wong, W. T., et al. (2016). Autophagy in sepsis: degradation into exhaustion? *Autophagy* 12 (7), 1073–1082. doi: 10.1080/15548627.2016.1179410

Ishimoto, Y., and Inagi, R. (2016). Mitochondria: a therapeutic target in acute kidney injury. *Nephrol. Dial. Transpl.* 31 (7), 1062–1069. doi: 10.1093/ndt/gfv317

Jou-Valencia, D., Molema, G., Popa, E., Aslan, A., van Dijk, F., Mencke, R., et al. (2018). Renal Klotho is reduced in septic patients and pretreatment with recombinant Klotho attenuates organ injury in lipopolysaccharide-challenged mice. *Crit. Care Med.* 46 (12), e1196–e1203. doi: 10.1097/ccm.0000000000003427

Kang, K., Gao, Y., Wang, S. C., Liu, H. T., Kong, W. L., Zhang, X., et al. (2018). Dexmedetomidine protects against lipopolysaccharide-induced sepsis-associated acute kidney injury *via an* α7 nAChR-dependent pathway. *Biomed. Pharmacother.* 106, 210–216. doi: 10.1016/j.biopha.2018.06.059

Kaushal, G. P., and Shah, S. V. (2016). Autophagy in acute kidney injury. *Kidney Int.* 89 (4), 779–791. doi: 10.1016/j.kint.2015.11.021

Kawazoe, Y., Miyamoto, K., Morimoto, T., Yamamoto, T., Fuke, A., Hashimoto, A., et al. (2017). Effect of dexmedetomidine on mortality and ventilator-free days in patients requiring mechanical ventilation with sepsis: a randomized clinical trial. *JAMA* 317 (13), 1321–1328. doi: 10.1001/jama.2017.2088

Kimura, T., Isaka, Y., and Yoshimori, T. (2017). Autophagy and kidney inflammation. *Autophagy* 13 (6), 997–1003. doi: 10.1080/15548627.2017.1309485

Kumar, S., Tripathy, S., Jyoti, A., and Singh, S. G. (2019). Recent advances in biosensors for diagnosis and detection of sepsis: a comprehensive review. *Biosens Bioelectron*, 124, 205–215. doi: 10.1016/j.bios.2018.10.034

Lowes, D. A., Webster, N. R., Murphy, M. P., and Galley, H. F. (2013). Antioxidants that protect mitochondria reduce interleukin-6 and oxidative stress, improve mitochondrial function, and reduce biochemical markers of organ dysfunction in a rat model of acute sepsis. *Br. J. Anaesth* 110 (3), 472–480. doi: 10.1093/bja/aes577

Maiuri, M. C., Zalckvar, E., Kimchi, A., and Kroemer, G. (2007). Self-eating and self-killing: crosstalk between autophagy and apoptosis. *Nat. Rev. Mol. Cell Biol.* 8 (9), 741–752. doi: 10.1038/nrm2239

Mei, S., Livingston, M., Hao, J., Li, L., Mei, C., and Dong, Z. (2016). Autophagy is activated to protect against endotoxic acute kidney injury. *Sci. Rep.* 6, 22171. doi: 10.1038/srep22171

Meng, L., Li, L., Lu, S., Li, K., Su, Z., Wang, Y., et al. (2018). The protective effect of dexmedetomidine on LPS-induced acute lung injury through the HMGB1-mediated TLR4/NF-κB and PI3K/Akt/mTOR pathways. *Mol. Immunol.* 94, 7–17. doi: 10.1016/j.molimm.2017.12.008

Munson, M. J., and Ganley, I. G. (2015). MTOR, PIK3C3, and autophagy: Signaling the beginning from the end. *Autophagy* 11 (12), 2375–2376. doi: 10.1080/15548627.2015.1106668

Parikh, S. M., Yang, Y., He, L., Tang, C., Zhan, M., and Dong, Z. (2015). Mitochondrial function and disturbances in the septic kidney. *Semin. Nephrol.* 35 (1), 108–119. doi: 10.1016/j.semnephrol.2015.01.011

Parzych, K. R., and Klionsky, D. J. (2014). An overview of autophagy: morphology, mechanism, and regulation. *Antioxid. Redox Signal.* 20 (3), 460–473. doi: 10.1089/ars.2013.5371

Plotnikov, E. Y., Pevzner, I. B., Zorova, L. D., Chernikov, V. P., Prusov, A. N., Kireev, I. I., et al. (2019). Mitochondrial damage and mitochondria-targeted antioxidant protection in LPS-induced acute kidney injury. *Antioxid. (Basel)* 8 (6), 176. doi: 10.3390/antiox8060176

Sorrentino, V., Romani, M., Mouchiroud, L., Beck, J. S., Zhang, H., D'Amico, D., et al. (2017). Enhancing mitochondrial proteostasis reduces amyloid-β proteotoxicity. *Nature* 552 (7684), 187–193. doi: 10.1038/nature25143

Sun, Y., Yao, X., Zhang, Q. J., Zhu, M., Liu, Z. P., Ci, B., et al. (2018). Beclin-1-dependent autophagy protects the heart during sepsis. *Circulation* 138 (20), 2247–2262. doi: 10.1161/circulationaha.117.032821

Sun, Y., Cai, Y., and Zang, Q. S. (2019). Cardiac autophagy in sepsis. *Cells* 8 (2), 141. doi: 10.3390/cells8020141

Tang, C., Han, H., Yan, M., Zhu, S., Liu, J., Liu, Z., et al. (2018). PINK1-PRKN/PARK2 pathway of mitophagy is activated to protect against renal ischemia-reperfusion injury. *Autophagy* 14 (5), 880–897. doi: 10.1080/15548627.2017.1405880

Wan, S. X., Shi, B., Lou, X. L., Liu, J. Q., Ma, G. G., Liang, D. Y., et al. (2016). Ghrelin protects small intestinal epithelium against sepsis-induced injury by enhancing the autophagy of intestinal epithelial cells. *Biomed. Pharmacother.* 83, 1315–1320. doi: 10.1016/j.biopha.2016.08.048

Wang, Y., Mao, X., Chen, H., Feng, J., Yan, M., Wang, Y., et al. (2019). Dexmedetomidine alleviates LPS-induced apoptosis and inflammation in macrophages by eliminating damaged mitochondria *via* PINK1 mediated mitophagy. *Int. Immunopharmacol.* 73, 471–481. doi: 10.1016/j.intimp.2019.05.027

Wei, M. C., Zong, W. X., Cheng, E. H., Lindsten, T., Panoutsakopoulou, V., Ross, A. J., et al. (2001). Proapoptotic BAX and BAK: a requisite gateway to mitochondrial dysfunction and death. *Science* 292 (5517), 727–730. doi: 10.1126/science.1059108

Whitworth, A. J., and Pallanck, L. J. (2017). PINK1/Parkin mitophagy and neurodegeneration-what do we really know *in vivo*? *Curr. Opin. Genet. Dev.* 44, 47–53. doi: 10.1016/j.gde.2017.01.016

Wu, Y., Yao, Y. M., and Lu, Z. Q. (2019). Mitochondrial quality control mechanisms as potential therapeutic targets in sepsis-induced multiple organ failure. *J. Mol. Med.* 97 (4), 451–462. doi: 10.1007/s00109-019-01756-2

Yao, Y., Hu, X., Feng, X., Zhao, Y., Song, M., Wang, C., et al. (2019). Dexmedetomidine alleviates lipopolysaccharide-induced acute kidney injury by inhibiting the NLRP3 inflammasome activation *via* regulating the TLR4/NOX4/NF-κB pathway. *J. Cell. Biochem.* 120 (10), 18509–18523. doi: 10.1002/jcb.29173

Zhong, Y., Wang, Q. J., Li, X., Yan, Y., Backer, J. M., Chait, B. T., et al. (2009). Distinct regulation of autophagic activity by Atg14L and Rubicon associated with Beclin 1-phosphatidylinositol-3-kinase complex. *Nat. Cell Biol.* 11 (4), 468–476. doi: 10.1038/ncb1854

Conflict of Interest: The authors declare that the research was conducted in the absence of any commercial or financial relationships that could be construed as a potential conflict of interest.

Copyright © 2020 Zhao, Feng, Li, Sha, Wang, Yang, Cui and Fan. This is an open-access article distributed under the terms of the Creative Commons Attribution License (CC BY). The use, distribution or reproduction in other forums is permitted, provided the original author(s) and the copyright owner(s) are credited and that the original publication in this journal is cited, in accordance with accepted academic practice. No use, distribution or reproduction is permitted which does not comply with these terms.

frontiers in Physiology

ORIGINAL RESEARCH
published: 27 February 2020
doi: 10.3389/fphys.2020.00172

IL-4 Receptor α Chain Protects the Kidney Against Tubule-Interstitial Injury Induced by Albumin Overload

*Diogo B. Peruchetti[1], João Luiz Silva-Filho[1], Rodrigo P. Silva-Aguiar[1], Douglas E. Teixeira[1], Christina M. Takiya[1], Mariana C. Souza[2], Maria das Graças Henriques[2], Ana Acacia S. Pinheiro[1,3] and Celso Caruso-Neves[1,3,4]**

[1] Instituto de Biofísica Carlos Chagas Filho, Universidade Federal do Rio de Janeiro, Rio de Janeiro, Brazil, [2] Instituto de Tecnologia em Fármacos, Fundação Oswaldo Cruz, Rio de Janeiro, Brazil, [3] Rio de Janeiro Innovation Network in Nanosystems for Health – NanoSAUiDE/FAPERJ, Rio de Janeiro, Brazil, [4] Instituto Nacional de Ciência e Tecnologia em Medicina Regenerativa, INCT-Regenera, Conselho Nacional de Desenvolvimento Científico e Tecnológico/MCTIC, Rio de Janeiro, Brazil

Increasing evidence has highlighted the role of tubule-interstitial injury (TII) as a vital step in the pathogenesis of acute kidney injury (AKI). Incomplete repair of TII during AKI could lead to the development of chronic kidney disease. Changes in albumin endocytosis in proximal tubule epithelial cells (PTECs) is linked to the development of TII. In this context, interleukin (IL)-4 has been shown to be an important factor in modulating recovery of TII. We have studied the possible role of IL-4 in TII induced by albumin overload. A subclinical AKI model characterized by albumin overload in the proximal tubule was used, without changing glomerular function. Four groups were generated: (1) CONT, wild-type mice treated with saline; (2) BSA, wild-type mice treated with 10 g/kg/day bovine serum albumin (BSA); (3) KO, IL4Rα$^{-/-}$ mice treated with saline; and (4) KO + BSA, IL4Rα$^{-/-}$ mice treated with BSA. As reported previously, mice in the BSA group developed TII without changes in glomerular function. The following parameters were increased in the KO + BSA group compared with the BSA group: (1) tubular injury score; (2) urinary γ-glutamyltransferase; (3) CD4^{+} T cells, dendritic cells, macrophages, and neutrophils are associated with increases in renal IL-6, IL-17, and transforming growth factor β. A decrease in M2-subtype macrophages associated with a decrease in collagen deposition was observed. Using LLC-PK1 cells, a model of PTECs, we observed that (1) these cells express IL-4 receptor α chain associated with activation of the JAK3/STAT6 pathway; (2) IL-4 alone did not change albumin endocytosis but did reverse the inhibitory effect of higher albumin concentration. This effect was abolished by JAK3 inhibitor. A further increase in urinary protein and creatinine levels was observed in the KO + BSA group compared with the BSA group, but not compared with the CONT group. These observations indicate that IL-4 has a protective role in the development of TII induced by albumin overload that is correlated with modulation of the pro-inflammatory response. We propose that megalin-mediated albumin endocytosis in PTECs could work as a sensor, transducer, and target during the genesis of TII.

Keywords: IL-4, tubule-interstitial injury, albumin overload, renal disease, proteinuria, albumin endocytosis, pro-inflammatory response, acute kidney injury

OPEN ACCESS

Edited by:
John D. Imig, Medical College of Wisconsin, United States

Reviewed by:
Ora Weisz, University of Pittsburgh, United States
Helen Grania Healy, Metro North Hospital and Health Service, Australia

***Correspondence:**
Celso Caruso-Neves
caruso@biof.ufrj.br

Specialty section:
This article was submitted to Renal and Epithelial Physiology, a section of the journal Frontiers in Physiology

Received: *03 October 2019*
Accepted: *13 February 2020*
Published: *27 February 2020*

Citation:
Peruchetti DB, Silva-Filho JL, Silva-Aguiar RP, Teixeira DE, Takiya CM, Souza MC, Henriques MdG, Pinheiro AAS and Caruso-Neves C (2020) IL-4 Receptor α Chain Protects the Kidney Against Tubule-Interstitial Injury Induced by Albumin Overload. Front. Physiol. 11:172. doi: 10.3389/fphys.2020.00172

INTRODUCTION

There is a strict correlation between AKI and CKD, a public health problem with a high level of morbidity and mortality (Liyanage et al., 2015; Negi et al., 2018). Increasing evidence has highlighted the role of TII as a vital step in the pathogenesis of AKI (Nakhoul and Batuman, 2011; Venkatachalam et al., 2015; Chevalier, 2016; Strausser et al., 2018). The incomplete repair of tubular injury during the course of AKI could lead to the development of CKD (Venkatachalam et al., 2015; Strausser et al., 2018). Several studies have demonstrated an important role of albumin overload in the PT in the development of TII (Gorriz and Martinez-Castelao, 2012; Erkan, 2013; Portella et al., 2013; Abreu et al., 2014; Landgraf et al., 2014; Teixeira et al., 2019). This mechanism requires changes in the albumin endocytosis machinery (Nakhoul and Batuman, 2011; Gorriz and Martinez-Castelao, 2012; Landgraf et al., 2014; Teixeira et al., 2019).

It is well known that albumin reabsorption in PT epithelial cells (PTECs) occurs by receptor-mediated endocytosis with megalin as the main receptor involved in this process (Gorriz and Martinez-Castelao, 2012; Erkan, 2013; Eshbach and Weisz, 2017). Some studies have shown that megalin works as sensor and integrator between changes in albumin concentration and PTEC injury (Caruso-Neves et al., 2006; Erkan, 2013; Peruchetti et al., 2014; Nielsen et al., 2016). This process is mediated by different cellular mechanisms triggered by changes in megalin expression (Caruso-Neves et al., 2006; Peruchetti et al., 2014). In a previous work, our group showed that megalin knockdown in LLC-PK1 cells mimicked the effect of pathologic albumin concentration on different signaling pathways, which could be correlated with cell apoptosis and a pro-inflammatory response (Caruso-Neves et al., 2006; Peruchetti et al., 2014). In addition, changes in megalin expression have been correlated with TII in Fanconi syndrome as well as autoimmune renal diseases (Piwon et al., 2000; Christensen et al., 2003; Batuman, 2007; Nakhoul and Batuman, 2011; Vicinanza et al., 2011; Gaide Chevronnay et al., 2014; Eshbach and Weisz, 2017; Wang et al., 2017; Cez et al., 2018).

The complete repair of tubular injury depends on the complex network involved in the early and resolution phase of the inflammatory response (Huen and Cantley, 2017; Lee et al., 2017). In this context, CD4+ T cells and macrophages have been shown to be important players in the initial and resolution phase of the inflammatory response during the development of TII (Huen and Cantley, 2017; Lee et al., 2017). Interestingly, it was shown that PTECs also participate in the activation of a pro-inflammatory response, secreting cytokines and chemokines after a specific signal such as exposure to albumin overload (Zoja et al., 1998; Donadelli et al., 2003; Takaya et al., 2003; Tang et al., 2003; Reich et al., 2005; Pearson et al., 2008; Gorriz and Martinez-Castelao, 2012; Erkan, 2013; Landgraf et al., 2014; Teixeira et al., 2019). PTECs could work as APCs, inducing an inflammatory phenotype with increasing CD4+ T cell responses (Breda et al., 2019).

Interleukin (IL)-4 has been shown to be an important factor in modulating the recovery of tubular injury in renal disease (Cao et al., 2011; Yan et al., 2015; Liang et al., 2017; Zhang et al., 2017). Using an AKI animal model, Zhang et al. (2017) showed that IL-4 induces polarization of the M2 macrophage phenotype, which was correlated with the recovery of tubular injury. In agreement, it was shown that STAT6-deficient mice develop more severe injury in an ischemia-reperfusion AKI animal model (Yokota et al., 2003). On the other hand, using a unilateral ureteral obstruction model, Liang et al. (2017) showed that the IL-4 receptor α chain/STAT6 pathway activates bone marrow-derived fibroblasts, leading to the development of fibrosis and aggravation of renal disease. These apparent contradictory results indicate that the final effect of IL-4 is more complex than has been described.

Based on this scenario, we decided to study the effect of IL-4 receptor α (IL-4Rα) chain on TII induced by albumin overload. To address this issue, a subclinical AKI (AKIsub) animal model in BALB/c (wild-type) or IL-4Rα chain deficient (IL4Rα$^{-/-}$) mice was used. In addition, LLC-PK1 cells were used as a model of PTECs to study the cellular response. It was observed that the IL-4Rα chain protects the development of TII induced by albumin overload. This process involves modulation of the albumin endocytosis machinery and a pro-inflammatory response.

MATERIALS AND METHODS

Reagents

Bovine serum albumin (BSA) fraction V (delipidated - #A9647), BSA conjugated to fluorescein isothiocyanate (BSA-FITC), CP-690550-10, collagenase and protease inhibitor cocktail (no. I3786) were purchased from Sigma-Aldrich (St. Louis, MO, United States). MK-2206 was purchased from Selleckchem (Houston, TX, United States). Sensiprot kit (ref. 36) was purchased from Labtest (Lagoa Santa, MG, Brazil). Creatinine kit (ref. 335) was purchased from Gold Analisa (Belo Horizonte, MG, Brazil). γ-GT kit (ref. K080) was purchased from Bioclin (Belo Horizonte, MG, Brazil). Recombinant porcine IL-4 was purchased from R&D Systems (Minneapolis, MN, United States). Polyclonal phospho-STAT6 (Tyr-641), polyclonal STAT6, polyclonal phospho-STAT3 (Ser-727), polyclonal STAT3, polyclonal phospho-ERK1/2 (Thr-202/Tyr-204), polyclonal phospho-PKB (Ser-473), polyclonal PKB, polyclonal ERK1/2, polyclonal inducible nitric oxide synthase (iNOS), polyclonal β-actin, and HRP-conjugated anti-rabbit IgG antibodies were purchased from Cell Signaling Technology (Danvers, MA, United States). Polyclonal Lrp2/megalin and polyclonal nephrin antibodies were purchased from Abcam (Cambridge, MA, United States). Polyclonal IL-4Rα and podocin antibodies were purchased from Santa Cruz Biotechnology (Dallas, TX,

Abbreviations: γ-GT, γ-glutamyl transferase; AKI, acute kidney injury; AKIsub, subclinical acute kidney injury; APC, antigen-presenting cells; CKD, chronic kidney disease; ERK1/2, extracellular signal-regulated protein kinases 1 and 2; IFN-γ, interferon-γ; IL, interleukin; JAK3, Janus kinase 3; pIgR, polymeric immunoglobulin receptor; PKB, protein kinase B; PT, proximal tubule; PTEC, proximal tubule epithelial cell; RANTES, regulated on activation, normal T cell expressed and secreted; STAT3, signal transducer and activator of transcription 3; STAT6, signal transducer and activator of transcription 6; TGF-β, transforming growth factor β; TII, tubule-interstitial injury; TNF-α, tumor necrosis factor α; UPCr, urinary protein/creatinine ratio.

United States). Monoclonal mouse IgG1 anti-mouse arginase-1 (clone 19, BD Transduction Laboratories), monoclonal rat IgG2a anti-mouse IA-IE (clone 2G9; Pharmingen), PE-conjugated rat IgG2b anti-mouse Ly-6G and Ly-6C (clone RB6-8C5; Pharmingen), PE-conjugated rat IgG2b anti-mouse CD11b (clone M1/70; Pharmingen), and PE-conjugated hamster IgG1 anti-mouse CD11c (clone HL3; Pharminge) were purchased from BD Bioscience (São Paulo, Brazil). Biotinylated anti-rabbit or anti-mouse IgG was purchased from Agilent Technologies (Santa Clara, CA, United States). Dulbecco's modified Eagle's medium (DMEM), phosphate-buffered saline (PBS), fetal bovine serum (FBS), 3,30-diaminobenzidine, UltraPure N,N'-methylene bisacrylamide, FITC-conjugated rat IgG2b anti-mouse CD4 (clone GK1.5; eBioscience), and PerCP-Cyanine5.5-conjugated IgG2a anti-mouse CD8a (clone 53-6.7; eBioscience) were purchased from Thermo Fisher Scientific (Waltham, MA, United States). LLC-PK1 cells were purchased from the ATCC (Rockville, MD, United States). All other reagents were of the highest purity available.

Animals

Male BALB/c mice (weighing 20–25 g), 8–11 weeks old, were used in all experiments. Wild-type (WT) BALB/c mice were obtained from the Institute of Science and Technology in Biomodels (ICTB) of the Oswaldo Cruz Foundation (FIOCRUZ), Rio de Janeiro, Brazil. IL-4Rα chain deficient mice (IL4Rα-/-, BALB/c-Il4ratm1Sz/J; backcrossed to BALB/c at least seven generations) were obtained from The Jackson Laboratories. All mice were housed, bred, and maintained in the animal care facility at the Federal University of Rio de Janeiro. The animals were accommodated in an air-conditioned environment (22–24°C) in a regular 12-h light/dark cycle with water and standard chow *ad libitum*. The presence or absence of any adverse clinical signs associated to this mouse strain was monitored as described previously (Teixeira et al., 2019). All procedures involving the handling of animals were conducted in accordance with the National Institutes of Health (NIH) Guide for the Care and Use of Laboratory Animals and were approved by the Institutional Ethics Committee of the Federal University of Rio de Janeiro (protocol number IBCCF098).

Subclinical AKI Animal Model

The AKIsub animal model was developed as described previously (Portella et al., 2013; Abreu et al., 2014; Landgraf et al., 2014; Peruchetti et al., 2019; Teixeira et al., 2019). Briefly, WT or IL4Rα-/- mice were used to generate four experimental groups: (1) CONT, WT mice treated with saline (used as vehicle); (2) BSA, WT mice treated with 10 g/kg/day BSA via intraperitoneal injection (ip) for 7 consecutive days; (3) KO, IL4Rα-/- mice treated with saline; and (4) KO + BSA, IL4Rα-/- mice treated with BSA. The animals were kept in the metabolic cage during all experiment and 24-h urine was collected at day 7. At the end of day 7, the animals were euthanized using a mixture of ketamine (240 mg/kg) and xylazine (15 mg/kg). The kidneys were removed and used for: (1) histomorphometry; (2) detection of specific proteins through immunohistochemistry and immunoblotting; (3) level of cytokines; and (4) immune cell infiltration.

Cell Culture

LLC-PK1 cells, a porcine PTEC line, were grown at 37°C in 5% CO2 in low-glucose DMEM supplemented with 10% FBS and 1% penicillin/streptomycin (Caruso-Neves et al., 2005, 2006; Lara et al., 2010; Lindoso et al., 2011; Peruchetti et al., 2011, 2014, 2018, 2019; Landgraf et al., 2014; Arnaud-Batista et al., 2016; Teixeira et al., 2019). After reach the confluence (85–90%), the serum-starved cells were treated with different compounds as indicated in the figure legends. Then, it was determined the rate of albumin endocytosis and detection of specific proteins through immunoblotting.

Renal Function Analysis

The renal function parameters were obtained as previously published (Portella et al., 2013; Abreu et al., 2014; Landgraf et al., 2014; Silva-Filho et al., 2016; Silva-Aguiar et al., 2018; Teixeira et al., 2019). Urine samples were used to assess the levels of γ-glutamyltransferase (γ-GT) activity, proteins and creatinine using commercial kits, according to the manufacturer's instructions. The creatinine clearance (CCr) and the ratio of urinary protein to creatinine (UPCr) were calculated using those parameters.

Histologic and Immunohistochemistry Studies

The histology and immunohistochemistry studies were performed as previously (Portella et al., 2013; Abreu et al., 2014; Landgraf et al., 2014; Silva-Filho et al., 2016; Silva-Aguiar et al., 2018; Teixeira et al., 2019). 5-μm-thick kidney sections stained with periodic acid-Schiff (PAS) were used for analysis of both glomerular and tubular structures. These sections were also used to determine megalin expression through immunohistochemistry. 8-μm-thick kidney sections were used to determine the cortical collagen deposition after Picrosirius red staining.

30 images were acquired randomly using a Nikon 80i eclipse microscope (Nikon, Japan) followed by quantification analysis using Image-Pro Plus software (Media Cybernetics, Rockville, MD, United States). To evaluate the possible changes in glomerular structure, both glomerular cellularity (number of glomerular cells) and mesangial expansion (intensity of mesangial matrix at glomerular tuft) were determined. To assess possible changes in tubular structure, a tubular injury score was used (Grgic et al., 2012). The red fibers intensity was measured in PicroSirius red-stained slices to determine the levels of collagen deposition (expressed as percentage of the interstitial area). The intensity of megalin-positive staining (expressed as arbitrary units) was measured as a ratio between the intensity of the positive area for megalin and total tissue area. All quantifications were performed in a blinded manner.

Immunoblotting

Immunoblotting was performed as described previously (Caruso-Neves et al., 2006; Lara et al., 2008; Peruchetti et al., 2011, 2014, 2018; Landgraf et al., 2014; Arnaud-Batista et al., 2016; Silva-Filho et al., 2016; Ribeiro et al., 2018; Silva-Aguiar et al., 2018;

Teixeira et al., 2019). Briefly, protein samples were obtained from LLC-PK1 cell lysate or renal cortex homogenate. Cell lysate and homogenate were clarified by centrifugation at 15,000 × *g* for 10 min at 4°C in an ice-cold solution described previously in the works above. The Folin phenol method was used to assess the total protein concentration (Lowry et al., 1951).

Proteins (30–60 μg) were resolved on 5% or 9% SDS-PAGE and transferred to PVDF membranes (Millipore). After blockade of non-specific binding, the membranes were incubated with specific primary antibodies and their respective HRP-conjugated IgG secondary antibodies, according to the manufacturer's instructions. ECL Prime was used to detect the proteins of interest (Peruchetti et al., 2018; Ribeiro et al., 2018; Silva-Aguiar et al., 2018; Teixeira et al., 2019). All the images were obtained using the Image Quant LAS4000 Image processing system (GE Healthcare Life Sciences, Pittsburgh, PA, United States) and processed by adjusting the brightness and contrast using NIH ImageJ software (version 1.6.0). It is important to mention that this image processing method was applied to every pixel in the original image without changing the information illustrated.

Assessment of Albumin Endocytosis

The rate of albumin endocytosis was assessed through the measurement of BSA-FITC uptake as described previously (Caruso-Neves et al., 2005; Peruchetti et al., 2018; Silva-Aguiar et al., 2018; Teixeira et al., 2019). Briefly, the cells were incubated with Ringer solution (12.4 mM HEPES–Tris (pH 7.4), 140 mM NaCl, 2.7 mM KCl, 1.8 mM CaCl2, 1 mM MgCl2, 5 mM glucose) containing 30 μg/mL BSA-FITC at 37°C for 30 min. After the reaction, the unbound BSA-FITC was washed extensively with ice-cold Ringer solution. Then, the cells were lysed using 0.1% Triton X-100 and the cell-associated fluorescence was determined using a microplate spectrofluorimeter (SpectraMax M2; Molecular Devices, Sunnyvale, CA, United States). BSA-FITC-specific uptake was calculated as the difference between the fluorescence intensity in the absence and in the presence of 30 mg/mL unlabeled BSA. The data obtained were further normalized by the total protein concentration and, then, expressed as arbitrary units.

Assessment of Renal Albumin-FITC Uptake

The renal cortex albumin-FITC uptake was measured as published previously (Silva-Aguiar et al., 2018; Teixeira et al., 2019). Briefly, mice received single intravenous injection of 5 μg/g BSA-FITC. After 15 min, renal cortexes slides were homogenized in ice-cold Ringer solution (20 mM HEPES–Tris (pH 7.4), 5 mM D(+)-glucose, 2.7 mM KCl, 140 mM NaCl, 1 mM MgCl2, 1.8 mM CaCl2, 1 mM PMSF and protease inhibitor cocktail 1×). After clarification, samples were used to determine the intensity of organ-associated fluorescence (excitation = 480 nm, emission = 520 nm) using SpectraMax M2 (Molecular Devices, Sunnyvale, CA, United States). The specific albumin-FITC uptake was further normalized by total protein concentration. Data were expressed as percentage of the controls.

Renal Cytokines

The levels of cortical cytokines were evaluated as described (Portella et al., 2013; Landgraf et al., 2014). The concentrations of IFN-γ, IL-4, IL-6, IL-10, IL-17, RANTES, TGF-β, and TNF-α were determined by cytometric bead array (BD Biosciences, San Jose, CA, United States). Data are represented by ratio between ng of cytokine/chemokine and mg of total proteins (ng/mg).

Immune Cell Infiltration

Immune cell infiltration in the renal tissue was assessed as described previously (Portella et al., 2013). Briefly, kidney thick sections were added in DMEM supplemented with 10 mM HEPES, 10 mM non-essential amino acids, 2 mM L-glutamine, 1 mM sodium pyruvate, 0.05 mM 2-mercaptoethanol, 100 U/mL penicillin, and 100 U/mL streptomycin. Then, the kidney slices were digested in a solution containing 0.1% collagenase (37°C for 60 min) with gentle shaking. After filtration, removal of erythrocytes and clarification, the cells were resuspended and washed with cold PBS. Then, the cells were incubated with Fc block (affinity purified anti-mouse CD16/CD32; eBioscience, San Diego, CA, United States) and with specific antibodies. The acquisition was obtained in FACSCalibur flow cytometer (Becton Dickinson, San Jose, CA, United States) followed by the analysis of surface markers in Summitt software as shown previously (Silva-Filho et al., 2013, 2017; Ribeiro et al., 2018). All data were collected and displayed on a log scale of increasing fluorescence intensity and presented as dot plots. The percentages of T cells (CD4+ and CD8+), macrophages (CD11b+), dendritic cells (CD11c+ IA-IE+) and neutrophils (Ly6G+) were determined in a specific gate.

Statistical Analysis

All data are expressed as means ± standard deviation (SD). For statistical analysis, it was used the GraphPad Prism 7 (version 7.00, GraphPad Software, San Diego, CA, United States)[1]. For comparison between two experimental groups (as shown in some experiments using LLC-PK1 cells), it was used the unpaired *t*-tests. For three or more experimental groups (as shown in some experiments using LLC-PK1 cells and the AKIsub animal model), it was used the one-way analysis of variance (ANOVA) test followed by the Newman-Keuls post test. $P < 0.05$ is used to determine statistical significance.

RESULTS

Tubule-Interstitial Injury Induced by Proximal Tubule Albumin Overload Is Worsened by IL-4Rα Deficiency

To address the role of IL-4R in the development of TII, we used BALB/c (WT) or IL4Rα$^{-/-}$ mice to generate four different experimental groups as described earlier. Initially, possible change in glomerular function was assessed (**Figure 1**). It was observed that the plasma creatinine level and creatinine

[1]www.graphpad.com

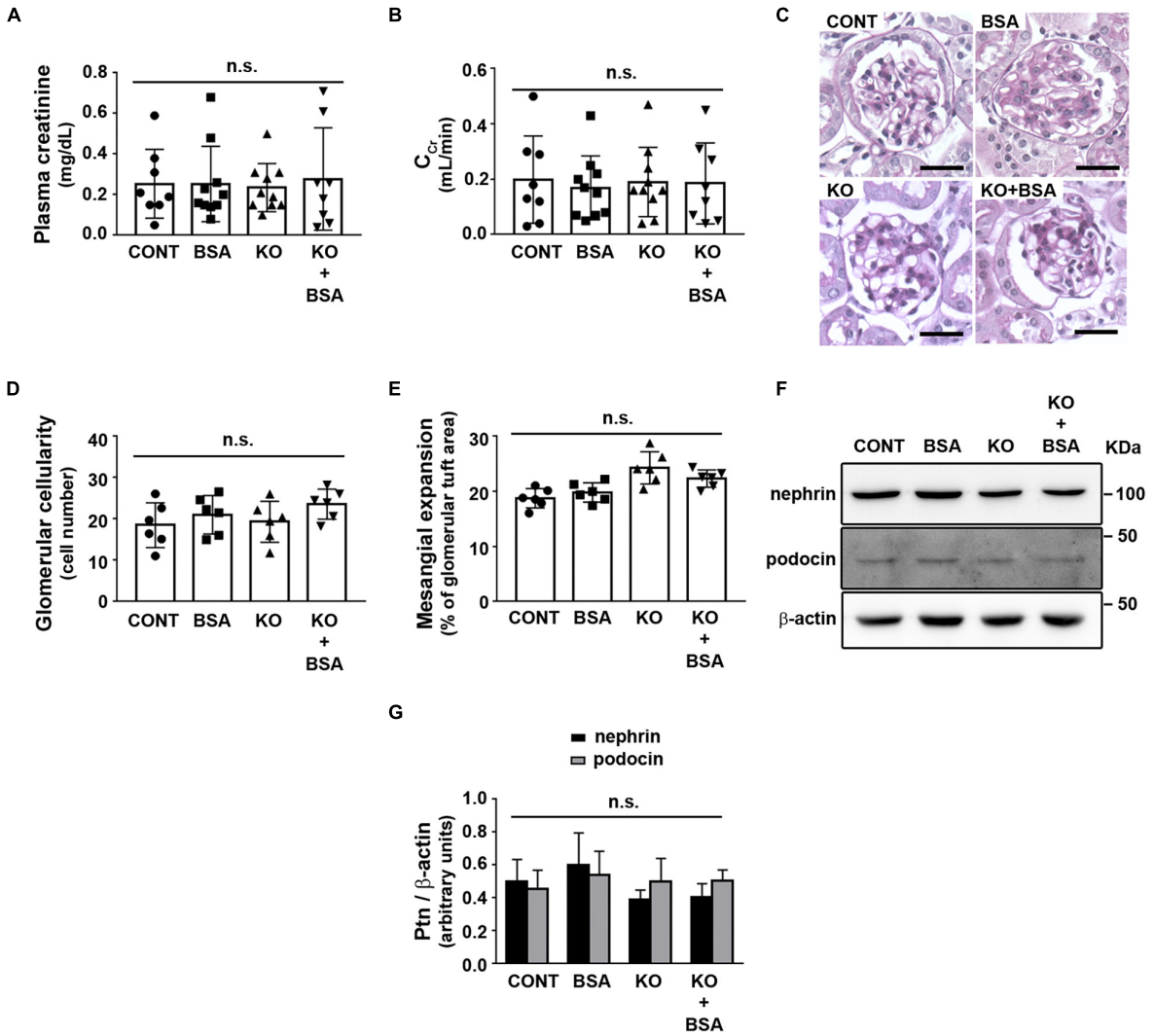

FIGURE 1 | IL-4Rα deficiency with or without subclinical AKI does not change glomerular function. Male BALB/c (wild-type) or IL-4Rα deficient (IL-4Rα$^{-/-}$) mice were used to develop a subclinical AKI animal model through the intraperitoneal injection of 10 g/kg/day BSA over 7 consecutive days (for details see section "Materials and Methods"). Four experimental groups were generated: (1) CONT, wild-type (WT) mice treated with saline (used as vehicle); (2) BSA, WT mice treated with BSA; (3) KO, IL4Rα$^{-/-}$ mice treated with saline; and (4) KO + BSA, IL4Rα$^{-/-}$ mice treated with BSA. **(A,B)** Assessment of glomerular function. **(A)** Plasma creatinine (n = 8). **(B)** Creatinine clearance (CCr, n = 8). **(C–E)** Evaluation of glomerular structure. **(C)** Representative images of glomeruli (scale bar represents 100 μm). **(D)** Glomerular cellularity (n = 6). **(E)** Measurement of mesangial expansion (n = 6). **(F,G)** Nephrin and podocin expression. **(F)** Representative images of four independent experiments. β-Actin was used as the load control. Ptn, protein. **(G)** Densitometry analyzes related to **(F)** (n = 4). The OD related to nephrin or podocin bands was normalized to the OD related to the β-actin band. The results are expressed as means ±SD. n.s., not significant.

clearance, markers of the glomerular flow rate, were not changed in any experimental groups (**Figures 1A,B**). In agreement, glomerular cellularity and mesangial expansion as well as podocin and nephrin expression were also not changed (**Figures 1C–G**).

The score index for tubular injury in the BSA-treated groups was increased and this effect was more pronounced in the KO + BSA group compared with the BSA group (**Figures 2A,B**). In agreement, γ-GT activity, a specific marker for PT cell injury, was higher in the KO + BSA group than in the BSA group (**Figure 2C**). No significant change in the score index for tubular injury or γ-GT activity, marker of PT injury, was observed in the KO group compared with the CONT group. Interestingly, collagen deposition was increased in the BSA-treated groups (BSA and KO + BSA). However, contrary to the results for other parameters, collagen deposition in the KO + BSA group was lower than that in the BSA group (**Figures 2D,E**).

Protein Handling in IL-4Rα Deficiency

Some groups, including our group, have proposed that there is a correlation among changes in albumin concentration in PT, megalin expression, and TII development (Caruso-Neves et al., 2006; Gorriz and Martinez-Castelao, 2012; Erkan, 2013; Peruchetti et al., 2014; Teixeira et al., 2019). Here, it was observed

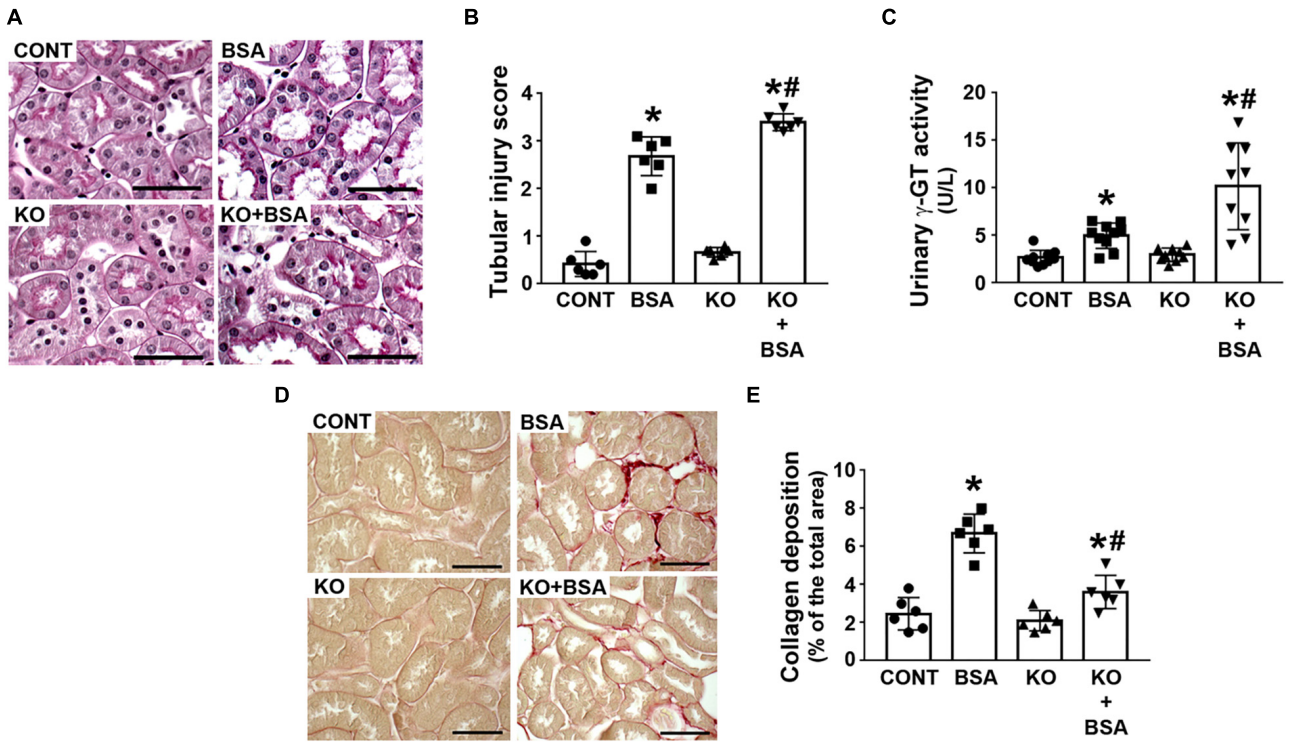

FIGURE 2 | IL-4Rα deficiency worsens tubule-interstitial injury in subclinical AKI. Mice were treated as described in **Figure 1**. **(A)** Representative images of the cortical tubular region. Kidney slices were stained with periodic acid-Schiff (PAS) (scale bar represents 50 μm). **(B)** Tubular injury score (n = 6). **(C)** Urinary γ-GT activity (n = 9). **(D)** Representative images of collagen fiber deposits (red color) in the renal cortex. Kidney slices were stained with Sirius red (scale bar represents 50 μm). **(E)** Quantitative analysis related to **(D)** (n = 6). The results are expressed as means ±SD. *P < 0.05 versus the CONT group; #P < 0.05 versus the BSA group.

that proteinuria was higher in the BSA and KO + BSA groups than in the CONT group, but was not changed in the KO group (**Figures 3A,B**). UPCr was measured to rule out the possible influence of urinary flow on proteinuria (**Figure 3C**). UPCr was increased in the BSA and KO + BSA groups compared with the CONT group. However, it was significantly higher in the KO + BSA group than in the BSA group, similarly to the trends observed for the score index for tubular injury and γ-GT activity. In the next step, albumin endocytosis in renal cortex was accessed (**Figure 3D**). It was decreased in BSA and KO + BSA groups when compared with CONT group (**Figure 3D**). Similarly, the expression of megalin, a protein endocytosis receptor, was also decreased in the BSA and KO + BSA groups (**Figures 3E–H**). Interestingly, the decrease in albumin endocytosis and megalin expression were more pronounced in the KO + BSA than in BSA group. Together these results indicate that IL-4/IL-4Rα pathway attenuate changes in PT albumin endocytosis machinery in TII induced by PT albumin overload.

IL-4 Modulates Albumin Endocytosis in Proximal Tubule Cells

We then investigated the possible effect of IL-4 on PT albumin endocytosis. LLC-PK1 cells, a model of PT cells, were used to address this question. Initially, it was shown that LLC-PK1 cells express the IL-4Rα chain, which was not changed when the cells were incubated overnight with 20 ng/mL IL-4 (**Figure 4A**). Furthermore, overnight incubation of LLC-PK1 cells with IL-4 led to increased STAT6 phosphorylation, associated with the IL-4Rα chain (**Figures 4B,C**). However, there was no change in the phosphorylation of PKB, STAT3, and ERK1/2.

Next, we wanted to determine if the cellular response triggered by IL-4 in LLC-PK1 cells modulated albumin endocytosis. Initially, incubation of LLC-PK1 cells with 20 ng/mL IL-4 overnight did not change albumin endocytosis (**Figure 4D**). When the cells were incubated overnight with a higher albumin concentration (20 mg/mL), mimicking the effect of albumin overload in PTs, albumin endocytosis was inhibited in 38% (**Figure 4D**). Interestingly, this effect was completely reversed by co-incubation of the LLC-PK1 cells with 20 ng/mL IL-4. These results are in accordance with the observation that proteinuria and UPCr were not changed in the KO group, but they were increased in the KO + BSA group. Furthermore, the molecular mechanism underlying the effect of IL-4 on albumin endocytosis involves STAT6 activation since 10^{-7} M CP-690550-10, a JAK3 inhibitor, completely abolished it. On the other hand, MK-2206, a PKB inhibitor, did not change the IL-4 effect (**Figure 4E**). So far, the results indicate that KO mice further increase TII induced by albumin overload, which could be associated with a decrease in the albumin endocytosis machinery.

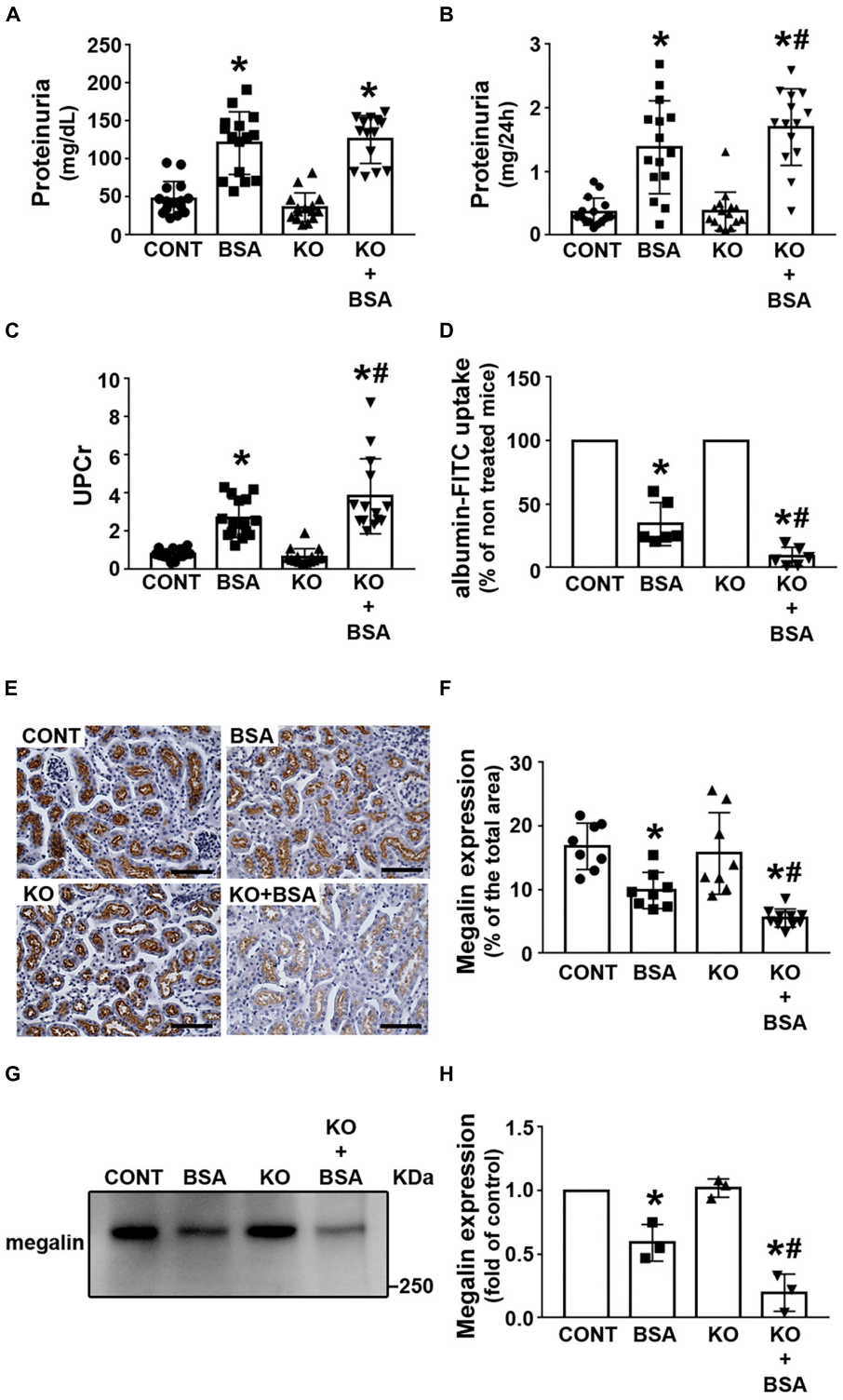

FIGURE 3 | IL-4Rα deficiency worsens proteinuria due to a decrease in megalin expression in subclinical AKI. Mice were treated as described in **Figure 1**. Measurement of proteinuria [**(A,B)**, $n = 15$] and the ratio of urinary proteins to creatinine [**(C)**, $n = 15$]. **(D)** *In vivo* albumin-FITC uptake ($n = 6$). **(E)** Representative megalin staining in the cortical area (bars represent 100 μm). **(F)** Quantitative analysis related to **(E)**. **(G)** Megalin expression in renal cortex was determined by immunoblotting ($n = 3$). **(H)** Quantitative analysis related to **(G)**. The results are expressed as means ±SD. *$P < 0.05$ versus the CONT group; #$P < 0.05$ versus the BSA group.

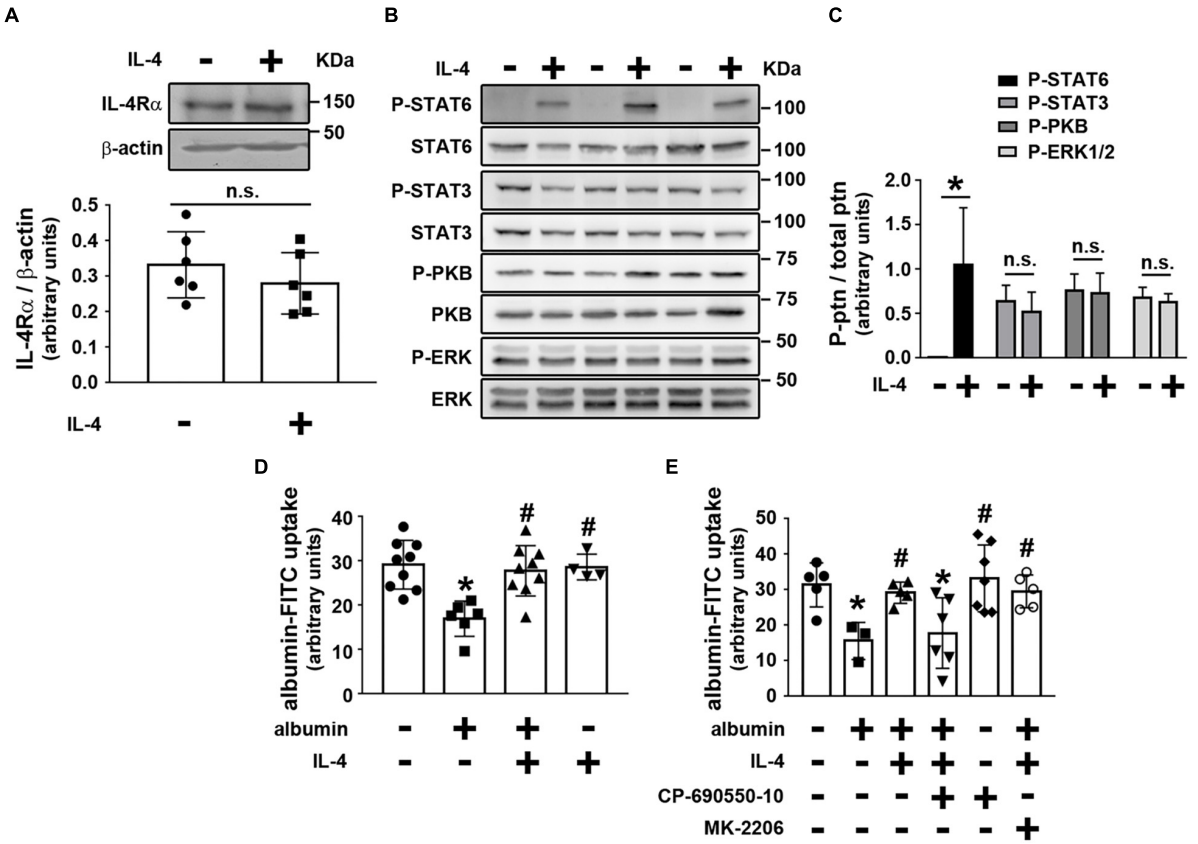

FIGURE 4 | IL-4 avoids the inhibitory effect of higher albumin concentration on albumin endocytosis through activation of the JAK3/STAT6 pathway. LLC-PK1 cells were grown in 24-well plates until 95% confluence was reached. Then, the cells were incubated with different compounds as indicated. **(A)** The effect of 20 ng/mL IL-4 on IL-4Rα chain expression (n = 6). β-actin was used as the load control. In upper panel is showed the representative images. In bottom panel is showed the densitometry analyzes. **(B,C)** The effect of IL-4 on the phosphorylation of STAT6 (Tyr641), STAT3 (Tyr705), PKB (Ser473), and ERK (Thr202/Tyr204). **(B)** Representative images of three independent experiments. **(C)** Densitometry analysis related to **(B)** (n = 3). Ptn, protein. All phosphorylated fractions of specific proteins were normalized by the total fraction of the respective proteins. **(D)** The effect of IL-4 on the inhibitory effect of 20 mg/mL albumin on albumin endocytosis (n = 9). Albumin endocytosis was measured by cell-associated fluorescence using albumin-FITC as a tracer. **(E)** The effect of 10^{-7} M CP-690550-10 (JAK3 inhibitor) or 10^{-7} M MK-2206 (PKB inhibitor) on the effect of IL-4 on albumin endocytosis (n = 6). The results are expressed as means ±SD. *P < 0.05 versus control; #P < 0.05 versus albumin; n.s., not significant.

Deficiency of IL-4Rα Enhances the Pro-inflammatory Response During Tubule-Interstitial Injury Induced by Albumin Overload

Figure 5 shows the cytokines and chemokines in the renal cortex homogenate for different experimental groups. The level of TNF-α, IL-6, IL-17, TGF-β, and RANTES was increased in the BSA-treated groups (BSA and KO + BSA; **Figures 5A–E**). A further increase in the IL-6, IL-17, TGF-β levels was observed in the KO + BSA group compared with the BSA group. In addition, the level of TGF-β was also increased in the KO group compared with the control group (**Figure 5D**). The levels of INF-γ and IL-10 were only increased in the KO groups (KO and KO + BSA; **Figures 5F,G**). On the other hand, the level of IL-4 was not changed in any experimental group (**Figure 5H**).

An increase in the frequency of CD4 + and CD8 + T cells as well as CD11c + IAE-IE + dendritic cells was observed in the BSA, KO, and KO + BSA groups compared with the CONT group (**Figures 6A–C**). However, the accumulation of all these cells, with the exception of CD8 + T cells, was higher in the KO + BSA group than in the BSA or KO groups separately. In addition, the level of Ly6G + neutrophils was increased only in the KO + BSA group (**Figure 6D**).

One important issue in the development of TII induced by PT albumin overload is the role of macrophages (Gorriz and Martinez-Castelao, 2012; Erkan, 2013; Portella et al., 2013; Abreu et al., 2014; Landgraf et al., 2014; Teixeira et al., 2019). Here, the CD11b + macrophage level was increased in the BSA, KO, and KO + BSA groups (**Figure 7A**). Further increase was observed in the KO + BSA group compared with the KO and BSA groups. To verify if the increase in total macrophages observed in the KO + BSA group correlated with possible changes in macrophage polarization, we assessed the expression of iNOS, a marker of M1-subtype macrophages, and arginase-1, a marker of M2-subtype macrophages. We observed no changes in iNOS expression in any

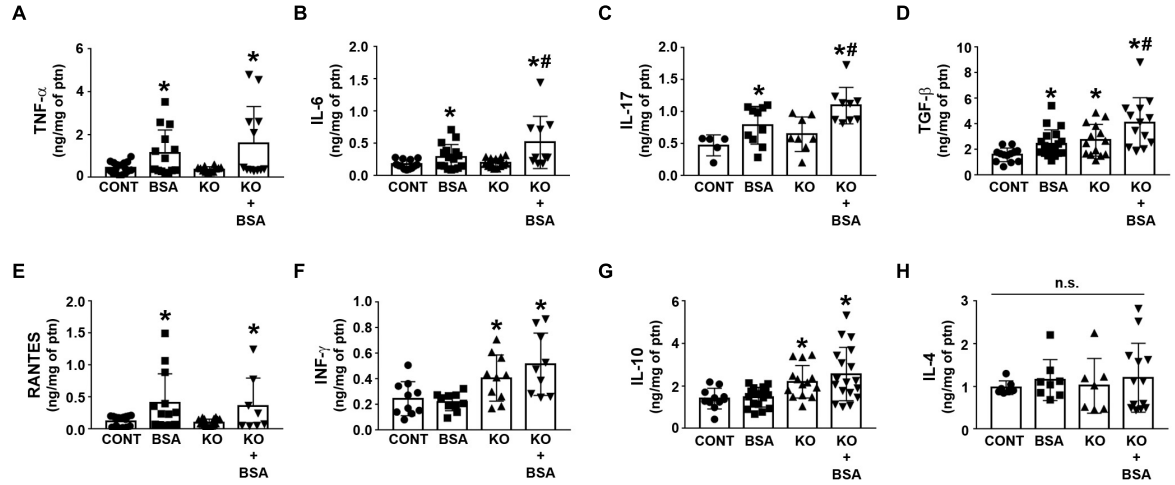

FIGURE 5 | IL-4Rα deficiency enhances renal pro-inflammatory cytokines in subclinical AKI. Mice were treated as described in **Figure 1**. Measurement of cortical TNF-α [**(A)**, $n = 12$], IL-6 [**(B)**, $n = 10$], IL-17 [**(C)**, $n = 9$], TGF-β [**(D)**, $n = 13$], RANTES [**(E)**, $n = 8$], IFN-γ [**(F)**, $n = 9$], IL-10 [**(G)**, $n = 18$], and IL-4 levels [**(H)**, $n = 13$] were determined by ELISA. The cytokine levels were normalized by the amount of total protein in the same samples. TNF-α, tumor necrosis factor alpha; IL, interleukin; TGF-β, transforming growth factor β; RANTES, regulated on activation, normal T cell expressed and secreted; INF-γ, interferon-γ. The results are expressed as means ±SD. *$P < 0.05$ versus the CONT group; #$P < 0.05$ versus the BSA group.

experimental group (**Figure 7B**). On the other hand, arginase-1 expression was increased in the BSA group (**Figure 7C**). Interestingly, arginase-1 expression was higher in the KO + BSA group than in the CONT group but lower than in the BSA group, showing a decrease in polarization of macrophages to the M2 phenotype in IL4Rα$^{-/-}$ mice.

DISCUSSION

Repair of tubular injury is a critical step for complete recovery from AKI (Venkatachalam et al., 2015; Strausser et al., 2018). The possible role of IL-4 in this process has been uncovered, although understanding the underlying mechanism is still a challenge. In the present study, we used a subclinical AKI animal model to study the role of IL-4 on TII induced by albumin overload. It was observed that IL-4 plays a protective role in tubular injury, and this effect is associated with PT albumin handling and regulation of the inflammatory response. These results open new avenues to understand the role of IL-4 on the course of AKI and, consequently, progression of renal disease.

In the present work, a subclinical AKI model characterized by overload of albumin in PTs without changing glomerular function was used (Ronco et al., 2012; Portella et al., 2013; Abreu et al., 2014; Landgraf et al., 2014; Teixeira et al., 2019; Vanmassenhove et al., 2019). This process results in tubular injury associated with modifications in the albumin reabsorption machinery, a pro-inflammatory response, and collagen deposition (Gorriz and Martinez-Castelao, 2012; Erkan, 2013; Portella et al., 2013; Abreu et al., 2014; Landgraf et al., 2014; Teixeira et al., 2019). Herein we observed that there is no change in apparent glomerular function measured by CCr and plasma creatinine. Ishola et al. (2006), using 129S2/Sv and C57BL/6J strains, showed that BSA overload animal model induced glomerular leakage of albumin without any changes in glomerular ultra-structure after 11 days measured by electron microscopy. The authors proposed that albumin overload in PT cells is a result of increased glomerular albumin permeability rather than by changes in glomerular ultrastructure. Nevertheless, the measurement of these parameters is not enough to assure that there is no change in glomerular function and structure in any way. In this context, it is a good animal model to study the possible effects of IL-4 on TII, independently of apparent glomerular changes. Accordingly, we observed that glomerular function was not changed in IL4Rα$^{-/-}$ mice. However, it is important to mention that the results obtained in the present study cannot exclude possible signals generated by glomerular cells during this experimental condition. In this context, it has been proposed that injuries in glomerular structure could be transmitted to tubular segments contributing to the tubule-interstitial injury (Theilig, 2010). Although further experiments are necessary to clarify this issue.

One crucial question in the pathogenesis of TII induced by albumin overload is how PTECs sense changes in the albumin concentration in PTs. It has been proposed that megalin is a sensor for this process, triggering cellular signaling coupled to misfunction of PTECs (Caruso-Neves et al., 2006; Erkan, 2013; Peruchetti et al., 2014; Nielsen et al., 2016). Our group showed that knockdown of megalin in LLC-PK1 cells mimicked the cellular response induced by higher albumin concentration (Peruchetti et al., 2014). This process was related to apoptosis of PTECs (Caruso-Neves et al., 2006; Teixeira et al., 2019). In agreement, we have shown here that in the AKIsub model, there was a decrease in megalin expression that was associated with a pro-inflammatory phenotype and development of TII. The induction of megalin expression in this animal model reduced proteinuria and tubule damage (Cabezas et al., 2011). In agreement, Koizumi et al. (2019)

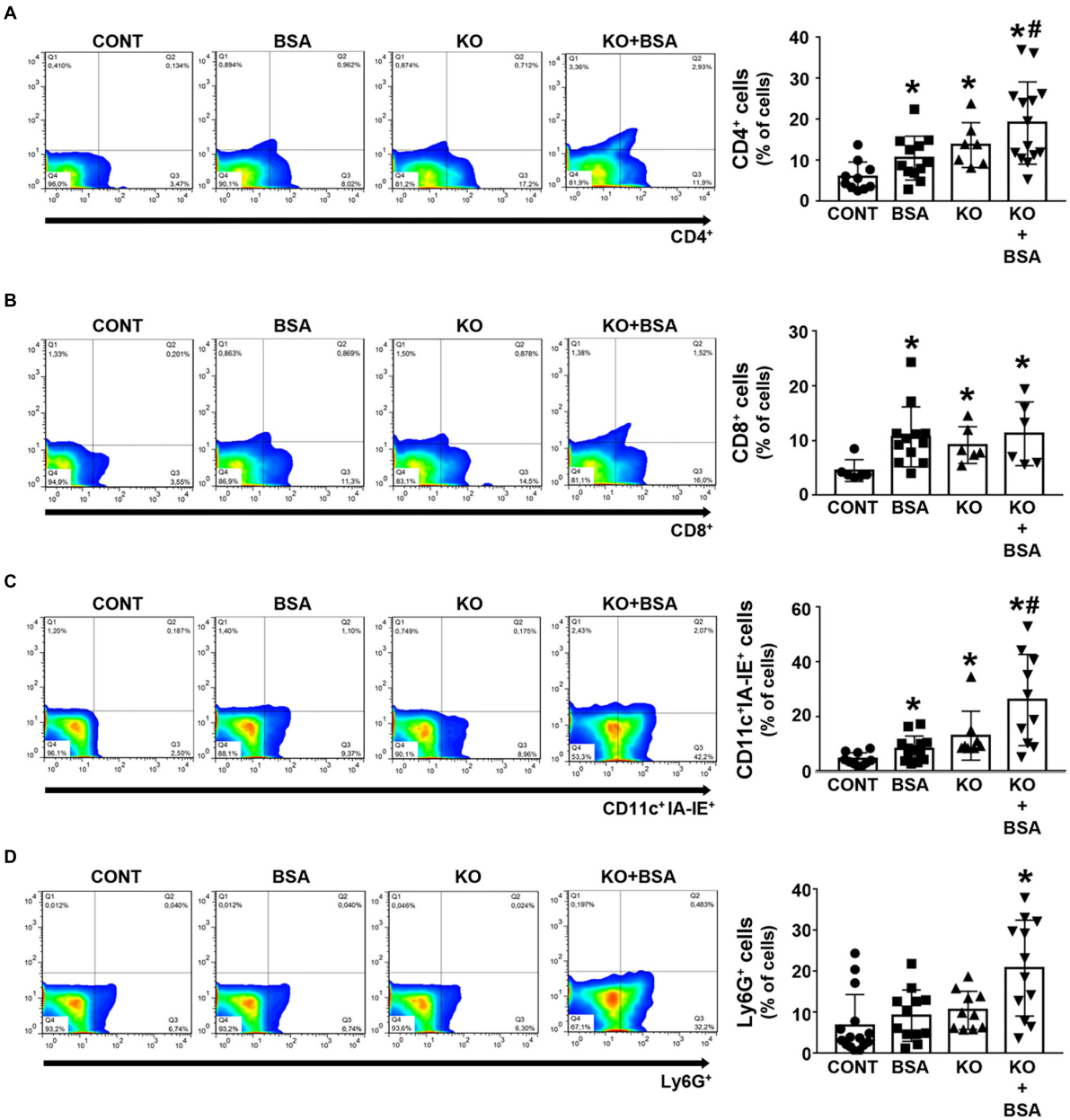

FIGURE 6 | IL-4Rα deficiency potentiates immune cell infiltration in subclinical AKI. Mice were treated as described in **Figure 1**. The kidneys were perfused with saline and digested with collagenase. The percentage of CD4 + T cells [**(A)**, $n = 14$], CD8 + T cells [**(B)**, $n = 8$], CD11c + IA-IE + dendritic cells [**(C)**, $n = 10$], and Ly6G + neutrophils [**(D)**, $n = 12$] were determined by flow cytometry. The results are expressed as means ±SD. $^*P < 0.05$ versus the CONT group; $\#P < 0.05$ versus the BSA group.

showed that PT specific knockout mice for megalin were more susceptible to tubule-interstitial damage in a model of podocyte injury.

Accordingly, with the view that megalin expression is associated with the development of TII, it has been shown that megalin is involved in the genesis of different renal diseases (Piwon et al., 2000; Christensen et al., 2003; Batuman, 2007; Nakhoul and Batuman, 2011; Vicinanza et al., 2011; Gaide Chevronnay et al., 2014; Eshbach and Weisz, 2017; Wang et al., 2017; Cez et al., 2018; Larsen et al., 2018; Peruchetti et al., 2018; Silva-Aguiar et al., 2018). Larsen et al. (2018) showed that megalin is the antigen target of human kidney anti-brush border antibody that causes a primary renal tubulointerstitial disease (ABBA disease). Furthermore, megalin has been proposed to be involved in Fanconi's syndrome and Dent's syndrome, correlated with the increase in the pro-inflammatory response and TII (Piwon et al., 2000; Christensen et al., 2003; Batuman, 2007; Nakhoul and Batuman, 2011; Vicinanza et al., 2011;

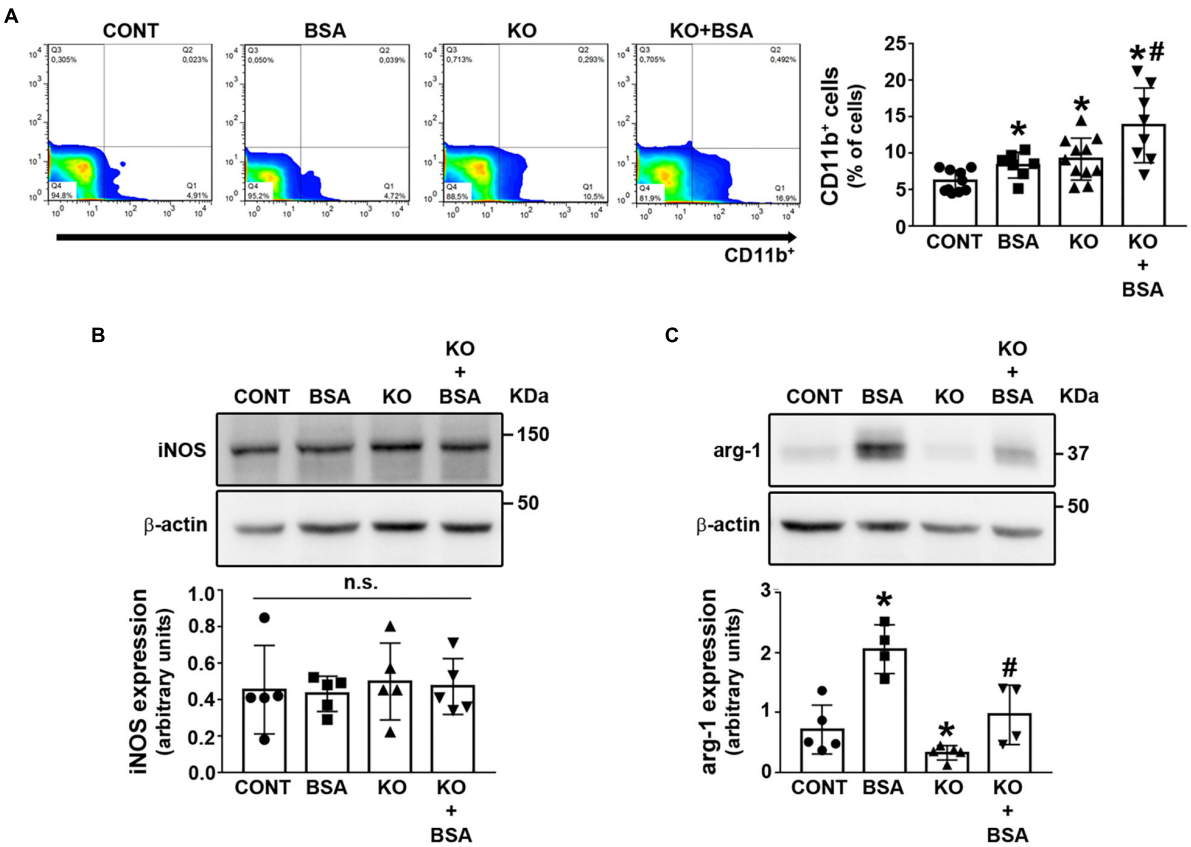

FIGURE 7 | IL-4Rα deficiency abolished the increase in M2-subtype macrophages in subclinical AKI. Mice were treated as described in **Figure 1**. The kidneys were perfused with saline and digested with collagenase. **(A)** The level of infiltrated CD11b+ macrophages was determined by flow cytometry (n = 8). The macrophage phenotype was determined by iNOS expression [**(B)**, *n* = 5] and arginase-1 expression [**(C)**, *n* = 4] through immunoblotting of the renal cortex. iNOS, a marker of M1-subtype cells; arginase-1, a marker of M2-subtype cells. The results are expressed as means ±SD. **P* < 0.05 versus the CONT group; #*P* < 0.05 versus the BSA group; n.s., not significant.

Gaide Chevronnay et al., 2014; Eshbach and Weisz, 2017; Wang et al., 2017; Cez et al., 2018).

But the mechanism involved in the decrease of megalin expression is not clear yet. An important link could be TGF-β secretion. Diwakar et al. (2007) using OK cells showed that albumin induces TGF-β secretion. Recently, Cabezas et al. (2019) using LLC-PK1 cells showed that TGF-β decreases megalin expression. Accordingly, we observed an increase in the TGF-β level in the BSA groups. On the other hand, the decrease in megalin expression was only observed when TII was induced despite an increase in the TGF-β level in IL4Rα$^{-/-}$ mice. In addition, IL-4 modulates the albumin uptake in LLC-PK1 cells only when the cells are exposed to a higher albumin concentration. These results indicate megalin-mediated albumin endocytosis is a component of a complex mechanism involved in the pathogenesis of TII induced by albumin overload.

Therefore, the modulation of albumin endocytosis by IL-4 is an attractive hypothesis in understanding the mechanism underlying the modulation of TII induced by albumin overload. Only few studies have shown the possible correlation between epithelial cell protein endocytosis and IL-4. Van Den Berg et al. (2002) showed that IL-4 increases intracellular trafficking of proteins in glomerular visceral epithelial cells. Olsan et al. (2015), using human autosomal-dominant polycystic kidney disease tissues, showed that STAT6 pathway activation induces an increase in renal pIgR, which is involved in renal cell IgA transport. Our data indicate that IL-4 has a protective effect against the decrease in megalin expression and PT albumin endocytosis induced by higher albumin concentration. This mechanism involves activation of the JAK3/STAT6 pathway and seems to be involved in a protective role of IL-4 on TII.

How PTEC mediates TII induced by albumin overload is not clear. Some studies have shown that PTECs could secrete cytokines and chemokines, which could mediate activation of the pro-inflammatory response (Zoja et al., 1998; Donadelli et al., 2003; Takaya et al., 2003; Tang et al., 2003; Reich et al., 2005; Pearson et al., 2008; Gorriz and Martinez-Castelao, 2012; Erkan, 2013; Portella et al., 2013; Landgraf et al., 2014; Teixeira et al., 2019). These observations bring a new concept to PTECs: they could be a sensor, transductor, effector, and the final target of different cytokines and chemokines involved in the development of TII. We showed that IL-4 binds to the receptor, triggers

a cellular response, and modulates PT endocytosis during the development of TII. We propose that besides immune cells, PTECs could work as a transducer in the effect of IL-4 on albumin endocytosis, pro-inflammatory response, and the development of TII. Accordantly, Breda et al. (2019) proposed that PTECs could work as APCs, inducing an inflammatory phenotype in CD4 + T cells.

Data from the literature indicate that macrophage infiltration during the pathogenesis of AKI is a critical process in the development and repair of TII (Huen and Cantley, 2017; Lee et al., 2017). M1 macrophage phenotypes are predominant at the early phase and switch to M2 phenotypes at a later phase of AKI (Huen and Cantley, 2017; Lee et al., 2017). Using a subclinical AKI model, our group showed that tubular injury induced by albumin overload encompasses a pro-inflammatory response followed by polarization of the M2 macrophage phenotype, an increase in renal TGF-β level, and collagen deposition (Landgraf et al., 2014; Teixeira et al., 2019). Here, we observed an increase in total macrophage infiltration but a decrease in M2 phenotypes associated with a decrease in collagen deposition in TII-induced IL4Ra$^{-/-}$ mice. In agreement, it has been proposed that IL-4 participates in the resolution phase, leading the polarization of M2 phenotype macrophages and promoting the recovery from AKI (Cao et al., 2011; Yan et al., 2015; Liang et al., 2017; Zhang et al., 2017). Furthermore, Lee et al. (2011) showed that macrophage ablation after established AKI worsened the tubular injury due to reduced M2 phenotype.

In parallel with the decrease in M2 macrophages, an increase in IL-6 and IL-17 cytokines was observed, as well as infiltrated CD4 + T cells, neutrophils, and dendritic cells in subclinical AKI developed in IL4Rα$^{-/-}$ mice. Interestingly, a further increase in TGF-β level was observed in IL4Rα$^{-/-}$ mice. Chung et al. (2018) using macrophage TGF-βRII$^{-/-}$ mice showed that TGF-β works as a chemoattractant mediating renal fibrosis and, consequently, the progression of renal disease. On the other hand, we showed that despite the increase in TGF-β level, there was a decrease in M2 phenotype macrophages associated with a reduction in collagen deposition and worsening TII. These results indicate that the resolution phase involves a more complex network than has been postulated. Probably, the final effect of the TGF-β level involves several coordinated actions. In agreement, it has been shown that IL-4 induces renal fibrosis depending on polarization to M2 phenotype macrophages and the activation of marrow-derived fibroblasts (Liang et al., 2017; Zhang et al., 2017). Further experiments are necessary to clarify this issue.

Our results indicate that IL-4 plays an important role in the balance between the initial and resolution phases of the inflammatory response. In a subclinical AKI model developed in IL4Rα$^{-/-}$ mice, there is an increase in the Th1 response associated with preponderance in M1 phenotype macrophages over the M2 phenotype, extending the early phase and delaying the resolution phase. Although, these conclusions are limited since we used one time point (day 7 of subclinical AKI) what does not allow us to determine longitudinal events of initial and resolution phases.

Based on the results obtained in the present work together with those published previously by other authors, we postulate

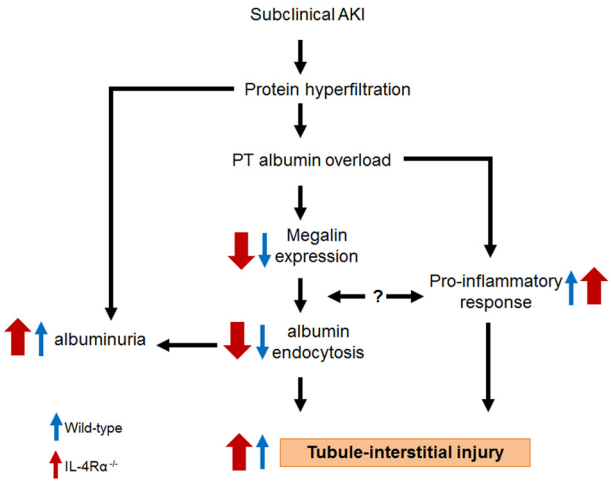

FIGURE 8 | Proposed model for the role of IL-4 on the tubule-interstitial injury induced by albumin overload in the proximal tubule. Blue arrow, wild-type mice. Red arrows, IL4Rα$^{-/-}$ mice.

a mechanism underlying the effect of IL-4 on the TII induced by albumin overload (**Figure 8**). IL-4 plays an important role in development of TII due to its action: (1) on the megalin expression, albumin endocytosis and, consequently on the albuminuria. This mechanism involves activation of JAK3/STAT6; (2) in modulating pro-inflammatory response. In this case, IL-4 attenuates the increase in cortical pro-inflammatory cytokines IL-6, IL-17 as well as the increase in TGF-β, a pro-fibrotic cytokine. Other possibility could be the direct effect of pro-inflammatory cytokines on the PT megalin expression and, consequently, on the albumin endocytosis. This process could form a dangerous loop aggravating TII. In conclusion, IL-4 attenuates the effect of albumin overload in both megalin expression and pro-inflammatory response what could explain why IL4Rα$^{-/-}$ mice has a more severe TII.

DATA AVAILABILITY STATEMENT

All datasets generated for this study are included in the article/supplementary material.

ETHICS STATEMENT

The animal study was reviewed and approved by the Institutional Ethics Committee of the Federal University of Rio de Janeiro (protocol number IBCCF098).

AUTHOR CONTRIBUTIONS

PA and CC-N conceived and designed the study. DP, JS-F, RS-A, DT, MS, and MH contributed to acquisition of the data. DP, JS-F, RS-A, DT, CT, AP, and CC-N contributed to analysis

and interpretation of the data. D-PB and CC-N wrote the first draft of the manuscript. All authors contributed to revision of the manuscript, read, and approved the submitted version.

FUNDING

This work was supported by grants from the following Brazilian agencies: Conselho Nacional de Desenvolvimento Científico e Tecnológico (www.cnpq.br), 304682/2015-2 to AP, 303793/2015-5 to CC-N, 423724/2018-5 to AP, 444194/2018-5 to CC-N and Fundação Carlos Chagas Filho de Amparo à Pesquisa do Estado do Rio de Janeiro–FAPERJ (www.faperj.br), E-26/2011.710/2015 to CC-N, E-26/202.950/2016 to AP, and E-26/202.833/2017 to CC-N.

ACKNOWLEDGMENTS

The authors would like to thank Dr. Fidel Zavala (Johns Hopkins University, Baltimore, MD, United States) for kindly providing the IL-4Rα$^{-/-}$ mice. The authors would also like to thank Mr. Mario Luiz da Silva Bandeira (FAPERJ TCT fellowship) for the excellent technical support.

REFERENCES

Abreu, T. P., Silva, L. S., Takiya, C. M., Souza, M. C., Henriques, M. G., Pinheiro, A. A., et al. (2014). Mice rescued from severe malaria are protected against renal injury during a second kidney insult. *PLoS One* 9:e93634. doi: 10.1371/journal.pone.0093634

Arnaud-Batista, F. J., Peruchetti, D. B., Abreu, T. P., do Nascimento, N. R., Malnic, G., Fonteles, M. C., et al. (2016). Uroguanylin modulates (Na++K+)ATPase in a proximal tubule cell line: interactions among the cGMP/protein kinase G, cAMP/protein kinase A, and mTOR pathways. *Biochim. Biophys. Acta* 1860, 1431–1438. doi: 10.1016/j.bbagen.2016.04.012

Batuman, V. (2007). Proximal tubular injury in myeloma. *Contrib. Nephrol.* 153, 87–104. doi: 10.1159/000096762

Breda, P. C., Wieck, T., Meyer-Schwesinger, C., Grahammer, F., Huber, T., Panzer, U., et al. (2019). Renal proximal tubular epithelial cells exert immunomodulatory function by driving inflammatory CD4+ T cell responses. *Am. J. Physiol. Renal Physiol.* 317, F77–F89. doi: 10.1152/ajprenal.00427.2018

Cabezas, F., Farfán, P., and Marzolo, M. P. (2019). Participation of the SMAD2/3 signalling pathway in the down regulation of megalin/LRP2 by transforming growth factor beta (TGF-ß1). *PLoS One* 14:e0213127. doi: 10.1371/journal.pone.0213127

Cabezas, F., Lagos, J., Céspedes, C., Vio, C. P., Bronfman, M., and Marzolo, M. P. (2011). Megalin/LRP2 expression is induced by peroxisome proliferator-activated receptor -alpha and -gamma: implications for PPARs' roles in renal function. *PLoS One* 6:e16794. doi: 10.1371/journal.pone.0016794

Cao, Q., Wang, C., Zheng, D., Wang, Y., Lee, V. W., Wang, Y. M., et al. (2011). IL-25 induces M2 macrophages and reduces renal injury in proteinuric kidney disease. *J. Am. Soc. Nephrol.* 22, 1229–1239. doi: 10.1681/ASN.2010070693

Caruso-Neves, C., Kwon, S. H., and Guggino, W. B. (2005). Albumin endocytosis in proximal tubule cells is modulated by angiotensin II through an AT2 receptor-mediated protein kinase B activation. *Proc. Natl. Acad. Sci. U.S.A.* 102, 17513–17518. doi: 10.1073/pnas.0507255102

Caruso-Neves, C., Pinheiro, A. A., Cai, H., Souza-Menezes, J., and Guggino, W. B. (2006). PKB and megalin determine the survival or death of renal proximal tubule cells. *Proc. Natl. Acad. Sci. U.S.A.* 103, 18810–18815. doi: 10.1073/pnas.0605029103

Cez, A., Brocheriou, I., Lescure, F. X., Adam, C., Girard, P. M., Pialoux, G., et al. (2018). Decreased expression of megalin and cubilin and altered mitochondrial activity in tenofovir nephrotoxicity. *Hum. Pathol.* 73, 89–101. doi: 10.1016/j.humpath.2017.12.018

Chevalier, R. L. (2016). The proximal tubule is the primary target of injury and progression of kidney disease: role of the glomerulotubular junction. *Am. J. Physiol. Renal Physiol.* 311, F145–F161. doi: 10.1152/ajprenal.00164.2016

Christensen, E. I., Devuyst, O., Dom, G., Nielsen, R., Van der Smissen, P., Verroust, P., et al. (2003). Loss of chloride channel ClC-5 impairs endocytosis by defective trafficking of megalin and cubilin in kidney proximal tubules. *Proc. Natl. Acad. Sci. U.S.A.* 100, 8472–8477. doi: 10.1073/pnas.1432873100

Chung, S., Overstreet, J. M., Li, Y., Wang, Y., Niu, A., Wang, S., et al. (2018). TGF-β promotes fibrosis after severe acute kidney injury by enhancing renal macrophage infiltration. *JCI Insight* 3:123563. doi: 10.1172/jci.insight.123563

Diwakar, R., Pearson, A. L., Colville-Nash, P., Brunskill, N. J., and Dockrell, M. E. (2007). The role played by endocytosis in albumin-induced secretion of TGF-beta1 by proximal tubular epithelial cells. *Am. J. Physiol. Renal Physiol.* 292, F1464–F1470.

Donadelli, R., Zanchi, C., Morigi, M., Buelli, S., Batani, C., Tomasoni, S., et al. (2003). Protein overload induces fractalkine upregulation in proximal tubular cells through nuclear factor kappaB- and p38 mitogen-activated protein kinase-dependent pathways. *J. Am. Soc. Nephrol.* 14, 2436–2446. doi: 10.1097/01.asn.0000089564.55411.7f

Erkan, E. (2013). Proteinuria and progression of glomerular diseases. *Pediatr. Nephrol.* 28, 1049–1058. doi: 10.1007/s00467-012-2335-1

Eshbach, M. L., and Weisz, O. A. (2017). Receptor-mediated endocytosis in the proximal tubule. *Annu. Rev. Physiol.* 79, 425–448. doi: 10.1146/annurev-physiol-022516-034234

Gaide Chevronnay, H. P., Janssens, V., Van Der Smissen, P., N'Kuli, F., Nuevo, N., Guiot, Y., et al. (2014). Time course of pathogenic and adaptation mechanisms in cystinotic mouse kidneys. *J. Am. Soc. Nephrol.* 25, 1256–1269. doi: 10.1681/ASN.2013060598

Gorriz, J. L., and Martinez-Castelao, A. (2012). Proteinuria: detection and role in native renal disease progression. *Transplant. Rev.* 26, 3–13. doi: 10.1016/j.trre.2011.10.002

Grgic, I., Campanholle, G., Bijol, V., Wang, C., Sabbisetti, V. S., Ichimura, T., et al. (2012). Targeted proximal tubule injury triggers interstitial fibrosis and glomerulosclerosis. *Kidney Int.* 82, 172–183. doi: 10.1038/ki.2012.20

Huen, S. C., and Cantley, L. G. (2017). Macrophages in renal injury and repair. *Annu. Rev. Physiol.* 79, 449–469. doi: 10.1146/annurev-physiol-022516-034219

Ishola, D. A. Jr., van der Giezen, D. M., Hahnel, B., Goldschmeding, R., Kriz, W., Koomans, H. A., et al. (2006). In mice, proteinuria and renal inflammatory responses to albumin overload are strain-dependent. *Nephrol. Dial. Transplant.* 21, 591–597. doi: 10.1093/ndt/gfi303

Koizumi, M., Ueda, K., Niimura, F., Nishiyama, A., Yanagita, M., Saito, A., et al. (2019). Podocyte injury augments intrarenal angiotensin II generation and sodium retention in a megalin-dependent manner. *Hypertension* 74, 509–517. doi: 10.1161/HYPERTENSIONAHA.118.12352

Landgraf, S. S., Silva, L. S., Peruchetti, D. B., Sirtoli, G. M., Moraes-Santos, F., Portella, V. G., et al. (2014). 5-Lypoxygenase products are involved in renal tubulointerstitial injury induced by albumin overload in proximal tubules in mice. *PLoS One* 9:e107549. doi: 10.1371/journal.pone.0107549

Lara, L. S., Correa, J. S., Lavelle, A. B., Lopes, A. G., and Caruso-Neves, C. (2008). The angiotensin receptor type 1-Gq protein-phosphatidyl inositol phospholipase Cbeta-protein kinase C pathway is involved in activation of proximal tubule Na+-ATPase activity by angiotensin(1-7) in pig kidneys. *Exp. Physiol.* 93, 639–647. doi: 10.1113/expphysiol.2007.040584

Lara, L. S., Vives, D., Correa, J. S., Cardozo, F. P., Marques-Fernades, M. F., Lopes, A. G., et al. (2010). PKA-mediated effect of MAS receptor in counteracting angiotensin II-stimulated renal Na+-ATPase. *Arch. Biochem. Biophys.* 496, 117–122. doi: 10.1016/j.abb.2010.02.005

Larsen, C. P., Trivin-Avillach, C., Coles, P., Collins, A. B., Merchant, M., Ma, H., et al. (2018). LDL receptor-related protein 2 (megalin) as a target antigen in human kidney anti-brush border antibody disease. *J. Am. Soc. Nephrol.* 29, 644–653. doi: 10.1681/ASN.2017060664

Lee, S., Huen, S., Nishio, H., Nishio, S., Lee, H. K., Choi, B. S., et al. (2011). Distinct macrophage phenotypes contribute to kidney injury and repair. *J. Am. Soc. Nephrol.* 22, 317–326. doi: 10.1681/ASN.2009060615

Lee, S. A., Noel, S., Sadasivam, M., Hamad, A. R. A., and Rabb, H. (2017). Role of immune cells in acute kidney injury and repair. *Nephron* 137, 282–286. doi: 10.1159/000477181

Liang, H., Zhang, Z., Yan, J., Wang, Y., Hu, Z., and Mitch, W. E. (2017). The IL-4 receptor α has a critical role in bone marrow-derived fibroblast activation and renal fibrosis. *Kidney Int.* 92, 1433–1443. doi: 10.1016/j.kint.2017.04.021

Lindoso, R. S., Araujo, D. S., Adão-Novaes, J., Mariante, R. M., Verdoorn, K. S., Fragel-Madeira, L., et al. (2011). Paracrine interaction between bone marrow-derived stem cells and renal epithelial cells. *Cell. Physiol. Biochem.* 28, 267–278. doi: 10.1159/000331739

Liyanage, T., Ninomiya, T., Jha, V., Neal, B., Patrice, H. M., Okpechi, I., et al. (2015). Worldwide access to treatment for end-stage kidney disease: a systematic review. *Lancet* 385, 1975–1982. doi: 10.1016/S0140-6736(14)61601-9

Lowry, O. H., Rosebrough, N. J., Farr, A. L., and Randall, R. J. (1951). Protein measurement with the Folin phenol reagent. *J. Biol. Chem.* 193, 265–275.

Nakhoul, N., and Batuman, V. (2011). Role of proximal tubules in the pathogenesis of kidney disease. *Contrib. Nephrol.* 169, 37–50. doi: 10.1159/000313944

Negi, S., Koreeda, D., Kobayashi, S., Yano, T., Tatsuta, K., Mima, T., et al. (2018). Acute kidney injury: epidemiology, outcomes, complications, and therapeutic strategies. *Semin. Dial.* 31, 519–527. doi: 10.1111/sdi.12705

Nielsen, R., Christensen, E. I., and Birn, H. (2016). Megalin and cubilin in proximal tubule protein reabsorption: from experimental models to human disease. *Kidney Int.* 89, 58–67. doi: 10.1016/j.kint.2015.11.007

Olsan, E. E., Matsushita, T., Rezaei, M., and Weimbs, T. (2015). Exploitation of the polymeric immunoglobulin receptor for antibody targeting to renal cyst lumens in polycystic kidney disease. *J. Biol. Chem.* 290, 15679–15686. doi: 10.1074/jbc.M114.607929

Pearson, A. L., Colville-Nash, P., Kwan, J. T., and Dockrell, M. E. (2008). Albumin induces interleukin-6 release from primary human proximal tubule epithelial cells. *J. Nephrol.* 21, 887–893.

Peruchetti, D. B., Cheng, J., Caruso-Neves, C., and Guggino, W. B. (2014). Mis-regulation of mammalian target of rapamycin (mTOR) complexes induced by albuminuria in proximal tubules. *J. Biol. Chem.* 289, 16790–16801. doi: 10.1074/jbc.M114.549717

Peruchetti, D. B., Freitas, A. C., Pereira, V. C., Lopes, J. V., Takiya, C. M., Nascimento, N. R. F., et al. (2019). PKB is a central molecule in the modulation of Na+-ATPase activity by albumin in renal proximal tubule cells. *Arch. Biochem. Biophys.* 674:108115. doi: 10.1016/j.abb.2019.108115

Peruchetti, D. B., Pinheiro, A. A., Landgraf, S. S., Wengert, M., Takiya, C. M., Guggino, W. B., et al. (2011). (Na+ + K+)-ATPase is a target for phosphoinositide 3-kinase/protein kinase B and protein kinase C pathways triggered by albumin. *J. Biol. Chem.* 286, 45041–45047. doi: 10.1074/jbc.M111.260737

Peruchetti, D. B., Silva-Aguiar, R. P., Siqueira, G. M., Dias, W. B., and Caruso-Neves, C. (2018). High glucose reduces megalin-mediated albumin endocytosis in renal proximal tubule cells through protein kinase B O-GlcNAcylation. *J. Biol. Chem.* 293, 11388–11400. doi: 10.1074/jbc.RA117.001337

Piwon, N., Günther, W., Schwake, M., Bösl, M. R., and Jentsch, T. J. (2000). ClC-5 Cl- -channel disruption impairs endocytosis in a mouse model for Dent's disease. *Nature* 408, 369–373. doi: 10.1038/35042597

Portella, V. G., Silva-Filho, J. L., Landgraf, S. S., de Rico, T. B., Vieira, M. A., Takiya, C. M., et al. (2013). Sepsis-surviving mice are more susceptible to a secondary kidney insult. *Crit. Care Med.* 41, 1056–1068. doi: 10.1097/CCM.0b013e3182746696

Reich, H., Tritchler, D., Herzenberg, A. M., Kassiri, Z., Zhou, X., Gao, W., et al. (2005). Albumin activates ERK via EGF receptor in human renal epithelial cells. *J. Am. Soc. Nephrol.* 16, 1266–1278. doi: 10.1681/asn.2004030222

Ribeiro, M. C., Peruchetti, D. B., Silva, L. S., Silva-Filho, J. L., Souza, M. C., Henriques, M. D. G., et al. (2018). LPS induces mTORC1 and mTORC2 activation during monocyte adhesion. *Front. Mol. Biosci.* 5:67. doi: 10.3389/fmolb.2018.00067

Ronco, C., Kellum, J. A., and Haase, M. (2012). Subclinical AKI is still AKI. *Crit. Care.* 16:313. doi: 10.1186/cc11240

Silva-Aguiar, R. P., Bezerra, N. C. F., Lucena, M. C., Sirtoli, G. M., Sudo, R. T., Zapata-Sudo, G., et al. (2018). O-GlcNAcylation reduces proximal tubule protein reabsorption and promotes proteinuria in spontaneously hypertensive rats. *J. Biol. Chem.* 293, 12749–12758. doi: 10.1074/jbc.RA118.001746

Silva-Filho, J. L., Caruso-Neves, C., and Pinheiro, A. A. (2017). Targeting angiotensin II type-1 receptor (AT1R) inhibits the harmful phenotype of *Plasmodium*-specific CD8+ T cells during blood-stage malaria. *Front. Cell. Infect. Microbiol.* 7:42. doi: 10.3389/fcimb.2017.00042

Silva-Filho, J. L., Peruchetti, D. B., Moraes-Santos, F., Landgraf, S. S., Silva, L. S., Sirtoli, G. M., et al. (2016). Group V secretory phospholipase A2 is involved in tubular integrity and sodium handling in the kidney. *PLoS One* 11:e0147785. doi: 10.1371/journal.pone.0147785

Silva-Filho, J. L., Souza, M. C., Ferreira-Dasilva, C. T., Silva, L. S., Costa, M. F., Padua, T. A., et al. (2013). Angiotensin II is a new component involved in splenic T lymphocyte responses during *Plasmodium berghei* ANKA infection. *PLoS One* 8:e62999. doi: 10.1371/journal.pone.0062999

Strausser, S. A., Nakano, D., and Souma, T. (2018). Acute kidney injury to chronic kidney disease transition: insufficient cellular stress response. *Curr. Opin. Nephrol. Hypertens.* 27, 314–322. doi: 10.1097/MNH.0000000000000424

Takaya, K., Koya, D., Isono, M., Sugimoto, T., Sugaya, T., Kashiwagi, A., et al. (2003). Involvement of ERK pathway in albumin-induced MCP-1 expression in mouse proximal tubular cells. *Am. J. Physiol. Renal Physiol.* 284, F1037–F1045.

Tang, S., Leung, J. C., Abe, K., Chan, K. W., Chan, L. Y., Chan, T. M., et al. (2003). Albumin stimulates interleukin-8 expression in proximal tubular epithelial cells in vitro and in vivo. *J. Clin. Invest.* 111, 515–527. doi: 10.1172/jci16079

Teixeira, D. E., Peruchetti, D. B., Silva, L. S., Silva-Aguiar, R. P., Oquendo, M. B., Silva-Filho, J. L., et al. (2019). Lithium ameliorates tubule-interstitial injury through activation of the mTORC2/protein kinase B pathway. *PLoS One* 14:e0215871. doi: 10.1371/journal.pone.0215871

Theilig, F. (2010). Spread of glomerular to tubulointerstitial disease with a focus on proteinuria. *Ann. Anat.* 192, 125–132. doi: 10.1016/j.aanat.2010.03.003

Van Den Berg, J. G., Aten, J., Annink, C., Ravesloot, J. H., Weber, E., and Weening, J. J. (2002). Interleukin-4 and -13 promote basolateral secretion of H(+) and cathepsin L by glomerular epithelial cells. *Am. J. Physiol. Renal Physiol.* 282, F26–F33.

Vanmassenhove, J., Van Biesen, W., Vanholder, R., and Lameire, N. (2019). Subclinical AKI: ready for primetime in clinical practice? *J. Nephrol.* 32, 9–16. doi: 10.1007/s40620-018-00566-y

Venkatachalam, M. A., Weinberg, J. M., Kriz, W., and Bidani, A. K. (2015). Failed tubule recovery, AKI-CKD transition, and kidney disease progression. *J. Am. Soc. Nephrol.* 26, 1765–1776. doi: 10.1681/ASN.2015010006

Vicinanza, M., Di Campli, A., Polishchuk, E., Santoro, M., Di Tullio, G., Godi, A., et al. (2011). OCRL controls trafficking through early endosomes via PtdIns4,5P2-dependent regulation of endosomal actin. *EMBO J.* 30, 4970–4985. doi: 10.1038/emboj.2011.354

Wang, J., Wen, Y., Zhou, M., Shi, X., Jiang, L., Li, M., et al. (2017). Ectopic germinal center and megalin defect in primary Sjogren syndrome with renal Fanconi syndrome. *Arthritis Res. Ther.* 19:120. doi: 10.1186/s13075-017-1317-x

Yan, J., Zhang, Z., Yang, J., Mitch, W. E., and Wang, Y. (2015). JAK3/STAT6 stimulates bone marrow-derived fibroblast activation in renal fibrosis. *J. Am. Soc. Nephrol.* 26, 3060–3071. doi: 10.1681/ASN.2014070717

Yokota, N., Burne-Taney, M., Racusen, L., and Rabb, H. (2003). Contrasting roles for STAT4 and STAT6 signal transduction pathways in murine renal ischemia-reperfusion injury. *Am. J. Physiol. Renal Physiol.* 285, F319–F325.

Zhang, M. Z., Wang, X., Wang, Y., Niu, A., Wang, S., Zou, C., et al. (2017). IL-4/IL-13-mediated polarization of renal macrophages/dendritic cells to an M2a phenotype is essential for recovery from acute kidney injury. *Kidney Int.* 91, 375–386. doi: 10.1016/j.kint.2016.08.020

Zoja, C., Donadelli, R., Colleoni, S., Figliuzzi, M., Bonazzola, S., Morigi, M., et al. (1998). Protein overload stimulates RANTES production by proximal tubular cells depending on NF-kappa B activation. *Kidney Int.* 53, 1608–1615. doi: 10.1046/j.1523-1755.1998.00905.x

Conflict of Interest: The authors declare that the research was conducted in the absence of any commercial or financial relationships that could be construed as a potential conflict of interest.

Copyright © 2020 Peruchetti, Silva-Filho, Silva-Aguiar, Teixeira, Takiya, Souza, Henriques, Pinheiro and Caruso-Neves. This is an open-access article distributed under the terms of the Creative Commons Attribution License (CC BY). The use, distribution or reproduction in other forums is permitted, provided the original author(s) and the copyright owner(s) are credited and that the original publication in this journal is cited, in accordance with accepted academic practice. No use, distribution or reproduction is permitted which does not comply with these terms.

frontiers in Medicine

REVIEW
published: 12 March 2020
doi: 10.3389/fmed.2020.00065

Defective Mitochondrial Fatty Acid Oxidation and Lipotoxicity in Kidney Diseases

Hee-Seong Jang[1], Mi Ra Noh[1], Jinu Kim[1,2,3] and Babu J. Padanilam[1,4]**

[1] Department of Cellular and Integrative Physiology, University of Nebraska Medical Center, Omaha, NE, United States, [2] Department of Anatomy, Jeju National University School of Medicine, Jeju, South Korea, [3] Interdisciplinary Graduate Program in Advanced Convergence Technology & Science, Jeju National University, Jeju, South Korea, [4] Internal Medicine, Section of Nephrology, University of Nebraska Medical Center, Omaha, NE, United States

The kidney is a highly metabolic organ and uses high levels of ATP to maintain electrolyte and acid-base homeostasis and reabsorb nutrients. Energy depletion is a critical factor in development and progression of various kidney diseases including acute kidney injury (AKI), chronic kidney disease (CKD), and diabetic and glomerular nephropathy. Mitochondrial fatty acid β-oxidation (FAO) serves as the preferred source of ATP in the kidney and its dysfunction results in ATP depletion and lipotoxicity to elicit tubular injury and inflammation and subsequent fibrosis progression. This review explores the current state of knowledge on the role of mitochondrial FAO dysfunction in the pathophysiology of kidney diseases including AKI and CKD and prospective views on developing therapeutic interventions based on mitochondrial energy metabolism.

Keywords: mitochondria, fatty acid β-oxidation, lipotoxicity, acute kidney injury, chronic kidney disease, diabetic nephropathy, polycystic kidney disease, glomerular nephropathy

OPEN ACCESS

Edited by:
John D. Imig,
Medical College of Wisconsin, United States

Reviewed by:
Jonatan Barrera-Chimal, National Autonomous University of Mexico, Mexico
Kirk Campbell, Icahn School of Medicine at Mount Sinai, United States

****Correspondence:***
Hee-Seong Jang
kiaroholic@gmail.com
Babu J. Padanilam
bpadanilam@unmc.edu

Specialty section:
This article was submitted to Nephrology, a section of the journal Frontiers in Medicine

Received: *01 December 2019*
Accepted: *13 February 2020*
Published: *12 March 2020*

Citation:
Jang HS, Noh MR, Kim J and Padanilam BJ (2020) Defective Mitochondrial Fatty Acid Oxidation and Lipotoxicity in Kidney Diseases. Front. Med. 7:65. doi: 10.3389/fmed.2020.00065

INTRODUCTION

The kidney demands a high energy supply to generate energy-required transport of glucose, ions, and nutrients from blood filtrate (1). Mitochondria is an essential organelle generating ATP through oxidative metabolism, as well as regulation of redox homeostasis and cell death signaling. Loss or depletion of ATP by renal tubular mitochondrial disturbance causes acute and chronic kidney diseases (2–5). Renal tubules, particularly proximal tubules that have abundant mitochondria, are metabolically active due to reabsorption of most glomerular filtrate. Because medullary region with pars recta adjunct proximal tubule has only 5–10% of total renal blood flow with tissue oxygen tension 10–20 mm Hg, the medullary proximal tubules are highly vulnerable to hypoxic condition such as ischemia/reperfusion injury (6, 7). Mitochondrial fatty acid β-oxidation (FAO) in proximal tubule is a major source of ATP generation, and its impairment is linked to ATP depletion-induced acute kidney injury (AKI) (1), lipotoxicity (8, 9), and its long-term sequelae leading to CKD (10). Several reports demonstrate that AKI is an independent risk factor for CKD (11–15), and thus promoting mitochondrial FAO is a first-rate option for preventing AKI and CKD. Recent reports indicate that podocytes are also highly sensitive to acute and chronic stimuli, because podocytes have a limited ability for adaptation to mitochondrial energy crisis (16). Here, we summarize the recent findings associated with mitochondrial dysregulation, particularly defective fatty acid (FA) metabolism and lipotoxicity in kidney diseases, which includes tubular and glomerular injury. We also discuss therapeutic strategies targeting mitochondrial energy metabolism in kidney diseases.

MITOCHONDRIAL ENERGETICS

The mitochondria are highly dynamic intracellular organelles that generate most of the ATP in tissues, including the kidney (17). The kidney has abundant mitochondria to produce high levels of ATP through oxidative phosphorylation, to accomplish the substantial passive or active reabsorption of components of the glomerular filtrate, including various ions, glucose, and nutrients. Oxidative phosphorylation yields 36 ATP per glucose, which is highly efficient compared to that of glycolysis generating only 2 ATP (18). The most efficient ATP-generating system in cell energy metabolism is FAO, which can generate 106–129 ATP, depending on the number of carbons in the FA chain. The proximal tubule transports ∼67% of glomerular filtrate and thus requires high levels of ATP for its function (19). The proximal tubule prefers FAO for ATP production and has low metabolic flexibility to glycolysis (6, 20). Moreover, it should be noted that the outer medullary proximal tubule has lower oxygen tension under normal conditions and thus less capacity to cope with hypoxic condition (6), which makes them highly sensitive to acute and chronic stimuli. On the other hand, distal tubule is less susceptible to acute stimuli such as ischemic injury and nephrotoxins, because it has better capacity for glycolytic adaptation during hypoxic/ischemic condition, despite its high energy requirement (6, 21, 22). The glomerular podocyte, which has less mitochondria than proximal tubule and depends on mitochondrial respiration for ∼75% of energy, also has high vulnerability to stimuli such as glycemic condition (16), but the mechanism of its susceptibility remains to be fully defined. In diseased kidneys with impaired FAO, glycolysis and glutaminolysis can serve as a significant energy source. For example, in polycystic kidney disease (PKD), metabolic reprogramming by increased glutaminolysis, as well as glycolysis, occurs to cope with impaired FAO (23). However, in the ischemic kidney, it has been reported that poly (ADP-ribose) Polymerase 1 and Tp53 induced glycolysis and apoptosis regulator are selectively activated in the injured proximal tubules and inhibit glycolysis during ischemic injury (24, 25). This will prevent compensation of ATP production by glycolysis and makes the proximal tubules extremely vulnerable. Intriguingly, recent reports suggest upregulation of glycolysis as a compensatory mechanism to adapt to reduced FAO during persistent acute tubular injury, which may be related with tubular repair mechanism, resulting in chronic inflammation and fibrosis progression (26–28). These studies indicate that adaptation of energy metabolism for loss of mitochondrial ATP could be compensated by other metabolic processes such as glycolysis or glutaminolysis, suggesting that regulatory mechanism of metabolic pathways can be a key to develop a valuable target for treatment of kidney diseases.

MITOCHONDRIAL FATTY ACID METABOLISM

Defective FA uptake, synthesis, and oxidation are tightly linked to development and progression of kidney diseases. In proximal tubular cells, FA can be taken up by membrane FA transport proteins, such as CD36 and FA-binding protein (FABP), as well as by reabsorption from glomerular filtrate by endocytosis of receptor-mediated FA-bound albumin (20, 29, 30). The kidney with AKI accumulates FAs in cytoplasm, which is a result of dysregulated FAO, leading to ATP depletion (1). Fatty acid is activated to acyl-CoA to make it permeable to the outer mitochondrial membrane (OMM) by acyl-CoA synthetases in the cytosol. Carnitine palmitoyltransferase-1 (Cpt-1), located on the OMM, catalyzes transesterification of the acyl-CoA to acylcarnitine (20, 21, 31). Acylcarnitine is shuttled across the inner mitochondrial membrane (IMM) through carnitine–acylcarnitine translocase. Acylcarnitine is reconverted to acyl-CoA by Cpt-2, an IMM protein. In the mitochondrial matrix, through β-oxidation, a serial cyclic process is trimmed the acyl-CoA to form molecules of acetyl-CoA (21). Finally, acetyl-CoA is fed into the tricarboxylic acid cycle, to generate NADH and $FADH_2$ that serve as electron donors to the electron transport chain for ATP production (20, 29, 31) (**Figure 1**). It is well-known that downregulated or deficient CPT-1 or CPT-2 is critical to impaired FAO in diverse kidney diseases, such as ischemic and cisplatin AKI and diabetic nephropathy (32–34).

It is well-recognized that peroxisome proliferator-activated receptor γ coactivator-1α (PGC-1α)–peroxisome proliferator-activated receptor α (PPARα) axis governs transcription and regulation of FAO genes in diverse tissues, including the kidney, and its regulation has been suggested as a therapeutic target of AKI and CKD (10, 20, 35–37). We (38) and others (39–42) suggested that defective mitochondrial FAO is critical to ischemic and cisplatin-induced AKI (**Figure 2**). Downregulation of activity and expression of PPARα and/or PGC-1α resulted in inhibited transcriptional regulation of FAO genes, such as Cpt-1 and medium chain–specific acyl-CoA dehydrogenase, leading to decreased mitochondrial FAO (38, 40, 45). Enhanced PPARα activation by fenofibrate protects histological and functional impairment in cisplatin AKI (46). However, the upstream signaling pathway that inhibits PPARα-regulated FAO in AKI is under investigation.

In our recent report (38), we hypothesized that mitochondrial interaction of proximal tubule cyclophilin D (CypD) and PPARα modulates FAO in cisplatin AKI. We demonstrated using genetic and pharmacological intervention, protein–protein interaction studies, and bioinformatics that mitochondrial CypD-PPARα binding, which modulates FAO, occurs in proximal tubule during cisplatin AKI. Mitochondrial translocation of PPARα, its binding to CypD, and sequestration led to inhibition of its nuclear translocation and transcription of PPARα-regulated FAO genes during cisplatin AKI, leading to reduced FAO, lipid accumulation, and lipotoxicity. Pharmacological or genetic inhibition of CypD promoted nuclear translocation of PPARα and enhanced the transcription of FAO genes and prevented cisplatin AKI (**Figure 2**).

In CKD, the PGC1α-PPARα axis and FAO key enzymes such as Cpt-1 are persistently decreased. In hypertensive and folic acid–induced CKD, tubular lipid accumulation related to defective FAO, along with tubular and functional impairment, is reported (10, 47). In proximal tubule exposed to FA, PPARα activation can eliminate ceramides, which are toxic

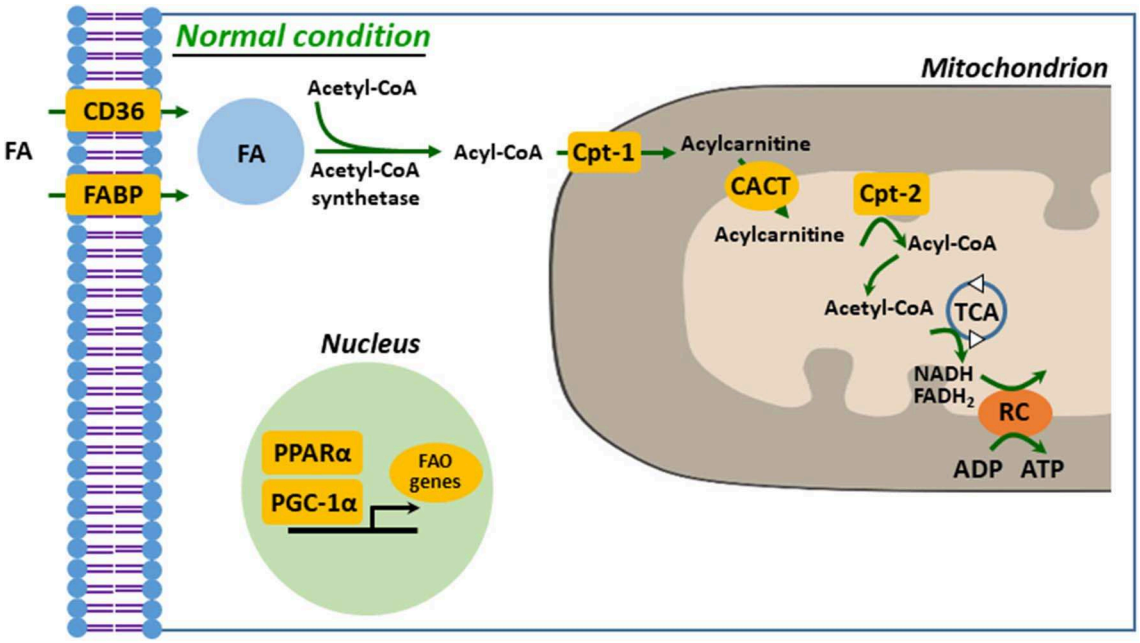

FIGURE 1 | Mitochondrial fatty acid oxidation in kidney tubule. FA enters into cytosol of renal proximal tubule cell (PTC) via FABP or CD36. In the cytosol, FA are converted from acetyl-CoA to acyl-CoA by acetyl-CoA synthetase and then transferred to mitochondrial matrix by carnitine shuttle, Cpt-1, CACT, and Cpt-2, step by step. Acyl-CoA undergoes β-oxidation to produce acetyl-CoA for TCA. NADH and FADH2 generated by TCA are used as electron donors for RC. FA, fatty acid; FAO, fatty acid β-oxidation; Cpt, carnitine *O*-palmitoyltransferase; CACT, carnitine-acylcarnitine translocase; TCA, tricarboxylic acid cycle; RC, respiratory chain.

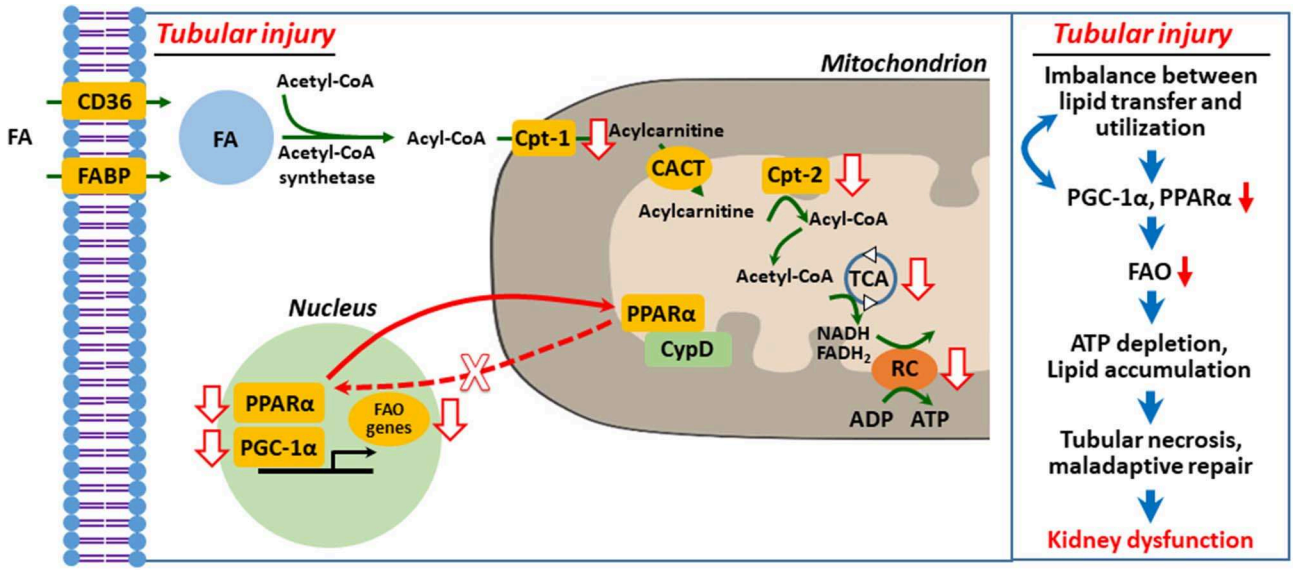

FIGURE 2 | Defective mitochondrial fatty acid oxidation and lipid accumulation in injured kidney tubular cell. Upon tubular injury, PPARα translocates to mitochondria and binds with cyclophilin D (CypD), resulting in mitochondrial sequestration and decreased transcriptional activity of PPARα for FAO genes (38). Inhibition of FAO genes depletes ATP by impaired FAO and that in turn induces PTC necrosis, maladaptive repair, and kidney dysfunction (1, 9, 20, 29, 36, 38, 39, 43, 44). FA, fatty acid; FAO, fatty acid β-oxidation; Cpt, carnitine *O*-palmitoyltransferase; CACT, carnitine-acylcarnitine translocase; TCA, tricarboxylic acid cycle; RC, respiratory chain.

metabolites contributing to lipotoxicity (20, 43, 48). On the other hand, in addition to its role in FAO, PGC-1α can act as a master regulator of mitochondrial biogenesis and NAD biosynthesis. This topic is reviewed in detail elsewhere (1, 8, 36, 37, 49).

GLOMERULAR/PODOCYTE INJURY

Glomerular podocytes are specialized epithelial cells, integrating structural and functional maintenance of glomerular filtration barrier. Podocytes consume high energy for their function,

which makes the cells highly susceptible to ATP depletion and to acute and chronic injury (16, 50, 51). Podocyte injury and loss contribute to initiation and progression of proteinuric glomerular diseases, including diabetic nephropathy, glomerular sclerosis, and membranous nephropathy (51–53). In hyperglycemic condition, mitochondrial FAO is enhanced in podocytes, but when both FAO and glycolysis were inhibited, it has a limited capacity to adapt to the changed condition and sensitize podocytes to apoptosis (16, 54). In addition, because mitochondrial respiration accounts for 75% of energy, podocytes have less glycolytic flexibility when mitochondrial function is impaired, resulting in energy deficit (16, 55). However, because glomerulus consists of other cells, including mesangial cell and endothelial cells, all of which could interact with podocytes, in diseased conditions, data from *in vitro* studies using only podocytes should be interpret cautiously (16). On the other hand, it seems that PPARα activation impedes the progression of diabetic nephropathy. PPARα is increased in the kidneys of streptozotocin-induced diabetic mouse model, but when PPARα was genetically deleted, the mice showed adverse effects, including glomerulosclerosis (56). Similar findings from types 1 and 2 diabetic animal models demonstrated that activation of PPARα by fibrates improved hyperglycemic and/or dislipidemic condition–induced glomerular injury and function along with lipid lowering effect (56–60). Although human data (61) revealed that fibrates improve diabetic nephropathy such as albuminuria, data from rodent studies demonstrate more effectiveness than those of clinical studies, suggesting that rodents are more sensitive to PPARα signaling. These data suggest that caution is needed to interpreting the effectiveness of fibrate treatment from animals to humans (61, 62).

GENETIC DISORDERS

Many genetic disorders are involved in initiation and progression of kidney diseases. Polycystic kidney disease due to mutations in PKD1 and PKD2, which produces polycystin 1 and 2, respectively, are the most common monogenic human kidney diseases, showing 100–1,000 fluid-filled renal cysts (63). A number of signaling pathways, including cAMP, calcium, cell cycle, mTORC1, and WNT signaling, are involved in PKD pathogenesis (63, 64). Recent reports demonstrated defective FAO, as well as glucose metabolism, can contribute to the pathogenesis of both human and animal autosomal dominant PKD (ADPKD) (64, 65). Polycystin proteins seem to be involved in mitochondrial function, because epithelial Pkd1 inactivation from proximal or distal tubule resulted in lower FAO with unchanged glycolysis (66, 67). It is reported that loss of Pkd1 drives cyst growth with declined FAO via direct repression of PPARα (23, 66). Upregulation of PPARα by fenofibrate enhanced FAO and showed beneficial effect in slowing PKD progression by suppressed renal cyst growth, fibrosis, and improved function in a slowly progressing orthologous model of ADPKD (68). On the other hand, the role of FAO in autosomal recessive PKD, a recessive form of PKD that is a rare genetic disorder characterized by enlarged kidney and biliary dysgenesis (63, 69), remains largely unknown.

LIPOTOXICITY

Although the causal relationship is unclear, a number of reports suggest that lipid accumulation in certain tissue and cell could be harmful and is referred to as lipotoxicity (43, 70, 71). The initial hypothesis regarding lipotoxicity was that intrarenal lipid accumulation can affect structure and function in renal cells, including proximal tubule cell (71, 72). Accumulation of triglyceride, which is produced by dysregulated glycerol and non-esterified FA (NEFA) presumably derived from impaired FA transport and/or FAO in cytoplasm causes lipotoxicity, contributing to decreased production of ATP and mitochondrial energy metabolism (43, 44). NEFA triggers mitochondrial dysfunction as a cause of energetic failure of proximal tubules during hypoxia/reoxygenation, and intracellular accumulation of NEFA and triglycerides with downregulation of mitochondrial FAO (43, 73). Accumulation of triglycerides is observed in tubule injured by ischemic, cisplatin, glycerol-induced, and septic AKI, as well as in kidneys with metabolic syndrome or fibrosis progression (10, 44, 71, 74). Lipid accumulation in ischemic proximal tubule may result in persistent energy depletion with NEFA-induced mitochondrial dysfunction (43). In parallel, high-fat diet or palmitic acid overload resulted in upregulation of inflammation, fibrosis, or cell death in kidneys (75–77). However, it is still under debate whether FA or triglyceride *per se* is toxic, but it is clear that intrarenal lipid accumulation, by as of yet undefined mechanisms, can represent characteristics of diseased status (43, 70, 78). Recent data show that in two CKD mouse models (diabetic nephropathy and folic acid nephropathy) lipid accumulation by kidney cell–specific overexpression of CD36, a key membrane protein for FA uptake in proximal tubule (79, 80), did not generate renal fibrosis (10). It is proposed that mitochondrial defects in energy production are more detrimental than the lipid accumulation in the cytoplasm. Further studies to define the causal relationship between lipid accumulation and energy depletion and the effect of lipotoxicity during AKI and CKD are warranted.

TARGETING MITOCHONDRIAL FATTY ACID METABOLISM IN KIDNEY DISEASES

A number of studies targeting mitochondrial dysfunction in kidney diseases have been investigated in both animals and human (29). The most treatable option targeting defective FAO in AKI and CKD to date is using agonists of PPARα, fibrates–fenofibrate, clofibrate, and others, despite its adverse effects (81, 82). Fibrates showed a preventive effect to tubular cell death and dysregulated intracellular lipid accumulation, in ischemic and cisplatin AKI models, and in high-fat diet or folic acid–induced CKD models (46, 83–86). However, fenofibrate treatment has adverse effects in kidney function as demonstrated by decreased glomerular filtrate rate and/or

increased serum creatinine independent of its lipid-lowering effect (82, 87–89). These data suggest that a better understanding of the molecular mechanism of PPARα agonists and its tissue specificity is required to assess the effectiveness of fenofibrate therapy. Another promising option to modulate FAO is to target FA synthase or transporter. Administration of 5A peptide, which targets CD36 to inhibit FA transport into cell, showed promising results by lowering intrarenal lipid level in subtotal nephrectomized mice kidneys (90). Like CD36 antagonist, a blocker of FA synthase, C75, showed beneficial effect in suppression of folic acid–induced kidney fibrosis progression (10).

Other treatment strategies targeting mitochondria, but not targeting FAO *per se*, include the use of SS-31 (Szeto-Schiller 31) and MitoQ or MitoT. SS-31, mitochondria-targeting tetrapeptides, preserved mitochondrial structure in both proximal tubules and podocytes and thus enhanced functional recovery from ischemic AKI and prevents its long-term consequences, including interstitial fibrosis and glomerulosclerosis (91, 92). In high-fat diet–mediated proximal tubule injury, SS-31 lowered intracellular lipid accumulation by suppressing disruption of mitochondrial function (93). Mitochondria-targeted lipophilic antioxidants, MitoQ and MitoT, protected tubular injury and kidney dysfunction through suppression of mitochondrial damage and oxidative stress and improvement of mitochondrial NADPH level in septic or cisplatin AKI (94, 95). One of the major barriers to develop treatment strategies targeting mitochondrial dysfunction in AKI and CKD is to take into consideration that mitochondria is an organelle regulating redox homeostasis by reactive oxygen species production and detoxification, and its dysregulation could increase oxidative stress (8, 96). Thus, an integrated understanding for mitochondrial biology, including mitochondrial energy metabolism and redox signaling, in particular in susceptible kidney segments, should be preceded to minimize the side effects of mitochondrial targeting in kidney diseases.

CONCLUSION

Mitochondrial dysregulation, resulting in loss of ATP, is critical to energy homeostasis and pathogenesis of kidney diseases. Acute and chronic disturbance of mitochondrial FA metabolism depletes ATP, leading to tubular and glomerular injury. Lipotoxicity via impaired FA metabolism could induce cell death and inflammation and promote the chronic progression of AKI to CKD. Unveiling the role and the related molecular mechanism of mitochondrial energy metabolism is required for the development of effective therapeutics in targeting tubular and glomerular injury in acute and chronic kidney diseases.

AUTHOR CONTRIBUTIONS

H-SJ and BP made substantial contributions to the conception and drafting the work and revising it critically for important intellectual content, provided approval for publication of the content, and agreed to be accountable for all aspects of the work in ensuring that questions related to the accuracy or integrity of any part of the work are appropriately investigated and resolved. MN and JK made contributions to drafting the work or revising it critically for important intellectual content and provided approval for publication of the content.

FUNDING

This work was supported by NIH grants DK-116987, DK-120533, DK120846, and American Heart Association (AHA) Grant in Aid 15GRNT25080031 (BP), AHA postdoctoral fellowship Grant 15POST25130003 (H-SJ), and grants (NRF-2016R1C1B2012080 and NRF-2019R1F1A1041410) from the National Research Foundation of Korea (JK).

REFERENCES

1. Bhargava P, Schnellmann RG. Mitochondrial energetics in the kidney. *Nat Rev Nephrol.* (2017) 13:629–46. doi: 10.1038/nrneph.2017.107
2. Basile DP, Anderson MD, Sutton TA. Pathophysiology of acute kidney injury. *Compr Physiol.* (2012) 2:1303–53. doi: 10.1002/cphy.c110041
3. Maekawa H, Inagi R. Pathophysiological role of organelle stress/crosstalk in AKI-to-CKD transition. *Semin Nephrol.* (2019) 39:581–8. doi: 10.1016/j.semnephrol.2019.10.007
4. Weinberg JM, Venkatachalam MA, Roeser NF, Saikumar P, Dong Z, Senter RA, et al. Anaerobic and aerobic pathways for salvage of proximal tubules from hypoxia-induced mitochondrial injury. *Am J Physiol Renal Physiol.* (2000) 279:F927–43. doi: 10.1152/ajprenal.2000.279.5.F927
5. Ying Y, Padanilam BJ. Regulation of necrotic cell death: p53, PARP1 and cyclophilin D-overlapping pathways of regulated necrosis? *Cell Mol Life Sci.* (2016) 73:2309–24. doi: 10.1007/s00018-016-2202-5
6. Bonventre JV, Yang L. Cellular pathophysiology of ischemic acute kidney injury. *J Clin Invest.* (2011) 121:4210–21. doi: 10.1172/JCI45161
7. Nourbakhsh N, Singh P. Role of renal oxygenation and mitochondrial function in the pathophysiology of acute kidney injury. *Nephron Clin Pract.* (2014) 127:149–52. doi: 10.1159/000363545
8. Hall AM, Schuh CD. Mitochondria as therapeutic targets in acute kidney injury. *Curr Opin Nephrol Hypertens.* (2016) 25:355–62. doi: 10.1097/MNH.0000000000000228
9. Stallons LJ, Funk JA, Schnellmann RG. Mitochondrial homeostasis in acute organ failure. *Curr Pathobiol Rep.* (2013) 1:169–77. doi: 10.1007/s40139-013-0023-x
10. Kang HM, Ahn SH, Choi P, Ko YA, Han SH, Chinga F, et al. Defective fatty acid oxidation in renal tubular epithelial cells has a key role in kidney fibrosis development. *Nat Med.* (2015) 21:37–46. doi: 10.1038/nm.3762
11. Basile DP, Bonventre JV, Mehta R, Nangaku M, Unwin R, Rosner MH, et al. Progression after AKI: understanding maladaptive repair processes to predict and identify therapeutic treatments. *J Am Soc Nephrol.* (2016) 27:687–97. doi: 10.1681/ASN.2015030309
12. Chawla LS, Eggers PW, Star RA, Kimmel PL. Acute kidney injury and chronic kidney disease as interconnected syndromes. *N Engl J Med.* (2014) 371:58–66. doi: 10.1056/NEJMra1214243
13. Coca SG, Singanamala S, Parikh CR. Chronic kidney disease after acute kidney injury: a systematic review and meta-analysis. *Kidney Int.* (2012) 81:442–8. doi: 10.1038/ki.2011.379
14. Jang HS, Kim JI, Han SJ, Park KM. Recruitment and subsequent proliferation of bone marrow-derived cells in the postischemic kidney are important to

the progression of fibrosis. *Am J Physiol Renal Physiol.* (2014) 306:F1451–61. doi: 10.1152/ajprenal.00017.2014
15. Venkatachalam MA, Weinberg JM, Kriz W, Bidani AK. Failed tubule recovery, AKI-CKD transition, and kidney disease progression. *J Am Soc Nephrol.* (2015) 26:1765–76. doi: 10.1681/ASN.2015010006
16. Muller-Deile J, Schiffer M. The podocyte power-plant disaster and its contribution to glomerulopathy. *Front Endocrinol.* (2014) 5:209. doi: 10.3389/fendo.2014.00209
17. Chandel NS. Evolution of mitochondria as signaling organelles. *Cell Metab.* (2015) 22:204–6. doi: 10.1016/j.cmet.2015.05.013
18. Mandel LJ. Primary active sodium transport, oxygen consumption, and ATP: coupling and regulation. *Kidney Int.* (1986) 29:3–9. doi: 10.1038/ki.1986.2
19. Koeppen BM, Stanton BA. *Renal Physiology.* 5th ed. Philadelphia, PA: Elsevier Mosby (2013).
20. Simon N, Hertig A. Alteration of fatty acid oxidation in tubular epithelial cells: from acute kidney injury to renal fibrogenesis. *Front Med.* (2015) 2:52. doi: 10.3389/fmed.2015.00052
21. Houten SM, Violante S, Ventura FV, Wanders RJ. The biochemistry and physiology of mitochondrial fatty acid beta-oxidation and its genetic disorders. *Annu Rev Physiol.* (2016) 78:23–44. doi: 10.1146/annurev-physiol-021115-105045
22. Weinberg JM, Molitoris BA. Illuminating mitochondrial function and dysfunction using multiphoton technology. *J Am Soc Nephrol.* (2009) 20:1164–6. doi: 10.1681/ASN.2009040419
23. Podrini C, Rowe I, Pagliarini R, Costa ASH, Chiaravalli M, Di Meo I, et al. Dissection of metabolic reprogramming in polycystic kidney disease reveals coordinated rewiring of bioenergetic pathways. *Commun Biol.* (2018) 1:194. doi: 10.1038/s42003-018-0200-x
24. Devalaraja-Narashimha K, Padanilam BJ. PARP-1 inhibits glycolysis in ischemic kidneys. *J Am Soc Nephrol.* (2009) 20:95–103. doi: 10.1681/ASN.2008030325
25. Kim J, Devalaraja-Narashimha K, Padanilam BJ. TIGAR regulates glycolysis in ischemic kidney proximal tubules. *Am J Physiol Renal Physiol.* (2015) 308:F298–308. doi: 10.1152/ajprenal.00459.2014
26. Lan R, Geng H, Singha PK, Saikumar P, Bottinger EP, Weinberg JM, et al. Mitochondrial pathology and glycolytic shift during proximal tubule atrophy after ischemic AKI. *J Am Soc Nephrol.* (2016) 27:3356–67. doi: 10.1681/ASN.2015020177
27. Lemos DR, McMurdo M, Karaca G, Wilflingseder J, Leaf IA, Gupta N, et al. Interleukin-1beta activates a MYC-dependent metabolic switch in kidney stromal cells necessary for progressive tubulointerstitial fibrosis. *J Am Soc Nephrol.* (2018) 29:1690–705. doi: 10.1681/ASN.2017121283
28. Wei Q, Su J, Dong G, Zhang M, Huo Y, Dong Z. Glycolysis inhibitors suppress renal interstitial fibrosis via divergent effects on fibroblasts and tubular cells. *Am J Physiol Renal Physiol.* (2019) 316:F1162–72. doi: 10.1152/ajprenal.00422.2018
29. Szeto HH. Pharmacologic approaches to improve mitochondrial function in AKI and CKD. *J Am Soc Nephrol.* (2017) 28:2856–65. doi: 10.1681/ASN.2017030247
30. Yang X, Okamura DM, Lu X, Chen Y, Moorhead J, Varghese Z, et al. CD36 in chronic kidney disease: novel insights and therapeutic opportunities. *Nat Rev Nephrol.* (2017) 13:769–81. doi: 10.1038/nrneph.2017.126
31. Aon MA, Bhatt N, Cortassa SC. Mitochondrial and cellular mechanisms for managing lipid excess. *Front Physiol.* (2014) 5:282. doi: 10.3389/fphys.2014.00282
32. Feingold KR, Wang Y, Moser A, Shigenaga JK, Grunfeld C. LPS decreases fatty acid oxidation and nuclear hormone receptors in the kidney. *J Lipid Res.* (2008) 49:2179–87. doi: 10.1194/jlr.M800233-JLR200
33. Idrovo JP, Yang WL, Nicastro J, Coppa GF, Wang P. Stimulation of carnitine palmitoyltransferase 1 improves renal function and attenuates tissue damage after ischemia/reperfusion. *J Surg Res.* (2012) 177:157–64. doi: 10.1016/j.jss.2012.05.053
34. Portilla D. Role of fatty acid beta-oxidation and calcium-independent phospholipase A2 in ischemic acute renal failure. *Curr Opin Nephrol Hypertens.* (1999) 8:473–7. doi: 10.1097/00041552-199907000-00012
35. Han SH, Wu MY, Nam BY, Park JT, Yoo TH, Kang SW, et al. PGC-1alpha protects from notch-induced kidney fibrosis development. *J Am Soc Nephrol.* (2017) 28:3312–22. doi: 10.1681/ASN.2017020130
36. Tran M, Parikh SM. Mitochondrial biogenesis in the acutely injured kidney. *Nephron Clin Pract.* (2014) 127:42–5. doi: 10.1159/000363715
37. Weinberg JM. Mitochondrial biogenesis in kidney disease. *J Am Soc Nephrol.* (2011) 22:431–6. doi: 10.1681/ASN.2010060643
38. Jang HS, Noh MR, Jung EM, Kim WY, Southekal S, Guda C, et al. Proximal tubule cyclophilin D regulates fatty acid oxidation in cisplatin-induced acute kidney injury. *Kidney Int.* (2020) 97:327–39. doi: 10.1016/j.kint.2019.08.019
39. Portilla D. Energy metabolism and cytotoxicity. *Semin Nephrol.* (2003) 23:432–8. doi: 10.1016/S0270-9295(03)00088-3
40. Portilla D, Dai G, McClure T, Bates L, Kurten R, Megyesi J, et al. Alterations of PPARalpha and its coactivator PGC-1 in cisplatin-induced acute renal failure. *Kidney Int.* (2002) 62:1208–18. doi: 10.1111/j.1523-1755.2002.kid553.x
41. Portilla D, Dai G, Peters JM, Gonzalez FJ, Crew MD, Proia AD. Etomoxir-induced PPARalpha-modulated enzymes protect during acute renal failure. *Am J Physiol Renal Physiol.* (2000) 278:F667–75. doi: 10.1152/ajprenal.2000.278.4.F667
42. Portilla D, Li S, Nagothu KK, Megyesi J, Kaissling B, Schnackenberg L, et al. Metabolomic study of cisplatin-induced nephrotoxicity. *Kidney Int.* (2006) 69:2194–204. doi: 10.1038/sj.ki.5000433
43. Weinberg JM. Lipotoxicity. *Kidney Int.* (2006) 70:1560–6. doi: 10.1038/sj.ki.5001834
44. Zager RA, Johnson AC, Hanson SY. Renal tubular triglyercide accumulation following endotoxic, toxic, and ischemic injury. *Kidney Int.* (2005) 67:111–21. doi: 10.1111/j.1523-1755.2005.00061.x
45. Tran MT, Zsengeller ZK, Berg AH, Khankin EV, Bhasin MK, Kim W, et al. PGC1alpha drives NAD biosynthesis linking oxidative metabolism to renal protection. *Nature.* (2016) 531:528–32. doi: 10.1038/nature17184
46. Nagothu KK, Bhatt R, Kaushal GP, Portilla D. Fibrate prevents cisplatin-induced proximal tubule cell death. *Kidney Int.* (2005) 68:2680–93. doi: 10.1111/j.1523-1755.2005.00739.x
47. Kim HJ, Moradi H, Yuan J, Norris K, Vaziri ND. Renal mass reduction results in accumulation of lipids and dysregulation of lipid regulatory proteins in the remnant kidney. *Am J Physiol Renal Physiol.* (2009) 296:F1297–306. doi: 10.1152/ajprenal.90761.2008
48. Kamijo Y, Hora K, Kono K, Takahashi K, Higuchi M, Ehara T, et al. PPARalpha protects proximal tubular cells from acute fatty acid toxicity. *J Am Soc Nephrol.* (2007) 18:3089–100. doi: 10.1681/ASN.2007020238
49. Ralto KM, Rhee EP, Parikh SM. NAD(+) homeostasis in renal health and disease. *Nat Rev Nephrol.* (2020) 16:99–111. doi: 10.1038/s41581-019-0216-6
50. Imasawa T, Rossignol R. Podocyte energy metabolism and glomerular diseases. *Int J Biochem Cell Biol.* (2013) 45:2109–18. doi: 10.1016/j.biocel.2013.06.013
51. Sieber J, Jehle AW. Free Fatty acids and their metabolism affect function and survival of podocytes. *Front Endocrinol.* (2014) 5:186. doi: 10.3389/fendo.2014.00186
52. Mallipattu SK, He JC. The podocyte as a direct target for treatment of glomerular disease? *Am J Physiol Renal Physiol.* (2016) 311:F46–51. doi: 10.1152/ajprenal.00184.2016
53. Reiser J, Altintas MM. Podocytes. *F1000Res.* (2016) 5:114. doi: 10.12688/f1000research.7255.1
54. Stieger N, Worthmann K, Teng B, Engeli S, Das AM, Haller H, et al. Impact of high glucose and transforming growth factor-beta on bioenergetic profiles in podocytes. *Metabolism.* (2012) 61:1073–86. doi: 10.1016/j.metabol.2011.12.003
55. Abe Y, Sakairi T, Kajiyama H, Shrivastav S, Beeson C, Kopp JB. Bioenergetic characterization of mouse podocytes. *Am J Physiol Cell Physiol.* (2010) 299:C464–76. doi: 10.1152/ajpcell.00563.2009
56. Park CW, Kim HW, Ko SH, Chung HW, Lim SW, Yang CW, et al. Accelerated diabetic nephropathy in mice lacking the peroxisome proliferator-activated receptor alpha. *Diabetes.* (2006) 55:885–93. doi: 10.2337/diabetes.55.04.06.db05-1329
57. Cernuda-Morollon E, Rodriguez-Pascual F, Klatt P, Lamas S, Perez-Sala D. PPAR agonists amplify iNOS expression while inhibiting

NF-kappaB: implications for mesangial cell activation by cytokines. *J Am Soc Nephrol.* (2002) 13:2223–31. doi: 10.1097/01.ASN.0000025786.87646.B1
58. Chen L, Zhang J, Zhang Y, Wang Y, Wang B. Improvement of inflammatory responses associated with NF-kappa B pathway in kidneys from diabetic rats. *Inflamm Res.* (2008) 57:199–204. doi: 10.1007/s00011-006-6190-z
59. Chen LL, Zhang JY, Wang BP. Renoprotective effects of fenofibrate in diabetic rats are achieved by suppressing kidney plasminogen activator inhibitor-1. *Vascul Pharmacol.* (2006) 44:309–15. doi: 10.1016/j.vph.2006.01.004
60. Muller DN, Theuer J, Shagdarsuren E, Kaergel E, Honeck H, Park JK, et al. A peroxisome proliferator-activated receptor-alpha activator induces renal CYP2C23 activity and protects from angiotensin II-induced renal injury. *Am J Pathol.* (2004) 164:521–32. doi: 10.1016/S0002-9440(10)63142-2
61. Kouroumichakis I, Papanas N, Zarogoulidis P, Liakopoulos V, Maltezos E, Mikhailidis DP. Fibrates: therapeutic potential for diabetic nephropathy? *Eur J Intern Med.* (2012) 23:309–16. doi: 10.1016/j.ejim.2011.12.007
62. Hennuyer N, Poulain P, Madsen L, Berge RK, Houdebine LM, Branellec D, et al. Beneficial effects of fibrates on apolipoprotein A-I metabolism occur independently of any peroxisome proliferative response. *Circulation.* (1999) 99:2445–51. doi: 10.1161/01.CIR.99.18.2445
63. Wilson PD. Polycystic kidney disease. *N Engl J Med.* (2004) 350:151–64. doi: 10.1056/NEJMra022161
64. Padovano V, Podrini C, Boletta A, Caplan MJ. Metabolism and mitochondria in polycystic kidney disease research and therapy. *Nat Rev Nephrol.* (2018) 14:678–87. doi: 10.1038/s41581-018-0051-1
65. Podrini C, Cassina L, Boletta A. Metabolic reprogramming and the role of mitochondria in polycystic kidney disease. *Cell Signal.* (2019) 67:109495. doi: 10.1016/j.cellsig.2019.109495
66. Hajarnis S, Lakhia R, Yheskel M, Williams D, Sorourian M, Liu X, et al. microRNA-17 family promotes polycystic kidney disease progression through modulation of mitochondrial metabolism. *Nat Commun.* (2017) 8:14395. doi: 10.1038/ncomms14395
67. Menezes LF, Lin CC, Zhou F, Germino GG. Fatty acid oxidation is impaired in an orthologous mouse model of autosomal dominant polycystic kidney disease. *EBioMedicine.* (2016) 5:183–92. doi: 10.1016/j.ebiom.2016.01.027
68. Lakhia R, Yheskel M, Flaten A, Quittner-Strom EB, Holland WL, Patel V. PPARalpha agonist fenofibrate enhances fatty acid beta-oxidation and attenuates polycystic kidney and liver disease in mice. *Am J Physiol Renal Physiol.* (2018) 314:F122–31. doi: 10.1152/ajprenal.00352.2017
69. Bergmann C. Genetics of autosomal recessive polycystic kidney disease and its differential diagnoses. *Front Pediatr.* (2017) 5:221. doi: 10.3389/fped.2017.00221
70. Bobulescu IA. Renal lipid metabolism and lipotoxicity. *Curr Opin Nephrol Hypertens.* (2010) 19:393–402. doi: 10.1097/MNH.0b013e32833aa4ac
71. Moorhead JF, Chan MK, El-Nahas M, Varghese Z. Lipid nephrotoxicity in chronic progressive glomerular and tubulo-interstitial disease. *Lancet.* (1982) 2:1309–11. doi: 10.1016/S0140-6736(82)91513-6
72. Ruan XZ, Varghese Z, Moorhead JF. An update on the lipid nephrotoxicity hypothesis. *Nat Rev Nephrol.* (2009) 5:713–21. doi: 10.1038/nrneph.2009.184
73. Feldkamp T, Kribben A, Roeser NF, Senter RA, Weinberg JM. Accumulation of nonesterified fatty acids causes the sustained energetic deficit in kidney proximal tubules after hypoxia-reoxygenation. *Am J Physiol Renal Physiol.* (2006) 290:F465–77. doi: 10.1152/ajprenal.00305.2005
74. Wahba IM, Mak RH. Obesity and obesity-initiated metabolic syndrome: mechanistic links to chronic kidney disease. *Clin J Am Soc Nephrol.* (2007) 2:550–62. doi: 10.2215/CJN.04071206
75. Jiang T, Wang Z, Proctor G, Moskowitz S, Liebman SE, Rogers T, et al. Diet-induced obesity in C57BL/6J mice causes increased renal lipid accumulation and glomerulosclerosis via a sterol regulatory element-binding protein-1c-dependent pathway. *J Biol Chem.* (2005) 280:32317–25. doi: 10.1074/jbc.M500801200
76. Katsoulieris E, Mabley JG, Samai M, Sharpe MA, Green IC, Chatterjee PK. Lipotoxicity in renal proximal tubular cells: relationship between endoplasmic reticulum stress and oxidative stress pathways. *Free Radic Biol Med.* (2010) 48:1654–62. doi: 10.1016/j.freeradbiomed.2010.03.021
77. Soumura M, Kume S, Isshiki K, Takeda N, Araki S, Tanaka Y, et al. Oleate and eicosapentaenoic acid attenuate palmitate-induced inflammation and apoptosis in renal proximal tubular cell. *Biochem Biophys Res Commun.* (2010) 402:265–71. doi: 10.1016/j.bbrc.2010.10.012
78. Listenberger LL, Han X, Lewis SE, Cases S, Farese RV Jr, Ory DS, et al. Triglyceride accumulation protects against fatty acid-induced lipotoxicity. *Proc Natl Acad Sci USA.* (2003) 100:3077–82. doi: 10.1073/pnas.0630588100
79. Baines RJ, Chana RS, Hall M, Febbraio M, Kennedy D, Brunskill NJ. CD36 mediates proximal tubular binding and uptake of albumin and is upregulated in proteinuric nephropathies. *Am J Physiol Renal Physiol.* (2012) 303:F1006–14. doi: 10.1152/ajprenal.00021.2012
80. Kennedy DJ, Chen Y, Huang W, Viterna J, Liu J, Westfall K, et al. CD36 and Na/K-ATPase-alpha1 form a proinflammatory signaling loop in kidney. *Hypertension.* (2013) 61:216–24. doi: 10.1161/HYPERTENSIONAHA.112.198770
81. Cases A, Coll E. Dyslipidemia and the progression of renal disease in chronic renal failure patients. *Kidney Int Suppl.* (2005) S87–93. doi: 10.1111/j.1523-1755.2005.09916.x
82. Keech A, Simes RJ, Barter P, Best J, Scott R, Taskinen MR, et al. Effects of long-term fenofibrate therapy on cardiovascular events in 9795 people with type 2 diabetes mellitus (the FIELD study): randomised controlled trial. *Lancet.* (2005) 366:1849–61. doi: 10.1016/S0140-6736(05)67667-2
83. Chung HW, Lim JH, Kim MY, Shin SJ, Chung S, Choi BS, et al. High-fat diet-induced renal cell apoptosis and oxidative stress in spontaneously hypertensive rat are ameliorated by fenofibrate through the PPARalpha-FoxO3a-PGC-1alpha pathway. *Nephrol Dial Transplant.* (2012) 27:2213–25. doi: 10.1093/ndt/gfr613
84. Sivarajah A, Chatterjee PK, Hattori Y, Brown PA, Stewart KN, Todorovic Z, et al. Agonists of peroxisome-proliferator activated receptor-alpha (clofibrate and WY14643) reduce renal ischemia/reperfusion injury in the rat. *Med Sci Monit.* (2002) 8:BR532–9.
85. Takahashi K, Kamijo Y, Hora K, Hashimoto K, Higuchi M, Nakajima T, et al. Pretreatment by low-dose fibrates protects against acute free fatty acid-induced renal tubule toxicity by counteracting PPARalpha deterioration. *Toxicol Appl Pharmacol.* (2011) 252:237–49. doi: 10.1016/j.taap.2011.02.012
86. Tanaka Y, Kume S, Araki S, Isshiki K, Chin-Kanasaki M, Sakaguchi M, et al. Fenofibrate, a PPARalpha agonist, has renoprotective effects in mice by enhancing renal lipolysis. *Kidney Int.* (2011) 79:871–82. doi: 10.1038/ki.2010.530
87. Frazier R, Mehta R, Cai X, Lee J, Napoli S, Craven T, et al. Associations of fenofibrate therapy with incidence and progression of CKD in patients with type 2 diabetes. *Kidney Int Rep.* (2019) 4:94–102. doi: 10.1016/j.ekir.2018.09.006
88. Group AS, Ginsberg HN, Elam MB, Lovato LC, Crouse JR 3rd, Leiter LA, et al. Effects of combination lipid therapy in type 2 diabetes mellitus. *N Engl J Med.* (2010) 362:1563–74. doi: 10.1056/NEJMoa1001282
89. Kim S, Ko K, Park S, Lee DR, Lee J. Effect of fenofibrate medication on renal function. *Korean J Fam Med.* (2017) 38:192–8. doi: 10.4082/kjfm.2017.38.4.192
90. Souza AC, Bocharov AV, Baranova IN, Vishnyakova TG, Huang YG, Wilkins KJ, et al. Antagonism of scavenger receptor CD36 by 5A peptide prevents chronic kidney disease progression in mice independent of blood pressure regulation. *Kidney Int.* (2016) 89:809–22. doi: 10.1016/j.kint.2015.12.043
91. Szeto HH, Liu S, Soong Y, Seshan SV, Cohen-Gould L, Manichev V, et al. Mitochondria protection after acute ischemia prevents prolonged upregulation of IL-1beta and IL-18 and arrests CKD. *J Am Soc Nephrol.* (2017) 28:1437–49. doi: 10.1681/ASN.2016070761
92. Szeto HH, Liu S, Soong Y, Wu D, Darrah SF, Cheng FY, et al. Mitochondria-targeted peptide accelerates ATP recovery and reduces ischemic kidney injury. *J Am Soc Nephrol.* (2011) 22:1041–52. doi: 10.1681/ASN.2010080808
93. Szeto HH, Liu S, Soong Y, Alam N, Prusky GT, Seshan SV. Protection of mitochondria prevents high-fat diet-induced glomerulopathy and proximal tubular injury. *Kidney Int.* (2016) 90:997–1011. doi: 10.1016/j.kint.2016.06.013
94. Kong MJ, Han SJ, Kim JI, Park JW, Park KM. Mitochondrial NADP(+)-dependent isocitrate dehydrogenase deficiency increases cisplatin-induced

oxidative damage in the kidney tubule cells. *Cell Death Dis.* (2018) 9:488. doi: 10.1038/s41419-018-0537-6

95. Lowes DA, Thottakam BM, Webster NR, Murphy MP, Galley HF. The mitochondria-targeted antioxidant MitoQ protects against organ damage in a lipopolysaccharide-peptidoglycan model of sepsis. *Free Radic Biol Med.* (2008) 45:1559–65. doi: 10.1016/j.freeradbiomed.2008.09.003
96. Cortassa S, O'Rourke B, Aon MA. Redox-optimized ROS balance and the relationship between mitochondrial respiration and ROS. *Biochim Biophys Acta.* (2014) 1837:287–95. doi: 10.1016/j.bbabio.2013.11.007

Conflict of Interest: The authors declare that the research was conducted in the absence of any commercial or financial relationships that could be construed as a potential conflict of interest.

Copyright © 2020 Jang, Noh, Kim and Padanilam. This is an open-access article distributed under the terms of the Creative Commons Attribution License (CC BY). The use, distribution or reproduction in other forums is permitted, provided the original author(s) and the copyright owner(s) are credited and that the original publication in this journal is cited, in accordance with accepted academic practice. No use, distribution or reproduction is permitted which does not comply with these terms.

frontiers in Physiology

ORIGINAL RESEARCH
published: 13 March 2020
doi: 10.3389/fphys.2020.00209

EDN1-AS, A Novel Long Non-coding RNA Regulating Endothelin-1 in Human Proximal Tubule Cells

*Lauren G. Douma[1,2], Kristen Solocinski[1], Sarah H. Masten[1], Dominique H. Barral[1], Sarah J. Barilovits[1], Lauren A. Jeffers[3], Kareme D. Alder[4], Ravi Patel[1], Charles S. Wingo[1], Kevin D. Brown[2], Brian D. Cain[2] and Michelle L. Gumz[1,2]**

[1] Department of Medicine, University of Florida, Gainesville, FL, United States, [2] Department of Biochemistry and Molecular Biology, University of Florida, Gainesville, FL, United States, [3] Department of Biochemistry, Cell and Developmental Biology, Emory University, Atlanta, GA, United States, [4] Yale University School of Medicine, New Haven, CT, United States

Endothelin-1 (ET-1) is a peptide hormone that functions as a vasoconstrictor in the vasculature, whereas in the collecting duct of the kidney it exerts blood pressure-lowering effects via natriuretic actions. Aberrant ET-1 signaling is associated with several pathological states including hypertension and chronic kidney disease. ET-1 expression is regulated largely through transcriptional control of the gene that encodes ET-1, *EDN1*. Here we report a long, non-coding RNA (lncRNA) that appears to be antisense to the *EDN1* gene, called *EDN1-AS*. Because *EDN1-AS* represents a potential novel mechanism to regulate ET-1 expression, we examined the regulation of *EDN1-AS* expression and action. A putative glucocorticoid receptor response (GR) element upstream of the predicted *EDN1-AS* transcription start site was identified using the ENCODE database and the UCSC genome browser. Two homozygous deletion clones of the element were generated using CRISPR/Cas9. This deletion resulted in a significant increase in the expression of *EDN1-AS,* which was associated with increased secretion of ET-1 peptide from HK-2 cells (two-fold increase in KO cells vs. CNTL, $n = 7$, $P < 0.05$). Phenotypic characterization of these CRISPR clones revealed a difference in cell growth rates. Using a standard growth assay, we determined that the KO1 clone exhibited a three-fold increase in growth over 8 days compared to control cells ($n = 4$, $P < 0.01$) and the KO2 clone exhibited a two-fold increase ($n = 4$, $P < 0.01$). These results support a role for *EDN1-AS* as a novel regulatory mechanism of ET-1 expression and cellular proliferation.

Keywords: kidney, long non-coding RNA, proximal tubule cells, CRISPR, circadian rhythm

OPEN ACCESS

Edited by:
John D. Imig, Medical College of Wisconsin, United States

Reviewed by:
Noriaki Emoto, Kobe Pharmaceutical University, Japan
Francois Verrey, University of Zurich, Switzerland

****Correspondence:***
Michelle L. Gumz
Michelle.Gumz@medicine.ufl.edu

Specialty section:
This article was submitted to Renal and Epithelial Physiology, a section of the journal Frontiers in Physiology

Received: *20 December 2019*
Accepted: *24 February 2020*
Published: *13 March 2020*

Citation:
Douma LG, Solocinski K, Masten SH, Barral DH, Barilovits SJ, Jeffers LA, Alder KD, Patel R, Wingo CS, Brown KD, Cain BD and Gumz ML (2020) EDN1-AS, A Novel Long Non-coding RNA Regulating Endothelin-1 in Human Proximal Tubule Cells. Front. Physiol. 11:209. doi: 10.3389/fphys.2020.00209

INTRODUCTION

ET-1 has many functions including vascular constriction, nervous system activation, and renal sodium secretion. The kidney is both a source and a target of ET-1, and the kidney has the highest concentrations of ET-1 found in the body (Kohan et al., 2011). The mechanisms of ET-1 action in the pathology of chronic kidney disease (CKD) involve increased cell proliferation, inflammation, and elaboration of the extracellular matrix (Speed and Pollock, 2013; Kohan and Barton, 2014; Reichetzeder et al., 2014). Mice overexpressing ET-1 developed chronic renal failure (Theuring et al., 1998). In humans, excess ET-1 levels are seen in all stages of CKD (Dhaun et al., 2009), and there are marked increases in urinary ET-1 secretion in CKD (Grenda et al., 2007).

ET-1 signaling works through two receptors, ETAR and ETBR, via paracrine and autocrine action (Dhaun and Webb, 2019). ETAR and ETBR exert largely opposite effects, and ET-1 stimulation of ETAR is primarily responsible for renal injury. Although regulation of ET-1 levels is widely attributed to control of transcription of the ET-1 gene (*EDN1*) (Stow et al., 2011), *EDN1* mRNA is also regulated at the post-transcriptional level by miRNAs (Jacobs et al., 2013, 2014).

The ET-1 pathway is a therapeutic target for many diseases. The ET receptor blocker Macitentan improved morbidity and mortality in pulmonary arterial hypertension patients (Pulido et al., 2013) whereas studies of ET-1 blockers in the kidney have been less successful. The endothelin axis is an important target in CKD, but pharmacological manipulation of endothelin receptors is associated with adverse side effects that have led to termination of clinical trials (Kohan and Pollock, 2013; Yuan et al., 2015). The ASCEND trial using ET-1 receptor blockers for CKD therapy was abandoned due to increased incidence of congestive heart failure (Reichetzeder et al., 2014). More recently, promising results emerged from SONAR, a trial for the ETA antagonist Atrasentan, which utilized an enrichment protocol to mitigate fluid retention side effects (Heerspink et al., 2019). Atrasentan reduced the risk for renal events in patients with type 2 diabetes mellitus, although the trial was ended early due to a less than expected number of end points. Given the critical role of ET-1 in renal function and CKD, alternative approaches are needed to translate ET-1 pathway inhibition to the bedside. With this goal in mind, we sought to better understand *EDN1* gene regulation in light of new findings regarding transcriptional control that continue to emerge from the Encyclopedia of DNA Elements (ENCODE).

Using the University of California-Santa Cruz (UCSC) Genome Browser to interrogate regulatory elements at the *EDN1* locus, we identified a putative promoter downstream of the promoter coding sequence. We hypothesized that this promoter may drive expression of a long non-coding (lnc) RNA. Here we describe a novel lncRNA that is antisense with respect to the ET-1 transcript, *EDN1-AS*. We also identified *EDN1-AS* expression in multiple human cell types including kidney. Using a human kidney proximal tubule cell line (HK-2), we show that CRISPR-mediated deletion of a regulatory element within the *EDN1-AS* promoter resulted in increased levels of *EDN1-AS*. This effect was associated with increased secretion of ET-1 peptide and increased cell proliferation.

MATERIALS AND METHODS

Analysis of EDN1 Chromatin State Using the UCSC Genome Browser

The human *EDN1* chromatin state was analyzed using the UCSC Genome Browser[1] (Karolchik et al., 2014). The EDN1-AS predicted promoter was identified using the Genome Segments and Broad Chromatin HMM tracks with HUVEC cell information selected. The Transcription Factor ChIP track and DNase Clusters track was also used to analyze transcriptional regulation of the predicted promoter site.

Cell Culture

HMEC cells were cultured in MEGM^{TM} Mammary Epithelial Cell Growth Medium with BulletKit^{TM} (Lonza) and 10% charcoal stripped FBS. S9 cells were cultured in F12 Ham Kaighn's modification (F12K) supplemented with 25 mM $NaHCO_3$, 4 mM glutamine, 1% Penicillin/Streptomycin and 10% FBS. HK-2 cells were cultured in DMEM/Hamm's F12 media supplemented with 10% FBS and 1% Penicillin/Streptomycin. HEK293 cells were cultured in DMEM containing 4.5 g/L glucose supplemented with 1% Penicillin/Streptomycin and 10% FBS. All cells were grown in a 37°C incubator, humidified at 5% CO_2.

RNA Isolation and DNase Treatment

RNA was isolated from cells using TRIzol (Ambion) per manufacturer instructions. In general, 1 ml TRIzol was used per well in a 6-well plate. Total RNA was treated with DNase (Ambion) per manufacturer instructions to remove genomic DNA. RNA from an adult human female kidney was purchased from Life Technologies.

Strand-Specific RT-PCR

Human strand-specific *EDN1-AS* primers (SS1-6; **Table 1**) were designed to lay down at locations progressively closer to the 5′ end of the *EDN1* gene for use in reverse transcriptase reactions. Reverse Transcriptase (RT) from Thermo Fisher was used as per manufacturer instructions. Oligo-dT primers were used as a positive control for any poly-adenylated tailed mRNA. All samples were used in –RT and + RT reactions. Primers have a complementary sequence to the *EDN1* sense strand so they will only anneal to antisense RNA. PCR primers (PCR1 and PCR2) were designed to amplify the same region of cDNA regardless of the strand-specific primer used.

TABLE 1 | *EDN1-AS* Strand-Specific RT-PCR primers and sequences.

***EDN1-AS* Strand-Specific RT Primers**		
Name	**Sequence (5′-3′)**	
SS1	GCAGTAAAATTATTTTCCTTTATATAACCGGC	
SS2	GTGTCAGCAGTAGATATAATATTTTCATGG	
SS3	CCAAGCTGAAAGGCAAGCCC	
SS4	AACCTATGCTGAGTTCCTCAAGGC	
SS5	CAGAAGAAGTTCAGAGGAACACCTAAG	
SS6	AATAACATTGTCTGGGGCTGGAA	
PCR Primers		
Name	**Sequence (5′-3′)**	**Product Size**
PCR1	GAAAGAGGTTGGATTGAATTTTGATGTAC	165 bp
PCR2	CAAAGCATGTTCTCAATTTCATTTAGAAATAC	
GAPDH Fwd	AAGAAATGTGCTTTGGGG	166 bp
GAPDH Rev	GACTCCACGACGTACTCA	
EDN1 Fwd	CAGAAGAAGTTCAGAGGAACACC	246 bp
EDN1 Rev	GGTTTGCATTCCAGAGCTTC	

[1]http://genome.ucsc.edu

Dexamethasone Treatment

HK-2 cells were grown to ∼80% confluence in 6-well cell culture plates. To synchronize the circadian clock in all cells, 100 nM Dexamethasone was added for 30 min and then media was changed. After 24 h, cells were trypsinized and RNA was isolated every 2 h for 24 h.

CRISPR/Cas9 gRNA Design

Guide RNA (gRNA) design, cloning and cell engineering was done as previously outlined (Dükel et al., 2016). Briefly, gRNAs were designed using the online tool CC Top ([2]Stemmer et al., 2015) using a ∼150 bp sequence of from the predicted human *EDN1-AS* promoter as input. The region was selected based on identified transcription factor binding sites hypothesized to be important to transcription regulation.

Generation of Recombinant LentiCRISPR Plasmids

gRNA sequences were synthesized as complementary oligonucleotides and included overhangs for insertion into BsmB1-digested LentiCRISPRv2 plasmid (Addgene catalog # 52961). Oligonucleotides were 5′ phosphorylated and annealed as outlined by the Zhang lab[3] and ligated to linearized LentiCRISPR v2 with Quick Ligase (NEB). Ligation reactions were transformed into Stbl3 bacteria following manufacturer instructions. Using this protocol, four (4) recombinant LentiCRISPR v2 plasmids (designated gRNA 1–4) were cloned and verified by automated Sanger sequencing.

Lentivirus Generation and Infection of Cells

HEK293 cells were co-transfected with the four LentiCRISPR + gRNA constructs (sgRNA 1, 2, 3, and 4) along with psPAX2 (Addgene #11260) and pMD2.G (Addgene #11259) for generation of pseudotyped lentiviral particles. Media containing virus particles was collected 72 h post-transfection and cleared viral supernatant was then added to HK-2 cells singly and pairwise (e.g., gRNA 1 + 2, 1 + 3, 1 + 4 etc.). 2 μg/ml puromycin was used for 2 weeks to select for cells transduced with virus.

Isolation of CRISPR/Cas9 KO HK-2 Cells

After puromycin selection, cells were plated into the first of 4 columns of a 96 well plate in 200 μl of media. Cells were then serial diluted into the following columns. After growth time, wells were inspected for the presence of one to three colonies of cells. These wells were then trypsinized with 1 drop of 0.25% Trypsin per well and plated into 10 cm dishes. Cells were allowed to grow undisturbed for 1 week until colony formation. Cloning rings were dipped in sterile vacuum grease to create a seal and pressed down over the colony. Media was aspirated and 1 drop of Trypsin was added. After ∼5 min, trypsinized cells were removed and plated in 6-well plate and allowed to grow. Genomic DNA was isolated from these cells and used for genotyping PCR.

Sequencing

Gel-purified PCR products from PCR reactions using genotyping primers GT1 and GT2 were cloned into the TA TOPO vector according to the manufacturer's instructions (Thermo Fisher). Cells with insert were identified by blue/white screening. Plasmids containing inserts were sent to GENEWIZ for sequencing using M13F and M13R primers. The resulting sequences were analyzed with Serial Cloner and sequences from NCBI and UCSC Genome Browser.

ET-1 ELISA

HK-2 cells were plated into 6-well Transwell plates (Corning) and grown to confluence. Media from HK-2 cell lines was spun down to remove cell debris and then frozen at −80°C until all samples were ready to use. ELISA for ET-1 was performed using the Human Endothelin-1 QuantiGlo ELISA Kit (R&D Systems) according to manufacturer instructions.

Growth Assay

HK-2 cells were counted and 20,000 cells were plated into 6-well Transwell dishes. Cells were grown under normal conditions for 2, 4, 6, and 8 days. After the specified amount of growth time, cells were treated with Trypsin, diluted, and counted using the BioRad TC20 Automated Cell Counter.

RESULTS

Predicted Promoter Region Downstream of the EDN1 Gene

The chromatin state of the human endothlien-1 gene (*EDN1*) gene was analyzed using the UCSC Genome Browser. The Genome Segments track and ChromHMM revealed a predicted promoter region with high confidence immediately downstream of the exon encoding the 3′ untranslated region (UTR) of *EDN1* (about 800 bp long) in human umbilical vein endothelial cells (HUVEC) (**Figure 1**). This region also contained large clusters of DNase sensitivity sites, suggesting that the chromatin is in an open state and transcription factors could bind to this region (**Figure 2**). Using the UCSC Genome Browser transcription factor binding site database created using data from chromatin immunoprecipitation (ChIP) assays (ENCODE) (Karolchik et al., 2014), multiple transcription factors including C-JUN, CCAAT/enhancer-binding protein β (CEBPβ), and Forkhead Box A1 (FOXA1) were shown to bind at the location of the predicted promoter region. Additionally, Transcription Factor II D (TFIID), Upstream Transcription Factor 1 (USF1), and Glucocorticoid Receptor (GR) are predicted to bind to this region, and these transcription factors are associated with sites of active transcription. RNA polymerase II was also shown to bind to the predicted promoter region. Based on this information, we hypothesized that the predicted downstream promoter contained a transcription start site and potentially could be a promoter for an antisense RNA.

[2]crispr.cos.uni-heidelberg.de

[3]https://www.addgene.org/crispr/zhang

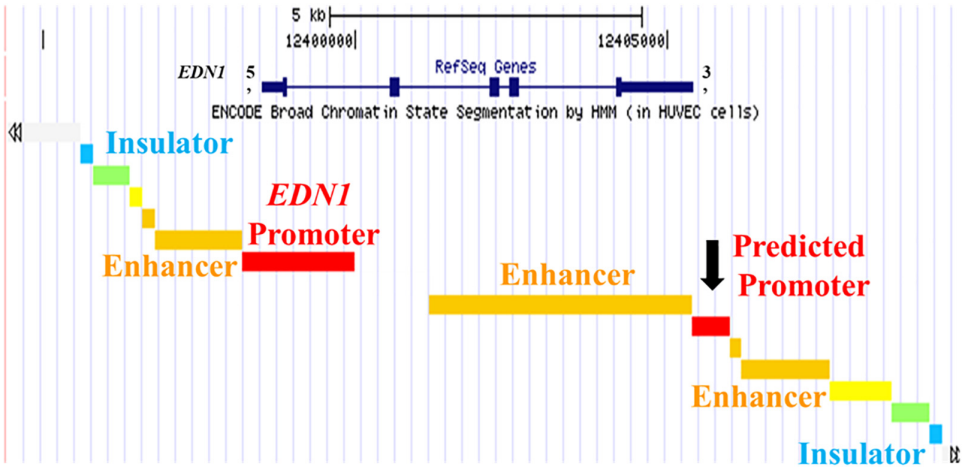

FIGURE 1 | UCSC Genome Browser Predicts Promoter in 3′ UTR of *EDN1* Gene. The University of California Santa Cruz (UCSC) Genome Browser with ENCODE broad chromatin state segmentation by HMM in human umbilical vein endothelial cells (HUVEC) cells shows a predicted promoter (black arrow) in the 3′ untranslated region (UTR) of the *EDN1* gene. The *EDN1* gene is shown at the top (navy blue) with boxes representing exons. The *EDN1* gene position is aligned with the genome segments in the ENCODE broad chromatin state track.

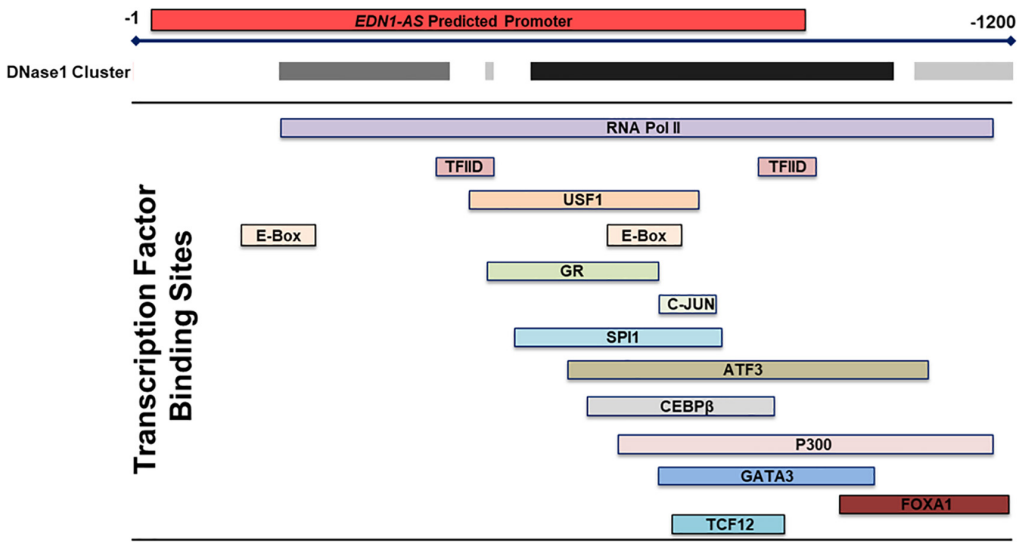

FIGURE 2 | Transcription Factor Binding Sites within the Predicted Promoter in the 3′ UTR of *EDN1*. Using the transcription factor binding sites track within the UCSC Genome Browser, multiple transcription factor binding sites were identified by ChIP within the 3′ UTR *EDN1* predicted promoter. Additionally, the DNase I cluster track showed multiple areas of high DNase sensitivity. The gray box indicates the extent of the hypersensitive region with darker boxes representing a stronger hypersensitivity signal. These data taken together suggests that this predicted promoter region is transcriptionally regulated and that the chromatin is in an open state.

EDN1 Anti-sense RNA Detectable in Human Cell Culture Models and Human RNA Samples

To determine if an antisense RNA is being transcribed from the *EDN1* downstream promoter, a strand-specific reverse transcriptase PCR (ssRT-PCR) strategy was designed (**Figure 3**). Primers for the reverse transcriptase reactions (RT) were designed to have a complementary sequence to the *EDN1* sense strand, so the primers will only anneal to RNA transcribed from the antisense strand (**Table 1**). Multiple strand-specific primers were designed at varying distances from the predicted promoter toward the 5′ end of the *EDN1* gene (SS1-6). Oligo dT primers were used as a positive control for the RT reactions. For each RT reaction, a –RT reaction was performed without the reverse transcriptase enzyme as a negative control to ensure the absence of genomic DNA contamination in our samples.

Total RNA was isolated from primary human mammary endothelial cells (HMEC), human kidney proximal tubule epithelial cells (HK-2), human bronchoendothelial cells (S9), and

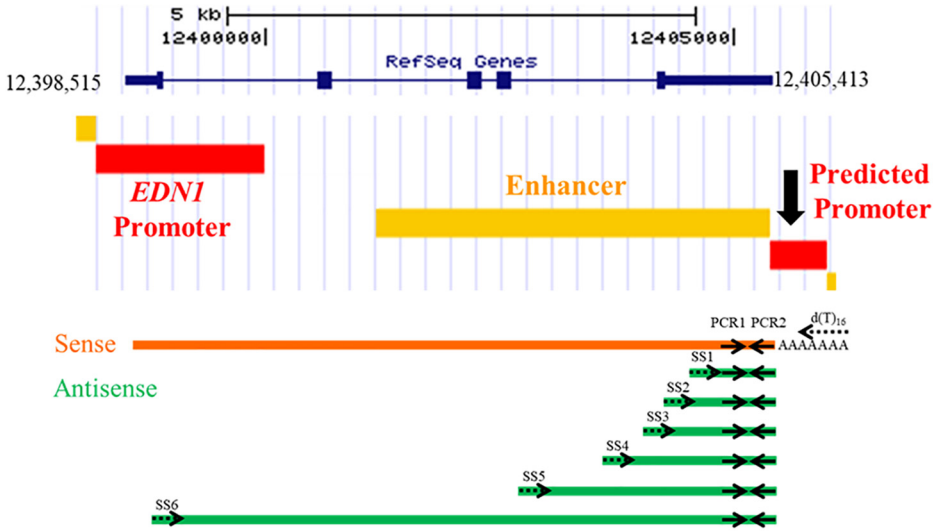

FIGURE 3 | Strand-Specific Reverse Transcriptase PCR Reactions. Strand-specific reverse transcriptase (RT) PCR reactions were designed using primers that would only anneal to an antisense transcript to *EDN1*. A total of 6 different strand-specific primers were used in the RT reactions (SS1–SS6, dotted arrows), which were progressively further away from the predicted 3′ UTR promoter region. For a positive RT control, oligo dT primers were used as it is known *EDN1* mRNA is poly-adenylated. After conversion of RNA into cDNA, PCR1 and PCR2 primers (solid arrows) were used in a PCR reaction to amplify any products generated. PCR1 and PCR2 amplify the same piece of cDNA regardless of the strand-specific primer used, so all bands visualized by gel electrophoresis are the same size (165 bp).

human embryonic kidney cells (HEK293). Additionally, human RNA from kidney tissue was obtained from Life Technologies. Each of the RNA samples was treated with DNase and then converted to cDNA using a strand-specific primer or an oligo dT primer. For every sample, both + RT and –RT reactions were performed. The resulting cDNA products were amplified in a PCR using the primers PCR1 and PCR2, which amplified the same region of cDNA regardless of the SS or oligo dT primer used. An antisense RNA transcript was detected in HMEC, HUVEC, HK-2, and S9 cell cultures (**Figures 4A,B**). The antisense transcript was also detected in human kidney tissue RNA samples (**Figure 4C**). Interestingly, this antisense RNA was not detected in HEK293 cells, but *EDN1* mRNA was also not detected in these cells (**Figure 4D**). These results demonstrate that there is an RNA transcribed in an antisense direction within the *EDN1* gene locus, and we have designated this transcript *EDN1-AS.* SS primers 4–6 (**Figure 3**) were designed to detect if the length of *EDN1-AS* spanned the entire *EDN1* coding region (**Figures 4B,C**). The results indicate that transcription of *EDN1-AS* proceeds at least as far as the first exon of *EDN1*.

EDN1-AS Exhibits Circadian Rhythm in Expression

We and others have shown that the *EDN1* gene is under the regulation of the circadian clock proteins (Hanai et al., 2005; Stow et al., 2012; Kozakai et al., 2014; Richards et al., 2014). Additionally, GR was shown to bind to the *EDN1-AS* promoter region and glucocorticoids have been shown to modulate the circadian clock (Balsalobre et al., 2000; Kino and Chrousos, 2010; Surjit et al., 2011). E-box response elements, to which circadian clock transcription factors bind, were also present in the predicted *EDN1-AS* promoter region. These data suggest that, similarly to the *EDN1* gene, *EDN1-AS* may be under control of the circadian clock and may display a circadian rhythm of expression. To determine if *EDN1-AS* exhibits a circadian rhythm of expression, a 24-h expression profile of the antisense transcript was generated (**Figure 5**). The HK-2 cells were treated with dexamethasone for 30 min to synchronize their circadian clocks (Feillet et al., 2014). Twenty-four hours after the dexamethasone treatment, RNA was isolated from the HK-2 cells every 2 h for 24 h and the ssRT-PCR protocol was performed as described above. RT reactions with random hexamers were also performed on the same samples in order to detect the levels of *GAPDH* expression as a control. As seen in **Figure 5**, *EDN1-AS* expression varies over a 24- h period.

CRISPR Deletion of EDN1-AS Regulatory Region

Since the expression of *EDN1-AS* seems to be under circadian regulation, we wanted to investigate the effect of removing the E-box response element and GR binding site in the predicted promoter region of *EDN1-AS.* In order to create a KO of this regulatory region in HK-2 cells, we utilized CRISPR/Cas9 technology. Guide RNAs (gRNAs) were designed using the online tool CC Top (Stemmer et al., 2015; **Table 2**). gRNAs were selected based on location and predicted off-target sites. If possible, only gRNAs with no off-target sites or those with sites only in regions between genes were chosen. No gRNAs were used that had predicted off-target sites in exonic or intronic regions of any gene to minimize possible off-target effects. Various combinations

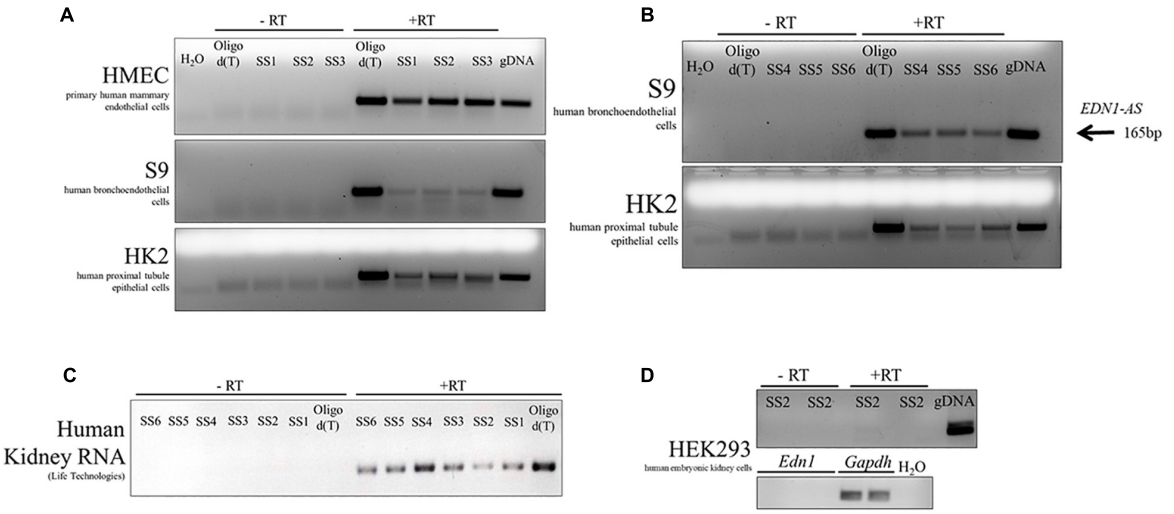

FIGURE 4 | Identification of *EDN1-AS* in Human Cell Culture Models and Human Kidney RNA. Strand-specific reactions were used to test various human cell culture models for the presence of an antisense transcript originating from the predicted promoter region. This transcript has been named *EDN1-AS*. Strand-specific RT primers SS1-3 were used to test for an antisense transcript in primary human mammary endothelial cells (HMEC), human bronchoendothelial cells (S9), and in human proximal tubule epithelial cells (HK2) **(A)**. Oligo dT primers were used as a positive control for the RT reactions. For each PCR reaction, water was used as a negative control and gDNA as a PCR positive control. For each of the strand-specific reactions, a no RT (-RT) control reaction was ran with the same cDNA sample. Strand-specific RT reactions using primers further away from the predicted promoter site (SS4–SS6) were designed to determine if the transcript spanned the entire length of the *EDN1* gene using available samples from S9 and HK2 cells **(B)**. All strand-specific RT primers (SS1–SS6) were used to determine if *EDN1-AS* could be detected in human kidney tissue RNA samples from Life Technologies **(C)**. *EDN1-AS* and *EDN1* transcripts could not be identified in human embryonic kidney cells (HEK293) **(D)**. All gels are representative of at least $n = 2$ per cell line.

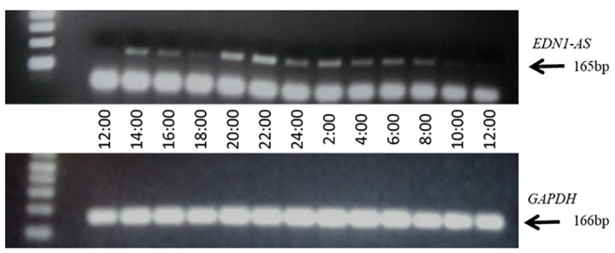

FIGURE 5 | *EDN1-AS* Exhibits a Circadian Rhythm of Expression. HK2 cells were treated with 100 nM dexamethasone for 30 min, after which media was replaced and cells incubated for 24 h. After 24 h (noon), RNA was isolated every 2 h for 24 h total. This RNA was used in strand-specific RT PCR reactions with either SS2 primer (to measure *EDN1-AS*) or random hexamer reactions (to measure *GAPDH*). For the PCR reactions, PCR1 and PCR2 primers were used in *EDN1-AS* reactions and GAPDH Fwd and GAPDH Rev primers were used in the *GAPDH* reactions. Gel representative of $n = 3$ independent experiments.

TABLE 2 | Guide RNAs for CRISPR/Cas9 and genotyping primers.

gRNAs	
Name	**Sequence (5′-3′)**
hEDN1AS CRISPR 1F	CACCGATAGAAAAGTGACAATTAGA
hEDN1AS CRISPR 1R	AAACTCTAATTGTCACTTTTCTATC
hEDN1AS CRISPR 2F	CACCGTTGATTTTATACTGCATTG
hEDN1AS CRISPR 2R	AAACCAATGCAGTATAAAATCAAC
hEDN1AS CRISPR 3F	CACCGGCCTGCTCAGAGCAAGTAG
hEDN1AS CRISPR 3R	AAACCTACTTGCTCTGAGCAGGCC
hEDN1AS CRISPR 4F	CACCGCCTGGTGTCTCTACCTCCAT
hEDN1AS CRISPR 4R	AAACATGGAGGTAGAGACACCAGGC

Genotyping Primers		
Name	**Sequence (5′-3′)**	**PCR Product**
GT1F	CATGCTTTGTTTTGCCTGTCA	709 bp
GT2R	AGGCAAAGTGGAGAGGAAGT	

of all the gRNAs were used in order to create a biallelic KO of the *EDN1-AS* regulatory region. The gRNA combination of gRNA 2 and 3 resulted in two HK-2 cell lines that had a homozygous deletion of an approximately 350 bp region within the predicted *EDN1-AS* promoter by genotyping PCR (**Figure 6**). Sanger sequencing using genomic DNA from these cell lines was used to confirm the KO region. In addition to the two homozygous KO cell lines, control (CNTL) cell lines that had undergone the CRISPR process, but did not have KO of the *EDN1-AS* regulatory region, were identified to use as control cells for future experiments.

KO of EDN1-AS Regulatory Region Results in Increased EDN1-AS and EDN1 Expression

To determine how the KO of the *EDN1-AS* regulatory region containing the predicted GR and circadian clock binding sites affected the expression of *EDN1-AS*, we performed our ssRT-PCR

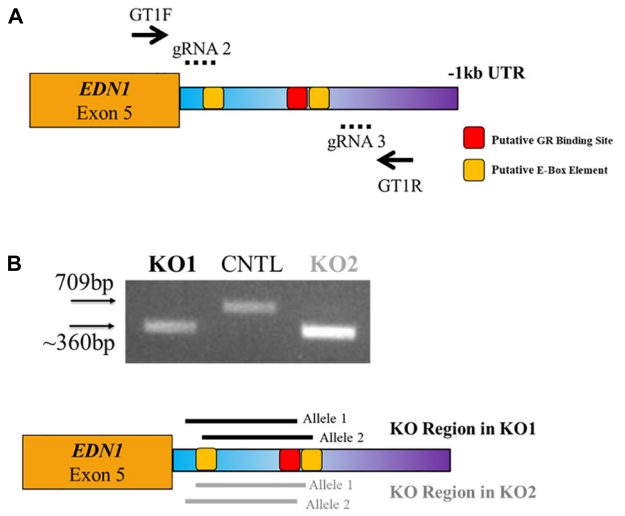

FIGURE 6 | CRISPR/Cas9 Targeted Deletion of GR and E-Box Regulatory Elements within the EDN1-AS Predicted Promoter Region. CRISPR/Cas9 technology was utilized to create biallelic KO of a portion of the predicted Edn1AS promoter region, which contained GR and E-Box regulatory sites. Four guide RNAs (gRNAs) were designed to create deletion of this region **(A)**. LentiCRISPR was used to deliver the gRNAs to HK2 cells. Puromycin was used to screen cells. Using genotyping primers, GT1F and GT1R (solid arrows), two clones were identified that had a KO of approximately 350 bp generated with gRNAs 2 and 3 (dotted lines) **(B)**. Sequencing results reviled KO1 has a biallelic KO of 297 bp with 64 bp additional KO 5′ of this region on one allele and 78 bp KO 3′ of this region on the other allele (black solid lines). KO2 has a biallelic KO of 310 bp with 46 bp additional KO 3′ of this region on one allele and 71 bp KO 5′ of this region on the other allele (gray solid lines). Both KOs have a deletion of the 1st E-Box response element and the GR element. In addition, we identified control (CNTL) cells that had undergone the CRISPR process, but retained WT copes of the *EDN1-AS* regulatory region.

protocol on the KO cell lines in addition to the CNTL cells. The CRISPR KO cells had higher expression of *EDN1-AS* compared to CNTL cells (**Figure 7A**). Secreted endothelin-1 peptide (ET-1) was measured to determine if the increase in expression of the *EDN1-AS* gene led to an increase in ET-1 peptide level. Briefly, KO and CNTL cells were plated into Transwell plates and media was collected from confluent cells. The media was then analyzed via an ET-1 ELISA to measure total ET-1 peptide levels. ET-1 peptide levels were normalized to total protein concentration measured by BCA assay. The CRISPR KO cells had a significant increase in total secreted ET-1 peptide levels compared to the CNTL cells (**Figure 7B**).

Increased ET-1 Production Associated With Increased Growth Rate

High expression of ET-1 in human proximal tubule cells, like HK-2 cells, is associated with increased cell proliferation (Zoja et al., 1995; Seccia et al., 2016). To determine if the increased ET-1 levels caused by KO of the *EDN1-AS* regulatory region affected cell proliferation, growth rates of the KO and CNTL cells were measured. Briefly, 20,000 cells were plated into 6-well dishes and counted after 2, 4, 6, and 8 days of growth. Both CRISPR KO cell lines grew significantly faster than the CNTL cells (**Figure 8**). Significant differences between individual KO cells and the CNTL cells total cell count were detected on day 6 and day 8.

DISCUSSION

Here we report the identification of a novel lncRNA, *EDN1-AS*, that is antisense to the ET-1 coding sequence. *EDN1-AS* is expressed in human mammary epithelial cells, human bronchoendothelial cells, human kidney proximal tubule cells, and in human kidney. Using a strand-specific RT-PCR approach, we demonstrated that *EDN1-AS* comprises the entire length of the *EDN1* sense coding sequence. *EDN1-AS* appears to exhibit rhythmic expression in HK-2 cells. CRISPR-mediated deletion of regulatory sequence upstream of *EDN1-AS* containing a GR element and an E-box resulted in increased expression of *EDN1-AS* in HK-2 cells. This effect was associated

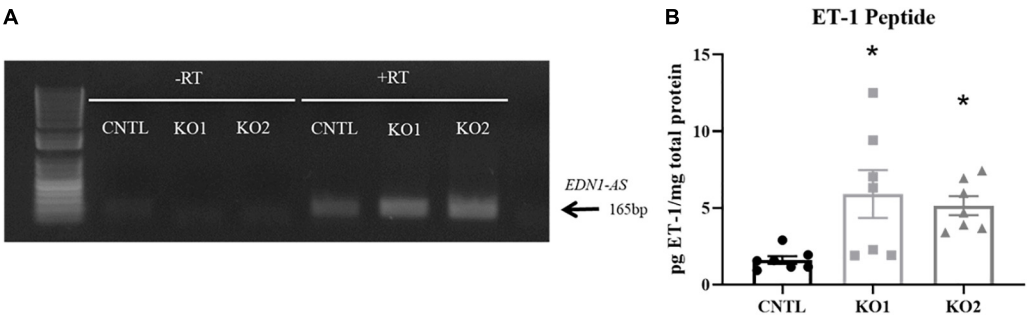

FIGURE 7 | CRISPR/Cas9 KO of *EDN1-AS* Regulatory Elements Results in Increased *EDN1-AS* and *EDN1* Expression. *EDN1-AS* expression levels were examined in CNTL and CRISPR/Cas9 KO cells by strand-specific RT PCR. For each reaction, 20 ng of cDNA was used in PCR reactions to amplify *EDN1-AS*. CRISPR/Cas9 KO cells had more *EDN1-AS* expression visualized by gel electrophoresis **(A)** (gel representative of $n = 3$ for CNTL and $n = 2$ for each KO cell line). To determine if these differences in *EDN1-AS* expression had an effect on *EDN1* expression, the product of the *EDN1* gene, endothelin-1 (ET-1) peptide was measured. Cells were placed in Transwells dishes and grown to confluence. Media from these cells was used in an endothelin-1 ELISA (R&D QuantiGlo ET-1 ELISA) to determine the amount of secreted ET-1 relativized to total protein concentration **(B)**. One-way ANOVA was used to determine significant differences between each KO and the CNTL cell line, $n = 7$ for each cell line. $^*P < 0.05$.

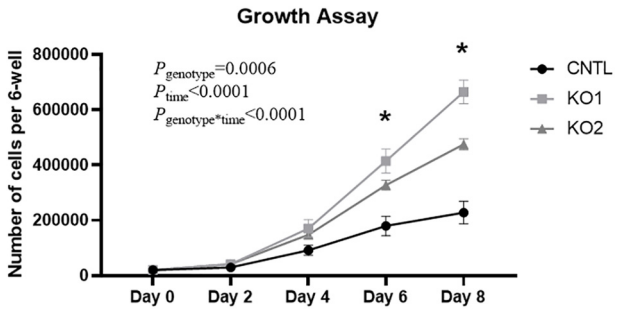

FIGURE 8 | KO of *EDN1-AS* Regulatory Elements Results in Increased Growth Rate of HK2 Proximal Tubule Cells. Because high expression of ET-1 is known to lead to cell proliferation in kidney proximal tubule cells, growth rate of CNTL and CRISPR/Cas9 KO cells was measured. 20,000 cells were plated into a 6-well dish and allowed to grow under normal conditions for 2, 4, 6, or 8 days. An automated cell counter was used to determine the total amount of cells in each well. Two-way ANOVA with repeated measures was used to determine genotype differences. *$P < 0.05$ by *T*-test within 1 day denotes that both KO cell lines are significantly different from the CNTL cell line, $n = 4$.

with increased ET-1 peptide secretion from the cells and increased growth rates.

CRISPR-mediated knockout of the region containing the predicted GR element and E-box resulted in increased expression of *EDN1-AS*, suggesting that the deleted regulatory region contains a repressive element. Given that GR elements can be bound by both GR and MR and these transcription factors can mediate positive and negative effects on gene regulation (Koning et al., 2019), this result is not surprising. Deletion of a GR element in the promoter of αENaC revealed a role for repressive regulation (Lin et al., 1999). Likewise, circadian clock proteins such as PER1 interact with E-box elements to mediate positive and negative effects on gene expression (Cox and Takahashi, 2019). Promoter analysis of the gonadotropin-releasing hormone demonstrated a key role for the E-box elements and a repressive role for PER1 (Resuehr et al., 2007). The concept that PER1 may mediate negative regulation of *EDN1-AS* is consistent with our previous observations that PER1 in the kidney mediates repression of the sense *EDN1* mRNA (Stow et al., 2012; Richards et al., 2014).

The non-coding RNA field has exploded in recent years due to the wealth of information provided by ENCODE. It is now estimated that more than 50% of the human genome is transcribed but only 1.2% of the genome encodes proteins (Ransohoff et al., 2018). Non-coding RNAs thus comprise a significant portion of the transcriptome, but our understanding of these RNA species is in its infancy. Some lncRNAs are natural antisense transcripts (NAT) because they arise by transcription of the strand opposite an mRNA (Khorkova et al., 2014). Our data suggest that *EDN1-AS* is a NAT with functional effects on ET-1 action. We estimate that the length of unprocessed *EDN1-AS* is at least 5 kb, based on the signal detected in HK2 and S9 cells and human kidney using SS6, which is located in the first exon of the sense *EDN1* sequence (**Figure 3**). The ssRT-PCR results in **Figure 4** demonstrate that *EDN1-AS* transcripts spanning the length of the *EDN1* gene are present in human kidney and bronchoendothelial cells. Whether or not *EDN1-AS* is subject to splicing or other post-transcriptional regulation remains to be determined.

Our report is the first description of an antisense lncRNA associated with the *EDN1* locus. According to LNCipedia, four lncRNAs have been identified near the *EDN1* gene (Volders et al., 2019). However, all four of these are associated with the sense strand. Functional relevance of these lncRNAs has not been described. Interestingly, a SNP in PHACTR, a gene ∼400,000 bp downstream of *EDN1,* has been associated with regulation of ET-1 levels (Gupta et al., 2017). This region appears to interact with an area of open chromatin located in a "gene desert" between the *EDN1* and *PHACTR* loci. These results, together with our current report, strongly suggest a new level of complexity in the regulation of *EDN1*.

A limitation of the current study is that the mechanism by which *EDN1-AS* affects ET-1 expression remains unclear. Many antisense RNAs act in an inhibitory manner, however, as the knowledge base regarding non-coding RNA increases, it is becoming increasingly clear that NATs act through myriad mechanisms (Wanowska et al., 2018). One example of a NAT that exerts positive effects on target mRNA expression is PTENP1, an antisense transcribed from the locus of the tumor suppressor gene PTEN. PTENP1 acts as a miRNA sponge for miR21, thus protecting the PTEN transcript from miRNA-mediated degradation (Wang et al., 2016). Another example of positive regulation by a NAT is BACE1-AS, which is transcribed from the β-amyloid cleaving enzyme 1 (BACE1) locus. BACE1-AS interacts with the BACE1 sense mRNA, masking a miRNA binding site and thus protecting BACE1 from miRNA-mediated degradation (Faghihi et al., 2010). BACE1-AS shows promise as a potential therapeutic in Alzheimer's disease (Ge et al., 2020). Given that ET-1 is subject to regulation by miRNA (Jacobs et al., 2013), it is tempting to speculate that *EDN1-AS* may function as a positive regulator of *EDN1* expression through a miRNA-protection mechanism. Future experiments are needed to test this hypothesis.

The lncRNAs are a newly recognized mechanism for gene regulation and are being explored as potential therapeutic targets in a variety of diseases (Li et al., 2018; Pecero et al., 2019; Wang et al., 2020), including diabetic nephropathy (Ge et al., 2019; Yang et al., 2019). A nucleic acid-based approach could allow greater specificity than pharmacological compounds, reducing side effects and allowing tissue-specific delivery (Sharma and Watts, 2015; Ku et al., 2016). Future studies are needed to determine whether or not manipulation of *EDN1-AS* could have therapeutic benefits. Although expression of *EDN1-AS* was confirmed in a variety of cell types and even in human kidney in the present study, the functional studies related to *EDN1-AS* are limited to HK-2 cells. In HK-2 cells, increased expression of *EDN1-AS* was associated with increased cell proliferation, which may have implications for manipulating *EDN1-AS* levels in a CKD setting.

DATA AVAILABILITY STATEMENT

The datasets generated for this study are available on request to the corresponding author.

AUTHOR CONTRIBUTIONS

LD, KS, LJ, CW, BC, KB, and MG conceived and designed research. LD, KS, SM, DB, SB, LJ, KA, RP, and KB performed experiments. LD, KS, SM, DB, and MG analyzed data. LD and MG interpreted results of experiments, prepared figures, and drafted manuscript. LD, SM, DB, SB, LJ, KB, BC, and MG edited and revised manuscript. LD, KS, SM, DB, SB, LJ, KA, RP, CW, KB, BC, and MG approved final version of manuscript.

FUNDING

This work was supported by the National Institutes of Health (NIH) R21AG052861 and 1R01DK109570-01A1 (MG), American Heart Association Grant-in-Aid (16GRNT31220009) (MG), University of Florida Department of Medicine Gatorade Trust (MG), American Heart Association Postdoctoral Fellowship Grants 18POST34030210 (LD), and NIH Grant T32-DK-104721 awarded to the University of Florida (UF) Division of Nephrology (LD).

REFERENCES

Balsalobre, A., Brown, S. A., Marcacci, L., Tronche, F., Kellendonk, C., Reichardt, H. M., et al. (2000). Resetting of circadian time in peripheral tissues by glucocorticoid signaling. *Science* 289, 2344–2347. doi: 10.1126/science.289.5488.2344

Cox, K. H., and Takahashi, J. S. (2019). Circadian clock genes and the transcriptional architecture of the clock mechanism. *J. Mol. Endocrinol.* 63, R93–R102. doi: 10.1530/JME-19-0153

Dhaun, N., Lilitkarntakul, P., MacIntyre, I. M., Muilwijk, E., Johnston, N. R., Kluth, D. C., et al. (2009). Urinary endothelin-1 in chronic kidney disease and as a marker of disease activity in lupus nephritis. *Am. J. Physiol. Ren. Physiol.* 296, F1477–F14783. doi: 10.1152/ajprenal.90713.2008

Dhaun, N., and Webb, D. J. (2019). Endothelins in cardiovascular biology and therapeutics. *Nat. Rev. Cardiol.* 16, 491–502. doi: 10.1038/s41569-019-0176-173

Dükel, M., Streitfeld, W. S., Tang, T. C. C., Backman, L. R. F., Ai, L., May, W. S., et al. (2016). The breast cancer tumor suppressor TRIM29 is expressed via ATM-dependent signaling in response to hypoxia. *J. Biol. Chem.* 291, 21541–21552. doi: 10.1074/jbc.M116.730960

Faghihi, M. A., Zhang, M., Huang, J., Modarresi, F., Van der Brug, M. P., Nalls, M. A., et al. (2010). Evidence for natural antisense transcript-mediated inhibition of microRNA function. *Genome Biol.* 11:R56. doi: 10.1186/gb-2010-11-5-r56

Feillet, C., Krusche, P., Tamanini, F., Janssens, R. C., Downey, M. J., Martin, P., et al. (2014). Phase locking and multiple oscillating attractors for the coupled mammalian clock and cell cycle. *Proc. Natl. Acad. Sci. U.S.A.* 111, 9828–9833. doi: 10.1073/pnas.1320474111

Ge, X., Xu, B., Xu, W., Xia, L., Xu, Z., Shen, L., et al. (2019). Long noncoding RNA GAS5 inhibits cell proliferation and fibrosis in diabetic nephropathy by sponging miR-221 and modulating SIRT1 expression. *Aging* 11, 8745–8759. doi: 10.18632/aging.102249

Ge, Y., Song, X., Liu, J., Liu, C., and Xu, C. (2020). The combined therapy of berberine treatment with lncRNA BACE1-as depletion attenuates Aβ25-35 induced neuronal injury through regulating the expression of miR-132-3p in neuronal cells. *Neurochem. Res.* doi: 10.1007/s11064-019-02947-6 [Epub ahead of print].

Grenda, R., Wuhl, E., Litwin, M., Janas, R., Sladowska, J., Arbeiter, K., et al. (2007). Urinary excretion of endothelin-1 (ET-1), transforming growth factor- 1 (TGF-1) and vascular endothelial growth factor (VEGF165) in paediatric chronic kidney diseases: results of the ESCAPE trial. *Nephrol. Dial. Transplant.* 22, 3487–3494. doi: 10.1093/ndt/gfm300

Gupta, R. M., Hadaya, J., Trehan, A., Zekavat, S. M., Roselli, C., Klarin, D., et al. (2017). A genetic variant associated with five vascular diseases is a distal regulator of endothelin-1 gene expression. *Cell* 170, 522–533.e15. doi: 10.1016/j.cell.2017.06.049

Hanai, S., Masuo, Y., Shirai, H., Oishi, K., Saida, K., and Ishida, N. (2005). Differential circadian expression of endothelin-1 mRNA in the rat suprachiasmatic nucleus and peripheral tissues. *Neurosci. Lett.* 377, 65–68. doi: 10.1016/j.neulet.2004.11.082

Heerspink, H. J. L., Parving, H. H., Andress, D. L., Bakris, G., Correa-Rotter, R., Hou, F. F., et al. (2019). Atrasentan and renal events in patients with type 2 diabetes and chronic kidney disease (SONAR): a double-blind, randomised, placebo-controlled trial. *Lancet* 393, 1937–1947. doi: 10.1016/S0140-6736(19)30772-X

Jacobs, M. E., Jeffers, L. A., Welch, A. K., Wingo, C. S., and Cain, B. D. (2014). MicroRNA regulation of endothelin-1 mRNA in renal collecting duct cells. *Life Sci.* 118, 195–199. doi: 10.1016/j.lfs.2014.03.003

Jacobs, M. E., Wingo, C. S., and Cain, B. D. (2013). An emerging role for microRNA in the regulation of endothelin-1. *Front. Physiol.* 4:22. doi: 10.3389/fphys.2013.00022

Karolchik, D., Barber, G. P., Casper, J., Clawson, H., Cline, M. S., Diekhans, M., et al. (2014). The UCSC genome browser database: 2014 update. *Nucleic Acids Res.* 42, D764–D770. doi: 10.1093/nar/gkt1168

Khorkova, O., Myers, A. J., Hsiao, J., and Wahlestedt, C. (2014). Natural antisense transcripts. *Hum. Mol. Genet.* 23, R54–R63. doi: 10.1093/hmg/ddu207

Kino, T., and Chrousos, G. P. (2010). Circadian CLOCK-mediated regulation of target-tissue sensitivity to glucocorticoids: implications for cardiometabolic diseases. *Endocr. Dev.* 20, 116–126. doi: 10.1159/000321232

Kohan, D. E., and Barton, M. (2014). Endothelin and endothelin antagonists in chronic kidney disease. *Kidney Int.* 86, 896–904. doi: 10.1038/ki.2014.143

Kohan, D. E., and Pollock, D. M. (2013). Endothelin antagonists for diabetic and non-diabetic chronic kidney disease. *Br. J. Clin. Pharmacol.* 76, 573–579. doi: 10.1111/bcp.12064

Kohan, D. E., Rossi, N. F., Inscho, E. W., and Pollock, D. M. (2011). Regulation of blood pressure and salt homeostasis by endothelin. *Physiol. Rev.* 91, 1–77. doi: 10.1152/physrev.00060.2009

Koning, A.-S. C. A. M., Buurstede, J. C., van Weert, L. T. C. M., and Meijer, O. C. (2019). Glucocorticoid and mineralocorticoid receptors in the brain: a transcriptional perspective. *J. Endocr. Soc.* 3, 1917–1930. doi: 10.1210/js.2019-2158

Kozakai, T., Sakate, M., Takizawa, S., Uchide, T., Kobayashi, H., Oishi, K., et al. (2014). Effect of feeding behavior on circadian regulation of endothelin expression in mouse colon. *Life Sci.* 118, 232–237. doi: 10.1016/j.lfs.2014.06.022

Ku, S. H., Jo, S. D., Lee, Y. K., Kim, K., and Kim, S. H. (2016). Chemical and structural modifications of RNAi therapeutics. *Adv. Drug Deliv. Rev.* 104, 16–28. doi: 10.1016/j.addr.2015.10.015

Li, Y., Liang, Y., Zhu, Y., Zhang, Y., and Bei, Y. (2018). Noncoding RNAs in cardiac hypertrophy. *J. Cardiovasc. Transl. Res.* 11, 439–449. doi: 10.1007/s12265-018-9797-x

Lin, H. H., Zentner, M. D., Ho, H. L., Kim, K. J., and Ann, D. K. (1999). The gene expression of the amiloride-sensitive epithelial sodium channel alpha-subunit is regulated by antagonistic effects between glucocorticoid hormone and ras pathways in salivary epithelial cells. *J. Biol. Chem.* 274, 21544–21554. doi: 10.1074/jbc.274.31.21544

Pecero, M. L., Salvador-Bofill, J., and Molina-Pinelo, S. (2019). Long non-coding RNAs as monitoring tools and therapeutic targets in breast cancer. *Cell. Oncol.* 42, 1–12. doi: 10.1007/s13402-018-0412-416

Pulido, T., Adzerikho, I., Channick, R. N., Delcroix, M., Galiè, N., Ghofrani, H.-A., et al. (2013). Macitentan and morbidity and mortality in pulmonary arterial hypertension. *N. Engl. J. Med.* 369, 809–818. doi: 10.1056/NEJMoa1213917

Ransohoff, J. D., Wei, Y., and Khavari, P. A. (2018). The functions and unique features of long intergenic non-coding RNA. *Nat. Rev. Mol. Cell Biol.* 19, 143–157. doi: 10.1038/nrm.2017.104

Reichetzeder, C., Tsuprykov, O., and Hocher, B. (2014). Endothelin receptor antagonists in clinical research — Lessons learned from preclinical and clinical kidney studies. *Life Sci.* 118, 141–148. doi: 10.1016/j.lfs.2014.02.025

Resuehr, D., Wildemann, U., Sikes, H., and Olcese, J. (2007). E-box regulation of gonadotropin-releasing hormone (GnRH) receptor expression in immortalized gonadotrope cells. *Mol. Cell. Endocrinol.* 278, 36–43. doi: 10.1016/j.mce.2007.08.008

Richards, J., Welch, A. K., Barilovits, S. J., All, S., Cheng, K. Y., Wingo, C. S., et al. (2014). Tissue-specific and time-dependent regulation of the endothelin axis by the circadian clock protein Per1. *Life Sci.* 118, 255–262. doi: 10.1016/j.lfs.2014.03.028

Seccia, T. M., Caroccia, B., Gioco, F., Piazza, M., Buccella, V., Guidolin, D., et al. (2016). Endothelin-1 drives epithelial-mesenchymal transition in hypertensive nephroangiosclerosis. *J. Am. Heart Assoc.* 5:721. doi: 10.1161/JAHA.116.003888

Sharma, V. K., and Watts, J. K. (2015). Oligonucleotide therapeutics: chemistry, delivery and clinical progress. *Future Med. Chem.* 7, 2221–2242. doi: 10.4155/fmc.15.144

Speed, J. S., and Pollock, D. M. (2013). Endothelin, kidney disease, and hypertension. *Hypertens* 61, 1142–1145. doi: 10.1161/HYPERTENSIONAHA.113.00595

Stemmer, M., Thumberger, T., Del Sol Keyer, M., Wittbrodt, J., and Mateo, J. L. (2015). CCTop: an intuitive, flexible and reliable CRISPR/Cas9 target prediction tool. *PLoS One* 10:e0124633. doi: 10.1371/journal.pone.0124633

Stow, L. R., Jacobs, M. E., Wingo, C. S., and Cain, B. D. (2011). Endothelin-1 gene regulation. *FASEB J.* 25, 16–28. doi: 10.1096/fj.10-161612

Stow, L. R., Richards, J., Cheng, K. Y., Lynch, I. J., Jeffers, L. A., Greenlee, M. M., et al. (2012). The circadian protein period 1 contributes to blood pressure control and coordinately regulates renal sodium transport genes. *Hypertension* 59, 1151–1156. doi: 10.1161/HYPERTENSIONAHA.112.190892

Surjit, M., Ganti, K. P., Mukherji, A., Ye, T., Hua, G., Metzger, D., et al. (2011). Widespread negative response elements mediate direct repression by agonist-liganded glucocorticoid receptor. *Cell* 145, 224–241. doi: 10.1016/j.cell.2011.03.027

Theuring, F., Thöne-Reinecke, C., Vogler, H., Schmager, F., Rohmeiss, P., Slowinski, T., et al. (1998). Pathophysiology in endothelin-1 transgenic mice. *J. Cardiovasc. Pharmacol.* 31(Suppl. 1), S489–S491. doi: 10.1097/00005344-199800001-199800140

Volders, P.-J., Anckaert, J., Verheggen, K., Nuytens, J., Martens, L., Mestdagh, P., et al. (2019). LNCipedia 5: towards a reference set of human long non-coding RNAs. *Nucleic Acids Res.* 47, D135–D139. doi: 10.1093/nar/gky1031

Wang, L., Zhang, N., Wang, Z., Ai, D.-M., Cao, Z.-Y., and Pan, H.-P. (2016). Pseudogene PTENP1 functions as a competing endogenous RNA (ceRNA) to regulate PTEN expression by sponging miR-499-5p. *Biochemistry* 81, 739–747. doi: 10.1134/S0006297916070105

Wang, Y., Wu, S., Zhu, X., Zhang, L., Deng, J., Li, F., et al. (2020). LncRNA-encoded polypeptide ASRPS inhibits triple-negative breast cancer angiogenesis. *J. Exp. Med.* 217, pii: e20190950. doi: 10.1084/jem.20190950

Wanowska, E., Kubiak, M. R., Rosikiewicz, W., Makałowska, I., and Szcześniak, M. W. (2018). Natural antisense transcripts in diseases: from modes of action to targeted therapies. *Wiley Interdiscip. Rev. RNA* 9:1461. doi: 10.1002/wrna.1461

Yang, J., Shen, Y., Yang, X., Long, Y., Chen, S., Lin, X., et al. (2019). Silencing of long noncoding RNA XIST protects against renal interstitial fibrosis in diabetic nephropathy via microRNA-93-5p-mediated inhibition of CDKN1A. *Am. J. Physiol. Renal Physiol.* 317, F1350–F1358. doi: 10.1152/ajprenal.00254.2019

Yuan, W., Li, Y., Wang, J., Li, J., Gou, S., and Fu, P. (2015). Endothelin-receptor antagonists for diabetic nephropathy: a meta-analysis. *Nephrology* 20, 459–466. doi: 10.1111/nep.12442

Zoja, C., Morigi, M., Figliuzzi, M., Bruzzi, I., Oldroyd, S., Benigni, A., et al. (1995). Proximal tubular cell synthesis and secretion of endothelin-1 on challenge with albumin and other proteins. *Am. J. Kidney Dis.* 26, 934–941. doi: 10.1016/0272-6386(95)90058-90056

Conflict of Interest: The authors declare that the research was conducted in the absence of any commercial or financial relationships that could be construed as a potential conflict of interest.

Copyright © 2020 Douma, Solocinski, Masten, Barral, Barilovits, Jeffers, Alder, Patel, Wingo, Brown, Cain and Gumz. This is an open-access article distributed under the terms of the Creative Commons Attribution License (CC BY). The use, distribution or reproduction in other forums is permitted, provided the original author(s) and the copyright owner(s) are credited and that the original publication in this journal is cited, in accordance with accepted academic practice. No use, distribution or reproduction is permitted which does not comply with these terms.

frontiers in Physiology

ORIGINAL RESEARCH
published: 13 March 2020
doi: 10.3389/fphys.2020.00138

Pharmacologic Blockade of 15-PGDH Protects Against Acute Renal Injury Induced by LPS in Mice

Shuying Miao[1,2,3†], Caihong Lv[1,3†], Ying Liu[1,3], Jie Zhao[4], Ting Li[5], Chunjiang Wang[6], Yunfei Xu[1,3], Xiaoli Wang[7], Xianzhong Xiao[1,3] and Huali Zhang[1,3*]*

[1] Department of Pathophysiology, Xiangya School of Medicine, Central South University, Changsha, China, [2] Department of Pathology, Nanjing Drum Tower Hospital, Nanjing University Medical School, Nanjing, China, [3] Sepsis Translational Medicine Key Lab of Hunan Province, Changsha, China, [4] Department of Neurosurgery, Xiangya Hospital, Central South University, Changsha, China, [5] Department of Physiology, Changzhi Medical College, Changzhi, China, [6] Department of Pharmacy, The Third Xiangya Hospital, Central South University, Changsha, China, [7] Department of Pathology and Pathophysiology, Jishou University, Jishou, China

OPEN ACCESS

Edited by:
Md Abdul Hye Khan, Medical College of Wisconsin, United States

Reviewed by:
Hee-Seong Jang, University of Nebraska Medical Center, United States
Hai-Jian Sun, Yong Loo Lin School of Medicine, National University of Singapore, Singapore

***Correspondence:**
Ying Liu
liu1977ying@126.com
Huali Zhang
zhanghuali@csu.edu.cn

[†] *These authors have contributed equally to this work*

Specialty section:
This article was submitted to Renal and Epithelial Physiology, a section of the journal Frontiers in Physiology

Received: *22 November 2019*
Accepted: *11 February 2020*
Published: *13 March 2020*

Citation:
Miao S, Lv C, Liu Y, Zhao J, Li T, Wang C, Xu Y, Wang X, Xiao X and Zhang H (2020) Pharmacologic Blockade of 15-PGDH Protects Against Acute Renal Injury Induced by LPS in Mice. Front. Physiol. 11:138. doi: 10.3389/fphys.2020.00138

Prostaglandin pathway plays multiple roles in various physiological and pathological conditions. The present study aimed to investigate the effect of 15-hydroxyprostaglandin dehydrogenase (15-PGDH), a key enzyme in the degradation of prostaglandins, on lipopolysaccharide (LPS)-induced acute kidney injury (AKI) in mice. In this study, male C57BL/6J mice were injected intraperitoneally with LPS (10 mg/kg). SW033291, a potent small-molecule inhibitor of 15-PGDH, was used to investigate the therapeutic potential of 15-PGDH inhibition on LPS-induced AKI. We discovered that the expression of 15-PGDH protein was upregulated in kidneys of LPS-stimulated mice, and it was mainly localized in the cytoplasm of renal tubular epithelial cells in renal cortex and outer medulla. SW033291 administration improved the survival rates of mice and attenuated renal injury of mice that were challenged by LPS. Additionally, inhibition of 15-PGDH also reversed LPS-induced apoptosis of renal cells, increased expression of anti-apoptotic protein Bcl-2, and downregulated expression of Fas, caspase-3, and caspase-8. Pretreatment of SW033291 enhanced autophagy in kidney cells after LPS stimulation. Our data also showed that inhibition of 15-PGDH relieved the level of lipid peroxidation and downregulated NADPH oxidase subunits induced by LPS in mice kidneys but had no significant effect on the release of inflammatory factors, such as IL-6, IL-1β, TNF-α, and MCP-1. Our study demonstrated that inhibition of 15-PGDH could alleviate LPS-induced AKI by regulating the apoptosis, autophagy, and oxidative stress rather than inflammation in mice.

Keywords: AKI, 15-PGDH, LPS, autophagy, apoptosis, oxidative stress

Abbreviations: AKI, acute kidney injury; LPS, lipopolysaccharide; 15-PGDH, 15-hydroxyprostaglandin dehydrogenase; MDA, malondialdehyde; SOD, superoxide dismutase; CAT, catalase; real-time PCR, real-time reverse transcriptase polymerase chain reaction; IL-6, interleukin-6; IL-1β, interleukin 1 beta; TNF-α, tumor necrosis factor-α; MCP-1, monocyte chemoattractant protein-1; ROS, reactive oxygen species; RNS, reactive nitrogen; PGE_2, Prostaglandin E_2; PGD2, Prostaglandin D2; PTGR2, prostaglandin reductase 2; RA, rheumatoid arthritis; TLR-4, Toll-like receptor 4.

INTRODUCTION

Acute kidney injury (AKI) is one of the most common and serious complications of sepsis with a high incidence and mortality rate. Sepsis accounts for up to 50% of cases of AKI in intensive care unit patients (Alobaidi et al., 2015). Mortality in patients with septic AKI is approximately doubled when compared with patients with sepsis alone (Jaworska et al., 2015; Thomas et al., 2015). However, little progress has been made toward the treatment of septic AKI in recent decades (Prowle, 2018). This may be related to the complex pathophysiological mechanism of septic AKI. Therefore, it is critical to further elucidate the mechanism of septic AKI.

It has been suggested that apoptosis, autophagy, oxidative damage, and inflammatory response are all involved in the development of AKI. Apoptosis and autophagy are common processes that maintain cellular metabolism and tissue homeostasis. A large number of studies show that renal tubular epithelial cells undergoing apoptosis can promote the development of renal dysfunction in ischemia-reperfusion (I/R) and septic AKI model (Lerolle et al., 2010). Autophagy is activated to prevent renal dysfunction from injury (Song et al., 2018). Studies have shown that renal tubular epithelium is the main site of oxidative stress, and reactive oxygen species (ROS) and reactive nitrogen (RNS) play important roles in acute renal tubular injury during sepsis (Pathak et al., 2012). In addition, systemic inflammatory response is closely related to septic AKI (Frei et al., 2010). When LPS enters the bloodstream, it forms a LPS/LBP/CD14 complex with lipopolysaccharide binding protein (LBP) and CD14, which in turn binds to toll-like receptor 4 (TLR-4) and activates the LPS signaling pathway, promoting the release of inflammatory factors, chemokines, and immune cell infiltration (Wu H. et al., 2007; Areschoug and Gordon, 2018).

15-hydroxyprostaglandin dehydrogenase (15-PGDH), a key enzyme in the degradation of prostaglandins, including prostaglandin E_2 (PGE_2), can catalyze the conversion of 15-hydroxy group of PGE_2 into a 15-keto group to produce a biologically inactive PG and antagonize the function of prostaglandin synthase COX-2 (Tai, 2011). Most previous studies have focused on the roles of COX-2 and its downstream prostaglandins, but there have been few studies on 15-PGDH. Recent studies have shown that 15-PGDH plays an important role in the development of inflammation-related diseases. In rheumatoid arthritis (RA), hydroxychloroquine can induce 15-PGDH expression through the MAP kinase pathway, while the exact role of PGDH as a potential target for RA treatment remains to be elucidated (Kim et al., 2015). Zhang et al. (2015) found that inhibition of 15-PGDH by selective inhibitor SW033291 or knockdown of 15-PGDH can promote the recovery of hematopoietic function. However, the biological function of 15-PGDH inhibition in AKI has not yet been reported. Therefore, we investigated the effect of 15-PGDH on AKI induced by lipopolysaccharide (LPS) in the hopes of determining whether 15-PGDH exerts its role by regulating information, autophagy, apoptosis, and oxidative stress. Our study provides new insights into the understanding on the pathogenesis and therapy of AKI caused by sepsis.

MATERIALS AND METHODS

Animals

C57BL/6J male mice aged 8–10 weeks (20–25 g) were purchased from Hunan Sleek Jingda Experimental Animal Co., Ltd. Mice were housed in a temperature-controlled room (25 ± 2°C) with relative humidity of 40∼60% on a 12 h light/dark cycle during the study. All animal experiments were approved by the Experimental Animal Ethics Committee of Central South University. The experimental mice were acclimatized for 7 days before administration of a 10 mg/kg dose of LPS or control saline.

For analysis of 15-PGDH expression in LPS-induced AKI, 12 mice were divided into four groups with three mice in each group ($n = 3$), and each mouse was administered intraperitoneally with 10 mg/kg body weight LPS (from *Escherichia coli* 0111:B4, Sigma-Aldrich, St. Louis, MO, United States) for 0, 6, 12, and 24 h, respectively. Under anesthesia, their eyeballs were removed for collection of blood, and tissues were collected for Western blot and immunohistochemistry.

For effect of SW033291 on inhibiting 15-PGDH, 30 mice were divided into five groups with six mice in each group ($n = 6$), and each mouse was administered intraperitoneally with 10 mg/kg body weight SW033291. Animals were sacrificed at 0, 3, 6, 12, and 24 h, followed by collection of kidneys for PGE_2 ELISA experiment. SW033291 was diluted according to Zhang et al. (2015).

For survival experiments, 100 mice were divided into four groups ($n = 20$ in control and SW033291 groups; $n = 43$ in LPS group; $n = 37$ in LPS + SW033291 group). Following LPS (10 mg/kg body weight), stimulated mice were treated with 10 mg/kg SW033291 or vehicle control twice daily for five doses. Then, mice survival was monitored and recorded daily. The other 70 mice were used to explore the role and mechanism of 15-PGDH on LPS-induced AKI, as described in the section below.

Serum and Tissue Samples

The mice were anesthetized, and the blood was collected for the assay of renal function. The kidneys were used for analysis of real-time PCR, Western blot, ELISA, HE staining, and immunohistochemistry.

Renal Function Test

Scr assay kit (C011-2-1) and BUN assay kit (C013-2-1) were acquired from Nanjing Jiancheng Bioengineering Institute. After the mice were anesthetized, blood was collected from the eyeballs of the mice for serum creatinine (Cr) and urea nitrogen (BUN) assay, according to the manufacturer's instructions. After sacrificed, the kidneys of each mouse were quickly removed and stored at −80°C.

Histological Data

After being fixed in 4% paraformaldehyde solution, the kidney tissue was dehydrated, transparent, paraffin embedded, and sliced. Then, HE staining was performed and observed under a microscope. Double-blind method was used to assess the renal tubular injury by the magnitude of tubular epithelial swelling, loss

of brush border, interstitial cell infiltration, tubular cell necrosis, vacuolation, and desquamation on the basis of the following scale: grade 0, no morphological deformities; grade 1, 1–25%; grade 2, 26–50%; grade 3, 51–75%; grade 4, 76–100% (Kojima et al., 2007; Havakhah et al., 2014).

Real-Time PCR

The total RNA from kidney tissue was isolated by using TRIzol. The isolated mRNA was used as a template to synthesize cDNA by using PrimeScriptTM RT Master Mix (Takara, Japan). Real-time PCR was performed by using the One Step SYBR® PrimeScript TM RT-PCR Kit in a Biosystems 7500 instrument. The amplification conditions were 95°C for 30 s, 95°C for 5 s, and 60°C for 34 s for 40 cycles. The primer sequences used were presented as follows (see **Table 1**).

Immunohistochemistry

The expressions of 15-PGDH in the kidneys were detected by immunohistochemistry. The antibody against 15-PGDH antibody (Cayman chemical, Item No.160615) was diluted at 1:100, and the experiment was manipulated according to the instructions of the EnVisionTM FLEX Mini Kit (Dako, K8024). Immunohistochemistry stained tissue sections were scored by two pathologists blinded to clinical and pathological data. According to the dyeing intensity: 0, no staining; 1+, weak; 2+, medium intensity; 3+, strong. Then, H-score was calculated according to the following formula: [1 × (% cells 1 +) + 2 × (% cells 2 +) + 3 × (% cells 3 +)] (Kim et al., 2019).

Western Blot

Proteins from the kidney samples of mice were extracted by sonicating the tissues in 1% PMSF-containing RIPA buffer and were centrifuged at 4°C for 10 min at 12,000 rpm. The protein concentration was determined by BCA method. Based on the protein concentration, 80–100 μg proteins were mixed with one quarter volume of 5× SDS loading buffer, boiled at 95°C for 10 min to denature the proteins. The proteins were subjected to SDS-PAGE and transferred to membrane. The membranes were blocked at room temperature for 1 h, washed with TBS-T (contains 0.1% Tween-20), and incubated with primary antibodies against 15-PGDH (1:1000 dilution, Cayman chemical, Item No.160615), caspase-3 (1:1000 dilution, proteintech, Item No.66470-2-Ig), microtubule-associated protein light chain 3 (LC-3B) (1:1000 dilution, CST, Item No. 3868), p62 (1:1000 dilution, CST, Item No. 5114), and β-actin (1:2000 dilution, Sigma-Aldrich, Item No. A1978), respectively, for overnight at 4°C. The membranes were then washed with TBST and incubated with secondary antibody for 1 h at RT, and signal was developed by adding the ECL luminescence substrate. The signal intensity of each protein was scanned by intensity-scanning software, and relative expression level of protein was calculated.

MDA Content, and SOD and CAT Activity

The kidney homogenates were prepared. The MDA content and the activities of SOD and CAT were determined according to the manufacturer's instructions (Nanjing Jiancheng Bioengineering Institute). The absorbance value (OD value) was measured with a microplate reader, and the MDA content and SOD and CAT activities were calculated according to the formula in the instructions.

Immunofluorescence

Paraffin sections were deparaffinized and rehydrated, further performed for antigen retrieval and blocked with goat serum for 30 min. The section samples were incubated with LC-3B primary antibody (1:100, CST) overnight at 4°C and washed three times with PBS (pH 7.4) at 5 min for each wash. Sections were then incubated with FITC-labeled anti-rabbit secondary antibody (1:400 dilution, MultiSciences) in the dark for 1 h at room temperature and washed three times with PBS (pH 7.4). The samples were counterstained with DAPI, mounted, and imaged under a fluorescence microscope. The nucleus stained with DAPI was blue under UV excitation, and the positive expression was shown as fluorescein-labeled red light.

TUNEL Assay

The apoptotic levels in the kidneys were measured according to the instruction of the TUNEL apoptosis detection kit (Roche). The percentage of apoptotic cells was calculated according to

TABLE 1 | The sequences of primers.

Primers	Species	Forward (5′–3′)	Reverse (5′–3′)
Caspase-3	Mouse	CTGACTGGAAAGCCGAAAC	GGACTGGATGAACCACGAC
Caspase-8	Mouse	GTTCAAAGTGCCCTTCCCTG	GTTCAAAGTGCCCTTCCCTG
iNOS	Mouse	CCACCAGGAGATGTTGAACTATGT	CTGTGGCTCTGACCCGTGAA
p47phox	Mouse	GATGGGAAATAGCCGGTGATA	CTATCTGGGCAAGGCTACGG
p40phox	Mouse	GGAGGAGGCTCTGCTGACTG	GTCCTCGTCCTCGGGAAAGT
gp91phox	Mouse	GTTCAAAGTGCCCTTCCCTG	TTGGCTGGGATCACAGGAAT
Catalase	Mouse	ATGGTAACTGGGATCTTGTGG	TTCAGGTGAGTCTGTGGGTT
SOD1	Mouse	CTGTACCAGTGCAGGACCTCA	CACCTTTGCCCAAGTCATCT
Fas	Mouse	GATCTGGGCTGTCCTGCCTCT	TTCACGAACCCGCCTCCTC
bcl2	Mouse	TTGTAATTCATCTGCCGCCG	AATGAATCGGGAGTTGGGGT
β-actin	Mouse	CATTGCTGACAGGATGCAGAAGG	TGCTGGAAGGTGGACAGTGAGG
15-PGDH	Mouse	CCAAGGTAG-CATTGGTGGAT	CCACATCACACTGGACGAAC

the number of apoptotic cells/total number of cells in randomly selected 5–10 fields.

Transmission Electron Microscope

Freshly isolated kidneys were quickly put into fixing buffer and fixed at 4°C for 2–4 h. After this, samples were transferred to Wuhan Goodbio Technology Co., Ltd., prepared as specimens, examined, and photographed under a transmission electron microscope.

Determination of PGE_2 Content

Pre-cooled 1 × PBS was added at a ratio of 1:10 to prepare tissue homogenates. The PGE_2 concentration of the renal tissue homogenate was determined according to the instruction of PGE_2 ELISA kit (Huamei Biology Company, Wuhan, China).

Statistical Analysis

GraphPad Prism version 5.02 (GraphPad Prism Software Inc, San Diego, CA, United States) was used for data analysis. All the experiments were repeated at least three times. Data were presented as mean ± SD. Statistical analysis was performed by ANOVA followed by Tukey's test. For the purpose of survival analysis, Kaplan-Meier method followed by log-rank test was applied to compare the survival rate between groups. A value of $P < 0.05$ was considered to be statistically significant.

RESULTS

Regulation of 15-PGDH in the Kidney of LPS-Induced AKI Mice

At first, we established an AKI mouse model using LPS. As shown in **Figure 1A**, the survival rate of mice in LPS group significantly decreased to 53% compared to the control group. Through HE staining, we observed marked edema, vacuolar degeneration, inflammatory cell infiltration, and the narrowing of tubular lumen at 12 and 24 h after LPS treatment, contrasting the normal renal morphology in vehicle-treated mice (**Figure 1B**). Accordingly, the serum levels of creatinine and urea nitrogen were significantly increased after LPS challenge compared to the control mice (**Figures 1C,D**). We determined the expression of 15-PGDH in kidney in response to LPS treatment. As shown in **Figures 1E,F**, LPS treatment significantly enhanced protein levels of 15-PGDH in kidneys; the highest level of 15-PGDH occurred at 12 h and lasted for 24 h. By immunohistochemistry, we found that 15-PGDH protein was mainly localized in the cytoplasm of renal tubular epithelial cells in renal cortex and outer medulla and that it had low expression levels in glomeruli and the inner medulla (**Figures 1G,H**).

Effect of SW033291 on Inhibiting 15-PGDH in Mice

As shown in **Figure 2A**, the PGE_2 content in kidney time-dependently increased with SW033291 treatment and peaked at 12 h. Strikingly, although the renal PGE_2 content in both control group and SW033291 group increased after 12 h treatment with LPS, the increase of PGE_2 content was higher in SW033291 group mice than that in control mice (**Figure 2B**). Furthermore, the mRNA and protein levels of 15-PGDH were significantly downregulated in kidney after SW033291 treatment (**Figures 2C,D**).

SW033291 Treatment Attenuated LPS-Induced AKI in Mice

SW033291 treatment enhanced the survival rate of LPS-treated mice from 30 to 49% (**Figure 3A**). Meanwhile, renal function assay showed that BUN and Cr levels were significantly increased after 6 h of LPS treatment compared with the control group and peaked at 12 h, whereas the BUN and Cr levels were significantly decreased after SW033291 treatment (**Figures 3B–E**). The decline in the BUN and Cr levels of mice with 10 mg/kg SW033291 treatment is more obvious than 5 mg/kg dose at 12 h (**Figures 3D,E**). HE staining showed that there were no significant pathological lesions in the kidneys of the control and SW033291 group mice. In LPS-treated group, the tubular epithelial cells of the mice were edematous with larger cellular volume, vacuolar degeneration and narrowed lumen of the renal tubules. It was also observed that the glomerular structure was disordered, accompanied by infiltration of scattered inflammatory cells and narrowing of the renal capsule. These pathological lesions were evidently alleviated after SW033291 treatment (**Figures 4I–Q**). PAS staining confirmed above findings in renal morphology (**Figures 4A–H**). These data indicated a protective effect of SW033291 against LPS-induced AKI.

SW033291 Treatment Alleviated the Apoptosis of Renal Cells in LPS-Induced AKI Mice

TUNEL assay showed enhanced renal cell apoptosis after intraperitoneal injection of LPS for 12 h in mice, but the apoptosis level was decreased significantly after SW033291 therapy (**Figures 5A,B**). After LPS stimulation, apoptosis-related protein cleaved-caspase-3 levels increased evidently, whereas SW033291 treatment showed a significant reduction of cleaved-caspase-3 protein expression levels (**Figures 5C,D**). At the same time, the elevated mRNA levels of Fas, caspase-3, and caspase-8 in kidney after LPS stimulation were all blunted by the pretreatment of SW033291 in line with the restoration of reduced mRNA expression of Bcl-2 (**Figures 5E–H**). All these data demonstrated an anti-apoptotic role of SW033291 in this experimental setting.

SW033291 Treatment Increased Autophagic Response in the Kidneys of LPS-Induced AKI Mice

As shown in **Figures 6A,B**, the expression of 15-PGDH protein was significantly upregulated by LPS treatment. In contrast, SW033291 treatment significantly suppressed 15-PGDH expression in LPS-treated mice. During the development of autophagy, cytosolic soluble LC3 (i.e., LC3-I) is converted to membrane-type LC3 (i.e., LC3-II) and localized on the autophagosome membrane. After LPS stimulation, the LC3-II/LC3-I ratio was significantly increased along with

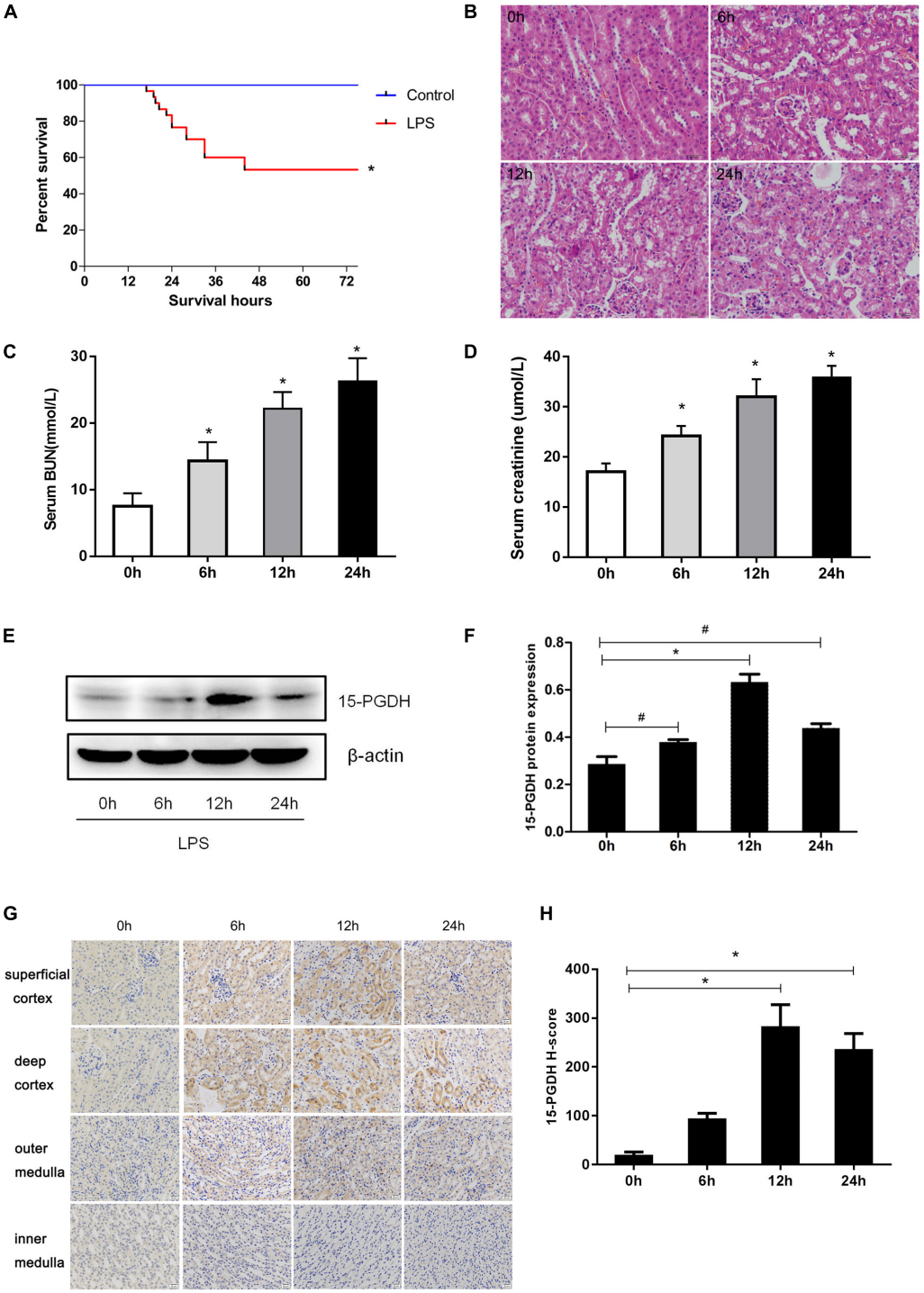

FIGURE 1 | Expression of 15-PGDH in the kidneys of LPS-induced AKI mice model. **(A)** Effect of LPS on the survival of mice (n = 30). **(B)** Effect of LPS on renal morphologic changes of mice (200×). **(C)** The levels of serum urea nitrogen (BUN) were measured at different time points (n = 6–10). **(D)** The levels of serum creatinine (Cr) were measured at different time points (n = 6–10). **(E)** The expression of 15-PGDH in renal tissues at different time points (0, 6, 12, and 24 h) after LPS (10 mg/kg) stimulation (n = 3). **(F)** The signal intensity ratio of 15-PGDH to β-actin in renal tissue (n = 3). **(G)** Effect of LPS (10 mg/kg) on the expression of 15-PGDH in mouse kidney tissue (200×). **(H)** Comparison of 15-PGDH IHC H-score after LPS (10 mg/kg) stimulation (n = 3). Scale = 20 μm. $^{*}P < 0.01$ (compared with 0 h), $^{\#}P < 0.05$ (compared with 0 h). Data are mean ± SD.

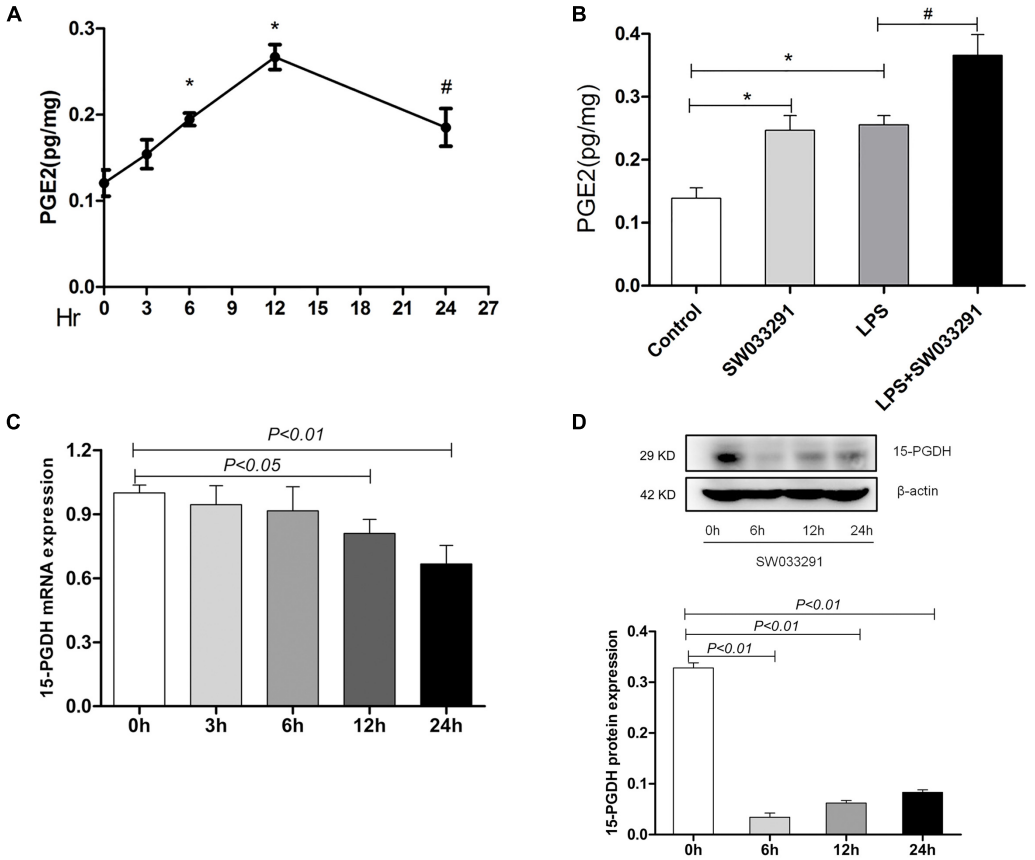

FIGURE 2 | Effect of SW033291 treatment on the blockade of 15-PGDH in the kidneys of mice. **(A)** Effect of SW033291 (10 mg/kg injected twice daily IP for five doses) treatment on renal PGE_2 content at 0, 3, 6, 12, and 24 h ($n = 6$). $^*P < 0.01$ vs. 0 h, $^{\#}P < 0.05$ vs. 0 h. **(B)** PGE_2 content in kidney tissue of mice induced by LPS (10 mg/kg) at 12 h ($n \geq 6$).$^*P < 0.01$ vs. Control, $^{\#}P < 0.05$ vs. LPS. **(C)** Expression of 15-PGDH mRNA after SW033291 (10 mg/kg) treatment at different time points ($n = 3$). **(D)** Expression of 15-PGDH protein after SW033291 (10 mg/kg) treatment at different time points ($n = 3$). Data are mean ± SD.

the enhanced P62 protein compared to the control group. Interestingly, SW033291 treatment resulted in a greater increment of the LC3-II/LC3-I ratio after stimulation with LPS (**Figures 6A–D**). By immunofluorescence, we further confirmed the regulatory role of SW033291 for LC3B in kidneys of AKI mice (**Figure 6E**). Transmission electron microscopy showed that SW033291 treatment evidently enhanced the number of autophagic vacuoles in kidney cells after LPS stimulation, which further confirmed a promoted autophagic response (**Figure 6F**).

SW033291 Treatment Ameliorated Oxidative Damage in the Kidneys of LPS-Induced AKI Mice

As shown in **Figures 7A–C**, compared with the control group, the MDA level in the kidney tissue of the LPS group was significantly increased, while the activity of antioxidant enzymes of SOD and CAT was evidently suppressed. Importantly, SW033291 treatment significantly decreased the MDA level and enhanced the activity of SOD and CAT in the kidneys of AKI mice (**Figures 7A–C**). In agreement with above findings, the mRNA levels of kidney NADPH oxidase subunits gp91phox, p40phox, and p47phox were strikingly upregulated after 12 h LPS challenge compared with the control group, which was significantly blunted after SW033291 treatment (**Figures 7D–F**). Similarly, the upregulated mRNA expression of iNOS was also reduced by the pretreatment of SW033291 (**Figure 7G**). Furthermore, we confirmed that the reduction of antioxidant genes of SOD1 and catalase in kidneys after a 12 h injection of LPS was significantly reversed by SW033291 (**Figures 7H,I**).

Effect of SW033291 Treatment of Inflammatory Response in the Kidneys of LPS-Induced AKI Mice

It has been shown that inflammation is a pathogenic factor of AKI. Meanwhile, prostaglandin E2 is a well-established inflammatory mediator. We evaluated whether inflammation was involved in the role of SW033291 in LPS-induced AKI. As shown in **Figure 8**, LPS treatment significantly enhanced the release of IL-6, IL-1β, TNF-α, and MCP-1 in the kidneys, while SW033291 treatment had no effect on the release of these inflammatory

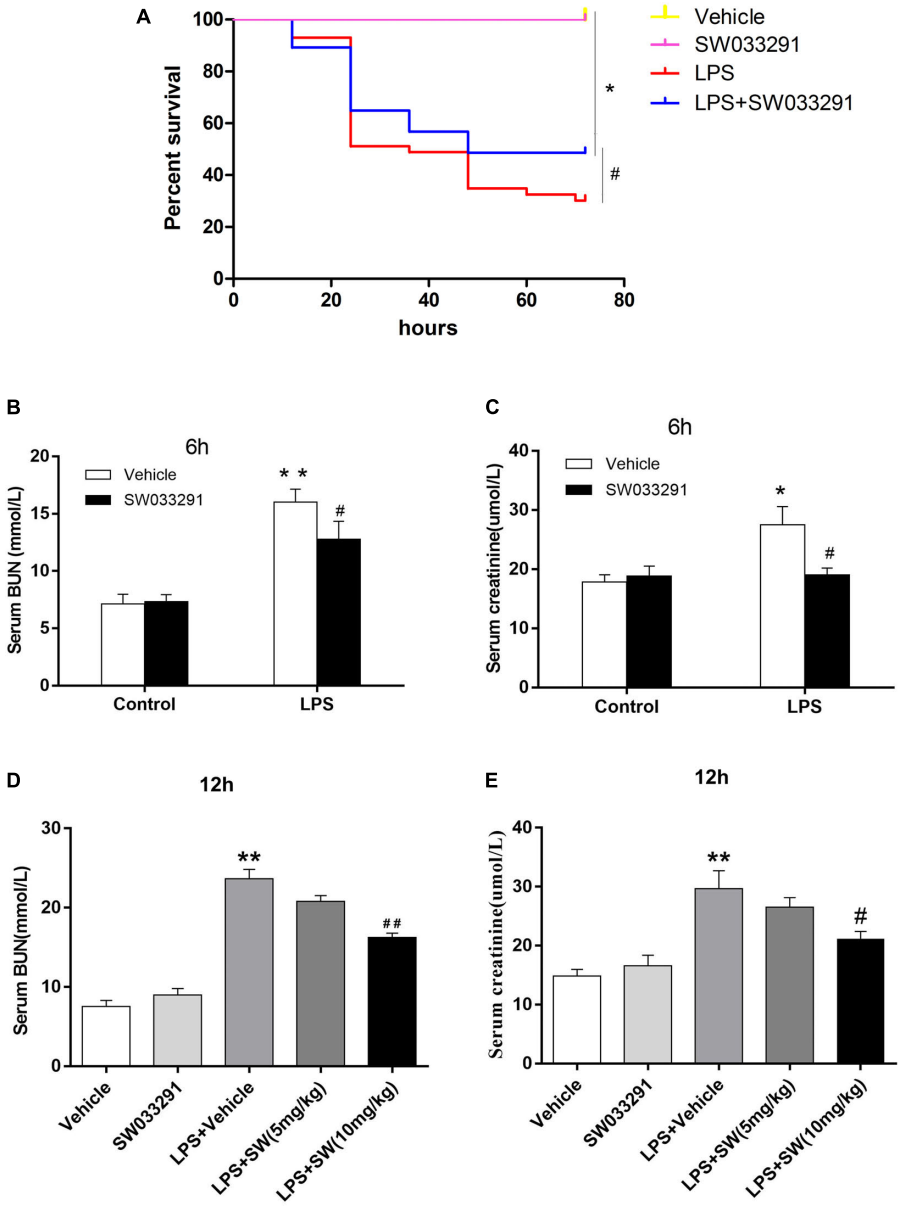

FIGURE 3 | Effect of SW033291 treatment on the survival rate and renal function in mouse sepsis model. **(A)** Effect of SW033291 (10 mg/kg injected twice daily IP for five doses) treatment on the survival of mice in sepsis model. $^{*}P < 0.01$ (compared with control group); $^{\#}P < 0.05$ (compared with LPS group). $n = 20$ in control and SW033291 groups; $n = 43$ in LPS group; $n = 37$ in LPS + SW033291 group; **(B,C)** Serum levels of BUN and Cr in mice with LPS-induced AKI after 6 h of SW033291 (10 mg/kg) treatment ($n \geq 6$). **(D,E)** Serum levels of BUN and Cr in mice with LPS-induced AKI after 12 h of SW033291 (5 mg/kg or 10 mg/kg) treatment ($n \geq 6$). $^{*}P < 0.05$, $^{**}P < 0.01$ (compared with control group); $^{\#}P < 0.05$, $^{\#\#}P < 0.01$ (compared with LPS group). Groups were compared by Two-Way ANOVA. Data are mean ± SD.

factors. These data suggested that the beneficial role of SW033291 in LPS-induced AKI could be independent of the inflammation.

DISCUSSION

In the present study, LPS intraperitoneal injection model has been successfully established for septic AKI research according to previous studies. Animals develop a series of systemic inflammation response that mimic clinical sepsis patients (Wu X. et al., 2007; Doi et al., 2009; Gong et al., 2016). The exact mechanisms of sepsis-induced AKI are complex and controversial. Various factors have been known to contribute to the pathologic process of LPS-induced AKI, such as renal cell apoptosis, oxidative stress, and endotoxin-induced complex inflammation (Zarjou and Agarwal, 2011; Prowle and Bellomo, 2015; Shum et al., 2016).

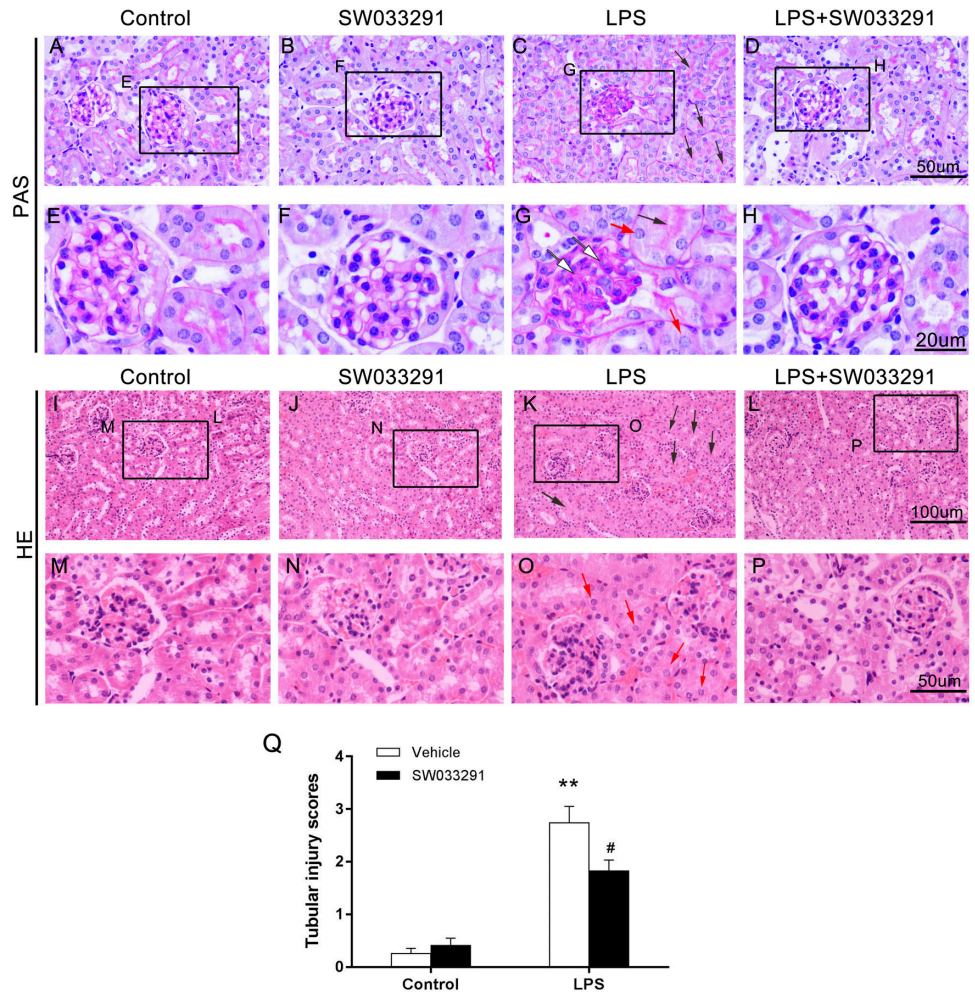

FIGURE 4 | Effect of SW033291 treatment on renal morphologic changes of AKI mice induced by LPS. **(A–D)** PAS staining (12 h) (400×); **(E–H)** Partial enlargement of PAS staining; (n = 3) **(I–L)** HE staining (12 h) (200×); **(M–P)** Partial enlargement of HE staining. (n = 3) The red arrow ([QSIImage]) indicates renal tubular epithelial cell edema; the black arrow ([QSIImage]) indicates tubular lumen shrinkage; the white arrow ([QSIImage]) indicates hyperplastic glomerular mesangial and thickened basement membrane. **(Q)** Shows the kidney tubular injury scores in mice with LPS-induced AKI after SW033291 (10 mg/kg) treatment, as described in section Materials and Methods (n = 3). $^{**}P < 0.01$ (compared with control group); $^{\#}P < 0.05$ (compared with LPS group). Data are mean ± SD.

15-PGDH is a key enzyme that expressed widely in mammalian tissues, such as lung, placenta, and kidney, and is mainly localized in the proximal tubules of renal cortex and the outer medullary thick ascending limb (Yao et al., 2008; Liu et al., 2014). In this study, for the first time we discovered that the expression of 15-PGDH protein was increased in kidneys of LPS-stimulated mice and that it was mainly localized in the cytoplasm of renal tubular epithelial cells in renal cortex and outer medulla. More importantly, we also found that the blockade of 15-PGDH could significantly alleviate the kidney damage and contribute to the survival rate of endotoxemic mice. There may be a negative correlation between 15-PGDH expression and kidney function and histology. Therefore, inhibition of 15-PGDH expression may be a potential target for relieving kidney damage. Studies have shown that the renal protective effect is shown by the reduction of apoptosis level in renal tubular epithelial cells in septic AKI (Lerolle et al., 2010; Wei et al., 2010). It has been documented that the apoptosis-associated genes, including Bcl-2, Bax, caspase-3, caspase-8, FasL, and Fas, are closely related to renal injury (Messaris et al., 2008; Lerolle et al., 2010). Our research is consistent with the literature, evidenced by the reduction of renal cell apoptosis in LPS-treated AKI mice after inhibition of 15-PGDH. Therefore, pharmacologic blockade of 15-PGDH may protect against kidney cells apoptosis and kidney injury and then contribute to the survival rate of endotoxemic mice. In agreement with our findings, previous studies have shown that the inhibition of 15-PGDH can promote tissue repair and regeneration after bone marrow transplantation, colitis and partial hepatectomy (Zhang et al., 2015), which also indicate that, in addition to alleviating kidney damage, inhibition of 15-PGDH may affect other organs, thereby improving survival rates in mice.

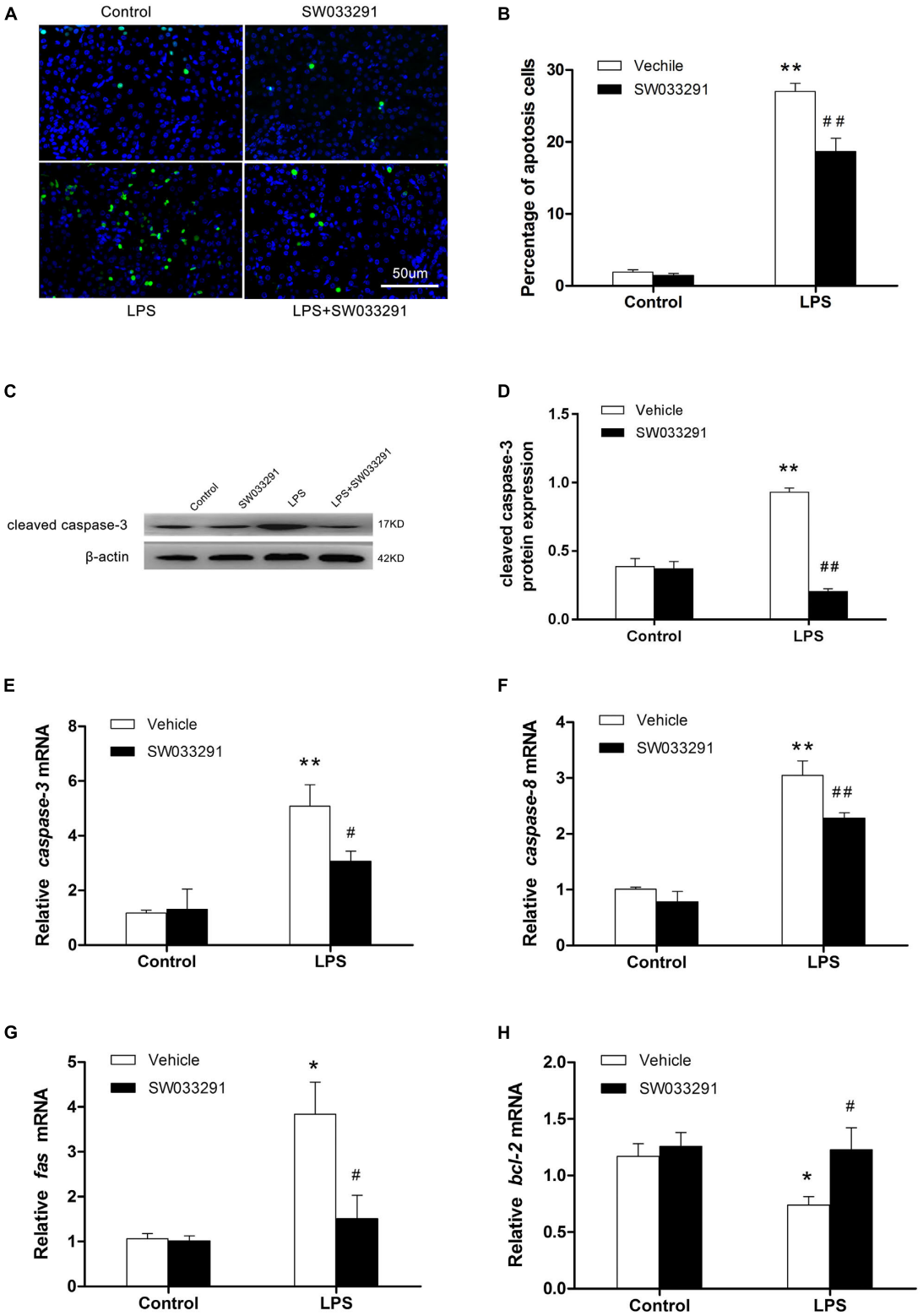

FIGURE 5 | SW033291 treatment alleviated the apoptosis of renal cells in LPS-induced AKI mice. **(A)** TUNEL staining shows the apoptotic renal cells after 12 h of SW033291 (10 mg/kg) treatment (400×). Scale bar: 50 μm. **(B)** Percentage of apoptotic cells ($n = 6$). **(C)** Western blot analysis of cleaved caspase-3 in each group after 12 h of SW033291 (10 mg/kg) treatment. **(D)** Density ratio of cleaved caspase-3/β-actin in each group ($n = 3$). **(E–H)** Real-time PCR was used to detect the apoptotic genes of caspase-3, caspase-8, Fas, and Bcl-2 ($n = 6$). $^{*}P < 0.05$, $^{**}P < 0.01$ vs. CON; $^{\#}P < 0.05$, $^{\#\#}P < 0.01$ vs. LPS. Data are mean ± SD.

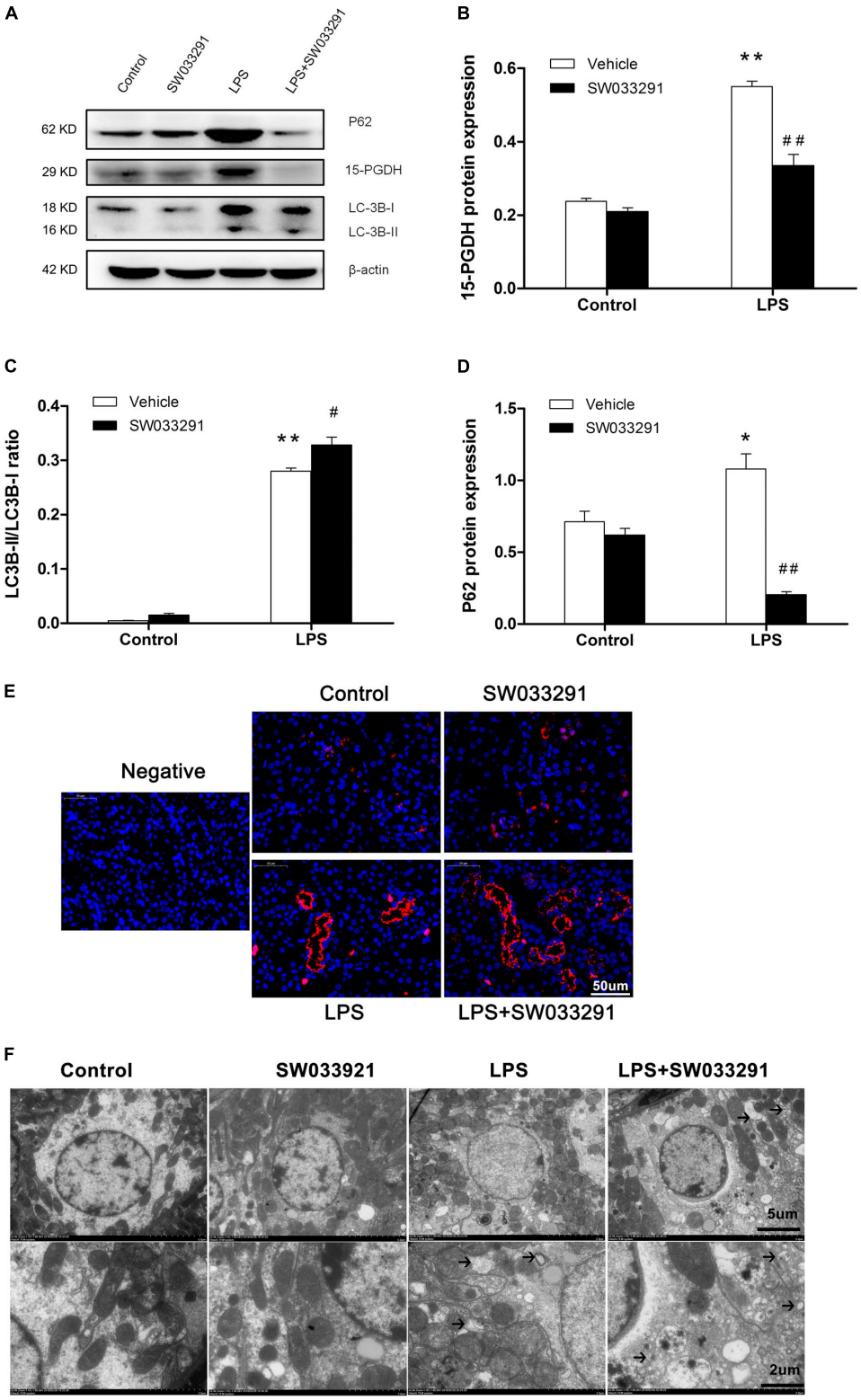

FIGURE 6 | Effect of SW033291 treatment on autophagic response in kidneys of LPS-induced AKI mice. **(A)** Western blotting was used to detect the protein expression of 15-PGDH, LC3B, and P62 in kidney tissues. **(B)** Density ratio of 15-PGDH/β-actin in each group. **(C)** Density ratio of LC3-II/LC3-I in each group. **(D)** Density ratio of P62/β-actin in each group. $^{*}P < 0.05$, $^{**}P < 0.01$ vs. CON; $^{\#}P < 0.05$, $^{\#\#}P < 0.01$ vs. LPS ($n = 3$). **(E)** Immunofluorescence analysis of kidney tissue from LPS-induced mice with or without SW033291 (10 mg/kg) treatment shows localization of LC3B. Scale bars: 50 μm, 400× ($n = 3$). **(F)** Autophagy level on renal tissue after SW033291 (10 mg/kg) treatment was observed by transmission electron microscope ($n = 3$). Autolysosomes indicated by arrowheads. Scale bars: 5 μm, 2 μm. Data are mean ± SD.

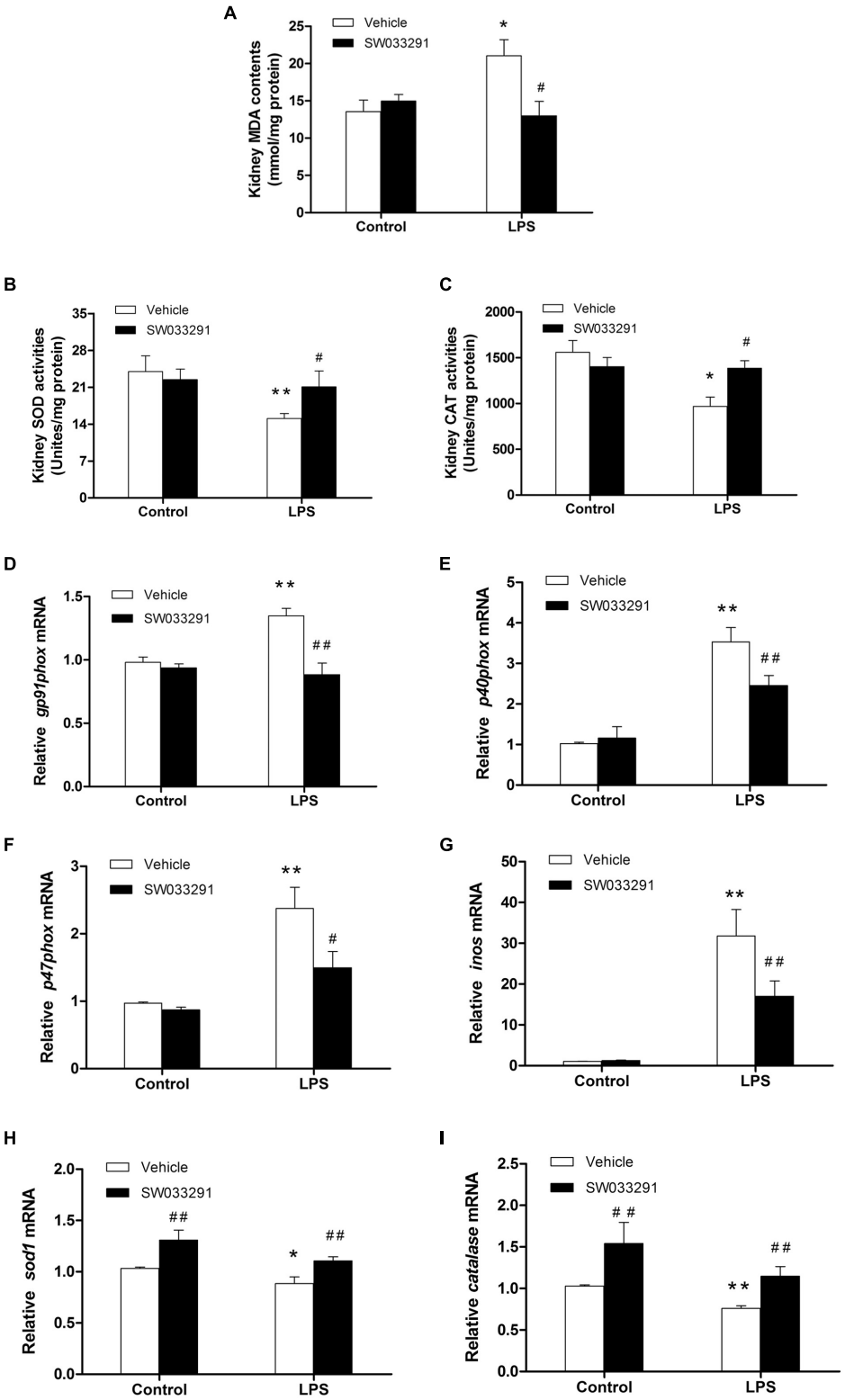

FIGURE 7 | Renal MDA level and the activity of SOD and CAT after SW033291 treatment. **(A)** Renal MDA level. **(B)** Renal SOD activity. **(C)** CAT activity. $^{*}P < 0.05$, $^{**}P < 0.01$ vs. CON; $^{\#}P < 0.05$, $^{\#\#}P < 0.01$ vs. LPS ($n \geq 6$). **(D–F)** Effect of SW033291 (10 mg/kg) treatment on the mRNA expression of NADPH oxidase subunits of gp91phox, p40phox, and p47phox in kidneys. **(G)** iNOS mRNA level. **(H,I)** Expression of antioxidant genes of SOD1 and catalase in the kidneys after SW033291 (10 mg/kg) treatment. $^{*}P < 0.05$, $^{**}P < 0.01$ vs. CON; $^{\#}P < 0.05$, $^{\#\#}P < 0.01$ vs. LPS; ($n = 6$). Data are mean ± SD.

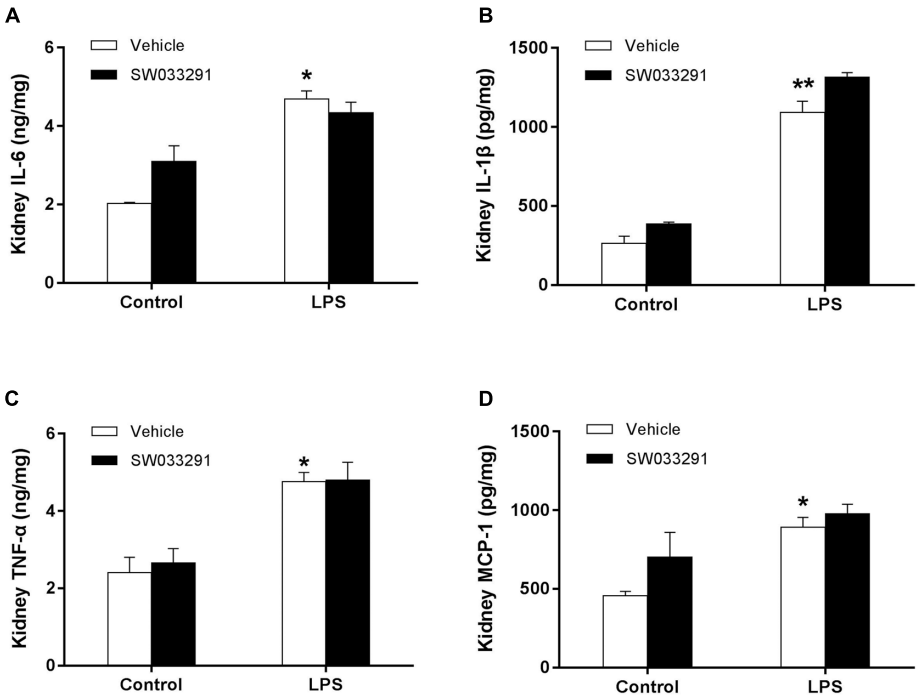

FIGURE 8 | Effect of 15-PGDH inhibition on the release of inflammatory cytokines in kidneys of AKI mice. **(A)** IL-6. **(B)** IL-1β. **(C)** TNF-α. **(D)** MCP-1. $^{*}P < 0.05$, $^{**}P < 0.01$ (compared with control group); ($n = 6$). Results were analyzed with Two-Way ANOVA. Data are mean ± SD.

The LC3-II/LC3-I ratio is usually used to estimate the level of autophagy (Dai et al., 2019; McCormick et al., 2019). Increased levels of LC3-II and decreased levels of p62/SQSTM1 are typically indicative of increased autophagic flux (Klionsky et al., 2016). In the present study, SW033291 treatment promoted LPS-induced autophagy. Studies have shown that autophagy is activated during AKI and protects kidney function (Suzuki et al., 2008; Turkmen et al., 2011). Li et al. (2017) found that increased autophagy could reduce the apoptosis of renal tubular epithelial cell after the occurrence of AKI induced by LPS. Therefore, autophagy may play a protective role in septic AKI via inhibiting apoptosis. These results suggest that inhibition of 15-PGDH may reduce the renal cells apoptosis, possibly related to autophagy.

One of the most important antioxidant enzymes, SOD can catalyze the conversion of harmful superoxide radicals to reduce the oxidative cell damage (Noor et al., 2002; Armogida et al., 2012). CAT can remove hydrogen peroxide and protect cells from damage. Thus, it was possible that inhibition of 15-PGDH reduced the production of oxygen free radicals in kidneys during endotoxemia and relieved the level of lipid peroxidation in the kidney, thereby attenuating the kidney injury. In this study, we also investigated the effect of 15-PGDH on NADPH oxidase subunits in the kidneys of mice treated with LPS. The results indicated that the SW033291 intervention could counteract the upregulation of the NADPH oxidase subunits gp91phox, p40phox, and p47phox induced by LPS. In addition, iNOS may be involved in 15-PGDH-mediated regulation of oxidative damage in AKI caused by LPS. A large amount of literature has indicated that RNS produced by iNOS in the kidney during sepsis could promote I/R-induced renal tubular injury, which was a key reason of AKI during sepsis (Walker et al., 2000; Noiri et al., 2001; Viñas and Sola, 2006; Wu and Mayeux, 2007). It has been shown that iNOS-derived NO/RNS may play a role in the pathogenesis of LPS-induced renal injury (Wang et al., 2003; Cuzzocrea et al., 2006). Selective inhibition of iNOS can reduce RNS production and improve sepsis-induced renal impairment (Heemskerk et al., 2009). The present study also found that inhibition of 15-PGDH could effectively reverse the downregulation of the antioxidation enzymes SOD1 and catalase induced by LPS. Antioxidants can reduce AKI caused

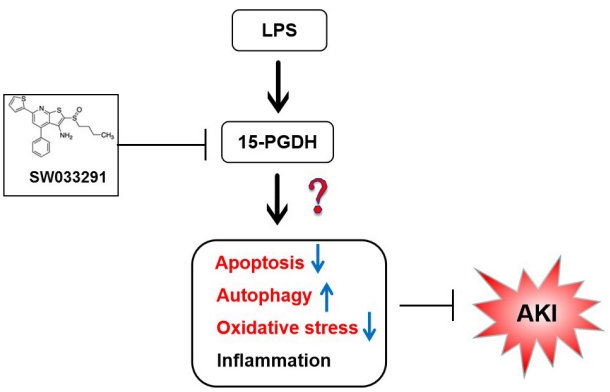

FIGURE 9 | The summary flow diagram.

by sepsis (Campos et al., 2012; Li et al., 2014). Therefore, 15-PGDH may promote the oxidative damage during LPS-induced AKI, and its mechanism may be related to the upregulation of NADPH oxidase subunits and iNOS and downregulation of the expression of antioxidant enzymes in the kidney. In oxaliplatin-resistant HT29 cells, PGE_2 levels were significantly elevated, with elevated COX-2 and reduced 15-PGDH expression. The COX-2/PGE2/EP4 signaling axis play an important role on oxaliplatin resistance via regulation of oxidative stress (Huang et al., 2019). In previous studies, injection of SW033291 [10 mg per kg of weight (mg/kg)] induced a significant increase of PGE_2 and Prostaglandin D2 (PGD2) levels, while PGF2a levels were mostly unaltered (Zhang et al., 2015). 15-PGDH catalyze the conversion of 15-hydroxy group of PGE_2 into 15-keto-PGE2 (15k-PGE2), which further catalyzed by prostaglandin reductase 2 (PTGR2). Exogenous 15k-PGE2 treatment or PTGR2 knockdown yielded the antioxidative transcription factor increase in LPS-stimulated RAW264.7 cells (Chen et al., 2018). Therefore, we speculate that 15-PGDH may regulate oxidative stress via COX-2/PGE2/EP4 signaling axis. However, other prostaglandins, such as PGD2, may play an important role, and the precise mechanism needs to be further investigated.

We also demonstrated that SW033291 treatment had no effect on the release of IL-6, IL-1β, TNF-α, and MCP-1. The effect of LPS is mediated by Toll-like receptor 4 (TLR-4) and the release of inflammatory cytokines, such as TNF-a (initiator of inflammatory response). Cunningham et al. (2004) found that LPS can induce systemic TNF-α releasing, promoting inflammatory cell infiltration and tubular cell apoptosis in septic AKI. These results indicate that 15-PGDH has little effect on the inflammatory response during LPS-induced AKI.

CONCLUSION

In summary, 15-PGDH expression was upregulated in kidneys of LPS-stimulated AKI mice, contributing to LPS-induced AKI. And such an effect may be related to apoptosis, autophagy, and oxidative damage (**Figure 9**). However, it is unclear whether there is interaction between apoptosis, autophagy, and oxidative damage, which needs to be further investigated. Our study provided new insights for the prevention and treatment of sepsis-related AKI.

DATA AVAILABILITY STATEMENT

The raw data supporting the conclusions of this article will be made available by the authors, without undue reservation, to any qualified researcher. Requests to access the datasets should be directed to YL, liu1977ying@126.com.

ETHICS STATEMENT

The animal study was reviewed and approved by the Experimental Animal Ethics Committee of Central South University.

AUTHOR CONTRIBUTIONS

SM, YL, HZ, and XX conceived and designed the experiments. SM, CL, JZ, TL, and YX executed the experiments and analyzed the samples. SM, CL, YL, XW, and CW analyzed the data. SM wrote the first version of the manuscript. All authors interpreted the data, critically revised the manuscript, and approved the final version of the manuscript.

FUNDING

The present study was supported by the National Natural Science Foundation of China (81571880 and 81373147) to YL, National Natural Science Foundation of China (81471897) to HZ, National Natural Science Foundation of China (81671895) to XX, and Natural Science Foundation of Hunan Province (2016JJ2157) to JZ. All of the funding bodies funded in the study design, collection, analysis, interpretation of data and writing the manuscript.

REFERENCES

Alobaidi, R., Basu, R. K., Goldstein, S. L., and Bagshaw, S. M. (2015). Sepsis-associated acute kidney injury. *Semin. Nephrol.* 35, 2–11. doi: 10.1016/j.semnephrol.2015.01.002

Areschoug, T., and Gordon, S. (2018). Pattern recognition receptors and their role in innate immunity: focus on microbial protein ligands. *Contrib. Microbiol.* 15, 45–60. doi: 10.1159/000135685

Armogida, M., Nisticò, R., and Mercuri, N. B. (2012). Therapeutic potential of targeting hydrogen peroxide metabolism in the treatment of brain ischaemia. *Br. J. Pharmacol.* 166, 1211–1224. doi: 10.1111/j.1476-5381.2012.01912.x

Campos, R., Shimizu, M. H., Volpini, R. A., Bragança, A. C., Andrade, L., Lopes, F. D., et al. (2012). N-acetylcysteine prevents pulmonary edema and acute kidney injury in rats with sepsis submitted to mechanical ventilation. *Am. J. Physiol. Lung Cell. Mol. Physiol.* 302, L640–L650. doi: 10.1152/ajplung.00097.2011

Chen, I. J., Hee, S. W., Liao, C. H., Lin, S. Y., Su, L., Shun, C. T., et al. (2018). Targeting the 15-keto-PGE2-PTGR2 axis modulates systemic inflammation and survival in experimental sepsis. *Free Radic. Biol. Med.* 15, 113–126. doi: 10.1016/j.freeradbiomed.2017.11.016

Cunningham, P. N., Wang, Y., Guo, R., He, G., and Quigg, R. J. (2004). Role of Toll-like receptor 4 in endotoxin-induced acute renal failure. *J. Immunol.* 172, 2629–2635. doi: 10.4049/jimmunol.172.4.2629

Cuzzocrea, S., Mazzon, E., Di Paola, R., Esposito, E., Macarthur, H., Matuschak, G., et al. (2006). A role for nitric oxide-mediated peroxynitrite formation in a model of endotoxin-induced shock. *J. Pharmacol. Exp. Ther.* 319, 73–81. doi: 10.1124/jpet.106.108100

Dai, Z., Zhu, B., Yu, H., Jian, X., Peng, J., Fang, C., et al. (2019). Role of autophagy induced by arecoline in angiogenesis of oral submucous fibrosis. *Arch. Oral Biol.* 102, 7–15. doi: 10.1016/j.archoralbio

Doi, K., Leelahavanichkul, A., Yuen, P. S., and Star, R. A. (2009). Animal models of sepsis and sepsis-induced kidney injury. *J. Clin. Invest.* 119, 2868–2878. doi: 10.1172/JCI39421

Frei, R., Steinle, J., Birchler, T., Loeliger, S., Roduit, C., Steinhoff, D., et al. (2010). MHC class II molecules enhance Toll-like receptor mediated innate immune responses. *PLoS One* 5:e8808. doi: 10.1371/journal.pone.0008808

Gong, C., Li, Z., Qin, C., Bu, X., and Yu, J. (2016). Hyperin protects against LPS-induced acute kidney injury by inhibiting TLR4 and NLRP3 signaling pathways. *Oncotarget* 7, 82602–82608. doi: 10.18632/oncotarget.13010

Havakhah, S., Sadeghnia, H. R., Hajzadeh, M. A., Roshan, N. M., Shafiee, S., Hosseinzadeh, H., et al. (2014). Effect of *Nigella sativa* on ischemia-reperfusion induced rat kidney damage. *Iran. J. Basic Med. Sci.* 17, 986–992.

Heemskerk, S., Masereeuw, R., Russel, F. G., and Pickkers, P. (2009). Selective iNOS inhibition for the treatment of sepsis-induced acute kidney injury. *Nat. Rev. Nephrol.* 5, 629–640. doi: 10.1038/nrneph.2009.155

Huang, H., Aladelokun, O., Ideta, T., Giardina, C., Ellis, L. M., and Rosenberg, D. W. (2019). Inhibition of PGE2/EP4 receptor signaling enhances oxaliplatin efficacy in resistant colon cancer cells through modulation of oxidative stress. *Sci. Rep.* 9:4954. doi: 10.1038/s41598-019-40848-4

Jaworska, K., Ratajczak, J., Huang, L., Whalen, K., Yang, M., Stevens, B. K., et al. (2015). Both PD-1 ligands protect the kidney from ischemia reperfusion injury. *J. Immunol.* 194, 325–333. doi: 10.4049/jimmunol.1400497

Kim, H. J., Lee, S., Lee, H. Y., Won, H., Chang, S. H., and Nah, S. S. (2015). 15-hydroxyprostaglandin dehydrogenase is upregulated by hydroxychloroquine in rheumatoid arthritis fibroblast-like synoviocytes. *Mol. Med. Rep.* 12, 4141–4148. doi: 10.3892/mmr.2015.3931

Kim, Y. B., Ahn, J. M., Bae, W. J., Sung, C. O., and Lee, D. (2019). Functional loss of ARID1A is tightly associated with high PD-L1 expression in gastric cancer. *Int. J. Cancer* 145, 916–926. doi: 10.1002/ijc.32140

Klionsky, D. J., Abdelmohsen, K., Abe, A., Abedin, M. J., Abeliovich, H., Acevedo Arozena, A., et al. (2016). Guidelines for the use and interpretation of assays for monitoring autophagy (3rd edition). *Autophagy* 12, 1–222. doi: 10.1080/15548627.2015.1100356

Kojima, I., Tanaka, T., Inagi, R., Kato, H., Yamashita, T., Sakiyama, A., et al. (2007). Protective role of hypoxia-inducible factor-2α against ischemic damage and oxidative stress in the kidney. *J. Am. Soc. Nephrol.* 18, 1218–1226. doi: 10.1681/ASN.2006060639

Lerolle, N., Nochy, D., Guérot, E., Bruneval, P., Fagon, J. Y., Diehl, J. L., et al. (2010). Histopathology of septic shock induced acute kidney injury: apoptosis and leukocytic infiltration. *Intensive Care Med.* 36, 471–478. doi: 10.1007/s00134-009-1723-x

Li, N., Xie, H., Li, L., Wang, J., Fang, M., Yang, N., et al. (2014). Effects of honokiol on sepsis-induced acute kidney injury in an experimental model of sepsis in rats. *Inflammation* 37, 1191–1199. doi: 10.1007/s10753-014-9845-x

Li, T., Liu, Y., Zhao, J., Miao, S., Xu, Y., Liu, K., et al. (2017). Aggravation of acute kidney injury by mPGES-2 down regulation is associated with autophagy inhibition and enhanced apoptosis. *Sci. Rep.* 7:10247. doi: 10.1038/s41598-017-10271-8

Liu, Y., Jia, Z., Sun, Y., Zhou, L., Downton, M., Chen, R., et al. (2014). Postnatal regulation of 15-hydroxyprostaglandin dehydrogenase in the rat kidney. *Am. J. Physiol. Renal Physiol.* 307, F388–F395. doi: 10.1152/ajprenal.00512.2013

McCormick, J. J., King, K. E., Dokladny, K., and Mermier, C. M. (2019). Effect of acute aerobic exercise and rapamycin treatment on autophagy in peripheral blood mononuclear cells of adults with prediabetes. *Can. J. Diabetes* 43, 457–463. doi: 10.1016/j.jcjd.2019.04.005

Messaris, E., Memos, N., Chatzigianni, E., Kataki, A., Nikolopoulou, M., Manouras, A., et al. (2008). Apoptotic death of renal tubular cells in experimental sepsis. *Surg. Infect. (Larchmt).* 9, 377–388. doi: 10.1089/sur.2006.018

Noiri, E., Nakao, A., Uchida, K., Tsukahara, H., Ohno, M., Fujita, T., et al. (2001). Oxidative and nitrosative stress in acute renal ischemia. *Am. J. Physiol. Renal Physiol.* 281, F948–F957. doi: 10.1152/ajprenal.2001.281.5.F948

Noor, R., Mittal, S., and Iqbal, J. (2002). Superoxide dismutase-applications and relevance to human diseases. *Med. Sci. Monit.* 8, RA210–RA215.

Pathak, E., MacMillan-Crow, L. A., and Mayeux, P. R. (2012). Role of mitochondrial oxidants in an in vitro model of sepsis-induced renal injury. *J. Pharmacol. Exp. Ther.* 340, 192–201. doi: 10.1124/jpet.111.183756

Prowle, J. R. (2018). Sepsis-associated AKI. *Clin. J. Am. Soc. Nephrol.* 13, 339–342. doi: 10.2215/CJN.07310717

Prowle, J. R., and Bellomo, R. (2015). Sepsis-associated acute kidney injury: macrohemodynamic and microhemodynamic alterations in the renal circulation. *Semin. Nephrol.* 35, 64–74. doi: 10.1016/j.semnephrol.2015.01.007

Shum, H. P., Yan, W. W., and Chan, T. M. (2016). Recent knowledge on the pathophysiology of septic acute kidney injury: a narrative review. *J. Crit. Care* 31, 82–89. doi: 10.1016/j.jcrc.2018.01.002

Song, Y., Tao, Q., Yu, L., Li, L., Bai, T., Song, X., et al. (2018). Activation of autophagy contributes to the renoprotective effect of postconditioning on acute kidney injury and renal fibrosis. *Biochem. Biophys. Res. Commun.* 504, 641–646. doi: 10.1016/j.bbrc.2018.09.003

Suzuki, C., Isaka, Y., Takabatake, Y., Tanaka, H., Koike, M., Shibata, M., et al. (2008). Participation of autophagy in renal ischemia/reperfusion injury. *Biochem. Biophys. Res. Commun.* 368, 100–106. doi: 10.1016/j.bbrc.2008.01.059

Tai, H. (2011). Prostaglandin catabolic enzymes as tumor suppressors. *Cancer Metastasis Rev.* 30, 409–417. doi: 10.1007/s10555-011-9314-z

Thomas, M. E., Blaine, C., Dawnay, A., Devonald, M. A., Ftouh, S., Laing, C., et al. (2015). The definition of acute kidney injury and its use in practice. *Kidney Int.* 87, 62–73. doi: 10.1038/ki.2014.328

Turkmen, K., Martin, J., Akcay, A., Nguyen, Q., Ravichandran, K., Faubel, S., et al. (2011). Apoptosis and autophagy in cold preservation ischemia. *Transplantation* 91, 1192–1197. doi: 10.1097/TP.0b013e31821ab9c8

Viñas, J. L., and Sola, A., (2006). Mitochondrial NOS upregulation during renal I/R causes apoptosis in a peroxynitrite-dependent manner. *Kidney Int.* 69, 1403–1409. doi: 10.1038/sj.ki.5000361

Walker, L. M., Walker, P. D., Imam, S. Z., Ali, S. F., and Mayeux, P. R. (2000). Evidence for peroxynitrite formation in renal ischemia-reperfusion injury: studies with the inducible nitric oxide synthase inhibitor L-N(6)-(1-Iminoethyl)lysine. *J. Pharmacol. Exp. Ther.* 295, 417–422.

Wang, W., Jittikanont, S., Falk, S. A., Li, P., Feng, L., Gengaro, P. E., et al. (2003). Interaction among nitric oxide, reactive oxygen species, and antioxidants during endotoxemia-related acute renal failure. *Am. J. Physiol. Renal Physiol.* 284, F532–F537. doi: 10.1152/ajprenal.00323.2002

Wei, Q., Bhatt, K., He, H. Z., Mi, Q. S., Haase, V. H., and Dong, Z. (2010). Targeted deletion of dicer from proximal tubules protects against renal ischemia-reperfusion injury. *J. Am. Soc. Nephrol.* 21, 756–761. doi: 10.1681/ASN.2009070718

Wu, H., Chen, G., Wyburn, K. R., Yin, J., Bertolino, P., Eris, J. M., et al. (2007). TLR4 activation mediates kidney ischemia/reperfusion injury. *J. Clin. Invest* 117, 2847–2859. doi: 10.1172/JCI31008

Wu, L., and Mayeux, P. R. (2007). Effects of the inducible nitric-oxide synthase inhibitor L-N(6)-(1-iminoethyl)-lysine on microcirculation and reactive nitrogen species generation in the kidney following lipopolysaccharide administration in mice. *J. Pharmacol. Exp. Ther.* 320, 1061–1067. doi: 10.1124/jpet.106.117184

Wu, X., Guo, R., Wang, Y., and Cunningham, P. N. (2007). The role of ICAM-1 in endotoxin-induced acute renal failure. *Am. J. Physiol. Renal Physiol.* 293, F1262–F1271. doi: 10.1152/ajprenal.00445.2006

Yao, B., Xu, J., Harris, R. C., and Zhang, M. Z. (2008). Renal localization and regulation of 15-hydroxyprostaglandin dehydrogenase. *Am. J. Physiol. Renal Physiol.* 294, F433–F439. doi: 10.1152/ajprenal.00436.2007

Zarjou, A., and Agarwal, A. (2011). Sepsis and acute kidney injury. *J. Am. Soc. Nephrol.* 22, 999–1006. doi: 10.1681/ASN.2010050484

Zhang, Y., Desai, A., Yang, S. Y., Bae, K. B., Antczak, M. I., Fink, S. P., et al. (2015). TISSUE REGENERATION. Inhibition of the prostaglandin-degrading enzyme 15-PGDH potentiates tissue regeneration. *Science* 348:aaa2340. doi: 10.1126/science.aaa2340

Conflict of Interest: The authors declare that the research was conducted in the absence of any commercial or financial relationships that could be construed as a potential conflict of interest.

Copyright © 2020 Miao, Lv, Liu, Zhao, Li, Wang, Xu, Wang, Xiao and Zhang. This is an open-access article distributed under the terms of the Creative Commons Attribution License (CC BY). The use, distribution or reproduction in other forums is permitted, provided the original author(s) and the copyright owner(s) are credited and that the original publication in this journal is cited, in accordance with accepted academic practice. No use, distribution or reproduction is permitted which does not comply with these terms.

frontiers in Pharmacology

REVIEW
published: 17 March 2020
doi: 10.3389/fphar.2020.00265

Recent Insights Into SREBP as a Direct Mediator of Kidney Fibrosis via Lipid-Independent Pathways

*Debra Dorotea[1], Daisuke Koya[2] and Hunjoo Ha[1]**

[1] Graduate School of Pharmaceutical Sciences, College of Pharmacy, Ewha Womans University, Seoul, South Korea,
[2] Department of Internal Medicine, Kanazawa Medical University, Ishikawa, Japan

Sterol regulatory-element binding proteins (SREBPs) are classical regulators of cellular lipid metabolism in the kidney and other tissues. SREBPs are currently recognized as versatile transcription factors involved in a myriad of cellular processes. Meanwhile, SREBPs have been recognized to mediate lipotoxicity, contributing to the progression of kidney diseases. SREBP1 has been shown to bind to the promoter region of TGFβ, a major pro-fibrotic signaling mechanism in the kidney. Conversely, TGFβ activates SREBP1 transcriptional activity suggesting a positive feedback loop of SREBP1 in TGFβ signaling. Public ChIP-seq data revealed numerous non-lipid transcriptional targets of SREBPs that plausibly play roles in progressive kidney disease and fibrosis. This review provides new insights into SREBP as a mediator of kidney fibrosis via lipid-independent pathways.

Keywords: SREBP, TGFβ, lipotoxicity, renal lipid, kidney fibrosis

OPEN ACCESS

Edited by:
Md. Abdul Hye Khan,
Medical College of Wisconsin,
United States

Reviewed by:
Chunming Cheng,
The Ohio State University Comprehensive Cancer Center,
United States
Xiang Cheng,
The Ohio State University,
United States

****Correspondence:***
Hunjoo Ha
hha@ewha.ac.kr

Specialty section:
This article was submitted to Renal Pharmacology, a section of the journal Frontiers in Pharmacology

Received: *07 November 2019*
Accepted: *24 February 2020*
Published: *17 March 2020*

Citation:
Dorotea D, Koya D and Ha H (2020) Recent Insights Into SREBP as a Direct Mediator of Kidney Fibrosis via Lipid-Independent Pathways. Front. Pharmacol. 11:265. doi: 10.3389/fphar.2020.00265

INTRODUCTION

Numerous studies have revealed the molecular mechanisms of sterol regulatory-element binding proteins (SREBPs) as transcription factors that critically regulate lipid homeostasis (Brown and Goldstein, 1997). The extended role of SREBPs within the last three decades has been attributed to its versatility in integrating multiple cellular signals to control, not only lipogenesis but also unexpected pathways that are important for diverse biological processes, such as endoplasmic reticulum (ER) stress, inflammation, autophagy, and apoptosis. Accordingly, SREBPs contribute to the pathogenesis of various diseases, such as diabetes mellitus, fatty liver disease, chronic kidney disease (CKD), neurodegenerative diseases, and cancers (Shimano and Sato, 2017).

CKD, a major public health problem in many countries (Webster et al., 2017), is defined by persistent urine abnormalities, structural abnormalities or impaired excretory renal function, which suggests a loss of functional nephrons (Romagnani et al., 2017). To date, renin-angiotensin system inhibitors are the mainstay of therapeutic options available to reduce albuminuria and slow the progression of CKD. However, these drugs show limitations in delaying the onset of kidney fibrosis, a common feature of end-stage kidney disease (Breyer and Susztak, 2016). Therefore, it remains interesting to explore the important target that mediates the disease progression, which can be further exploited to develop novel disease-modifying therapies.

Various factors, such as infiltrating immune cells, albuminuria, and glucosuria in diabetes, have been well recognized to activate proximal tubular epithelial cells, resulting in the secretion of pro-inflammatory and pro-fibrotic mediators that further promote interstitial inflammation and fibrosis development (Romagnani et al., 2017). Meanwhile, lipid accumulation in tubular cells has been associated with an increase in reactive oxygen species production, the loss of ATP production, apoptosis, and elevated inflammatory cytokines, which contribute to the development of tissue

fibrosis (Simon and Hertig, 2015). In earlier studies, SREBP1 activation was shown to induce lipotoxicity that consequently extended SREBP-related pathology to include inflammation and fibrosis in the kidney (Sun et al., 2002). SREBP1 was further revealed to bind to the promoter region of transforming growth factor (TGF)β, a major pro-fibrotic signaling mechanism in the kidney (Uttarwar et al., 2012). Thus, SREBPs appear to mediate the progression of CKD via both lipid-dependent and -independent pathways. This review summarized the recent findings involving the TGFβ signaling pathway as a regulatory target of SREBP and predicts other putative target genes of SREBP in mediating kidney fibrosis.

SREBPS AS CLASSIC MEDIATORS OF LIPOTOXICITY

The SREBP Family

SREBPs are a family of membrane-bound transcription factors involved in lipid homeostasis. Three isoforms of SREBPs, SREBP1a, -1c, and -2, are encoded by two different genes. SREBP1a and -1c originate from different promotors of sterol regulatory element-binding transcription factor (SREBF)1 genes, whereas SREBP2 is derived from the SREBF2 gene (Goldstein et al., 2006). SREBP1a stimulates global lipid synthesis in proliferating cells, and SREBP1c plays a major role in the nutritional regulation of fatty acid and triglyceride (TG) synthesis in lipogenic organs, such as the liver. In contrast, SREBP2 ubiquitously regulates sterol synthesis in tissues (Shimano et al., 1997; Horton et al., 2002).

SREBPs are bHLH-LZ (basic-helix-loop-helix-leucine zipper) transcription factors, synthesized as inactive precursors bound to ER membranes. Each precursor is organized into three domains: (1) an NH2-terminal domain containing the transactivation domain, a region rich in serine and proline, and the bHLH-LZ region for DNA binding and dimerization; (2) two hydrophobic transmembrane segments projected into the ER lumen; and (3) a COOH-terminal domain (Goldstein et al., 2006; **Figure 1**).

Proteolytic Activation of SREBPs

Under basal conditions, the C-terminal domain of SREBPs binds to SREBP-cleavage activating protein (SCAP) in the ER membrane. This SREBP-SCAP complex interacts with insulin-induced gene 1 protein (INSIG1) and INSIG2 (Yabe et al., 2002; Yang et al., 2002). In the presence of high cellular cholesterol and oxycholesterol levels, INSIGs become stable and bind to SREBP-SCAP creating a complex retained in the ER membrane. When the level of sterols is low, INSIGs are ubiquitylated by the associated E3 ligases and rapidly degraded (Gong et al., 2006). Meanwhile, the proteolytic activation of SREBP1 is induced by insulin and high glucose and inhibited by polyunsaturated fatty acids (PUFAs) (Nakakuki et al., 2014; Cheng et al., 2015). Insulin-induced Akt activation is shown to decrease INSIG2a protein pools, resulting in increased ER-to-Golgi transport of the SCAP-SREBP1c complex (Yellaturu et al., 2009). SCAP escorts SREBP insertion on ER transport vesicles containing COP II vesicle coat protein. The SREBP-SCAP complex is then transported to the Golgi apparatus (Sun et al., 2005). In the Golgi, the ER luminal loop of SREBP is initially cleaved by site-1 protease (S1P), a membrane-bound serine protease. Subsequent cleavage by site-2 protease (S2P), a Zn^{2+} metalloprotease, generates transcriptionally active N-terminal domains (Ye et al., 2000), which are translocated to the nucleus mediated via importin β (Lee et al., 2003) (**Figure 2**).

Several kinases have also been reported to be involved in the regulation of proteolytic activation. PAS kinase (PASK), a serine/threonine kinase, is required for the proteolytic maturation of SREBP1c in cultured cells and mice and rat liver. However, the detailed signaling mechanism and its effect on the stability or transcriptional activity of nuclear SREBP1c have not been fully investigated (Wu et al., 2014), whereas AMP-activated protein kinase (AMPK) has been recently identified as an upstream regulator of INSIG1. AMPK phosphorylates INSIG1 (Thr222), abrogates its interaction with E3 ubiquitin ligase gp78, and represses its ubiquitination and degradation. Increased INSIG1 stabilization eventually inhibits the cleavage and processing of SREBP1 (Han et al., 2019).

Regulation of SREBPs Synthesis and Nuclear Activity

SREBP1c gene transcription is activated by the liver X receptor (LXR), which is modulated by insulin, PUFAs, and oxysterols. The LXR-retinoid X receptor heterodimer interacts with the LXR-responsive elements located in the SREBP1c promoter, initiating SREBP1c gene transcription (Yoshikawa et al., 2001). Activation of the farnesoid X receptor (FXR) induces small heterodimer partner (SHP) expression, leading to inhibition of LXR and reduced SREBP1c expression (Watanabe et al., 2004; **Figure 3**).

The transcription of SREBP target genes is tightly regulated by nuclear SREBP stability (Hirano et al., 2001). Mammalian target of rapamycin complex 1 (mTORC1), a major downstream element of insulin-induced phosphatidylinositol 3-kinase (PI3K)/Akt, activates SREBP1 depending on its S6-kinase 1 activity (Düvel et al., 2010). mTORC1 also promotes SREBP via the phosphorylation of lipin1, a phosphatidic acid phosphatase. Dephosphorylated lipin-1 triggers lipin-1 nuclear localization, reduces nuclear SREBP, and alters the localization of SREBP to the nuclear periphery (Peterson et al., 2011). In addition, nuclear SREBPs undergo post-translational modifications. Glycogen synthase kinase 3 (GSK3) phosphorylates nuclear SREBP1a (Ser-434), which serves as a recognition motif for Fbw7 ubiquitin ligases, leading to SREBP1a degradation (Bengoechea-Alonso and Ericsson, 2009). AMPK directly phosphorylates both precursor and nuclear SREBP1c (Ser372), decreasing SREBP1c cleavage and nuclear translocation (Li Y. et al., 2011). NAD^{+}-dependent deacetylase Sirtuin 1 (SIRT1) deacetylates and inhibits SREBP1c transactivation by enhancing ubiquitination (Bengoechea-Alonso and Ericsson, 2009; **Figure 3**).

Furthermore, cyclin-dependent kinase 8 (CDK8) and its regulatory partner cyclin C (CycC) have been identified to cause the phosphorylation of nuclear SREBP1c at a conserved

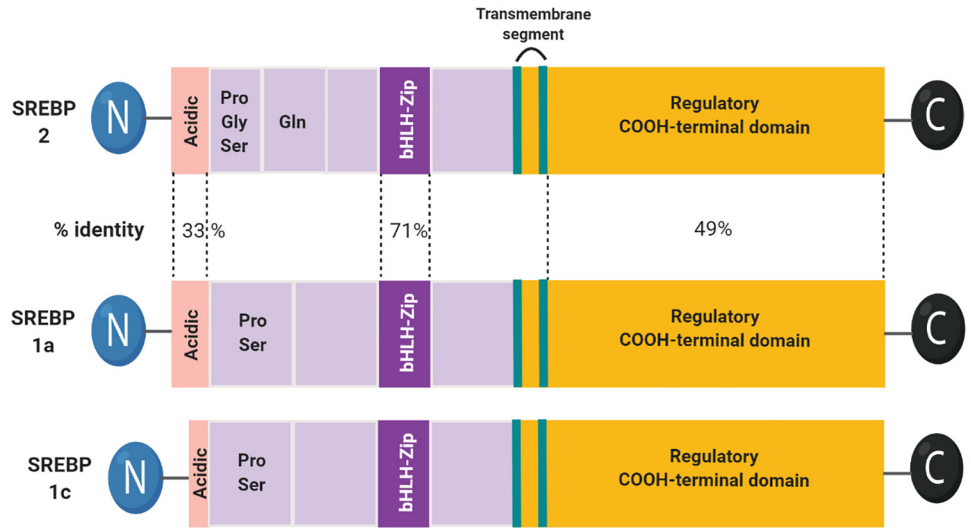

FIGURE 1 | Domain structure of the SREBP family. The structure of SREBP1c is highly similar to SREBP1a. SREBP1c has a shorter transactivation domain in the N-terminus.

threonine residue (T402), leading to increased nuclear SREBP1c ubiquitination and degradation. Interestingly, CDK8 and CycC are negatively regulated by feeding and insulin, the most widely studied stimuli that promote SREBP1 activation (Zhao et al., 2012). Protein kinase A (PKA) also regulates nuclear SREBP1c stability. Under fasting conditions, glucagon-induced PKA activation stimulates the phosphorylation of SREBP1c (Ser308) (Lee et al., 2014) and SREBP1a (Ser331/332) (Dong et al., 2014). This promotes the sumoylation of SREBP1c at Lys98 by the mammalian protein inhibitor of activated STAT (PIAS)y, a SUMO E3 ligase. Sumoylated SREBP1c is readily degraded by ubiquitination, which leads to decreased hepatic lipid metabolism (Lee et al., 2014).

Classical DNA Binding Sites of SREBPs

Intra-nuclear SREBPs were initially found to bind to HMG CoA reductase (HMGCR) and LDL receptor (LDLR) gene promoters, known as sterol response elements (SREs). The original SRE sequence is 5′-ATCACCCCAC-3′ (Hua et al., 1993). In addition to non-palindromic SREs, the SREBPs bind to and activate classic palindromic E-boxes (CAXXTG sequence) containing promoter (Kim et al., 1995). This dual binding specificity allows SREBPs to bind with various cholesterolgenic and lipogenic genes, whose SREs are relatively similar to the original SRE sequence found in the LDLR gene. The sequences of the SREBP binding and activation sites vary considerably and are designated SRE-like sequences (Shimano, 2001; **Figure 4**).

SREBP1 activates lipogenic genes, whereas SREBP2 is more specific for cholesterolgenic genes. SREBP1a and -2 are equally active for SRE, whereas SREBP1c is inactive. However, only SREBP1a and -1c are active for E-box (Amemiya-Kudo et al., 2000). Due to the high similarity between the N-terminal domains of the three isoforms, all SREBP isoforms can activate each of their target genes but with different efficacies. As SREBP1c contains a shorter transactivation domain, it is weaker than SREBP1a and SREBP2. In contrast, the C-terminal domains of SREBP1 and SREP-2 are relatively less conserved compared to other domains, which may lead to minor differences in the sterol regulation mechanism (Shimano et al., 1997; Pai et al., 1998).

SREBPs Mediate Renal Lipotoxicity

Altered lipid metabolism has been linked to the progression of both acute and CKDs. Microarray analysis of human kidney biopsies in the Nephroseq database[1] revealed a higher expression of SREBF1 and SREBF2 in patients with CKD or diabetic kidney disease (DKD) than in normal patients according to the results reported in *Ju CKD Glom* (Ju et al., 2013), *Nakagawa CKD* (Nakagawa et al., 2015), and *Woroniecka Diabetes Glom* (Woroniecka et al., 2011; Na et al., 2015). Furthermore, nutrient and genetic manipulations in experimental animal studies have demonstrated increased SREBP expression, which was associated with renal lipid accumulation, as well as progressive kidney injuries (**Table 1**).

The accumulation of non-esterified fatty acids and their metabolites in the kidney leads to cellular dysfunction and death through various mechanisms, such as altered mitochondrial energy coupling, excessive reactive oxygen species generation, and stimulation of ER stress (Murea et al., 2010). Defective fatty acid oxidation (FAO) in renal tubular epithelial cells particularly plays a crucial role in the progression of kidney fibrosis. Genome-wide transcriptome studies of fibrotic human kidneys revealed a lower expression of key enzymes and regulators of FAO (Kang et al., 2015). Kidney biopsies of patients with DKD demonstrated abnormal lipid metabolism, which was

[1]http://www.nephroseq.org/

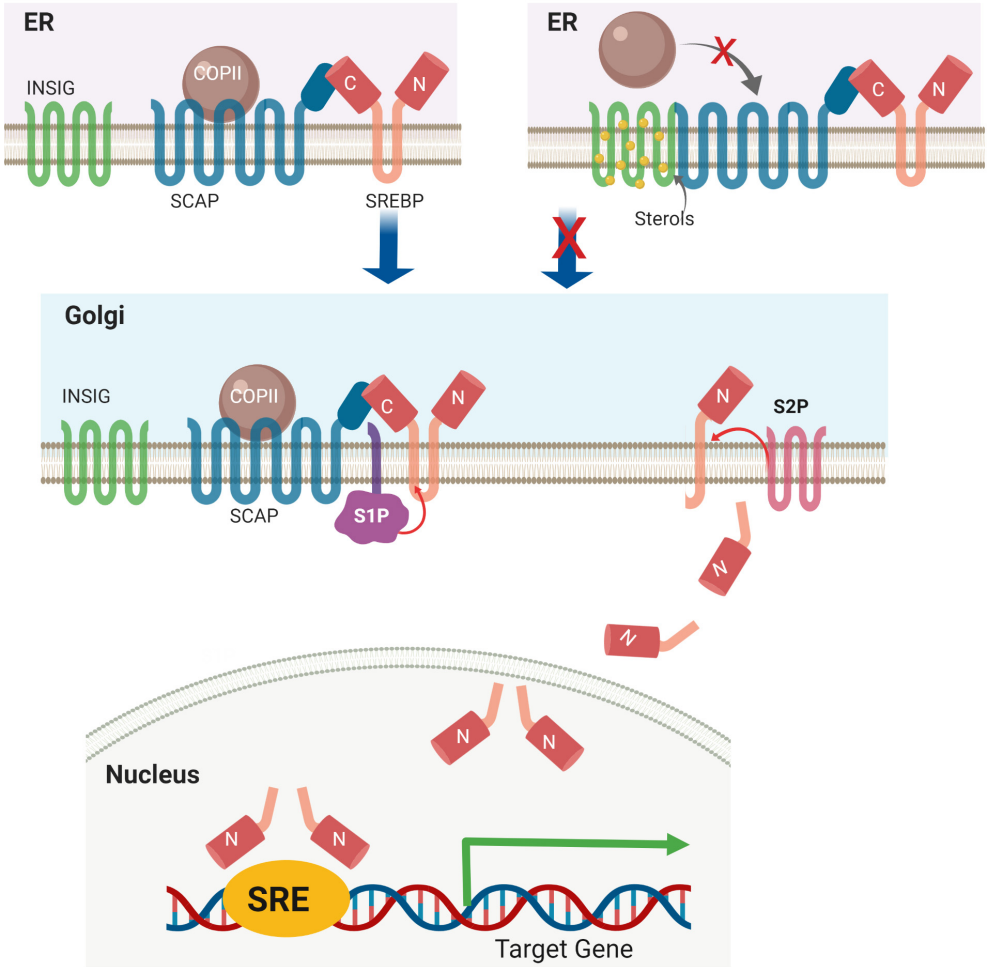

FIGURE 2 | Sterol-mediated proteolytic activation of SREBP. Under basal conditions, the SREBP-SCAP-INSIG complex is retained in the ER membrane. High levels of cellular sterol induce INSIG degradation, followed by translocation of the SREBP-SCAP complex from the ER to the Golgi apparatus. In the Golgi, SREBP is activated via a two-step proteolytic mechanism with S1P and S2P.

significantly correlated with a decline in glomerular filtration rate and kidney inflammation. The genes involved in the FAO pathway, TG hydrolysis, and cholesterol efflux were downregulated, whereas the cholesterol uptake receptor-related gene expression was elevated in the kidneys of human DKD patients (Herman-Edelstein et al., 2014).

SREBP-Induced Lipotoxicity Also Applies to Other Organs

In addition to kidney diseases, which are the focus of our review, the lipid accumulation induced by SREBP has been demonstrated to aggravate disease progression in other organs, such as the liver and lungs. Increased SREBP activity in the liver causes hepatic steatosis (Shimomura et al., 1999a), that can eventually progress to liver fibrosis and liver failure (Cohen et al., 2009). Specifically in the liver, the synthesis and proteolytic processing of SREBP1c is mainly triggered by insulin (Shimomura et al., 1999b; Brown and Goldstein, 2008). When insulin resistance is evident in peripheral tissues, insulin continues to activate SREBP1c transcription and proteolytic cleavage. Thus, the upregulated nuclear SREBP1c enhances lipogenic gene expression, fatty acid synthesis, and TG accumulation (Shimomura et al., 1999a, 2000). Meanwhile, lipid homeostasis in the lung is precisely regulated to maintain proper lung function, partially regulated by SREBP1c expression. The deletion of SCAP was shown to inhibit SREBP activity in alveolar type 2 cells and enhance neutral lipid accumulation in the lung fibroblasts of fetal and postnatal mice (Besnard et al., 2009). Double Insig1 and Insig2 gene deletions in alveolar type 2 cells activated SREBP1, leading to cholesterol esters and TG accumulation in type 2 epithelial cells and alveolar macrophages. Enhancing lipogenesis in respiratory epithelial cells resulted in lipotoxicity-related lung inflammation, airspace abnormalities, and tissue remodeling (Plantier et al., 2012). Aside from this lipid-dependent pathway, to our knowledge, there has been no study in the liver and lungs elucidating the mechanism of SREBP in mediating fibrotic signaling through a lipid-independent pathway.

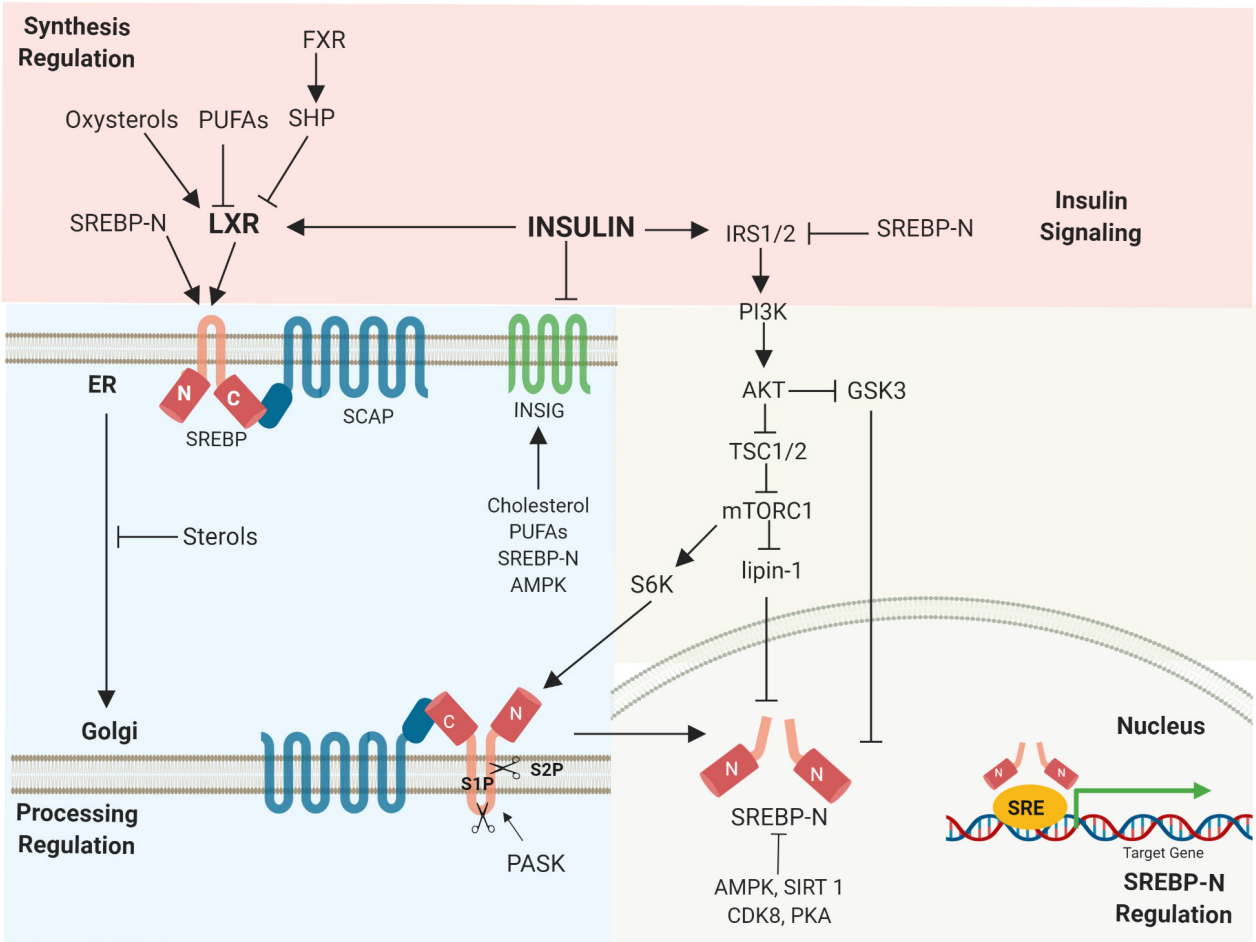

FIGURE 3 | Regulation of SREBPs occurs at various stages. Multiple signals regulate SREBP synthesis, proteolytic activation, transcriptional activity, as well as degradation. Activated, nuclear SREBP is tightly controlled by post-translational modifications.

SREBP AS A PRO-FIBROTIC MEDIATOR IN THE KIDNEY

Although most of the early works have already shown the role of SREBP in lipotoxicity-induced progressive tissue injuries and fibrosis development, a plausible role for SREBP in directly mediating the activation of fibrotic signaling has been underscored. SREBP was initially reported to induce extracellular matrix (ECM) gene transcription in fibroblasts. The promoter of collagen (col) VI (α1) contains a growth arrest-responsive region (GARR), comprised of repeat GA-box motifs (GGGGAGGG). In NIH3T3 fibroblasts cultured in serum-free medium, SREBP bound to GARR and induced Col VI (α1) transcription (Ferrari et al., 2004). Plasminogen activator inhibitor 1 (PAI1), a serine protease with pro-fibrotic properties, has been also identified as a transcriptional target of SREBP1c in 3T3-L1 adipocytes (Lay et al., 2002). Following these precedent reports, a series of studies in the kidney were performed to further demonstrate a transcriptional effect of SREBP on the fibrotic signaling pathway.

Non-sterol-mediated SREBP Activation

As described in the previous section, the activation of SREBP is classically regulated by cellular sterol levels. Other tissue-injury stimuli, such as mechanical cues (Liu et al., 2002; Lin et al., 2003) and high glucose (HG) (Hasty et al., 2000; Guillet-Deniau et al., 2004; Uttarwar et al., 2012), have been reported to induce SREBP activation, as well. However, the signaling mechanism of non-sterol-mediated SREBP activation appears to depend on the type of stimulus. SREBP1 activation in endothelial cells exposed to shear stress requires signaling via β1 integrin, focal adhesion kinase, and c-Src (Liu et al., 2002). The shear stress activates SREBP2 in vascular endothelial cells via RhoA/Rho-kinase signaling. The Rho-ROCK-LIMK-cofilin pathway enhances the actin assembly needed for SREBP transport from the ER to Golgi (Lin et al., 2003). In recent work, ECM stiffening and geranylgeranylated RhoA-dependent acto-myosin contraction were also shown to activate AMPK, resulting in inhibition of SREBP1 activation (Bertolio et al., 2019).

Glucose has been shown to activate SREBP1 in renal tubular epithelial cell lines (Jun et al., 2009). Several studies

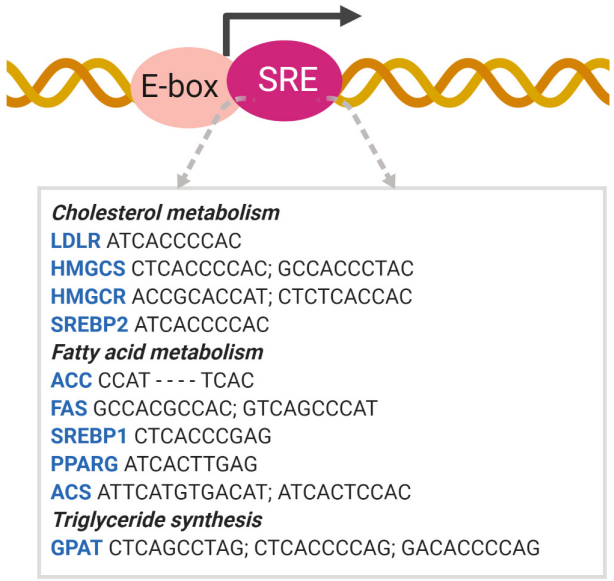

FIGURE 4 | SREBP binds to the SRE promoter. SREBP binding to the SRE promoter activates the transcription of target genes involved in lipid metabolism (Shimano, 2001). ACC acetyl-CoA carboxylase; ACS acetyl-CoA synthetase; GPAT glycerol-3-phosphate acyltransferase; HMGCS HMG-CoA synthase; PPAR peroxisome proliferator-activated receptor.

have suggested that epidermal growth factor receptor (EGFR)/PI3K/Akt (Wu et al., 2007, 2009) and RhoA/Rho-kinase (Peng et al., 2008) signaling mediate HG-induced TGFβ upregulation and ECM accumulation in the kidney. A mechanistic study with primary rat mesangial cells (MCs) confirmed the role of these signaling in mediating HG-induced SREBP1 activation, which leads to TGFβ activation. S1P and SCAP were required for SREBP1 activation, as it was blocked by chemical inhibitors of S1P and SCAP (Wang T. N. et al., 2015). Despite the technical limitations associated with the differentiation of the two isoforms of SREBP1, these studies suggested that multiple factors activate SREBP1, which is associated with kidney injuries. By utilizing more recent and sensitive techniques, it remains challenging to differentiate the SREBP isoforms activated by specific stimuli and the respective downstream signaling in the kidney.

SREBP Regulates TGFβ Activity

Particularly in the kidney, SREBP has then been shown to be activated by several non-sterol stimuli and to contribute to the activation of fibrotic signaling, i.e., TGFβ, a multifunctional cytokine that classically plays a major role in progressive kidney fibrosis (Sureshbabu et al., 2016).

SREBP Induces TGFβ Transcriptional Activity

HG increased TGFβ activity via SREBP1 activation in primary rat MCs. As early as 30 min and persisting up to 6 h, 30 mM HG activated SREBPs based on the detection of its mature form (nSREBP1), whereas SREBP2 was not activated. HG promoted SREBP1 binding to the TGFβ promoter, which contains a putative SREBP1 binding site, SRE. This binding was halted by fatostatin and dominant-negative SREBP1a Y335A. Connective tissue growth factor (CTGF) was detected as the downstream target of TGFβ activation. Interestingly, TGFβ promoter analysis revealed that a potential SRE site was within the first 100 base pairs of the start codon. The site is located apparently in close proximity to the Sp1 site, a well-known coactivator of SREBP (Uttarwar et al., 2012).

Angiotensin (Ang)-II also stimulated SREBP1-induced TGFβ signaling in primary rat MC cultures. Treatment with 100 nM Ang II induced SREBP1 maturation, activated SREBP1 as detected by responsive SRE, and increased the SREBP downstream target, fatty acid synthase (FAS), leading to lipid accumulation. Then, Ang II activated two parallel signals essential for TGFβ promoter activation, ER stress-induced SREBP1 activation and EGFR-mediated activation of co-transcription factor Sp1. ER stress and SREBP1 activation were detected in the glomeruli of Ang II infused mice. SREBP1 inhibition by fatostatin prevented Ang II-induced TGFβ upregulation and ECM accumulation. Mechanistically, Ang II-induced SREBP1 activation in MC culture required angiotensin (AT)1 receptor/PI3K/Akt signaling (Wang T. N. et al., 2015). PI3K and Akt are the downstream signaling molecules of AT1 receptor via coupling to G-proteins that positively regulate SREBP activation (Yellaturu et al., 2009; Uttarwar et al., 2012). Ang II-induced ER stress, exhibited by increased p-eIF2α and GRP78 expression, also activated SREBP1 in MC culture. Inhibition of ER stress or SREBP1 prevented Ang II-induced SREBP1 binding to the TGFβ promoter (Wang T. N. et al., 2015). Another study showed that ER stress decreased INSIG via eIF2α translational inhibition, resulting in the proteolytic activation of SCAP/SREBP. GRP78 retained SCAP/SREBP1 in the ER via direct interaction, which was disrupted during ER stress (Colgan et al., 2011). However, this Ang II/ER stress/SREBP activation needs to be confirmed in experimental animal models to provide stronger evidence. As Ang II might also induce ER stress in podocytes (Ha et al., 2015) and proximal tubular epithelial cells (Wang J. et al., 2015), other studies with these kidney cell subtypes are needed, as well. EGFR may be an important second signal in TGFβ upregulation via activation of the SREBP1 co-transcription factor Sp1. However, EGFR was not required for either SREBP1 activation or TGFβ promoter binding by SREBP1 (Wang T. N. et al., 2015).

A recent study suggested the role of lysophosphatidic acid (LPA) in SREBP-induced TGFβ activity (Li et al., 2017). LPA is a small, ubiquitous phospholipid that mediates pro-inflammatory and pro-fibrotic signaling in the kidney (Zhang et al., 2017). TGFβ and Smad-2/3 phosphorylation were upregulated in the renal cortex of db/db mice and SV40 MES13 MCs stimulated with LPA. LPA bound to its receptor and activated PI3K/Akt phosphorylation, leading to phosphorylation of GSK3β at Ser9. The inactive, phosphorylated GSK3β decreased SREBP1 degradation, induced its nuclear translocation, and eventually triggered TGFβ transcriptional activity. Inhibition of either LPA receptor or SCAP by fatostatin significantly decreased TGFβ signaling and ECM accumulation in mesangial cells (Li et al., 2017).

TABLE 1 | SREBPs and their target gene expressions mediating renal lipid accumulation and disease progression.

Experimental condition	SREBP in kidney	Expression of target genes	Lipid content in kidney	Renal pathology	Metabolic changes	References
TYPE 1 DIABETES MELLITUS						
STZ*-induced SD* rats	P: ↑1	P: ↑ FAS	TG ↑2-fold	↑ Proteinuria P: ↑ COL4A1, FN1*		Sun et al., 2002
Ins2 Akita mice	P: ↑1, 2		TC* ↑1.6-fold, TG ↑1.4-fold	↑ Urinary albumin/creatinine P: ↑ COL4A1, FN1* R: ↑ *Tgfb, Pai1, Vegf*, Tnfa* R: ↓ *Synpo*, Nphs2**		Proctor et al., 2006
OVE26 mice	R: ↑1c, 2	R: ↑*Acc, Fas, Hmgcr* R: ↑ *Pparg*		R: ↑ *Fn1*, Col4a1, Il6, Tnfa* R: ↓ *Synpo*, Nphs2**		Proctor et al., 2006
TYPE 2 DIABETES MELLITUS						
FVB$^{db/db}$mice	P: ↑ n 1,2	R: ↑ *Fas, Acc, Hmgcr, Ldlr*	TC* ↑2.2-fold TG ↑2.4-fold	↑ Urinary albumin/creatinine ↑ GBM* thickness, podocyte foot process length R: ↑ *Tgfb, Pai1, Vegf**	BW* TC* ↑2.1-fold TG ↑1.6-fold	Wang et al., 2005
C57BL/6J mice with HFD*	P: ↑n1,2 R: ↑1a, 1c, 2	R: ↑ *Fas, Acc, Hmgcr*	TC* ↑1.2-fold TG ↑3-fold	↑ Urinary albumin/creatinine P: ↑ COL4A1, FN1*, PAI1, VEGF*	BW* TC* ↑1.4-fold TG ↑1.2-fold Insulin ↑13.4-fold	Jiang et al., 2005c
STZ*-induced SD* rats fed with HFD*& sucrose diet	P: ↑2, n2 R: ↑2	P: ↑ HMGCR, LDLR		↑ Serum Creatinine, BUN*, Albuminuria, Urinary NGAL*	TC* ↑6.8-fold TG ↑5-fold LDL* ↑6.2-fold	Sun et al., 2013
HYPERTENSION						
AngII infused SD* rats	P: ↑1		TC* ↑1.5-fold TG ↑1.5-fold	P: ↑ TGFB	BP* TC* ↑1.3-fold TG ↑2-fold	Saito et al., 2005
AGING						
C57BL/6 mice, 23 months vs. 3 months	P: ↑n1, n2 R: ↑1c	P: ↑ HMGCR R: ↑ *Hmgcr, Ldlr*	TC* ↑3-fold TG ↑3-fold	↑ Urinary albumin/creatinine ↑ GBM* thickness, podocyte width and effacement P: ↑ COL4A1, FN1*		Jiang et al., 2005a
F344BN rats, 24 months vs. 4 months	P: ↑n1, n2	P: ↑ HMGCR	TC* ↑1.5-fold TG ↑2.6-fold	↑ Urinary albumin/creatinine P: ↑ COL4A1, FN1* CTGF, PAI1, VEGF*	TC* ↑1.5-fold TG ↑2-fold Leptin ↑5.6-fold	Jiang et al., 2005b
SD* rats, 24 months vs. 6 months	P: ↑1		TG ↑2-fold	↑ Serum Urea, Serum KIM1* P: ↑ COL1A1, COL4A1, FN1*		Chung et al., 2018
GENETICALLY MODIFIED MICE						
Transgenic SREBP1a	P: ↑ 1	R: ↑*Fas, Acc*	TC* ↑1.2-fold TG ↑2.5-fold	↑ Urinary albumin/Creatinine P: ↑ COL4A1, FN1* TGFB, VEGF*	Liver TG ↑20-fold TC* ↑3.5-fold	Sun et al., 2002
SREBP1c knockout			TG ↓ 1.7-fold (vs WT* in HFD* group)	R: ↓ *Col4a1, Fn1*, Pai1, Vegf** (vs WT* in HFD* group)	TG ↓ ↑1.7-fold TC* ↓1.2-fold (vs WT* in ND* group)	Jiang et al., 2005c

**BP, blood pressure; BUN, blood urea nitrogen; BW, body weight; FN1, fibronectin; GBM, glomerular basement membrane; HFD, high-fat diet; KIM1, kidney injury molecule; LDL, low-density lipoprotein; n,nucleus; ND, normal diet; NGAL, neutrophil gelatinase-associated lipocalin; NPHS2, stomatin family member, podocin; P, protein; R, mRNA; SD rats, Sprague Dawley rats; STZ, streptozotocin; SYNPO,synaptopodin; TC, total cholesterol; VEGF, vascular endothelial growth factor; WT, wild-type.*

One should be aware that the cited evidence linking SREBP and TGFβ activation was derived from different experimental conditions or biological contexts. Those studies utilized EMSA and ChiP to discover the binding site motif, but the methods were limited by the skewed distribution of the genomic sequence and the inability to distinguish direct and indirect binding of the transcription factor (Lambert et al., 2018). A combination of methods with different throughput and information content, e.g., ChiP combined with SELEX, protein binding microarray/PBM, and MITOMI, are ideally necessary to determine and validate the precise genomic binding site of the transcription factor and how the transcription factor binding ultimately relates to the regulation of transcription (Geertz and Maerkl, 2010; Lambert et al., 2018).

A Vicious Cycle of SREBP1 and TGFβ Activation

Active SREBP1a, but not SREBP1c, activates the TGFβ-responsive reporter plasmid p3TP-lux carrying the promoter region of PAI1 (Chen et al., 2014). Due to its additional N-terminal residues, SREBP1a can bind to co-transcriptional factors, such as CREB-binding protein (CBP), making it a more potent transcriptional factor than SREBP1c (Toth et al., 2004). However, TGFβ activates not only its canonical pro-fibrotic downstream target, Smad3, but also non-canonical SREBP1, which requires SCAP, S1P, and P13K/Akt signaling (**Figure 5**). TGFβ-induced PI3K/Akt signaling acts as a critical regulator of Smad3-CBP interaction and Smad3 acetylation, which results in the upregulation of PAI1 expression (Das et al., 2008). Moreover, TGFβ-induced PI3K/Akt signaling stimulated acetylation of SREBP1a in the lysine residue (K333) by the acetyltransferase CBP, which enhanced the nuclear stability of SREBP1a. The active SREBP1a was further bound to E-box, which was adjacent to the Smad-binding element (SBE). TGFβ, interestingly, induced a direct association between Smad3 and acetylated SREBP1a in this adjacent area and the interaction between these two transcription factors was crucial in regulating the transcriptional activity of TGFβ (Chen et al., 2014). Along with previous observations suggesting that SREBP1 mediates the upregulation of TGFβ transcriptional activity (Uttarwar et al., 2012; Wang T. N. et al., 2015; Li et al., 2017), a positive feedback loop may exist in which SREBP1 exacerbates both TGFβ transcriptional activity and the response, to trigger progressive fibrosis (**Figure 5**).

SREBP Prevents Exosomal Degradation of TGFβ Receptor (TβR)

As discussed above, SREBP1 coordinates TGFβ signaling via its interaction with Smad3 (Chen et al., 2014). The activation of Smad2/3 can be controlled at various levels, for example, via the turnover of TβRI and TβRII (Huang and Chen, 2012). SREBP1 inhibition by either fatostatin or SREBP1 siRNA decreased TβRI expression and halted TGFβ/Smad3 signaling. However, SREBP1 did not regulate TβRI via transcription, proteasomal/lysosomal degradation, or proteolytic cleavage (Van Krieken et al., 2017).

Lipid rafts and caveolar endocytosis have been associated with the downregulation of TβRI (Huang and Chen, 2012; Lan and Chung, 2012). Cyclodextrin-induced lipid raft disruption prevented TβRI decreases, suggesting that SREBP1 regulated the cell surface expression of TβRI in a lipid-raft dependent manner. However, TβRI expression in MCs was found to be independent of caveolae since SREBP1 inhibition still induced TβRI downregulation in caveolin-1 knockout MCs. SREBP1 may act as an important cell surface retention factor for TβRI by preventing its secretion in the exosome (**Figure 5**). SREBP1 inhibition induced TβRI secretion into exosomes, which has been implicated in intracellular organelle transfer (Van Krieken et al., 2017). However, this study did not exclude the plausible re-fusion of exosomes containing TβRI in the adjacent MCs.

POTENTIAL TARGETS OF SREBPS: BEYOND LIPID METABOLISM

In a study by Seo et al. (2009), the genome-wide analysis of SREBP1 binding in mouse liver chromatin revealed a preference for proximal binding of the promoter to a new motif (5′-ACTACANNTCCC-3′). Since then, many putative target genes of SREBPs have been shown to act beyond lipid metabolism, such as in autophagy (Seo et al., 2009), ER stress (Sanchez-Alvarez et al., 2014), as well as metabolic circadian rhythm (Gilardi et al., 2014).

Identification of Non-lipogenic Target Genes of SREBPs

Having been identified to promote the transcriptional activity of TGFβ, we wondered whether other pro-fibrotic mediators could also be targets of SREBP regulation. Here, the potential SREBF target genes were identified using a data-mining suite powered by full integration of public chromatin immunoprecipitation (ChIP)-sequencing data, namely ChIP-Atlas[2]. The transcription regulatory peaks were examined from around ± 5 kb of the transcription start sequence of the coding genes (**Figure 6**). However, it should be noted that the genes listed as target genes are not necessarily functional targets of a given transcriptional regulator, suggesting that the actual regulation of potential target genes should be experimentally verified (Oki et al., 2018).

Potential Targets of SREBPs for the Regulation of Fibrosis Development

As summarized in **Table 2**, SREBFs are predicted to regulate various non-lipogenic genes in diverse tissues and cell lines. Among those genes, we discuss several SREBP target genes that are plausibly involved in the pathogenesis of tissue fibrosis. These target genes would be interesting to be directly investigated in an experimental disease model of either kidney or other organs.

Claudin 34D (*CLDN34D*)

Claudins are a family of tight-junction membrane proteins that have not been clearly elucidated in the kidney. Genetic mutations in claudin-16 and -19 cause familial hypomagnesemia and hypercalciuria with nephrocalcinosis,

[2]https://chip-atlas.org/

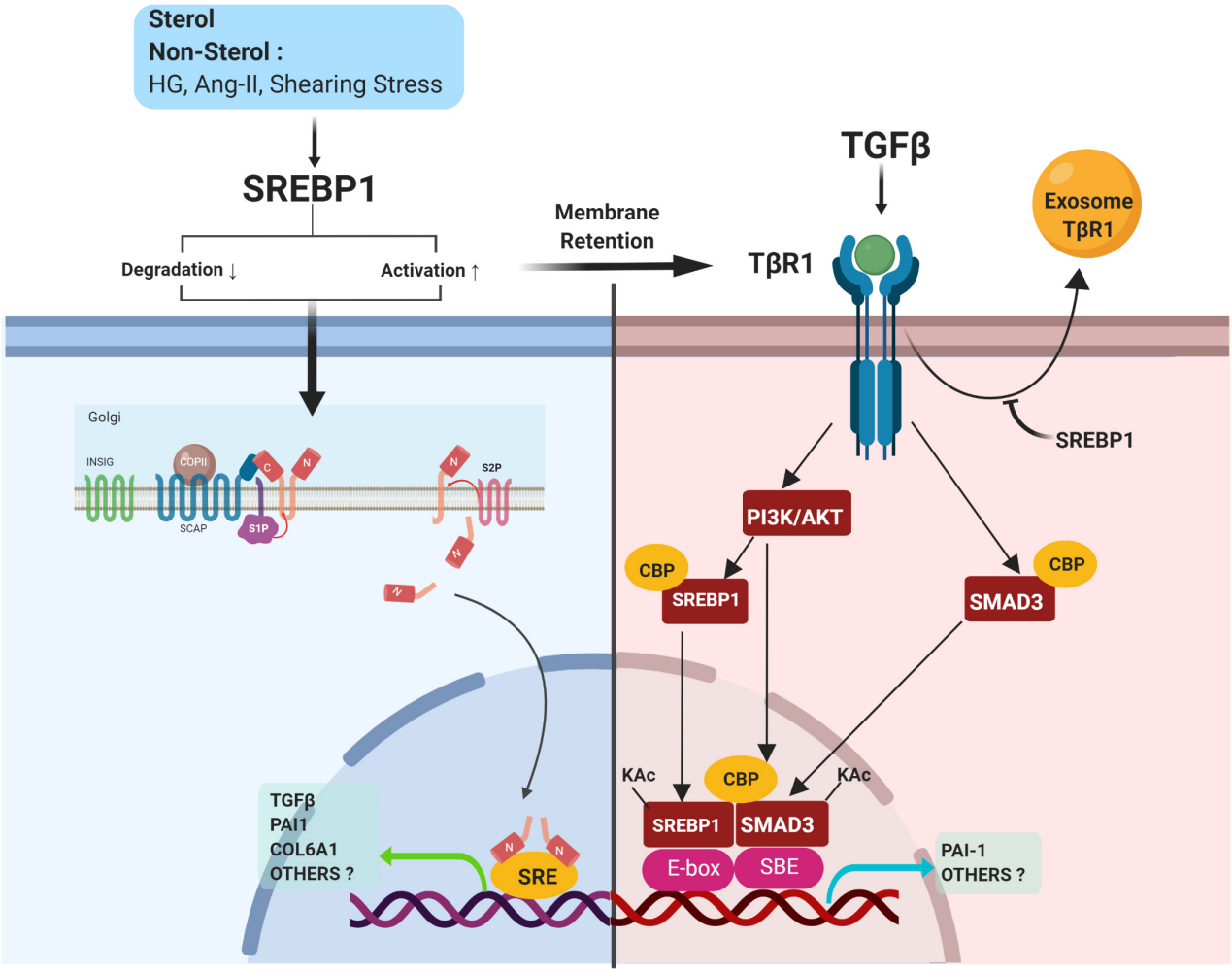

FIGURE 5 | SREBP1 directly activates pro-fibrotic signaling. SREBP activation is induced by either sterol or non-sterol stimuli, resulting in fibrotic signaling. In the kidney, SREBP1 regulates TGFβ activity via 1) induction of TGFβ transcriptional activity, 2) a positive feedback loop with TGFβ/Smad3 signaling, and 3) prevention of exosomal degradation of the TGFβ-receptor.

whereas polymorphisms in claudin-14 are associated with the risk of kidney stones (Li J. et al., 2011; Yu, 2015). In the lung, the disruption of claudin-18 expression stimulates pulmonary fibrosis or chronic obstructive pulmonary disease (Schlingmann et al., 2015). Furthermore, claudin modification has been established in several cancers, including gastric cancer, via the activation of epithelial-to-mesenchymal transition (EMT), a mechanism that is also involved in the progression of fibrosis (Rendon-Huerta et al., 2013).

Syndecan Binding Protein (Syntenin) 2 (*SDCBP2*)

Syntenin was initially identified as a protein linking syndecan-mediated signaling to the cytoskeleton (Grootjans et al., 1997). Syntenin positively regulates TGFβ-mediated Smad activation and EMT by preventing the caveolin-1-mediated internalization of TβRI (Hwangbo et al., 2016). Thus, this adapter protein might contribute to tissue fibrosis.

Elastin Microfibril Interfacer 2 (*EMILIN2*)

EMILIN is an elastic fiber-associated glycoprotein (Doliana et al., 2001). In the kidney, it is localized to the glomeruli and occurs predominantly in mesangial cells (Sterzel et al., 2000). EMILIN2 binds to the TNF-related apoptosis-inducing ligand (TRAIL) death receptor (DR) 4 and partially with DR5 to activate the extrinsic apoptotic pathway. EMILIN2 knockdown results in enhanced cell survival and its overexpression triggers massive apoptosis (Mongiat et al., 2007). These additional mechanisms of ECM in modulating cell survival require further exploration in kidney diseases.

Death Associated Protein Kinase 3 (*DAPK3*)

DAPK is a calcium/calmodulin-regulated serine/threonine kinase that mediates cell death. Deletion of the kinase domain in DAPK attenuates tubular cell apoptosis in renal ischemia-reperfusion injury (Kishino et al., 2004). DAPK3 induces

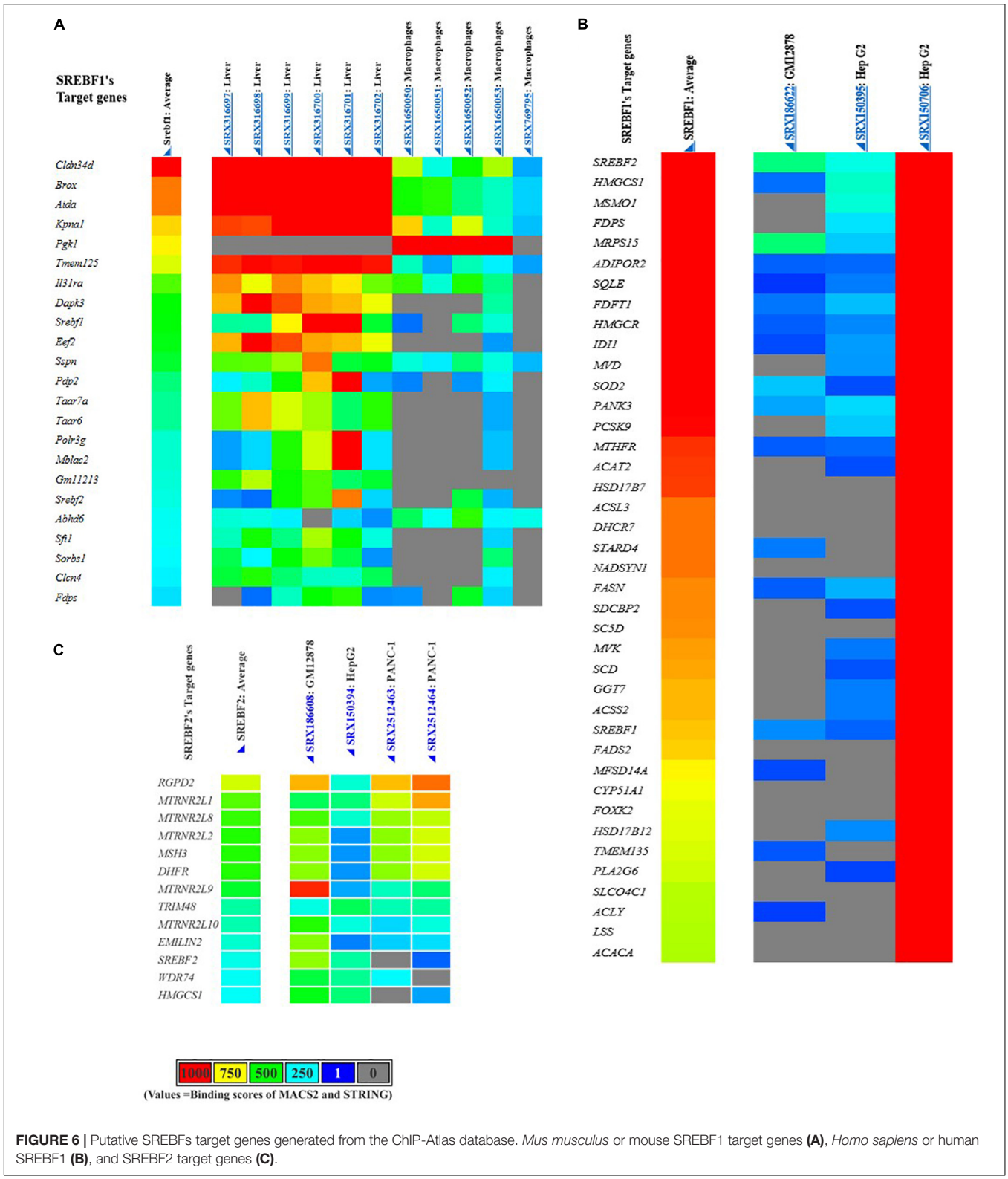

FIGURE 6 | Putative SREBFs target genes generated from the ChIP-Atlas database. *Mus musculus* or mouse SREBF1 target genes **(A)**, *Homo sapiens* or human SREBF1 **(B)**, and SREBF2 target genes **(C)**.

apoptosis or autophagy with or without caspase proteins. It also mediates inflammatory signals L13a (ribosome protein), ERK, and interferon-γ-activated inhibition of translation (Elbadawy et al., 2018). However, it is unclear whether DAPK3 is a potential target for kidney protection against cell death.

TABLE 2 | Lipid and non-lipid targets of SREBF genes generated from the Chip-Atlas database (https://chip-atlas.org/).

Biological Function	Target Genes
SREBF1 MUS MUSCULUS	
Lipid biosynthesis	*Srebf1; Srebf2*
Non-lipid targets	
Antiport system	*Clcn4*
Associated protein of endosomal sorting complex	*Brox*
Cytoskeleton and ECM	*Sspn*
RNA polymerase activity	*Polr3g*
Essential factor for protein synthesis	*Eef2*
Cell matrix adhesion	*Sorbs1; Cldn34d*
Glycolytic enzyme	*Pgk1*
Hydrolase activity	*Mblac2*
Induction of apoptosis	*Dapk3*
Interleukin-31 receptor signaling	*Il31ra*
Lipase activity	*Abhd6*
Nuclear protein import	*Kpna1*
Phosphatase activity	*Pdp2*
Structural protein of centrosome	*Sfi1*
Trace-amine receptor	*Taar6; Taar7a*
Transmembrane protein	*Tmem125*
Ventralizing factor in embryogenesis	*Aida*
SREBF1 HOMO SAPIENS	
Lipid biosynthesis	*ACACA, ACAT2, ACLY, ACSL3, ACSS2, CYP51A1, DHCR7, FADS2, FAS, FDFT1, FDPS, HMGCR, HMGCS1, HSD17B12, HSD17B7, IDI1, LSS, MSMO1, MVD, MVK, SC5D, SCD, SQLE, SREBF1, SREBF2, STARD4*
Non-lipid targets	
Adiponectin signaling	*ADIPOR2*
Biosynthesis of coenzyme A	*PANK3*
Cell matrix adhesion	*SDCBP2*
Glutathione metabolism	*SOD2*
Mitochondrial translation	*MRPS15*
Peroxisome organization, mitochondrial fission	*TMEM135*
Phospholipase activity	*PLA2G6*
Transcriptional regulator	*FOXK2*
Transmembrane transporter	*SLCO4C1*
SREBF2 HOMO SAPIENS	
Lipid biosynthesis	*SREBF2; HMGCS1*
Non-lipid targets	
Anti-apoptotic	*MT-RNR2L*
De novo synthesis of purines, thymidylic acid	*DHFR*
DNA mismatch repair	*MSH3*
ECM constituent	*EMILIN2*
Ribosome biogenesis	*WDR74*

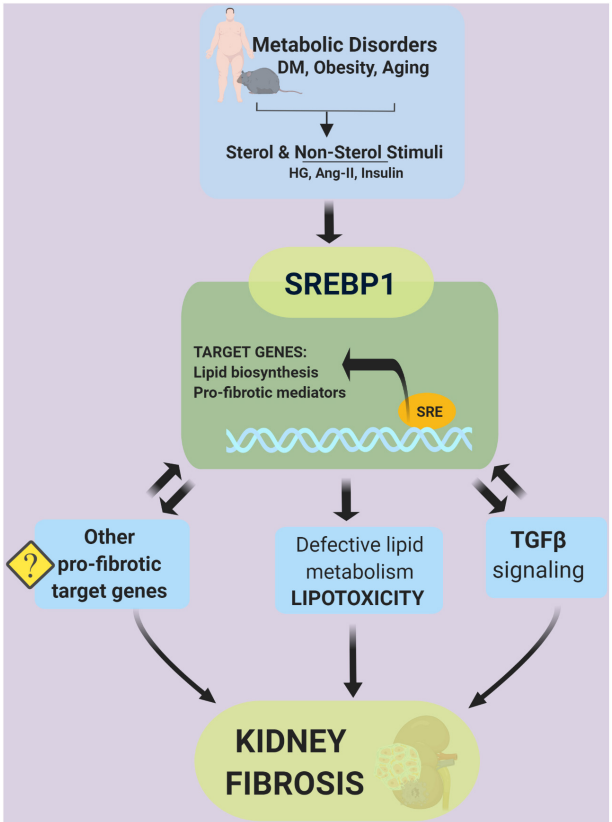

FIGURE 7 | SREBPs mediate kidney fibrosis via lipid-dependent and -independent pathways.

Transmembrane Protein 135 (*TMEM135*)

TMEM135 is an LXR-inducible regulator of peroxisome catabolic and anabolic processes mediated via the auxiliary matrix protein import pathway. It also regulates mitochondrial dynamics to protect the retina against oxidative stress and progressive retinal aging (Lee et al., 2016). Overexpression of TMEM135 increases mitochondrial fragmentation, as well as collagen accumulation and hypertrophy in the heart (Lewis et al., 2018). However, the role of TMEM135 in modulating mitochondria or peroxisomal function in kidney tissue remains elusive.

FUTURE DIRECTIONS AND CONCLUSION

Given the importance of SREBP in mediating lipid biosynthesis, which converges with various pathological signaling mechanisms, targeting SREBP is an important pharmacological strategy to attenuate the progression of kidney diseases. The available small-molecule inhibitors of SREBP activation have been comprehensively reviewed elsewhere (Watanabe and Uesugi, 2013). However, fatostatin is the only SREBP inhibitor extensively studied in kidney diseases. It inhibits the ER-Golgi translocation of SREBPs by binding to SCAP at a site distinct from the sterol-binding domain. Decreased SREBP maturation attenuates the progression of tubulointerstitial fibrosis induced by unilateral obstructive injury (Mustafa et al., 2016) and

kidney injury in hypertensive mice (Wang T. N. et al., 2015). In type 1 diabetic mice, 12-week fatostatin treatment blocked renal SREBP1 and SREBP2 expression. However, hyperfiltration, albuminuria, and kidney fibrosis were not attenuated in the diabetic mice. Non-diabetic mice treated with fatostatin exhibited hyperfiltration and increases in glomerular volume to levels seen in diabetic mice, which were associated with increased kidney inflammation and a trend toward fibrosis (Van Krieken et al., 2018). Thus, the efficacy of other SREBP inhibitors and the specific roles of SREBP in the pathogenesis of DKD and CKD remain to be investigated.

Genome-wide analysis, *in vitro*, and *in vivo* studies have demonstrated the versatility of SREBPs in mediating diverse biological processes. Particularly in the kidney, SREBP1 acts as an activator of pro-fibrotic signaling by binding to the promoter area of fibrosis-related genes, i.e., TGFβ. The precise elucidation of non-lipid and direct or indirect targets of SREBPs that mediate the development of fibrosis remains a challenge. Emerging data suggest that continued investigation of the SREBP pathway and the discovery of its small molecule inhibitors will facilitate the amelioration of kidney disease via lipid-dependent and -independent pathways (**Figure 7**).

AUTHOR CONTRIBUTIONS

DD conceived and wrote the manuscript, and designed the figures. DK and HH provided critical revisions of the manuscript. HH made the final approval of the version to be published.

FUNDING

The preparation of this review was supported by grants from the Korean Health Technology R&D Project through the Korean Health Industry Development Institute (HI18C0695).

REFERENCES

Amemiya-Kudo, M., Shimano, H., Yoshikawa, T., Yahagi, N., Hasty, A. H., Okazaki, H., et al. (2000). Promoter analysis of the mouse sterol regulatory element-binding protein-1c gene. *J. Biol. Chem.* 275, 31078–31085. doi: 10.1074/jbc.M005353200

Bengoechea-Alonso, M. T., and Ericsson, J. (2009). A phosphorylation cascade controls the degradation of active SREBP1. *J. Biol. Chem.* 284, 5885–5895. doi: 10.1074/jbc.M807906200

Bertolio, R., Napoletano, F., Mano, M., Maurer-Stroh, S., Fantuz, M., Zannini, A., et al. (2019). Sterol regulatory element binding protein 1 couples mechanical cues and lipid metabolism. *Nat. Commun.* 10:1326. doi: 10.1038/s41467-019-09152-7

Besnard, V., Wert, S. E., Stahlman, M. T., Postle, A. D., Xu, Y., Ikegami, M., et al. (2009). Deletion of Scap in alveolar type II cells influences lung lipid homeostasis and identifies a compensatory role for pulmonary lipofibroblasts. *J. Biol. Chem.* 284, 4018–4030. doi: 10.1074/jbc.M805388200

Breyer, M. D., and Susztak, K. (2016). The next generation of therapeutics for chronic kidney disease. *Nat. Rev. Drug Discov.* 15, 568–588. doi: 10.1038/nrd.2016.67

Brown, M. S., and Goldstein, J. L. (1997). The SREBP pathway: regulation of cholesterol metabolism by proteolysis of a membrane-bound transcription factor. *Cell* 89, 331–340. doi: 10.1016/S0092-8674(00)80213-5

Brown, M. S., and Goldstein, J. L. (2008). Selective versus total insulin resistance: a pathogenic paradox. *Cell Metab.* 7, 95–96. doi: 10.1016/j.cmet.2007.12.009

Chen, G., Wang, T., Uttarwar, L., Vankrieken, R., Li, R., Chen, X., et al. (2014). SREBP-1 is a novel mediator of TGFβ1 signaling in mesangial cells. *J. Mol. Cell Biol.* 6, 516–530. doi: 10.1093/jmcb/mju041

Cheng, C., Ru, P., Geng, F., Liu, J., Yoo, J. Y., Wu, X., et al. (2015). Glucose-mediated N-glycosylation of SCAP is essential for SREBP-1 activation and tumor growth. *Cancer Cell* 28, 569–581. doi: 10.1016/j.ccell.2015.09.021

Chung, K. W., Lee, E. K., Lee, M. K., Oh, G. T., and Yu, B. P. (2018). Impairment of PPARα and the fatty acid oxidation pathway aggravates renal fibrosis during aging. *J. Am. Soc. Nephrol.* 29, 1223–1237. doi: 10.1681/ASN.2017070802

Cohen, J. C., Horton, J. D., and Hobbs, H. H. (2009). Human fatty liver disease: old questions and new insights. *Science* 332, 1519–1523. doi: 10.1126/science.1204265

Colgan, S. M., Al-Hashimi, A. A., and Austin, R. C. (2011). Endoplasmic reticulum stress and lipid dysregulation. *Expert Rev. Mol. Med.* 13, 1–14. doi: 10.1017/S1462399410001742

Das, F., Ghosh-Choudhury, N., Venkatesan, B., Li, X., Mahimainathan, L., and Choudhury, G. G. (2008). Akt kinase targets association of TGF-β induced expression of CBP with SMAD 3 to regulate plasminogen activator inhibitor-1. *J. Cell. Physiol.* 214, 513–527. doi: 10.1002/JCP

Doliana, R., Bot, S., Mungiguerra, G., Canton, A., Paron Cilli, S., and Colombatti, A. (2001). Isolation and characterization of EMILIN-2, a new component of the growing EMILINs family and a member of the EMI domain-containing superfamily. *J. Biol. Chem.* 276, 12003–12011. doi: 10.1074/jbc.M011591200

Dong, Q., Giorgianni, F., Deng, X., Beranova-Giorgianni, S., Park, E. A., Raghow, R., et al. (2014). Phosphorylation of sterol regulatory element binding protein-1a by protein kinase A (PKA) regulates transcriptional activity. *Biochem. Biophys. Res. Commun.* 449, 449–454. doi: 10.1016/j.bbrc.2014.05.046

Düvel, K., Yecies, J. L., Menon, S., Raman, P., Lipovsky, A. I., Souza, A. L., et al. (2010). Activation of a metabolic gene regulatory network downstream of mTOR complex 1. *Mol. Cell* 39, 171–183. doi: 10.1016/j.molcel.2010.06.022

Elbadawy, M., Usui, T., Yamawaki, H., and Sasaki, K. (2018). Novel functions of death-associated protein kinases through mitogen-activated protein kinase-related signals. *Int. J. Mol. Sci.* 19:E3031. doi: 10.1080/00927879708826060

Ferrari, A., Maretto, S., Girotto, D., Volpin, D., and Bressan, G. M. (2004). SREBP contributes to induction of collagen VI transcription by serum starvation. *Biochem. Biophys. Res. Commun.* 313, 600–605. doi: 10.1016/j.bbrc.2003.11.159

Geertz, M., and Maerkl, S. J. (2010). Experimental strategies for studying transcription factor-DNA binding specificities. *Brief. Funct. Genomics* 9, 362–373. doi: 10.1093/bfgp/elq023

Gilardi, F., Migliavacca, E., Naldi, A., Baruchet, M., Canella, D., Le Martelot, G., et al. (2014). Genome-wide analysis of SREBP1 activity around the clock reveals its combined dependency on nutrient and circadian signals. *PLoS Genet.* 10:e1004155. doi: 10.1371/journal.pgen.1004155

Goldstein, J. L., DeBose-Boyd, R. A., and Brown, M. S. (2006). Protein sensors for membrane sterols. *Cell* 124, 35–36. doi: 10.1016/j.cell.2005.12.022

Gong, Y., Lee, J. N., Lee, P. C. W., Goldstein, J. L., Brown, M. S., and Ye, J. (2006). Sterol-regulated ubiquitination and degradation of Insig-1 creates a convergent mechanism for feedback control of cholesterol synthesis and uptake. *Cell Metab.* 3, 15–24. doi: 10.1016/j.cmet.2005.11.014

Grootjans, J. J., Zimmermann, P., Reekmans, G., Smets, A., Degeest, G., Dürr, J., et al. (1997). Syntenin, a PDZ protein that binds syndecan cytoplasmic domains. *Proc. Natl. Acad. Sci. U.S.A.* 94, 13683–13688. doi: 10.1073/pnas.94.25.13683

Guillet-Deniau, I., Pichard, A.-L., Koné, A., Esnous, C., Nieruchalski, M., Girard, J., et al. (2004). Glucose induces de novo lipogenesis in rat muscle satellite cells through a sterol-regulatory-element-binding-protein-1c-dependent pathway. *J. Cell Sci.* 117, 1937–1944. doi: 10.1242/jcs.01069

Ha, T.-S., Park, H.-Y., Seong, S.-B., and Ahn, H. Y. (2015). Angiotensin II induces endoplasmic reticulum stress in podocyte, which would be further augmented by PI3-kinase inhibition. *Clin. Hypertens.* 21:13. doi: 10.1186/s40885-015-0018-5

Han, Y., Hu, Z., Cui, A., Liu, Z., Ma, F., Xue, Y., et al. (2019). Post-translational regulation of lipogenesis via AMPK-dependent phosphorylation of insulin-induced gene. *Nat. Commun.* 10:623. doi: 10.1038/s41467-019-08585-4

Hasty, A. H., Shimano, H., Yahagi, N., Amemiya-Kudo, M., Perrey, S., Yoshikawa, T., et al. (2000). Sterol regulatory element-binding protein-1 is regulated by glucose at the transcriptional level. *J. Biol. Chem.* 275, 31069–31077. doi: 10.1074/jbc.M003335200

Herman-Edelstein, M., Scherzer, P., Tobar, A., Levi, M., and Gafter, U. (2014). Altered renal lipid metabolism and renal lipid accumulation in human diabetic nephropathy. *J. Lipid Res.* 55, 561–572. doi: 10.1194/jlr.P040501

Hirano, Y., Yoshida, M., Shimizu, M., and Sato, R. (2001). Direct demonstration of rapid degradation of nuclear sterol regulatory element-binding proteins by the ubiquitin-proteasome pathway. *J. Biol. Chem.* 276, 36431–36437. doi: 10.1074/jbc.M105200200

Horton, J. D., Goldstein, J. L., and Brown, M. S. (2002). SREBPs: activators of the complete program of cholesterol and fatty acid synthesis in the liver. *J. Clin. Invest.* 109, 1125–1131. doi: 10.1172/JCI200215593

Hua, X., Yokoyama, C., Wu, J., Briggs, M. R., Brown, M. S., Goldstein, J. L., et al. (1993). SREBP-2, a second basic-helix-loop-helix-leucine zipper protein that stimulates transcription by binding to a sterol regulatory element. *Proc. Natl. Acad. Sci. U.S.A.* 90, 11603–11607. doi: 10.1073/pnas.90.24.11603

Huang, F., and Chen, Y.-G. (2012). Regulation of TGF-β receptor activity. *Cell Biosci.* 2:9. doi: 10.1186/2045-3701-2-9

Hwangbo, C., Tae, N., Lee, S., Kim, O., Park, O., Kim, J., et al. (2016). Syntenin regulates TGF-β1-induced Smad activation and the epithelial-to-mesenchymal transition by inhibiting caveolin- mediated TGF-β type I receptor internalization. *Oncogene* 35, 389–401. doi: 10.1038/onc.2015.100

Jiang, T., Liebman, S. E., Lucia, M. S., Li, J., and Levi, M. (2005a). Role of altered renal lipid metabolism and the sterol regulatory element binding proteins in the pathogenesis of age-related renal disease. *Kidney Int.* 68, 2608–2620. doi: 10.1111/j.1523-1755.2005.00733.x

Jiang, T., Liebman, S. E., Lucia, M. S., Phillips, C. L., and Levi, M. (2005b). Calorie restriction modulates renal expression of sterol regulatory element binding proteins, lipid accumulation, and age-related renal disease. *J. Am. Soc. Nephrol.* 16, 2385–2394. doi: 10.1681/ASN.2004080701

Jiang, T., Wang, Z., Proctor, G., Moskowitz, S., Liebman, S. E., Rogers, T., et al. (2005c). Diet-induced obesity in C57BL/6J mice causes increased renal lipid accumulation and glomerulosclerosis via a sterol regulatory element-binding protein-1c-dependent pathway. *J. Biol. Chem.* 280, 32317–32325. doi: 10.1074/jbc.M500801200

Ju, W., Greene, C. S., Eichinger, F., Nair, V., Hodgin, J. B., Bitzer, M., et al. (2013). Defining cell-type specificity at the transcriptional level in human disease. *Genome Res.* 23, 1862–1873. doi: 10.1101/gr.155697.113

Jun, H., Song, Z., Chen, W., Zanhua, R., Yonghong, S., Shuxia, L., et al. (2009). In vivo and in vitro effects of SREBP-1 on diabetic renal tubular lipid accumulation and RNAi-mediated gene silencing study. *Histochem. Cell Biol.* 131, 327–345. doi: 10.1007/s00418-008-0528-2

Kang, H. M., Ahn, S. H., Choi, P., Ko, Y. A., Han, S. H., Chinga, F., et al. (2015). Defective fatty acid oxidation in renal tubular epithelial cells has a key role in kidney fibrosis development. *Nat. Med.* 21, 37–46. doi: 10.1038/nm.3762

Kim, J. B., Spotts, G. D., Halvorsen, Y.-D., Hsiu-Ming, S., Ellenberger, T., Towle, H. C., et al. (1995). Dual DNA binding specificity of ADD1/SREBP1 controlled by a single amino acid in the basic helix-loop-helix domain. *Mol. Cell. Biol.* 15, 2582–2588. doi: 10.1038/news.2009.50

Kishino, M., Yukawa, K., Hoshino, K., Kimura, A., Shirasawa, N., Otani, H., et al. (2004). Deletion of the kinase domain in death-associated protein kinase attenuates tubular cell apoptosis in renal ischemia-reperfusion injury. *J. Am. Soc. Nephrol.* 15, 1826–1834. doi: 10.1097/01.ASN.0000131527.59781.F2

Lambert, S. A., Jolma, A., Campitelli, L. F., Das, P. K., Yin, Y., Albu, M., et al. (2018). The human transcription factors. *Cell* 172, 650–665. doi: 10.1016/j.cell.2018.01.029

Lan, H. Y., and Chung, A. C. K. (2012). TGF-β/Smad signaling in kidney disease. *Semin. Nephrol.* 32, 236–243. doi: 10.1016/j.semnephrol.2012.04.002

Lay, S., Le Lefrère, I., Trautwein, C., Dugail, I., and Krief, S. (2002). Insulin and sterol-regulatory element-binding protein-1c (SREBP-1c) regulation of gene expression in 3T3-L1 adipocytes: identification of CCAAT/enhancer-binding protein β as an SREBP-1c target. *J. Biol. Chem.* 277, 35625–35634. doi: 10.1074/jbc.M203913200

Lee, G. Y., Jang, H., Lee, H., Huh, Y., Choi, S., Chung, J., et al. (2014). PIASy-mediated sumoylation of SREBP1c regulates hepatic lipid metabolism upon fasting signaling. *Mol. Cell. Biol.* 34, 926–938. doi: 10.1128/MCB.01166-13

Lee, S. J., Sekimoto, T., Yamashita, E., Nagoshi, E., Nakagawa, A., Imamoto, N., et al. (2003). The structure of importin-β bound to SREBP-2: nuclear import of a transcription factor. *Science* 302, 1571–1576. doi: 10.1126/science.1088372

Lee, W. H., Higuchi, H., Ikeda, S., Macke, E. L., Takimoto, T., Pattnaik, B. R., et al. (2016). Mouse Tmem135 mutation reveals a mechanism involving mitochondrial dynamics that leads to age-dependent retinal pathologies. *eLife* 5:19264. doi: 10.7554/eLife.19264

Lewis, S. A., Takimoto, T., Mehrvar, S., Higuchi, H., Doebley, A. L., Stokes, G., et al. (2018). The effect of Tmem135 overexpression on the mouse heart. *PLoS One* 13:e0201986. doi: 10.1371/journal.pone.0201986

Li, H. Y., Oh, Y. S., Choi, J. W., Jung, J. Y., and Jun, H. S. (2017). Blocking lysophosphatidic acid receptor 1 signaling inhibits diabetic nephropathy in db/db mice. *Kidney Int.* 91, 1362–1373. doi: 10.1016/j.kint.2016.11.010

Li, J., Ananthapanyasut, W., and Yu, A. S. L. (2011). Claudins in renal physiology and disease. *Pediatr. Nephrol.* 26, 2133–2142. doi: 10.1007/s00467-011-1824-y

Li, Y., Xu, S., Mihaylova, M. M., Zheng, B., Hou, X., Jiang, B., et al. (2011). AMPK phosphorylates and inhibits SREBP activity to attenuate hepatic steatosis and atherosclerosis in diet-induced insulin-resistant mice. *Cell Metab.* 13, 376–388. doi: 10.1016/j.cmet.2011.03.009

Lin, T., Zeng, L., Liu, Y., DeFea, K., Schwartz, M. A., Chien, S., et al. (2003). Rho-ROCK-LIMK-cofilin pathway regulates shear stress activation of sterol regulatory element binding proteins. *Circ. Res.* 92, 1296–1304. doi: 10.1161/01.RES.0000078780.65824.8B

Liu, Y., Chen, B. P. C., Lu, M., Zhu, Y., Stemerman, M. B., Chien, S., et al. (2002). Shear stress activation of SREBP1 in endothelial cells is mediated by integrins. *Arterioscler. Thromb. Vasc. Biol.* 22, 76–81. doi: 10.1161/hq0102.101822

Mongiat, M., Ligresti, G., Marastoni, S., Lorenzon, E., Doliana, R., and Colombatti, A. (2007). Regulation of the extrinsic apoptotic pathway by the extracellular matrix glycoprotein EMILIN2. *Mol. Cell. Biol.* 27, 7176–7187. doi: 10.1128/MCB.00696-07

Murea, M., Freedman, B. I., Parks, J. S., Antinozzi, P. A., Elbein, S. C., and Ma, L. (2010). Lipotoxicity in diabetic nephropathy: the potential role of fatty acid oxidation. *Clin. J. Am. Soc. Nephrol.* 5, 2373–2379. doi: 10.2215/CJN.08160910

Mustafa, M., Wang, T. N., Chen, X., Gao, B., and Krepinsky, J. C. (2016). SREBP inhibition ameliorates renal injury after unilateral ureteral obstruction. *Am. J. Physiol. Physiol.* 311, F614–F625. doi: 10.1152/ajprenal.00140.2016

Na, J., Sweetwyne, M. T., Park, A. S. D., Susztak, K., and Cagan, R. L. (2015). Diet-induced podocyte dysfunction in drosophila and mammals. *Cell Rep.* 12, 636–647. doi: 10.1016/j.celrep.2015.06.056

Nakagawa, S., Nishihara, K., Miyata, H., Shinke, H., Tomita, E., Kajiwara, M., et al. (2015). Molecular markers of tubulointerstitial fibrosis and tubular cell damage in patients with chronic kidney disease. *PLoS One* 10:0136994. doi: 10.1371/journal.pone.0136994

Nakakuki, M., Kawano, H., Notsu, T., Imada, K., Mizuguchi, K., and Shimano, H. (2014). A novel processing system of sterol regulatory element-binding protein-1c regulated by polyunsaturated fatty acid. *J. Biochem.* 155, 301–313. doi: 10.1093/jb/mvu019

Oki, S., Ohta, T., Shioi, G., Hatanaka, H., Ogasawara, O., Okuda, Y., et al. (2018). ChIP-Atlas: a data-mining suite powered by full integration of public ChIP-seq data. *EMBO Rep.* 19:e46255. doi: 10.15252/embr.201846255

Pai, J. T., Guryev, O., Brown, M. S., and Goldstein, J. L. (1998). Differential stimulation of cholesterol and unsaturated fatty acid biosynthesis in cells expressing individual nuclear sterol regulatory element-binding proteins. *J. Biol. Chem.* 273, 26138–26148. doi: 10.1074/jbc.273.40.26138

Peng, F., Wu, D., Gao, B., Ingram, A. J., Zhang, B., Chorneyko, K., et al. (2008). RhoA/Rho-kinase contribute to the pathogenesis of diabetic renal disease. *Diabetes Metab. Res. Rev.* 57, 1683–1692. doi: 10.2337/db07-1149

Peterson, T. R., Sengupta, S. S., Harris, T. E., Carmack, A. E., Kang, S. A., Balderas, E., et al. (2011). mTOR complex 1 regulates lipin 1 localization to control the SREBP pathway. *Cell* 146, 408–420. doi: 10.1016/j.cell.2011.06.034

Plantier, L., Besnard, V., Xu, Y., Ikegami, M., Wert, S. E., Hunt, A. N., et al. (2012). Activation of sterol-response element-binding proteins (SREBP) in alveolar

type II cells enhances lipogenesis causing pulmonary lipotoxicity. *J. Biol. Chem.* 287, 10099–10114. doi: 10.1074/jbc.M111.303669

Proctor, G., Jiang, T., Iwahashi, M., Wang, Z., Li, J., and Levi, M. (2006). Regulation of renal fatty acid and cholesterol metabolism, inflammation, and fibrosis in Akita and OVE26 mice with type 1 diabetes. *Diabetes Metab. Res. Rev.* 55, 2502–2509. doi: 10.2337/db05-0603

Rendon-Huerta, E., Chavarria-Velazquez, C., and Montaño, L. (2013). Claudins, inflammation and epithelial-mesenchymal transition in gastric tissue. *J. Gastrointest. Dig. Syst.* 3:4. doi: 10.4172/2161-069X.1000149

Romagnani, P., Remuzzi, G., Glassock, R., Levin, A., Tonelli, M., Massy, Z., et al. (2017). Chronic kidney disease. *Nat. Rev. Dis. Prim.* 23:17088. doi: 10.1038/nrdp.2017.88

Saito, K., Ishizaka, N., Hara, M., Matsuzaki, G., Sata, M., Mori, I., et al. (2005). Lipid accumulation and transforming growth factor-β upregulation in the kidneys of rats administered angiotensin II. *Hypertension* 46, 1180–1185. doi: 10.1161/01.HYP.0000184653.75036.d5

Sanchez-Alvarez, M., Finger, F., Del Mar Arias-Garcia, M., Bousgouni, V., Pascual-Vargas, P., and Bakal, C. (2014). Signaling networks converge on TORC1-SREBP activity to promote endoplasmic reticulum homeostasis. *PLoS One* 9:0101164. doi: 10.1371/journal.pone.0101164

Schlingmann, B., Molina, S. A., and Koval, M. (2015). Claudins: gatekeepers of lung epithelial function. *Semin. Cell Dev. Biol.* 42, 47–57. doi: 10.1016/j.semcdb.2015.04.009

Seo, Y., Kim, H., Infante, A. M., Im, S., Xie, X., and Osborne, T. F. (2009). Genome-wide analysis of SREBP-1 binding in mouse liver chromatin reveals a preference for promoter proximal binding to a new motif. *Proc. Natl. Acad. Sci. U.S.A.* 106, 13765–13769. doi: 10.1073/pnas.0904246106

Shimano, H. (2001). Sterol regulatory element-binding proteins (SREBPs) as regulators of lipid metabolism. *Prog. Lipid Res.* 40, 439–452. doi: 10.1016/s0163-7827(01)00010-8

Shimano, H., Horton, J. D., Shimomura, I., Hammer, R. E., Brown, M. S., and Goldstein, J. L. (1997). Isoform 1c of sterol regulatory element binding protein is less active than isoform 1a in livers of transgenic mice and in cultured cells. *J. Clin. Invest.* 99, 846–856. doi: 10.1172/JCI119248

Shimano, H., and Sato, R. (2017). SREBP-regulated lipid metabolism: convergent physiology-divergent pathophysiology. *Nat. Rev. Endocrinol.* 13, 710–730. doi: 10.1038/nrendo.2017.91

Shimomura, I., Bashmakov, Y., and Horton, J. D. (1999a). Increased levels of nuclear SREBP-1c associated with fatty livers in two mouse models of diabetes mellitus. *J. Biol. Chem.* 274, 30028–30032. doi: 10.1074/jbc.274.42.30028

Shimomura, I., Bashmakov, Y., Ikemoto, S., Horton, J. D., Brown, M. S., and Goldstein, J. L. (1999b). Insulin selectively increases SREBP-1c mRNA in the livers of rats with streptozotocin-induced diabetes. *Proc. Natl. Acad. Sci. U.S.A.* 96, 13656–13661. doi: 10.1073/pnas.96.24.13656

Shimomura, I., Matsuda, M., Hammer, R. E., Bashmakov, Y., Brown, M. S., and Goldstein, J. L. (2000). Decreased IRS-2 and increased SREBP-1c lead to mixed insulin resistance and sensitivity in livers of lipodystrophic and ob/ob mice. *Mol. Cell* 6, 77–86. doi: 10.1016/S1097-2765(05)00010-9

Simon, N., and Hertig, A. (2015). Alteration of fatty acid oxidation in tubular epithelial cells: from acute kidney injury to renal fibrogenesis. *Front. Med.* 2:52. doi: 10.3389/fmed.2015.00052

Sterzel, R. B., Hartner, A., Schlötzer-Schrehardt, U., Voit, S., Hausknecht, B., Doliana, R., et al. (2000). Elastic fiber proteins in the glomerular mesangium in vivo and in cell culture. *Kidney Int.* 58, 1588–1602. doi: 10.1046/j.1523-1755.2000.00320.x

Sun, H., Yuan, Y., and Sun, Z. L. (2013). Cholesterol contributes to diabetic nephropathy through SCAP-SREBP-2 pathway. *Int. J. Endocrinol.* 2013:592576. doi: 10.1155/2013/592576

Sun, L., Halaihel, N., Zhang, W., Rogers, H., and Levi, M. (2002). Role of sterol regulatory element-binding protein 1 in regulation of renal lipid metabolism and glomerulosclerosis in diabetes mellitus. *J. Biol. Chem.* 277, 18919–18927. doi: 10.1074/jbc.M110650200

Sun, L. P., Li, L., Goldstein, J. L., and Brown, M. S. (2005). Insig required for sterol-mediated inhibition of Scap/SREBP binding to COPII proteins in vitro. *J. Biol. Chem.* 280, 26483–26490. doi: 10.1074/jbc.M504041200

Sureshbabu, A., Muhsin, S. A., and Choi, M. E. (2016). TGF-β signaling in the kidney: profibrotic and protective effects. *Am. J. Physiol. Ren. Physiol.* 310, F596–F606. doi: 10.1152/ajprenal.00365.2015

Toth, J. I., Datta, S., Athanikar, J. N., Freedman, L. P., and Osborne, T. F. (2004). Selective coactivator interactions in gene activation by SREBP-1a and -1c. *Mol. Cell. Biol.* 24, 8288–8300. doi: 10.1128/MCB.24.18.8288

Uttarwar, L., Gao, B., Ingram, A. J., and Krepinsky, J. C. (2012). SREBP-1 activation by glucose mediates TGF-β upregulation in mesangial cells. *Am. J. Physiol. Ren. Physiol.* 302, F329–F341. doi: 10.1152/ajprenal.00136.2011

Van Krieken, R., Chen, G., Gao, B., Read, J., Al Saleh, H. A., Li, R., et al. (2017). Sterol regulatory element binding protein (SREBP)-1 is a novel regulator of the transforming growth factor (TGF)-β receptor I (TβRI) through exosomal secretion. *Cell. Signal.* 29, 158–167. doi: 10.1016/j.cellsig.2016.11.004

Van Krieken, R., Marway, M., Parthasarathy, P., Mehta, N., Ingram, A., Gao, B., et al. (2018). Inhibition of SREBP with fatostatin does not attenuate early diabetic nephropathy in male mice. *Endocrinology* 159, 1479–1495. doi: 10.1210/en.2018-00093

Wang, J., Wen, Y., Lv, L. L., Liu, H., Tang, R. N., Ma, K. L., et al. (2015). Involvement of endoplasmic reticulum stress in angiotensin II-induced NLRP3 inflammasome activation in human renal proximal tubular cells in vitro. *Acta Pharmacol. Sin.* 36, 821–830. doi: 10.1038/aps.2015.21

Wang, T. N., Chen, X., Li, R., Gao, B., Mohammed-Ali, Z., Lu, C., et al. (2015). SREBP-1 mediates angiotensin II-induced TGF-β1 upregulation and glomerular fibrosis. *J. Am. Soc. Nephrol.* 26, 1839–1854. doi: 10.1681/ASN.2013121332

Wang, Z., Jiang, T., Li, J., Proctor, G., McManaman, J. L., Lucia, S., et al. (2005). Regulation of renal lipid metabolism, lipid accumulation, and glomerulosclerosis in FVBdb/db mice with type 2 diabetes. *Diabetes Metab. Res. Rev.* 54, 2328–2335. doi: 10.2337/diabetes.54.8.2328

Watanabe, M., Houten, S. M., Wang, L., Moschetta, A., Mangelsdorf, D. J., Heyman, R. A., et al. (2004). Bile acids lower triglyceride levels via a pathway involving FXR. SHP, and SREBP-1c. *J. Clin. Invest.* 113, 1408–1418. doi: 10.1172/JCI21025

Watanabe, M., and Uesugi, M. (2013). Small-molecule inhibitors of SREBP activation-potential for new treatment of metabolic disorders. *Medchemcomm* 4, 1422–1433. doi: 10.1039/c3md00177f

Webster, A. C., Nagler, E. V., Morton, R. L., and Masson, P. (2017). Chronic kidney disease. *Lancet* 389, 1238–1252. doi: 10.1016/S0140-6736(16)32064-5

Woroniecka, K. I., Park, A. S. D., Mohtat, D., Thomas, D. B., Pullman, J. M., and Susztak, K. (2011). Transcriptome analysis of human diabetic kidney disease. *Diabetes Metab. Res. Rev.* 60, 2354–2369. doi: 10.2337/db10-1181

Wu, D., Peng, F., Zhang, B., Ingram, A. J., Gao, B., and Krepinsky, J. C. (2007). Collagen I induction by high glucose levels is mediated by epidermal growth factor receptor and phosphoinositide 3-kinase/Akt signalling in mesangial cells. *Diabetologia* 50, 2008–2018. doi: 10.1007/s00125-007-0721-1

Wu, D., Peng, F., Zhang, B., Ingram, A. J., Kelly, D. J., Gilbert, R. E., et al. (2009). PKC-β1 mediates glucose-induced Akt activation and TGF-β1 upregulation in mesangial cells. *J. Am. Soc. Nephrol.* 20, 554–566. doi: 10.1681/ASN.2008040445

Wu, X., Romero, D., Swiatek, W. I., Dorweiler, I., Kikani, C. K., Sabic, H., et al. (2014). PAS kinase drives lipogenesis through SREBP-1 maturation. *Cell Rep.* 8, 242–255. doi: 10.1016/j.celrep.2014.06.006

Yabe, D., Brown, M. S., and Goldstein, J. L. (2002). Insig-2, a second endoplasmic reticulum protein that binds SCAP and blocks export of sterol regulatory element-binding proteins. *Proc. Natl. Acad. Sci. U.S.A.* 99, 12753–12758. doi: 10.1073/pnas.162488899

Yang, T., Espenshade, P. J., Wright, M. E., Yabe, D., Gong, Y., Aebersold, R., et al. (2002). Crucial step in cholesterol homeostasis: sterols promote binding of SCAP to INSIG-1, a membrane protein that facilitates retention of SREBPs in ER. *Cell* 110, 489–500. doi: 10.1016/s0092-8674(02)00872-3

Ye, J., Dave, U., Grishin, N., Goldstein, J., and Brown, M. (2000). Asparagine-proline sequence within membrane-spanning segment of SREBP triggers intramembrane cleavage by site-2 protease. *Proc. Natl. Acad. Sci. U.S.A.* 97, 5123–5128. doi: 10.1073/pnas.97.10.5123

Yellaturu, C. R., Deng, X., Park, E. A., Raghow, R., and Elam, M. B. (2009). Insulin enhances the biogenesis of nuclear sterol regulatory element-binding protein (SREBP)-1c by posttranscriptional down-regulation of Insig-2A and

its dissociation from SREBP cleavage-activating protein (SCAP)·SREBP-1c complex. *J. Biol. Chem.* 284, 31726–31734. doi: 10.1074/jbc.M109.050914

Yoshikawa, T., Shimano, H., Amemiya-Kudo, M., Yahagi, N., Hasty, A. H., Matsuzaka, T., et al. (2001). Identification of liver X receptor-retinoid X receptor as an activator of the sterol regulatory element-binding protein 1c gene promoter. *Mol. Cell. Biol.* 21, 2991–3000. doi: 10.1128/MCB.21.9.2991

Yu, A. S. L. (2015). Claudins and the kidney. *J. Am. Soc. Nephrol.* 26, 11–19. doi: 10.1681/ASN.2014030284

Zhang, M.-Z., Wang, X., Yang, H., Fogo, A. B., Murphy, B. J., Kaltenbach, R., et al. (2017). Lysophosphatidic acid receptor antagonism protects against diabetic nephropathy in a type 2 diabetic model. *J. Am. Soc. Nephrol.* 28, 3300–3311. doi: 10.1681/ASN.2017010107

Zhao, X., Ji, J., Yang, F., Zhao, X., Feng, D., Wang, Q., et al. (2012). Regulation of lipogenesis by cyclin-dependent kinase 8 – mediated control of SREBP-1. *J. Clin. Invest.* 122, 2417–2427. doi: 10.1172/JCI61462

Conflict of Interest: The authors declare that the research was conducted in the absence of any commercial or financial relationships that could be construed as a potential conflict of interest.

Copyright © 2020 Dorotea, Koya and Ha. This is an open-access article distributed under the terms of the Creative Commons Attribution License (CC BY). The use, distribution or reproduction in other forums is permitted, provided the original author(s) and the copyright owner(s) are credited and that the original publication in this journal is cited, in accordance with accepted academic practice. No use, distribution or reproduction is permitted which does not comply with these terms.

APPENDIX

Abbreviations: ABHD6, abhydrolase domain containing 6; ACACA, acetyl-Coa carboxylase alpha; ACAT, acetyl-Coa acetyltransferase; ACC, acetyl-CoA carboxylase; ACLY, ATP citrate lyase; ACOX, acyl-CoA oxidase; ACS, acetyl-CoA synthetase; ACSL, acyl-CoA synthetase long-chain family member; ACSS, acyl-CoA synthetase short-chain family member; ADIPOR2, adiponectin receptor; AIDA, axin interactor, dorsalization associated; AMPK, AMP-activated protein kinase; Ang II, angiotensin II; AT1, angiotensin II type 1; BROX BRO1, domain and CAAX motif containing; CBP, CREB-binding protein; CDK8, cyclin-dependent kinase 8; ChIP, chromatin immunoprecipitation; CKD, chronic kidney disease; CLCN4, chloride voltage-gated channel 4; CLDN34D, claudin 34D; COL, collagen; CPT, carnitine palmitoyltransferase; CTGF, connective tissue growth factor; CYP51A1, cytochrome P450 family 51 subfamily A member 1; DAPK3, death-associated protein kinase 3; DHCR7, 7-dehydrocholesterol reductase; DHFR, dihydrofolate reductase; DKD, diabetic kidney disease; ECM, extracellular matrix; EEF2, eukaryotic translation elongation factor 2; EMILIN2, elastin microfibril interfacer 2; EMT, epithelial-to-mesenchymal transition; ER, endoplasmic reticulum; FADS2, fatty acid desaturase; FAO, fatty acid oxidation; FAS, fatty acid synthase; FDFT1, farnesyl diphosphate farnesyl transferase; FDPS, farnesyl diphosphate synthase; FOXK2, forkhead box K2; FXR, farnesoid x receptor; GARR, growth arrest-responsive region; GM11213, predicted gene 11213; GPAT, glycerol-3-phosphate acyltransferase; GSK, glycogen synthase kinase; HG, high glucose; HMGCR, 3-hydroxy-3-methylglutaryl-Coa reductase; HMGCS, 3-hydroxy-3-methylglutaryl-CoA synthase; HNF4α, hepatocyte nuclear factor-4α; HSD17B, hydroxysteroid 17-beta dehydrogenase; IDI1, isopentenyl-diphosphate delta isomerase; IL31RA, interleukin 31 receptor A; INSIG, insulin-induced gene; KPNA1, karyopherin subunit alpha 1; LDLR, LDL receptor; LPA, lysophosphatidic acid; LSS, lanosterol synthase; LXR, liver X receptor; LXRE LXR-responsive elements; MBLAC2, metallo-beta-lactamase domain containing 2; MC, mesangial cell; MEF, mouse embryonic fibroblast; MRPS15, mitochondrial ribosomal protein S1; MSH3, MutS homolog; MSMO1, methylsterol monooxygenase; mTORC1, mammalian target of rapamycin complex 1; MT-RNR2L, MT-RNR2 like; MVD, mevalonate diphosphate decarboxylase; MVK, mevalonate kinase; PAI1, plasminogen activator inhibitor 1; PANK3, pantothenate kinase; PCSK9, proprotein convertase subtilisin/kexin type 9; PDP2, pyruvate dehydrogenase phosphatase catalytic subunit 2; PGC1α, proliferator-activated receptor-gamma coactivator 1; PGK1, phosphoglycerate kinase 1; PI3K, phosphatidylinositol 3-kinase; PKA, protein kinase A; PLA2G6, phospholipase A2 group 6; POLR3G, RNA polymerase 3 subunit G; PPAR, peroxisome proliferator-activated receptor; PUFAs, polyunsaturated fatty acids; S1P, site-1 protease; S2P, site-2 protease; SCAP, SREBP cleavage-activating protein; SCD, stearoyl-CoA desaturase; SDCBP2, syndecan binding protein; SFI1, SFI1 centrin binding protein; SIRT1, sirtuin 1; SLCO4C1, solute carrier organic anion transporter family member 4C1; SOD2, superoxide dismutase; SORBS1, sorbin and SH3 domain containing 1; SQLE, squalene epoxidase; SRE, sterol response element; SREBF, sterol regulatory element-binding transcription factor; SREBP, sterol regulatory element-binding protein; SSPN, sarcospan; STARD4, StAR-related lipid transfer domain containing; TAAR, trace amine-associated receptor; TC, total cholesterol; TG, triglyceride; TGFβ, transforming growth factor β; TMEM, transmembrane protein; TSC1/2, tuberous sclerosis complex 1/2; TβRI, TGFβ receptor I; WDR74, WD repeat domain 74.

frontiers in Physiology

ORIGINAL RESEARCH
published: 03 April 2020
doi: 10.3389/fphys.2020.00285

Resolvin D1 Protects Against Ischemia/Reperfusion-Induced Acute Kidney Injury by Increasing Treg Percentages via the ALX/FPR2 Pathway

*Hong Luan[1], Chuanxiao Wang[2], Jianping Sun[1], Long Zhao[1], Lin Li[1], Bin Zhou[1], Shihong Shao[3], Xuefei Shen[1] and Yan Xu[1]**

[1] Department of Nephrology, The Affiliated Hospital of Qingdao University, Qingdao, China, [2] Department of Thoracic Surgery, Qingdao Municipal Hospital, School of Medicine, Qingdao University, Qingdao, China, [3] Department of Pathology, The Affiliated Hospital of Qingdao University, Qingdao, China

OPEN ACCESS

Edited by:
John D. Imig, Medical College of Wisconsin, United States

Reviewed by:
Antonio Recchiuti, Università degli Studi G. d'Annunzio Chieti e Pescara, Italy
Vasundhara Kain, University of Alabama at Birmingham, United States

***Correspondence:**
Yan Xu
xuyanqyfy@126.com

Specialty section:
This article was submitted to Renal and Epithelial Physiology, a section of the journal Frontiers in Physiology

Received: *13 December 2019*
Accepted: *13 March 2020*
Published: *03 April 2020*

Citation:
Luan H, Wang C, Sun J, Zhao L, Li L, Zhou B, Shao S, Shen X and Xu Y (2020) Resolvin D1 Protects Against Ischemia/Reperfusion-Induced Acute Kidney Injury by Increasing Treg Percentages via the ALX/FPR2 Pathway. Front. Physiol. 11:285. doi: 10.3389/fphys.2020.00285

Aims: To evaluate whether Resolvin D1 attenuates ischemia/reperfusion-induced (IRI) acute kidney injury (AKI) via affecting Tregs.

Materials and Methods: The IRI-AKI mouse model was established, and RvD1 was injected into the mouse tail vein. Further, the renal function, histological changes, injury markers and serum cytokines were detected at 24 and 72 h after IRI. Flow cytometry was used to categorize regulatory T cells (Tregs) in the spleen and kidney. Treg cells were stripped with the anti-CD25 antibody blocker PC61 to assess its role in the protective effect of RvD1 on IRI mice. $CD4^+$ T cells were obtained from spleen monocytes by magnetic bead sorting and differentiated into induced Treg (iTreg) cells. The effect of RvD1 on iTreg cell differentiation was observed *in vitro*. In addition, neutralizing antibodies against the orphan receptor G-protein-coupled receptor 32 (anti-GPR32) and LXA4 receptor (anti-ALX/FPR2), both RvD1 receptor blockers, were used to evaluate the effect of RvD1 on iTreg cell differentiation. Boc-1, an ALX/FPR2 receptor inhibitor, was administered via the tail vein to observe its effects on the ameliorative efficacy of RvD1 in IRI-AKI mice *in vivo*.

Results: *In vivo*, RvD1 increased Treg percentages, alleviated renal tubular injury and reduced the serum levels of IFN-γ, TNF-α and IL-6 in IRI-AKI mice, while PC61 depleted the number of Tregs and reversed the protective effects of RvD1. *In vitro*, RvD1 induced the generation of iTregs. Importantly, preincubation with anti-ALX/FPR2 neutralizing antibodies but not with anti-GPR32 neutralizing antibodies, abrogated the enhancement activity of RvD1 on iTregs. In addition, *in vivo* blockade of the receptor ALX/FPR2 by Boc-1 reversed the beneficial effects of RvD1 on the splenic and kidney Treg percentages, renal tubular injury and serum IFN-γ, TNF-α, and IL-6 levels.

Conclusion: Our study demonstrates that RvD1 protects against IRI-AKI by increasing the percentages of Tregs via the ALX/FPR2 pathway.

Keywords: acute kidney injury, Resolvin D1, regulatory T cells, ischemia-reperfusion injury, LXA4 receptor

INTRODUCTION

Ischemia/reperfusion injury (IRI) is the primary cause of acute kidney injury (AKI), occurs in major operations (Mehta et al., 2015). Numerous IRI animal models and human histopathological studies have shown that the inflammatory response mediated by innate and adaptive immunity is an important pathophysiological change in ischemic AKI. Th1, Th2, and Th17 cells and regulatory T cells (Tregs), which are all $CD4^+$ T lymphocyte subsets, act as a bridge between innate and adaptive immunity and participate in the pathological process of ischemic AKI.

Resolvins are a new family of endogenous lipid mediators that are derived from docosahexaenoic acid (DHA) and eicosapentaenoic acid (EPA) (Serhan et al., 2002). Resolvins include the D series (RvD) and E series and can alleviate inflammation (Weylandt et al., 2012). Resolvin D1 (RvD1) is biosynthesized from ω-3 DHA, and its effect is dependent on the LXA4 receptor (ALX/FPR2) and orphan receptor G-protein-coupled receptor 32 (GPR32) (Krishnamoorthy et al., 2010). RvD1 can promote neutrophil migration and enhance macrophage phagocytosis in an ALX/FPR2-dependent manner, which contributes to the resolution of inflammation (Hong et al., 2003; Sun et al., 2007; Spite et al., 2009). RvD1 improves the cardiorenal microenvironment to clear myocardial infarction-induced inflammation by increasing neutrophil and macrophages numbers and facilitates renoprotective mechanisms to limit cardiorenal syndrome (Halade et al., 2018).

Recently, RvDs were found to be effective in IRI-AKI and to function by reducing leukocyte influx and prohibiting postischemic kidney fibrosis (Duffield et al., 2006). Chen et al. (2014) also demonstrated that aspirin-triggered RvD1 is a potent anti-inflammatory mediator in lipopolysaccharide-induced AKI. Furthermore, a recent study reported that RvD1 can also modulate adaptive immunity, including affecting the balance between pathogenic Th1/Th17 cells and tolerogenic Tregs (Chiurchiu et al., 2016). Tregs are commonly known to play critical roles in controlling inflammation and maintaining immunological tolerance in various immune disease models. According to three recent studies, Tregs suppress innate immunity in the kidneys and play protective roles in the repair of ischemic AKI and in renal ischemic preconditioning (Gandolfo et al., 2009; Kinsey et al., 2009, 2010). Therefore, we propose that the beneficial effect of RvD1 on inflammatory regression may involve not only peripheral inflammatory cells but also Tregs. In this study, we sought to investigate whether RvD1 attenuates IRI-AKI via affecting Tregs. This study demonstrates for the first time that RvD1 alleviates IRI-AKI possibly by increasing Tregs percentages via the ALX/FPR2 pathway.

MATERIALS AND METHODS

Mice, Procedures and Interventions

Eight-week-old male C57BL/6 mice were purchased from Slake Laboratory Animal Company, Shanghai, China. All mice were fed a standard laboratory diet, provided unlimited access to drinking water, and housed in 50% humidity at room temperature on a 12 h/12 h light/dark cycle. Animal care was performed according to criteria established by the Animal Care Committee of Qingdao University. The IRI-AKI model was established by clamping the mouse bilateral renal pedicle for 60 min. In the sham operation group, a similar procedure was used except for clamping of the renal pedicle. RvD1 (Cayman Chemical, 5 μg/kg/d) or vehicle was administered through the tail vein at 30 min, 24 and 48 h after reperfusion. The dosage of RvD1 was selected based on previous reports (Kinsey et al., 2009). In some cases, RvD1 was given together with Boc-1 (a specific antagonist of ALX, China Peptide Co., 5 mg/kg/d). Blood, the kidneys, and spleen specimens were collected at the designated time points for further analysis. PC61 (BioLegend, San Diego, CA, United States, 100 μg), an anti-CD25 antibody, was used to deplete Tregs *in vivo* and was administered to the mice via the tail vein after reperfusion (Pasare and Medzhitov, 2004; Hu et al., 2013). Animals in the control group were given rat IgG (BioLegend, CA, United States).

Histology

All mice were sacrificed at selected intervals. The kidneys were sequentially harvested, fixed with 4% paraformaldehyde, dehydrated and paraffin embedded. The paraffin tissue was sliced into 3 mm sections and stained with periodate acid-Schiff (PAS) for histological analysis. The histological evaluation was performed by grading tubular necrosis, cast formation, tubular dilation, and the loss of the brush border in a blinded manner to determine acute tubular necrosis (ATN) scores. Ten non-overlapping fields (400×) were randomly selected and scored as follows: 0 = no injury; 1 = less than 10%; 2 = 11% to 25%; 3 = 26% to 45%; 4 = 46% to 75%; and 5 = more than 76%.

Biochemical Analysis

Blood samples were collected at 24 and 72 h and analyzed with a serum creatinine (Scr) kit (BioAssay Systems, Hayward, CA, United States).

Single-Cell Suspensions From the Spleen and Kidneys

Single-cell suspensions of splenocytes and kidney cells were harvested from C57BL/6 mice as described previously (Zhang et al., 2014). Briefly, the spleen was finely minced with PBS, sequentially passed through a 200-mesh sieve and lysed with a red blood cell lysis buffer (BioLegend, San Diego, CA, United States). Kidney suspensions were additionally incubated with collagenase I (Sigma-Aldrich, 1.6 mg/ml) and DNase I (Sigma-Aldrich, 200 μg/ml) in RPMI-1640 medium (HyClone, Logan, UT, United States) at 37°C for 30 min. Then, cells were successively filtered through 70 and 40 μm mesh successively, and lysed with red blood cell lysis buffers.

$CD4^+$ T Cell Isolation and Intervention

Single-cell suspensions of splenocytes were harvested as described above. According to the manufacturer's instructions, $CD4^+$ T cells were purified with an EasySep Mouse $CD4^+$ T cell enrichment kit (STEMCELL Technologies, Canada), and

the purity was confirmed to be greater than 90% confirmed by FACS (Zhang et al., 2014). The purified naïve $CD4^+$ T cells were cultured in RPMI-1640 medium supplemented with 10% fetal bovine serum (HyClone) at a density of 1×10^5 in a 5% CO_2 humidified incubator at 37°C. In addition, $CD4^+$ T cells were induced by incubation with an anti-CD3 antibody (2.5 μg/ml, Invitrogen), an anti-CD28 antibody (5 μg/ml, Invitrogen), IL-2 (20 U/ml, Miltenyi Biotec) and TGF-β (2 ng/ml, Miltenyi Biotec) in the presence or absence of 10 nM RvD1 for 5 days (Chiurchiu et al., 2016). Cultures were supplemented with RvD1 every other day. After 5 days, cells were collected for FACS and real-time PCR analyses. In some cases, the purified naïve $CD4^+$ T cells were preincubated with anti-GPR32 neutralizing antibodies (2 μg/ml, GeneTex) and/or anti-ALX/FPR2 neutralizing antibodies (2 μg/ml, Genovac) for 30 min before the incubation with RvD1 or vehicle and then stimulated with anti-CD3/CD28, IL-2, and TGF-β.

Flow Cytometry

First, cells were incubated with Cytofix/Cytoperm (BioLegend) to permeabilize the cell membranes for 20 min at 4°C. Then, cells surfaces were stained with FITC-conjugated anti-CD4 and PE-conjugated anti-Foxp3 antibodies (eBiosciences, CA) according to the instructions. Finally, cytometry was performed with the BD FACS Calibur System (BD Bioscience). The plots were gated for $CD4^+$ lymphocytes, and Tregs were identified as $CD4^+Foxp3^+$ T cells.

Real-Time PCR

Total RNA was extracted with Trizol reagent, and cDNA was obtained by reverse transcription of 1 μg RNA according to the manufacturer's instructions. Foxp3, KIM-1, Nephrin and β-actin were amplified by real-time fluorescence quantitative PCR kits (Takara Corporation, Japan) using SYBR Green master mix (Finnzyme, New England Biolabs). Relative mRNA levels were calculated by the $2^{-\Delta\Delta Ct}$ method and normalized to those of β-actin. The sequences of primers used for quantitative reverse transcription-polymerase chain reaction (RT-PCR) are listed in **Table 1**.

Cytokines Enzyme-Linked Immunosorbent Assay (ELISA)

The concentrations of IFN-γ, IL-10, IL-6, and TNF-α in blood samples were determined by ELISA kits (eBioscience) according to the manufacturer's instructions. The absorbance of the final reactant was quantified at 450 nm with an ELISA plate reader (BioTek).

TABLE 1 | The sequences of primers used for RT-PCR.

Gene	Sense (5′→3′)	Antisense (5′→3′)
Foxp3	GCACAAGTGCTTTGTGCGA GT	TGTCTGTGGTTGCAGACGTTGT
KIM-1	ACATATCGTGGAATCACAACGAC	ACTGCTCTTCTGATAGGTGACA
Nephrin	CAGGGAAGACAGCAACAAACAA	CAGGTTTTCAGATAGAGCCCAGA
β-actin	CTGAGAGGGAAATCGTGCGT	CCACAGGATTCCATACCCAAGA

Statistical Analysis

Values are expressed as the means ± SDs and represented by at least three independent experiments. A least significant difference (LSD) *t*-test or a one-way analysis of variance (ANOVA) was performed to compare differences among diverse groups using SPSS 13.0 software. Significance levels were set at $P < 0.05$ for all data analyses.

RESULTS

RvD1 Alleviated Renal Injury in IRI-AKI

Duffield et al. (2006) demonstrated that IRI-AKI could result in the biosynthesis and release of RvD and protectins. To investigate the efficacy of RvD1 in IRI-AKI, mice were subjected to bilateral renal ischemia for 60 min. RvD1 was applied to the IRI mice via tail vein injection after reperfusion. The morphology and ultrastructure of kidney cells were nearly intact in the sham group, while IRI of the kidney resulted in protein cast formation, tubular epithelial cell sloughing, loss of the brush border, tubule dilation and infiltration of multiple inflammatory cells after 72 h. However, RvD1 administration significantly protected against tubule injury induced by IRI (**Figure 1A**). The semiquantitative assessment of ATN showed a lower score in the RvD1 group than in the IRI group (**Figure 1B**). In addition to the benefits to structural damage, RvD1 improved renal functions, which included reduced Scr levels at 24 and 72 h after reperfusion (**Figure 1C**). In addition, the mRNA level of kidney injury molecule-1 (KIM-1), a sensitive and specific biomarker for the early prediction of renal tubule injury (Vaidya et al., 2010), was increased at 24 and 72 h after reperfusion. As expected, RvD1 reduced the KIM-1 mRNA level compared with that in the IRI group (**Figure 1D**). Nephrin, a structural protein, plays an important role in maintaining the glomerular filtration barrier of the podocyte slit diaphragm (Kawachi et al., 1995; Ruotsalainen et al., 1999). It serves as an early marker of podocyte injury, and its reduced levels are largely associated with the loss of podocyte mass (Aaltonen et al., 2001). In our study, the nephrin mRNA levels were reduced at 24 and 72 h after reperfusion compared with those in the sham group; however, higher nephrin mRNA levels were observed in the RvD1-treated group (**Figure 1E**). Moreover, RvD1 administration reduced the levels of the proinflammatory cytokines IFN-γ, IL-6, and TNF-α but increased the level of the anti-inflammatory cytokine IL-10 in the serum (**Figure 1F**). In summary, these results suggested that RvD1 can alleviate renal lesions and protect renal function in IRI-AKI.

RvD1 Increased the Percentages of Tregs in IRI-AKI

$Foxp3^+$ Tregs inhibit innate and adaptive immune responses, which play important roles in ischemic preconditioning and ischemic AKI repair (Gandolfo et al., 2009; Kinsey et al., 2010). Therefore, we tested whether RvD1 administration could upregulate the proportions of Tregs in IRI-AKI mice. Single cells isolated from the spleen were detected by FACS

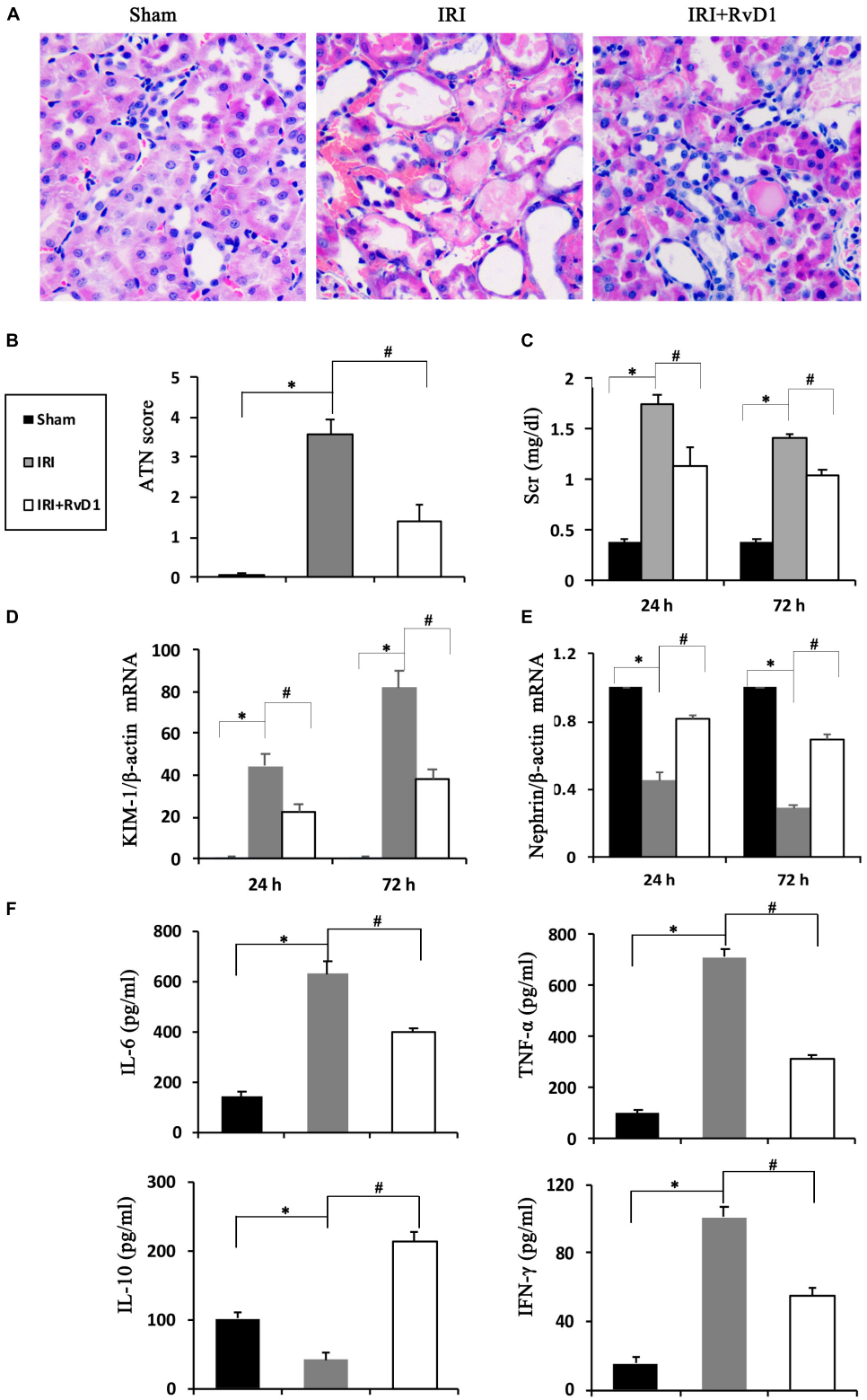

FIGURE 1 | RvD1 protected against renal injury in IRI-AKI mice. The IRI-AKI model was established by clamping the bilateral renal pedicles for 60 min. RvD1 (5 μg/kg/d) or vehicle was administered to the mice via the tail vein at 30 min, 24 and 48 h after reperfusion. **(A)** Kidneys were stained by PAS (original magnification, 400×). **(B)** ATN scores at 72 h after reperfusion. **(C)** Serum creatinine levels at 24 and 72 h after reperfusion. The relative mRNA expression of KIM-1 **(D)** and Nephrin **(E)** at 72 h after reperfusion. **(F)** Serum IL-6, TNF-α, IL-10, and IFN-γ levels at 72 h after reperfusion as determined by ELISA. Values are expressed as the means ± SDs, n = 6–8 per group. $^{*}P < 0.05$ versus sham; $^{\#}P < 0.05$ versus IRI.

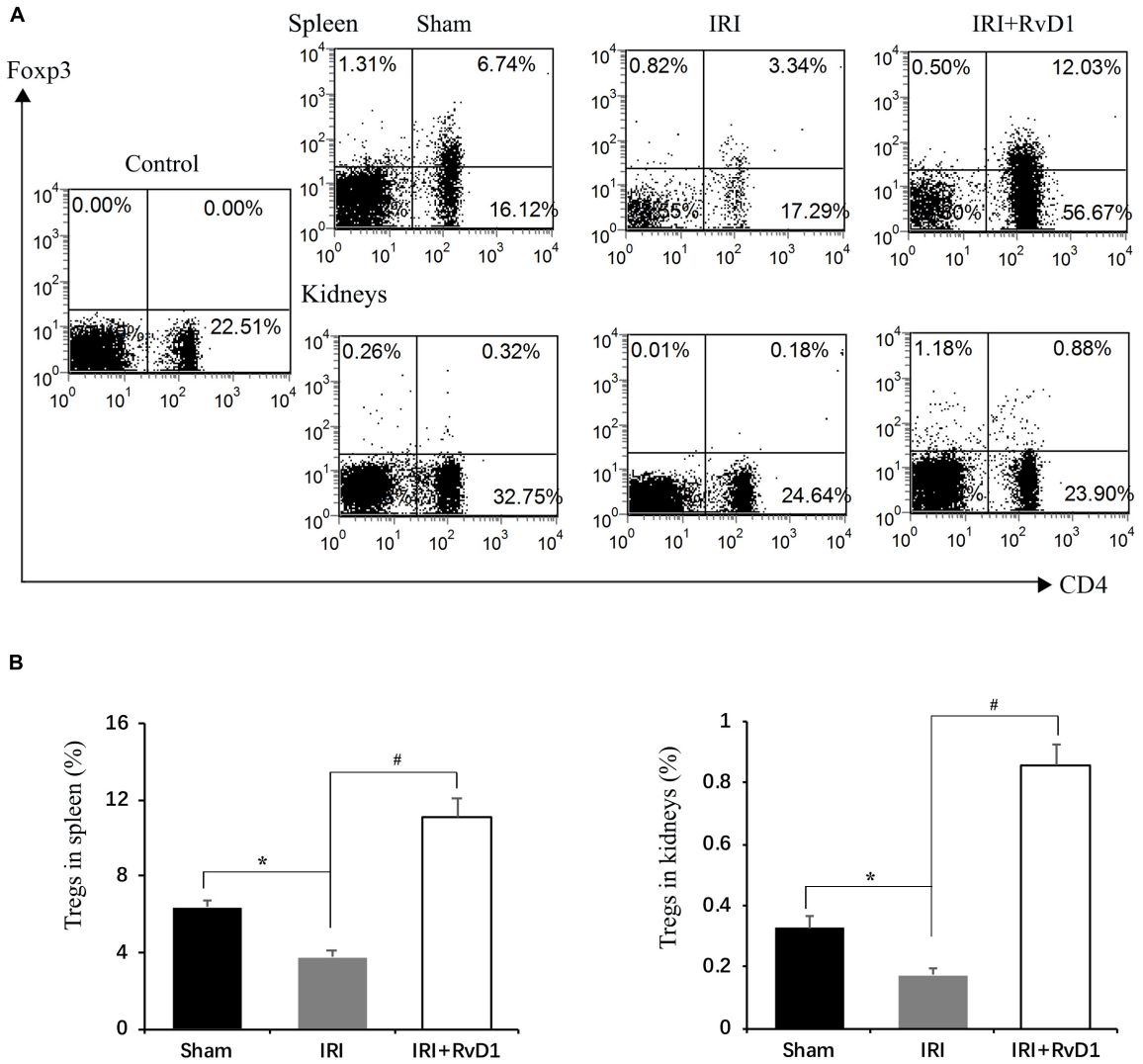

FIGURE 2 | RvD1 increased the percentages of Tregs in IRI-AKI mice. At 72 h after reperfusion, single-cell suspensions were harvested from splenocytes and kidney cells. **(A)** Representative flow cytometry analysis of $CD4^+Foxp3^+$T cells obtained from the spleen or kidneys in IRI-AKI mice. The plots are gated for $CD4^+$lymphocytes. The data are representative of 3 independent experiments. **(B)** Percentages of $CD4^+Foxp3^+$T cells in the spleen and kidneys of IRI-AKI mice. Values are expressed as the means ± SDs, n = 6–8 per group. $^*P < 0.05$ versus sham; $^\#P < 0.05$ versus IRI.

to assess $CD4^+Foxp3^+$ T cell percentages. We found that RvD1 increased Treg percentages in the spleen after 72 h of continuous administration (**Figures 2A,B**). Additionally, the Treg percentages in the kidneys increased after RvD1 administration (**Figures 2A,B**), although a small number of Tregs were observed in the kidneys of the IRI-AKI mice. Therefore, these results indicated that RvD1 enhances the Treg percentages in both the kidneys and spleen in IRI-AKI mice.

Depletion of Tregs Reversed the Beneficial Effects of RvD1 on IRI-AKI

To further define the role of Tregs in the beneficial effects of RvD1 on IRI-AKI, Tregs were depleted *in vivo*. PC61 (an anti-CD25 antibody, 100 μg) can reportedly effectively remove Tregs *in vivo* without affecting non-Tregs (Pasare and Medzhitov, 2004; Hu et al., 2013). After PC61 administration, the percentages of Tregs in the spleen and kidneys were significantly reduced in IRI-AKI mice (**Figures 3A,B**), which indicated that the depletion of Tregs was successful. In the IRI-AKI mice administered RvD1, PC61 reversed the beneficial effects of RvD1 on IRI-AKI, which included aggravated tubular injury (**Figure 4A**), increased ATN scores (**Figure 4B**) and renal function deterioration (**Figure 4C**). Moreover, higher KIM-1 mRNA levels (**Figure 4D**) and lower nephrin mRNA levels (**Figure 4E**) were observed in the PC61 group than in the rat IgG group. In addition, compared with rat IgG, PC61 treatment increased the levels of the proinflammatory cytokines IFN-γ, IL-6, and TNF-α but decreased the level of the anti-inflammatory cytokine IL-10 (**Figure 4F**). These experimental results demonstrate that the

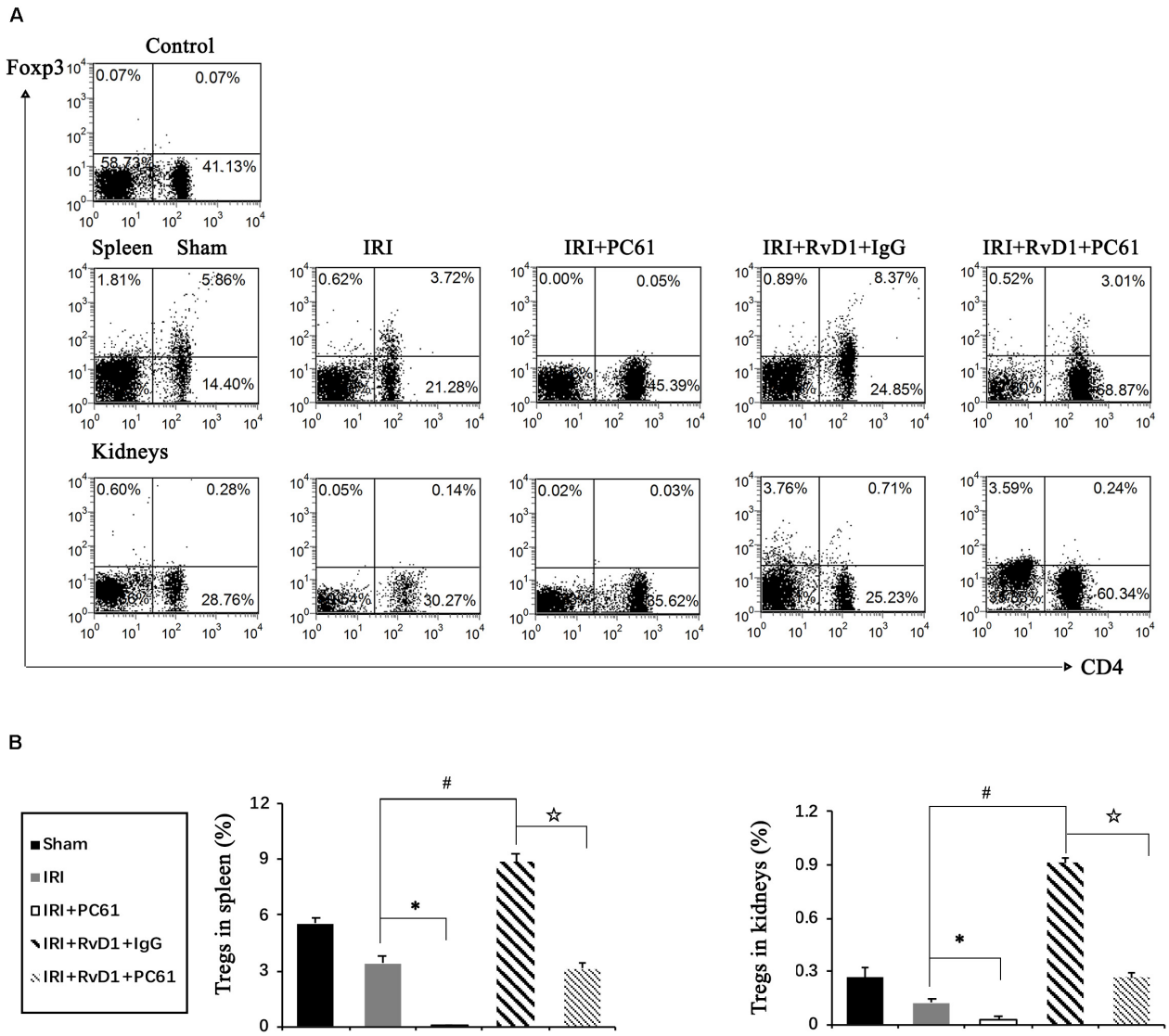

FIGURE 3 | PC61 administration reduced Treg percentages in the spleen and kidneys of IRI-AKI mice. The IRI-AKI model was established, and PC61 or rat IgG was administered via the tail vein after RvD1 or vehicle interventions. Single-cell suspensions were generated from the spleen and kidneys at 72 h after reperfusion. **(A)** Representative flow cytometry analysis of $CD4^+Foxp3^+$ T cells obtained from the spleen or kidneys of IRI-AKI mice treated with or without RvD1, PC61 or rat IgG. The plots are gated for $CD4^+$lymphocytes. The data are representative of 3 independent experiments. **(B)** The percentage of $CD4^+Foxp3^+$ T cells in the spleen or kidneys. Values are expressed as the means ± SDs, n = 6–8 per group. $^*P < 0.05$, IRI + PC61 versus IRI; $^{\#}P < 0.05$, IRI + RvD1 + IgG versus IRI; $^{☆}P < 0.05$, IRI + RvD1 + IgG versus IRI + RvD1 + PC61.

protection of RvD1 in IRI-AKI is related to the increased percentage of Tregs.

RvD1 Induced the Generation of Induced Tregs (iTregs) via ALX/FPR2 Receptors

Further, we conducted another study to explore whether RvD1 could affect the generation of iTregs, which develop from naïve $CD4^+$ T cells under antigen and TGF-β stimulation (Chiurchiu et al., 2016). To this end, naïve $CD4^+$ T cells were stimulated with RvD1 or vehicle under Treg-inducing conditions *in vitro* (**Figure 5A**). At 96 h, the percentages of $CD4^+Foxp3^+$ Tregs (**Figures 5B,C**), Foxp3 mRNA expression (**Figure 5E**), and serum IL-10 levels (**Figure 5D**) were all increased in the presence of RvD1 compared with the control vehicle. These results suggest that RvD1 affects not only the induction of Tregs but also their specific functional properties.

To verify the potential molecular mechanism of RvD1 in iTreg regulation, we assessed the role of RvD1 receptors in iTregs. GPR32 and ALX/FPR2 are known receptors of RvD (Krishnamoorthy et al., 2010; Norling et al., 2012) and because Chiurchiu et al. demonstrated that iTregs express both GPR32 and ALX/FPR2 (Chiurchiu et al., 2016), we focused on

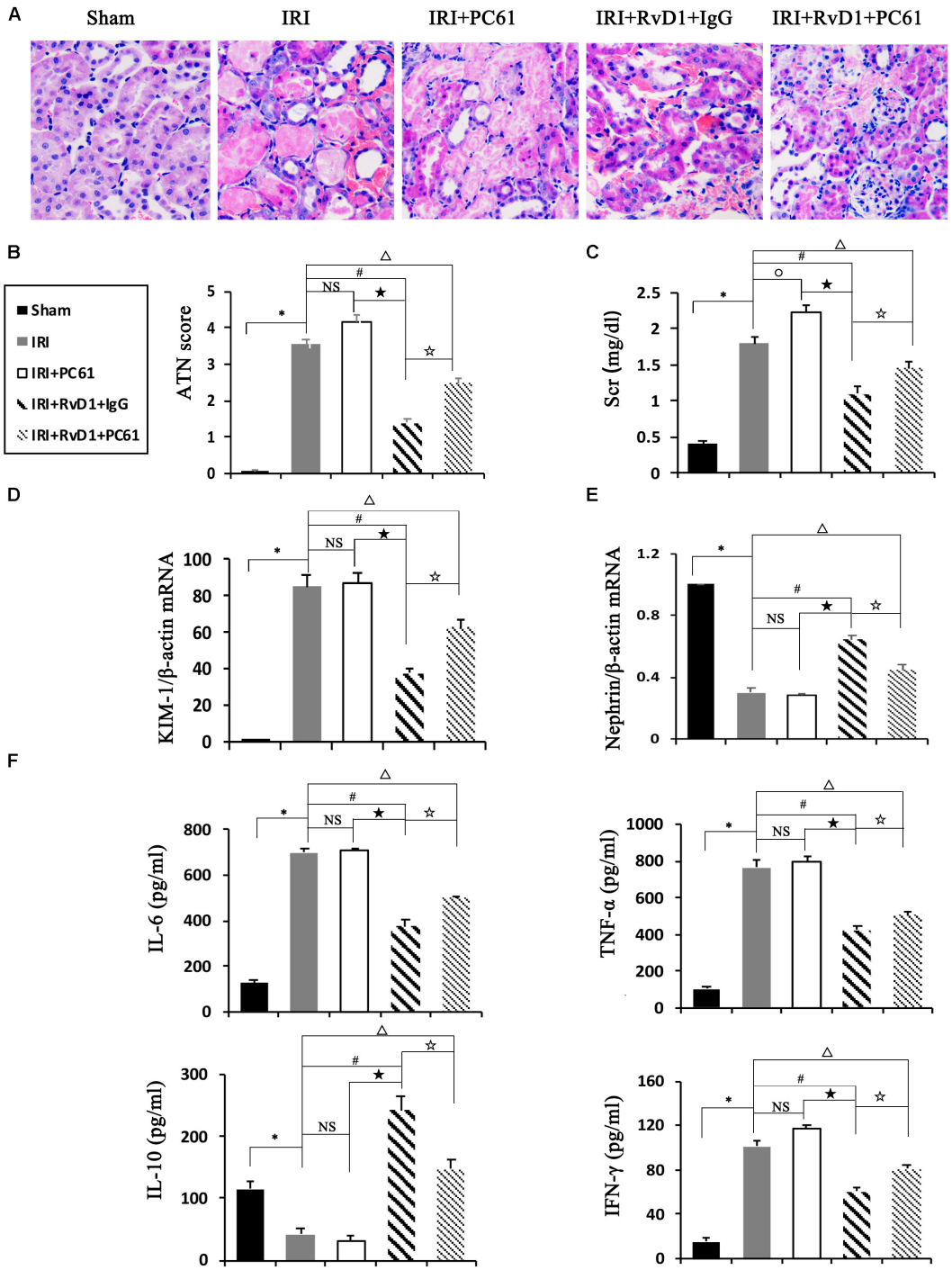

FIGURE 4 | PC61 reversed the beneficial effects of RvD1 on IRI-AKI. **(A)** Kidneys were stained by PAS (original magnification, 400×). **(B)** ATN scores at 72 h after reperfusion. **(C)** Serum creatinine levels at 72 h after reperfusion. The relative mRNA expression of KIM-1 **(D)** and Nephrin **(E)** at 72 h after reperfusion. **(F)** Serum IL-6, TNF-α, IL-10 and IFN-γ levels at 72 h after reperfusion as determined by ELISA. Values are expressed as the means ± SDs, n = 6–8 per group. $^{*}P < 0.05$, IRI versus Sham; $^{\#}P < 0.05$, IRI + RvD1 + IgG versus IRI; $^{\bigstar}P < 0.05$, IRI + PC61 versus IRI + RvD1 + IgG; $^{\star}P < 0.05$, IRI + RvD1 + IgG versus IRI + RvD1 + PC61; $^{\Delta}P < 0.05$, IRI + RvD1 + PC61 versus IRI; $^{\circ}P < 0.05$, IRI + PC61 versus IRI; NS: not significant.

these receptors. Interestingly, preincubation with anti-ALX/FPR2 neutralizing antibodies alone or in combination with anti-GPR32 neutralizing antibodies abrogated the enhancement effect of RvD1 on iTregs, while anti-GPR32 neutralizing antibodies alone did not (**Figures 5B–E**). This result suggests that the receptor ALX/FPR2 mediates the effects of RvD1 on iTregs *in vitro*.

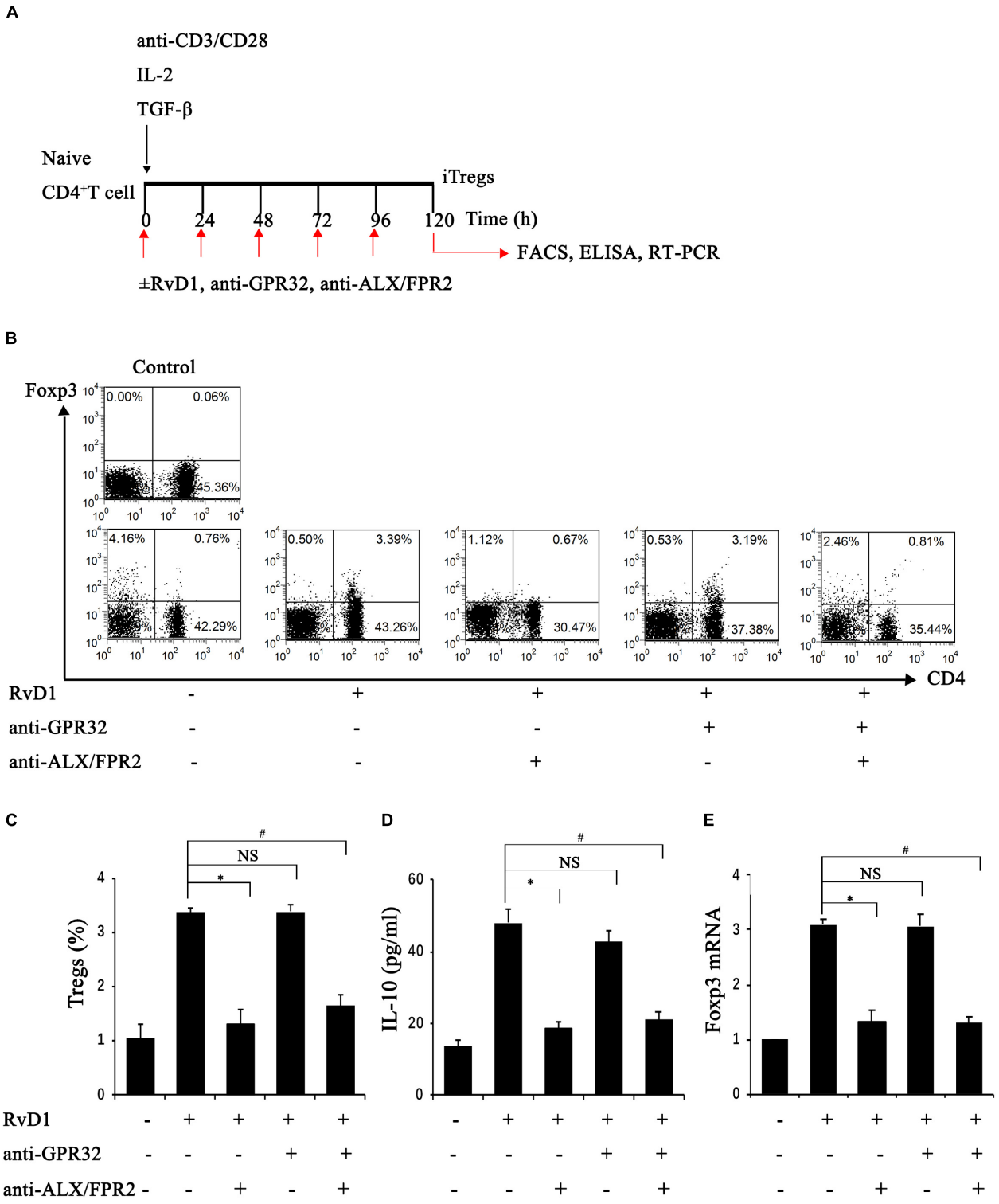

FIGURE 5 | RvD1 induced the generation of iTregs via the receptor ALX/FPR2. **(A)** The sketch map of iTreg generation. **(B)** Representative flow cytometry analysis of iTregs generated with or without RvD1, an anti-GPR32 neutralizing antibody, or an anti-ALX/FPR2 neutralizing antibody at 96 h after incubation under the condition of iTreg generation. The plots are gated for $CD4^+$ lymphocytes. The data are representative of 3 independent experiments. **(C)** The percentage of iTregs. **(D)** IL-10 levels in the supernatants of iTregs as determined by ELISA. **(E)** The mRNA expression of Foxp3 in iTregs as determined by RT-PCR. Values are expressed as the means ± SDs, $n = 6$ per group. $^*P < 0.05$, RvD1 versus RvD1 + anti-ALX/FPR2 antibody; $^\#P < 0.05$, RvD1 versus RvD1 + anti-ALX/FPR2 antibody + anti-GPR32 antibody; NS: not significant, RvD1 versus RvD1 + anti-GPR32 antibody.

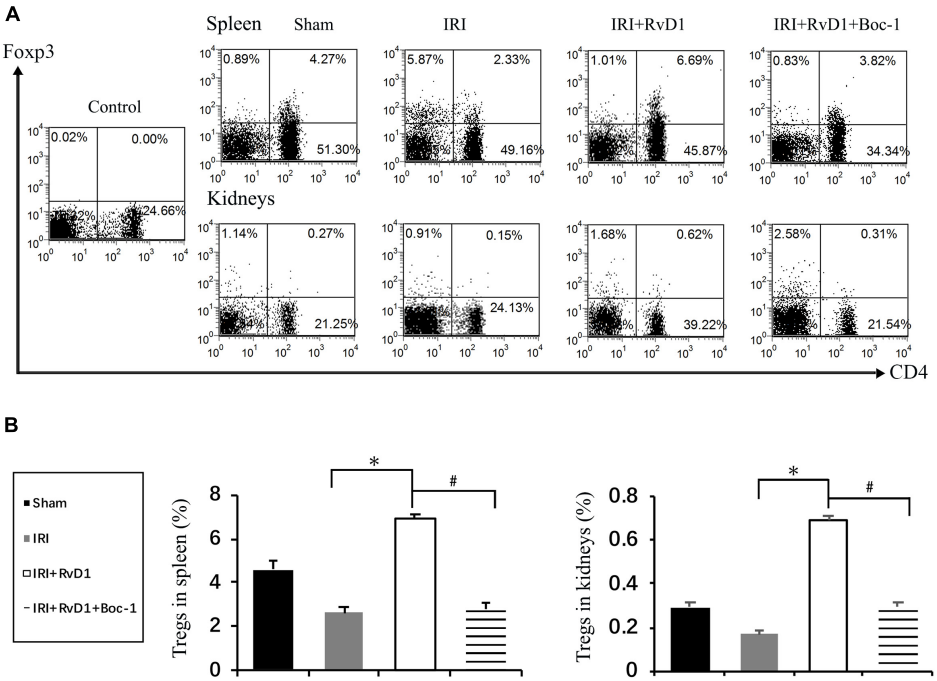

FIGURE 6 | Boc-1 abrogated the effect of RvD1 on the spleen and kidney cell Treg percentages. The IRI-AKI model was established and Boc-1 was administered via the tail vein after RvD1 or vehicle interventions. **(A)** Representative flow cytometry analysis of $CD4^+Foxp3^+$ T cells obtained from the spleen or kidneys of IRI-AKI mice treated with or without RvD1 or Boc-1. The plots are gated for $CD4^+$ lymphocytes. The data are representative of 3 independent experiments. **(B)** The percentage of $CD4^+Foxp3^+$ T cells in the spleen or kidneys. Values are expressed as the means ± SDs, n = 6–8 per group. $^*P < 0.05$, IRI versus IRI + RvD1; $^\#P < 0.05$, IRI + RvD1 versus IRI + RvD1 + Boc-1.

Boc-1 Reversed the Protective Effect of RvD1 on IRI-AKI

Boc-1 is a selective RvD1-receptor ALX/FPR2 antagonist. To further verify that RvD1 increases the percentage of Tregs through the ALX/FPR2 pathway *in vivo*, Boc-1 was administered to IRI-AKI mice. We found that Boc-1 reduced the Treg percentages in the spleen and kidneys of IRI-AKI mice treated with RvD1 (**Figure 6**). Additionally, compared with RvD1 treatment, the administration of Boc-1 *in vivo* led to pathological changes (widespread protein cast, tubular necrosis and inflammatory cell infiltration; **Figure 7A**), increased in ATN scores (**Figure 7B**), renal dysfunction (manifested as high levels of Scr; **Figure 7C**) and inflammatory cytokines infiltration (high serum levels of IFN-γ, IL-6 and TNF-α; **Figure 7F**). Moreover, Boc-1 treatment increased the mRNA levels of KIM-1 (**Figure 7D**) but reduced those of Nephrin (**Figure 7E**) compared to those in the RvD1 treatment group. This result demonstrated that Boc-1 reversed the protective effect of RvD1 on IRI-AKI.

DISCUSSION

RvD1, one of the most extensively studied resolvins, can promote the resolution of inflammation by inhibiting inflammatory cell infiltration, downregulating cytokine secretion and promoting neutrophil apoptosis (Schwab et al., 2007). It is reported to play protective roles in a variety of disease models, including acute lung injury, peritonitis, wound infection, insulin resistance and atherosclerosis models (Bento et al., 2011; Weylandt et al., 2012). In the field of nephrology, RvD1 can also preserve renal function and inhibit fibrosis in multiple kidney diseases, such as obstructive nephropathy (Qu et al., 2012), adriamycin-induced AKI (Zhang et al., 2013), lipopolysaccharide (LPS)-induced AKI (Chen et al., 2014), paraquat-induced AKI (Hu et al., 2019), and IRI-AKI (Duffield et al., 2006). In our research, RvD1 administration alleviated renal injury and protected renal function in IRI-AKI, results that were identical to those of previous studies.

In addition to limiting inflammation, RvD1 also plays an important role in adaptive immune mediation. Chiurchiu et al. reported that RvD1 could promote the generation of $Foxp3^+$ Tregs (Chiurchiu et al., 2016). Luo et al. suggested that RvD1 could increase Treg activity and the macrophage phagocytosis of apoptotic T cells, which was shown to contribute to disease recovery in rats with experimental autoimmune neuritis (Luo et al., 2016). Tregs are lymphocytes with immunosuppressive properties that are commonly identified by their expression of CD4 and CD25 on the cell surface and upregulated levels of the transcription factor Foxp3 (Fontenot et al., 2003). With the development of a tissue digestion and sieving technique followed by flow cytometry, Tregs were discovered in the normal kidney (Ascon et al., 2006). Despite less infiltration in the normal kidney (less than 1% as assessed by FACS) (Gandolfo et al., 2009; Kinsey et al., 2009), Tregs still play an important role in many kidney

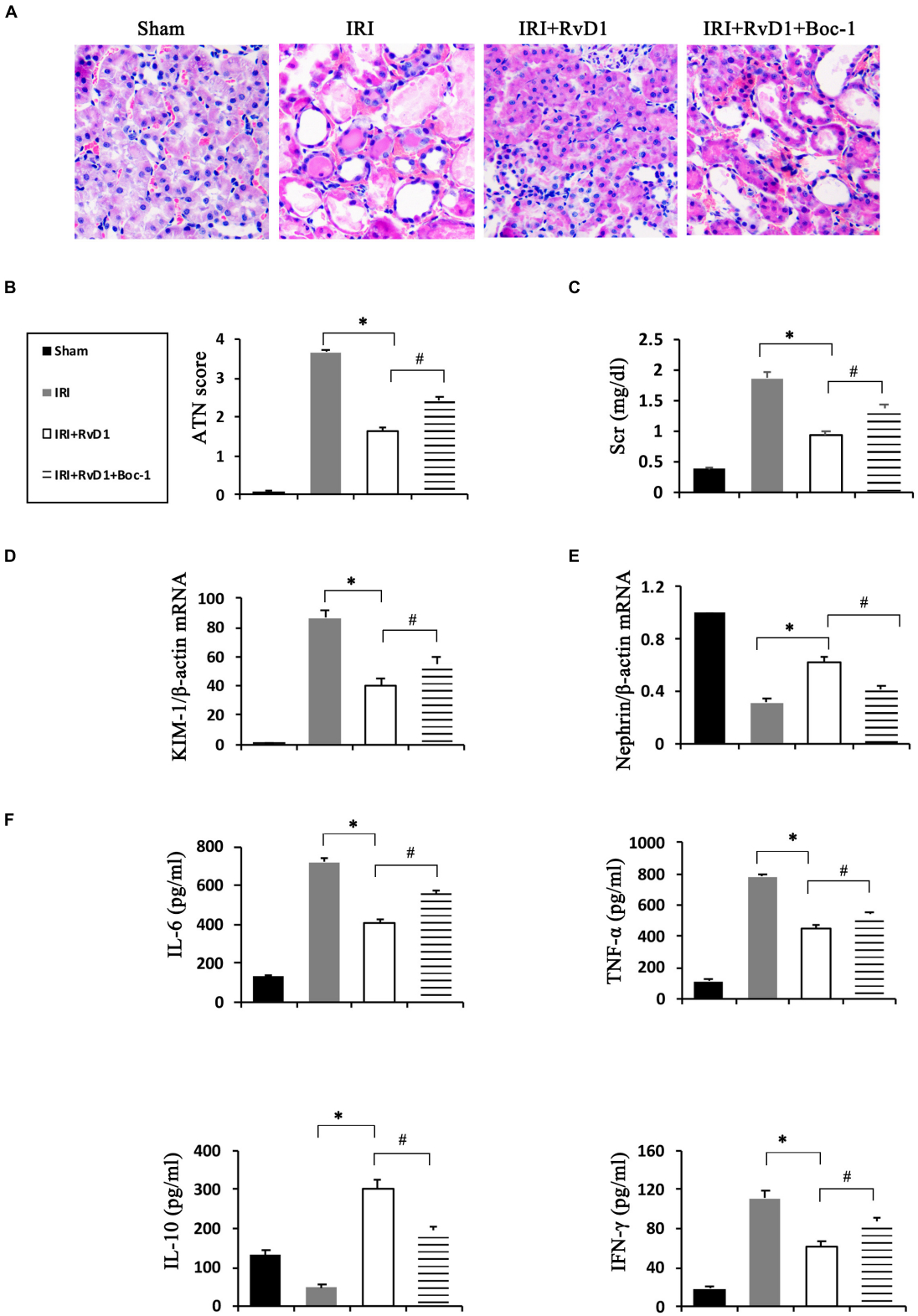

FIGURE 7 | Boc-1 reversed the improved therapeutic efficacy of RvD1 in IRI-AKI. **(A)** Kidneys were stained by PAS (original magnification, 400×). **(B)** ATN scores at 72 h after reperfusion. **(C)** Serum creatinine levels at 72 h after reperfusion. The relative mRNA expression of KIM-1 **(D)** and Nephrin **(E)** at 72 h after reperfusion. **(F)** Serum IL-6, TNF-α, IL-10 and IFN-γ levels at 72 h after reperfusion as determined by ELISA. Values are expressed as the means ± SDs, n = 6–8 per group. $^{*}P < 0.05$, IRI versus IRI + RvD1; $^{\#}P < 0.05$, IRI + RvD1 versus IRI + RvD1 + Boc-1.

diseases, such as AKI and progression to CKD. Tregs suppress innate immunity and participate in the repair of ischemic AKI and in renal ischemic preconditioning (Gandolfo et al., 2009; Kinsey et al., 2009, 2010). Our studies demonstrated that RvD1 administration could increase the Treg percentages in the spleen and kidneys of IRI-AKI mice. However, whether the increased percentages of Tregs were important for the protective effect of RvD1 remained unknown. To better understand the causal relationship between the induction of Treg activity by RvD1 and its renal protective effect, PC61, an anti-CD25 antibody, was used to deplete Tregs, which mitigated the effect of RvD1 on ischemic injury. These results suggest that the increased percentages of Tregs induced by RvD1 treatment may contribute to the beneficial effects of RvD1 on IRI-AKI.

Treg depletion experiments are complex. The administration of PC61 to IRI-AKI mice slightly increased the average ATN score and the inflammatory cytokine levels compared with those in IRI group, but the differences were not statistically significant. This result was consistent with those reported by Bai et al. (2018) and Gandolfo et al. (2009). However, Gandolfo reported that PC61 administration reduced Scr levels within 1 day, increased tubular damage in the outer medulla after 3 days and persistently increased tubular damage after 10 days in IRI-AKI mice, while Treg transfer was associated with histological changes only at 10 days. These results suggested that Treg depletion and transfer require some time to become effective, which may be related to the lower number of Tregs in the kidney. These studies may further explain our results, and we hypothesized that as the IRI time extends in mice, the effect of PC61 on renal pathology will gradually appear. In addition, the treatment of Tregs-depleted mice with RvD1 had some protective effects in histopathology, renal function and inflammatory cytokines levels compared with those in the IRI group. Therefore, we speculate that RvD1 protects IRI-AKI mice by increasing the numbers of not only Tregs but also other cells, such as TH1 and Th17 cells.

The mechanism of Treg amplification in mice treated with RvD1 may be associated with the proliferation of preexisting Tregs or the transformation of naïve $CD4^+$ T cells. Recently, Chiurchiu et al. reported that RvD1 could enhance the *de novo* generation of $Foxp3^+$ Tregs and further confirmed the conclusion drawn *in vivo* regarding $Elovl2^{-/-}$ mice, which are deficient for elongase 2, the key enzyme involved in the synthesis of DHA (the precursor of RvD) (Chiurchiu et al., 2016). *In vitro*, we further evaluated whether RvD1 could affect the transformation of non-Tregs to Tregs. iTregs develop from naïve $CD4^+$ T cells under stimulation by antigen and TGF-β (Yamagiwa et al., 2001). Therefore, purified naïve $CD4^+$ T cells were incubated with RvD1 under the condition of Treg induction. Our data showed that RvD1 could potentiate iTreg differentiation, with significantly higher Foxp3 mRNA expression levels compared to those in the control group. The GPR32 and ALX/FPR2 are two receptors that have been shown to transmit RvD1 signals, but only ALX/FPR2 has been identified in rodents (Recchiuti, 2013). Interestingly, after the addition of an anti-ALX/FPR2 neutralizing antibody, the Treg percentage, Foxp3 mRNA level and IL-10 level were reduced. However, this effect was not observed after the additional application of an anti-GPR32 neutralizing antibody. Furthermore, *in vivo* studies showed that the administration of Boc-1, a selective RvD1-receptor ALX/FPR2 antagonist, reduced the percentages of Tregs in the spleen and kidneys of IRI-AKI mice treated with RvD1 and reversed the beneficial effects of RvD1 on tubular injury. Therefore, these results suggest that RvD1 enhances the generation of iTregs and the protective efficacy of RvD1 against IRI-AKI via the ALX/FPR2 pathway.

In summary, our studies demonstrated that RvD1 administration improved renal injury in IRI-AKI. This amelioration efficacy was associated with an increased percentage of Tregs induced by the ALX/FPR2 pathway.

DATA AVAILABILITY STATEMENT

The raw data supporting the conclusion of this article will be made available by the authors, without undue reservation, to any qualified researcher.

ETHICS STATEMENT

The animal study was reviewed and approved by the Animal Care Committee of Qingdao University.

AUTHOR CONTRIBUTIONS

HL and YX designed the study and wrote the manuscript. CW and LZ contributed to the original data. SS performed the pathological image analysis. LL and BZ contributed to the flow cytometry analysis. XS performed the cell experiments. JS performed the ELISA and RNA data analysis.

FUNDING

This study was funded by grants (Nos. 81470973 and 81800601) from the National Natural Science Foundation of China.

REFERENCES

Aaltonen, P., Luimula, P., Astrom, E., Palmen, T., Gronholm, T., Palojoki, E., et al. (2001). Changes in the expression of nephrin gene and protein in experimental diabetic nephropathy. *Lab. Invest.* 81, 1185–1190. doi: 10.1038/labinvest.3780332

Ascon, D. B., Lopez-Briones, S., Liu, M., Ascon, M., Savransky, V., Colvin, R. B., et al. (2006). Phenotypic and functional characterization of kidney-infiltrating lymphocytes in renal ischemia reperfusion injury. *J. Immunol.* 177, 3380–3387. doi: 10.4049/jimmunol.177.5.3380

Bai, M., Zhang, L., Fu, B., Bai, J., Zhang, Y., Cai, G., et al. (2018). IL-17A improves the efficacy of mesenchymal stem cells in ischemic-reperfusion renal injury

by increasing Treg percentages by the COX-2/PGE2 pathway. *Kidney Int.* 93, 814–825. doi: 10.1016/j.kint.2017.08.030

Bento, A. F., Claudino, R. F., Dutra, R. C., Marcon, R., and Calixto, J. B. (2011). Omega-3 fatty acid-derived mediators 17(R)-hydroxy docosahexaenoic acid, aspirin-triggered resolvin D1 and resolvin D2 prevent experimental colitis in mice. *J. Immunol.* 187, 1957–1969. doi: 10.4049/jimmunol.1101305

Chen, J., Shetty, S., Zhang, P., Gao, R., Hu, Y., Wang, S., et al. (2014). Aspirin-triggered resolvin D1 down-regulates inflammatory responses and protects against endotoxin-induced acute kidney injury. *Toxicol. Appl. Pharmacol.* 277, 118–123. doi: 10.1016/j.taap.2014.03.017

Chiurchiu, V., Leuti, A., Dalli, J., Jacobsson, A., Battistini, L., Maccarrone, M., et al. (2016). Proresolving lipid mediators resolvin D1, resolvin D2, and maresin 1 are critical in modulating T cell responses. *Sci. Transl. Med.* 8:353ra111. doi: 10.1126/scitranslmed.aaf7483

Duffield, J. S., Hong, S., Vaidya, V. S., Lu, Y., Fredman, G., Serhan, C. N., et al. (2006). Resolvin D series and protectin D1 mitigate acute kidney injury. *J. Immunol.* 177, 5902–5911. doi: 10.4049/jimmunol.177.9.5902

Fontenot, J. D., Gavin, M. A., and Rudensky, A. Y. (2003). Foxp3 programs the development and function of CD4+CD25+ regulatory T cells. *Nat. Immunol.* 4, 330–336. doi: 10.1038/ni904

Gandolfo, M. T., Jang, H. R., Bagnasco, S. M., Ko, G. J., Agreda, P., Satpute, S. R., et al. (2009). Foxp3+ regulatory T cells participate in repair of ischemic acute kidney injury. *Kidney Int.* 76, 717–729. doi: 10.1038/ki.2009.259

Halade, G. V., Kain, V., and Serhan, C. N. (2018). Immune responsive resolvin D1 programs myocardial infarction-induced cardiorenal syndrome in heart failure. *FASEB J.* 32, 3717–3729. doi: 10.1096/fj.201701173RR

Hong, S., Gronert, K., Devchand, P. R., Moussignac, R. L., and Serhan, C. N. (2003). Novel docosatrienes and 17S-resolvins generated from docosahexaenoic acid in murine brain, human blood, and glial cells, Autacoids in anti-inflammation. *J. Biol. Chem.* 278, 14677–14687. doi: 10.1074/jbc.M300218200

Hu, J., Zhang, L., Wang, N., Ding, R., Cui, S., Zhu, F., et al. (2013). Mesenchymal stem cells attenuate ischemic acute kidney injury by inducing regulatory T cells through splenocyte interactions. *Kidney Int.* 84, 521–531. doi: 10.1038/ki.2013.114

Hu, X., Liang, Y., Zhao, H., and Zhao, M. (2019). Effects of AT-RvD1 on paraquat-induced acute renal injury in mice. *Int. Immunopharmacol.* 67, 231–238. doi: 10.1016/j.intimp.2018.12.029

Kawachi, H., Abrahamson, D. R., St John, P. L., Goldstein, D. J., Shia, M. A., Matsui, K., et al. (1995). Developmental expression of the nephritogenic antigen of monoclonal antibody 5-1-6. *Am. J. Pathol.* 147, 823–833.

Kinsey, G. R., Huang, L., Vergis, A. L., Li, L., and Okusa, M. D. (2010). Regulatory T cells contribute to the protective effect of ischemic preconditioning in the kidney. *Kidney Int.* 77, 771–780. doi: 10.1038/ki.2010.12

Kinsey, G. R., Sharma, R., Huang, L., Li, L., Vergis, A. L., Ye, H., et al. (2009). Regulatory T cells suppress innate immunity in kidney ischemia-reperfusion injury. *J. Am. Soc. Nephrol.* 20, 1744–1753. doi: 10.1681/ASN.2008111160

Krishnamoorthy, S., Recchiuti, A., Chiang, N., Yacoubian, S., Lee, C. H., Yang, R., et al. (2010). Resolvin D1 binds human phagocytes with evidence for proresolving receptors. *Proc. Natl. Acad. Sci. U.S.A.* 107, 1660–1665. doi: 10.1073/pnas.0907342107

Luo, B., Han, F., Xu, K., Wang, J., Liu, Z., Shen, Z., et al. (2016). Resolvin D1 programs inflammation resolution by increasing TGF-beta expression induced by dying cell clearance in experimental autoimmune neuritis. *J. Neurosci.* 36, 9590–9603. doi: 10.1523/JNEUROSCI.0020-16.2016

Mehta, R. L., Cerda, J., Burdmann, E. A., Tonelli, M., Garcia-Garcia, G., Jha, V., et al. (2015). International Society of Nephrology's 0by25 initiative for acute kidney injury (zero preventable deaths by 2025): a human rights case for nephrology. *Lancet* 385, 2616–2643. doi: 10.1016/S0140-6736(15)60126-X

Norling, L. V., Dalli, J., Flower, R. J., Serhan, C. N., and Perretti, M. (2012). Resolvin D1 limits polymorphonuclear leukocyte recruitment to inflammatory loci: receptor-dependent actions. *Arterioscler. Thromb. Vasc. Biol.* 32, 1970–1978. doi: 10.1161/ATVBAHA.112.249508

Pasare, C., and Medzhitov, R. (2004). Toll-dependent control mechanisms of CD4 T cell activation. *Immunity* 21, 733–741. doi: 10.1016/j.immuni.2004.10.006

Qu, X., Zhang, X., Yao, J., Song, J., Nikolic-Paterson, D. J., and Li, J. (2012). Resolvins E1 and D1 inhibit interstitial fibrosis in the obstructed kidney via inhibition of local fibroblast proliferation. *J. Pathol.* 228, 506–519. doi: 10.1002/path.4050

Recchiuti, A. (2013). Resolvin D1 and its GPCRs in resolution circuits of inflammation. *Prostaglandins Other Lipid Mediat.* 107, 64–76. doi: 10.1016/j.prostaglandins.2013.02.004

Ruotsalainen, V., Ljungberg, P., Wartiovaara, J., Lenkkeri, U., Kestila, M., Jalanko, H., et al. (1999). Nephrin is specifically located at the slit diaphragm of glomerular podocytes. *Proc. Natl. Acad. Sci. U.S.A.* 96, 7962–7967. doi: 10.1073/pnas.96.14.7962

Schwab, J. M., Chiang, N., Arita, M., and Serhan, C. N. (2007). Resolvin E1 and protectin D1 activate inflammation-resolution programmes. *Nature* 447, 869–874. doi: 10.1038/nature05877

Serhan, C. N., Hong, S., Gronert, K., Colgan, S. P., Devchand, P. R., Mirick, G., et al. (2002). Resolvins: a family of bioactive products of omega-3 fatty acid transformation circuits initiated by aspirin treatment that counter proinflammation signals. *J. Exp. Med.* 196, 1025–1037. doi: 10.1084/jem.20020760

Spite, M., Summers, L., Porter, T. F., Srivastava, S., Bhatnagar, A., and Serhan, C. N. (2009). Resolvin D1 controls inflammation initiated by glutathione-lipid conjugates formed during oxidative stress. *Br. J. Pharmacol.* 158, 1062–1073. doi: 10.1111/j.1476-5381.2009.00234.x

Sun, Y. P., Oh, S. F., Uddin, J., Yang, R., Gotlinger, K., Campbell, E., et al. (2007). Resolvin D1 and its aspirin-triggered 17R epimer. Stereochemical assignments, anti-inflammatory properties, and enzymatic inactivation. *J. Biol. Chem.* 282, 9323–9334. doi: 10.1074/jbc.M609212200

Vaidya, V. S., Ozer, J. S., Dieterle, F., Collings, F. B., Ramirez, V., Troth, S., et al. (2010). Kidney injury molecule-1 outperforms traditional biomarkers of kidney injury in preclinical biomarker qualification studies. *Nat. Biotechnol.* 28, 478–485. doi: 10.1038/nbt.1623

Weylandt, K. H., Chiu, C. Y., Gomolka, B., Waechter, S. F., and Wiedenmann, B. (2012). Omega-3 fatty acids and their lipid mediators: towards an understanding of resolvin and protectin formation. *Prostaglandins Other Lipid Mediat.* 97, 73–82. doi: 10.1016/j.prostaglandins.2012.01.005

Yamagiwa, S., Gray, J. D., Hashimoto, S., and Horwitz, D. A. (2001). A role for TGF-beta in the generation and expansion of CD4+CD25+ regulatory T cells from human peripheral blood. *J. Immunol.* 166, 7282–7289. doi: 10.4049/jimmunol.166.12.7282

Zhang, Q., Luan, H., Wang, L., He, F., Zhou, H., Xu, X., et al. (2014). Galectin-9 ameliorates anti-GBM glomerulonephritis by inhibiting Th1 and Th17 immune responses in mice. *Am. J. Physiol. Renal Physiol.* 306, F822–F832. doi: 10.1152/ajprenal.00294.2013

Zhang, X., Qu, X., Sun, Y. B., Caruana, G., Bertram, J. F., Nikolic-Paterson, D. J., et al. (2013). Resolvin D1 protects podocytes in adriamycin-induced nephropathy through modulation of 14-3-3beta acetylation. *PLoS One* 8:e67471. doi: 10.1371/journal.pone.0067471

Conflict of Interest: The authors declare that the research was conducted in the absence of any commercial or financial relationships that could be construed as a potential conflict of interest.

Copyright © 2020 Luan, Wang, Sun, Zhao, Li, Zhou, Shao, Shen and Xu. This is an open-access article distributed under the terms of the Creative Commons Attribution License (CC BY). The use, distribution or reproduction in other forums is permitted, provided the original author(s) and the copyright owner(s) are credited and that the original publication in this journal is cited, in accordance with accepted academic practice. No use, distribution or reproduction is permitted which does not comply with these terms.

frontiers in Medicine

ORIGINAL RESEARCH
published: 07 April 2020
doi: 10.3389/fmed.2020.00109

Baseline Soluble Anti-erythropoietin Antibody Level Is an Independent Associated Factor for Follow-Up Erythropoietin Demand in Maintenance Dialysis Patients With End-Stage Renal Disease: A Prospective Cohort Study

*Ying Zhang[1], Shi-Zhu Bian[2], Kun Yang[1], Yiqing Wang[1], Sha Tang[1], Weili Wang[1], Daihong Wang[1], Ling Nie[1] and Jinghong Zhao[1]**

[1] Department of Nephrology, Institute of Nephrology of Chongqing and Kidney Center of PLA, Xinqiao Hospital, Army Medical University (Third Medical University), Chongqing, China, [2] Department of Cardiology, Institute of Cardiovascular Diseases of PLA, Xinqiao Hospital, Army Medical University (Third Military Medical University), Chongqing, China

OPEN ACCESS

Edited by:
Xueying Zhao,
Morehouse School of Medicine,
United States

Reviewed by:
Praveen Kumar Potukuchi,
University of Tennessee Health Science Center (UTHSC),
United States
Daw-Yang Hwang,
National Health Research Institutes, Taiwan

***Correspondence:**
Jinghong Zhao
zhaojh@tmmu.edu.cn

Specialty section:
This article was submitted to Nephrology, a section of the journal Frontiers in Medicine

Received: *09 November 2019*
Accepted: *10 March 2020*
Published: *07 April 2020*

Citation:
Zhang Y, Bian S-Z, Yang K, Wang Y, Tang S, Wang W, Wang D, Nie L and Zhao J (2020) Baseline Soluble Anti-erythropoietin Antibody Level Is an Independent Associated Factor for Follow-Up Erythropoietin Demand in Maintenance Dialysis Patients With End-Stage Renal Disease: A Prospective Cohort Study. Front. Med. 7:109. doi: 10.3389/fmed.2020.00109

Aims: The aim of this study was to identify the predictive role of baseline anti-erythropoietin (anti-EPO) antibody levels in follow-up EPO demand in maintenance dialysis patients with end-stage renal disease (ESRD).

Methods: Baseline routine blood parameters, clinical data, dialysis-related parameters, EPO, anti-EPO antibody, and anti-EPO-receptor antibody were also measured. Differences in the abovementioned variables were compared among four intervals of the EPO demand index (EDI). Further univariate and adjusted logistic regression analyses were performed to identify the independent predictors for higher EPO demand.

Results: The predialysis potassium ion concentration was significantly higher in the fourth quartile (Q4) population than in the other three populations ($p < 0.05$). Furthermore, the anti-EPO antibody level showed significant differences among the four intervals ($p = 0.006$). The baseline anti-EPO antibody level was correlated with the follow-up EDI ($r^2 = 0.0377$, $p = 0.030$). Furthermore, the follow-up EDI was significantly higher in the anti-EPO antibody-positive group ($p = 0.02$). Age (OR = 1.071, $p = 0.005$), ferritin (OR = 1.001, $p = 0.038$), potassium ion concentration before dialysis (OR = 2.781, $p = 0.012$), dialysis duration (OR = 1.025, $p = 0.030$), and anti-EPO antibody level (OR = 7.694, $p = 0.004$) were potential predictors for higher EPO demand. After adjustment, age (OR = 1.072, $p = 0.026$), potassium ion concentration before dialysis (OR = 3.425, $p = 0.013$), and EPO level (OR = 5.27, $p = 0.007$) were independent predictors for higher EDI demand.

Conclusion: The baseline anti-EPO antibody level combined with an older age and a higher predialysis potassium ion concentration are independent predictors for a higher follow-up EPO demand in maintenance dialysis patients with ESRD.

Keywords: anti-erythropoietin antibody, predictor, erythropoietin demand, maintenance dialysis, cohort study

INTRODUCTION

Anemia is considered the most frequent complication in patients with end-stage renal disease (ESRD), especially in the subpopulation on maintenance dialysis (1). It has also been identified as an independent risk factor/predictor for major cardiovascular events, including heart failure and atherosclerosis (2). Anemia in ESRD patients has also been demonstrated to be caused mainly by insufficient synthesis of erythropoietin (EPO) combined with erythropoietin resistance as well as a higher erythropoietin demand (3).

It has been demonstrated that up to 10% of patients in the erythropoietin-stimulating agent (ESA)-treated population have a lower erythropoietin response (1, 4, 5). Furthermore, an imbalance between the production of EPO and the demand for EPO is another pivotal reason for anemia in patients treated with ESA.

Erythropoietin demand reflects the need for erythropoietin (including endogenous and exogenous EPO) in ESRD patients in order to produce sufficient Hb to eliminate anemia (6, 7). Previous studies have shown that maintenance of dialysis patients with ESRD may be characterized by a greater erythropoietin demand or require a larger amount of ESA (1, 6). The erythropoietin demand index (EDI) is an indicator of the requirement for EPO, which is calculated as plasma erythropoietin units divided by the hemoglobin value (1).

The erythropoietin demand is a critical risk factor for cardiovascular disease; thus, it is urgent to identify the main causes for erythropoietin demand and epidemiology of increased EPO demand in maintenance dialysis patients with ESRD and its risk predictors/factors (2, 4). However, the risk factors and predictors for increased erythropoietin demand have been comprehensively investigated.

In recent decades, the anti-EPO antibody and anti-EPO receptor (anti-EPOR) antibody have been reported to be associated with EPO resistance (8–10). In addition, they may play an important role in anemia among maintenance dialysis patients combined with insufficient EPO production (6, 11). Furthermore, the roles of anti-EPO and anti-EPOR antibodies in EPO demand have not been identified. Thus, we performed the current prospective cohort study to identify the predictive role of anti-EPO and anti-EPOR antibodies in EPO demand in maintenance dialysis patients.

METHODS

Study Design and Population

Our present research is a prospective cohort study in consecutive patients with ESRD who were undergoing maintenance dialysis at Xinqiao Hospital, Army Medical University (Third Military Medical University) from March 1, 2016, to July 1, 2019. A total of 129 consecutive patients were included in our cohort according to the inclusion and exclusion criteria. Most of the subjects were followed up within 39 months (fewer of them were followed up within 2 months). Median and quartiles of the follow-up time were 39 (39–39) months. During a median of 39 months of follow-up, nine patients were excluded or lost to follow-up.

The inclusion criterion was ESRD patients who were undergoing maintenance dialysis. The exclusion criteria were as follows: severe hepatic dysfunction ($n = 2$), death during hospitalization ($n = 2$), advanced cancer ($n = 1$), or severe infection (1). Additionally, three patients were lost to follow-up in the cohort, as shown in **Figure 1**.

All patients provided written informed consent. Our present research complied with the Declaration of Helsinki with respect to human investigations and was approved by the ethics committee of Xinqiao Hospital, Army Medical University (Third Military Medical University).

Procedures and Clinical Data Collection

The selected maintenance dialysis patients were viewed in clinical reception by our trained physicians, Dr. Ying Zhang and Dr. Yiqing Wang, by using standardized case file records to record demographic data (age, height, and weight), lifestyle factors (smoking and alcohol consumption status), prevalent diseases (hypertension, cardiovascular diseases, and other diseases), family histories, and medication use (antihypertension drugs, anticoagulants, and phosphate binders), as well as EPO usage.

Biomarker Variable Determination

Venous blood samples were obtained from the patients in the early morning after at least 12-h fasting at both cross sections (after entrance to the cohort and follow-up cross section) within a median of 39 months of follow-up (from 2 to 39 months).

First, we performed routine blood examination [tests of red blood cell count (RBC), mean corpuscular volume (MCV), concentration of hemoglobin (Hb), mean corpuscular hemoglobin (MCH), hematocrit (HCT), MCH concentration (MCHC), red blood cell distribution width (RDW), white blood cell count (WBC), platelet count (PLT), plateletcrit (PCT), and platelet distribution width (PDW)] by using an automated hematology corpuscle analyzer (AU400; Olympus Optical, Co., Tokyo, Japan).

Second, we measured plasma creatinine (Cr, enzyme method), UA (colorimetry), parathyroid hormone (PTH; chemiluminescent immunoassay), and ferritin (chemiluminescent immunoassay) concentrations by using Roche Diagnostics GmbH products (Abbott, i2000, USA).

Third, we also performed examinations of serum iron concentration (FERENE methods, Beckman AU5821), blood urea nitrogen concentration (BUN), potassium concentration (K^+), and sodium concentration (Na^+) by using indirect ion-selective electrode methods (EX-Z, JOKOH, Japan). Serum calcium concentration (Ca^{2+}) was measured by using Tri-azo methods, and phosphate concentration (P) was measured with a phosphomolybdate ultraviolet method (Roche Diagnostics GmbH, USA).

Finally, EPO, anti-EPO antibody, and anti-EPOR antibody were measured using ELISA kits (Recombinant Human Erythropoietin, BioLegend and Recombinant Human R Erythropoietin, RD Systems, USA). Each

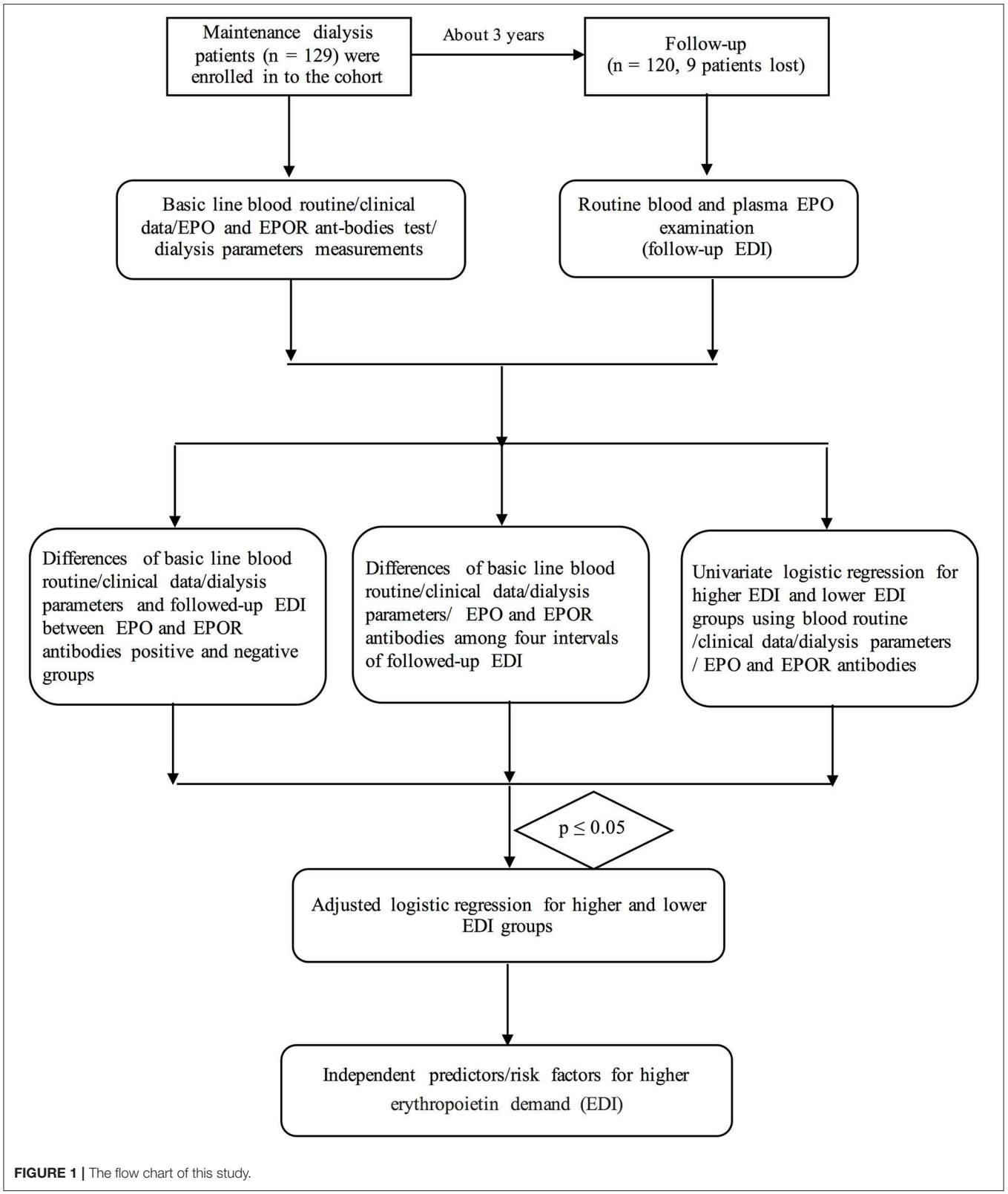

FIGURE 1 | The flow chart of this study.

sample was assayed in duplicate to measure the exact concentrations of endogenous EPO, anti-EPO antibody, and anti-EPOR antibody.

All of the biochemical variables were measured from blood specimens in the Clinical Laboratory Department, Xinqiao Hospital.

Definition of the Variables

KT/V was calculated as ln(posturea/preurea) – 0.008 *ultrafiltration time + (4 – 3.5 *posturea/preurea) *(ultrafiltration volume/postweight). Follow-up EPO demand was assessed by using the endogenous EPO level divided by Hb (EDI). Anti-EPO antibody positive (EPOA+) was defined as an optical density (OD) >0.5526 [the mean ± 3 standard deviations (SDs) in 55 age-matched healthy volunteers]; otherwise, it was defined as anti-EPO antibody negative (EPOA–). Similarly, EPOR antibody positive (EPOA+) was defined as an OD >0.5356 (the mean ± 3 SDs in 55 age-matched healthy volunteers); otherwise, it was defined as anti-EPOR negative (EPORA–).

Statistical Analysis

Continuous variables (such as age and BMI) that are normally distributed were expressed as the means ± SD. The differences between two groups or among four EDI intervals of these variables were compared using independent Student's *t*-test or one-way ANOVA [comparisons between two intervals were made using least significant difference (LSD) methods]. The Wilcoxon rank sum test was used to compare the non-normally distributed variables (comparisons among four intervals were performed by using one-way ANOVA after transformation to normality). Furthermore, the chi-square test or Fisher's exact test (if there were less than five cases) was employed to assess dichotomous variables. Univariate logistic regression analyses were performed to primarily screen the risk factors for EPO demand. Variables with $p < 0.05$ in comparisons among different EDI groups or in the univariate logistic regression were included in multivariate (adjusted) logistic regression analyses to identify independent associated factors of higher EPO demand. The regressions were performed using ordinal logistic regression analyses, and we have just listed the Q4 EDI vs. other intervals (Q1–Q3) owing to too many data. Furthermore, the generalized linear model's analyses have also been performed to determine the OR and its 95% CI. All of the statistical analyses were performed with SPSS 22.0 for MAC statistical software (California, USA).

TABLE 1 | Characteristics of the patients.

Basic information of the patient (n = 120)	
Age (years)	48.17 ± 13.55
BMI (kg/m^2)	21.97 ± 3.24
Gender (female)	48 (40%)
Smoker (cases and %)	7 (5.8%)
Alcohol use (cases and %)	5 (3.3%)
Dialysis duration (month)	34.50 (22–65)
Anemia (cases and %)	77 (64.2%)
Hypertension (cases and %)	38 (31.7%)
ACEI/ARB (cases and %)	18 (15.0%)
CCB (cases and %)	30 (25%)
β receptor blocker (cases and %)	19 (15.8%)

ACEI, angiotensin-converting enzyme inhibitor; ARB, angiotensin receptor blocker; CCB, calcium channel blockers.

RESULTS

At the follow-up cross section, 120 patients were included in the statistical analysis. The basic characteristics of the patients are listed in **Table 1**. The mean age of the subjects was 48.17 ± 13.55 years, and the BMI was 21.97 ± 3.24 kg/m^2. A total of 77 patients were diagnosed with anemia (64.2%). Hypertension status and drug use are also shown in **Table 1**. The follow-up endogenous EPO was 18.05 (10.70–18.88) g/dl in these maintenance dialysis patients.

Differences in Baseline Parameters Among the Four Intervals of Follow-Up Erythropoietin Demand Index

The EDI was divided into four quartile intervals, and we compared the differences among various groups. The patients in the Q4 and Q3 groups were significantly older than those in the Q2 and Q1 groups (p-values were <0.05; **Table 2**).

In the routine blood tests, only Hb showed significant differences among different EDI intervals. The Hb concentration was significantly higher in the Q1 EDI group at 10.95 (9.82–12.02). Other routine blood test parameters, including HCT, MCV, MCH, MCHC, RDW-CV, WBC, PCT, PLT, mean platelet volume (MPV), and PDW, showed no differences among the various intervals of EDI.

The serum iron, ferritin, and PTH levels were similar in the groups (all p-values were >0.05).

In the dialysis parameters, the dialysis duration showed no differences among the four intervals ($p = 0.179$). Predialysis, the potassium ion concentration was significantly higher in the Q4 population than in the other three populations (all p-values were <0.05). However, other predialysis parameters, including the concentrations of urea, Cr, uric acid, calcium ion, serum phosphate, and serum sodium, as well as TCO_2, showed no differences among these populations (all of the p-values were >0.05). Furthermore, the postdialysis-related variables were all similar among various populations, including concentrations of urea, Cr, uric acid, calcium ion, serum phosphate, potassium ion, and serum sodium, as well as TCO_2.

Unfortunately, we found no difference in either ultrafiltration volume or KT/V value ($p > 0.05$). Focusing on the target level of anti-EPO and anti-EPOR antibodies, only anti-EPO antibody showed significant differences among the four intervals ($p = 0.006$); that is, the levels of anti-EPO antibody were significantly higher in the Q2, Q3, and Q4 populations than in the Q1 subgroup (all p-values were <0.05). However, the anti-EPO antibody levels were similar among the three subgroups (Q2, Q3, and Q4, **Table 2**).

TABLE 2 | Differences of basic line routine blood, clinical data, dialysis parameters, EPO, and EPOR antibodies among four intervals of follow-up EDI.

	Overall (n = 120)	Q1 (n = 30)	Q2 (n = 30)	Q3 (n = 30)	Q4 (n = 30)	p-value (among four intervals)
DEMOGRAPHICS						
Age (years)	48.17 ± 13.55	43.01 ± 12.52	46.00 ± 14.10	51.33 ± 15.03*	52.34 ± 10.53#	0.020
BMI (kg/m^2)	21.97 ± 3.24	21.74 ± 3.16	22.51 ± 3.10	21.99 ± 3.62	21.63 ± 3.15	0.730
BASELINE DATA IN THE INITIAL OF THE STUDY						
Blood routine examination parameters						
RBC (10^{12}/L)	3.45 ± 0.61	3.59 ± 0.64	3.48 ± 0.51	3.40 ± 0.64	3.34 ± 0.63	0.407
Hb (g/dl)	10.40 (9.02–11.58)	10.95 (9.82–12.02)	10.45 (9.12–11.18)	10.20 (9.08–11.42)	10.30 (8.38–11.6.5)*#Δ	0.012
Hct (L/L)	33.52 ± 5.38	34.61 ± 6.13	33.31 ± 5.10	33.31 ± 4.97	32.85 ± 5.36	0.623
MCV (fl)	98.10 (93.60–102.27)	96.65 (93.025–99.05)	96.60 (92.75–203.77)	98.95 (92.70–102.15)	99.25 (95.00–103.27)	0.520
MCH (pg)	30.95 (29.15–32.27)	30.50 (29.25–31.20)	30.95 (28.95–32.35)	31.30 (29.62–32.67)	31.05 (29.70–32.95)	0.542
MCHC (g/dl)	313.00 (307.25–321.75)	313.50 (309.75–321.25)	311.00 (307.00–321.50)	315.00 (308.75–322.25)	311.50 (303.00–320.50)	0.227
RDW-CV (%)	14.43 ± 1.39	14.62 ± 1.32	14.41 ± 1.34	14.12 ± 1.26	14.56 ± 1.64	0.512
WBC (10^9/L)	6.26 ± 1.66	6.36 ± 1.82	6.20 ± 1.45	6.20 ± 1.78	6.30 ± 1.65	0.997
PCT (%)	0.155 (0.122–0.190)	0.160 (0.120–0.190)	0.165 (0.125–0.192)	0.140 (0.117–0.210)	0.160 (0.130–0.190)	0.970
PLT (10^9/L)	177.50 (134.00–215.75)	163.00 (135.75–219.25)	185.50 (132.50–212.50)	156.50 (121.75–221.75)	185.50 (131.00–214.50)	0.988
MPV (fl)	9.14 ± 1.35	9.20 ± 1.38	9.12 ± 1.42	9.08 ± 1.31	9.12 ± 1.37	0.988
PDW (%)	16.30 (16.00–16.60)	16.30 (15.90–16.50)	16.30 (16.00–16.50)	16,45 (16.07–16.77)	16.25 (16.00–16.52)	0.865
Clinical data						
Serum iron (μmol/L)	13.37 (10.00–15.30)	13.45 (10.77–16.25)	11.25 (8.67–13.45)	12.20 (10.07–17.45)	13.45 (10.25–17.82)	0.113
Ferritin (μg/L)	383.28 (161.19–656.76)	344.80 (91.56–560.51)	298.30 (162.85–524.19)	414.53 (213.26–631.64)	524.17 (265.50–838.53)	0.069
PTH (pg/ml)	499.5 (237.75–800.5)	433.00 (243.75–846.5)	414.5 (228.75–849.75)	641.73 (247.5–1,065.25)	431.5 (229.25–671.75)	0.509
Dialysis parameters						
Dialysis duration (months)	34.5 (22.0–65.0)	26.0 (16.25–46.5)	37.5 (23.75–52.75)	34.0 (21.75–66.25)	47.5 (22.75–75.0)*	0.179
Ultrafiltration volume (L)	2.00 (0.00–2.80)	2.55 (0.00–2.92)	2.40 (0.00–3.00)	1.70 (0.00–2.72)	2.00 (0.00–2.800)	0.640
Predialysis						
Urea (μmol/L)	26.42 ± 5.88	26.85 ± 5.19	26.84 ± 6.70	25.45 ± 5.68	26.52 ± 6.03	0.772
Cr (μmol/L)	1,030.20 ± 248.52	1,091.82 ± 230.90	1,086.84 ± 298.61	967.02 ± 219.54	975.12 ± 219.66	0.076
Uric acid (μmol/L)	506.47 ± 90.20	519.92 ± 99.62	519.67 ± 101.75	481.23 ± 62.02	505.06 ± 90.74	0.302
Calcium ion (mmol/L)	2.24 (2.07–2.35)	2.25 (2.07–2.35)	2.25 (2.11–2.35)	2.24 (2.07–2.39)	2.15 (2.00–2.33)	0.496
Serum phosphate (mmol/L)	2.21 (1.74–2.63)	2.42 (1.98–2.70)	2.08 (1.74–2.55)	1.94 (1.66–2.50)	2.31 (1.73–2.65)	0.240
Potassium ion (mmol/L)	5.15 ± 0.77	5.00 ± 0.68	5.01 ± 0.76	5.08 ± 0.79	5.52 ± 0.76*#	0.024
Serum sodium (mmol/L)	137.86 ± 3.00	137.27 ± 2.69	138.10 ± 2.34	138.81 ± 3.20	137.25 ± 3.50	0.132
TCO_2 (mmol/L)	20.41 ± 3.07	20.55 ± 3.32	19.78 ± 2.62	20.99 ± 3.72	20.33 ± 2.51	0.500
Postdialysis						
Urea (mmol/L)	9.09 ± 3.04	9.26 ± 2.64	9.64 ± 3.74	8.53 ± 2.69	8.89 ± 3.00	0.853
Cr (μmol/L)	388.20 ± 140.76	402.51 ± 137.07	420.17 ± 157.01	371.64 ± 130.28	358.47 ± 135.73	0.309
Uric acid (μmol/L)	141.99 ± 40.82	138.97 ± 44.22	145.83 ± 42.70	138.39 ± 41.98	144.75 ± 35.37	0.853
Calcium ion (mmol/L)	2.38 (2.26–2.49)	2.40 (2.27–2.45)	2.40 (2.28–2.50)	2.32 (2.16–2.45)	2.35 (2.17–2.51)	0.509
Serum phosphate (mmol/L)	0.83 (0.65–1.01)	0.84 (0.71–0.97)	0.82 (0.60–0.98)	0.82 (0.62–1.01)	0.91 (0.66–1.11)	0.877
Potassium ion (mmol/L)	3.51 ± 0.38	3.49 ± 0.37	3.43 ± 0.35	3.51 ± 0.37	3.61 ± 0.42	0.310
Serum sodium (mmol/L)	138.70 ± 2.56	138.88 ± 2.55	138.83 ± 2.16	139.07 ± 2.57	137.99 ± 2.90	0.369
TCO_2 (μmol/L)	26.38 ± 3.37	26.34 ± 3.89	26.06 ± 2.78	27.25 ± 3.44	25.87 ± 3.29	0.403
Weight (kg)	59.06 ± 10.46	58.64 ± 10.98	62.15 ± 11.43	38.38 ± 9.33	57.05 ± 9.83	0.275
KT/V	1.22 (1.08–1.45)	1.20 (1.04–1.49)	1.24 (1.05–1.45)	1.21 (1.08–1.43)	1.24 (1.14–1.45)	0.879

(Continued)

TABLE 2 | Continued

	Overall (n = 120)	Q1 (n = 30)	Q2 (n = 30)	Q3 (n = 30)	Q4 (n = 30)	p-value (among four intervals)
EPO and EPOR antibodies						
EPOA OD	0.428 (0.314–0.542)	0.357 (0.266–0.447)	0.426 (0.316–0.574)*	0.468 (0.367–0.546)*	0.456 (0.382–0.616)*	0.006
EPORA OD	0.359 (0.226–0.562)	0.413 (0.336–0.577)	0.305 (0.208–0.445)	0.413 (0.187–0.613)	0.421 (0.289–0.578)	0.387

Cr, creatinine; EDI, erythropoietin demand index; EPO, erythropoietin, mIU/ml; EPOA, EPO antibody; EPOA+, EPO antibody positive; EPORA, EPOR antibody; EPORA+, EPOR antibody positive; Hb, hemoglobin; Hct, hematocrit; MCH, mean corpuscular hemoglobin; MCHC, mean corpuscular hemoglobin concentration; MCV, mean corpuscular volume; OD, optical density; PCT, plateletcrit; PDW, platelet distribution width; PLT, platelet; PTH, parathyroid hormone; RBC, red blood cell; RDW, red blood cell distribution width; WBC, white blood cell.
**$p \leq 0.05$ compared with Q1.*
#$p \leq 0.05$ compared with Q2.
Δ$p \leq 0.05$ compared with Q3.

Differences in Baseline Parameters Between Erythropoietin and Erythropoietin Receptor Antibodies Positive and Negative Groups

We further analyzed the differences in baseline parameters between EPO/EPOR antibody-positive and EPO/EPOR antibody-negative groups. First, age and BMI showed no difference between the EPOA+ and EPOA– groups or between the EPORA+ and EPORA– groups.

In the routine blood examination parameters, we found that only RDW was significantly higher in the EPOA+ group than in the EPOA– group (14.87 ± 1.57% vs. 14.28 ± 1.31%, $p = 0.046$). Only one variable (MPV) was significantly higher in the EPORA+ group than in the EPORA– group (9.65 ± 1.70 vs. 8.94 ± 1.14 fl, $p = 0.010$). However, none of the other routine blood examination parameters showed any differences between the EPORA+ and EPORA– individuals ($p > 0.05$).

Moreover, neither clinical data (serum iron, ferritin, and PTH) nor dialysis-related parameters showed any differences between the EPOA+ and EPORA+ populations.

Regarding the EPORA groups, we found that ferritin and TCO_2 (both predialysis and postdialysis) showed differences between the EPORA+ and EPORA– populations. Other clinical data and dialysis-related parameters were similar in the two groups (**Table 3**).

Associations Between Erythropoietin Demand Index and Erythropoietin/Erythropoietin Receptor Antibodies

To identify the associations between EDI and anti-EPO/anti-EPOR antibody levels, we further compared the EDI between the EPOA + and EPOA– groups (as well as between the EPORA+ and EPORA– groups). As shown in **Figure 2**, the baseline EPO antibody level is correlated with follow-up EDI ($r^2 = 0.0377$, $p = 0.03$), whereas the baseline anti-EPOR antibody level was not correlated with EDI ($r^2 = 0.0009$, $p = 0.73$). Furthermore, in **Figure 3**, we found that the follow-up EDI was significantly higher in the EPOA+ group than in the EPOA– group ($p = 0.02$, **Figure 3A**). However, there were no significant differences between the EPORA+ and EPORA– groups. In addition, follow-up EDI was similar in the EPOA+ combined with EPORA+ group and EPOA– combined EPORA– group (**Figures 3B–D**). The correlations between the follow-up EDI and other parameters are shown in **Table S1**.

Univariate and Adjusted Regressions for the Higher Erythropoietin Demand Index Group

To identify the predictive roles of EPO and other potential factors, we performed univariate logistic regression for each parameter between the higher and lower erythropoietin demand (Q4 of EDI vs. Q1 of EDI). Other analyses between Q3 EDI and Q1 EDI are shown in the **Appendix**.

In the univariate logistic regression analyses, we found that age (OR = 1.071, 95% CI 95% CI: 1.021–1.123, $p = 0.005$), ferritin (OR = 1.001, 95% CI: 1.000–1.003, $p = 0.038$), potassium ion concentration before dialysis (OR = 2.781, 95% CI: 1.255–6.162, $p = 0.012$), dialysis duration (OR = 1.025, 95% CI: 1.002–1.048, $p = 0.030$), and EPOA OD value (OR = 7.694, 95% CI: 2.109–67.277, $p = 0.004$) were potential associated factors for higher erythropoietin demand (**Table 4**).

To identify the independent associated factors of higher erythropoietin demand, variables that showed differences among various intervals of EDI or that had a p-value of <0.05 in univariate logistic regression analyses were included in the adjusted logistic regression. Ultimately, age (OR = 1.072, 95% CI: 1.008–1.140, $p = 0.026$), potassium ion concentration before dialysis (OR = 3.425, 95% CI: 1.297–9.040, $p = 0.013$), and EPOA OD value (OR = 5.27, 95% CI: 2.577–6.733, $p = 0.007$) were found to be independent associated factors of higher erythropoietin demand (**Table 5**).

The ordinal logistic regression analyses have found that the baseline EPO antibody level (OR = 5.328, 95% CI: 1.072–8.735, $p = 0.045$), ferritin (OR = 6.746, 95% CI: 1.028–9.976, $p = 0.044$), and PTH (OR= 0.064, 95% CI: 0.009–0.148, $p = 0.035$) were independently associated with higher EDI (**Tables S4, S5**).

TABLE 3 | Differences of basic line blood routine, clinical data, and dialysis parameters between EPO and EPOR antibody positive and negative groups.

	EPOA – group ($n = 91$)	EPOA + group ($n = 29$)	*P*	EPORA – group ($n = 87$)	EPORA + group ($n = 33$)	*P*
DEMOGRAPHICS						
Age (years)	47.69 ± 12.90	49.67 ± 15.55	0.494	46.95 ± 12.81	51.07 ± 15.06	0.109
BMI (kg/m^2)	21.65 ± 3.05	22.96 ± 3.66	0.059	21.74 ± 3.12	22.56 ± 3.52	0.220
BASELINE DATA IN THE INITIAL OF THE STUDY						
Routine blood examination parameters						
RBC (10^{12}/L)	3.44 ± 0.58	3.49 ± 0.69	0.720	3.51 ± 0.61	3.30 ± 0.59	0.099
Hb (g/dl)	104.00 (92.00–116.00)	100.00 (87.00–114.00)	0.306	104.00 (93.00–117.00)	103.00 (86.00–115.00)	0.389
Hct (L/L)	33.58 ± 5.36	33.31 ± 5.52	0.813	34.04 ± 5.31	32.14 ± 5.39	0.085
MCV (fl)	98.60 (93.60–102.90)	95.70 (93.00–102.10)	0.445	98.30 (94.00–102.20)	97.90 (92.55–102.45)	0.624
MCH (pg)	31.00 (29.40–32.30)	30.50 (28.60–31.85)	0.343	31.00 (29.10–32.10)	30.50 (29.25–32.85)	0.911
MCHC (g/dl)	314.00 (308.00–322.00)	311.00 (304.50–321.00)	0.447	313.00 (308.00–320.00)	316.00 (305.50–323.50)	0.379
RDW-CV (%)	14.28 ± 1.31	14.87 ± 1.57	0.046*	14.32 ± 1.33	14.70 ± 1.53	0.182
WBC (10^9/L)	6.32 ± 1.65	6.09 ± 1.70	0.525	6.28 ± 1.73	6.23 ± 1.50	0.887
PCT (%)	0.160 (0.130–0.200)	0.150 (0.105–0.180)	0.218	0.150 (0.130–0.190)	0.160 (0.110–0.205)	1.000
PLT (10^9/L)	178.00 (135.00–223.00)	176.73 (122.50–195.00)	0.186	177.00 (136.00–216.00)	179.00 (114.50–204.50)	0.389
MPV (fl)	9.12 ± 1.36	9.19 ± 1.34	0.811	8.94 ± 1.14	9.65 ± 1.70	0.010
PDW (%)	16.30 (16.00–16.50)	16.40 (16.10–16.70)	0.286	16.30 (16.00–16.60)	16.30 (15.65–16.65)	0.699
Clinical data						
Serum iron (μmol/L)	13.30 (10.00–15.80)	13.45 (9.65–13.70)	0.773	10.10 (13.45–15.80)	12.50 (9.50–14.25)	0.530
Ferritin (μg/L)	377.70 (151.26–618.55)	483.24 (170.46–765.79)	0.405	344.85 (155.85–524.19)	524.19 (182.59–1,183.17)	0.025*
PTH (pg/ml)	431.00 (237.00–772.00)	536.00 (238.00–981.00)	0.654	406.00 (233.00–710.00)	641.73 (363.50–1,028.50)	0.068
Dialysis parameters						
Dialysis duration (month)	35.0 (22.0–59.0)	34.00 (22.00–70.50)	0.832	34.00 (22.00–59.00)	39.00 (22.00–71.50)	0.352
Ultrafiltration volume (L)	2.00 (0.00–2.80)	2.40 (0.00–2.85)	0.744	2.20 (0.00–2.80)	1.00 (0.00–2.85)	0.223
Predialysis						
Urea (μmol/L)	26.02 ± 5.74	27.65 ± 6.24	0.196	26.43 ± 5.68	26.36 ± 6.46	0.950
Cr (μmol/L)	1,023.62 ± 241.80	1,050.86 ± 272.01	0.609	1,038.00 ± 243.08	1,009.64 ± 265.12	0.579
Uric acid (μmol/L)	506.80 ± 94.92	505.42 ± 74.92	0.943	507.83 ± 87.80	502.89 ± 97.55	0.790
Calcium ion (mmol/L)	2.24 (2.07–2.35)	2.22 (2.08–2.31)	0.773	2.22 (2.08–2.35)	2.25 (2.05–2.38)	0.962
Serum phosphate (mmol/L)	2.23 (1.74–2.64)	2.20 (1.74–2.61)	0.806	2.20 (1.74–2.64)	2.35 (1.74–2.63)	0.791
Potassium ion (mmol/L)	5.17 ± 0.80	5.08 ± 0.69	0.546	5.21 ± 0.80	4.99 ± 0.67	0.162
Serum sodium (mmol/L)	137.88 ± 3.06	137.78 ± 2.84	0.881	137.80 ± 2.87	138.00 ± 3.36	0.744
TCO_2 (mmol/L)	20.25 ± 3.27	20.90 ± 2.34	0.327	19.95 ± 2.91	21.63 ± 3.20	0.007**
Postdialysis						
Urea (mmol/L)	8.90 ± 2.92	9.65 ± 3.39	0.254	9.06 ± 3.04	9.15 ± 3.10	0.889
Cr (μmol/L)	385.12 ± 138.25	397.85 ± 150.48	0.673	388.50 ± 142.43	387.39 ± 138.42	0.969
Uric acid (μmol/L)	140.39 ± 42.93	146.98 ± 33.51	0.452	139.20 ± 37.67	149.32 ± 48.03	0.227
Calcium ion (mmol/L)	2.38 (2.26–2.46)	2.37 (2.26–2.56)	0.734	2.39 (2.28–2.50)	2.35 (2.17–2.47)	0.448
Serum phosphate (mmol/L)	0.830 (0.650–0.980)	0.847 (0.705–1.080)	0.334	0.830 (0.660–0.980)	0.920 (0.560–1.045)	0.881
Potassium ion (mmol/L)	3.52 ± 0.39	3.48 ± 0.35	0.609	3.54 ± 0.39	3.43 ± 0.34	0.188
Serum sodium (mmol/L)	138.70 ± 2.67	138.69 ± 2.22	0.990	138.72 ± 2.63	138.63 ± 2.40	0.863
TCO_2 (μmol/L)	26.21 ± 3.48	26.91 ± 3.01	0.334	25.99 ± 3.22	27.42 ± 3.60	0.037*
Weight (kg)	58.57 ± 10.09	60.57 ± 11.61	0.372	58.81 ± 10.35	59.69 ± 10.89	0.683
KT/V	1.22 (1.09–1.45)	1.21 (1.01–1.45)	0.963	1.28 (1.11–1.46)	1.15 (1.04–1.37)	0.090

Cr, creatinine; EPO, erythropoietin, mIU/ml; EPOA, EPO antibody; EPOA+, EPO antibody positive; EPORA, EPOR antibody; EPORA+, EPOR antibody positive; Hb, hemoglobin; Hct, hematocrit; MCH, mean corpuscular hemoglobin; MCHC, mean corpuscular hemoglobin concentration; MCV, mean corpuscular volume; OD, optical density; PCT, plateletcrit; PDW, platelet distribution width; PLT, platelet; PTH, parathyroid hormone; RBC, red blood cell; RDW, red blood cell distribution width; WBC, white blood cell.

**$p \leq 0.05$ between two groups.*

***$p \leq 0.01$ between two groups.*

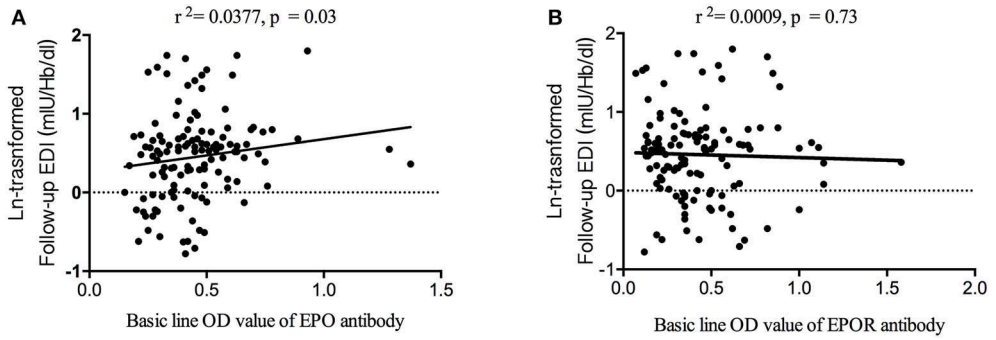

FIGURE 2 | Correlation between follow-up EDI and baseline anti-EPO and anti-EPOR antibodies. **(A)** The baseline anti-EPO antibody level was correlated with follow-up EDI. **(B)** The baseline anti-EPOR antibody level was not correlated with follow-up EDI. EDI, erythropoietin demand index; EPO, erythropoietin; EPOR, erythropoietin receptor.

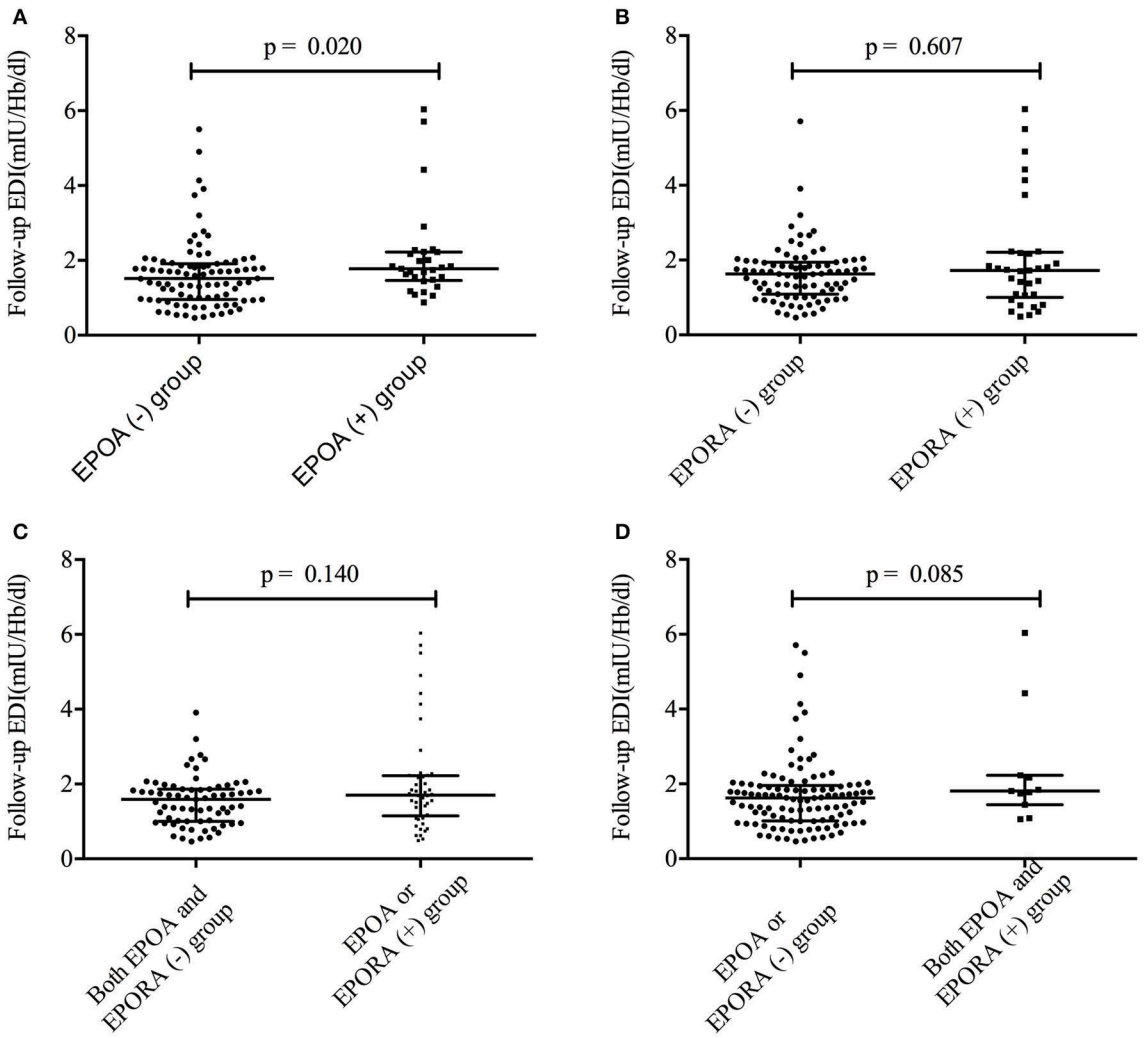

FIGURE 3 | The follow-up EDI was different between the different groups. **(A)** The follow-up EDI was different between the EPOA+ and EPOA– groups. **(B)** The follow-up EDI was not different between the EPORA+ and EPORA– groups. **(C)** Follow-up EDI showed no difference between the EPOA/EPORA+ group and the EPOA– (plus EPORA–) group. **(D)** Follow-up EDI showed no difference between the EPOA+ (plus EPORA+) group and the EPOA–/EPORA– group. EDI, erythropoietin demand index; EPOA–, EPOA negative; EPOA, erythropoietin antibody; EPOA+, EPOA positive.

TABLE 4 | Univariate regressions for higher EDI (Q4).

Variables	β	*P*	OR	95% CI	
				Lower border	Upper border
DEMOGRAPHICS					
Age (years)	0.068	0.005**	1.071	1.021	1.123
BMI (kg/m^2)	−0.011	0.899	0.990	0.841	1.165
BASELINE DATA IN THE INITIAL OF THE STUDY					
Blood routine examination parameters					
RBC (10^{12}/L)	−0.642	0.129	0.526	0.230	1.205
Hb (g/dl)	−0.023	0.146	0.977	0.948	1.008
Hct (L/L)	−0.055	0.239	0.947	0.864	1.037
MCV (fl)	0.057	0.156	1.058	0.979	1.145
MCH (pg)	0.084	0.409	1.087	0.891	1.326
MCHC (g/dl)	−0.023	0.316	0.977	0.933	1.023
RDW (%)	0.025	0.902	1.026	0.686	1.535
WBC (10^9/L)	−0.020	0.893	0.980	0.730	1.317
PCT (%)	−0.587	0.916	−0.556	0.000	32,573.031
PLT (10^9/L)	−0.000	1.000	1.000	0.991	1.009
MPV (fl)	−0.042	0.825	0.957	0.659	1.394
PDW (%)	0.025	0.902	1.026	0.686	1.535
Clinical data					
Serum iron (μmol/L)	0.048	0.302	1.049	0.958	1.149
Ferritin (μg/L)	0.001	0.038*	1.001	1.000	1.003
PTH (pg/ml)	−0.001	0.137	0.999	0.998	1.000
Dialysis parameters					
Dialysis duration (month)	0.025	0.030*	1.025	1.002	1.048
Ultrafiltration volume (L)	−0.071	0.703	0.931	0.646	1.342
Predialysis					
Urea (μmol/L)	−0.011	0.816	0.989	0.903	1.084
Cr (μmol/L)	−0.002	0.055	0.998	0.995	1.000
Uric acid (μmol/L)	−0.002	0.541	0.998	0.993	1.004
Calcium ion (mmol/L)	−1.197	0.272	0.302	0.036	2.553
Serum phosphate (mmol/L)	0.137	0.712	1.147	0.554	2.376
Potassium ion (mmol/L)	1.023	0.012*	2.781	1.255	6.162
Serum sodium (mmol/L)	−0.001	0.987	0.999	0.847	1.178
TCO_2 (mmol/L)	−0.027	0.765	0.974	0.817	1.160
Postdialysis					
Urea (mmol/L)	−0.048	0.606	0.953	0.793	1.144
Cr (μmol/L)	−0.002	0.215	0.997	0.993	1.001
Uric acid (μmol/L)	0.004	0.572	1.004	0.991	1.017
Calcium ion (mmol/L)	−1.142	0.394	0.319	0.023	4.407
Serum phosphate (mmol/L)	0.569	0.587	1.767	0.227	13.751
Potassium ion (mmol/L)	0.790	0.237	2.204	0.594	8.175
Serum sodium (mmol/L)	−0.123	0.210	0.884	0.729	1.072
TCO_2 (μmol/L)	−0.038	0.608	0.963	0.834	1.112
Weight (kg)	−0.015	0.549	0.985	0.937	1.035
KT/V	0.333	0.707	1.396	0.246	7.931
EPO and EPOR antibodies					
EPORA OD	0.098	0.937	1.103	0.097	12.596
EPOA OD	2.126	0.004**	7.694	2.109	67.277

The regressions were performed using the Q1 interval as the reference, with Q4 as the higher EDI. The regressions between Q3 and Q1 were appended in the ***Appendix****.*
Cr, creatinine; EDI, erythropoietin demand index; EPO, erythropoietin, mIU/ml; EPOA, EPO antibody; EPOA+, EPO antibody positive; EPORA, EPOR antibody; EPORA+, EPOR antibody positive; Hb, hemoglobin; Hct, hematocrit; MCH, mean corpuscular hemoglobin; MCHC, mean corpuscular hemoglobin concentration; MCV, mean corpuscular volume; OD, optical density; PCT, plateletcrit; PDW, platelet distribution width; PLT, platelet; PTH, parathyroid hormone; RBC, red blood cell; RDW, red blood cell distribution width; WBC, white blood cell.
$^*p \leq 0.05$.
$^{**}p \leq 0.01$.

TABLE 5 | Adjusted regressions.

Variables	β	*P*	OR	95% CI	
				Lower border	Upper border
Age	0.070	0.026*	1.072	1.008	1.140
Predialysis Potassium ion	1.231	0.013*	3.425	1.297	9.040
EPOA OD	1.990	0.007**	5.27	2.577	6.733

The regressions were performed using the Q1 interval as the reference, with Q4 as the higher EDI. The regressions between Q3 and Q1 were appended in the ***Appendix****.*
EDI, erythropoietin demand index; EPOA, erythropoietin antibody; OD, optical density.
$^{*}p \leq 0.05$.
$^{**}p \leq 0.01$.

DISCUSSION

In the present cohort study lasting a median of 39 months, we found differences in age, baseline Hb, baseline predialysis potassium ion concentration, and baseline anti-EPO antibody level among four follow-up EDI intervals. Furthermore, EDI was significantly higher in the EPOA+ group than in the EPOA– group, and it was associated with the anti-EPO antibody level. Further analyses indicated that age, potassium ion concentration before dialysis, and anti-EPO antibody OD level were independent associated factors of higher EPO demand or higher EDI.

As mentioned in the *Introduction*, anemia is one of the most frequent complications accompanying ESRD, especially in the maintenance dialysis patient subpopulation (1, 7, 11, 12). In the present study, more than half of the maintenance dialysis patients had various severities of anemia. It is known that patients with ESRD produce insufficient EPO due to kidney dysfunction to satisfy the higher need for EPO resulting in anemia. It is also the most important reason for use of ESA.

Age has been considered a non-modifiable risk factor for various diseases, including anemia and renal dysfunction (13, 14). Without exception, we found that older patients with ESRD who underwent maintenance dialysis were characterized by a higher EDI, indicating a greater requirement for EPO. We also found that age may be the potential risk factor for higher EPO demand in the primary screening univariate regression analysis. Final adjusted analyses identified the independently predictive role of age in the higher EPO demand after 39 months.

EPO demand is directly calculated by Hb; thus, it may be related to baseline routine blood parameters, especially RBC and Hb variables. We found that the baseline Hb concentration was significantly higher in the lower follow-up EPO demand group. However, in the latter analyses, baseline Hb concentration showed no association with EPO demand. Neither was it an independent associated factor of higher EPO demand. Serum iron, ferritin, and PTH were also considered in the analyses; however, they were not associated with follow-up EDI. Although iron is one of the basic elements for the production of Hb, we did not find an association between iron and EPO demand (15).

We also attempted to identify the association between dialysis parameters (separated into predialysis and postdialysis). We revealed one novel finding that the predialysis potassium concentration was significantly higher in the higher EDI group. Further analyses also indicated that the predialysis potassium concentration was an independent associated factor/risk factor of higher EPO demand. Our present study identified a novel risk factor for follow-up EDI/EPO demand and predialysis potassium concentration. However, the mechanisms underlying this association have not been uncovered and may be associated with the renewal of erythrocytes and their energy demand (16). Others' studies have shown that potassium ion transport may play an important role in the production of erythrocytes as well as Hb (16–18). Furthermore, the associations have also been reported between potassium levels and Hb in the red cell units that undergo changes during storage and processing (19).

Anti-EPO antibodies have been reported in a small number of chronic renal disease patients who were administered EPO α (8). Others' studies have also found that anti-EPO antibody prevalence in ESRD patients who receive ESA may be associated with EPO resistance and demand, resulting in anemia (9, 20). Studies in patients with some autoimmune diseases and patients with HIV revealed high levels of anti-EPO antibodies (8, 21). Thus, EPO antibodies may participate in a variety of diseases. Importantly, we have identified that the baseline anti-EPO antibody level was associated with follow-up EPO demand. Previous studies suggest that EPO is associated with Hb loss (22). In addition, EPO antibodies have been demonstrated to mediate pure red cell aplasia after treatment with recombinant EPO products (22, 23). Furthermore, anemia treated with ESAs continuously failed to obtain a sustained response, which may also be caused by EPO antibodies. Finally, we identified that a higher baseline anti-EPO antibody level was an independent risk factor for higher EPO demand, which may provide a novel strategy for prevention or risk classification of anemia as well as the direction of ESA use.

LIMITATIONS

We performed this prospective cohort study in 129 consecutive patients with ESRD who were undergoing dialysis and identified the predialysis potassium concentration, baseline anti-EPO antibody level, and age as independent risk factors for higher

EPO demand. However, there are still three limitations to this study. First, the population size is relatively small. Second, there are many other factors that may be associated with EPO demand that should be included; however, we have not considered all of them owing to limited time and finances. Finally, the mechanisms underlying the associations between anti-EPO antibody and EPO demand have not been investigated, which warrants basic molecular research.

CONCLUSION

The baseline anti-EPO antibody level combined with an older age and a higher predialysis potassium ion concentration are independent risk factors for a higher follow-up EPO demand in maintenance dialysis patients with ESRD, which also indicated that a lower baseline anti-EPO antibody level was an independent associated factor of lower EPO demand. The novel risk factors identified in this study may allow prevention or risk classification of anemia as well as guidance for ESA use.

DATA AVAILABILITY STATEMENT

The datasets generated for this study are available on request to the corresponding author.

ETHICS STATEMENT

The studies involving human participants were reviewed and approved by the ethics committee of Xinqiao Hospital, Army Medical University (Third Military Medical University). The patients/participants provided their written informed consent to participate in this study.

AUTHOR CONTRIBUTIONS

YZ and JZ participated in the design of the study. YZ and S-ZB also drafted the manuscript and performed the statistical analysis. JZ reviewed and revised this manuscript critically for important intellectual content. YZ, ST, and KY collected the baseline history and baseline demographic data and the measurements of EPO and EPOR antibodies. The laboratory measurements were performed by YZ, YW, LN, and DW. The dialysis-related data were obtained by YW and WW.

FUNDING

This study was supported by the National Natural Science Foundation of China (grant no. 81400736) and Xinqiao Hospital, Army Medical University (grant no. 2016YLC36). We would like to thank all the individuals who participated in this study for their support.

SUPPLEMENTARY MATERIAL

The Supplementary Material for this article can be found online at: https://www.frontiersin.org/articles/10.3389/fmed.2020.00109/full#supplementary-material

REFERENCES

1. Yokoro M, Nakayama Y, Yamagishi SI, Ando R, Sugiyama M, Ito S, et al. Asymmetric dimethylarginine contributes to the impaired response to erythropoietin in CKD-Anemia. *J Am Soc Nephrol.* (2017) 28:2670–80. doi: 10.1681/ASN.2016111184
2. Okazaki M, Komatsu M, Kawaguchi H, Tsuchiya K, Nitta K. Erythropoietin resistance index and the all-cause mortality of chronic hemodialysis patients. *Blood Purif.* (2014) 37:106–12. doi: 10.1159/000358215
3. Afsar B, Saglam M, Yuceturk C, Agca E. The relationship between red cell distribution width with erythropoietin resistance in iron replete hemodialysis patients. *Eur J Intern Med.* (2013) 24:e25–9. doi: 10.1016/j.ejim.2012.11.017
4. Guerrero-Riscos MA, Montes-Delgado R, Seda-Guzman M, Praena-Fernandez JM. Erythropoietin resistance and survival in non-dialysis patients with stage 4-5 chronic kidney disease and heart disease. *Nefrologia.* (2012) 32:343–52. doi: 10.3265/Nefrologia.pre2012.Jan.11111
5. Khankin EV, Mutter WP, Tamez H, Yuan HT, Karumanchi SA, Thadhani R. Soluble erythropoietin receptor contributes to erythropoietin resistance in end-stage renal disease. *PLoS ONE.* (2010) 5:e9246. doi: 10.1371/journal.pone.0009246
6. Priyadarshi A, Shapiro JI. Erythropoietin resistance in the treatment of the anemia of chronic renal failure. *Semin Dial.* (2006) 19:273–8. doi: 10.1111/j.1525-139X.2006.00172.x
7. Sharma RK, Chakrabarti S. Anaemia secondary to erythropoietin resistance: important predictor of adverse outcomes in chronic obstructive pulmonary disease. *Postgrad Med J.* (2016) 92:636–9. doi: 10.1136/postgradmedj-2015-133814
8. Helegbe GK, Huy NT, Yanagi T, Shuaibu MN, Kikuchi M, Cherif MS, et al. Anti-erythropoietin antibody levels and its association with anaemia in different strains of semi-immune mice infected with plasmodium berghei ANKA. *Malar J.* (2013) 12:296. doi: 10.1186/1475-2875-12-296
9. Oh JG, Seong J, Han S, Heo TH. Development of an anti-EPO antibody detection kit based on lab-on-a-chip and bridging antibody technologies. *Biologicals.* (2018) 5:48–12. doi: 10.1016/j.biologicals.2018.05.005
10. Wang T, Hao SF, Fu R, Wang HQ, Shao ZH. Significance of anti-EPO receptor antibody in immune-related pancytopenia. *Zhonghua Yi Xue Za Zhi.* (2017) 97:1406–10. doi: 10.3760/cma.j.issn.0376-2491.2017.18.011
11. Okonko DO, Marley SB, Anker SD, Poole-Wilson PA, Gordon MY. Erythropoietin resistance contributes to anaemia in chronic heart failure and relates to aberrant JAK-STAT signal transduction. *Int J Cardiol.* (2013) 164:359–64. doi: 10.1016/j.ijcard.2011.07.045
12. Mallick S, Rafiroiu A, Kanthety R, Iqbal S, Malik R, Rahman M. Factors predicting erythropoietin resistance among maintenance hemodialysis patients. *Blood Purif.* (2012) 33:238–44. doi: 10.1159/000335256
13. Treister-Goltzman Y, Peleg R, Biderman A. A comparative study of iron deficiency anemia in bedouin and jewish women of childbearing age in Southern Israel. *Popul Health Manag.* (2019). doi: 10.1089/pop.2019.0177. [Epub ahead of print].
14. Hamarneh Z, Symonds EL, Kholmurodova F, Cock C. Older age, symptoms or anemia: which factors increase colorectal cancer risk with a positive fecal immunochemical test? *J Gastroenterol Hepatol.* (2019). doi: 10.1111/jgh.14888. [Epub ahead of print].
15. Jiang X, Gao M, Chen Y, Liu J, Qi S, Ma J, et al. EPO-dependent induction of erythroferrone drives hepcidin suppression and systematic iron absorption under phenylhydrazine-induced hemolytic anemia. *Blood Cells Mol Dis.* (2016) 58:45–51. doi: 10.1016/j.bcmd.2016.02.005
16. Duhm J, Gobel BO, Beck FX. Sodium and potassium ion transport accelerations in erythrocytes of DOC, DOC-salt, two-kidney, one clip, and

spontaneously hypertensive rats. Role of hypokalemia and cell volume. *Hypertension.* (1983) 5:642–52. doi: 10.1161/01.HYP.5.5.642
17. Fincher RK, Strong JS, Jackson JL. Accuracy of measurements of hemoglobin and potassium in blood samples from peripheral catheters. *Am J Crit Care.* (1998) 7:439–43. doi: 10.4037/ajcc1998.7.6.439
18. Saini N, Basu S, Kaur R, Kaur J. Assessment of changes in plasma hemoglobin and potassium levels in red cell units during processing and storage. *Transfus Apher Sci.* (2015) 52:319–25. doi: 10.1016/j.transci.2015.01.009
19. Wang K, Wu J, Xu J, Gu S, Li Q, Cao P, et al. Correction of anemia in chronic kidney disease with angelica sinensis polysaccharide via restoring EPO production and improving iron availability. *Front Pharmacol.* (2018) 9:803. doi: 10.3389/fphar.2018.00803
20. Lee H, Yang J, Kim H, Kwon JW, Oh KH, Joo KW, et al. Improvement in erythropoieis-stimulating agent-induced pure red-cell aplasia by introduction of darbepoetin-alpha when the anti-erythropoietin antibody titer declines spontaneously. *J Korean Med Sci.* (2010) 25:1676–79. doi: 10.3346/jkms.2010.25.11.1676
21. Schecter JM, Mears JG, Alobeid B, Gaglio PJ. Anti-erythropoietin antibody-mediated pure red cell aplasia in a living donor liver transplant recipient treated for hepatitis C virus. *Liver Transpl.* (2007) 13:1589–92. doi: 10.1002/lt.21332
22. Tsubata EK, Kawamura S, Ishimoto T, Tomiyama-Miyaji Y, Watanabe C, Sekikawa H, et al. Protection against malaria by anti-erythropoietin antibody due to suppression of erythropoiesis in the liver and at other sites. *Immunol Cell Biol.* (2005) 83:638–42. doi: 10.1111/j.1440-1711.2005.01385.x
23. Macdougall IC, Casadevall N, Locatelli F, Combe C, London GM, Di Paolo S, et al. Incidence of erythropoietin antibody-mediated pure red cell aplasia: the prospective immunogenicity surveillance registry (PRIMS). *Nephrol Dial Transplant.* (2015) 30:451–60. doi: 10.1093/ndt/gfu297

Conflict of Interest: The authors declare that the research was conducted in the absence of any commercial or financial relationships that could be construed as a potential conflict of interest.

Copyright © 2020 Zhang, Bian, Yang, Wang, Tang, Wang, Wang, Nie and Zhao. This is an open-access article distributed under the terms of the Creative Commons Attribution License (CC BY). The use, distribution or reproduction in other forums is permitted, provided the original author(s) and the copyright owner(s) are credited and that the original publication in this journal is cited, in accordance with accepted academic practice. No use, distribution or reproduction is permitted which does not comply with these terms.

frontiers in Physiology

ORIGINAL RESEARCH
published: 29 May 2020
doi: 10.3389/fphys.2020.00560

NBCe2 (*Slc4a5*) Is Expressed in the Renal Connecting Tubules and Cortical Collecting Ducts and Mediates Base Extrusion

*Dagne Barbuskaite[1], Fredrik D. Pedersen[2], Henriette L. Christensen[2], Laura Ø. Johnsen[2], Jeppe Praetorius[2] and Helle H. Damkier[1,2]**

[1] Department of Cellular and Molecular Medicine, Faculty of Health and Medical Sciences, University of Copenhagen, Copenhagen, Denmark, [2] Department of Biomedicine, Health, Aarhus University, Aarhus, Denmark

Arterial hypertension, is a common disorder with multiple and variable etiologies. Single nucleotide polymorphism analyses have detected an association between variants in the gene encoding the electrogenic Na^+:HCO_3^- cotransporter NBCe2 (*Slc4a5*), and salt-sensitive hypertension. Mice with genetic deletion of NBCe2 are hypertensive, and the cause of the blood pressure (BP) increase is believed to arise from a lack of renal NBCe2 function. The exact cellular expression of NBCe2 in the kidney tubular system is, however, not determined. Here, we find NBCe2 to be expressed predominantly in isolated connecting tubules (CNT) and cortical collecting ducts (CD) by RT-PCR. In isolated renal CNT and CCD, genetic deletion of NBCe2 leads to decreased net base extrusion. To determine the role of renal NBCe2 in the development of hypertension, we generated CNT and intercalated cell NBCe2 knockout mice by crossing an *Slc4a5* lox mouse with mice expressing cre recombinase under the V-ATPase B1 subunit promotor. Although the mice displayed changes in the expression of renal membrane transporters, we did not detect hypertension in these mice by tail cuff recordings. In conclusion, while global NBCe2 deletion certainly causes hypertension this study cannot confirm the role of renal NBCe2 expression in blood pressure regulation.

Keywords: NBCe2, kidney, blood pressure, *Slc4a5*, hypertension

OPEN ACCESS

Edited by:
Md Abdul Hye Khan, Medical College of Wisconsin, United States

Reviewed by:
Francesco Trepiccione, Second University of Naples, Italy
Matthew A. Bailey, The University of Edinburgh, United Kingdom

****Correspondence:***
Helle H. Damkier
hd@biomed.au.dk

Specialty section:
This article was submitted to Renal and Epithelial Physiology, a section of the journal Frontiers in Physiology

Received: *28 January 2020*
Accepted: *04 May 2020*
Published: *29 May 2020*

Citation:
Barbuskaite D, Pedersen FD, Christensen HL, Johnsen LØ, Praetorius J and Damkier HH (2020) NBCe2 (Slc4a5) Is Expressed in the Renal Connecting Tubules and Cortical Collecting Ducts and Mediates Base Extrusion. Front. Physiol. 11:560. doi: 10.3389/fphys.2020.00560

INTRODUCTION

Hypertension, defined as a chronically elevated blood pressure (BP), is one of the most common chronic disorders in the developed world, affecting nearly one billion people worldwide (Writing Group Members et al., 2016). Hypertension has a significant heritability factor, as more and more genes are being identified as hypertension susceptibility genes. *Slc4a5*, encoding the sodium bicarbonate cotransporter NBCe2, was shown to be significantly associated with BP increases (Barkley et al., 2004; Hunt et al., 2006), and a salt-sensitivity trait (Carey et al., 2012; Taylor et al., 2012) by several genome wide association studies. Studies of NBCe2 knockout (NBCe2 ko) mice confirmed this observation. In the pioneering study by Groger et al. (2012) an NBCe2 ko was generated by excising the 7th coding exon, which resulted in increased BP at day and night time, metabolic acidosis, increased arterial natriuretic peptide, hyporeninemia, hypoaldosteronism, and increased glomerular filtration rate. A quite different phenotype was observed in the studies by Wen et al. (2015b) in the same ko model, but backcrossed to a C57Bl/6 background for at least 6

generations, resulting in a BP phenotype only on an acidic diet. The authors showed that NBCe2 dysfunction leads to increased activity of epithelial sodium channels (ENaC) in the kidney, as well as increased uncleaved α-ENaC expression and decreased NCC expression (Iversen et al., 2013). In the latter study of NBCe2 dysfunction, NBCe2 ko was reported to cause distal renal tubular acidosis and increased H^+-ATPase expression. Additionally, the two studies by Wen et al. report different results on the same NBCe2 ko mouse model: in the first study, decreased urinary (Na^+), and increased (K^+) excretion was reported and blood (Na^+) and (K^+) was unchanged, whereas the authors report decreased blood (K^+), and increased blood (Na^+), with no changes in urine concentration in the second study. The explanation for the observed NBCe2 ko phenotype was also different: Gröger et al. reasoned that lack of NBCe2, that supposedly reabsorbs bicarbonate in the collecting duct (CD), causes upregulation of another sodium bicarbonate transporter (NBCn1). Due to different transport stoichiometry increased activity of NBCn1 results in increased sodium reabsorption. Wen et al. suggested a different role for NBCe2. They propose NBCe2 to be expressed on the basolateral membrane in the principal cells and have a role in intracellular pH regulation, thus having most activity during acidosis, and causing intracellular sodium loading and inhibition of luminal ENaC activity. Such different interpretation of the results arises from overall lack of information about the exact renal NBCe2 expression site.

NBCe2 mediates electrogenic Na^+:HCO_3^- transport (Sassani et al., 2002), and can operate in both a 1:2 (Virkki et al., 2002; Shao et al., 2009), and 1:3 (Pushkin et al., 2000; Millar and Brown, 2008) manner, but the transport stoichiometry as well as directionality have not been defined for the renal NBCe2. In addition, there is a lack of coherence regarding NBCe2 localization in the kidney. The expression of NBCe2 has been reported in nearly all kidney nephron segments and CDs, indicating that some species-specificity might be present. In humans, NBCe2 has been immunolocalized in the intercalated cells of the CD (Damkier et al., 2007), and in the proximal tubules (PT; Gildea et al., 2015). In isolated rat tubules, NBCe2 mRNA expression was detected in cortical thick ascending limb (cTAL), medullary thick ascending limb (mTAL), PT, and cortical CD (Xu et al., 2003) but the purity of the micro-isolated renal tubules was not reported. In mouse, *in situ* hybridization studies showed that NBCe2 co-localizes with AQP2, which indicates expression in the principal cells of the CD (Groger et al., 2012). NBCe2 was also detected in micro-isolated connecting tubules (CNT; Wen et al., 2015a), again without reporting how the purity of the samples was tested. Finally, a transcriptome study evaluating renal CD cells revealed that *Slc4a5* expression was detected only in a few of the α- and β-intercalated cell (2/87 and 1/23, respectively) as well as principal cell (2/74) samples (Chen et al., 2017). Thus, it is complicated to establish a physiological and pathophysiological role for NBCe2 in the kidney without knowledge on which tubule segments express the protein, what membrane domain it localizes to, and finally the transport direction of NBCe2 at these sites.

In the current study, we evaluate the NBCe2 expression in isolated renal tubules and detect expression only in cells from CNT and CCD. Using intracellular pH recordings of isolated CNT and CDs, we determine that global lack of NBCe2 expression leads to impaired base extrusion capacity. We find decreased expression of γ-ENaC and increased expression of NBCn1 in global NBCe2 ko mice. Finally, we crossed floxed NBCe2 mice with a mouse expressing cre recombinase driven by the V-ATPase B1 promotor. This $Slc4a5^{(lox/lox)cre(Atp6v1b1)}$ mouse model showed decreased expression of α-ENaC but increased expression of γ-ENaC. Furthermore, the expression of the acid/base transporters AE2, V-ATPase, and pendrin were decreased in this model. Finally, tail cuff BP measurements confirmed hypertension in the global NBCe2 knockout mouse, but surprisingly the kidney-specific NBCe2 knockout mice did not display a BP phenotype. Our study suggests that a lack of NBCe2 expression in the CNT and CD does not seem to be associated with the hypertension observed in global NBCe2 knockouts. This suggests that another organ or cell type is involved in the BP regulation in the global NBCe2 knockout mouse.

MATERIALS AND METHODS

Experimental Animals

All animal experiments and protocols were approved by the Danish Animal Experiments Inspectorate. Mice were fed a standard rodent pellet diet (0.4% sodium) *ad libitum*, had free access to tap water and were exposed to a 12 h:12 h light-dark cycle. Only male mice were used throughout the study.

Transgenic mice, expressing enhanced green fluorescent protein (eGFP) in particular renal tubule segments were used for kidney tubule isolation. Mice expressing eGFP under the parvalbumin (PV-eGFP) promoter (Markadieu et al., 2012) were used for collection of distal convoluted tubules (DCT). Transgenic mice expressing eGFP driven by the transient receptor potential subfamily V, member 5 gene (TRPV5; Hofmeister et al., 2009) were used to collect late DCT, CNT, and CDs.

The breeding and genotyping of NBCe2 ko mice on a mixed C57Bl/6J-129S1/Sv genetic background have previously been described (Christensen et al., 2018). Briefly, the 13th exon of the *Slc4a5* gene was floxed with LoxP sites, and the generated $Slc4a5^{flx}$ mice were crossed with a tamoxifen-inducible ubiquitin promoter-driven Cre-recombinase expressing mouse strain. Mice carrying the $Slc4a5^{flx}$ allele were also used to generate kidney specific knockout mice. Intercalated cell specific kidney knockout mice were generated by crossing mice with the $Slc4a5^{flx}$ allele, and mice expressing Cre recombinase under endogenous Atp6v1b1 promoter/enhancer elements (Miller et al., 2009) resulting in $Slc4a5^{(lox/lox)cre(Atp6v1b1)}$. In the following, this strain will be named $NBCe2^{B1-VATPasecre}$ mice. Throughout the study, mice carrying $Slc4a5^{(lox/lox)}$ without cre expression or wildtype mice expressing only cre are used as controls and will be named "control." In all experiments, littermates are used as controls in order to ensure similar genetic background when comparing phenotypes.

NBCe2 Expression in Micro-Isolated Mouse Kidney Tubules and Cells

The kidney tubule isolation procedure was adapted from Hofmeister et al. (2009). Transgenic TRPv5-promoter driven eGFP expressing mice (CNT/CCD-GFP) and parvalbumin-promoter driven eGFP expressing mice (DCT-GFP) were anesthetized by isoflurane inhalation and perfused through the left ventricle with isolation buffer (in mM: 150 Na^+, 3.6 K^+, 1.0 Mg^{2+},1.3 Ca^{2+}, 140 Cl^-, 0.4 $H_2PO_4^-$, 1.6 HPO_4^{2-}, 1.0 SO_4^{2-}, 10 acetate$^-$, 1.3 gluconate$^-$, 1.0 α-ketoglutarate, and 5 glycine) supplemented with 48 mg/l trypsin inhibitor, 25 mg/l DNase I, 1 mg/ml collagenase B (Roche Diagnostics), and 1 mg/ml pronase (Roche Diagnostics) at pH 7.4 and 37°C. Kidneys were dissected and placed in the enzyme-supplemented isolation buffer and spun at 850 rpm for 10 min. To isolate inner medullary CDs, 1 mg/ml Hyaluronidase was added. Half volume of the tubule suspension was transferred into ice-cold isolation buffer containing 0.5 mg/ml albumin. Equal volume of isolation solution was added to the remaining tubule suspension and spun for an additional 5 min. This procedure was repeated three times resulting in 4 tubule fractions. PT, thick ascending limbs of loop of Henle (TAL), and glomeruli (Gl) were selected under a dissection microscope (Leica MZ125) according to their morphology. DCT and CNT/CD were collected according to fluorescence. Neither the DCT nor CNT/CD collected fractions were pure, thus we determined NBCe2 by fluorescence activated cell sorting (FACS) DCT and CNT/CD tubules.

For FACS (Jensen et al., 2012), the isolation buffer was supplemented with 1 μl/ml proteinase K (Roche Diagnostics), and mice were perfused as described above. The perfused kidneys were dissected, sliced, and incubated in isolation solution for 45 min on a shaking table at 37°C. To obtain single cells, tubules were digested twice in a trypsin/ethylenediaminetetraacetic acid (EDTA) solution (Invitrogen, ThermoFisher, Roskilde, Denmark) at 37°C for 5 min. The cell suspension was passed through a 40 μm filter, and propidium iodide was added before the FACS for exclusion of dead cells. Tubules were sorted into fluorescein-positive and fluorescein-negative samples by 4-way purity sorting on a FACS Aria III (BD Biosciences, Lyngby, Denmark). The tubules were sorted using a 100 μm nozzle, at 20 psi and 30 kHz. For FACS on kidney cells from TRPv5-eGFP mice, 25,739,077 events were recorded, and 109,449 CNT/CCD-GFP positive (+) cells were collected with a recount purity of 94.5%, and 4,604,668 negative eGFP(–) cells were collected with 100.0% purity, respectively. For FACS on kidney cells from parvalbumin-eGFP mice, 21,309,632 events were recorded, and 105,884 DCT-GFP positive (+) cells were collected with a recount purity of 94.0%, and 3,914,983 negative eGFP (–) cells were collected with 99.7% purity, respectively. Collected tubule samples were placed in RNAlater solution (Invitrogen) for later analysis by RT-PCR.

Reverse Transcription Polymerase Chain Reaction (RT-PCR)

The purity of the collected renal tubules and the expression of NBCe2 was determined by RT-PCR (see **Supplementary Table S1** for primer sequences and product sizes). RNA from the tubules was purified using an RNeasy micro kit (Qiagen, Copenhagen, Denmark) according to the manufacturer's instructions. The concentration of purified RNA was determined by absorbance at 260 nm using a NanoDrop ND-2000 (Fisher Scientific) and 20–40 ng of RNA was reverse transcribed by iScript Reverse Transcription Supermix (Bio Rad, Copenhagens, Denmark). PCR amplification was performed for each transcript by mixing cDNA with 1 pmol of primers and 5× HOT FIREPol Blend Master Mix (Solis BioDyne). The PCR reaction was performed for 35 cycles after 15 min at 95°C: denaturation was performed for 30 s at 95°C, annealing at 60°C for 30 s, and elongation at 72°C for 1 min. PCR products were mixed with 2 μl of DNA Gel Loading Dye (6×; Thermo Scientific) containing 0.05% 10000 × GelRed (Biotium, BioNordika Denmark, Herlev, Denmark) nucleic acid gel stain, separated by 1% agarose gel electrophoresis, and photographed under ultraviolet illumination.

Intracellular pH Measurements in Distal Renal Tubules

Isolated renal tubules were resuspended in a HEPES-buffered solution (HBS; see **Supplementary Table S2**), plated on Cell-tak (corning^{TM}, Fisher Scientific)-covered coverslips and allowed to attach for 10 min at 37°C. Cells were loaded with the pH-sensitive BCECF (10 μM, Thermo Fisher Scientific, Roskilde, Denmark) for 10 min or carboxy-SNARF (2 μM, Thermo Fisher Scientific) for 30 min. Coverslips were mounted in a closed perfusion chamber (RC-21BR; Harvard Apparatus, Holliston, MA, United States) and placed on an inverted microscope stage inside a 37°C dark chamber. Tubules were allowed to equilibrate in HBS before the protocols were performed. CNT/CCD segments were identified by branching appearance and the occurrence of intercalated cells not readily retaining the fluorescent dyes.

Intracellular pH with BCECF was recorded similar to a previous study (Hofmeister et al., 2012). In short, the tubules were imaged at the stage of a Nikon Eclipse microscope provided with a Nikon Plan Apo VC 60×/1.4NA oil-immersion objective. Till Vision software (Till Photonics) was used to control the monochromator wavelength (alternating between 490 nm and 440 nm), frequency (1 Hz), exposure time (20 ms), and binning (to 640 × 480 pixel images). A 12-bit cooled monochrome CCD camera (Imago, Till Photonics) recorded the light emission at 510–535 nm and data was collected from user defined regions of interest (ROIs) of individual tubule cells after background subtraction. Sample size (*n*) refers to the mean values from at least three individual cells from one mouse. In separate experiments the fluorescence ratio was calibrated to pH by clamping pH_i stepwise from pH 8 to 6 in a high K^+ containing HBS with 10 μM nigericin (Sigma-Aldrich, Soeborg, Denmark) similar to (Boyarsky et al., 1988).

To determine acid-extrusion, the tubules were acidified by superfusion with a HEPES buffered solution containing 20 mM NH_4Cl (HBS NH_4Cl) for 3 min followed by a washout of NH_4Cl using a Na^+ free bicarbonate buffered solution (BBS $0Na^+$, see **Supplementary Table S2**). After reaching a new steady state, a Na^+ containing bicarbonate solution was added (BBS,

Supplementary Table S2) and the Na^+ dependent pH recovery was determined as the dpH_i/dt after re-addition of Na^+.

For pH_i recordings using carboxy-SNARF, the tubules were imaged using an iMic microscope (Till Photonics) with an Olympus UApo N340, 40×/1.35 NA oil-immersion objective. Till Vision software (Till Photonics) was used to control the monochromator wavelength for excitation alternating between 485 nm and 555 nm, exposure time (25 ms), frequency (0.25 Hz), and binning (to 256 × 256 pixel images). Light emission (565–615 nm) was recorded by a 14-bit cooled monochrome EMCCD camera ($iXon^{EM+}$, Andor technology, Belfast, United Kingdom) with 4 times EM gain. Data was collected from ROIs of individual tubule cells after background subtraction. The excitation fluorescence ratio (485/555 nm) was calibrated to pHi by stepwise shifts from pH 8.4 to 7 in high K^+ containing HBS with 10 μ M nigericin.

To determine base extrusion, the tubules were superfused with a bicarbonate buffered solution (BBS, **Supplementary Table S2**). Base extrusion was determined as the dpH_i/dt following peak alkalization induced by removal of Cl^- in a bicarbonate buffered solution (BBS 0Cl, **Supplementary Table S2**).

The intrinsic buffering capacity was determined by recording of pH_i changes while stepwise decreasing NH_4^+ from 20 to 0 mM as previously described (Boyarsky et al., 1988; Hofmeister et al., 2012).

All experiments were performed in the presence of 2.5 mM probenecid (Thermo Fisher Scientific) to inhibit dye extrusion by organic anion-transporters. CNT/CD tubules were selected based on morphology similar to a previous study (Hofmeister et al., 2012).

Immunoblotting

Mouse kidney was homogenized in an ice-cold dissection buffer (0.3 mol/L sucrose, 25 mol/L imidazole, 1 mmol/L EDTA, and pH 7.2) containing 8.4 mol/L leupeptin (Calbiochem) and 0.4 mmol/L Pefabloc (Roche) protease inhibitors, as well as PhosSTOP (Roche, Sigma Aldrich, Soeborg, Denmark) phosphatase inhibitor (1 tablet/10 ml buffer). Samples were centrifuged at 4000 *g* for 15 min at 4°C, and the sample buffer was added to the supernatant (0.1 mol/L sodium dodecyl sulfate and 0.04 mol/L dithiothreitol, pH 6.8). The protein samples were heated at 65°C for 15 min and separated by 4–15% gradient polyacrylamide gel electrophoresis (Bio Rad, mini-protean TGX). Then samples were electro transferred by the Transblot turbo system (Bio Rad) onto a PVDF (Ambion, ThermoFisher, Roskilde, Denmark) membrane, which was then blocked with 5% milk in PBS-T (in mmol/L: 167 Na^+, 2.8 $H_2PO_4^-$, 7.2 HPO_4^{2-}, and pH 7.4 with 0.1% vol/vol Tween), and incubated with primary antibody in PBS with 1% bovine serum albumin (BSA), and 2 mmol/L NaN_3 overnight at 4°C. The primary antibodies used in the study were characterized elsewhere: NBCe2 (Christensen et al., 2018), α-ENaC (Sorensen et al., 2013), the 82 kDa band represents uncleaved and the 25 kDa band cleaved α-ENaC (Michlig et al., 2005), γ-ENaC (Masilamani et al., 1999) [the uncleaved form is seen at 95 kDa and the cleaved form at 65 kDa (Harris et al., 2008)], and H^+-ATPase (Toyomura et al., 2000). The day after, membranes were rinsed, and incubated with horseradish peroxidase-conjugated anti-rabbit secondary antibody (Dako) diluted 1:3000 in 5% milk in PBS-T at room temperature. The membranes were incubated with the Pierce ECL Plus Western Blotting Substrate (Thermo Scientific) and imaged with the Epson perfection V700 Photo scanner (Seiko Epson Corporation, Suwa, Japan). Labeling density was quantified using Quantity One 4.6.9 software (Bio Rad Laboratories).

Metabolic Cages, Blood Gas and Electrolyte Analysis

Mice were placed in metabolic cages (Techniplast, Scanbur, Karlslunde, Denmark) and given three days to acclimatize. Baseline parameters (food intake, water intake, and urine output) as well as urine composition (pH, electrolyte concentration, and osmolality) were determined on day 4. In the metabolic acidosis experiments, the animals were placed in metabolic cages and given 3 days to acclimatize. This was followed by induction of metabolic acidosis by adding 2% NH_4Cl to the standard chow for 4 days. The collected urine samples were centrifuged at 1000 × *g* for 1 min. Urine pH was measured with a pH-meter (Metrohm, Glostrup, Denmark), whereas ionic composition (Na^+, K^+, and Cl^-) was analyzed at the Medical Research Council Harwell, United Kingdom. Osmolality was measured in 3 × mqH_2O diluted urine by using a freezing point depression osmometer (model 3320, Advanced Instruments). All urine samples containing feces and larger food products were excluded. The blood samples were collected with heparin-containing PICO syringes (Radiometer, Broenshoej, Denmark) by drawing the blood from the right heart atrium of isoflurane anesthetized mice. The blood gas analysis was performed on FLEX blood gas analyzer (Radiometer).

Blood Pressure Measurement

Systemic BP was measured non-invasively in 1- to 4-month-old $NBCe2^{B1-V\ ATPase\ cre}$ and global NBCe2 ko mice by determining the tail blood volume with a volume pressure recording sensor and an occlusion tail-cuff (CODA System, Kent Scientific, Torrington, CT, United States). Non-anaesthetized mice were placed in a restrainer, and warmed for 5 min on a heating pad. An occlusion cuff and a volume pressure cuff were placed on the tail of the mouse, and the BP was measured. The mice were first placed 10–15 min in the restrainer in order to reduce the stress response to the procedure. In order to further lower the stress response, mice were trained by daily BP measurements for 8–13 days. Measurements were performed at the same time each day in the afternoon when activity in the animal facility was low. The mice were handled by the same researcher each day. There was no statistically significant difference in BP when comparing within the same genotype over duration of the measurement period (not shown). To avoid a systematic bias in the tail cuff equipment, mice were randomly switched between individual cuffs from day to day. One full measurement consisted of 10 acclimation cycles and 10 measurement cycles. Daily values of systolic, diastolic and

mean arterial BP were calculated as an average value of the 10 measurement cycles.

Statistical Analysis

All data is represented as an average ± SEM. Semi-quantification of immunoblotting and NBCe2 ko BP measurements and metabolic cages data were analyzed by an unpaired two-tailed *t*-test and $p < 0.05$ was considered statistically significant.

RESULTS

NBCe2 Expression in the Kidney Is Restricted to Cells From CNT and CCD Principal Cells

NBCe2 expression was determined in isolated mouse kidney tubules and FACS isolated fluorescent tubular cells. Fractions enriched for PT and TAL were collected under a dissection microscope determined by morphology. PT fractions were chosen by the most prominent RT-PCR signal for NBCe1 and AQP1, whereas TAL fractions were chosen by the most prominent signal for NKCC2 and CLC2. DCT fractions were obtained either by morphology or from parvalbumin-promoter driven eGFP expressing mouse tubules. Conversely CNT/CCD fractions were obtained from the branching morphology or from TRPv5-promoter driven eGFP expressing mouse tubules. Although most fractions showed contamination from other tubular segments, NBCe2 expression only coincided with DCT, or CNT/CCD markers. No NBCe2 was detected in TAL and glomeruli in contrast to a whole kidney sample (**Figure 1A**). Similarly, two PT isolates did not reveal NBCe2 expression in contrast to a choroid plexus sample (**Figure 1B**). FACS-sorted single cells enriched for CNT/CD showed amplification of a NBCe2 signal (**Figure 1C**). Weak reaction product was observed in both DCT-GFP(–) cells and TRPv5-GFP(–) cells. As described in Methods, these fractions showed a high level of purity and leave little room for false-positive and false-negative results. The high cycle number necessary to detect NBCe2 in the kidney suggests a relatively low expression level.

Global NBCe2 Deletion Results in Decreased Base Extrusion From CNT/CCD

In the choroid plexus, NBCe2 exports Na^+, and HCO_3^- from the epithelial cell across the luminal membrane (Millar and Brown, 2008). We have previously demonstrated that knockout of NBCe2 in the choroid plexus leads to decreased net base extrusion and increased acid extrusion due to the lack of an effective base extruder (Christensen et al., 2018).

In the kidney, the membrane localization of NBCe2 protein in the renal tubules is not known. Using an NBCe2 antibody that specifically recognizes NBCe2 in the choroid plexus, we are unable to determine the subcellular localization of NBCe2 in kidney epithelial cells. We do observe immunoreactivity in PT and DCT similar to what has previously been published by other research groups (Gildea et al., 2015). However, the renal staining is remarkably also present in the kidneys from NBCe2 knockout mice (**Supplementary Figure S1**). Together, the high cycle number necessary for the detection of NBCe2 by RT-PCR and the lack of detection of renal NBCe2 by immunohistochemistry and immunoblotting suggest a low renal expression level as compared to the choroid plexus.

Similar to the question of subcellular localization, the net transport direction of ions through NBCe2 in the kidney is not known. To investigate the contribution of NBCe2 to base extrusion, intracellular pH was monitored first in either SNARF-loaded or BCECF-loaded isolated tubules (CNT/CCD) from NBCe2 knockout and wild type mice.

Intracellular pH was increased by removal of Cl^- from a HCO_3^- buffered solution (**Figure 2A**). Baseline pH assessed in BBS was not significantly different between the two genotypes [NBCe2 wt: 7.51 ± 0.07 ($n = 7$); NBCe2 ko: 7.56 ± 0.07 ($n = 6$), $p = 0.64$]. The removal of Cl^- created a gradient for Cl^- out of the cell through the anion exchanger that in return imports HCO_3^- which increases pH_i. The pH_i recovery from this point would be mediated by Cl^- independent Na^+-dependent HCO_3^- *export* (i.e., outward NBC activity). The pH_i recovery rate following peak alkalization was decreased by 87% compared to wild type (**Figures 2A,B**). A different way of assessing NBC activity is to record the Na^+-dependent HCO_3^- *import* (net acid extrusion) after acidification. The acid extrusion showed a 45% increase in the tubules from NBCe2 knockout but the difference was not statistically significant (**Figures 2C,D**), but would suggest the lack of NBCe2 mediated HCO_3^- efflux. In order to rule out that the difference in pH_i regulation is caused by differences in the buffering capacity of the tubules, the intrinsic buffering capacity was determined. No difference in intrinsic buffering capacity was detected in tubules isolated from knockout and wildtype mice (not shown). Thus, NBCe2 appears to be mediating outward Na^+:HCO_3^- cotransport in these renal tubules.

Regulation of Transporters in Kidneys of NBCe2 ko Mice

Previous studies have shown differences in expression of the electroneutral Na^+ and HCO_3^- cotransporter NBCn1 as well as the epithelial sodium channel, ENaC, in kidney from NBCe2 knockout mice. We determined the expression of transporters involved in Na^+ and HCO_3^- handling in our knockout model. Contrary to previous studies, we found decreased abundance of the γENaC, but no difference in abundance of the α or β subunits (**Figures 3A–D**). We find increased expression of the Na^+ and HCO_3^- cotransporter NBCn1 (**Figure 3E**) but no difference in expression of the Cl^-/HCO_3^- exchangers pendrin and AE2 (**Figures 3F,G**).

NBCe2 Kidney Cell-Specific ko Mice

Since NBCe2 expression and function was only observed in the CNT/CCD, we generated kidney cell specific knockout mice by targeting cells of the CNT and CDs. We have previously shown that NBCe2 is expressed in intercalated cells in the human kidney (Damkier et al., 2007), while previous studies have suggested *slc4a5* mRNA in principal cells

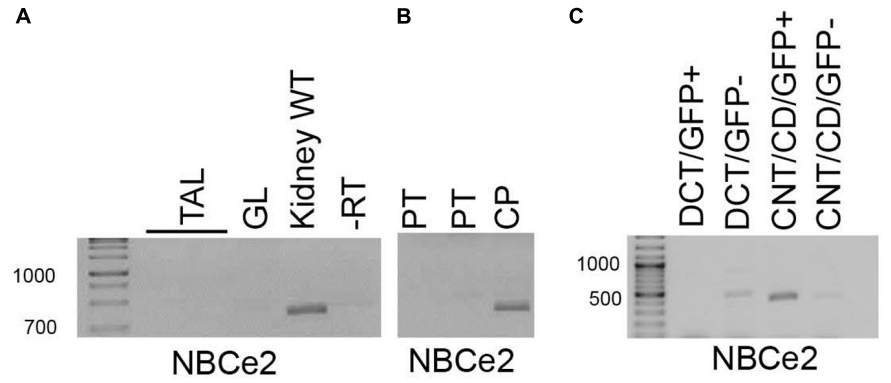

FIGURE 1 | RT-PCR analysis of micro-isolated renal tubules. NBCe2 amplicons were only observed in whole kidney samples and were absent from samples of thick ascending limb (TAL) and glomeruli (GL; **A**). Similarly, a NBCe2 product was absent in samples from proximal tubule (PT) but the present in the positive control, the choroid plexus (CP; **B**). Finally, NBCe2 product was successfully amplified from samples enriched for connecting tubule and collecting duct (CNT/CD) fraction **(C)**. -RT: no reverse transcriptase; DCT-GFP(+); and CNT/CCD-GFP(+): fluorescence positive fraction of FACS sorting, DCT-GFP(–), and CNT/CCD-GFP(–): fluorescence negative fraction of FACS sorting using kidney cells from mice expressing eGFP under control of the parvalbumin (DCT) and TRPv5 (CNT/CCD) promotor, respectively.

(Groger et al., 2012). The NBCe2$^{B1-VATPasecre}$ model expresses cre recombinase under the endogenous *Atp6v1b1* promoter, resulting in recombination in the intercalated cells of the CNT, CD, as well as in 50% of principal cells within the CNT (Miller et al., 2009). We attempted to evaluate the extent of knockout by qPCR but did not obtain a sufficient NBCe2 signal for quantitation. As previously mentioned, a recently characterized NBCe2 specific antibody (Christensen et al., 2018) failed to produce anti-NBCe2 staining in the kidney. The antibody is directed at the N-terminal domain of mouse NBCe2 and should recognize the renal NBCe2 variant. The immunostaining was tested in paraffin sections with target retrieval in high and low pH, as well as in cryostat sections, yet no NBCe2 specific signal was observed. In addition, a proximity ligation assay (PLA, Duolink, Sigma Aldrich) was used in order to amplify the NBCe2 antibody's binding, but without success apart from the choroid plexus control labeling. Therefore, we were unable to assess the degree of NBCe2 knockout in NBCe2$^{B1-VATPase\ cre}$ mice.

Kidney Cell-Specific NBCe2 Deletion Causes Significant Changes in Expression of Renal Membrane Transporters

As it was impossible to evaluate the knockdown degree in the cre model, we evaluated whether the mouse model showed a transporter expression phenotype similar to the global knockout mouse. The expression of some ion transporters, typical for principal and intercalated cells was assessed by semi-quantification from immunoblotting. Unlike the global NBCe2 ko, a significant decrease in cleaved (p = 0.005), uncleaved (p = 0.04), and total (p = 0.011) α-ENaC protein was observed (n = 6 for both genotypes) in NBCe2$^{B1-VATPasecre}$ (**Figure 4**). The uncleaved (p = 0.037) and total γ-ENaC (p = 0.049) expression was increased at the protein level, whereas the H^+-ATPase protein expression was decreased (p = 0.030) in NBCe2$^{B1-VATPasecre}$. Thus, the NBCe2$^{B1-VATPasecre}$ ko model offers a renal expression pattern separate from that of kidneys from control and global NBCe2 ko mice.

Kidney Cell-Specific NBCe2 Deletion Causes Minor Alterations in Water and Electrolyte Handling

The baseline renal function was studied in the global NBCe2 ko mice by measuring the basic urine and blood electrolyte parameters. We have previously reported that global NBCe2 ko results in elevated blood pCO_2 and HCO_3^- (Hofmeister et al., 2009), yet no other parameters statistically differed in this ko model (**Table 1**).

In order to evaluate the cell-type specific NBCe2 knockout effect on renal function, we placed NBCe2$^{B1-VATPasecre}$ mice in metabolic cages to assess baseline water and food intake, urine output and pH, and urine and blood electrolyte composition. NBCe2$^{B1-VATPasecre}$ mice had significantly elevated blood potassium levels with no signs of hemolysis in the samples, whereas the urine potassium level showed a decreaseing tendency (**Table 2**). NBCe2$^{B1-VATPasecre}$ mice had a numerical but non-statistically significant change in base excess and anion gap in same direction as the global NBCe2 ko.

Increased Blood Pressure in Global NBCe2 Knockout Mice Is Absent in Kidney Cell Targeted ko

To ensure that the tail cuff method is sensitive enough to detect NBCe2 mediated increase in BP, we assessed the BP in NBCe2 ko. As expected, a significantly increased BP was observed in the global NBCe2 ko model (83 ± 1.8 mmHg for wt, 117 ± 7.0 mmHg for ko, n = 12 in both groups, $p = 1.8 \times 10^{-11}$, **Figures 5A,B**). We then determined the

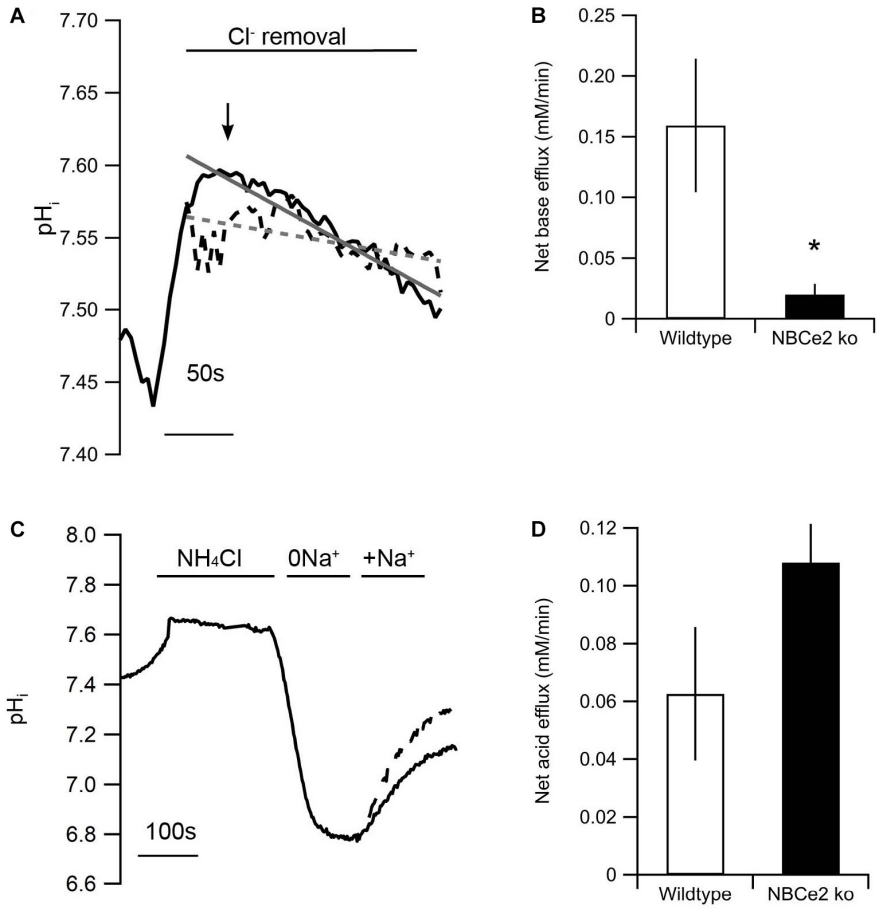

FIGURE 2 | Knockout of NBCe2 results in decreased base extrusion in distal renal tubules. **(A)** Representative traces of intracellular pH (pH_i) recordings of SNARF loaded isolated distal renal tubules from NBCe2 ko (dotted black line) and wild type mice (full black line). The gray lines show a line fit of the trace from the NBCe2 ko (dotted gray line) and wildtype (full line). Baseline pH_i was determined in CO_2/HCO_3^- buffered saline solution followed by determination of the alkalization induced by removing Cl^- in the continued presence of CO_2/HCO_3^-. The rate of base extrusion was determined as the dpH_i/dt after peak alkalization (arrow). **(B)** Mean values of the net base efflux ± SEM at the peak of Cl^- removal. **(C)** Representative traces of pH_i recordings of BCECF loaded isolated distal renal tubules from NBCe2 ko (dotted line) and wild type mice (full line). Baseline pH_i was determined in a HEPES buffered saline solution. Intracellular pH was decreased by an NH_4Cl prepulse followed by a washout in Na^+ free ($0Na^+$) solution. The rate of acid extrusion was determined as the dpH_i/dt after addition of a Na^+ and HCO_3^- containing solution ($+Na^+$). **(D)** Mean values of net acid efflux ± SEM after addition of Na^+.

average BP in $NBCe2^{B1-VATPasecre}$ mice by the same method. The mean arterial BP was not increased in the kidney cell-targeted ko model (119 ± 2.0 mmHg for wt, n = 9; 120 ± 2.3 mmHg for $NBCe2^{B1-VATPasecre}$, n = 8; p = 0.569, **Figures 5C,D**).

DISCUSSION

In the present study, we show that the renal cortical NBCe2 expression is restricted to the CNT and CD in mice. Exploiting a cell-specific cre mouse model, we targeted deletion of NBCe2 to cells of the CNT/CCD of mouse kidney. The genetic manipulation resulted in altered expression of various sodium and acid-base transporting proteins expressed in the kidney tubules in question. We did, however, not find evidence for increased BP in these mice or changes in basic physiological parameters. This suggests that other organs or cell types are mediating the hypertension observed in the global NBCe2 ko mouse.

We exploited a method for the selection of renal tubules by combining manual tubule collection by morphology, and by FACS sorting of the eGFP expressing tubules. We assessed the purity of the samples by evaluating the expression of tubule segment specific transporters. Previous studies have reported NBCe2 expression in both the proximal part of nephron [PT (Gildea et al., 2015), TAL (Xu et al., 2003)] and in distal nephron and CDs (Damkier et al., 2007; Groger et al., 2012; Wen et al., 2015a), perhaps representing inter-species variation. In the current study, we show that renal cortical NBCe2 is not expressed in the mouse PT, TAL, or DCT, but is only detected in the CNT/CD fractions. Our experiments suggest that it should be a prerequisite to evaluate isolated tubule purity, as only a small fraction of collected samples showed segment-specific expression

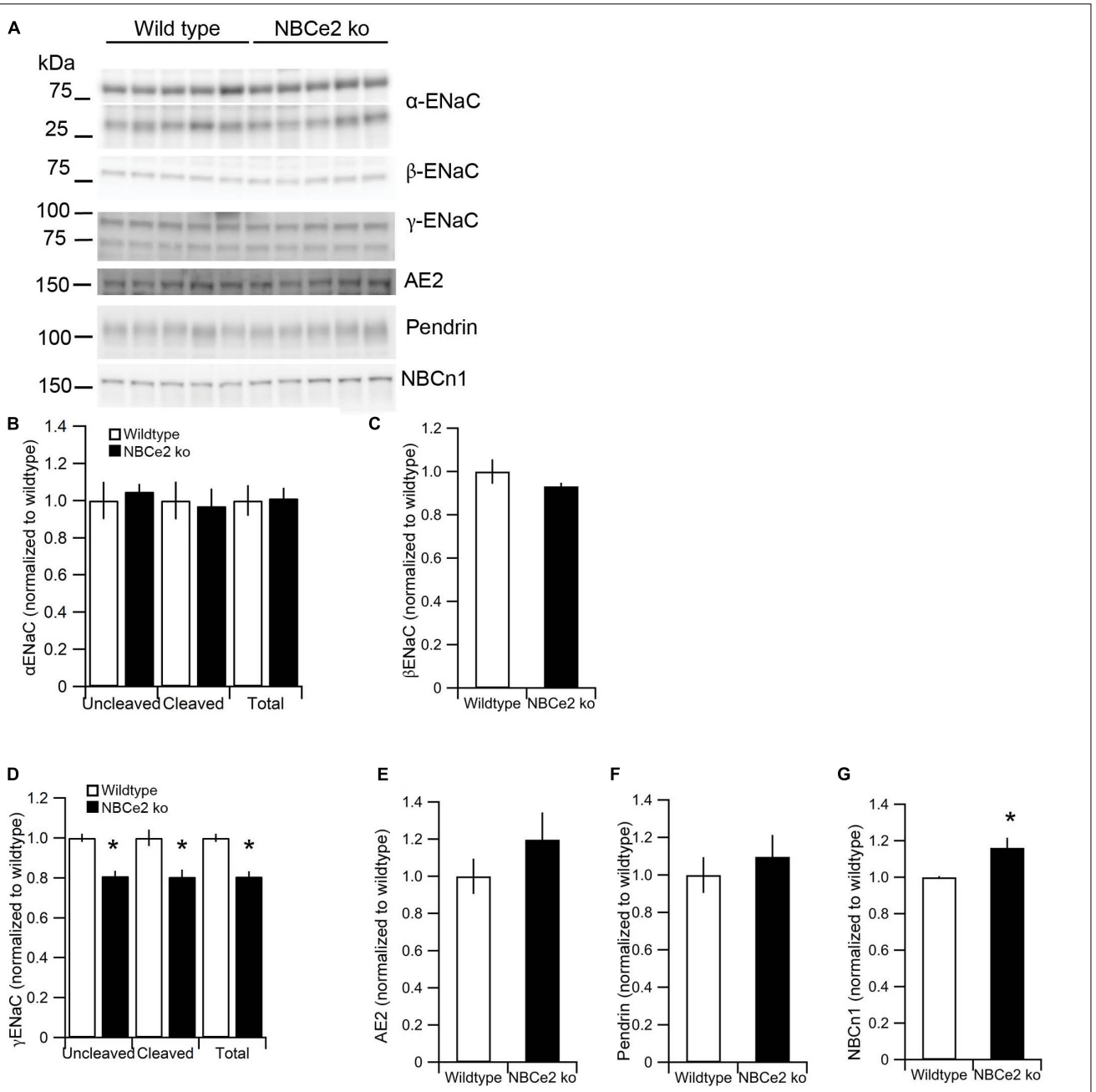

FIGURE 3 | Expression of sodium and bicarbonate transporters in NBCe2 knockout mice. Immunoblotting analysis of kidney protein samples from wildtype (white bars) and NBCe2 global knockout mice (NBCe2 ko, black bars). Blots show immunoreactivity for α, β, and γ-ENaC, NBCn1, pendrin, and AE2 **(A)**. Semi-quantitative analysis of uncleaved (95 kDa band), cleaved (65 kDa band), and total α-ENaC **(B)**, βENaC **(C)** uncleaved (85 kDa band), cleaved (70 kDa band), and total γ-ENaC **(D)**, AE2 **(E)**, pendrin **(F)**, and NBCn1 **(G)**. Data is presented as mean intensity normalized to the control mice ± SEM.

of transporter mRNA. Although we did not achieve completely pure fractions, we can at least exclude NBCe2 expression in the proximal part of the nephron and confirm its expression in the CNT and CD.

Our functional data indicate that NBCe2 in the CNT/CCD has a similar transport direction as in the choroid plexus: a net outward transport of Na^+ and HCO_3^-. Base extrusion is greatly diminished in alkalized cells and net acid extrusion is numerically increased in acidified cells (however, the latter not significantly). The phenotype could be a result of increased or decreased activity of other acid-base transporters in the cells. In fact, we also found that the abundance of the electroneutral Na^+;HCO_3^- importer NBCn1 is increased similar to previous publications. NBCn1 is expressed in the basolateral membrane of intercalated cells where it is responsible for the import of HCO_3^- from the blood to the cell (Vorum et al., 2000). The previous

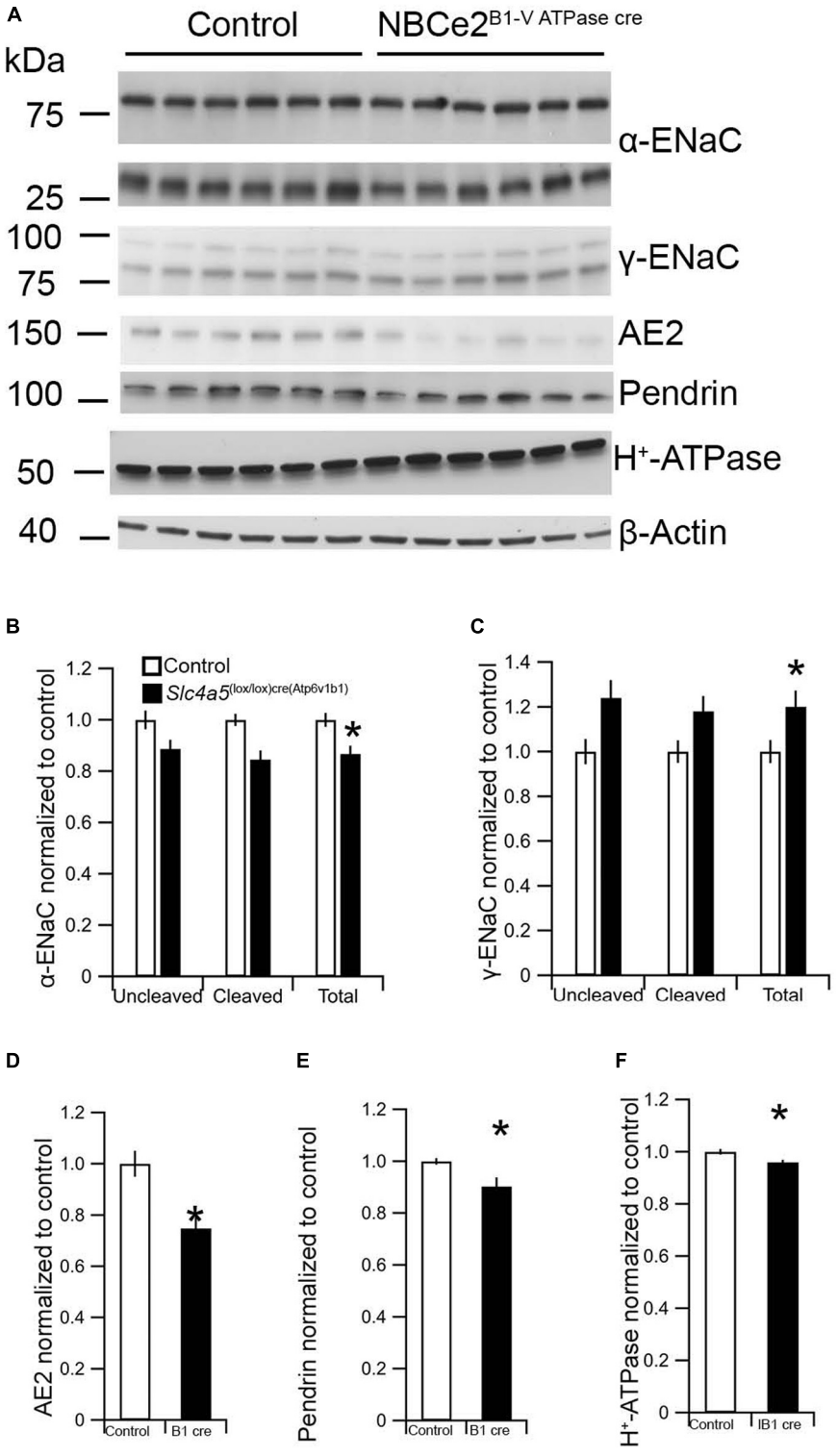

FIGURE 4 | Expression of renal α and β-ENaC as well as H^+–ATPase in $NBCe2^{B1-VATPasecre}$ mice. Immunoblotting analysis of kidney protein samples from wildtype (white bars) and $NBCe2^{B1-VATPasecre}$ (black bars). Blots show immunoreactivity for α and β-ENaC, AE2, pendrin, H^+-ATPase, and β-actin **(A)**. Semi-quantitative analysis of uncleaved (95 kDa band), cleaved (65 kDa band), and total α-ENaC relative to β-actin **(B)**; uncleaved (93 kDa band), cleaved (75 kDa band), and total β-ENaC relative to β-actin **(C)**, AE2 **(D)**, pendrin **(E)**, and H^+-ATPase **(F)** relative to β-actin. Data is presented as mean intensity normalized to the control mice ± SEM.

TABLE 1 | Baseline parameters in the full NBCe2 ko mice.

Baseline parameters			
	WT	**KO**	
Food intake, g/day	3.33 ± 0.21	3.29 ± 0.25	n.s.
Water intake, g/day	6.28 ± 0.86	6.14 ± 0.94	n.s.
Urine output (ml/day)	1.41 ± 0.39	1.47 ± 0.37	n.s.
Urine pH	7.50 ± 0.24	7.50 ± 0.20	n.s.
Plasma parameters			
Potassium, mmol/l	6.05 ± 0.14	6.18 ± 0.72	n.s.
Blood pH	7.43 ± 0.02	7.43 ± 0.01	n.s.
pCO_2, kPa (mmHg)	4.4 ± 0.3 (33 ± 2.3)	3.4 ± 0.3 (25.5 ± 2.3)	0.035
$StHCO_{3-}$, mM	23.1 ± 0.5	20.2 ± 0.7	0.004
Base excess	-2.28 ± 1.12	-4.32 ± 0.85	n.s.
n	5	5	

TABLE 2 | Baseline blood and urine parameters in the $NBCe2^{B1-VATPase\ cre}$ mice.

Baseline parameters			
	Control	**$NBCe2^{B1-VATPasecre}$**	
Mouse weight (g)	25.0 ± 0.1	25.2 ± 0.6	n.s.
Food intake, g/day	5.0 ± 0.7	5.5 ± 0.4	n.s.
Water intake, g/day	4.8 ± 0.4	3.5 ± 0.4	n.s.
Urine output ml/g body weight	0.06 ± 0.02	0.06 ± 0.01	n.s.
Urine parameters			
Sodium, mmol/24 h	0.08 ± 0.01	0.12 ± 0.02	n.s.
Potassium, mmol/24 h	0.38 ± 0.01	0.45 ± 0.04	n.s.
Chloride, mmol/24 h	0.22 ± 0.02	0.26 ± 0.02	n.s.
pH	7.37 ± 0.55	7.46 ± 0.17	n.s.
Osmolality (mosm/l)	1990 ± 414	1948 ± 140	n.s.
Plasma parameters			
Sodium, mmol/l	147 ± 2	144 ± 1	n.s.
Potassium, mmol/l	6.1 ± 0.3	7.1 ± 0.2	$p = 0.03$
Chloride, mmol/l	110 ± 2	112 ± 1	n.s
Calcium, mmol/l	1.3 ± 0.01	1.3 ± 0.02	n.s.
pH	7.42 ± 0.01	7.45 ± 0.01	n.s.
Hematocrit, %	40 ± 2	33 ± 4	n.s.
Base excess	-0.77 ± 1.22	-1.32 ± 0.91	n.s.
Anion gap	20.4 ± 1.3	15.14 ± 2.8	n.s.
n	3	5	

study also showed that AE1 is increased in NBCe2 knockout mice (Groger et al., 2012). These two transporters have opposite effects on basolateral base extrusion.

Our RT-PCR results suggest that renal cortical NBCe2 expression is confined to the CNT and CDs. We thus generated a kidney cell specific NBCe2 ko model to further explore the role of NBCe2 by crossing our floxed NBCe2 mouse with a mouse expressing cre recombinase driven by the H^+-ATPase B1 subunit. This model expresses cre recombinase in all intercalated cells and approximately 50% of the principal cells of the CNT (Ramkumar et al., 2018). Unfortunately, both quantitative PCR and immuno-based techniques failed to detect NBCe2 in the kidney and we were not able to determine the degree of NBCe2 knockdown in the mice. We speculate that the reason why we cannot detect NBCe2 using QPCR and immunohistochemistry is that the abundance of NBCe2 in the kidney is very low. If only a few copies of mRNA are present in the tubules, it would be difficult to get a valid and comparable result with the QPCR from a whole kidney. In comparison, QPCR from the choroid plexus which also expresses NBCe2 gives a stable signal (Christensen et al., 2018). Using RT-PCR of isolated tubules, we are able to detect the level of NBCe2 only with a high cycle number in the PCR. The immunohistochemistry using a previously validated anti-NBCe2 antibody did not detect specific NBCe2 signal in the renal tubules. Increasing the antibody concentration resulted in more background staining and several antigen retrieval methods did not get rid of the background. With a low amount of protein, it would be impossible to detect specific NBCe2 immunoreactivity. In contrast using the same antibody for the choroid plexus revealed intense anti-NBCe2 staining, supporting the notion of a low renal NBCe2 expression level.

Although we cannot estimate how much NBCe2 was excised in our model, we do see changes in the expression of some sodium and acid-base transporters in the kidneys from the $NBCe2^{B1-VATPasecre}$ mouse. This suggests that recombination events have taken place and accounts for the observed expression changes. The cre recombinase in the B1 cre mouse is active in both intercalated cells of the CD as well as principal cells in the CNT (Miller et al., 2009). Previous publications using this cre model has resulted in up to 55–80% reduction in the target protein (Poulsen et al., 2016; Ramkumar et al., 2018). The fact that the $NBCe2^{B1-VATPasecre}$ mouse presents with a phenotype suggests that functionally relevant NBCe2 could be expressed in the intercalated cells as well as in principal cells of the CNT.

The $NBCe2^{B1-VATPasecre}$ mice show a different expression pattern of transporters compared to the global knockout. The α-ENaC expression is decreased, whereas uncleaved and total γ-ENaC are increased. The full knockouts, however, show decreased expression of γ-ENaC but normal levels of the α and β subunits of ENaC. In the previously reported NBCe2 knockout mice α-ENaC was found to be increased. The discrepancy between the two knockout mice could be explained by differences in the knockout strategy or differences in animal housing (e.g., sodium content in the chow) in the laboratories.

Additionally in the $NBCe2^{B1-VATPasecre}$ mouse, we observed a significant decrease in V-ATPase expression, which is opposite to the effect observed in previously published full NBCe2 ko mice on an acidic diet (Wen et al., 2015a) where an increased expression is observed. We also found a decreased abundance of two of the anion exchangers, AE2 and pendrin. Both of these are found to be expressed at normal levels in the global NBCe2 knockout mouse. The difference in expression pattern of other proteins could potentially explain the lack of a BP phenotype increase in the $NBCe2^{B1-VATPasecre}$. For example, a decrease in pendrin could potentially have an opposing effect on BP (López-Cayuqueo et al., 2018). Ablation of pendrin is known to result in lowering of BP (Trepiccione et al., 2017) as pendrin is known to affect ENaC mediated by changing urinary HCO_3 (Pech et al., 2010). We cannot explain the discrepancy in pendrin expression in the full knockout and the $NBCe2^{B1-VATPasecre}$ mouse. The possible

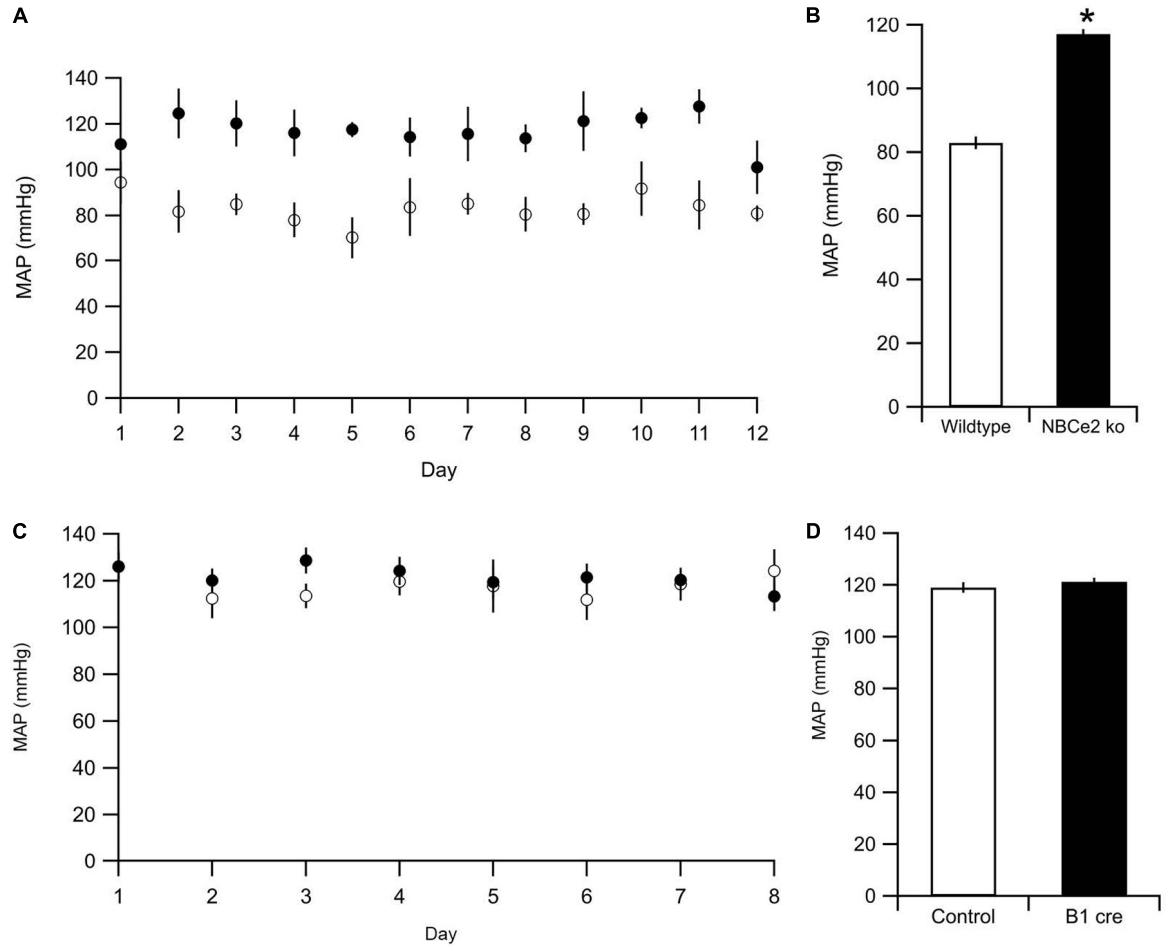

FIGURE 5 | Blood pressure measurements of NBCe2 mice. **(A)** Blood pressure was determined by tail cuff in WT (white dots) and NBCe2 ko mice (black dots). **(B)** Summarized results of mean arterial pressure over the entire 12-day period. **(C)** Blood pressure was determined by tail cuff in control (white dots) and NBCe2$^{B1-VATPasecre}$ (black dots) for eight consecutive days. Dots indicate the mean values ± SEM. **(D)** Summarized results of the mean arterial pressure (MAP) over the entire 8-day period.

interplay between NBCe2 expression in principal cells of the CNT and pendrin in the intercalated cells needs to be further investigated.

The metabolic cage data showed only minor changes in water and electrolyte parameters. We observed increased plasma K^+ in the NBCe2$^{B1-VATPasecre}$ model, which is opposite to what was seen in the study by Wen et al. (2015a). Stimulation with aldosterone or increased ENaC activity in the principal cells usually results in potassium wasting, as increased sodium uptake via apical ENaC channels stimulates basolateral Na^+ excretion into the blood in exchange for K^+. We observe the opposite effect, i.e., an increase in plasma K^+ and a decreased cleaved α-ENaC expression in the global NBCe2 ko model, which might suggest a reduction of ENaC activity as a response to the increase in BP. No significant differences were observed during baseline metabolic assessment in the global NBCe2 ko model, apart from the previously reported decrease in blood pCO_2 and HCO_3^-.

In accordance to previous studies, full NBCe2 ko resulted in significantly increased BP, as measured by the tail-cuff method, whereas kidney-targeted NBCe2 ko did not present with this trait. We did not assess the BP in our kidney ko models on an acidic diet. Although the BP assessment by tail-cuff is not as accurate as telemetric measurements, the difference between the full NBCe2 ko and kidney cell-targeted NBCe2 ko is clearly evident.

It is possible that the discrepancy between the full ko and the B1-cre model is caused by insufficient knockdown of NBCe2 in the kidney. This would result in a different phenotype than that of a global NBCe2 knockout. Another explanation is that dysfunctional kidney NBCe2 might not be the only cause of the increased BP observed in full NBCe2 ko, as NBCe2 expression is close to undetectable in the mouse kidney, and kidney cell targeted NBCe2 ko had no apparent BP phenotype. In addition to the kidney, NBCe2 is expressed in the liver and in especially high abundance in the choroid plexus of the brain. The choroid plexus secretes the majority of the cerebrospinal fluid. Changes in cerebrospinal fluid electrolytes have previously been shown to affect the central regulation of BP through activation of the sympathetic nervous system. While this study clearly shows

that the renal NBCe2 may play a role in local regulation of HCO_3^- in the kidney tubule cells, further investigations are necessary to understand the pathogenesis and possible treatment of this particular cause of hypertension in relation to dysfunctional NBCe2.

In conclusion, renal NBCe2 expression seems to be confined to CNT and CD, and thus, we cannot confirm previous reports of NBCe2 expression in proximal or distal tubules. In isolated CNT and CCD, NBCe2 mediates outward Na^+-dependent HCO_3^- transport from either the basolateral or luminal membrane. Targeted knockout of NBCe2 in intercalated cells led to a different pattern of changes in renal transport protein expression levels than observed in global NBCe2 knockout mice. The targeted knockout of NBCe2 in CNT/CCD did not lead to the hypertensive phenotype observed in the global NBCe2 knockout. Thus, we speculate that the BP elevation in NBCe2 knockout mice does not arise from lack of NBCe2 expression in the CNT and CD, but indicate that other cell types or potentially other organ systems are involved in the NBCe2 dependent BP regulation.

DATA AVAILABILITY STATEMENT

The datasets generated for this study are available on request to the corresponding author.

ETHICS STATEMENT

The animal study was reviewed and approved by The Danish Animal Experiments Inspectorate.

AUTHOR CONTRIBUTIONS

HD and JP contributed to the conception and design of the work. DB, FP, HC, LJ, and HD contributed to the acquisition of the data. All authors contributed to the analysis and interpretation of the data for the manuscript. DB drafted the initial manuscript and HD and JP revised it critically for important intellectual content. All authors contributed to manuscript revision, read and approved the submitted version.

FUNDING

DB was funded by a Ph.D. stipend from the Faculty of Health and Medical Sciences and the Department of Cellular and Molecular Medicine, University of Copenhagen. FP was funded by a research year scholarship from the independent research fund Denmark/Medical and Health Sciences. HC and LJ were funded by Ph.D. stipends from the Faculty of Health, Aarhus University. The project was supported by grants to HD from the independent research fund Denmark/Medical and Health Sciences, the Danish Heart association, læge Sofus Carl Emil Friis og hustru Olga Friis' legat, Vera og Carl Johan Michaelsens Legat, Lundbeckfonden, and Aase og Ejnar Danielsen fonden.

ACKNOWLEDGMENTS

We thank Helle Hoyer, Inger Merete S. Paulsen, Christian V. Westberg, and Helle S. Gittins for expert technical assistance and training.

SUPPLEMENTARY MATERIAL

The Supplementary Material for this article can be found online at: https://www.frontiersin.org/articles/10.3389/fphys.2020.00560/full#supplementary-material

REFERENCES

Barkley, R. A., Chakravarti, A., Cooper, R. S., Ellison, R. C., Hunt, S. C., Province, M. A., et al. (2004). Positional identification of hypertension susceptibility genes on chromosome 2. *Hypertension* 43, 477–482. doi: 10.1161/01.HYP.0000111585.76299.f7

Boyarsky, G., Ganz, M. B., Sterzel, R. B., and Boron, W. F. (1988). pH regulation in single glomerular mesangial cells. II. Na+-dependent and -independent Cl(-)-HCO3- exchangers. *Am. J. Physiol.* 255(6 Pt 1), C857–C869. doi: 10.1152/ajpcell.1988.255.6.C857

Carey, R. M., Schoeffel, C. D., Gildea, J. J., Jones, J. E., McGrath, H. E., Gordon, L. N., et al. (2012). Salt sensitivity of blood pressure is associated with polymorphisms in the sodium-bicarbonate cotransporter. *Hypertension* 60, 1359–1366. doi: 10.1161/HYPERTENSIONAHA.112.196071

Chen, L., Lee, J. W., Chou, C. L., Nair, A. V., Battistone, M. A., Paunescu, T. G., et al. (2017). Transcriptomes of major renal collecting duct cell types in mouse identified by single-cell RNA-seq. *Proc. Natl. Acad. Sci. U.S.A.* 114, E9989–E9998. doi: 10.1073/pnas.1710964114

Christensen, H. L., Barbuskaite, D., Rojek, A., Malte, H., Christensen, I. B., Fuchtbauer, A. C., et al. (2018). The choroid plexus sodium-bicarbonate cotransporter NBCe2 regulates mouse cerebrospinal fluid pH. *J. Physiol.* 596, 4709–4728. doi: 10.1113/JP275489

Damkier, H. H., Nielsen, S., and Praetorius, J. (2007). Molecular expression of SLC4-derived Na+-dependent anion transporters in selected human tissues. *Am. J. Physiol. Regul. Integr. Comp. Physiol.* 293, R2136–R2146. doi: 10.1152/ajpregu.00356.2007

Gildea, J. J., Xu, P., Carlson, J. M., Gaglione, R. T., Bigler Wang, D., Kemp, B. A., et al. (2015). The sodium-bicarbonate cotransporter NBCe2 (slc4a5) expressed in human renal proximal tubules shows increased apical expression under high-salt conditions. *Am. J. Physiol. Regul. Integr. Comp. Physiol.* 309, R1447–R1459. doi: 10.1152/ajpregu.00150.2015

Groger, N., Vitzthum, H., Frohlich, H., Kruger, M., Ehmke, H., Braun, T., et al. (2012). Targeted mutation of SLC4A5 induces arterial hypertension and renal metabolic acidosis. *Hum. Mol. Genet.* 21, 1025–1036. doi: 10.1093/hmg/ddr533

Harris, M., Garcia-Caballero, A., Stutts, M. J., Firsov, D., and Rossier, B. C. (2008). Preferential assembly of epithelial sodium channel (ENaC) subunits in Xenopus oocytes: role of furin-mediated endogenous proteolysis. *J. Biol. Chem.* 283, 7455–7463. doi: 10.1074/jbc.M707399200

Hofmeister, M. V., Damkier, H. H., Christensen, B. M., Olde, B., Fredrik Leeb-Lundberg, L. M., Fenton, R. A., et al. (2012). 17beta-Estradiol induces nongenomic effects in renal intercalated cells through G protein-coupled estrogen receptor 1. *Am. J. Physiol. Renal Physiol.* 302, F358–F368. doi: 10.1152/ajprenal.00343.2011

Hofmeister, M. V., Fenton, R. A., and Praetorius, J. (2009). Fluorescence isolation of mouse late distal convoluted tubules and connecting tubules: effects of

vasopressin and vitamin D3 on Ca2+ signaling. *Am. J. Physiol. Renal Physiol.* 296, F194–F203. doi: 10.1152/ajprenal.90495.2008

Hunt, S. C., Xin, Y., Wu, L. L., Cawthon, R. M., Coon, H., Hasstedt, S. J., et al. (2006). Sodium bicarbonate cotransporter polymorphisms are associated with baseline and 10-year follow-up blood pressures. *Hypertension* 47, 532–536. doi: 10.1161/01.HYP.0000196949.26088.3c

Iversen, N. K., Frische, S., Thomsen, K., Laustsen, C., Pedersen, M., Hansen, P. B., et al. (2013). Superparamagnetic iron oxide polyacrylic acid coated gamma-Fe2O3 nanoparticles do not affect kidney function but cause acute effect on the cardiovascular function in healthy mice. *Toxicol. Appl. Pharmacol.* 266, 276–288. doi: 10.1016/j.taap.2012.10.014

Jensen, T. B., Pisitkun, T., Hoffert, J. D., Jensen, U. B., Fenton, R. A., Praetorius, H. A., et al. (2012). Assessment of the effect of 24-hour aldosterone administration on protein abundance in fluorescence-sorted mouse distal renal tubules by mass spectrometry. *Nephron Physiol.* 121, 9–15. doi: 10.1159/000346832

López-Cayuqueo, K. I., Chavez-Canales, M., Pillot, A., Houillier, P., Jayat, M., Baraka-Vidot, J., et al. (2018). A mouse model of pseudohypoaldosteronism type II reveals a novel mechanism of renal tubular acidosis. *Kidney Int.* 94, 514–523. doi: 10.1016/j.kint.2018.05.001

Markadieu, N., San-Cristobal, P., Nair, A. V., Verkaart, S., Lenssen, E., Tudpor, K., et al. (2012). A primary culture of distal convoluted tubules expressing functional thiazide-sensitive NaCl transport. *Am. J. Physiol. Renal Physiol.* 303, F886–F892. doi: 10.1152/ajprenal.00114.2012

Masilamani, S., Kim, G. H., Mitchell, C., Wade, J. B., and Knepper, M. A. (1999). Aldosterone-mediated regulation of ENaC alpha, beta, and gamma subunit proteins in rat kidney. *J. Clin. Invest.* 104, R19–R23. doi: 10.1172/JCI7840

Michlig, S., Harris, M., Loffing, J., Rossier, B. C., and Firsov, D. (2005). Progesterone down-regulates the open probability of the amiloride-sensitive epithelial sodium channel via a Nedd4-2-dependent mechanism. *J. Biol. Chem.* 280, 38264–38270. doi: 10.1074/jbc.M506308200

Millar, I. D., and Brown, P. D. (2008). NBCe2 exhibits a 3 HCO3(-):1 Na+ stoichiometry in mouse choroid plexus epithelial cells. *Biochem. Biophys. Res. Commun.* 373, 550–554. doi: 10.1016/j.bbrc.2008.06.053

Miller, R. L., Lucero, O. M., Riemondy, K. A., Baumgartner, B. K., Brown, D., Breton, S., et al. (2009). The V-ATPase B1-subunit promoter drives expression of Cre recombinase in intercalated cells of the kidney. *Kidney Int.* 75, 435–439. doi: 10.1038/ki.2008.569

Pech, V., Pham, T. D., Hong, S., Weinstein, A. M., Spencer, K. B., Duke, B. J., et al. (2010). Pendrin modulates ENaC function by changing luminal HCO3. *J. Am. Soc. Nephrol.* 21, 1928–1941. doi: 10.1681/ASN.2009121257

Poulsen, S. B., Praetorius, J., Damkier, H. H., Miller, L., Nelson, R. D., Hummler, E., et al. (2016). Reducing alphaENaC expression in the kidney connecting tubule induces pseudohypoaldosteronism type 1 symptoms during K+ loading. *Am. J. Physiol. Renal Physiol.* 310, F300–F310. doi: 10.1152/ajprenal.00258.2015

Pushkin, A., Abuladze, N., Newman, D., Lee, I., Xu, G., and Kurtz, I. (2000). Cloning, characterization and chromosomal assignment of NBC4, a new member of the sodium bicarbonate cotransporter family. *Biochim. Biophys. Acta* 1493, 215–218. doi: 10.1016/s0167-4781(00)00149-4

Ramkumar, N., Stuart, D., Mironova, E., Abraham, N., Gao, Y., Wang, S., et al. (2018). Collecting duct principal, but not intercalated, cell prorenin receptor regulates renal sodium and water excretion. *Am. J. Physiol. Renal Physiol.* 315, F607–F617. doi: 10.1152/ajprenal.00122.2018

Sassani, P., Pushkin, A., Gross, E., Gomer, A., Abuladze, N., Dukkipati, R., et al. (2002). Functional characterization of NBC4: a new electrogenic sodium-bicarbonate cotransporter. *Am. J. Physiol. Cell Physiol.* 282, C408–C416. doi: 10.1152/ajpcell.00409.2001

Shao, X. S., Kao, L. Y., Abuladze, N., and Kurtz, I. (2009). Stoichiometry and Inhibitory Pharmacology Of Electrogenic Sodium Bicarbonate Cotransporter NBC4c (NBCe2-C) expressed in HEK-293 cells. *FASEB J.* 23:LB1-1039.5.

Sorensen, M. V., Grossmann, S., Roesinger, M., Gresko, N., Todkar, A. P., Barmettler, G., et al. (2013). Rapid dephosphorylation of the renal sodium chloride cotransporter in response to oral potassium intake in mice. *Kidney Int.* 83, 811–824. doi: 10.1038/ki.2013.14

Taylor, J. Y., Wu, C. Y., Darling, D., Sun, Y. V., Kardia, S. L., and Jackson, J. S. (2012). Gene-environment effects of SLC4A5 and skin color on blood pressure among African American women. *Ethn. Dis.* 22, 155–161.

Toyomura, T., Oka, T., Yamaguchi, C., Wada, Y., and Futai, M. (2000). Three subunit a isoforms of mouse vacuolar H(+)-ATPase. Preferential expression of the a3 isoform during osteoclast differentiation. *J. Biol. Chem.* 275, 8760–8765. doi: 10.1074/jbc.275.12.8760

Trepiccione, F., Soukaseum, C., Baudrie, V., Kumai, Y., Teulon, J., Villoutreix, B., et al. (2017). Acute genetic ablation of pendrin lowers blood pressure in mice. *Nephrol. Dial. Transplant.* 32, 1137–1145. doi: 10.1093/ndt/gfw393

Virkki, L. V., Wilson, D. A., Vaughan-Jones, R. D., and Boron, W. F. (2002). Functional characterization of human NBC4 as an electrogenic Na+-HCO cotransporter (NBCe2). *Am. J. Physiol. Cell Physiol.* 282, C1278–C1289. doi: 10.1152/ajpcell.00589.2001

Vorum, H., Kwon, T. H., Fulton, C., Simonsen, B., Choi, I., Boron, W., et al. (2000). Immunolocalization of electroneutral Na-HCO(3)(-) cotransporter in rat kidney. *Am. J. Physiol. Renal Physiol.* 279, F901–F909. doi: 10.1152/ajprenal.2000.279.5.F901

Wen, D., Yuan, Y., Cornelius, R. J., Li, H., Warner, P. C., Wang, B., et al. (2015a). Deficient acid handling with distal RTA in the NBCe2 knockout mouse. *Am. J. Physiol. Renal Physiol.* 309, F523–F530. doi: 10.1152/ajprenal.00163.2015

Wen, D., Yuan, Y., Warner, P. C., Wang, B., Cornelius, R. J., Wang-France, J., et al. (2015b). Increased epithelial sodium channel activity contributes to hypertension caused by Na+-HCO3- cotransporter electrogenic 2 deficiency. *Hypertension* 66, 68–74. doi: 10.1161/HYPERTENSIONAHA.115.05394

Writing Group Members, Mozaffarian, D., Benjamin, E. J., Go, A. S., Arnett, D. K., Blaha, M. J., et al. (2016). Heart disease and stroke statistics-2016 update: a report from the american heart association. *Circulation* 133, e38–e360. doi: 10.1161/CIR.0000000000000350

Xu, J., Wang, Z., Barone, S., Petrovic, M., Amlal, H., Conforti, L., et al. (2003). Expression of the Na+-HCO-3 cotransporter NBC4 in rat kidney and characterization of a novel NBC4 variant. *Am. J. Physiol. Renal Physiol.* 284, F41–F50. doi: 10.1152/ajprenal.00055.2002

Conflict of Interest: The authors declare that the research was conducted in the absence of any commercial or financial relationships that could be construed as a potential conflict of interest.

Copyright © 2020 Barbuskaite, Pedersen, Christensen, Johnsen, Praetorius and Damkier. This is an open-access article distributed under the terms of the Creative Commons Attribution License (CC BY). The use, distribution or reproduction in other forums is permitted, provided the original author(s) and the copyright owner(s) are credited and that the original publication in this journal is cited, in accordance with accepted academic practice. No use, distribution or reproduction is permitted which does not comply with these terms.

frontiers in Physiology

ORIGINAL RESEARCH
published: 22 July 2020
doi: 10.3389/fphys.2020.00853

Enhanced Myogenic Constriction in the SHR Preglomerular Vessels Is Mediated by Thromboxane A2 Synthesis

*Samera Nademi[1], Chao Lu[2] and Jeffrey G. Dickhout[1,2]**

[1] Department of Medicine, Division of Nephrology, McMaster University, Hamilton, ON, Canada, [2] St. Joseph's Healthcare Hamilton, Hamilton, ON, Canada

Background: Spontaneously Hypertensive Rats (SHR) have chronically elevated blood pressures at 30 weeks of age (systolic: 191.0 ± 1.0, diastolic: 128.8 ± 0.9). However, despite this chronic malignant hypertension, SHR kidneys remain relatively free of pathology due to having an augmented myogenic constriction (MC). We hypothesized that the enhanced MC in the SHR preglomerular vessels was due to increased prostaglandin and decreased nitric oxide (NO) synthesis, providing renal protection.

Methods: SHR and Wistar Kyoto (WKY) arcuate and mesenteric arteries were treated with indomethacin (prostaglandin synthesis inhibitor), N omega-nitro-L-arginine (L-NNA, NO synthase inhibitor), and nifedipine (L-type calcium channel blocker); and MC was measured in these vessels. The role of endothelium in MC was examined by removing endothelium from WKY and SHR preglomerular and mesenteric arteries using human hair, and measuring MC. We also studied the source of prostaglandin in the SHR by treating endothelium-removed arcuate arteries with indomethacin and furegrelate (thromboxane synthase inhibitor).

Results: MC was enhanced in the SHR preglomerular vessels but not the mesenteric arteries. Indomethacin and LNNA removed the enhanced MC in the SHR. Nifedipine also inhibited MC in both WKY and SHR arcuate and mesenteric arteries. Removing endothelium did not change MC in either arcuate or mesenteric arteries of WKY and SHR rats; and did not remove the augmented MC in the SHR arcuate arteries. Indomethacin and furegrelate decreased MC in endothelium-removed SHR arcuate arteries and obliterated the enhanced MC in the SHR.

Conclusion: The enhanced MC in the SHR arcuate arteries was due to thromboxane A2 synthesis from the tunica media and/or adventitia layers. MC was not dependent on endothelium, but was dependent on L-type calcium channels. Nevertheless, SHR arcuate arteries displayed differential intracellular calcium signaling compared to the WKYs.

Keywords: myogenic constriction, renal autoregulation, preglomerular arteries, hypertension, prostaglandin, thromboxane A2, nitric oxide, endothelium

OPEN ACCESS

Edited by:
John D. Imig,
Medical College of Wisconsin, United States

Reviewed by:
Hendrik Buikema,
University Medical Center Groningen, Netherlands
Ning Xia,
Johannes Gutenberg University of Mainz, Germany

***Correspondence:**
Jeffrey G. Dickhout
jdickhou@stjosham.on.ca

Specialty section:
This article was submitted to Renal and Epithelial Physiology, a section of the journal Frontiers in Physiology

Received: *22 November 2019*
Accepted: *25 June 2020*
Published: *22 July 2020*

Citation:
Nademi S, Lu C and Dickhout JG (2020) Enhanced Myogenic Constriction in the SHR Preglomerular Vessels Is Mediated by Thromboxane A2 Synthesis. Front. Physiol. 11:853. doi: 10.3389/fphys.2020.00853

INTRODUCTION

In 1901, Bayliss observed that small resistant arteries from different vascular beds of rabbits, cats, and dogs decreased in diameter when he increased intraluminal pressure, and increased diameter with decreasing pressure. Bayliss believed that this response was "myogenic in nature," and thus later this phenomenon was termed myogenic constriction (MC) (Bayliss, 1902; Saboliæ et al., 1995). MC is stretch-induced reduction in small arteriole diameters in order to regulate the amount of intraluminal blood flow (Kaplan and Palmer, 2001). In the kidneys, renal blood flow autoregulation is an important homeostatic mechanism that protects the delicate glomerular capillaries from fluctuations in the systematic blood pressure, allowing the kidneys to maintain a constant blood flow and glomerular filtration rate (GFR). MC is one of the two mechanisms through which kidneys autoregulate their blood flow (the other mechanism is tubuloglomerular feedback). The significance of MC can be realized from consequences of its' dysfunction or augmentation. Impaired MC has been observed in variety of diseases such as diabetes, low-renin and salt-sensitive hypertensions (i.e., in African Americans), and chronic kidney disease (CKD) (Carlström et al., 2015; Atala, 2016; Le Goff et al., 2016). On the Contrary, enhanced myogenic constriction protects the kidneys from renal injury. It has been observed that some chronically hypertensive human (i.e., essential hypertensives) and rats (i.e., Spontaneously hypertensive rats, SHR) do not develop significant renal injuries despite highly elevated blood pressures. It appears that this renal protection is due to an augmented MC response in the pre-glomerular vessels (Arendshorst and Beierwaltes, 1979; Imig et al., 1996; Griffin et al., 2001; Loutzenhiser et al., 2002, 2004, 2006; Bidani and Griffin, 2004). We hypothesized that the enhanced MC found in the SHR rats is due to increased prostaglandin H2 (PGH2) and decreased nitric oxide (NO) synthesis in the endothelium compared to their normotensive controls, Wistar Kyoto (WKY) rats. To test this hypothesis, we treated SHR and WKY arcuate and mesenteric arteries with indomethacin and N omega-nitro-L-arginine (LNNA, NO synthase inhibitor) and measured MC. We also examined the role of endothelium in the SHR enhanced MC by removing the endothelium, based on a method that was described by Osol involving the use of human hair (Osol et al., 1989), and measured MC in SHR and WKY arcuate and mesenteric arteries. We utilized both younger and older animals since the augmentation of MC in the SHR may be the result of endothelial dysfunction.

TABLE 1 | Average age and characteristics of the rats that were used in this study.

	Older Rats (30–40 weeks)				Younger Rats (12–16 weeks)			
	Avg. Age (weeks)	SBP (mmHg)	DBP (mmHg)	BW (g)	Avg. Age (weeks)	SBP (mmHg)	DBP (mmHg)	BW (g)
WKY	34.6 ± 0.5 (*n* = 18)	143.3 ± 6.1 (*n* = 18)	93.4 ± 4.8 (*n* = 18)	439.2 ± 5.6 (*n* = 15)	13.8 ± 0.6 (*n* = 11)	142.7 ± 4.9 (*n* = 5)	85.5 ± 5.8 (*n* = 5)	240.2 ± 30.54 (*n* = 5)
SHR	35.95 ± 0.2 (*n* = 12)	197.4 ± 6.0 (*n* = 12) *	149.1 ± 6.0 (*n* = 12) *	425.2 ± 10.2 (*n* = 12)	13.1 ± 0.4 (*n* = 18)	197.4 ± 7.1 (*n* = 5)*	142.8 ± 8.0 (*n* = 5)*	262.4 ± 39.01 (*n* = 5)

*Values are expressed as mean ± SEM; "n": number of animals. Independent two-tailed T-test was used to assess significance between WKY and SHR of the same age and parameter. *P ≤ 0.05 was deemed significant.*

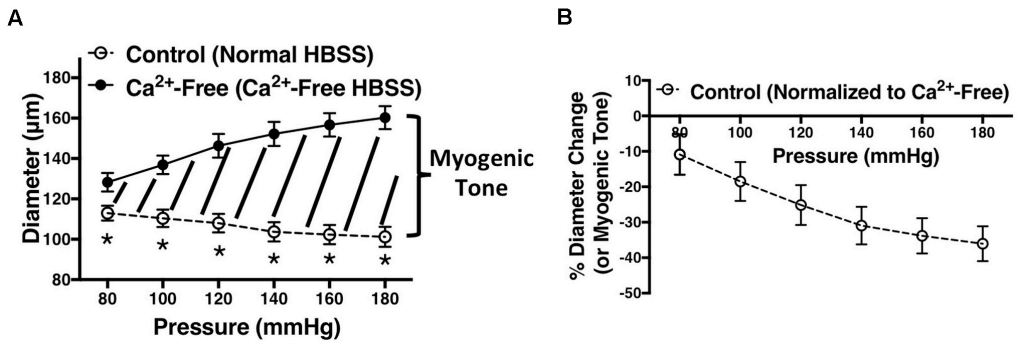

FIGURE 1 | Demonstration of how figures in this manuscript were generated. **(A)** Vessel diameters were recorded at different intraluminal pressures (P80 to P180 mmHg) in the presence of normal HBSS (control) or calcium (Ca^{2+})-free HBSS. The area in between the two graphs (graph of normal HBSS and Ca^{2+}-free HBSS) represents myogenic tone. **(B)** Myogenic tone was calculated as percent diameter change by subtracting lumen diameter at each pressure point in Ca^{2+}-free HBSS ($D_{n\ (Ca2+\ free)}$) from the lumen diameter at the same pressure point in normal HBSS (D_n), divided by the diameter in Ca^{2+}-free HBSS ($D_{n\ (Ca2+\ free)}$), and multiplied by 100 (% Diameter Change $= \left(\frac{D_n - D_{n\ (Ca-Free)}}{D_{n\ (Ca-Free)}}\right) * 100$). Two-way ANOVA and Holm-Sidak *post hoc* test were used to assess significance between two population means at each pressure point; denoted by $^*P \leq 0.05$. Graphs were made using WKY arcuate arteries. $N_{WKY} = 5$, $n_{WKY} = 5$ ("N": number of vessels, "*n*": number of animals).

We hypnotized this dysfunction would be more severe in the old animals, since they would have been exposed to elevated blood pressure for a longer period of time.

MATERIALS AND METHODS

Animal Studies

Older (30 to 40 weeks old) and younger (12 to 16 weeks old) male WKY and SHR rats were utilized for the vessel studies. Rats' blood pressure was measured using tail cuff plethysmography (Kent Scientific, CODA system) and their body weights were recorded (**Table 1**). All rats were bred at McMaster University Central Animal Facility and maintained at St Joseph's Healthcare Hamilton Animal Facility. All animal work was performed with McMaster University Animal Research Ethics Board's approval and in accordance with their guidelines. Animals were housed with a 12-hour light-dark cycle and had free access to food and drinking water. After anesthetizing the rodents with isoflurane and perfusing the vasculature with Hank's basic salt solution (HBSS) to remove blood, arcuate and second branch mesenteric arteries were dissected out of their kidneys and mesenteries, respectively, to conduct vascular studies, as previously (Dickhout and Lee, 1997).

Myogenic Response Measurements in Endothelium-Intact Arteries

Renal arcuate and second-branch mesenteric arteries were dissected out of their tissues and transferred into a pressure myograph chamber (PMC) containing 37°C oxygenated HBSS. The PMC was connected to a PS-200 system and a peristaltic pump with a servo-controller to pressurize the arteries (Living Systems, Burlington, VT, United States), and a Leica WILD M3C microscope and Hitachi KP-113 CCD camera to video-record the vessels. In the PMC, the arteries were mounted on a glass micropipette, a blind-sac was created, and the vessels were allowed 30 min to equilibrate to 80 mmHg pressure (P80 mmHg) as previously described (Dickhout and Lee, 1997). To test the functional presence of the endothelium, 3 μM phenylephrine (endothelium-independent vasoconstrictor) was

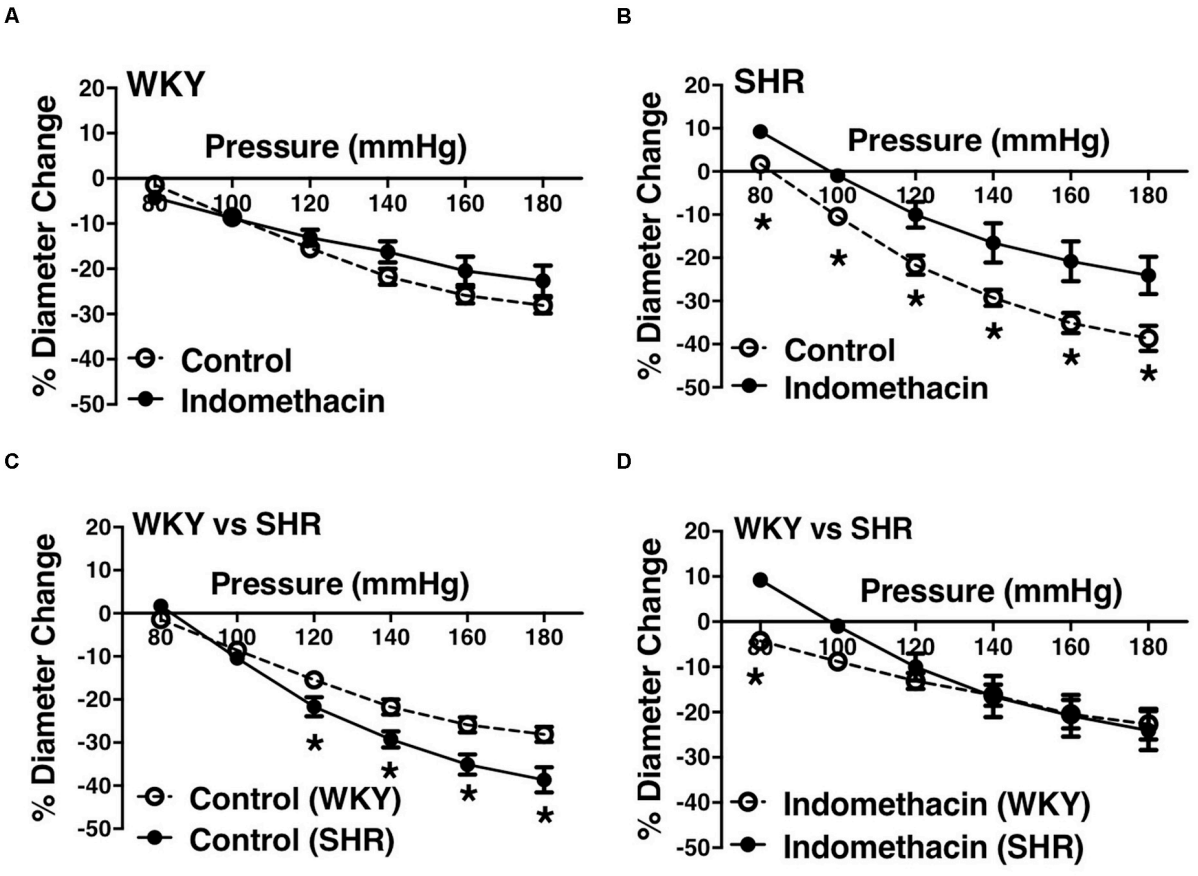

FIGURE 2 | Effects of inhibiting cyclooxygenase 1 and 2 (prostaglandin H2 synthesis) in WKY and SHR preglomerular arteries (30–40 weeks-old rats). **(A)** Effect of indomethacin (10 μM) on WKY arcuate artery myogenic constriction (MC). **(B)** Effect of indomethacin (10 μM) on SHR arcuate artery MC. **(C)** Comparison of MC between WKY and SHR arcuate arteries. **(D)** Comparison of MC between WKY and SHR arcuate arteries that were treated with 10 μM indomethacin. Two-way ANOVA and Holm-Sidak *post hoc* test were used to assess significance; denoted by $^*P \leq 0.05$. $N_{WKY} = 9$, $N_{SHR} = 5$, $n_{WKY} = 7$, $n_{SHR} = 5$ ("N": number of vessels, "*n*": number of animals).

added to pre-constrict the arteries followed by 10 μM carbachol (endothelium-dependent vasodilator), and the diameter-changes were recorded. The chamber was subsequently washed with HBSS and vessels were re-allowed 30 min to equilibrate at P80 mmHg. MC was measured by increasing intraluminal pressure in 20 mmHg increments until 180 mmHg with 5-minute-intervals between each pressure change and the lumen diameters were recorded (E-intact MC). To investigate the effects of prostanoid and NO synthesis, 10 μM indomethacin and 100 μM LNNA, respectively, and independently were added to the PMC, the vessels were allowed 30 min to equilibrate, and MC was measured as described. Passive diameter at each pressure point was measured by replacing HBSS with Ca^{2+}-Free HBSS containing 5 mM Ca^{2+} chelator, ethylene glycol tetraacetic acid (EGTA), and re-measuring MC as aforementioned. MC measurements in this study were conducted serially in the following order: normal HBSS (control), drug-treated HBSS, and Ca^{2+}-Free HBSS (passive diameter). To investigate the dependency of MC on endothelium, the tunica intima was denuded from the arteries using a human hair.

Removing Endothelium Using Human Hair

A human hair was glued to a small petri dish and the arteries were moved through the length of the hair about 10 times, according to a method that was described by Osol et al. (1989). The arteries were then re-mounted in the PMC, remnant endothelium was flushed out for 5 min with HBSS, the blind-sac was re-created, and the vessels were allowed 30 min to equilibrate at P80 mmHg. To test the functional absence of the endothelium, 3 μM phenylephrine was added to pre-constrict the arteries followed by 10 μM carbachol and the diameter-changes were recorded. MC was then re-measured (E-removed MC) as described above.

Myogenic Response Measurements in Endothelium-Removed Arteries

To investigate the effects of prostaglandin and thomboxane A2 (TXA2) synthesis on endothelium-removed vessels, 10 μM indomethacin and 100 μM furegrelate, respectively, and

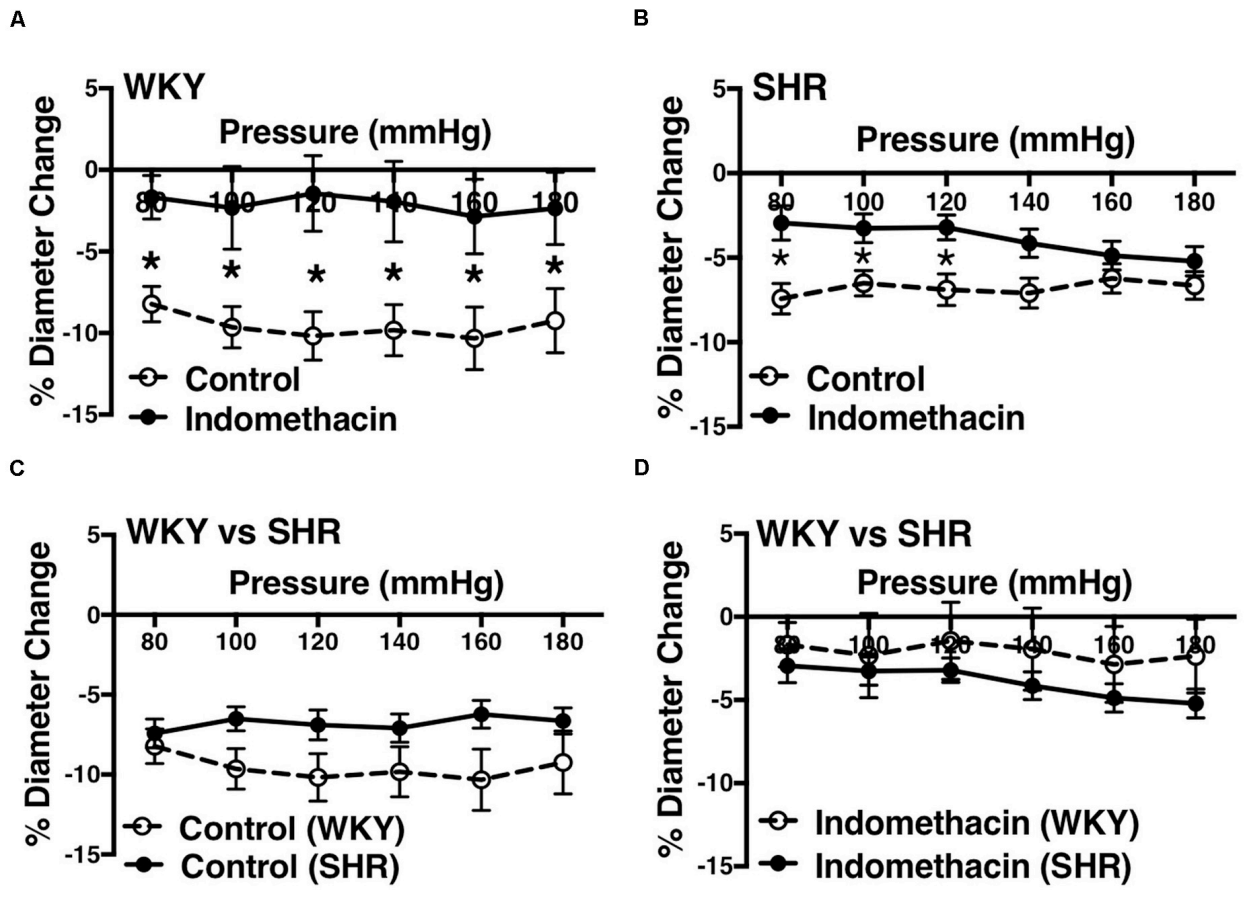

FIGURE 3 | Effects of inhibiting cyclooxygenase 1 and 2 (prostaglandin H2 synthesis) in WKY and SHR mesenteric arteries (30–40 weeks-old rats). **(A)** Effect of indomethacin (10 μM) on WKY mesenteric artery myogenic constriction (MC). **(B)** Effect of indomethacin (10 μM) on SHR mesenteric artery MC. **(C)** Comparison of MC between WKY and SHR mesenteric arteries. **(D)** Comparison of MC between WKY and SHR mesenteric arteries that were treated with 10 μM indomethacin. Two-way ANOVA and Holm-Sidak *post hoc* test were used to assess significance; denoted by $^*P \leq 0.05$. $N_{WKY} = 8$, $N_{SHR} = 17$, $n_{WKY} = 5$, $n_{SHR} = 6$ ("N": number of vessels, "*n*": number of animals).

independently were added to the PMC, the vessels were allowed 30 min to adjust, and MC was measured as previously explained. Passive diameter at each pressure point was measured at the end of each experiment by replacing HBSS with Ca^{2+}-free HBSS (5 mM EGTA). Physical absence of the endothelium was further investigated.

Scanning Electron Microscopy (SEM) to Ensure Physical Absence of Endothelium

Endothelium-removed and -intact arcuate arteries were cut in half, fixed with 2% glutaraldehyde (in 0.1 M sodium cacodylate buffer), post-fixed with 2% osmium tetroxide, dehydrated with increasing ethanol concentration, critical point dried, mounted onto microscope stubs, and examined under SEM.

Data and Statistical Analysis

Percent diameter change was calculated by subtracting lumen diameter at each pressure point in Ca^{2+}-free HBSS ($D_{n\ (Ca2+\ free)}$) from the lumen diameter at the same pressure point in normal HBSS (D_n), divided by the diameter in Ca^{2+}-free HBSS ($D_{n\ (Ca2+\ free)}$), and multiplied by 100 (% Diameter Change $= \left(\frac{D_n - D_{n\ (Ca-Free)}}{D_{n\ (Ca-Free)}}\right)^* 100$); this is illustrated in **Figures 1A,B**. Percent relaxation due to carbachol was calculated by subtracting lumen diameter at P80 mmHg after adding carbachol (D_{after}) from lumen diameter before adding carbachol (D_{before}), divided by diameter before carbachol (D_{before}), and multiplied by 100 (% Carbachol Relaxation $= \left(\frac{D_{before} - D_{after}}{D_{before}}\right)^* 100$). Paired *t*-test was used to compare carbachol-induced responses before and after endothelium removal. Independent *t*-test was used to compare WKY and SHR population means. Two-way ANOVA was used to compare MC from different rat strains or treatments. If differences were found by ANOVA, *post hoc* comparisons at different pressure points (Holm-Sidak *post hoc* test) were conducted to determine differences in the means. Significant differences were evaluated using GraphPad prism and 95% confidence intervals. *P*-values less than or equal to 0.05 were deemed statistically significant.

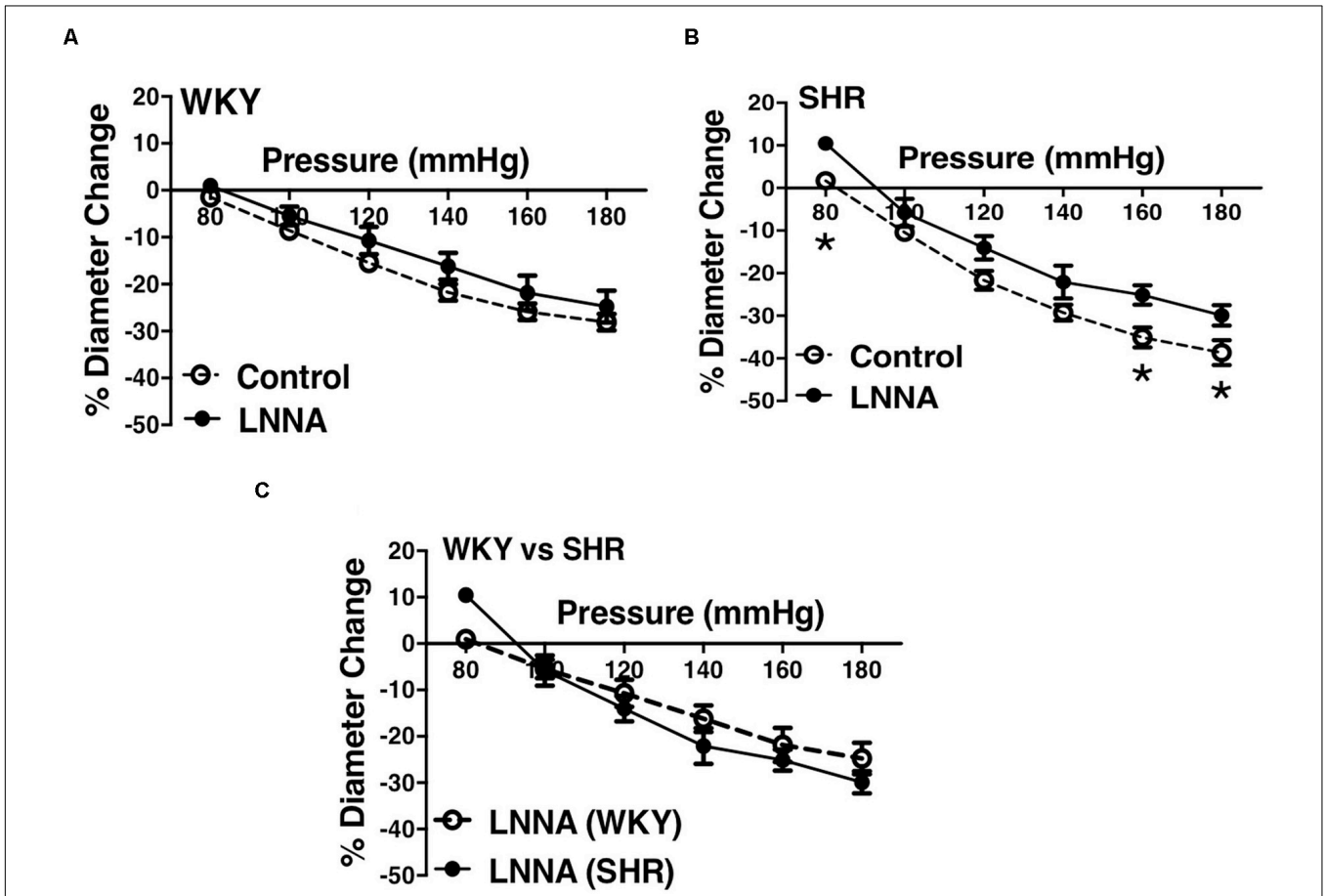

FIGURE 4 | Effects of nitric oxide synthase inhibition on MC of preglomerular arteries in WKY and SHR rats (30–40 weeks-old rats). **(A)** Effect of N omega-nitro-L-arginine (LNNA, 100 μM) on myogenic constriction (MC) of WKY arcuate arteries. **(B)** Effect of LNNA (100 μM) on MC of SHR arcuate arteries. **(C)** Comparing MC in WKY and SHR arcuate arteries that were treated with LNNA (100 μM). Two-way ANOVA and Holm-Sidak *post hoc* test were used to assess significance; denoted by $^*P \leq 0.05$. $N_{WKY} = 7$, $N_{SHR} = 6$, $n_{WKY} = 7$, $n_{SHR} = 6$ ("N": number of vessels, "*n*": number of animals).

Reagents

The following reagents were purchased from Sigma-Aldrich: phenylephrine (P6126), carbachol (C4382), furegrelate (F3764), indomethacin (I7378), LNNA (N5501), and EGTA (E3889).

RESULTS

Effects of Inhibiting PGH2 and NO Synthesis on Endothelium-Intact Vessels Derived From Older Rats

We used indomethacin, a non-selective cyclooxygenase (COX-1 and COX-2) inhibitor, to block PGH2 synthesis (Lucas, 2016). Indomethacin reduced MC in the SHR but not the WKY arcuate arteries (**Figures 2A,B**). SHR arcuate arteries demonstrated an enhanced MC compared to the WKY arteries (**Figure 2C**), and the augmented MC in the SHR was abolished by indomethacin treatment (**Figure 2D**). Comparably, indomethacin decreased MC in both SHR and WKY mesenteric arteries (**Figures 3A,B**). Nevertheless, an enhanced MC was not observed in the SHR mesenteric arteries compared to the WKY (**Figure 3C**). Also, indomethacin-treated SHR and WKY mesenteric vessels showed similar MC (**Figure 3D**). We also investigated the effects of blocking nitric oxide synthase (NOS) by LNNA on MC in the SHR and WKY rats. Similar to the indomethacin, LNNA reduced MC in the SHR arcuate arteries at P80, P160, and P180 mmHg; but did not change MC in the WKY pre-glomerular vessels (**Figures 4A,B**). LNNA also removed the augmented MC in the SHR arcuate arteries compared to the WKY (**Figure 4C**). In mesenteric arteries, LNNA treatment did not change MC in either WKY or SHR, and there were no differences between WKY and SHR LNNA-treated vessels (**Figures 5A–D**).

Effects of Inhibiting L-Type Calcium Channels on MC in Endothelium-Intact Vessels

L-type Ca^{2+} channel blocker, nifedipine, significantly reduced MC in both WKY and SHR arcuate (**Figures 6A,B**) and mesenteric arteries (**Figures 7A,B**) of older rats. Nonetheless in older rats, nifedipine-treated SHR arcuate arteries showed

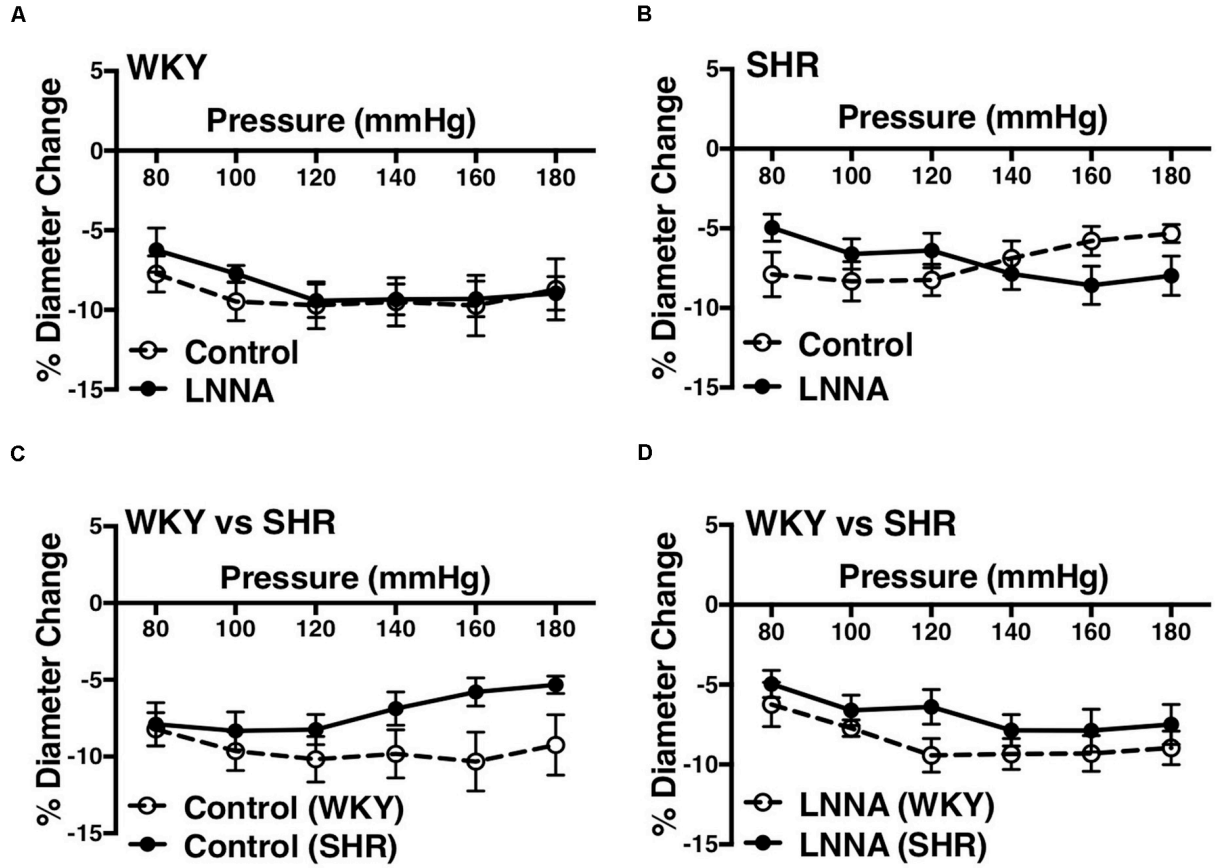

FIGURE 5 | Effects of nitric oxide synthase inhibition on MC of mesenteric arteries in WKY and SHR rats (30–40 weeks-old rats). **(A)** Effect of N omega-nitro-L-arginine (LNNA, 100 μM) on myogenic constriction (MC) of WKY mesenteric arteries. **(B)** Effect of LNNA (100 μM) on MC of SHR mesenteric arteries. **(C)** Comparison of MC between WKY and SHR mesenteric arteries. **(D)** Comparing MC in WKY and SHR mesenteric arteries that were treated with LNNA (100 μM). Two-way ANOVA and Holm-Sidak *post hoc* test were used to assess significance; denoted by $^*P \leq 0.05$. $N_{WKY} = 7$, $N_{SHR} = 6$, $n_{WKY} = 5$, $n_{SHR} = 6$ ("N": number of vessels, "*n*": number of animals).

significantly more MC compared to the WKY arcuate arteries (**Figure 6C**) at P140 to P180 mmHg; this difference was not observed in the SHR and WKY mesenteric arteries (**Figure 7C**). Further, we also investigated the effects of nifedipine in arcuate arteries from younger WKY and SHR rats (12–16 weeks old). Similar to the older rats (30–40 weeks old), nifedipine blocked MC in both WKY and SHR arcuate arteries of the younger rats (**Figures 8A,B**). However, there were no differences between nifedipine-treated WKY and SHR arcuate arteries (**Figure 8C**).

Endothelium Was Successfully Removed Using Human Hair

Scanning Electron Microscopy micrographs showed complete physical absence of the endothelium in WKY arcuate arteries. The endothelium was oriented longitudinally, whereas the smooth muscle cell (SMC) layer was oriented cross-sectionally (**Figure 9A**). WKY and SHR pre-constricted arcuate arteries (by 3 μM phenylephrine) showed almost no relaxation to 10 μM carbachol after removing the endothelium. WKY endothelium-intact arcuate vessels showed significantly more relaxation compared to SHR endothelium-intact vessels (**Figure 9B**). Pre-constricted mesenteric arteries (by 3 μM phenylephrine) in WKY and SHR also showed lack of relaxation to 10 μM carbachol after removing the endothelium. There were no statistically significant differences between WKY and SHR endothelium-intact carbachol-induced relaxation (**Figure 9C**).

Effects of Removing Endothelium on Myogenic Constriction in the WKY and SHR

Removing endothelium did not change MC in the WKY and SHR arcuate (**Figures 10A,B**) and mesenteric arteries (**Figures 11A,B**). Moreover, SHR endothelium-intact arcuate arteries demonstrated enhanced MC compared to the WKY endothelium-intact arcuate arteries at P140 to P180 mmHg (**Figure 10C**), but this enhancement was absent in the SHR mesenteric arteries (**Figure 11C**). Denuding endothelium did not remove the augmented MC in the SHR arcuate arteries (**Figure 10D**). Furthermore, MC was similar in endothelium -removed WKY and SHR mesenteric arcades (**Figure 11D**).

Effects of Inhibiting Prostaglandin H2 and Thromboxane A2 Synthesis in Endothelium-Removed Arcuate Arteries of Younger SHRs

Similar to the older rats (30–40 weeks old), arcuate arteries of younger SHR rats (12–16 weeks old) showed enhanced MC at

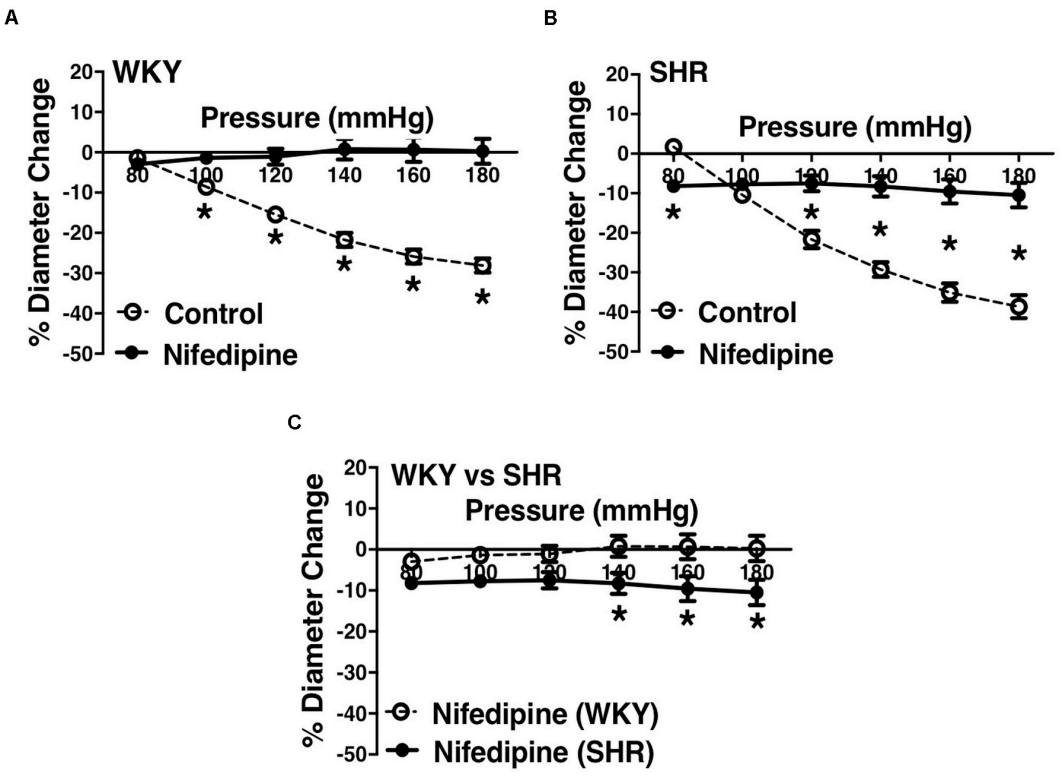

FIGURE 6 | Effects of L-type calcium channel blockade on arcuate arteries of WKY and SHR older rats (30–40 weeks-old). **(A)** Effect of nifedipine (10 μM) on myogenic constriction (MC) of WKY arcuate arteries. **(B)** Effect of nifedipine (10 μM) on MC of SHR arcuate arteries. **(C)** Comparing MC in WKY and SHR preglomerular arteries that were treated with nifedipine (10 μM). Two-way ANOVA and Holm-Sidak *post hoc* test were used to assess significance; denoted by $^*P \leq 0.05$. $N_{WKY} = 7$, $N_{SHR} = 5$, $n_{WKY} = 4$, $n_{SHR} = 4$ ("N": number of vessels, "*n*": number of animals).

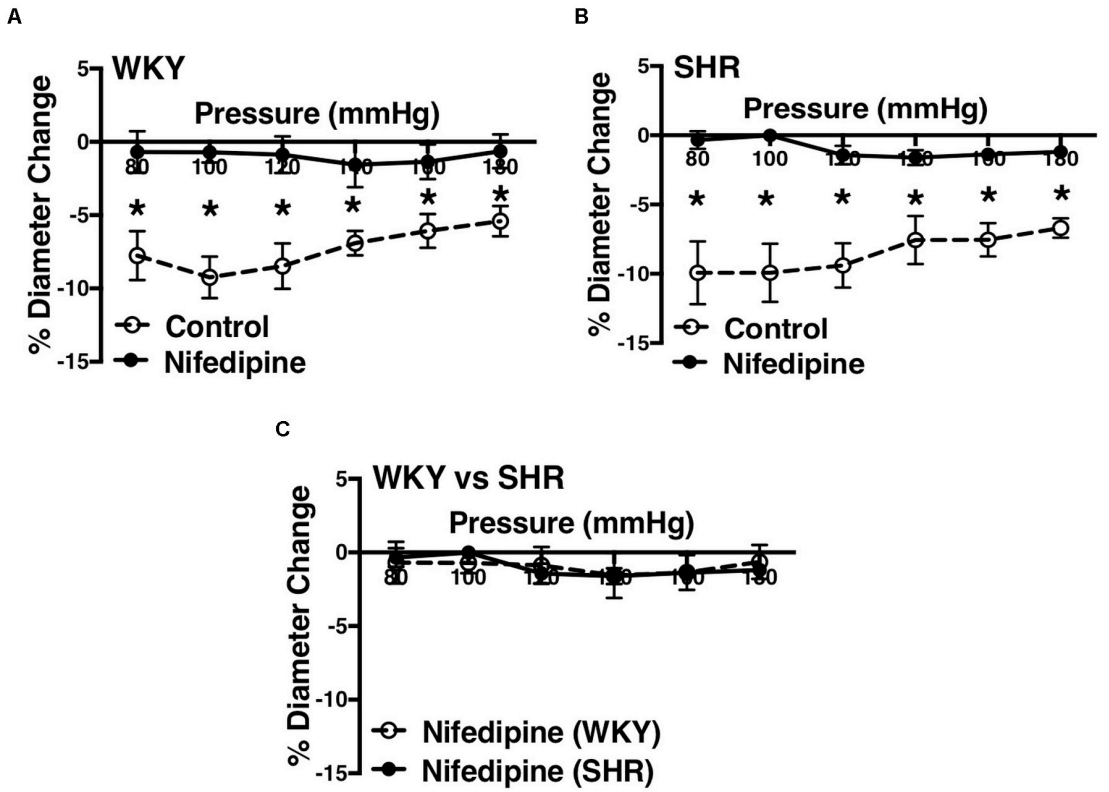

FIGURE 7 | Effects of L-type calcium channel blockade on mesenteric arteries of WKY and SHR older rats (30–40 weeks-old). **(A)** Effect of nifedipine (1 μM) on myogenic constriction (MC) of WKY mesenteric arteries. **(B)** Effect of nifedipine (1 μM) on MC of SHR mesenteric arteries. **(C)** Comparing MC in WKY and SHR mesenteric arteries that were treated with nifedipine (1 μM). Two-way ANOVA and Holm-Sidak *post hoc* test were used to assess significance; denoted by $^{*}P \leq 0.05$. $N_{WKY} = 9$, $N_{SHR} = 8$, $n_{WKY} = 5$, $n_{SHR} = 4$ ("N": number of vessels, "*n*": number of animals).

P140, P160, and P180 mmHg (**Figure 12A**). Inhibiting PGH2 synthesis by indomethacin in endothelium-removed arcuate arteries significantly decreased MC at P160 and P180 mmHg in the SHR (compared to both E-intact and E-removed vessels) but did not change MC in the WKY (**Figures 12B,C**). Similarly, inhibiting TXA2 synthesis by furegrelate in endothelium-removed arcuate arteries also significantly decreased MC at P120 to P180 mmHg (compared to both E-intact and E-removed vessels), but did not change MC in the WKY (**Figures 12D,E**). There were no differences in endothelium-removed arcuate arteries that had been treated with indomethacin or furegrelate in either WKY or SHR (**Figures 12F,G**). Similar to the older rats (**Figure 10D**), MC was still enhanced in the endothelium-removed SHR arcuate arteries compared to the endothelium-removed WKY arcuate arteries (**Figure 13A**). Treating SHR endothelium-removed preglomerular arteries with indomethacin and furegrelate obliterated the enhanced MC in these vessels compared to the WKY arcuate arteries (**Figures 13B,C**).

DISCUSSION

We observed an augmented MC in the SHR pre-glomerular arteries compared to the WKY pre-glomerular arteries of both younger and older rats (**Figures 2C**, **4C**, **10C**, **12A**). This augmented MC was absent in the SHR mesenteric vessels (**Figures 3C**, **5C**, **11C**). We also found that inhibiting prostaglandin synthesis (by indomethacin) obliterated the enhanced MC that was observed in the SHR preglomerular arteries (**Figure 2D**) by reducing MC in these vessels (**Figure 2B**). L-type Ca^{2+} channel blocker, nifedipine, reduced MC in all vessels (**Figures 6A,B**, **7A,B**, **8A,B**), although SHR arcuate arteries of older rats showed more myogenic tone than WKY arcuate arteries after treating with nifedipine (**Figure 6C**). Our work showed that MC in WKY and SHR arcuate and mesenteric arteries is independent of endothelium as removing endothelium did not change MC (**Figures 10A,B**, **11A,B**). As well, removing endothelium did not eradicate the enhanced MC in the SHR preglomerular vessels (**Figure 10D**), suggesting that this augmentation is endothelium-independent. Our results also showed that indomethacin (PGH2 synthesis inhibitor) and furegrelate (TXA2 synthase inhibitor) abolished the enhanced MC in the SHR independently from endothelium (**Figures 12C,E**) suggesting that the source of TXA2 synthesis in the SHR pre-glomerular arteries is the tunica media and/or adventitia layers, and not the endothelium (**Figure 14**). In omental arteries, thromboxane synthase has been found in both

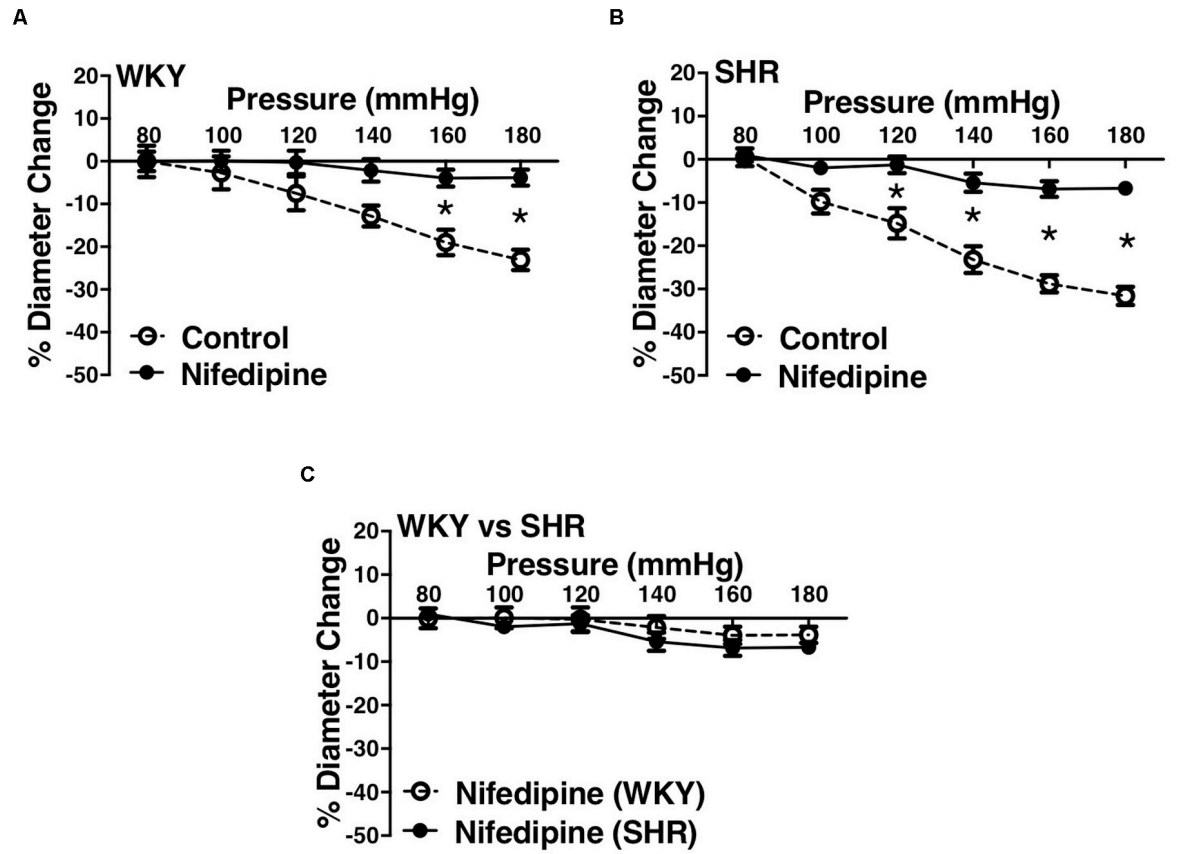

FIGURE 8 | Effects of L-type calcium channel blockade on arcuate arteries of WKY and SHR younger rats (12–16 weeks-old). **(A)** Effect of nifedipine (10 μM) on myogenic constriction (MC) of WKY arcuate arteries. **(B)** Effect of nifedipine (10 μM) on MC of SHR arcuate arteries. **(C)** Comparing MC in WKY and SHR arcuate arteries that were treated with nifedipine (10 μM). Two-way ANOVA and Holm-Sidak *post hoc* test were used to assess significance; denoted by $^*P \leq 0.05$. $N_{WKY} = 5$, $N_{SHR} = 5$, $n_{WKY} = 5$, $n_{SHR} = 5$ ("N": number of vessels, "*n*": number of animals).

the tunica media and adventitia layers in both normal and preeclamptic women (Mousa et al., 2012). This is the first study, to our knowledge, to show that MC is independent of endothelium in arcuate and mesenteric arteries of WKY and SHR rats. We were also the first to show that the enhanced MC in the SHR arcuate arteries was due to increased TXA2 synthesis.

The Enhanced Myogenic Constriction in the SHR

Several studies investigated the reason for the observed enhanced MC during chronic hypertension in different vascular beds. Huang et al. (1993) examined WKY and SHR cremaster muscle arteriole responses to indomethacin (PGH2 synthesis inhibitor) and SQ 29,548 (PGH2 receptor blocker), as well as the effects of endothelium removal (Huang et al., 1993). Contrary to our results, they suggested that increased PGH2 production from endothelium was responsible for the observed enhanced MC in the SHR cremaster muscle arterioles. This could be because different vascular beds display different vasoactive mechanisms in the endothelium and vascular SMCs (Ferrer et al., 1995; Thorin et al., 1997; Hill et al., 2001). Other studies conducted in skeletal muscle arterioles and aorta showed that in hypertension, endothelium synthesizes endothelin (Schiffrin and Thibault, 1991; Lemne et al., 1994; Schiffrin et al., 1997) and TXA2 (formed from PGH2) (Mayhan, 1992; Ungvari and Koller, 2000) which increase sensitivity of smooth muscle contractile apparatus, inducing greater contractions in response to similar raise in intracellular calcium in the SHR SMC layer compared to the Wistar Rats (WR) (Ungvari and Koller, 2000). This is consistent with our findings that also suggest a heightened intracellular calcium response in the SHR preglomerular arteries versus the WKY, as nifedipine-treated SHR vessels showed higher myogenic tone compared to the WKY nifedipine-treated vessels (**Figure 6C**). This enhanced sensitivity of SHR pre-glomerular arteries to intracellular calcium-rise may be due to activation of Rho-kinase pathway in SMCs (Uehata et al., 1997; Homma et al., 2013). Moreover, diminished NO signaling in skeletal muscle arterioles of hypertensive rats (i.e., Zucker Diabetic Fatty rats) has been shown to contribute to the exaggerated MC (Lesniewski et al., 2008), which is contrary to our finding that NO synthesis may have a small constrictor effect on the SHR arcuate arteries at high intraluminal pressures (P160 and P180

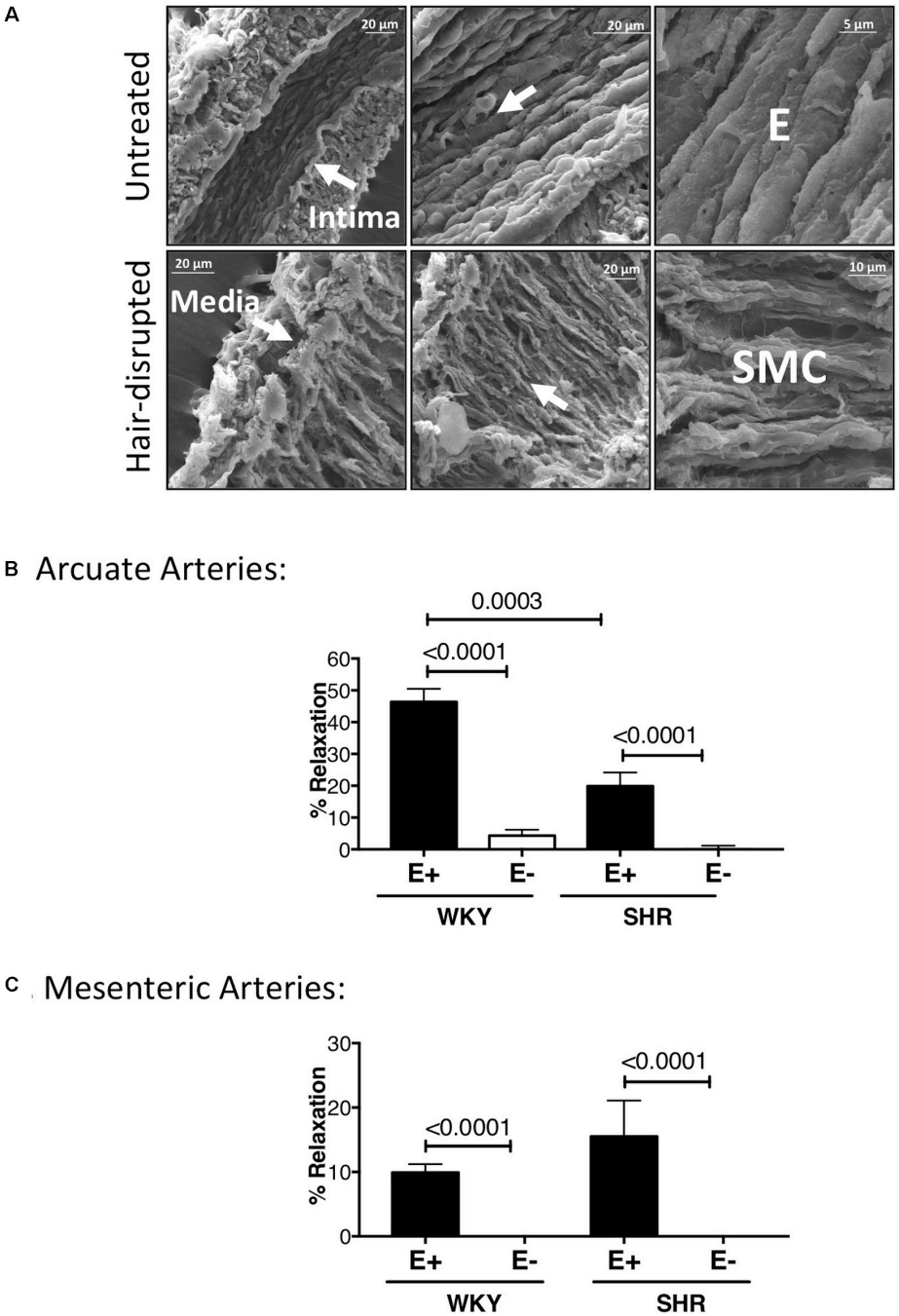

FIGURE 9 | Scanning Electron Micrographs and carbachol treatments demonstrating physical and functional removal of endothelium. **(A)** Scanning Electron Microscopy (SEM) showing intact tunica intima (consisting of endothelium, E) and media (consisting of smooth muscle cells) in untreated, but only tunica media in hair-disrupted WKY arcuate arteries. Micrographs were magnified between 700 to 15000 times. **(B)** Percent carbachol-induced relaxation (10 μM) in WKY and SHR arcuate arteries that were pre-constricted with 3 μM phenylephrine at P80 mmHg. **(C)** Percent carbachol-induced relaxation (10 μM) in WKY and SHR mesenteric arteries that were pre-constricted with 3 μM phenylephrine at P80 mmHg. Paired *t*-test was used to compare endothelium-intact (E+) and endothelium-removed (E-) arteries in the same animal strain. Unpaired *t*-test was used to compare E + and E- arteries in different animal strains. $^*P \leq 0.05$; for arcuate arteries: $N_{WKY} = 10$, $N_{SHR} = 10$, $n_{WKY} = 5$, $n_{SHR} = 4$; for mesenteric arteries: $N_{WKY} = 11$, $N_{SHR} = 5$, $n_{WKY} = 5$, $n_{SHR} = 4$; ("N": number of vessels; "*n*": number of animals).

mmHg) (**Figure 4B**). No is predominantly produced by the endothelium and is very unstable with a half-life of seconds (Butler et al., 1995; Schini, 1996; Jeremy et al., 1999). After being produced, NO can rapidly react with oxygen species (O_2, O_2^- and H_2O_2) and thiol groups to produce nitrite, nitrate, peroxynitrite (ONOO), and nitrosothiols. The effects of

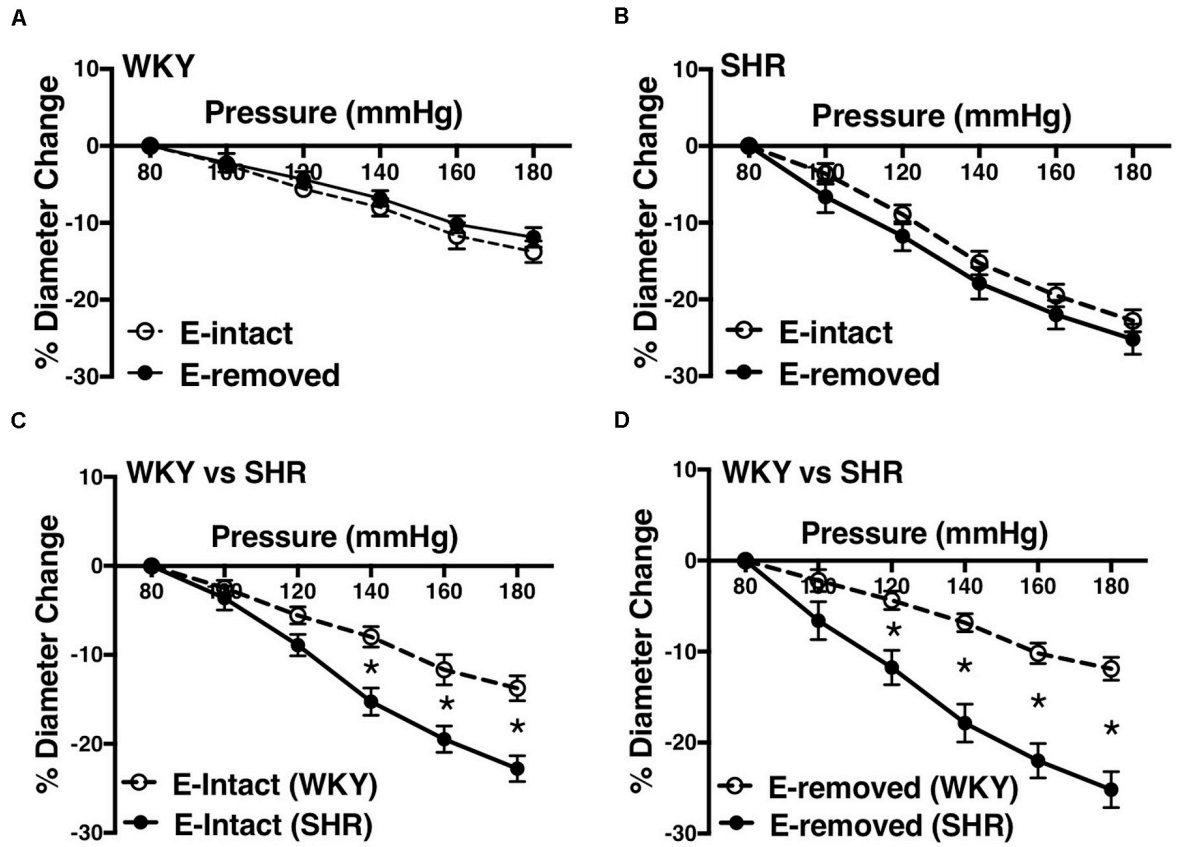

FIGURE 10 | Effects of removing endothelium from WKY and SHR preglomerular arteries using human hair (30–40 weeks-old rats). **(A)** Effect of removing endothelium in WKY arcuate arteries. **(B)** Effect of removing endothelium in SHR arcuate arteries. **(C)** Comparison of myogenic constriction (MC) in endothelium-intact (E-intact) WKY and SHR arcuate arteries. **(D)** Comparison of MC in endothelium-removed (E-removed) WKY and SHR arcuate arteries. Two-way ANOVA and Holm-Sidak *post hoc* test was used to assess significance; denoted by $^*P \leq 0.05$. $N_{WKY} = 10$, $N_{SHR} = 10$, $n_{WKY} = 5$, $n_{SHR} = 4$; ("N": number of vessels; "*n*": number of animals).

NO on vessels can be mediated by the potential presence of thiol and oxygen species (Darley-Usmar et al., 1995; Jeremy et al., 1999). The small vasoconstrictor effects of NO (at high intraluminal pressures) that was observed in this study may be due to the reaction of NO with superoxide to create peroxynitrite in the SHR vessels (Carlisle et al., 2016) and thereby augmenting constrictor responses (Bagi et al., 2002). The resulting peroxynitrite may promote the release of TXA2 leading to arteriolar constriction, as was shown in gracilis muscle arterioles of hyperhomocysteinemia (induced by methionine diet) mouse model (Bagi et al., 2002). As well, in rat models of high-fat high-sucrose (HFHS) and levothyroxine (L-T_4) diets, endothelium-denuded thoracic aortic rings from HFHS + LT_4 rats showed stronger vasoconstriction than HFHS rats due to increase NO and superoxide production that led to peroxynitrite formation, independent from the endothelium (Hu et al., 2014). Other contributing mechanisms to the enhanced MC have also been reported such as increased superoxide generation through activation of Nicotinamide Adenine Dinucleotide Phosphate (NADPH) oxidase in afferent arterioles (Ren et al., 2010); increased activation of angiotensin II type 1 receptor in cremaster muscle arteries (Hong et al., 2017); and increased production of 20-hydroxyeicosatrienoic acid (20-HETE) through activation of cytochrome P450 in afferent and cerebral arterioles (Imig et al., 1993, 1994, 1996; Szarka et al., 2017). Consistent with our observation of an augmented MC in the SHR arcuate arteries, (Imig et al., 1993), found an enhanced MC in the SHR (4-week-old prehypertensive SHRs) interlobular as well as proximal and distal portions of the afferent arterioles of juxtamedullary glomeruli. The researchers also discovered that inhibiting cytochrome P-450 enzyme (with ketoconazole or 7-ethoxyresorufin) had variable effects in different segments of the preglomerular arteries. In interlobular, proximal afferent, and distal afferent arterioles, inhibiting cytochrome P-450 did not remove, removed, and partially removed the enhanced MC in the SHR arterioles, respectively, compared to the WKY arteries (Imig et al., 1993). These findings suggest that cytochrome P-450 metabolites of arachidonic acid have a critical role in the enhanced MC in the SHR preglomerular vessels (Imig et al., 1996). To investigate if the enhanced MC in the SHR vessels is endothelium-dependent, we removed the endothelium using human hair.

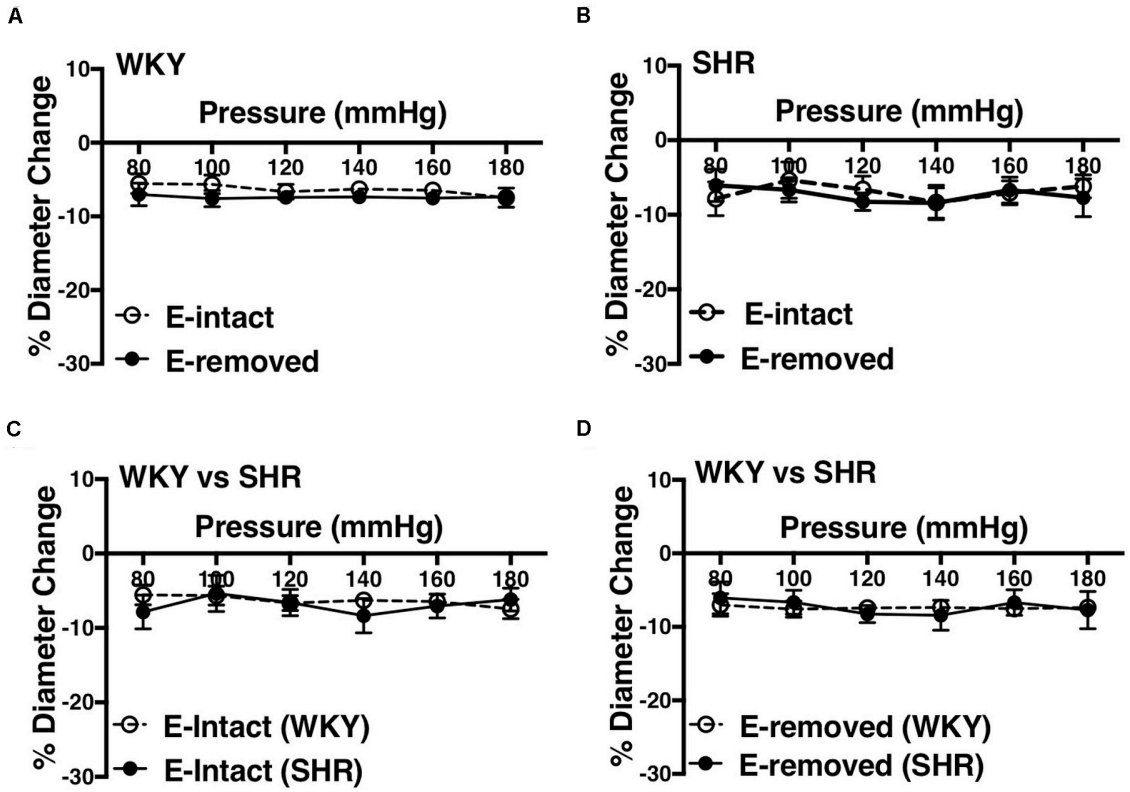

FIGURE 11 | Effects of removing endothelium from WKY and SHR mesenteric arteries using human hair (30–40 weeks-old rats). **(A)** Effect of removing endothelium in WKY mesenteric arteries. **(B)** Effect of removing endothelium in SHR mesenteric arteries. **(C)** Comparison of myogenic constriction (MC) in endothelium-intact (E-intact) WKY and SHR mesenteric arteries. **(D)** Comparison of MC in endothelium-removed (E-removed) WKY and SHR mesenteric arteries. Two-way ANOVA and Holm-Sidak *post hoc* test was used to assess significance; denoted by $^*P \leq 0.05$. $N_{WKY} = 11$, $N_{SHR} = 5$, $n_{WKY} = 6$, $n_{SHR} = 4$; ("N": number of vessels; "*n*": number of animals).

Removing the Endothelium

Endothelium can be removed from blood vessels by chemical or physical means. Chemical methods include using collagenase, elastase, or antibodies. Collagenase and elastase are enzymes that dissolve intercellular matrix between endothelium, but might also damage the vascular SMC layer (Osol et al., 1989). Antibodies against specific endothelial antigens may also not completely remove the endothelium (Juncos et al., 1995). Physical methods of denuding endothelium involve abrading the inner surface of the vessel by an applicator such as cotton, filter paper (Molina et al., 1992), wood, wire, air bolus, or human hair; most of which are fragile or difficult to apply to small arteries (Osol et al., 1989) such as preglomerular vessels. Air bolus injections also are appropriate methods for large arteries, but may not completely remove the endothelium in small arterioles (Ralevic et al., 1989). In 1989, Osol et al. suggested an effective method for removing endothelium from small arteries involving human hair, which provided sufficient degree of abrasion to damage the endothelium but not the vascular SMC layer. After reviewing the aforementioned methods, we decided to use human hair to mechanically abrade endothelium from preglomerular and mesenteric arteries in order to investigate the role of endothelium in MC.

Role of Endothelium in MC

Even though MC is essential in renal autoregulation, its dependency on endothelium is controversial. Studies in different species and tissues have reported that endothelium removal abolished (Harder, 1987; Katusic et al., 1987; Rubanyi, 1988; Kuo et al., 1990; Hughes and Bund, 2002), enhanced (Garcia-Roldan and Bevan, 1990; Juncos et al., 1995; Scotland et al., 2001; Gschwend et al., 2003; Huang et al., 2005; Chaston et al., 2013), reduced (Huang et al., 2005), or did not change (Hwa and Bevan, 1986; Falcone et al., 1991; Scotland et al., 2001; Daneshtalab and Smeda, 2010) MC. This controversy may be because endothelial cells can release different vasoactive substances in variable quantities in different vascular beds or even different sections of the same vascular bed (Ferrer et al., 1995; Thorin et al., 1997; Hill et al., 2001). Thus, it is important to investigate the function of endothelium in different vascular beds. In rabbit afferent arterioles, (Juncos et al., 1995) reported that removing endothelium enhanced MC in free-flow vessels but did not change MC in no-flow arteries. Nevertheless, the authors used factor VIII-related antigen antibodies which did not completely remove the endothelium, revealed in their transmission electron micrographs (Juncos et al., 1995). Another study conducted by Harder demonstrated a dependency

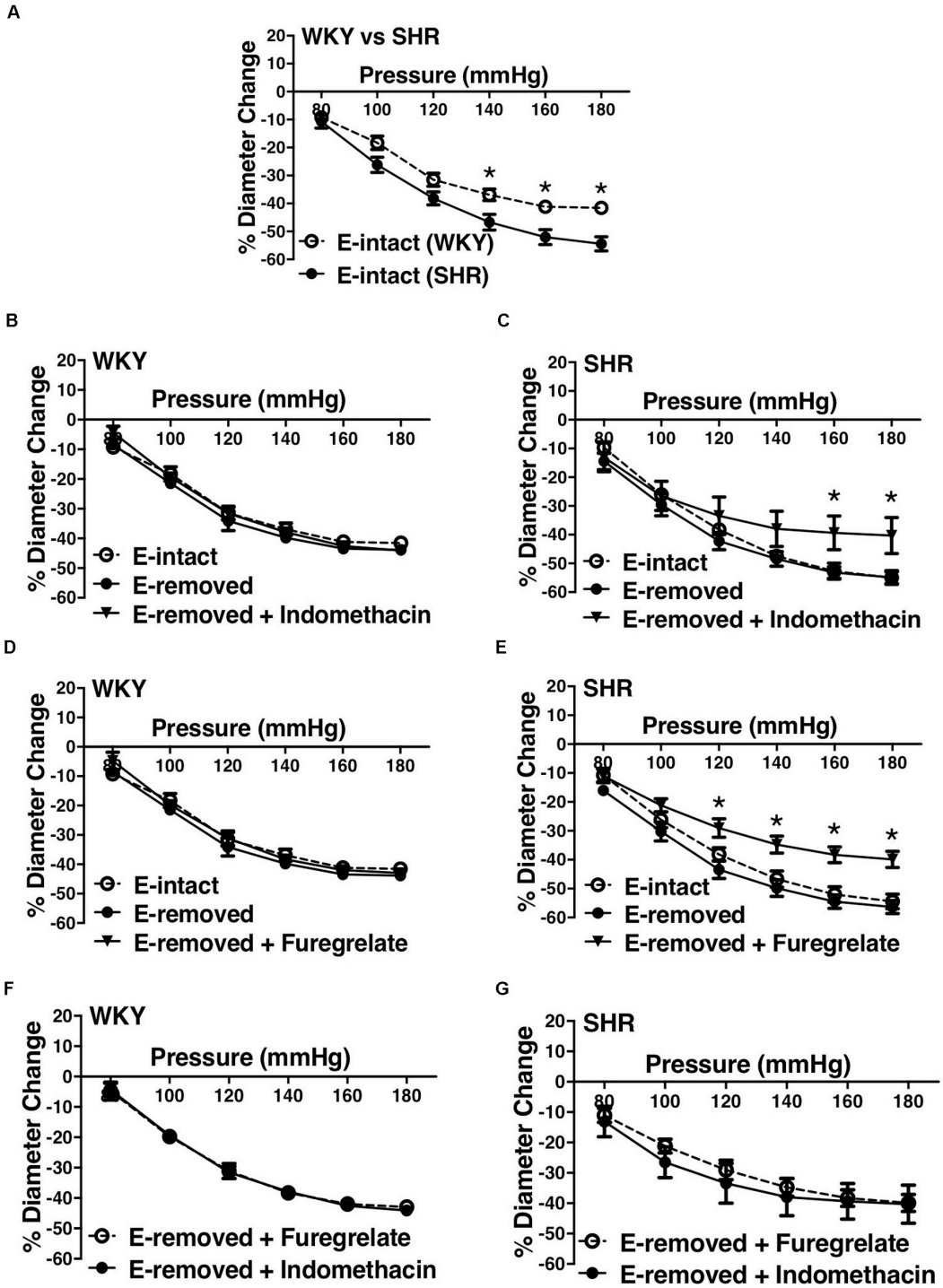

FIGURE 12 | Effects of inhibiting cyclooxygenase 1 and 2 (prostaglandin H2 synthesis) and thromboxane synthetase on arcuate arteries of young WKY and SHR rats (12–16 weeks-old). **(A)** Myogenic constriction (MC) comparison between endothelium-intact (E-intact) WKY and SHR arcuate arteries. **(B,C)** Comparing WKY and SHR arcuate arteries with E-intact, endothelium-removed (E-removed), and E-removed that were treated with indomethacin (prostaglandin H2 synthesis inhibitor, 10 μM). Star,"*", depicts significant differences between indomethacin-treated vessels with when they had their E-removed and E-intact ($P \leq 0.05$). **(D,E)** Comparing WKY and SHR arcuate arteries with E-intact, E-removed, and E-removed that were treated with furegrelate (thromboxane A2 synthesis inhibitor, 100 μM). Star,"*", depicts significant differences between furegrelate-treated vessels with when they had their E-removed and E-intact ($P \leq 0.05$). **(F,G)** Comparing WKY and SHR E-removed arcuate arteries that were treated with either indomethacin or furegrelate. Two-way ANOVA and Holm-Sidak *post hoc* test was used to assess significance. $N_{WKY} = 9$, $N_{SHR} = 10$, $n_{WKY} = 6$, $n_{SHR} = 9$; ("N": number of vessels; "*n*": number of animals).

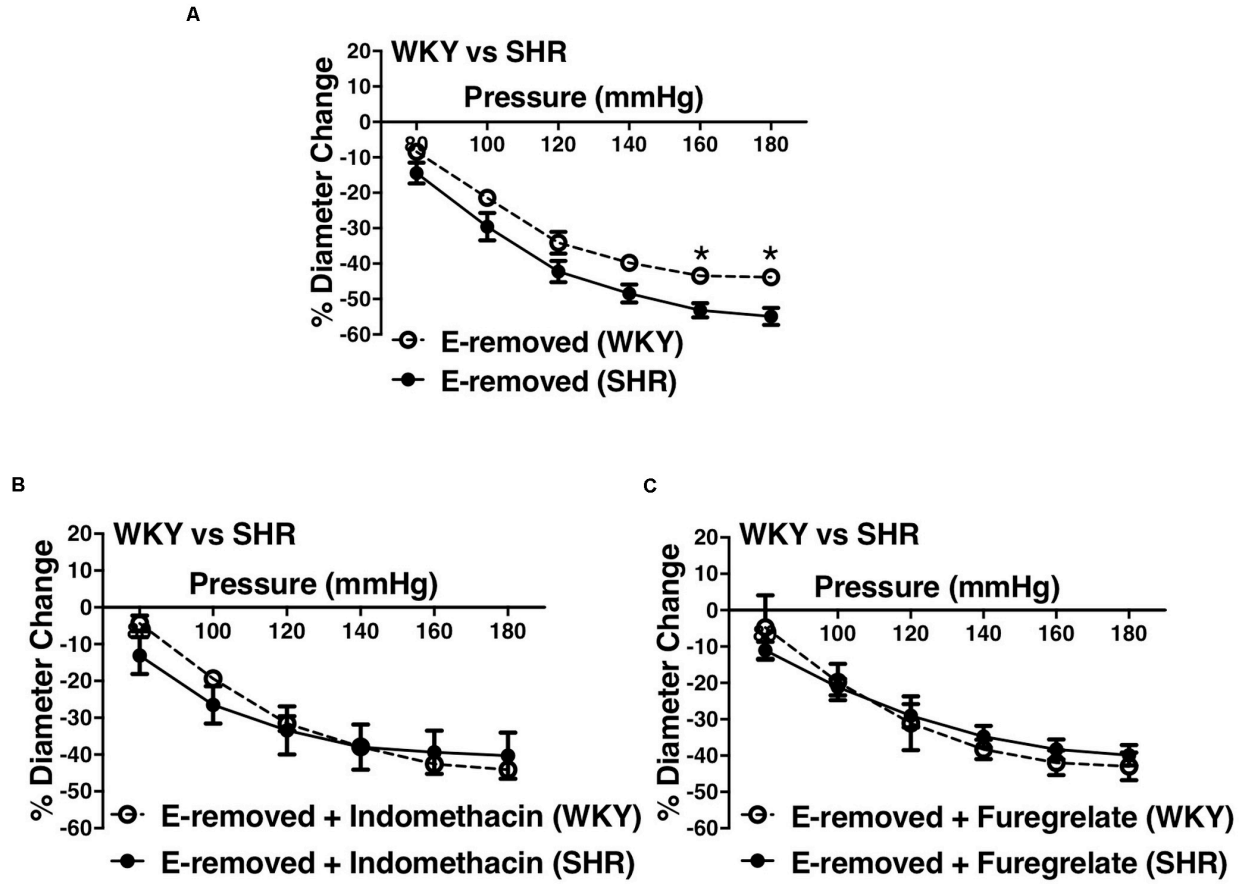

FIGURE 13 | Enhanced myogenic constriction (MC) in the young SHR arcuate arteries, compared to the WKY, was abolished with inhibiting prostaglandin H2 synthesis (by indomethacin) and thromboxane A2 synthesis (by furegrelate) independent from endothelium. **(A)** MC is enhanced in the endothelium-removed (E-removed) SHR arcuate arteries compared with E-removed WKY arcuate arteries at high intraluminal pressures. **(B)** Treating E-removed SHR arcuate arteries with 10 μM indomethacin abolished the enhanced MC compared to the WKY arcuate arteries. **(C)** Treating E-removed SHR arcuate arteries with 100 μM furegrelate abolished the enhanced MC compared to the WKY arcuate arteries. Two-way ANOVA and Holm-Sidak *post hoc* test was used to assess significance; denoted by $^*P \leq 0.05$. $N_{WKY} = 9$, $N_{SHR} = 10$, $n_{WKY} = 6$, $n_{SHR} = 9$; ("N": number of vessels; "*n*": number of animals).

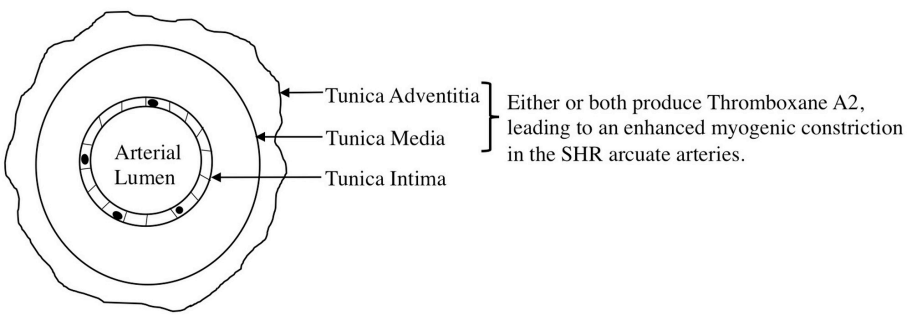

FIGURE 14 | Proposed mechanism for the enhanced myogenic constriction in the SHR arcuate arteries. Tunica intima, Tunica media, and tunica adventitia are composed of endothelial cells, smooth muscle cells, and connective tissue, respectively.

of MC on endothelium in cat cerebral arteries. Harder subjected these arteries to 40 to 60 mmHg pressure and recorded a depolarization of 0.35 mV/mmHg, which was abolished when he removed the endothelium (Harder, 1987). In mesenteric arteries, endothelial cells may have roles in MC under hypoxic conditions. Earley and Walker (2002) exposed Sprague-Dawley rats to chronic hypoxia and found that myogenic responsiveness in their mesenteric arteries

was abolished. This obliteration was restored by removing the endothelium.

NSAIDs in Hypertension and CKD

Non-steroidal anti-inflammatory drugs (NSAIDs) are a class of drugs that block prostaglandins synthesis by inhibiting COX-1 and COX-2 enzymes. While healthy people rarely have adverse renal side effects upon using NSAIDs, individuals (particularly elderly patients) who have hypertension and CKD may develop acute kidney failure (Hörl, 2010). In fact, administering indomethacin to renal failure rat models (Sprague–Dawley rats that have been administered adenine to have chronic renal failure) significantly decreased their survival rate (Kadowaki et al., 2012). Every year, about 2.5 million Americans who use NSAIDs experience renal-related side effects (Sandhu and Heyneman, 2004).

CONCLUSION

Myogenic constriction is augmented in the SHR preglomerular arteries but not the mesenteric arteries, compared to the WKY respective vessels. The augmented MC in the SHR pre-glomerular vessels appears to be due to increased prostanoid production, particularly TXA2 synthesis, from the tunica media and/or adventitia layers. Moreover, MC is not dependent on the endothelium in the WKY and SHR pre-glomerular and mesenteric arteries, as removing endothelium did not change the MC. L-type Ca^{2+} channels are critical to MC as inhibiting them tremendously decreases MC in both WKY and SHR arcuate and mesenteric arteries. Nevertheless, SHR pre-glomerular arteries seem to have a differential intracellular Ca^{2+} signaling at higher intraluminal pressures (P140-P180 mmHg) compared to the WKY vessels.

DATA AVAILABILITY STATEMENT

All datasets generated for this study are included in the article/supplementary material.

ETHICS STATEMENT

The animal study was reviewed and approved by McMaster University Animal Research Ethics Board.

AUTHOR CONTRIBUTIONS

SN and CL performed the experiments, analyzed the data, and interpreted the results. SN prepared the figures and drafted the manuscript. SN and JD edited and revised the manuscript. All authors approved the final version of the manuscript, contributed to the article and approved the submitted version. JD conceived and designed the research.

FUNDING

This work was supported by the Canadian Institutes of Health Research grants to JD (PJT148499). Financial support from St. Joseph's Healthcare Hamilton, salary support from St. Joseph's Healthcare Hamilton, and Division of Nephrology in the Department of Medicine at McMaster University are also acknowledged by JD.

REFERENCES

Arendshorst, W. J., and Beierwaltes, W. H. (1979). Renal and nephron hemodynamics in spontaneously hypertensive rats. *Am. J. Physiol. Ren. Physiol.* 236, F246–F251.

Atala, A. (2016). Re: a structured interdomain linker directs self-polymerization of human uromodulin. *J. Urol.* 196:958. doi: 10.1016/j.juro.2016.06.027

Bagi, Z., Ungvari, Z., and Koller, A. (2002). Xanthine oxidase–derived reactive oxygen species convert flow-induced arteriolar dilation to constriction in hyperhomocysteinemia: possible role of peroxynitrite. *Arterioscler. Thromb. Vasc. Biol.* 22, 28–33. doi: 10.1161/hq0102.101127

Bayliss, W. M. (1902). On the local reactions of the arterial wall to changes of internal pressure. *J. Physiol.* 28, 220–231. doi: 10.1113/jphysiol.1902.sp000911

Bidani, A. K., and Griffin, K. A. (2004). Pathophysiology of hypertensive renal damage: implications for therapy. *Hypertension* 44, 595–601. doi: 10.1161/01.hyp.0000145180.38707.84

Butler, A. R., Flitney, F. W., and Williams, D. L. H. (1995). NO, nitrosonium ions, nitroxide ions, nitrosothiols and iron-nitrosyls in biology: a chemist's perspective. *Trends Pharmacol. Sci.* 16, 18–22. doi: 10.1016/s0165-6147(00)88968-3

Carlisle, R. E., Werner, K. E., Yum, V., Lu, C., Tat, V., Memon, M., et al. (2016). Endoplasmic reticulum stress inhibition reduces hypertension through the preservation of resistance blood vessel structure and function. *J. Hypertens.* 34, 1556–1569. doi: 10.1097/hjh.0000000000000943

Carlström, M., Wilcox, C. S., and Arendshorst, W. J. (2015). Renal autoregulation in health and disease. *Physiol. Rev.* 95, 405–511. doi: 10.1152/physrev.00042.2012

Chaston, D. J., Baillie, B. K., Grayson, T. H., Courjaret, R. J., Heisler, J. M., Lau, K. A., et al. (2013). Polymorphism in endothelial connexin40 enhances sensitivity to intraluminal pressure and increases arterial stiffness. *Arterioscler. Thromb. Vasc. Biol.* 33, 962–970. doi: 10.1161/atvbaha.112.300957

Daneshtalab, N., and Smeda, J. S. (2010). Alterations in the modulation of cerebrovascular tone and blood flow by nitric oxide synthases in SHRsp with stroke. *Cardiovasc. Res.* 86, 160–168. doi: 10.1093/cvr/cvp395

Darley-Usmar, V., Wiseman, H., and Halliwell, B. (1995). Nitric oxide and oxygen radicals: a question of balance. *FEBS lett.* 369, 131–135. doi: 10.1016/0014-5793(95)00764-z

Dickhout, J. G., and Lee, R. M. (1997). Structural and functional analysis of small arteries from young spontaneously hypertensive rats. *Hypertension* 29, 781–789. doi: 10.1161/01.hyp.29.3.781

Earley, S., and Walker, B. R. (2002). Endothelium-dependent blunting of myogenic responsiveness after chronic hypoxia. *Am. J. Physiol. Heart Circ. Physiol.* 283, H2202–H2209.

Falcone, J. C., Davis, M. J., and Meininger, G. A. (1991). Endothelial independence of myogenic response in isolated skeletal muscle arterioles. *Am. J. Physiol. Heart Circ. Physiol.* 260, H130–H135.

Ferrer, M., Encabo, A., Conde, M. V., Marín, J., and Balfagón, G. (1995). Heterogeneity of endothelium-dependent mechanisms in different rabbit arteries. *J. Vas. Res.* 32, 339–346. doi: 10.1159/000159108

Garcia-Roldan, J.-L., and Bevan, J. A. (1990). Flow-induced constriction and dilation of cerebral resistance arteries. *Circ. Res.* 66, 1445–1448. doi: 10.1161/01.res.66.5.1445

Griffin, K. A., Churchill, P. C., Picken, M., Webb, R. C., Kurtz, T. W., and Bidani, A. K. (2001). Differential salt-sensitivity in the pathogenesis of renal damage in SHR and stroke prone SHR. *Am. J. Hypertens.* 14, 311–320. doi: 10.1016/s0895-7061(00)01282-6

Gschwend, S., Henning, R. H., Pinto, Y., Zeeuw, D. D., Gilst, W. V., and Buikema, H. (2003). Myogenic constriction is increased in mesenteric resistance arteries from rats with chronic heart failure: instantaneous counteraction by acute AT1 receptor blockade. *Br. J. Pharmacol.* 139, 1317–1325. doi: 10.1038/sj.bjp.0705367

Harder, D. R. (1987). Pressure-induced myogenic activation of cat cerebral arteries is dependent on intact endothelium. *Circ. Res.* 60, 102–107. doi: 10.1161/01.res.60.1.102

Hill, C. E., Phillips, J. K., and Sandow, S. L. (2001). Heterogeneous control of blood flow amongst different vascular beds. *Med. Res. Rev.* 21, 1–60. doi: 10.1002/1098-1128(200101)21:1<1::aid-med1>3.0.co;2-6

Homma, K., Hayashi, K., Wakino, S., Tokuyama, H., Kanda, T., Tatematsu, S., et al. (2013). Rho-kinase contributes to pressure-induced constriction of renal microvessels. *Keio J. Med.* 63, 1–12. doi: 10.2302/kjm.2013-0001-oa

Hong, K., Li, M., Nourian, Z., Meininger, G. A., and Hill, M. A. (2017). Angiotensin II type 1 receptor mechanoactivation involves rgs5 (regulator of g protein signaling 5) in skeletal muscle arteries: impaired trafficking of RGS5 in hypertension. *Hypertension* 70, 1264–1272. doi: 10.1161/hypertensionaha.117.09757

Hörl, W. H. (2010). Nonsteroidal anti-inflammatory drugs and the kidney. *Pharmaceuticals* 3, 2291–2321. doi: 10.3390/ph3072291

Hu, D., Peng, J., Zhang, X., Zheng, H., Yan, S., Zhang, Y., et al. (2014). Thyroid hormone exacerbates vasoconstriction in insulin resistance: the role of ONOO(-). *Eur. J. Pharmacol.* 730, 41–50. doi: 10.1016/j.ejphar.2014.02.018

Huang, A., Sun, D., and Koller, A. (1993). Endothelial dysfunction augments myogenic arteriolar constriction in hypertension. *Hypertension* 22, 913–921. doi: 10.1161/01.hyp.22.6.913

Huang, A., Sun, D., Yan, C., Falck, J. R., and Kaley, G. (2005). Contribution of 20-HETE to augmented myogenic constriction in coronary arteries of endothelial NO synthase knockout mice. *Hypertension* 46, 607–613. doi: 10.1161/01.hyp.0000176745.04393.4d

Hughes, J. M., and Bund, S. J. (2002). Arterial myogenic properties of the spontaneously hypertensive rat. *Exper. Physiol.* 87, 527–534. doi: 10.1113/eph8702399

Hwa, J. J., and Bevan, J. A. (1986). Stretch-dependent (myogenic) tone in rabbit ear resistance arteries. *Am. J. Physiol. Heart Circ. Physiol.* 250, H87–H95.

Imig, J. D., Falck, J. R., Gebremedhin, D., Harder, D. R., and Roman, R. J. (1993). Elevated renovascular tone in young spontaneously hypertensive rats. Role of cytochrome P-450. *Hypertension* 22, 357–364. doi: 10.1161/01.hyp.22.3.357

Imig, J. D., Zou, A., Ortiz De Montellano, P., Sui, Z., and Roman, R. J. (1994). Cytochrome P-450 inhibitors alter afferent arteriolar responses to elevations in pressure. *Am. J. Physiol. Heart Circ. Physiol.* 266, H1879–H1885.

Imig, J. D., Zou, A. P., Stec, D. E., Harder, D. R., Falck, J. R., and Roman, R. J. (1996). Formation and actions of 20-hydroxyeicosatetraenoic acid in rat renal arterioles. *Am. J. Physiol. Regul. Integr. Compar. Physiol.* 270, R217–R227.

Jeremy, J. Y., Rowe, D., Emsley, A. M., and Newby, A. C. (1999). Nitric oxide and the proliferation of vascular smooth muscle cells. *Cardiovasc. Res.* 43, 580–594. doi: 10.1016/s0008-6363(99)00171-6

Juncos, L. A., Garvin, J., Carretero, O. A., and Ito, S. (1995). Flow modulates myogenic responses in isolated microperfused rabbit afferent arterioles via endothelium-derived nitric oxide. *J. Clin. Invest.* 95, 2741–2748. doi: 10.1172/jci117977

Kadowaki, D., Sumikawa, S., Arimizu, K., Taguchi, K., Kitamura, K., Ishitsuka, Y., et al. (2012). Effect of acetaminophen on the progression of renal damage in adenine induced renal failure model rats. *Life Sci.* 91, 1304–1308. doi: 10.1016/j.lfs.2012.09.018

Kaplan, N. M., and Palmer, B. F. (2001). Impaired renal autoregulation: implications for the genesis of hypertension and hypertension-induced renal injury. *Am. J. Med. Sci.* 321, 388–400. doi: 10.1097/00000441-200106000-00005

Katusic, Z. S., Shepherd, J. T., and Vanhoutte, P. M. (1987). Endothelium-dependent contraction to stretch in canine basilar arteries. *Am. J. Physiol.* 252, H671–H673.

Kuo, L., Davis, M. J., and Chilian, W. M. (1990). Endothelium-dependent, flow-induced dilation of isolated coronary arterioles. *Am. J. Physiol. Heart Circ. Physiol.* 259, H1063–H1070.

Le Goff, X., Chesnel, F., Delalande, O., Couturier, A., Dreano, S., Le Goff, C., et al. (2016). Aggregation dynamics and identification of aggregation-prone mutants of the von Hippel-Lindau tumor suppressor protein. *J. Cell Sci.* 129, 2638–2650. doi: 10.1242/jcs.184846

Lemne, C. E., Lundeberg, T., Theodorsson, E., and De Faire, U. (1994). Increased basal concentrations of plasma endothelin in borderline hypertension. *J. Hypertens.* 12, 1069–1074.

Lesniewski, L. A., Donato, A. J., Behnke, B. J., Woodman, C. R., Laughlin, M. H., Ray, C. A., et al. (2008). Decreased NO signaling leads to enhanced vasoconstrictor responsiveness in skeletal muscle arterioles of the ZDF rat prior to overt diabetes and hypertension. *Am. J. Physiol. Heart Circ. Physiol.* 294, H1840–H1850.

Loutzenhiser, R., Bidani, A., and Chilton, L. (2002). Renal myogenic response: kinetic attributes and physiological role. *Circ. Res.* 90, 1316–1324. doi: 10.1161/01.res.0000024262.11534.18

Loutzenhiser, R., Bidani, A., and Wang, X. (2004). Systolic pressure and the myogenic response of the renal afferent arteriole. *Acta Physiol. Scand.* 181, 407–413. doi: 10.1111/j.1365-201x.2004.01312.x

Loutzenhiser, R., Griffin, K. A., and Bidani, A. K. (2006). Systolic blood pressure as the trigger for the renal myogenic response: protective or autoregulatory? *Curr. Opin. Nephrol. Hyperten.* 15, 41–49. doi: 10.1097/01.mnh.0000199011.41552.de

Lucas, S. (2016). The pharmacology of indomethacin. *Headache J. Head Face Pain* 56, 436–446.

Mayhan, W. G. (1992). Role of prostaglandin H2-thromboxane A2 in responses of cerebral arterioles during chronic hypertension. *Am. J. Physiol. Heart Circ. Physiol.* 262, H539–H543.

Molina, R., Hidalgo, A., and De Boto García, M. J. (1992). Influence of mechanical endothelium removal techniques and conservation conditions on rat aorta responses. *Methods Find. Exper. Clin. Pharmacol.* 14, 91–96.

Mousa, A. A., Strauss, J. F., and Walsh, S. W. (2012). Reduced methylation of the thromboxane synthase gene is correlated with its increased vascular expression in preeclampsia. *Hypertension* 59, 1249–1255. doi: 10.1161/hypertensionaha.111.188730

Osol, G., Cipolla, M., and Knutson, S. (1989). A new method for mechanically denuding the endothelium of small (50–150 μm) arteries with a human hair. *J. Vasc. Res.* 26, 320–324. doi: 10.1159/000158781

Ralevic, V., Kristek, F., Hudlicka, O., and Burnstock, G. (1989). A new protocol for removal of the endothelium from the perfused rat hind-limb preparation. *Circ. Res.* 64, 1190–1196. doi: 10.1161/01.res.64.6.1190

Ren, Y., D'ambrosio, M. A., Liu, R., Pagano, P. J., Garvin, J. L., and Carretero, O. A. (2010). Enhanced myogenic response in the afferent arteriole of spontaneously hypertensive rats. *Am. J. Physiol. Heart Circ. Physiol.* 298, H1769–H1775.

Rubanyi, G. M. (1988). Endothelium-dependent pressure-induced contraction of isolated canine carotid arteries. *Am. J. Physiol. Heart Circ. Physiol.* 255, H783–H788.

Saboliæ, I., Katsura, T., Verbavatz, J.-M., and Brown, D. (1995). The AQP2 water channel: effect of vasopressin treatment, microtubule disruption, and distribution in neonatal rats. *J. Membr. Biol.* 143, 165–175. doi: 10.1007/bf00233445

Sandhu, G. K., and Heyneman, C. A. (2004). Nephrotoxic potential of selective cyclooxygenase-2 inhibitors. *Ann. Pharm.* 38, 700–704. doi: 10.1345/aph.1d296

Schiffrin, E. L., Deng, L. Y., Sventek, P., and Day, R. (1997). Enhanced expression of endothelin-1 gene in resistance arteries in severe human essential hypertension. *J. Hyperten.* 15, 57–63. doi: 10.1097/00004872-199715010-00005

Schiffrin, E. L., and Thibault, G. E. L. (1991). Plasma endothelin in human essential hypertension. *Am. J. Hypertens.* 4, 303–308. doi: 10.1093/ajh/4.4.303

Schini, V. (1996). "The L-Arginine-Nitric oxide pathway in the vascular smooth muscle: Regulation and pathophysiological significance," in *Vascular Endothelium* (Springer), 320–320.

Scotland, R. S., Chauhan, S., Vallance, P. J., and Ahluwalia, A. (2001). An endothelium-derived hyperpolarizing factor–like factor moderates myogenic constriction of mesenteric resistance arteries in the absence of endothelial nitric oxide synthase–derived nitric oxide. *Hypertension* 38, 833–839. doi: 10.1161/hy1001.092651

Szarka, N., Amrein, K., Horvath, P., Ivic, I., Czeiter, E., Buki, A., et al. (2017). Hypertension-induced enhanced myogenic constriction of cerebral arteries is preserved after traumatic brain injury. *J. Neurotraum.* 34, 2315–2319. doi: 10.1089/neu.2016.4962

Thorin, E., Shatos, M. A., Shreeve, S. M., Walters, C. L., and Bevan, J. A. (1997). Human vascular endothelium heterogeneity: a comparative study of cerebral and peripheral cultured vascular endothelial cells. *Stroke* 28, 375–381. doi: 10.1161/01.str.28.2.375

Uehata, M., Ishizaki, T., Satoh, H., Ono, T., Kawahara, T., Morishita, T., et al. (1997). Calcium sensitization of smooth muscle mediated by a Rho-associated protein kinase in hypertension. *Nature* 389:990. doi: 10.1038/40187

Ungvari, Z., and Koller, A. (2000). Endothelin and prostaglandin H2/thromboxane A2 enhance myogenic constriction in hypertension by increasing Ca2+ sensitivity of arteriolar smooth muscle. *Hypertension* 36, 856–861. doi: 10.1161/01.hyp.36.5.856

Conflict of Interest: The authors declare that the research was conducted in the absence of any commercial or financial relationships that could be construed as a potential conflict of interest.

Copyright © 2020 Nademi, Lu and Dickhout. This is an open-access article distributed under the terms of the Creative Commons Attribution License (CC BY). The use, distribution or reproduction in other forums is permitted, provided the original author(s) and the copyright owner(s) are credited and that the original publication in this journal is cited, in accordance with accepted academic practice. No use, distribution or reproduction is permitted which does not comply with these terms.

frontiers in Pharmacology

ORIGINAL RESEARCH
published: 29 July 2020
doi: 10.3389/fphar.2020.01136

Trimetazidine Inhibits Renal Tubular Epithelial Cells to Mesenchymal Transition in Diabetic Rats *via* Upregulation of Sirt1

Yong Yang[1,2], *Yong Wang*[1,2], *Zuowen He*[1,2], *Yunchang Liu*[1,2], *Chen Chen*[1,2], *Yan Wang*[1,2], *Dao Wen Wang*[1,2] *and Hong Wang*[1,2]*

[1] Division of Cardiology, Department of Internal Medicine, Tongji Hospital, Tongji Medical College, Huazhong University of Science and Technology, Wuhan, China, [2] Hubei Key Laboratory of Genetics and Molecular Mechanisms of Cardiologic Disorders, Huazhong University of Science and Technology, Wuhan, China

Trimetazidine (TMZ), as a metabolic regulator, is effective in treatment of coronary atherosclerotic heart disease with rare side effects in the clinic for long years. Interestingly, studies have shown that TMZ protects against several acute kidney injuries (AKI). However, the effect of TMZ on chronic kidney diseases (CKD) remains unknown. This study aimed to investigate the role of TMZ in diabetic nephropathy (DN) and its potential mechanisms. A rat model of DN was established in male Sprague-Dawley rats by streptozotocin (STZ) intraperitoneal injection. Experimental rats were separated into three groups: control, DN and DN + TMZ treatment. Metabolic parameters, pathological features and renal function markers were evaluated after 20 weeks of diabetes induction. *In vitro* experiments, the effect of TMZ on high fat and high glucose (HFG) induced or TGFβ1-induced epithelial-to-mesenchymal transition (EMT) was examined in HK-2 cells. Our results showed that TMZ could maintain renal function without affecting hemodynamic and plasma metabolic levels in diabetic rats. The effect was associated with a reversion of pathological progression of DN, especially for tubulointerstitial fibrosis. EMT is an important contributor to renal fibrosis. In this study, we investigated the role of TMZ in the process of EMT in DN. Mechanistically; TMZ attenuated HFG-induced EMT by relieving oxidative stress *via* deacetylation forkhead box O1 (FoxO1) in a Sirt1-dependent pathway. And it suppressed TGFβ1-induced EMT by deacetylating Smd4 in a Sirt1-dependent manner. Moreover, our study found that TMZ upregulated Sirt1 expression by increasing the expression of nicotinamide phosphoribosyl transferase (Nampt), which is a rate limiting enzyme for nicotinamide adenine dinucleotide (NAD^+) generation by salvage pathway. And the increased NAD^+ promoted Sirt1 expression. In conclusion, TMZ can prevent renal dysfunction and pathogenesis of tubulointerstitial fibrosis in DN, partly by inhibition of EMT *via* FoxO1/ROS pathway and TGFβ/Smad pathway in a Nampt/NAD^+/Sirt1 dependent manner.

Keywords: diabetic nephropathy, epithelial-to-mesenchymal transition, trimetazidine, Sirt1, reactive oxygen species

OPEN ACCESS

Edited by:
John D. Imig,
Medical College of Wisconsin, United States

Reviewed by:
Regalla Kumarswamy, Centre for Cellular & Molecular Biology (CCMB), India
Ariela Benigni, Mario Negri Pharmacological Research Institute (IRCCS), Italy

***Correspondence:**
Hong Wang
hong_wang1988@126.com

Specialty section:
This article was submitted to Renal Pharmacology, a section of the journal Frontiers in Pharmacology

Received: *17 October 2019*
Accepted: *13 July 2020*
Published: *29 July 2020*

Citation:
Yang Y, Wang Y, He Z, Liu Y, Chen C, Wang Y, Wang DW and Wang H (2020) Trimetazidine Inhibits Renal Tubular Epithelial Cells to Mesenchymal Transition in Diabetic Rats via Upregulation of Sirt1. Front. Pharmacol. 11:1136. doi: 10.3389/fphar.2020.01136

INTRODUCTION

Diabetic nephropathy (DN) is the leading cause of end-stage renal disease and increases the risk of death (Tuttle et al., 2014; Webster et al., 2017; Li et al., 2019). Glomerular lesions were previously considered the primary cause of renal function decline in the process of DN. However, the kidney is mainly composed of renal tubules, and the renal tubules are more sensitive to the injury of metabolic disorders than glomeruli (Gilbert, 2017). Emerging evidence suggests that renal tubular lesions play an important role in the occurrence and progression of this disease (Vaidya et al., 2011; Gilbert, 2017; Zeni et al., 2017). For example, tubulointerstitial fibrosis, which is the common final outcome of tubular lesions, is the most important predictor of the progression of DN (Taft et al., 1994; Grgic et al., 2012; Okada et al., 2012).

Renal tubular epithelial cells (TECs) can convert to myofibroblasts *via* a process known as epithelial-to-mesenchymal transition (EMT), which is characterized by the loss of an epithelial marker and an increased mesenchymal phenotype, results in increased production of extracellular matrix (ECM) and contributes to the development of chronic kidney diseases (CKD) (Hay and Zuk, 1995). Studies have shown that renal fibrosis could be ameliorated by blunting EMT in a variety of kidney diseases (Yang and Liu, 2002; Grande et al., 2015). In diabetes, high fat and high glucose (HFG) led to elevated levels of reactive oxygen species (ROS), transforming growth factor-β1 (TGFβ1), and other factors, thereby inducing EMT in TECs (Ha and Lee, 2003; Hills and Squires, 2011; Chen et al., 2018). And inhibition of EMT could alleviate renal dysfunction and the progression of tubulointerstitial fibrosis in DN (Shi et al., 2017; Zhao et al., 2017).

Trimetazidine (TMZ), a piperazine derivative, has been widely used in the treatment of coronary atherosclerotic heart disease *via* shifting cardiac energy metabolism from fatty acid oxidation to glucose oxidation (Kantor et al., 2000; Ferrari et al., 2019). TMZ can also alleviate fibrosis in diabetic cardiomyopathy (Zhang et al., 2016) or inhibit cardiac fibrosis induced by pressure-overload (Liu et al., 2010). Other than the beneficial effects on the heart, studies have shown the protective effects of TMZ on acute kidney injuries (AKI), such as contrast nephropathy, drug-induced nephrotoxicity, and ischemia/reperfusion injury (Hauet et al., 2000; Satyanarayana and Chopra, 2002; Onbasili et al., 2007). However, whether TMZ has a positive effect on CKD, specifically in cases of renal fibrosis and EMT, is rarely studied.

Sirt1, a protein deacetylase, is an essential modulator of cellular energy metabolism and aging (Rahman and Islam, 2011; Catana et al., 2018; Vasquez and Tomanek, 2019). It has been shown to suppress oxidative stress in kidney injuries (Wu et al., 2012; Dong et al., 2014) and is capable of inhibiting multiple organ fibrosis (Simic et al., 2013). Previous article showed that TMZ had an anti-ROS effect in sepsis-induced myocardial dysfunction *via* the activation of Sirt1 (Chen et al., 2016). We suspected that TMZ may affect the expression level of Sirt1 in DN and had a protective effect. ROS pathway and TGFβ/Samd pathway play a crucial role in the process of organ fibrosis (Xu et al., 2009; Wu et al., 2012). Transcriptional factor FoxO1 is regulated by Sirt1 and plays a role in anti-oxidative stress in DN (Wu et al., 2012), and Sirt1 inhibits the TGFβ/Smad pathway by deacetylating Smad2/3/4/7 (Garcia-Vizcaino et al., 2017; Wang et al., 2018). We speculated that Sirt1/FoxO1/ROS pathway and Sirt1/TGFβ/Smad pathway may be involved in the regulation of DN by TMZ. In the current study, we confirmed that TMZ could ameliorate renal fibrosis by inhibiting EMT and prevent the progression of CKD in a STZ-induced diabetic rat model. To further study the underlying mechanism, we investigated the role of Sirt1 in the process of EMT and how TMZ affects Sirt1 expression. Sirt1/FoxO1/ROS pathway and Sirt1/TGFβ/Smad pathway were involved in the inhibitory effect of TMZ on EMT in DN. In addition, our findings revealed that TMZ upregulates Sirt1 expression through the Nampt/NAD^+ pathway.

MATERIALS AND METHODS

Reagents

Streptozotocin (STZ, V900890) was purchased from Sigma-Aldrich (St. Louis, MO). TMZ was provided by Servier (Tianjin China). Sirt1 siRNA and non-targeted siRNA were purchased from RiboBio (Guangzhou China). Lipofectamine™ 2000 Transfection Reagent (11668019) was from Invitrogen (Carlsbad, CA, USA). Antibodies against Sirt1 (A11267), FN (A12932), Sirt3 (A5718), and pan-acetyl lysine (A2391) were purchased from Abclonal (Cambridge, MA, USA). Antibodies against E-cadherin (20874-1-AP), Col1a1 (A1352), α-SMA (55135-1-AP), TGFβ1 (21898-1-AP), FoxO1 (18592-1-AP), Smad4 (10231-1-AP), Nampt (11776-1-AP), and β-actin (60008-1-Ig) were purchased from Proteintech Group (Wuhan, China). Antibody against TGFβRI (sc-518018) was from Santa Cruz Biotechnology (Dallas, TX, USA). Antibody against p-Ampk (50081) was from Cell Signaling Technology (Danvers, MA, USA). Dihydroethidium (DHE, S0063), N-acetyl-L-cysteine (NAC, S0077), hydrogen peroxide detection kit (S0038), Sod activity detection kit (S0101), and NAD^+/NADH detection kit (S0175) were from Beyotime Biotechnology (Shanghai China). NAD^+ (HY-B0445), FK866 (HY-50876), and Compound C (CC, HY-13418) were purchased from MedChemExpress (Shanghai China).

Animals and Experimental Protocol

Male Sprague-Dawley rats (8 weeks old, 200–220 g) were purchased from Hubei Research Centre of Laboratory Animals (Wuhan, China). Diabetes was induced by intraperitoneal injection of STZ (55 mg/kg in 0.1 mol/L citrate buffer, adjusted to pH 4.5). Rats in the control group received equal volumes of citrate buffer (n = 7). Diabetes was verified 72 h later after STZ injection by measuring blood glucose levels. Rats with fasting blood glucose > 11.1 mmol/L were selected as qualified diabetic models and used in the study (n = 15). Two weeks after the onset of diabetes, diabetic rats were randomly divided into two groups: rats in the DN group (n = 8) received vehicle (0.9% saline

solution), and rats in the DN + TMZ group (n = 7) received TMZ (5 mg/kg/day), respectively. The medications were given by oral gavage. After 20 weeks of treatment, blood and urine samples were taken for metabolite measurements. The rats were then sacrificed, and tissue samples were collected and stored at −80°C for paraffin embedding or snap frozen. All animal studies were approved by the Animal Research Committee of Tongji Medical College and followed the guidelines of the National Institutes of Health.

Analysis of Plasma and Urine Metabolites

Plasma levels of glucose, triglyceride, cholesterol, creatinine, and urea nitrogen and urine levels of albumin, creatinine, and N-acetyl-β-D-glucosaminidase (β-NAG) were detected using assay kits from Nanjing Jiancheng Bioengineering Institute (Nanjing, China) following the manufacturer's instructions.

Histology and Immunohistochemical Staining

Kidney tissues were fixed with 4% paraformaldehyde, then dehydrated and embedded in paraffin. Sections (4 mm thick) were subjected to hematoxylin-eosin (HE), periodic acid Schiff (PAS), and Sirius Red staining. Glomerular area, mesangial area/glomerular area, and proximal tubular inner diameter were measured as previously described (Gotoh et al., 2010; Wu et al., 2015; Irsik et al., 2018). Glomerular collagen content percentage was calculated by comparing the Sirius Red staining positive area in glomeruli to the total glomerular area. Tubulointerstitial collagen content percentage was calculated by comparing the Sirius Red staining positive area in the renal tubulointerstitium to the total renal tubular interstitial area. The ultrastructure of the kidney was observed using a transmission electron microscope (TEM; Hitachi, Tokyo, Japan), according to the method described previously (Kalimuthu et al., 2018). Immunohistochemistry and immunofluorescence staining were conducted as described previously (Oshimori and Fuchs, 2012; Wang et al., 2019).

Cell Culture, Transfection, and Treatment

HK-2 cell lines were purchased from the Cell Bank of the Chinese Academy of Sciences (Shanghai, China), and grown in DMEM/F12 supplemented with 10% FBS. Cells were transfected with siRNA against human Sirt1 (si-Sirt1, 100 nM) or negative control (si-NC, 100 nM), using Lipofectamine 2000, according the manufacturer's protocol. After transfection, cells were incubated with normal glucose (5 mM) or high fat (100 μM Palmitic acid) and high glucose (30 mM) for 48 h and then collected.

Western Blotting

Kidney tissues and cells were collected using Protein or IP lysate (Beyotime Technology, Shanghai, China). The protein concentration was measured by BCA kit (Boster, Wuhan, China). A total of 10% gradient gels were used. The α-SMA antibody was diluted at 1:3,000, the β-actin antibody at 1:5,000, and the others at 1:1,000. Density analysis of the bands was performed using Gel Pro analysis software.

Detection of Oxidative Stress Indexes

In order to reflect the degree of oxidative stress in tissues and cells under different treatment conditions, H_2O_2 levels, Sod activity, and DHE staining were all used for detection, according to the kit instructions.

Protein Acetylation Assay

Forkhead box O1 (FoxO1) and Smad4 acetylation were measured by immunoprecipitation of collected protein lysate using antibody against FoxO1 and Smad4 respectively. Thereafter, acetylated-FoxO1 and acetylated-Smad4 were assessed with anti-pan acetyl lysine antibody.

Detection of NAD^+/NADH

The levels of nicotinamide adenine dinucleotide (NAD^+) and NADH in kidney tissue and HK-2 cells were detected by the NAD^+/NADH assay kit, according to the manufacturer's instructions. In brief, renal cortex (10 mg/sample) and HK-2 cells (1×10^6 cells/sample) were lysed with 200 μl of NAD^+/NADH extraction reagent. In order to detect the total amount of NAD^+ and NADH, 20 μl of lysate was added to a 96-well plate. To determine the content of NADH, the lysates was incubated at 60°C for 30 min to remove NAD^+, and then 20 μl of supernatant was added to a 96-well plate. Subsequently, 90 μl of alcohol dehydrogenase working solution was added and incubated at 37°C for 10 min. Finally, 10 μl of color reagent was added to the 96-well plate and incubated at 37°C for 30 min. The absorbance was measured at 450 nm. According to the standard curve, the total content of NAD^+/NADH and the content of NADH were calculated. The NAD^+ content was equal to the total content minus the NADH content.

Statistics

Results were expressed as mean ± SEM. One-way analysis of variance (ANOVA) with Newman-Keuls post analysis was used to compare the means of three or more different treatment groups. A $P < 0.05$ was considered to be significant.

RESULTS

TMZ Mitigated Renal Dysfunction in STZ-Induced Diabetic Rats

After 20 weeks of STZ injection, metabolic indices associated with diabetes were measured. The weight gain of these rats was significantly reduced, but blood glucose, serum triglyceride and cholesterol levels were markedly increased. Treatment with TMZ in diabetic rats did not change these metabolic indices or blood pressure (**Table 1**). All renal function parameters measured in the study, including plasma creatinine, blood urea nitrogen, urine albumin to urine creatinine ratio, and urine β-NAG to urine creatinine ratio were significantly increased in diabetic rats compared with normal control rats. Interestingly, treating with TMZ blunted these changes markedly (**Figures 1A–D**).

These results indicate that diabetic rats induced by STZ injection experience a remarkable decline in renal function,

TABLE 1 | Biochemical and physical parameters of diabetic rats after TMZ treatment.

Group	Control	DN	DN + TMZ
N	7	8	7
Body weight (g)	566.57 ± 12.30	296.00 ± 15.69*	296.57 ± 9.42
Plasma glucose (mM)	5.84 ± 0.21	26.50 ± 2.56*	26.04 ± 2.81
Plasma triglyceride (mM)	1.29 ± 0.13	3.70 ± 1.02*	3.21 ± 0.79
Plasma cholesterol (mM)	2.02 ± 0.24	4.18 ± 0.41*	4.40 ± 0.44
SBP (mmHg)	141.29 ± 3.65	144.00 ± 3.28	140.60 ± 6.32
DBP (mmHg)	105.67 ± 2.32	95.96 ± 4.38	99.33 ± 4.98

SBP, systolic blood pressure; DBP, diastolic blood pressure.
*Values represent mean ± SEM. *P < 0.05 (one-way ANOVA with Newman-Keuls post analysis).*

which can be mitigated by treating with TMZ independent of affecting blood pressure and systemic metabolic levels.

TMZ Attenuated Glomerular and Tubulointerstitial Remodeling in STZ-Induced Diabetic Rats

To investigate the effects of TMZ on renal pathological changes in STZ-induced diabetic rats, tissue sections of glomeruli and renal tubules were assessed. Glomerular area, ratio of mesangial area to glomerular area, and ratio of glomerular collagen fiber area to glomerular area (glomerular collagen content percentage) were calculated to evaluate glomerular remodeling. In HE-stained tissue sections, the glomerular area was significantly increased in STZ-injected rats compared to control rats, and treating with TMZ had no effect on glomerular enlargement induced by STZ injection (**Figure 2A-a**). Glomerular mesangial expansion was evaluated by PAS staining. Compared with the control group, the ratio of mesangial area to glomerular area increased significantly in diabetic rats, and was ameliorated by treatment of TMZ (**Figure 2A-b**). Sirius Red staining was used to assess the deposition of glomerular collagen fibers. STZ injection significantly increased the glomerular collagen area, while TMZ treatment partially reversed the collagen deposition (**Figure 2A-c**). To observe the changes of glomerular ultrastructure, transmission electron microscopy (TEM) was used in the experiment. In diabetic rats, the shape of podocytes was irregular and flattened. TMZ treatment alleviated these changes (**Figure 2A-d**).

To evaluate pathological changes of the renal tubules, renal tubular vacuolization, proximal tubule inner diameter, renal interstitial collagen deposition, and renal tubule ultrastructure were investigated. Compared with the control rats, a large

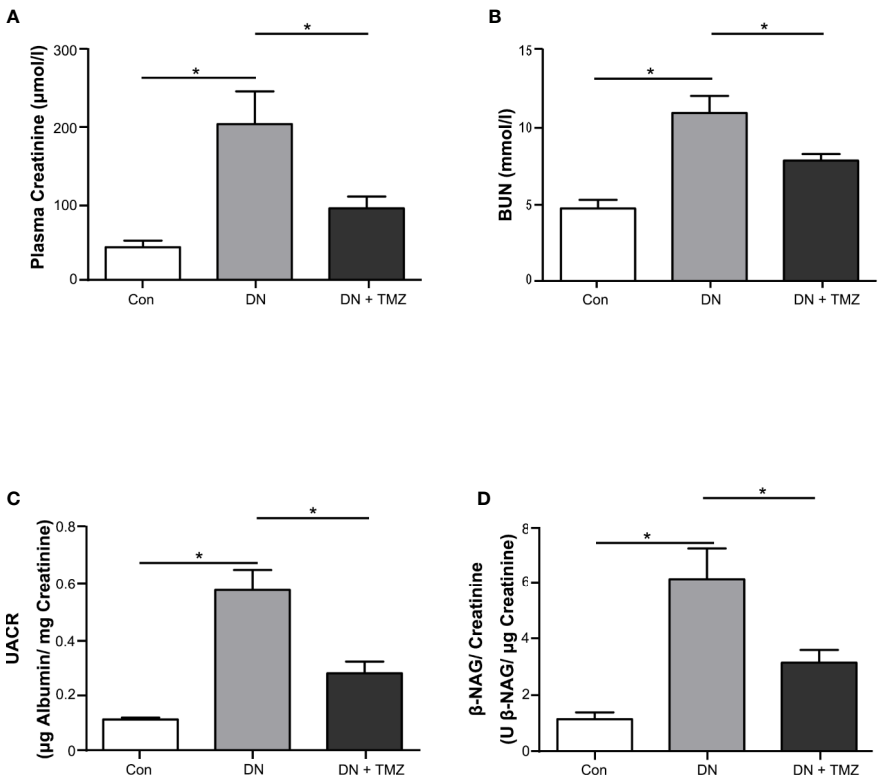

FIGURE 1 | Trimetazidine (TMZ) preserved renal function in streptozotocin (STZ)-induced diabetic rats. Plasma and urine were collected before the experimental rats sacrificed. **(A, B)** Plasma creatinine and BUN determined after 20 weeks of TMZ treatment. **(C, D)** Calculated values of UACR and β-NAG/creatinine in urine samples. BUN, blood urea nitrogen; UACR, urine albumin to urine creatinine ratio; β-NAG, N-acetyl-β-D-glucosaminidase; Con, control group; DN, diabetic nephropathy group; DN + TMZ, TMZ-treated DN group. Data in **(A–D)** were expressed as mean ± SEM (n = 7–8). *$P < 0.05$ (one-way ANOVA with Newman-Keuls post analysis).

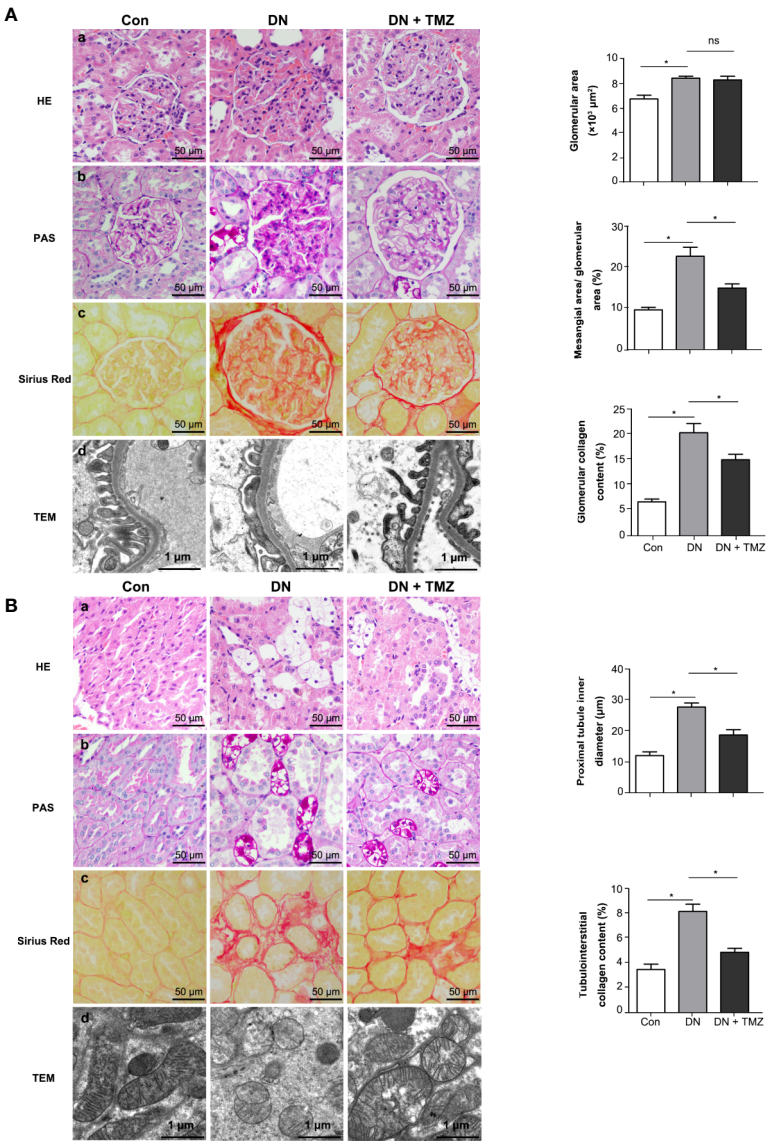

FIGURE 2 | Trimetazidine (TMZ) attenuated glomerular and tubular interstitial remodeling in streptozotocin (STZ)-induced diabetic rats. **(A)** Pathological examination of glomeruli. (a–c) Representative images of HE, PAS, and Sirius Red staining of glomeruli from different groups (left panel). Scale bar, 50 μm. Bar graphs representing analyzed glomerular area, the ratio of mesangial area to glomerular area, glomerular collagen content percentage (right panel). Data were expressed as mean ± SEM (n = 5, the value of each variable was derived from the average of 20 glomeruli per rat). *$P < 0.05$ (one-way ANOVA with Newman-Keuls post analysis). (d) Representative images of TEM of glomeruli from different groups. Scale bar, 1 μm. **(B)** Pathological detection of tubulointerstitium. (a–c) Representative images of HE, PAS and Sirius Red staining of tubulointerstitium from different groups. Scale bar, 50 μm (left panel). Bar graphs representing analyzed proximal tubule inner diameter, tubulointerstitial collagen content percentage. Data were expressed as mean ± SEM (n = 5, the value of each variable was derived from the average of 20 analyses per rat). *$P < 0.05$ (one-way ANOVA with Newman-Keuls post analysis). (d) Representative images of TEM of renal tubules from different groups. Scale bar, 1 μm. HE, hematoxylin-eosin staining; PAS, periodic acid schiff staining; Con, control group; DN, diabetic nephropathy group; DN + TMZ, TMZ-treated DN group.

number of vacuolated TECs were observed in STZ-induced diabetic rats. This morphological alteration in renal tubular cells was ameliorated by the administration of TMZ (**Figure 2B-a**). In addition, there was a notable increase of the inner diameter of the tubules in the kidneys of diabetic rats, while it was apparently reduced following TMZ treatment (**Figure 2B-b**). On the other hand, collagen deposition increased distinctly in the tubulointerstitial of diabetic rats. This change was also significantly ameliorated in the TMZ treated group (**Figure 2B-c**). The mitochondria were elongated and the mitochondrial crest was clear in the normal group. While in the DN group, the mitochondria were small and round, and the mitochondrial crest was unclear. TMZ treatment improved the mitochondrial morphological changes (**Figure 2B-d**).

These data suggest that STZ-induced diabetic rats experience significant pathological alterations on both glomeruli and renal tubules. TMZ treatment can effectively reverse these changes, at least in part. Particularly, the protective effects of TMZ on DN may be more prominent on the renal tubules than glomeruli.

TMZ Suppressed Renal Tubular EMT

To investigate whether the beneficial effect of TMZ against tubulointerstitial fibrosis was *via* inhibiting EMT in renal tubule, markers of fibrosis and EMT were measured. Immunohistochemical staining of renal tissue sections showed that the expression levels of FN and Col1a1 were predominantly increased in renal tubules of rats that had experienced STZ-injection, while these were markedly decreased after TMZ treatment (**Figure 3A**). Immunofluorescent staining of EMT markers, including E-cadherin and α-SMA, showed that expression of E-cadherin was decreased and expression of α-SMA was increased in renal tubules of rats with STZ-injection, whereas these changes were reversed by TMZ treatment (**Figure 3B**). *In vitro* experiments, HFG-induced EMT in HK-2 cells, characterized by decreased E-cadherin and elevated α- SMA. However, as the treatment concentration of TMZ increased, these alterations were gradually reversed (**Figure 3C**). Vimentin is another marker of cells of mesenchymal origin; β-catenin and E-cadherin are connected in the cytoplasm, and the reduction of E-cadherin will cause the translocation of β-catenin from the cytoplasm to the nucleus (Simic et al., 2013). Vimentin and β-catenin are two other markers of EMT. In this study, their changes were consistent with E-cadherin and α-SMA (**Supplementary Figure 1**).

These results suggest that EMT in tubulointerstitial fibrosis is involved in STZ-induced DN and that treating with TMZ could attenuate this pathological progression.

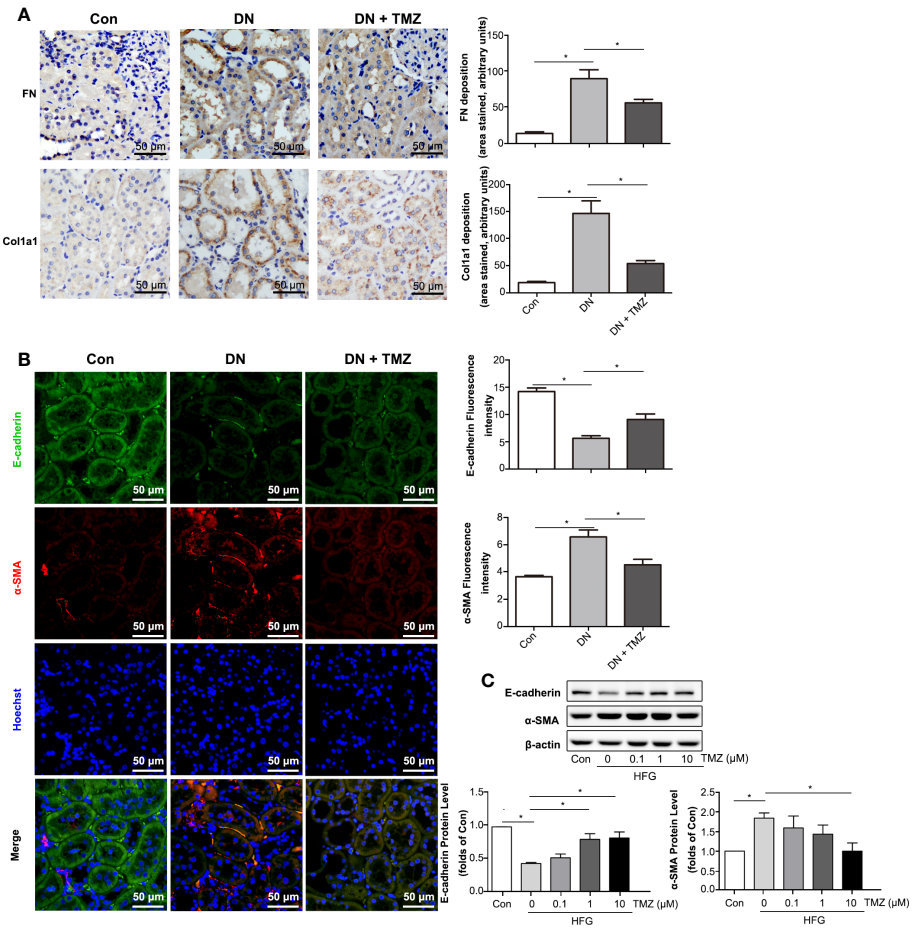

FIGURE 3 | Trimetazidine (TMZ) suppressed renal tubular EMT. **(A)** Relative FN and Col1a1 expression levels in renal cortex measured by immunohistochemical staining. Scale bar, 50 μm. The bar graph illustrated the quantitative analysis of FN and Col1a1 staining. **(B)** Representative images of immunofluorescence staining for E-cadherin (green), α-SMA (red), and Hoechst (blue). Scale bar, 50 μm. The bar graph on the right showed the quantitative analysis of E-cadherin and α-SMA staining. **(A, B)** Con, control group; DN, diabetic nephropathy group; DN + TMZ, TMZ-treated DN group. **(C)** Western blots analysis of the expression of E-cadherin and α-SMA in HK-2 cells treated with different concentrations of TMZ and exposed to HFG for 48 hours. Con, normal control; HFG, high fat and high glucose. Data are expressed as mean ± SEM (n = 3), **P* < 0.05 (one-way ANOVA with Newman-Keuls post analysis).

TMZ Suppressed EMT by Reducing ROS Production

Oxidative stress has been shown to be associated with EMT. Therefore, DHE staining, H_2O_2 level, and Sod activity were performed to investigate the effect of TMZ treatment on ROS production. Results showed that ROS production greatly increased in the kidney tissues of diabetic rats, while TMZ treatment ameliorated the generation of ROS (**Figures 4A–C**). Similarly, TMZ treatment could also inhibit the production of ROS induced by HFG in cultured HK-2 cells (**Figure 4D**). Furthermore, a ROS scavenger called NAC was used to verify whether ROS played a key role in HFG-induced EMT in HK-2 cells. The results showed that NAC could significantly reverse HFG-induced EMT (**Figure 4E**). Therefore, we propose that TMZ may inhibit EMT in DN by reducing ROS levels.

TMZ Reduced HFG-Induced ROS Generation and EMT Depending on Upregulation of Sirt1

Previous studies have shown that Sirt1 and Sirt3 have anti-oxidant activity (Wu et al., 2012). We wondered if they were involved in EMT in DN. In addition, they are regulated by the energy state (Noriega et al., 2011), and TMZ is an energy regulator. Therefore, we suspect that TMZ may affect the

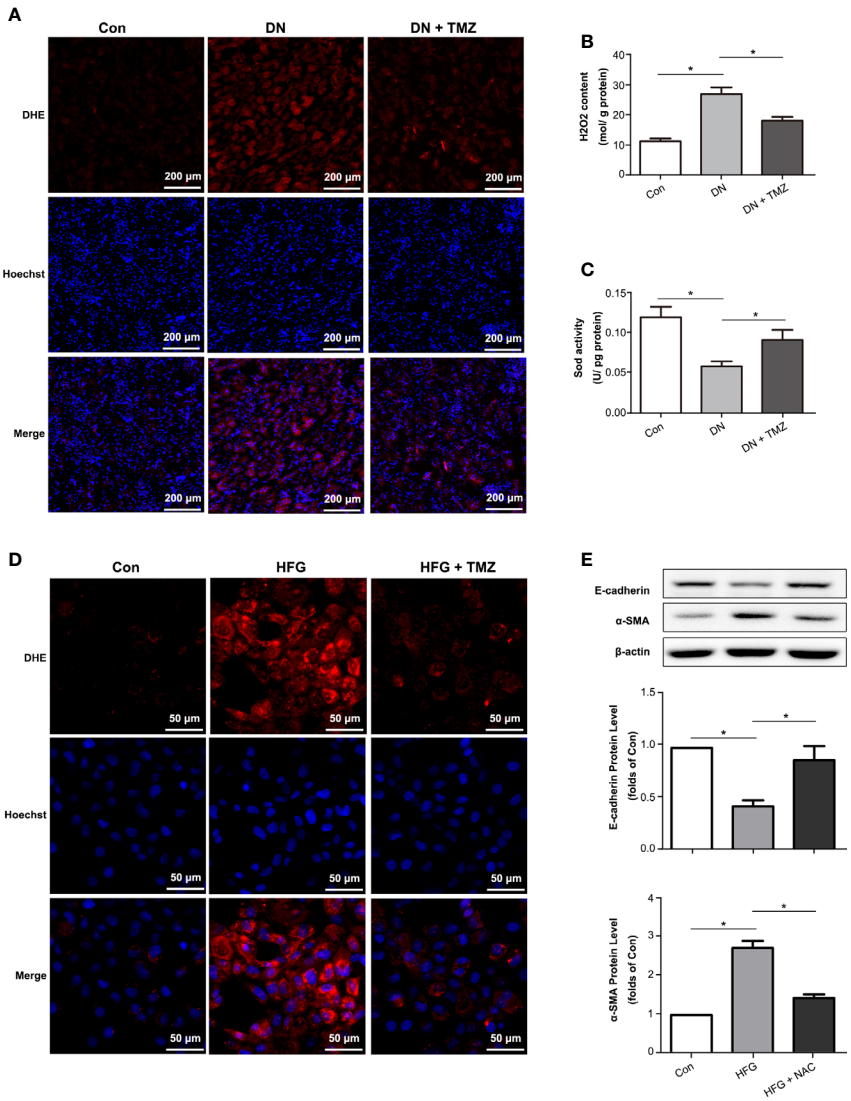

FIGURE 4 | Trimetazidine (TMZ) suppressed HFG-induced EMT by reducing ROS levels in diabetic nephropathy. **(A)** Images of DHE fluorescence in renal cortex from different groups. Scale bar, 200 μm. **(B)** H_2O_2 content in renal cortex from different groups. **(C)** Sod activity in renal cortex from different groups. **(A–C)** Con, control group; DN, diabetic nephropathy group; DN + TMZ, TMZ treated DN group. Data were expressed as mean ± SEM (n = 3), $^*P < 0.05$ (one-way ANOVA with Newman-Keuls post analysis). **(D)** Images of DHE fluorescence in HK-2 cells treated with HFG and/or TMZ. Scale bar, 50 μm. **(E)** Western blots analysis of E-cadherin and α-SMA in HK-2 cells treated with HFG and/or NAC. **(B, C)** Con, normal control; HFG, high fat and high glucose; HFG + NAC, high fat and high glucose group treated with NAC. Data were expressed as mean ± SEM (n = 3), $^*P < 0.05$ (one-way ANOVA with Newman-Keuls post analysis).

expression level of them. In our study, both Sirt1 and Sirt3 were significantly down-regulated in DN, and TMZ intervention could significantly restore the expression level of Sirt1. Although the level of Sirt3 was increased in the TMZ treatment group, it was not as obvious as that of Sirt1 (**Figure 5A-a**). Therefore, we mainly study from the perspective of Sirt1. *In vitro* experiments, the Sirt1 protein level was significantly decreased in HK-2 cells when exposed to the HFG environment, and this change was ameliorated by TMZ incubation in a dose-dependent manner (**Figure 5A-b**). DHE fluorescence revealed that the inhibitory effect of TMZ on the ROS production was weakened when Sirt1 was silenced (si-Sirt1) in HFG treated HK-2 cells (**Figure 5B**). After silencing Sirt1, upregulation of E-cadherin and downregulation of α-SMA by TMZ treatment were reversed. This suggested that silencing Sirt1 blunted the role of TMZ in the inhibition of the EMT program induced by HFG (**Figure 5C**). Transcriptional factor FoxO1 is regulated by Sirt1 and plays a role in antioxidative stress (Wu et al., 2012). Therefore, acetylated FoxO1 and the expression level of Sod2, the downstream of antioxidant gene of FoxO1, were examined. While HFG increased the level of acetylated FoxO1, TMZ could inhibit acetylation of FoxO1 and this effect was reversed

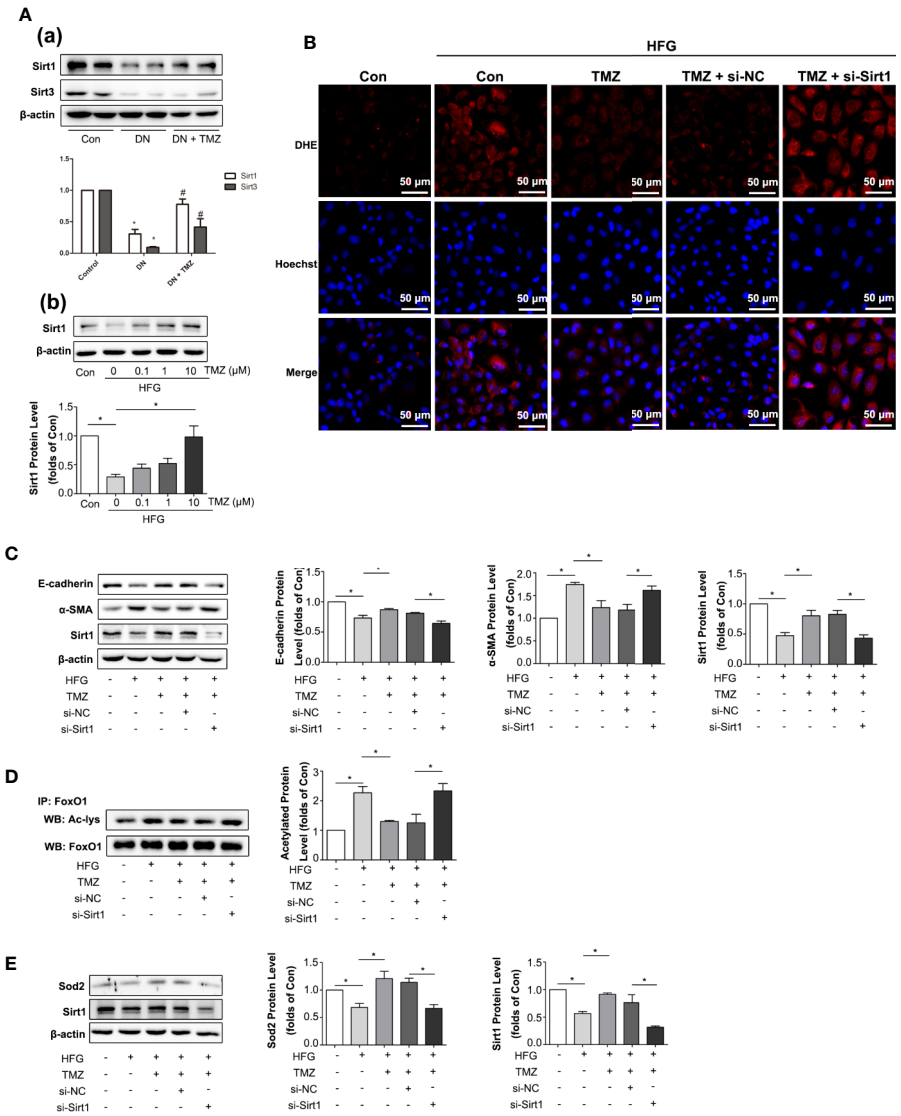

FIGURE 5 | Trimetazidine (TMZ) reduced HFG-induced ROS generation and EMT depending on upregulation of Sirt1. **(A-a)** Western blots analysis of Sirt1 and Sirt3 in the kidneys of diabetic rats and TMZ treated rats. **(A-b)** Western blots analysis of Sirt1 in HK-2 cells treated with HFG and different concentrations of TMZ for 48 h. **(B–E)** HK-2 cells were treated with or without HFG, TMZ, si-NC and si-Sirt1 for 48 h. **(B)** Images of DHE fluorescence. Scale bar, 50 μm. **(C)** Western blots analysis of E-cadherin, α-SMA and Sirt1. **(D)** The relative expression level of acetylated-FoxO1 measured by IP. **(E)** Western blots analysis of Sod2 and Sirt1. Con, normal control; HFG, high fat and high glucose; IP, immunoprecipitation; WB, western blot; Ac-lys, acetyl lysine level. Data were expressed as mean ± SEM (n = 3), $^{*}P < 0.05$ (one-way ANOVA with Newman-Keuls post analysis).

by silencing Sirt1 (**Figure 5D**). Furthermore, the elevated expression of downstream gene Sod2 was seen by TMZ treatment but diminished after silencing Sirt1 (**Figure 5E**).

These data suggest that HFG induces EMT program in HK-2 cells by enhancing FoxO1 acetylation and reducing expression of its downstream antioxidant proteins, whereas TMZ reverses this process through Sirt1/FoxO1/ROS pathway, specifically by inhibiting the acetylation of FoxO1.

TMZ Reduced TGFβ1-Induced EMT Depending on Sirt1 Upregulation

TGFβ1 serves as one of the most important cytokines in the process of EMT in kidney (Xu et al., 2009; Iwano, 2010). We then investigated whether TMZ played the role in inhibition EMT through Sirt1/TGFβ1 pathway. We first assessed the expression levels of TGFβ1 and TGFβRI in HK-2 cells after exposure to HFG. The results showed HFG could apparently increase the expression level of TGFβ1 and TGFβRI. However, TMZ had no effect on the elevation of TGFβ1 and TGFβRI induced by HFG (**Figure 6A**). TGFβ1 could induce EMT in HK-2 cells, verified by the decreased expression of E-cadherin and the increased expression level of α-SMA that was seen in a dose dependent manner. These results were accompanied with downregulation of Sirt1 protein levels (**Figure 6B**). Although TMZ had no effect on expression of TGFβ1 and TGFβRI, TMZ intervention could alleviate TGFβ1-induced EMT verified by corresponding changes of E-cadherin and α-SMA expression. Moreover, the effect of TMZ on TGFβ1-induced EMT declined after silencing Sirt1. It suggested that TMZ affected TGFβ1-induced EMT *via* upregulating Sirt1 (**Figure 6C**). Further experiments found TGFβ1 could increase the level of acetylated Smad4, which was reversed after TMZ treatment. However, the effect of TMZ on acetylation of Smad4 was declined after silencing Sirt1 (**Figure 6D**).

These results indicate that HFG can induce EMT *via* the TGFβ1 pathway. TMZ doesn't affect TGFβ1 or TGFβRI but rather through deacetylation of Smad4 in a Sirt1 dependent way, thereby attenuating TGFβ1-induced EMT.

TMZ Upregulated Sirt1 Expression in a Nampt/NAD$^+$ Dependent Manner in DN

Nicotinamide adenine dinucleotide (NAD^+) is known for as an essential coenzyme that mediates redox reactions. In addition, it is a substrate for NAD^+-dependent enzyme such as sirtuins and

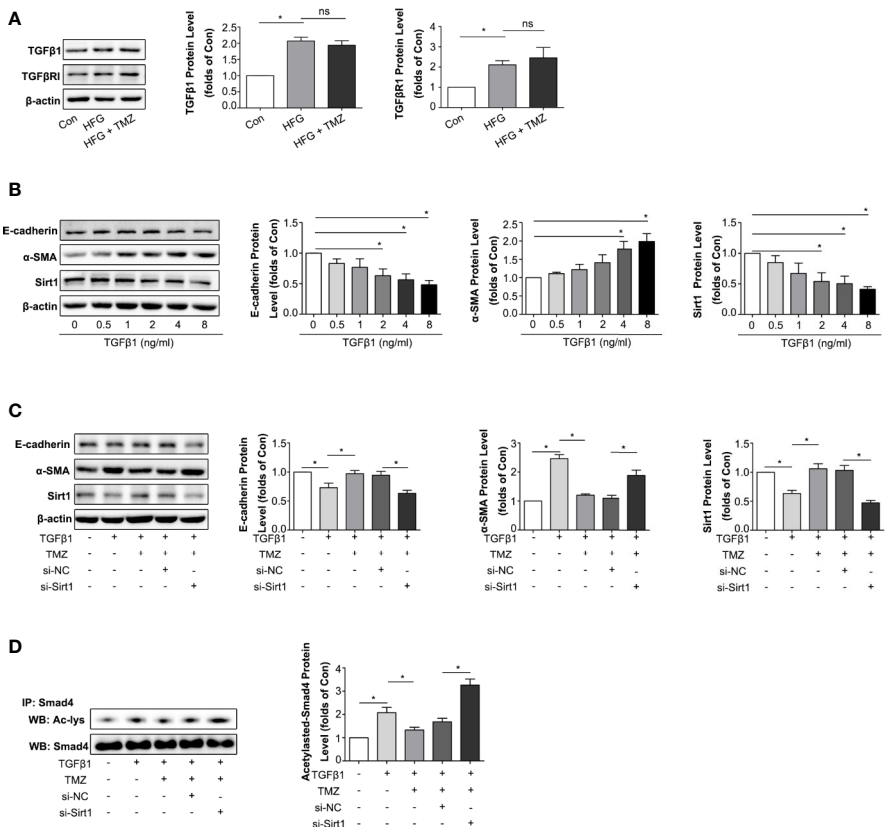

FIGURE 6 | Trimetazidine (TMZ) reduced TGFβ1 induced EMT by a restoration of Sirt1 expression. **(A)** Western blots analysis of TGFβ1 and TGFβRI in HK-2 cells treated with HFG and/or TMZ. **(B)** Western blots analysis of E-cadherin, α-SMA and Sirt1 in HK-2 cells treated with different concentrations of TGFβ1. **(C, D)** HK-2 cells were treated with or without TGFβ1, TMZ, si-NC and si-Sirt1 for 48 h. **(C)** Western blots analysis of E-cadherin, α-SMA and Sirt1. **(D)** The relative expression level of acetylated-Smad4 measured by IP. Con, normal control; IP, immunoprecipitation; WB, western blot; Ac-lys, acetyl lysine level. Data were expressed as mean ± SEM (n ≥ 3), $^*P < 0.05$ (one-way ANOVA with Newman-Keuls post analysis).

PARPs (Garten et al., 2015). It has been reported that NAD^+ affects not only Sirt1 activity, but also its expression level (Revollo and Li, 2013). NADH is the reduced state of NAD^+, which has the opposite effect on Sirt1 expression (Hayashida et al., 2010). As a metabolic regulator, TMZ may regulate intracellular NAD^+ level by affecting cellular redox status. In this study, we detected the levels of NAD^+ and NADH in TMZ treated diabetic rats. The results showed that TMZ increased the content of NAD^+ and the ratio of NAD^+ to NADH (NAD^+/NADH) in diabetic rats (**Figure 7A**). There are many factors that can regulate the NAD^+ content in cells, of which Nampt and p-Ampk are two important ones (Belenky et al., 2007; Canto et al., 2009). Therefore, we tested their expression. The results showed that TMZ treatment increased the expression of both (**Figures 7B, C**). Inhibiting their activity could significantly reduce the content of NAD^+, and FK866 (an inhibitor of Nampt) was more effective than Compound C (CC, an inhibitor of Ampk) (**Figure 7D**). Administration of different concentrations of NAD^+ in HFG-treated HK-2 cells could increase the expression of Sirt1 in a concentration-dependent manner (**Figure 7E**). After the administration of Nampt and Ampk inhibitor, respectively, the up-regulation effect of TMZ on Sirt1 was weakened by FK866 rather than CC (**Figure 7F**). A possible explanation is that CC raised NAD^+/NADH (**Figure 7D**). Correspondingly, NAD^+ supplementation rescued the inhibitory effect of FK866 on Sirt1 expression (**Figure 7F**).

These results indicated that regulation of TMZ on Sirt1 expression is dependent on the Nampt/NAD^+ pathway.

DISCUSSION

In this study, we aimed to investigate the effects of TMZ on DN, specifically on EMT and renal fibrosis. We found that treatment with TMZ could alleviate renal insufficiency and renal pathological remodeling in rats experiencing DN by STZ. This worked partially by the inhibition of EMT. Sirt1/FoxO1/ROS and Sirt1/TGFβ1/Smad4 pathways were involved in the inhibition of EMT by TMZ treatment, and Nampt/NAD^+ pathway was related to how TMZ affects Sirt1 expression in DN (**Figure 8**).

TMZ is recognized as an anti-ischemic agent because of its metabolic benefits in treating myocardial ischemia. Studies also suggest the beneficial effect of TMZ on other heart diseases, including ischemia reperfusion injury, hypertrophic cardiomyopathy, diabetic cardiomyopathy, and chronic heart failure (D'Hahan et al., 1997; Zhang et al., 2012; Liu et al., 2016; Zhang et al., 2016). The possible role of TMZ in kidney diseases has been suggested by a few studies, which indicate that TMZ may have protective effects on drug or contrast induced nephrotoxicity (Satyanarayana and Chopra, 2002; Chander et al., 2003; Onbasili et al., 2007) and kidney transplant reperfusion injury (Hauet et al., 2000; Faure et al., 2003). The mechanisms are related to the inhibition of inflammatory reactions, reductions in oxidation stress, anti-apoptosis, and improvements in endothelial dysfunction (Onay-Besikci and Ozkan, 2008; Chrusciel et al., 2014). All of these studies were conducted with a focus on AKI. However, the role of TMZ in CKD has rarely been reported. We speculated that TMZ may also have protective effects on CKD. In this study, we observed that early administration of TMZ could alleviate renal insufficiencies and pathological remodeling in STZ-induced diabetic rats. Interestingly, the beneficial effects of TMZ on DN were more prominent in renal tubules than glomeruli. A previous study by Tugba Karadeniz *et al.* reported similar effects of TMZ on DN as well as the finding that TMZ was more protective of the renal tubular and interstitial region by reducing FN and i-NOS expression (Karadeniz et al., 2014). Different from their work, our study focused on the inhibition of tubulointerstitial fibrosis by TMZ.

Our results indicated that TMZ could inhibit tubulointerstitial fibrosis dramatically in diabetic rats. Renal fibrosis represents the final common pathway of CKD, which is mediated by fibroblast activation and their subsequent transformations into myofibroblasts. This results in excessive secretion of ECM, including FN, Col1a1, and ColIV (Eddy, 2014). Other than residual renal fibroblasts, myofibroblasts originated from TECs *via* a process called as EMT also plays an important role in the deposition of ECM (Stahl and Felsen, 2001; Kalluri and Neilson, 2003). We then specifically examined the role of TMZ on EMT program. Our findings suggest that the administration of TMZ can inhibit EMT in diabetic rats and in cultured cells exposed to HFG. Previous study has shown that ROS makes great contribution to EMT program in DN (Ha and Lee, 2003). Meanwhile, TMZ has been shown to have an evident antioxidant effect by inhibiting NADPH oxidase (Liu et al., 2010) or activating the Nrf2/Ho-1 pathway (Wan et al., 2017). These findings suggest that TMZ may inhibit EMT in DN through its antioxidant effect. In our study, TMZ treatment reduced ROS level in DN (**Figure 4**), and TMZ inhibited HFG-induced ROS and EMT production depending on Sirt1 protein level in HK-2 cells (**Figure 5**). Sirt3 also plays an important role in anti-ROS (Morigi et al., 2018). In our study, although Sirt3 decreased significantly as Sirt1 in DN, it increased slightly after TMZ intervention (**Figure 5A-a**). Therefore, Sirt3 may play a weak antioxidant role here. Mitochondria are the main place where cells produce ROS. Due to abnormal mitochondrial morphology and dysfunction, excessive ROS are produced in DN (Sharma, 2016). In present study, TMZ improved mitochondrial morphological abnormalities in renal tubular cells in DN. PGC1α plays an important role in regulating mitochondrial production and function (Scarpulla, 2008). Our results showed that TMZ reduced the acetylation level of PGC1α (**Supplementary Figure 3**). Therefore, TMZ may partially improve the mitochondrial function through the PGC1α pathway, thereby reducing intracellular ROS level.

Down-regulation of Sirt1 expression in proximal tubules has been found in diabetic rats and over-expressing Sirt1 in proximal tubules could prevent kidney injury (Hasegawa et al., 2013). Moreover, Sirt1 inhibits organ fibrosis (Simic et al., 2013) and suppresses oxidative stress (Wu et al., 2012; Zhu et al., 2019), and is regulated by the energy status of the cells (Noriega et al., 2011). TMZ as a metabolic regulator through inhibiting fatty acid

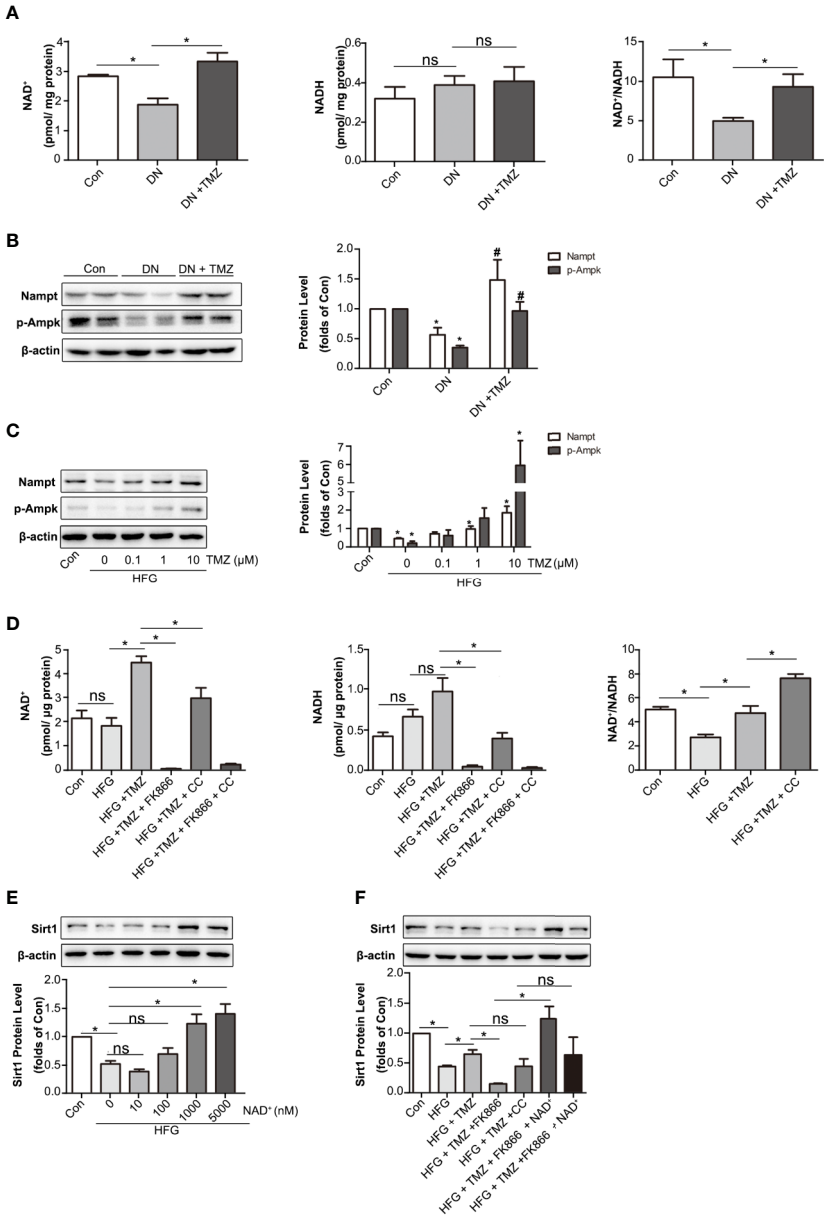

FIGURE 7 | Trimetazidine (TMZ) upregulated Sirt1 expression depending on Nampt/NAD^+ pathway in diabetic nephropathy. **(A)** The content of NAD^+ and NADH in TMZ treated DN, and the ratio of NAD^+ and NADH. **(B)** Western blots analysis of Nampt and p-Ampk in TMZ treated DN. **(C)** Western blots analysis of Nampt and p-Ampk in HK-2 cells treated with different concentrations of TMZ and exposed to HFG for 48 hours. **(D)** The content of NAD^+ and NADH in HK-2 cells with different treatment, and the ratio of NAD^+ and NADH. HK-2 cells were treated with 10 μM TMZ and exposed to HFG for 48 h. Nampt activity and Ampk activity were inhibited by FK866 and CC, respectively. **(E)** Western blots analysis of Sirt1 in HK-2 cells treated with different concentrations of NAD^+ and exposed to HFG for 48 hours. **(F)** Western blots analysis of Sirt1 in HK-2 cells with different treatment. CC, Compound c. Data were expressed as mean ± SEM (n ≥ 3), ***P* < 0.05 (one-way ANOVA with Newman-Keuls post analysis).

oxidation (Kantor et al., 2000; Lopaschuk et al., 2003), so it may regulate Sirt1 expression. In this study, we examined whether Sirt1 could be the action target of TMZ. First, TMZ administration could reverse the decline of Sirt1 *in vivo* and *in vitro* (**Figure 5A**). Second, the effect of TMZ on inhibiting the ROS production and subsequently EMT program induced by HFG *in vitro* was mediated *via* upregulating Sirt1 (**Figures 5B, C**). Third, TMZ reduced the acetylation level of FoxO1 *via* a restoration of Sirt1 expression and then increased the expression of the downstream antioxidant protein Sod2 (**Figures 5D, E**). Therefore, the Sirt1/FoxO1 pathway was involved in the inhibition of ROS production by TMZ. Forth, Although TMZ

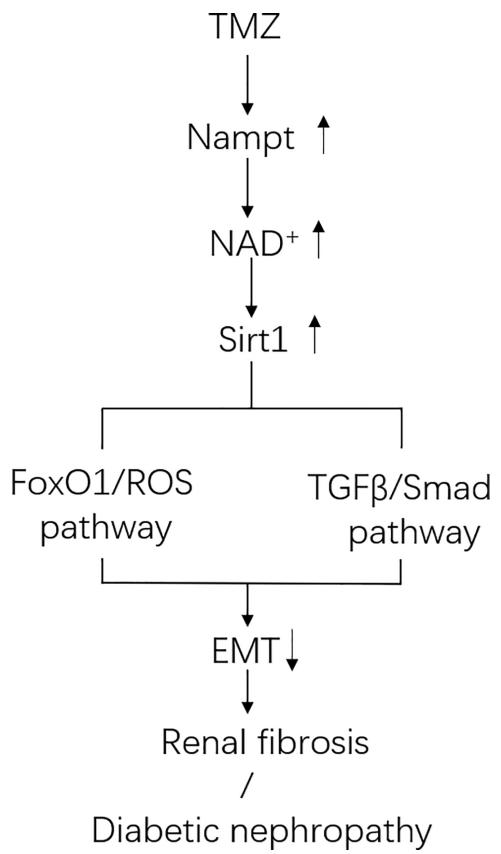

FIGURE 8 | Schematic of pathways involved in Trimetazidine (TMZ)-mediated EMT inhibition in DN. In diabetic environment, ROS pathway and TGFβ/Smad pathway together induce tubule epithelial cells (TECs) to produce EMT. TMZ inhibits EMT generation by suppressing these two pathways *via* upregulating Sirt1 expression in TECs in DN (Sirt1 inhibits the ROS pathway by deacetylating FoxO1, and inhibits TGFβ/Smad pathway by deacetylating Smad4). Both the expression and activity of Sirt1 are regulated by NAD^+. The generation of NAD^+ depends on *de novo* synthesis and salvage pathway, and the latter is its main source. Nampt is the rate-limiting enzyme of the salvage pathway. TMZ promotes NAD^+ production in DN by up-regulating Nampt expression. In conclusion, TMZ inhibits EMT generation by upregulating Sirt1 expression depending on Nampt/NAD^+ pathway in DN.

treatment did not affect HFG-induced upregulation of TGFβ1 and TGFβRI expression, we found it could relieve TGFβ1-induced EMT by reducing acetylated Smad4 level *via* upregulating Sirt1 (**Figure 6**). Therefore, Sirt1/TGFβ1/Smad4 pathway was also involved in the inhibition of EMT by TMZ. In conclusion, our results suggest that Sirt1 may be the key player for the anti-fibrotic effect of TMZ in DN.

In TGFβ/Smad pathway, TGFβ stimulated receptor complex leads to phosphorylation activation of Smad2 and Smad3. Phosphorylated Smad2 and Smad3 form a complex with Smad4 and enter the nucleus, and act as a transcriptional regulator to promote the expression of pro-fibrotic genes. In contrast, the inhibitory Smad6 and Smad7 suppress Smad2/3 activation (Xu et al., 2009). To date, Smad2/3/4/7 have been reported to be deacetylated by Sirt1 (Kume et al., 2007; Simic et al., 2013; Garcia-Vizcaino et al., 2017; Bugyei-Twum et al., 2018). A previous study showed Sirt1 inhibited TGFβ-induced apoptosis in glomerular mesangial cells *via* Smad7 deacetylation (Kume et al., 2007). There are some reports about the deacetylation of Smad2/3 by Sirt1 (Garcia-Vizcaino et al., 2017; Zhang et al., 2017; Bugyei-Twum et al., 2018). However, the deacetylation of Sirt1 on Smad2 is controversial (Simic et al., 2013; Chen et al., 2014). What is clearer is that Sirt1 can obviously deacetylate Smad4 (Simic et al., 2013; Chen et al., 2014). And Smad4, as a common mediator Smad, is necessary for the translocation of TGFβ/Smad family signals into the nucleus. In this study, in order to illustrate the effect of Sirt1 on TGFβ/Smad pathway in DN, we selected only Smad4 for this study. Other Smads, such as Smad2/3/7 may also be involved in the regulation of EMT by TMZ.

It has been reported that NAD^+ affects both Sirt1 activity and its expression level (Hayashida et al., 2010; Revollo and Li, 2013). In our study, TMZ increased NAD^+ content in DN. In order to investigate how TMZ affects NAD^+ content, we conducted a study on Nampt and p-Ampk. The generation of NAD^+ depends on *de novo* synthesis and salvage pathway, and the latter is its main source. Nampt is the rate-limiting enzyme of the salvage pathway (Belenky et al., 2007). Previous literature reported that Ampk increased NAD^+ content by increasing mitochondrial β-oxidation (Canto et al., 2009). In our study, only the effect of Nampt on Sirt1 expression was observed, Probably because Ampk reduced NAD^+/NADH (**Figure 7D**), or because of TMZ inhibition of β-oxidation. In previous studies, although inhibition of Nampt showed deleterious effects, the expression of Nampt was elevated in DN (Yilmaz et al., 2008; Benito-Martin et al., 2014). However, in our study, the expression of Nampt was decreased in DN (**Figures 7B, C**). This may be due to the decreased expression of Nampt in the later stages of DN. The study by Muraoka et al. explained this phenomenon (Muraoka et al., 2019).

In our study, TMZ showed a deacetylation effect by promoting Sirt1 expression. In order to observe whether the combination of TMZ and Sirt1 agonist has a synergistic effect, we administrated both TMZ and RSV in diabetic rats. The results showed both TMZ and RSV could relieve renal insufficiency, ROS, and EMT. However, the combination of the two showed no obvious synergistic effect (**Supplementary Figure 2**). The possible explanation is that, because they have the same mechanism of action, and the dosage of TMZ and RSV has reached the highest concentration of their effect in our experimental design, therefore, the combination of the two does not see a stronger anti-EMT effect.

Currently, the treatment of DN mainly consists of four parts: glycemic control, blood pressure control, inhibition of the renin-angiotensin system, and cardiovascular risk reduction (Umanath and Lewis, 2018). To date, no therapy specifically targeted at renal fibrosis is known. Although new hypoglycemic drugs with additional mechanisms are being tested for DN, such as SGLT2

inhibitor and GLP-1 activator (Warren et al., 2019), drugs targeting at renal fibrosis are needed to be used as adjuvant treatments to prevent the development and progression of DN. Our study demonstrates the renal protective effect of TMZ in relieving tubulointerstitial fibrosis in diabetic rats. Moreover, TMZ rarely has side effects in clinical practice in the past years. Therefore, TMZ is promising as a new adjuvant therapy for DN in the future. In our study, we found that TMZ was a potential Sirt1 agonist. Sirt1 has a protective effect on multiple organs, especially the heart (Gomes et al., 2019). Most patients with chronic renal failure are accompanied by cardiac insufficiency. Therefore, long-term use of TMZ in patients with DN may benefit from multiple organs and display a better result.

In conclusion, our study provides experimental evidences suggesting that TMZ can attenuate the development and the progression of renal dysfunction in DN. The underlying mechanism comes from TMZ's inhibition of tubulointerstitial fibrosis by blunting EMT. In detail, TMZ inhibits ROS pathway and TGFβ/Smad pathway to relieve EMT in a diabetic environment by upregulating Sirt1. Further clinical research will be needed to verify if TMZ is an effective adjuvant drug, in combination with hypoglycemic agents and other treatments, against DN.

LIMITATIONS

Our study focused on the effect of TMZ on diabetic renal tubular EMT. We did not examine the possible effect of TMZ on other pathological processes, such as apoptosis and inflammation. We also did not investigate the mechanisms of fibroblasts activation other than EMT. Future studies should consider these aspects in order to better understand the role of TMZ in DN.

DATA AVAILABILITY STATEMENT

All datasets generated for this study are included in the article/ **Supplementary Material**.

ETHICS STATEMENT

The animal study was reviewed and approved by The Animal Research Committee of Tongji Medical College.

AUTHOR CONTRIBUTIONS

YY contributed to the design of the study, data collection and drafting of this paper. YoW, ZH and YL participated in performing the study. CC, YaW and DW participated in designed the study. HW contributed to the design, organization of the work and prepared the manuscript.

FUNDING

This work was supported by National Natural Science Foundation of China (number: 81570367 and 81900341).

SUPPLEMENTARY MATERIAL

The Supplementary Material for this article can be found online at: https://www.frontiersin.org/articles/10.3389/fphar.2020.01136/full#supplementary-material

REFERENCES

Belenky, P., Bogan, K. L., and Brenner, C. (2007). NAD+ metabolism in health and disease. *Trends Biochem. Sci.* 32 (1), 12–19. doi: 10.1016/j.tibs.2006.11.006

Benito-Martin, A., Ucero, A. C., Izquierdo, M. C., Santamaria, B., Picatoste, B., Carrasco, S., et al. (2014). Endogenous NAMPT dampens chemokine expression and apoptotic responses in stressed tubular cells. *Biochim. Biophys. Acta* 1842 (2), 293–303. doi: 10.1016/j.bbadis.2013.11.022

Bugyei-Twum, A., Ford, C., Civitarese, R., Seegobin, J., Advani, S. L., Desjardins, J. F., et al. (2018). Sirtuin 1 activation attenuates cardiac fibrosis in a rodent pressure overload model by modifying Smad2/3 transactivation. *Cardiovasc. Res.* 114 (12), 1629–1641. doi: 10.1093/cvr/cvy131

Canto, C., Gerhart-Hines, Z., Feige, J. N., Lagouge, M., Noriega, L., Milne, J. C., et al. (2009). AMPK regulates energy expenditure by modulating NAD+ metabolism and SIRT1 activity. *Nature* 458 (7241), 1056–1060. doi: 10.1038/nature07813

Catana, C. S., Atanasov, A. G., and Berindan-Neagoe, I. (2018). Natural products with anti-aging potential: Affected targets and molecular mechanisms. *Biotechnol. Adv.* 36 (6), 1649–1656. doi: 10.1016/j.biotechadv.2018.03.012

Chander, V., Singh, D., and Chopra, K. (2003). Attenuation of glycerol-induced acute renal failure in rats by trimetazidine and deferoxamine. *Pharmacology* 67 (1), 41–48. doi: 10.1159/000066785

Chen, I. C., Chiang, W. F., Huang, H. H., Chen, P. F., Shen, Y. Y., and Chiang, H. C. (2014). Role of SIRT1 in regulation of epithelial-to-mesenchymal transition in oral squamous cell carcinoma metastasis. *Mol. Cancer* 13, 254. doi: 10.1186/1476-4598-13-254

Chen, J., Lai, J., Yang, L., Ruan, G., Chaugai, S., Ning, Q., et al. (2016). Trimetazidine prevents macrophage-mediated septic myocardial dysfunction via activation of the histone deacetylase sirtuin 1. *Br. J. Pharmacol.* 173 (3), 545–561. doi: 10.1111/bph.13386

Chen, Q., Su, Y., Ju, Y., Ma, K., Li, W., and Li, W. (2018). Astragalosides IV protected the renal tubular epithelial cells from free fatty acids-induced injury by reducing oxidative stress and apoptosis. *BioMed. Pharmacother.* 108, 679–686. doi: 10.1016/j.biopha.2018.09.049

Chrusciel, P., Rysz, J., and Banach, M. (2014). Defining the role of trimetazidine in the treatment of cardiovascular disorders: some insights on its role in heart failure and peripheral artery disease. *Drugs* 74 (9), 971–980. doi: 10.1007/s40265-014-0233-5

Dong, Y. J., Liu, N., Xiao, Z., Sun, T., Wu, S. H., Sun, W. X., et al. (2014). Renal protective effect of sirtuin 1. *J. Diabetes Res.* 2014, 843786. doi: 10.1155/2014/843786

D'Hahan, N., Taouil, K., Dassouli, A., and Morel, J. E. (1997). Long-term therapy with trimetazidine in cardiomyopathic Syrian hamster BIO 14:6. *Eur. J. Pharmacol.* 328 (2-3), 163–174. doi: 10.1016/s0014-2999(97)83042-7

Eddy, A. A. (2014). Overview of the cellular and molecular basis of kidney fibrosis. *Kidney Int. Suppl. (2011)* 4 (1), 2–8. doi: 10.1038/kisup.2014.2

Faure, J. P., Baumert, H., Han, Z., Goujon, J. M., Favreau, F., Dutheil, D., et al. (2003). Evidence for a protective role of trimetazidine during cold ischemia: targeting inflammation and nephron mass. *Biochem. Pharmacol.* 66 (11), 2241–2250. doi: 10.1016/j.bcp.2003.07.011

Ferrari, R., Pavasini, R., Camici, P. G., Crea, F., Danchin, N., Pinto, F., et al. (2019). Anti-anginal drugs-beliefs and evidence: systematic review covering 50 years of

medical treatment. *Eur. Heart J.* 40 (2), 190–194. doi: 10.1093/eurheartj/ehy504

Garcia-Vizcaino, E. M., Liarte, S., Alonso-Romero, J. L., and Nicolas, F. J. (2017). Sirt1 interaction with active Smad2 modulates transforming growth factor-beta regulated transcription. *Cell Commun. Signal* 15 (1), 50. doi: 10.1186/s12964-017-0205-y

Garten, A., Schuster, S., Penke, M., Gorski, T., de Giorgis, T., and Kiess, W. (2015). Physiological and pathophysiological roles of NAMPT and NAD metabolism. *Nat. Rev. Endocrinol.* 11 (9), 535–546. doi: 10.1038/nrendo.2015.117

Gilbert, R. E. (2017). Proximal Tubulopathy: Prime Mover and Key Therapeutic Target in Diabetic Kidney Disease. *Diabetes* 66 (4), 791–800. doi: 10.2337/db16-0796

Gomes, P., Leal, H., Mendes, A. F., Reis, F., and Cavadas, C. (2019). Dichotomous Sirtuins: Implications for Drug Discovery in Neurodegenerative and Cardiometabolic Diseases. *Trends Pharmacol. Sci.* 40 (12), 1021–1039. doi: 10.1016/j.tips.2019.09.003

Gotoh, N., Yan, Q., Du, Z., Biemesderfer, D., Kashgarian, M., Mooseker, M. S., et al. (2010). Altered renal proximal tubular endocytosis and histology in mice lacking myosin-VI. *Cytoskeleton (Hoboken)* 67 (3), 178–192. doi: 10.1002/cm.20435

Grande, M. T., Sanchez-Laorden, B., Lopez-Blau, C., De Frutos, C. A., Boutet, A., Arevalo, M., et al. (2015). Snail1-induced partial epithelial-to-mesenchymal transition drives renal fibrosis in mice and can be targeted to reverse established disease. *Nat. Med.* 21 (9), 989–997. doi: 10.1038/nm.3901

Grgic, I., Campanholle, G., Bijol, V., Wang, C., Sabbisetti, V. S., Ichimura, T., et al. (2012). Targeted proximal tubule injury triggers interstitial fibrosis and glomerulosclerosis. *Kidney Int.* 82 (2), 172–183. doi: 10.1038/ki.2012.20

Ha, H., and Lee, H. B. (2003). Reactive oxygen species and matrix remodeling in diabetic kidney. *J. Am. Soc. Nephrol.* 14 (8 Suppl 3), S246–S249. doi: 10.1097/01.asn.0000077411.98742.54

Hasegawa, K., Wakino, S., Simic, P., Sakamaki, Y., Minakuchi, H., Fujimura, K., et al. (2013). Renal tubular Sirt1 attenuates diabetic albuminuria by epigenetically suppressing Claudin-1 overexpression in podocytes. *Nat. Med.* 19 (11), 1496–1504. doi: 10.1038/nm.3363

Hauet, T., Goujon, J. M., Vandewalle, A., Baumert, H., Lacoste, L., Tillement, J. P., et al. (2000). Trimetazidine reduces renal dysfunction by limiting the cold ischemia/reperfusion injury in autotransplanted pig kidneys. *J. Am. Soc. Nephrol.* 11 (1), 138–148.

Hay, E. D., and Zuk, A. (1995). Transformations between epithelium and mesenchyme: normal, pathological, and experimentally induced. *Am. J. Kidney Dis.* 26 (4), 678–690. doi: 10.1016/0272-6386(95)90610-x

Hayashida, S., Arimoto, A., Kuramoto, Y., Kozako, T., Honda, S., Shimeno, H., et al. (2010). Fasting promotes the expression of SIRT1, an NAD+ -dependent protein deacetylase, via activation of PPARalpha in mice. *Mol. Cell Biochem.* 339 (1-2), 285–292. doi: 10.1007/s11010-010-0391-z

Hills, C. E., and Squires, P. E. (2011). The role of TGF-beta and epithelial-to mesenchymal transition in diabetic nephropathy. *Cytokine Growth Factor Rev.* 22 (3), 131–139. doi: 10.1016/j.cytogfr.2011.06.002

Irsik, D. L., Romero-Aleshire, M. J., Chavez, E. M., Fallet, R. W., Brooks, H. L., Carmines, P. K., et al. (2018). Renoprotective impact of estrogen receptor-alpha and its splice variants in female mice with type 1 diabetes. *Am. J. Physiol. Renal Physiol.* 315 (3), F512–F520. doi: 10.1152/ajprenal.00231.2017

Iwano, M. (2010). EMT and TGF-beta in renal fibrosis. *Front. Biosci. (Schol Ed)* 2, 229–238. doi: 10.2741/s60

Kalimuthu, S., Gangadaran, P., Rajendran, R. L., Zhu, L., Oh, J. M., Lee, H. W., et al. (2018). A New Approach for Loading Anticancer Drugs Into Mesenchymal Stem Cell-Derived Exosome Mimetics for Cancer Therapy. *Front. Pharmacol.* 9, 1116. doi: 10.3389/fphar.2018.01116

Kalluri, R., and Neilson, E. G. (2003). Epithelial-mesenchymal transition and its implications for fibrosis. *J. Clin. Invest.* 112 (12), 1776–1784. doi: 10.1172/JCI20530

Kantor, P. F., Lucien, A., Kozak, R., and Lopaschuk, G. D. (2000). The antianginal drug trimetazidine shifts cardiac energy metabolism from fatty acid oxidation to glucose oxidation by inhibiting mitochondrial long-chain 3-ketoacyl coenzyme A thiolase. *Circ. Res.* 86 (5), 580–588. doi: 10.1161/01.res.86.5.580

Karadeniz, T., Cavusoglu, T., Turkmen, E., Uyanikgil, Y., Karadeniz, M., Akdemir, O., et al. (2014). Experimental comparison of protective characteristics of enalapril and trimetazidine in diabetic nephropathy. *Ren Fail* 36 (8), 1283–1290. doi: 10.3109/0886022X.2014.930331

Kume, S., Haneda, M., Kanasaki, K., Sugimoto, T., Araki, S., Isshiki, K., et al. (2007). SIRT1 inhibits transforming growth factor beta-induced apoptosis in glomerular mesangial cells via Smad7 deacetylation. *J. Biol. Chem.* 282 (1), 151–158. doi: 10.1074/jbc.M605904200

Li, S., Wang, J., Zhang, B., Li, X., and Liu, Y. (2019). Diabetes Mellitus and Cause-Specific Mortality: A Population-Based Study. *Diabetes Metab. J.* 43 (3), 319–341. doi: 10.4093/dmj.2018.0060

Liu, X., Gai, Y., Liu, F., Gao, W., Zhang, Y., Xu, M., et al. (2010). Trimetazidine inhibits pressure overload-induced cardiac fibrosis through NADPH oxidase-ROS-CTGF pathway. *Cardiovasc. Res.* 88 (1), 150–158. doi: 10.1093/cvr/cvq181

Liu, Z., Chen, J. M., Huang, H., Kuznicki, M., Zheng, S., Sun, W., et al. (2016). The protective effect of trimetazidine on myocardial ischemia/reperfusion injury through activating AMPK and ERK signaling pathway. *Metabolism* 65 (3), 122–130. doi: 10.1016/j.metabol.2015.10.022

Lopaschuk, G. D., Barr, R., Thomas, P. D., and Dyck, J. R. (2003). Beneficial effects of trimetazidine in ex vivo working ischemic hearts are due to a stimulation of glucose oxidation secondary to inhibition of long-chain 3-ketoacyl coenzyme a thiolase. *Circ. Res.* 93 (3), e33–e37. doi: 10.1161/01.RES.0000086964.07404.A5

Morigi, M., Perico, L., and Benigni, A. (2018). Sirtuins in Renal Health and Disease. *J. Am. Soc. Nephrol.* 29 (7), 1799–1809. doi: 10.1681/ASN.2017111218

Muraoka, H., Hasegawa, K., Sakamaki, Y., Minakuchi, H., Kawaguchi, T., Yasuda, I., et al. (2019). Role of Nampt-Sirt6 Axis in Renal Proximal Tubules in Extracellular Matrix Deposition in Diabetic Nephropathy. *Cell Rep.* 27199-212 (1), e195. doi: 10.1016/j.celrep.2019.03.024

Noriega, L. G., Feige, J. N., Canto, C., Yamamoto, H., Yu, J., Herman, M. A., et al. (2011). CREB and ChREBP oppositely regulate SIRT1 expression in response to energy availability. *EMBO Rep.* 12 (10), 1069–1076. doi: 10.1038/embor.2011.151

Okada, T., Nagao, T., Matsumoto, H., Nagaoka, Y., Wada, T., and Nakao, T. (2012). Histological predictors for renal prognosis in diabetic nephropathy in diabetes mellitus type 2 patients with overt proteinuria. *Nephrol. (Carlton)* 17 (1), 68–75. doi: 10.1111/j.1440-1797.2011.01525.x

Onay-Besikci, A., and Ozkan, S. A. (2008). Trimetazidine revisited: a comprehensive review of the pharmacological effects and analytical techniques for the determination of trimetazidine. *Cardiovasc. Ther.* 26 (2), 147–165. doi: 10.1111/j.1527-3466.2008.00043.x

Onbasili, A. O., Yeniceriglu, Y., Agaoglu, P., Karul, A., Tekten, T., Akar, H., et al. (2007). Trimetazidine in the prevention of contrast-induced nephropathy after coronary procedures. *Heart* 93 (6), 698–702. doi: 10.1136/hrt.2006.097477

Oshimori, N., and Fuchs, E. (2012). Paracrine TGF-beta signaling counterbalances BMP-mediated repression in hair follicle stem cell activation. *Cell Stem Cell* 10 (1), 63–75. doi: 10.1016/j.stem.2011.11.005

Rahman, S., and Islam, R. (2011). Mammalian Sirt1: insights on its biological functions. *Cell Commun. Signal* 9, 11. doi: 10.1186/1478-811X-9-11

Revollo, J. R., and Li, X. (2013). The ways and means that fine tune Sirt1 activity. *Trends Biochem. Sci.* 38 (3), 160–167. doi: 10.1016/j.tibs.2012.12.004

Satyanarayana, P. S., and Chopra, K. (2002). Oxidative stress-mediated renal dysfunction by cyclosporine A in rats: attenuation by trimetazidine. *Ren Fail* 24 (3), 259–274. doi: 10.1081/jdi-120005360

Scarpulla, R. C. (2008). Transcriptional paradigms in mammalian mitochondrial biogenesis and function. *Physiol. Rev.* 88 (2), 611–638. doi: 10.1152/physrev.00025.2007

Sharma, K. (2016). Obesity and Diabetic Kidney Disease: Role of Oxidant Stress and Redox Balance. *Antioxid. Redox Signal* 25 (4), 208–216. doi: 10.1089/ars.2016.6696

Shi, L., Zhao, C., Wang, H., Lei, T., Liu, S., Cao, J., et al. (2017). Dimethylarginine Dimethylaminohydrolase 1 Deficiency Induces the Epithelial to Mesenchymal Transition in Renal Proximal Tubular Epithelial Cells and Exacerbates Kidney Damage in Aged and Diabetic Mice. *Antioxid. Redox Signal* 27 (16), 1347–1360. doi: 10.1089/ars.2017.7022

Simic, P., Williams, E. O., Bell, E. L., Gong, J. J., Bonkowski, M., and Guarente, L. (2013). SIRT1 suppresses the epithelial-to-mesenchymal transition in cancer metastasis and organ fibrosis. *Cell Rep.* 3 (4), 1175–1186. doi: 10.1016/j.celrep.2013.03.019

Stahl, P. J., and Felsen, D. (2001). Transforming growth factor-beta, basement membrane, and epithelial-mesenchymal transdifferentiation: implications for fibrosis in kidney disease. *Am. J. Pathol.* 159 (4), 1187–1192. doi: 10.1016/s0002-9440(10)62503-5

Taft, J. L., Nolan, C. J., Yeung, S. P., Hewitson, T. D., and Martin, F. I. (1994). Clinical and histological correlations of decline in renal function in diabetic patients with proteinuria. *Diabetes* 43 (8), 1046–1051. doi: 10.2337/diab.43.8.1046

Tuttle, K. R., Bakris, G. L., Bilous, R. W., Chiang, J. L., de Boer, I. H., Goldstein-Fuchs, J., et al. (2014). Diabetic kidney disease: a report from an ADA Consensus Conference. *Am. J. Kidney Dis.* 64 (4), 510–533. doi: 10.1053/j.ajkd.2014.08.001

Umanath, K., and Lewis, J. B. (2018). Update on Diabetic Nephropathy: Core Curriculum 2018. *Am. J. Kidney Dis.* 71 (6), 884–895. doi: 10.1053/j.ajkd.2017.10.026

Vaidya, V. S., Niewczas, M. A., Ficociello, L. H., Johnson, A. C., Collings, F. B., Warram, J. H., et al. (2011). Regression of microalbuminuria in type 1 diabetes is associated with lower levels of urinary tubular injury biomarkers, kidney injury molecule-1, and N-acetyl-beta-D-glucosaminidase. *Kidney Int.* 79 (4), 464–470. doi: 10.1038/ki.2010.404

Vasquez, M. C., and Tomanek, L. (2019). Sirtuins as regulators of the cellular stress response and metabolism in marine ectotherms. *Comp. Biochem. Physiol. A Mol. Integr. Physiol.* 236, 110528. doi: 10.1016/j.cbpa.2019.110528

Wan, P., Su, W., Zhang, Y., Li, Z., Deng, C., and Zhuo, Y. (2017). Trimetazidine protects retinal ganglion cells from acute glaucoma via the Nrf2/Ho-1 pathway. *Clin. Sci. (Lond.)* 131 (18), 2363–2375. doi: 10.1042/CS20171182

Wang, D., Jiang, X., Lu, A., Tu, M., Huang, W., and Huang, P. (2018). BMP14 induces tenogenic differentiation of bone marrow mesenchymal stem cells in vitro. *Exp. Ther. Med.* 16 (2), 1165–1174. doi: 10.3892/etm.2018.6293

Wang, T., Gao, Y., Wang, X., Shi, Y., Xu, J., Wu, B., et al. (2019). Calpain-10 drives podocyte apoptosis and renal injury in diabetic nephropathy. *Diabetes Metab. Syndr. Obes.* 12, 1811–1820. doi: 10.2147/DMSO.S217924

Warren, A. M., Knudsen, S. T., and Cooper, M. E. (2019). Diabetic nephropathy: an insight into molecular mechanisms and emerging therapies. *Expert Opin. Ther. Targets* 23 (7), 579–591. doi: 10.1080/14728222.2019.1624721

Webster, A. C., Nagler, E. V., Morton, R. L., and Masson, P. (2017). Chronic Kidney Disease. *Lancet* 389 (10075), 1238–1252. doi: 10.1016/S0140-6736(16)32064-5

Wu, L., Zhang, Y., Ma, X., Zhang, N., and Qin, G. (2012). The effect of resveratrol on FoxO1 expression in kidneys of diabetic nephropathy rats. *Mol. Biol. Rep.* 39 (9), 9085–9093. doi: 10.1007/s11033-012-1780-z

Wu, P., Wang, Y., Davis, M. E., Zuckerman, J. E., Chaudhari, S., Begg, M., et al. (2015). Store-Operated Ca2+ Channels in Mesangial Cells Inhibit Matrix Protein Expression. *J. Am. Soc. Nephrol.* 26 (11), 2691–2702. doi: 10.1681/ASN.2014090853

Xu, J., Lamouille, S., and Derynck, R. (2009). TGF-beta-induced epithelial to mesenchymal transition. *Cell Res.* 19 (2), 156–172. doi: 10.1038/cr.2009.5

Yang, J., and Liu, Y. (2002). Blockage of tubular epithelial to myofibroblast transition by hepatocyte growth factor prevents renal interstitial fibrosis. *J. Am. Soc. Nephrol.* 13 (1), 96–107.

Yilmaz, M. I., Saglam, M., Qureshi, A. R., Carrero, J. J., Caglar, K., Eyileten, T., et al. (2008). Endothelial dysfunction in type-2 diabetics with early diabetic nephropathy is associated with low circulating adiponectin. *Nephrol. Dial. Transplant.* 23 (5), 1621–1627. doi: 10.1093/ndt/gfm828

Zeni, L., Norden, A. G. W., Cancarini, G., and Unwin, R. J. (2017). A more tubulocentric view of diabetic kidney disease. *J. Nephrol.* 30 (6), 701–717. doi: 10.1007/s40620-017-0423-9

Zhang, L., Lu, Y., Jiang, H., Zhang, L., Sun, A., Zou, Y., et al. (2012). Additional use of trimetazidine in patients with chronic heart failure: a meta-analysis. *J. Am. Coll. Cardiol.* 59 (10), 913–922. doi: 10.1016/j.jacc.2011.11.027

Zhang, L., Ding, W. Y., Wang, Z. H., Tang, M. X., Wang, F., Li, Y., et al. (2016). Early administration of trimetazidine attenuates diabetic cardiomyopathy in rats by alleviating fibrosis, reducing apoptosis and enhancing autophagy. *J. Transl. Med.* 14 (1), 109. doi: 10.1186/s12967-016-0849-1

Zhang, Y., Connelly, K. A., Thai, K., Wu, X., Kapus, A., Kepecs, D., et al. (2017). Sirtuin 1 Activation Reduces Transforming Growth Factor-beta1-Induced Fibrogenesis and Affords Organ Protection in a Model of Progressive, Experimental Kidney and Associated Cardiac Disease. *Am. J. Pathol.* 187 (1), 80–90. doi: 10.1016/j.ajpath.2016.09.016

Zhao, Y., Yin, Z., Li, H., Fan, J., Yang, S., Chen, C., et al. (2017). MiR-30c protects diabetic nephropathy by suppressing epithelial-to-mesenchymal transition in db/db mice. *Aging Cell* 16 (2), 387–400. doi: 10.1111/acel.12563

Zhu, Y., Wang, K., Ma, Z., Liu, D., Yang, Y., Sun, M., et al. (2019). SIRT1 activation by butein attenuates sepsis-induced brain injury in mice subjected to cecal ligation and puncture via alleviating inflammatory and oxidative stress. *Toxicol. Appl. Pharmacol.* 363, 34–46. doi: 10.1016/j.taap.2018.10.013

Conflict of Interest: The authors declare that the research was conducted in the absence of any commercial or financial relationships that could be construed as a potential conflict of interest.

Copyright © 2020 Yang, Wang, He, Liu, Chen, Wang, Wang and Wang. This is an open-access article distributed under the terms of the Creative Commons Attribution License (CC BY). The use, distribution or reproduction in other forums is permitted, provided the original author(s) and the copyright owner(s) are credited and that the original publication in this journal is cited, in accordance with accepted academic practice. No use, distribution or reproduction is permitted which does not comply with these terms.

Advantages of publishing in Frontiers

OPEN ACCESS
Articles are free to read for greatest visibility and readership

FAST PUBLICATION
Around 90 days from submission to decision

HIGH QUALITY PEER-REVIEW
Rigorous, collaborative, and constructive peer-review

TRANSPARENT PEER-REVIEW
Editors and reviewers acknowledged by name on published articles

Frontiers
Avenue du Tribunal-Fédéral 34
1005 Lausanne | Switzerland

Visit us: www.frontiersin.org
Contact us: info@frontiersin.org | +41 21 510 17 00

REPRODUCIBILITY OF RESEARCH
Support open data and methods to enhance research reproducibility

DIGITAL PUBLISHING
Articles designed for optimal readership across devices

FOLLOW US
@frontiersin

IMPACT METRICS
Advanced article metrics track visibility across digital media

EXTENSIVE PROMOTION
Marketing and promotion of impactful research

LOOP RESEARCH NETWORK
Our network increases your article's readership